# EMERGING INFECTIOUS DISEASES®

Vectorborne Infectious Diseases
February 2021

Ted Geisel (aka Dr. Seuss) illustration; Munro Leaf, text; United States War Department Special Services Division and Government Printing Office.
*This is Ann–: she drinks blood!* (1943) (detail). Photomechanical print (poster): 35 inches x 47 inches/89 cm x 120 cm. National Library of Medicine, Bethesda, Maryland, USA. Public domain image.

EMERGING INFECTIOUS DISEASES®



Emerging Infectious Diseases is published monthly by the Centers for Disease Control and Prevention, 1600 Clifton Rd NE, Mailstop H16-2, Atlanta, GA 30329-4027, USA. Telephone 404-639-1960; email, eideditor@cdc.gov

# EMERGING INFECTIOUS DISEASES®

Vectorborne Infectious Diseases February 2020


## On the Cover

**Ted Geisel (aka Dr. Seuss) illustration; Munro Leaf, text; United States War Department Special Services Division and Government Printing Office.** ***This is Ann–: she drinks blood!*** **(1943)** (detail). Photomechanical print (poster): 35 inches x 47 inches/89 cm x 120 cm. National Library of Medicine, Bethesda, Maryland, United States. Public domain image.

## Synopses



## Research

EMERGING INFECTIOUS DISEASES®
February 2020

## Dispatches

## Research Letters



EMERGING INFECTIOUS DISEASES®
February 2020



## Books and Media



## About the Cover



### Etymologia

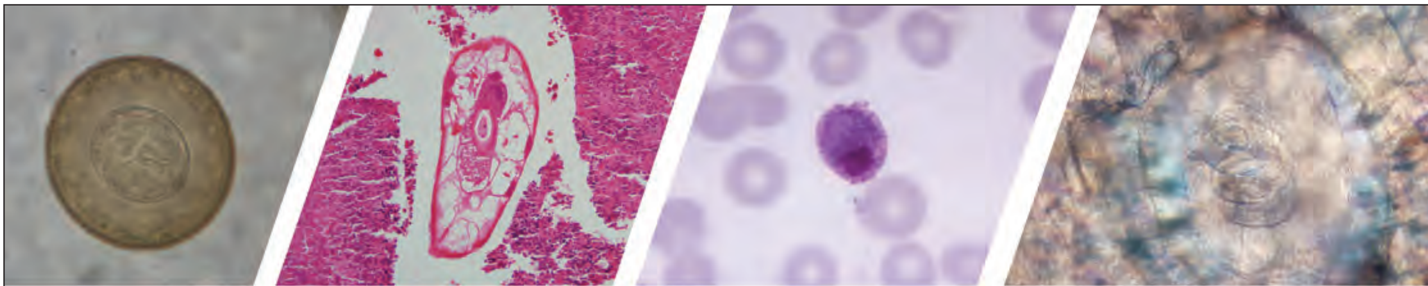

# DPDx

## Diagnostic Assistance and Training in Laboratory Identification of Parasites

A free service of CDC available to laboratorians, pathologists, and other health professionals in the United States and abroad

- Diagnosis from photographs of worms, histological sections, fecal, blood, and other specimen types
- Expert diagnostic review
- Formal diagnostic laboratory report
- Submission of samples via secure file share

Visit the DPDx website for information on laboratory diagnosis, geographic distribution, clinical features, parasite life cycles, and training via Monthly Case Studies of parasitic diseases.

www.cdc.gov/dpdx
dpdx@cdc.gov

CS272346-DE

**U.S. Department of Health and Human Services**
Centers for Disease Control and Prevention

# Childcare Exposure to Severe Acute Respiratory Syndrome Coronavirus 2 for 4-Year-Old Presymptomatic Child, South Korea

Yoonsun Yoon,[1] Gwang-Jun Choi,[1] Ji Yeong Kim, Kyung-Ran Kim, Hwanhee Park, Jae Kyung Chun,[2] Yae-Jean Kim[2]

Data on transmission of severe acute respiratory syndrome coronavirus 2 (SARS-CoV-2) from preschool-age children to children and adults are limited. We investigated SARS-CoV-2 exposure at a childcare center in South Korea. A 4-year-old child, probably infected by his grandmother, attended the center during the presymptomatic period (February 19–21, 2020). Fever developed on February 22, and he was given a diagnosis SARS-CoV-2 infection on February 27. At the center, 190 persons (154 children and 36 adults) were identified as contacts; 44 (23.2%) were defined as close contacts (37 children and 7 adults). All 190 persons were negative for SARS-CoV-2 on days 8–9 after the last exposure. Two close contacts (1 child and 1 adult) showed development of symptoms on the last day of quarantine. However, subsequent test results were negative. This investigation adds indirect evidence of low potential infectivity in a childcare setting with exposure to a presymptomatic child.

The exact number of global confirmed cases of coronavirus disease (COVID-19) in children is unknown. Since the first case report in a child, 2.2%–6.7% of reported cases from China, the United States, the European Union, and the United Kingdom have occurred in children (*1–3*). In South Korea, 14,305 SARS-CoV-2 cases were diagnosed as of July 31, 2020 (*4*). Of these cases, 1,028 were in children ≤19 years of age; the proportions of cases for persons ≤19 years of age was 7.2% and for persons for ≤9 years of age was 1.7% (*4*). The proportion of COVID-19 cases in children in South Korea was higher than that for China (2.2%) and the United States (5.1%) (*1,2*). This proportion was comparable to that for the European Union and the United Kingdom (6.7%) (*3*).

Respiratory virus infection among young children in childcare settings is a major epidemiologic consideration. Children are believed to be vectors for transmission of many respiratory viral diseases, including influenza and infection with respiratory syncytial virus (*5–7*). However, there are few data on SARS-CoV-2 transmission among young children.

In South Korea, the first imported case of SARS-CoV-2 from Wuhan, China, was reported on January 20, 2020 (*8*). The first case in a child from South Korea was diagnosed on February 18 (*9*). A religious group–related large outbreak in Daegu (a city with a population of 2.4 million in the southeastern part of the country) started on February 18 (*9*); a total of 5,212 patients were eventually found to have COVID-19 related to the religious group outbreak (*10*). Social distancing measures, including temporary closure of childcare centers, were initiated in Daegu immediately. However, other regions with no confirmed patients with COVID-19 remained open, including Miryang-si (population 108,600, 60 km from Daegu). The first patient with COVID-19 in Miryang-si was a 35-year-old man given a diagnosis on February 26, when there were 710 confirmed cases in Daegu (*11*). Subsequently, his 4-year-old son was given a diagnosis of COVID-19. The child had attended a childcare center during his presymptomatic period (February 19–21). In this study, we report the results of an epidemiologic investigation of potential exposure to a presymptomatic child who attended a childcare center in South Korea.

Author affiliations: Samsung Medical Center, Sungkyunkwan University School of Medicine, Seoul, South Korea (Y. Yoon, K.-R. Kim, H. Park, Y.-J. Kim); Division of Infectious Disease Control, Daegu Metropolitan City, Daegu, South Korea (G.-J. Choi); Miryang-si Public Health Center, Miryang, South Korea (J.Y. Kim, J.K. Chun)

DOI: https://doi.org/10.3201/eid2702.203189

[1]These authors contributed equally to this article.

[2]These senior authors contributed equally to this article.

## Materials and Methods

### Setting

On February 27, 2020, the Miryang-si Public Health Center was notified of a confirmed case of a 4-year-old child with COVID-19 and possible exposure of children and adult staff by this child at a childcare center. The childcare center consisted of 17 classes divided by age group from <1 to 7 years. Children usually stayed at the center from 8:00 AM to 6:00 PM, depending on schedules of parents. The index case-patient attended a class for 4- or 5-year-old children that had 13 classmates and 2 teachers. Each classroom had its own toilet, and children ate lunch and snacks in their classrooms with classmates and teachers. The center also has shuttle buses that can transport an average of 20 children, 2 teachers, and 1 driver.

Under the guidance of local health authorities, wearing masks, more frequent hand hygiene, and disinfection of the environment were required before the child tested positive. Adult staff at the center wore masks, but mask wearing by children were not consistent.

### Epidemiologic Investigation and Case Definition

An epidemiologic investigation was conducted. Close contacts were identified by trained epidemic intelligence officers on the basis of surveillance by closed-circuit television, childcare schedules, and statements from teachers. Close contact was defined as a person who had face-to-face contact for ≥15 minutes or who had direct physical contact with the index case-patient. Persons who used the same shuttle bus were also considered to be close contacts.

### Response Measures

After the index case-patient was identified, the center was closed. All potentially exposed persons were quarantined at home for 14 days.

Symptoms of close contacts were actively monitored by the local health authority through phone calls twice a day. For the remaining persons, passive reporting through self-assessment for fever or a defined set of newly present symptoms indicative of COVID-19 was conducted. Acute respiratory symptoms included fever, sore throat, rhinorrhea, myalgia, dyspnea, or cough.

All children and staff members (n = 190) at the center were tested 8–9 days after the last exposure for SARS-CoV-2, which was the earliest time point on which we could perform PCR considering the median incubation period for COVID-19 (*12*). The tests were performed at a drive-through test facility (*13*) or the COVID-19 screening clinic of Miryang-si Public Health Center. All samples were collected by obtaining nasopharyngeal swab specimens and tested by using real-time reverse transcription PCRs for SARS-CoV-2.

### Data Collection and Analysis

We obtained information on demographic characteristics and presence of symptoms by using standardized epidemiologic investigation forms. The investigation was a part of a public health response and was not considered research subject to institutional review board approval; therefore, written informed consent was not required. Personal information was accessed only by the public health officer of Miryang-si and epidemic intelligence officer of Daegu. Participant confidentiality was maintained throughout the study.

## Results

### Family Exposure

The index case-patient was a 4-year-old boy who lived in Miryang-si and was suspected of contracting the virus from his grandmother, who lived in Daegu. His grandmother attended the religious services on February 12 and 16 that were related to the large religious group outbreak in Daegu. He had contact with his grandmother on February 12 and 15 when he visited Daegu with his father. However, he and his father did not attend the religious service. His grandmother also came to the child's house and stayed in Miryang-si during February 17–27.

The index case-patient showed development of fever (temperature 39°C) on February 22 and a cough on February 24. He was treated by a pediatrician on February 23 and 25. His father also showed development of fever, cough, and myalgia. The father was confirmed to have COVID-19 on February 26 (cycle threshold [$C_t$] value for envelope gene 19.0, positive cutoff value 40.0). The child and his asymptomatic grandmother were confirmed to have COVID-19 on February 27. The $C_t$ value was 24.6 (positive cutoff value 37.0) for the child and 32.7 (positive cutoff value 37.0) for the grandmother. His grandmother was asymptomatic during this entire period (Figure 1).

### Childcare Exposure

The index case-patient attended the childcare center on February 19–21 during a presymptomatic period before his fever developed (Figure 1). He traveled to the center by shuttle bus; the bus ride took ≈30 minutes in each direction. On the shuttle bus from

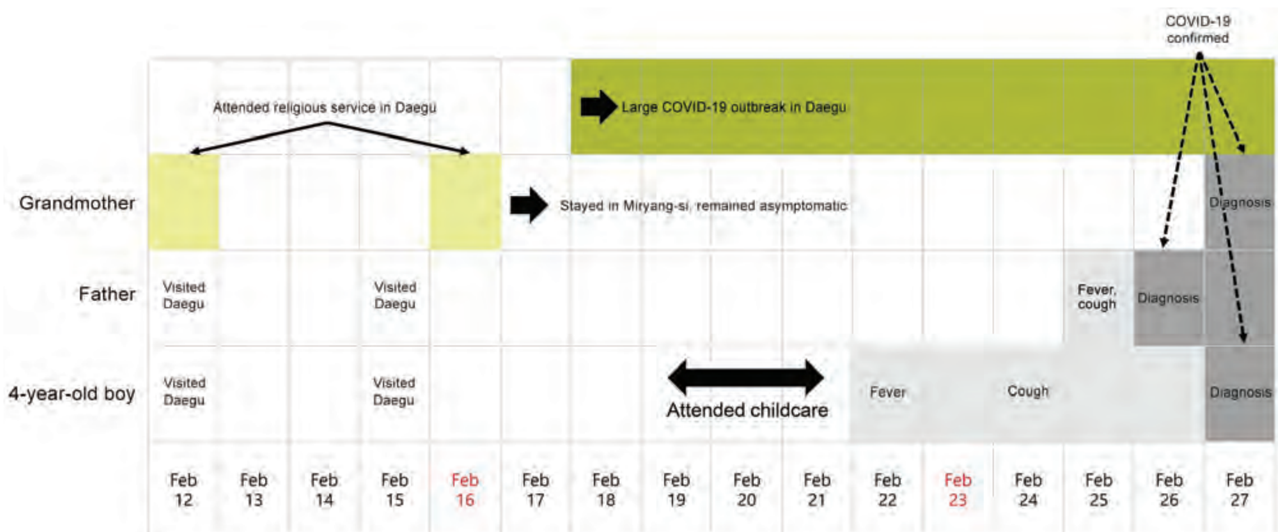


**Figure 1.** Timeline of family exposure and progress of symptoms until diagnosis of a 4-year-old child (index case-patient) and adult family members, South Korea. The index case-patient attended a childcare center during February 19–21, 2020. He showed development of fever on February 22. His father was given a diagnosis of COVID-19 on February 26. The index case-patient and his grandmother were given a diagnosis on February 27. The asymptomatic grandmother was suspected to be the primary case-patient in the family because she attended a religious service in Daegu, where a large outbreak occurred. Sundays are indicated in red. COVID-19, coronavirus disease.

his house to the center, 9 children, 2 teachers, and 1 bus driver were exposed. On the shuttle bus from the center to his house, an additional 15 children and 2 teachers were exposed. The boy attended the center for an average of ≈8 hours/day, and he had lunch and 2 snack times/day with his classmates in his classroom. He used the toilet in the classroom ≈5 times/day. There was no outside activity because of cold weather. Thirteen classmates of similar ages and 2 teachers were exposed to the index case-patient in the same classroom. Among these persons, 1 child was also exposed on the shuttle bus. Closed-circuit television review additionally identified a friend from another class who visited his classroom and played with him.

A total of 190 persons (154 children and 36 adults) at the center were identified as potential contacts (Figure 2). The median age of exposed children was 4.1 years (range 0.9–7.2 years), and 75 (49%) were male. The median age of exposed adults was 42.0 years (range 22.1–64.8 years), and 3 (8%) were male. Of the 190 contacts, 44 (23.2%) were exposed to the index case-patient and considered close contacts: 37 (84.0%) children and 7 (16.0%) adults (1 bus driver and 6 teachers).

After the investigation, all 190 exposed persons had PCR testing for SARS-CoV-2 on the 8th and 9th days after the last exposure; 185 were tested in a drive-through test center, and 5 were tested in the COVID-19 screening clinic of Miryang-si Public Health Center. Among close contacts, 1 classmate and 1 teacher in the class of the index case-patient showed development of cough on the last day of quarantine (14 days from the last exposure). However, subsequent testing of nasopharyngeal swab specimens for these 2 persons showed negative results. The investigation and monitoring ended on March 6, 2020, which was 14 days after the last day the child attended the center, which was 1 day before fever onset. There were no laboratory-confirmed secondary cases of COVID-19 during this exposure. Although 2 close contacts showed development of symptoms during the quarantine period and were retested, test results for these close contacts were negative.

## Discussion

We describe a childcare center exposure of SARS-CoV-2 for a 4-year-old presymptomatic child and the subsequent investigation, with detailed information on exposure types and durations among exposed children and adult staff members. Among all 190 persons at the center who were tested and monitored, no secondary cases were identified.

There are few data on childcare exposure to SARS-CoV-2 among young children. Recently, a few reports were published from the United States and Australia. In Rhode Island, USA, 666 of 891 childcare programs reopened as of July 31, 2020 (*14*). Local health authorities required strict regulations, including restricting the maximum number of persons in a

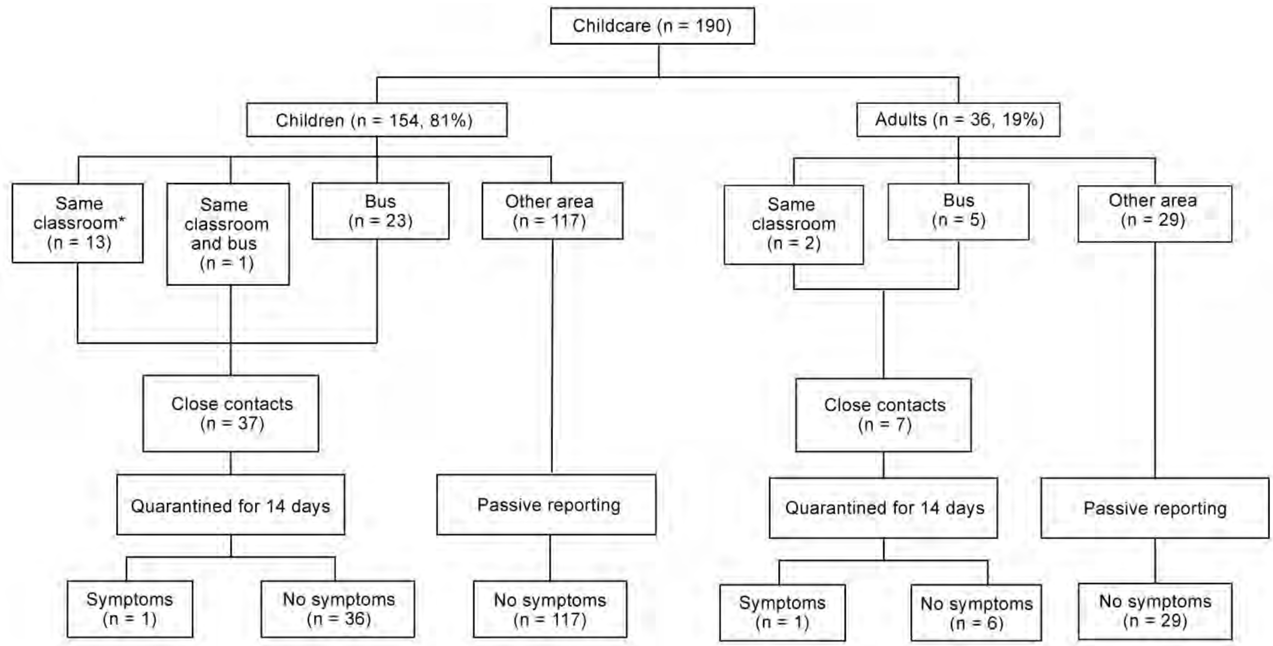


**Figure 2.** Persons exposed to severe acute respiratory syndrome coronavirus 2 (SARS-CoV-2) (154 children and 36 adults) in a childcare center and a shuttle bus, South Korea. All exposed persons underwent testing for SARS-CoV-2 and showed negative results. Close contacts (37 children and 7 adults) were quarantined for 14 days, and persons who had symptoms during the quarantine period were retested; all had negative results. *One child was exposed when she visited the classroom of the index case-patient.

class, limiting switching between classes, staff use of masks, daily symptom monitoring of staff and attendees, and enhanced disinfection of the center (*14*). During June 1–July 31, a total of 52 laboratory-confirmed or probable COVID-19 cases, including cases in 30 children, were identified. Among the 666 reopened childcare centers, staff members and attendees from 29 (4.0%) centers were exposed to SARS-CoV-2 (*14*). Epidemiologic investigation showed that there was 1 case without further transmission at 20 (69.0%) of these 29 centers. In 5 (17.0%) of the 29 programs, 2–5 COVID-19 cases/program were identified; however, there was no evidence of childcare-related transmission. Childcare-related transmission occurred at 4 (14.0%) of the 29 programs (2–10 COVID-19 cases/program); 2 of these programs did not adhere strictly to regulations (*14*). Therefore, of the 86% of childcare programs in the study that had COVID-19 cases, there were no instances of secondary transmission. In addition, a 2-year-old child attended childcare for 6 days while potentially infectious and did not produce secondary transmission.

In Salt Lake City, Utah, USA, during April 1–July 10, 2020, small-to-large outbreaks occurred in 3 childcare facilities for which complete investigation data were available (*15*). All 3 outbreaks were linked to index cases in adult staff members (*15*). Childcare-related transmission occurred; there were 2–15 COVID-19 cases/facility (*15*). The facility that had 15 patients given a diagnosis of COVID-19 did not require wearing masks for staff members and children. A total of 12 children (age range 8 months–10 years) were probably infected with SARS-CoV-2 at childcare centers (*15*). A total of 83 household and nonhousehold contacts were exposed to these 12 case-patients. Among those 83 contacts, 5 probable and 7 confirmed patients with COVID-19 were identified, including parents and siblings (*15*).

In New South Wales, Australia, 10 childcare centers for children age 6 weeks–5 years had exposure to COVID-19 cases during January 25–April 10, 2020 (*16*). The primary cases were defined as initial infectious cases in this setting (*16*). Of those 10 centers, the exposure occurred by primary pediatric cases in 3 centers (30.0%). At these 3 centers, 85 children and 37 adults were defined as being close contacts and quarantined (*16*). Among these persons, 17 (20.0%) of 85 children and 11 (30.0%) of 37 adults were tested, and all showed negative results (*16*). Overall, secondary transmission occurred in only 1 center, in which the primary case-patient was a 49-year-old woman (staff member). Of 37 close contacts at that childcare center, 6 staff and 7 children were infected with SARS-CoV-2 (*16*). However, there was little evidence of child-to-child transmission or child-to-adult transmission in that epidemiologic investigation (*16*).

Our findings, along with literature discussed, might suggest potential low transmissibility of SARS-CoV-2 among young children in childcare settings. However, there might be differences in background COVID-19 situations between countries in which studies were conducted. Our epidemiologic investigation was conducted at the early stages of the pandemic, when a large outbreak first started in Daegu and the virus rapidly spread to nearby cities. Public awareness, mitigation measures, and public health responses were believed to be incomplete at that time. The study from Australia was conducted in communities that had low transmission rates and good public health responses (*17*). Although the studies from the United States showed that a few child-to-child or child-to-adult transmissions probably occurred in childcare centers, community transmission rates were higher in that country, which might confound true transmission rates from pediatric patients with COVID-19 in childcare settings. In addition, less strict adherence to precautions in some childcare facilities could have also affected the childcare-related transmission (*14*,*15*).

There were also a few reports of school exposure in older children during the early period of the COVID-19 pandemic. A report of a cluster in the French Alps included a 9-year-old boy who did not transmit SARS-CoV-2 to any other persons, although 112 persons at 3 different schools had contact with him (*18*). However, detailed information on exposure at schools was not available for that study. In a report from New South Wales, Australia, there were several high schools and 1 primary school in which many children and adolescents were exposed to a child (index-patient[s]) but few secondary cases resulted (*19*). In 15 schools (10 high school and 5 primary schools), 18 COVID-19 cases (in 9 students and 9 staff) were identified during March 5–April 3, 2020. Of 863 identified close contacts, only 2 secondary cases, both in children, resulted from transmission in the school setting; 1 case-patient was infected by another child and the other case-patient by an adult staff member. However, there were no details on exposure setting. In Ireland, for notifications of SARS-CoV-2 infection before school closure in March 2020, there was no transmission from 3 children (index case-patients) among 905 contacts in the school settings (*20*). All children who had COVID-19 in Ireland attended schools during the presymptomatic and symptomatic periods, and other children were exposed in a variety of settings, including music lessons (woodwind instruments) and choir practice, both of which are high-risk activities for virus transmission. Studies in France (*18*) and Ireland (*20*) performed laboratory tests only for symptomatic persons and might have underestimated asymptomatic or paucisymptomatic patients. In comparison, we collected test results on all persons at the childcare center in our study.

There have been reports demonstrating that children are not the main drivers of the COVID-19 outbreak (*21*,*22*), but it is unclear whether these findings are caused by low susceptibility, low transmissibility, or both. An age-structured mathematical model estimated that persons <20 years of age have lower susceptibility to SARS-CoV-2 infection than adults (*23*). Different immune responses or host factors of children have been also suggested as possible mechanisms of their low susceptibility (*24*,*25*). However, an epidemiologic study from China reported a conflicting finding that SARS-CoV-2 exposure rates for children were comparable to those for adults (*26*).

Because children who had COVID-19 had milder symptoms and a high proportion of subclinical infections, viral load and transmissibility during the asymptomatic or presymptomatic period is of particular interest (*23*,*27*,*28*). Several studies of adult patients showed that viral shedding of SARS-CoV-2 peaked at ≈1–2 days before symptom onset, and a substantial proportion of transmission probably occurred during presymptomatic or asymptomatic periods in the index case-patient (*29*,*30*). In children, SARS-CoV-2 RNA was also detected at a comparably high level, as in adults, at the time of diagnosis (*31*). However, more data are needed on whether young children have a high level of virus during the presymptomatic period, as in adults, and can transmit the virus to others.

In our study, the index child was present at a childcare for an average of 8 hours/day and had several meals/snacks with his young classmates at a close distance, with probable close physical contact. However, there were no additional cases.

This study had a few limitations. First, this study was a single epidemiologic investigation of SARS-CoV-2 exposure at 1 childcare center. More data on transmission from young pediatric index case-patients to other children and adults in educational settings are needed. Second, it was not proven that the index case-patient in this report was shedding virus during the presymptomatic period.

Closing childcare or schools has probably reduced transmission of SARS-CoV-2 in children (*32*). However, decisions regarding reopening schools or childcare centers are critical in many countries that are considering the social, educational, and economic benefits to society and children (*33*). Our investigation adds indirect evidence of low potential infectivity among children in a childcare setting when exposed to a presymptomatic child. Therefore, there might be a chance to safely reopen childcares if certain conditions are satisfied, including such infection prevention protocols as good personal hygiene practices, wearing masks, daily symptom monitoring of staff members and attendees, and disinfection of possibly contaminated surfaces and items.

### Acknowledgments

We thank the children, their parents, childcare staff, and public health officials in Miryang-si and Gyeongsangnam-do for their cooperation and Kyong Ran Peck for discussions and critical feedback.

## About the Author

Dr. Yoon is a clinical fellow in the Division of Pediatric Infectious Disease and Immunodeficiency, Department of Pediatrics, Samsung Medical Center, Seoul, South Korea. Her primary research interest is respiratory virus infections.

### References

1. Stokes EK, Zambrano LD, Anderson KN, Marder EP, Raz KM, El Burai Felix S, et al. Coronavirus disease 2019 case surveillance—United States, January 22–May 30, 2020. MMWR Morb Mortal Wkly Rep. 2020;69:759–65. https://doi.org/10.15585/mmwr.mm6924e2
2. Wu Z, McGoogan JM. Characteristics of and important lessons from the coronavirus disease 2019 (COVID-19) outbreak in China: summary of a report of 72,314 cases from the Chinese Center for Disease Control and Prevention. JAMA. 2020;323:1239–42. https://doi.org/10.1001/jama.2020.2648
3. European Centre for Disease Prevention and Control. COVID-19 surveillance report week 34, 2020 [cited 2020 Aug 28]. https://covid19-surveillance-report.ecdc.europa.eu/
4. Korea Centers for Disease Control and Prevention. Daily cumulative confirmed data, March 1 to July 31, 2020, Korea [cited 2020 Jul 31]. https://www.cdc.go.kr/board/board.es?mid=a20501000000&bid=0015
5. Martin ET, Fairchok MP, Stednick ZJ, Kuypers J, Englund JA. Epidemiology of multiple respiratory viruses in childcare attendees. J Infect Dis. 2013;207:982–9. https://doi.org/10.1093/infdis/jis934
6. Chu HY, Kuypers J, Renaud C, Wald A, Martin E, Fairchok M, et al. Molecular epidemiology of respiratory syncytial virus transmission in childcare. J Clin Virol. 2013;57:343–50. https://doi.org/10.1016/j.jcv.2013.04.011
7. Bin Nafisah S, Alamery AH, Al Nafesa A, Aleid B, Brazanji NA. School closure during novel influenza: a systematic review. J Infect Public Health. 2018;11:657–61. https://doi.org/10.1016/j.jiph.2018.01.003
8. Kim JY, Choe PG, Oh Y, Oh KJ, Kim J, Park SJ, et al. The first case of 2019 novel coronavirus pneumonia imported into Korea from Wuhan, China: implication for infection prevention and control measures. J Korean Med Sci. 2020;35:e61. https://doi.org/10.3346/jkms.2020.35.e61
9. Korean Society of Infectious Diseases, Korean Society of Pediatric Infectious Diseases, Korean Society of Epidemiology, Korean Society for Antimicrobial Therapy, Korean Society for Healthcare-Associated Infection Control and Prevention, Korea Centers for Disease Control and Prevention. Report on the epidemiological features of coronavirus disease 2019 (COVID-19) outbreak in the Republic of Korea from January 19 to March 2, 2020. J Korean Med Sci. 2020;35:e112. https://doi.org/10.3346/jkms.2020.35.e112
10. Korea Center for Disease and Control and Prevention. Daily cumulative confirmed data as of April 30, 2020 [cited 2020 Apr 30]. https://www.cdc.go.kr/board/board.es?mid=a20501000000&bid=0015
11. Korea Center for Disease and Control and Prevention. Daily cumulative confirmed data as of February 27, 2020 [cited 202 Feb 27]. https://www.cdc.go.kr/board/board.es?mid=a20501000000&bid=0015
12. Lauer SA, Grantz KH, Bi Q, Jones FK, Zheng Q, Meredith HR, et al. The incubation period of coronavirus disease 2019 (COVID-19) from publicly reported confirmed cases: estimation and application. Ann Intern Med. 2020;172:577–82. https://doi.org/10.7326/M20-0504
13. Kwon KT, Ko JH, Shin H, Sung M, Kim JY. Drive-through screening center for COVID-19: a safe and efficient screening system against massive community outbreak. J Korean Med Sci. 2020;35:e123. https://doi.org/10.3346/jkms.2020.35.e123
14. Link-Gelles R, DellaGrotta AL, Molina C, Clyne A, Campagna K, Lanzieri TM, et al. Limited secondary transmission of SARS-CoV-2 in child care programs—Rhode Island, June 1–July 31, 2020. MMWR Morb Mortal Wkly Rep. 2020;69:1170–2. https://doi.org/10.15585/mmwr.mm6934e2
15. Lopez AS, Hill M, Antezano J, Vilven D, Rutner T, Bogdanow L, et al. Transmission dynamics of COVID-19 outbreaks associated with child care facilities—Salt Lake City, Utah, April–July 2020. MMWR Morb Mortal Wkly Rep. 2020;69:1319–23. https://doi.org/10.15585/mmwr.mm6937e3
16. Macartney K, Quinn HE, Pillsbury AJ, Koirala A, Deng L, Winkler N, et al.; NSW COVID-19 Schools Study Team. Transmission of SARS-CoV-2 in Australian educational settings: a prospective cohort study. Lancet Child Adolesc Health. 2020;4:807–16. https://doi.org/10.1016/S2352-4642(20)30251-0
17. McAnulty JM, Ward K. Suppressing the epidemic in New South Wales. N Engl J Med. 2020;382:e74. https://doi.org/10.1056/NEJMc2011592
18. Danis K, Epaulard O, Bénet T, Gaymard A, Campoy S, Botelho-Nevers E, et al.; Investigation Team. Cluster of coronavirus disease 2019 (COVID-19) in the French Alps, February 2020. Clin Infect Dis. 2020;71:825–32. https://doi.org/10.1093/cid/ciaa424
19. National Centre for Immunisation Research and Surveillance. COVID-19 in schools: the experience in NSW, 2020 [cited 2020 Jul 4]. http://www.ncirs.org.au/covid-19-in-schools
20. Heavey L, Casey G, Kelly C, Kelly D, McDarby G. No evidence of secondary transmission of COVID-19 from children attending school in Ireland, 2020. Euro Surveill. 2020;25. https://doi.org/10.2807/1560-7917.ES.2020.25.21.2000903
21. Lee B, Raszka WV Jr. COVID-19 transmission and children: the child is not to blame. Pediatrics. 2020;146:e2020004879. https://doi.org/10.1542/peds.2020-004879
22. Ludvigsson JF. Children are unlikely to be the main drivers of the COVID-19 pandemic: a systematic review. Acta Paediatr. 2020;109:1525–30. https://doi.org/10.1111/apa.15371

23. Davies NG, Klepac P, Liu Y, Prem K, Jit M, Eggo RM; CMMID COVID-19 working group. Age-dependent effects in the transmission and control of COVID-19 epidemics. Nat Med. 2020;26:1205–11. https://doi.org/10.1038/s41591-020-0962-9
24. Carsetti R, Quintarelli C, Quinti I, Piano Mortari E, Zumla A, Ippolito G, et al. The immune system of children: the key to understanding SARS-CoV-2 susceptibility? Lancet Child Adolesc Health. 2020;4:414–6. https://doi.org/10.1016/S2352-4642(20)30135-8
25. Bunyavanich S, Do A, Vicencio A. Nasal gene expression of angiotensin-converting enzyme 2 in children and adults. JAMA. 2020;323:2427–9. https://doi.org/10.1001/jama.2020.8707
26. Bi Q, Wu Y, Mei S, Ye C, Zou X, Zhang Z, et al. Epidemiology and transmission of COVID-19 in 391 cases and 1286 of their close contacts in Shenzhen, China: a retrospective cohort study. Lancet Infect Dis. 2020;20:911–9. https://doi.org/10.1016/S1473-3099(20)30287-5
27. Lu X, Zhang L, Du H, Zhang J, Li YY, Qu J, et al.; Chinese Pediatric Novel Coronavirus Study Team. SARS-CoV-2 infection in children. N Engl J Med. 2020;382:1663–5. https://doi.org/10.1056/NEJMc2005073
28. Han MS, Choi EH, Chang SH, Jin BL, Lee EJ, Kim BN, et al. Clinical characteristics and viral RNA detection in children with coronavirus disease 2019 in the Republic of Korea. JAMA Pediatr. 2020. https://doi.org/10.1001/jamapediatrics.2020.3988
29. He X, Lau EH, Wu P, Deng X, Wang J, Hao X, et al. Temporal dynamics in viral shedding and transmissibility of COVID-19. Nat Med. 2020;26:672–5. https://doi.org/10.1038/s41591-020-0869-5
30. Arons MM, Hatfield KM, Reddy SC, Kimball A, James A, Jacobs JR, et al.; Public Health–Seattle and King County and CDC COVID-19 Investigation Team. Presymptomatic SARS-CoV-2 infections and transmission in a skilled nursing facility. N Engl J Med. 2020;382:2081–90. https://doi.org/10.1056/NEJMoa2008457
31. Han MS, Seong MW, Kim N, Shin S, Cho SI, Park H, et al. Viral RNA load in mildly symptomatic and asymptomatic children with COVID-19, Seoul, South Korea. Emerg Infect Dis. 2020;26:2497–9. https://doi.org/10.3201/eid2610.202449
32. Auger KA, Shah SS, Richardson T, Hartley D, Hall M, Warniment A, et al. Association between statewide school closure and COVID-19 incidence and mortality in the US. JAMA. 2020;324:859–70. https://doi.org/10.1001/jama.2020.14348
33. Levinson M, Cevik M, Lipsitch M. Reopening primary schools during the pandemic. N Engl J Med. 2020;383:981–5. https://doi.org/10.1056/NEJMms2024920


Address for correspondence: Yae-Jean Kim, Department of Pediatrics, Samsung Medical Center, Sungkyunkwan University, 81 Irwon-ro, Gangnam-gu, Seoul 06351, South Korea; email: yaejeankim@skku.edu

SYNOPSIS

# Characteristics of Patients Co-infected with Severe Acute Respiratory Syndrome Coronavirus 2 and Dengue Virus, Buenos Aires, Argentina, March–June 2020

Lucila M. Carosella, Daniel Pryluka, Aldo Maranzana, Laura Barcan, Rosana Cuini, Cristina Freuler, Alfredo Martinez, Tomás Rivero Equiza, Carolina Rodriguez Peria, Diego Yahni, Martin E. Stryjewski, for the COVIDENGUE Study Group[1]

An epidemic of dengue virus and severe acute respiratory syndrome coronavirus 2 (SARS-CoV-2) co-infections occurred in Argentina during 2020. We describe the clinical characteristics and outcomes in a cohort of patients hospitalized because of co-infection. We retrospectively identified 13 patients from different hospitals in Buenos Aires who had confirmed infection with SARS-CoV-2 and dengue virus and obtained clinical and laboratory data from clinical records. All patients had febrile disease when hospitalized. Headache was a common symptom. A total of 8 patients had respiratory symptoms, 5 had pneumonia, and 3 had rash. Nearly all patients had lymphopenia when hospitalized. No patients were admitted to an intensive care unit or died during follow up. Co-infection with SARS-CoV-2 and dengue virus can occur in patients living in areas in which both viruses are epidemic. The outcome of these patients did not seem to be worse than those having either SARS-CoV-2 or dengue infection alone.

Severe acute respiratory syndrome coronavirus 2 (SARS-CoV-2), which produces coronavirus disease (COVID-19), and dengue caused an epidemic in Argentina during 2020. During March 3–October 25, 2020, a total of 1,090,589 confirmed cases of infection with SARS-CoV-2 were reported in this country. Of these cases, 143,990 were reported in Ciudad Autónoma de Buenos Aires (*1*). During January 4–June 13, 2020, there were ≈7,300 confirmed cases of dengue virus infection in this city (*2*).

Although co-infection with these 2 virus is a major concern, it has only been reported in individual patients (*3*–*5*). Information from cohorts of co-infected patients is still lacking. We describe the clinical characteristics and outcomes in a cohort of patients co-infected with SARS-CoV-2 and dengue virus in Buenos Aires.

## Methods

Using a network of colleagues (COVIDENGUE Study Group), we retrospectively identified patients co-infected with SARS-CoV-2 and dengue virus during March–June 2020. Seven sites were in Buenos Aires, and an additional site was in the surrounding area. Through June 30, 2020, healthcare admission was mandated in Argentina for any patient with confirmed COVID-19. Therefore, all patients had complete information regarding signs and symptoms at hospitalization, as well as their hospital course. Clinical data were obtained in a predesigned clinical report form by reviewing medical records.

Infection with SARS-CoV-2 was diagnosed by using real-time PCR of nasopharyngeal swab specimens, as approved by the Ministry of Health in reference laboratories. Dengue was diagnosed by either detec-

Author affiliations: Centro de Educación Médica e Investigaciones Clínicas, Buenos Aires, Argentina (L.M. Carosella, A. Martinez, T. Rivero Equiza, M.E. Stryjewski); Sanatorio Otamendi, Buenos Aires (D. Pryluka); General Hospital de Agudos Parmenio Piñero Gobierno de la Ciudad, Buenos Aires (A. Maranzana); Hospital Italiano de Buenos Aires, Buenos Aires (L. Barcan); Hospital de Agudos Dr. Teodoro Álvarez, Buenos Aires (R. Cuini); Hospital Alemán, Buenos Aires (C. Freuler); Sanatorio de Los Arcos, Buenos Aires (C. Rodriguez Peria), Sanatorio Mutual del Transporte Automotor, Buenos Aires (D. Yahni)

DOI: https://doi.org/10.3201/eid2702.203439

[1]Members of the COVIDENGUE Study Group are listed at the end of this article.

tion of nonstructural protein 1 (NS1), real-time PCR, or serologic conversion. Severe dengue was defined by presence of respiratory distress, severe bleeding, or organ impairment. Mild COVID-19 was defined by absence of pneumonia or pneumonia without impairment in oxygenation for otherwise stable patients. Patients requiring supplemental oxygen were considered to have moderate-to-severe COVID-19. Patients were followed up for 4 weeks from their initial hospitalizations. Descriptive statistics were used. This study was approved by the Ethic Committee of Centro de Educación Médica e Investigaciones Clínicas (Buenos Aires, Argentina).

## Results

A total of 13 patients who had co-infections with SARS-CoV-2 and dengue virus were identified. Most patients were relatively young (median age 37 years), 46% were female, and 54% reported ≥1 concurrent condition. All patients had febrile disease at hospitalization (Table). The median duration of fever was 7 days; 9 (69%) patients had fever for ≥5 days. Headache was a common symptom among co-infected patients. A total of 8 patients (62%) had respiratory symptoms. Symptoms of lower respiratory tract infection were present in 4 (31%) patients; 5 (38%) patients had ground glass opacities consistent with viral pneumonia on computed tomography (CT) scans. Two patients had bilateral infiltrates on a chest radiograph or computed tomography. Rash appeared in 3 patients early in the course of the disease and before resolution of fever. Two of these patients had concomitant pneumonia and rash. Lymphopenia was observed in all but 1 patient (92%), and thrombocytopenia was observed in 46%.

Among patients with fever ≤5 days, suspicion of dengue was based on a history of recent mosquito bite (2 patients), frontal headache (3 patients), intense myalgia (3 patients), or thrombocytopenia (2 patients). All patients had a diagnosis of COVID-19 by real-time PCR of nasopharyngeal swabs specimens. Dengue was diagnosed by detection of NS1 in >50% of co-infected patients; 4 cases were diagnosed by real-time PCR of serum and 1 by serologic conversion. The patient who had serologic conversion had a first serum sample negative for IgM and IgG. One week later, a second serum sample was positive for both antibodies. All but 1 patient (92%) had mild COVID-19. No patients had severe dengue infection, required admission to an intensive care unit, or died during follow up. All patients fully recovered from their symptoms after 4 weeks.

## Discussion

This report of patients co-infected with SARS-CoV-2 and dengue virus provides several useful observations. First, in geographic areas in which both viruses

**Table.** Clinical characteristics and laboratory parameters at hospitalization for 13 patients co-infected with SARS-CoV-2 and dengue virus, Buenos Aires, Argentina, March–June 2020*

| Characteristics | Value |
|---|---|
| Age, y | 37 (29–50) |
| Sex | |
| F | 6 (46) |
| M | 7 (54) |
| Concurrent condition† | 7 (54) |
| Signs or symptoms | |
| Fever at hospitalization | 13 (100) |
| Median temperature at hospitalization, °C | 38.0 (38.0–38.8) |
| Median duration of fever, d | 7 (4–9) |
| Cough | 3 (23) |
| Headache | 8 (61) |
| Myalgia | 7 (54) |
| Rash | 3 (23) |
| Chills | 3 (23) |
| Dyspnea | 2 (15) |
| Diarrhea | 2 (15) |
| Odinophagia | 2 (15) |
| Nasal congestion | 2 (15) |
| Anosmia | 1 (8) |
| Dysgeusia | 1 (8) |
| Arthralgia | 1 (8) |
| Nausea or vomiting | 1 (8) |
| Pneumonia | 5 (38) |
| Bilateral | 2 (15) |
| Laboratory findings | |
| Median hematocrit, % | 44 (36–46) |
| Median hemoglobin, g/dL | 14.1 (13.0–15.0) |
| Median leukocytes × $10^3$ cells/μL | 4.3 (2.26–7.9) |
| Leukopenia, <4 × $10^3$ cells/μL | 4 (31) |
| Median lymphocyte count × $10^3$ cells/μL | 0.81 (4.1–1.16) |
| Lymphopenia, <1.5 × $10^3$ cells/μL | 12 (92) |
| Platelets ×$10^3$/μL | 172 (116–196) |
| <150 ×$10^3$/μL | 6 (46) |
| <100 ×$10^3$/μL | 3 (23) |
| Abnormal AST level | 6 (46) |
| Abnormal ALT level | 6 (46) |
| Diagnosis of dengue | |
| NS1 detection | 8 (61) |
| Real-time PCR | 4 (31) |
| Serologic conversion | 1 (8) |
| Clinical outcomes | |
| Need for supplemental oxygen | 1 (8) |
| ICU | 0 |
| Median length of stay in hospital, d | 12 (10–14) |
| Severe dengue | 0 |
| Hospital discharge | 13 (100) |
| Full recovery at follow-up at 4 wk | 13 (100) |
| Rehospitalization at 4 wk | 0 |
| Death | 0 |
| Therapy for infection with SARS-CoV-2 | |
| Lopinavir/ritonavir | 3 (23) |
| Hydroxychloroquine | 1 (8) |
| Antimicrobial drug therapy | 6 (46) |

*Values are no. (%) or median IQR. ALT, alanine aminotransferase; AST, aspartate aminotransferase, ICU, intensive care unit; IQR, interquartile range; SARS-CoV-2, severe acute respiratory syndrome coronavirus 2.
†Includes obesity 3; chronic obstructive pulmonary disease 2; hypertension 2; smoking 2; diabetes 1; and cirrhosis 1.

are circulating, co-infections can occur. This concerning possibility, which might impose an additional burden on healthcare systems, has been reported previously (*6*). In Latin America, >3 million cases of dengue were reported during 2019 (*7*). Dengue virus circulates epidemically in Argentina, particularly in the northeastern region of this country (*8*). The most recent epidemic occurred in 2016 (*2*). In Buenos Aires, the number of cases reported during 2017–2019 was relatively low. For example, during 2018 only 151 cases were reported and during 2019 only 51 cases in this city. However, during 2020, the magnitude of the dengue epidemic in Buenos Aires surpassed case counts for the preceding 10 years. Therefore, given the current circulation of SARS-CoV-2 at high levels, a new epidemic of dengue virus during early 2021 (warm months) could substantially increase the risk for co-infections.

Second, in this scenario of concomitant circulation of SARS-CoV-2 and dengue virus, the distinction between clinical diseases among febrile patients is crucial. Certain clinical characteristics among these co-infected patients are relevant. All patients who had co-infections had fever at hospitalization, and most had fever duration for ≥5 days. Also, >50% of patients with COVID-19 did not have fever at admission (*9*). Prolonged fever has been associated with more severe disease in patients with COVID-19 (*10*). Therefore, for most patients with mild COVID-19 in this study, prolonged fever was a clinical clue for suspecting co-infection. Other than fever, headache was the most common symptom in patients with co-infection. Although headache is common in patients who have dengue infection (>90%) (*11*) it is less commonly observed in patients with COVID-19 (≈13%) (*9*). For some co-infected patients, a clinical overlap based on hallmarks of both diseases was also noted. For example, 2 patients had pneumonia, suggesting COVID-19, as well as a rash, which can be a hallmark of dengue virus infection. The duration of fever longer than expected for mild COVID-19, headache, rash, or absence of respiratory symptoms should raise the suspicion of a concomitant infection with dengue virus. Therefore, clinical suspicion based on epidemiologic grounds might alert clinicians to order tests for both viruses.

Third, all patients had favorable outcomes for both COVID-19 and dengue virus infections. There is conflictive data on the clinical outcome of co-infection with dengue and other viruses (*12*–*14*). All but 1 of our patients had mild COVID-19, and none had severe dengue. Our preliminary findings, based on limited data, do not suggest that co-infection with dengue and SARS-CoV-2 viruses worsens clinical outcomes.

Our study had several limitations. False-positive IgM results for dengue have been described for 2 patients who had COVID-19 (*15*). However, only 1 of our patients had a serologic diagnosis of dengue, and this diagnosis was based on serologic conversion for IgM and IgG. Almost all our patients had positive results for virus NS1 tests or real-time PCR of serum for dengue. Because these tests for dengue have high specificity for acute infection (*16*), a false-positive diagnosis is unlikely (*17*). Immune response was not evaluated in our study. Analyzing the immune activation for these co-infected patients would help to clarify the clinical outcomes of these patients who have simultaneous viral infections.

Finally, our data are limited by a small sample size. Our observation on the unaltered clinical course of COVID-19 concomitant with dengue infection needs to be confirmed in larger cohorts of patients, including a comparative analysis of persons infected only with SARS-CoV-2 or dengue virus, and patients who are co-infected with both viruses.

In conclusion, co-infection with SARS-CoV-2 and dengue virus can occur in patients living in areas in which both viruses are epidemic. Some clinical clues can orient physicians to suspect both diseases. Based on limited data, our study suggests that the clinical outcome of these co-infected patients may not be worse than for patients who have either SARS-CoV-2 or dengue infection alone.

Members of the COVIDENGUE Study Group: Claudio Basile, Pablo Bonvehi, Patricia Chabay, Mariana De Paz, Cecilia Ezcurra, Diana Ferreño, Margarita Gaset, Daniel Lopez, Cecilia Losada, Veronica Paz, Sandra Paz, and Pedro Wainer.

M.E.S. is a consultant to Basilea and a speaker for Pfeizer.

## About the Author

Dr. Carosella is a chief resident of internal medicine at the Centro de Educación Médica e Investigaciones Clínicas, Buenos Aires, Argentina. Her primary research interests are cardiology and COVID-19.

### References

1. Ministry of Health. Argentina. Daily reported [in Spanish] [cited 2020 Oct 26]. https://www.argentina.gob.ar/coronavirus/informes-diarios/reportes/octubre2020
2. Weekly Epidemiological Bulletin. Autonomous city of Buenos Aires [in Spanish] [cited 2020 Nov 17]. https://www.buenosaires.gob.ar/sites/gcaba/files/bes_200_se_23_vf.pdf
3. Bicudo N, Bicudo E, Costa JD, Castro JA, Barra GB. Co-infection of SARS-CoV-2 and dengue virus: a clinical

challenge. Braz J Infect Dis. 2020;24:452–4. https://doi.org/10.1016/j.bjid.2020.07.008
4. Epelboin L, Blondé R, Nacher M, Combe P, Collet L. COVID-19 and dengue co-infection in a returning traveller. J Travel Med. 2020;27:taaa114. https://doi.org/10.1093/jtm/taaa114
5. Pontes RL, de Brito BB, da Silva FA, Figueredo MS, Correia TM, Teixeira AF, et al. Coinfection by SARS-CoV-2 and dengue virus in a dual viral circulation setting. Travel Med Infect Dis. 2020;37:101862. https://doi.org/10.1016/j.tmaid.2020.101862
6. Lorenz C, Azevedo TS, Chiaravalloti-Neto F. COVID-19 and dengue fever: a dangerous combination for the health system in Brazil. Travel Med Infect Dis. 2020;35:101659. https://doi.org/10.1016/j.tmaid.2020.101659
7. Gutierrez L. PAHO/WHO Data. Dengue cases. Pan American Health Organization/World Health Organization [in Spanish] [cited 2020 Nov 17]. https://www.paho.org/data/index.php/es/temas/indicadores-dengue/dengue-nacional/9-dengue-pais-ano.html?start=1
8. Integrated Surveillance Bulletin. Ministry of Health, Argentina [in Spanish] [cited 2020 Nov 17]. https://www.argentina.gob.ar/sites/default/files/biv_500_se_24.pdf
9. Guan WJ, Ni ZY, Hu Y, Liang WH, Ou CQ, He JX, et al.; China Medical Treatment Expert Group for Covid-19. Clinical characteristics of coronavirus disease 2019 in China. N Engl J Med. 2020;382:1708–20. https://doi.org/10.1056/NEJMoa2002032
10. Ng DH, Choy CY, Chan YH, Young BE, Fong SW, Ng LF, et al. Fever patterns, cytokine profiles, and outcomes in COVID-19. Open Forum Infect Dis. 2020;7:ofaa375.
11. Domingues RB, Kuster GW, Onuki de Castro FL, Souza VA, Levi JE, Pannuti CS. Headache features in patients with dengue virus infection. Cephalalgia. 2006;26:879–82. https://doi.org/10.1111/j.1468-2982.2006.01100.x
12. Carrillo-Hernández MY, Ruiz-Saenz J, Villamizar LJ, Gómez-Rangel SY, Martínez-Gutierrez M. Co-circulation and simultaneous co-infection of dengue, chikungunya, and Zika viruses in patients with febrile syndrome at the Colombian–Venezuelan border. BMC Infect Dis. 2018;18:61. https://doi.org/10.1186/s12879-018-2976-1
13. Vogels CB, Rückert C, Cavany SM, Perkins TA, Ebel GD, Grubaugh ND. Arbovirus coinfection and co-transmission: a neglected public health concern? PLoS Biol. 2019;17:e3000130. https://doi.org/10.1371/journal.pbio.3000130
14. Perdigão AC, Ramalho IL, Guedes MI, Braga DN, Cavalcanti LP, Melo ME, et al. Coinfection with influenza A(H1N1)pdm09 and dengue virus in fatal cases. Mem Inst Oswaldo Cruz. 2016;111:588–91. https://doi.org/10.1590/0074-02760160140
15. Yan G, Lee CK, Lam LTM, Yan B, Chua YX, Lim AY, et al. Covert COVID-19 and false-positive dengue serology in Singapore. Lancet Infect Dis. 2020;20:536. https://doi.org/10.1016/S1473-3099(20)30158-4
16. Tang KF, Ooi EE. Diagnosis of dengue: an update. Expert RevAnti Infect Ther. 2012;10:895–907. https://doi.org/10.1586/eri.12.76
17. Chaterji S, Allen JC Jr, Chow A, Leo YS, Ooi EE. Evaluation of the NS1 rapid test and the WHO dengue classification schemes for use as bedside diagnosis of acute dengue fever in adults. Am J Trop Med Hyg. 2011;84:224–8. https://doi.org/10.4269/ajtmh.2011.10-0316


Address for correspondence: Martin E. Stryjewski, Centro de Educación Médica e Investigaciones Clínicas, Coronel Diaz 2423, Buenos Aires 1425, Argentina; email: stryj002@gmail.com

# Characteristics and Timing of Initial Virus Shedding in Severe Acute Respiratory Syndrome Coronavirus 2, Utah, USA

Nathaniel M. Lewis, Lindsey M. Duca, Perrine Marcenac, Elizabeth A. Dietrich, Christopher J. Gregory, Victoria L. Fields, Michelle M. Banks, Jared R. Rispens, Aron Hall, Jennifer L. Harcourt, Azaibi Tamin, Sarah Willardson, Tair Kiphibane, Kimberly Christensen, Angela C. Dunn, Jacqueline E. Tate, Scott Nabity, Almea M. Matanock, Hannah L. Kirking

Virus shedding in severe acute respiratory syndrome coronavirus 2 (SARS-CoV-2) can occur before onset of symptoms; less is known about symptom progression or infectiousness associated with initiation of viral shedding. We investigated household transmission in 5 households with daily specimen collection for 5 consecutive days starting a median of 4 days after symptom onset in index patients. Seven contacts across 2 households implementing no precautionary measures were infected. Of these 7, 2 tested positive for SARS-CoV-2 by reverse transcription PCR on day 3 of 5. Both had mild, nonspecific symptoms for 1–3 days preceding the first positive test.SARS-CoV-2 was cultured from the fourth-day specimen in 1 patient and from the fourth- and fifth-day specimens in the other. We also describe infection control measures taken in the households that had no transmission. Persons exposed to SARS-CoV-2 should self-isolate, including from household contacts, wear a mask, practice hand hygiene, and seek testing promptly.

The coronavirus disease (COVID-19) outbreak first recognized in Wuhan, China, in December 2019 is now a global pandemic (*1*). Serial intervals for transmission have been estimated (*2*,*3*), and presymptomatic transmission from confirmed case-patients to others has been documented (*4*–*8*). In addition, studies suggest that virus shedding can begin before the onset of symptoms (*7*,*8*) and extend beyond the resolution of symptoms (*9*). However, data on the initiation and progression of viral shedding in relation to symptom onset and infectiousness are limited. Intensive early monitoring of household members through serial (i.e., daily) collection of a respiratory tract specimen for testing by real-time reverse transcription PCR (rRT-PCR), which could clarify the characteristics of initial viral shedding, has rarely been implemented, although serial self-collection of nasal and saliva samples was used in a recent study (*10*). To examine the transmission dynamics of severe acute respiratory syndrome coronavirus 2 (SARS-CoV-2) and guide public health recommendations, we describe initial detection and progression of SARS-CoV-2 viral shedding, as indicated by rRT-PCR positivity for SARS-CoV-2 and cycle threshold ($C_t$) values, in relation to exposure to an index patient, symptom onset and duration, and transmission to household contacts who underwent intensive early monitoring with viral cultures.

Author affiliations: Centers for Disease Control and Prevention, Atlanta, Georgia, USA (N.M. Lewis, L.M. Duca, P. Marcenac, E.A. Dietrich, C.J. Gregory, V.L. Fields, M.M. Banks, J.R. Rispens, A. Hall, J.L. Harcourt, A. Tamin, J.E. Tate, S. Nabity, A.M. Matanock, H.L. Kirking); Utah Department of Health, Salt Lake City, Utah, USA (N.M. Lewis, K. Christensen, A.C. Dunn); Davis County Health Department, Clearfield, Utah, USA (S. Willardson); Salt Lake County Health Department, Salt Lake City (T. Kiphibane)

DOI: https://doi.org/10.3201/eid2702.203517

## Methods

Index patients with laboratory-confirmed SARS-CoV-2 infection were reported to 2 health departments in the Salt Lake City, Utah, USA, metropolitan area during April 19–25, 2020. Households were recruited through convenience sampling with assistance from health department staff and were considered eligible if the index patient was not hospitalized, lived with ≥2 additional persons, and tested positive for SARS-CoV-2 by rRT-PCR in a respiratory tract specimen collected ≤5 days before enrollment. A sample size of 5 households was chosen because of time constraints and workload capacity; we also took into consideration the likelihood of observing secondary transmission within households, on the basis of the estimated secondary attack rate in a larger household transmission investigation conducted by the Centers for Disease Control and Prevention (CDC) (*11*). CDC investigation staff visited all enrolled households (day 0) within 2–4 days of diagnosis (within 3–5 days of symptom onset) and conducted daily visits on 4 subsequent days (days 1–4) and a final visit on day 14.

Before the day 0 visit, questionnaires were administered to all index patients and household contacts by telephone to request demographic information and data on symptoms, exposure to the index patient and others outside the household, and any previous SARS-CoV-2 testing. A household-level questionnaire, completed by the index patient or self-declared head of household, documented the home's square footage; the number of persons per bedroom and bathroom; isolation measures undertaken by the index patient; and extent of household use of gloves, masks, or cloth face coverings after symptom onset in the index patient. A household-level closeout questionnaire reassessing isolation measures and glove and face mask use during the observation period was completed on the day 14 visit. In addition, during the day 0 and day 14 visits, nasopharyngeal swab specimens and blood samples were collected from all index patients and household contacts. During day 1–4 follow-up visits, nasopharyngeal swab specimens were collected daily from non–index patient household members, including those with SARS-CoV-2 test results pending or confirmed from specimens collected at other facilities before the investigation. If symptoms occurred in a household contact during days 1–14 that were not reported on day 0, investigation staff conducted an interim household visit, during which nasopharyngeal swab specimens were collected from all household members, including the index patient.

During days 1–4, if a household contact had an inconclusive result (1 of 2 target gene regions positive for SARS-CoV-2 by rRT-PCR assay) or positive result (both target gene regions positive) after an rRT-PCR–negative test (i.e., first detection of viral shedding), the associated specimen and all subsequent daily specimens from the person were submitted for viral culture to evaluate infectiousness. Results that were inconclusive by rRT-PCR were categorized as negative unless a positive viral culture was obtained from the same specimen. Specimens positive by rRT-PCR that were collected on day 14 with $C_t$ values <35 were also cultured. For household contacts, the date of first positive test was defined as the day on which the first SARS-CoV-2–positive specimen was collected. The Utah Public Health Laboratory (UPHL) tested specimens by using the CDC 2019 novel coronavirus (2019-nCoV) real-time RT-PCR assay (*12*); viral cultures were performed at CDC (*13*). Nasopharyngeal specimens were transported at 4°C in viral transport media, first from households to UPHL and then (if applicable) onward to CDC for viral culture. Blood samples were processed by UPHL; serum samples were subsequently shipped to CDC and tested by using a CDC-developed SARS-CoV-2 ELISA kit (B. Freeman, unpub. data, https://doi.org/10.1101/2020.04.24.057323).

During days 0–14, all index patients and household members completed a daily symptom diary. Symptoms were grouped according to Council of State and Territorial Epidemiologists (CSTE) categories of classic (cough, shortness of breath, or discomfort while breathing), nonclassic ($\geq$2 of measured or subjective fever, chills, headache, myalgia, sore throat, loss of taste, or loss of smell), and asyndromic (symptoms other than CSTE classic or nonclassic) (*14*). Symptom onset was defined as the first day of any reported symptom. Onset of viral shedding was defined as the date of first detection of SARS-CoV-2 by rRT-PCR in the nasopharynx. Presymptomatic shedding was defined as symptom onset $\geq$1 day after the first positive SARS-CoV-2 result by rRT-PCR. $C_t$ values were categorized as low (<20), medium (20–30), and high (>30). Lower $C_t$ values indicated that more viral RNA was detected in the specimen.

This protocol was reviewed by CDC human subjects research officials, and the activity was deemed nonresearch as part of the COVID-19 public health response. Verbal assent to participate was initially obtained by telephone during questionnaire administration, and written consent was collected during the first visit.

## Results

During April 19–25, 2020, a total of 5 households were enrolled, each consisting of an index case-patient and a median of 3 household members (range 2–4 persons). All index patients had the earliest symptom onset in their households. The day 0 visit occurred a median of 4 days (range 3–5 days) after symptom onset in the index patient. Secondary transmission was observed in 2 (40%) of the 5 households (HH-02 and HH-05), consisting of 7 (100%) of 7 contacts in these 2 households and 7 (47%) of 15 total household contacts in the study. The 8 contacts from the remaining

3 households did not become infected during the investigation (Figure 1). The median number of days between symptom onset in index patients and symptom onset in SARS-CoV-2–positive household contacts was 4 days (range 2–5 days). Eighty percent of index patients (4/5) were men and boys, and 80% of household contacts (12/15 [80%]) were women and girls (Table). The median age of index patients was 35 years (range 16–46 years). Of household contacts who tested positive, median age was 16 years (range 7–45 years); of household contacts who tested negative, median age was 45 years (range 14–67 years). Forty percent (2/5) of index patients, 43% (3/7) of SARS-CoV-2–positive household contacts, and 75% (6/8) of SARS-CoV-2–negative contacts reported ≥1 underlying medical condition.

Participants with a COVID-19 diagnosis had similar symptom profiles: headache was reported by 12/12 (100%); subjective fever, chills, fatigue, and nasal congestion were each reported by 10/12 (80%); myalgia was reported by 8/12 (67%); and partial loss of smell was reported by 7/12 (58%) (Appendix Figure, https://wwwnc.cdc.gov/EID/article/27/2/20-3517-App1.pdf). Classic symptoms were less common: dry cough was reported by 6/12 (50%); and productive cough, shortness of breath, and

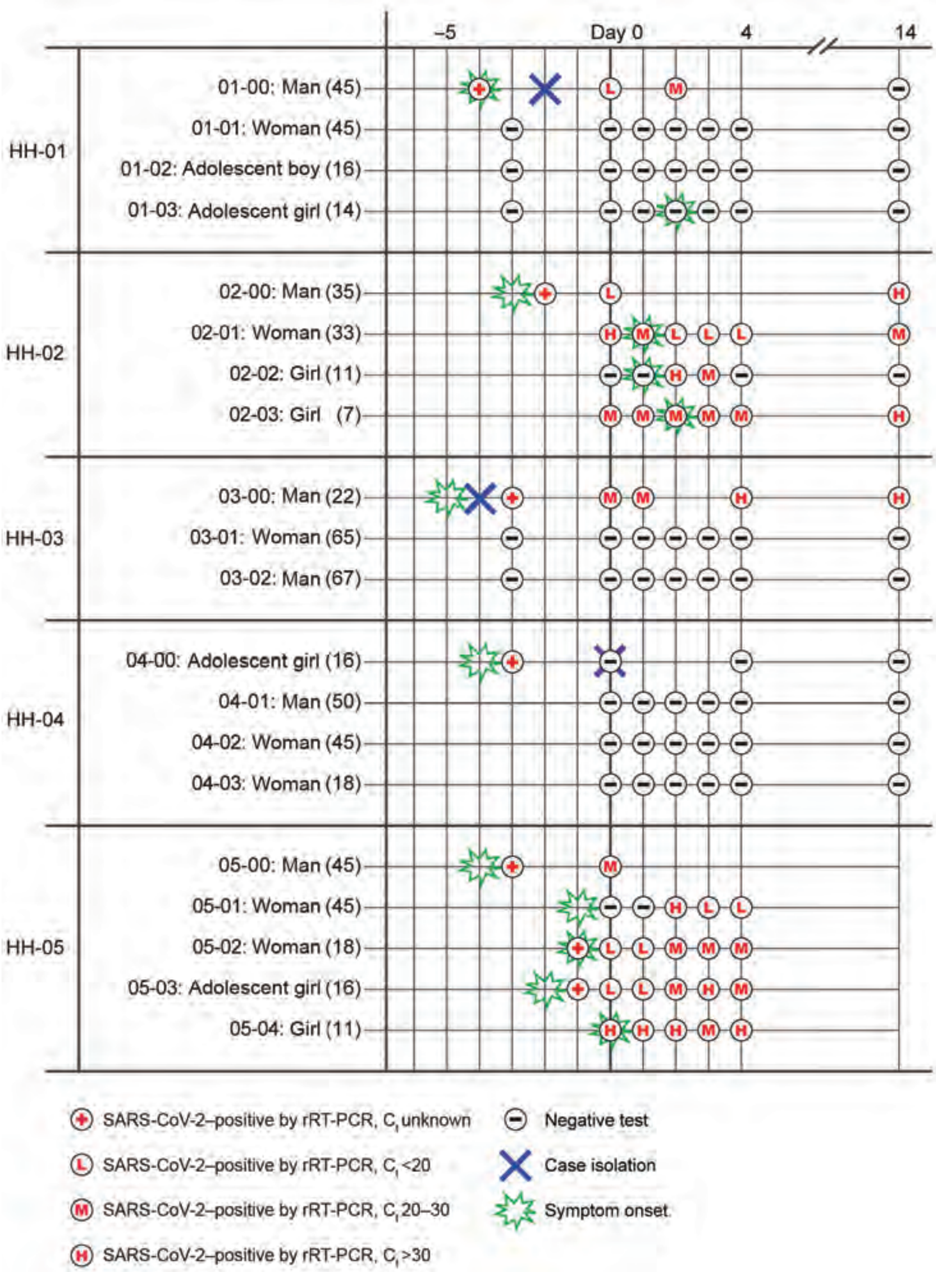


**Figure 1.** Results of rRT-PCR for SARS-CoV-2 and symptom onset among index case-patients, SARS-CoV-2–positive household contacts, and SARS-CoV-2–negative household contacts in study of initial virus shedding in SARS-CoV-2, Utah, USA, April–May 2020. The timelines of symptom onset and testing dates preceding and during the 15-day study period are ordered by individual households (HH-01–HH-05). Sex and age (in parentheses) are listed to the left. Symptom onset date is only included for household members who tested positive at any time during the study period or for whom onset of symptoms consistent with coronavirus disease prompted an interim visit from investigators. HH-05 opted out of day 14 nasopharyngeal specimen collection. $C_t$, cycle threshold; HH, household; rRT-PCR, real-time reverse transcription PCR; SARS-CoV-2, severe acute respiratory syndrome coronavirus 2.

**Table.** Characteristics and symptoms of index case-patients and household contacts testing positive or negative for severe acute respiratory syndrome coronavirus 2 by real-time reverse transcription PCR in study of initial virus shedding in SARS-CoV-2, Utah, USA, April–May 2020*

| Characteristic | No. (%) | | |
|---|---|---|---|
| | Index case-patients, n = 5 | SARS-CoV-2–positive contacts, n = 7 | SARS-CoV-2–negative contacts, n = 8 |
| Age group, y | | | |
| <18 | 1 (20.0) | 4 (57.1) | 2 (25.0) |
| 18–49 | 4 (80.0) | 3 (42.9) | 3 (37.5) |
| 50–64 | 0 | 0 | 1 (12.5) |
| ≥65 | 0 | 0 | 2 (25.0) |
| Sex | | | |
| M | 4 (80.0) | 0 | 3 (37.5) |
| F | 1 (20.0) | 7 (100.0) | 5 (62.5) |
| Race or ethnicity | | | |
| Non-Hispanic white | 5 (100.0) | 7 (100.0) | 7 (87.5) |
| Hispanic | 0 | 0 | 1 (12.5) |
| Underlying medical conditions | | | |
| Any underlying condition | 2 (40.0) | 3 (42.9) | 6 (75.0) |
| Any chronic lung disease | 1 (20.0) | 0 | 2 (25.0) |
| Diabetes mellitus | 0 | 1 (14.3) | 0 |
| Any cardiovascular disease | 0 | 0 | 5 (62.5) |
| Any chronic renal disease | 0 | 0 | 1 (12.5) |
| Any immunocompromised condition | 1 (20.0) | 0 | 1 (12.5) |
| Other chronic condition | 1 (20.0) | 2 (28.6) | 1 (12.5) |
| No underlying medical condition | 3 (60.0) | 4 (57.1) | 2 (25.0) |
| Smoking or vaping status | | | |
| Former history of smoking or vaping | 1 (20.0) | 0 | 1 (12.5) |
| Interactions with index case-patient | | | |
| Intimate physical contact | N/A | 6 (85.7) | 2 (25.0) |
| Close contact only | N/A | 1 (14.3) | 4 (50.0) |
| No interaction reported | N/A | 0 | 2 (25.0) |
| Symptoms | | | |
| Any symptom | 5 (100.0) | 7 (100.0) | 7 (87.5) |
| CSTE categories | | | |
| Classic† | 4 (80.0) | 5 (71.4) | 2 (25.0) |
| Nonclassic‡ | 4 (80.0) | 7 (100.0) | 5 (62.5) |
| Asyndromic§ | 5 (100.0) | 7 (100.0) | 7 (87.5) |
| Other categories | | | |
| Neurologic¶ | 5 (100.0) | 7 (100.0) | 4 (50.0) |
| Lower respiratory# | 4 (80.0) | 6 (85.7) | 2 (25.0) |
| Upper respiratory** | 4 (80.0) | 6 (85.7) | 7 (87.5) |
| Constitutional†† | 4 (80.0) | 7 (100.0) | 5 (62.5) |
| Gastrointestinal‡‡ | 3 (60.0) | 2 (28.6) | 3 (37.5) |

*CSTE, Council of State and Territorial Epidemiologists; SARS-CoV-2, severe acute respiratory syndrome coronavirus disease 2.
†Cough, shortness of breath, or discomfort breathing.
‡≥2 of fever, myalgia, headache, chills, loss of taste or smell, or sore throat.
§Any symptoms other than classic or nonclassic: fatigue, runny nose, nasal congestion, chest pain, wheezing, nausea or vomiting, or diarrhea.
¶Loss of taste (partial or complete), loss of smell (partial or complete), or headache.
#Discomfort while breathing, wheezing, shortness of breath, chest pain, or cough (dry or productive).
**Sore throat, nasal congestion, or runny nose.
††Chills, fever (measured or subjective), fatigue, or myalgia.
‡‡Abdominal pain, nausea or vomiting, or diarrhea.

discomfort while breathing were each reported by <50% of those infected (Appendix Figure). Measured fever, sore throat, partial or full loss of taste, runny nose, chest pain, wheezing, nausea or vomiting, abdominal pain, and diarrhea were each reported by ≤33%. Nonclassic and asyndromic symptoms were also reported by SARS-CoV-2–negative household contacts (Appendix Figure). Median duration of illness was 7 days (range 2–14 days) among SARS-CoV-2–positive contacts and 11 days (range 4–19 days) among index case-patients. None of the 12 participants who tested positive for SARS-CoV-2 were hospitalized or experienced complications from pneumonia. Four (33%) of 12 tested positive on day 14, 3 (25%) were negative on day 14, and 5 (42%) refused swab tests on day 14. Among the 4 participants (02-00, 02-01, 02-03, and 03-00) with day 14 specimens positive for SARS-CoV-2 by rRT-PCR, 3 with $C_t$ values <35 were cultured and viable virus was detected in 0/3 (0%). None of the 8 household members who tested negative by rRT-PCR tested positive by ELISA on day 0 or 14, suggesting no previous or undetected infections.

The 3 households (60%) that did not experience transmission (HH-01, HH-03, and HH-04) instituted household-level isolation practices. In HH-01, the index patient (01-00) moved out of the family home to a trailer on the property on the day of symptom onset (day –4), which coincided with the collection at a drive-through facility of the first specimen to test positive by rRT-PCR. He did report having had intimate contact (e.g., hugging or kissing) after symptom onset but before diagnosis with 1 household member (01-01). The index patient wore gloves but no face mask on the few occasions he entered the family home. Household members also increased handwashing after diagnosis in the index patient. In HH-03, all household members had close contact (i.e., ≥10 minutes within 6 feet) with the index patient

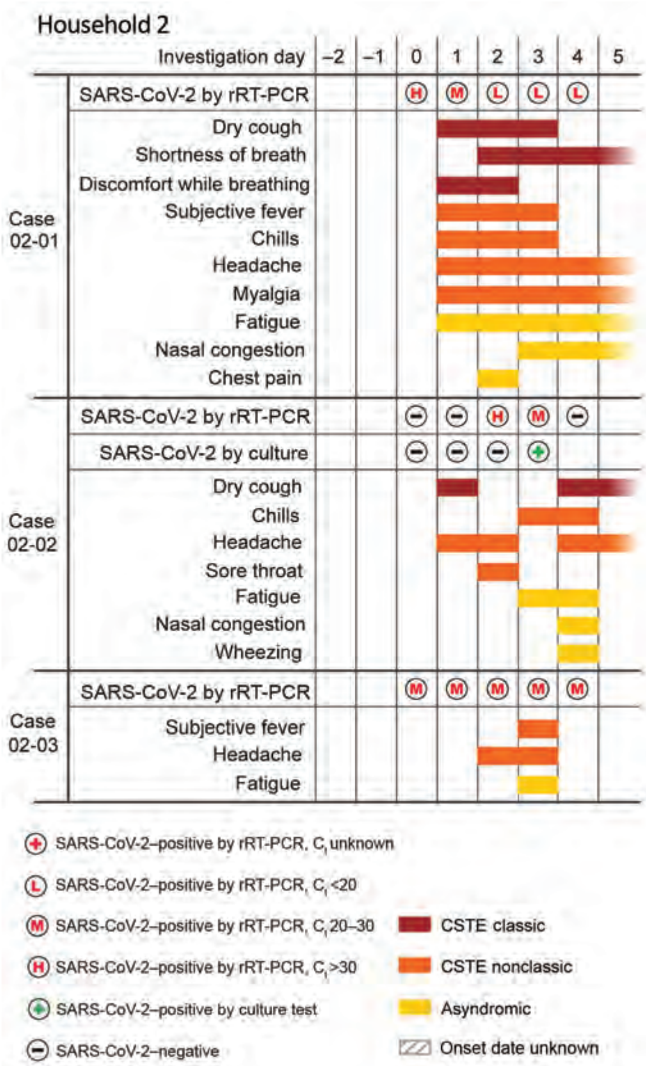


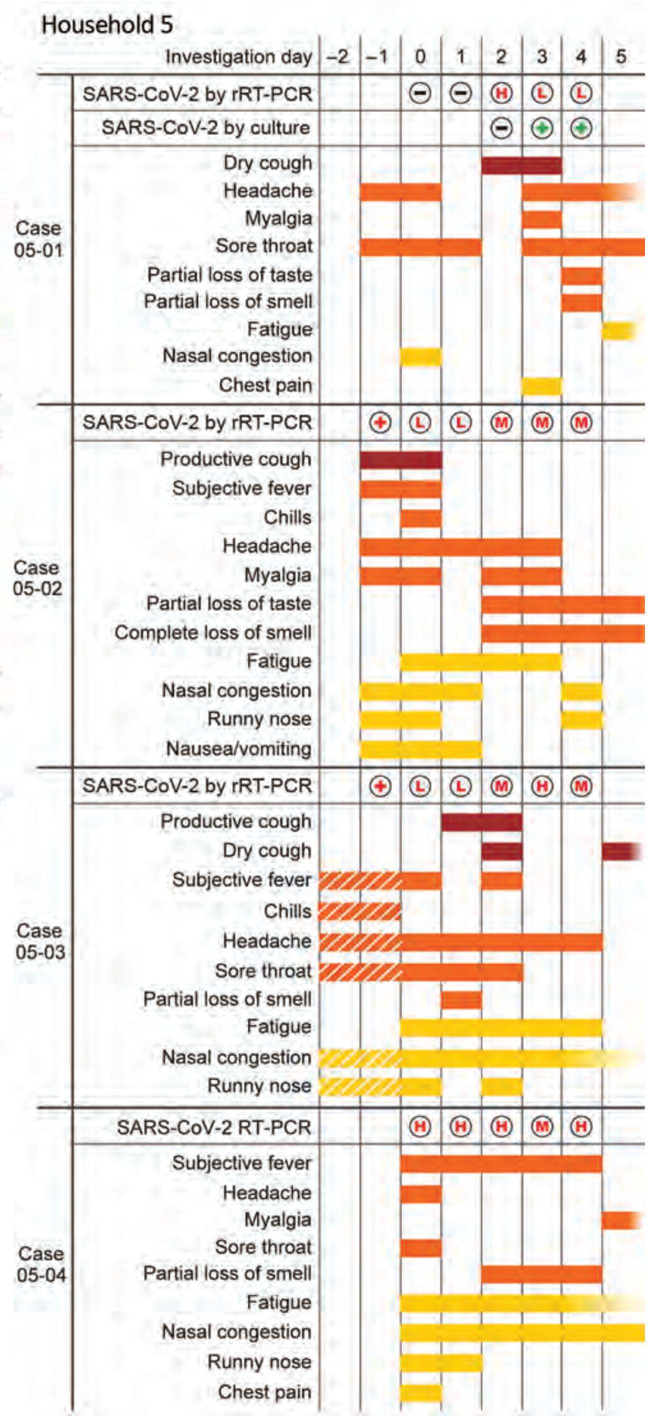


**Figure 2.** Symptom timing, symptom type, cycle threshold values, and viral culture results among household contacts positive for SARS-CoV-2 by rRT-PCR in study of initial virus shedding in SARS-CoV-2, Utah, USA, April–May 2020. The symptom onset and progression of 7 SARS-CoV-2–positive household contacts in households 2 and 5 (HH-02 and HH-05), who tested positive by real-time reverse transcription PCR, are detailed from first symptom onset to the end of the daily swabbing period (days 0–4). Fading bars indicate symptoms persisting after day 5. CSTE, Council of State and Territorial Epidemiologists; $C_t$, cycle threshold; rRT-PCR, real-time reverse transcription PCR; SARS-CoV-2, severe acute respiratory syndrome coronavirus 2

(03-00) between her symptom onset and the diagnosis; however, after diagnosis, the index patient used a separate bathroom (in addition to having her own bedroom) and ate meals separately from household contacts. Household contacts also increased disinfection of surfaces and handwashing after diagnosis in the index patient. In HH-04, between symptom onset and diagnosis in the index patient, 2 household contacts (04-02 and 04-03) had close contact with the index patient, and 1 contact (04-01) had intimate contact with the index patient. After diagnosis, the index patient stayed in a separate bedroom throughout the day (including for meals) but did not have access to a separate bathroom. He wore an N95 mask and gloves when leaving his room. Household members also disinfected surfaces regularly.

The 2 households (40%) where all contacts became infected (HH-02 and HH-05) did not institute household-level isolation practices, and all contacts had ongoing exposure to the index patient (Figure 2). During the investigation period, all members of both households were out of work and school because of school closures and stay-at-home recommendations in Salt Lake County. During the period from symptom onset in the index patient to enrollment in our study, all 7 (100%) contacts in these 2 households reported close contact with the index patient. During the same period, 6/7 (85%) household contacts who tested positive also reported intimate contact with the index patient after symptom onset, compared with 2/8 (25%) of household members who tested negative.

In HH-02, which consisted of a male index patient, his wife, and their 2 children, all 3 household contacts tested positive within 5 days of symptom onset in the index patient. Two of the contacts (02-01 and 02-03) shed virus while presymptomatic, and their symptoms did not occur until after their first SARS-CoV-2–positive test by rRT-PCR. The 33-year-old wife (02–01), who had ongoing exposure to the index patient for the duration of his illness, had $C_t$ values that progressed from high (i.e., lower viral load) on her first positive test (day 0) to low (i.e., higher viral load) on her third test (day 2), when she first reported a combination of classic and nonclassic symptoms and fatigue. She remained SARS-CoV-2–positive by rRT-PCR at day 14, with a medium $C_t$ value but no viable virus detected from culture. The second household member with presymptomatic virus shedding was a 7-year-old girl (02-03) whose daily $C_t$ values were consistently medium during days 0–4. After testing positive for 2 days (days 0–1), she first reported nonclassic symptoms on day 2 and was symptomatic for only 2 days. She also remained positive at day 14, with a high $C_t$ value and no viable virus detected from culture. The third household member, an 11-year-old girl (02-02), converted to rRT-PCR–positive (day 2) after testing negative for 2 days (days 0–1). She reported classic and nonclassic symptoms (dry cough and headache) on day 1. On day 2, she tested positive with a high $C_t$ value and reported onset of a sore throat. On day 3, she tested positive with a medium $C_t$ value, reported onset of chills and fatigue, and had a positive viral culture, before testing negative again on day 4.

Household 5 (HH-05) consisted of a male index patient, his wife, an adult child, and 2 adolescent children. All 4 household contacts tested positive for SARS-CoV-2 by rRT-PCR within 6 days of symptom onset in the index patient. Although all household contacts sought drive-through testing the day before the investigation began (day –1), only the 18-year-old woman (05-02) and the 16-year-old girl (05-03) met symptom criteria for testing; consequently, both had 1 positive test result before the investigation. The 16-year-old girl (05-03) reported nonclassic and asyndromic symptoms (day –2) starting the day before her first positive test by rRT-PCR (day –1) administered at the drive-through facility. Her next 2 positive tests, administered by the investigation team on day 0 and day 1, had low Ct values and coincided with the onset of fatigue (day 0) and cough (day 1). The 18-year-old woman (05-02) and 11-year-old girl (05-04) each reported symptoms starting the same day as their first rRT-PCR–positive tests, with 1 (05-02) administered at a drive-through facility (day –1) and the other (05-04) by the investigation team (day 0). Although they had a range of nonclassic and asyndromic symptoms during illness, the 18-year-old female (05-02) had a cough at onset (day –1) and low $C_t$ values for her first 2 team-administered tests (days 0–1), whereas the 11-year-old girl had generally milder illness and high $C_t$ values (i.e., lower viral load) for 4 of 5 tests. The 45-year-old woman (05-01) tested negative for 2 days (days 0–1) and had nonclassic and asyndromic symptoms for 3 days (days –1 to 1) before her first positive test on day 2; on that day, she tested positive with a high $C_t$ value and reported onset of a cough. Her next 2 positive tests (days 3–4) had low $C_t$ values, coinciding with onset of additional symptoms (chest pain, myalgia, and loss of taste and smell) and positive viral cultures on both days. All HH-05 members refused testing by nasopharyngeal swab on day 14 because of concerns about the potential need to self-isolate beyond 14 days after an initial positive test, which was the required isolation period at the time in Salt Lake County.

## Discussion

In our study, we found that symptoms of secondary SARS-CoV-2 infection occurred in 7 household contacts of index COVID-19 patients starting <2 days before and ≤3 days after the observed initiation of viral shedding. The median interval of 4 days between symptom onset in index patients and symptom onset in their respective SARS-CoV-2–positive household contacts was similar to that reported in other household studies (*10,11,15*). Timely enrollment in our investigation (median 4 days after symptom onset in the index patient), however, allowed us to observe the timing and characteristics of initial viral shedding with a level of granularity not attained in previous studies.

For the household members (02-02 and 05-01) in whom we observed the initiation of viral shedding (i.e., SARS-CoV-2–positive result by rRT-PCR after a negative test), the first day of shedding corresponded with a high $C_t$ value, and the second day of shedding corresponded with a lower $C_t$ value, a positive viral culture, and the onset of new symptoms. These observations suggest that although the initiation of shedding marks the beginning of potential infectiousness, higher likelihood of virus transmission (indicated by positive viral culture) might coincide with lower $C_t$ values and the appearance of additional symptoms (*16*). Although 4 persons continued shedding virus >12 days after onset of symptoms, no culturable and potentially infectious virus could be isolated from the specimens collected.

For the 2 household members (02-01 and 02-03) in whom we observed presymptomatic viral shedding, initial shedding corresponded with medium or high $C_t$ values and occurred for 1–2 days before symptom onset. In 1 patient (02-01), the onset of symptoms coincided with a progression from high to medium $C_t$ value, and new, additional symptoms coincided with further progression from medium to low $C_t$ values. These findings mirror previous observations of presymptomatic shedding but suggest that viral load might increase as symptoms appear or progress. Among all SARS-CoV-2–positive contacts, symptoms were generally mild and sometimes transient. Of note, only 4 of 7 cases reported classic lower respiratory symptoms. In HH-02, the 2 contacts (02-01 and 02-02) who reported lower respiratory symptoms had them at illness onset, alongside several other symptoms. In HH-05, of the 3 contacts who had lower respiratory symptoms (05-01, 05-02, 05-03), two (05-01 and 05-03) reported them several days after symptom onset. Reports of symptoms by household contacts who remained SARS-CoV-2–negative could suggest other viral illnesses, allergies, underlying medical conditions, or stress-related effects of living with a person with COVID-19 (*17*).

Our findings suggest that household-level isolation practices could have been effective in preventing transmission. Findings from the 2003 SARS-CoV-1 epidemic showed that isolation of a patient before peak shedding was effective in reducing household transmission (*18*), and our results suggest that adopting precautionary measures can be effective in preventing secondary household transmission. In the households where no transmission was experienced, providing an index patient with separate sleeping quarters and avoiding face-to-face interactions (e.g., shared mealtimes) appeared sufficient to prevent transmission, even in households where close or intimate contact had occurred before diagnosis. Our findings show, however, that some persons infected with SARS-CoV-2 could begin shedding virus before being prompted to isolate by the onset of symptoms. In contrast to the households with no transmission, which consisted primarily of adults, the 2 households with secondary transmission to all contacts consisted of parents and their adolescent or preadolescent children. In these households, childcare needs and difficulties maintaining full isolation caused members to eschew precautionary practices, particularly after other household members were known to be infected.

Our study has some limitations. First, our household case-series was small because of the intensive nature of our early monitoring protocol; it was also biased toward index patients who were sufficiently symptomatic to be tested but whose disease was not severe enough to require hospitalization. Second, although all SARS-CoV-2–positive contacts had symptom onset ≥2 days (the estimated minimum incubation period) after the corresponding index patient, we cannot rule out the possibility of transmission from 1 presymptomatic household contact to another contact. Finally, symptom data relied on self-reporting, and symptoms might have been present before or after they were reported by patients. Three (20%) of 15 household contacts were children <13 years of age, who might have had more difficulty recognizing and reporting symptoms. Patient subjectivity could contribute to whether virus shedding or symptom onset is observed first.

In conclusion, our findings indicate that shedding of the SARS-CoV-2 virus might occur early in the disease course before symptom onset and clinical diagnosis, or it could occur when symptoms are mild or even absent. Persons with confirmed COVID-19 or who have had close contact with someone with confirmed COVID-19 should limit close contact with others, including household members, for 14 days. Persons who have been exposed to SARS-CoV-2 should be vigilant to the onset of mild symptoms; if they have not already limited close contact with household members or other persons, the onset of even mild symptoms should prompt additional caution and efforts to limit close contact. In addition, wearing masks or cloth face covers, practicing hand hygiene, and disinfecting surfaces regularly might reduce risk for transmission in households (*19*). Stay-at-home orders and at-home self-treatment of COVID-19 in the United States requires clear communication of such guidelines to prevent household transmission.

## About the Author

Dr. Lewis is an Epidemic Intelligence Service officer with the Centers for Disease Control and Prevention, assigned to the Utah Department of Health in Salt Lake City, Utah. His research interests include the role of social and environmental context in the spread of infectious diseases.

## References


1. Centers for Disease Control and Prevention. Coronavirus disease 2019 (COVID-19). United States COVID-19 cases and deaths by state [cited 2020 Jun 15]. https://www.cdc.gov/coronavirus/2019-ncov/cases-updates/cases-in-us.html
2. You C, Deng Y, Hu W, Sun J, Lin Q, Zhou F, et al. Estimation of the time-varying reproduction number of COVID-19 outbreak in China. Int J Hyg Environ Health. 2020;228:113555. https://doi.org/10.1016/j.ijheh.2020.113555
3. Ganyani T, Kremer C, Chen D, Torneri A, Faes C, Wallinga J, et al. Estimating the generation interval for coronavirus disease (COVID-19) based on symptom onset data, March 2020. Euro Surveill. 2020;25:2000257. https://doi.org/10.2807/1560-7917.ES.2020.25.17.2000257
4. Arons MM, Hatfield KM, Reddy SC, Kimball A, James A, Jacobs JR, et al.; Public Health–Seattle and King County and CDC COVID-19 Investigation Team. Presymptomatic SARS-CoV-2 infections and transmission in a skilled nursing facility. N Engl J Med. 2020;382:2081–90. https://doi.org/10.1056/NEJMoa2008457
5. Pan X, Chen D, Xia Y, Wu X, Li T, Ou X, et al. Asymptomatic cases in a family cluster with SARS-CoV-2 infection. Lancet Infect Dis. 2020;20:410–1. https://doi.org/10.1016/S1473-3099(20)30114-6
6. Qian G, Yang N, Ma AHY, Wang L, Li G, Chen X, et al. COVID-19 transmission within a family cluster by presymptomatic carriers in China. Clin Infect Dis. 2020;71:861–2.
7. Cheng HY, Jian SW, Liu DP, Ng TC, Huang WT, Lin HH; Taiwan COVID-19 Outbreak Investigation Team. Contact tracing assessment of COVID-19 transmission dynamics in Taiwan and risk at different exposure periods before and after symptom onset. JAMA Intern Med. 2020;180:1156–63. https://doi.org/10.1001/jamainternmed.2020.2020
8. He X, Lau EHY, Wu P, Deng X, Wang J, Hao X, et al. Temporal dynamics in viral shedding and transmissibility of COVID-19. Nat Med. 2020;26:672–5. https://doi.org/10.1038/s41591-020-0869-5
9. Wölfel R, Corman VM, Guggemos W, Seilmaier M, Zange S, Müller MA, et al. Virological assessment of hospitalized patients with COVID-2019. Nature. 2020;581:465–9. https://doi.org/10.1038/s41586-020-2196-x
10. Grijalva CG, Rolfes MA, Zhu Y, McLean HQ, Hanson KE, Belongia EA, et al. Transmission of SARS-COV-2 infections in households—Tennessee and Wisconsin, April–September 2020. MMWR Morb Mortal Wkly Rep. 2020;69:1631–4.
11. Lewis N, Chu V, Ye D, Conners EE, Gharpure R, Laws RL, et al. Household transmission of SARS-CoV-2 in the United States. Clin Infect Dis. 2020 Aug 16 [Epub ahead of print]. https://doi.org/10.1093/cid/ciaa1166
12. Centers for Disease Control and Prevention. CDC 2019-Novel Coronavirus (2019-nCoV) Real-time RT-PCR diagnostic panel. Instructions for use [cited 2020 Jun 30]. https://www.fda.gov/media/134922/download
13. Harcourt J, Tamin A, Lu X, Kamili S, Sakthivel SK, Murray J, et al. Severe acute respiratory syndrome coronavirus 2 from patient with coronavirus disease, United States. Emerg Infect Dis. 2020;26:1266–73. https://doi.org/10.3201/eid2606.200516
14. Council of State and Territorial Epidemiologists. Technical guidance interim-20-ID-01: standardized surveillance case definition and national notification for 2019 novel coronavirus disease (COVID-19) [cited 2020 Jul 8]. https://cdn.ymaws.com/www.cste.org/resource/resmgr/2020ps/interim-20-id-01_covid19.pdf
15. Wu J, Huang Y, Tu C, Bi C, Chen Z, Luo L, et al. Household transmission of SARS-CoV-2, Zhuhai, China, 2020. Clin Infect Dis. 2020 May 11 [Epub ahead of print].
16. Lui G, Ling L, Lai CK, Tso EY, Fung KS, Chan V, et al. Viral dynamics of SARS-CoV-2 across a spectrum of disease severity in COVID-19. J Infect. 2020;81:318–356.
17. Schimmenti A, Billieux J, Starcevic V. The four horsemen of fear: an integrated model of understanding fear experiences during the COVID-19 pandemic. Clin Neuropsychiatry. 2020;17:41–5.
18. Wilder-Smith A, Chiew CJ, Lee VJ. Can we contain the COVID-19 outbreak with the same measures as for SARS? Lancet Infect Dis. 2020;20:e102–7. https://doi.org/10.1016/S1473-3099(20)30129-8
19. Centers for Disease Control and Prevention. Coronavirus disease 2019 (COVID-19). How to protect yourself and others [cited 2020 Jun 29]. https://www.cdc.gov/coronavirus/2019-ncov/prevent-getting-sick/prevention.html


Address for correspondence: Nathaniel M. Lewis, Utah Department of Health, 288 N 1460 W, Salt Lake City, UT 84116, USA, email: CDCeisnml@utah.gov

# Zika Virus–Associated Birth Defects, Costa Rica, 2016–2018

Adriana Benavides-Lara, María de la Paz Barboza-Arguello, Mauricio González-Elizondo, Marcela Hernández-deMezerville, Helena Brenes-Chacón, Melissa Ramírez-Rojas, Catalina Ramírez-Hernández, Nereida Arjona-Ortegón, Shana Godfred-Cato, Diana Valencia, Cynthia A. Moore, Alejandra Soriano-Fallas

## Medscape EDUCATION ACTIVITY

In support of improving patient care, this activity has been planned and implemented by Medscape, LLC and Emerging Infectious Diseases. Medscape, LLC is jointly accredited by the Accreditation Council for Continuing Medical Education (ACCME), the Accreditation Council for Pharmacy Education (ACPE), and the American Nurses Credentialing Center (ANCC), to provide continuing education for the healthcare team.

Medscape, LLC designates this Journal-based CME activity for a maximum of 1.00 ***AMA PRA Category 1 Credit(s)*™**. Physicians should claim only the credit commensurate with the extent of their participation in the activity.

Successful completion of this CME activity, which includes participation in the evaluation component, enables the participant to earn up to 1.0 MOC points in the American Board of Internal Medicine's (ABIM) Maintenance of Certification (MOC) program. Participants will earn MOC points equivalent to the amount of CME credits claimed for the activity. It is the CME activity provider's responsibility to submit participant completion information to ACCME for the purpose of granting ABIM MOC credit.

All other clinicians completing this activity will be issued a certificate of participation. To participate in this journal CME activity: (1) review the learning objectives and author disclosures; (2) study the education content; (3) take the post-test with a 75% minimum passing score and complete the evaluation at http://www.medscape.org/journal/eid; and (4) view/print certificate. For CME questions, see page 679.

**Release date: January 21, 2021; Expiration date: January 21, 2022**

### Learning Objectives

Upon completion of this activity, participants will be able to:

- Describe epidemiologic features and prevalence of Zika-related birth defects (ZBD) and microcephaly among live-born infants in Costa Rica, March 2016 to March 2018, according to a descriptive analysis
- Determine clinical and test findings of live-born infants with ZBD in Costa Rica, March 2016 to March 2018, according to a descriptive analysis
- Identify clinical and public health implications of features of ZBD among live-born infants in Costa Rica, March 2016 to March 2018, according to a descriptive analysis.

### CME Editor

**P. Lynne Stockton Taylor, VMD, MS, ELS(D),** Technical Writer/Editor, Emerging Infectious Diseases. *Disclosure: P. Lynne Stockton Taylor, VMD, MS, ELS(D), has disclosed no relevant financial relationships.*

### CME Author

**Laurie Barclay, MD,** freelance writer and reviewer, Medscape, LLC. *Disclosure: Laurie Barclay, MD, has disclosed no relevant financial relationships.*

### Authors

*Disclosures:* ***Adriana Benavides-Lara, MD, MSc; María de la Paz Barboza Arguello, MSc; Mauricio González Elizondo, MSc; Marcela Hernández-deMezerville, MD; Helena Brenes-Chacón; Alejandra Soriano, MD; Melissa Ramírez Rojas, MD, MSc; Nereida Arjona Ortegón, MD; Catalina Ramírez-Hernández, MD, MSc; Shana Godfred-Cato, DO; Diana Valencia, MS;*** *and* ***Cynthia A. Moore, MD, PhD, h****ave disclosed no relevant financial relationships.*

Author affiliations: Instituto Costarricense de Investigación y Enseñanza en Nutrición y Salud, Cartago, Costa Rica (A. Benavides-Lara, M.P. Barboza-Arguello, M. González-Elizondo); Caja Costarricense del Seguro Social, San José, Costa Rica (M. Hernández-deMezerville, H. Brenes-Chacón, C. Ramírez-Hernández, N. Arjona Ortegón, A. Soriano-Fallas); Ministry of Health, San José (M. Ramírez-Rojas); Centers for Disease Control and Prevention, Atlanta, Georgia, USA (S. Godfred-Cato, D. Valencia, C.A. Moore)

DOI: https://doi.org/10.3201/eid2702.202047

After Zika virus (ZIKV) infection in Costa Rica was confirmed in January 2016, the national surveillance system was enhanced to monitor associated birth defects. To characterize the ZIKV outbreak among live-born infants during March 2016–March 2018, we conducted a descriptive analysis. Prevalence of ZIKV-associated birth defects was 15.3 cases/100,000 live births. Among 22 infants with ZIKV-associated birth defects, 11 were designated as confirmed (positive for ZIKV) and 11 were designated as probable cases (negative for ZIKV or not tested, but mother was exposed to ZIKV during pregnancy). A total of 91% had microcephaly (head circumference >2 SDs below mean for age and sex), 64% severe microcephaly (head circumference ≥3 SDs below mean for age and sex), 95% neurodevelopmental abnormalities, 82% brain anomalies, 41% eye abnormalities, and 9% hearing loss. Monitoring children for ≥1 year can increase identification of ZIKV-associated abnormalities in addition to microcephaly.

Zika virus (ZIKV) is an RNA virus of the Flaviviridae family and is transmitted primarily by mosquitos of the genus *Aedes* (*Stegomyia*). The virus was discovered in Uganda in 1947 (*1*) and isolated from humans in Nigeria in 1953; in subsequent years, small clusters of infection in humans from Africa and Asia were reported (*2*). ZIKV outbreaks were identified in Yap in 2007 and in French Polynesia in 2013–2014 (*2*–*4*). In 2015, ZIKV reached the continental Americas, and an outbreak in Brazil was identified (*5*). In September 2015, an increased number of children were born with microcephaly and other central nervous system (CNS) defects in countries where ZIKV was circulating (*6*–*8*).

An article published in early 2017 described the most severe phenotype of ZIKV-associated birth defects (ZBD) (*9*). The 5 key characteristics of that phenotype are severe microcephaly with collapse of the skull and redundancy of the scalp consistent with the fetal brain disruption sequence (*10*), thinning of the cerebral cortex and subcortical calcifications, macular scarring with focal retinal pigment mottling, congenital joint contractures, and hypertonia with symptoms of extrapyramidal involvement. These findings were noted to be more characteristic of ZIKV infection than other congenital infections; however, they did not constitute a case definition. Several subsequent studies supported that these defects were associated with ZIKV infection during pregnancy (*11*–*13*).

In Costa Rica, microcephaly has been monitored by the national birth defects surveillance system (NBDSS) since 1985. Before the ZIKV epidemic, Costa Rica was among countries with the highest prevalence of microcephaly in Latin America; microcephaly prevalence during 2011–2015 was 4.2 cases/10,000 live births (95% CI 3.6–4.9 cases/10,000 live births; n = 153; annual median 31) (*14*). In January 2016, the National Virology Reference Center (Cartago, Costa Rica), in coordination with the NBDSS, implemented laboratory-based surveillance for ZIKV disease; in February 2016, the NBDSS, along with health authorities, initiated ZBD surveillance (Figure 1). To characterize the effects of the Zika virus outbreak on live-born infants, we reviewed enhanced surveillance data for birth defects and the clinical characteristics of infants with confirmed and probable ZBD born in Costa Rica during March 2016–March 2018. In accordance with the Costa Rican Biomedical Research Legislation, Article 7, the analysis of surveillance data was registered in the National Council of Health Investigation.

## Methods

### Birth Defects Surveillance System

We conducted a descriptive analysis based on retrospective data collected for the NBDSS during the study period. The Costa Rican Birth Defects Register Center is an NBDSS that collects information on internal and external birth defects for all live-born infants up to 1 year of age. Passive reporting is mandatory for public and private hospitals; live-birth coverage is 96%. In February 2016, birth defect surveillance was enhanced by creation of a protocol that established the follow-up of cases, including laboratory tests for ZIKV and other differential diagnoses (*18*). Cases reported to the NBDSS were reviewed and classified by a multidisciplinary team in Costa Rica and by subject matter experts from the US Centers for Disease Control and Prevention.

### Microcephaly

Microcephaly is defined as head circumference measurement >2 SDs below the mean for a given age and sex (*19*); it is severe when the circumference is ≥3 SDs below the mean for a given age and sex. For infants born at term, we used World Health Organization growth charts (*20*). For preterm infants, microcephaly was defined as head circumference below the third percentile according to the Fenton Growth Charts (https://live-ucalgary.ucalgary.ca/resource/preterm-growth-chart/preterm-growth-chart). Congenital and postnatal-onset microcephaly were included.

### Suspected Cases

All potential cases of ZBD were reported to NBDSS. These reports were reviewed to determine whether they met the criteria for a suspected case of ZBD. Suspected cases were those that met ≥1 of the following criteria:

- Live-born infants with microcephaly, regardless of laboratory findings in the mother or infant, or maternal symptoms of ZIKV (rash and fever) during pregnancy
- Any live-born infant with ≥2 of the following findings (or 1 + microcephaly), regardless of laboratory findings in the mother or infant or maternal ZIKV symptoms during pregnancy:
    - CNS: intracerebral calcifications, cerebellar hypoplasia, thinning of the cerebral cortex, corpus callosum anomalies, ventriculomegaly or increased extra-axial fluid, abnormal pattern of cerebral gyri (e.g., polymicrogyria, lissencephaly), and specific neurodevelopmental findings (e.g., psychomotor development delay, spasticity, persistent irritability, seizures, swallowing disorders, movement abnormalities, or extrapyramidal changes)
    - Sensorineural deafness
    - Eye: structural abnormalities (e.g., microphthalmia, coloboma, cataracts or intraocular calcifications; posterior pole anomalies such as chorioretinal atrophy, optic nerve abnormalities, focal retinal pigment mottling)
    - Arthrogryposis or multiple joint contractures affecting ≥1 major joint or talipes equinovarus
- Live-born infants without microcephaly but with any major birth defect not consistent with a ZBD (e.g., significant cardiac defect) or with specific neurodevelopmental findings mentioned above, born to a mother with probable or confirmed ZIKV infection during pregnancy (defined as a mother with symptomatic ZIKV infection during pregnancy and/or a strong epidemiologic link to ZIKV during pregnancy [lives in high ZIKV–endemic area or has close contact with ZIKV–positive person] with or without positive laboratory test result for ZIKV during pregnancy)

For all suspected case-patients, a serum sample, urine sample, or both were collected from the infant before hospital discharge. Samples were tested for ZIKV RNA by using established singleplex real-time reverse transcription PCR (rRT-PCR) (*3*). Serum was tested in parallel with Zika IgM Antibody Capture ELISA (*3*,*21*). The NBDSS was immediately notified, the case was reviewed, and the infant was referred to a pediatrician and the congenital infection clinic (CIC). A multidisciplinary assessment of the child was conducted and included evaluation by pediatricians and the CIC; laboratory testing for syphilis, toxoplasmosis, rubella, and cytomegalovirus infection; cranial ultrasonography; and indirect ophthalmologic examination and neonatal auditory screening by otoacoustic emissions, followed by auditory brainstem response. Referral to a geneticist, pediatric cardiologist, neurodevelopmental specialist, or pediatric neurologist was dependent on examination findings. Thus, some of the children underwent complementary testing such as chromosomal or fluorescence in situ hybridization analysis, cardiac or abdominal ultrasonography, computerized tomography, and specialized neurodevelopmental assessments.

### Classification and Characterization of Suspected Cases

All clinical, epidemiologic, and laboratory data for suspected cases were reviewed. Cases were classified as confirmed, probable, excluded, and not classifiable (Figure 2) as follows:

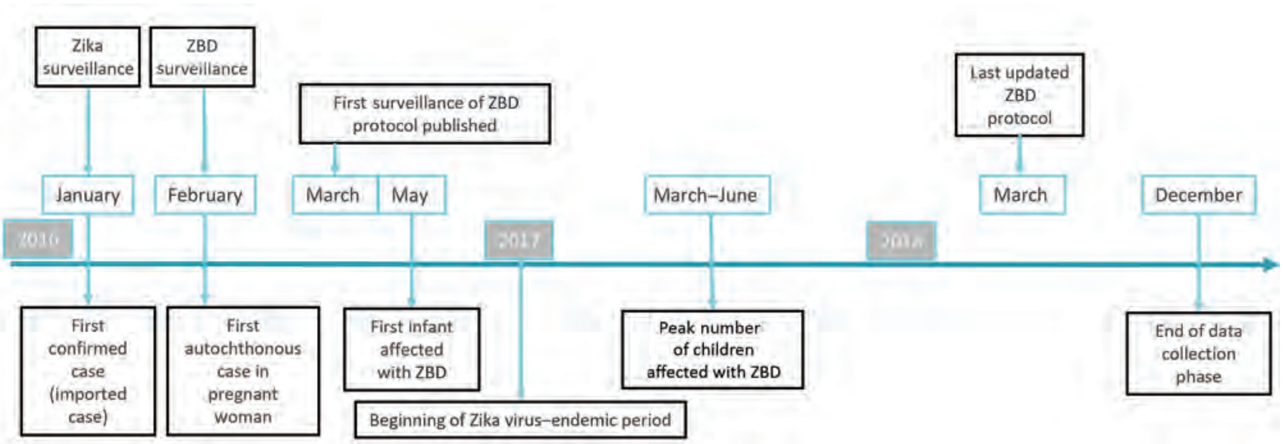


**Figure 1.** Key events involving ZBD surveillance, Costa Rica, March 2016–March 2018. In Costa Rica, laboratory testing using real-time reverse transcription PCR was implemented in late January 2016 (*15*–*17*). Although the first autochthonous case in Costa Rica was detected in a pregnant woman in February 2016 (*16*), a case was published in the United States about a traveler infected in December 2015 in Costa Rica (*17*). ZBD, Zika virus–associated birth defects.

- Confirmed case-patients were infants with ZBD (clinical criteria) for whom a sample taken before hospital discharge was positive for ZIKV by rRT-PCR or IgM ELISA (laboratory criteria) and who had an epidemiologic link (mother with ZIKV symptoms or was ZIKV positive by rRT-PCR during pregnancy or was from a highly ZIKV–endemic community).
- Probable case-patients were infants with ZBD (clinical criteria) who had negative ZIKV results by rRT-PCR or IgM ELISA or were not tested but whose mother had laboratory-confirmed ZIKV infection or symptoms compatible with ZIKV infection or had an epidemiologic link, and no other cause for the birth defect was identified.
- Excluded case-patients were infants with birth defects not related to ZIKV infection, who had negative laboratory results for ZIKV by rRT-PCR and IgM ELISA or were not tested and whose mother had negative ZIKV results, no symptoms of ZIKV infection, or no clear exposure to ZIKV during pregnancy. Excluded cases also included infants who had other known etiologies for microcephaly or the birth defect or had a presumed syndrome of undetermined cause. This group also included infants with a diagnosis of microcephaly at birth whose head circumference by 1 year of age was <2 SDs below the mean (and did not have any other birth defects).

Not classifiable case-patients were infants with insufficient information to be appropriately included in the previous categories.

### Analysis

We calculated population-based birth prevalence and 95% CI for confirmed and probable cases of ZBD and microcephaly during the period of enhanced surveillance and compared the prevalence ratio for microcephaly with the baseline prevalence during 2011–2015. We also calculated the distributions of specific birth defects and neurodevelopmental abnormalities among infants with ZBD. Total births for the period were obtained from the National Institute of Statistics and Censuses (http://www.inec.go.cr). To characterize infants with ZBD, we used the mother's province of origin; mother's history of exposure to ZIKV during pregnancy (associated symptoms or laboratory confirmation); and the infant's head circumference, weight, length, gestational age, ZIKV molecular and serologic test results, other reported birth defects, and neurodevelopmental anomalies.

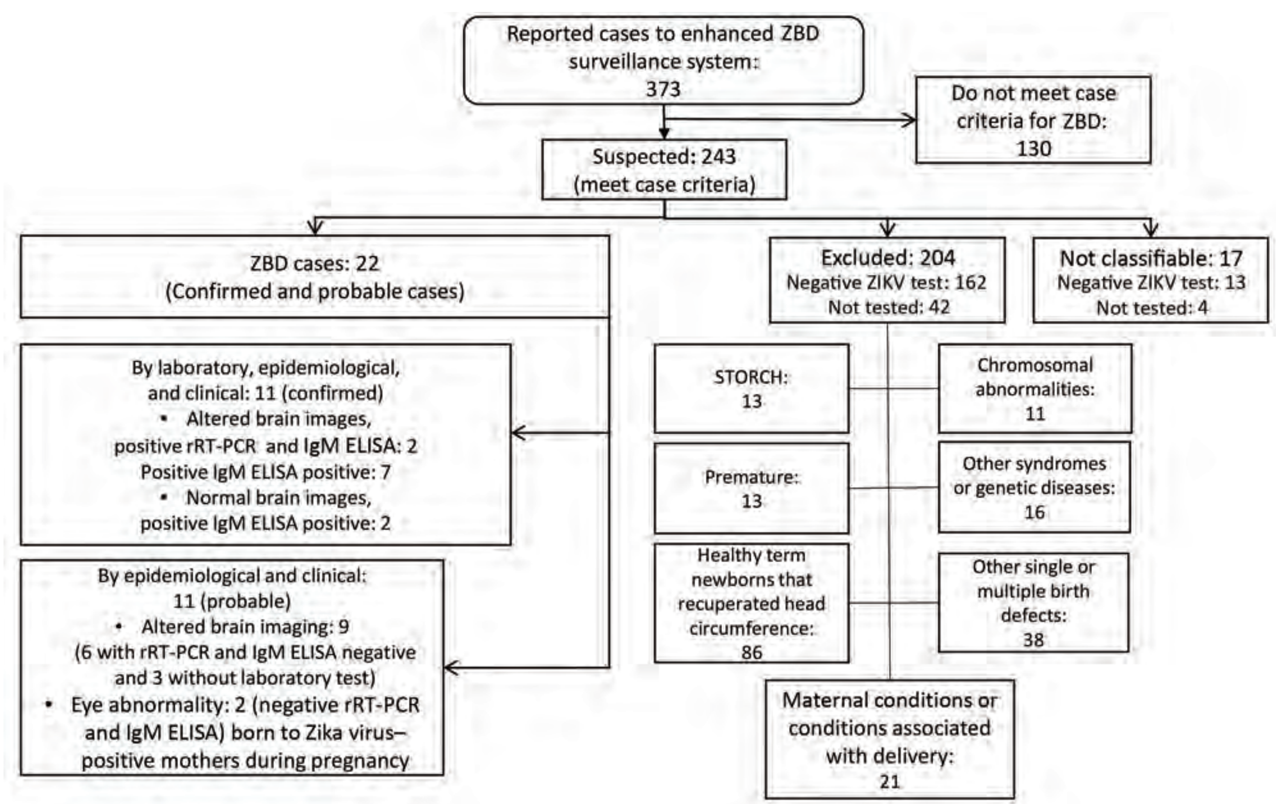


**Figure 2.** Reported cases and classification of suspected cases of ZBD according to protocol, Costa Rica, March 2016–March 2018. rRT-PCR, real-time reverse transcription PCR; STORCH, syphilis, toxoplasmosis, rubella, cytomegalovirus, and hepatitis B (note that Costa Rica does not include hepatitis B in its standard evaluations); ZBD, Zika virus–associated birth defects.

## Results

Of 373 potential cases reported to the NBDSS, 243 met the criteria for a suspected case (Figure 2); 150 (62%) of the 243 infants were female. Compared with microcephaly baseline data for Costa Rica (22), the birth prevalence of microcephaly increased from 4.2 (95% CI 3.6–4.9) cases/10,000 live births during 2011–2015 to 15.5 (95% CI 13.5–17.5) cases/10,000 live births during the Zika outbreak (March 2016–March 2018); prevalence ratio was 3.7 (95% CI 3.0–4.5).

**Table 1**. Distribution of 204 excluded cases according to exclusion criteria for Zika virus–associated birth defects, Costa Rica, March 2016–March 2018*

| Category, cause | No. cases |
|---|---|
| Chromosome anomaly, n = 11 | |
| Ring chromosome 4. Possible Wolf-Hirschhorn | 1 |
| Mosaic 47,XYY/46,XY | 1 |
| Trisomy 13 | 5 |
| Trisomy 18 | 1 |
| Trisomy 21 | 3 |
| STORCH, n = 13 | |
| Congenital syphilis | 2 |
| Congenital toxoplasmosis | 6 |
| Rubella | 0 |
| Congenital cytomegalovirus | 4 |
| Congenital hepatitis B | 1 |
| Birth defects (isolated, multiple nonsyndromic), n = 38 | |
| Anencephaly and rachischisis | 3 |
| Congenital heart defect | 7 |
| Craniosynostosis | 1 |
| Gastroschisis | 2 |
| Hydranencephaly and hydrocephaly | 4 |
| Microcephaly, constitutional or familial | 11 |
| Multiple malformations of unknown cause | 8 |
| Partial agenesis of the corpus callosum | 1 |
| Cleft palate | 1 |
| Diseases, maternal conditions, or problems at delivery, n = 27 | |
| Maternal alcoholism or drug use | 7 |
| Hypoxic encephalopathy or acute fetal distress at birth | 5 |
| Maternal ossifying myositis | 1 |
| Maternal hyperthyroidism | 1 |
| Pregnancy-induced hypertension with or without pre-eclampsia | 9 |
| Maternal chronic arterial hypertension | 2 |
| Maternal tuberculosis | 1 |
| Maternal epilepsy | 1 |
| Other genetic diseases or other specific syndromes of the infant, n = 16 | |
| Crouzon syndrome | 1 |
| Septo-optic dysplasia | 1 |
| Holoprosencephaly | 8 |
| Cystic fibrosis | 1 |
| Roberts syndrome (possible) | 1 |
| Meckel Gruber syndrome (possible) | 1 |
| Aicardi Goutières syndrome (probable) | 1 |
| Russel Silver syndrome | 1 |
| Familial syndrome not specified | 1 |
| Newborn with microcephaly with subsequent normal head circumference and no other findings, n = 99† | |
| Term newborns‡ | 86 |
| Premature newborns | 13 |
| Total excluded cases | 204 |

*STORCH, syphilis, toxoplasmosis, rubella, cytomegalovirus, and hepatitis B. Note that Costa Rica does not include hepatitis B in its standard evaluations.
†Newborns that do not belong to any other category of causes.
‡Includes 56 with and 30 without intrauterine growth restriction.

### Evaluation of Suspected ZBD Cases

A pediatric infectious disease specialist at the CIC examined 40% (96/243) of the infants with suspected ZBD ≥1 time; a pediatrician evaluated the rest. The most frequent birth defect was microcephaly; 88% (213/243) had microcephaly at birth. Among those, 26% (55/213) had severe microcephaly. Postnatal-onset microcephaly developed in 5% (12/243), and no microcephaly but other criteria that met the definition of suspected ZBD was found for 7% (18/243). A total of 9% (22/243)of suspected cases-infants were classified as having confirmed or probable ZBD, 84% (204/243) were excluded, and 7% (17/243) were not classifiable (Table 1; Figure 2).

For 79% (193/243) of newborns, ≥1 ZIKV laboratory test was performed by urine or serum rRT-PCR or by serum IgM ELISA. Cerebrospinal fluid from 4 infants was available for testing. Serologic tests for other congenital infections were completed for syphilis (65%, 159/243), rubella (87%, 211/243), cytomegalovirus infection (69%, 168/243), and toxoplasmosis (68%, 166/243).

Among infants with suspected ZBD, 68% (165/243) underwent head ultrasonography or computed tomography (CT), 56% (136/243) underwent indirect ophthalmologic evaluation, 46% (113/243) had hearing screened by otoacoustic emissions, and 31% (75/243) underwent auditory brain response testing. Diagnostic auditory brain response testing was also performed for those with confirmed and probable ZBD.

### Confirmed and Probable Cases of ZIKV-Associated Birth Defects

The prevalence of ZBD during March 2016–March 2018 was 15.3 (95% CI 8.9–21.7) cases/100,000 live births, based on 22 confirmed and probable cases among 143,930 live births (Figure 3). Proportion of deaths within the first year of life among infants with ZBD was 13.6% (3/22). All death cases were classified as probable. These infants had cerebral anomalies, microcephaly, hypertonia, multiple joint contractures (n = 2), and optic nerve hypoplasia (n = 1), and were born to immigrant mothers from highly ZIKV-endemic areas.

Most infants with ZBD were full-term newborns (95%, 21/22) and had weight appropriate for gestational age (68%, 15/22). The average weight (± SD) at birth was 2,818 g (± 657 g, range 1,560–3,940 g), and height was 44.2 cm (± 3.1 cm, range 41–53 cm).

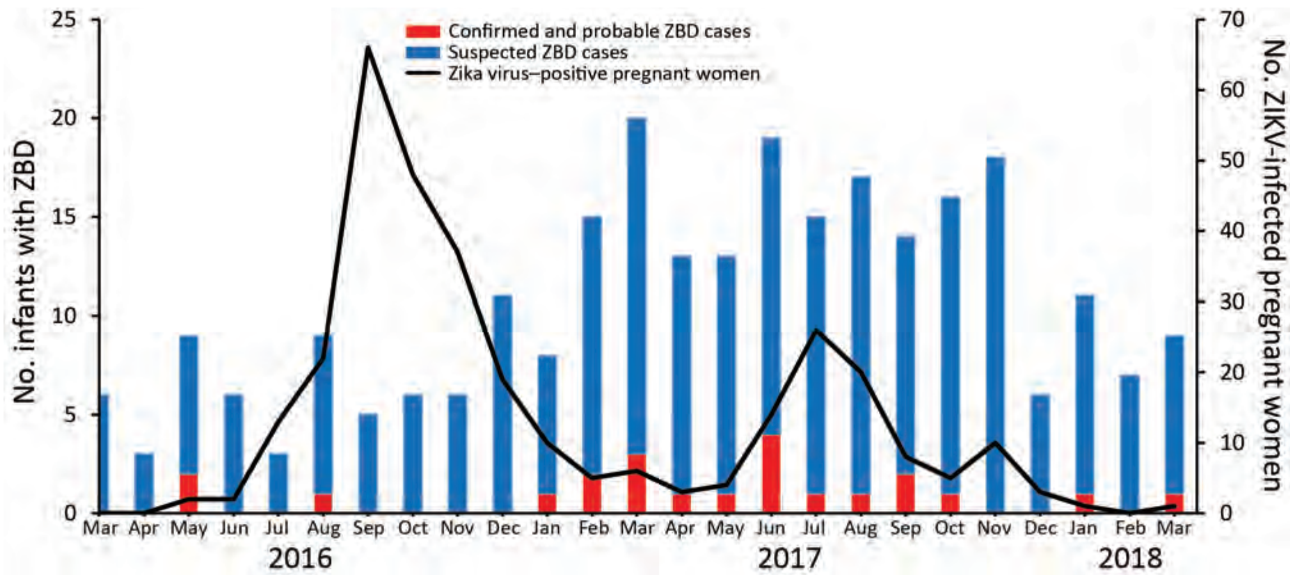


**Figure 3.** Distribution of infants with reported ZBD and pregnant women with Zika virus infection, by month, Costa Rica, March 2016–March 2018. The peak of Zika virus infection among pregnant women occurred in September 2016; the highest number of suspected cases of ZBD occurred 6 months later, March–October 2017. ZBD, Zika virus–associated birth defects.

Eleven infants classified as confirmed were positive for ZIKV (9 by IgM ELISA and 2 by IgM ELISA and rRT-PCR; Figure 2); among 11 infants classified as probable, 7 had negative test results (4 by rRT-PCR and IgM ELISA and 3 by rRT-PCR alone) and 4 did not undergo laboratory testing.

The provinces registering the highest prevalence of ZBD were Limón (58.8 cases/100,000 live births) and Puntarenas (37.1 cases/100,000 live births) (Figure 4). Among mothers of infants with ZBD, 64% had symptoms, 27% during the first trimester and 37% during the second trimester; 23% of the mothers had positive ZIKV rRT-PCR results during pregnancy (Table 2). Among infants with ZBD, 91% (20/22) had microcephaly (Table 3); onset was postnatal for 9% (2/22 cases). Two infants who did not have microcephaly were born to mothers who had confirmed ZIKV infection during the second trimester of pregnancy. One of these infants had cortical atrophy seen with head ultrasonography, scarring of the macula, strabismus, central hypotonia and peripheral hypertonia, swallowing difficulties, epilepsy and global neurodevelopmental delay; the other infant had normal brain images and neurodevelopment, but atrophic scarring involved the macula of both eyes.

Head ultrasonography was performed for 21 of the 22 infants classified as confirmed and probable cases (6 of them also underwent CT, magnetic resonance imaging, or both), and the other underwent head CT. Among these infants, 82% (18/22) had evidence of ≥1 brain defect. Those without brain defects evident by imaging had defects in the eye, body tone, or neurodevelopment.

Ophthalmologic evaluation was performed for 91% (20/22) of infants classified as confirmed and probable cases; eye anomaly was detected for 45% (9/20). Sensorineural deafness was present in 9% (2/22); however, only 15/22 (68%) underwent audiologic evaluation with diagnostic auditory brain response testing. At least 1 neurodevelopmental anomaly was present in 95% (21/22) of infants; most (82%) had body tone anomalies (mainly hypertonia or spasticity) and possible neurodevelopmental delay. Other frequent manifestations included multiple contractures, seizures, movement anomalies, swallowing anomalies, and possible visual impairment (strabismus, nystagmus, or failure to fix and follow).

## Discussion

In Costa Rica, most infants with ZBD were born ≈1 year after the onset of autochthonous circulation of ZIKV and 6 months after peak incidence of ZIKV infection among pregnant women. Similar findings have been observed in Brazil, Colombia, and the United States, where the peak incidence was observed ≈6 months after the ZIKV epidemic, corroborating a temporal link between ZIKV infection and associated birth defects (*7*,*23*,*24*). Most infants with ZBD were born to mothers who reported symptoms in the first and second trimesters of pregnancy (64%), consistent with other reports (*25*–*29*); however, because 36%

were born to mothers who were asymptomatic, the proportion of infections in early to mid-pregnancy is probably greater.

The birth prevalence of infants with confirmed and probable ZBD during the enhanced surveillance period was 15.3 (95% CI 8.9–21.7) cases/100,000 live births. Birth prevalence of microcephaly, which was monitored before the ZIKV outbreak in Costa Rica, increased by almost 4-fold after the ZIKV outbreak, from 4.2 cases/10,000 live births to 15.5 cases/10,000 live births. Although we recognize that the birth prevalence of this defect may be underreported during non–ZIKV-epidemic times, these data are consistent with the experience in other countries, where the prevalence of microcephaly increased >4-fold (Colombia, French Polynesia, United States) (*7*,*24*,*25*) and up to 9-fold (Brazil) (*30*,*31*). Heightened awareness of the possible association between congenital ZIKV infection and microcephaly, as well as country-specific protocols to improve identification of this traditionally underascertained birth defect, probably contributed to increased prevalence estimates (*32*). Additional efforts were necessary to differentiate microcephaly as a component of ZBD from microcephaly from other causes in Costa Rica and in other ZIKV-affected locations. Consistent with published case series from Brazil (*11*,*12*) and from the US Zika Pregnancy and Infant Registry (*26*), we found that the most frequent clinical finding was microcephaly and most cases were classified as severe. The percentage of brain abnormalities was similar to what has been published (*11*,*26*,*33*), and among infants who underwent neuroimaging, the

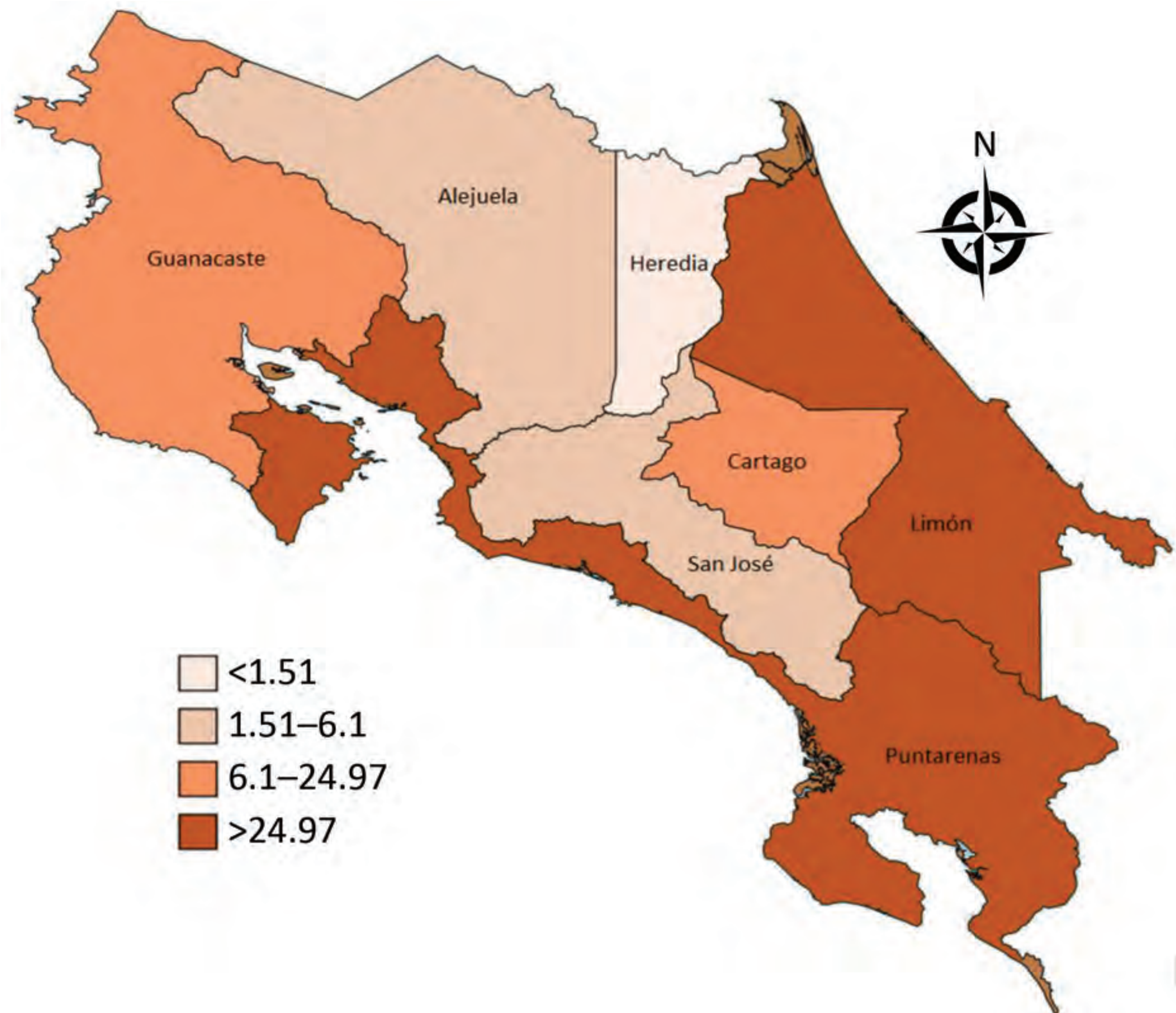


**Figure 4.** Prevalence of Zika-virus–associated birth defects (no. cases/100,000 live births), by province, Costa Rica, March 2016–March 2018. Cases are distributed by place of residence of the mother, not by place of birth. The 2 provinces in which prevalence of Zika virus–associated birth defects was highest (Puntarenas and Limón) are on the coast and have a humid tropical climate.

**Table 2.** Distribution of confirmed and probable ZIKV-associated birth defects, by trimester of infection for presence of ZIKV symptoms and laboratory confirmation for the mother, Costa Rica, March 2016–March 2018*

| | Mothers by trimester of symptom onset | | | | | | | | | |
|---|---|---|---|---|---|---|---|---|---|---|
| | ZIKV positive through rRT-PCR of maternal sample | | | | Without laboratory evidence in maternal sample | | | | | |
| | Trimester | | | | Trimester | | | | | |
| Cases | I | II | III | Subtotal | I | II | III | Subtotal | Asymptomatic mothers, subtotal | Total |
| Confirmed† | 2 | 1 | 0 | 3 | 4 | 2 | 0 | 6 | 2 | 11 |
| Probable‡ | 0 | 2 | 0 | 2 | 0 | 3 | 0 | 3 | 6 | 11 |
| Total, no. (%) | 2 (9) | 3 (14) | 0 | 5 (23) | 4 (18) | 5 (23) | 0 | 9 (41) | 8 (36) | 22 (100) |

*Samples were taken only from pregnant women with symptoms. rRT-PCR, real-time reverse transcription PCR; ZIKV, Zika virus.
†Designated as an infant with ZIKV-associated birth defects (clinical criteria), who was positive for ZIKV by rRT- PCR or IgM-ELISA in a sample taken before hospital discharge (laboratory criteria) and had an epidemiologic link (mother with ZIKV symptoms or positive rRT-PCR during pregnancy or from a high ZIKV-endemic community).
‡Designated as an infant with ZIKV-associated birth defects who was negative for ZIKV by rRT-PCR or IgM-ELISA or was not tested but whose mother had laboratory-confirmed ZIKV infection or had symptoms compatible with ZIKV infection or had a clear exposure to ZIKV during pregnancy and no other cause that could explain the birth defect.

most common findings were ventriculomegaly and cerebral calcifications, consistent with results of a recent meta-analysis (*34*). Two case-patients did not have microcephaly; both were born to mothers who had confirmed ZIKV infection during the second trimester of pregnancy, and both had other clinical findings consistent with congenital ZIKV infection. These findings have also been reported in studies from Brazil (*33*), where up to 1 in 5 infants with confirmed or probable ZBD had a normal head circumference (*12*).

Anomalies of the eye have also been associated with congenital ZIKV infection. Among the infants with eye anomalies in our study, most common were anomalies of the fundus, primarily chorioretinal scars or abnormal macular pigmentation and papillary/optic nerve atrophy. Several case series reported the same findings for 24%–55% of case-patients (*9*), mainly children of mothers infected with ZIKV during the first trimester (*35*,*36*). ZIKV-associated eye defects were found without microcephaly in 10/24 (42%) infants born to mothers with rRT-PCR–confirmed ZIKV infection during pregnancy; 8 (33%) of these infants had no abnormal brain findings (*36*), consistent with what we found for 1 infant with a confirmed case.

Sensorineural deafness was detected in 13% of infants by diagnostic auditory brain response testing. One study that specifically evaluated hearing loss in children with birth defects found sensorineural deafness in 6% by using auditory brain response testing (*37*); most cases also had neurodevelopmental anomalies previously described in the literature (*9*–*12*,*26*,*38*). The most frequent neurodevelopmental anomalies were tone abnormalities (primarily hypertonia), movement anomalies, and congenital joint contractures. Some neurologic and developmental alterations associated with microcephaly are secondary to CNS damage caused by ZIKV. Described in our case series and in other studies, these alterations include movement abnormalities and posturing (50%), swallowing abnormalities (41%), and epilepsy (36%) (*39*).

Our descriptive analysis is subject to limitations. Findings are based on a passive surveillance system enhanced with confirmation of the diagnosis; thus, information depends on the completeness of reporting, case ascertainment, and workup of suspected cases to verify microcephaly and determine which cases are probably ZIKV associated. The NBDSS collects data on live births only; findings are not generalizable to stillbirths and miscarriages. Comparing the prevalence of ZBD among countries is difficult because surveillance system methods and definitions of microcephaly and suspected cases vary and evaluations and criteria used to define ZBD might differ substantially (*40*). Another consideration is the known limitations of ZIKV laboratory tests (*41*–*43*). Among infants with ZBD, 50% had a positive ZIKV laboratory test result, all by ZIKV IgM ELISA and only 1 by rRT-PCR. Nonspecific reactivity resulting in a false-positive IgM result might have led to misclassification of cases as confirmed; however, false-positive IgM results seem unlikely, given the timing of ZIKV testing in these infants. Eleven infants with ZBD but without laboratory evidence were classified as probable cases. Of these, 7 had negative results by rRT-PCR, IgM ELISA, or both. The low detection of laboratory evidence for ZIKV infection in these infants probably reflects recognized challenges of laboratory testing, including the unknown sensitivity and specificity of testing of infants (*41*,*42*). In addition, given possible cross-reactivity for other flaviviruses and the need to prioritize resources, we did not conduct plaque-reduction neutralization tests. To help address laboratory limitations, we used the combination of clinical, epidemiologic, and laboratory data to classify cases. However, we cannot exclude an alternate etiology for birth defects in infants classified as having probable cases.

The Pan American Health Organization recommends surveillance of ZIKV disease in pregnant women and monitoring outcomes of infants born with brain anomalies (*44*). Many countries have implemented surveillance to monitor infants of ZIKV-positive mothers to capture cases of ZBD, to determine the risk for birth defects, and to examine neurodevelopmental anomalies (*25*,*30*,*32*). Population-based birth defects surveillance programs along with monitoring pregnant women with ZIKV disease provide an example of a complementary approach to ascertaining exposures and outcomes to better monitor new and emerging threats during pregnancy and effects on infants (*45*). Costa Rica National Guidelines established laboratory sampling and monitoring of every child born to symptomatic women (*46*). In our analysis, 23% of mothers of infants with confirmed and probable ZBD had a positive laboratory test result for ZIKV (Table 2); had the enhanced birth defects surveillance system not been implemented, 77% of cases would not have been linked to ZIKV. In addition, 60%–80% of ZIKV infections are asymptomatic, and in Costa Rica, the laboratory test for ZIKV is performed only for symptomatic pregnant women. Given these challenges, the benefit of combining an intensified birth defects surveillance system with surveillance of pregnant women with laboratory-confirmed ZIKV infection, as was done in Costa Rica and Colombia (*29*), is very useful, especially for countries with few resources.

The success of surveillance for ZBD in Costa Rica depended on the strict application of standard operating procedures and the active participation of healthcare personnel to enhance ascertainment of component anomalies, such as microcephaly, and to identify infants with sufficient evidence of a confirmed or probable ZIKV etiology for their birth

**Table 3.** Cases of Zika virus–associated birth defects and neurodevelopmental abnormalities, Costa Rica, March 2016–March 2018*

| Clinical and neuroimaging features | No. (%) cases | | |
|---|---|---|---|
| | Confirmed, n = 11 | Probable, n = 11 | Total, n = 22 |
| Brain defects | 9 (82) | 9 (82) | 18 (82) |
| Ventriculomegaly/Hydrocephaly | 8 (73) | 4 (36) | 12 (55) |
| Intracranial calcifications | 8 (73) | 3 (27) | 11 (50) |
| Cerebral atrophy | 4 (36) | 6 (55) | 10 (45) |
| Corpus callosum abnormalities | 4 (36) | 4 (36) | 8 (36) |
| Abnormal cortical formation | 3 (27) | 3 (27) | 6 (27) |
| Cerebellar abnormalities | 2 (18) | 0 | 2 (9) |
| Porencephaly | 0 | 1 (9) | 1 (5) |
| Other | 0 | 2 (18) | 2 (9) |
| No brain defects | 2 (18) | 2 (18) | 4 (18) |
| Eye anomalies | 5 (45) | 4 (36) | 9 (41) |
| Chorioretinal scarring in the macula | 4 (36) | 2 (18) | 6 (27) |
| Optic nerve | 3 (27) | 2 (18) | 5 (23) |
| Other | 0 | 0 | 0 |
| No eye anomalies | 6 (55) | 5 (45) | 11 (50) |
| No data reported† | 0 | 2 (18) | 2 (9) |
| Microcephaly | 11 (100) | 9 (82) | 20 (91) |
| Severe | 9 (82) | 5 (45) | 14 (64) |
| Mild–moderate | 2 (18) | 4 (36) | 6 (27) |
| No microcephaly | 0 | 2 (18) | 2 (9) |
| Hearing abnormalities, ABR evaluation | 2 (18) | 0 | 2 (9) |
| Sensorineural hearing loss | 2 (18) | 0 | 2 (9) |
| No hearing abnormalities | 7 (64) | 6 (55) | 13 (59) |
| Not evaluated by ABR‡ | 2 (18) | 5 (45) | 7 (32) |
| Neurodevelopmental abnormalities | 11 (100) | 9 (82) | 21 (95) |
| Body tone abnormalities | 10 (91) | 8 (73) | 18 (82) |
| Possible developmental delay§ | 10 (91) | 8 (73) | 18 (82) |
| Possible visual impairment | 8 (73) | 4 (36) | 12 (55) |
| Congenital contractures | 5 (45) | 5 (45) | 10 (45) |
| Seizures, excluding febrile | 7 (64) | 1 (9) | 8 (36) |
| Movement abnormalities | 6 (55) | 5 (45) | 11 (50) |
| Swallowing abnormalities | 6 (55) | 3 (27) | 9 (41) |
| No abnormalities | 0 | 1 (9) | 1 (5) |
| No data reported† | 0 | 1 (9) | 1 (5) |

*ABR, auditory brain response test.
†These infants had a normal result for newborn hearing screening by otoacoustic emissions testing and were not evaluated by ABR because they were lost to follow-up. Three infants did not have any hearing screening because they died soon after birth.
‡Includes infants for whom an evaluation was not performed or records were not obtainable.
§For 4 children (1 with a confirmed case and 3 with a possible case), developmental delay was not evaluated by any specific method.

defects. Thus, global establishment and strengthening of NBDSS is essential, as recommended by the World Health Organization at its 63rd World Health Assembly (Resolution WHA63.17, https://apps.who.int/gb/ebwha/pdf_files/WHA63-REC1/WHA63_REC1-en.pdf). Microcephaly is not the only congenital anomaly that should be monitored after ZIKV infection; other birth defects, such as congenital brain and eye defects and joint contractures, should also be monitored. Monitoring children born to ZIKV-positive mothers and those with ZBD or neurodevelopmental anomalies through at least the first year of life can increase identification of additional associated abnormalities such as deafness, eye or vision anomalies, postnatal onset of microcephaly, and substantial neurodevelopmental abnormalities. Other neurodevelopmental disabilities might become apparent after 1 year of age; thus, following children to 3 years of age is valuable and may enhance surveillance of ZBD and neurodevelopmental outcomes in Costa Rica.

## About the Author

Dr. Benavides-Lara is a pediatrician and epidemiologist who directs the Costa Rican Birth Defects Register Center in Cartago, Costa Rica. Her primary research interest is epidemiological investigations of birth defects.

## References

1. Dick GWA, Kitchen SF, Haddow AJ. Zika virus (I). Isolations and serological specificity. Trans R Soc Trop Med Hyg. 1952;46:509–20. https://doi.org/10.1016/0035-9203(52)90042-4
2. Petersen LR, Jamieson DJ, Powers AM, Honein MA. Zika virus. N Engl J Med. 2016;374:1552–63. https://doi.org/10.1056/NEJMra1602113
3. Lanciotti RS, Kosoy OL, Laven JJ, Velez JO, Lambert AJ, Johnson AJ, et al. Genetic and serologic properties of Zika virus associated with an epidemic, Yap State, Micronesia, 2007. Emerg Infect Dis. 2008;14:1232–9. https://doi.org/10.3201/eid1408.080287
4. Aubry M, Teissier A, Huart M, Merceron S, Vanhomwegen J, Roche C, et al. Zika virus seroprevalence, French Polynesia, 2014–2015. Emerg Infect Dis. 2017;23:669–72. https://doi.org/10.3201/eid2304.161549
5. Campos GS, Bandeira AC, Sardi SI. Zika virus outbreak, Bahia, Brazil. Emerg Infect Dis. 2015;21:1885–6. https://doi.org/10.3201/eid2110.150847
6. Schuler-Faccini L, Ribeiro EM, Feitosa IM, Horovitz DD, Cavalcanti DP, Pessoa A, et al.; Brazilian Medical Genetics Society–Zika Embryopathy Task Force. Possible association between Zika virus infection and microcephaly—Brazil, 2015. MMWR Morb Mortal Wkly Rep. 2016;65:59–62. https://doi.org/10.15585/mmwr.mm6503e2
7. Cuevas EL, Tong VT, Rozo N, Valencia D, Pacheco O, Gilboa SM, et al. Preliminary report of microcephaly potentially associated with Zika virus infection during pregnancy—Colombia, January–November 2016. MMWR Morb Mortal Wkly Rep. 2016;65:1409–13. https://doi.org/10.15585/mmwr.mm6549e1
8. Kleber de Oliveira W, Cortez-Escalante J, De Oliveira WT, do Carmo GM, Henriques CM, Coelho GE, et al. Increase in reported prevalence of microcephaly in infants born to women living in areas with confirmed Zika virus transmission during the first trimester of pregnancy—Brazil, 2015. MMWR Morb Mortal Wkly Rep. 2016;65:242–7. https://doi.org/10.15585/mmwr.mm6509e2
9. Moore CA, Staples JE, Dobyns WB, Pessoa A, Ventura CV, da Fonseca EB, et al. Characterizing the pattern of anomalies in congenital Zika syndrome for pediatric clincians. JAMA Pediatr. 2017;171:288–95. https://doi.org/10.1001/jamapediatrics.2016.3982
10. Russell LJ, Weaver DD, Bull MJ, Weinbaum M, Opitz JM. In utero brain destruction resulting in collapse of the fetal skull, microcephaly, scalp rugae, and neurologic impairment: the fetal brain disruption sequence. Am J Med Genet. 1984;17:509–21. https://doi.org/10.1002/ajmg.1320170213
11. del Campo M, Feitosa IML, Ribeiro EM, Horovitz DDG, Pessoa ALS, França GVA, et al.; Zika Embryopathy Task Force-Brazilian Society of Medical Genetics ZETF-SBGM. The phenotypic spectrum of congenital Zika syndrome. Am J Med Genet A. 2017;173:841–57. https://doi.org/10.1002/ajmg.a.38170
12. França GVA, Schuler-Faccini L, Oliveira WK, Henriques CMP, Carmo EH, Pedi VD, et al. Congenital Zika virus syndrome in Brazil: a case series of the first 1501 livebirths with complete investigation. Lancet. 2016;388:891–7. https://doi.org/10.1016/S0140-6736(16)30902-3
13. Rice ME, Galang RR, Roth NM, Ellington SR, Moore CA, Valencia-Prado M, et al. Vital signs: Zika-associated birth defects and neurodevelopmental abnormalities possibly associated with congenital Zika virus infection—U.S. territories and freely associated states, 2018. MMWR Morb Mortal Wkly Rep. 2018;67:858–67. https://doi.org/10.15585/mmwr.mm6731e1
14. Orioli IM, Dolk H, Lopez-Camelo JS, Mattos D, Poletta FA, Dutra MG, et al. Prevalence and clinical profile of microcephaly in South America pre-Zika, 2005-14: prevalence and case-control study. BMJ. 2017;359:j5018. https://doi.org/10.1136/bmj.j5018
15. Costa Rica Bicentennial Government. First imported case of Zika in Costa Rica [in Spanish] [cited 2019 Aug 14]. https://presidencia.go.cr/comunicados/2016/01/primer-caso-importado-de-zika-en-costa-rica/
16. Ávalos A. Pregnant woman becomes first native case of Zika in Costa Rica [in Spanish] [cited 2019 Aug 14]. https://www.nacion.com/el-pais/salud/embarazada-se-convierte-en-primer-caso-autoctono-de-zika-en-costa-rica/PSI4Z6V75ZGARLKBA62NAH6INA/story/
17. Chen LH. Zika virus infection in a Massachusetts resident after travel to Costa Rica: a case report. Ann Intern Med. 2016;164:574–576. https://doi.org/10.7326/L16-0075
18. Ministerio de Salud de Costa Rica, Instituto Costarricense de Investigación y Enseñanza en Nutrición y Salud, Caja Costarricense del Seguro Social. Surveillance protocol for microcephaly and congenital syndrome associated with Zika virus in Costa Rica [in Spanish] [cited 2019 Sep 14]. https://www.ministeriodesalud.go.cr/index.php/vigilancia-de-la-salud/normas-protocolos-y-guias/malformaciones-congenitas/3786-protocolo-vigilancia-zika-congenito-microcefalia-marzo-2018/file
19. World Health Organization. Birth defects surveillance: a manual for programme managers [cited 2019 Sep 14].

https://apps.who.int/iris/bitstream/handle/10665/110223/9789241548724_eng.pdf
20. World Health Organization Multicentre Growth Reference Study Group. WHO child growth standards: methods and development [cited 2019 Aug 14]. https://www.who.int/childgrowth/standards/second_set/technical_report_2/en
21. Centers for Disease Control and Prevention. CDC instructions for Zika MAC-ELISA protocol. 2018 Feb 2 [cited 2019 Aug 21]. https://www.cdc.gov/zika/pdfs/zika-mac-elisa-instructions-for-use.pdf
22. Benavides-Lara A, Barboza-Arguello MP. Abbreviated report of microcephaly cases reported to Costa Rican Birth Defects Register Center, Costa Rica 2011–2017 [in Spanish] [cited 2019 Aug 14]. https://www.inciensa.sa.cr/vigilancia_epidemiologica/informes_vigilancia/2018/Malformaciones%20Congenitas/Reporte%20abreviado%20de%20Microcefalia%20en%20Costa%20Rica%202011-2017.pdf
23. de Oliveira WK, de França GVA, Carmo EH, Duncan BB, de Souza Kuchenbecker R, Schmidt MI, et al. Infection-related microcephaly after the 2015 and 2016 Zika virus outbreaks in Brazil: a surveillance-based analysis. Lancet. 2017;390:861–70. https://doi.org/10.1016/S0140-6736(17)31368-5
24. Smoots AN, Olson SM, Cragan J, Delaney A, Roth NM, Godfred-Cato S, et al. Population-based surveillance for birth defects potentially related to Zika virus infection—22 states and territories, January 2016–June 2017. MMWR Morb Mortal Wkly Rep. 2020;69:67–71. https://doi.org/10.15585/mmwr.mm6903a3
25. Besnard M, Eyrolle-Guignot D, Guillemette-Artur P, Lastère S, Bost-Bezeaud F, Marcelis L, et al. Congenital cerebral malformations and dysfunction in fetuses and newborns following the 2013 to 2014 Zika virus epidemic in French Polynesia. Euro Surveill. 2016;21:30181. https://doi.org/10.2807/1560-7917.ES.2016.21.13.30181
26. Honein MA, Dawson AL, Petersen EE, Jones AM, Lee EH, Yazdy MM, et al.; US Zika Pregnancy Registry Collaboration. Birth defects among fetuses and infants of US women with evidence of possible Zika virus infection during pregnancy. JAMA. 2017;317:59–68. https://doi.org/10.1001/jama.2016.19006
27. Shapiro-Mendoza CK, Rice ME, Galang RR, Fulton AC, VanMaldeghem K, Prado MV, et al.; Zika Pregnancy and Infant Registries Working Group. Pregnancy outcomes after maternal Zika virus infection during pregnancy—U.S. Territories, January 1, 2016–April 25, 2017. MMWR Morb Mortal Wkly Rep. 2017;66:615–21. https://doi.org/10.15585/mmwr.mm6623e1
28. Cauchemez S, Besnard M, Bompard P, Dub T, Guillemette-Artur P, Eyrolle-Guignot D, et al. Association between Zika virus and microcephaly in French Polynesia, 2013-15: a retrospective study. Lancet. 2016;387:2125–32. https://doi.org/10.1016/S0140-6736(16)00651-6
29. Pacheco O, Beltrán M, Nelson CA, Valencia D, Tolosa N, Farr SL, et al. Zika virus disease in Colombia—preliminary report [cited 2019 Jun 14]. http://www.nejm.org/doi/10.1056/NEJMoa1604037
30. Kleber de Oliveira W, Cortez-Escalante J, Gonçalves WT, Ikeda do Carmo GM, Henriques CMP, Coelho GE, et al. Increase in reported prevalence of microcephaly in infants born to women living in areas with confirmed Zika virus transmission during the first trimester of pregnancy—Brazil, 2015. MMWR Morb Mortal Wkly Rep. 2016;65:242–7. http://dx.doi.org/10.15585/mmwr.mm6509e2
31. Marinho F, de Araújo VEM, Porto DL, Ferreira HL, Coelho MRS, Lecca RCR, et al. Microcephaly in Brazil: prevalence and characterization of cases from the Live Birth Information System (Sinasc), 2000–2015 [in Portuguese]. Epidemiol Serv Saude. 2016;25:701–12. https://doi.org/10.5123/S1679-49742016000400004
32. Dufort E, White J. Pre-Zika microcephaly in Brazil: closer to the elusive baseline and new questions raised. Pediatrics. 2018;141:e20173811. https://doi.org/10.1542/peds.2017-3811
33. van der Linden V, Pessoa A, Dobyns W, Barkovich AJ, Júnior HV, Filho EL, et al. Description of 13 infants born during October 2015–January 2016 with congenital Zika virus infection without microcephaly at birth—Brazil. MMWR Morb Mortal Wkly Rep. 2016;65:1343–8. https://doi.org/10.15585/mmwr.mm6547e2
34. Nithiyanantham SF, Badawi A. Maternal infection with Zika virus and prevalence of congenital disorders in infants: systematic review and meta-analysis. Can J Public Health. 2019;110:638–48 [cited 2019 Aug 5]. https://doi.org/10.17269/s41997-019-00215-2
35. de Paula Freitas B, Zin A, Ko A, Maia M, Ventura CV, Belfort R. Anterior-segment ocular findings and microphthalmia in congenital Zika syndrome. Ophthalmology. 2017;124:1876–8. https://doi.org/10.1016/j.ophtha.2017.06.009
36. Zin AA, Tsui I, Rossetto J, Vasconcelos Z, Adachi K, Valderramos S, et al. Screening criteria for ophthalmic manifestations of congenital Zika virus infection. JAMA Pediatr. 2017;171:847–54. https://doi.org/10.1001/jamapediatrics.2017.1474
37. Leal MC, Muniz LF, Ferreira TSA, Santos CM, Almeida LC, Van Der Linden V, et al. Hearing loss in Infants with microcephaly and evidence of congenital Zika virus infection—Brazil, November 2015–May 2016. MMWR Morb Mortal Wkly Rep. 2016;65:917–9. https://doi.org/10.15585/mmwr.mm6534e3
38. de Fatima Vasco Aragao M, van der Linden V, Brainer-Lima AM, Coeli RR, Rocha MA, Sobral da Silva P, et al. Clinical features and neuroimaging (CT and MRI) findings in presumed Zika virus related congenital infection and microcephaly: retrospective case series study. BMJ. 2016;353:i1901. https://doi.org/10.1136/bmj.i1901
39. Wheeler AC. Development of infants with congenital Zika syndrome: what do we know and what can we expect? Pediatrics. 2018;141(Suppl 2):S154–160. https://doi.org/10.1542/peds.2017-2038D
40. Tinker SC, Gilboa S, Reefhuis J, Jenkins MM, Schaeffer M, Moore CA. Challenges in studying modifiable risk factors for birth defects. Curr Epidemiol Rep. 2015;2:23–30. https://doi.org/10.1007/s40471-014-0028-y
41. Singh RK, Dhama K, Karthik K, Tiwari R, Khandia R, Munjal A, et al. Advances in diagnosis, surveillance, and monitoring of Zika virus: an update. Front Microbiol. 2018;8:2677. https://doi.org/10.3389/fmicb.2017.02677
42. Adebanjo T, Godfred-Cato S, Viens L, Fischer M, Staples JE, Kuhnert-Tallman W, et al. Update: interim guidance for the diagnosis, evaluation, and management of infants with possible congenital Zika virus infection—United States, October 2017. MMWR Morb Mortal Wkly Rep. 2017;66:1089–99. https://doi.org/10.15585/mmwr.mm6641a1
43. Eppes C, Rac M, Dunn J, Versalovic J, Murray KO, Suter MA, et al. Testing for Zika virus infection in pregnancy: key concepts to deal with an emerging epidemic. Am J Obstet Gynecol. 2017;216:209–25. https://doi.org/10.1016/j.ajog.2017.01.020
44. Pan American Health Organization. Guidelines for surveillance of Zika virus disease and its complications. 2018

edition [cited 2019 Aug 5]. http://iris.paho.org/xmlui/bitstream/handle/123456789/49518/9789275120194_eng.pdf
45. Gilboa SM, Mai CT, Shapiro-Mendoza CK, Cragan JD, Moore CA, Meaney-Delman DM, et al. Population-based pregnancy and birth defects surveillance in the era of Zika virus. Birth Defects Res. 2017;109:372–8. https://doi.org/10.1002/bdr2.1007
46. Ministerio de Salud (Costa Rica). National guidelines for the comprehensive approach of pregnant women and newborn, related to Zika infection [in Spanish] [cited 2019 Aug 5]. https://www.ministeriodesalud.go.cr/index.php/vigilancia-de-la-salud/normas-protocolos-y-guias/enfermedades-de-transmision-vectorial/3054-lineamientos-nacionales-para-el-abordaje-integral-de-la-mujer-embarazada-y-el-recien-nacido-relacionado-con-la-infeccion-del-zika/file

Address for correspondence: Adriana Benavides-Lara, Costa Rican Birth Defects Register Center, Costa Rican Institute of Research and Education in Nutrition and Health, Cartago, Costa Rica; email: abenavides@inciensa.sa.cr

# *Plasmodium ovale wallikeri* and *P. ovale curtisi* Infections and Diagnostic Approaches to Imported Malaria, France, 2013–2018

Valentin Joste, Justine Bailly, Véronique Hubert, Cécile Pauc, Mathieu Gendrot, Emilie Guillochon, Marylin Madamet, Marc Thellier, Eric Kendjo, Nicolas Argy, Bruno Pradines, Sandrine Houzé, on behalf of the French National Reference Center for Imported Malaria Study Group[1]

Medscape EDUCATION **ACTIVITY**

In support of improving patient care, this activity has been planned and implemented by Medscape, LLC and Emerging Infectious Diseases. Medscape, LLC is jointly accredited by the Accreditation Council for Continuing Medical Education (ACCME), the Accreditation Council for Pharmacy Education (ACPE), and the American Nurses Credentialing Center (ANCC), to provide continuing education for the healthcare team.

Medscape, LLC designates this Journal-based CME activity for a maximum of 1.00 ***AMA PRA Category 1 Credit(s)™***. Physicians should claim only the credit commensurate with the extent of their participation in the activity.

Successful completion of this CME activity, which includes participation in the evaluation component, enables the participant to earn up to 1.0 MOC points in the American Board of Internal Medicine's (ABIM) Maintenance of Certification (MOC) program. Participants will earn MOC points equivalent to the amount of CME credits claimed for the activity. It is the CME activity provider's responsibility to submit participant completion information to ACCME for the purpose of granting ABIM MOC credit.

All other clinicians completing this activity will be issued a certificate of participation. To participate in this journal CME activity: (1) review the learning objectives and author disclosures; (2) study the education content; (3) take the post-test with a 75% minimum passing score and complete the evaluation at http://www.medscape.org/journal/eid; and (4) view/print certificate. For CME questions, see page 680.

**Release date: January 22, 2021; Expiration date: January 22, 2022**

**Learning Objectives**

Upon completion of this activity, participants will be able to:

- Describe epidemiologic and clinical characteristics of *Plasmodium ovale curtisi* (POC) and *P. ovale wallikeri* (POW) in infected patients who were treated in France from January 2013 to December 2018, according to a retrospective multicenter analysis
- Determine diagnostic test and gene sequencing findings of patients infected with POC and POW who were treated in France from January 2013 to December 2018, according to a retrospective multicenter analysis
- Identify treatment and clinical implications of characteristics of POC and POW in infected patients treated in France from January 2013 to December 2018, according to a retrospective multicenter analysis

**CME Editor**

**Jude Rutledge, BA,** Technical Writer/Editor, Emerging Infectious Diseases. *Disclosure: Jude Rutledge has disclosed no relevant financial relationships.*

**CME Author**

**Laurie Barclay, MD,** freelance writer and reviewer, Medscape, LLC. *Disclosure: Laurie Barclay, MD, has disclosed no relevant financial relationships.*

**Authors**

*Disclosures:* ***Valentin Joste, PharmD; Justine Bailly, MSc; Véronique Hubert, MS; Cecile Pauc; Mathieu Gendrot, MSc; Emilie Guillochon, MSc; Marylin Madamet, PhD; Marc Thellier, MD, MSc; Eric Kendjo, MSc, PhD; Nicolas Argy, PharmD, PhD; Bruno Pradines, PharmD, PhD;*** *and* ***Sandrine Houzé, PhD,*** *have disclosed no relevant financial relationships.*

Author affiliations: Centre National de Référence du Paludisme, Paris, France (V. Joste, J. Bailly, V. Hubert, C. Pauc, N. Argy, S. Houzé); Université de Paris, Paris (N. Argy, S. Houzé); Laboratoire de Parasitologie-Mycologie, Paris (V. Joste, N. Argy, S. Houzé); Institut de Recherche Biomédicale des Armées, Marseille, France (M. Gendrot, M. Madamet, B. Pradines); Aix–Marseille Université, Marseille (M. Gendrot, M. Madamet, B. Pradines); Instituts Hospitalo–Universitaires Méditerranée Infection, Marseille (M. Gendrot, M. Madamet, B. Pradines); Centre National de Référence du Paludisme, Marseille (M. Madamet, B. Pradines); Sorbonne Université, Paris, France (M. Thellier, E. Kendjo)

DOI: https://doi.org/10.3201/eid2702.202143

[1]Additional members of the French National Reference Center for Imported Malaria Study Group who contributed data are listed at the end of this article.

We retrospectively analyzed epidemiologic, clinical, and biologic characteristics of 368 *Plasmodium ovale wallikeri* and 309 *P. ovale curtisi* infections treated in France during January 2013–December 2018. *P. ovale wallikeri* infections displayed deeper thrombocytopenia and shorter latency periods. Despite similar clinical manifestations, *P. ovale wallikeri*–infected patients were more frequently treated with artemisinin-based combination therapy. Although the difference was not statistically significant, *P. ovale wallikeri*–infected patients were 5 times more frequently hospitalized in intensive care or intermediate care and had a higher proportion of severe thrombocytopenia than *P. ovale curtisi*–infected patients. Rapid diagnostic tests that detect aldolase were more efficient than those detecting *Plasmodium* lactate dehydrogenase. Sequence analysis of the *potra* gene from 90 *P. ovale* isolates reveals an insufficient polymorphism for relapse typing.

Malaria is a vectorborne disease caused by *Plasmodium*, a parasite transmitted by *Anopheles* mosquitoes. In 2018, malaria was responsible for ≈228 million cases and 405,000 deaths worldwide (*1*). *Plasmodium ovale* is endemic in Africa and represents the main agent of relapsing malaria (*2*). In mainland France, *P. ovale* was responsible for ≈6% of imported malaria cases in 2018 (*3*). Since the 2017 France updates for *Plasmodium* infection management recommendations, first-line treatment of *P. ovale* infections is based on chloroquine- or artemisinin-based combination therapy (ACT), instead of atovaquone/proguanil (*4*).

Because of low parasite density and poor efficiency of rapid diagnostic test (RDT) detection (*5*), *P. ovale* infections are difficult to diagnose. Consequently, infections caused by *P. ovale* remain poorly studied, and little is known about the global burden of the disease worldwide or its geographic distribution.

Since 2010, *P. ovale* has been divided into 2 species, *Plasmodium ovale wallikeri* and *P. ovale curtisi*, on the basis of gene polymorphisms (*6*–*8*). *P. ovale wallikeri* appears to cause malaria infections with a shorter latency period (*9*,*10*) and with deeper thrombocytopenia than *P. ovale curtisi* (*11*,*12*). Both *P. ovale wallikeri* (*13*) and *P. ovale curtisi* (*14*) can be responsible for a clinical relapse event, defined as renewed asexual parasitemia originating from liver dormancies (*2*). Relapse characterization relies on microscopic diagnosis and medical history. No consensus molecular method for *P. ovale* spp. relapse typing is reported. However, *P. ovale* tryptophan–rich antigen (*potra*) gene sequencing has previously been used for genotyping purpose (*13*,*14*).

At the microscopic level, the only observable difference between the species is a lack of Schüffner granulations in *P. ovale wallikeri* infected erythrocytes (*15*). However, this feature is rare and difficult to see, which makes *P. ovale* species distinction almost impossible even for an experienced microscopist. Molecular biology is a promising tool and is both sensitive and specific for the differentiation of *P. ovale wallikeri* from *P. ovale curtisi*. The first nested PCR that discriminates *P. ovale wallikeri* and *P. ovale curtisi* was developed in 2007 (*16*), and the first quantitative PCR (qPCR) was developed in 2013 (*17*).

In this study, we conducted a large retrospective multicenter analysis of imported *P. ovale* cases. Epidemiologic, clinical, and biologic characteristics of 309 *P. ovale curtisi*– and 368 *P. ovale wallikeri*–infected patients treated in France during January 2013–December 2018 were analyzed. The effectiveness of Rapid Diagnostic Test (RDT) and the polymorphism of *potra* gene were also investigated.

## Methods

### Sample Selection

France's National Malaria Reference Center (FF-NMRC) is in charge of epidemiologic surveillance of imported malaria in France. Whole blood samples of patients with *Plasmodium* infections were received from hospital correspondents in France. FNMRC correspondents also reported demographic, epidemiologic, clinical, and biologic data through a reporting website. We retrospectively selected all the reported and PCR-confirmed *P. ovale* infections that occurred during January 2013–December 2018.

### DNA Extraction

DNA was extracted from 200 µL of whole blood samples by using Magnapure automaton (Roche Diagnostics, https://diagnostics.roche.com) and eluted in 100 µL of elution buffer, =according to the manufacturer's instructions. DNA was stored at –20°C until further analysis.

### Diagnosis of *P. ovale* Infection

The diagnosis of *P. ovale* infection was made by the hospital correspondent and confirmed by FNMRC with a thin blood smear reading, a thick blood smear reading, or both. Thick blood smears were considered positive if >1 trophozoïtes was visualized after examination of 1,000 leukocytes. Thin blood smears were used to confirm Plasmodium species identification. Parasite density was calculated by using the formula parasite density (parasites per µL) = patient leukocyte count (per µL) × (no. parasites counted)/(no. leucocytes counted), according to World Health Organization (WHO) recommendations (*18*). Parasitemia was calculated by counting the percentage of infected red blood cells on thin blood smears according to WHO recommendations (*18*). All *P. ovale* infections were confirmed with nested PCR (*19*,*20*) during 2013–2014, with qPCR–Taqman (Launch Diagnostics, https://www.launchdiagnostics.com) during 2015–2017, and with Bio-Evolution (https://www.bio-evolution.net/index.php) in 2018.

### *P. ovale curtisi* and *P. ovale wallikeri* differentiation

qPCR–high-resolution melting (HRM) targeting the 18S rRNA gene was performed to differentiate *P. ovale wallikeri* from *P. ovale curtisi* by using Plasmo1_F and Plasmo2_R primers. The method development and validation was described previously (*21*). In brief, qPCR-HRM results were compared with nested PCR results from Calderaro et al. (*16*), and they displayed similar species determination. In all studied samples, *P. ovale wallikeri* and *P. ovale curtisi* melting plots displayed 2 specific melting temperatures (Tm) as $Tm_1$ and $Tm_2$, and the ΔTm between the 2 Tm was calculated.

For uncertain results (i.e., only 1 Tm on melting plot analysis [*21*]), nested PCR was performed by using rPLU1 and rPLU5 primers in the first PCR reaction and rOVA1/rOVA2 for *P. ovale curtisi* amplification or rOVA1v/rOVA2v for *P. ovale wallikeri* amplification in second PCR reaction (*16*). PCR products were visualized on 1% agarose gel stained with GelRed (https://biotium.com). We used *P. ovale wallikeri* and *P. ovale curtisi* isolates as positive controls and water as a negative control for each qPCR-HRM run.

## RDT Efficiency in *P. ovale wallikeri* and *P. ovale curtisi* Detection

We evaluated the efficiency of 4 different RDTs detecting pan-*Plasmodium* proteins (aldolase or *Plasmodium* lactate dehydrogenase [pLDH]) for the detection of *P. ovale wallikeri* and *P. ovale curtisi*. Vikia Malaria Ag Pf/Pan (bioMérieux, https://www.biomerieux.com) (*22*) and Binax Now Pf/Pan (Abbott, https://www.abbott.com) (*23*) were used for aldolase detection (aldolase-RDT). Palutop+4 Pan/Pv/Pf (Biosynex, https://www.biosynex.com) (*24*) and Core Malaria Pan/Pv/Pf (Core Diagnostics, https://www.corediagnostics.net) were used for pLDH protein detection (pLDH-RDT). Results were interpreted according to the manufacturer's instructions.

## Data Collection

Each hospital correspondent sent an EDTA blood sample of a patient infected with *P. ovale* to FNMRC. This process was completed by using the online patient form containing multiple data, including demographic data (place of birth, ethnicity, age, and sex), epidemiologic data (trip purpose, visited country, duration of travel, and use of prophylaxis or bed nets), biologic data (parasite count, RDT results, leukocytes, hemoglobin and platelet counts, with severe thrombopenia defined as <50 G/L [*25*], and date of diagnosis), and clinical data (date of symptom onset, fever, headache, asthenia, and arthralgia or myalgia, as well as free symptomatology description for other symptoms, antimalarial treatment used, hospital or ambulatory regimen, and duration of hospitalization). Severe malaria biologic and clinical signs, adapted from the severe *P. falciparum* WHO recommendations (*4*,*26*), and relapsing *P. ovale* infection, defined as new *P. ovale* infection after a first completed and effective antimalarial treatment (*27*), were reported.

The latency period was calculated for each infection by subtracting the date of return from travel to the onset of the symptoms as defined by Rojo-Marcos et al. (*11*,*12*). The period of high malaria transmission in West Africa was defined as August–November on the basis of Nabarro et al. definition (*10*). The delay between symptom onset and diagnosis was also determined. We looked for false or incomplete microscopic diagnosis (*Plasmodium* spp.) to estimate the potential effect on *P. ovale* microscopic diagnosis of the described lack of Schüffner granulations in *P. ovale wallikeri*–infected erythrocytes (*15*).

No specific consent was required from patients because the parasitologic data were collected from the FNMRC database and analyzed in accordance with the common public health mission of all National Reference Centers in France, in coordination with the Santé Publique France organization for malaria surveillance and care. The study of the biologic samples obtained from routine medical care was considered as noninterventional research accordingly to article L1221–1.1 of the public health code in France and only requires the nonopposition of the patient during sampling (per article L1211–2 of the public health code). All data collected were anonymized before analysis.

## *potra* Sequencing and Analysis

We amplified *potra* fragments as previously described (*28*). Bidirectional sequencing reaction was performed for the secondary *potra* fragment. Gene sequences were analyzed with Sequencher 5.0 (Genecodes, http://www.genecodes.com). Isolates from GenBank under accession nos. HM594183 (*28*), MG588152, and MG588154 (*29*) were used as *P. ovale curtisi* reference sequences; HM594180 (*28*) and MG588148–150 (*29*) were used as *P. ovale wallikeri* reference sequences.

### Statistical Analysis

*P. ovale wallikeri* and *P. ovale curtisi* infections were compared in terms of demographic, epidemiologic, clinical, and biologic characteristics. The Kolmogorov-Smirnov test with the Lilliefors correction was used to verify the normality of variables distributions, and the Levene test was used to verify the homogeneity of the variances. If both criteria were validated, a Student *t*-test was used; otherwise, a Mann-Whitney U-test was performed to compare medians. Proportions were compared by using the $\chi^2$ or Fisher exact test according to sample size (>5 or ≤5). R software was used to perform statistical tests (*30*).

## Results

### *P. ovale* Sample Selection

During January 2013–December 2018, 15,028 *Plasmodium* spp. infection cases were reported to FNMRC, including 765 *P. ovale* infections. Seventeen cases were excluded from the analysis because blood sample were unavailable. After exclusion of co-infections and inclusion of 59 *P. ovale* initially misdiagnosed (confirmed by PCR), 677 *P. ovale* cases from 63 different hospitals in France were finally included (Figure 1). By using qPCR-HRM for species differentiation, we identified 368 *P. ovale wallikeri* and 309 *P. ovale curtisi* infections. The 2 species segregated perfectly in qPCR-HRM; *P. ovale wallikeri* had a ΔTm of 1.62–2.69, and *P. ovale curtisi* had a ΔTm of 2.84–4.22.

### Patients' Demographic and Epidemiologic Characteristics

*P. ovale wallikeri* and *P. ovale curtisi* showed similar repartition by month, except for October, which showed an increase in *P. ovale wallikeri* infections and a decrease in *P. ovale curtisi* cases (Figure 2, panel A). Among *P. ovale* cases, the proportion of *P. ovale wallikeri* infections increased from 44% to 59% during January 2013–December 2018 (Figure 2, panel B).

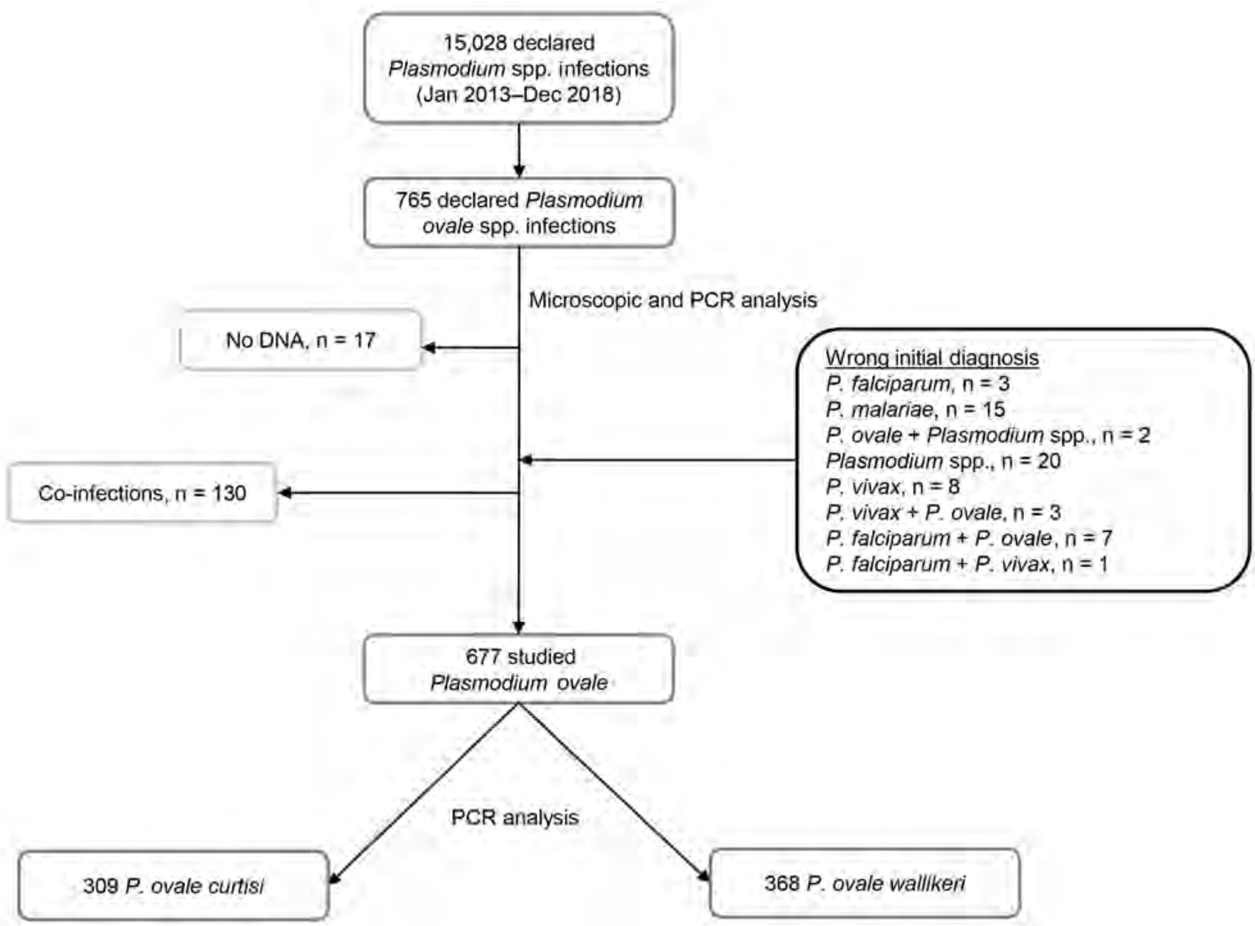


**Figure 1.** Flow-chart of the retrospective study analyzing characteristics of *Plasmodium ovale wallikeri* and *P. ovale curtisi* infections treated in France during January 2013–December 2018. All reported *P. ovale* infection cases were confirmed with microscopy and PCR analysis, and co-infections were excluded. A total of 59 *P. ovale* isolates initially misdiagnosed by the hospital correspondent were added. A total of 677 *P. ovale* infection cases were included in the study.

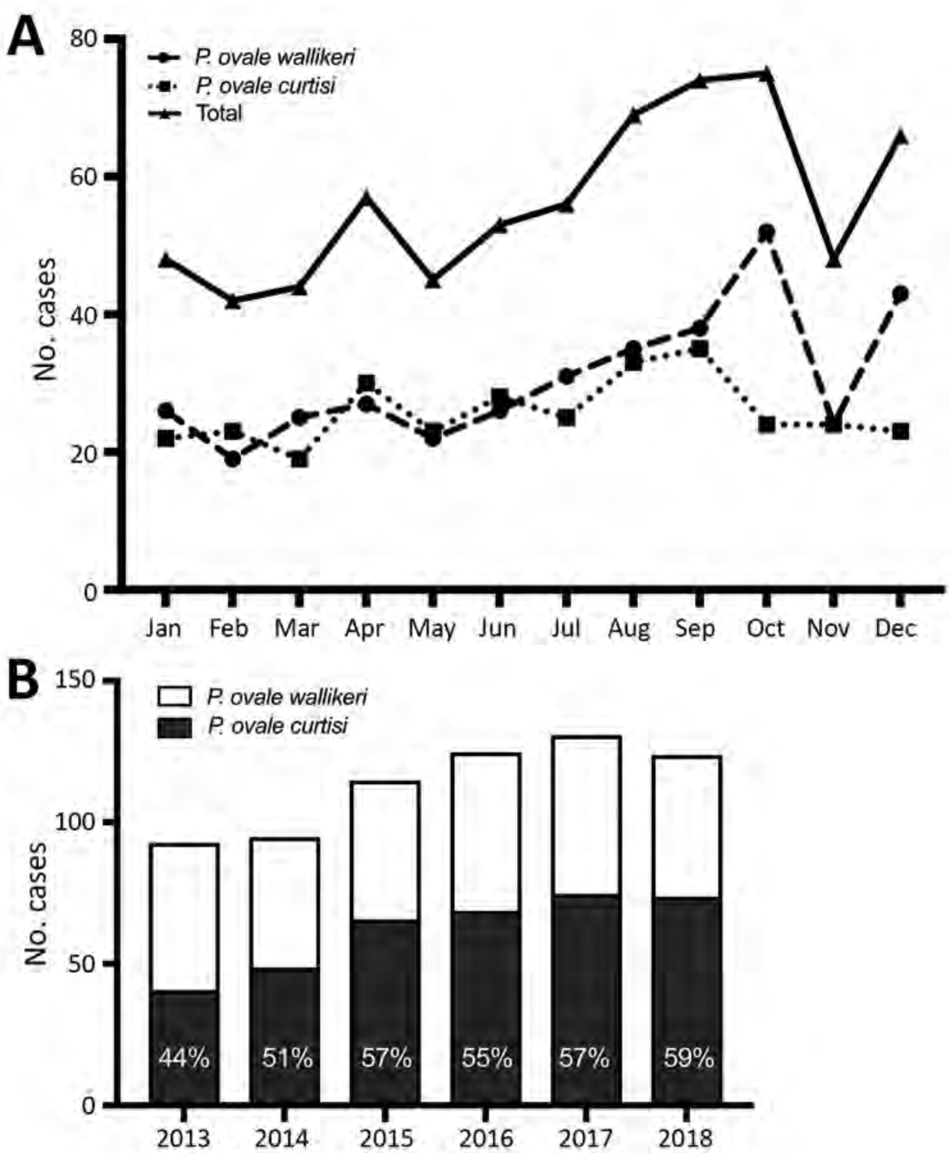


**Figure 2.** Number of *Plasmodium ovale* infection cases included in a study analyzing characteristics of *P. ovale wallikeri* and *P. ovale curtisi* infections treated in France during January 2013–December 2018, by month of inclusion (A) and year of inclusion (B).

*P. ovale wallikeri*– and *P. ovale curtisi*–infected patients did not display any differences in demographic and epidemiologic characteristics (Table 1). Countries of contamination were not statistically different between imported *P. ovale curtisi* and *P. ovale wallikeri* cases ($p = 0.52$) (Figure 3; Appendix Table 1, https://wwwnc.cdc.gov/EID/article/27/2/20-2143-App1.pdf).

For well-followed chemoprophylaxis ($n = 77$), the main treatments used were doxycycline (48%), atovaquone/proguanil (25%), and mefloquine (18%). No statistically significant differences were observed in the percentage of infection between those treatments.

### *P. ovale* Diagnosis

Parasite densities for *P. ovale curtisi* and *P. ovale wallikeri* infections were similar (median 4,500 parasites/µL [interquartile range (IQR) 1,094–10,197 parasites/µL] for *P. ovale curtisi* vs. median 3,970 parasites/µL [IQR 598–9,240 parasites/µL] for *P. ovale wallikeri*). We noted 8.5% of species misidentification for *P. ovale curtisi* and 9% for *P. ovale wallikeri* (Figure 1).

### Aldolase and pLDH-RDT Efficiency

We compared the diagnostic performance of aldolase-RDTs and pLDH-RDTs for *P. ovale* diagnosis. Aldolase-RDTs detection were more efficient in *P. ovale* spp. detection than pLDH-RDTs ($p<0.001$); no differences between the 2 species were observed. *P. ovale wallikeri* was more frequently detected with pLDH-RDT than *P. ovale curtisi* ($p<0.001$) (Table 2). The positivity of aldolase and pLDH-RDTs were

**Table 1.** Demographic and epidemiologic characteristics of patients infected with *Plasmodium ovale wallikeri* and *P. ovale curtisi*, France, January 2013–December 2018*

| Characteristic | *P. ovale curtisi*, n = 309 | *P. ovale wallikeri*, n = 368 | p value |
|---|---|---|---|
| Age, y, median (IQR) | 31 (21–47) | 34 (21–47) | 0.973 |
| Sex, % | | | 0.716 |
| M | 63.4 | 61.4 | |
| F | 36.6 | 38.6 | |
| Ethnicity | | | 0.502 |
| Black | 200 (74.3) | 239 (75.7) | |
| White | 64 (23.8) | 68 (21.5) | |
| Asian | 2 (0.7) | 1 (0.3) | |
| Other | 3 (1.2) | 8 (2.5) | |
| If African, place of birth | | | 0.420 |
| Africa | 144 (83.2) | 164 (80) | |
| Nonendemic country | 29 (16.8) | 41 (20) | |
| Type of patient | | | 0.192 |
| Immigrant† | 23 (11.6) | 21 (8.6) | |
| Traveler‡ | 137 (68.8) | 187 (77.3) | |
| Visiting friends or relatives | 109 (79.6) | 152 (81.3) | |
| Tourism | 6 (4.4) | 8 (4.3) | |
| Work | 22 (16) | 27 (14.4) | |
| Resident | 19 (9.5) | 20 (8.3) | |
| Expatriate | 6 (38.6) | 10 (50) | |
| Humanitarian | 13 (61.4) | 10 (50) | |
| Military | 20 (10.1) | 14 (5.8) | |
| Duration of travel, d, median (IQR) | 58 (29–91) | 50 (24–91) | 0.106 |
| Chemoprophylaxis | | | 0.882 |
| Yes | 97 (40) | 123 (39.3) | |
| Complete | 35 (44.9) | 42 (43.8) | |
| Incomplete | 43 (55.1) | 54 (56.2) | |
| Prematurely stopped | 26 (60.5) | 36 (66.7) | |
| Occasionally taking | 17 (39.5) | 18 (33.3) | |
| No data | 19 (NA) | 27 (NA) | |
| No | 146 (60) | 190 (60.7) | |
| Using bed nets | | | 0.119 |
| Yes | 48 (26.7) | 41 (20.2) | |
| No | 130 (73.3) | 162 (79.8) | |

*Values are no. (%) patients except as indicated. IQR, interquartile range; NA, not available.
†A person who was born and lived in Africa.
‡A person who lived in a non–*Plasmodium*-endemic country.

strongly associated with parasite density. Percentage of positive RDT results increased with parasite density for both pLDH-RDT and aldolase-RDT (Table 2). A positive aldolase-RDT result was associated with a parasite density significantly higher than with a negative aldolase-RDT result for both species (median 6,612 parasites/µL [IQR 2,410–14,175 parasites/µL] for *P. ovale wallikeri* vs. median 1,287 parasites/µL [IQR 450–4,500 parasites/µL] for *P. ovale curtisi*; p<0.001) (Figure 4). Similarly, the parasite density of positive pLDH-RDT *P. ovale wallikeri* samples were significantly higher than those of negative pLDH-RDT (median 11,000 parasites/µL [IQR 3,960–52,910 parasites/µL] vs. median 3,227 parasites/µL [IQR 551–7,118] parasites/µL; p<0.001). Vikia (bioMérieux) aldolase-RDT had a greater accuracy for detecting *P. ovale* infections compared than did Binax Now (Abbott) (59.3% vs. 40.9%; p<0.001) and a better sensitivity (median 4,230 parasites/µL [IQR 1,205–9,450 parasites/µL] for positive Vikia vs. median 8350 parasites/µL [IQR 4,032–16,166 parasites/µL] for positive Binax Now; p<0.001).

## Biologic and Clinical Characteristics

Patients infected with *P. ovale wallikeri* displayed deeper thrombocytopenia than those with *P. ovale curtisi* (Table 3), but reported symptomatology and disease severity did not differ. *P. ovale wallikeri* infections had shorter latency periods and a higher proportion of latency periods <50 days (p<0.001) (Table 3). Compared with patients who did not take prophylactic treatment, patients who reported well-managed prophylactic treatment had longer latency periods (median 90 days [IQR 47–177 days] vs. median 30 days [IQR 8–125 days]; p<0.001). Uncompleted prophylactic treatment did not extend latency period (median 33 days [IQR 17–112 days] vs. median 30 days [IQR 8–125 days]; p = 0.34). Military patients had longer latency periods than other patients (median 109 days [IQR 57–159 days] vs. median 40 days [IQR 12–142 days]; p = 0.0018), as did Caucasian versus African patients (median 84 days [IQR 28–140 days] vs. median 42 days [IQR 12–147 days]; p = 0.005 days). In the African population, no differences were found

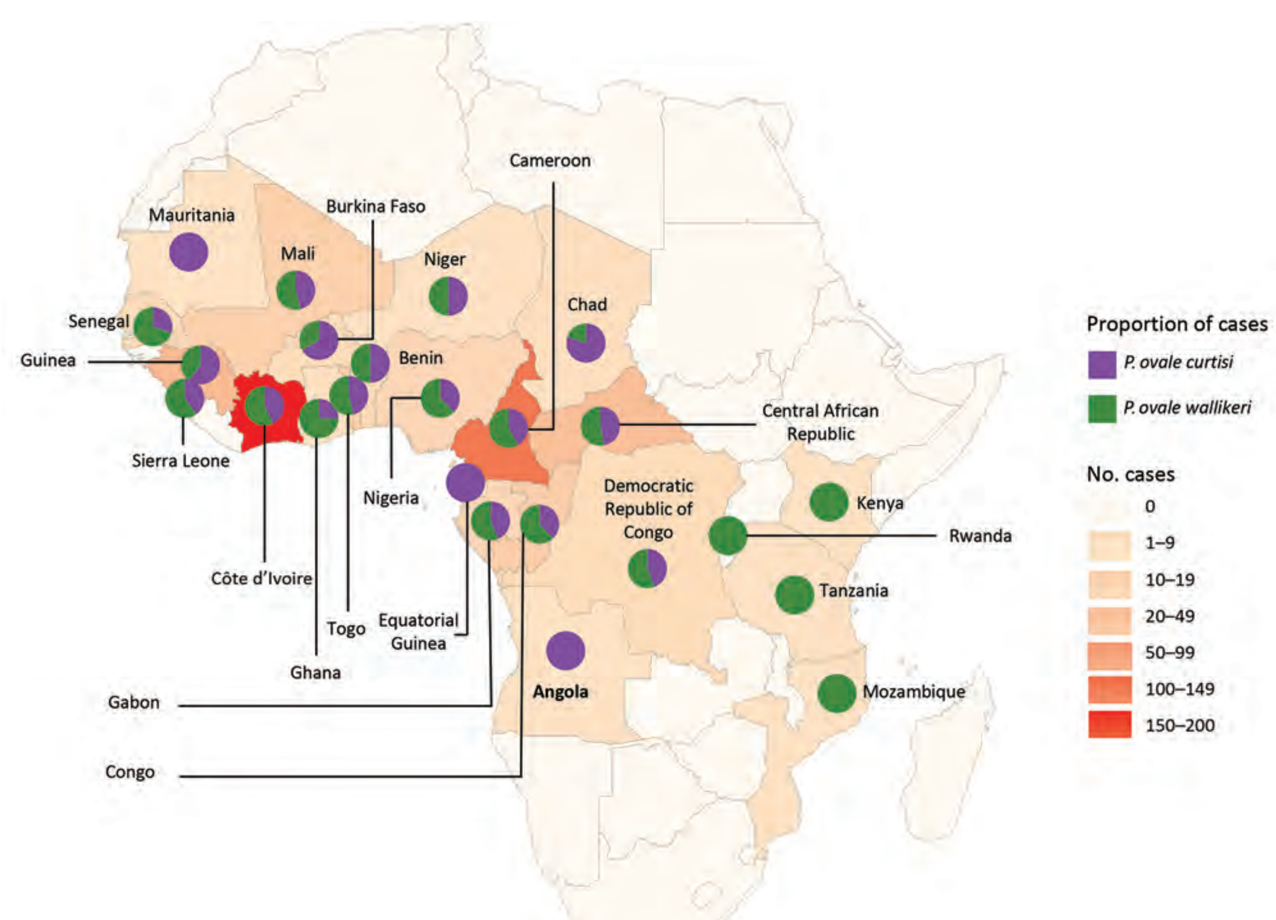


**Figure 3.** Geographic repartition of the origin countries of imported *Plasmodium ovale wallikeri* and *P. ovale curtisi* infection cases into France, January 2013–December 2018. Pie charts showed the repartition of cases between both species in each country.

between African-born patients and others (mean 53 days [IQR 12–170 days] vs. mean 35 days [IQR 11–117 days]). The latency period was shorter in symptomatic patients returning from West Africa during the malaria season than in low-transmission or no-transmission seasons (median 27 days [IQR 10–67 days] vs. median 90 days [IQR 17–158 days]; p<0.001) (Appendix Figure). *P. ovale wallikeri* infections and *P. ovale curtisi* infections were each responsible for 16 reported clinical relapses.

### Patient Care

A similar proportion of patients were hospitalized in the *P. ovale curtisi* and *P. ovale wallikeri* groups. Eight malaria case-patients with WHO-defined severe criteria (*26*) were reported during the period analysis (Table 3). *P. ovale wallikeri*–infected patients were 5 times more likely to be hospitalized in intensive or intermediate care than *P. ovale curtisi*–infected patients (Table 3). A higher percentage of *P. ovale wallikeri* infections were treated with ACT (29.2% vs. 17.1%;

**Table 2**. Comparison of aldolase and pLDH-RDT efficiency in *Plasmodium ovale wallikeri* and *P. ovale curtisi* infection diagnosis, France, January 2013–December 2018*

| RDT result | Parasite density, parasites/µL | LDH | | | Aldolase | | |
|---|---|---|---|---|---|---|---|
| | | *P. ovale* | *P. ovale wallikeri* | *P. ovale curtisi* | *P. ovale* | *P. ovale wallikeri* | *P. ovale curtisi* |
| Positive | | 55 (10.6) | 45 (16) | 10 (4.2) | 211 (47.8) | 120 (50) | 91 (45.3) |
| | <1,000 | 5 (3.9) | 3 (3.9) | 2 (3.9) | 25 (19.5) | 16 (20) | 9 (17.6) |
| | 1,000–5,000 | 15 (9.4) | 14 (15) | 1 (1.5) | 65 (40.6) | 42 (54.5) | 23 (33.8) |
| | 5,000–10,000 | 6 (7.8) | 5 (12) | 1 (2.8) | 44 (57.1) | 24 (66.7) | 20 (57.1) |
| | 10,000–50,000 | 16 (16.2) | 11 (20) | 5 (11.4) | 67 (67.7) | 29 (78.4) | 38 (86.4) |
| | >50,000 | 13 (86.7) | 12 (86) | 1 (100) | 10 (100) | 9 (100) | 1 (100) |
| Negative | | 465 (89.4) | 237 (84) | 228 (95.8) | 230 (52.2) | 120 (50) | 110 (54.7) |
| p value | | | <0.001 | | | 0.322 | |

*Values are no. (%) patients except as indicated. LDH, lactate dehydrogenase; pLDH, plasmodium lactate dehydrogenase; RDT, rapid diagnostic test.
†Proportions of positive and negative LDH or aldolase-RDT were compared for *P. ovale wallikeri* and *P. ovale curtisi* by using a $\chi^2$ test.

p<0.001), but no association was found between ACT treatment and parasite density, between ACT treatment and platelet count, or between ACT treatment and positive and negative RDTs. Patients treated with ACT did have shorter latency periods than other patients (median 33 days [IQR 11–111 days] vs. 54 days [IQR 15–170 days]; p = 0.025) and patients with latency periods <50 days were more often treated with ACT than others (28.6% vs. 20.3%; p = 0.048). This high proportion of ACT prescription was highest in patients with latency periods <50 days and platelet counts <60 G/L (52.3% vs. 22.7%; p = 0.002).

New recommendations from the Infectious Diseases Society in France (La Société de Pathologie Infectieuse de Langue Française) edited in 2017 (*4*) had a clear effect on *P. ovale* infection treatment (Figure 5), including replacement of atovaquone/proguanil by artemisinin-based combination therapy. However, little change in rates of chloroquine prescription occurred (52.5% before the revisions and 47.2% after).

For the period analyzed, no statistically significant relationship was found between the number of included *P. ovale* infection cases per hospital and the percentage of patients receiving ACT treatment. We also analyzed the relation between the total number of included *Plasmodium* infection cases per hospital and the percentage of intensive care or intermediate care hospitalizations and did not find any statistically significant relation (data not shown).

### *potra* Sequencing and Analysis

In total, 49 *potra* genes were sequenced from *P. ovale wallikeri* and 41 *potra* genes were sequenced from *P. ovale curtisi*. Three different genotypes (299, 317, and 335 bp) were identified in *P. ovale curtisi* and 4 different genotypes (245, 263, 263′, and 281 bp) in *P. ovale wallikeri* (Table 4). The major genotypes were $(MANPIN)_1(AITPIN)_2$ for *P. ovale wallikeri* and $(TINPIN)_3(TITPIS)_1$ for *P. ovale curtisi*. No association was found between country of contamination and *potra* genotype.

## Discussion

Our findings show that patients infected with *P. ovale wallikeri* displayed deeper thrombocytopenia than those infected with *P. ovale curtisi* (p<0.001) and had a shorter latency period (p<0.001). Those features of *P. ovale wallikeri* infection are currently debated in the literature, with some studies describing deeper thrombocytopenia (*11*,*12*) and shorter latency periods (*9*) and other finding refuting any differences between the 2 species (*31*).

We reported 1.2% of patients with diagnosed *P. ovale* infection having severe criteria of malaria

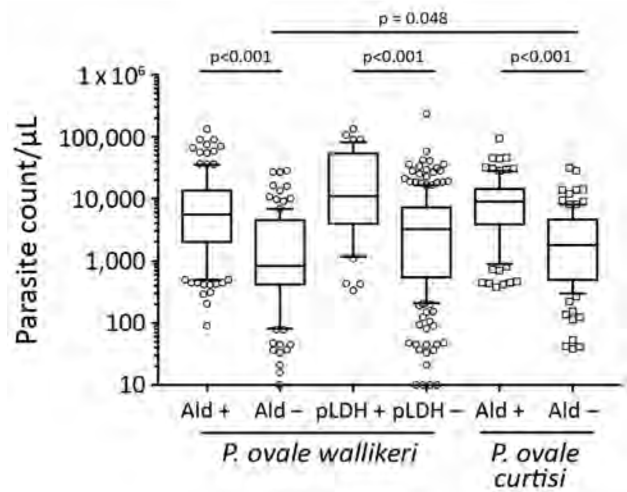


**Figure 4.** Comparison of parasite count according to RDT results in study analyzing characteristics of *Plasmodium ovale wallikeri* and *P. ovale curtisi* infections treated in France during January 2013–December 2018. Upper half of each box indicates quartile 3, and lower half indicates quartile 1. Horizontal bar dividing each box indicate median. Error bars range from 10th to 90th percentile. Ald, aldolase RDTs; pLDH, plasmodium lactate dehydrogenase RDTs; Poc, *P. ovale curtisi*; Pow, *P. ovale wallikeri*; RDT, rapid diagnostic test.

(*26*), a similar percentage to the data reported by the malaria surveillance in the United States (*32*) or by Kotepui et al. (*33*). Seven *P. ovale wallikeri*– and 1 *P. ovale curtisi*–infected patients were hospitalized in intensive or intermediate care. Six of those patients did not have WHO-defined severe malaria criteria (*26*). Hospitalization in intensive or intermediate care for non–WHO-defined severe malaria was previously described in uncomplicated malaria patients with *P. falciparum* (*34*) or *P. vivax* (*35*) infections. We examined the hospitalization information of 5,227 uncomplicated malaria patients (all infected with *Plasmodium* species) for the study period in the FNMRC database. Among these patients, 180 (3.6%) were hospitalized in intensive or intermediate care with a median length of hospital stay shorter to that observed with severe malaria patients (median 2 days [IQR 1–3 days] vs. median 3 days [IQR 2–4 days]; p<0.001).

In June 2017, La Société de Pathologie Infectieuse de Langue Française updated malaria management recommendations (*4*) and proposed the use of ACT as first-line treatment for all *Plasmodium* spp. infections and placed atovaquone/proguanil as a second-line treatment. Our data confirmed that physicians followed the new guidelines with a clear change between ACT and atovaquone/proguanil prescription frequency (Figure 5). *P. ovale wallikeri* infections

**Table 3**. Biologic and clinical characteristics of *Plasmodium ovale wallikeri* and *P. ovale curtisi* infections, France, January 2013–December 2018*

| Characteristic | *P. ovale curtisi*, n = 309 | *P. ovale wallikeri*, n = 368 | p value |
|---|---|---|---|
| Parasite density, parasites/µL, median (IQR) | 4,500 (1,094–10,197) | 3,970 (598–9,240) | 0.112 |
| Leucocyte count, G/L, median (IQR) | 5.6 (4.4–7.1) | 5.2 (4.1–6.5) | 0.0501 |
| Hemoglobin, g/L, median (IQR) | 127 (113–140) | 126 (114–139) | 0.855 |
| Platelet count, G/L, median (IQR) | 111 (84–145) | 94 (70–130) | <0.001 |
| <75 | 56 (19.4) | 104 (31) | |
| 75–150 | 168 (58.1) | 174 (51.9) | 0.003 |
| >150 | 65 (22.5) | 57 (17.1) | |
| Severe thrombocytopenia | 13 (4.5) | 25 (7.5) | 0.123 |
| Diagnostic delay, d, median (IQR) | 5 (3–7) | 4 (2–7) | 0.583 |
| Delay between return from endemic country and onset of symptoms, d, median (IQR) | 72 (18–208) | 34 (10–95) | <0.001 |
| <50 days | 87 (42.4) | 150 (59.5) | <0.001 |
| Symptoms | | | |
| Fever | 262 (95.6) | 316 (97.8) | 0.125 |
| Arthralgia or myalgia | 120 (54.8) | 138 (57.7) | 0.525 |
| Asthenia | 108 (58) | 133 (61.3) | 0.506 |
| Headache | 151 (68.6) | 201 (75.3) | 0.103 |
| Anorexia | 5 | 4 | |
| Diarrhea | 13 | 18 | |
| Abdominal pain | 28 | 29 | |
| Nausea | 16 | 20 | |
| Vomiting | 24 | 13 | |
| Cough | 6 | 12 | |
| Clinical categorization | | | 0.927 |
| Uncomplicated malaria | 293 (97.7) | 335 (97.4) | |
| Severe malaria | 3 (1) | 5 (1.5) | |
| Asymptomatic | 4 (1.3) | 4 (1.1) | |
| Admission to hospital | 158 (55.4) | 196 (60.3) | 0.243 |
| Duration of hospitalization, d, median (IQR) | 2 (1–3) | 3 (1–4) | 0.0732 |
| Intensive- or intermediate-care hospitalization | 1 (2.2) | 7 (11.3) | 0.134 |
| Conventional hospitalization | 46 (97.8) | 55 (88.7) | |
| Treatment | | | 0.00359 |
| Chloroquine | 147 (54.8) | 152 (47.8) | |
| Artemisinin therapy | 46 (17.1) | 93 (29.2) | |
| Artemeter/lumefantrine | 11 (25.5) | 39 (41.9) | |
| Artesunate | 2 (4.3) | 5 (5.4) | |
| Arteminol/piperaquine | 33 (70.2) | 49 (52.7) | |
| Atovaquone/proguanil | 64 (23.9) | 64 (20.1) | |
| Mefloquine | 3 (1.2) | 0 (0) | |
| Quinine | 8 (3) | 9 (2.9) | |

*Values are no. (%) patients except as indicated. IQR, interquartile range.

were treated more often with ACT. To explain this phenomenon, we compared the antimalarial treatment used according to the platelet counts, parasite density, pLDH-RDTs results, and latency period duration. No association was observed between the type of antimalarial treatment and platelet counts, parasite density, or pLDH-RDTs results, but we highlighted a relationship between ACT treatment and shorter latency period (p = 0.048). The combination of low platelet count and short latency delay in *Plasmodium* infections are suggestive of *P. falciparum* infection (*36*). In the context of emergency care before species confirmation, those features might have influenced the prescription of ACT. Because they were seen more frequently in *P. ovale wallikeri* infections, we assumed that this tendency could partially explain that most of the ACT treatment administered occurred in the *P. ovale wallikeri* group.

About 44% of patients that took a prophylactic treatment reported taking their medication regularly, as prescribed. The latency period was longer in those patients (p<0.001). Because prophylactic treatments are not effective against liver-dormant forms of *P. ovale* (*2*) and did not protect patients from relapsing malaria, those results are not surprising. This phenomenon is well-illustrated in military patients, a population with a higher rate of chemoprophylaxis treatment (85%) and greater compliance with the drug regimen (62%) who had longer latency periods than other patients (p<0.001).

Most of the *P. ovale* cases we analyzed were originally diagnosed by microscopic analysis. Species misidentification occurred for 8.8% of the samples, and the main misidentification was between *P. malariae* and *P. ovale*. In endemic settings, microscopic analysis or PCR diagnosis are not always available in remote setting.

Simple and affordable point-of-care compatible diagnostic tools are required. Although RDTs are widely spread nowadays in malaria-endemic countries, their efficiency for *P. ovale* diagnosis is not sufficiently studied compared with that for *P. falciparum* of *P. vivax* diagnosis. To supplement this deficiency, we analyzed the ability of aldolase and pLDH-RDTs to detect *P. ovale wallikeri* and *P. ovale curtisi* infection (Table 2). Aldolase-RDTs detection was definitively more accurate for *P. ovale* diagnosis than pLDH-RDTs (p<0.001). pLDH-RDTs used in this study (Palutop+4 [Biosynex] and Core Malaria [Core Diagnostics, https://www.corediagnostics.net]) were more efficient in diagnosing *P. ovale wallikeri* than *P. ovale curtisi* infection, but their performance remained extremely low (≈16% of infections diagnosed). This discrepancy might be explained by lactate dehydrogenase protein polymorphisms in *P. ovale* (*37*) affecting affinity of RDT-antibodies for *P. ovale* lactate dehydrogenase (*38*). Tang et al. (*39*) compared the efficiency of several pLDH-RDTs and confirmed variable diagnostic performance for *P. ovale*. In contrast, aldolase-RDTs had similar efficiency in detection of both species (50% for *P. ovale wallikeri* and 41.2% for *P. ovale curtisi*) that increased with parasite density (Table 2; Figure 4). Vikia demonstrated better performances than BinaxNow in *P. ovale* spp. detection (p<0.001).

The ability of *P. ovale* to establish liver-dormant forms (hypnozoïtes) induces relapse episodes of fever and parasitemia (*2*,*40*). Relapsing malaria was observed in only 3.5% of the included patients, a lower prevalence than previously reported (*14*). This difference is probably linked to the recommendations in France that advises systematic primaquine treatment of all *P. ovale*–infected patients, even for the first episode (except for major contraindication such as G6PD deficiency, pregnancy, and breastfeeding) (*4*). Currently, diagnosis of *P. ovale* infection relapse is mainly based on clinical data. *potra* gene sequencing has been used to distinguish reinfection from relapse by genotyping the initial and corresponding relapse sample (*13*,*14*). We evaluated the polymorphism of *potra* genes in 80 samples and, as previously described, identified a limited number of polymorphisms

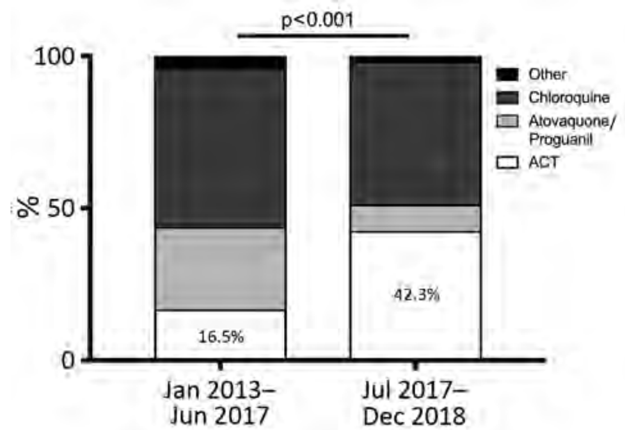


**Figure 5.** Effects of the new ACT treatment recommendations for *Plasmodium* spp. infections from La Société de Pathologie Infectieuse de Langue Française, revised in June 2017. ACT, chloroquine- or artemisinin-based combination therapy.

(Table 4) (*28*). Our results, combined with those of Zhou et al. (*29*), demonstrate that the *potra* gene is not a satisfying genetic marker of relapse. New genetic markers, such as microsatellite typing, need to be developed for *P. ovale* genotyping, as was previously done for *P. falciparum* (*41*,*42*) and *P. vivax* (*43*,*44*).

A limitation of our study is that, because of uncompleted online patient form filling (Appendix Table 2), we might lack statistical power to highlight differences in some rare infections features, such as hospitalization in intensive or intermediate care. In addition, our study is retrospective and might suffer from missing data about infection characteristics. Furthermore, we collected *P. ovale* isolates from Africa only.

In conclusion, our large retrospective study on *P. ovale wallikeri* and *P. ovale curtisi* infections confirmed that patients infected with *P. ovale wallikeri* display deeper thrombocytopenia and shorter latency periods. In addition, we found that physicians in France used more ACT to treat *P. ovale wallikeri* than *P. ovale curtisi* infections. This difference might be linked to the lower platelet level and shorter latency period seen with *P. ovale wallikeri* infections. in addition, we described a higher rate in intensive or intermediate

**Table 4**. Analysis of the *potra* fragment polymorphisms sequenced for *Plasmodium ovale wallikeri* and *P. ovale curtisi*, France, January 2013–December 2018

| Species | Size, bp | Dominant amino acid repeat | No. (%) samples | GenBank accession no. of reference sequence |
|---|---|---|---|---|
| *P. ovale wallikeri* | 245 | $(MANPIN)_1(AITPIN)_2$ | 43 (88) | HMG594180 |
| | 263 | $(MANPIN)_1(AITPIN)_3$ | 2 (4) | MG588149 |
| | 263 | $(MANPIN)_2(AITPIN)_2$ | 1 (2) | MG588148 |
| | 281 | $(MANPIN)_2(AITPIN)_3$ | 3 (6) | MG588150 |
| *P. ovale curtisi* | 299 | $(TINPIN)_3(TITPIS)_1$ | 26 (63) | MG588152 |
| | 317 | $(TINPIN)_3(TITPIS)_2$ | 13 (32) | HM594183 |
| | 335 | $(TINPIN)_4(TITPIS)_2$ | 2 (5) | MG588154 |

care admission in *P. ovale wallikeri*–infected patients. Because of missing data and lack of power, this observation was not statistically significant and needs to be confirmed by a large, prospective study.

Additional members of the French National Reference Center for Imported Malaria Study Group who contributed data: Chantal Garabedian (Aix-en-Provence), Alain Domergue (Aix-en-Provence), Sylvain Clauser (Boulogne), Patrice Agnamey (Amiens), Céline Damiani (Amiens), Ludovic de Gentile (Angers), Marc Pihet (Angers), Anne Marfaing-Koka (Clamart), Anthony Marteau (Avicenne Hospital, Bobigny), Izri Arezki (Avicenne Hospital, Bobigny), Cecile Ficko (Bégin Hospital, Vincennes), Sébastien Larréché (Bégin Hospital, Vincennes), Adela Enache Angoulvant (Kremlin-Bicêtre), Nadia Guennouni (Kremlin-Bicêtre), Thierry Pistone (Bordeaux), Valérie Fuster-Dumas (Bordeaux), Denis Malvy (Bordeaux), Dorothée Quinio (Brest), Gilles Nevez (Brest), Didier Raffenot (Chambéry), Olivier Rogeaux (Chambéry), Céline Nourrisson (Clermont-Ferrand), Naima Dahane (Cochin Hospital, Paris), Angèle Li (Creil), Bernadette Cuisenier (Dijon), Louise Basmacyan (Dijon), Annie Motard-Picheloup (Fréjus St-Raphaël), Cécile Garnaud (Grenoble), Céline Dard (Grenoble), Dominique Maubon (Grenoble), Eric Dannaoui (Hôpital Européen Georges Pompidou Hospital, Paris), Françoise Botterel (Créteil), Dieudonné Bemba (Bondy), Isabelle Poilane (Bondy), Ana Mendes-Moreira (La Rochelle), Gauthier Pean-de-Ponfilly (Lariboisière Hospital, Paris), Bruno Megarbane (Lariboisière Hospital, Paris), Céline Mesnil (Lariboisière Hospital, Paris), Muriel Silva (Le Havre), Céline Malassigne (Le Havre), Pascal Penn (Le Mans), Anne-Sophie Deleplancque (Lille), Boualem Sendid (Lille), Marie-Laure Darde (Limoges), Marie-Fleur Durieux (Limoges), Martine Bloc'h (Colombes), Luce Landraud (Colombes), Stéphane Picot (Lyon), Pauline Tirard-Collet (Lyon), Léo Vidoni (Lyon), Marie-Laure Bigel (Mantes-la-Jolie), Hélène Savini (HIA Laveran, Marseille), Coralie l'Ollivier (Marseille), Nicole Desbois-Nogard Nicole (Martinique), Hélène Broutier (Meaux), Patrick Bastien (Montpellier), Alain Gravet (Mulhouse), Caroline Lohmann (Mulhouse), Anne Debourgogne (Nancy), Fakhri Jeddi (Nantes), Rose-Anne Lavergne (Nantes), Marie-Elisabeth Bougnoux (Necker Hospital, Paris), Emilie Sitterle (Necker Hospital, Paris), Christelle Pomares Estran (Nice), Pascal Delaunay (Nice), Milène Sasso (Nîmes), Victor Mercier (Nîmes), Laurence Lachaud (Nîmes) Bernadette Buret (Niort), Didier Poisson (Orléans), Jérôme Guinard (Orléans), Aurélie Guigon (Orléans), Oussama Mouri (Pitié-Salpétrière Hospital, Paris), Estelle Perraud-Cateau (Poitiers), Gwénaël le Moal (Poitiers), Antoine Huguenin (Reims), Sorya Belaz (Rennes), Anne Delaval (Aulnay-sous-bois), Cécile Leprince (Aulnay-sous-bois), Jean-Yves Siriez (Robert Debré Hospital, Paris), Lauren Pull (Robert Debré Hospital, Paris), Odile Fenneteau (Robert Debré Hospital, Paris), Loïc Favennec (Rouen), Gilles Gargala (Rouen), Ghania Belkadi (Saint-Antoine Hospital, Paris), Cécile Tournus (Saint-Denis), Samia Hamane (Saint-Louis Hospital, Paris), Stéphane Bretagne (Saint-Louis Hospital, Paris), Julie Brunet (Strasbourg), Ahmed Abou-Bacar (Strasbourg), Guillaume Menard (Toulon), Pamela Chauvin (Toulouse), Faïza Ajana (Tourcoing), Pierre Patoz (Tourcoing), Nathalie Desuremain (Trousseau Hospital, Paris), Pierre Mornand (Trousseau Hospital, Paris), Farida Moreau-Benaoudia (Troyes), Maxime Thouvenin (Troyes), Gisèle Dewulf (Valenciennes), Edith Mazars (Valenciennes), Odile Eloy (Le Chesnay), Sylvie Maurellet Evrard (Villeneuve St-Georges), Alice Raffetin (Villeneuve St-Georges), Pauline Caraux-Paz (Villeneuve St-Georges).


### Acknowledgments

We thank the hospital correspondents who sent us *P. ovale* samples and filled in the online patient forms. We also thank Claire Kamaliddin and Alexandre Lampros for their assistance in translation and review of the manuscript.


## About the Author

Dr. Joste is resident in pathology and laboratory medicine and is a medical microbiologist. At the time of this study, he worked at the French National Malaria Reference Center at Bichat Hospital, Paris, France. His research interests include the diagnosis and epidemiology of *Plasmodium ovale* spp. infection.

### References


1. World Health Organization. World malaria report 2019 [cited 2020 Jan 7]. https://www.who.int/publications-detail/world-malaria-report-2019
2. Markus MB. Do hypnozoites cause relapse in malaria? Trends Parasitol. 2015;31:239–45. https://doi.org/10.1016/j.pt.2015.02.003
3. Centre National de Référence du Paludisme. Rapport d'activité annuel 2018 [cited 2020 Jan 7]. https://anofel.net/wp-content/uploads/2019/07/ra_cnr_2018_CNPaludisme.pdf
4. Bouchaud O, Bruneel F, Caumes E, Houzé S, Imbert P, Pradines B, et al. Management and prevention of imported malaria. 2018 update of the 2007 French clinical guidelines. Med Mal Infect. 2020;50:161–93. https://doi.org/10.1016/j.medmal.2019.10.009
5. Yerlikaya S, Campillo A, Gonzalez IJ. A systematic review: performance of rapid diagnostic tests for the detection of *Plasmodium knowlesi, Plasmodium malariae*, and *Plasmodium ovale* monoinfections in human blood. J Infect Dis. 2018;218:265–76. https://doi.org/10.1093/infdis/jiy150
6. Sutherland CJ, Tanomsing N, Nolder D, Oguike M, Jennison C, Pukrittayakamee S, et al. Two nonrecombining

sympatric forms of the human malaria parasite *Plasmodium ovale* occur globally. J Infect Dis. 2010;201:1544–50. https://doi.org/10.1086/652240
7. Tachibana M, Tsuboi T, Kaneko O, Khuntirat B, Torii M. Two types of *Plasmodium ovale* defined by SSU rRNA have distinct sequences for ookinete surface proteins. Mol Biochem Parasitol. 2002;122:223–6. https://doi.org/10.1016/S0166-6851(02)00101-9
8. Win TT, Jalloh A, Tantular IS, Tsuboi T, Ferreira MU, Kimura M, et al. Molecular analysis of *Plasmodium ovale* variants. Emerg Infect Dis. 2004;10:1235–40. https://doi.org/10.3201/eid1007.030411
9. Nolder D, Oguike MC, Maxwell-Scott H, Niyazi HA, Smith V, Chiodini PL, et al. An observational study of malaria in British travellers: *Plasmodium ovale wallikeri* and *Plasmodium ovale curtisi* differ significantly in the duration of latency. BMJ Open. 2013;3:e002711. https://doi.org/10.1136/bmjopen-2013-002711
10. Nabarro LEB, Nolder D, Broderick C, Nadjm B, Smith V, Blaze M, et al. Geographical and temporal trends and seasonal relapse in *Plasmodium ovale* spp. and *Plasmodium malariae* infections imported to the UK between 1987 and 2015. BMC Med. 2018;16:218. https://doi.org/10.1186/s12916-018-1204-6
11. Rojo-Marcos G, Rubio-Muñoz JM, Ramírez-Olivencia G, García-Bujalance S, Elcuaz-Romano R, Díaz-Menéndez M, et al. Comparison of imported *Plasmodium ovale curtisi* and *P. ovale wallikeri* infections among patients in Spain, 2005-2011. Emerg Infect Dis. 2014;20:409–16. https://doi.org/10.3201/eid2003.130745
12. Rojo-Marcos G, Rubio-Muñoz JM, Angheben A, Jaureguiberry S, García-Bujalance S, Tomasoni LR, et al.; TropNet Plasmodium ovale investigator group. Prospective comparative multi-centre study on imported *Plasmodium ovale wallikeri* and *Plasmodium ovale curtisi* infections. Malar J. 2018;17:399. https://doi.org/10.1186/s12936-018-2544-6
13. Veletzky L, Groger M, Lagler H, Walochnik J, Auer H, Fuehrer H-P, et al. Molecular evidence for relapse of an imported *Plasmodium ovale wallikeri* infection. Malar J. 2018;17:78. https://doi.org/10.1186/s12936-018-2226-4
14. Groger M, Veletzky L, Lalremruata A, Cattaneo C, Mischlinger J, Manego Zoleko R, et al. Prospective Clinical and Molecular Evaluation of Potential *Plasmodium ovale curtisi* and *wallikeri* Relapses in a High-transmission Setting. Clin Infect Dis. 2019;69:2119–26. https://doi.org/10.1093/cid/ciz131
15. Phuong MS, Lau R, Ralevski F, Boggild AK. Parasitological correlates of *Plasmodium ovale curtisi* and *Plasmodium ovale wallikeri* infection. Malar J. 2016;15:550. https://doi.org/10.1186/s12936-016-1601-2
16. Calderaro A, Piccolo G, Perandin F, Gorrini C, Peruzzi S, Zuelli C, et al. Genetic polymorphisms influence *Plasmodium ovale* PCR detection accuracy. J Clin Microbiol. 2007;45:1624–7. https://doi.org/10.1128/JCM.02316-06
17. Calderaro A, Piccolo G, Gorrini C, Rossi S, Montecchini S, Dell'Anna ML, et al. Accurate identification of the six human *Plasmodium* spp. causing imported malaria, including *Plasmodium ovale wallikeri* and *Plasmodium knowlesi.* Malar J. 2013;12:321. https://doi.org/10.1186/1475-2875-12-321
18. World Health Organization. Basic malaria microscopy. Part I: learner's guide. Second edition [cited 2020 Jun 15]. https://www.who.int/malaria/publications/atoz/9241547820
19. Snounou G, Singh B. Nested PCR analysis of *Plasmodium* parasites. Methods Mol Med. 2002;72:189–203.
20. Fuehrer H-P, Stadler M-T, Buczolich K, Bloeschl I, Noedl H. Two techniques for simultaneous identification of *Plasmodium ovale curtisi* and *Plasmodium ovale wallikeri* by use of the small-subunit rRNA gene. J Clin Microbiol. 2012;50:4100–2. https://doi.org/10.1128/JCM.02180-12
21. Joste V, Kamaliddin C, Kendjo E, Hubert V, Argy N, Houzé S. Distinction of *Plasmodium ovale wallikeri* and *Plasmodium ovale curtisi* using quantitative Polymerase Chain Reaction with High Resolution Melting revelation. Sci Rep. 2018;8:300. https://doi.org/10.1038/s41598-017-18026-1
22. Chou M, Kim S, Khim N, Chy S, Sum S, Dourng D, et al. Performance of "VIKIA Malaria Ag Pf/Pan" (IMACCESS®), a new malaria rapid diagnostic test for detection of symptomatic malaria infections. Malar J. 2012;11:295. https://doi.org/10.1186/1475-2875-11-295
23. Nkrumah B, Acquah SE, Ibrahim L, May J, Brattig N, Tannich E, et al. Comparative evaluation of two rapid field tests for malaria diagnosis: Partec Rapid Malaria Test® and Binax Now® Malaria Rapid Diagnostic Test. BMC Infect Dis. 2011;11:143. https://doi.org/10.1186/1471-2334-11-143
24. van Dijk DPJ, Gillet P, Vlieghe E, Cnops L, van Esbroeck M, Jacobs J. Evaluation of the Palutop+4 malaria rapid diagnostic test in a non-endemic setting. Malar J. 2009;8:293. https://doi.org/10.1186/1475-2875-8-293
25. Lampah DA, Yeo TW, Malloy M, Kenangalem E, Douglas NM, Ronaldo D, et al. Severe malarial thrombocytopenia: a risk factor for mortality in Papua, Indonesia. J Infect Dis. 2015;211:623–34. https://doi.org/10.1093/infdis/jiu487
26. Severe malaria. Trop Med Int Health. 2014;19(Suppl 1):7–131. https://doi.org/10.1111/tmi.12313_2
27. White NJ, Imwong M. Relapse. Adv Parasitol. 2012;80:113–50. https://doi.org/10.1016/B978-0-12-397900-1.00002-5
28. Oguike MC, Betson M, Burke M, Nolder D, Stothard JR, Kleinschmidt I, et al. *Plasmodium ovale curtisi* and *Plasmodium ovale wallikeri* circulate simultaneously in African communities. Int J Parasitol. 2011;41:677–83. https://doi.org/10.1016/j.ijpara.2011.01.004
29. Zhou R, Liu Y, Li S, Zhao Y, Huang F, Yang C, et al. Polymorphisms analysis of the *Plasmodium ovale* tryptophan-rich antigen gene (potra) from imported malaria cases in Henan Province. Malar J. 2018;17:127. https://doi.org/10.1186/s12936-018-2261-1
30. Wickham H, Henry L. tidyr: easily tidy data with "spread()" and "gather()" functions. R package version 0.8.1 [cited 2020 Jan 7]. https://CRAN.R-project.org/package=tidyr
31. Frickmann H, Wegner C, Ruben S, Loderstädt U, Tannich E. A comparison of two PCR protocols for the differentiation of *Plasmodium ovale* species and implications for clinical management in travellers returning to Germany: a 10-year cross-sectional study. Malar J. 2019;18:272. https://doi.org/10.1186/s12936-019-2901-0
32. Mace KE, Arguin PM, Lucchi NW, Tan KR. Malaria surveillance—United States, 2016. MMWR Surveill Summ. 2019;68:1–35. https://doi.org/10.15585/mmwr.ss6805a1
33. Kotepui M, Kotepui KU, Milanez GD, Masangkay FR. Severity and mortality of severe *Plasmodium ovale* infection: A systematic review and meta-analysis. PLoS One. 2020;15:e0235014. https://doi.org/10.1371/journal.pone.0235014
34. Schwake L, Streit JP, Edler L, Encke J, Stremmel W, Junghanss T. Early treatment of imported falciparum malaria in the intermediate and intensive care unit setting: an 8-year single-center retrospective study. Crit Care. 2008;12:R22. https://doi.org/10.1186/cc6796
35. Lança EFC, Magalhães BML, Vitor-Silva S, Siqueira AM, Benzecry SG, Alexandre MAA, et al. Risk factors and characterization of *Plasmodium vivax*–associated admissions

to pediatric intensive care units in the Brazilian Amazon. PLoS One. 2012;7:e35406. https://doi.org/10.1371/journal.pone.0035406
36. Robinson P, Jenney AW, Tachado M, Yung A, Manitta J, Taylor K, et al. Imported malaria treated in Melbourne, Australia: epidemiology and clinical features in 246 patients. J Travel Med. 2001;8:76–81. https://doi.org/10.2310/7060.2001.24309
37. Talman AM, Duval L, Legrand E, Hubert V, Yen S, Bell D, et al. Evaluation of the intra- and inter-specific genetic variability of *Plasmodium* lactate dehydrogenase. Malar J. 2007;6:140. https://doi.org/10.1186/1475-2875-6-140
38. Bauffe F, Desplans J, Fraisier C, Parzy D. Real-time PCR assay for discrimination of *Plasmodium ovale curtisi* and *Plasmodium ovale wallikeri* in the Ivory Coast and in the Comoros Islands. Malar J. 2012;11:307. https://doi.org/10.1186/1475-2875-11-307
39. Tang J, Tang F, Zhu H, Lu F, Xu S, Cao Y, et al. Assessment of false negative rates of lactate dehydrogenase-based malaria rapid diagnostic tests for *Plasmodium ovale* detection. PLoS Negl Trop Dis. 2019;13:e0007254. https://doi.org/10.1371/journal.pntd.0007254
40. Robinson LJ, Wampfler R, Betuela I, Karl S, White MT, Li Wai Suen CSN, et al. Strategies for understanding and reducing the *Plasmodium vivax* and *Plasmodium ovale* hypnozoite reservoir in Papua New Guinean children: a randomised placebo-controlled trial and mathematical model. PLoS Med. 2015;12:e1001891. https://doi.org/10.1371/journal.pmed.1001891
41. Leclerc MC, Durand P, de Meeûs T, Robert V, Renaud F. Genetic diversity and population structure of *Plasmodium falciparum* isolates from Dakar, Senegal, investigated from microsatellite and antigen determinant loci. Microbes Infect. 2002;4:685–92. https://doi.org/10.1016/S1286-4579(02)01587-3
42. Su X, Wellems TE. Toward a high-resolution *Plasmodium falciparum* linkage map: polymorphic markers from hundreds of simple sequence repeats. Genomics. 1996;33:430–44. https://doi.org/10.1006/geno.1996.0218
43. Gunawardena S, Karunaweera ND, Ferreira MU, Phone-Kyaw M, Pollack RJ, Alifrangis M, et al. Geographic structure of *Plasmodium vivax*: microsatellite analysis of parasite populations from Sri Lanka, Myanmar, and Ethiopia. Am J Trop Med Hyg. 2010;82:235–42. https://doi.org/10.4269/ajtmh.2010.09-0588
44. Orjuela-Sánchez P, Brandi MC, Ferreira MU. Microsatelliteanalysis of malaria parasites. Methods Mol Biol. 2013; 1006:247–58. https://doi.org/10.1007/978-1-62703-389-3_17

Address for correspondence: Valentin Joste, Hôpital Bichat-Claude Bernard, Service de Parasitologie–Mycologie, 46 rue Henri Huchard, 75018 Paris, France; email: valentinjoste@gmail.com

# Symptom Profiles and Progression in Hospitalized and Nonhospitalized Patients with Coronavirus Disease, Colorado, USA, 2020

Grace M. Vahey,[1] Kristen E. Marshall,[1] Emily McDonald, Stacey W. Martin, Jacqueline E. Tate, Claire M. Midgley, Marie E. Killerby, Breanna Kawasaki, Rachel K. Herlihy, Nisha B. Alden, J. Erin Staples, on behalf of the Colorado Investigation Team[2]

To improve recognition of coronavirus disease (COVID-19) and inform clinical and public health guidance, we randomly selected 600 COVID-19 case-patients in Colorado. A telephone questionnaire captured symptoms experienced, when symptoms occurred, and how long each lasted. Among 128 hospitalized patients, commonly reported symptoms included fever (84%), fatigue (83%), cough (73%), and dyspnea (72%). Among 236 nonhospitalized patients, commonly reported symptoms included fatigue (90%), fever (83%), cough (83%), and myalgia (74%). The most commonly reported initial symptoms were cough (21%–25%) and fever (20%–25%). In multivariable analysis, vomiting, dyspnea, altered mental status, dehydration, and wheezing were significantly associated with hospitalization, whereas rhinorrhea, headache, sore throat, and anosmia or ageusia were significantly associated with nonhospitalization. General symptoms and upper respiratory symptoms occurred earlier in disease, and anosmia, ageusia, lower respiratory symptoms, and gastrointestinal symptoms occurred later. Symptoms should be considered alongside other epidemiologic factors in clinical and public health decisions regarding potential COVID-19 cases.

Severe acute respiratory syndrome coronavirus 2 (SARS-CoV-2), the virus that causes coronavirus disease (COVID-19), was first detected in China in December 2019 (*1*,*2*). Within 1 month, COVID-19 cases were reported in numerous countries, including the United States (*3*). By the end of January 2020, the World Health Organization (WHO) declared the COVID-19 outbreak a public health emergency of international concern (*4*). After WHO's declaration, rapid acceleration of virus transmission in many parts of the world led WHO to characterize COVID-19 as a global pandemic in March (*5*). As of December 4, the United States had reported >14 million COVID-19 cases and ≈275,000 associated deaths (*6*). The large number of cases and deaths has created an unprecedented burden on the nation's healthcare system, necessitating triage of patients and the prioritization of testing.

Initially, the most common symptoms of COVID-19 were reported to be fever, cough, and dyspnea (*7*–*9*). However, asymptomatic infections and additional symptoms common to other viral respiratory illnesses have been reported, including chills, fatigue, myalgia, sore throat, nasal congestion, rhinorrhea, nausea, vomiting, and diarrhea (*10*). Persons with COVID-19 have also reported anosmia (loss of smell) and ageusia (loss of taste) more frequently than with other viral respiratory diseases (*11*).

Although ≈80% of persons with COVID-19 experience mild disease (*12*), to date most published reports of COVID-19 symptoms are derived from case-series and cross-sectional analyses of medical record reviews, primarily among hospitalized patients. Literature regarding symptoms experienced by nonhospitalized COVID-19 patients is growing, but information summarizing symptom duration,

Author affiliations: Centers for Disease Control and Prevention, Fort Collins, Colorado, USA (G.M. Vahey, E. McDonald, S.W. Martin, J.E. Staples); Centers for Disease Control and Prevention, Atlanta, Georgia, USA (K.E. Marshall, J.E. Tate, C.M. Midgley, M.E. Killerby); Colorado Department of Public Health and Environment, Denver, Colorado, USA (K.E. Marshall, B. Kawasaki, R.K. Herlihy, N.B. Alden)

DOI: https://doi.org/10.3201/eid2702.203729

[1]These authors contributed equally to this article.

[2]Members of the team are listed at the end of this article.

progression, and statistical comparison to hospitalized patients remains limited. To improve COVID-19 disease recognition, which can help mitigate its spread, particularly for mild cases, and inform clinical and public health guidance, we interviewed hospitalized and nonhospitalized COVID-19 patients in Colorado to determine the symptoms they experienced and when these symptoms occurred during their course of illness.

## Methods

### Sample

Hospitalized and nonhospitalized patients were identified from laboratory-confirmed COVID-19 cases reported to the Colorado Electronic Disease Reporting System (CEDRS) as of April 5, 2020. Based on data available in CEDRS, patients were considered eligible if they had known hospitalization status; had self-reported illness onset during March 9–31, 2020; and resided in 1 of the 9 counties (Adams, Arapahoe, Boulder, Denver, Douglas, El Paso, Jefferson, Larimer, and Weld) that account for ≈80% of Colorado's population. March 9 was selected because it was the date on which testing for SARS-CoV-2 became more widely available in Colorado and was no longer restricted to suspected cases requiring hospitalization or having an epidemiologic link to a confirmed case, though travel to an area with ongoing community transmission was required for testing early in this period. To obtain interviews from at least 300 patients (200 nonhospitalized and 100 hospitalized), we used stratified, simple random sampling to select 600 patients (using a 2:1 ratio) from 1,738 COVID-19 cases meeting inclusion criteria.

### Data Collection

At least 3 attempts were made to contact each selected patient on at least 2 separate days, at different times of the day, during April 10–30, 2020. For contacted patients who consented, a trained public health official administered a standardized questionnaire by telephone to obtain demographic information, verify hospitalization status and date of illness onset, and determine whether the patient had experienced any of 30 symptoms during their illness. For patients whose hospitalization status differed between CEDRS data and interview, we confirmed status using electronic medical records. For all deceased patients, minors, and persons unable to be interviewed (e.g., those with dementia), a proxy (i.e., relative or caregiver) was interviewed. Patients were asked what their first and subsequent symptoms were, and for each reported symptom, when it occurred relative to onset of illness and how long it lasted. No follow-up contact was made once the questionnaire was completed.

### Statistical Analysis

Data were entered into a Research Electronic Data Capture database (*13*,*14*). Frequencies and percentages were calculated and stratified by hospitalization status. We calculated odds ratios (ORs), 95% CIs, and p values to identify COVID-19 symptoms associated with hospitalization. Multivariable logistic regression was conducted to construct a model examining association of all symptoms with hospitalization status, while adjusting for demographic variables associated with hospitalization for COVID-19 (i.e., male sex, age $\geq$65 years, and Hispanic ethnicity) (Appendix Table, https://wwwnc.cdc.gov/EID/article/27/2/20-3729-App1.pdf). A reduced multivariable model was constructed by using purposeful selection to identify a subset of symptoms from the full model that had statistically significant association (*15*). In multivariable models, anosmia and ageusia were combined because of a high degree of collinearity; no other significant collinearity was identified.

Median and interquartile ranges (IQRs) were calculated for duration and timing of individual symptoms in relation to overall onset of illness. To account for patients who died and the large proportion of patients who were still symptomatic at the time of interview, we used survival analysis to calculate estimated median illness duration compared by hospitalization status. For participants still experiencing symptoms at interview, individual symptom duration was truncated to the date of interview because a low proportion (<10%) of patients reported individual symptoms still occurring at that time. Symptoms were categorized by organ system based on codes from the International Classification of Diseases, 10th Revision, Clinical Modification. Statistical analyses were conducted by using SAS 9.4 (SAS Institute, https://www.sas.com) and R version 3.6.3 software (https://r-project.org) (*16*). Significance was defined as $\alpha = 0.05$, and all testing was 2-sided.

### Ethics Considerations

This investigation received a nonresearch determination as a public health response from human subjects advisors at the Centers for Disease Control and Prevention. The investigation was considered a public health response to a notifiable disease by the Colorado Department of Public Health and Environment.

## Results

### The Patients

Of 600 randomly selected case-patients, 364 (61%) completed the interview, 46 (8%) were ineligible (because onset date was before March 9 or they were asymptomatic), 57 (10%) declined to participate, and 133 (22%) were unreachable. Median age of the 364 participating patients was 50 years (range 2 months–94 years); 187 (51%) were male, 288 (79%) identified as white, and 75 (21%) identified as Hispanic. Almost all patients (345 [95%]) reported having health insurance; 128 (35%) patients were hospitalized, and 18 (5%) died. Compared with nonhospitalized patients, hospitalized patients were older and more likely to be Black; they were also more likely to be male (Table 1). Compared with patients who declined to participate or were unreachable, investigation participants resided proportionately in the same counties and had similar hospitalization rates (35% vs. 31%) and case-fatality ratios (5% vs. 8%), but they were older than nonparticipating patients (median age 50 vs. 43 years).

Among 364 participating patients, interviews were conducted with 322 (88%) patients and proxies for 42 (12%) patients. Patients who were interviewed directly reported a higher median number of symptoms (13 [IQR 9–16]) than proxies reported (6 [IQR 4–10]). Proxies were interviewed more frequently for hospitalized patients than for nonhospitalized patients (Table 1) and more often for participants ≥65 years of age (30/85 [35%]) than for those <65 years (12/279 [4%]). Median number of days from illness onset to interview (33 days) did not differ by hospitalization status.

### Frequency of Symptoms

Based on International Classification of Diseases, Tenth Revision, Clinical Modification, categorization of symptoms, general systemic symptoms (i.e., fever, chills, myalgia, headache, or anorexia) were commonly reported among both hospitalized (122 [95%]) and nonhospitalized (234 [99%]) patients (Table 2). Symptoms associated with potential lower respiratory tract infection (cough, dyspnea, wheezing, or chest pain) were reported by 116 (91%) of hospitalized patients and 213 (90%) of nonhospitalized patients. Cognition and perception symptoms (altered mental status, anosmia, or ageusia) were reported by 87 (68%) hospitalized and 165 (70%) nonhospitalized patients. More nonhospitalized patients (158 [67%]) reported upper respiratory tract infection symptoms (i.e., rhinorrhea, nasal congestion, or sore throat) than were reported by hospitalized patients (60 [47%]). Gastrointestinal symptoms (i.e., nausea, vomiting, diarrhea, or abdominal pain) were reported by 58% of participants, regardless of hospitalization status.

The most frequently reported symptoms were similar for hospitalized and nonhospitalized participants (Table 2). Among 128 hospitalized patients, the most commonly reported symptoms were fever (108 [84%]), fatigue (106 [83%]), cough (93 [73%]), and dyspnea (92 [72%]). Among 236 nonhospitalized patients, the most commonly reported symptoms were fatigue (213 [90%]), fever (196 [83%]), cough (196 [83%]), and myalgia (175 [74%]). Ageusia was reported by 149 (63%) nonhospitalized and 63 (49%) hospitalized patients, and anosmia by 131 (56%) nonhospitalized and 45 (35%) hospitalized patients. A total of 123 (96%) hospitalized patients and 229 (97%) nonhospitalized

**Table 1.** Demographics, interview information, hospitalization status, and outcome of 364 patients with laboratory-confirmed coronavirus disease by hospitalization status, Colorado, USA, March 2020

| Characteristic | No. (%) Hospitalized, n = 128 | No. (%) Nonhospitalized, n = 236 |
|---|---|---|
| Sex | | |
| M | 79 (62) | 108 (46) |
| F | 49 (38) | 127 (54) |
| Other | 0 (0) | 1 (<1) |
| Age group, y | | |
| ≤18 | 3 (2) | 1 (<1) |
| 19–44 | 23 (18) | 118 (50) |
| 45–64 | 50 (39) | 84 (36) |
| ≥65 | 52 (41) | 33 (14) |
| Race* | | |
| White | 95 (74) | 193 (82) |
| Black | 13 (10) | 12 (5) |
| Asian | 9 (7) | 9 (4) |
| Pacific Islander | 1 (1) | 3 (1) |
| American Indian | 2 (2) | 2 (1) |
| Other | 9 (7) | 18 (8) |
| Unknown | 4 (3) | 4 (2) |
| Ethnicity | | |
| Non-Hispanic or Latino | 86 (67) | 163 (69) |
| Hispanic or Latino | 29 (23) | 46 (19) |
| Unknown | 13 (10) | 27 (11) |
| Health insurance status and type | | |
| Insured* | 118 (92) | 227 (96) |
| Private | 64 (50) | 184 (78) |
| Medicare | 41 (32) | 21 (9) |
| Medicaid | 22 (17) | 13 (6) |
| Military or Tricare | 5 (4) | 11 (5) |
| Not specified | 1 (1) | 2 (1) |
| Not insured | 8 (6) | 6 (3) |
| Unknown | 2 (2) | 3 (1) |
| Interview type | | |
| Patient interview | 96 (75) | 226 (96) |
| Proxy interview | 32 (25) | 10 (4) |
| Outcome | | |
| Survived | 113 (88) | 233 (99) |
| Died | 15 (12) | 3 (1) |

*Options were not mutually exclusive.

patients reported fever, cough, or dyspnea. Of the 12 participants not reporting these symptoms, the most commonly reported symptoms were fatigue (7 patients), anosmia (6 patients), ageusia (6 patients), anorexia (6 patients), and diarrhea (5 patients).

Participants who reported altered mental status and vomiting had at least twice the odds of being hospitalized (Table 2). Patients reporting wheezing and dyspnea also had higher odds of hospitalization. In contrast, patients who reported lymphadenopathy, anosmia, rhinorrhea, myalgia, headache, sore throat, or nasal congestion had less than half the odds of hospitalization. Patients reporting fatigue, dry cough, and ageusia also had lower odds of hospitalization.

When we controlled for all reported symptoms and characteristics included in the reduced multivariable logistic regression model, we found that participants who reported vomiting (OR 2.46 [95% CI 1.2–5.06]), dyspnea (OR 2.32 [95% CI 1.26–4.37]), altered mental status (OR 2.12 [95% CI 1.18–3.83]), dehydration (OR 1.88 [95% CI 1.1–3.26]), and wheezing (OR 1.88 [95% CI 1.03–3.43]) had higher odds of

**Table 2.** Frequency and duration of symptoms reported by 364 hospitalized and nonhospitalized patients with laboratory-confirmed coronavirus disease, Colorado, USA, March 2020*

| | Hospitalized, n = 128 | | Nonhospitalized, n = 236 | | | |
|---|---|---|---|---|---|---|
| Symptoms | No. (%) | Median symptom duration (IQR) | No. (%) | Median symptom duration (IQR) | Crude OR (95% CI) | p value |
| Symptom groups | | | | | | |
| Any general symptom† | 122 (95) | NC | 234 (99) | NC | NC | NC |
| Any LRI symptom‡ | 116 (91) | NC | 213 (90) | NC | NC | NC |
| Any cognitive or perception symptom§ | 87 (68) | NC | 165 (70) | NC | NC | NC |
| Any URI symptom¶ | 60 (47) | NC | 158 (67) | NC | NC | NC |
| Any GI symptom# | 74 (58) | NC | 136 (58) | NC | NC | NC |
| Individual symptoms | | | | | | |
| Fever** | 108 (84) | ** | 196 (83) | ** | 1.10 (0.61–2.01) | 0.74 |
| Fatigue | 106 (83) | 14 (9–27) | 213 (90) | 12 (7–15) | 0.52 (0.28–0.98) | 0.04 |
| Any cough†† | 93 (73) | NC | 196 (83) | NC | NC | NC |
| Dry cough | 79 (62) | 10 (7–22) | 175 (74) | 10 (5–18) | 0.56 (0.35–0.89) | 0.01 |
| Chills | 84 (66) | 7 (3–10) | 169 (72) | 3 (2–7) | 0.76 (0.48–1.20) | 0.24 |
| Myalgia | 72 (56) | 11 (7–15) | 175 (74) | 5 (3–9) | 0.45 (0.28–0.71) | <0.01 |
| Anorexia | 89 (70) | 12 (7–17) | 150 (64) | 7 (4–11) | 1.31 (0.83–2.09) | 0.25 |
| Dyspnea | 92 (72) | 10 (5–19) | 144 (61) | 10 (6–14) | 1.63 (1.03–2.62) | 0.04 |
| Headache | 66 (52) | 8 (4–14) | 166 (70) | 7 (3–14) | 0.45 (0.29–0.70) | <0.01 |
| Ageusia | 63 (49) | 14 (8–21) | 149 (63) | 10 (7–20) | 0.57 (0.37–0.87) | 0.01 |
| Sweats | 70 (55) | 7 (3–10) | 134 (57) | 3 (2–7) | 0.92 (0.60–1.42) | 0.70 |
| Anosmia | 45 (35) | 14 (7–24) | 131 (56) | 10 (7–21) | 0.43 (0.28–0.67) | <0.01 |
| Diarrhea | 60 (47) | 7 (3–13) | 104 (44) | 3 (2–6) | 1.12 (0.73–1.73) | 0.61 |
| Arthralgia | 45 (35) | 13 (7–17) | 100 (42) | 5 (4–10) | 0.74 (0.47–1.15) | 0.18 |
| Dehydration | 54 (42) | 10 (4–14) | 76 (32) | 5 (3–10) | 1.54 (0.98–2.40) | 0.06 |
| Chest pain | 42 (33) | 10 (5–16) | 85 (36) | 7 (4–14) | 0.87 (0.55–1.36) | 0.54 |
| Rhinorrhea | 31 (24) | 7 (3–12) | 97 (41) | 7 (4–14) | 0.46 (0.28–0.73) | <0.01 |
| Sore throat | 28 (22) | 8 (4–15) | 91 (39) | 4 (2–7) | 0.45 (0.27–0.72) | <0.01 |
| Nasal congestion | 28 (22) | 7 (3–14) | 86 (36) | 7 (5–14) | 0.49 (0.29–0.79) | <0.01 |
| Nausea | 41 (32) | 7 (3–12) | 69 (29) | 4 (2–7) | 1.14 (0.71–1.81) | 0.58 |
| Wheezing | 44 (34) | 12 (5–16) | 54 (23) | 9 (6–14) | 1.77 (1.10–2.84) | 0.02 |
| Productive cough | 37 (29) | 10 (7–28) | 58 (25) | 10 (5–16) | 1.25 (0.77–2.02) | 0.37 |
| Altered mental status | 39 (30) | 7 (3–16) | 39 (17) | 6 (3–12) | 2.21 (1.33–3.69) | <0.01 |
| Abdominal pain | 18 (14) | 9 (7–20) | 49 (21) | 3 (2–5) | 0.62 (0.34–1.11) | 0.12 |
| Conjunctivitis | 16 (13) | 7 (3–12) | 36 (15) | 5 (3–10) | 0.79 (0.41–1.47) | 0.47 |
| Vomiting | 24 (19) | 4 (2–6) | 24 (10) | 2 (1–4) | 2.04 (1.10–3.77) | 0.02 |
| Lymphadenopathy | 7 (5) | 7 (6–13) | 37 (16) | 6 (3–10) | 0.31 (0.12–0.68) | <0.01 |
| Rash | 9 (7) | 4 (2–7) | 24 (10) | 5 (3–10) | 0.67 (0.29–1.44) | 0.32 |
| Hemoptysis | 8 (6) | 7 (4–9) | 7 (3) | 3 (3–9) | 2.18 (0.77–6.36) | 0.14 |
| Seizures | 3 (2) | 7 (4–10) | 0 | NC | NC | NC |

*GI, gastrointestinal; IQR, interquartile range; LRI, lower respiratory tract infection; NC, not calculated; OR, odds ratio; URI, upper respiratory tract infection.
†General symptoms included fever, chills, sweats, myalgia, headache, fatigue, arthralgia, dehydration, anorexia, and lymphadenopathy.
‡ LRI symptoms included cough (dry and productive), dyspnea, wheezing, hemoptysis, and chest pain.
§Cognition and perception symptoms included anosmia, ageusia, and altered mental status.
¶URI symptoms included nasal congestion, rhinorrhea, and sore throat.
#GI symptoms included nausea, vomiting, diarrhea, and abdominal pain.
**Fever was collected individually as subjective or measured. Values were combined given potential bias because hospitalized patients were more likely to have their temperature measured compared with nonhospitalized patients, who more commonly reported subjective fever only. The median duration of both subjective and measured fevers in nonhospitalized patients was 4 d (IQR 2–7 d). In hospitalized patients, the median duration of measured fever was 7 d [IQR 3–11 d] and subjective fever was 8 d (IQR 4–13 d).
††Any cough is a combination of dry cough, productive cough, and hemoptysis, which are also reported individually.

hospitalization, as did participants who were male (OR 2.13 [95% CI 1.27–3.62]) or ≥65 years of age (OR 3.93 [95% CI 2.16–7.27]) (Figure 1). Patients reporting rhinorrhea (OR 0.43 [95% CI 0.24–0.74]), headache (OR 0.47 [95% CI 0.27–0.82]), sore throat (OR 0.5 [95% CI 0.28–0.87]), and anosmia or ageusia (OR 0.57 [95% CI 0.33–0.96]) had lower odds of hospitalization.

### Temporal Occurrence of Symptoms

The most common initial symptoms for hospitalized and nonhospitalized patients were cough (25% for hospitalized and 21% for nonhospitalized patients) and fever (25% for hospitalized and 20% for nonhospitalized patients) (Table 3). No participants reported conjunctivitis, rash, or lymphadenopathy as an initial symptom of their illness. Patients reporting sore throat as their initial symptom had lower odds of being hospitalized (OR 0.28 [95% CI 0.11–0.74]); no other initial symptom was associated with hospitalization status.

Little variation was observed between hospitalized and nonhospitalized patients in terms of symptom progression (Figure 2). Upper respiratory symptoms and general systemic symptoms were reported early in the course of disease; many patients reported these types of symptoms within 1 day of illness onset. Symptoms related to cognition, perception, and lower respiratory tract (except cough) were generally reported to occur 2–4 days after illness onset. Gastrointestinal symptoms were reported to occur ≈3–6 days after illness onset, and rash generally appeared last.

Among 346 surviving patients, 134 (39%) were still symptomatic at time of interview. The estimated median duration of illness was 18 days longer in hospitalized patients (36 days; p<0.01) than in patients who were not hospitalized (18 days; p<0.01) (Appendix Figure). The median duration of most individual symptoms was ≤10 days; notable exceptions were fatigue for both hospitalized (14 days [IQR 9–27 days]) and nonhospitalized (12 days [IQR 7–15 days]) participants and, among hospitalized patients, anosmia (14 days [IQR 7–24 days]), ageusia (14 days [IQR 8–21 days]), arthralgia (13 days [IQR 7–17 days]), anorexia (12 days [IQR 7–17 days]), wheezing (12 days [IQR 5–16 days]), and myalgia (11 days [IQR 7–15 days]) (Table 2). The median durations of chills, myalgia, sweats, diarrhea, arthralgia, dehydration, sore throat, abdominal pain, vomiting, and hemoptysis for hospitalized patients were ≥2 times those of nonhospitalized patients.

## Discussion

We found that persons with COVID-19 in Colorado commonly reported fever, cough, or dyspnea, similar to findings in previous reports (*7–9*,*17*). However, we also identified several other symptoms (i.e., fatigue, chills, myalgia, anorexia, and headache) that occurred with similar frequency, and we noted differences in the frequency of symptoms reported by hospitalized and nonhospitalized participants.

In general, we found higher frequencies of symptoms than previously reported (*18–21*). This discrepancy is likely in part a result of our approach of collecting symptom data through standardized interviews compared with other reports that are based on data extracted from medical records. Data taken from medical records generally capture the most prominent symptoms reported when a patient seeks care and might not capture initial nonspecific symptoms or symptoms that occur later in the course of illness. For example, a medical chart review of 242 hospitalized patients with symptomatic COVID-19 in China found the most common symptoms at admission were fever (90%), cough (38%), and fatigue (16%), compared with

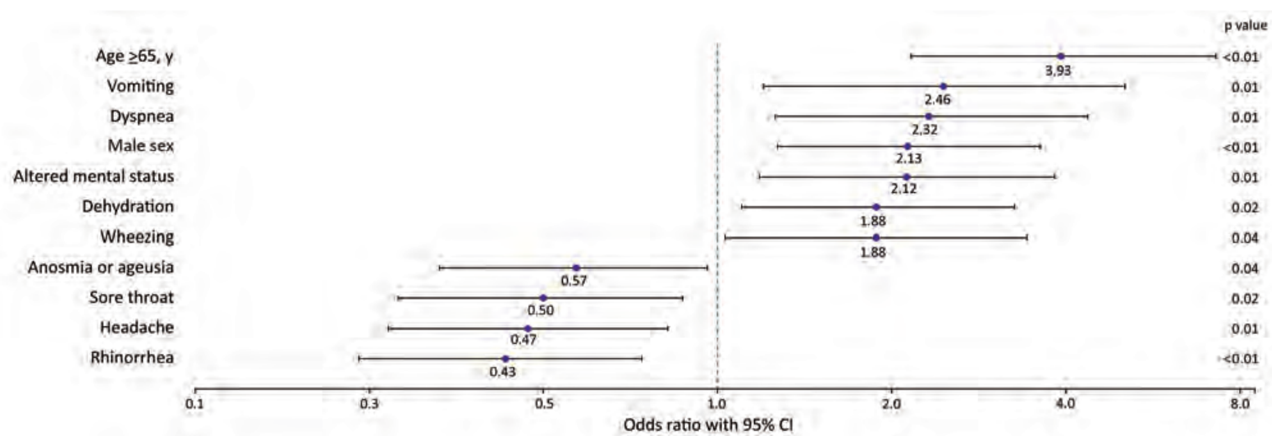


**Figure 1.** Coronavirus disease symptoms significantly associated with hospitalization in reduced multivariable model (n = 364 patients), Colorado, March 2020.

**Table 3.** Initial symptom reported by 364 hospitalized and nonhospitalized patients with laboratory-confirmed coronavirus disease, Colorado, USA, March 2020*

| Symptom | No. (%) Hospitalized, n = 128 | No. (%) Nonhospitalized, n = 236 |
|---|---|---|
| Cough | 32 (25) | 49 (21) |
| Fever | 32 (25) | 47 (20) |
| Fatigue | 17 (13) | 44 (19) |
| Headache | 14 (11) | 45 (19) |
| Myalgia | 14 (11) | 38 (16) |
| Sore throat† | 5 (4) | 30 (13) |
| Chills | 11 (9) | 19 (8) |
| Nasal congestion | 2 (2) | 12 (5) |
| Dyspnea | 8 (6) | 6 (3) |
| Ageusia | 1 (1) | 7 (3) |
| Diarrhea | 2 (2) | 6 (3) |
| Anosmia | 1 (1) | 6 (3) |
| Rhinorrhea | 2 (2) | 5 (2) |
| Chest pain | 1 (1) | 5 (2) |
| Abdominal pain | 3 (2) | 2 (1) |
| Altered mental status | 4 (3) | 1 (<1) |
| Sweats | 2 (2) | 2 (1) |
| Wheezing | 1 (1) | 2 (1) |
| Vomiting | 2 (2) | 1 (<1) |
| Dehydration | 1 (1) | 1 (<1) |
| Anorexia | 1 (1) | 1 (<1) |
| Nausea | 0 | 1 (<1) |
| Seizures | 1 (1) | 0 |
| Conjunctivitis | 0 | 0 |
| Rash | 0 | 0 |
| Lymphadenopathy | 0 | 0 |

*Reported symptoms are not mutually exclusive.
†Indicates statistical significance with nonhospitalization.

rates of fever (84%), cough (73%), and fatigue (83%) in the hospitalized participants in our analysis (*18*). However, the higher frequencies of certain symptoms in our analysis might also be because of differences in the populations studied and their disease severity. For instance, the frequency of ageusia and anosmia among nonhospitalized patients in this analysis was similar to previous reports of patients with mild COVID-19 (*22*–*26*) but was higher than a smaller cohort of hospitalized patients in another study (*19*).

Patients in our cohort reported high frequencies of general symptoms and lower respiratory tract symptoms, including cough. More than half of our patients reported ≥1 gastrointestinal symptom regardless of hospitalization status, which was similar to findings from previous reports examining symptoms through interviews with hospitalized and nonhospitalized patients (*17*,*26*). The rates of gastrointestinal symptoms in this analysis are higher than a previous report that found 35% of persons receiving outpatient care for COVID-19 had diarrhea, nausea, or vomiting documented in their charts (*27*) and another study in which 19% of hospitalized COVID-19 patients had chart-documented diarrhea or abdominal pain at admission (*28*). One explanation for the differences in reported gastrointestinal symptoms is that these symptoms occur later in illness and might be absent when the patient initially seeks care. This progression was documented recently in a prospective investigation of nonhospitalized COVID-19 patients, in which only 23% of patients reported gastrointestinal symptoms at the time of their first positive SARS-CoV-2 test but 53% of all patients experienced gastrointestinal symptoms at some point in their illness (*22*). Other studies have found patients with gastrointestinal symptoms were more likely to seek medical care ≥1 week after onset of illness, compared with those without gastrointestinal symptoms, who were more likely to seek care <1 week after illness onset (*27*,*28*).

When comparing the frequency of reported symptoms between hospitalized and nonhospitalized patients, we found that patients reporting certain lower respiratory symptoms (wheezing and dyspnea), altered mental status, vomiting, and dehydration had higher odds of hospitalization. This finding is not surprising, because many of these symptoms would likely prompt a clinician to recommend inpatient management. Similarly, in a convenience sample of symptomatic persons with COVID-19 from 16 US states, dyspnea was more commonly reported by hospitalized patients, and anosmia, ageusia, and rhinorrhea were more commonly reported by nonhospitalized patients (*17*). Among all symptoms we associated with hospitalization, only dyspnea has been statistically associated with more serious disease, as measured by intensive-care unit admission (*29*).

A notable finding from our analysis was that upper respiratory tract symptoms were more commonly reported by nonhospitalized patients. This finding could aid in clinicians' recognition of less severe disease and therefore help mitigate the spread of infection. Other nonspecific symptoms reported very commonly or rarely (namely, fatigue, dry cough, myalgia, and lymphadenopathy) were no longer significantly associated with nonhospitalization on multivariable analysis. Our findings among nonhospitalized patients are consistent with recent reports from Europe, South Korea, and the United States that found that upper respiratory symptoms, such as nasal congestion and rhinorrhea, were common among persons with mild or moderate COVID-19 (*22*,*30*,*31*). These findings suggest that potential differences in route of infection (i.e., contact with respiratory droplets vs. inhalation of aerosolized viral particles) could be related to the pathogenesis and severity of COVID-19, although other factors also

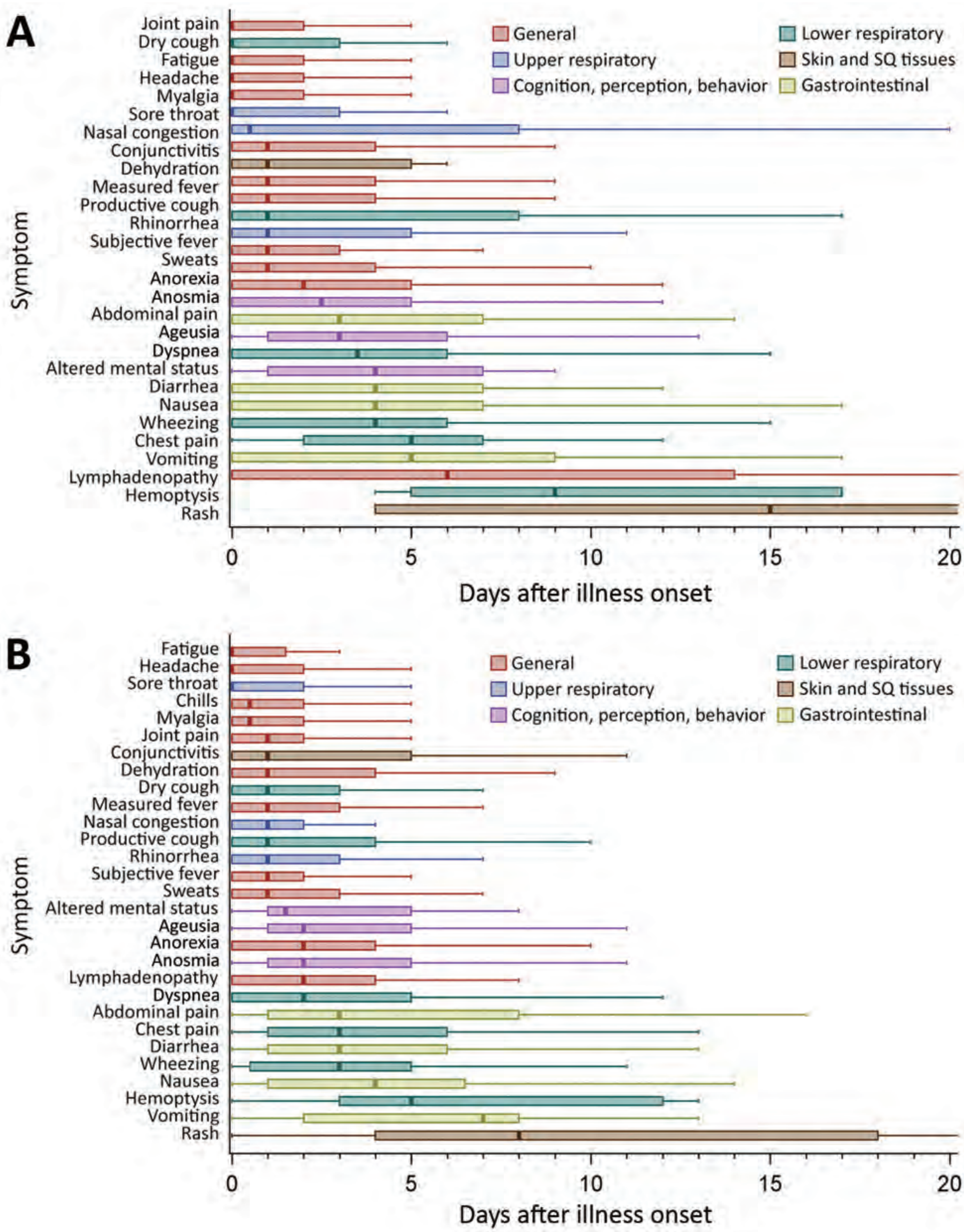


**Figure 2.** Days from coronavirus disease onset to individual symptom onset, by hospitalization status (n = 364 patients), Colorado, March 2020. Symptom progression is shown for hospitalized patients (A) and nonhospitalized patients (B). Lines within boxes indicate median for each symptom, and boxes represent interquartile range. Outliers (defined as >1.5× interquartile range >75th percentile) not shown in figure. SQ, subcutaneous.

likely contribute, such as age, underlying medical conditions, and viral strain. These findings also support the concept that COVID-19 manifests in 1 of 3 general patterns of illness: mild illness primarily consisting of upper respiratory symptoms, non–life-threatening pneumonia, and severe pneumonia with acute respiratory distress syndrome (*32*).

We found the most commonly reported initial symptoms for COVID-19 patients were cough or fever. These symptoms were also the most common initial symptoms reported by 48 healthcare personnel with COVID-19 in King County in Washington state (*33*). However, no single symptom was reported by more than one quarter of our participating patients as their initial symptom, suggesting the absence of a hallmark symptom at the beginning of disease.

In regards to symptom progression over the course of illness, upper respiratory symptoms, general systemic symptoms, and cough were reported to have occurred early in illness. These symptoms were followed by other lower respiratory symptoms, altered mental status, anosmia, ageusia, and, finally, gastrointestinal symptoms and rash. The timing of anosmia and ageusia in our analysis is similar to previous reports, which found a mean of 3 days from illness onset to anosmia and ageusia in hospitalized and nonhospitalized COVID-19 patients (*34*,*35*). The later occurrence of gastrointestinal symptoms and rash among our participants could be related directly to the virus, linked to interventions (e.g., use of antimicrobial drugs or other medications), or, in the case of gastrointestinal symptoms, related to hypoxia (*36*–*39*). We identified an overall progression of reported symptoms that is consistent with, although more detailed than, a recent metaanalysis of symptoms among persons with COVID-19 (*20*). In addition, symptom onset and progression in this investigation is similar to what has been described for severe acute respiratory syndrome (SARS), caused by SARS-CoV (*40*,*41*). SARS has been described to manifest with an initial phase of fever, cough, sore throat, and myalgia, followed by dyspnea, hypoxia, and diarrhea, and, in some patients, a final phase of acute respiratory distress syndrome (*42*).

In our investigation, the median duration of most symptoms was ≤10 days. However, estimated duration of illness was >1 month in hospitalized patients, twice as long as in nonhospitalized patients; this pattern was also observed for many individual symptoms. Duration of individual symptoms experienced by nonhospitalized patients was slightly longer in our analysis than in 2 previous reports of nonhospitalized COVID-19 patients; however, the symptoms with the longest duration were similar (cough, anosmia, and ageusia) and methods differed slightly between analyses (*24*,*43*). A report on symptoms experienced by nonhospitalized COVID-19 patients in Utah found a median duration of symptoms of 16 days, which is similar to our findings for nonhospitalized patients (*22*). Published data on COVID-19 symptoms in 2 studies of hospitalized patients in China found that fever duration was substantially longer in those with more severe disease (*18*,*44*).

Our investigation has some limitations. First, interviews were conducted several weeks after illness onset, which enabled accurate classification of patients by hospitalization status and data collection on all symptoms and their duration (*45*). However, this timing might result in incomplete recall and recall bias, which could affect the accuracy of reported symptoms and their timing, particularly among hospitalized patients, who might be more likely to remember more severe symptoms (*46*). Future prospective studies using methods such as symptom diaries or serial interviews could reduce recall bias. Second, a higher proportion of proxies were interviewed on behalf of hospitalized case-patients. However, when proxies were removed from the reduced multivariable model, the ORs were relatively stable, indicating the proxies did not affect the association of symptoms with hospitalization. In addition, although clinical manifestation of viral respiratory diseases can differ by age, we were unable to compare symptoms across different age groups because of the high percentage of proxy interviews for patients ≥65 years of age, which resulted in fewer symptoms being reported in that age group. Our findings might not apply to all populations because of differences in age distribution, disease severity, testing practices, and socioeconomic status. Finally, because symptoms such as seizure and hemoptysis were experienced by a small number of participants, we were limited in our ability to draw conclusions about their duration and associations with hospitalization status.

Overall, in this study, patients with COVID-19 commonly reported fever, cough, or dyspnea. However, other symptoms occurred frequently, less than one quarter of participants reported any 1 individual symptom as their initial symptom, and the frequency of symptoms reported by hospitalized and nonhospitalized patients was notably different. A person's symptoms should be considered alongside local disease prevalence and other epidemiologic factors (e.g., age, underlying conditions, and exposures to known and suspected COVID-19 cases) for clinical decision-making, such as testing and differentia diagnosis, and for determining appropriate public health action for persons with potential COVID-19. Clinicians should consider COVID-19 in addition to other common respiratory pathogens in patients with mild or nonspecific symptoms to help mitigate the spread of the disease. Furthermore, public health messaging should continue to encourage social distancing, use of masks, and good hand hygiene for everyone and self-isolation for anyone with potential COVID-19 symptoms.

Members of the Colorado Investigation Team: Alison J. Basile, Alyssa R. Beck, Karen L. Boroughs, Paul L. Burns, Cathy L. Buschmeier, Nathaniel M. Byers, Amanda E. Calvert, Trudy V. Chambers, David T. Dennis, Mary Ellen Fernandez, Katherine T. Ficalora, Kelly A. Fitzpatrick, Shannon Fleck-Derderian, Erik S. Foster, Christin H. Goodman, Garrett Heck, Claire Y.-H. Huang, Amy J. Lambert, Aine Lehane, Jennifer A. Lehman, Kristine Lindell, Nicole P. Lindsey, Sarah E. Maes, Courtney C. Nawrocki, Nancy H. Nay, Kathleen A. Orloski, Lynn Osikowicz, Christina Parise, Lara C. Perinet, Mark A. Pilgard, Jordan A. Powers, María F. Rizzo, Brandy J. Russell, Tracey M. Semcer, Benjamin Skinner, and Melanie Spillane.

### Acknowledgments

The authors thank Sarabeth Mathis for her assistance with database development and the Centers for Disease Control and Prevention (CDC) Emergency Operations Center staff for facilitating deployment of personnel and equipment for this investigation.

R.H. and N.A. received CDC funding through the Emerging Infection Program and Epidemiology and Laboratory Capacity Cooperative Agreement for work related to coronavirus disease. The case investigations, analysis, and manuscript preparation were completed as part of official duties at CDC and Colorado Department of Public Health and Environment. The CDC and Colorado Department of Public Health and Environment staff designed and conducted this investigation; received, managed, analyzed, and interpreted the data; prepared, reviewed, and approved the manuscript; and played a role in the decision to submit the manuscript for publication.

## About the Author

Dr. Vahey is an Epidemic Intelligence Service officer in the Division of Vector-Borne Diseases, National Center for Emerging and Zoonotic Infectious Diseases, Centers for Disease Control and Prevention, Fort Collins, Colorado. Her research interests include infectious disease epidemiology and One Health. Dr. Marshall is an Epidemic Intelligence Service officer in the Communicable Diseases Branch at the Colorado Department of Public Health and Environment in Denver. Her research interests include network science and infectious disease epidemiology.

### References

1. World Health Organization. Coronavirus disease 2019 (COVID-19) situation report—1. Geneva: The Organization; 2020 [cited 2020 Jun 11]. https://www.who.int/docs/default-source/coronaviruse/situation-reports/20200121-sitrep-1-2019-ncov.pdf
2. Coronaviridae Study Group of the International Committee on Taxonomy of Viruses. The species severe acute respiratory syndrome-related coronavirus: classifying 2019-nCoV and naming it SARS-CoV-2. Nat Microbiol. 2020;5:536–44. https://doi.org/10.1038/s41564-020-0695-z
3. Holshue ML, DeBolt C, Lindquist S, Lofy KH, Wiesman J, Bruce H, et al.; Washington State 2019-nCoV Case Investigation Team. First case of 2019 novel coronavirus in the United States. N Engl J Med. 2020;382:929–36. https://doi.org/10.1056/NEJMoa2001191
4. World Health Organization. Coronavirus disease 2019 (COVID-19) situation report—11. Geneva: The Organization; 2020 [cited 2020 Jun 11]. https://www.who.int/docs/default-source/coronaviruse/situation-reports/20200131-sitrep-11-ncov.pdf
5. World Health Organization. Coronavirus disease 2019 (COVID-19) situation report—51. Geneva: The Organization; 2020 [cited 2020 Jun 11]. https://www.who.int/docs/default-source/coronaviruse/situation-reports/20200311-sitrep-51-covid-19.pdf
6. Centers for Disease Control and Prevention. Coronavirus disease 2019 (COVID-19). United States COVID-19 cases and deaths by state [cited 2020 Dec 04]. https://www.cdc.gov/coronavirus/2019-ncov/cases-updates/cases-in-us.html
7. Garg S, Kim L, Whitaker M, O'Halloran A, Cummings C, Holstein R, et al. Hospitalization rates and characteristics of patients hospitalized with laboratory-confirmed coronavirus disease 2019—COVID-NET, 14 states, March 1–30, 2020. MMWR Morb Mortal Wkly Rep. 2020;69:458–64. https://doi.org/10.15585/mmwr.mm6915e3
8. Goyal P, Choi JJ, Pinheiro LC, Schenck EJ, Chen R, Jabri A, et al. Clinical characteristics of Covid-19 in New York City. N Engl J Med. 2020;382:2372–4. https://doi.org/10.1056/NEJMc2010419
9. Guan WJ, Ni ZY, Hu Y, Liang WH, Ou CQ, He JX, et al.; China Medical Treatment Expert Group for Covid-19. Clinical characteristics of coronavirus disease 2019 in China. N Engl J Med. 2020;382:1708–20. https://doi.org/10.1056/NEJMoa2002032
10. Centers for Disease Control and Prevention. Coronavirus disease 2019 (COVID-19). Symptoms of coronavirus [cited 2020 May 28]. https://www.cdc.gov/coronavirus/2019-ncov/symptoms-testing/symptoms.html
11. Beltrán-Corbellini Á, Chico-García JL, Martínez-Poles J, Rodríguez-Jorge F, Natera-Villalba E, Gómez-Corral J, et al. Acute-onset smell and taste disorders in the context of COVID-19: a pilot multicentre polymerase chain reaction based case-control study. Eur J Neurol. 2020 Apr 22 [Epub ahead of print].
12. Wu Z, McGoogan JM. Characteristics of and important lessons from the coronavirus disease 2019 (COVID-19) outbreak in China: summary of a report of 72,314 cases from the Chinese Center for Disease Control and Prevention. JAMA.

2020;323:1239 [Epub ahead of print]. https://doi.org/10.1001/jama.2020.2648 PMID 32091533
13. Harris PA, Taylor R, Thielke R, Payne J, Gonzalez N, Conde JG. Research Electronic Data Capture (REDCap)—a metadata-driven methodology and workflow process for providing translational research informatics support. J Biomed Inform. 2009;42:377–81. https://doi.org/10.1016/j.jbi.2008.08.010
14. Harris PA, Taylor R, Minor BL, Elliott V, Fernandez M, O'Neal L, et al.; REDCap Consortium. The REDCap Consortium: building an international community of software platform partners. J Biomed Inform. 2019;95:103208. https://doi.org/10.1016/j.jbi.2019.103208
15. Bursac Z, Gauss CH, Williams DK, Hosmer DW. Purposeful selection of variables in logistic regression. Source Code Biol Med. 2008;3:17. https://doi.org/10.1186/1751-0473-3-17
16. R Core Team. R: a language and environment for statistical computing. Version 3.6.3 [cited 2020 Jun 15]. http://www.R-project.org
17. Burke RM, Killerby ME, Newton S, Ashworth CE, Berns AL, Brennan S, et al.; Case Investigation Form Working Group. Symptom profiles of a convenience sample of patients with COVID-19-United States, January–April 2020. MMWR Morb Mortal Wkly Rep. 2020;69:904–8. https://doi.org/10.15585/mmwr.mm6928a2
18. Chen J, Qi T, Liu L, Ling Y, Qian Z, Li T, et al. Clinical progression of patients with COVID-19 in Shanghai, China. J Infect. 2020;80:e1–6. https://doi.org/10.1016/j.jinf.2020.03.004
19. Giacomelli A, Pezzati L, Conti F, Bernacchia D, Siano M, Oreni L, et al. Self-reported olfactory and taste disorders in patients with severe acute respiratory coronavirus 2 infection: a cross-sectional study. Clin Infect Dis. 2020;71:889–90. https://doi.org/10.1093/cid/ciaa330
20. Gaythorpe K, Imai N, Cuomo-Dannenburg G, Baguelin M, Bhatia S, Boonyasiri A, et al. Report 8: symptom progression of COVID-19. London: Imperial College London; 2020 [cited 2020 Jul 2]. http://hdl.handle.net/10044/1/77344
21. Grant MC, Geoghegan L, Arbyn M, Mohammed Z, McGuinness L, Clarke EL, et al. The prevalence of symptoms in 24,410 adults infected by the novel coronavirus (SARS-CoV-2; COVID-19): a systematic review and meta-analysis of 148 studies from 9 countries. PLoS One. 2020;15:e0234765. https://doi.org/10.1371/journal.pone.0234765
22. Yousaf AR, Duca LM, Chu V, Reses HE, Fajans M, Rabold EM, et al. A prospective cohort study in non-hospitalized household contacts with SARS-CoV-2 infection: symptom profiles and symptom change over time. Clin Infect Dis. 2020 Jul 28 [Epub ahead of print]. https://doi.org/10.1093/cid/ciaa1072
23. Adorni F, Prinelli F, Bianchi F, Giacomelli A, Pagani G, Bernacchia D, et al. Self-reported symptoms of SARS-CoV-2 infection in a nonhospitalized population in Italy: cross-sectional study of the EPICOVID19 web-based survey. JMIR Public Health Surveill. 2020;6:e21866. https://doi.org/10.2196/21866
24. Bergquist SH, Partin C, Roberts DL, O'Keefe JB, Tong EJ, Zreloff J, et al. Non-hospitalized adults with COVID-19 differ noticeably from hospitalized adults in their demographic, clinical, and social characteristics. SN Compr Clin Med. 2020 Aug 14 [Epub ahead of print].
25. Sierpiński R, Pinkas J, Jankowski M, Zgliczyński WS, Wierzba W, Gujski M, et al. Sex differences in the frequency of gastrointestinal symptoms and olfactory or taste disorders in 1,942 nonhospitalized patients with coronavirus disease 2019 (COVID-19). Pol Arch Intern Med. 2020;130:501–5.
26. Spinato G, Fabbris C, Polesel J, Cazzador D, Borsetto D, Hopkins C, et al. Alterations in smell or taste in mildly symptomatic outpatients with SARS-CoV-2 infection. JAMA. 2020;323:2089–90. https://doi.org/10.1001/jama.2020.6771
27. Nobel YR, Phipps M, Zucker J, Lebwohl B, Wang TC, Sobieszczyk ME, et al. Gastrointestinal symptoms and COVID-19: case-control study from the United States. Gastroenterology. 2020;159:373–375.e2. https://doi.org/10.1053/j.gastro.2020.04.017
28. Pan L, Mu M, Yang P, Sun Y, Wang R, Yan J, et al. Clinical characteristics of COVID-19 patients with digestive symptoms in Hubei, China: a descriptive, cross-sectional, multicenter study. Am J Gastroenterol. 2020;115:766–73. https://doi.org/10.14309/ajg.0000000000000620
29. Jain V, Yuan JM. Predictive symptoms and comorbidities for severe COVID-19 and intensive care unit admission: a systematic review and meta-analysis. Int J Public Health. 2020;65:533–46. https://doi.org/10.1007/s00038-020-01390-7
30. Lechien JR, Chiesa-Estomba CM, Place S, Van Laethem Y, Cabaraux P, Mat Q, et al.; COVID-19 Task Force of YO-IFOS. Clinical and epidemiological characteristics of 1,420 European patients with mild-to-moderate coronavirus disease 2019. J Intern Med. 2020;288:335–44. https://doi.org/10.1111/joim.13089
31. Kim GU, Kim MJ, Ra SH, Lee J, Bae S, Jung J, et al. Clinical characteristics of asymptomatic and symptomatic patients with mild COVID-19. Clin Microbiol Infect. 2020;26:948.e1–3. https://doi.org/10.1016/j.cmi.2020.04.040
32. Heymann DL, Shindo N; WHO Scientific and Technical Advisory Group for Infectious Hazards. COVID-19: what is next for public health? Lancet. 2020;395:542–5. https://doi.org/10.1016/S0140-6736(20)30374-3
33. Chow EJ, Schwartz NG, Tobolowsky FA, Zacks RLT, Huntington-Frazier M, Reddy SC, et al. Symptom screening at illness onset of health care personnel with SARS-CoV-2 infection in King County, Washington. JAMA. 2020;323:2087–9. https://doi.org/10.1001/jama.2020.6637
34. Speth MM, Singer-Cornelius T, Oberle M, Gengler I, Brockmeier SJ, Sedaghat AR. Olfactory dysfunction and dinonasal dymptomatology in COVID-19: prevalence, severity, timing, and associated characteristics. Otolaryngol Head Neck Surg. 2020;163:114–20. https://doi.org/10.1177/0194599820929185
35. Paderno A, Mattavelli D, Rampinelli V, Grammatica A, Raffetti E, Tomasoni M, et al. Olfactory and gustatory outcomes in COVID-19: a prospective evaluation in nonhospitalized subjects. Otolaryngol Head Neck Surg. 2020 Jun 20 [Epub ahead of print].
36. Criado PR, Abdalla BMZ, de Assis IC, van Blarcum de Graaff Mello C, Caputo GC, Vieira IC. Are the cutaneous manifestations during or due to SARS-CoV-2 infection/COVID-19 frequent or not? Revision of possible pathophysiologic mechanisms. Inflamm Res. 2020;69:745–56. https://doi.org/10.1007/s00011-020-01370-w
37. Fruehauf H, Vavricka SR, Lutz TA, Gassmann M, Wojtal KA, Erb A, et al. Evaluation of acute mountain sickness by unsedated transnasal esophagogastroduodenoscopy at high altitude. Clin Gastroenterol Hepatol. 2020;18:2218–2225.e2. https://doi.org/10.1016/j.cgh.2019.11.036
38. Galván Casas C, Català A, Carretero Hernández G, Rodríguez-Jiménez P, Fernández-Nieto D, Rodríguez-Villa Lario A, et al. Classification of the cutaneous manifestations of COVID-19: a rapid prospective nationwide consensus study in Spain with 375 cases. Br J Dermatol. 2020;183:71–7. https://doi.org/10.1111/bjd.19163

39. Cao B, Wang Y, Wen D, Liu W, Wang J, Fan G, et al. A trial of lopinavir-ritonavir in adults hospitalized with severe Covid-19. N Engl J Med. 2020;382:1787–99. https://doi.org/10.1056/NEJMoa2001282
40. Weiss SR, Leibowitz JL. Coronavirus pathogenesis. Adv Virus Res. 2011;81:85–164. https://doi.org/10.1016/B978-0-12-385885-6.00009-2
41. Cheng VC, Lau SK, Woo PC, Yuen KY. Severe acute respiratory syndrome coronavirus as an agent of emerging and reemerging infection. Clin Microbiol Rev. 2007;20:660–94. https://doi.org/10.1128/CMR.00023-07
42. Peiris JS, Chu CM, Cheng VC, Chan KS, Hung IFN, Poon LLM, et al.; HKU/UCH SARS Study Group. Clinical progression and viral load in a community outbreak of coronavirus-associated SARS pneumonia: a prospective study. Lancet. 2003;361:1767–72. https://doi.org/10.1016/S0140-6736(03)13412-5
43. Tenforde MW, Kim SS, Lindsell CJ, Billig Rose E, Shapiro NI, Files DC, et al.; IVY Network Investigators; CDC COVID-19 Response Team; IVY Network Investigators. Symptom duration and risk factors for delayed return to usual health among outpatients with COVID-19 in a multistate health care systems network—United States, March–June 2020. MMWR Morb Mortal Wkly Rep. 2020;69:993–8. https://doi.org/10.15585/mmwr.mm6930e1
44. Zhou F, Yu T, Du R, Fan G, Liu Y, Liu Z, et al. Clinical course and risk factors for mortality of adult inpatients with COVID-19 in Wuhan, China: a retrospective cohort study. Lancet. 2020;395:1054–62. https://doi.org/10.1016/S0140-6736(20)30566-3
45. Giorgi Rossi P, Marino M, Formisano D, Venturelli F, Vicentini M, Grilli R; Reggio Emilia COVID-19 Working Group. Characteristics and outcomes of a cohort of COVID-19 patients in the Province of Reggio Emilia, Italy. PLoS One. 2020;15:e0238281. https://doi.org/10.1371/journal.pone.0238281
46. Van den Bergh O, Walentynowicz M. Accuracy and bias in retrospective symptom reporting. Curr Opin Psychiatry. 2016;29:302–8. https://doi.org/10.1097/YCO.0000000000000267


Address for correspondence: Grace M. Vahey, Centers for Disease Control and Prevention, 3156 Rampart Rd, Fort Collins, CO 80521, USA; email: gvahey@cdc.gov

# Addressing COVID-19 Misinformation on Social Media Preemptively and Responsively

Emily K. Vraga, Leticia Bode

Efforts to address misinformation on social media have special urgency with the emergence of coronavirus disease (COVID-19). In one effort, the World Health Organization (WHO) designed and publicized shareable infographics to debunk coronavirus myths. We used an experiment to test the efficacy of these infographics, depending on placement and source. We found that exposure to a corrective graphic on social media reduced misperceptions about the science of 1 false COVID-19 prevention strategy but did not affect misperceptions about prevention of COVID-19. Lowered misperceptions about the science persisted ≥1 week later. These effects were consistent when the graphic was shared by the World Health Organization or by an anonymous Facebook user and when the graphics were shared preemptively or in response to misinformation. Health organizations can and should create and promote shareable graphics to improve public knowledge.

The uncertainty around the emergence of severe acute respiratory syndrome coronavirus 2, a novel coronavirus that causes coronavirus disease (COVID-19), has led to the rapid and widespread diffusion of misinformation about the virus, its origins, and effective prevention and treatment strategies (*1*,*2*). Misinformation is not a new problem, but it poses particular challenges for infectious disease management when public acceptance is required for prevention behaviors such as social distancing or wearing a mask.

As part of the effort to promote good information over misinformation, the World Health Organization (WHO) has created and publicized shareable infographics ("mythbusters") that debunk specific myths about COVID-19 (*3*). Research regarding the efficacy of health organization websites designed to debunk misinformation has yielded mixed results. Material from the Centers for Disease Control and Prevention (CDC) regarding the influenza vaccine successfully reduced misperceptions that the vaccine can cause influenza or is unsafe but also reduced intentions to get the vaccine among those concerned about its side effects (*4*). Likewise, WHO material debunking Zika virus rumors did not affect most targeted misperceptions and also reduced the accuracy of related beliefs about Zika virus (*5*). These examples reinforce concern that repeating false information, even to correct it, can strengthen belief in the myths (*6*,*7*).

In this study, we considered the effectiveness of sharing WHO's myth correction graphics on social media specifically. This project differed from previous research in 2 ways. First, the graphic used in every correction was clearly labeled as coming from WHO, which may boost effectiveness compared with research that did not prominently display the source of the corrective material (*4*,*5*). Second, we considered exposure to someone sharing a specific correction graphic on social media, rather than to website material more generally. Previous research has found that observational correction, which occurs when persons see misinformation being corrected on social media and update their own attitudes in response, is effective for emerging infectious disease topics such as Zika virus (*8*,*9*) and for infectious diseases such as influenza (*10*). We aimed to determine the effectiveness of social media sharing of a graphic that debunks 2 related coronavirus myths.

## Methods

### Study Design

In this study we considered the effectiveness of sharing a WHO graphic (on social media) that debunks 2 related coronavirus myths: that taking a hot bath both raises body temperature and prevents coronavirus infection (Figure). Scientific evidence suggests that hot baths can minimally affect body temperature; studies have found a change of roughly 0.5°C –1.0°C in body

Author affiliations: University of Minnesota, Minneapolis, Minnesota, USA (E.K. Vraga); Georgetown University, Washington, DC, USA (L. Bode)

DOI: https://doi.org/10.3201/eid2702.203139

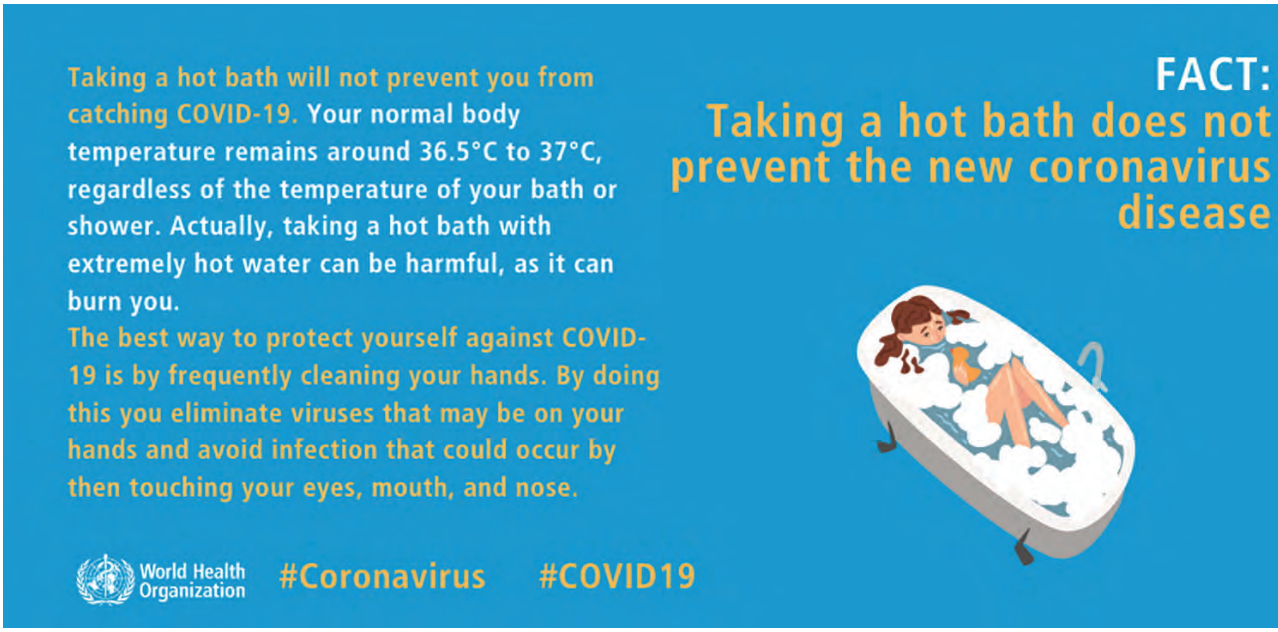


**Figure.** Original World Health Organization myth buster graphic used in study of addressing COVID-19 misinformation on social media. COVID-19, coronavirus disease.

temperature (*11*,*12*). Temperatures needed to deactivate coronavirus are typically >56°C (*13*–*15*), which exceed safe bath temperatures; scalding is likely within 10 minutes at 48°C (*16*). In other words, this graphic explains the science for why hot baths do not prevent COVID-19 and directly disputes the prevention efficacy of baths. The graphic follows many best practices for combating misinformation: it is fact-based, colorful, simple, and easy to understand; focuses on the fact rather than the myth; and includes a label signaling that it comes from an expert source (*7*,*9*,*10*). These aspects fulfill many of the 5 Cs of correction: is consensus based, includes corroborating evidence, and is consistent, coherent, and credible (*6*). Addressing the science behind why hot baths do not prevent COVID-19 infection also corroborates the argument with a science-based alternative explanation shown to boost correction effectiveness (*6*,*7*,*17*). Therefore, we expected that exposure to a post containing this graphic would reduce the 2 misperceptions among persons targeted by the graphic as compared with persons who did not see any information on the topic.

Such a graphic might be shared in multiple ways, which we also tested. The first factor manipulates whether the graphic was shared preemptively on a social media feed, compared with whether it was shared in response to misinformation on the topic (we refer to this as placement). When offered preemptively, a user shares the graphic as a social media post without addressing the misinformation directly. In this case, it might function like a fact check, addressing an inaccurate claim made elsewhere but not directly linking to that claim on the social media platform (*18*–*20*). Alternatively, the graphic could be shared in response to someone posting misinformation. These responsive corrections are a relatively common behavior (*21*) and reduce belief in misinformation among other social media users who witness the correction (*8*,*9*,*22*). Given the relative dearth of research in this space, we explored whether preemptive or responsive posting strategies are more effective in reducing misperceptions.

The second factor manipulates who shares the information. Previous research on correction has emphasized the ability of an expert source like WHO to address misinformation (*7*,*22*,*23*) but offers mixed evidence about the effectiveness of a single user in correcting misinformation on social media (*22*,*24*). Therefore, we expect that a graphic shared by WHO will more effectively reduce misperceptions than the same graphic (still with WHO branding) shared by an unknown Facebook user.

In addition, we explored the combination of these 2 elements: who shared a graphic and whether it was shared in response or preemptively. Although it is not clear how these 2 elements interact, several possibilities seem plausible. For instance, it might seem strange to see a powerful organization like WHO responding directly to misinformation, making this form of correction less effective for WHO but not for users. Alternatively, research suggests that a user debunking a myth preemptively using facts might be less effective than when sharing a correction after misinformation (*24*), but we do not have research to determine whether this pattern should similarly hold for organizations. Although research does not clearly specify what to expect, the interaction between source and type of sharing is worth exploring.

Finally, not enough correction research has been done to investigate the enduring effect of exposure to misinformation and its correction. Some research suggests that corrections fade over time, and the myth could actually be reinforced through an illusory truth effect of seeing misinformation repeated (*6*,*7*). Alternatively, if the correction follows best practices by emphasizing facts and providing an alternative explanation, as we believe the WHO graphic does, lowered misperceptions may endure over time. Therefore, we tested whether the effects of correction endure over 1 week.

### Experimental Design

An experimental design enabled us to best consider the effects of who corrected and whether the correction was in response to misinformation or independent of it. This experiment received approval from the Institutional Review Board at the University of Minnesota on April 27, 2020.

We fielded a survey experiment to 1,596 participants during May 4–5, 2020 (wave 1) using Amazon's Mechanical Turk service (https://www.mturk.com). Of these, 1,453 were willing to continue participation and 1,419 passed an attention check in the first wave of the study; these participants were contacted 1 week later (on May 12, with a recontact on May 14) for a follow-up survey (wave 2). A total of 1,122 participants (79%) completed wave 2 an average of 7.5 days later (mean 7.54, SD 0.75).

Each participant viewed a screenshot of a Facebook feed and was asked to read it as if it were on their own feed (Appendix 1, https://wwwnc.cdc.gov/EID/article/27/2/20-3139-App1.pdf). The experiment consisted of 6 experimental conditions (Appendix 2, https://wwwnc.cdc.gov/EID/article/27/2/20-3139-App2.pdf): a pure control condition, a misinformation-only condition, and 4 correction conditions manipulated in a crossed factorial design with the 2 factors we described earlier: placement (preemptive versus responsive) and source (WHO versus user).

In the pure control condition, participants viewed 5 control posts on the simulated feed. In the misinformation-only condition, they viewed the same 5 posts, with the addition of a misinformation post: a status posted by a user saying "This is such an easy thing to do! Take a hot bath to keep yourself healthy and protect you from coronavirus!" on a bright pink background.

For all correction conditions, participants viewed the same WHO infographic, which prominently labels the source, to isolate the effects of who is sharing the graphic rather than the graphic itself. Those who viewed the preemptive correction saw the correction infographic as the second post in the feed, posted either by WHO or by a social media user but with no misinformation post as part of the feed. Those who viewed the responsive correction saw the misinformation post described earlier, with the corrective graphic posted in response, either by a user or by WHO in the form of a WHO "info bot." Although no such bot exists as far as we know, WHO and Facebook have partnered to offer a Facebook messenger bot to answer user questions about coronavirus (*25*), so this sort of correction is plausible, if not currently being deployed. Moreover, a bot offers a scalable and realistic responsive mechanism, rather than assuming that WHO would directly respond to individual Facebook users on their official feeds.

After exposure to the simulated Facebook feed in wave 1, participants answered questions regarding their beliefs regarding the myths targeted by the WHO graphic to measure misperceptions about body temperature and COVID-19 prevention (Appendix 3, https://wwwnc.cdc.gov/EID/article/27/2/20-3139-App3.pdf). These questions were replicated in wave 2 of the study.

### Sample Characteristics

Of the 1,596 participants who completed our initial survey, participants skewed male (62.9%) and highly educated (72% had a bachelor's degree or higher). Participants averaged 37 years of age (mean 36.94 years, SD 11.31 years), were relatively diverse in terms of race and ethnicity (18.5% African-American, 7.9% Asian-American, 70.6% White; 21.3% considered themselves Hispanic or Latino) and income (median $50,000–$75,000) and leaned Democratic (5-point scale, mean 3.73, SD 2.00) and liberal (5-point scale, mean 3.69, SD 1.93). These characteristics were consistent among participants who completed the second wave of the study (Appendix 2 Table 1).

### Statistical Analysis

We performed 2 sets of analyses based on our preregistration (*26*). First, we compared each of the experimental conditions to the pure control condition using linear regression to determine whether the corrections reduced misperceptions as compared with baseline beliefs (absent any information regarding hot baths or COVID-19). We replicated these analyses for wave 2. Second, we isolated the effects of source and placement using a regression approach (not preregistered) excluding both the control and misinformation-only conditions, and entering 2 factors (placement and source) as well as the interaction between the two.

## Results

### Wave 1

First, we tested the effects of correction on misperceptions related to the effects of a hot bath on body temperature and COVID-19 prevention for wave 1. We limited these regression analyses to the 1,543 persons who passed a premanipulation attention check (Appendix 4, https://wwwnc.cdc.gov/EID/article/27/2/20-3139-App4.pdf). Exposure to the WHO graphic in any condition reduced misperceptions that a hot bath will raise body temperature as compared with the control, but had no effects on misperceptions that a hot bath will prevent COVID-19 infection (Table 1). When comparing the types of correction to each other, we found no differences by either source or placement, nor by the interaction between the 2 categories (Table 2). In other words, corrections were equally effective for body temperature misperceptions (and ineffective for COVID-19 prevention misperceptions) whether they came from a user or from WHO and when they were preemptive as well as responsive.

### Wave 2

We replicated these analyses with the 1,110 participants who completed the follow-up survey and passed the attention check for wave 2 (12 participants failed the attention check in wave 2), controlling for the amount of time between taking the 2 waves of the survey. We found that exposure to the WHO preemptive, WHO responsive, or user responsive corrections all produced lower misperceptions than the control condition at wave 2 for body temperature misperceptions (Table 3). We also found that those exposed to the WHO responsive correction had significantly lower COVID-19 prevention misperceptions 1 week later than those in the control condition; results showed an average decline of 11% in COVID-19 prevention misperceptions from the control to the WHO responsive correction. However, the overall model predicting COVID-19 misperceptions was not significant, meaning that there were no differences in means averaged across the 6 experimental conditions even though there was a significant difference in directly comparing the WHO responsive correction to control condition, so this result must be interpreted with caution. We again found no significant differences in either type of misperceptions based on the source of the graphic (WHO versus Facebook user) or whether it was offered preemptively or responsively (Table 4).

## Discussion

Efforts to address misinformation on social media have taken on special urgency with the emergence of COVID-19. Mitigating the risks associated with COVID-19 requires sustained public action, so misinformation that promotes false preventives or cures can hinder necessary behaviors to reduce the spread of the disease. In this study, we tested whether sharing graphics from WHO designed to address COVID-19 misinformation can reduce misperceptions. Our results suggest that although these graphics do not affect all misperceptions, reductions in misperceptions that do occur persist over time.

Notably, exposure to the WHO graphic in any form reduced immediate misperceptions about the science of a false preventive for COVID-19 (that a hot bath can raise body temperature), and this reduction was maintained for at least 1 week for 3 of the 4 correction conditions. This finding suggests that understanding of

**Table 1.** Comparing participants in correction conditions to control condition for wave 1 using regression analysis in study of addressing COVID-19 misinformation on social media*

| | Body temperature | | COVID-19 prevention | |
|---|---|---|---|---|
| Condition | Beta | SE | Beta | SE |
| Pure control [reference] | – | – | – | – |
| Misinformation only | –0.06 | 0.08 | –0.13 | 0.09 |
| WHO preemptive | –0.40‡ | 0.09 | –0.12 | 0.09 |
| User preemptive | –0.26† | 0.08 | –0.10 | 0.09 |
| WHO responsive | –0.46‡ | 0.08 | –0.14 | 0.09 |
| User responsive | –0.30‡ | 0.08 | –0.05 | 0.09 |
| Adjusted $R^2$ | 0.028‡ | | 0.000 | |

*Adjusted $R^2$ indicates the variance explained by the overall model. COVID-19, coronavirus disease; WHO, World Health Organization.
†p<0.01.
‡p<0.001.

**Table 2.** Comparing participants among the 4 correction conditions for wave 1 using regression analysis in study of addressing COVID-19 misinformation on social media*

| | Body temperature | | COVID-19 prevention | |
|---|---|---|---|---|
| Condition | Beta | SE | Beta | SE |
| WHO (vs. user) | –0.13 | 0.11 | –0.03 | 0.11 |
| Responsive (vs. preemptive) | –0.04 | 0.11 | 0.05 | 0.11 |
| Interaction | –0.03 | 0.15 | –0.06 | 0.16 |
| Adjusted $R^2$ | 0.002 | | 0.000 | |

*Adjusted $R^2$ indicates the variance explained by the overall model. COVID-19, coronavirus disease; WHO, World Health Organization.

the science behind why hot baths do not prevent COVID-19 prevention does not deteriorate rapidly.

Although these effects on reducing science-related misperceptions show the promise of the WHO graphics as myth busters on social media, we did not see a parallel reduction in the related misperceptions regarding prevention efficacy (that a hot bath will prevent COVID-19 infection). We offer several post hoc explanations for these findings. First, we suspect that a floor effect may partially explain these null effects; even in the control condition in wave 1, participants were largely well informed, rating the argument that a hot bath can prevent COVID-19 infection as at least probably false (55.8% had an average score $\leq$2 or less on a scale of 1, definitely false, to 5, definitely true). In contrast, only 17.5% believed that the claim that a hot bath can raise body temperature was probably false, offering more leverage to change beliefs. Second, motivated reasoning may make persons more resistant to updating beliefs as issues around COVID-19 and the WHO become more politicized in the United States (*27*); this motivated reasoning is likely less operant for the science of why such prevention is not effective. Third, persons may have thought that the science regarding hot baths and their effects on body temperature is better established given longstanding research (*11*,*12*), boosting confidence in the validity of the correction. Given high levels of scientific as well as public uncertainty regarding COVID-19 (*28*), the public may have been less convinced regarding the scientific evidence that a hot bath does not prevent COVID-19.

Finally, the fact that a hot bath does not raise body temperature may not be the only (or even the most prominent) reason that persons may believe that taking a hot bath decreases the risk of COVID-19 infection. A supplemental analysis (Appendix 5 Table 1, https://wwwnc.cdc.gov/EID/article/27/2/20-3139-App5.pdf) provides some evidence for this explanation. In the pure control condition, the correlation between misperceptions that a hot bath raises body temperature and a hot bath can prevent COVID-19 is not significant (Pearson's correlation coefficient $r = 0.06$; p = 0.16). In the misinformation-only condition, the correlation is not significantly stronger than in the control condition (p = 0.27). However, for both WHO correction conditions, the correlation is significantly stronger than both the pure control and misinformation conditions ($p<0.05$). This preliminary evidence suggests that the correction, especially when shared by WHO, helps participants mentally link the science claim and the prevention claim; however, this explanation accounts for, at most, 18% of variance in COVID-19 prevention beliefs. Therefore, the explanation for why hot baths do not prevent COVID-19 is not the only factor in persons' beliefs about prevention efficacy.

These effects were consistent whether the graphic was shared by WHO itself or by another user. We suspect the similar effects between users and WHO, in contrast to earlier research suggesting experts were more effective than users (*22*,*23*), may result from the prominent labeling of WHO within the graphic itself, boosting the credibility of the post. Therefore,

**Table 3.** Comparing participants in correction conditions to control condition for wave 2 using regression analysis in study of addressing COVID-19 misinformation on social media*

| | Body temperature | | COVID-19 prevention | |
|---|---|---|---|---|
| Condition | Beta | SE | Beta | SE |
| Time gap | 0.05 | 0.04 | –0.01 | 0.04 |
| Pure control [reference] | – | – | – | – |
| Misinformation only | –0.09 | 0.10 | –0.20 | 0.10 |
| WHO preemptive | –0.29† | 0.11 | –0.13 | 0.11 |
| User preemptive | –0.08 | 0.11 | –0.09 | 0.10 |
| WHO responsive | –0.35† | 0.11 | –0.22‡ | 0.10 |
| User responsive | –0.21‡ | 0.11 | –0.10 | 0.11 |
| Adjusted $R^2$ | 0.010† | | 0.001 | |

*Adjusted $R^2$ indicates the variance explained by the overall model. COVID-19, coronavirus disease; WHO, World Health Organization.
†$p<0.01$.
‡$p<0.05$.

**Table 4.** Comparing participants among the 4 correction conditions for wave 2 using regression analysis in study of addressing COVID-19 misinformation on social media*

| | Body temperature | | COVID-19 prevention | |
|---|---|---|---|---|
| Condition | Beta | SE | Beta | SE |
| Gap | 0.09 | 0.06 | –0.01 | 0.06 |
| WHO (vs. user) | –0.21 | 0.13 | –0.05 | 0.13 |
| Responsive (vs. preemptive) | –0.14 | 0.13 | –0.01 | 0.13 |
| Interaction | 0.08 | 0.19 | –0.07 | 0.18 |
| Adjusted $R^2$ | 0.006 | | 0.000 | |

*Adjusted $R^2$ indicates the variance explained by the overall model. COVID-19, coronavirus disease; WHO, World Health Organization.

mobilizing users to share WHO's graphics may produce similar effects in reducing misperceptions.

We found limited evidence that preemptive corrections differ in their effectiveness from reactive corrections. Preemptive and responsive corrections are equally effective when considering whether hot baths affect body temperature, both immediately and over time. Likewise, both are unsuccessful in affecting misperceptions about the efficacy of hot baths to prevent COVID-19 infection immediately after exposure to the correction. If preemptive corrections are effective in reducing misperceptions for (some) myths, persons need not wait until seeing someone share misinformation but can share the posts created by official expert organizations to address misperceptions in society at large. Thus, more attention is needed to find ways to motivate persons to share those types of corrections on their feeds.

However, the reactive correction addresses both the prevention efficacy of a hot bath (which is raised by the misinformation post) and the science behind this explanation, which is not addressed in the misinformation post. If the misinformation had also offered an explanation for why a hot bath supposedly reduces COVID-19 risk through raising body temperature, perhaps a reactive correction would be more effective. Although research suggests that false cures and preventives are a major subset of COVID-19 misinformation (*2*), these studies do not elaborate on whether the misinformation contains false claims about the science behind the myth. We suspect that providing false explanations is a subset of misinformation claims and therefore chose to have the misinformation post include only the COVID-19 prevention myth to enhance external validity. Best practices for correction suggest that including an alternative explanation and corroborating evidence enhances the power of corrections (*6*,*7*,*17*). Furthermore, emerging research suggests that correcting a related myth not raised in the misinformation can reduce misperceptions on that related myth, serving as an alternative form of preemptive correction (*29*).

We did find 1 case in which a responsive correction from WHO may be more effective than the other corrections: exposure to the WHO responsive condition reduces misperceptions that a hot bath can prevent COVID-19 infection as compared with the control condition 1 week later, although this result must be interpreted with caution given the insignificance of the model overall and the limited amount of variance explained. If this result holds, it could be that the WHO responsive condition is the most memorable, and therefore had the most lasting effect on misperceptions, which future research should test.

We also found that both body temperature and COVID-19 prevention misperceptions were lower in wave 2 than in wave 1 for both the control and misinformation conditions (Appendix 5 Table 2). We suspect that the debriefing that all participants viewed at the end of wave 1 of the study, which included the WHO graphic and explained the myth, functioned as a correction itself (as intended to reduce potential misperceptions). Therefore, it is noteworthy that some correction conditions reduced hot bath misperceptions even further in wave 2 compared with the control, which reinforces the value of multiple corrections (*7*,*22*).

This study's limitations suggest caution in interpreting our findings. First, we relied on a diverse but unrepresentative sample of the US public, most notably skewing educated and male. Future research should explore these effects among a representative sample and samples outside the United States, including countries where the worst of the pandemic has passed and ones that are struggling to contain new outbreaks, to examine how these contexts affect the relationships we observed here. Second, although our study suggests that the WHO graphics have potential given their effects on body temperature misperceptions, low levels of initial belief that hot baths can prevent COVID-19 limited our ability to perceive potential effects on prevention efficacy. Similarly, the post promoting misinformation about hot baths preventing COVID-19 was largely not persuasive in generating misperceptions. Future research should consider efforts to debunk more prominent or plausible COVID-19 myths. Third, we selected a myth with little partisan divide; we cannot speak to whether these graphics would be effective for politically polarized myths (*11*). Fourth, the effect sizes explained were relatively small, so corrections should be deployed as part of a larger health communication strategy for promoting accurate COVID-19 information.

Despite these limitations, this study offers several practical and theoretical advancements. First, we found little evidence of a backfire effect in promoting misperceptions of sharing the WHO's infographics on social media. This finding not only fits with increasing evidence about the rarity of backfire effects (*30*) but is also reassuring that sharing the graphics at least does no harm. Second, we find that preemptively sharing these graphics can be effective. Users and organizations can debunk misinformation circulating in society by sharing high-quality information on social media emphasizing the facts without waiting to see it shared directly in their feeds, which expands the opportunities for observational correction to occur. Third, we found that a WHO bot that directly responds to misinformation may be a particularly effective technique. Partnerships with platforms may enable these automated responses to prominent myths, furthering the reach of expert organizations. Creating easily shared graphics that promote facts in spaces in which misinformation abounds appears promising as part of a broader strategy to enable more efficient and effective corrections on social media.

Funding for this project was provided by the University of Minnesota and Georgetown University.

## About the Authors

Dr. Vraga is an associate professor at the Hubbard School of Journalism and Mass Communication at the University of Minnesota, where she holds the Don and Carole Larson Professorship in Health Communication. Her research tests methods to correct health misinformation on social media, to limit biased processing of news messages, and to encourage attention to more diverse content online.

Dr. Bode is a Provost's Distinguished Associate Professor in the Communication, Culture, and Technology master's program at Georgetown University. She researches the intersection of communication, technology, and political behavior, emphasizing the role communication and information technologies may play in the acquisition, use, effects, and implications of political information and misinformation.

## References


1. Starbird K, Spiro E, West J. This covid-19 misinformation went viral. Here's what we learned. 2020 May 8 [cited 2020 Jun 8]. https://www.washingtonpost.com/politics/2020/05/08/this-covid-19-misinformation-went-viral-heres-what-we-learned/
2. Brennen JS, Simon FM, Howard PN, Nielsen RK. Types, sources, and claims of COVID-19 misinformation. Reuters Institute. 2020 [cited 2020 Apr 15]. http://www.primaonline.it/wp-content/uploads/2020/04/COVID-19_reuters.pdf
3. World Health Organization. Coronavirus disease (COVID-19) advice for the public: myth busters. 2020 [cited 2020 Apr 2]. https://www.who.int/emergencies/diseases/novel-coronavirus-2019/advice-for-public/myth-busters
4. Nyhan B, Reifler J. Does correcting myths about the flu vaccine work? An experimental evaluation of the effects of corrective information. Vaccine. 2015;33:459–64. https://doi.org/10.1016/j.vaccine.2014.11.017
5. Carey JM, Chi V, Flynn DJ, Nyhan B, Zeitzoff T. The effects of corrective information about disease epidemics and outbreaks: evidence from Zika and yellow fever in Brazil. Sci Adv. 2020;6:eaaw7449. https://doi.org/10.1126/sciadv.aaw7449
6. Schwarz N, Newman E, Leach W. Making the truth stick and the myths fade: lessons from cognitive psychology. Behav Sci Policy. 2016;2:85–95. https://doi.org/10.1353/bsp.2016.0009
7. Lewandowsky S, Ecker UK, Seifert CM, Schwarz N, Cook J. Misinformation and its correction: continued influence and successful debiasing. Psychol Sci Public Interest. 2012;13:106–31. https://doi.org/10.1177/1529100612451018
8. Bode L, Vraga EK. See something, say something: correction of global health misinformation on social media. Health Commun. 2018;33:1131–40. https://doi.org/10.1080/10410236.2017.1331312
9. Vraga EK, Bode L. I do not believe you: how providing a source corrects health misperceptions across social media platforms. Inf Commun Soc. 2018;21:1337–53. https://doi.org/10.1080/1369118X.2017.1313883
10. Vraga EK, Bode L, Tully M. Creating news literacy messages to enhance expert corrections of misinformation on Twitter. Commun Res. 2020 Jan 30 [Epub ahead of print]. https://doi.org/10.1177/0093650219898094
11. Dorsey CM, Teicher MH, Cohen-Zion M, Stefanovic L, Satlin A, Tartarini W, et al. Core body temperature and sleep of older female insomniacs before and after passive body heating. Sleep. 1999;22:891–8. https://doi.org/10.1093/sleep/22.7.891
12. Dorsey CM, Lukas SE, Teicher MH, Harper D, Winkelman JW, Cunningham SL, et al. Effects of passive body heating on the sleep of older female insomniacs. J Geriatr Psychiatry Neurol. 1996;9:83–90. https://doi.org/10.1177/089198879600900203
13. Duan SM, Zhao XS, Wen RF, Huang JJ, Pi GH, Zhang SX, et al.; SARS Research Team. Stability of SARS coronavirus in human specimens and environment and its sensitivity to heating and UV irradiation. Biomed Environ Sci. 2003;16:246–55.
14. Darnell ME, Subbarao K, Feinstone SM, Taylor DR. Inactivation of the coronavirus that induces severe acute respiratory syndrome, SARS-CoV. J Virol Methods. 2004;121:85–91. https://doi.org/10.1016/j.jviromet.2004.06.006
15. Chan KH, Sridhar S, Zhang RR, Chu H, Fung AY, Chan G, et al. Factors affecting stability and infectivity of SARS-CoV-2. J Hosp Infect. 2020;106:226–31. https://doi.org/10.1016/j.jhin.2020.07.009
16. Shields WC, McDonald E, Frattaroli S, Perry EC, Zhu J, Gielen AC. Still too hot: examination of water temperature and water heater characteristics 24 years after manufacturers adopt voluntary temperature setting. J Burn Care Res. 2013;34:281–7. https://doi.org/10.1097/BCR.0b013e31827e645f

17. Walter N, Murphy ST. How to unring the bell: a meta-analytic approach to correction of misinformation. Commun Monogr. 2018;85:423–41. https://doi.org/10.1080/03637751.2018.1467564
18. Amazeen MA, Thorson E, Muddiman A, Graves L. Correcting political and consumer misperceptions: the effectiveness and effects of rating scale versus contextual correction formats. Journalism Mass Commun Q. 2018;95:28–48. https://doi.org/10.1177/1077699016678186
19. Hameleers M, van der Meer TGLA. Misinformation and polarization in a high-choice media environment: how effective are political fact-checkers? Communic Res. 2020;47:227–50. https://doi.org/10.1177/0093650218819671
20. Walter N, Cohen J, Holbert RL, Morag Y. Fact-checking: a meta-analysis of what works and for whom. Polit Commun. 2020;37:350–75. https://doi.org/10.1080/10584609.2019.1668894
21. Bode L, Vraga EK. Americans are fighting coronavirus misinformation on social media. 2020 May 7 [cited 2020 May 22]. https://www.washingtonpost.com/politics/2020/05/07/americans-are-fighting-coronavirus-misinformation-social-media/
22. Vraga EK, Bode L. Using expert sources to correct health misinformation in social media. Sci Commun. 2017;39:621–45. https://doi.org/10.1177/1075547017731776
23. van der Meer TGLA, Jin Y. Seeking formula for misinformation treatment in public health crises: the effects of corrective information type and source. Health Commun. 2020;35:560–75. https://doi.org/10.1080/10410236.2019.1573295
24. Vraga EK, Kim SC, Cook J, Bode L. Testing the effectiveness of correction placement and type on Instagram. Int J Press/Polit. 2020;25:632–52. https://doi.org/10.1177/1940161220919082
25. World Health Organization. WHO launches a chatbot on Facebook Messenger to combat COVID-19 misinformation. 2020 Apr 15 [cited 2020 Jun 4]. https://www.who.int/news-room/feature-stories/detail/who-launches-a-chatbot-powered-facebook-messenger-to-combat-covid-19-misinformation
26. Open Science Framework. Using expert graphics to debunk COVID-19 misinformation on Facebook. 2020 [cited 2020 May 5]. https://osf.io/gvucy
27. Pew Research Center for the People and the Press. Republicans, Democrats move even further apart in coronavirus concerns. 2020 Jun 25 [cited 2020 Jun 26]. https://www.people-press.org/2020/06/25/republicans-democrats-move-even-further-apart-in-coronavirus-concerns
28. Balog-Way DH, McComas KA. COVID-19: Reflections on trust, tradeoffs, and preparedness. J Risk Res. 2020 Apr 27 [Epub ahead of print]. https://doi.org/10.1080/13669877.2020.1758192
29. Bode L, Vraga EK, Tully M. Do the right thing: tone may not affect correction of misinformation on social media. Harvard Kennedy School Misinformation Review. 2020 Jun 11 [cited 2020 Jun 24]. https://misinforeview.hks.harvard.edu/article/do-the-right-thing-tone-may-not-affect-correction-of-misinformation-on-social-media
30. Wood T, Porter E. The elusive backfire effect: mass attitudes' steadfast factual adherence. Polit Behav. 2019;41:135–63. https://doi.org/10.1007/s11109-018-9443-y


Address for correspondence: Emily Vraga, University of Minnesota, 338 Murphy Hall, 206 Church St, Minneapolis, MN 55455, USA; email: ekvraga@umn.edu

# Universal Admission Screening for SARS-CoV-2 Infections among Hospitalized Patients, Switzerland, 2020

Thomas Scheier, Adrian Schibli, Geri Eich, Christian Rüegg, Frank Kube, Adrian Schmid, Urs Karrer, Aline Wolfensberger, Hugo Sax, Peter W. Schreiber

Switzerland began a national lockdown on March 16, 2020, in response to the rapid spread of severe acute respiratory syndrome coronavirus 2 (SARS-CoV-2). We assessed the prevalence of SARS-CoV-2 infection among patients admitted to 4 hospitals in the canton of Zurich, Switzerland, in April 2020. These 4 acute care hospitals screened 2,807 patients, including 2,278 (81.2%) who did not have symptoms of coronavirus disease (COVID-19). Overall, 529 (18.8%) persons had ≥1 symptom of COVID-19, of whom 60 (11.3%) tested positive for SARS-CoV-2. Eight asymptomatic persons (0.4%) also tested positive for SARS-CoV-2. Our findings indicate that screening on the basis of COVID-19 symptoms, regardless of clinical suspicion, can identify most SARS-CoV-2–positive persons in a low-prevalence setting.

In late 2019, a pneumonia of unknown etiology emerged in Wuhan, Hubei Province, China. In early 2020, public health officials identified the illness as coronavirus disease (COVID-19) and its causative agent as severe acute respiratory syndrome coronavirus 2 (SARS-CoV-2). The World Health Organization declared a pandemic on March 11, 2020 (*1*–*3*), in response to the rapid international spread of COVID-19.

The transmission mode of SARS-CoV-2 is not fully understood; it is thought to be spread mostly by respiratory droplets and direct contact (*4*–*6*). The median incubation period is ≈5 days (*7*,*8*). Among symptomatic patients, men are affected slightly more frequently than women (*9*,*10*). COVID-19 has many manifestations, ranging from mild upper airway symptoms to acute respiratory distress syndrome. Common signs and symptoms of COVID-19 include fever, cough, sputum production, and fatigue (*11*,*12*). A high proportion of hospitalized COVID-19 patients have concurrent conditions such as arterial hypertension, diabetes mellitus, or coronary heart disease (*13*–*17*).

Author affiliations: University Hospital Zurich, Zurich, Switzerland (T. Scheier, A. Wolfensburger, H. Sax, P.W. Schreiber); University of Zurich (T. Scheier, A. Wolfensburger, H. Sax, P.W. Schreiber); City Hospital Triemli, Zurich (A. Schibli, G. Eich); GZO Wetzikon, Wetzikon, Switzerland (C. Rüegg, F. Kube); Cantonal Hospital Winterthur, Winterthur, Switzerland (A. Schmid, U. Karrer)

DOI: https://doi.org/10.3201/eid2702.202318

In March 2020, Rothe et al. published evidence of asymptomatic SARS-CoV-2 transmission (*18*), and evidence that asymptomatic or presymptomatic persons can transmit SARS-CoV-2 infection has continued to increase (*19*,*20*). In many healthcare settings, the number of persons with asymptomatic SARS-CoV-2 infection is unknown. Asymptomatic persons and healthcare workers can contract and spread the infection among hospitalized patients. Many hospitalized patients, who frequently are >65 years of age, have concurrent conditions, or both, are at risk for severe COVID-19.

In consideration of these circumstances, hospitals must take precautions to prevent the spread of SARS-CoV-2. For example, some hospitals might screen patients for SARS-CoV-2 infection within 24 hours before an elective intervention (*21*). Some well-resourced healthcare settings in high incidence areas might benefit from testing patients without COVID-19 symptoms (*22*). In the canton of Zurich, Switzerland, 4 hospitals introduced universal admission screening of all hospitalized patients in April 2020. We used the results of this screening to assess SARS-CoV-2 prevalence among hospitalized patients and to evaluate the additional yield of a universal screening strategy compared to a symptom-driven approach.

## Methods and Materials

### Study Population Characteristics

The canton of Zurich is a region in northeast Switzerland that has a population of ≈1.5 million inhabitants. The canton has 32 registered hospitals, of which 31 publicly report annual discharge numbers. These 31 hospitals discharged 237,919 patients in 2018 (*23*). During April 1–24, 2020, four hospitals conducted universal admission screening for SARS-CoV-2 (Table 1). The participating sites included the 3 largest hospitals in the canton, which accounted for ≈44% of discharges in 2018 (Table 1). Screening periods ranged from 11–24 days. The Zurich Cantonal Ethics Commission (Req-2020–00441) waived the requirement for a formal ethical evaluation according to the Swiss Human Research Act.

### Testing for SARS-CoV-2

During the screening period, the hospitals tested all patients ≥16 years of age for SARS-CoV-2 infection, regardless of signs or symptoms. At the time, the health authorities of the canton supported the policy of universal admission screening. Hospital staff informed admitted patients about SARS-CoV-2 testing as a new routine diagnostic procedure. Staff collected a nasopharyngeal swab sample from each patient and tested the samples by PCR. A single laboratory conducted diagnostic procedures for the University Hospital of Zurich (USZ) and GZO Wetzikon (GZO). The other 2 hospitals, City Hospital Triemli (STZ) and Cantonal Hospital Winterthur (KSW), sent samples to separate laboratories. The laboratory that conducted diagnostic procedures for USZ and GZO also tested and confirmed all SARS-CoV-2–positive samples from patients at STZ and a random subset of SARS-CoV-2–positive samples from patients at KSW. PCR methods varied among the participating study sites (Appendix Table 1, https://wwwnc.cdc.gov/EID/article/27/2/20-2318-App1.pdf).

### Symptom Information Collection

Hospital staff assessed each patient for signs and symptoms of COVID-19 at admission. In accordance with guidance provided by the Swiss Federal Office for Public Health, staff considered cough, dyspnea, temperature ≥38.0°C or feeling feverish, sore throat, and myalgia as possible signs and symptoms of COVID-19 (*24*). The assessment focused on symptoms at the time of the nasopharyngeal sample. Staff also noted whether suspected COVID-19 was the primary reason for admission. Before beginning the study, all participating sites agreed to prospectively collect these variables and document them in medical records. Staff extracted these data from the medical records and entered them into an electronic case report form. When information in the medical chart was inconclusive, we contacted the treating physician or the patient for clarification. At admission, patients were categorized as asymptomatic, (i.e., absence of all COVID-19 signs or symptoms) or symptomatic (i.e., presence of ≥1 COVID-19 sign or symptom). We compared our results with cantonal data (COVID-19 Informationen Schweiz, https://www.corona-data.ch).

### Statistical Analyses

We analyzed deidentified patient data submitted through an electronic case report form. We conducted statistical analysis using R version 3.3.2 (The R Foundation, https://www.r-project.org). We analyzed the medians and interquartile ranges of continuous variables and frequencies of categorical variables.

## Results

### Incidence of COVID-19

In the canton of Zurich, which has ≈1.5 million inhabitants, the first case of COVID-19 was documented on February 27, 2020 (*25*; Figure 1). The daily incidence of new SARS-CoV-2 infections peaked at 364 cases on March 23, 2020. During the screening period (April 1–24, 2020), the median daily incidence was 40 cases (interquartile range [IQR] 27–87 cases), corresponding to a rate of 2.7 cases/100,000 inhabitants (COVID-19 Informationen Schweiz, https://www.corona-data.ch).

### Study Population

Hospital staff screened 2,807 patients for SARS-CoV-2 infection (Table 2). The median age was 60 years (IQR 39–74 years); 1,368 (48.7%) patients were men

**Table 1.** Characteristics of 4 hospitals in study on severe acute respiratory syndrome coronavirus 2, canton of Zurich, Switzerland, 2020

| Hospital | No. beds | No. patients in 2018 | Screening period |
|---|---|---|---|
| GZO Wetzikon | 156 | 10,368 | 2020 Apr 8–2020 Apr 24 |
| Cantonal Hospital Winterthur | 445 | 27,451 | 2020 Apr 9–2020 Apr 19 |
| City Hospital Triemli | 396 | 24,335 | 2020 Apr 8–2020 Apr 24 |
| University Hospital of Zurich | 941 | 41,916 | 2020 Apr 1–2020 Apr 24 |

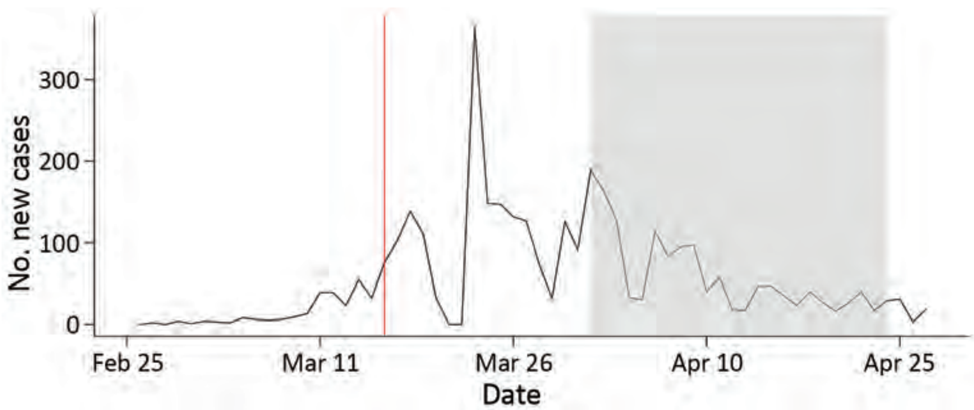


**Figure 1.** Incidence of severe acute respiratory syndrome coronavirus 2 infection, canton of Zurich, Switzerland, 2020. Data reported as absolute number of daily new diagnosed cases. Red vertical line indicates start of lockdown in Switzerland. Gray shading indicates study period.

and 1,439 (51.3%) women. At admission, 529 (18.8%) patients had ≥1 sign or symptom of COVID-19: 205 (7.3%) had temperatures ≥38.0°C or felt feverish, 192 (6.8%) had cough, 282 (10.0%) had dyspnea, 30 (1.1%) had sore throats, and 27 (1.0%) had myalgia. A total of 164 patients (5.8% of the whole study population) were hospitalized primarily for suspected COVID-19.

### PCR Results

Overall, 68 (2.4%) patients tested positive for SARS-CoV-2 RNA by PCR. Of the 529 patients with ≥1 sign or symptom of COVID-19, 60 (11.3%) tested positive. In contrast, only 8 (0.4%) of 2,278 patients without symptoms tested positive (Table 2). SARS-CoV-2 infection was diagnosed in 6 (8.8%) patients at GZO, 6 (8.8%) patients at KSW, 16 (23.5%) patients at STZ, and 40 (58.8%) patients at USZ. Asymptomatic SARS-CoV-2–positive patients were identified at all 4 hospitals: 1 (12.5%) patient at GZO, 3 (37.5%) patients at KSW, 1 (12.5%) patient at STZ, and 3 (37.5%) patients at USZ.

Of the 164 patients admitted primarily for suspected COVID-19, 52 (31.7%) tested positive for SARS-CoV-2 infection by PCR. Of all SARS-CoV-2–infected patients, 38 (55.9%) had temperatures ≥38.0°C or felt feverish, 40 (58.8%) had cough, 27 (39.7%) had dyspnea, 8 (11.8%) had sore throats, and 13 (19.1%) had myalgia. Among symptomatic COVID-19 patients, the most common manifestations were cough and fever (27; 45%), cough and dyspnea (17; 28.3%), and dyspnea and fever (14; 23.3%) (Figure 2). The absence of COVID-19 signs or symptoms yielded a negative predictive value of 99.6% for SARS-CoV-2–infection.

## Discussion

In this prospective multicenter study, hospital staff tested 2,807 patients, of whom 2,278 (81.2%) did not have signs or symptoms of COVID-19. In total, 68 (2.4%) patients tested positive for SARS-CoV-2 infection by PCR. Of SARS-CoV-2–positive patients, 8 (11.8%) were asymptomatic, corresponding to 0.4% of patients without

**Table 2.** Characteristics of hospitalized patients in study on severe acute respiratory syndrome coronavirus 2, canton of Zurich, Switzerland, 2020*

| | | PCR results for severe acute respiratory syndrome coronavirus 2 | |
|---|---|---|---|
| Characteristic | Total | Negative | Positive |
| Total | 2,807 | 2,739 (97.6) | 68 (2.4) |
| Hospital | | | |
| GZO Wetzikon | 283 | 277 (97.9) | 6 (2.1) |
| Cantonal Hospital Winterthur | 409 | 403 (98.5) | 6 (1.5) |
| City Hospital Triemli | 583 | 567 (97.3) | 16 (2.7) |
| University Hospital Zurich | 1,532 | 1,492 (97.4) | 40 (2.6) |
| Median age, y (IQR) | 60 (39–74) | 60 (39–74) | 54.5 (44.5–69) |
| Sex | | | |
| M | 1,368 | 1,330 (97.2) | 38 (2.8) |
| F | 1,439 | 1,409 (97.9) | 30 (2.1) |
| Symptoms | | | |
| Any symptom of coronavirus disease | 529 | 469 (88.7) | 60 (11.3) |
| Fever/feeling feverish | 205 | 167 (81.5) | 38 (18.5) |
| Cough | 192 | 152 (79.2) | 40 (20.8) |
| Dyspnea | 282 | 255 (90.4) | 27 (9.6) |
| Sore throat | 30 | 22 (73.3) | 8 (26.7) |
| Myalgia | 27 | 14 (51.9) | 13 (48.1) |

*Values are no. (%) except as indicated.

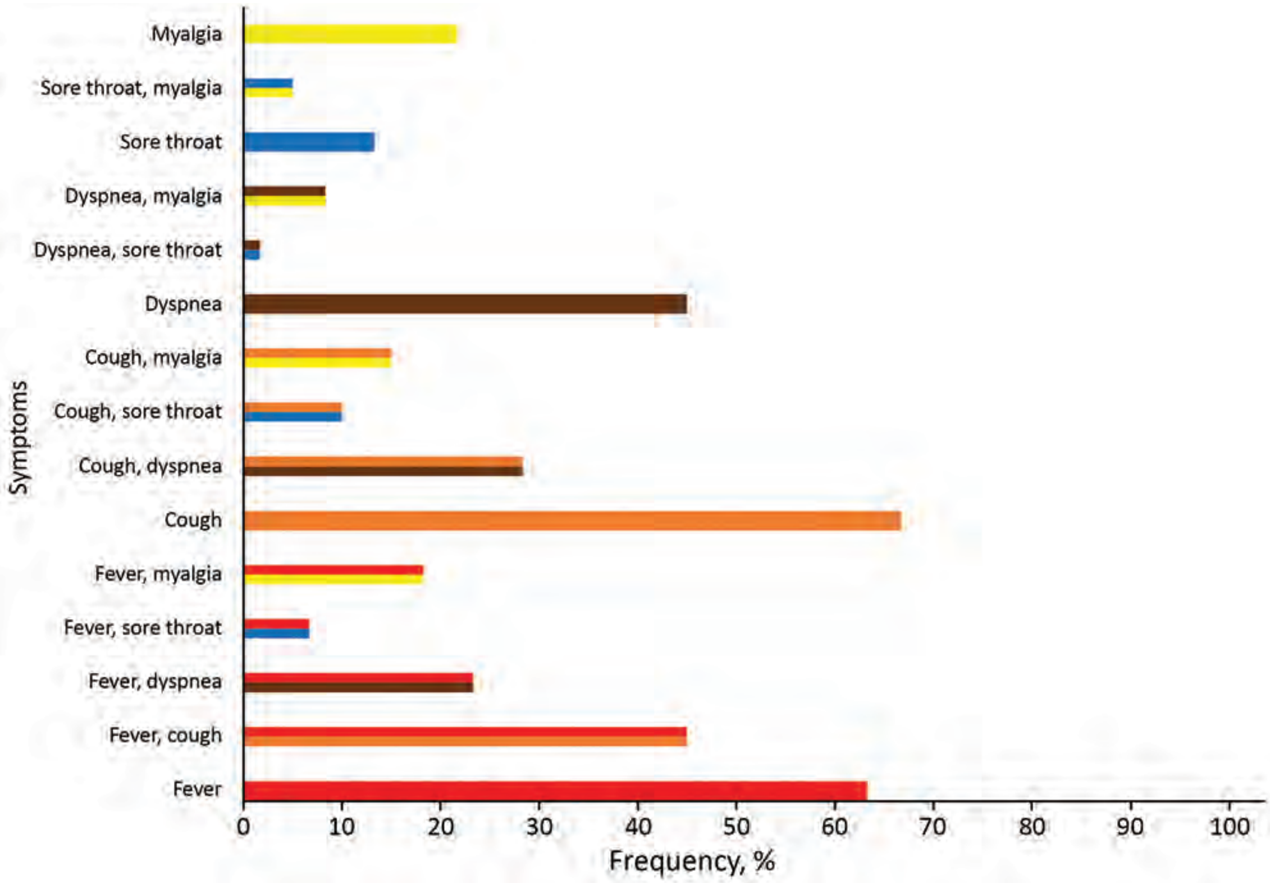


**Figure 2.** Frequency of ≥1 symptom of coronavirus disease among patients with symptomatic severe acute respiratory syndrome coronavirus 2 infection, canton of Zurich, Switzerland, 2020. Red indicates fever/feeling feverish; orange indicates cough; brown indicates dyspnea; blue indicates sore throat; yellow indicates myalgia. Unicolor bars indicate 1 symptom; multicolor bars indicate combination of ≥2 symptoms.

signs or symptoms of COVID-19. We found that 99.6% of patients without COVID-19 signs or symptoms tested negative for SARS-CoV-2 infection.

On March 16, 2020, the rapid increase in COVID-19 incidence prompted the government of Switzerland to implement and enforce preventive measures including social distancing and the closure of restaurants, bars, entertainment businesses (e.g., cinemas, libraries, museums), and all shops that could not guarantee a minimum distance of 2 meters between persons (*26*). These measures contributed to a sharp decline in COVID-19 incidence. In the canton of Zurich, the incidence of COVID-19 decreased after March 23, 2020, ≈1 week after the lockdown began in Switzerland. This study started on April 1, 2020, ≈2 weeks after the beginning of lockdown.

Because of the successful control measures for COVID-19 and the low prevalence of influenza and other respiratory viruses, <20% of the study population had signs or symptoms of COVID-19. Among all persons with SARS-CoV-2 infection, the most frequent symptoms were cough (58.8%) and fever (55.9%), consistent with other reports (*9*,*11*).

We conducted this study because of reports of a large proportion of persons with asymptomatic SARS-CoV-2 infection (*18*,*19*,*27*). In this study, only 0.4% of persons without signs or symptoms of COVID-19 tested positive for SARS-CoV-2 infection. More than 88% of SARS-CoV-2–positive persons had ≥1 sign or symptom of COVID-19. Our findings are in contrast to Sutton et al. (*28*), who found that 33 (15.4%) of 214 pregnant women tested positive for SARS-CoV-2 infection at time of hospitalization for delivery. Only 4 of those women had COVID-19 symptoms at admission; symptoms developed in 3 more women in the following days. During the study period in New York, NY, USA, from March 22–April 4, a median of 4,958 persons (59 cases/100,000 inhabitants) tested positive for SARS-CoV-2 infection each day (*28*). This rate is ≈22 times higher than that for the canton of Zurich (median 2.7 cases/100,000 inhabitants) during the period of our study (*29*,*30*). Similarly, Kimball et al. (*31*) reported that 23 (30.3%) of 76 residents in a skilled nursing home tested positive for SARS-CoV-2 infection during a local COVID-19 outbreak. At the time of testing, 13 (56.5%) SARS-CoV-2–positive persons were asymptomatic or had stable, chronic symptoms; COVID-19 symptoms developed in 10 of these 13 previously asymptomatic persons during the 7 days after testing (*31*). The delayed development of symptoms probably indicates that the cases were diagnosed during a presymptomatic period. Another recent study tested for SARS-CoV-2 infection among different subsets of the population in Iceland (*32*). In an open invitation sample of residents of Iceland with no or mild respiratory symptoms (*32*), 87 (0.8%) tested positive for SARS-CoV-2 infection; 36 (41.4%) of these persons were asymptomatic. Researchers also tested a random sample of 2,283 persons living in Iceland, of whom 13 (0.6%) tested positive for SARS-CoV-2 infection; 7 (53.8%) of these persons were asymptomatic. Both sample populations had a 0.3% proportion of persons with asymptomatic SARS-CoV-2 infections (36/10,797 persons in the open invitation sample and 7/2,283 persons in the random sample) (*32*), which is similar to the proportions in our findings (8/2,807 persons; 0.3%). The difference in the proportions of asymptomatic persons among those with SARS-CoV-2 infection (11.8% in this study vs. 41.4% in the open invitation and 53.8% in the random samples from Iceland) (*32*) might have been caused by an overrepresentation of symptomatic persons in our study because COVID-19–compatible symptoms are probably more common among admitted hospital patients.

Identifying and isolating persons with SARS-CoV-2 infection is critical to containing COVID-19. Because of limited testing capacity, healthcare providers must use resources strategically (*33*). Our findings indicate that screening on the basis of COVID-19 symptoms, regardless of clinical suspicion, can identify nearly all SARS-CoV-2–infected persons in the studied epidemiologic setting. Because COVID-19 has a broad spectrum of clinical manifestations, healthcare providers should screen patients for symptoms at admission. By only testing symptomatic patients, healthcare providers can use >80% fewer tests; however, this strategy would not identify 0.4% of SARS-CoV-2 infections. For every ≈285 persons without symptoms whom we tested, we identified 1 asymptomatic SARS-CoV-2 infection. Whether asymptomatic persons are as infectious as symptomatic persons is unknown. At the time of this study, no quantitative SARS-CoV-2 reporting existed; this lack of data hindered a comparison of viral replication between asymptomatic and symptomatic persons. Additional studies on this topic are urgently needed.

Our study has limitations. First, all participants were tested only once for SARS-CoV-2 infection at admission; no routine follow-up tests were scheduled, regardless of patient signs or symptoms. The lack of follow-up testing might have missed some cases of SARS-CoV-2 infection. Second, we did not collect information on the patients' potential exposures to SARS-CoV-2 or any other agents of respiratory illness. Third, different laboratories conducted the PCRs with different methods. However, we ensured the validity of results from different laboratories by retesting a subset of SARS-CoV-2–positive samples at another laboratory. Fourth, our findings must be considered in the epidemiologic context; they do not apply to high-prevalence settings with active outbreaks. Fifth, we did not collect information about patients' COVID-19 symptoms during the previous 2 weeks. We also did not conduct follow-up evaluations of symptoms in patients who were asymptomatic at admission. Further studies should evaluate whether these asymptomatic patients might have been presymptomatic or recovering from COVID-19 at admission. Sixth, we did not collect information on ageusia and anosmia, which were later described as characteristic symptoms among mild and moderate cases of COVID-19 (*34*). Including these variables might have increased the number of symptomatic persons among SARS-CoV-2–infected patients.

This prospective study benefited from a multicenter design and the availability of data on regional incidence of COVID-19. We selected study sites that accounted for ≈44% of all patient discharges in the canton in 2018 and included the 3 largest hospitals (*23*) and were therefore representative of the canton of Zurich. In addition, no admitted patients refused to participate in the screening for SARS-CoV-2.

In conclusion, universal testing for SARS-CoV-2 of all patients at hospital admission in this region of Switzerland did not identify a substantial number of asymptomatic infections in a low-prevalence setting. Future studies are needed to delineate the role of asymptomatic SARS-CoV-2–infected persons as transmitters in the current pandemic.

**Acknowledgments**

We thank Lauren Clack for providing feedback on grammar and spelling.

P.W.S. and A.W. have received grants from the career funding program "Filling the Gap" of the Medical Faculty of the University of Zurich. These grants were made outside of the context of the submitted work.

## About the Author

Dr. Scheier is an infectious disease fellow at the University Hospital Zurich, Zurich. His research focuses on epidemiology of emerging infections.

### References


1. World Health Organization. Rolling updates on coronavirus disease (COVID-19). 2020 [cited 2020 Apr 18]. https://www.who.int/emergencies/diseases/novel-coronavirus-2019/events-as-they-happen
2. European Centre for Disease Prevention and Control. Rapid risk assessment: Coronavirus disease 2019 (COVID-19) in the EU/EEA and the UK—ninth update. 2020 [cited 2020 Apr 24]. https://www.ecdc.europa.eu/en/publications-data/rapid-risk-assessment-coronavirus-disease-2019-covid-19-pandemic-ninth-update
3. World Health Organization. Naming the coronavirus disease (COVID-19) and the virus that causes it. 2020 [cited 2020 May 5]. https://www.who.int/emergencies/diseases/novel-coronavirus-2019/technical-guidance/naming-the-coronavirus-disease-(covid-2019)-and-the-virus-that-causes-it
4. World Health Organization. Modes of transmission of virus causing COVID-19: implications for IPC precaution recommendations. 2020 Mar 29 [cited 2020 Apr 23]. https://www.who.int/news-room/commentaries/detail/modes-of-transmission-of-virus-causing-covid-19-implications-for-ipc-precaution-recommendations
5. National Center for Immunization and Respiratory Diseases. How COVID-19 spreads. 2020 [cited 2020 May 5]. https://www.cdc.gov/coronavirus/2019-ncov/prevent-getting-sick/how-covid-spreads.html?CDC_AA_refVal=https%3A%2F%2Fwww.cdc.gov%2Fcoronavirus%2F2019-ncov%2Fprepare%2Ftransmission.html
6. World Health Organization. Report of the WHO-China Joint Mission on Coronavirus Disease 2019 (COVID-19). 2020 Feb [cited 2020 May 5]. https://www.who.int/docs/default-source/coronaviruse/who-china-joint-mission-on-covid-19-final-report.pdf
7. Ganyani T, Kremer C, Chen D, Torneri A, Faes C, Wallinga J, et al. Estimating the generation interval for coronavirus disease (COVID-19) based on symptom onset data, March 2020. Euro Surveill. 2020;25:2000257. https://doi.org/10.2807/1560-7917.ES.2020.25.17.2000257
8. Lauer SA, Grantz KH, Bi Q, Jones FK, Zheng Q, Meredith HR, et al. The incubation period of coronavirus disease 2019 (COVID-19) from publicly reported confirmed cases: estimation and application. Ann Intern Med. 2020;172:577–82; Epub ahead of print. https://doi.org/10.7326/M20-0504
9. Guan W-J, Ni Z-Y, Hu Y, Liang W-H, Ou C-Q, He J-X, et al.; China Medical Treatment Expert Group for Covid-19. Clinical characteristics of coronavirus disease 2019 in China. N Engl J Med. 2020;382:1708–20. https://doi.org/10.1056/NEJMoa2002032
10. Goyal P, Choi JJ, Pinheiro LC, Schenck EJ, Chen R, Jabri A, et al. Clinical characteristics of COVID-19 in New York City. N Engl J Med. 2020;382:2372–4. https://doi.org/10.1056/NEJMc2010419
11. Wang D, Hu B, Hu C, Zhu F, Liu X, Zhang J, et al. Clinical characteristics of 138 hospitalized patients with 2019 novel coronavirus–infected pneumonia in Wuhan, China. JAMA. 2020;323:1061–9. https://doi.org/10.1001/jama.2020.1585
12. Yang X, Yu Y, Xu J, Shu H, Xia J, Liu H, et al. Clinical course and outcomes of critically ill patients with SARS-CoV-2 pneumonia in Wuhan, China: a single-centered, retrospective, observational study. Lancet Respir Med. 2020;8:475–81; Epub ahead of print. https://doi.org/10.1016/S2213-2600(20)30079-5
13. Zhou F, Yu T, Du R, Fan G, Liu Y, Liu Z, et al. Clinical course and risk factors for mortality of adult inpatients with COVID-19 in Wuhan, China: a retrospective cohort study. [Erratum in: Lancet. 2020;395:1038]. Lancet. 2020;395:1054–62. https://doi.org/10.1016/S0140-6736(20)30566-3
14. Docherty AB, Harrison EM, Green CA, Hardwick HE, Pius R, Norman L, et al.; ISARIC4C investigators. Features of 20133 UK patients in hospital with covid-19 using the ISARIC WHO Clinical Characterisation Protocol: prospective observational cohort study. BMJ. 2020;369:m1985. https://doi.org/10.1136/bmj.m1985
15. Grasselli G, Zangrillo A, Zanella A, Antonelli M, Cabrini L, Castelli A, et al.; COVID-19 Lombardy ICU Network. Baseline characteristics and outcomes of 1,591 patients infected with SARS-CoV-2 admitted to ICUs of the Lombardy region, Italy. JAMA. 2020;323:1574–81. https://doi.org/10.1001/jama.2020.5394
16. Chow N, Fleming-Dutra K, Gierke R, Hall A, Hughes M, Pilishvili T, et al.; CDC COVID-19 Response Team. Preliminary estimates of the prevalence of selected underlying health conditions among patients with coronavirus disease 2019—United States, February 12–March 28, 2020. MMWR Morb Mortal Wkly Rep. 2020;69:382–6. https://doi.org/10.15585/mmwr.mm6913e2
17. Istituto Superiore di Sanità. Characteristics of SARS-CoV-2 patients dying in Italy: report based on available data on July 22nd, 2020. [cited 2020 Aug 10]. https://www.epicentro.iss.it/en/coronavirus/bollettino/Report-COVID-2019_22_july_2020.pdf
18. Rothe C, Schunk M, Sothmann P, Bretzel G, Froeschl G, Wallrauch C, et al. Transmission of 2019-nCoV infection from an asymptomatic contact in Germany. N Engl J Med. 2020;382:970–1. https://doi.org/10.1056/NEJMc2001468
19. Furukawa NW, Brooks JT, Sobel J. Evidence supporting transmission of severe acute respiratory syndrome coronavirus 2 while presymptomatic or asymptomatic. Emerg Infect Dis. 2020;26: Epub ahead of print. 10.3201/eid2607.201595 https://doi.org/10.3201/eid2607.201595
20. Wiersinga WJ, Rhodes A, Cheng AC, Peacock SJ, Prescott HC. Pathophysiology, transmission, diagnosis, and treatment of coronavirus disease 2019 (COVID-19): a review. JAMA. 2020;324:782–93. https://doi.org/10.1001/jama.2020.12839
21. Al-Muharraqi MA. Testing recommendation for COVID-19 (SARS-CoV-2) in patients planned for surgery - continuing the service and 'suppressing' the pandemic. Br J Oral Maxillofac Surg. 2020;58:503–5. https://doi.org/10.1016/j.bjoms.2020.04.014
22. European Society of Cardiology. ESC Guidance for the Diagnosis and Management of CV Disease during the COVID-19 Pandemic. 2020 [cited 2020 May 11]. https://www.escardio.org/Education/COVID-19-and-Cardiology/ESC-COVID-19-Guidance
23. Kanton Zürich Gesundheitsdirektion. Healthcare 2019 acute somatics rehabilitation psychiatry [in German]. 2020 [cited 2020 Aug 10]. https://www.zh.ch/content/dam/zhweb/bilder-dokumente/themen/gesundheit/gesundheitsversorgung/spitaeler_kliniken/daten_und_

statistik_der_listenspitaeler/gesundheitsversorgungsbericht/gesundheitsversorgungsbericht_2019.pdf
24. Bundesamt für Gesundheit. COVID-19: Empfehlungen zum Umgang mit erkrankten Personen und Kontakten ab 19. Bern (Switzerland): Eidgenössisches Departement des Innern; 2020.
25. Kanton Zürich. Coronavirus: first case in the Canton of Zurich [in German]. 2020 Feb 27 [cited 2020 Nov 11]. https://www.zh.ch/de/news-uebersicht/medienmitteilungen/2020/02/coronavirus-erster-fall-im-kanton-zuerich.html
26. Der Bundesrat. Coronavirus: federal council declares the extraordinary situation and tightened the measures [in German]. 2020 Mar 17 [cited 2020 May 4]. https://www.admin.ch/gov/de/start/dokumentation/medienmitteilungen.msg-id-78454.html
27. Arons MM, Hatfield KM, Reddy SC, Kimball A, James A, Jacobs JR, et al.; Public Health–Seattle and King County and CDC COVID-19 Investigation Team. Presymptomatic SARS-CoV-2 infections and transmission in a skilled nursing facility. N Engl J Med. 2020;382:2081–90. https://doi.org/10.1056/NEJMoa2008457
28. Sutton D, Fuchs K, D'Alton M, Goffman D. Universal screening for SARS-CoV-2 in women admitted for delivery. N Engl J Med. 2020;382:2163–4. https://doi.org/10.1056/NEJMc2009316
29. New York City Department of Health and Mental Hygiene. COVID-19: data. 2020 [cited 2020 May 5]. https://www1.nyc.gov/site/doh/covid/covid-19-data.page#download
30. New York City Department of City Planning. Population—current and projected populations. 2018 [cited 2020 Apr 28]. https://www1.nyc.gov/site/planning/planning-level/nyc-population/current-future-populations.page
31. Kimball A, Hatfield KM, Arons M, James A, Taylor J, Spicer K, et al.; Public Health – Seattle & King County; CDC COVID-19 Investigation Team. Asymptomatic and presymptomatic SARS-CoV-2 infections in residents of a long-term care skilled nursing facility—King County, Washington, March 2020. MMWR Morb Mortal Wkly Rep. 2020;69:377–81. https://doi.org/10.15585/mmwr.mm6913e1
32. Gudbjartsson DF, Helgason A, Jonsson H, Magnusson OT, Melsted P, Norddahl GL, et al. Spread of SARS-CoV-2 in the Icelandic population. N Engl J Med. 2020;382:2302–15. https://doi.org/10.1056/NEJMoa2006100
33. World Health Organization. Laboratory testing strategy recommendations for COVID-19. 2020 [cited 2020 May 4]. https://apps.who.int/iris/bitstream/handle/10665/331509/WHO-COVID-19-lab_testing-2020.1-eng.pdf
34. Lechien JR, Chiesa-Estomba CM, De Siati DR, Horoi M, Le Bon SD, Rodriguez A, et al. Olfactory and gustatory dysfunctions as a clinical presentation of mild-to-moderate forms of the coronavirus disease (COVID-19): a multicenter European study. Eur Arch Otorhinolaryngol. 2020;277:2251–61. https://doi.org/10.1007/s00405-020-05965-1

Address for correspondence: Peter Schreiber, University Hospital Zurich, Division of Infectious Diseases and Hospital Epidemiology, Raemistrasse 100, Zurich 8091, Switzerland; email: peterwerner.schreiber@usz.ch

# Excess Deaths during Influenza and Coronavirus Disease and Infection-Fatality Rate for Severe Acute Respiratory Syndrome Coronavirus 2, the Netherlands

Liselotte van Asten, Carel N. Harmsen, Lenny Stoeldraijer, Don Klinkenberg, Anne C. Teirlinck, Marit M.A. de Lange, Adam Meijer, Jan van de Kassteele, Arianne B. van Gageldonk-Lafeber, Susan van den Hof, Wim van der Hoek

Since the 2009 influenza pandemic, the Netherlands has used a weekly death monitoring system to estimate deaths in excess of expectations. We present estimates of excess deaths during the ongoing coronavirus disease (COVID-19) epidemic and 10 previous influenza epidemics. Excess deaths per influenza epidemic averaged 4,000. The estimated 9,554 excess deaths (41% in excess) during the COVID-19 epidemic weeks 12–19 of 2020 appeared comparable to the 9,373 excess deaths (18%) during the severe influenza epidemic of 2017–18. However, these deaths occurred in a shorter time, had a higher peak, and were mitigated by nonpharmaceutical control measures. Excess deaths were 1.8-fold higher than reported laboratory-confirmed COVID-19 deaths (5,449). Based on excess deaths and preliminary results from seroepidemiologic studies, we estimated the infection-fatality rate to be 1%. Monitoring of excess deaths is crucial for timely estimates of disease burden for influenza and COVID-19. Our data complement laboratory-confirmed COVID-19 death reports and enable comparisons between epidemics.

Influenza and coronavirus disease (COVID-19) are respiratory illnesses that show a high burden of disease. Comparison of their effect on death rates is critical in light of the discussion, especially early in the COVID-19 pandemic, whether deaths from COVID-19 are comparable to or higher than deaths from influenza. With the yearly influenza season nearing the Northern Hemisphere, the comparison of burden will remain essential because the 2 viruses might continue to affect populations.

Author affiliations: National Institute for Public Health and the Environment, Bilthoven, the Netherlands (L. van Asten, D. Klinkenberg, A.C. Teirlinck, M.M.A. de Lange, A. Meijer, J. van de Kassteele, A.B. van Gageldonk-Lafeber, S. van den Hof, W. van der Hoek); Statistics Netherlands, the Hague, the Netherlands (C.N. Harmsen, L. Stoeldraijer)

DOI: https://doi.org/10.3201/eid2702.202999

The ongoing COVID-19 pandemic and previous seasonal influenza epidemics have led to deaths exceeding the levels that are normally expected in a certain period (i.e., excess deaths) (*1*,*2*). Although the contribution of either COVID-19 or influenza (*3*,*4*) to excess all-cause deaths can only be estimated, this information is pivotal for real-time monitoring of the impact and severity of any epidemic (*5*) by providing timely and inclusive estimates (*6*). In the case of influenza, there is no alternative to estimates because only a fraction of patients with influenza-like illness (ILI) or severe acute respiratory infections are tested for influenza virus infection (*7*). Thus, the number of laboratory-confirmed influenza deaths is not a useful indicator and it is also delayed. COVID-19, which must be reported, is subject to closer monitoring and more extensive laboratory testing than influenza in most countries. However, as with influenza, deaths from laboratory-confirmed cases of COVID-19 are an underestimate of the total number of deaths from this disease.

We provide an estimate of the excess deaths observed during the COVID-19 epidemic in the Netherlands in March–May 2020, in comparison with excess deaths observed during the previous 10 influenza epidemics. In addition, we compared the excess COVID-19 death estimates with reported COVID-19 deaths and provide a timely preliminary estimate of the infection-fatality rate of COVID-19.

## Methods

### Data

To estimate excess deaths during influenza and COVID-19 epidemics and their relationship with reported COVID-19 deaths, we used the following resources. First, weekly number of deaths are monitored at the National Institute for Public Health and the Environment (Bilthoven, the Netherlands [RIVM]) by using death registrations from Statistics Netherlands with a 100% coverage of the country (total 2019 population 17.3 million). The monitoring was implemented in 2009 during the influenza pandemic (*1*,*8*,*9*). RIVM receives data from Statistics Netherlands every Thursday. For our analyses, we used data and results from this system for 2010–2020 (2020 data through week 25, ending June 17). Aggregated weekly numbers (running from Thursday through Wednesday for the most up-to-date reporting) were used (Monday–Sunday definitive numbers available at https://opendata.cbs.nl).

Second, influenza epidemic weeks (2010–2020) are defined and reported weekly and yearly by the national sentinel influenza surveillance system (*7*). In this system, the incidence of medically attended ILI incidence is registered by Nivel Primary Care Database based on its sentinel general practitioner practices (*10*). A subgroup of patients with ILI and other acute respiratory infections is swabbed for laboratory testing. Swab specimens are analyzed for influenza virus, respiratory syncytial virus, rhinovirus, enterovirus, and, since February 2020, severe acute respiratory syndrome coronavirus 2 (SARS-CoV-2). This system covers 0.7%–0.8% of the population of the Netherlands and is nationally representative for age, sex, regional distribution, and population density (*11*). When ILI incidence is above the preset threshold for $\geq$2 consecutive weeks (*12*), and when influenza virus is detected in samples from patients who have ILI, an influenza epidemic is declared and reported.

Third, patients with laboratory confirmed COVID-19 diagnosis must be reported to regional public health services and their data are entered into a national database maintained by RIVM (February 2020, https://www.rivm.nl/en/novel-coronavirus-covid-19/current-information; open data at https://data.rivm.nl). Records include date of death, if applicable. Because most persons are not deceased when first reported, record completion requires follow-up of patients. For our study, reports by date of death were aggregated weekly from Thursday through Wednesday to enable comparison with death monitoring.

### Defining Periods of Influenza, COVID-19, and Mixed Epidemics

The 2020 seasonal influenza epidemic was short and mild, running from week 5 through week 7. On Thursday, February 27, 2020, the first new SARS-CoV-2 infection was detected in the Netherlands (https://www.rivm.nl/coronavirus-covid-19/grafieken). This infection was at the end of calendar week 9, or week 10 in our weekly Thursday–Wednesday aggregations: February 27–March 4 (Table 1). The seasonal influenza epidemic appeared to resurface briefly in weeks 10 and 11 (February 27–March 11) and overlapped with the first 2 full weeks for reported COVID-19 patients. Therefore, we analyzed separately the cumulated excess deaths for these 2 weeks of mixed epidemics. Fear of coronavirus infection might have motivated persons who had ILI but who would not otherwise have sought care to visit their physician, causing or heightening an increase in the ILI surveillance data. However, a true resurfacing of influenza could not be ruled out; although not common, resurfacing has occurred (*13*,*14*). In both weeks (weeks 10–11 2020), influenza virus was detected in swabbed ILI patients (40% in week 10). In week 11, SARS-CoV-2 was detected in primary care, although at less than half the level of influenza: 10% vs. 25% of ILI patients (*15*) (but based on low numbers of swabbed patients). We counted excess deaths during the COVID-19 epidemic from week 12 through week 19 (March 12–May 6). By week 20, death levels had returned to expected levels, although COVID-19 death reports persisted at low levels (≈0.07 deaths/100,000 persons; https://www.rivm.nl/coronavirus-covid-19/grafieken).

### Death Monitoring

Once a week, the number of reported deaths is checked for excess above the number of expected deaths. For our analyses, we used deaths reported within 3 weeks (as were 99% of all deaths reported). Because data are received on Thursday morning, weekly numbers are aggregated from Thursdays through Wednesdays. A weekly email bulletin reporting the findings is sent to the Infectious Disease Early Warning Unit (at RIVM), and a short summary is placed weekly on the website (https://www.rivm.nl/monitoring-sterftecijfers-nederland). Any known concurrent and possibly related events are also reported. Data are sent weekly to EuroMOMO, (https://www.euromomo.eu), which monitors excess deaths at the level of Europe.

We used linear regression models to estimate current weekly baseline deaths on the basis of the preceding 5-year data wherein previous events were removed. Any deaths above the expected level was

**Table 1.** Total, excess, and reported COVID-19 deaths during 25 weeks of the COVID-19 epidemic, the Netherlands*

| Week† | Week start (Thursday) | Week end (Wednesday) | No. observed all-cause deaths | No. expected all-cause deaths (baseline) | No. excess deaths | % Above expected | No. reported COVID-19 deaths | Ratio (excess vs. reported COVID-19 deaths) |
|---|---|---|---|---|---|---|---|---|
| 1 | 2019 Dec 26 | 2020 Jan 1 | 2,982 | 2,972 | 10 | 0 | NA | NA |
| 2 | 2020 Jan 2 | 2020 Jan 8 | 3,166 | 2,985 | 181 | 6 | NA | NA |
| 3 | 2020 Jan 9 | 2020 Jan 15 | 3,342 | 2,996 | 346 | 12 | NA | NA |
| 4 | 2020 Jan 16 | 2020 Jan 22 | 2,986 | 3,004 | −18 | −1 | NA | NA |
| 5 | 2020 Jan 23 | 2020 Jan 29 | 3,119 | 3,010 | 109 | 4 | NA | NA |
| 6 | 2020 Jan 30 | 2020 Feb 5 | 3,179 | 3,012 | 167 | 6 | NA | NA |
| 7 | 2020 Feb 6 | 2020 Feb 12 | 3,152 | 3,012 | 140 | 5 | NA | NA |
| 8 | 2020 Feb 13 | 2020 Feb 19 | 3,106 | 3,009 | 97 | 3 | NA | NA |
| 9 | 2020 Feb 20 | 2020 Feb 26 | 2,973 | 3,002 | −29 | −1 | NA | NA |
| 10 | 2020 Feb 27 | 2020 Mar 4 | 3,104 | 2,992 | 112 | 4 | 0 | NA |
| 11 | 2020 Mar 5 | 2020 Mar 11 | 3,081 | 2,980 | 101 | 3 | 7 | 14.5 |
| 12 | 2020 Mar 12 | 2020 Mar 18 | 3,286 | 2,964 | 322 | 11 | 99 | 3.3 |
| 13 | 2020 Mar 19 | 2020 Mar 25 | 3,941 | 2,946 | 995 | 34 | 502 | 2.0 |
| 14 | 2020 Mar 26 | 2020 Apr 1 | 4,764 | 2,926 | 1,838 | 63 | 1,003 | 1.8 |
| 15 | 2020 Apr 2 | 2020 Apr 8 | 5,143 | 2,903 | 2,240 | 77 | 1,144 | 2.0 |
| 16 | 2020 Apr 9 | 2020 Apr 15 | 4,565 | 2,879 | 1,686 | 59 | 941 | 1.8 |
| 17 | 2020 Apr 16 | 2020 Apr 22 | 4,109 | 2,853 | 1,256 | 44 | 837 | 1.5 |
| 18 | 2020 Apr 23 | 2020 Apr 29 | 3,692 | 2,827 | 865 | 31 | 558 | 1.5 |
| 19 | 2020 Apr 30 | 2020 May 6 | 3,153 | 2,801 | 352 | 13 | 365 | 1.0 |
| 20 | 2020 May 7 | 2020 May 13 | 2,876 | 2,774 | 102 | 4 | 240 | 0.4 |
| 21 | 2020 May 14 | 2020 May 20 | 2,788 | 2,748 | 40 | 1 | 136 | 0.3 |
| 22 | 2020 May 21 | 2020 May 27 | 2,694 | 2,723 | NA | NA | 112 | −0.3 |
| 23 | 2020 May 28 | 2020 Jun 3 | 2,690 | 2,700 | NA | NA | 61 | −0.2 |
| 24 | 2020 Jun 4 | 2020 Jun 10 | NA | 2,679 | NA | NA | 45 | NA |
| 25 | 2020 Jun 11 | 2020 Jun 17 | NA | 2,660 | NA | NA | 26 | NA |

*COVID-19, coronavirus disease; NA, not applicable.
†Week as defined in the death surveillance (running Thursday through Wednesday).

considered excess deaths and significantly increased when above the upper 95% prediction limit. In addition, a range of excess deaths was provided by calculating excess deaths as observed deaths minus the upper limit and observed deaths minus the lower limit. We provide further details of the statistical model and additional calculations (Appendix, https://wwwnc.cdc.gov/EID/article/27/2/20-2999-App1.pdf).

## Results

The average weekly number of deaths was 2,797 during 2010–2020. Death numbers were generally higher in winter than in summer months and showed an upward trend over time, related to an aging population.

### Excess Deaths

Using our death algorithm, we found that excess deaths were found during all previous influenza epidemics except that during 2013–2014 (Figure 1). For influenza, deaths reached their highest weekly peak during the 2017–2018 epidemic when 4,049 deaths were observed in week 10, and 2,860 deaths was the expected baseline (deaths reported within 3 weeks).

Excess deaths were found during the COVID-19 epidemic (weeks 12–19 2020; Thursday, March 12, through Wednesday, May 6) and reached its peak in week 15 (April 2–8) with 5,143 deaths; 2,903 was the expected baseline level (thus 77% in excess) for deaths reported within 3 weeks (Figure 2). COVID-19 excess deaths peaked 5–6 weeks after the first COVID-19 patient was detected on February 27. By week 20, deaths were not greatly increased beyond expected levels, but reports of COVID-19 deaths continued at low levels.

No COVID-19 deaths were reported in week 10 (February 27–March 4); 7 were reported in week 11 (March 5–11), the first 2 COVID-19 weeks with a concurrent influenza epidemic. Reported COVID-19 deaths increased to 99 in the ensuing week 12 (March 12–18) by which time the influenza epidemic had receded. Reported COVID-19 deaths peaked at 1,144 in week 15 (April 2–8), coinciding with peak excess deaths.

### Ratio of Excess Deaths to COVID-19 Deaths

Excess deaths were 3.3 times higher than reported COVID-19 deaths in week 12 (March 12–18) but then stabilized at 1.8–2.0 times higher in the ensuing 4 weeks (weeks 13–16; ratio 2.0 during peak deaths in week 15) (Figure 3). The ratio then further decreased to 1.5 in weeks 17 and 18 (April 16–29) and had decreased to 1 in week 19 (April 30–May 6), the final week with excess deaths for our model.

### Accumulated Excess Deaths

On average, ≈4,000 accumulated excess deaths were observed during influenza epidemics, but numbers

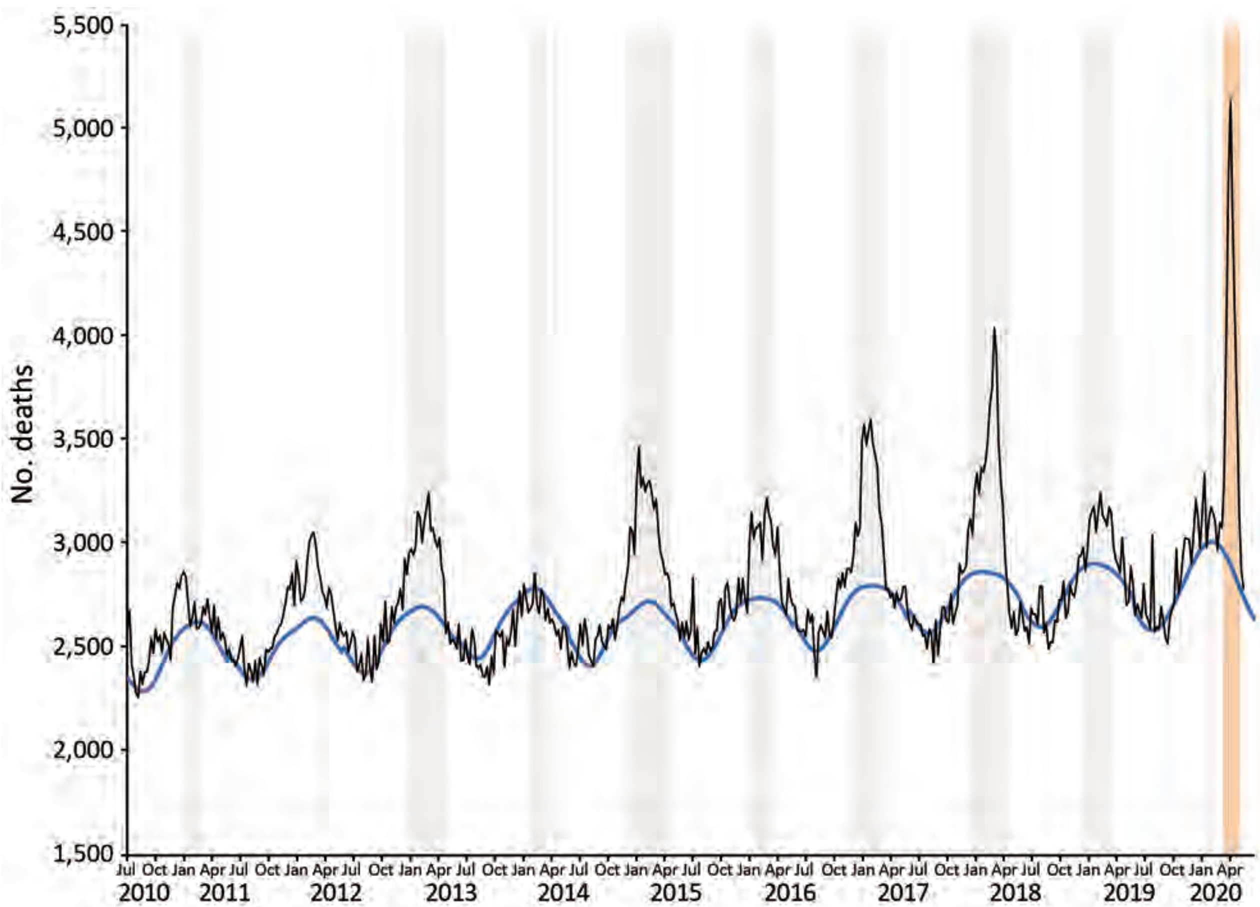


**Figure 1.** Excess deaths during influenza and coronavirus disease (COVID-19) and infection-fatality rate for severe acute respiratory syndrome coronavirus 2, the Netherlands. Weekly and expected number of deaths, 2010–2020. Black line indicates weekly number of deaths, and blue line indicates expected number of weekly deaths. Gray vertical bars indicate influenza epidemic weeks, and orange vertical bar indicates COVID-19 epidemic week 12–19 (March 12–May 6); excluding week 10–11, which overlapped with an influenza epidemic flare-up. Weeks run Thursday through Wednesday.

varied considerably from 1 epidemic to another (Table 2). During the 2013–14 influenza epidemic, observed deaths were around baseline levels. During the other influenza epidemics, excess deaths varied from the lowest estimates of 404–600 (2010–2011, 2011–2012, and 2019–2020) up to 9,373 (range 6,439–12,306) during 2017–2018. During the 2017–18 epidemic, the accumulated all-cause deaths were 60,790, or 18% higher than the expected baseline level of 51,417. Influenza epidemic duration varied from 2 to 21 weeks; longer epidemics tended to show higher excess deaths.

The total number of excess deaths during weeks 12–19 (March 12–May 6) of the COVID-19 epidemic was estimated to be 9,554 (range 8,271–10,838) (Table 2), which is almost twice (1.8 times) the total of 5,449 reported COVID-19 deaths during the same period. A total of 32,654 accumulated all-cause deaths were observed during this period, whereas accumulated expected deaths were 23,099 (deaths reported within 3 weeks). Thus, observed deaths were an overall 41% higher than expected baseline levels. In the 2 weeks that had a mixed influenza and COVID-19 epidemics (weeks 10 and 11; February 27–March 11, 2020), excess deaths totaled 213 (range –115 to 541).

### Estimated SARS-CoV-2 Infection-Fatality Rate

The assumption that all 9,554 excess deaths were associated directly with COVID-19 infections is an oversimplification, but enables a provisional estimate of the infection-fatality rate. In April 2020, the first 2 national serologic surveys by Sanquin (*20*) and Pienter (*21*) provided provisional estimates of the proportion of persons who had SARS-CoV-2 antibodies: 3% of adult blood donors (*20*) and 4% of a random population sample (*21*). A second blood donor survey reported a subsequent preliminary estimate of 5.5% on the basis of blood samples drawn May 10–20, 2020 (*22*). This finding suggests that up

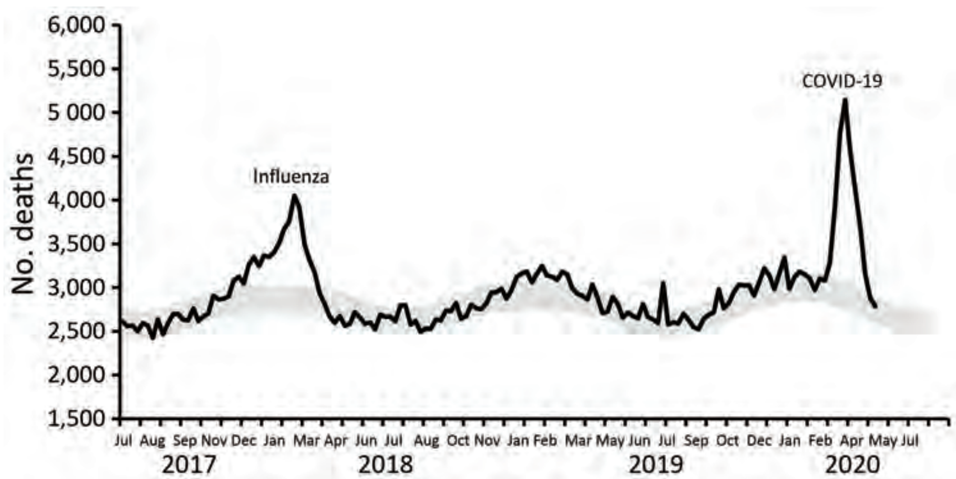


**Figure 2.** Excess deaths during influenza and COVID-19 and infection-fatality rate for severe acute respiratory syndrome coronavirus 2, the Netherlands. Weekly deaths and expected baseline deaths (July 2017–June 2020). Black line indicates weekly number of deaths (black line). Weeks run Thursday through Wednesday. Gray shading indicates lower and upper limits of expected baseline weekly deaths. COVID-19, coronavirus disease.

to 5.5% of the general population had experienced a SARS-CoV-2 infection by early May 2020. Of the total population size of 17.3 million (Statistics Netherlands, 2019), 5.5% corresponds to an estimated 951,500 coronavirus-infected persons (0.055 × 17.3 million = 951,500), thus placing the preliminary estimated overall infection-fatality rate at 1% (9,554 excess deaths/951,500 infected persons).

### Estimated Potential COVID-19 Deaths without Control Measures

A series of hygiene, social-distancing and partial lockdown measures have been implemented since March 9, 2020 (week 11; March 5–11 for our data). These measures and dates include cease handshaking, March 9; work from home, March 12; closure of schools and bars/restaurants, March 15; and stay-at-home advised and contact professions banned, March 23. During the COVID-19 epidemic, the RIVM provided weekly analyses and forecasts of the epidemic in the form of estimates of the virus reproduction number and projections of intensive care admissions by using a dynamic transmission model fitted to intensive care data (*23*). On the basis of the estimated reproduction number before the start of control measures (≈2–2.5), and model simulations in absence of control, it is expected that the epidemic would have infected 75%–80% of the population by early June 2020. This range is ≈14 times the 5.5% (*22*) seroprevalence found in May 2020. Assuming the same estimated infection-fatality rate, this rate would have resulted in 9,554 × 14, or 134,000, excess deaths if no control measures had been in place. This value is 0.78% of the population of the Netherlands.

## Discussion

Excess deaths varied considerably among influenza epidemics; the highest level in the past 10 years was observed during the influenza epidemic of 2017–18; there were an estimated 9,373 excess deaths in 18

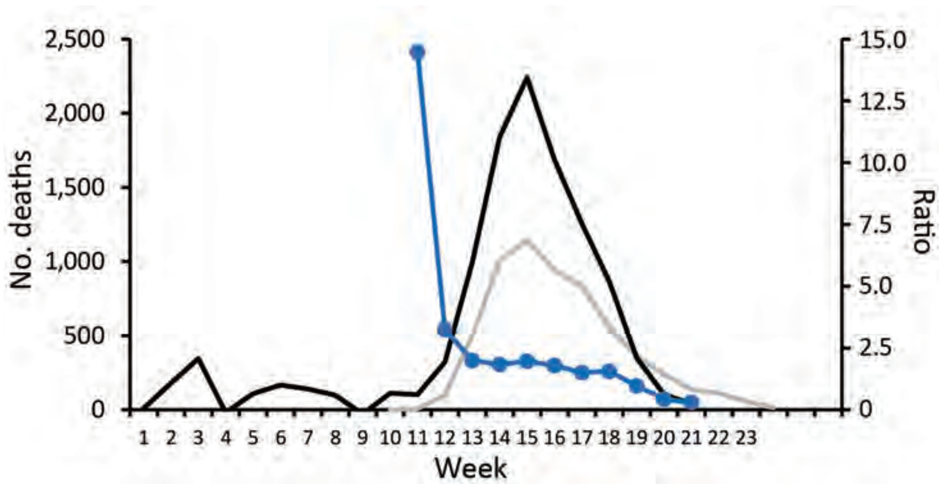


**Figure 3.** Excess deaths during influenza and coronavirus disease (COVID-19) and infection-fatality rate for severe acute respiratory syndrome coronavirus 2, the Netherlands. Excess deaths, reported COVID-19 deaths, and ratio between the 2 items (weeks 1–25, 2020). Black lines indicates excess deaths, gray line indicates COVID-19 reported deaths, and blue line indicates the ratio. Excess deaths were estimated with deaths reported within 3 weeks (and thus not yet available for week 24–25). The ratio for week 11 was 14.5, during the second (and final) week of the mixed influenza and COVID-19 epidemic.

weeks. The excess deaths for COVID-19 was similar in number to this large influenza epidemic, but its 9,554 excess deaths occurred in a much shorter time period (8 weeks) and reached a higher weekly peak (5,143) than during the influenza epidemic (4,049). In addition, the measures implemented to control the COVID-19 epidemic presumably prevented many infections (*24*) and deaths. Thus, the effect of COVID-19 on deaths is potentially much higher than that of seasonal influenza. The joint effect of influenza and COVID-19 epidemics on deaths is not yet known because they hardly overlapped during the past influenza season. To avoid miscomparisons (*25*), we compared excess deaths from influenza and COVID-19 by using the same data (all-cause deaths) and the same statistical method.

The case-fatality rate (CFR), calculated as the proportion of laboratory-confirmed COVID-19 cases that are fatal, is a commonly used measure of the severity of the COVID-19 epidemic. However, the CFR is greatly affected by testing and reporting practices and therefore cannot be used for comparisons over time and among countries. Some countries report only laboratory-confirmed cases, whereas other countries report clinically suspected patients and deaths. In addition, countries that test persons who have mild symptoms will have lower CFRs than countries that restrict testing to severely ill persons. We therefore calculated the infection-fatality rate on the basis of excess deaths and results of seroepidemiologic studies, a measure suitable for international comparisons.

The serologic surveys from which we used the estimated proportion of the population infected with SARS-CoV-2 are still in progress, and follow-up results will help to further improve the infection-fatality rate estimate. Cross-reactivity of laboratory tests might have caused an underestimation of the infection-fatality rate, whereas delayed antibody production after infection might have caused an overestimation. Additional study is required to better

**Table 2.** Excess deaths during influenza epidemics and the COVID-19 epidemic, the Netherlands*

| Season | Influenza strains† | Influenza vaccine match‡ | Vaccinated, % of target group§ | Epidemic duration, weeks | Excess deaths: No. (range)¶ | Excess deaths: % Above expected deaths |
|---|---|---|---|---|---|---|
| 2010–2011 | A(H1N1)pdm09 dominance followed by B Victoria dominance | Match | 69 | 7 | 416 (−722 to 1,555) | 2 |
| 2011–2012 | A(H3N2) dominance | Mismatch | 66 | 2 | 600 (308–892) | 11 |
| 2012–2013 | Mixed A(H1N1)pdm09 and A(H3N2) dominance followed by mixed B Yamagata and Victoria dominance | Mismatch | 62 | 18 | 6,318 (3,790–8,846) | 13 |
| 2013–2014 | Mixed dominance with slightly more A(H3N2) than A(H1N1)pdm09 | Mismatch | 60 | 11 | −581 (−1,927 to –765) | −2.1 |
| 2014–2015 | A(H3N2) dominance followed by B Yamagata dominance | Mismatch | 57 | 21 | 8,574 (5,831–11,316) | 15 |
| 2015–2016 | A(H1N1)pdm09 dominance followed by B Victoria dominance | Match | 56 | 11 | 3,883 (2,390–5, 375) | 13 |
| 2016–2017 | A(H3N2) | Match | 54 | 15 | 7,527 (5,236–9,817) | 18 |
| 2017–2018 | B Yamagata dominance; at end of season mixed AH3N2 and A(H1N1)pdm09 dominance | Mismatch; match# | 50 | 18 | 9,373 (6,439–12,306) | 18 |
| 2018–2019 | Mixed A(H1N1)pdm09 and AH3N2 dominance | Match | 51 | 14 | 2,858 (499–5,217) | 7 |
| 2019–2020 | Mixed A(H1N1)pdm09 and AH3N2 dominance | Match | 53 | 3** | 404 (−97 to –905) | 4 |
| 2019–2020 | Mixed Influenza and COVID-19 epidemic (weeks 10 and 11, 2020) | Match | NA | 2 | 213 (−115 to −541) | 4 |
| 2019–2020 | COVID-19 (selected weeks: 12–19, 2020) | NA | NA | 8†† | 9,554 (8,271–10,838) | 41 |
| 2010–2020 | Influenza seasonal average | NA | NA | 12 | 3,995 | 10 |

*COVID-19, coronavirus disease; NA, not applicable; pdm, pandemic.
†COVID-19 or influenza epidemic (influenza strains as reported in the Annual report: surveillance of influenza and other respiratory infections in the Netherlands).
‡Vaccine match with the dominant influenza strain(s).
§Persons $\geq$60 years of age or with concurrent conditions and increased risk for influenza complications, % as reported previously (*16*–*19*).
¶Number of deaths above expected baseline number of deaths (observed minus expected deaths). The range is approximated by the lower limit minus observed and the upper limit minus observed.
#Mismatch: Yamagata was not included in the vaccine; match: for both influenza A H1 and H3 strains.
**Excluding weeks 10 and 11 in 2020, which were both COVID-19 and influenza epidemic weeks (COVID-19: week 12–19: Thursday March 12–Wednesday May 6).
††Weeks with high excess deaths in the first wave of the COVID-19 epidemic.

estimate the number of COVID-19 deaths averted in the Netherlands.

We used a ratio of ≈14-fold higher expected excess deaths (134,000, or 0.78% of the population) in the absence of mitigation measures. This ratio is crude and not published but aligns with estimates from 11 other countries in Europe, which report COVID-19 deaths ranging from 0.22% to 1.1% of the population had there been no interventions (*26*). Without mitigation measures, persons might also have changed behavior, which would have affected the currently assumed ratio of 14.

The death surveillance system in the Netherlands was set up during the 2009 influenza pandemic to track the effect and burden of any epidemic and to signal any unexpected or undetected events (*1*,*8*,*9*). All calculations of excess deaths in this study and in our death surveillance are estimations and thus provide only a preliminary estimate of excess deaths from COVID-19. The straightforward linear regression model with linear and harmonic terms assumes a normal error distribution with constant variance, an approximation we deemed applicable to high numbers of weekly deaths.

There is no standard for determining actual expected levels of deaths and various calculations exist, even within the same country (*27*). Our method is similar to the regression method used by the EuroMOMO network (*28,29*) and similar to Serfling-type regression models (i.e., including seasonality by using sine and cosine terms) (*30*–*32*). However, the true baseline level of deaths during winter in the presence of influenza epidemics remains difficult to estimate. Removing seasons (*28*) or extremes to estimate the baseline warrants additional future sensitivity analyses. Our model detects no excess deaths in 2013–14, corresponding to a previous estimate of no influenza-associated intensive care admissions in that season (*33*). By accumulating the difference between the observed number of deaths and the upper (or lower) limit of the predicted baseline number of deaths, we only approximated the 95% prediction intervals. The intervals obtained in this way are too wide because nonlinearities in the calculation are neglected. Instead, in the future, by applying Monte Carlo simulation, we could obtain a better approximation of the 95% prediction intervals.

Weekly excess deaths from COVID-19 were usually 1.5–2-fold higher than those reported, indicating the extent of potential underreporting or underdetection of COVID-19 deaths. This discrepancy was greater at the beginning of excess deaths (at the peak of the COVID-19 epidemic), most likely because many regional public health services were unable to follow all the reported patients for disease outcome, including death status. All excess deaths during weeks 12–19 were most likely caused by direct and indirect effects of SARS-CoV-2 infections. No other outbreaks or extreme weather events were present during the epidemic weeks. Reported circulation of many other infectious diseases was actually lower than expected (*34*), probably because of partial lockdown, social distancing, and hygiene instructions.

We currently do not know the distribution of direct versus indirect effects of the COVID-19 epidemic on deaths. A major indirect factor to be explored is the postponement of regular medical care, especially during the peak of the epidemic. Hospitals were overburdened and halted admissions for nonurgent care. Also, healthcare-seeking behavior changed in patients with nonrespiratory symptoms because they feared getting COVID-19 in hospitals or putting additional pressure on the healthcare system. Other indirect effects on deaths might have been caused by shifts (up or down) in occurrence of potentially fatal events, such as accidents and suicides. In-depth analyses of death-cause data will shed more light on these events.

Several other issues should also be elucidated in further studies. First, we provided an indication of excess deaths in the total population of the Netherlands, but it occurred mostly, but not exclusively, in the elderly (groups ≥65 years of age) during the influenza epidemics and the COVID-19 epidemic. Age-specific results warrant further investigation and reporting, as do regional differences (*35*). Second, our analyses provide estimates specific to the Netherlands. Data for the Netherlands are also included in the EuroMOMO death monitoring, which pools data from 24 countries and provides death surveillance at a level for Europe. Third, influenza epidemics, which are well monitored, are the most frequent infectious disease events coinciding with excess deaths in the Netherlands. However, influenza epidemics often coincide with other respiratory infections in winter or (occasionally) cold weather. Influenza is a well-known contributor to excess deaths, but our methods did not disentangle its contribution from that of other respiratory infections and events. Fourth, the estimate of COVID-19 excess deaths was based on data for weeks 12–19, after which overall death rates returned to baseline levels. However, COVID-19 deaths were still reported at low levels (e.g., 45 during week 24), and we do not know how COVID-19 deaths will continue to evolve.

Although COVID-19 incidence has greatly decreased because of social distancing and lockdowns, measures are still in place to reduce virus transmission. The 9,554 excess deaths (March 12–May 6) are a slight underestimation of the total excess during the entire COVID-19 epidemic because we excluded the first 2 weeks in which influenza and COVID-19 epidemics coincided. With excess deaths at 213 during those weeks, this exclusion underestimates COVID-19 excess deaths by at most 2%. An additional 1% underestimation is caused by using deaths reported within 3 weeks (i.e., 99% of deaths reported), which is an input parameter for the weekly algorithm in death monitoring. Finally, further quantification of years of life lost because of COVID-19 is required because such loss may be considerable (*36*).

Influenza vaccination is available in the Netherlands for risk groups (persons $\geq$60 years of age or those with underlying conditions) to reduce severe sequelae of influenza infections, but coverage is rather low (51% in 2019) (*33*–*36*). Vaccination is only partially effective, and the effectiveness varies by season because of virus strain variability and varying vaccine match (Table 2). COVID-19 vaccination is not yet available. Social distancing and lockdown measures have had a large effect on decreasing the epidemic and thus also COVID-19 deaths. If some or all of these measures stay in place, they might likewise decrease influenza virus circulation and thus severe sequelae of infection in the upcoming winter season, as observed in Hong Kong, China, at the beginning of the COVID-19 epidemic (*37*).

The 2019–2020 influenza season just preceding the COVID-19 epidemic was short and relatively mild; there were 404 excess deaths compared with an average of 4,000 in seasons over the past 10 years. It is unknown whether excess deaths would have differed had the COVID-19 epidemic been preceded by a more severe influenza epidemic or a colder winter. It is likewise unclear how SARS-CoV-2 and influenza virus infections might interact and affect deaths, should epidemics occur simultaneously. In our study, the short mixed-epidemic period of 2 weeks did not involve full combined virus circulation because the influenza epidemic was decreasing and the COVID-19 epidemic was just getting started.

In conclusion, estimation of excess deaths complements the reporting of laboratory-confirmed COVID-19 deaths, indicating the potential magnitude of underreporting and underdetection of COVID-19 deaths. These estimates also provide a timely indication of the combined direct and indirect effects of the COVID-19 epidemic on population deaths. In the coming weeks and months, monitoring of deaths remains key to the timely monitoring of the effects of COVID-19 and influenza. COVID-19 might have a long-lasting effect, potentially becoming endemic with yearly recurrence(s), similar to influenza. It remains to be seen whether the effect of COVID-19 on deaths remains greater than that of influenza. Monitoring of excess deaths can provide input for public health and economic decisions. This monitoring also remains essential for monitoring the effects of any other events and outbreaks and for detecting any unexpected and unforeseen increases in deaths.

This study was supported by the National Institute for Public Health and the Environment; support was made available by the Ministry of Health, Welfare and Sport (project no. D/111001/01/CO).

L.vA. and W.vdH. designed the research study; L.vA. drafted the manuscript; L.vA. performed statistical analyses; J.vdK. provided statistical support; and L.vA., C.N.H., L.S., D.K., A.C.T., M.dL., A.M., J.vdK, A.vG., S.vdH., and W.vdH. contributed to writing the paper. All coauthors read and approved the final manuscript.

## About the Author

Dr. van Asten is a research scientist at the National Institute for Public Health and the Environment, Bilthoven, the Netherlands. Her primary research interests are epidemiology of infectious diseases, surveillance, and respiratory infections.

## References

1. van Asten L, de Lange M, Teirlinck A, Stoeldraijer L, Harmsen C, van der Hoek W. Mortality surveillance in the Netherlands: severity of winter 2016/2017. Online J Public Health Inform. 2018;10. https://doi.org/10.5210/ojphi.v10i1.8946
2. Vestergaard LS, Nielsen J, Krause TG, Espenhain L, Tersago K, Bustos Sierra N, et al. Excess all-cause and influenza-attributable mortality in Europe, December 2016 to February 2017. Euro Surveill. 2017;22:30506. https://doi.org/10.2807/1560-7917.ES.2017.22.14.30506
3. van Asten L, van den Wijngaard C, van Pelt W, van de Kassteele J, Meijer A, van der Hoek W, et al. Mortality attributable to 9 common infections: significant effect of influenza A, respiratory syncytial virus, influenza B, norovirus, and parainfluenza in elderly persons. J Infect Dis. 2012;206:628–39. https://doi.org/10.1093/infdis/jis415
4. Nielsen J, Mazick A, Andrews N, Detsis M, Fenech TM, Flores VM, et al. Pooling European all-cause mortality: methodology and findings for the seasons 2008/2009 to 2010/2011. Epidemiol Infect. 2013;141:1996–2010. https://doi.org/10.1017/S0950268812002580
5. Leon DA, Shkolnikov VM, Smeeth L, Magnus P, Pechholdová M, Jarvis CI. COVID-19: a need for real-time

monitoring of weekly excess deaths. Lancet. 2020;395:e81. https://doi.org/10.1016/S0140-6736(20)30933-8
6. Olson DR, Huynh M, Fine A, Baumgartner J, Castro A, Chan HT, et al.; New York City Department of Health and Mental Hygiene (DOHMH) COVID-19 Response Team. Preliminary estimate of excess mortality during the COVID-19 outbreak—New York City, March 11–May 2, 2020. MMWR Morb Mortal Wkly Rep. 2020;69:603–5. https://doi.org/10.15585/mmwr.mm6919e5
7. Reukers DF, Brandsema L, Dijkstra PS, Donker F, van Gageldonk-Lafeber GA, Hooiveld AB, et al. Annual report. Surveillance of influenza and other respiratory infections in the Netherlands: winter 2018/2019. RIVM: Bilthoven (the Netherlands); 2019 [cited 2020 Nov 15]. https://www.rivm.nl/bibliotheek/rapporten/2019-0079.pdf
8. van Asten LW, Harmsen C, van Gageldonk C, van Pelt R, van Vliet W, van der Sande H, et al. M., Syndromic surveillance with death data: is crude mortality data suitable for real time surveillance? Advances in Disease Surveillance. 2007;4:269.
9. van Asten L, de Lange M, Harmsen C, van den Wijngaard K, Kretzschmar M, van der Hoek W. Mortality monitoring in the Netherlands. Online J Public Health Inform. 2014;6. https://doi.org/10.5210/ojphi.v6i1.5130
10. Teirlinck AC, van Asten L, Brandsema PS, Dijkstra F, Donker GA, Euser SM, et al. Annual report: surveillance of influenza and other respiratory infections in the Netherlands: winter 2014/2015; 2015. Rijksinstituut voor Volksgezondheid en Milieu (RIVM) [cited 2020 Nov 15]. https://www.rivm.nl/bibliotheek/rapporten/2015-0042.pdf
11. Donker G. Nivel primary care registry: sentinels 2018; 2019 [in Dutch] [cited 2020 Nov 16]. https://nivel.nl/en/publicatie/nivel-zorgregistraties-eerste-lijn-peilstations-2018
12. Vega T, Lozano JE, Meerhoff T, Snacken R, Mott J, Ortiz de Lejarazu R, et al. Influenza surveillance in Europe: establishing epidemic thresholds by the moving epidemic method. Influenza Other Respir Viruses. 2013;7:546–58. https://doi.org/10.1111/j.1750-2659.2012.00422.x
13. Dijkstra F, van Gageldonk-Lafeber AB, Brandsema P, Friesema IH, Robert-Du Ry van Beest Holle M, van der Lubben IM, et al. Year report. Respiratory infections 2007/2008; 2008. RIVM, Bilthoven, the Netherlands [cited 2020 Nov 16]. https://www.rivm.nl/bibliotheek/rapporten/210231003.pdf
14. Teirlinck A, van Asten L, Brandsema P, Dijkstra F. Annual report: surveillance of respiratory infections 2013/2014; 2014 [in Dutch] [cited 2020 Nov 16]. https://www.rivm.nl/bibliotheek/rapporten/150002006.pdf
15. Bulletin of Influenza Surveillance. Number of ILI patients above epidemic threshold, 2020 [in Dutch] [cited 2020 Nov 15]. https://www.nivel.nl/sites/default/files/influenza-nieuwsbrief/NB_2019_2020_no5.pdf
16. Tacken M, Mulder J, Visscher S, Tiersma W, Donkers J, Verheij R, et al. Monitoring the influenza vaccination coverage 2009; 2010 [in Dutch] [cited 2020 Nov 15]. https://www.nivel.nl/sites/default/files/bestanden/LINH%20griepmonitoring%202009%20rapport.pdf
17. Heins MJ, Hooiveld M, Davids R, Korevaar JC. Influenza vaccination coverage in the Dutch National Programme for Influenza Prevention, 2016; 2017 [cited 2020 Nov 16]. https://nivel.nl/sites/default/files/bestanden/Monitor_Vaccinatiegraad_Nationaal_Programma_Grieppreventie_2016.pdf.
18. Heins M, Hooiveld M, Korevaar J. Vaccine Coverage Dutch National Influenza Prevention Program 2018: brief monitor, 2019 [cited 2020 Nov 15]. https://www.nivel.nl/nl/publicatie/vaccine-coverage-dutch-national-influenza-prevention-program-2018-brief-monitor
19. Heins MJ, Hooiveld M, Davids R, Korevaar JC. Vaccine Coverage Dutch National Influenza Prevention Program 2019: brief monitor, 2020 [cited 2020 Nov 15]. https://www.nivel.nl/nl/publicatie/vaccine-coverage-dutch-national-influenza-prevention-program-2019-brief-monitor
20. Sanquin. Approximately 3% of blood donors have antibodies against SARS-CoV-2, April 16, 2020 [in Dutch] [cited 2020 Nov 15]. https://www.sanquin.nl/over-sanquin/nieuws/2020/04/sanquin-ongeveer-3-van-donors-heeft-corona-antistoffen
21. RIVM. Preliminary results from the Pienter corona study, 2020 [in Dutch] [cited 2020 Nov 15] https://www.rivm.nl/pienter-corona-studie/voorlopige-resultaten
22. Sanquin. Approximately 5% of blood donors have antibodies against SARS-CoV-2; June 3, 29020 [in Dutch] [cited 2020 Nov 15]. https://www.sanquin.nl/over-sanquin/persberichten/2020/06/ongeveer-5-procent-van-bloeddonors-heeft-corona-antistoffen
23. van Dissel J. COVID 19 presentation for the House of Representatives of the Netherlands, May 20, 2020 [in Dutch]. National Institute for Public Health and the Environment (RIVM) [cited 2020 Nov 15]. https://www.tweedekamer.nl/kamerstukken/detail?id=2020D19084&did=2020D19084
24. Hsiang S, Allen D, Annan-Phan S, Bell K, Bolliger I, Chong T, et al. The effect of large-scale anti-contagion policies on the COVID-19 pandemic. Nature. 2020;584:262–7. https://doi.org/10.1038/s41586-020-2404-8
25. Faust JS, Del Rio C. Assessment of deaths from COVID-19 and from seasonal influenza. JAMA Intern Med. 2020; 180:1045–6. https://doi.org/10.1001/jamainternmed.2020.2306
26. Flaxman S, Mishra S, Gandy A, Unwin HJ, Mellan TA, Coupland H, et al.; Imperial College COVID-19 Response Team. Estimating the effects of non-pharmaceutical interventions on COVID-19 in Europe. Nature. 2020;584:257–61. https://doi.org/10.1038/s41586-020-2405-7
27. Thompson WW, Weintraub E, Dhankhar P, Cheng PY, Brammer L, Meltzer MI, et al. Estimates of US influenza-associated deaths made using four different methods. Influenza Other Respir Viruses. 2009;3:37–49. https://doi.org/10.1111/j.1750-2659.2009.00073.x
28. Molbak K, Espenhain L, Nielsen J, Tersago K, Bossuyt N, Denissov G, et al. Excess mortality among the elderly in European countries, December 2014 to February 2015. Euro Surveill. 2015;20:21065. https://doi.org/10.2807/1560-7917.ES2015.20.11.21065
29. Nielsen J, Vestergaard LS, Richter L, Schmid D, Bustos N, Asikainen T, et al. European all-cause excess and influenza-attributable mortality in the 2017/18 season: should the burden of influenza B be reconsidered? Clin Microbiol Infect. 2019;25:1266–76. https://doi.org/10.1016/j.cmi.2019.02.011
30. Serfling RE. Methods for current statistical analysis of excess pneumonia-influenza deaths. Public Health Rep. 1963;78:494–506. https://doi.org/10.2307/4591848
31. Baghdadi Y, Gallay A, Caserio-Schönemann C, Fouillet A. Evaluation of the French reactive mortality surveillance system supporting decision making. Eur J Public Health. 2019;29:601–7. https://doi.org/10.1093/eurpub/cky251
32. Green HK, Andrews N, Fleming D, Zambon M, Pebody R. Mortality attributable to influenza in England and Wales prior to, during and after the 2009 pandemic. PLoS One. 2013;8:e79360. https://doi.org/10.1371/journal.pone.0079360

33. van Asten L, Luna Pinzon A, van de Kassteele J, Donker G, de Lange DW, Dongelmans DA, et al. The association between influenza infections in primary care and intensive care admissions for severe acute respiratory infection (SARI): a modelling approach. Influenza Other Respir Viruses. 2020;14:575–86. https://doi.org/10.1111/irv.12759
34. Nivel. Nivel primary care database: weekly numbers [cited 2020 Nov 15]. https://www.nivel/nl/surveillance
35. Michelozzi P, de'Donato F, Scortichini M, De Sario M, Noccioli F, Rossi P, et al. Mortality impacts of the coronavirus disease (COVID-19) outbreak by sex and age: rapid mortality surveillance system, Italy, 1 February to 18 April 2020. Euro Surveill. 2020;25. https://doi.org/10.2807/1560-7917.ES.2020.25.19.2000620
36. Hanlon P, Chadwick F, Shah A, Wood R, Minton J, McCartney G, et al. COVID-19: exploring the implications of long-term condition type and extent of multimorbidity on years of life lost: a modelling study. Wellcome Open Research. 2020;5:75. https://doi.org/10.12688/wellcomeopenres.15849.1
37. Cowling BJ, Ali ST, Ng TW, Tsang TK, Li JCM, Fong MW, et al. Impact assessment of non-pharmaceutical interventions against coronavirus disease 2019 and influenza in Hong Kong: an observational study. Lancet Public Health. 2020;5:e279–88. https://doi.org/10.1016/S2468-2667(20)30090-6


Address for correspondence: Liselotte van Asten, Centre for Infectious Disease Control Netherlands, National Institute for Public Health and the Environment (RIVM), PO.Box 1, 3720 BA Bilthoven, the Netherlands; email: liselotte.van.asten@rivm.nl

# Rapid Transmission of Severe Acute Respiratory Syndrome Coronavirus 2 in Detention Facility, Louisiana, USA, May–June, 2020

Megan Wallace,[1] Allison E. James,[1] Rachel Silver, Mitsuki Koh, Farrell A. Tobolowsky, Sean Simonson, Jeremy A. W. Gold, Rena Fukunaga, Henry Njuguna, Keith Bordelon, Jonathan Wortham, Melissa Coughlin, Jennifer L. Harcourt, Azaibi Tamin, Brett Whitaker, Natalie J. Thornburg, Ying Tao, Krista Queen, Anna Uehara, Clinton R. Paden, Jing Zhang, Suxiang Tong, Danielle Haydel, Ha Tran, Kaylee Kim, Kiva A. Fisher, Mariel Marlow, Jacqueline E. Tate, Reena H. Doshi, Theresa Sokol, Kathryn G. Curran

To assess transmission of severe acute respiratory syndrome coronavirus 2 (SARS-CoV-2) in a detention facility experiencing a coronavirus disease outbreak and evaluate testing strategies, we conducted a prospective cohort investigation in a facility in Louisiana, USA. We conducted SARS-CoV-2 testing for detained persons in 6 quarantined dormitories at various time points. Of 143 persons, 53 were positive at the initial test, and an additional 58 persons were positive at later time points (cumulative incidence 78%). In 1 dormitory, all 45 detained persons initially were negative; 18 days later, 40 (89%) were positive. Among persons who were SARS-CoV-2 positive, 47% (52/111) were asymptomatic at the time of specimen collection; 14 had replication-competent virus isolated. Serial SARS-CoV-2 testing might help interrupt transmission through medical isolation and quarantine. Testing in correctional and detention facilities will be most effective when initiated early in an outbreak, inclusive of all exposed persons, and paired with infection prevention and control.

Correctional and detention facilities face unique challenges for controlling severe acute respiratory syndrome coronavirus 2 (SARS-CoV-2), the virus that causes coronavirus disease (COVID-19). These challenges include an inability for incarcerated or detained persons to socially distance and an ongoing risk for virus introduction caused by staff movement outside and within the facilities (*1,2*). These inherent difficulties underpin increased rates of SARS-CoV-2 infections and deaths among incarcerated and detained persons compared with the general population; 146,472 cases and 1,122 deaths in this population were reported in the United States as of October 20, 2020 (*3,4*). The Centers for Disease Control and Prevention (CDC) released interim guidance for management of COVID-19 in correctional and detention facilities; however, some facilities reported limitations to fully implementing the guidance (*5–7*). In addition, the potential for asymptomatic and presymptomatic transmission limits the effectiveness of symptom screening to identify cases and halt transmission (*8–10*). In other congregate settings, serial testing and physically separating persons based on their SARS-CoV-2 test results have been used to interrupt transmission (*11,12*).

We investigated a COVID-19 outbreak in a detention center in Louisiana, USA (facility X) and used a serial testing strategy to identify infections and interrupt transmission in affected dormitories. All residents of affected dormitories underwent SARS-CoV-2 testing to assess the extent of transmission within the dormitory, to cohort detained persons based on their test result to prevent transmission, and to evaluate the utility of serial testing in this setting. We report the findings of this investigation; initial results were previously reported (*13*).

Author affiliations: Centers for Disease Control and Prevention, Atlanta, Georgia, USA (M. Wallace, A.E. James, R. Silver, M. Koh, F.A. Tobolowsky, J.A.W. Gold, R. Fukunaga, H. Njuguna, K. Bordelon, J. Wortham, M. Coughlin, J.L. Harcourt, A. Tamin, B. Whitaker, N.J. Thornburg, Y. Tao, K. Queen, A. Uehara, C.R. Paden, J. Zhang, S. Tong, K. Kim, K.A. Fisher, M. Marlow, J.E. Tate, R.H. Doshi, K.G. Curran); Louisiana Department of Health, New Orleans, Louisiana, USA (S. Simonson, D. Haydel, H. Tran, T. Sokol)

DOI: https://doi.org/10.3201/eid2702.204158

[1]These authors contributed equally to this article.

By March 17, 2020, in response to emergence of COVID-19 in Louisiana, facility X ceased travel of detained persons outside the facility, halted visitors and transfers between facilities, and prohibited movement of detained persons within the facility. On March 29, a staff member showed symptoms consistent with COVID-19; this staff member later tested positive for SARS-CoV-2. On April 7, facility X medical staff identified the first COVID-19 case in a detained person residing in dormitory A. After this diagnosis, staff began active daily monitoring for fever (temperature >100.4°F) and blood oxygen saturation levels (pulse oximeter reading <90%) to detect suspected cases among persons in affected dormitories. On April 9, additional cases were identified in dormitories B and C; the first cases were identified in dormitory D on April 17 and in dormitory E on April 23.

The Louisiana Department of Health requested CDC assistance; a team arrived and began an investigation on May 7. By that date, 3 staff members and 35 detained persons showed development of symptoms and later tested positive for SARS-CoV-2; 5 of 18 dormitories were affected.

## Methods

### Population

Facility X is a medium-security local jail that houses up to 800 detained persons. Before the COVID-19 pandemic, the facility operated at nearly 100% capacity. On May 7, the facility was at ≈85% capacity because of a reduction in occupancy in response to COVID-19. Detained persons from 6 dormitories (A–F) were enrolled in this prospective cohort investigation. Five dormitories (A–E) had detained persons with laboratory-confirmed COVID-19 cases; dormitory F, which housed a detained person with COVID-19 symptoms and negative SARS-CoV-2 test results, was enrolled because of proximity to dormitories A, B, and D. All detained persons with suspected and confirmed COVID-19 were moved to medical isolation, and persons within the dormitories were quarantined as a cohort.

### Testing Strategy and Cohorting by Test Result

Nasopharyngeal swab specimens were collected for initial SARS-CoV-2 testing on day 0 for all consenting persons residing in dormitories A–F (Figure 1). Persons who had positive results by real-time reverse transcription PCR (rRT-PCR) were moved to the designated SARS-CoV-2–positive dormitories upon facility receipt of results (<24 hours after specimen collection). Serial testing was offered on day 4 to detained persons who tested negative for SARS-CoV-2 on day 0, and again on day 14 for persons who tested negative on day 4. To assess persistence of viral shedding, detained persons testing positive on day 0 or day 4 were offered testing 14–15 days and 19–27 days after their first positive test result.

In dormitory F, where all detained persons tested negative for SARS-CoV-2 on day 0, a serial testing strategy was not used. Rather, a second survey and repeat test was conducted on day 18.

### Dormitory Survey and Symptoms, Concurrent Conditions, and Behavioral Risk Assessment

The investigation team administered a structured dormitory survey among facility staff to assess physical layout, capacity, activities, and practices. During day 0 testing, detained persons completed a self-administered, paper-based questionnaire of demographics, symptoms in the preceding 2 months and 2 weeks, facility exposures, and preventive measures. On the day of each subsequent test, detained persons received an abbreviated self-administered, paper-based questionnaire of symptoms experienced since the last testing day. The team verbally verified responses with detained persons and assisted as necessary. Medical history data were abstracted from facility medical records. Data were deidentified and entered into a secure database (Research Electronic Data Capture, version 8.8.0; Vanderbilt University, https://redcap.vanderbilt.edu).

### Laboratory Testing

Nasopharyngeal swab specimens collected for the investigation during May 7–June 3 were immediately placed on dry ice and sent by courier to the Louisiana Office of Public Health Laboratory for SARS-CoV-2 testing by using the CDC 2019-Novel Coronavirus (2019-nCoV) Real-Time rRT-PCR Diagnostic Panel. Cycle threshold ($C_t$) values for 2 viral nucleocapsid protein genes (N1 and N2) were obtained for each specimen; $C_t$ values <40 cycles for both N1 and N2 were considered positive for SARS-CoV-2 (*14*). All samples that were positive at the Louisiana Office of Public Health Laboratory were refrozen and shipped to CDC for viral culture by using Vero-CCL-81 cells (*15*). Positive viral culture for SARS-CoV-2 replication-competent virus was confirmed in cells that showed a cytopathic effect by using rRT-PCR.

Nucleic acid was extracted from 41 rRT-PCR–positive specimens or isolates and subjected to Oxford Nanopore MinION Sequencing (https://nanoporetech.com) according to published protocols (*16*); consensus sequences were generated by using Minimap version 2.17 (https://github.com/lh3/minimap2) and Samtools version 1.9 (http://www.

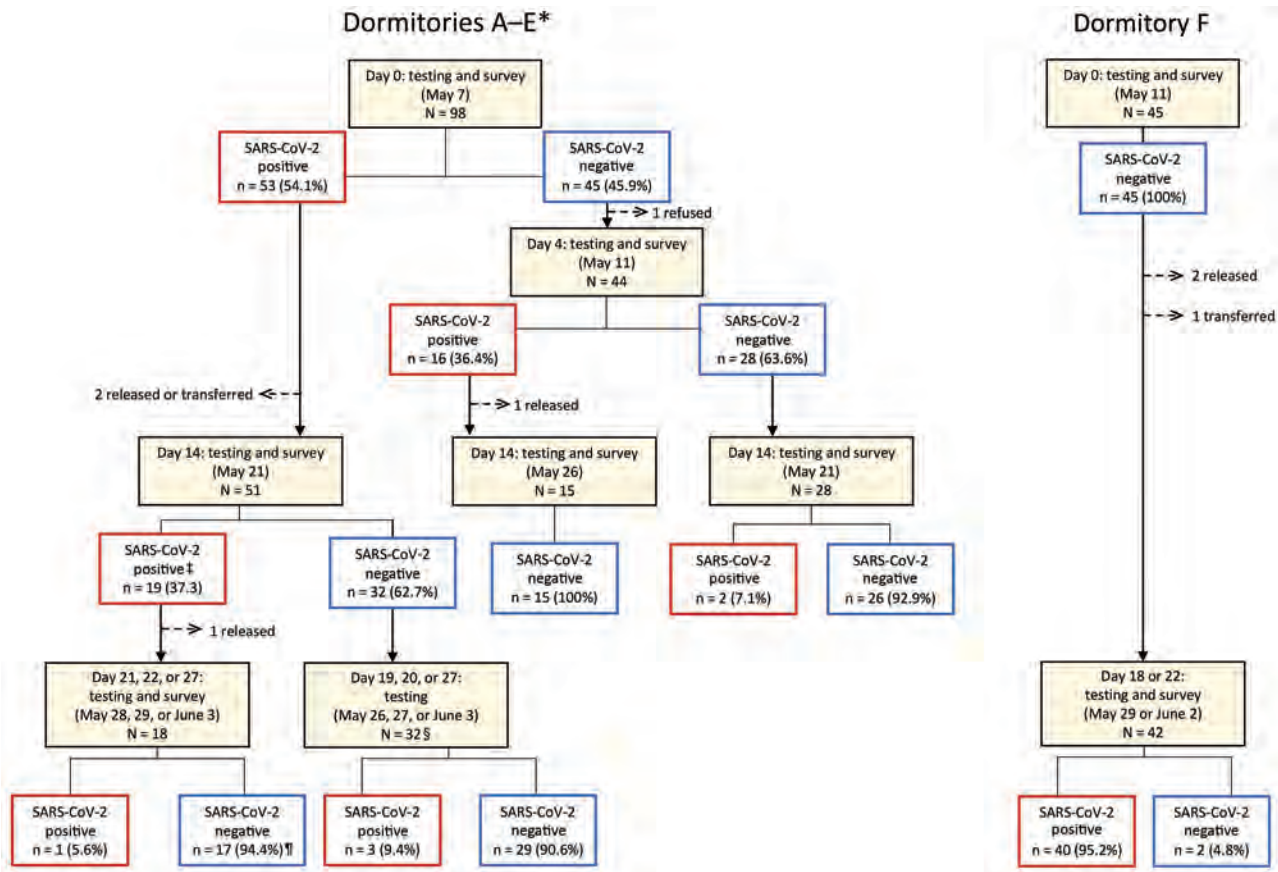


**Figure 1.** Rapid transmission of SARS-CoV-2 in detention facility, Louisiana, USA, May–June 2020. Enrollment and follow-up at each timepoint for detained persons (n = 143) in dormitories A–E and F. The sequence of testing for all enrolled dormitories is shown, along with the number of persons who were positive or negative for SARS-CoV-2 by real-time reverse transcription PCR and percentage of total at each timepoint. Red boxes indicate SARS-CoV-2 positive, and blue boxes indicate SARS-CoV-2 negative. *The first positive test result for SARS-CoV-2 among persons detained occurred on the following dates in each dormitory: April 7 in A, April 9 in B and C, April 17 in D, and April 23 in E. Introduction in dormitory F likely occurred between May 11 and May 29. †One inconclusive result was considered negative; ‡One inconclusive result was considered positive. §16 persons were tested on May 26 only, 14 on May 27 only, and 2 on May 26 and June 3. ¶10 persons were tested on May 28 only, 1 on May 29 only, 1 on June 3 only, and 6 on May 28 and June 3. SARS-CoV-2, severe acute respiratory syndrome coronavirus 2.

htslib.org). Representative full-genome sequences were downloaded on August 28, 2020, from GISAID (https://www.gisaid.org), and phylogenetic relations were inferred by using maximum-likelihood analyses implemented in TreeTime (http://evol.bio.lmu.de/_statgen/software/treetime) and the Nextstrain pipeline (*17*). Sequences were submitted to GenBank and GISAID.

## Analyses

We performed descriptive analyses for the population demographics (age, sex, race/ethnicity), underlying medical conditions (respiratory disease, diabetes, hypertension, other cardiovascular disease, other condition), obesity (body mass index >30 kg/m$^2$), tobacco use, and dormitory characteristics (capacity at start of the investigation, toilets/sinks, showers per person). Overall cumulative incidence and dormitory cumulative incidence for each test day were calculated.

We calculated descriptive statistics for $C_t$ values and culture results, stratified by symptom status. The rRT-PCR analyses used the $C_t$ value reported for the N1 genetic target because N1 and N2 approximate each another (*18*). Persons were categorized as presymptomatic, symptomatic, postsymptomatic, or asymptomatic on the basis of symptoms at sample collection. Any CDC-listed coronavirus symptom with a reported onset date on or after March 29, 2020, the illness onset date of the first reported COVID-19 case in the facility, was included in analyses (*19*). Persons were classified as symptomatic if they reported ≥1 present or ongoing symptom. If 2 courses of illness were distinguishable from the symptom data, in which multiple symptoms were reported to occur with symptom onsets ≥14 days apart and the first course of illness (earlier dated symptoms) was reported to have resolved, only the symptoms reported closer to the date of testing were used for classification. Postsymptomatic persons were those who reported symptoms that had resolved before the first positive test result or before the start of the investigation (day 0) for those who were tested and remained negative during the investigation. Persons reporting symptoms whose surveys were missing current symptom status were considered symptomatic if the onset date was ≤10 days the start of the investigation. Presymptomatic persons reported ≥1 symptom with onset after their first positive test result and had no previously reported symptoms. Asymptomatic persons reported no symptoms throughout the investigation. Persons were classified as having an unknown symptom status if any symptom data were missing and no symptoms were reported. $C_t$ value and culture results were graphed by days from symptom onset and original dormitory.

To compare individual symptoms, facility exposures (bunk sleeping location, travel out of dormitory, exposure to someone visibly ill), and preventive measures (handwashing, mask use) by SARS-CoV-2 test result, we performed bivariate analyses by using Fisher exact tests for proportions. Analyses were completed by using R statistical software version 4.0.0 (The R Foundation, https://www.r-project.org) and SAS 9.4 software version 6.2.92 (SAS Institute Inc., https://www.sas.com).

### Ethics

This activity was determined to meet the requirements of public health surveillance as defined in 45 CFR 46.102(l) (2). All persons provided voluntary oral consent for testing and to complete questionnaires.

## Results

### Dormitory and Detained Persons Characteristics

All 143 detained persons from 6 dormitories were invited for testing, and 143 (100%) participated in the day 0 testing and survey (Figure 1). Median age was 33 (interquartile range 28–42) years, and most (136, 95%) were male (Table 1). Most (102, 71%) were Black non-Hispanic persons, and 36 (25%) were White non-Hispanic persons. One third (49, 34%) of the 143 detained persons had an underlying medical condition. Dormitory E was the only female dormitory. Dormitory C had the highest median age (45 years; interquartile range 35–52 years) and the highest proportion (7/11; 64%) of persons with underlying medical conditions. Dormitory E had the lowest percent occupancy (7/22; 32%), whereas dormitory F was near full capacity (45/50; 90%). All dormitories had 3–4 shared toilets and sinks and 2–3 shared showers.

**Table 1.** Characteristics of detained persons tested for SARS-CoV-2 in a correctional facility, Louisiana, USA, by dormitory, May–June 2020*

| Characteristic | Dormitory A, n = 20 | Dormitory B, n = 23 | Dormitory C, n = 11 | Dormitory D, n = 37 | Dormitory E, n = 7 | Dormitory F, n = 45 | Total, N = 143 |
|---|---|---|---|---|---|---|---|
| Median age, y (IQR) | 37 (29–47) | 31 (29–36) | 45 (35–52) | 31 (29–39) | 37 (29–47) | 32 (24–41) | 33 (28–42) |
| Sex | | | | | | | |
| M | 20 (100) | 23 (100) | 11 (100) | 37 (100) | 0 | 45 (100) | 136 (95) |
| F | 0 | 0 | 0 | 0 | 7 (100) | 0 | 7 (5) |
| Race/ethnicity | | | | | | | |
| White non-Hispanic | 10 (50) | 6 (26) | 7 (64) | 5 (14) | 2 (29) | 5 (11) | 36 (25) |
| Black non-Hispanic | 10 (50) | 16 (70) | 4 (36) | 30 (81) | 5 (71) | 37 (82) | 102 (71) |
| Asian non-Hispanic | 0 | 0 | 0 | 1 (3) | 0 | 0 | 1 (1) |
| Hispanic/Latino | 0 | 0 | 0 | 1 (3) | 0 | 3 (8) | 4 (3) |
| Underlying health condition | | | | | | | |
| Any | 8 (40) | 7 (30) | 7 (64) | 14 (38) | 3 (43) | 10 (22) | 49 (34) |
| Respiratory disease | 3 (15) | 3 (13) | 3 (27) | 5 (14) | 1 (14) | 3 (7) | 18 (13) |
| Asthma | 1 (5) | 1 (4) | 3 (27) | 4 (11) | 0 | 3 (7) | 12 (8) |
| Diabetes | 1 (5) | 0 | 3 (27) | 0 | 2 (29) | 1 (2) | 7 (5) |
| Hypertension | 3 (15) | 3 (13) | 5 (45) | 7 (19) | 2 (29) | 7 (15) | 27 (19) |
| Other CVD | 0 | 1 (4) | 0 | 2 (5) | 0 | 1 (2) | 4 (3) |
| Other† | 4 (15) | 2 (8) | 1 (9) | 2 (5) | 0 | 1 (2) | 10 (7) |
| Obesity, BMI >30 kg/m$^2$ | 6 (30) | 7 (30) | 1 (9) | 7 (19) | 2 (29) | 6 (13) | 29 (20) |
| Any past tobacco use | 12 (60) | 5 (22) | 8 (73) | 14 (38) | 4 (57) | 17 (38) | 60 (42) |
| Dormitory | | | | | | | |
| Capacity at start of study | 20/30 (67) | 23/30 (77) | 11/22 (50) | 37/50 (74) | 7/22 (32) | 45/50 (90) | NA |
| Toilets/sinks | 3 | 3 | 4 | 3 | 4 | 3 | NA |
| Showers/person | 3 | 3 | 2 | 3 | 2 | 2 | NA |

*Values are no. (%) or no. unless indicated otherwise. BMI, body mass index; CVD, cardiovascular disease; IQR, interquartile range; NA, not applicable; SARS-CoV-2, severe acute respiratory syndrome coronavirus 2.
†Includes liver disease, immunosuppressive disorder, and neurologic disease.

### Serial Testing

In dormitories A–E, 53 (54%) persons tested positive on day 0 (Table 2). Among persons with negative test results from day 0 testing in dormitories A–E (n = 45), 16 (36%) had SARS-CoV-2 detected on day 4 testing. Two additional persons tested positive for SARS-CoV-2 on day 14, both of whom originally resided in dormitory B. No SARS-CoV-2 infections (0/45) were detected during the day 0 testing in dormitory F. However 40 (89%) of 45 persons tested positive for SARS-CoV-2 on day 18. No detained persons testing positive for SARS-CoV-2 from any dormitory required hospitalization during their illness.

The overall cumulative incidence during May 7–June 3 of SARS-CoV-2 infection for all dormitories was 78% (111/143). Dormitory E had the lowest cumulative incidence (57; 4/7), and dormitory F had the highest cumulative incidence (89%; 40/45). Day 0 testing in dormitory E was initiated 14 days after the diagnosis of the first known COVID-19 case in the dormitory, and dormitories A–D had reported cases 20–30 days before the investigation.

Of 111 detained persons with SARS-CoV-2-positive test results, 66 persons received a second test (day 14) and 50 people received a third test (during days 19–27) during the investigation (Figure 1). Nineteen (29%) of 66 persons had positive test results 14 days after the first positive test result, and 4 (8%) of 50 persons had positive test results ≈3 weeks after first testing positive, 3 of whom had negative results on day 14.

### Symptom and Behavioral Risk Assessment

Among 111 detained persons who tested positive for SARS-CoV-2, 21 (19%) were symptomatic at the time of their first positive test result, and 27 (24%) reported symptoms that had resolved before their first positive test result (Table 3). The most commonly reported symptoms among persons with SARS-CoV-2 infection were headache (32%), loss of taste or smell (31%), and nasal congestion (26%); measured fever (5%) and dyspnea (8%) were less commonly reported (Appendix Table 1, https://wwwnc.cdc.gov/EID/article/27/2/20-4158-App1.pdf). Forty-nine (44%) detained persons who tested positive for SARS-CoV-2 were asymptomatic and 3 (3%) were presymptomatic. Symptom onset among presymptomatic persons was 0–7 days from the day of first positive specimen collection. Among 32 detained persons with negative test results, 8 (25%) were symptomatic and 9 (28%) were postsymptomatic. No enrolled detained persons were hospitalized or died. No major differences in handwashing practices, mask use, and movement within the facility were reported by those who tested positive compared with those who tested negative (Appendix Table 2).

### $C_t$ Values and Viral Culture

Median $C_t$ values were lowest among presymptomatic persons (30.6, range 20.0–31.1) and highest among postsymptomatic persons (33.2, range 25.2–37.5) ($p = 0.03$). The overall ranges for $C_t$ values were similar for symptomatic (19.7–36.3) and asymptomatic persons (19.8–36.9). Among the 51 symptomatic SARS-CoV-2–positive persons, positive rRT-PCR results occurred 7 days before symptom onset to 48 days after symptom onset (Figure 2, panel A).

Among 111 specimens that resulted in the first positive results for detained persons, 110 were submitted for viral culture and 25 (23%) had replication-competent virus isolated (Table 3). Replication-competent virus isolates were obtained from 25% (12/48) of nasopharyngeal swab specimens from asymptomatic persons, 67% (2/3) from presymptomatic persons, 29% (6/21) from symptomatic persons, and 11% (3/27) from postsymptomatic persons. Among persons reporting symptoms, specimens with replication-competent virus were collected during 6 days before to 4 days after symptom onset. Two postsymptomatic persons reported symptom resolution the day of testing; for the third person, date of symptom resolution was unknown.

**Table 2.** Cumulative incidence of SARS-CoV-2 infection in 143 detained persons by time point and original dormitory in a correctional facility, Louisiana, USA, May–June, 2020*

| Dormitory | Days since first positive test result for SARS-CoV-2 | SARS-CoV-2 positive, no. (%) | | | | Cumulative incidence by dormitory and overall, no. positive/no. tested (%) |
|---|---|---|---|---|---|---|
| | | Day 0 | Day 4 | Day 14 | Day 18 | |
| A, n = 20 | 30 | 13/20 (65) | 2/7 (29) | 0/5 (0) | NA | 15/20 (75) |
| B, n = 23 | 28 | 10/23 (43) | 4/13 (31) | 2/9 (22) | NA | 16/23 (70) |
| C, n = 11 | 28 | 6/11 (55) | 3/5 (60) | 0 /2 (0) | NA | 9/11 (82) |
| D, n = 37 | 20 | 20/37 (54) | 7/16 (44) | 0/10 (0) | NA | 27/37 (73) |
| E, n = 7 | 14 | 4/7 (57) | 0/3 (0) | 0/3 (0) | NA | 4/7 (57) |
| F, n = 45 | Unknown† | 0/45 (0) | NA | NA | 40/45 (89) | 40/45 (89) |
| Cumulative incidence by day | | 53/143 (37) | 16/44 (36) | 2/29 (7) | 40/45 (89) | 111/143 (78) |

*NA, not applicable; SARS-CoV-2, severe acute respiratory syndrome coronavirus 2.
†Introduction in dormitory F occurred at some point between day 0 and day 18.

**Table 3.** Symptom status of 143 detained persons at time of testing for SARS-CoV-2 and throughout course of investigation in a correctional facility, Louisiana, USA, May–June 2020*

| | SARS-CoV-2 testing results from first positive test result | | | |
|---|---|---|---|---|
| Symptom status† | SARS-CoV-2 positive, no. (%) | Median $C_t$ values (range)‡ | Culture positive, no. (%)§ | SARS-CoV-2 negative, no. (%) |
| Presymptomatic | 3 (3) | 30.6 (20.0–31.1) | 2 (8) | NA |
| Symptomatic | 21 (19) | 32.7 (19.7–36.3) | 6 (24) | 8 (25) |
| Postsymptomatic | 27 (24) | 33.2 (25.2–37.5) | 3 (12) | 9 (28) |
| Asymptomatic | 49 (44) | 32.9 (19.8–36.9)¶ | 12 (48)# | 12 (34) |
| Unknown | 11 (10) | 33.1 (25.1–35.7) | 2 (8) | 3 (9) |
| Overall | 111 (78) | 33 (19.7–37.5) | 25 (23) | 32 (22) |

*SARS-CoV-2 testing was conducted by using the Centers for Disease Control and Prevention 2019-Novel Coronavirus (2019-nCoV) Real-Time RT-PCR Diagnostic Panel. The $C_t$ values reported for nucleocapsid protein gene 1 target are shown. $C_t$, cycle threshold; NA, not applicable; SARS-CoV-2, severe acute respiratory syndrome coronavirus 2.
†Symptom status at time of first positive test result or throughout the investigation for persons remaining SARS-CoV-2 negative. Presympomatic: at least 1 symptom started after positive test result and no symptoms before positive test result; symptomatic: at least 1 symptom ongoing at time of test result (first positive, or any negative test result); postsymptomatic: at least 1 symptom started before test result (first positive result) or before investigation start date (continuous negative results); asymptomatic: no symptoms before test result (first positive result or before each negative test result); unknown: at least 1 symptom is unknown during at least 1 interview. Symptoms assessed: fever, subjective fever, cough, shortness of breath, chills, myalgia, sore throat, loss of taste or smell, or diarrhea
‡Tukey's test for significance, p = 0.03.
§Viral culture positive for replication-competent virus.
¶One person missing a $C_t$ value on the initial day this person tested positive.
#One specimen from an asymptomatic person who was positive by real-time reverse transcription PCR was not submitted for culture.

The $C_t$ values at the first positive test result and the proportion of specimens with positive viral culture for SARS-CoV-2 varied by dormitory (Figure 2, panel B). The median $C_t$ value for 53 specimens collected from detained persons in dormitories A–E was 33.6 (range 20.0–37.5); 2 (4%) samples from persons in dormitories D and E were replication competent. The median $C_t$ value for 39 samples from detained persons in dormitory F was 29.3 (range 19.7–34.3). Of these samples, 23 (59%) were replication competent.

Of 22 persons that had positive test results ≥14 days after the first positive test, 4 remained rRT-PCR positive for SARS-CoV-2 ≈3 weeks after first testing positive. Virus isolation was attempted but was not successful for any of the specimens from repeat-positive persons.

### Phylogenetic Analysis

We compared sequencing results for 41 specimens collected from persons in dormitories A (n = 2), D (n = 5), E (n = 2), and F (n = 32) at facility X during May 7–29 with each other and representative sequences from GISAID. All sequences clustered together within clade 20C and among other sequences reported from Louisiana (Appendix Figure). A phylogenetic tree illustrated 3 groups: 1 with sequences from persons in dormitories D and E, a second with sequences from persons in dormitories A and D, and a third with sequences from persons in dormitory F. Two identical SARS-CoV-2 sequences were identified from a person in dormitory D and a person from dormitory E. The third group differed from the first cluster by ≥6 nt and from the second cluster by 2 nt mutations.

## Discussion

Through serial testing of detained persons from quarantined dormitories at a Louisiana detention facility, we identified rapid and widespread SARS-CoV-2 transmission, a large number of asymptomatic infections, and shedding of replication-competent virus in persons with asymptomatic and presymptomatic infections. Despite early adoption of certain prevention and mitigation measures, the cumulative incidence among affected dormitories in facility X was 78%. Of persons who tested positive for SARS-CoV-2, 47% (52/111) were asymptomatic, of which 12 had positive viral culture results with replication-competent virus, indicating infectiousness. In this relatively young population, $C_t$ values were similar regardless of symptom status; the lowest $C_t$ values were among persons with presymptomatic infection, indicating high viral load (*20*). These findings add to the evidence that presymptomatic and asymptomatic persons can transmit SARS-CoV-2 (*8*).

This investigation demonstrated the usefulness of testing shortly after SARS-CoV-2 introduction and at multiple time points to comprehensively identify infections and mitigate transmission. Serial testing identified 52% (58/111) of the COVID-19 cases identified during the investigation. In dormitories A–E, 2 of 53 positive samples from day 0 testing had replication-competent virus, suggesting many persons in these dormitories were convalescent. In dormitory F, 89% (40/45) of residents tested positive for SARS-CoV-2 18 days after all testing negative on day 0; 59% had replication-competent virus. The timing of initial testing in dormitories A–E (2–4 weeks after the first case) and the long

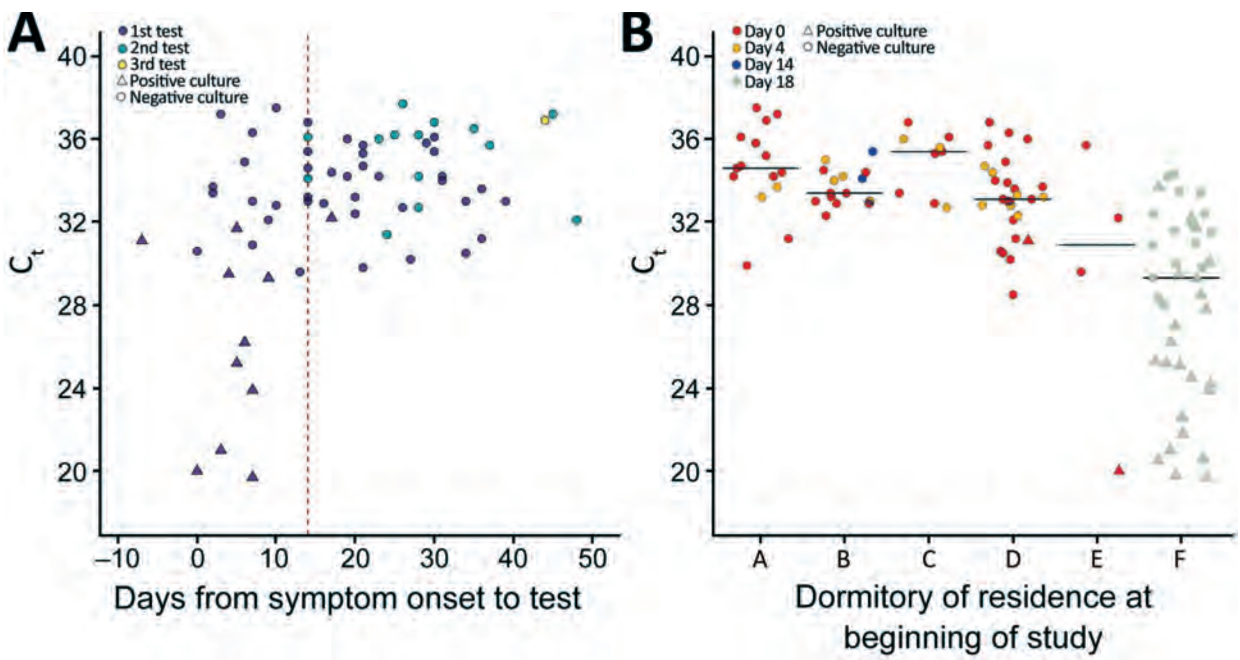


**Figure 2.** Rapid transmission of severe acute respiratory syndrome coronavirus 2 (SARS-CoV-2) in detention facility, Louisiana, USA, May–June 2020. A) $C_t$ values and viral culture results by days from symptom onset of any symptom in SARS-CoV-2–positive detained persons. Nucleocapsid protein 1 target $C_t$ values and viral culture results of 66 specimens from 51 persons who were positive for SARS-CoV-2 by days from reported symptom onset. $C_t$ values and viral culture results are also shown for 14 of the 51 specimens from persons who were positive a second time, and for 1 specimen that remained positive for a third test. Vertical dashed line indicates day 14 to depict the recommended medical isolation timeframe from symptom onset for persons in congregate settings. Shapes indicate culture results, and colors indicate day of positive test result. One positive test result is not included because $C_t$ values were not reported. B) $C_t$ values and viral culture results for SARS-CoV-2–positive detained persons at the time of first sample collection according to dormitory residence and day of first positive result. Nucleocapsid protein 1 target $C_t$ values and viral culture results of the first SARS-CoV-2–positive test result for 110 detained persons is shown by dormitory of residence at the time of first sample collection. Horizontal lines indicate median $C_t$ values for first positive samples from residents in each dormitory. One positive test result from a dormitory F resident is not included because $C_t$ value was not reported. $C_t$ , cycle threshold.

testing interval (18 days) in dormitory F limited the usefulness of serial testing to provide data needed to mitigate transmission. Once SARS-CoV-2 introduction into a correctional or detention facility is suspected or confirmed, widespread testing of detained persons and staff at short intervals could quickly identify infections and inform cohorting by infection status to prevent further transmission. In nursing homes, facilitywide testing closer in time to the identification of a COVID-19 case was associated with fewer cases within the facility (*21*). Facilities with resource constraints for which widespread testing is not feasible should work with the local health department to determine the most effective testing strategy for their facility.

To complement symptom screening and address the challenges of early detection of SARS-CoV-2, correctional and detention facilities might consider both periodic testing at regular intervals (e.g., 7–14 days) and serial testing of close contacts at short intervals (e.g., 3–4 days) to identify newly acquired infections, infections missed in previous rounds of testing, and new introductions (*8,12,20*). Increased dormitory density might also be a risk factor for viral transmission; the lowest cumulative incidence occurred in dormitory E, which had lowest occupancy. Some facilities have reduced occupancy as a mitigation strategy (*6*). Novel testing approaches (e.g., pooled testing), point-of-care rapid antigen assays, and less intrusive specimen collection methods are urgently needed to enable efficient SARS-CoV-2 testing. This investigation found no differences in handwashing and mask use between persons who tested positive or negative for SARS-CoV-2. A small proportion overall (13%) reported always using a mask which, along with close living quarters, might have limited the effectiveness of these personal mitigation measures.

During follow-up, 22 persons tested positive ≥14 days after their first positive result and 1 person tested positive 48 days after symptom onset. Four persons had positive rRT-PCR results ≈3 weeks after the first positive result, which was longer than that seen in previous investigations of patients with mild illness (*22,23*). However, replication-competent virus was not isolated from these specimens or any specimens collected >9 days after symptom onset. This finding lends support to facilities using symptom-based criteria for release after 10 days of isolation, with resolution of fever and improvement of other symptoms, instead of test-based criteria (*24*).

Phylogenetic analysis identified 3 distinct clusters of SARS-CoV-2 infection from 41 specimens collected within the same month from detained persons in dormitories A, D, E, and F. Given the genetic distance between the groups within a short time period and the overall diversity of sequences from the COVID-19 outbreak, there was likely >1 introduction of SARS-CoV-2 into the facility before May 29. In addition to mitigation measures to prevent SARS-CoV-2 spread within a facility, measures should be taken to limit introductions into the facility, including routine symptom screening and test-ing at entry, use of face masks, and systematic assignment of staff to specific dormitories.

We identified 4 primary limitations to this investigation. First, serial testing was initiated 2–4 weeks after the first case was identified in dormitories A–E, which limited our ability to assess the impact of testing and cohorting on preventing transmission if most detained persons had been infected before the investigation. In addition, persons who tested negative for SARS-CoV-2, including 53% who reported COVID-19 symptoms, might have had COVID-19 and cleared their infections by the time of testing, leading to an underestimation of the prevalence of SARS-CoV-2 infection. No antibody testing was performed; thus, the extent of prior infection cannot be estimated. Second, detained persons might have limited recall of mild symptoms and symptom timing, particularly symptoms occurring >2 weeks before testing, potentially resulting in an overestimation of the prevalence of asymptomatic infection. Also, follow-up symptom assessments were not conducted among persons with positive test results from dormitory F, thus potential presymptomatic detained persons remained classified as asymptomatic. Third, given our inclusion of symptoms reported up to 6 weeks before testing, misclassification of symptoms caused by other pathogens or allergies could have occurred. Finally, no systematic testing of facility staff or detained persons in other dormitories was part of this investigation.

In correctional and detention facilities, prevention and mitigation of SARS-CoV-2 transmission requires a combination of measures (*5*). Testing is necessary to identify asymptomatic and presymptomatic persons who can silently transmit the infection. Although symptom screening alone was not sufficient to identify SARS-CoV-2 infections, it could serve as a signal for SARS-CoV-2 introduction and initiation of widespread testing. To increase sensitivity of symptom screening, screenings should use an expanded COVID-19 symptom list based on the latest evidence and guidance, and barriers to symptom reporting, such as medical care costs or concerns over medical isolation, should be minimized (*18,25,26*). Multiple rounds of widespread testing for detained persons and staff might be necessary for early detection of virus introduction, particularly when there are high rates of transmission in the surrounding community and ongoing risk for reintroduction. When initiated early in an outbreak, results from serial testing 3–4 days after an exposed person first tests negative for SARS-CoV-2, paired with mitigation strategies, might help limit transmission among detained persons. SARS-CoV-2 testing in these congregate settings will likely be most effective when timed soon after viral introduction, inclusive of all potentially exposed staff and detained persons, and combined with infection control mitigation strategies such as medical isolation and quarantine.

### Acknowledgments

We thank persons incarcerated and detained at the detention facility, detention facility staff members, Louisiana Department of Health officials, Louisiana Office of Public Health Laboratory officials, Lauren Franco, Julian Grass, Jennifer Huang, Hannah Kirking, Eric Manders, Claire Midgely, Erin Moritz, Amy Schumacher, Margaret Williams, the Public Health Institute, and the CDC COVID-19 Epidemiology Task Force for participating in this study.

## About the Authors

Dr. Wallace is an Epidemic Intelligence Officer in the Division of Viral Diseases, National Center for Immunization and Respiratory Diseases, Centers for Disease Control and Prevention, Atlanta, GA. Her primary research interests include infectious disease epidemiology and public health practice infrastructure.

Dr. James is an Epidemic Intelligence Service Officer with the Centers for Disease Control and Prevention, Atlanta, GA, currently assigned to the Arkansas Department of Health, Little Rock, AR. Her primary research interest is emerging communicable diseases.

## References


1. Hawks L, Woolhandler S, McCormick D. COVID-19 in prisons and jails in the United States. JAMA Intern Med. 2020;180:1041–2. https://doi.org/10.1001/jamainternmed.2020.1856
2. Bick JA. Infection control in jails and prisons. Clin Infect Dis. 2007;45:1047–55. https://doi.org/10.1086/521910
3. Saloner B, Parish K, Ward JA, DiLaura G, Dolovich S. COVID-19 cases and deaths in federal and state prisons. JAMA. 2020;324:602–3. https://doi.org/10.1001/jama.2020.12528
4. Law UCLA. UCLA law COVID-19 behind bars data project, 2020 [cited 2020 Nov 2]. https://law.ucla.edu/academics/centers/criminal-justice-program/ucla-covid-19-behind-bars-data-project
5. Centers for Disease Control and Prevention. Interim guidance on management of coronavirus disease 2019 (COVID-19) in correctional and detention facilities, 2020 [cited 2020 Nov 2]. https://www.cdc.gov/coronavirus/2019-ncov/community/correction-detention/guidance-correctional-detention.html
6. Wallace M, Marlow M, Simonson S, Walker M, Christophe N, Dominguez O, et al. Public health response to COVID-19 cases in correctional and detention facilities—Louisiana, March–April 2020. MMWR Morb Mortal Wkly Rep. 2020;69:594–8. https://doi.org/10.15585/mmwr.mm6919e3
7. Centers for Disease Control and Prevention. Interim considerations for SARS-CoV-2 testing in correctional and detention facilities, 2020 [cited 2020 Nov 21]. https://www.cdc.gov/coronavirus/2019-ncov/community/correction-detention/testing.html
8. Arons MM, Hatfield KM, Reddy SC, Kimball A, James A, Jacobs JR, et al.; Public Health–Seattle and King County and CDC COVID-19 Investigation Team. Presymptomatic SARS-CoV-2 infections and transmission in a skilled nursing facility. N Engl J Med. 2020;382:2081–90. https://doi.org/10.1056/NEJMoa2008457
9. Furukawa NW, Brooks JT, Sobel J. Evidence supporting transmission of severe acute respiratory syndrome coronavirus 2 while presymptomatic or asymptomatic. Emerg Infect Dis. 2020;26. https://doi.org/10.3201/eid2607.201595
10. Hagan LM, Williams SP, Spaulding AC, Toblin RL, Figlenski J, Ocampo J, et al. Mass testing for SARS-CoV-2 in 16 prisons and jails—six jurisdictions, United States, April–May 2020. MMWR Morb Mortal Wkly Rep. 2020;69:1139–43. https://doi.org/10.15585/mmwr.mm6933a3
11. Dora AV, Winnett A, Jatt LP, Davar K, Watanabe M, Sohn L, et al. Universal and serial laboratory testing for SARS-CoV-2 at a long-term care skilled nursing facility for veterans—Los Angeles, California, 2020. MMWR Morb Mortal Wkly Rep. 2020;69:651–5. https://doi.org/10.15585/mmwr.mm6921e1
12. Tobolowsky FA, Gonzales E, Self JL, Rao CY, Keating R, Marx GE, et al. COVID-19 outbreak among three affiliated homeless service sites—King County, Washington, 2020. MMWR Morb Mortal Wkly Rep. 2020;69:523–6. https://doi.org/10.15585/mmwr.mm6917e2
13. Njuguna H, Wallace M, Simonson S, Tobolowsky FA, James AE, Bordelon K, et al. Serial laboratory testing for SARS-CoV-2 infection among incarcerated and detained persons in a correctional and detention facility—Louisiana, April–May 2020. MMWR Morb Mortal Wkly Rep. 2020;69:836–40. https://doi.org/10.15585/mmwr.mm6926e2
14. Lu X, Wang L, Sakthivel SK, Whitaker B, Murray J, Kamili S, et al. US CDC real-time reverse transcription PCR panel for detection of severe acute respiratory syndrome coronavirus 2. Emerg Infect Dis. 2020;26:1654–65. https://doi.org/10.3201/eid2608.201246
15. Harcourt J, Tamin A, Lu X, Kamili S, Sakthivel SK, Murray J, et al. Severe acute respiratory syndrome coronavirus 2 from patient with coronavirus disease, United States. Emerg Infect Dis. 2020;26:1266–73. https://doi.org/10.3201/eid2606.200516
16. Paden CR, Tao Y, Queen K, Zhang J, Li Y, Uehara A, et al. Rapid, sensitive, full-genome sequencing of severe acute respiratory syndrome coronavirus 2. Emerg Infect Dis. 2020;26:2401–5. https://doi.org/10.3201/eid2610.201800
17. Hadfield J, Megill C, Bell SM, Huddleston J, Potter B, Callender C, et al. Nextstrain: real-time tracking of pathogen evolution. Bioinformatics. 2018;34:4121–3. https://doi.org/10.1093/bioinformatics/bty407
18. Centers for Disease Control and Prevention. 2019-novel coronavirus (2019-NCoV) real-time RT-PCR diagnostic panel. Instructions for use, 2020 [cited 2020 Nov 2]. https://www.fda.gov/media/134922/download
19. Centers for Disease Control and Prevention. Symptoms of coronavirus, 2020 [cited 2020 Nov 2]. https://www.cdc.gov/coronavirus/2019-ncov/symptoms-testing/symptoms.html?CDC_AA_refVal=https%3A%2F%2Fwww.cdc.gov%2Fcoronavirus%2F2019-ncov%2Fabout%2Fsymptoms.html
20. Sethuraman N, Jeremiah SS, Ryo A. Interpreting diagnostic tests for SARS-CoV-2. JAMA. 2020;323:2249–51. https://doi.org/10.1001/jama.2020.8259
21. Hatfield KM, Reddy SC, Forsberg K, Korhonen L, Garner K, Gulley T, et al. Facility-wide testing for SARS-CoV-2 in nursing homes—seven U.S. jurisdictions, March–June 2020. MMWR Morb Mortal Wkly Rep. 2020;69:1095–9. https://doi.org/10.15585/mmwr.mm6932e5
22. Liu Y, Yan LM, Wan L, Xiang TX, Le A, Liu JM, et al. Viral dynamics in mild and severe cases of COVID-19. Lancet Infect Dis. 2020;20:656–7. https://doi.org/10.1016/S1473-3099(20)30232-2
23. Zheng S, Fan J, Yu F, Feng B, Lou B, Zou Q, et al. Viral load dynamics and disease severity in patients infected with SARS-CoV-2 in Zhejiang Province, China, January–March 2020: retrospective cohort study. BMJ. 2020;369:m1443. https://doi.org/10.1136/bmj.m1443
24. Centers for Disease Control and Prevention. Discontinuation of isolation for persons with COVID-19 not in healthcare settings, 2020 [cited 2020 Nov 2]. https://www.cdc.gov/coronavirus/2019-ncov/hcp/disposition-in-home-patients.html
25. Dawson P, Rabold EM, Laws RL, Conners EE, Gharpure R, Yin S, et al. Loss of taste and smell as distinguishing symptoms of COVID-19. Clin Infect Dis. 2020 Jun 21 [Epub ahead of print]. https://doi.org/10.1093/cid/ciaa799
26. Tenforde MW, Kim SS, Lindsell CJ, Billig Rose E, Shapiro NI, Files DC, et al.; IVY Network Investigators; CDC COVID-19 Response Team; IVY Network Investigators. Symptom duration and risk factors for delayed return to usual health among outpatients with COVID-19 in a multistate health care systems network—United States, March–June 2020. MMWR Morb Mortal Wkly Rep. 2020;69:993–8. https://doi.org/10.15585/mmwr.mm6930e1


Address for correspondence: Megan Wallace, Centers for Disease Control and Prevention, 1600 Clifton Rd NE, Atlanta, GA 30329-4027, USA; email:phu3@cdc.gov

# Plasma MicroRNA Profiling of *Plasmodium falciparum* Biomass and Association with Severity of Malaria Disease

Himanshu Gupta,[1,2] Mercedes Rubio,[1] Antonio Sitoe, Rosauro Varo, Pau Cisteró, Lola Madrid, Inocencia Cuamba, Alfons Jimenez, Xavier Martiáñez-Vendrell, Diana Barrios, Lorena Pantano, Allison Brimacombe, Mariona Bustamante, Quique Bassat,[3] Alfredo Mayor[3]

Severe malaria (SM) is a major public health problem in malaria-endemic countries. Sequestration of *Plasmodium falciparum*–infected erythrocytes in vital organs and the associated inflammation leads to organ dysfunction. MicroRNAs (miRNAs), which are rapidly released from damaged tissues into the host fluids, constitute a promising biomarker for the prognosis of SM. We applied next-generation sequencing to evaluate the differential expression of miRNAs in SM and in uncomplicated malaria (UM). Six miRNAs were associated with in vitro *P. falciparum* cytoadhesion, severity in children, and *P. falciparum* biomass. Relative expression of hsa-miR-4497 quantified by TaqMan-quantitative reverse transcription PCR was higher in plasma of children with SM than those with UM ($p<0.048$) and again correlated with *P. falciparum* biomass ($p = 0.033$). These findings suggest that different physiopathological processes in SM and UM lead to differential expression of miRNAs and pave the way for future studies to assess their prognostic value in malaria.

Author affiliations: ISGlobal, Hospital Clinic—Universitat de Barcelona, Barcelona, Spain (H. Gupta, M. Rubio, R. Varo, P. Cisteró, A. Jimenez, X. Martiáñez-Vendrell, D. Barrios, A. Brimacombe, M. Bustamante, Q. Bassat, A. Mayor); Centro de Investigação em Saúde de Manhiça (CISM), Maputo, Mozambique (A. Sitoe, R. Varo, L. Madrid, I. Cuamba, Q. Bassat, A. Mayor); Spanish Consortium for Research in Epidemiology and Public Health (CIBERESP), Madrid, Spain (A. Jimenez, M. Bustamante, Q. Bassat, A. Mayor); Harvard T.H. Chan School of Public Health Department of Biostatistics, Boston, Massachusetts, USA (L. Pantano); Universitat Pompeu Fabra (UPF), Barcelona (M. Bustamante); Institut Català de Recerca en Estudis Avançats (ICREA), Barcelona (Q. Bassat); Hospital Sant Joan de Déu—University of Barcelona Pediatrics Department, Barcelona (Q. Bassat)

DOI: https://doi.org/10.3201/eid2702.191795

Case-fatality rates for *Plasmodium falciparum* severe malaria (SM) remain unacceptably high in young children in Africa (*1*). Early detection and prompt treatment of SM are critical to improve the prognosis of sick children. Unfortunately, clinical signs and symptoms in many malaria patients, particularly early in the infection, may not adequately indicate whether the infection will trigger severe or life-threatening disease. Moreover, in malaria-endemic areas, where immunity to malaria is progressively acquired, detecting peripheral *P. falciparum* parasitemia in sick children does not necessarily prove that malaria is the cause of the severe pathology observed, given that many persons may carry parasites without expressing clinical malarial disease (*2*).

Sequestration of *P. falciparum*–infected erythrocytes (iEs) (*3*) in vital organs is considered a key pathogenic event leading to SM, as has been shown in postmortem parasite counts in patients who died with cerebral malaria (*4,5*). This extensive sequestration of parasitized erythrocytes in the microvasculature, together with the production of inflammatory mediators, leads to the dysfunction of one or more peripheral organs, such as the lungs (acute respiratory distress syndrome), kidneys (acute kidney injury) or brain (coma) (*6,7*). This tissue-specific tropism of *P. falciparum* parasites is mediated by the *P. falciparum* erythrocyte membrane protein 1 (PfEMP1), which can bind to different host receptors on the capillary endothelium, uninfected erythrocytes, and platelets (*8,9*); such receptors include endothelial receptor of

[1]These authors contributed equally to this article.

[2]Current affiliation: London School of Hygiene and Tropical Medicine, London, UK.

[3]These senior authors contributed equally to this article.

protein C (ePCR), gC1qR, intercellular adhesion molecule-1, CD36, chondroitin sulfate A, or complement receptor 1 (*10*).

Efforts have been made to identify biomarkers of SM that could be used for early diagnosis and for reducing severity of disease (*11*). Several biomarkers related to endothelial activation and immune dysfunction have been associated with different malaria-derived severe pathologies (*11–14*). Plasma level of histidine-rich protein 2 (HRP2), a parasite-specific protein secreted by the parasite during its blood cycle, has been used as a biomarker of total parasite biomass (circulating and sequestered parasites) (*15*,*16*) and therefore as a prognostic marker of the total parasite biomass and as a better proxy marker for SM than peripheral parasitemia (*16*). Organ damage and pathological disease states have also been associated with the rapid release of microRNAs (miRNAs), a class of endogenous small noncoding RNAs (18–24 nt), into circulation (*17*). Because secreted miRNAs can be detected in biologic fluids such as plasma (*18*), they are currently being explored (*17*) as promising noninvasive biomarkers to monitor organ functionality and tissue pathophysiological status. The content of miRNAs in the host is influenced by host-pathogen interactions (*19*). Sequestration of erythrocytes infected with *P. berghei* in mice brains has been demonstrated to modify the miRNA expression in cells (*20*). Similarly, sequestration of *P. vivax* gametocytes in bone marrow has been associated with transcriptional changes of miRNAs involved in erythropoiesis (*21*). The evidence suggests that *Plasmodium* parasites, although unable to produce miRNAs (*22*), could affect the production of organ-specific host miRNAs, pointing toward the potential of these small molecules to detect SM associated organ injury (*23*) and to confirm the contribution of malaria in the chain of events leading to death through the analysis of postmortem tissues (*23*).

Our study hypothesis is that miRNA levels in plasma are differentially expressed among children with severe and uncomplicated malaria because of the parasite sequestration in vital organs of severely ill children. To identify promising biomarkers for SM, we conducted a small RNA next-generation sequencing study to select miRNAs that were differentially expressed by human brain endothelial (HBE) cells exposed to *P. falciparum* iEs selected for cytoadhesion to ePCR, the main host receptor associated with SM (*9*), compared with HBE cells exposed to noncytoadherent iEs and noninfected erythrocytes (niEs). We also compared children who had SM with children who had UM (Figure 1). miRNAs that were differentially expressed in both analyses, together with the *P. falciparum* biomass-associated miRNAs (correlation coefficient >0.50 [*24*]), were quantitatively confirmed in

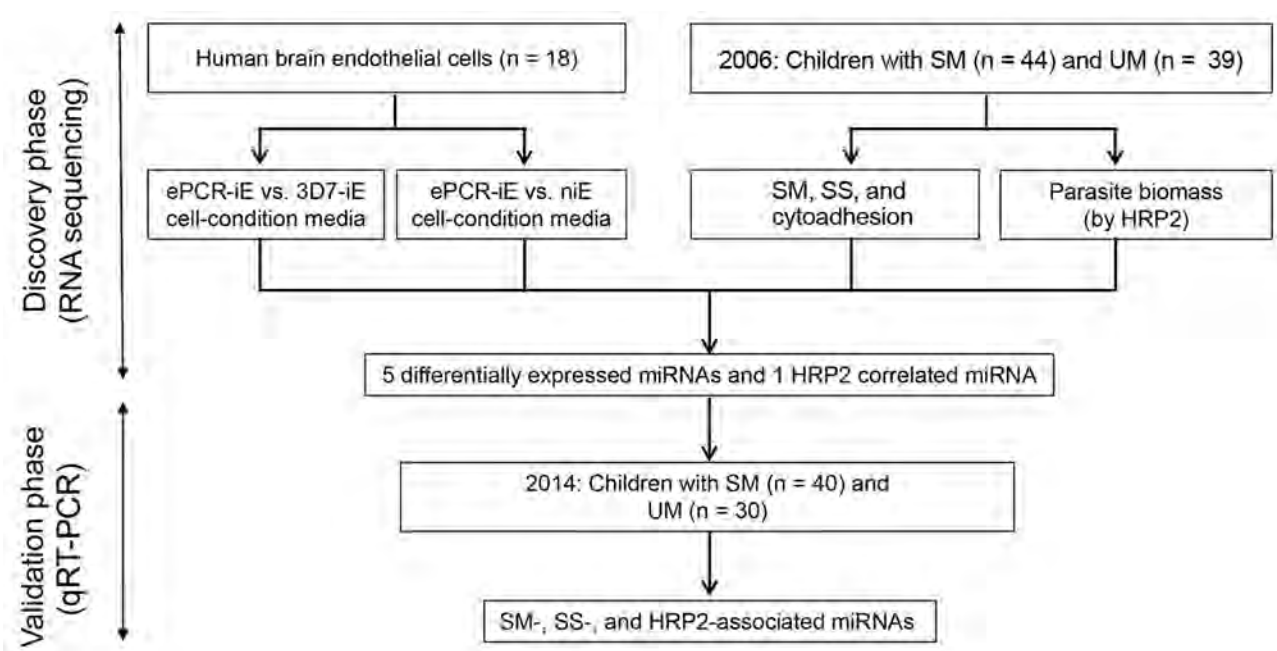


**Figure 1.** Schematic representation of study design to identify miRNA-based biomarkers of SM. ePCR, endothelial protein-C receptor (a binding *Plasmodium falciparum* strain-FCR3); HRP2, histidine-rich protein 2; iE, infected erythrocyte; miRNA, microRNA; niE, noninfected erythrocyte; SM, severe malaria; SS, severity symptoms; UM, uncomplicated malaria; 3D7, a nonbinding *P. falciparum* strain.

an independent validation cohort set of children with SM and UM using TaqMan quantitative reverse transcription PCR (qRT-PCR).

## Materials and Methods

### Study Population

Plasma samples used to assess miRNA levels were collected in 2 case–control studies conducted in Manhiça District in southern Mozambique during 2006 (n = 113) and 2014 (n = 91). In brief, the cases were children <5 years of age admitted to Manhiça District Hospital for SM and controls were outpatient children with UM (Appendix, https://wwwnc.cdc.gov/EID/27/2/19-1795-App1.pdf). The National Mozambican Ethical Review Committee (Mozambique) and Hospital Clínic (Barcelona, Spain) approved study protocols for each of the case–control studies. A signed written informed consent was obtained from each participant's guardian or parent during the original studies.

### Parasitological Determinations

We prepared thick and thin blood films to quantify *P. falciparum* parasitemia. We used approximately half of a 60µL dried blood drop on Whatman-903 filter paper to extract parasite DNA and performed real-time quantitative PCR (qPCR) targeting the *P. falciparum* 18S rRNA gene (*25,26*). HRP2 levels were quantified using commercially available ELISA kits and an in-house highly sensitive quantitative bead suspension array (qSA) based on Luminex technology (Appendix).

### *P. falciparum* Cytoadhesion Assays

We performed cytoadhesion assays to discover the differential expression of miRNAs (Appendix). HBE cells were incubated with *P. falciparum* iEs at the trophozoite stage of the ePCR binding FCR3 strain (ePCR-iE, which expresses the PfEPM1 protein that binds to ePCR receptor) and the 3D7 strain (3D7-iE, a strain without the protein that binds to ePCR receptor). Noninfected erythrocytes were used as negative control. The cell-conditioned media of each group were collected after 1 h (t1) and 24 h of stimulation (t24) and subjected to RNA extraction followed by small-RNA sequencing.

### Molecular Procedures, Gene Target Prediction and Data Analysis

RNA was extracted from cell-conditioned media (3 mL) by using the miRNeasy tissues/cells kit (QIAGEN, https://www.qiagen.com) and from plasma samples (1 mL) by using the miRNeasy plasma/serum kit, with the use of 5µg UltraPure glycogen/sample. Given that the plasma samples were conserved in heparin, RNA was precipitated with lithium chloride as described previously (*27*). Purified RNA was subjected to library preparation, pooling, and sequencing using a HiSeq 2000 (Illumina, https://www.illumina.com) platform, following the protocol for small RNAs (*28*) (Appendix). We used a previously published pipeline (*28*) to assess the sequencing quality, identification, and quantification of small RNAs, normalization and other species RNA contamination (Appendix). To detect miRNAs and isomiRs, reads were mapped to the precursors and annotated to miRNAs or isomiRs using miRBase version 21 with the miraligner (*29*). DESeq2 R package version 1.10.1 (R3.3.2; https://www.r-project.org/about.html) (*30*) was used to perform an internal normalization.

In the 2014 study, we used 50 µL of plasma with no hemolysis for RNA extraction as described, then conducted qRT-PCR (Appendix). We calculated miRNA relative expression levels (RELs) by the $2^{-\Delta C_t}$ method, where $\Delta C_t$ = cycle threshold ($C_t$) (miRNA) – mean $C_t$ (endogenous controls; ECs), considering efficiencies of 100% for all the miRNAs and ECs (*31*).

The selected miRNAs were screened through different gene target prediction programs such as DIANA-microT-CDS (http://www.microrna.gr/microT-CDS), MiRDIP (http://ophid.utoronto.ca/mirDIP), MirGate (http://mirgate.bioinfo.cnio.es), and TargetScan (http://www.targetscan.org) (Appendix). We assessed differential expression of miRNAs and isomiRs using DESEq2 and IsomiRs packages in R (*29,32*) (Appendix). All statistical analyses were performed using R version 3.3.2, and graphs were prepared with GraphPad version 6 (https://www.graphpad.com).

## Results

### Discovery Phase

#### miRNA Expression by HBE Cells

The ePCR binding *P. falciparum* strain (FCR3; ePCR-iE) showed higher levels of cytoadhesion to HBE cells (mean 32.60, SD 4.87 iE/500 cells) than a nonbinding *P. falciparum* (3D7; 3D7-iE) strain (mean 3.20, SD 1.06 iE/500 cells; p = 0.001) and noninfected erythrocytes (mean 3.12, SD 0.39 iE/500 cells; p = 0.001) (Appendix Figure 1). We sequenced 3 replicates of the media collected from each cytoadhesion assay after 1 h (t1) and 24 h (t24), giving a total of >200 million reads/lane, with a mean of 12.10 million reads (SD 13.31) per sample (Table 1; Figure 2, panel A; Appendix Table

**Table 1.** Quality control and mapped reads in different species of small RNAs from cell-conditioned media of human brain endothelial cells and plasma samples in children with uncomplicated and severe malaria, Mozambique*

| | Cell condition | | | | | | | |
|---|---|---|---|---|---|---|---|---|
| | niE | | 3D7-iE | | ePCR-iE | | | |
| Read type | t1, n = 3 | t24, n = 3 | t1, n = 3 | t24, n = 3 | t1, n = 3 | t24, n = 3 | UM, n = 39 | SM, n = 44 |
| Total reads, millions (SD) | 8.70 (3.55) | 16.71 (14.59) | 10.43 (3.48) | 25.86 (28.14) | 4.78 (2.13) | 6.11 (1.18) | 10.90 (9.69) | 9.26 (6.06) |
| Quality filtered, counts (SD) | 46.00 (36.72) | 33.33 (29.67) | 14.67 (23.69) | 125.67 (217.66) | 10.67 (2.31) | 16.33 (25.70) | 557.62 (1,200.76) | 615.75 (1,163.62) |
| Complexity filtered, counts (SD) | 910.67 (775.48) | 745.00 (659.60) | 369.33 (567.40) | 3168.67 (5,438.11) | 220.67 (163.57) | 308.00 (526.55) | 535.97 (884.46) | 506.23 (455.16) |
| Size filtered, millions (SD) | 0.63 (0.34) | 2.26 (2.99) | 0.68 (0.40) | 2.12 (2.92) | 0.90 (0.48) | 0.49 (0.50) | 1.94 (1.51) | 2.39 (1.82) |
| Good-quality reads† | | | | | | | | |
| Millions (SD) | 8.07 (3.35) | 14.44 (11.60) | 9.75 (3.10) | 23.74 (25.23) | 3.88 (2.00) | 5.62 (0.84) | 8.96 (8.89) | 6.88 (4.64) |
| Percentage (SD) | 92.62 (2.54) | 90.35 (6.98) | 93.93 (2.37) | 94.15 (3.26) | 79.60 (8.86) | 92.62 (6.35) | 77.76 (15.31) | 74.95 (11.08) |
| miRNA | | | | | | | | |
| Millions (SD) | 0.26 (0.19) | 1.09 (1.57) | 0.27 (0.19) | 0.98 (1.14) | 0.25 (0.07) | 0.15 (0.13) | 2.05 (2.50) | 1.33 (1.42) |
| Percentage (SD) | 3.02 (1.73) | 4.97 (4.92) | 2.47 (1.52) | 3.75 (0.54) | 7.41 (3.44) | 2.47 (1.97) | 22.43 (16.01) | 20.21 (13.22) |
| rRNA | | | | | | | | |
| Millions (SD) | 2.34 (1.82) | 3.12 (2.71) | 1.57 (1.72) | 5.74 (9.19) | 0.72 (0.38) | 0.90 (1.08) | 0.92 (0.97) | 0.81 (0.72) |
| Percentage (SD) | 24.72 (16.01) | 20.36 (14.62) | 14.84 (15.37) | 13.41 (15.42) | 19.55 (5.14) | 15.13 (16.99) | 11.11 (7.75) | 11.49 (5.78) |
| tRNA | | | | | | | | |
| Millions (SD) | 1.72 (0.58) | 3.37 (1.51) | 3.75 (1.80) | 6.35 (3.00) | 0.84 (0.64) | 2.47 (1.47) | 1.13 (1.17) | 1.14 (0.94) |
| Percentage (SD) | 27.51 (23.37) | 32.53 (27.16) | 41.04 (20.74) | 43.47 (23.59) | 18.65 (9.43) | 45.24 (26.80) | 13.93 (6.85) | 17.79 (7.70) |
| Unknown | | | | | | | | |
| Millions (SD) | 3.75 (1.92) | 6.86 (6.80) | 4.16 (1.67) | 10.66 (12.55) | 2.07 (0.97) | 2.11 (0.67) | 4.87 (5.88) | 3.59 (2.62) |
| Percentage (SD) | 44.76 (6.35) | 42.14 (11.63) | 41.65 (5.12) | 39.37 (8.36) | 54.40 (3.75) | 37.15 (7.89) | 52.53 (16.01) | 50.51 (13.55) |

*Reads were obtained from cell-conditioned media of human brain endothelial cells exposed to cytoadherent *P. falciparum*–infected and noninfected erythrocytes, and plasma of Mozambique children with SM and UM. Three replicates of the media were collected from each cytoadhesion assay after 1 (t1) and 24 (t24) hours. ePCR-iE, adherent FCR3 expression endothelial receptor of protein C-infected erythrocytes; miRNA, microRNA; niE, noninfected erythrocytes; SM, severe malaria; UM, uncomplicated malaria; 3D7-iE, nonadherent 3D7-infected erythrocytes.
†Reads after filtering low quality, low complexity, and short (<18-nt) sequences.

1). The mean percentage of miRNAs in the media samples analyzed was 4.01% (SD 2.93%); a mean of 203 (SD 93.82, range 101–465) distinct miRNAs were detected (Appendix Table 1). The 10 most expressed miRNAs for all samples at t1 and t24 time points are described in Figure 2, panel B. No contamination with RNA from other species was observed.

One hour after incubating the HBE cells with *P. falciparum* infected and noninfected erythrocytes, 111 miRNAs were found to be differentially expressed in cell-condition media of niE and ePCR-iE; 76 of them were downregulated and 35 upregulated in ePCR-iE compared with niE (Figure 2, panel C; Appendix Table 2). At this same time point, 100 miRNAs were differentially expressed in cell-condition media of 3D7-iE and ePCR-iE; 67 were downregulated and 33 upregulated in ePCR-iE compared with 3D7-iE (Figure 2, panel D; Appendix Table 3). Overall, 89 miRNAs were differentially expressed in ePCR-iE compared with both niE and 3D7-iE; 28 of those were upregulated and 61 downregulated in ePCR-iE. There were no differentially expressed miRNAs between niE and 3D7-iE cell-condition media. At t24, only hsa-miR-451a was significantly upregulated in cell-condition media of ePCR-iE with respect to niE ($p<0.001$) and 3D7-iE ($p = 0.023$). We found no significantly different miRNAs between niE and 3D7-iE cell-condition media. All differentially expressed isomiRs originated from the selected miRNAs; none of them presented any modifications in the seed region.

#### miRNAs Expression in Plasmas from Children with Malaria of Varying Severity

Out of 113 plasma samples collected from children with SM (N = 57) and UM (N = 56) in Mozambique in 2006, 11 samples were discarded, 5 because of hemolysis ($OD_{414}>0.2$) (*33*) and 6 because no peak was observed between 133–150 nt (typical size for miRNAs plus library adaptors) on the bioanalyzer results after library preparation. Among the 102 sequenced samples (SM = 53, UM = 49), 19 samples (9 SM, 10 UM) were further excluded because of the low number of miRNA reads (<10,000 reads). In total, samples from 83 children (44 with SM and 39 with UM) were included in the analysis (Table 2).

The sequencing of the 83 plasma samples yielded a mean of 9.42 (SD 6.4) million reads per sample (Table 1; Figure 2, panel A; Appendix Table 4). The mean percentage of miRNAs per plasma samples was 20.5% (SD 13.2%), with a mean of 395 (SD 169, range 116–786) distinct miRNAs detected (Appendix Table 4). The total number of miRNAs detected across samples was 1,450. The 10 most expressed miRNAs can be found in Figure 2, panel B. No contamination with RNA from other species was observed.

We found hsa-miR-122–5p upregulated in children with SM (Table 3). In the subanalysis by signs of severity, 5 miRNAs were associated with severe anemia (SA), prostration, and acute respiratory distress (ARD) (Table 3). Twelve miRNAs were associated

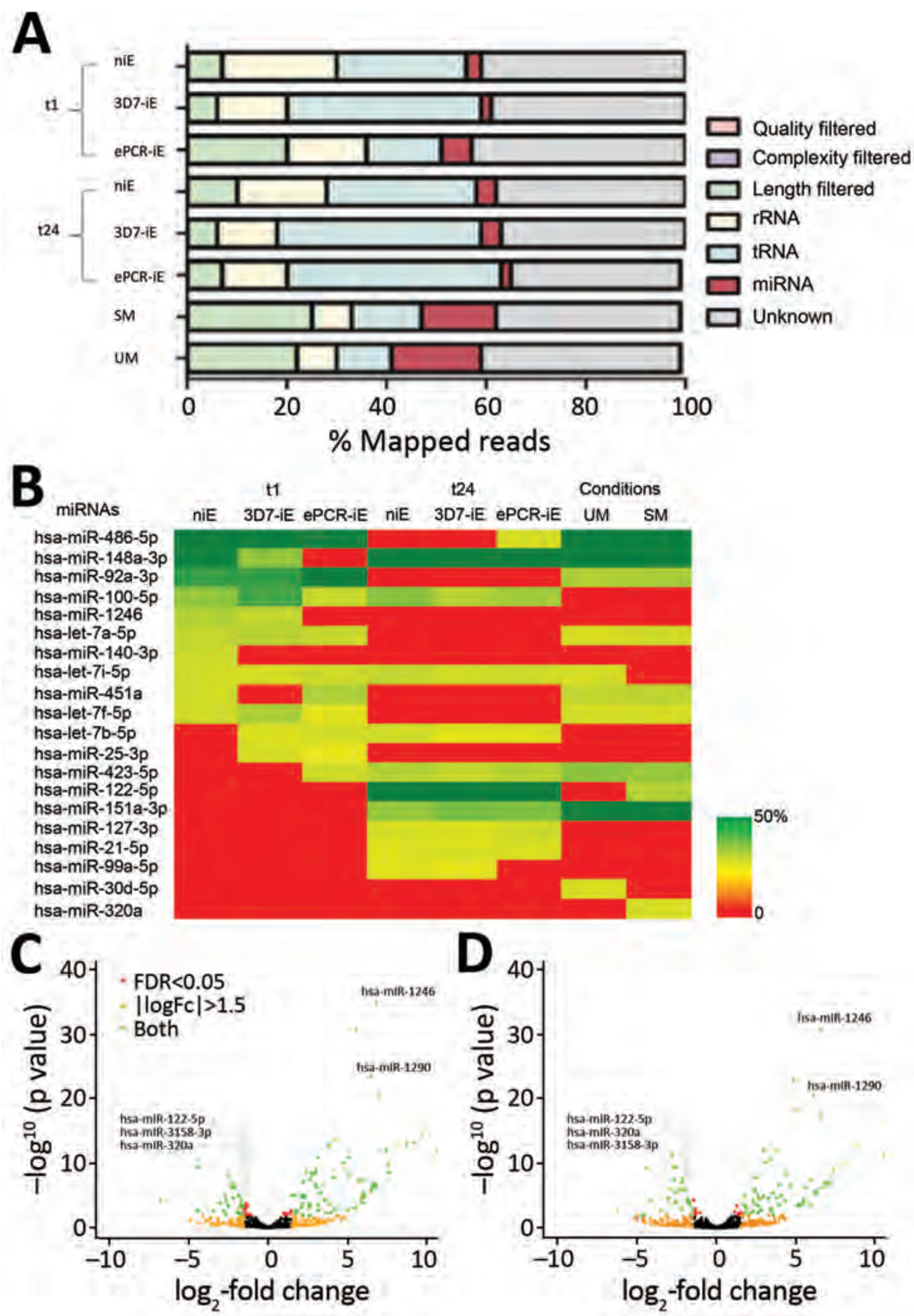


**Figure 2.** RNA sequencing of human brain endothelial (HBE) cell media and plasma from children recruited in 2006, Mozambique. A) Percentage of mapped reads in different species of small RNAs, for both in vitro and ex vivo approaches. B) Ten most expressed miRNAs in HBE cell medias and plasmas. Color-coded cells show the percentage of each assay/condition (columns) for each miRNA (rows). C) Volcano plot of differentially expressed miRNAs in cell-condition media of niEs versus cell-condition media of iEs with the FCR3-ePCR strain (ePCR-iE) incubated with HBE cells. D) Volcano plot of differentially expressed miRNAs in cell-condition media of iEs with 3D7 strain (3D7-iE) versus cell-condition media of iEs with the FCR3-ePCR strain (ePCR-iE) incubated with HBE cells. Comparisons depicted in C and D were adjusted for multiple testing by the Benjamini-Hochberg method. Negative $log_2$-fold change indicates overexpression in ePCR-iE samples. ePCR, endothelial protein-C receptor (a binding *Plasmodium falciparum* strain); HRP2, histidine-rich protein 2; iE, infected erythrocyte; miRNA, microRNA; SM, severe malaria; UM, uncomplicated malaria.

**Table 2.** Characteristics of children with severe and uncomplicated malaria recruited for case–control studies in 2006 and 2014, Mozambique*

| | 2006 | | | 2014 | | |
|---|---|---|---|---|---|---|
| Characteristic | UM, n = 39 | SM, n = 44 | p value | UM, n = 30 | SM, n = 40 | p value |
| Age, y, mean (SD)† | 2.3 (1.1) | 2.4 (1.3) | 0.671 | 2.2 (1.3) | 2.8 (1.2) | 0.419 |
| Sex, no. (%) | | | | | | |
| M | 24 (62) | 28 (64) | 1.000 | 18 (60) | 21 (52.5) | 0.532 |
| F | 15 (38) | 16 (36) | | 12 (40) | 19 (47.5) | |
| HRP2, ng/mL, GM (SD) | 71.3 (10.7) | 331.4 (40.7) | <0.001 | 24.1 (4.9) | 78.7 (12.2) | 0.038 |
| qPCR, parasites/μL, GM (SD) | 2,084.9 (302.5) | 7,976.1 (1,079.6) | 0.004 | 72,845.9 (7,193.9) | 94,099.6 (8,716.0) | 0.549 |
| Splenomegaly, no. (%) | | | | | | |
| No | 33 (85) | 21 (48) | 0.001 | ND | 27 (67.5) | NA |
| Yes | 6 (15) | 23 (52) | | ND | 13 (32.5) | |
| Hepatomegaly, no. (%) | | | | | | |
| No | 38 (97) | 35 (80) | 0.016 | ND | 35 (87.5) | NA |
| Yes | 1 (3) | 9 (20) | | ND | 5 (12.5) | |
| Hyperlactatemia, no. (%) | | | | | | |
| No | 10 (26) | 5 (11) | 0.152 | 26 (86.7) | 27 (67.5) | 0.064 |
| Yes | 29 (74) | 39 (89) | | 4 (13.3) | 13 (32.5) | |
| Temperature, °C, mean (SD) | 38.0 (1.6) | 38.5 (1.1) | 0.093 | 38.0 (1.3) | 38.2 (1.4) | 0.437 |
| Weight, kg, mean (SD) | 11.3 (2.8) | 11.0 (2.8) | 0.599 | 12.3 (2.9) | 12.7 (3.3) | 0.476 |
| Platelets, $10^9$/L, mean (SD) | 156.7 (86.8) | 115.8 (66.8) | 0.018 | 149.0 (89.7) | 95.3 (69.3) | 0.001 |
| Glucose, mM, mean (SD)‡ | 6.2 (1.5) | 5.9 (1.8) | 0.391 | 6.6 (1.3) | 6.0 (2.6) | 0.165 |
| WBC, $10^9$/L, mean (SD) | 9.9 (4.1) | 10.2 (3.9) | 0.774 | 9.7 (3.8) | 9.6 (5.0) | 0.929 |
| Neutrophils, %, mean (SD)§ | 54.1 (16.7) | 54.4 (14.3) | 0.940 | 50.7 (20.6) | 58.9 (13.7) | 0.447 |
| Lymphocytes, %, mean (SD)¶ | 39.4 (17.9) | 36.3 (12.6) | 0.374 | 26.1 (17.1) | 25.6 (12.2) | 0.995 |
| Lactate, mM, mean (SD) | 3.0 (1.7) | 4.7 (3.6) | 0.009 | 2.8 (2.2) | 3.6 (2.4) | 0.035 |
| Severe malaria syndromes, no. (%) | | | | | | |
| Prostration | | 33 (75.0) | | | 30 (75.0) | |
| Acute respiratory distress | | 18 (40.9) | | | 19 (47.5) | |
| Severe anemia | | 17 (38.6) | | | 7 (17.5) | |
| Multiple seizures | | 11 (25.0) | | | 24 (60.0) | |
| Cerebral malaria | | 2 (4.5) | | | 7 (17.5) | |
| Hypoglycemia | | 2 (4.5) | | | 2 (5.0) | |

*Data were gathered in a discovery study in 2006 and validation study in 2014. GM, geometric mean; HRP2, histidine-rich protein 2: NA, not applicable; ND, not determined; SM, severe malaria; UM, uncomplicated malaria; WBC, white blood cells.
†No data for 1 sample (UM = 1) in 2014 study.
‡No data for 3 samples (SM = 2; UM = 1) in 2014 study.
§No data for 4 samples (SM = 4) in 2014 study.
¶No data for 3 samples (SM = 3) in 2014 study.

with PM-agglutination and cytoadhesion to g1CqR (Table 3). We observed no associations between miRNA counts and other cytoadhesion data such as rosetting and binding to CD36 and to CD54. After adjusting for multiple comparisons, we found 3/1,450 miRNAs identified in RNA sequencing data, hsa-miR-10b-5p, hsa-miR-378a-3p, and hsa-miR-4497, correlated with HRP2 levels determined by qSA Spearman analysis (Figure 3). We observed similar correlations when HRP2 levels were determined by ELISA (Appendix Table 5). miRNAs were neither associated with hepatomegaly nor with splenomegaly. All differentially expressed isomiRs between children with SM and those with UM belong to the differentially expressed miRNAs, with no modifications in the seed region.

### Validation Cohort

Among the 89 miRNAs differentially expressed in cell-condition media of HBE cells exposed to niE and 3D7-iE compared with ePCR-iE, we confirmed 5 miRNAs to be differentially expressed between children with SM and UM. These 5 miRNAs (hsa-miR-122–5p, hsa-miR-320a, hsa-miR-1246, hsa-miR-1290 and hsa-miR-3158–3p), along with hsa-miR-4497 miRNA, which had a correlation coefficient with HRP2 >0.5 (Figure 3), were selected for TaqMan qRT-PCR validation in an independent cohort of children with SM and UM recruited in 2014. Among the 91 plasma samples collected from these children, 21 were discarded because of hemolysis ($OD_{414}$>0.2) (33). Of the 70 remaining samples, 40 were collected from children with SM and 30 from children with UM (Table 2).

All samples tested by qRT-PCR amplified the exogenous control (ath-miR-159a) with a $C_t$ value<18 and a coefficient of variance (CV) <5%, suggesting the correct RNA extraction and cDNA preparation. We selected 3 ECs, hsa-miR-191–5p (CV = 4.8%, baseMean = 3953.3, $log_2$-fold change [FC] −0.02, SD 0.56), hsa-miR-30d-5p (CV = 4.9%, baseMean = 14172.31, FC 0.01, SD 0.61), and hsa-miR-148a-3p (CV = 5%, baseMean = 111593.08, FC 0.11, SD 0.82) as a panel for qRT-PCR analysis. Among these, the NormFinder stability value was 0.044 for the combination of hsa-miR-30d-5p and hsa-miR-191–5p, and thus we selected those 2 ECs. No statistically significant differences were found when we compared $C_t$ values of the exogenous controls and 2 endogenous controls between SM and UM samples (Appendix Figure 2). We performed standard curves for all miRNAs (ECs and selected miRNAs), giving efficiencies of 91.1%–103.8% (Appendix Table 6), which were assumed as 100% to calculate the relative expression values using the $2^{-\Delta C_t}$ method (*31*).

The relative expression levels of hsa-miR-3158–3p and hsa-miR-4497 were significantly higher in children with SM than UM ($p<0.05$) (Figure 4). We found that hsa-miR-3158–3p levels were higher in children who had prostration, multiple seizures, and ARD compared with those who had UM ($p<0.05$; Figure 5). Severe anemia and ARD symptoms were associated with higher hsa-miR-4497 levels ($p<0.05$; Figure 5). No such associations were observed for cerebral malaria and hypoglycemia. RELs of hsa-miR-3158–3p and hsa-miR-4497 were found positively correlated with HRP2 levels quantified by qSA ($p<0.05$; Figure 6). Similar correlations were observed when HRP2 levels were determined by ELISA (Appendix Table 5).

### miRNA Gene Target Prediction

We identified a total of 87 putative targets for hsa-miR-3158–3p and hsa-miR-4497 miRNAs, none of which were shared by both miRNAs (Appendix Table 7). We predicted 45 experimentally validated mRNA targets for hsa-miR-3158–3p and 42 for hsa-miR-4497; the predicted targets were found to be involved in a broad range of biologic processes (Appendix Table 8). However, significance was lost when adjusted by the Benjamini-Hochberg method; none of the target genes were clustered under the KEGG pathway with $p<0.05$.

## Discussion

Because of their specificity to cell type (*17*), microRNAs can reflect disease states and organ damage. Consequently, they have the potential to provide a new screening method for early detection of pathological *P. falciparum* sequestration and could become an effective prognosis tool for severe malaria.

**Table 3.** Association of miRNA levels with severe malaria, symptoms of severity, and *Plasmodium falciparum* cytoadhesion among children with uncomplicated and severe malaria, Mozambique*

| Characteristic | miRNA | baseMean | $\log_2$-fold change | Adjusted p value |
|---|---|---|---|---|
| Clinical data | | | | |
| SM, n = 44 vs. 39 UM | | | | |
| All | hsa-miR-122-5p | 19,929.69 | 1.67 | 0.001 |
| SA, n = 17 vs. 39 UM | | | | |
| | hsa-miR-4492 | 17.34 | 2.81 | 0.046 |
| | hsa-miR-4497 | 293.66 | 2.18 | 0.046 |
| Prostration, n = 33 vs. 39 UM | | | | |
| | hsa-miR-122-5p | 20,677 | 1.89 | 0.001 |
| | hsa-miR-6087 | 5.36 | 2.39 | 0.033 |
| | hsa-miR-511-5p | 126.67 | 1.36 | 0.040 |
| Acidosis or respiratory distress, n = 18 vs. 39 UM | | | | |
| | hsa-miR-122-5p | 13,367.43 | 2.21 | <0.001 |
| | hsa-miR-4497 | 272.39 | 2.05 | 0.07 |
| Cytoadhesion data | | | | |
| Platelet-mediated agglutination, n = 50 vs. 19 UM | | | | |
| | hsa-miR-3158-3p | 1,180.96 | –2.26 | <0.001 |
| | hsa-miR-320a | 22,005.69 | –1.48 | 0.001 |
| | hsa-miR-4492 | 18.33 | 2.78 | 0.002 |
| | hsa-miR-1290 | 1,011.34 | –1.38 | 0.014 |
| | hsa-miR-320b | 1,191.44 | –1.23 | 0.014 |
| | hsa-miR-320c | 408.32 | –1.29 | 0.014 |
| | hsa-miR-1246 | 3,907.45 | –1.32 | 0.019 |
| | hsa-miR-6741-5p | 48.11 | –1.81 | 0.023 |
| | hsa-miR-1228-5p | 82.73 | –1.88 | 0.023 |
| | hsa-miR-3195 | 16.35 | 2.21 | 0.023 |
| | hsa-miR-7706 | 334.86 | –1.00 | 0.023 |
| gC1qR, n = 35 vs. 34 UM | | | | |
| | hsa-miR-1-3p | 622.35 | 2.09 | 0.003 |

*Positive fold change indicates overexpression in severe malaria and symptoms of severity compared to UM as well as parasites showing cytoadhesion compared to none. Total number of miRNAs in RNA sequencing data was 1,450. p value adjusted for multiple testing by the Benjamini-Hochberg method. baseMean, mean normalized expression of the miRNAs in all the samples; miRNA, microRNA; SA, severe anemia, SM, severe malaria; UM, uncomplicated malaria.

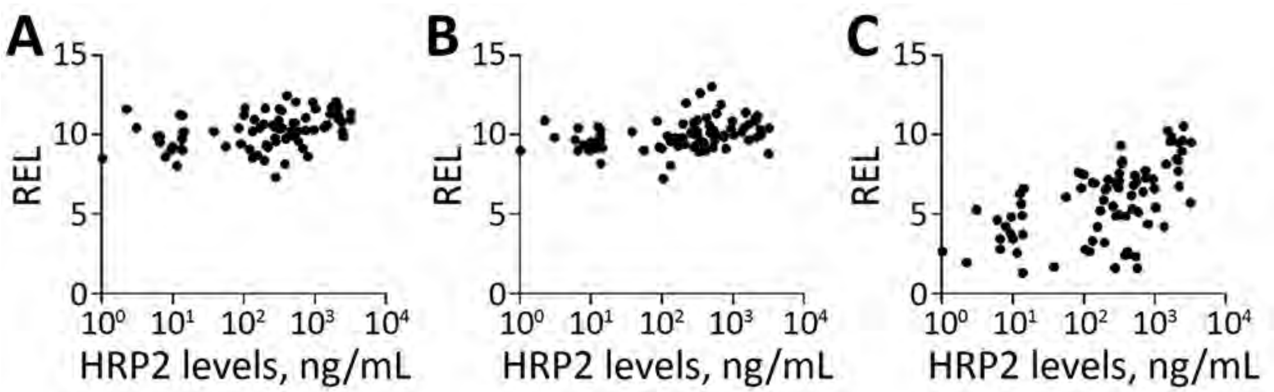


**Figure 3.** Spearman correlations between HRP2 levels and relative expression levels (RELs) of 3 miRNA in plasma samples from children with malaria, 2006, Mozambique. A) hsa-miR-10b-5p; B) hsa-miR-378a-3p; C) hsa-miR-4497. HRP2 levels and miRNA RELs were log transformed. The correlation analysis was adjusted for multiple testing by the Benjamini-Hochberg method. HRP2, histidine-rich protein 2; miRNA, microRNA; REL, relative expression levels.

Moreover, the detection of miRNAs associated with organ damage in host biofluids may provide an alternative to postmortem autopsies for determining the presence of parasites in host vital organs. This approach creates new opportunities to develop malaria diagnostic tools that can guide treatment decisions, and to understand the role of human miRNAs in several disease conditions (*23*).

In the discovery phase, 89 miRNAs were found to be differentially expressed in the media of HBE cells after incubation with an ePCR-cytoadherent *P. falciparum* strain compared with noncytoadherent parasites and noninfected erythrocytes. In addition, 15 miRNAs in plasma samples obtained from children were associated with SM, with specific severity symptoms, and with the cytoadherent *P. falciparum*

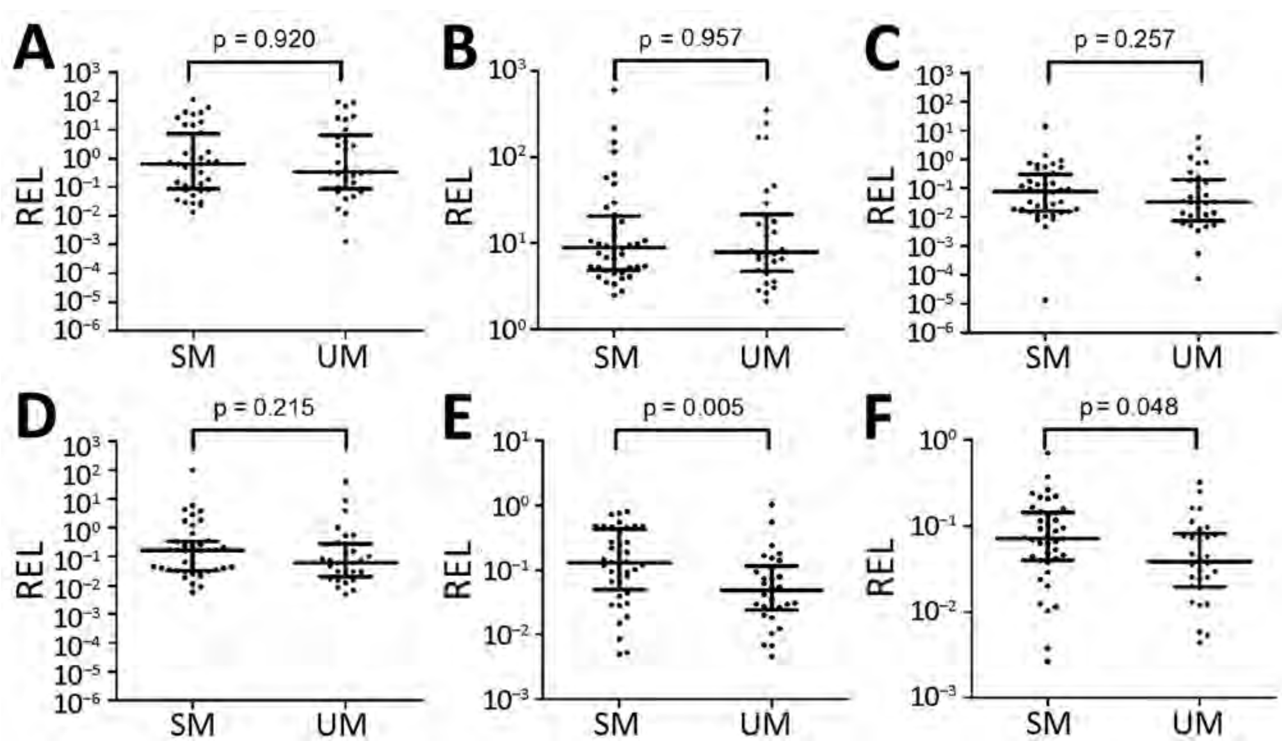


**Figure 4.** MiRNA validation in plasma samples of children with malaria, 2014, Mozambique. A) hsa-miR-122-5p; B) hsa-miR-320a; C) hsa-miR-1246; D) hsa-miR-1290; E) hsa-miR-3158-3p; F) hsa-miR-4497. RELs were calculated with respect to the mean of 2 endogenous controls (hsa-miR-30d-5p and hsa-miR-191–5p) and compared between children with SM and UM. Statistical differences were obtained by using the Mann-Whitney U test. Error bars represent medians and interquartile ranges. HRP2, histidine-rich protein 2; miRNA, microRNA; REL, relative expression levels; SM, severe malaria; UM, uncomplicated malaria.

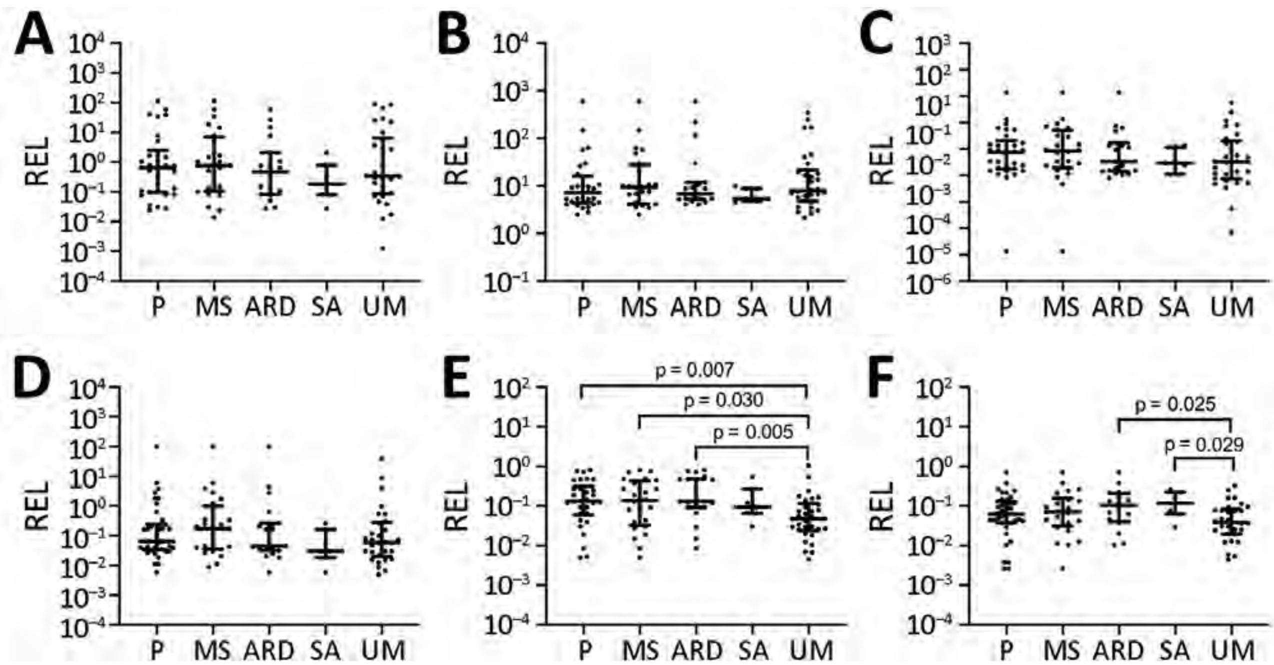


**Figure 5.** Association of microRNA levels with symptoms of severity in children with malaria, Mozambique, 2014. A) hsa-miR-122-5p; B) hsa-miR-320a; C) hsa-miR-1246; D) hsa-miR-1290; E) hsa-miR-3158-3p; F) hsa-miR-4497. RELs were calculated with respect to the mean of 2 endogenous controls (hsa-miR-30d-5p and hsa-miR-191–5p) and compared between children with UM and symptoms of severity. Distributions were compared using Mann-Whitney U test. Error bars represent medians and interquartile ranges. p values are shown for significant comparisons. ARD, acidosis or acute respiratory distress; MS, multiple seizures; P, prostration; REL, relative expression levels; SA, severe anemia; UM, uncomplicated malaria.

phenotype, compared with UM and noncytoadherent parasites. In the validation phase, we confirmed the higher abundance of hsa-miR-3158–3p and hsa-miR-4497 in children with SM than in children with UM. Prostration, multiple seizures, SA, and ARD symptoms of severity were associated with higher levels of hsa-miR-3158–3p and hsa-miR-4497. hsa-miR-4497 levels were also positively correlated with the parasite biomass as quantified by the levels of HRP2 in both the discovery and validation phases. Overall, these findings suggest that different physiopathological processes in SM and UM lead to differential expression of miRNAs in plasma.

HBE cells released a high number of the miRNAs when they were stimulated with an ePCR binding *P. falciparum* strain within the first hour of incubation. After 24 hours, the system stabilized; 1 miRNA (hsa-miR-451a) was found at higher levels in cell-conditioned media of HBE cells incubated with an ePCR binding strain than in cells stimulated with nonadherent (3D7-iE) or noninfected erythrocytes. miR-451 has been implicated in translocation to form a chimera with *Plasmodium* mRNAs to block their translation (*34*) and was also found to be abundant in sickle erythrocytes (*35*). In addition, it has been shown that parasites could reduce miR-451 levels in host fluids (*36*). However, this finding was not confirmed in plasmas from the children in this study. Five miRNA levels were higher in children with SM and severity symptoms (prostration, SA, and ARD) than in children with UM. *P. falciparum* cytoadhesion phenotypes (PM-agglutination and cytoadhesion to gC1qR) were also associated with the differential expression of miRNAs, suggesting that the interaction between PfEMP1 and host receptors leads to the secretion to plasma of specific miRNAs. Moreover, 3 miRNAs (hsa-miR-10b-5p, hsa-miR-378a-3p, and hsa-miR-4497) were positively correlated with HRP2 levels.

We selected 6 candidate miRNAs identified in the discovery phase to determine the validity of the previous results in an independent cohort of children in Mozambique. The relative expression of hsa-miR-3158–3p and hsa-miR-4497 was significantly higher in children with SM than in those with UM; hsa-miR-3158–3p levels were higher in children with prostration, multiple seizures, and ARD, and hsa-miR-4497 in children with SA and ARD. To our knowledge, hsa-miR-3158–3p, which is widely expressed in skin, spleen, kidney, and brain tissues (*37*), has been associated with bipolar disorders (*38*) but not with

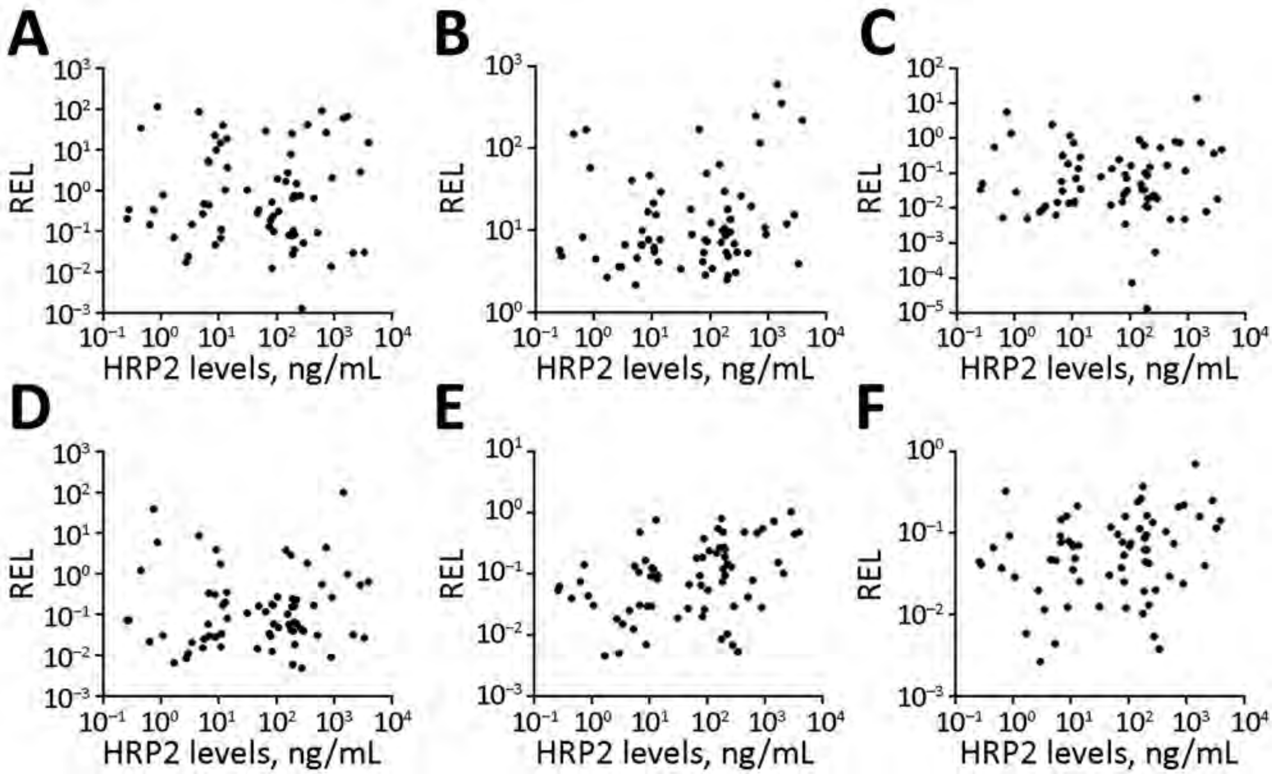


**Figure 6.** Spearman correlations between HRP2 levels and microRNA RELs in plasma samples from children with malaria, Mozambique, 2014. A) hsa-miR-122-5p; B) hsa-miR-320a; C) hsa-miR-1246; D) hsa-miR-1290; E) hsa-miR-3158-3p; F) hsa-miR-4497. HRP2 levels and microRNA RELs were log transformed. HRP2, histidine-rich protein 2; REL, relative expression levels.

other infectious diseases. Further validation is required for hsa-miR-3158–3p because the levels of this miRNA were found to be downregulated in the plasma from children recruited in 2006 with positive PM-agglutination compared with no PM-agglutination, a *P. falciparum* cytoadhesion phenotype which has been associated with malaria severity (*39*). However, the positive correlation of hsa-miR-4497 with HRP2 levels, which was consistently observed in the cohorts of children from 2006 and 2014, suggested that increasing parasite biomass associated with parasite sequestration may lead to higher levels of secretion of this specific miRNA by damaged tissues. The miRNA hsa-miR-4497 is widely expressed in the lymph nodes and spleen, kidney, and liver tissues (*37*). Overall, this study shows that hsa-miR-4497, which is also associated with SM, might be an interesting proxy marker of malaria severity. However, hsa-miR-4497 has been identified as a tumor suppressor (*40*) and associated with *Mycobacterium tuberculosis* infection (*41*). Therefore, longitudinal studies are required to assess the prognostic value of this miRNA, as well as to estimate its differential expression in children with severity due to nonmalarial infections.

Few of the most expressed miRNAs found in our study, which represent 70% of the total miRNA counts in plasma samples, have been previously reported as highly abundant in plasma samples (*28,42*). According to public data deposited in the miRmine database (*43*), hsa-miR-486–5p and hsa-miR-451a are the 2 most abundant miRNAs in plasma; both were among the 10 most expressed miRNAs in our study. Although no data are available on miRNAs from cell-conditioned media of HBE cells, miRNA data from other cell types, such as primary tissue explants, primary stromal cells, and breast cancer cell lines, also show low miRNA yield (*44*), similar to this study. Our observation indicates that RNA sequencing data obtained in this study is of good quality and can be used for posterior analysis with high confidence.

The first limitation of our study is that we used only HBE cells and ePCR binding parasites for the in vitro assay and therefore may have missed miRNAs produced by other parasite-host interactions contributing to SM. Second, plasma samples used in this study were collected retrospectively. Therefore, factors before small RNA sequencing and TaqMan-qRT-PCR, such as time taken between centrifugation, storage, and storage temperature, might have varied among the samples, affecting miRNA plasma levels (*45,46*). However, confirmation of findings in both the study cohorts suggest a minimal effect of preanalysis conditions in the results. Third, variations in the number of miRNAs identified in replicates of in vitro experiments may have led to the loss of some miRNAs. Fourth, the lack of tissue samples from organs with *P. falciparum* sequestration restricted the histological confirmation of identified miRNAs, and the presence of co-infections other than blood culture positive bacteremia cannot be neglected in the studied plasma samples. Finally, the association of each miRNA with specific symptoms that are part of the SM case definition may need further validation using a larger sample size, considering that our numbers were relatively small for individual SM criteria. In addition, future studies using machine-learning approaches would enable the identification of a combination of miRNAs that may detect SM pathologies.

In conclusion, the profiling of miRNAs in media from HBE cells after incubation with a cytoadherent *P. falciparum* strain and in plasma from children with different clinical manifestations enabled us to identify promising miRNA candidates for characterizing severe malaria, specifically hsa-miR-4497. This study is a base for future analyses to understand the value of these miRNAs as a prognostic biomarker and for disentangling the etiology of SM.


### Acknowledgments

We thank the children who participated in the study; the staff of the Manhiça District Hospital; the clinical officers, field supervisors, and data managers; G. Cabrera, L. Mussacate, N. Ernesto José, and A. Nhabomba for their contribution to the collection of parasites; and L. Puyol for her laboratory management, as well as everyone who supported this study directly or indirectly. We also thank Ruhi Sikka, Varun Sharma, Rebecca Smith-Aguasca, Malia Skjefte, and Catriona Patterson for their useful comments on this manuscript.

This work was supported by the Instituto de Salud Carlos III (PI13/01478 cofunded by the Fondo Europeo de Desarrollo Regional [FEDER], grant no. CES10/021-I3SNS to A.M. and no. CP11/00269 from the Miguel Servet program to Q.B.). H.G. was supported by the Science and Engineering Research Board (SERB), Department of Science & Technology, Government of India (Overseas Postdoctoral Fellowship, SB/OS/PDF043/201516), January 2017–January 2019. ISGlobal is a member of the CERCA Programme, Generalitat de Catalunya (http://cerca.cat/en/suma). CISM is supported by the Government of Mozambique and the Spanish Agency for International Development (AECID). This research is part of ISGlobal's Program on the Molecular Mechanisms of Malaria, which is partially supported by the Fundación Ramón Areces.

H.G. and M.R. carried out the molecular analysis and results interpretation and wrote the first draft of this manuscript. P.C. also carried out molecular analysis and conducted cytoadhesion assays. A.S., R.V., L.M., and I.C. participated in fieldwork; collected clinical and epidemiological data, plasma samples, and dried blood drop filter papers; and performed microscopy. A.J., X.M.V., and D.B. participated in HRP2 analysis. M.R., P.C., H.G., L.P., A.B., and M.B. participated in bioinformatics and statistical analyses. Q.B. and A.M. participated in the study design, supervision, funding acquisition, project administration and coordinated all the stages of the project. All authors reviewed and approved the final manuscript. The datasets analyzed in this study are available from the corresponding author on request.


## About the Author

Dr. Gupta is a molecular biologist and an early career malaria disease researcher. His research focuses on host and parasite factors associated with severe malaria, and on the use of molecular tools for the active surveillance of emerging drug resistance, gene deletions, and afebrile malaria in malaria-endemic regions.

### References


1. Dondorp AM, Fanello CI, Hendriksen IC, Gomes E, Seni A, Chhaganlal KD, et al.; AQUAMAT group. Artesunate versus quinine in the treatment of severe falciparum malaria in African children (AQUAMAT): an open-label, randomised trial. Lancet. 2010;376:1647–57. https://doi.org/10.1016/S0140-6736(10)61924-1
2. Gravenor MB, van Hensbroek MB, Kwiatkowski D. Estimating sequestered parasite population dynamics in cerebral malaria. Proc Natl Acad Sci U S A. 1998;95:7620–4. https://doi.org/10.1073/pnas.95.13.7620
3. Miller LH, Baruch DI, Marsh K, Doumbo OK. The pathogenic basis of malaria. Nature. 2002;415:673–9. https://doi.org/10.1038/415673a
4. Dorovini-Zis K, Schmidt K, Huynh H, Fu W, Whitten RO, Milner D, et al. The neuropathology of fatal cerebral malaria in Malawian children. Am J Pathol. 2011;178:2146–58. https://doi.org/10.1016/j.ajpath.2011.01.016
5. Nagatake T, Hoang VT, Tegoshi T, Rabbege J, Ann TK, Aikawa M. Pathology of falciparum malaria in Vietnam. Am J Trop Med Hyg. 1992;47:259–64. https://doi.org/10.4269/ajtmh.1992.47.259
6. Milner DA Jr, Whitten RO, Kamiza S, Carr R, Liomba G, Dzamalala C, et al. The systemic pathology of cerebral malaria in African children. Front Cell Infect Microbiol. 2014;4:104. https://doi.org/10.3389/fcimb.2014.00104
7. White NJ, Turner GD, Day NP, Dondorp AM. Lethal malaria: Marchiafava and Bignami were right. J Infect Dis. 2013;208:192–8. https://doi.org/10.1093/infdis/jit116

8. Rowe JA, Claessens A, Corrigan RA, Arman M. Adhesion of *Plasmodium falciparum*-infected erythrocytes to human cells: molecular mechanisms and therapeutic implications. Expert Rev Mol Med. 2009;11:e16. https://doi.org/10.1017/S1462399409001082
9. Turner L, Lavstsen T, Berger SS, Wang CW, Petersen JE, Avril M, et al. Severe malaria is associated with parasite binding to endothelial protein C receptor. Nature. 2013;498:502–5. https://doi.org/10.1038/nature12216
10. Jensen AR, Adams Y, Hviid L. Cerebral *Plasmodium falciparum* malaria: The role of PfEMP1 in its pathogenesis and immunity, and PfEMP1-based vaccines to prevent it. Immunol Rev. 2020;293:230–52. https://doi.org/10.1111/imr.12807
11. Sahu PK, Satpathi S, Behera PK, Mishra SK, Mohanty S, Wassmer SC. Pathogenesis of cerebral malaria: new diagnostic tools, biomarkers, and therapeutic approaches. Front Cell Infect Microbiol. 2015;5:75. https://doi.org/10.3389/fcimb.2015.00075
12. Erdman LK, Petes C, Lu Z, Dhabangi A, Musoke C, Cserti-Gazdewich CM, et al. Chitinase 3-like 1 is induced by *Plasmodium falciparum* malaria and predicts outcome of cerebral malaria and severe malarial anaemia in a case–control study of African children. Malar J. 2014;13:279. https://doi.org/10.1186/1475-2875-13-279
13. Lucchi NW, Jain V, Wilson NO, Singh N, Udhayakumar V, Stiles JK. Potential serological biomarkers of cerebral malaria. Dis Markers. 2011;31:327–35. https://doi.org/10.1155/2011/345706
14. Tahar R, Albergaria C, Zeghidour N, Ngane VF, Basco LK, Roussilhon C. Plasma levels of eight different mediators and their potential as biomarkers of various clinical malaria conditions in African children. Malar J. 2016;15:337. https://doi.org/10.1186/s12936-016-1378-3
15. Dondorp AM, Desakorn V, Pongtavornpinyo W, Sahassananda D, Silamut K, Chotivanich K, et al. Estimation of the total parasite biomass in acute falciparum malaria from plasma PfHRP2. PLoS Med. 2005;2:e204. https://doi.org/10.1371/journal.pmed.0020204
16. Hendriksen IC, Mwanga-Amumpaire J, von Seidlein L, Mtove G, White LJ, Olaosebikan R, et al. Diagnosing severe falciparum malaria in parasitemic African children: a prospective evaluation of plasma PfHRP2 measurement. PLoS Med. 2012;9:e1001297. https://doi.org/10.1371/journal.pmed.1001297
17. Cortez MA, Bueso-Ramos C, Ferdin J, Lopez-Berestein G, Sood AK, Calin GA. MicroRNAs in body fluids—the mix of hormones and biomarkers. Nat Rev Clin Oncol. 2011;8:467–77. https://doi.org/10.1038/nrclinonc.2011.76
18. Mitchell PS, Parkin RK, Kroh EM, Fritz BR, Wyman SK, Pogosova-Agadjanyan EL, et al. Circulating microRNAs as stable blood-based markers for cancer detection. Proc Natl Acad Sci U S A. 2008;105:10513–8. https://doi.org/10.1073/pnas.0804549105
19. Hakimi MA, Cannella D. Apicomplexan parasites and subversion of the host cell microRNA pathway. Trends Parasitol. 2011;27:481–6. https://doi.org/10.1016/j.pt.2011.07.001
20. El-Assaad F, Hempel C, Combes V, Mitchell AJ, Ball HJ, Kurtzhals JA, et al. Differential microRNA expression in experimental cerebral and noncerebral malaria. Infect Immun. 2011;79:2379–84. https://doi.org/10.1128/IAI.01136-10
21. Baro B, Deroost K, Raiol T, Brito M, Almeida AC, de Menezes-Neto A, et al. *Plasmodium vivax* gametocytes in the bone marrow of an acute malaria patient and changes in the erythroid miRNA profile. PLoS Negl Trop Dis. 2017;11:e0005365. https://doi.org/10.1371/journal.pntd.0005365
22. Xue X, Zhang Q, Huang Y, Feng L, Pan W. No miRNA were found in *Plasmodium* and the ones identified in erythrocytes could not be correlated with infection. Malar J. 2008;7:47. https://doi.org/10.1186/1475-2875-7-47
23. Rubio M, Bassat Q, Estivill X, Mayor A. Tying malaria and microRNAs: from the biology to future diagnostic perspectives. Malar J. 2016;15:167. https://doi.org/10.1186/s12936-016-1222-9
24. StatsTutor. Spearman's correlation. 2011 [cited 2020 Nov 23]. http://www.statstutor.ac.uk/resources/uploaded/spearmans.pdf
25. Mayor A, Serra-Casas E, Bardají A, Sanz S, Puyol L, Cisteró P, et al. Sub-microscopic infections and long-term recrudescence of *Plasmodium falciparum* in Mozambican pregnant women. Malar J. 2009;8:9. https://doi.org/10.1186/1475-2875-8-9
26. Taylor SM, Mayor A, Mombo-Ngoma G, Kenguele HM, Ouédraogo S, Ndam NT, et al. A quality control program within a clinical trial consortium for PCR protocols to detect *Plasmodium* species. J Clin Microbiol. 2014;52:2144–9. https://doi.org/10.1128/JCM.00565-14
27. Wang J, Chen J, Chang P, LeBlanc A, Li D, Abbruzzesse JL, et al. MicroRNAs in plasma of pancreatic ductal adenocarcinoma patients as novel blood-based biomarkers of disease. Cancer Prev Res (Phila). 2009;2:807–13. https://doi.org/10.1158/1940-6207.CAPR-09-0094
28. Rubio M, Bustamante M, Hernandez-Ferrer C, Fernandez-Orth D, Pantano L, Sarria Y, et al. Circulating miRNAs, isomiRs, and small RNA clusters in human plasma and breast milk. PLoS One. 2018;13:e0193527. https://doi.org/10.1371/journal.pone.0193527
29. Pantano L, Estivill X, Martí E. SeqBuster, a bioinformatic tool for the processing and analysis of small RNAs datasets, reveals ubiquitous miRNA modifications in human embryonic cells. Nucleic Acids Res. 2010;38:e34. https://doi.org/10.1093/nar/gkp1127
30. Love MI, Huber W, Anders S. Moderated estimation of fold change and dispersion for RNA-seq data with DESeq2. Genome Biol. 2014;15:550. https://doi.org/10.1186/s13059-014-0550-8
31. Marabita F, de Candia P, Torri A, Tegnér J, Abrignani S, Rossi RL. Normalization of circulating microRNA expression data obtained by quantitative real-time RT-PCR. Brief Bioinform. 2016;17:204–12. https://doi.org/10.1093/bib/bbv056
32. Pantano L, Estivill X, Martí E. A non-biased framework for the annotation and classification of the non-miRNA small RNA transcriptome. Bioinformatics. 2011;27:3202–3. https://doi.org/10.1093/bioinformatics/btr527
33. Kirschner MB, Edelman JJ, Kao SC, Vallely MP, van Zandwijk N, Reid G. The impact of hemolysis on cell-free microRNA biomarkers. Front Genet. 2013;4:94. https://doi.org/10.3389/fgene.2013.00094
34. LaMonte G, Philip N, Reardon J, Lacsina JR, Majoros W, Chapman L, et al. Translocation of sickle cell erythrocyte microRNAs into *Plasmodium falciparum* inhibits parasite translation and contributes to malaria resistance. Cell Host Microbe. 2012;12:187–99. https://doi.org/10.1016/j.chom.2012.06.007
35. Chen SY, Wang Y, Telen MJ, Chi JT. The genomic analysis of erythrocyte microRNA expression in sickle cell diseases. PLoS One. 2008;3:e2360. https://doi.org/10.1371/journal.pone.0002360
36. Rathjen T, Nicol C, McConkey G, Dalmay T. Analysis of short RNAs in the malaria parasite and its red blood cell host. FEBS Lett. 2006;580:5185–8. https://doi.org/10.1016/j.febslet.2006.08.063

37. Ludwig N, Leidinger P, Becker K, Backes C, Fehlmann T, Pallasch C, et al. Distribution of miRNA expression across human tissues. Nucleic Acids Res. 2016;44:3865–77. https://doi.org/10.1093/nar/gkw116
38. Maffioletti E, Cattaneo A, Rosso G, Maina G, Maj C, Gennarelli M, et al. Peripheral whole blood microRNA alterations in major depression and bipolar disorder. J Affect Disord. 2016;200:250–8. https://doi.org/10.1016/j.jad.2016.04.021
39. Mayor A, Hafiz A, Bassat Q, Rovira-Vallbona E, Sanz S, Machevo S, et al. Association of severe malaria outcomes with platelet-mediated clumping and adhesion to a novel host receptor. PLoS One. 2011;6:e19422. https://doi.org/10.1371/journal.pone.0019422
40. Chen X, Zhang L, Tang S. MicroRNA-4497 functions as a tumor suppressor in laryngeal squamous cell carcinoma via negatively modulation the GBX2. Auris Nasus Larynx. 2019;46:106–13. https://doi.org/10.1016/j.anl.2018.05.005
41. Das K, Saikolappan S, Dhandayuthapani S. Differential expression of miRNAs by macrophages infected with virulent and avirulent *Mycobacterium tuberculosis*. Tuberculosis (Edinb). 2013;93(Suppl):S47–50. https://doi.org/10.1016/S1472-9792(13)70010-6
42. Tonge DP, Gant TW. What is normal? Next generation sequencing-driven analysis of the human circulating miRNAOme. BMC Mol Biol. 2016;17:4. https://doi.org/10.1186/s12867-016-0057-9
43. Panwar B, Omenn GS, Guan Y. miRmine: a database of human miRNA expression profiles. Bioinformatics. 2017;33:1554–60. https://doi.org/10.1093/bioinformatics/btx019
44. Glynn CL, Khan S, Kerin MJ, Dwyer RM. Isolation of secreted microRNAs (miRNAs) from cell-conditioned media. MicroRNA. 2013;2:14–9. https://doi.org/10.2174/2211536611302010003
45. Glinge C, Clauss S, Boddum K, Jabbari R, Jabbari J, Risgaard B, et al. Stability of circulating blood-based microRNAs—pre-analytic methodological considerations. PLoS One. 2017;12:e0167969. https://doi.org/10.1371/journal.pone.0167969
46. Sourvinou IS, Markou A, Lianidou ES. Quantification of circulating miRNAs in plasma: effect of preanalytical and analytical parameters on their isolation and stability. J Mol Diagn. 2013;15:827–34. https://doi.org/10.1016/j.jmoldx.2013.07.005

Address for correspondence: Himanshu Gupta, ISGlobal, Hospital Clínic, Universitat de Barcelona, Carrer Rosselló 153 (CEK Bldg), E-08036 Barcelona, Spain; email: himanshu.gupta@isglobal.org or himanshugupta.hcu@gmail.com

# Increasing Incidence of Invasive Group A *Streptococcus* Disease in First Nations Population, Alberta, Canada, 2003–2017

Gregory J. Tyrrell, Christopher Bell, Lea Bill, Sumana Fathima

The incidence of invasive group A *Streptococcus* (iGAS) disease in the general population in Alberta, Canada, has been steadily increasing. To determine whether rates for specific populations such as First Nations are also increasing, we investigated iGAS cases among First Nations persons in Alberta during 2003–2017. We identified cases by isolating GAS from a sterile site and performing *emm* typing. We collected demographic, social, behavioral, and clinical data for patients. During the study period, 669 cases of iGAS in First Nations persons were reported. Incidence increased from 10.0 cases/100,000 persons in 2003 to 52.2 cases/100,000 persons in 2017. The 2017 rate was 6 times higher for the First Nations population than for non–First Nations populations (8.7 cases/100,000 persons). The 5 most common *emm* types from First Nations patients were 59, 101, 82, 41, and 11. These data indicate that iGAS is severely affecting the First Nations population in Alberta, Canada.

GAS disease is caused by the gram-positive coccus bacterium *Streptococcus pyogenes*; invasive GAS (iGAS) disease is typically defined as identification of GAS from any sterile site, including blood, cerebrospinal fluid, brain, and deep tissues. GAS affects persons worldwide and causes a wide array of diseases including pharyngitis, skin infections (e.g., impetigo and cellulitis), bacteremia, pneumonia, septic arthritis, rheumatic fever, rheumatic heart disease, and the severe invasive diseases necrotizing fasciitis and streptococcal toxic shock syndrome (*1*,*2*). The epidemiology of many of these diseases varies by region; pharyngitis is more common in high-income countries, and diseases such as impetigo are more common in tropical climates and low-income countries (*3*,*4*). In 2005, the mortality rate associated with GAS disease (noninvasive and invasive) was ≈500,000 deaths/year (*2*).

GAS bacteria can be typed by identifying variability in the DNA sequence at the tip of a coiled-coil protein on the bacteria's surface (the M protein), which is encoded by the *emm* gene. Worldwide, there are >240 *emm* types (*5*,*6*). Prevalence of *emm* types varies according to population and geography (*7*). In addition, the diversity of *emm* types is greater in developing countries and less in more developed countries (*8*–*10*).

Previous studies have shown that rates of iGAS disease are higher for indigenous populations than for other populations (*11*–*15*). Examples include Native Americans in Arizona and Alaska and indigenous communities in parts of Australia and northwestern Ontario, Canada. For parts of the country such as western Canada, detailed descriptive data on iGAS in the indigenous population are lacking. We previously reported increased age-standardized rates of iGAS in Alberta's general population and increasing incidence from a low of 4.2 cases/100,000 persons in 2003 to a high of 10.2 cases/100,000 persons in 2017 (*16*). On the basis of that finding, we explored whether iGAS rates also increased for the First Nations population of Alberta during the same period.

## Methods

### Case and Population Data

All iGAS cases were identified by diagnostic microbiology laboratories in Alberta, where iGAS disease is listed as a Public Health Notifiable Disease (https://open.alberta.ca/publications/streptococcal-disease-

Author affiliations: University of Alberta, Edmonton, Alberta, Canada (G.J. Tyrrell); Alberta Precision Laboratories–Public Health–Alberta Health Services, Edmonton (G.J. Tyrrell); Alberta Ministry of Health, Edmonton (C. Bell, S. Fathima); Alberta First Nations Information Governance Center, Siksika, Alberta, Canada (L. Bill)

DOI: https://doi.org/10.3201/eid2702.201945

group-a-invasive). All cases identified by diagnostic microbiology laboratories are required to be reported to the Alberta Ministry of Health. Confirmed iGAS cases are defined as identification of GAS from any typically sterile site, including blood, cerebrospinal fluid, brain, deep tissues, and joints (https://open.alberta.ca/publications/streptococcal-disease-group-a-invasive). After initially identifying iGAS isolates, diagnostic microbiology laboratories in Alberta informed provincial public health officials, and trained public health nurses collected clinical and risk factor data according to routine notifiable disease requirements by using a notifiable disease reporting form (https://open.alberta.ca/publications/ndr-manual-9th-edition). Clinical (including risk factors) and laboratory data were electronically captured in the Alberta Health Communicable Disease Reporting System (CDRS), an electronic database held by Alberta Health and used to capture data regarding cases of reported communicable disease. Staff at Alberta Health reviewed each incident case for data quality and completeness in the CDRS.

For the risk factor analysis, we defined addiction abuse as a primary chronic neurobiological disease with genetic, psychosocial, and environmental factors and behaviors leading to impaired control over drug use, compulsive use, continued use despite harm, and craving. Subsets of addiction abuse were alcohol abuse and drug use. Alcohol abuse was defined as the overindulgence in alcohol, leading to effects that are detrimental to the person's physical and mental health. Drug use was defined as the use of all drugs that were acquired unlawfully. Deaths were determined at the time of data collection by Alberta Health.

In Canada, there are 3 groups of aboriginal peoples: First Nations, Inuit, and Métis (https://www.rcaanc-cirnac.gc.ca/eng/1100100013785/1529102490303). Only cases in First Nations persons, Inuit, and Métis were captured in this analysis. To identify cases in First Nations persons only, we extracted all iGAS cases during 2003–2017 from the CDRS and used a Unique Lifetime Identifier number to link them to the Alberta Health First Nations identifiers registry held by Alberta Health. The First Nations registry includes anyone ever registered as having First Nations status. For statistical analyses, we used deidentified and aggregated data. The First Nations population of Alberta in 2003 was 140,436; in 2017, the population was 164,786 (http://www.ahw.gov.ab.ca/IHDA_Retrieval). An ethical framework for information and knowledge-sharing for this project was provided by the principles of OCAP (Ownership, Control, Access and Possession) within Alberta First Nations (http://afnigc.ca/main/index.php?id=resources&content=community%20resources).

### *emm* Typing of iGAS Isolates

All GAS isolates from persons with invasive cases are required to be submitted to the Provincial Public Health Laboratory for *emm* typing. The method used to type iGAS isolates from 2003 through September 2006 was a previously described serologic typing assay (*17*). From October 2006 through 2017, *emm* typing was conducted by DNA sequencing of the M serotype specific region of the *emm* gene as previously described (*17*–*19*). Assignment of *emm*-cluster type was performed as previously described (*20*). In brief, after the *emm* type was identified, it was matched to an *emm*-cluster type on the basis of the typing scheme of Sanderson-Smith et al. (*20*).

### Statistical Analyses

During 2003–2017, First Nations population estimates in Alberta were extracted from the online Interactive Health Data Application database (http://www.ahw.gov.ab.ca/IHDA_Retrieval). We calculated incidence rates by age group and by year of diagnosis, expressed as cases per 100,000 persons. Data were analyzed by using SAS version 9.3 (SAS Institute Inc., https://www.sas.com) and graphed by using OriginLab software 2018 (OriginLab Corporation, https://www.originlab.com). To compare clinical presentations and *emm* clusters between First Nations and non–First Nations persons, we conducted Fisher exact *t* tests. We considered $p<0.05$ to be statistically significant.

## Results

### Incidence

Over the 15 years reviewed, we found 669 cases of iGAS in the First Nations population in Alberta; mean annual incidence rate was 28.6 cases/100,000 persons. The number of cases in 2003 was 14, which by 2017 increased to 86. In 2017, the incidence rate for the Alberta First Nations population (52.2 cases/100,000 persons) was 6 times greater than that for non–First Nations populations (8.7 cases/100,000 persons) (Figure 1). By First Nations age group, incidence was highest among persons <1 year of age (71.2 cases/100,000 persons), followed by persons ≥60 years of age (65.8 cases/100,000 persons) (Figure 2, panel A). iGAS incidence among First Nations persons of all age groups was higher than that among non–First Nations persons (Figure 2). Incidence rates varied by season; the number of cases of iGAS among First Nations persons was

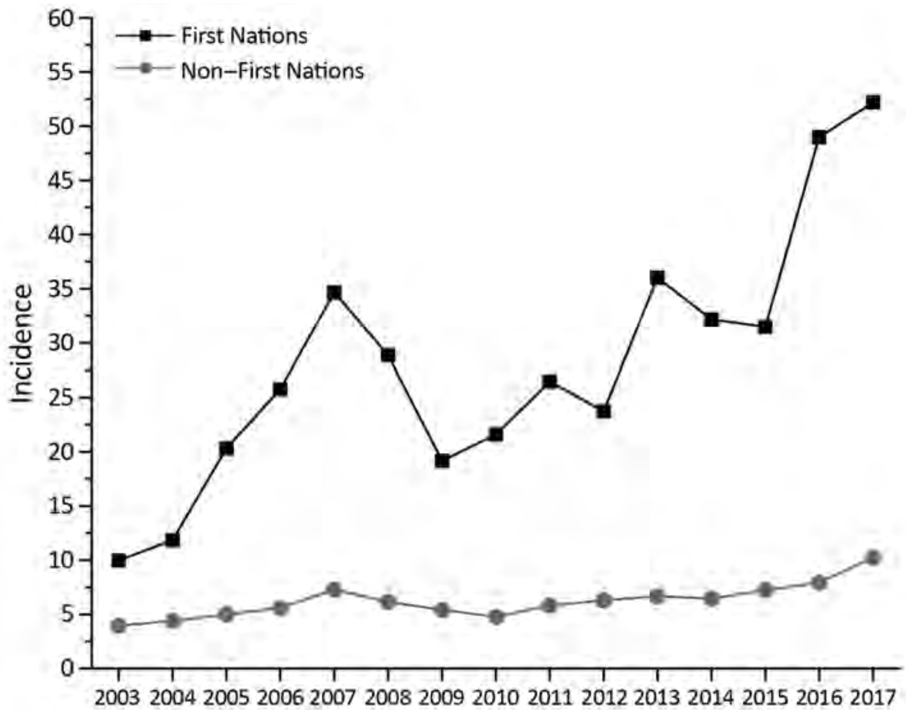


**Figure 1.** Incidence (cases/100,000 population) of invasive group A *Streptococcus* disease for First Nations and non–-First Nations populations, Alberta, Canada, 2003–2017. The incidence rate for the First Nations population climbed from a low of 10.0 in 2003 to a high of 52.2 in 2017. This rate contrasts with that for the non–First Nations population (3.7 in 2003 and 8.7 in 2017).

lowest during May and June (Figure 3), similar to what has been reported for the general population (*16*).

### Case Demographics, Clinical Manifestations, and Risk Factor Analyses

The median age of First Nations persons with iGAS disease was 38.5 years, younger than the overall median age of 45 years for persons with iGAS disease previously reported for the overall Alberta population (*16*). The proportion of First Nations iGAS patients who were male (54.8%) was similar to the proportion of non–First Nations patients who were male (58.5%). A total of 24 deaths among First Nations patients were attributed to iGAS; case-fatality rate was 3.6%. In comparison, the case-fatality rate among non–First Nations persons was 7.0%. By age group, of the 24 First Nations persons who died, 2 were children (<1 through 2 years of age). The remaining 22 First Nations persons who died were ≥35 years of age (Figure 2, panel A). For all age groups, case-fatality rates were higher among non–First Nations than among First Nations persons (Figure 2, panels A and B).

We observed little difference between First Nations and non–First Nations populations with respect to clinical diagnosis (Table 1). The percentage of soft tissue infections was higher for the First Nations population

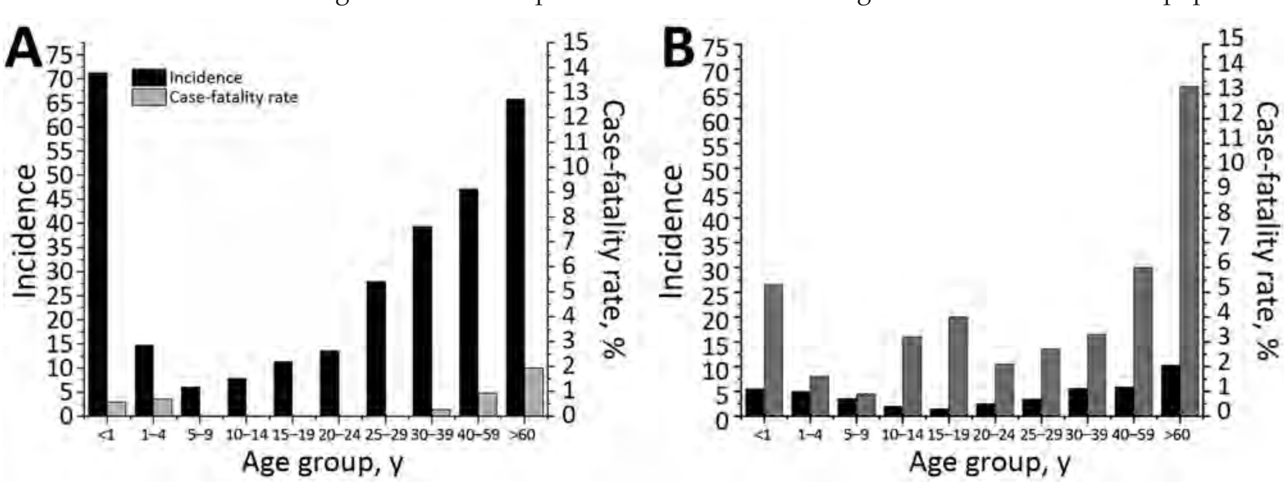


**Figure 2.** Incidence (cases/100,000 population) and case-fatality rates for invasive group A *Streptococcus* disease for First Nations (A) and non–First Nations (B) populations, by age group, Alberta, Canada, 2003–2017.

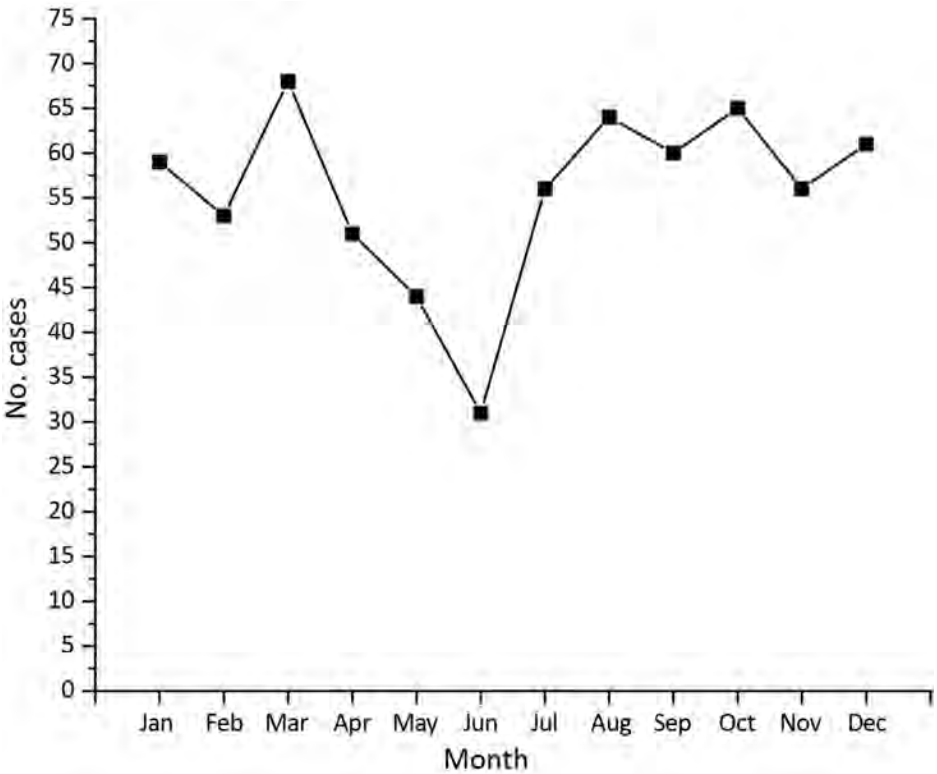


**Figure 3.** Seasonality of invasive group A *Streptococcus* disease in the First Nations population, Alberta, Canada, 2003–2017.

than the non–First Nations population (18.8% vs. 10.8%, p<0.001; Table 1). Frequency of streptococcal toxic shock syndrome was greater in the non–First Nations population than in the First Nations population (6.4% vs. 2.3%, p<0.001; Table 1). The most prevalent risk factors for the First Nations population over the 15-year study period were addiction abuse, alcohol abuse, drug use, nonsurgical wounds, homelessness, diabetes mellitus, and hepatitis C (*16*) (Table 2).

### *emm* Types and *emm* Cluster Descriptions

For the 15-year study period, we observed a difference in the distribution of *emm* types between First Nations and non–First Nations populations in Alberta. The most prevalent *emm* type among the First Nations population was *emm*59, which accounted for 13.5% of all *emm* types, followed by *emm*101 (8.4%) and 82 (7.4%) (Table 3, Figure 4). This finding was in contrast to that for the non–First Nations population,

**Table 1.** Invasive group A *Streptococcus* disease in First Nations and non–First Nations persons, by clinical diagnosis, Alberta, Canada, 2003-2017*

| System, clinical condition | First Nations, no. (%) cases | Non–First Nations, no. (%) cases | p value† |
|---|---|---|---|
| Blood, brain, sterile tissue | | | |
| Septicemia/bacteremia | 319 (37.8) | 1570 (42.8) | 0.011 |
| Streptococcal toxic shock syndrome | 19 (2.3) | 235 (6.4) | <0.001 |
| Meningitis | 9 (1.1) | 16 (0.4) | 0.061 |
| Peritonitis | 5 (0.6) | 24 (0.7) | 0.886 |
| Encephalitis | 1 (0.1) | 0 | 0.373 |
| Skin/soft tissue | | | |
| Cellulitis | 146 (17.3) | 633 (17.3) | 0.971 |
| Soft tissue infection | 159 (18.8) | 397 (10.8) | <0.001 |
| Necrotizing fasciitis | 60 (7.1) | 266 (7.3) | 0.989 |
| Respiratory | | | |
| Pneumonia | 50 (5.9) | 291 (7.9) | 0.054 |
| Epiglottitis | 2 (0.2) | 11 (0.3) | 0.824 |
| Bone | | | |
| Joint | 63 (7.5) | 192 (5.2) | 0.016 |
| Osteomyelitis | 10 (1.2) | 27 (0.8) | 0.272 |
| Unknown | 2 (0.2) | 0 | 0.069 |
| Total | 845 (100) | 3,688 (100) | Not applicable |

*Patients may have multiple clinical manifestations (193 patients had 2 clinical manifestations, 39 patients had 3, 2 patients had 4, and 1 had 5).
†By Fisher exact test.

for which the top 3 *emm* types were *emm*1 (22.1%), 28 (9.9%), 3 (5.1%), and 59 (5.1%).

*emm* cluster types differed substantially between First Nations and non–First Nations populations (Table 4). These differences were notable for cluster types A-C3, D4, E3, E4, and E6. The cluster types associated with the greatest number of cases for the First Nations population were D4 (*emm*41, 53, 80, 83, 91, 101) and E6 (*emm*11, 59, 75, 81, 94), representing 50.6% of the cases in this group. Twelve other clusters represented the remaining 49.4% (30 other *emm* types) of typed cases.

## Discussion

Our data illustrate the extent to which rates of iGAS disease are disproportionately higher for the First Nations population than the non–First Nations population in Alberta. For 2017, rates for the First Nations population (52.2 cases/100,000 persons) were 6-fold higher than rates for non–First Nations populations (8.7 cases/100,000 persons). Rates were also very high for First Nations children <1 year of age (71.2 cases/100,000 persons), in contrast to previously published rates for children in the 0 to 1–year age group of the general Alberta population (9.7 cases/100,000 persons [*16*]). Our results are similar to those reported for First Nations groups elsewhere. For example, another study in Canada found that, from 2009 through 2014, northwestern Ontario reported an elevated annualized rate of 56.2 cases/100,000 persons for the First Nations communities (*14*), similar to the rates we report for First Nations populations. With respect to other indigenous groups elsewhere, iGAS rates for the Aboriginal population in Australia during 2011–2013 were as high as 70.0 cases/100,000 persons, 8-fold higher than rates for the non-Aboriginal population (*21*). A previous study from Alaska found that during 2001–2013, the incidence rate for Alaska Natives was 13.7 cases/100,000 persons, compared with a rate of 3.9 cases/100,000 persons for non–Alaska Natives (*15*). Reported rates for Alaska Native children (39.9 cases/100,000 persons) have been higher than those reported for non–Alaska Native children (4.2 cases/100,000 persons) (*15*).

**Table 2.** Risk factors for First Nations and non–First Nations persons with invasive group A *Streptococcus* disease, Alberta, Canada, 2003-2017*

| | No. (%) | |
|---|---|---|
| Risk factor | First Nations, n = 669 | Non–First Nations, n = 2,315 |
| Diabetes | 103 (15.4) | 176 (7.6) |
| Hepatitis C | 101 (15.1) | 181 (7.8) |
| Immunocompromised | 41 (6.1) | 238 (10.3) |
| Nonsurgical wound | 165 (24.7) | 543 (23.5) |
| Surgical wound | 43 (6.4) | 133 (5.7) |
| Addiction abuse | 250 (37.4) | 390 (16.8) |
| Alcohol abuse | 188 (28.1) | 90 (3.9) |
| Drug use | 126 (18.8) | 307 (13.3) |
| Homelessness | 117 (17.5) | 257 (11.1) |

*Percentages may add up to >100% because each patient may have multiple risk factors.

Drivers of the higher rates in the First Nations populations are not completely clear, although specific risk factors probably contribute. Risk factor data for iGAS in the First Nations population in our study frequently indicated nonsurgical wounds, addiction abuse (of which alcohol use and drug use are subsets), and homelessness. Other studies have noted high rates of GAS skin infections (e.g., cellulitis and abscesses) among persons who were experiencing homelessness and injected drugs (*22*–*24*). Recently,

**Table 3.** Number of *emm* gene types in group A *Streptococcus* from First Nations persons with invasive disease, by year, Alberta, Canada, 2003–2017*

| *emm* type | 2003 | 2004 | 2005 | 2006 | 2007 | 2008 | 2009 | 2010 | 2011 | 2012 | 2013 | 2014 | 2015 | 2016 | 2017 | Total |
|---|---|---|---|---|---|---|---|---|---|---|---|---|---|---|---|---|
| 59 | 0 | 0 | 1 | 0 | 7 | 18 | 12 | 4 | 3 | 1 | 3 | 1 | 4 | 10 | 13 | 77 |
| 101 | 0 | 0 | 0 | 0 | 0 | 1 | 4 | 1 | 4 | 2 | 1 | 2 | 9 | 14 | 10 | 48 |
| 82 | 1 | 3 | 0 | 3 | 7 | 2 | 1 | 0 | 2 | 3 | 6 | 2 | 2 | 7 | 3 | 42 |
| 41 | 1 | 1 | 4 | 2 | 2 | 1 | 0 | 0 | 0 | 3 | 3 | 11 | 4 | 4 | 2 | 38 |
| 11 | 0 | 0 | 0 | 2 | 0 | 0 | 0 | 0 | 2 | 5 | 3 | 0 | 5 | 9 | 11 | 37 |
| 1 | 0 | 1 | 1 | 1 | 4 | 2 | 1 | 2 | 3 | 1 | 5 | 5 | 1 | 0 | 4 | 31 |
| 83 | 0 | 1 | 2 | 2 | 6 | 2 | 0 | 0 | 1 | 3 | 1 | 1 | 2 | 3 | 5 | 29 |
| 77 | 0 | 1 | 0 | 1 | 0 | 0 | 1 | 2 | 2 | 5 | 11 | 2 | 0 | 0 | 1 | 26 |
| 53 | 0 | 0 | 0 | 2 | 2 | 1 | 2 | 2 | 5 | 1 | 5 | 3 | 0 | 0 | 0 | 23 |
| 74 | 0 | 0 | 0 | 0 | 0 | 0 | 0 | 0 | 0 | 0 | 0 | 0 | 0 | 5 | 17 | 22 |
| 89 | 0 | 0 | 2 | 1 | 2 | 0 | 1 | 2 | 4 | 0 | 1 | 1 | 1 | 0 | 1 | 16 |
| 91 | 0 | 0 | 0 | 3 | 1 | 0 | 0 | 0 | 1 | 2 | 3 | 1 | 3 | 2 | 0 | 16 |
| 12 | 0 | 0 | 1 | 1 | 1 | 0 | 0 | 2 | 4 | 0 | 1 | 0 | 1 | 3 | 1 | 15 |
| 114 | 0 | 2 | 1 | 2 | 3 | 0 | 0 | 2 | 1 | 0 | 0 | 2 | 1 | 0 | 0 | 14 |
| 3 | 1 | 0 | 0 | 1 | 1 | 0 | 0 | 0 | 1 | 0 | 0 | 0 | 5 | 3 | 0 | 12 |
| 22 | 1 | 0 | 0 | 0 | 0 | 0 | 0 | 2 | 0 | 0 | 2 | 3 | 1 | 2 | 1 | 12 |
| 87 | 0 | 0 | 0 | 1 | 1 | 0 | 0 | 2 | 3 | 0 | 1 | 2 | 1 | 1 | 0 | 12 |
| 80 | 0 | 0 | 1 | 0 | 0 | 4 | 0 | 2 | 1 | 1 | 2 | 0 | 0 | 1 | 0 | 12 |
| Other | 4 | 3 | 7 | 5 | 6 | 4 | 3 | 3 | 3 | 3 | 4 | 5 | 3 | 9 | 11 | 73 |
| Nontypable | 2 | 4 | 2 | 6 | 0 | 1 | 0 | 0 | 0 | 0 | 0 | 0 | 0 | 0 | 0 | 15 |
| Total | 10 | 16 | 22 | 33 | 43 | 36 | 25 | 26 | 40 | 30 | 52 | 41 | 43 | 73 | 80 | 570 |

**emm* types found in >10 cases are shown.

work by the Active Bacterial Core surveillance program in the United States showed that skin infections and skin breakdown were common among iGAS patients who were injection drug users or experiencing homelessness (*25*). These studies suggest that skin infections in vulnerable populations with these risk factors provide routes for iGAS infections.

A role of skin infections is also suggested when *emm* types are grouped by *emm* clusters. Grouping *emm* types by cluster shows that the bulk of disease among the First Nations population was focused on cluster *emm* types that are considered to be associated with skin-related infections (D clusters) and generalist strains (E clusters), as opposed to throat-related clusters (A–C) (*26*). This finding may suggest that in this population, skin-to-skin transmission occurs more frequently than respiratory route transmission. Opportunities for skin-to-skin transmission can include overcrowded households, as has been documented in Australia for the Aboriginal population, in whom the high burden of iGAS disease associated with skin and soft tissue infections is related to overcrowded or inadequate housing (*27,28*). With respect to other potential risk factors, risk for iGAS has been found to be significantly increased for close contacts of iGAS patients (≈2,000 times higher than background incidence) (*29,30*). Overcrowding and inadequate housing have also been documented among First Nations populations in Canada (*31*). Overcrowding has been considered endemic to First Nations populations in Canada and can probably lead to higher rates of disease than in non–First Nations populations (*31*). However, the numbers of persons living in households was not a demographic captured in this study; therefore, whether overcrowding was a contributor for this study remains unclear.

When we examined specific clinical conditions, we found additional contrasts in iGAS disease between First Nations and non–First Nations groups. Soft tissue and joint infections occurred with more statistically significant frequency in the First Nations population than in the non–First Nations population, whereas septicemia/bacteremia and streptococcal toxic shock syndrome occurred with more frequency in the non–First Nations population than in the First Nations population. The reasons for these differences are not clear and may be multifactorial. We did not expect to find that streptococcal toxic shock syndrome occurred more frequently in the non–First Nations population. A different *emm* type distribution may account for some of these differences.

Prevalence of *emm*1 was greater for the non–First Nations population (>22%) than for the First Nations population (<6%). *emm*1 is a major contributor to streptococcal toxic shock syndrome and is the most frequent *emm* type isolated from persons in the

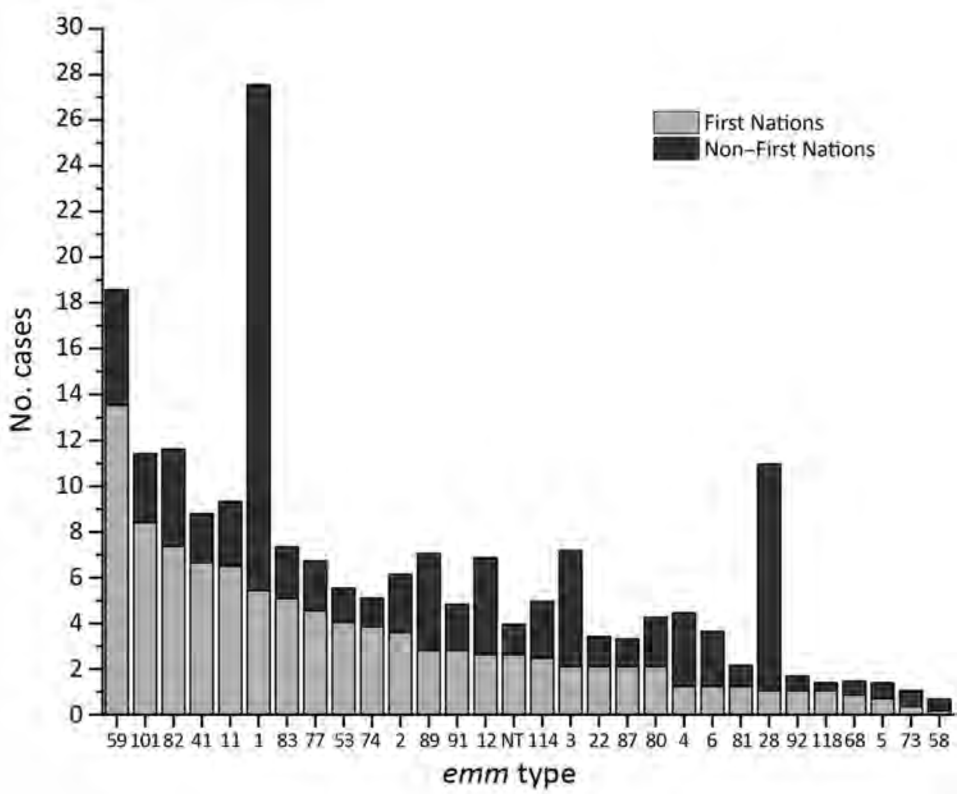


**Figure 4.** Group A *Streptococcus emm* types from First Nations persons and non–First Nations with invasive disease, Alberta, Canada, 2003–2017.

**Table 4.** *emm* clusters among group A *Streptococcus* from First Nations and non–First Nation persons with invasive disease, Alberta, Canada, 2003–2017

| Cluster type | First Nations, no. (%) | Non–First Nations, no. (%) | Total cases | p value |
|---|---|---|---|---|
| A-C3 | 32 (5.8) | 568 (22.7) | 600 | <0.001 |
| A-C4 | 15 (2.7) | 141 (5.6) | 156 | 0.004 |
| A-C5 | 12 (2.2) | 130 (5.2) | 142 | 0.001 |
| D2 | 1 (0.2) | 2 (0.1) | 3 | 0.902 |
| D3 | 0 | 3 (0.2) | 3 | 0.948 |
| D4 | 166 (30.0) | 310 (12.4) | 476 | <0.001 |
| E1 | 7 (1.3) | 83 (3.1) | 90 | 0.008 |
| E2 | 18 (3.3) | 64 (2.6) | 82 | 0.435 |
| E3 | 65 (11.7) | 199 (8.0) | 264 | 0.007 |
| E4 | 79 (14.3) | 616 (24.6) | 695 | <0.001 |
| E5 | 0 | 5 (0.2) | 5 | 0.736 |
| E6 | 125 (22.6) | 268 (10.7) | 393 | <0.001 |
| M5 | 4 (0.7) | 18 (0.7) | 22 | 0.787 |
| M6 | 7 (1.3) | 62 (2.5) | 69 | 0.100 |
| M23 | 1 (0.2) | 0 | 1 | 0.362 |
| M74 | 22 (4.0) | 32 (1.3) | 54 | <0.001 |
| M111 | 0 | 1 (0.1) | 1 | 0.408 |
| M122 | 0 | 1 (0.1) | 1 | 0.408 |
| M218 | 0 | 1 (0.1) | 1 | 0.408 |
| Total | 554 (100) | 2,504 (100) | 3,058 | Not applicable |

non–First Nations population in Alberta (*16*,*32*). The reason(s) behind the decreased presence of *emm*1 in the First Nations population despite it being the dominant *emm* type in the non–First Nations population are not clear.

In contrast to the lower frequency of streptococcal toxic shock syndrome is the higher frequency of soft tissue infections in the First Nations population. Our data show that *emm*59 was the most prevalent *emm* type in the First Nations population, and it has previously been shown that *emm*59 displays a tropism for skin infections (*33*,*34*). Since 2006, when a large outbreak of *emm*59 was first reported, *emm*59 has become an established *emm* type causing diseases such as skin and soft tissue infections throughout western Canada and the United States, whereas previously it was relatively rare (*33*,*35*–*37*). The *emm*59 cases reported here are probably derived from that original outbreak in 2006–2009 because before then, *emm*59 was uncommon.

Also notable is the striking difference in percentage of *emm*28 cases between First Nations (≈1%) versus non–First Nations (≈10%) populations. Our previous survey of the overall population indicated that *emm*28 was the second most common *emm* type after *emm*1 (*16*). *emm*28 falls within the E4 cluster categorizing this *emm* type as a generalist (*20*). The reason for the large difference in *emm*28 prevalence between the 2 populations is not clear.

The high iGAS incidence rate in the Alberta First Nations population illustrates the need for an effective GAS vaccine. One vaccine that has undergone phase 1 clinical trials is a polypeptide vaccine composed of 30 *emm* types (*38*). An assessment of the *emm* types contained in this 30-valent M protein–based GAS vaccine shows that this vaccine would include ≈53% of the *emm* types found in the Alberta First Nations population (*38*). If cross-protection against nonvaccine *emm* types based on immunogenicity in rabbits were included, this coverage rate would increase to 62.3% (*38*). In comparison, the 30-valent M-protein–based vaccine would include 77.1% of the *emm* types found in the non–First Nations population; if cross-protection with non-vaccine *emm* types were included, this percentage would increase to 79.8%. These comparisons do not include potential cross-protection through coverage of *emm* clusters. These *emm* type differences would have to be taken into account for the First Nations population should an *emm* type–based vaccine such as this be introduced into the Alberta population.

In summary, iGAS rates in the First Nations community in Alberta are high, at ≈50 cases/100,000 persons. Marked differences in iGAS disease in the First Nations population include more skin and soft tissue infections and fewer streptococcal toxic shock syndrome cases than in the non–First Nations population. Of note, substantial *emm* differences between the 2 populations could have potential implications for future vaccines.


## Acknowledgments

We thank the clinical diagnostic microbiology laboratories in Alberta for identifying iGAS isolates and submitting these to the Provincial Public Health Laboratory for *emm* typing.

This work was supported by Alberta Health and Alberta Precision Laboratories–Public Health, Alberta Health

Services, and the AMR-One Health Consortium Major Innovation Fund program of the Ministry of Jobs, Economy and Innovation, government of Alberta.

## About the Author

Dr. Tyrrell is a professor and divisional director in the Division of Diagnostic and Applied Microbiology, Department of Laboratory Medicine and Pathology, University of Alberta, Edmonton. His primary research interests are epidemiology of GAS, *Streptococcus pneumoniae*, and pathogenesis of group B streptococci.

## References

1. Cunningham MW. Pathogenesis of group A streptococcal infections. Clin Microbiol Rev. 2000;13:470–511. https://doi.org/10.1128/CMR.13.3.470
2. Carapetis JR, Steer AC, Mulholland EK, Weber M. The global burden of group A streptococcal diseases. Lancet Infect Dis. 2005;5:685–94. https://doi.org/10.1016/S1473-3099(05)70267-X
3. Bowen AC, Tong SYC, Chatfield MD, Carapetis JR. The microbiology of impetigo in indigenous children: associations between *Streptococcus pyogenes*, *Staphylococcus aureus*, scabies, and nasal carriage. BMC Infect Dis. 2014;14:727. https://doi.org/10.1186/s12879-014-0727-5
4. Steer AC, Jenney AWJ, Kado J, Batzloff MR, La Vincente S, Waqatakirewa L, et al. High burden of impetigo and scabies in a tropical country. PLoS Negl Trop Dis. 2009;3:e467. https://doi.org/10.1371/journal.pntd.0000467
5. Bessen DE, Smeesters PR, Beall BW. Molecular epidemiology, ecology and evolution of group A streptococci. Microbiol Spec. 2018;6. https://doi.org/10.1128/microbiolspec.CPP3-0009-2018
6. Centers for Disease Control and Prevention. *Streptococcus pyogenes* (group A *Streptococcus*) [cited 2019 Oct 19]. https://www.cdc.gov/streplab/groupa-strep/index.html
7. Steer AC, Law I, Matatolu L, Beall BW, Carapetis JR. Global *emm* type distribution of group A streptococci: systematic review and implications for vaccine development. Lancet Infect Dis. 2009;9:611–6. https://doi.org/10.1016/S1473-3099(09)70178-1
8. Tewodros W, Kronvall G. M protein gene (*emm* type) analysis of group A beta-hemolytic streptococci from Ethiopia reveals unique patterns. J Clin Microbiol. 2005;43:4369–76. https://doi.org/10.1128/JCM.43.9.4369-4376.2005
9. Smeesters PR, Vergison A, Campos D, de Aguiar E, Miendje Deyi VY, Van Melderen L. Differences between Belgian and Brazilian group A *Streptococcus* epidemiologic landscape. PLoS One. 2006;1:e10. https://doi.org/10.1371/journal.pone.0000010
10. Sakota V, Fry AM, Lietman TM, Facklam RR, Li Z, Beall B. Genetically diverse group A streptococci from children in far-western Nepal share high genetic relatedness with isolates from other countries. J Clin Microbiol. 2006;44:2160–6. https://doi.org/10.1128/JCM.02456-05
11. Hoge CW, Schwartz B, Talkington DF, Breiman RF, MacNeill EM, Englender SJ. The changing epidemiology of invasive group A streptococcal infections and the emergence of streptococcal toxic shock-like syndrome. A retrospective population-based study. JAMA. 1993;269:384–9. https://doi.org/10.1001/jama.1993.03500030082037
12. Marshall CS, Cheng AC, Markey PG, Towers RJ, Richardson LJ, Fagan PK, et al. Acute post-streptococcal glomerulonephritis in the Northern Territory of Australia: a review of 16 years data and comparison with the literature. Am J Trop Med Hyg. 2011;85:703–10. https://doi.org/10.4269/ajtmh.2011.11-0185
13. Harris AM, Yazzie D, Antone-Nez R, Dinè-Chacon G, Kinlacheeny JB, Foley D, et al. Community-acquired invasive GAS disease among Native Americans, Arizona, USA, Winter 2013. Emerg Infect Dis. 2015;21:177–9. https://doi.org/10.3201/eid2101.141148
14. Bocking N, Matsumoto C, Loewen K, Teatero S, Marchand-Austin A, Gordon J, et al. High incidence of invasive group A streptococcal infections in remote First Nations communities in Northwestern Ontario, Canada. Open Forum Infect Dis. 2016 ;4:ofw243. https://doi.org/10.1093/ofid/ofw243
15. Rudolph K, Bruce MG, Bruden D, Zulz T, Reasonover A, Hurlburt D, et al. Epidemiology of invasive group A streptococca l disease in Alaska, 2001–2013. J Clin Microbiol. 2016;54:134–41. https://doi.org/10.1128/JCM.02122-15
16. Tyrrell GJ, Fathima S, Kakulphimp J, Bell C. Increasing rates of invasive group A streptococcal disease in Alberta, Canada, 2003–2017. Open Forum Infect Dis. 2018;5:ofy177. https://doi.org/10.1093/ofid/ofy177
17. Tyrrell GJ, Lovgren M, Kress B, Grimsrud K. Invasive group A streptococcal disease in Alberta, Canada (2000 to 2002). J Clin Microbiol. 2005;43:1678–83. https://doi.org/10.1128/JCM.43.4.1678-1683.2005
18. Centers for Disease Control and Prevention. Protocol for *emm* typing [cited 2020 Feb 7]. https://www.cdc.gov/streplab/protocol-emm-type.html
19. Centers for Disease Control and Prevention. *Streptococcus pyogenes emm* sequence database, 2018 [cited 2020 Mar 1]. https://www.cdc.gov/streplab/groupa-strep/emm-typing-protocol.html
20. Sanderson-Smith M, De Oliveira DMP, Guglielmini J, McMillan DJ, Vu T, Holien JK, et al.; M Protein Study Group. A systematic and functional classification of *Streptococcus pyogenes* that serves as a new tool for molecular typing and vaccine development. J Infect Dis. 2014;210:1325–38. https://doi.org/10.1093/infdis/jiu260
21. Boyd R, Patel M, Currie BJ, Holt DC, Harris T, Krause V. High burden of invasive group A streptococcal disease in the Northern Territory of Australia. Epidemiol Infect. 2016;144:1018–27. https://doi.org/10.1017/S0950268815002010
22. Gittzus JWJ, White J, Caine L, Hansen K, Daly E, Chan B, et al. An outbreak of invasive group A streptococcal infections in injection drug users. Open Forum Infect Dis. 2017;4(suppl_1):S241. https://doi.org/10.1093/ofid/ofx163.511
23. Bundle N, Bubba L, Coelho J, Kwiatkowska R, Cloke R, King S, et al. Ongoing outbreak of invasive and non-invasive disease due to group A *Streptococcus* (GAS) type *emm*66 among homeless and people who inject drugs in England and Wales, January to December 2016. Euro Surveill. 2017;22:1–6. https://doi.org/10.2807/1560-7917.ES.2017.22.3.30446
24. Dickson C, Pham MT, Nguyen V, Brubacher C, Silverman MS, Khaled K, et al. Community outbreak of invasive group A *streptococcus* infection in Ontario, Canada. Can Commun Dis Rep. 2018;44:182–8. https://doi.org/10.14745/ccdr.v44i78a06
25. Valenciano SJ, Onukwube J, Spiller MW, Thomas A, Como-Sabetti K, Schaffner W, et al. Invasive group A streptococcal infections among people who inject drugs and people experiencing homelessness in the United States,

2010–2017. Clin Infect Dis. 2020:ciaa787. https://doi.org/in10.1093/cid/ciaa787
26. McMillan DJ, Drèze P-A, Vu T, Bessen DE, Guglielmini J, Steer AC, et al. Updated model of group A *Streptococcus* M proteins based on a comprehensive worldwide study. Clin Microbiol Infect. 2013;19:E222–9. https://doi.org/10.1111/1469-0691.12134
27. Steer AC, Carapetis JR, Nolan TM, Shann F. Systematic review of rheumatic heart disease prevalence in children in developing countries: the role of environmental factors. J Paediatr Child Health. 2002;38:229–34. https://doi.org/10.1046/j.1440-1754.2002.00772.x
28. Jaine R, Baker M, Venugopal K. Acute rheumatic fever associated with household crowding in a developed country. Pediatr Infect Dis J. 2011;30:315–9. https://doi.org/10.1097/INF.0b013e3181fbd85b
29. O'Grady KA, Kelpie L, Andrews RM, Curtis N, Nolan TM, Selvaraj G, et al. The epidemiology of invasive group A streptococcal disease in Victoria, Australia. Med J Aust. 2007;186:565–9. https://doi.org/10.5694/j.1326-5377.2007.tb01054.x
30. Mearkle R, Saavedra-Campos M, Lamagni T, Usdin M, Coelho J, Chalker V, et al. Household transmission of invasive group A *Streptococcus* infections in England: a population-based study, 2009, 2011 to 2013. Euro Surveill. 2017;22:30532. https://doi.org/10.2807/1560-7917.ES.2017.22.19.30532
31. Anaya J. The situation of indigenous peoples in Canada [cited 2020 Aug 1]. http://unsr.jamesanaya.org/?cat=11
32. Nasser W, Beres SB, Olsen RJ, Dean MA, Rice KA, Long SW, et al. Evolutionary pathway to increased virulence and epidemic group A *Streptococcus* disease derived from 3,615 genome sequences. Proc Natl Acad Sci U S A. 2014;111:E1768–76. https://doi.org/10.1073/pnas.1403138111
33. Tyrrell GJ, Lovgren M, St Jean T, Hoang L, Patrick DM, Horsman G, et al. Epidemic of group A *Streptococcus* M/*emm*59 causing invasive disease in Canada. Clin Infect Dis. 2010;51:1290–7. https://doi.org/10.1086/657068
34. Fittipaldi N, Beres SB, Olsen RJ, Kapur V, Shea PR, Watkins ME, et al. Full-genome dissection of an epidemic of severe invasive disease caused by a hypervirulent, recently emerged clone of group A *Streptococcus*. Am J Pathol. 2012;180:1522–34. https://doi.org/10.1016/j.ajpath.2011.12.037
35. Brown CC, Olsen RJ, Fittipaldi N, Morman ML, Fort PL, Neuwirth R, et al. Spread of virulent group A *Streptococcus* type *emm*59 from Montana to Wyoming, USA. Emerg Infect Dis. 2014;20:679–81. https://doi.org/10.3201/eid2004.130564
36. Engelthaler DM, Valentine M, Bowers J, Pistole J, Driebe EM, Terriquez J, et al. Hypervirulent *emm*59 clone in invasive group A *Streptococcus* outbreak, southwestern United States. Emerg Infect Dis. 2016;22:734–8. https://doi.org/10.3201/eid2204.151582
37. Chochua S, Metcalf BJ, Li Z, Rivers J, Mathis S, Jackson D, et al. Population and whole genome sequence based characterization of invasive group A streptococci recovered in the United States during 2015. mBio. 2017;8:e01422–17. https://doi.org/10.1128/mBio.01422-17
38. Dale JB, Penfound TA, Chiang EY, Walton WJ. New 30-valent M protein-based vaccine evokes cross-opsonic antibodies against non-vaccine serotypes of group A streptococci. Vaccine. 2011;29:8175–8. https://doi.org/10.1016/j.vaccine.2011.09.005

Address for correspondence: Gregory J. Tyrrell, University of Alberta Hospital, ProvLab, 2B3.08 WMC, 8440-112 St, Edmonton, AB T6G 2J2, Canada; email: gjt@ualberta.ca

# Effects of Social Distancing Measures during the First Epidemic Wave of Severe Acute Respiratory Syndrome Infection, Greece

Vana Sypsa, Sotirios Roussos, Dimitrios Paraskevis, Theodore Lytras, Sotirios Tsiodras,[1] Angelos Hatzakis[1]

Greece imposed a nationwide lockdown in March 2020 to mitigate transmission of severe acute respiratory syndrome coronavirus 2 during the first epidemic wave. We conducted a survey on age-specific social contact patterns to assess effects of physical distancing measures and used a susceptible-exposed-infectious-recovered model to simulate the epidemic. Because multiple distancing measures were implemented simultaneously, we assessed their overall effects and the contribution of each measure. Before measures were implemented, the estimated basic reproduction number ($R_0$) was 2.38 (95% CI 2.01–2.80). During lockdown, daily contacts decreased by 86.9% and $R_0$ decreased by 81.0% (95% credible interval [CrI] 71.8%–86.0%); each distancing measure decreased $R_0$ by 10%–24%. By April 26, the attack rate in Greece was 0.12% (95% CrI 0.06%–0.26%), one of the lowest in Europe, and the infection fatality ratio was 1.12% (95% CrI 0.55%–2.31%). Multiple social distancing measures contained the first epidemic wave in Greece.

Coronavirus disease (COVID-19), caused by severe acute respiratory syndrome coronavirus 2 (SARS-CoV-2), emerged in China in December 2019 (*1*) and by September 14, 2020, had spread worldwide, causing >28.6 million cases and >917,000 deaths (*2*). To suppress the epidemic curve, public health authorities needed to use the strongest possible mitigation strategies until effective therapies and vaccines are available. Central mitigation strategies include nonpharmaceutical interventions, such as travel-related restrictions, case-based, and social distancing interventions. Social distancing aims to decrease social contacts and reduce transmission (*3*).

Author affiliations: National and Kapodistrian University of Athens, Athens, Greece (V. Sypsa, S. Roussos, D. Paraskevis, S. Tsiodras, A. Hatzakis); National Public Health Organization, Athens (T. Lytras); European University Cyprus, Nicosia, Cyprus (T. Lytras)

DOI: https://doi.org/10.3201/eid2702.203412

In Greece, the first COVID-19 case was reported on February 26, 2020 (*4*). Soon after, several social distancing, travel-related, and case-based interventions were implemented. A nationwide lockdown restricting all nonessential movement throughout the country began on March 23 (Figure 1). By the end of April, the first epidemic wave had waned, and withdrawal of physical distancing interventions became a social priority.

Despite an ongoing severe financial crisis and an older population, Greece has been noted as an example of a country with successful response against COVID-19 (*5*). However, given the resurgence of cases in Greece and other countries, careful consideration and close monitoring are needed to inform strategies for resuming and maintaining social and economic activities.

We describe a survey implemented during lockdown in Greece and assess the effects of physical distancing measures on contact behavior. We used these data and mathematical modeling to obtain estimates for the first epidemic wave in the country, during February–April 2020, to assess the effects of all social distancing measures, and to assess the relative contribution of each measure towards the control of COVID-19.

## Materials and Methods

### Social Contacts Survey

We conducted a phone survey during March 31–April 7, 2020, to estimate the number of social contacts and age mixing of the population on a weekday during the lockdown and on the same day of the week before the pandemic, during mid-January 2020, by using contact diaries (Appendix Figure 1, https://wwwnc.cdc.gov/EID/

[1]These senior authors contributed equally to this article.

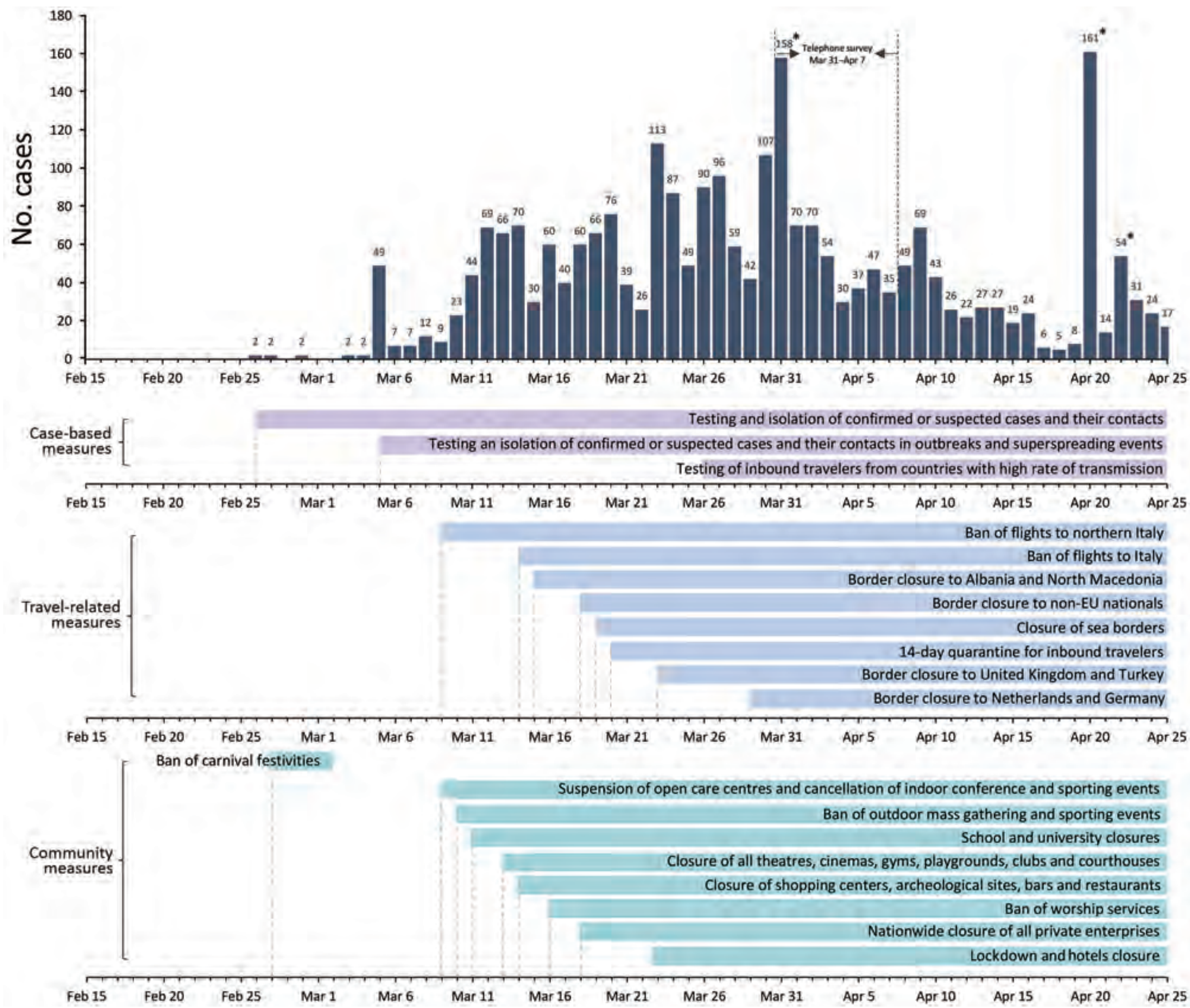


**Figure 1.** Daily number of coronavirus disease cases by date of sampling for laboratory testing (25) and timeline of key measures, Greece. Dates of telephone survey are indicated. Asterisks indicate spikes in the number of diagnosed cases at the end of March and late April that correspond to clusters of cases in 3 settings: a ship, a refugee camp, and a clinic. EU, European Union.

article/27/2/20-3412-App1.pdf). Participants provided oral informed consent. We defined contact as either skin-to-skin contact or a 2-way conversation with ≥3 words spoken in the physical presence of another person (*6*). For each contact, we recorded information on the contact person's age and location of the contact, such as home, school, workplace, transportation, leisure, or other. We planned to recruit 600 participants of all ages residing in Athens by using proportional quota sampling and oversampling among persons 0–17 years of age.

We estimated the average number of contacts for the prepandemic and lockdown periods. We defined 6 age groups to build age-specific contact matrices, adjusting for the age distribution of the population of Greece, by using socialmixr in R software (R Foundation for Statistical Computing, https://www.r-project.org).

### Estimating the Course of the First Epidemic Wave and Assessing Effects of Social Distancing

To estimate the course of the epidemic, we first estimated the basic reproduction number ($R_0$), the average number of secondary cases 1 case would produce in a completely susceptible population in the absence of control measures. Then, we used social contacts matrices to assess the effects of physical distancing measures on $R_0$. Finally, we simulated the course of the epidemic using a susceptible-exposed-infectious-recovered (SEIR) model.

### Estimating $R_0$

We estimated $R_0$ based on the number of confirmed cases with infection onset dates before the first social distancing measures were adopted, up to March 9, and accounted for imported cases. We used a maximum-likelihood method to obtain the $R_0$ and 95% CI, assuming that the serial interval distribution is known (*7*). We used the daily number of cases by date of symptom onset and inferred infection dates assuming an average incubation period of 5 days (*8*,*9*). We assumed a gamma distributed serial interval with a mean of 6.67 (SD 4.85) days, in accordance with other studies (*10*,*11*; D. Cereda et al., unpub. data, https://arxiv.org/abs/2003.09320). As a sensitivity analysis, we estimated $R_0$ assuming a shorter serial interval of 4.7 days (Appendix) (*12*).

### Assessing Effects of Social Distancing on $R_0$

Primary social distancing measures implemented in Greece began on March 11. These measures and the dates implemented were closing all educational establishments on March 11; theatres, courthouses, cinemas, gyms, playgrounds, and nightclubs on March 13; shopping centers, cafes, restaurants, bars, museums, and archaeological sites on March 14; suspending services in churches on March 16; closing all private enterprises, with some exceptions, on March 18; and, finally, restricting all nonessential movement throughout the country on March 23 (Figure 1; Appendix Table 1).

We assessed the effects of these measures on $R_0$ through the social contact matrices obtained before and during lockdown, as used in other studies (*13*,*14*). For respiratory-spread infectious agents, $R_0$ is a function of the age-specific number of daily contacts, the probability that a single contact leads to transmission, and the total duration of infectiousness; thus, $R_0$ is proportional to the dominant eigenvalue of the social contact matrix (*15*). If the other 2 parameters did not change before and during social distancing measures, the relative reduction, $\delta$, in $R_0$ is equivalent to the reduction in the dominant eigenvalue of the contact matrices obtained for the 2 periods (Appendix) (*14*,*16*). To account for a lower susceptibility for children than for adults, we introduced an age-dependent proportionality factor, $s_i$, measuring susceptibility to infection of persons in age group $i$, as in other studies (*13*,*17*). We performed the analysis using a conservative estimate for $s_i$, and considered the susceptibility among persons 0–17 years of age to be 0.34 compared with persons ≥18 years of age (Appendix Table 2) (*13*).

We estimated the relative reduction in $R_0$ in 2 periods: the period of initial measures until the day before lockdown (March 11–22), which included closure of schools, entertainment venues, and shops (reduction $\delta_1$); and the period of lockdown (March 23–April 26) (reduction $\delta_2$). Because we did not assess social contacts during the period of initial measures, we created a synthetic contact matrix by assuming no school contacts because of school closures, and a reduction in leisure and work contacts (*18*–*20*) (Appendix). To assess uncertainty, we performed a nonparametric bootstrap on contact data by participant to estimate the mean and 95% credible interval (95% CrI) of $\delta_1$ and $\delta_2$ (n = 1,000 bootstrap samples).

### Simulating the Epidemic in Greece

We used a SEIR model to simulate the outbreak from the beginning of local transmission until April 26, 2020, the day before the originally planned date to ease lockdown measures. Susceptible persons (S) become infected at a rate $\beta$ and move to the exposed state (E) as infected but not infectious. Exposed persons become infectious at a rate $\sigma$, and a proportion $p$ will eventually develop symptoms ($p$ = 80%) (*21*). To account for asymptomatic transmission during the incubation period, we introduce a compartment for infectious presymptomatic persons ($I_{pre}$). $I_{pre}$ cases become symptomatic infectious ($I_{symp}$) cases at a rate of $\sigma_s$. We assumed that infectiousness can occur 1.5 days before the onset of symptoms (*22*–*24*). The remainder ($1 - p$) will be true asymptomatic or subclinical cases ($I_{asymp}$). We assumed that the infectiousness of subclinical cases relative to symptomatic cases was $q$ = 50% (*24*). Symptomatic cases recover (R) at a rate of $\gamma_s$, and asymptomatic cases recover (R) at a rate of $\gamma_{asymp}$ (Table 1; Figure 2; Appendix).

We derived the transmission rate $\beta$ from $R_0$ and parameters related to the duration of infectiousness (Appendix). We incorporated uncertainty in $R_0$ by drawing values uniformly from the estimated 95% CI (2.01–2.80). We modeled the effect of measures by multiplying $\beta$ by the parameters $\delta_1$ and $\delta_2$; in which $\delta_1$ corresponds to the reduction of $R_0$ in the period of initial social distancing measures, where $\delta_1$ was drawn from a normal distribution with a mean of 42.7% (SD 1.7%); and $\delta_2$ corresponds to the reduction of $R_0$ during lockdown, for which $\delta_2$ was drawn from a normal distribution of 81.0% (SD 1.6%) estimated from the bootstrap on the contact data. To account for the uncertainty in $R_0$, $\delta_1$, and $\delta_2$, we performed 1,000 simulations of the model and obtained median estimates and 95% CrIs.

We obtained the infection fatality ratio (IFR) and the cumulative proportion of critically ill patients by dividing the reported number of deaths and of

**Table 1.** Parameters of the susceptible-exposed-infectious-recovered model used to assess effects of social distancing measures during the first epidemic wave of coronavirus disease, Greece

| Epidemiologic parameters | Value | Comments and references |
| --- | --- | --- |
| $R_0$ (95% CI) | 2.38 (2.01–2.80) | Estimated from data on the number of confirmed cases in Greece by accounting for imported cases and assuming gamma distributed serial interval with mean 6.67 days (SD 4.88 days) (D. Cereda et al., unpub. data, https://arxiv.org/abs/2003.09320) and aligned with other studies (*10*,*11*) |
| Latent period ($1/\sigma$) | 3.5 days | Based on an average incubation time of ≈5 days (*8*,*9*) and assuming that infectiousness starts 1.5 days prior to the symptom onset (*22*–*24*) |
| Percentage (*p*) infected cases developing symptoms | 80 | From K. Mizumoto et al. (*21*), the estimated proportion of true asymptomatic cases was 20.6% assuming a mean incubation period of 5.5 days |
| Symptomatic cases | | |
| Length of infectiousness before symptoms, d ($1/\sigma_s$) | 1.5 | (*22*–*24*) |
| Duration of infectious period from development of symptoms to recovery, d ($1/\gamma_s$) | 4.5 | To obtain a serial interval of ≈6 days (*8*,*9*) |
| True asymptomatic cases | | |
| Infectiousness (*q*) of asymptomatic vs. symptomatic persons, % | 50 | (*24*) |
| Duration of infectious period until recovery ($1/\gamma_{asymp}$) | 6 days | The same duration of infectiousness as for symptomatic cases = $1/\sigma_s + 1/\gamma_s$ |

critically ill patients (*25*) by the total number of cases predicted by the model. We used a lag of 18 days for deaths and 14 days for critically ill patients based on unpublished data on hospitalized patients from the National Public Health Organization in Greece. To validate our findings, we used a reverse approach; we applied a published estimate of the IFR (*26*) to the number of infections predicted by the model and compared the resulting cumulative and daily number of deaths to the observed deaths (Appendix Table 3).

### Effects of Social Distancing Interventions

Because multiple social distancing measures were implemented simultaneously, to delineate the effects of each measure on $R_0$, we used information from the

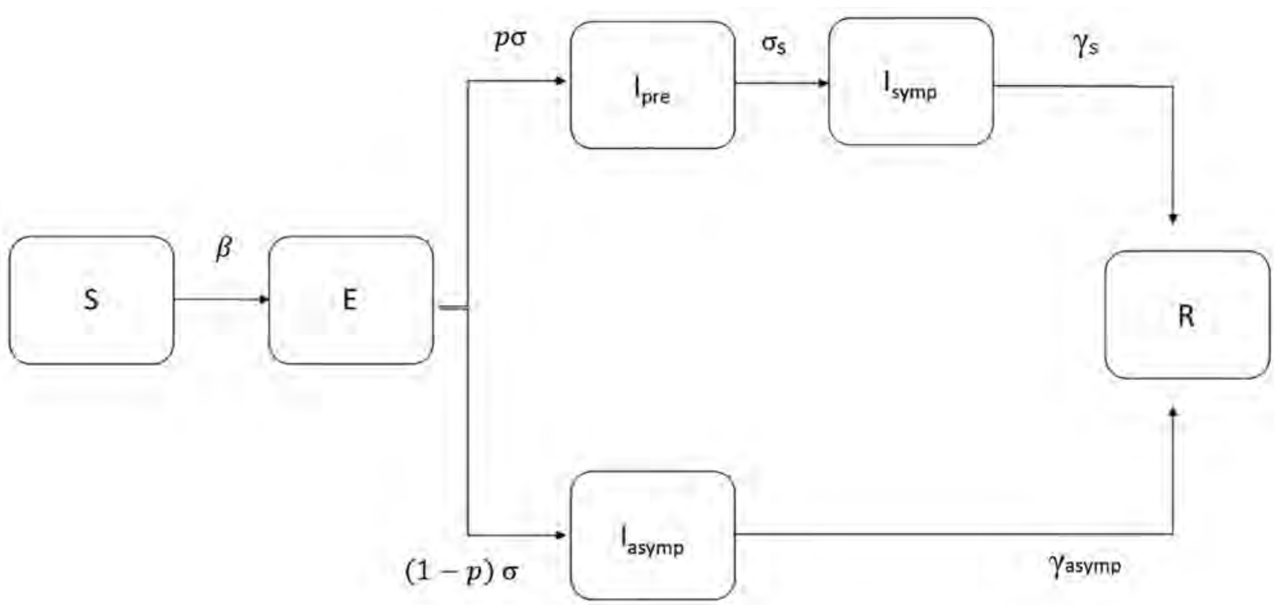


**Figure 2.** Modified susceptible-exposed-infectious-recovered (SEIR) model used to estimate the course of the first epidemic wave of coronavirus disease, Greece. Cases are classified into susceptible (S), exposed (E), infectious (I, which is divided into 3 conditions: $I_{pre}$, before developing symptoms, $I_{symp}$ for clinically ill, or $I_{asymp}$ for true asymptomatic), and recovered (R). We assumed that a proportion (*p*) of exposed cases will develop symptoms and that infectiousness can occur before the onset of symptoms. β is the rate at which persons become infected and move to E; exposed individuals become infectious at a rate σ and presymptomatic infectious cases develop symptoms at a rate $\sigma_s$; $\gamma_{asymp}$ is the rate of recovery for asymptomatic persons; $\gamma_s$ is the rate of recovery for symptomatic persons.

contacts reported on a regular weekday in January 2020 and mimicked the impact of each intervention by excluding or reducing subsets of corresponding social contacts (*16*,*17*,*19*,*20*) (Appendix). We also assessed scenarios with less disruptive social distancing measures (Appendix). In addition, we evaluated the increase in effective reproduction number ($R_t$) for varying levels of infection control measures (hand hygiene, use of facemasks, and maintaining distance ≥1.5 m) when social distancing measures are partially lifted after lockdown (Appendix).

## Results

### Social Contacts before and during Lockdown

In total, 602 persons provided contact diaries and reported 12,463 contacts before the pandemic and 1,743 during lockdown (Table 2). The mean daily number of contacts declined from 20.7 before to 2.9 during lockdown; when adjusted for the age distribution of the population, the reduction was 19.9 before and 2.6 during lockdown (86.9%).

We noted a change in age-mixing patterns in the contact matrices (Figure 3, panel A). In the prepandemic period, the diagonal of the contact matrix depicts the assortativity by age; participants tended to associate more with people of similar age (Figure 3, panel A). When social distancing measures were put into effect, the assortativity by age disappeared and contacts occurred mainly between household members (Figure 3, panels B–D).

### $R_0$ and Effects of Social Distancing Measures

Before lockdown, the estimated $R_0$ was 2.38 (95% CI 2.01–2.80). During the first period of social distancing measures, in which schools, entertainment venues, and shops were closed, $R_0$ was estimated to decrease by 42.7% (95% CrI 34.9%–51.3%); under lockdown, $R_0$ decreased by 81.0% (95% CrI 71.7%–86.1%). Thus, the cumulative measures implemented during lockdown would have reduced $R_0$ to <1.0 even if the initial $R_0$ had been as high as 5.3 (95% CrI 3.5–7.2). Estimated $R_t$ was 1.13 (95% CrI 1.38–1.61) during the period of the initial measures but was 0.46 (95% CrI 0.35–0.57) during lockdown (Figure 4, panel A).

### Contribution of Each Social Distancing Measure

We assessed the effect of each measure separately and in combinations (Figure 5). During lockdown, the estimated reduction in $R_0$ attributed to each measure was 10.3% (95% CrI 5.2%–20.3%) for the decline in work contacts, 18.5% (95% CrI 10.7%–26.3%) for school closures, and 24.1% (95% CrI 14.8%–34.3%) for the decline in leisure activity contacts. Thus, each measure separately would have reduced $R_0$ to <1.0 if the initial $R_0$ had been as high as 1.11 for the decline in work contacts, 1.23 for school closures, and 1.32 for the decline in leisure activity contacts. A combination of measures could be effective if the initial $R_0$ had been as high as 1.78 for interventions reducing work and school contacts, 1.72 for reducing work and leisure contacts, and 1.43 for reducing school and leisure contacts.

We assessed alternative scenarios with less disruptive social distancing measures. A 50% reduction in school contacts, such as smaller class sizes; 20% in work contacts, such as teleworking for part of the population or rotating weekly schedules in which employees telework some days and work onsite other days; and 20% in leisure activities could reduce $R_0$ to <1.0 for initial levels as high as 1.32 (95% CrI 1.27–1.38). An even larger decline in leisure activities (50%) could successfully reduce an initial $R_0$ as high as 1.48 (95% CrI 1.35–1.62).

Finally, we assessed the increase in $R_t$ when measures were partially lifted after lockdown. To mimic the measures implemented after lockdown in Greece, we assumed that contacts at work would return to

**Table 2.** Number of contacts on a weekday during lockdown, March 31–April 7, 2020, and on the corresponding day in January 2020 before the coronavirus disease epidemic in Athens, Greece

| | Mid-January 2020 | | | During lockdown | | |
|---|---|---|---|---|---|---|
| Covariate | Participants, no. (%) | No. (%) | Mean (95% CI) | No. (%) | Mean (95% CI) | Reduction of reported contacts, % |
| Overall | 602 (100.0) | 12,463 (100.0) | 20.7 (18.9–22.5) | 1,743 (100.0) | 2.9 (2.6–3.2) | 86.0* |
| Sex | | | | | | |
| M | 295 (49.0) | 6,218 (49.9) | 21.1 (18.3–23.9) | 934 (53.6) | 3.2 (2.7–3.6) | 85.0 |
| F | 307 (51.0) | 6,245 (50.1) | 20.3 (18.0–22.7) | 809 (46.4) | 2.6 (2.2–3.1) | 87.1 |
| Age, y | | | | | | |
| 0–4 | 20 (3.3) | 386 (3.1) | 19.3 (12.8–25.8) | 53 (3.0) | 2.7 (2.2–3.1) | 86.3 |
| 5–11 | 58 (9.6) | 2,020 (16.2) | 34.8 (29.1–40.6) | 168 (9.6) | 2.9 (2.6–3.2) | 91.7 |
| 12–17 | 83 (13.8) | 2,758 (22.1) | 33.2 (28.4–38.1) | 275 (15.8) | 3.3 (2.3–4.3) | 90.0 |
| 18–29 | 74 (12.3) | 1,316 (10.6) | 17.8 (14.4–21.1) | 361 (20.7) | 4.9 (3.1–6.7) | 72.6 |
| 30–64 | 209 (34.7) | 4,852 (38.9) | 23.2 (19.5–26.9) | 529 (30.4) | 2.5 (2.2–2.9) | 89.1 |
| ≥65 | 158 (26.3) | 1,131 (9.1) | 7.2 (5.4–8.9) | 357 (20.5) | 2.3 (1.8–2.7) | 68.4 |

*The reduction in the reported contacts becomes 86.9% after adjusting for the age distribution of the population of Greece.

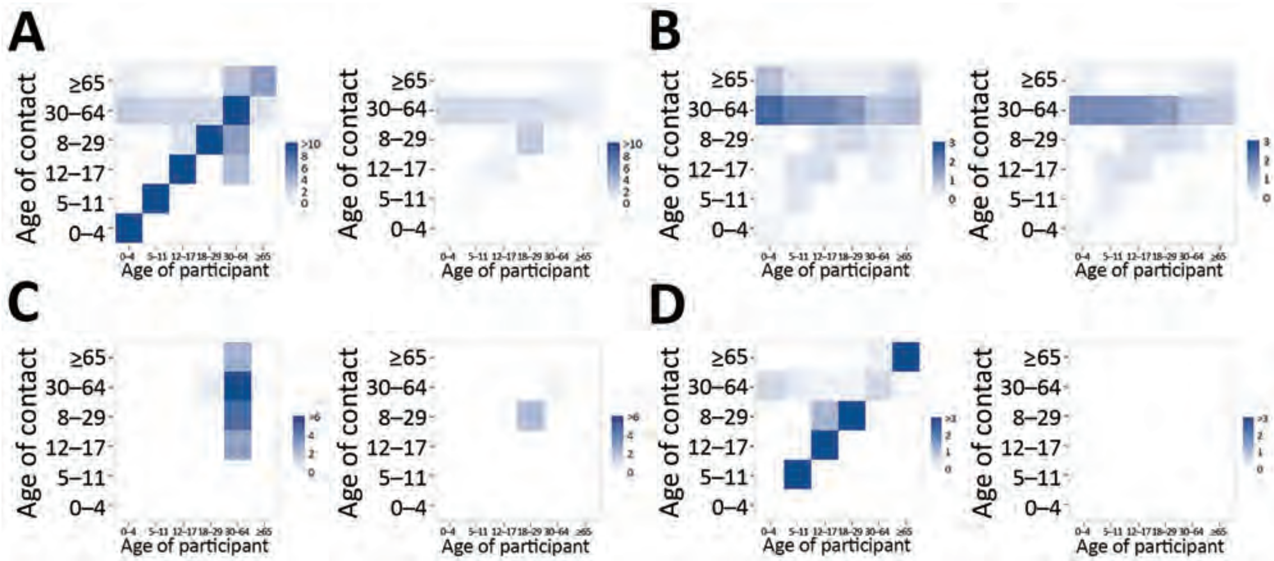

**Figure 3.** Side-by-side comparisons of age-specific contact matrices in Greece before the coronavirus disease pandemic (January 2020; left) and during lockdown (April 2020; right). A) All contacts; B) contacts at home; C) contacts at work; and D) contacts during leisure activities. Each cell represents the average daily number of reported contacts, stratified by the age group of the participants and their corresponding contacts. In panel A, the diagonal of the contact matrix corresponds to contacts between persons in the same age group, the bottom left corner of the matrix corresponds to contacts between school-age children, and the central part corresponds to contacts mainly in the work environment.

levels 50% lower than pre-pandemic, school to 50%, and leisure to 60%. For instance, class sizes were reduced 50% when schools reopened in May. Under this scenario, $R_t$ would remain <1.0 assuming ≥20% reduction in susceptibility as a result of infection control measures, including hand hygiene, use of face masks, and maintaining physical distances ≥1.5 meters (Figure 6). Under milder social distancing measures, infection control policies would need to be much more effective (Appendix Figure 2).

**Model Predictions on the Epidemic during February 15–April 26**

By April 26, 2020, Greece had 2,517 diagnosed COVID-19 cases, 23.0% of which were imported, and 134 deaths (Figure 1) (*25*). The corresponding naive case-fatality ratio (CFR) was 5.3%. Based on our SEIR model, the cumulative number of infections during February 15–April 26 would be 13,189 (95% CrI 6,206–27,700) (Figure 4, panel B), which corresponds to an attack rate (AR) of 0.12% (95% CrI

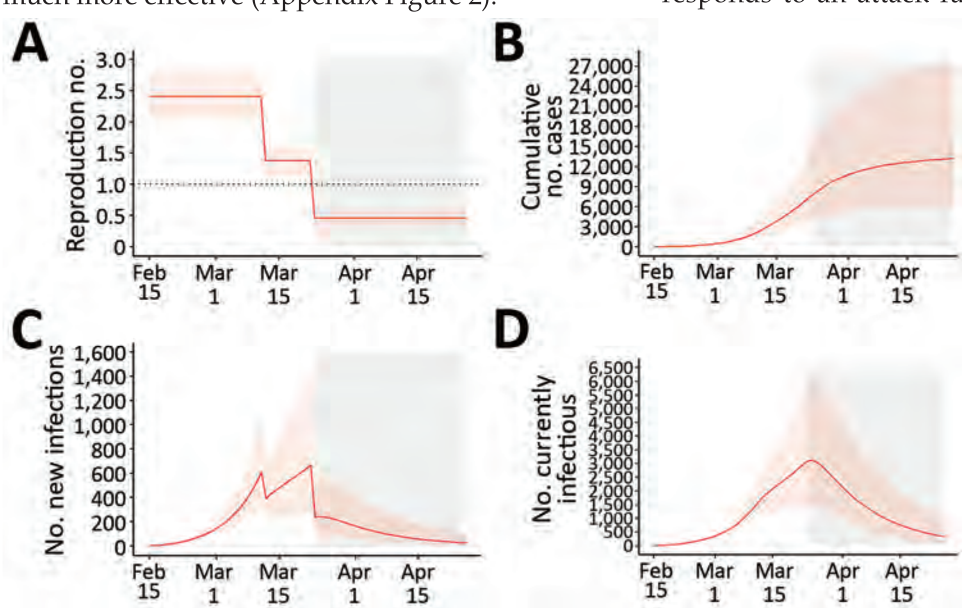

**Figure 4.** The first wave of the coronavirus disease epidemic in Greece (February 15–April 26, 2020), estimated from 1,000 susceptible-exposed-infectious-recovered (SEIR) model simulations. A) Effective reproduction number; B) cumulative number of cases; C) new infections; and D) number of infectious persons by date. Orange lines represent the median estimates, and the light orange shaded areas indicate 95% credible intervals. Gray areas indicate the period of restrictions of all nonessential movement in the country (i.e., lockdown).

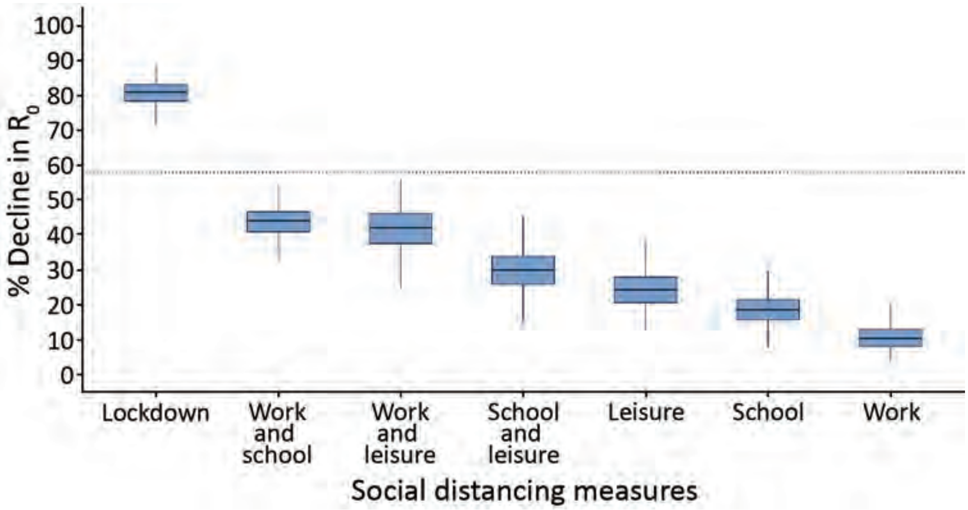


**Figure 5.** The percenage decline of $R_0$ associated with multiple social distancing measures during coronavirus disease lockdown in Greece and the relative contribution of each measure or combination of measures implemented. Boxplots demonstrate distribution of the estimated percent decline from nonparametric bootstrap on the social contacts data based on 1,000 bootstrap samples. $R_0$ reduction during lockdown was obtained by comparing social contacts data collected for April 2020 versus January 2020. The other estimates were derived by using the information from contact diaries in January 2020 corresponding to a regular school or work day and excluding or reducing subsets of social contacts at school, work, home, and leisure activities, based on observations during lockdown. Because contact with a particular person can take place in multiple settings, we assigned contacts at multiple locations to a single location by using the following hierarchical order: home, work, school, leisure activities, transportation, and other locations. Dotted line indicates the minimum reduction needed to bring $R_0$ from 2.38 to <1. Box top and bottom lines indicate 25th and 75th percentiles; horizontal lines within boxes indicate medians; whiskers indicate 25th/75th percentile plus 1.5 times the interquartile range. $R_0$, basic reproduction number.

0.06%–0.26%). The estimated case ascertainment rate was 19.1% (95% CrI 9.1%–40.6%). By the end of April, 25 (95% CrI 6–97) new infections per day and 329 (95% CrI 97–1,027) total infectious cases were estimated (Figure 4, panels C, D).

On the basis of the number of deaths and critically ill patients reported in Greece by April 26, and using the number of infections obtained from the model as denominator, we estimated the IFR to be 1.12% (95% CrI 0.55%–2.31%) and the cumulative proportion of critically ill patients to be 1.55% (95% CrI 0.75%–3.22%). As a validation, we estimated the number of deaths by applying a published age-adjusted estimated IFR to the number of infections predicted by the model (Appendix Table 3). The predicted number of deaths was 137 (95% CrI 66–279) compared with the reported number of 134 deaths (Appendix Figure 3). As a sensitivity analysis, we simulated the epidemic and calculated IFR and AR assuming a shorter mean serial interval of 4.7 days. We obtained similar results for the AR and the IFR as when the serial interval was 6.67 days (Appendix Figure 4).

## Discussion

Greece and other countries managed to successfully slow the first wave of the SARS-CoV-2 epidemic early in 2020. Assessing the burden of infection and death in the population and quantifying the effects of social distancing was necessary because the stringent measures taken had major economic costs and restricted individual freedom. In addition, several countries, including Greece, began seeing COVID-19 cases increase after resuming economic activities and travel, indicating the need to reimplement some types of location-specific physical distancing measures.

We assessed the effects of social distancing by using a social contacts survey to directly measure participants' contact patterns during lockdown in a sample including children. To our knowledge, only 2 other diary-based social contacts surveys have been implemented during COVID-19 lockdown, 1 in China (*13*) and 1 in the United Kingdom (*14*); only the study from China included children. Our study had common findings with the other 2: a large reduction in the number of contacts, 86.9% in Greece, 86.4%–90.3% in China, and 73.1% in United Kingdom; and assortativity by age (i.e., contacts between people of the same age group) disappeared during lockdown and contacts were mainly among household members. Other studies have assessed the impact of social distancing indirectly by using contact data from prepandemic periods and assuming that interventions reduce social mixing in different contexts (*18*,*20*,*27*).

We estimated that $R_0$ declined by 81% and reached 0.46 during lockdown. This finding agrees with findings from a study pooling information from 11 countries in Europe, which also reported an 81% reduction in $R_0$ (*28*) and with estimates from China (*3*,*29*), the United Kingdom (76.2%; *14*), and France (77%; *30*). In our analysis, we assumed lower susceptibility among children because of support from a growing body of evidence (*13*,*17*,*31*–*33*; K. Mizumoto et al., unpub. data, https://doi.org/10.1101/2020.03.09.20033142).

We further attempted to delineate the effects of each measure. For example, many countries, including Greece, instituted large-scale or national school closures (*34*). We estimated that each measure alone could reduce an $R_0$ of ≈1.1–1.3 to <1.0. Only multiple social distancing measures would be effective for reducing an $R_0$ at the initial level (2.38) observed in Greece. The finding concerning an 18.5% reduction in $R_0$ related to school closures agrees with recent studies suggesting that this measure likely is much less effective for COVID-19 than for influenza-like infections (*17*,*28*). Concerning the course of the epidemic after lockdown, moderately relaxing social distancing could be safe if ongoing infection control strategies are adopted; milder social distancing measures would demand stricter infection control policies.

By May 18, 2020, Greece had one of the lowest reported COVID-19 death rates in Europe, 15.2 deaths/1 million population (*35*) (Appendix Table 4). Our IFR estimate of 1.12% was similar to that anticipated for the population of Greece based on a published estimate adjusting for demography (*26*). In addition, the estimated AR of 0.12% (95% CrI 0.06%–0.26%) was one of the lowest in Europe (*28*,*36*). Other researchers have applied back calculation of infections from reported deaths (*28*), and the resulting infection AR was almost identical (0.13%) (*36*). Our estimate is further confirmed by a serosurvey in residual serum samples that identified 0.25% (95% CI 0.02%–0.50%) seroprevalence in Greece in April 2020 (*37*). The number of infectious cases subsided considerably towards the end of April; however, even during this period with low transmission levels, 2 local outbreaks were identified, 1 in a refugee camp and 1 in a private healthcare unit, thus increasing the number of diagnosed cases in the respective days (Figure 1). An increasing number of reports around the world suggest the significance of superspreading events (*38*–*41*), and caution should be exercised to prevent or recognize these events early.

The first limitation of our study was that, due to the absence of prepandemic data on social contacts, we asked respondents to report their contacts ≈2 months prior to the survey to ensure reports were not affected by increased awareness of the pandemic. Recall bias might be observed, although to what direction is not clear. A general limitation in contact diaries is that participants record a fraction of their contacts (*42*). However, biases in participant recall are difficult to quantify, especially for those with many contacts in different settings. For example, short-lived contacts and work contacts are more likely to be underreported (*42*). Thus, recall bias could be different among children and adults and in various settings. In addition, underreporting might have occurred before and during lockdown because of many social contacts before the pandemic or because participants were afraid to disclose contacts during lockdown. Second, the survey was conducted in a sample from the Athens metropolitan area and not from the whole country. However, no consistent relationship has been found between social contacts and urbanization (*43*). In addition, most (79%) of the population of Greece lives in urban areas, and Athens accounts for 35% of the population. Furthermore, the observed reduction of social contacts during lockdown was similar to other surveys (*13*,*14*). Third, estimated $R_0$ depends on the serial interval. Because no data from a local study of

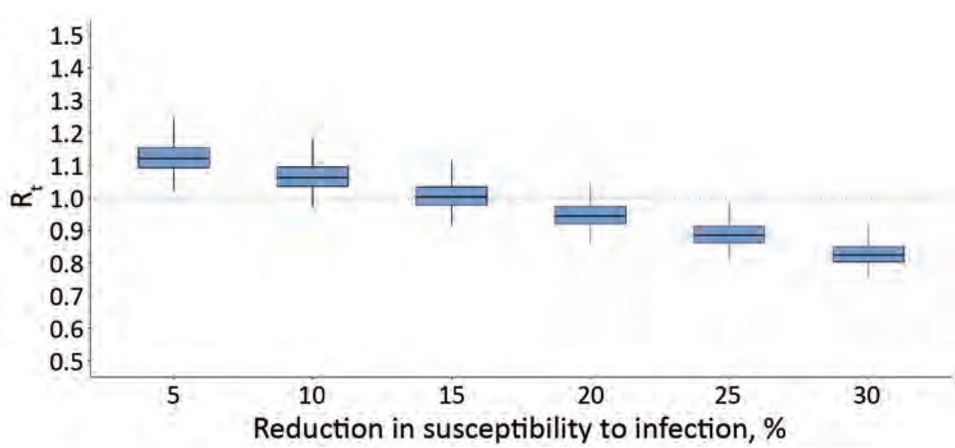


**Figure 6.** Estimated $R_t$ after the partial lifting of social distancing measures at the end of the first coronavirus disease epidemic wave in Greece for varying effectiveness levels of infection control measures, such as hand hygiene, use of masks, maintaining social distances, in reducing susceptibility to infection. $R_t$ during lockdown was 0.46. For the partial lifting of measures, we hypothesized a scenario in which contacts at work and school contacts will return to 50% lower than pre-epidemic levels and leisure activities will return to 60% lower than pre-epidemic levels. Dotted line indicates the threshold of $R_t$ = 1. Boxplots of the distribution of the estimated Rt from nonparametric bootstrap on the social contacts data based on 1,000 bootstrap samples. Box top and bottom lines indicate 25th and 75th percentiles; horizontal lines within boxes indicate medians; whiskers indicate 25th/75th percentile plus 1.5 times the interquartile range. $R_t$, effective reproduction number.

infector–infectee pairs were available, the distribution of the serial interval was based on previous estimates (*10*,*11*; D. Cereda et al., unpub. data, https://arxiv.org/abs/2003.09320). The estimated $R_0$ aligned with estimates obtained in China (*44*) and Italy (*45*), and we accounted for the uncertainty in this value. We also repeated the analysis assuming a shorter serial interval (*12*), which resulted in a lower reproduction number. Fourth, in assessing the effect of each social distancing measure separately, we should note that an interrelation exists between the different measures and our approach might be an approximation. For example, school closure alone might result in increases in leisure contacts or decline in work contacts because parents need to be home with younger children. Fifth, as elsewhere, we assumed that changes in social contacts occur as soon as interventions take place, rather than gradually during lockdown dates (*28*), which could be valid for some interventions, such as school closure, but not for others. Finally, we did not consider case-based interventions that might have affected contacts, such as isolation of confirmed cases and quarantine of close contacts. In Greece, narrow testing criteria were applied beginning March 16 and elderly or severely ill persons, other high-risk groups, and healthcare personnel were tested but others were not; also, the testing capacity during March and April was low.

Overall, the social distancing measures Greece put in place in early March 2020 had a substantial impact on contact patterns and reduced $R_0$ to <1.0. By the end of April, the spread of COVID-19 was contained in Greece, and the country had one of the lowest ARs in Europe after the first pandemic wave. However, as social distancing and travel restrictions are relaxed, close monitoring of $R_t$ is essential in order to adapt interventions over time without having to resort to stringent measures. Measuring social mixing patterns and adherence to infection control measures through repeated surveys can be additional tools for real-time monitoring of the epidemic potential in the months to come.

This article was preprinted at https://doi.org/10.1101/2020.05.27.20114017.

### Acknowledgments

We thank the personnel of the National Public Health Organization for performing the epidemiological surveillance of SARS-CoV-2 in Greece.

The social contacts survey was funded by the Hellenic Scientific Society for the Study of AIDS and Sexually Transmitted Diseases, Athens.

### About the Author

Dr. Sypsa is an associate professor of epidemiology and medical statistics in the Medical School of the National and Kapodistrian University of Athens in Greece. Her research interests include the epidemiology and mathematical modeling of hepatitis C, HIV, influenza, and other infectious diseases, as well as infectious diseases among prisoners and persons who inject drugs.

### References

1. Wu F, Zhao S, Yu B, Chen YM, Wang W, Song ZG, et al. A new coronavirus associated with human respiratory disease in China. Nature. 2020;579:265–9. https://doi.org/10.1038/s41586-020-2008-3
2. World Health Organization. Weekly epidemiological update: coronavirus disease 2019 (COVID-19), 14 September 2020 [cited 2020 Sep 18]. https://www.who.int/docs/default-source/coronaviruse/situation-reports/20200914-weekly-epi-update-5.pdf
3. Leung K, Wu JT, Liu D, Leung GM. First-wave COVID-19 transmissibility and severity in China outside Hubei after control measures, and second-wave scenario planning: a modelling impact assessment. Lancet. 2020;395:1382–93. https://doi.org/10.1016/S0140-6736(20)30746-7
4. National Public Health Organisation. Epidemiological surveillance of COVID-19—daily report 26 March 2020 [in Greek] [cited 2020 Jul 10]. https://eody.gov.gr/wp-content/uploads/2020/03/covid-gr-daily-report-20200320.pdf
5. Perrigo B, Hincks J. Greece has an elderly population and a fragile economy. How has it escaped the worst of the coronavirus so far? Time. 2020 Apr 21 [cited 2020 Jul 10]. https://time.com/5824836/greece-coronavirus
6. Mossong J, Hens N, Jit M, Beutels P, Auranen K, Mikolajczyk R, et al. Social contacts and mixing patterns relevant to the spread of infectious diseases. PLoS Med. 2008;5:e74. https://doi.org/10.1371/journal.pmed.0050074
7 White LF, Wallinga J, Finelli L, Reed C, Riley S, Lipsitch M, et al. Estimation of the reproductive number and the serial interval in early phase of the 2009 influenza A/H1N1 pandemic in the USA. Influenza Other Respir Viruses. 2009;3:267–76. https://doi.org/10.1111/j.1750-2659.2009.00106.x
8. Li Q, Guan X, Wu P, Wang X, Zhou L, Tong Y, et al. Early transmission dynamics in Wuhan, China, of novel coronavirus-infected pneumonia. N Engl J Med. 2020;382:1199–207. https://doi.org/10.1056/NEJMoa2001316
9. Lauer SA, Grantz KH, Bi Q, Jones FK, Zheng Q, Meredith HR, et al. The incubation period of coronavirus disease 2019 (COVID-19) from publicly reported confirmed cases: estimation and application. Ann Intern Med. 2020;172:577–82. https://doi.org/10.7326/M20-0504
10. Bi Q, Wu Y, Mei S, Ye C, Zou X, Zhang Z, et al. Epidemiology and transmission of COVID-19 in 391 cases and 1286 of their close contacts in Shenzhen, China: a retrospective cohort study. Lancet Infect Dis. 2020;20:911–9. https://doi.org/10.1016/S1473-3099(20)30287-5
11. Lavezzo E, Franchin E, Ciavarella C, Cuomo-Dannenburg G, Barzon L, Del Vecchio C, et al.; Imperial College COVID-19 Response Team. Suppression of a SARS-CoV-2 outbreak in the Italian municipality of Vo'. Nature. 2020;584:425–9. https://doi.org/10.1038/s41586-020-2488-1
12. Nishiura H, Linton NM, Akhmetzhanov AR. Serial interval of novel coronavirus (COVID-19) infections. Int J Infect Dis. 2020;93:284–6. https://doi.org/10.1016/j.ijid.2020.02.060

13. Zhang J, Litvinova M, Liang Y, Wang Y, Wang W, Zhao S, et al. Changes in contact patterns shape the dynamics of the COVID-19 outbreak in China. Science. 2020;368:1481–6. https://doi.org/10.1126/science.abb8001
14. Jarvis CI, Van Zandvoort K, Gimma A, Prem K, Klepac P, Rubin GJ, et al.; CMMID COVID-19 working group. Quantifying the impact of physical distance measures on the transmission of COVID-19 in the UK. BMC Med. 2020;18:124. https://doi.org/10.1186/s12916-020-01597-8
15. Wallinga J, Teunis P, Kretzschmar M. Using data on social contacts to estimate age-specific transmission parameters for respiratory-spread infectious agents. Am J Epidemiol. 2006;164:936–44. https://doi.org/10.1093/aje/kwj317
16. Hens N, Ayele GM, Goeyvaerts N, Aerts M, Mossong J, Edmunds JW, et al. Estimating the impact of school closure on social mixing behaviour and the transmission of close contact infections in eight European countries. BMC Infect Dis. 2009;9:187. https://doi.org/10.1186/1471-2334-9-187
17. Davies NG, Klepac P, Liu Y, Prem K, Jit M, Eggo RM; CMMID COVID-19 working group. Age-dependent effects in the transmission and control of COVID-19 epidemics. Nat Med. 2020;26:1205–11. https://doi.org/10.1038/s41591-020-0962-9
18. Davies NG, Kucharski AJ, Eggo RM, Gimma A, Edmunds WJ, Jombart T, et al.; Centre for the Mathematical Modelling of Infectious Diseases COVID-19 working group. Effects of non-pharmaceutical interventions on COVID-19 cases, deaths, and demand for hospital services in the UK: a modelling study. Lancet Public Health. 2020;5:e375–85. https://doi.org/10.1016/S2468-2667(20)30133-X
19. Willem L, Van Hoang T, Funk S, Coletti P, Beutels P, Hens N. SOCRATES: an online tool leveraging a social contact data sharing initiative to assess mitigation strategies for COVID-19. BMC Res Notes. 2020;13:293. https://doi.org/10.1186/s13104-020-05136-9
20. Prem K, Liu Y, Russell TW, Kucharski AJ, Eggo RM, Davies N, et al.; Centre for the Mathematical Modelling of Infectious Diseases COVID-19 Working Group. The effect of control strategies to reduce social mixing on outcomes of the COVID-19 epidemic in Wuhan, China: a modelling study. Lancet Public Health. 2020;5:e261–70. https://doi.org/10.1016/S2468-2667(20)30073-6
21. Mizumoto K, Kagaya K, Zarebski A, Chowell G. Estimating the asymptomatic proportion of coronavirus disease 2019 (COVID-19) cases on board the Diamond Princess cruise ship, Yokohama, Japan, 2020. Euro Surveill. 2020;25:2000180. https://doi.org/10.2807/1560-7917.ES.2020.25.10.2000180
22. He X, Lau EHY, Wu P, Deng X, Wang J, Hao X, et al. Temporal dynamics in viral shedding and transmissibility of COVID-19. Nat Med. 2020;26:672–5. https://doi.org/10.1038/s41591-020-0869-5
23. Ganyani T, Kremer C, Chen D, Torneri A, Faes C, Wallinga J, et al. Estimating the generation interval for coronavirus disease (COVID-19) based on symptom onset data, March 2020. Euro Surveill. 2020;25:2000257. https://doi.org/10.2807/1560-7917.ES.2020.25.17.2000257
24. Li R, Pei S, Chen B, Song Y, Zhang T, Yang W, et al. Substantial undocumented infection facilitates the rapid dissemination of novel coronavirus (SARS-CoV2). Science. 2020;368:489–93. https://doi.org/10.1126/science.abb3221
25. National Public Health Organisation. Epidemiological surveillance of COVID-19—daily report 26 [in Greek]. April 2020 [cited 2020 Jul 10]. https://eody.gov.gr/wp-content/uploads/2020/04/covid-gr-daily-report-20200426.pdf
26. Verity R, Okell LC, Dorigatti I, Winskill P, Whittaker C, Imai N, et al. Estimates of the severity of coronavirus disease 2019: a model-based analysis. Lancet Infect Dis. 2020;20:669–77. https://doi.org/10.1016/S1473-3099(20)30243-7
27. Di Domenico L, Pullano G, Sabbatini CE, Boëlle PY, Colizza V. Impact of lockdown on COVID-19 epidemic in Île-de-France and possible exit strategies. BMC Med. 2020;18:240. https://doi.org/10.1186/s12916-020-01698-4
28. Flaxman S, Mishra S, Gandy A, Unwin HJT, Mellan TA, Coupland H, et al.; Imperial College COVID-19 Response Team. Estimating the effects of non-pharmaceutical interventions on COVID-19 in Europe. Nature. 2020;584:257–61. https://doi.org/10.1038/s41586-020-2405-7
29. Pan A, Liu L, Wang C, Guo H, Hao X, Wang Q, et al. Association of public health interventions with the epidemiology of the COVID-19 outbreak in Wuhan, China. JAMA. 2020;323:1915–23. https://doi.org/10.1001/jama.2020.6130
30. Salje H, Tran Kiem C, Lefrancq N, Courtejoie N, Bosetti P, Paireau J, et al. Estimating the burden of SARS-CoV-2 in France. Science. 2020;369:208–11. https://doi.org/10.1126/science.abc3517
31. Jing QL, Liu MJ, Zhang ZB, Fang LQ, Yuan J, Zhang AR, et al. Household secondary attack rate of COVID-19 and associated determinants in Guangzhou, China: a retrospective cohort study. Lancet Infect Dis. 2020;20:1141–50. https://doi.org/10.1016/S1473-3099(20)30471-0
32. Li W, Zhang B, Lu J, Liu S, Chang Z, Peng C, et al. The characteristics of household transmission of COVID-19. Clin Infect Dis. 2020;71:1943–6. https://doi.org/10.1093/cid/ciaa450
33. Danis K, Epaulard O, Bénet T, Gaymard A, Campoy S, Botelho-Nevers E, et al.; Investigation Team. Cluster of coronavirus disease 2019 (Covid-19) in the French Alps, February 2020. Clin Infect Dis. 2020;71:825–32. https://doi.org/10.1093/cid/ciaa424
34. Viner RM, Russell SJ, Croker H, Packer J, Ward J, Stansfield C, et al. School closure and management practices during coronavirus outbreaks including COVID-19: a rapid systematic review. Lancet Child Adolesc Health. 2020;4:397–404. https://doi.org/10.1016/S2352-4642(20)30095-X
35. European Centre for Disease Prevention and Control. Daily number of new reported cases of COVID-19 by country worldwide. 2020 May 20 [cited 2020 May 20]. https://www.ecdc.europa.eu/en/publications-data/download-todays-data-geographic-distribution-covid-19-cases-worldwide
36. Imperial College London. COVID-19 model, estimates as of 4th of May 2020; Greece [cited 2020 Apr 25]. https://mrc-ide.github.io/covid19estimates/#/details/Greece
37. Bogogiannidou Z, Vontas A, Dadouli K, Kyritsi MA, Soteriades S, Nikoulis DJ, et al. Repeated leftover serosurvey of SARS-CoV-2 IgG antibodies, Greece, March and April 2020. Euro Surveill. 2020;25. https://doi.org/10.2807/1560-7917.ES.2020.25.31.2001369
38. Arons MM, Hatfield KM, Reddy SC, Kimball A, James A, Jacobs JR, et al.; Public Health–Seattle and King County and CDC COVID-19 Investigation Team. Presymptomatic SARS-CoV-2 infections and transmission in a skilled nursing facility. N Engl J Med. 2020;382:2081–90. https://doi.org/10.1056/NEJMoa2008457
39. Kimball A, Hatfield KM, Arons M, James A, Taylor J, Spicer K, et al.; Public Health–Seattle & King County; CDC COVID-19 Investigation Team. Asymptomatic and presymptomatic SARS-CoV-2 infections in residents of a long-term care skilled nursing facility—King County, Washington, March 2020. MMWR Morb Mortal Wkly Rep. 2020;69:377–81. https://doi.org/10.15585/mmwr.mm6913e1

40. Park SY, Kim Y-M, Yi S, Lee S, Na B-J, Kim CB, et al. Coronavirus disease outbreak in call center, South Korea. Emerg Infect Dis. 2020;26:1666–70. https://doi.org/10.3201/eid2608.201274
41. McMichael TM, Currie DW, Clark S, Pogosjans S, Kay M, Schwartz NG, et al.; Public Health–Seattle and King County, EvergreenHealth, and CDC COVID-19 Investigation Team. Epidemiology of Covid-19 in a long-term care facility in King County, Washington. N Engl J Med. 2020;382:2005–11. https://doi.org/10.1056/NEJMoa2005412
42. Read JM, Edmunds WJ, Riley S, Lessler J, Cummings DA. Close encounters of the infectious kind: methods to measure social mixing behaviour. Epidemiol Infect. 2012;140:2117–30. https://doi.org/10.1017/S0950268812000842
43. Hoang T, Coletti P, Melegaro A, Wallinga J, Grijalva CG, Edmunds JW, et al. A systematic review of social contact surveys to inform transmission models of close-contact infections. Epidemiology. 2019;30:723–36. https://doi.org/10.1097/EDE.0000000000001047
44. Kucharski AJ, Russell TW, Diamond C, Liu Y, Edmunds J, Funk S, et al.; Centre for Mathematical Modelling of Infectious Diseases COVID-19 working group. Early dynamics of transmission and control of COVID-19: a mathematical modelling study. Lancet Infect Dis. 2020;20:553–8. https://doi.org/10.1016/S1473-3099(20)30144-4
45. Giordano G, Blanchini F, Bruno R, Colaneri P, Di Filippo A, Di Matteo A, et al. Modelling the COVID-19 epidemic and implementation of population-wide interventions in Italy. Nat Med. 2020;26:855–60. https://doi.org/10.1038/s41591-020-0883-7

Address for correspondence: Vana Sypsa, Medical School, Department of Hygiene, Epidemiology and Medical Statistics, Building No. 12, M. Asias 75, Athens 11527, Greece; email: vsipsa@med.uoa.gr

# Role of *Burkholderia pseudomallei*–Specific IgG2 in Adults with Acute Melioidosis, Thailand

Panjaporn Chaichana, Kemajittra Jenjaroen, Suchintana Chumseng, Manutsanun Sumonwiriya, Patpong Rongkard, Barbara Kronsteiner, Prapit Teparrukkul, Direk Limmathurotsakul, Nicholas P.J. Day, Narisara Chantratita, Susanna J Dunachie

Melioidosis is a life-threatening infectious disease caused by the gram-negative bacillus *Burkholderia pseudomallei*. An effective vaccine is needed, but data on protective immune responses in human melioidosis are lacking. We used ELISA and an antibody-dependent cellular phagocytosis assay to identify the major features of protective antibodies in patients with acute melioidosis in Thailand. We found that high levels of *B. pseudomallei*–specific IgG2 are associated with protection against death in a multivariable logistic regression analysis adjusting for age, diabetes, renal disease, and neutrophil count. Serum from melioidosis survivors enhanced bacteria uptake into human monocytes expressing FcγRIIa-H/R131, an intermediate-affinity IgG2-receptor, compared with serum from nonsurvivors. We did not find this enhancement when using monocytes carrying the low IgG2–affinity FcγRIIa-R131 allele. The findings indicate the importance of IgG2 in protection against death in human melioidosis, a crucial finding for antibody-based therapeutics and vaccine development.

Melioidosis is a major cause of fatal community-acquired septicemia in highly endemic areas, including northeast Thailand and north Australia (*1*,*2*). Melioidosis is now known to be endemic in ≥45 countries across tropical regions (*3*). A formal modeling framework predicted the global burden to be 165,000 human melioidosis cases per year, with a case-fatality rate of 54%. The causative agent of melioidosis, the highly pathogenic gram-negative bacillus *Burkholderia pseudomallei*, is classified as a Tier 1 Select Agent by the US Centers for Disease Control and Prevention (https://www.cdc.gov/selectagent/index.html). *B. pseudomallei* intrinsically is resistant to first-line commonly available antimicrobial drugs, making a prophylactic vaccine the most desirable approach for disease control.

Author affiliations: Mahidol-Oxford Tropical Medicine Research Unit, Bangkok, Thailand (P. Chaichana, K. Jenjaroen, S. Chumseng, M. Sumonwiriya, P. Rongkard, D. Limmathurotsakul, N.P.J. Day, N. Chantratita, S.J. Dunachie); University of Oxford, Oxford, England (P. Rongkard, B. Kronsteiner, D. Limmathurotsakul, N.P.J. Day, S. Dunachie); Sunpasithiprasong Hospital, Ubon Ratchathani, Thailand (P. Teparrukkul)

DOI: https://doi.org/10.3201/eid2702.200213

Growing evidence supports the effects of cellular adaptive immunity in human defense against *B. pseudomallei* infection (*4*–*6*), but additional evidence also points to the role of protective antibodies against fatal melioidosis. For instance, animal studies have demonstrated that passive transfer of antibodies specific to the bacterial lipopolysaccharide (LPS) or capsular polysaccharide (CPS) can protect mice (*7*–*9*) or a diabetic rat model (*10*) from intranasal or intraperitoneal challenge of *B. pseudomallei* at lethal doses. Intraperitoneal or subcutaneous immunization of mice with *B. pseudomallei* LPS, CPS (*11*), or CPS covalently linked to recombinant CRM197 diphtheria toxin mutant (CPS-CRM197) plus hemolysin coregulated protein 1 (Hcp1) (*12*) provided an optimal protective antibody response. In addition, results from studies of human melioidosis patients demonstrated that elevated levels of anti-oligo polysaccharide (OPS) II (*13*) and anti-LPSII IgG (*14*) were correlated with survival. Previous studies demonstrated that IgG1 and IgG2 are the predominant antibodies in response to the culture filtrate antigen (*15*,*16*). A recent study in a population from the same region showed differences in IgG subclass effects in response to 2 key antigens in *B. pseudomallei*, Hcp1 and OPS (*17*), and IgG3 responses to Hcp1 correlated with melioidosis survival. However, little data on the mechanistic effects of IgG subclasses in human melioidosis are available.

Clarifying the mechanistic role of immunoglobulin-mediated protection against melioidosis would provide crucial information for developing an effective vaccine and therapeutic monoclonal antibodies. We report on the role of *B. pseudomallei*–specific IgG2 subclass and its high binding activating Fc gamma receptor (FcγR) IIa polymorphism H131 in protection against death in human melioidosis during the acute phase.

## Materials and Methods

### Ethics Statement

The study was approved by the ethics committees of the Faculty of Tropical Medicine, Mahidol University (submission no. TMEC 12–014) and Sunpasithiprasong Hospital, Ubon Ratchathani (reference no. 018/2555), and by the Oxford Tropical Research Ethics Committee (reference no. 64–11). We conducted the study according to the principles of the Declaration of Helsinki 2008 (https://www.wma.net) and the International Conference on Harmonization Good Clinical Practice guidelines (https://ichgcp.net). We received written informed consent from all patients enrolled in the study.

### Serum Sample Collection

We enrolled 200 adult inpatients with acute melioidosis ≥18 years of age at Sunpasithiprasong Hospital at a median of 5 days (range 2–13 days; interquartile range [IQR] 3–6 days) after admission, as described previously (*4*,*18*). We recruited healthy controls among donors at the hospital's blood donation clinic. We defined melioidosis as isolation of *B. pseudomallei* from any clinical sample submitted to the laboratory, including blood, sputum, pus, urine, throat or endotracheal swabs, or bronchoalveolar lavage. Among 200 enrolled patients, 6 patients were lost to follow-up, with survival status unknown, so they were excluded from the analysis. Of 194 patients included, 61 had insufficient stored serum specimens for IgG subclass assays; hence, we analyzed serum samples from 139 subjects.

### Antigen Preparation

We prepared whole-cell antigen from wild type strain *B. pseudomallei* K96243, an isolate from a patient in northeast Thailand, which was modified from a previous study (*19*,*20*). In brief, we grew the bacteria in rice medium at 37°C for 14 days, then heat-inactivated the bacteria at 121°C for 30 min. We centrifuged the whole-cell heat-inactivated (HIA) *B. pseudomallei* at 2,000 × *g* for 1 h, then used the supernatant as an antigen. We aliquoted and kept the supernatant at −20°C until used. We quantitated the protein concentration of the antigens in the supernatant by using the Pierce BCA Protein Assay Kit (Thermo Fisher Scientific, https://www.thermofisher.com) according to the manufacturer's protocol.

### ELISA

We used ELISA to measure serum levels of IgM and IgG specific to *B. pseudomallei*. We added whole cells of HIA *B. pseudomallei* to wells of Nunc MaxiSorp flat bottom 96-Well immunoplates (Thermo Fisher Scientific) at a concentration of 200 ng/well and incubated the plates overnight at 4°C. Between each step, we washed the ELISA plate 3 times with 300 μL of washing buffer consisting of 0.05% Tween-20 in phosphate buffered saline (PBS; Sigma-Aldrich, https://www.sigmaaldrich.com). After blocking with 5% skimmed milk in PBS for 2 h at 37°C, we diluted the serum 1:100 and added it to the plate in duplicate, then incubated for 1 h. We diluted the horseradish peroxidase (HRP) enzyme–conjugated antihuman IgM or IgG (Sigma-Aldrich) 1:2,000 and then added it to the ELISA plate before incubating for 1 h. We developed the ELISA by using 3,3′,5,5′-tetramethylbenzidine (TMB; Thermo Fisher Scientific) substrate and determined the absorbance value (optical density = 450 nm) by using a Multiskan GO microplate spectrometer (Thermo Fisher Scientific).

For IgG subclasses, we blocked the overnight precoated ELISA plate with 1% bovine serum albumin (BSA) in PBS for 2 h. We then diluted the serum 1:100 for detecting IgG1, IgG3, and IgG4 or 1:2,000 for detecting IgG2, and then added the serum to the ELISA plate. After 1-h incubation, we diluted the biotin-conjugated antihuman IgG1, IgG2, IgG3, or IgG4 1:1,000 and added them to the plate before incubating for 1 h. Then we added streptavidin-HRP (Mabtech, https://www.mabtech.com) to the plate and incubated for 1 h and developed by using TMB as we described in the previous paragraph.

### Genomic Methods

We extracted genomic DNA from blood samples by using the QIAamp DNA Blood Midi kit (QIAGEN, https://www.qiagen.com) according to the manufacturer's instructions, then stored at −20°C. We genotyped the *FCGR2A* c.535A>G (rs1801274) single nucleotide variant (SNV) by using the TaqMan SNP genotyping assay (Applied Biosystems, https://www.thermofisher.com) on a CFX96 Touch Real-Time PCR Detection System (Bio-Rad, http://www.bio-rad.com). The SNV context sequence was AATGGAAAATCCCAGAAATTCTCCC(A/G)TTTGGATCCCACCTTCTCCATCCCA.

### Antibody-Dependent Cellular Phagocytosis

We labeled the bacteria by incubating with fluorescein isothiocyanate (FITC) for 30 min in the dark at room temperature, then washed the bacteria with PBS and immediately used the bacteria in the assay. We incubated FITC-labeled *B. pseudomallei* with HIA serum samples (10% vol/vol) or Roswell Park Memorial Institute (RPMI) 1640 medium (Sigma-Aldrich) as a control at 37°C for 1 h. We then added opsonized FITC-labeled *B. pseudomallei* to human monocyte cell lines, THP-1 (FcγRIIa-R-H131 genotype) or U937 (FcγRIIa-R131 genotype), at a multiplicity of infection (MOI) of 5 CFUs/cell. After incubation at 37°C for 30 min, we immediately transferred cells to ice to stop phagocytosis. We washed the cells twice with cold PBS. We then added cold trypan blue (Sigma-Aldrich) to the cells and incubated for 10 min on ice to quench the FITC signal of bound *B. pseudomallei* on cell surface. Next, we washed the cells twice with cold PBS and incubated with BD Cytofix Fixation Buffer (Becton Dickinson, https://www.bd.com) cold fixative buffer at 4°C for 15 min. We then washed the cells twice with cold MACSQuant Running Buffer (Miltenyi Biotec, https://www.miltenyibiotec.com), and analyzed the cells by using the MACSQuant Analyzer 10 (Miltenyi Biotec). We expressed results as fold-change in enhancement of phagocytosis calculated by dividing the percentage of infected cells in the presence of serum by those in the absence of serum samples in the RPMI-1640 control.

### Statistics

We reported nonnormally distributed continuous data as median and IQR. We analyzed the statistical significance of differences by using Mann-Whitney U-test for 2 groups and the Kruskal-Wallis 1-way ANOVA to test the mean difference among 3 groups in GraphPad Prism Version 6 (GraphPad Software Inc., https://www.graphpad.com). We calculated the percentage of coefficient of variation (CV) in ELISA by dividing SD of measurement by mean of measurement multiplied by 100. The cutoff was 10% intra-assay CV and 15% for inter-assay CV. We performed univariable and multivariable logistic regression adjusting for age, diabetes, pre-existing renal disease, and neutrophil counts by using Stata version 14.0 for Windows (StataCorp LLC, https://www.stata.com).

## Results

### Elevated IgG2 Levels in Patients Who Survived Melioidosis

The characteristics of patients with acute melioidosis enrolled in the study were previously described (*4*,*18*). Among 194 patients in the cohort, median age was 56 years (range 19–89 years; IQR 46–63 years); 129 (66.5%) were men and 65 (33.5%) were women. Underlying conditions among patients included diabetes (57.7%), renal disease (17.5%), and heart disease (11.8%) (Table 1). Forty-nine (25%) persons died within 28 days despite receiving appropriate antimicrobial drug treatment.

Serum levels of IgM specific to whole-cell HIA *B. pseudomallei* were not statistically significantly different between survivors (median 0.28, IQR 0.13–1.00) and nonsurvivors (median 0.31, IQR 0.08–0.52; p = 0.18) (Figure 1, panel A). Similarly, anti–HIA *B. pseudomallei* IgG levels were not different between survivors (median 2.32, IQR 1.10–2.94) and nonsurvivors (median 2.12, IQR 1.42–2.50; p = 0.29) (Figure 1, panel B). As expected, HIA *B. pseudomallei*–specific IgM and IgG levels in patients with melioidosis, including those who died and survived, were much higher than those in healthy controls (Figure 1, panels A, B).

We then measured anti–HIA *B. pseudomallei* IgG subclasses in serum samples from melioidosis patients to determine whether IgG subclasses are associated with survival. We found statistically significantly higher IgG2 levels (median 1.30, IQR 0.45–2.04) against whole-cell heat-killed *B. pseudomallei* in serum from survivors than in serum from nonsurvivors (median 0.59, IQR 0.26–1.51; p = 0.047) (Figure 1, panel D). Levels of IgG1, IgG3, and IgG4 subclasses were comparable between groups (Figure 1, panels C, E, F).

### IgG2 Level Associated with Protection against Death

In a univariable model, we found that increasing IgG2 levels in serum samples was statistically significantly associated with survival (odds ratio [OR] 0.63, 95% CI 0.43–0.92). In previous studies of the same cohort, we found that age, pre-existing renal disease, and neutrophil count were associated with a 28-day mortality rate of 26% (*4*,*18*). We next tested the association of the IgG2 levels with death by using a multivariable

**Table 1.** Baseline demographic characteristics of patients with acute melioidosis, Thailand

| Characteristic | No. patients (%), n = 194 |
|---|---|
| Deaths | 49 (25.3) |
| Median age, y (IQR) | 56 (46–63) |
| Sex | |
| M | 129 (66.5) |
| F | 65 (33.5) |
| Underlying conditions | |
| Diabetes | 112 (57.7) |
| Renal disease | 34 (17.5) |
| Heart disease | 23 (11.8) |
| Chronic liver disease | 7 (3.6) |
| Previous melioidosis | 5 (2.6) |
| Clinical manifestation | |
| Bacteremia | 99 (51.0) |
| Pneumonia | 48 (24.7) |

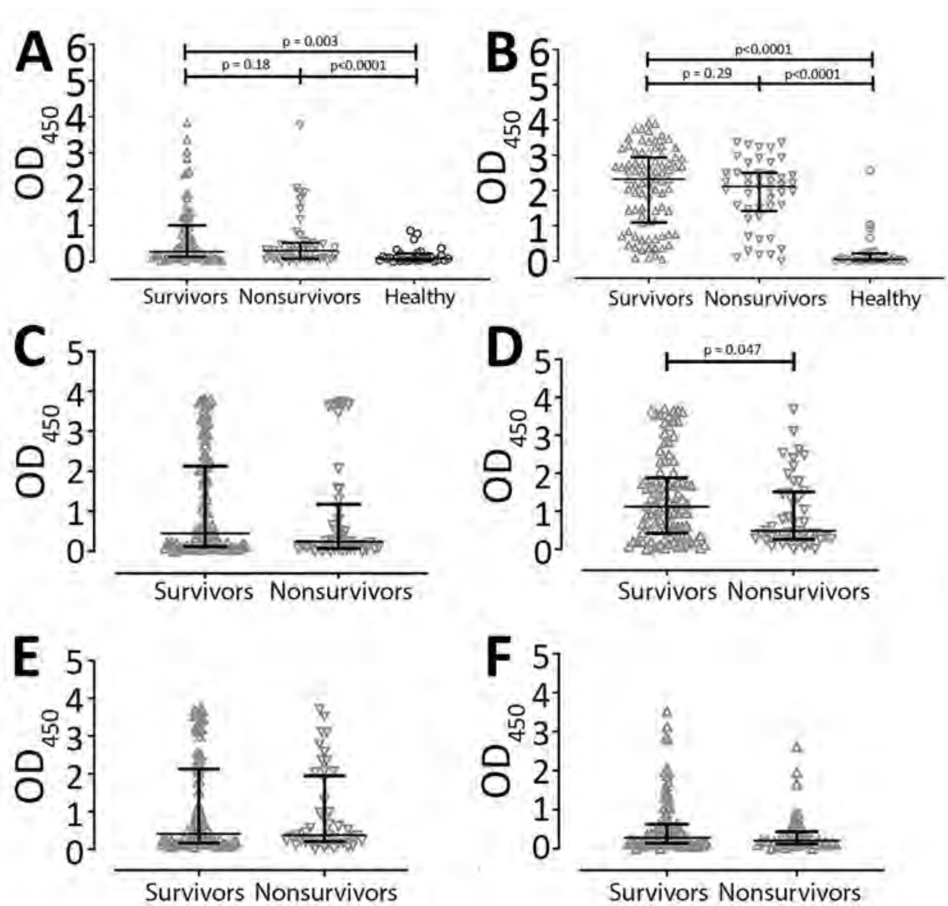


**Figure 1.** Comparison of serum levels of *Burkholderia pseudomallei*–specific antibody subclasses between 94 survivors and 45 nonsurvivors of acute melioidosis, Thailand. A) IgM; B) total IgG; C) IgG1; D) IgG2; E) IgG3; and F) IgG4. Serum levels were tested by using indirect ELISA on heat-killed whole cell *B. pseudomallei*. We used Kruskal-Wallis 1-way ANOVA to compare >2 groups and Mann-Whitney U to compare 2 groups. Antibody levels in healthy endemic controls (n = 30) are shown for comparison for total IgM and IgG only. $OD_{450}$, optical density at 450 nm.

model adjusting for age, diabetes, pre-existing renal disease, and neutrophil count (Table 2). Our results demonstrate that elevated IgG2 levels correlate with survival (OR 0.50, 95% CI 0.30–0.83).

### Serum from Survivors Enhanced Phagocytosis in THP-1 Human Monocytic Cells

IgG2 has the least functional potency of the subclasses due to low affinity binding between its Fc region and activating FcγRs expressed on effector innate immune cells (*21*,*22*). A single-nucleotide polymorphism (SNP) resulting in a histidine (H) residue instead of an arginine (R) at position 131 improves affinity for human IgG2 and affects effector function (*23*). We performed antibody-dependent cellular phagocytosis (ADCP) assays by using 2 monocyte cell lines: U937 cells, containing a homozygous low-affinity R131 allele, and THP-1 cells, containing heterozygous intermediate-affinity H/R131 alleles of FcγRIIa.

**Table 2.** Multivariable-adjusted logistic regression for melioidosis mortality rates, Thailand*

| | Mortality rate | |
|---|---|---|
| Variable | Adjusted OR (95% CI) | p value |
| Serum IgG2 level | 0.50 (0.30–0.83) | 0.007 |
| Age ≥45 y | 0.36 (0.10–1.30) | 0.120 |
| Diabetes | 0.92 (0.34–2.53) | 0.876 |
| Preexisting renal disease | 9.41 (2.48–35.80) | 0.001 |
| Neutrophil count/µL | | |
| >4,000–8,000 | Referent | <0.001 |
| ≤4,000 | 4.66 (0.52–41.50) | |
| >8,000–12,000 | 19.00 (3.40–106.33) | |
| ≥12,000 | 14.78 (2.78–78.73) | |

*OR, odds ratio.

The ADCP activities of antibodies were not statistically significantly different between serum from survivors (median 37.63, IQR 19.88–82.62) and nonsurvivors (median 45.34, IQR 21.51–93.67) in U937 containing the low-affinity FcγRIIa-R131 phenotype (p = 0.68) (Figure 2, panel A). In contrast, we did find a statistically significant difference in phagocytic activity between survivors (median 89.66, IQR 69.03–120.30) and nonsurvivors (median 52.43, IQR 37.14–105.10) when we used THP-1 expressing intermediate affinity FcγRIIA-H/R131 (p<0.001) (Figure 2, panel B).

### Association between Enhanced Phagocytosis in THP-1 and Bacteremia

When we used U937 cells, we did not see a statistically significant difference in ADCP activity between patients without bacteremia (median 60.95,

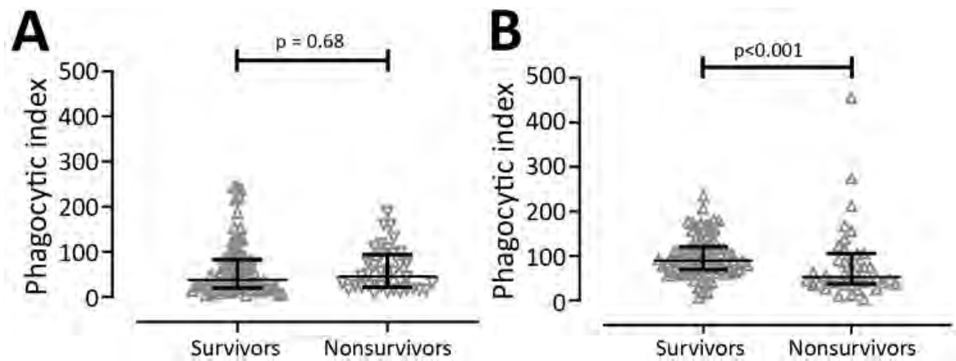


**Figure 2.** Comparison of antibody-dependent cellular phagocytosis (ADCP) activity between 82 survivors and 38 nonsurvivors of acute melioidosis, Thailand. ADCP activity was tested by using U937 (A) and THP-1 (B) human monocytic cell lines. Heat-inactivated serum samples were incubated with live fluorescein isothiocyanate–labeling *Burkholderia pseudomallei* before transfer to the cells, and the percentage of *B. pseudomallei* uptake by cells was analyzed by flow cytometer. We used the Mann-Whitney U test for statistical comparison.

IQR 18.18–93.38) and those with bacteremia (median 30.68, IQR 20.22–76.03; p = 0.12) (Figure 3, panel A). Furthermore, the ADCP activity in THP-1 of serum from patients without bacteremia (median 90.18, IQR 61.62–135.5) was higher than in those with bacteremia (median 75.38, IQR 41.39–106.80), but this difference did not reach statistical significance (p = 0.07) (Figure 3, panel B).

#### FcγRIIa Genotype Distribution among Cohort Patients

The genotype distribution was 63.4% FcγRIIa-H131/H131, 29.3% FcγRIIa-H131/R131, and 7.3% FcγRIIa-R131/R131 and exhibited a 9:4:1 ratio in our melioidosis cohort. The frequency of the FcγRIIa-H131 allele overall in our cohort was 78%. However, we did not find a substantial association between this FcγRIIa polymorphism and death, bacteremia, diabetes status, or preexisting renal disease in our cohort (data not shown).

### Discussion

Our major finding in this study is the elevated level of serum IgG2 against whole-cell HIA *B. pseudomallei* lysate in melioidosis patients who survived the disease compared with fatal cases. We confirmed the association between elevated IgG2 level and survival in a multivariable logistic regression analysis adjusting for age, diabetes, preexisting renal disease, and neutrophil count. Some studies provide evidence for a role of IgG2 in protection against various microorganismal infections, including *Plasmodium falciparum* malaria (*24*), and encapsulated bacteria, including *Streptococcus pneumoniae* (*25*,*26*), *Haemophilus influenza* (*26*,*27*), and *Neisseria meningitidis* (*28*). The IgG2 in those studies mainly recognized CPS epitopes that are highly repeated T-independent antigens. Previous work did not show a correlation between IgG2 responses to Hcp1 or OPS and survival (*14*), so the IgG2 responses to whole-cell *B. pseudomallei* in our study are likely to be against other antigens yet to be tested. Ongoing work also will address whether protective IgG2 also bind to carbohydrate epitopes on the outside surface of *Burkholderia* spp.

A large body of literature supports IgG2 having no or lower relative binding affinity for activating FcγRs when compared with other IgG subclasses (*21*,*29*). Nevertheless, IgG2 has been shown to possess opsonophagocytosis capacity in some studies (*27*,*28*,*30*). These conflicting results might be explained by the presence of a guanine to adenine SNP resulting in replacement

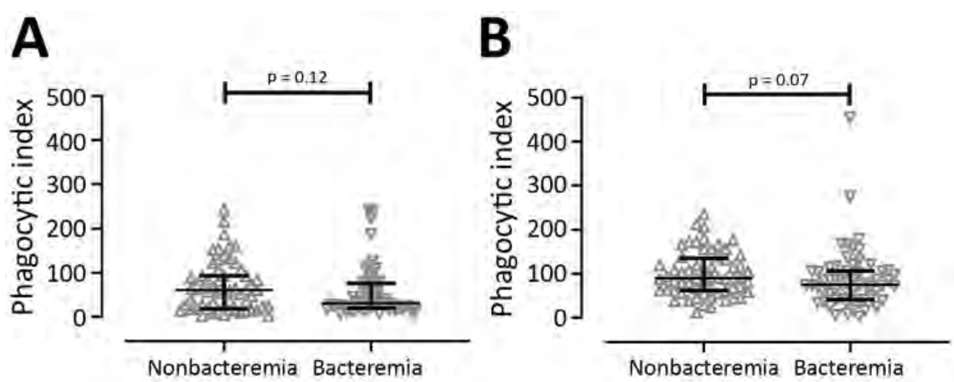


**Figure 3.** Comparison of antibody-dependent cellular phagocytosis (ADCP) activity between 61 patients without bacteremia and 59 patients with bacteremia among patients with acute melioidosis, Thailand. ADCP activity was tested by using U937 (A) and THP-1 (B) human monocytic cell lines. We used the Mann-Whitney U test for statistical comparison.

of arginine (R) with histidine (H) at residue 131 of FcγRIIa. The product of FcγRIIa-H131, which has been reported in 67% of persons with Chinese ethnicity (*31*), 45% of White populations, and 41% of Black populations (*32*), were found to bind IgG2-immune complex more efficiently than those of R131 (*33*,*34*), hence enhancing phagocytosis. Therefore, the considerable association between elevated IgG2 and protection against death in this cohort could be partly due to an increase of IgG2–mediated phagocytosis of the bacteria to effector innate immune cells via FcγRIIA, which 78% of our cohort possessed.

We used 2 types of human monocytic cells expressing different FcγRIIa phenotypes to compare ADCP activity between patients who survived the disease and those who did not. U937 cells are homozygous for low-affinity FcγRIIa-H/R131 phenotype, whereas THP-1 cells are heterozygous for intermediate-affinity FcγRIIa-H/R131 phenotype. We demonstrated that serum from survivors with much higher levels of IgG2 subclass could enhance *B. pseudomallei* uptake into THP-1 cells compared with those from nonsurvivors. Conversely, we did not find a difference in ADCP activity in U937 cells between survivors and nonsurvivors. When using U937 cells, comparable phagocytic activities of serum samples between survivors and nonsurvivors might be due to the comparable levels of IgG1or IgG3 that can effectively interact with FcγRIIa-R131. The phagocytic activities of IgG1 and IgG3 imply that higher IgG2 levels can enhance ADCP activity in effector innate immune cells carrying the FcγRIIa-H131 allele and that this ADCP activity was associated with protection against death in acute melioidosis patients.

Elevated ADCP activity of serum samples from patients without bacteremia almost reached statistical significance ($p = 0.07$) compared with those from patients with bacteremia when we used THP-1 cells but not when we used U937 cells. The ADCP activity results imply that the immune complex in circulating blood can be removed more effectively in persons with the FcγRIIa-H131 phenotype.

One limitation of this study is that we used different cell types, which might have different genetic and phenotypic backgrounds resulting in different outcomes of ADCP activity in serum from survivors and nonsurvivors. This finding should be confirmed in U937 cells transfected with the FcγRIIa-H131 receptor. In addition, IgG2 serum samples from patients also contain the other 3 IgG subclasses, IgG1, IgG3, and IgG4, and IgM and IgA that might influence outcomes. In addition, the antibody-dependent phagocytosis activity of serum in this study was tested solely in human monocytic cells, U937 and THP-1, whereas FcγRIIa also is constitutively expressed on the surface of other effective immune cells including dendritic cells, neutrophils, and B cells.

We did not find a statistically significant association between FcγRIIa-H131 phenotype and ADCP activity in either THP-1 or U937 cells when adjusting for death, diabetes status, and pre-existing renal disease. This result might be due to a low number of patients with the FcγRIIa-R131 phenotype (7.3%) in our cohort; therefore, we did not have the statistical power to detect a difference in outcome.

In conclusion, the data in this study emphasize the role of IgG subclasses in clinical outcomes of infectious diseases. The relationship between elevated IgG2 levels and protection against death in melioidosis is comparable with those in other encapsulated bacterial infections. The relationship between elevated IgG2 levels and protection against death in melioidosis constitutes critical information for selecting the appropriate antibody subclasses for therapeutic antibody and vaccine development, in particular for patients with the FcγRIIa-H131 phenotype.

### Acknowledgments

We are grateful for the help and support from all participants and staff at Sunpasitthiprasong Hospital and the Mahidol-Oxford Tropical Medicine Research Unit (MORU), which receives core support from the Wellcome Trust.

P.C. received financial support from the Global Challenges Research Fund Networks in Vaccines Research and Development VALIDATE Network, which was cofunded by the Medical Research Council and Biotechnology and Biological Sciences Research Council, a funding award from the United Kingdom that is part of the European & Developing Countries Clinical Trials Programme 2 and supported by the European Union. S.J.D. received financial support from Wellcome Trust Intermediate Clinical Fellowship award (no. WT100174/Z/12/Z).

## About the Author

Dr. Chaichana is a postdoctoral fellow at Mahidol-Oxford Tropical Medicine Research Unit, Mahidol University, Bangkok, Thailand. Her research interests focus on the humoral immune response and antibody-based therapeutics to tropical bacterial diseases.

### References

1. Currie BJ, Fisher DA, Howard DM, Burrow JN, Lo D, Selva-Nayagam S, et al. Endemic melioidosis in tropical northern Australia: a 10-year prospective study and review of the

literature. Clin Infect Dis. 2000;31:981–6. https://doi.org/10.1086/318116
2. Chaowagul W, White NJ, Dance DA, Wattanagoon Y, Naigowit P, Davis TM, et al. Melioidosis: a major cause of community-acquired septicemia in northeastern Thailand. J Infect Dis. 1989;159:890–9. https://doi.org/10.1093/infdis/159.5.890
3. Limmathurotsakul D, Golding N, Dance DAB, Messina JP, Pigott DM, Moyes CL, et al. Predicted global distribution of *Burkholderia pseudomallei* and burden of melioidosis. Nat Microbiol. 2016;1:15008. PubMed https://doi.org/10.1038/nmicrobiol.2015.8
4. Jenjaroen K, Chumseng S, Sumonwiriya M, Ariyaprasert P, Chantratita N, Sunyakumthorn P, et al. T-cell responses are associated with survival in acute melioidosis patients. PLoS Negl Trop Dis. 2015;9:e0004152. https://doi.org/10.1371/journal.pntd.0004152
5. Nithichanon A, Rinchai D, Buddhisa S, Saenmuang P, Kewcharoenwong C, Kessler B, et al. Immune control of *Burkholderia pseudomallei*—common, high-frequency T-cell responses to a broad repertoire of immunoprevalent epitopes. Front Immunol. 2018;9:484. https://doi.org/10.3389/fimmu.2018.00484
6. Tippayawat P, Pinsiri M, Rinchai D, Riyapa D, Romphruk A, Gan YH, et al. *Burkholderia pseudomallei* proteins presented by monocyte-derived dendritic cells stimulate human memory T cells in vitro. Infect Immun. 2011;79:305–13. https://doi.org/10.1128/IAI.00803-10
7. Jones SM, Ellis JF, Russell P, Griffin KF, Oyston PCF. Passive protection against *Burkholderia pseudomallei* infection in mice by monoclonal antibodies against capsular polysaccharide, lipopolysaccharide or proteins. J Med Microbiol. 2002;51:1055–62. https://doi.org/10.1099/0022-1317-51-12-1055
8. Bottex C, Gauthier YP, Hagen RM, Finke EJ, Splettstösser WD, Thibault FM, et al. Attempted passive prophylaxis with a monoclonal anti-*Burkholderia pseudomallei* exopolysaccharide antibody in a murine model of melioidosis. Immunopharmacol Immunotoxicol. 2005;27:565–83. https://doi.org/10.1080/08923970500493995
9. AuCoin DP, Reed DE, Marlenee NL, Bowen RA, Thorkildson P, Judy BM, et al. Polysaccharide specific monoclonal antibodies provide passive protection against intranasal challenge with *Burkholderia pseudomallei*. PLoS One. 2012;7:e35386. https://doi.org/10.1371/journal.pone.0035386
10. Bryan LE, Wong S, Woods DE, Dance DA, Chaowagul W. Passive protection of diabetic rats with antisera specific for the polysaccharide portion of the lipopolysaccharide isolated from *Pseudomonas pseudomallei*. Can J Infect Dis. 1994;5:170–8. https://doi.org/10.1155/1994/856850
11. Nelson M, Prior JL, Lever MS, Jones HE, Atkins TP, Titball RW. Evaluation of lipopolysaccharide and capsular polysaccharide as subunit vaccines against experimental melioidosis. J Med Microbiol. 2004;53:1177–82. https://doi.org/10.1099/jmm.0.45766-0
12. Burtnick MN, Shaffer TL, Ross BN, Muruato LA, Sbrana E, DeShazer D, et al. Development of subunit vaccines that provide high-level protection and sterilizing immunity against acute inhalational melioidosis. Infect Immun. 2017;86:e00724-17. https://doi.org/10.1128/IAI.00724-17
13. Ho M, Schollaardt T, Smith MD, Perry MB, Brett PJ, Chaowagul W, et al. Specificity and functional activity of anti-*Burkholderia pseudomallei* polysaccharide antibodies. Infect Immun. 1997;65:3648–53. https://doi.org/10.1128/IAI.65.9.3648-3653.1997
14. Charuchaimontri C, Suputtamongkol Y, Nilakul C, Chaowagul W, Chetchotisakd P, Lertpatanasuwun N, et al. Antilipopolysaccharide II: an antibody protective against fatal melioidosis. Clin Infect Dis. 1999;29:813–8. https://doi.org/10.1086/520441
15. Vasu C, Vadivelu J, Puthucheary SD. The humoral immune response in melioidosis patients during therapy. Infection. 2003;31:24–30. https://doi.org/10.1007/s15010-002-3020-2
16. Chenthamarakshan V, Kumutha MV, Vadivelu J, Puthucheary SD. Distribution of immunoglobulin classes and IgG subclasses against a culture filtrate antigen of *Burkholderia pseudomallei* in melioidosis patients. J Med Microbiol. 2001;50:55–61. https://doi.org/10.1099/0022-1317-50-1-55
17. Pumpuang A, Phunpang R, Ekchariyawat P, Dulsuk A, Loupha S, Kwawong K, et al. Distinct classes and subclasses of antibodies to hemolysin co-regulated protein 1 and O-polysaccharide and correlation with clinical characteristics of melioidosis patients. Sci Rep. 2019;9:13972. https://doi.org/10.1038/s41598-019-48828-4
18. Chaichana P, Chantratita N, Brod F, Koosakulnirand S, Jenjaroen K, Chumseng S, et al. A nonsense mutation in TLR5 is associated with survival and reduced IL-10 and TNF-α levels in human melioidosis. PLoS Negl Trop Dis. 2017;11:e0005587. https://doi.org/10.1371/journal.pntd.0005587
19. Wuthiekanun V, Langa S, Swaddiwudhipong W, Jedsadapanpong W, Kaengnet Y, Chierakul W, et al. Short report: melioidosis in Myanmar: forgotten but not gone? Am J Trop Med Hyg. 2006;75:945–6. https://doi.org/10.4269/ajtmh.2006.75.945
20. Alexander AD, Huxsoll DL, Warner AR Jr, Shepler V, Dorsey A. Serological diagnosis of human melioidosis with indirect hemagglutination and complement fixation tests. Appl Microbiol. 1970;20:825–33. https://doi.org/10.1128/AM.20.5.825-833.1970
21. Bruhns P, Iannascoli B, England P, Mancardi DA, Fernandez N, Jorieux S, et al. Specificity and affinity of human Fcgamma receptors and their polymorphic variants for human IgG subclasses. Blood. 2009;113:3716–25. https://doi.org/10.1182/blood-2008-09-179754
22. Warmerdam PA, van de Winkel JG, Vlug A, Westerdaal NA, Capel PJ. A single amino acid in the second Ig-like domain of the human Fc gamma receptor II is critical for human IgG2 binding. J Immunol. 1991;147:1338–43.
23. Arthur MF, Yee HMP, Zuniga R, Salmon JE, Musher DM. Association between FcgRIIa-R131 allotype and bacteremic pneumococcal pneumonia. Clin Infect Dis. 2000;30:25–8. PubMed https://doi.org/10.1086/313588
24. Aucan C, Traoré Y, Tall F, Nacro B, Traoré-Leroux T, F umoux F, et al. High immunoglobulin G2 (IgG2) and low IgG4 levels are associated with human resistance to *Plasmodium falciparum* malaria. Infect Immun. 2000;68:1252–8. https://doi.org/10.1128/IAI.68.3.1252-1258.2000
25. Shackelford PG, Granoff DM, Polmar SH, Scott MG, Goskowicz MC, Madassery JV, et al. Subnormal serum concentrations of IgG2 in children with frequent infections associated with varied patterns of immunologic dysfunction. J Pediatr. 1990;116:529–38. https://doi.org/10.1016/S0022-3476(05)81598-7
26. Siber GR, Schur PH, Aisenberg AC, Weitzman SA, Schiffman G. Correlation between serum IgG-2 concentrations and the antibody response to bacterial polysaccharide antigens. N Engl J Med. 1980;303:178–82. https://doi.org/10.1056/NEJM198007243030402
27. Amir J, Scott MG, Nahm MH, Granoff DM. Bactericidal and opsonic activity of IgG1 and IgG2 anticapsular antibodies to

*Haemophilus influenzae* type b. J Infect Dis. 1990;162:163–71. https://doi.org/10.1093/infdis/162.1.163
28. Aase A, Michaelsen TE. Opsonophagocytic activity induced by chimeric antibodies of the four human IgG subclasses with or without help from complement. Scand J Immunol. 1994;39:581–7. https://doi.org/10.1111/j.1365-3083.1994.tb03416.x
29. Bindon CI, Hale G, Brüggemann M, Waldmann H. Human monoclonal IgG isotypes differ in complement activating function at the level of C4 as well as C1q. J Exp Med. 1988;168:127–42. https://doi.org/10.1084/jem.168.1.127
30. Sawada S, Kawamura T, Masuho Y. Immunoprotective human monoclonal antibodies against five major serotypes of Pseudomonas aeruginosa. J Gen Microbiol. 1987; 133:3581–90.
31. Nagelkerke SQ, Tacke CE, Breunis WB, Tanck MWT, Geissler J, Png E, et al.; International Kawasaki Disease Genetics Consortium. Extensive ethnic variation and linkage disequilibrium at the *FCGR2/3* locus: different genetic associations revealed in Kawasaki disease. Front Immunol. 2019;10:185. https://doi.org/10.3389/fimmu.2019.00185
32. van Schie RC, Wilson ME. Evaluation of human FcgammaRIIA (CD32) and FcgammaRIIIB (CD16) polymorphisms in Caucasians and African-Americans using salivary DNA. Clin Diagn Lab Immunol. 2000;7:676–81. https://doi.org/10.1128/CDLI.7.4.676-681.2000
33. Parren PW, Warmerdam PA, Boeije LC, Arts J, Westerdaal NA, Vlug A, et al. On the interaction of IgG subclasses with the low affinity Fc gamma RIIa (CD32) on human monocytes, neutrophils, and platelets. Analysis of a functional polymorphism to human IgG2. J Clin Invest. 1992;90:1537–46. https://doi.org/10.1172/JCI116022
34. van Sorge NM, van der Pol W-L, van de Winkel JG. FcgammaR polymorphisms: Implications for function, disease susceptibility and immunotherapy. Tissue Antigens. 2003;61:189–202. https://doi.org/10.1034/j.1399-0039.2003.00037.x

Address for correspondence: Susanna J. Dunachie, Center for Tropical Medicine and Global Health, Peter Medawar Building for Pathogen Research, South Parks Road, Oxford OX1 3SY, UK; email: susie.dunachie@ndm.ox.ac.uk

# etymologia

## *Falciparum* [fal-ʹsɪ-pə-rəm]

Aparna Tiwari, Abhinav Sinha

From the Latin *falx* or *falci* (sickle or scythe-shaped) and *parum* (like or equal to another) or *parere* (to bring forth or bear). The species *falciparum* in the genus *Plasmodium* is the parasite that causes malignant tertian malaria in humans.

There were many terms suggested for this parasite, such as *Ematozoo falciforme* by Antolisei and Angelini in 1890 and Haemotozoon falciforme by Thayer and Hewetson in 1895, because of its sickle-shaped gametocytes, the sexual stage of *falciparum* parasites. However, the term *falciparum*, suggested by William Henry Welch in 1897, was eventually accepted. In 1954, *Plasmodium falciparum* (previously *Laverania malariae*) was approved by International Commission on Zoological Nomenclature.

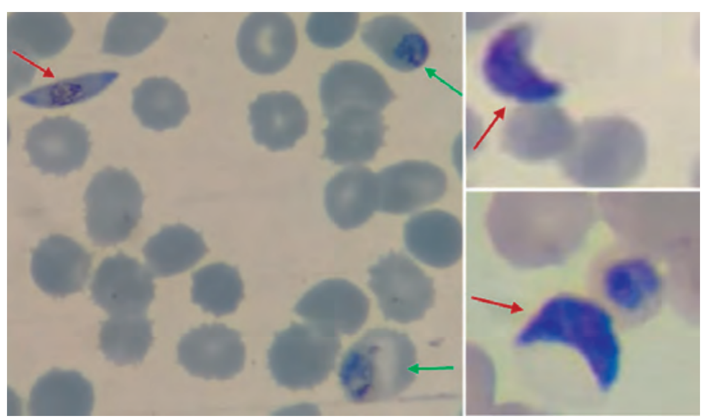

**Figure.** Giemsa-stained thin blood smear of *Plasmodium falciparum* (original magnification ×1,000). Red arrows indicate gametocytes, and green arrows indicate trophozoite stages. Photograph provided by A. Tiwari.

### Sources

1. Bruce-Chwatt LJ. *Falciparum* nomenclature. Parasitol Today. 1987;3:252. https://doi.org/10.1016/0169-4758(87)90153-0
2. Christophers R, Sinton JA. Correct name of malignant tertian parasite. BMJ. 1938;2:1130–4. https://doi.org/10.1136/bmj.2.4065.1130
3. Dorland's illustrated medical dictionary. 32nd ed. Philadelphia: Saunders/Elsevier; 2012. p. 678.

Author affiliations: Council of Scientific and Industrial Research, New Delhi, India (A. Tiwari); India Council of Medical Research– National Institute of Malaria Research, New Delhi (A. Tiwari, A. Sinha)

DOI: https://doi.org/10.3201/eid2702.ET2702

Address for correspondence: Aparna Tiwari, India Council of Medical Research–National Institute of Malaria Research, New Delhi 110077, India; email: aparna@nimr.org.in

# *Plasmodium falciparum* Histidine-Rich Protein 2 and 3 Gene Deletions in Strains from Nigeria, Sudan, and South Sudan

Christiane Prosser, Karryn Gresty, John Ellis, Wieland Meyer, Karen Anderson, Rogan Lee, Qin Cheng

Deletion of histidine-rich protein genes *pfhrp2/3* in *Plasmodium falciparum* causes infections to go undetected by HRP2-based malaria rapid diagnostic tests. We analyzed *P. falciparum* malaria cases imported to Australia (n = 210, collected 2010–2018) for their *pfhrp2/3* status. We detected gene deletions in patients from 12 of 25 countries. We found >10% *pfhrp2*-deletion levels in those from Nigeria (13.3%, n = 30), Sudan (11.2%, n = 39), and South Sudan (17.7%, n = 17) and low levels of *pfhrp3* deletion from Sudan (3.6%) and South Sudan (5.9%). No parasites with *pfhrp2/3* double deletions were detected. Microsatellite typing of parasites from Nigeria, Sudan, and South Sudan revealed low relatedness among gene-deleted parasites, indicating independent emergences. The gene deletion proportions signify a risk of false-negative HRP2-RDT results. This study's findings warrant surveillance to determine whether the prevalence of gene-deleted parasites justifies switching malaria rapid diagnostic tests in Nigeria, Sudan, and South Sudan.

During 2000–2015, global malaria incidence and death rates were reduced by more than half (*1*). Malaria control efforts are credited with increasing life expectancy by 5% globally and by 12.3% in sub–Saharan Africa, where ≈90% of the disease burden is located (*2*). Gains in malaria control have been attributed primarily to the implementation of key intervention measures including insecticide-treated netting, indoor residual spraying, combination medicines, and diagnostic tests. Malaria decline has been more gradual, or has stalled, in endemic regions with limited access to these interventions (*3*).

Rapid diagnostic tests (RDTs) are recommended, and have become essential, for malaria case management in many regions because they meet the challenges for remote and low-resource settings. These tests are affordable, easy to transport and store, and less skill- and resource-demanding than microscopy, but they offer comparable sensitivity to quality microscopy (*4*). These RDTs are used, along with Giemsa-stained blood films, for diagnosis of imported malaria in pathology laboratories in Australia (including those of the Australian Defence Force) (*5*). A preliminary diagnosis using RDTs is made and the diagnosis confirmed by stained thick and thin films. False-negative tests from RDTs will result in delayed treatment, which may affect the patient's clinical outcomes.

Histidine-rich protein 2 (HRP2)–based RDTs are largely preferred for detecting *P. falciparum* malaria because of their superior sensitivity and heat-stability profile over *Plasmodium* lactate dehydrogenase (pLDH) or aldolase (*6*). HRP2-based tests detect the HRP2 antigen (and, to a lesser extent, HRP3, because of cross-reactivity) at levels as low as ≈1 ng/mL blood; however, in practice, the detection limit of HRP2-based tests is reportedly comparable with that of quality microscopy (≈200 parasites/μL) (*7*). This level is adequate for case management but much less sensitive than molecular methods. RDTs have been reported to have failed to detect a substantial proportion of asymptomatic infections (*8*).

Parasite deletion of the genes *pfhrp2* and *pfhrp3* has been implicated in false-negative results using

Author affiliations: Australian Defence Force Malaria and Infectious Disease Institute, Brisbane, Queensland, Australia (C. Prosser, K. Gresty, K. Anderson, Q. Cheng); Westmead Institute for Medical Research, Westmead, New South Wales, Australia (C. Prosser, W. Meyer); University of Sydney, Sydney, New South Wales, Australia (C. Prosser, W. Meyer, R. Lee); QIMR–Berghofer Medical Research Institute, Brisbane (K. Gresty, K. Anderson, Q. Cheng); University of Technology Sydney, Sydney (J. Ellis); Westmead Hospital, Westmead (W. Meyer); Marie Bashir Institute for Infectious Diseases and Biosecurity, University of Sydney, Sydney (W. Meyer); Centre for Infectious Diseases and Microbiology Laboratory Services, ICPMR, Westmead Hospital, Westmead (R. Lee)

DOI: https://doi.org/10.3201/eid2702.191410

HRP2-based RDTs. There are recent reports of *pfhrp2*-deleted parasites in several countries in Africa (*9*–*15*), as well as India (*16*), China and Myanmar (*17*), and countries in South America, including Peru (*18*). Single *pfhrp2* gene deletions represent an increased risk for RDT failure, especially in cases of low parasitemia or inferior RDTs (*19*). In the instance of a double deletion of *pfhrp2* and *pfhrp3,* the parasite is undetectable with HRP2-based RDTs (*20*). Because RDTs are the mainstay diagnostic tool for many endemic countries, loss of effectiveness constitutes a public health emergency and poses a major challenge to *P. falciparum* control and elimination efforts. For countries reliant on RDTs, gene-deletion prevalence data are needed to inform case management policy.

The World Health Organization has estimated a threshold of 5% of parasites lacking HRP2 as the point at which false negatives from lack of antigen expression would likely exceed the rate of false negatives observed using alternative RDTs and, as such, the point at which HRP2-based tests are no longer recommended for that location (*21*). Therefore, surveillance is critical to estimate whether the prevalence of parasites with gene deletions has reached the threshold for switching RDTs and is recommended to focus primarily on locations or nearby locations where gene deletions have been detected. Imported cases of malaria are a resource to detect gene deletions in countries of origin and the outcomes can prompt large-scale surveillance.

When case management policies for imported malaria are developed, regional *pfhrp2*/*pfhrp3* deletion levels should also be considered. The lack of clarity regarding the status of many endemic regions has fueled concern on the part of physicians. In settings where only RDTs are used for diagnosis, laboratories need to be aware of the possibility of false negatives when testing samples with >5% rate of HRP2 deletion. Consequently, we investigated the *pfhrp2*/*pfhrp3* status of malaria cases imported from travelers, immigrants, and refugees entering Australia to identify evidence for *pfhrp2* and *pfhrp3* deletions in *P. falciparum* from malaria-endemic countries.

## Methods

### Sample Collection and DNA Extraction

Malaria cases in Australia require that a blood sample be sent to a regional reference laboratory for confirmation and storage. We determined *Plasmodium* spp. infection and species by microscopy (Giemsa-stained thick and thin smears) and confirmed them by PCR (*22*) at the New South Wales Health Pathology Parasitology Laboratory at Westmead Hospital (Westmead, New South Wales, Australia). We aliquoted whole blood from archived *P. falciparum*–positive samples from imported malaria cases (n = 210) and recorded deidentified patient information. We extracted genomic DNA from whole blood using QIAamp mini DNA kits (QIAGEN, https://www.qiagen.com) according to the manufacturer's directions. We assessed DNA quality by subjecting DNA to agarose gel electrophoresis. We measured DNA concentrations by spectrophotometric analysis using a Nanodrop Spectrophotometer ND-1000 (Thermo Fisher, https://www.thermofisher.com) at 260 nm and 280 nm. We included genomic DNA from *P. falciparum* laboratory reference strains in each PCR assay as experimental controls for various *pfhrp2/pfhrp3* deletion statuses: 3D7 (*pfhrp2* +/*pfhrp3* +), HB3 (*pfhrp2* +/*pfhrp3* −), 3BD5 (*pfhrp2* −/*pfhrp3* −), Dd2 (*pfhrp2* −/*pfhrp3* +), and D10 (*pfhrp2* −/*pfhrp3* +). We stored samples at −20°C before use.

### Characterization of *pfhrp2* and *pfhrp3*

We investigated the status (presence/absence) of *pfhrp2* (PlasmoDB gene ID Pf3D7_0831800) and *pfhrp3* (PlasmoDB gene ID Pf3D7_1372200) genes by amplifying across exon 1–exon 2 and exon 2, as previously described (*10*; Appendix Table, https://wwwnc.cdc.gov/EID/article/27/2/19-1410-App1.pdf). Samples were considered to contain the *pfhrp2*- or *pfhrp3*-deleted parasites when there was a negative PCR result for exon 1 or exon 2 of the gene, or both, along with a positive PCR amplifying all 3 single-copy reference genes: merozoite surface protein 1 (*pfmsp1*), merozoite surface protein 2 (*pfmsp2*), and glutamate-rich protein (*pfglurp*). The use of the comparable single copy reference gene assays as a DNA quality control has been observed in several studies reporting *P. falciparum* with and without deletions to show a concordant limit of detection when the genes are present (*23*).

### Rapid Diagnostic Testing

We used SD Bioline (Standard Diagnostics, https://www.globalpointofcare.abbott) HRP2-based malaria RDTs according to the manufacturer's instructions to test thawed whole blood samples that had been determined to contain *P. falciparum* with gene deletions (when whole blood was available). We performed additional tests on *pfhrp2/pfhrp3* positive and negative samples at various parasite densities, and we conducted comparative tests using BinaxNOW (Inverness Medical Binax, https://www.globalpointofcare.abbott) and Carestart (AccessBio, https://accessbiodiagnostics.net) HRP2-based malaria RDTs.

### Microsatellite Analysis

We conducted microsatellite analysis as described elsewhere (*10*). In brief, for each sample originating from Sudan, South Sudan, or Nigeria, we analyzed 7 neutral microsatellite markers (TA1, PolyA, PfPK2, TA109, 2490, 313, and 383). We amplified markers per PCR conditions and primers listed (Appendix Table). We sized amplicons using an ABI 3100 Genetic Analyzer (Applied Biosystems, https://www.thermofisher.com). We scored alleles manually using Peak Scanner Software version 1.0 (Applied Biosystems), including a minimum peak height of 300 relative fluorescence units (Appendix Figure 1). To exclude artifactual stutter peaks (likely polymerase slippage on extended tandem repeats, which are frequent in *Plasmodium* genomes), we disregarded peaks less than one third of the predominant peak (*24*).

### Genetic Diversity Phylogenetic Analysis

We produced a predominant haplotype for each sample based on the sizes of the 7 microsatellite markers. We used PHYLOViZ software (*25*) using a minimum spanning tree approach to compare the genetic diversity and genetic relatedness of the Sudan, South Sudan, and Nigeria cohorts within this study and to compare with parasites from Eritrea and Peru (haplotypes characterized in a previous study [*10*]). We standardized values for the microsatellite marker sizes against the *P. falciparum* 3D7 reference strain. We used FSTAT to calculate microsatellite allele frequencies at each locus, average number of alleles, and expected and observed heterozygosity (*26*).

## Results

### Patient Data Analysis

This study included parasite samples from persons from 25 countries, with most (194/210) originating from countries in Africa. A large proportion of the patient cohort traveled to Australia from Nigeria (n = 30) or Sudan (n = 39); for all other countries of origin, n<20. The clinical state, when known, was predominantly symptomatic travelers who came to the hospital; however, the cohort included ≥15 potentially asymptomatic samples collected during refugee screening (n = 8 within the cohort from South Sudan). The study population was composed of 149 male patients, 53 female patients, and 8 patients with unknown gender; age range was 6 months to 79 years at the time of infection (median age 42 years). Of the samples collected, 75.2% had a parasitemia ranging from 0.01% (≈500 parasites/µL) to 30.1% (1,505,000 parasites/µL), with a mean of 1.34 ± 3.00%, 67,000 parasites/µL; 24.8% had a parasitemia <0.01%. Only 48% of patients (when reported) had used chemoprophylaxis (doxycycline, artemether/lumefantrine, or mefloquine), and instances of concurrent conditions were low (reported in <5% of cases, most commonly dengue fever; Appendix Table 2).

### Presence/Absence of *pfhrp2* and *pfhrp3*

We observed *pfhrp2* or *pfhrp3* deletion (together with positive *pfmsp1*, *pfmsp2*, and *pfglurp* results) in 24 of 210 parasite samples from 12 of 25 countries of origin (Table 1). Results from assays amplifying exon 2 of *pfhrp2* and *pfhrp3* matched the findings from assays amplifying across exon 1–2, suggesting whole rather than partial gene deletion. We observed *pfhrp2*-deleted parasites in 3 samples from Nigeria (3/30, 10%), 4 samples from Sudan (4/39, 10.26%), and 4 samples from South Sudan (4/17, 17.65%) (Figure 1). We observed a single sample with *pfhrp2*-deletion in specimens originating from Ghana (1/17, 5.88%), Kenya (1/18, 5.55%), Mali (1/3, 33.33%), Togo (1/1, 100%), and Zambia (1/5, 20%). We found 3 samples (3/27) of unknown African origins to be *pfhrp2*-deleted.

We observed a single sample with *pfhrp3* deletion per origin in parasites from Sudan (1/39, 2.56%), South Sudan (1/17, 5.88%), Tanzania (1/4, 25%), Sumatra (1/2, 50%), and Peru (1/1, 100%). No parasites were observed to have both the *pfhrp2* and *pfhrp3* gene deletion.

### Rapid Diagnostic Test Results

We tested 20 gene deletion blood samples with HRP2 RDTs (18 *pfhrp2* deleted, 2 *pfhrp3* deleted). Of these, 16 samples produced a positive Pf band using HRP2-based SD BioLine malaria RDTs (14 *pfhrp2* deleted, 2 *pfhrp3* deleted). Of the 16 gene deletion parasites detected by HRP2 RDT, 10 samples had a parasitemia ≥1000/µL. Four of 18 *pfhrp2*-deleted parasites failed to be detected by HRP2 RDTs; 3 of these 4 cases had a parasitemia level <500/µL (Table 2). Only 9 of 20 samples gave a positive pan band; 8 of the 9 had a parasitemia level ≥2,000/µL.

### Microsatellite Analysis

We amplified and scored 7 microsatellite loci for each sample from Sudan, South Sudan, and Nigeria (n = 86), finding 88 unique haplotypes. Two samples shared a haplotype, and we observed 2 instances of multiple haplotype infection. All 7 microsatellite markers were found to be polymorphic. We found a mean of 11 alleles per locus, a range from 6 (microsatellite markers TA109 and 2490) to 16 (microsatellite marker 383) distinct alleles. We found the genetic relatedness of *P. falciparum* populations to correspond weakly with country of origin (represented by small clusters of 2–3 haplotypes), as compared with the population structure of parasites from Eritrea (Figure 2, panel A). Unlike large clustering of *pfhrp2/3*-deleted parasites in Eritrea, *pfhrp2*- or *pfhrp3*-deleted parasites within the cohorts from Sudan, South Sudan, and Nigeria were not found to be more closely related to each other than to *pfhrp2/pfhrp3*-positive parasites within their cohort (Figure 2, panel B). The expected heterozygosity of populations (by country and by deletion status) did not exceed the observed heterozygosity for any cohort.

## Discussion

Increasing availability and use of HRP2-based malaria RDTs in Africa has been pivotal to improving case management over the past 20 years (*27*). Evaluation of compliance to RDT outcomes in sub-Saharan Africa found that protocols often varied among health-care workers, particularly in the case of negative RDT results (*28*). Increased rates of RDT false-negative results may undermine confidence in adherence to World Health Organization guidelines (*29*) and would threaten the recent gains in malaria control.

Several countries relying on HRP2-based malaria RDTs lack molecular data on parasite *pfhrp2* and *pfhrp3* deletion. Sudan and South Sudan had no previously reported data regarding *pfhrp2* and *pfhrp3* status. We observed the presence of both *pfhrp2* and *pfhrp3*-deleted parasites in this study, although no double deletions were detected. The presence of these parasites is not altogether unexpected given the low level of *pfhrp2*- and *pfhrp3*-deleted parasites previously found in natural *P. falciparum* populations (*30*) and the presence of these parasites in neighboring endemic regions (*10*). The levels of *pfhrp2* deletion raise concerns: 10.3% observed from Sudan (mean collection date 2016), and 17.5% from South Sudan (mean collection date 2017–2018) (Figure 1). Mathematical modeling predicts rapid (≈3 years) selection for widespread *pfhrp2*-deletion within a population subjected to HRP2-based RDT use, with a baseline *pfhrp2*-deletion level lower than what we observed

**Table 1.** Summary of *pfhrp2/pfhrp3* gene deletion screening results showing *pfhrp2/pfhrp3* status for *Plasmodium* spp. isolates, by parasite country of origin, Australia*

| Source | Country/strain name | No. cases | pfhrp2/pfhrp3 status, no. (%) | | | % Symptomatic | % Refugee |
|---|---|---|---|---|---|---|---|
| | | | +/– | –/+ | –/– | | |
| Africa | Cameroon | 3 | 0 | 0 | 0 | 66.6 | 33.3 |
| | Gambia | 5 | 0 | 0 | 0 | 100 | 0 |
| | Ghana | 17 | 0 | 1 (0.06) | 0 | 100 | 0 |
| | Ivory Coast | 2 | 0 | 0 | 0 | 100 | 0 |
| | Kenya | 18 | 0 | 1 (0.06) | 0 | 100 | 0 |
| | Madagascar | 1 | 0 | 0 | 0 | 100 | 0 |
| | Malawi | 6 | 0 | 0 | 0 | 33.3 | 66.6 |
| | Mali | 3 | 0 | 1 (33.3) | 0 | 100 | 0 |
| | Nigeria | 30 | 0 | 4 (13.3) | 0 | 100 | 0 |
| | Sierra Leone | 13 | 0 | 0 | 0 | 92.3 | 7.7 |
| | South Africa | 2 | 0 | 0 | 0 | 100 | 0 |
| | South Sudan | 17 | 1 (5.9) | 3 (17.6) | 0 | 52.9 | 47.1 |
| | Sudan | 39 | 1 (2.6) | 4 (10.3) | 0 | 100 | 0 |
| | Sumatra | 2 | 1 (50) | 0 | 0 | 100 | 0 |
| | Togo | 1 | 0 | 1 (100) | 0 | 100 | 0 |
| | Tanzania | 4 | 1 (25) | 0 | 0 | 100 | 0 |
| | Uganda | 2 | 0 | 0 | 0 | 100 | 0 |
| | Zambia | 5 | 0 | 1 (20) | 0 | 100 | 0 |
| | Zimbabwe | 1 | 0 | 0 | 0 | 100 | 0 |
| | Unknown† | 27 | 0 | 3 (11.1) | 0 | 100 | 0 |
| Asia | Cambodia | 1 | 0 | 0 | 0 | 100 | 0 |
| | India | 3 | 0 | 0 | 0 | 100 | 0 |
| | Indonesia | 1 | 0 | 0 | 0 | 100 | 0 |
| | Papua New Guinea | 5 | 0 | 0 | 0 | 100 | 0 |
| | Thailand | 1 | 0 | 0 | 0 | 100 | 0 |
| South America | Peru | 1 | 1 (100) | 0 | 0 | 100 | 0 |
| Laboratory strains | 3D7 | 1 | 0 | 0 | 0 | NA | NA |
| | 3BD5 | 1 | 0 | 0 | 1 (100) | NA | NA |
| | D10 | 1 | 0 | 1 (100) | 0 | NA | NA |
| | Dd2 | 1 | 0 | 1 (100) | 0 | NA | NA |
| | HB3 | 1 | 0 | 1 (100) | 0 | NA | NA |

*NA, not applicable.
†Cases in which clinical notes state African origins but do not specify a country.

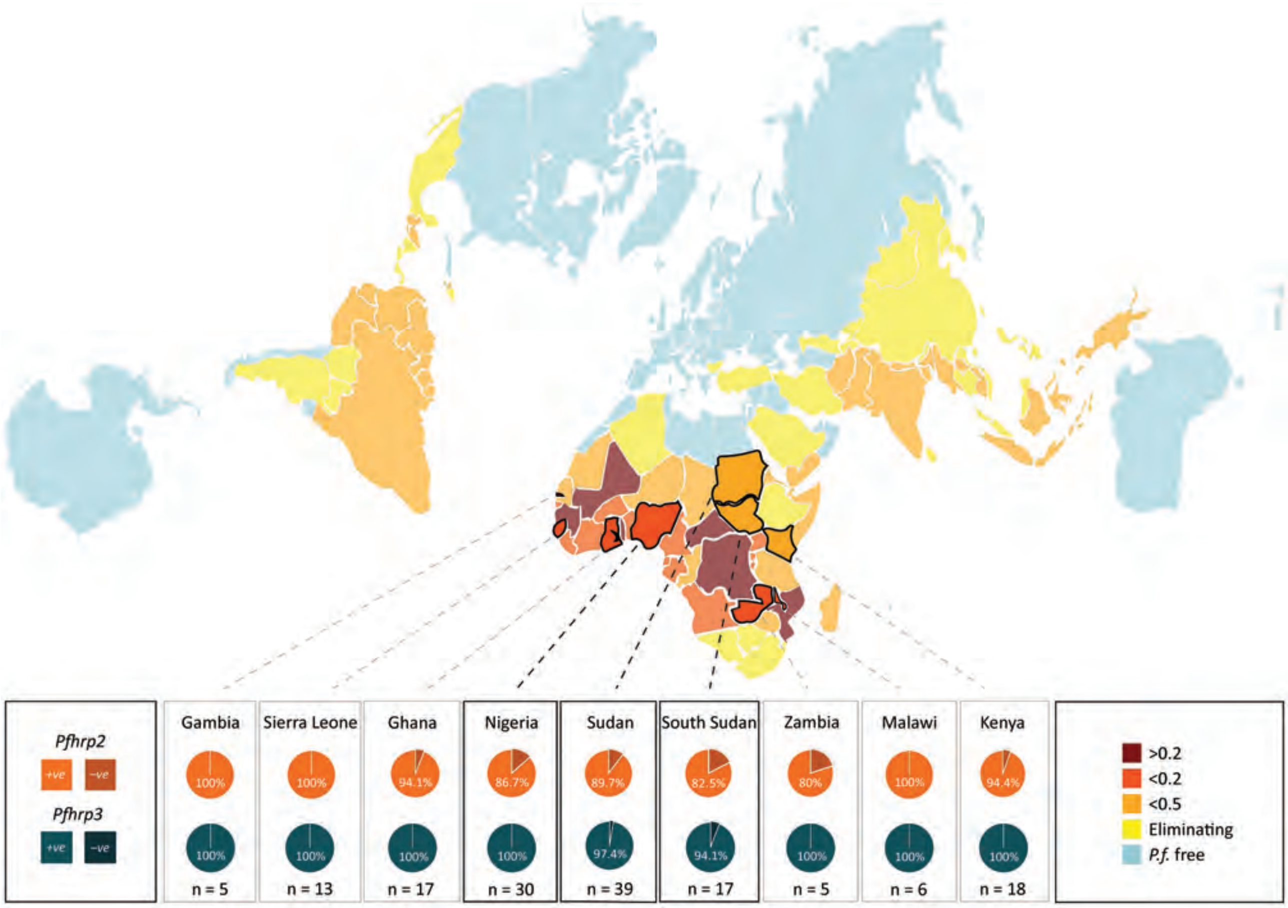


**Figure 1.** Summary of *pfhrp2* and *pfhrp3* deletion key results showing *pfhrp2* and *pfhrp3* deletion results for *Plasmodium* spp. isolates, by parasite country of origin (where n>4), Australia. National *P. falciparum* endemicity depicted is measured as population-weighted mean *P. falciparum* infection rate of children 2–10 years of age, using data available from the Malaria Atlas Project (http://www.map.ox.ac.uk). Data were mapped using the AuthaGraph world map projection to more truthfully visualize the potential paths of dissemination and adjacency of various endemic zones, as this is considered the most accurate representation of land proportions and relative orientations (https://hrcak.srce.hr/185867). *P.f.*, *P. falciparum*.

in parasites originating from Sudan and South Sudan (*31*). In addition, this region of Africa experiences a great deal of human migration (*32*,*33*), notably in Sudan's neighbor Eritrea (where *pfhrp2*/*pfhrp3* double deletion parasites are prevalent [*10*]), increasing the risk for deletion-parasite dissemination.

Samples originating from Nigeria (n = 30) were collected during 2011–2015 (1 sample from 2011 was, to our knowledge, the earliest reported *pfhrp2*-deleted parasite from Nigeria); however, the proportion of *pfhrp2*-deleted parasites observed (13.3%) is similar to the 17% observed in a 2019 study of contemporary parasites from Nigeria (likewise finding no double deletion) (*14*). Countries in western Africa, such as Nigeria, often make use of exclusively HRP2-based RDTs (no pan–*Plasmodium* spp. antigen target); because reliance on *P. falciparum*–only RDTs would further exacerbate the public health consequences of *pfhrp2*/*pfhrp3*-deleted parasites, ongoing monitoring in these locations is warranted (*31*).

No gene-deleted parasites were observed within the cohorts from several countries (Cameroon, Gambia, Côte d'Ivoire, Madagascar, Malawi, Sierra Leone, South Africa, Sumatra, Uganda, Zimbabwe, and all countries in Asia); in 6 countries in Africa, a single gene-deleted parasite was found (*pfhrp2*: Ghana, Kenya, Mali, Togo, and Zambia; *pfhrp3*: Tanzania). The sample sizes are insufficient to comment on regional proportions. Baselines for these regions are undetermined, although a low level of false-negative results using HRP2-based RDTs has been reported in rural Ghana (*34*), and varying levels (0%–30%) of *pfhrp2* deletion have been observed in regions of Kenya (*12*). *pfhrp2/pfhrp3* double-deleted parasites have been observed within the China–Myanmar border area, where baseline *pfhrp2*-deleted parasite proportions were as low as 4% (*17*). The observation of a low level of gene-deleted parasites in this study emphasizes the need to monitor *pfhrp2/pfhrp3* status for early detection of emergent double deletions in the countries of origin.

SD BioLine and Carestart HRP2-based tests consistently produced the same outcome, but those results occasionally differed from results from BinaxNOW, which was less sensitive (Table 2). Subjecting the selected samples to testing with HRP2-based SD BioLine malaria RDTs corroborated the hypothesis that infections by *pfhrp2*-deleted parasites may occasionally fail to be detected, particularly in cases of low parasite density (<1,000/µL) and less-sensitive RDT varieties. Indeed, most *pfhrp2*-negative/*pfhrp3*-positive samples tested positive with HRP2-based SD BioLine malaria RDTs when parasitemia was >1000 parasites/µL, which suggests that HRP3 cross-reaction with HRP2-based tests acts as a failsafe, in cases of adequate parasite density (generally observed to be >1,000 parasites/µL [*14*]). *pfhrp2*-deleted parasites, in the absence of a double deletion, may suffer a loss of sensitivity, but these assays remain a viable interim option for remote and low-resource settings.

*P. falciparum* and pan–*Plasmodium* spp. RDTs failing to detect *pfhrp2/3*-deleted *P. falciparum* through pan–*Plasmodium* spp. pLDH likely reflects the freezing/thawing of whole blood samples, which is reported to degrade the antigen and to cause hemolysis of the blood, leading to sample inhibition (*35*). Freeze-thawing of archived blood is not observed to degrade HRP2 appreciably (*7*).

The main purpose of microsatellite analysis was to compare the genetic relatedness between parasites with gene deletions reported from different areas globally so that we could determine whether parasites with gene deletions were of de novo emergence. For this purpose, we used the same set of microsatellite markers that have been used in other parts of the world, including South America, and included a common control of 3D7 parasite in each run at different laboratories to calibrate outcomes. Microsatellite analyses found high heterogeneity of *P. falciparum* populations within and between Sudan, South Sudan, and Nigeria. The lack of genetic relatedness

**Table 2.** Assessment of HRP2-based SD BioLine RDT for *pfhrp2/pfhrp3* deletion genotypes for *Plasmodium* spp. isolates, by parasite country of origin, Australia*

| Country | Sample ID | Collection year | Parasitemia, % erythrocytes | Parasites/µL blood | Genotype, *pfhrp2/pfhrp3* | BioLine RDT† Pan | BioLine RDT† *Pf* |
|---|---|---|---|---|---|---|---|
| Sudan | BDA1 | 2016 | 0.16 | 8,000 | +/+ | 1 | 2 |
| Sudan | BDA2 | 2016 | 0.79 | 39,500 | –/+ | 1 | 3 |
| Sudan | BDA3 | 2016 | 0.3 | 15,000 | –/+ | 0 | 1 |
| Sudan | BDA4 | 2016 | 0.02 | 1,000 | –/+ | 0 | 1 |
| Sudan | BDA37 | 2014 | <0.01 | NA | –/+ | 0 | 0 |
| South Sudan | BDD4 | 2018 | 1.24 | 62,000 | +/– | 1† | 3 |
| South Sudan | BDC98 | 2018 | 0.5 | 25,000 | –/+ | 1 | 1 |
| South Sudan | BDB94 | 2017 | 0.5 | 25,000 | –/+ | 1 | 1 |
| South Sudan | BDB99 | 2017 | <0.01 | NA | –/+ | 0 | 1† |
| Nigeria | BDA24 | 2015 | 1.1 | 55,000 | –/+ | 0 | 1 |
| Nigeria | BDA92 | 2012 | 4 | 200,000 | –/+ | 1 | 1 |
| Nigeria | BDA91 | 2012 | 2.5 | 125,000 | –/+ | 1 | 1 |
| Nigeria | BDB31 | 2011 | 0.08 | 4,000 | –/+ | 0 | 0 |
| Kenya | BDA42 | 2014 | 0.12 | 6,000 | –/+ | 2 | 1 |
| Kenya | BDB19 | 2011 | <0.01 | NA | +/+ | 0 | 3 |
| Ghana | BDA5 | 2016 | <0.01 | NA | –/+ | 1‡ | 1‡ |
| Tanzania | BDA28 | 2015 | <0.01 | NA | –/+ | 0 | 1 |
| Zambia | BDA31 | 2015 | 0.2 | 10,000 | –/+ | 0 | 1 |
| Togo | BDA50 | 2014 | 0.27 | 13,500 | –/+ | 0 | 1 |
| Peru | BDA52 | 2014 | 0.4 | 20,000 | +/– | 1 | 3 |
| Papua New Guinea | BDB6 | 2012 | 2.81 | 140,500 | +/+ | 1‡ | 2 |
| Papua New Guinea | BDB5 | 2012 | <0.01 | NA | +/+ | 1‡ | 1 |
| Africa | BDA99 | 2012 | 0.46 | 23,000 | +/+ | 0 | 3 |
| Africa | BDA90 | 2012 | 1.2 | 60,000 | +/+ | 0 | 3 |
| Africa | BDA100 | 2012 | <0.01 | NA | +/+ | 0 | 1 |
| Africa | BDB11 | 2011 | <0.01 | NA | –/+ | 0 | 0 |
| Africa | BDB46 | 2010 | 0.01 | 500 | –/+ | 0 | 0 |

*Gray shading signifies a negative result with both the pan-pLDH and pfHRP2 antigen tests on the RDT. Africa indicates unknown country of origin. ID, identification; NA, not applicable; pan, pan–*Plasmodium* spp.; *Pf*, *P. falciparum*; pfHRP2, *Plasmodium falciparum* histidine-rich protein 2; pLDH, *Plasmodium* lactate dehydrogenase; RDT, rapid diagnostic test.
†0–4 result scored by World Health Organization guidelines.
‡Sample results matched outcomes using CareStart Malaria RDT, whereas parasites were not detected by BinaxNOW RDT (Appendix Figures 2, 3, https://wwwnc.cdc.gov/EID/article/27/2/19-1410-App1.pdf).


**Figure 2.** Minimum spanning tree of microsatellite allelic data showing genetic relatedness of *Plasmodium falciparum* populations from Sudan, South Sudan, Nigeria, and Eritrea (A), and *pfhrp2* and *pfhrp3* deletion status of haplotypes (B) (positive: gene present; negative: gene absent). Numbered circles represent specific haplotypes. Plots were generated using PHYLOViZ software (*25*) with a cutoff value of 2 (minimum differences for 2 microsatellite loci) depicted as lines connecting haplotypes and a cutoff value of 3 depicted as haplotype circle arrangements/proximities.

observed between gene-deleted parasites, including between the gene-deleted parasites observed in this study and those analyzed within Eritrea in a previous study (*10*), suggests independent, de novo emergence of parasites with gene deletions. The high level of genetic diversity may reflect the broad geographic and temporal sampling range, as well as the heterogenicity, of natural *P. falciparum* populations in areas with moderate or high transmission intensities.

We analyzed microsatellite peaks for the presence of multiple peaks (indicating multiple unique haplotypes within an individual infection). Three samples had evidence of infection by multiple strains with cocirculating strains potentially present at lower density; all other samples had no secondary peaks exceeding our thresholds for calling (this necessary threshold may prevent the detection of minor alleles). Although it detected few multiclonal infections in this sample set, microsatellite analysis was able to detect a very high level of heterogeneity (88 haplotypes/86 samples) within and between countries, demonstrating the quality of the analysis. The low level of multiple clone infections may reflect the source of samples. For instance, Nigeria is a high-transmission country with a high median multiplicity of infection; however, the Nigerian cohort was composed of travelers or immigrants to Australia who returned home for family events, usually traveling for <2 weeks.

A notable consideration when interpreting results from this study is the opportunity sampling. Using imported *P. falciparum* from travelers provided small sample sizes for most countries of origin and a broad collection timeframe (2010–2018). The sampling timeframe does not capture the true prevalence of *pfhrp2* and *pfhrp3* deletion in contemporary parasite populations or allow us to consider the effects of seasonal profiles (*38*). As a result, the cohort is not representative of cases within endemic regions, which is noteworthy because *pfhrp2/3* deletion needs to be interpreted considering clinical relevance. Deletion proportions between symptomatic and asymptomatic patients within groups were too small and too often status unknown for meaningful analysis. This limitation restricts the conclusions that can be drawn from the screening results, although analyses of imported malaria cases in persons entering Australia has the added benefit of informing local case management.

Because clinicians' notes informed patient data, the specific geographic origins were limited to the country level (and, in 27 cases, were reported only as having origins in Africa). To the best of our knowledge, travelers contracted malaria parasites from their country of origin. However, we cannot exclude the possibility that parasites were contracted from another endemic region. Specimens from South Sudan were obtained primarily from refugees who had reported staying in camps for long periods (3–12 months), including settlements bordering Uganda and Ethiopia. Therefore, parasites may have originated from bordering endemic regions.

Malaria control is complicated in regions bordering other endemic nations by human–vector migration. Border regions are often rural, which may lead to high transmission coupled with inadequate health services (*36*). Similarly, the remoteness, limited resources, and political complexity of border regions often produces suboptimal surveillance responses (*37*). Given the genetic exchange expected between adjacent parasite populations, monitoring of *pfhrp2* and *pfhrp3* for Sudan and South Sudan would ideally be coordinated together with neighboring countries.

In conclusion, analysis of imported *P. falciparum* cases revealed *pfhrp2* and *pfhrp3* deletion from 12 countries, including levels of *pfhrp2*-deleted parasites exceeding 10% from Nigeria, Sudan, and South Sudan, where *pfhrp2*-based malaria RDT failure would constitute a major public health threat. These nations require urgent prevalence surveys and ongoing monitoring for early detection of emergent double deletion parasites.

### About the Author

Ms. Prosser is a PhD candidate at Sydney Medical School at the University of Sydney; she is conducting research at the Westmead Institute for Medical Research Westmead and is a scientific officer at the Australian Defence Force Malaria and Infectious Disease Institute. Her primary research interests are malaria drug resistance and diagnostics, molecular epidemiology, and public health.

### References

1. World Health Organization. World malaria report 2015. Geneva: The Organization; 2016.
2. World Health Organization. Strategy for malaria elimination in the Greater Mekong Subregion: 2015–2030. Manila: WHO Regional Office for the Western Pacific; 2015.
3. World Health Organization. World malaria report 2019. Geneva: The Organization; 2019.
4. Batwala V, Magnussen P, Hansen KS, Nuwaha F. Cost-effectiveness of malaria microscopy and rapid diagnostic tests versus presumptive diagnosis: implications for malaria control in Uganda. Malar J. 2011;10:372. https://doi.org/10.1186/1475-2875-10-372
5. Australian Government Department of Health. Malaria laboratory case definition (LCD) 2018 [updated 2019 Jan 2] [cited 2019 Sep 15]. https://www1.health.gov.au/internet/main/publishing.nsf/Content/cda-phlncd-malaria.htm
6. Jimenez A, Rees-Channer RR, Perera R, Gamboa D, Chiodini PL, Gonzalez IJ, et al. Analytical sensitivity of current best-in-class malaria rapid diagnostic tests. Malar J. 2017;16:128. https://doi.org/10.1186/s12936-017-1780-5
7. Das S, Peck RB, Barney R, Jang IK, Kahn M, Zhu M, et al. Performance of an ultra-sensitive *Plasmodium falciparum* HRP2-based rapid diagnostic test with recombinant HRP2, culture parasites, and archived whole blood samples. Malar J. 2018;17:118. https://doi.org/10.1186/s12936-018-2268-7
8. Donald W, Pasay C, Guintran J-O, Iata H, Anderson K, Nausien J, et al. The utility of malaria rapid diagnostic tests as a tool in enhanced surveillance for malaria elimination in Vanuatu. PLoS One. 2016;11:e0167136. https://doi.org/10.1371/journal.pone.0167136
9. Parr JB, Verity R, Doctor SM, Janko M, Carey-Ewend K, Turman BJ, et al. Pfhrp2-deleted *Plasmodium falciparum* parasites in the Democratic Republic of the Congo: a national cross-sectional survey. J Infect Dis. 2017;216:36–44. https://doi.org/10.1093/infdis/jiw538
10. Berhane A, Anderson K, Mihreteab S, Gresty K, Rogier E, Mohamed S, et al. Major threat to malaria control programs by *Plasmodium falciparum* lacking histidine-rich protein 2, Eritrea. Emerg Infect Dis. 2018;24:462–70. https://doi.org/10.3201/eid2403.171723
11. Amoah LE, Abankwa J, Oppong A. *Plasmodium falciparum* histidine rich protein-2 diversity and the implications for PfHRP 2: based malaria rapid diagnostic tests in Ghana. Malar J. 2016;15:101. https://doi.org/10.1186/s12936-016-1159-z
12. Beshir KB, Sepulveda N, Bharmal J, Robinson A, Mwanguzi J, Busula AO, et al. *Plasmodium falciparum* parasites with histidine-rich protein 2 (*pfhrp2*) and *pfhrp3*

gene deletions in two endemic regions of Kenya. Sci Rep. 2017;7:14718. https://doi.org/10.1038/s41598-017-15031-2
13. Kozycki CT, Umulisa N, Rulisa S, Mwikarago EI, Musabyimana JP, Habimana JP, et al. False-negative malaria rapid diagnostic tests in Rwanda: impact of *Plasmodium falciparum* isolates lacking hrp2 and declining malaria transmission. Malar J. 2017;16:123. https://doi.org/10.1186/s12936-017-1768-1
14. Funwei R, Nderu D, Nguetse CN, Thomas BN, Falade CO, Velavan TP, et al. Molecular surveillance of *pfhrp2* and *pfhrp3* genes deletion in *Plasmodium falciparum* isolates and the implications for rapid diagnostic tests in Nigeria. Acta Trop. 2019;196:121–5. https://doi.org/10.1016/j.actatropica.2019.05.016
15. Agaba BB, Yeka A, Nsobya S, Arinaitwe E, Nankabirwa J, Opigo J, et al. Systematic review of the status of *pfhrp2* and *pfhrp3* gene deletion, approaches and methods used for its estimation and reporting in *Plasmodium falciparum* populations in Africa: review of published studies 2010–2019. Malar J. 2019;18:355. https://doi.org/10.1186/s12936-019-2987-4
16. Bharti PK, Chandel HS, Ahmad A, Krishna S, Udhayakumar V, Singh N. Prevalence of *pfhrp2* and/or *pfhrp3* gene deletion in *Plasmodium falciparum* population in eight highly endemic states in India. PLoS One. 2016; 11:e0157949. https://doi.org/10.1371/journal.pone.0157949
17. Li P, Xing H, Zhao Z, Yang Z, Cao Y, Li W, et al. Genetic diversity of *Plasmodium falciparum* histidine-rich protein 2 in the China-Myanmar border area. Acta Tropica. 2015;152:26–31. https://doi.org/10.1016/j.actatropica.2015.08.003
18. Akinyi S, Hayden T, Gamboa D, Torres K, Bendezu J, Abdallah JF, et al. Multiple genetic origins of histidine-rich protein 2 gene deletion in *Plasmodium falciparum* parasites from Peru. Sci Rep. 2013;3:2797. https://doi.org/10.1038/srep02797
19. Gendrot M, Fawaz R, Dormoi J, Madamet M, Pradines B. Genetic diversity and deletion of *Plasmodium falciparum* histidine-rich protein 2 and 3: a threat to diagnosis of *P. falciparum* malaria. Clin Microbiol Infect. 2019;25:580–5. https://doi.org/10.1016/j.cmi.2018.09.009
20. World Health Organization. False-negative RDT results and implications of new reports of *P. falciparum* histidine-rich protein 2/3 gene deletions. WHO reference no. WHO/HTM/GMP/2017.18. Geneva: The Organization; 2017.
21. World Health Organization, Foundation for Innovative New Diagnostics, United States Centers for Disease Control and Prevention. Malaria rapid diagnostic test performance. Results of WHO product testing of malaria RDTs: round 7 (2015–2016). Geneva: The Organization; 2017.
22. Padley D, Moody AH, Chiodini PL, Saldanha J. Use of a rapid, single-round, multiplex PCR to detect malarial parasites and identify the species present. Ann Trop Med Parasitol. 2003;97:131–7. https://doi.org/10.1179/000349803125002977
23. Cheng Q, Gatton ML, Barnwell J, Chiodini P, McCarthy J, Bell D, et al. *Plasmodium falciparum* parasites lacking histidine-rich protein 2 and 3: a review and recommendations for accurate reporting. Malar J. 2014;13:283. https://doi.org/10.1186/1475-2875-13-283
24. Anderson TJ, Haubold B, Williams JT, Estrada-Franco JG, Richardson L, Mollinedo R, et al. Microsatellite markers reveal a spectrum of population structures in the malaria parasite *Plasmodium falciparum*. Mol Biol Evol. 2000;17:1467–82. https://doi.org/10.1093/oxfordjournals.molbev.a026247
25. Ribeiro-Goncalves B, Francisco AP, Vaz C, Ramirez M, Carrico JA. PHYLOViZ Online: web-based tool for visualization, phylogenetic inference, analysis and sharing of minimum spanning trees. Nucleic Acids Res. 2016;44: W246–51. https://doi.org/10.1093/nar/gkw359
26. Goudet J. FSTAT (version 1.2): a computer program to calculate F-statistics. J Hered. 1995;86:485–6. https://doi.org/10.1093/oxfordjournals.jhered.a111627
27. World Health Organization. World Malaria Report 2017. Geneva: The Organization; 2017.
28. Boyce MR, O'Meara WP. Use of malaria RDTs in various health contexts across sub-Saharan Africa: a systematic review. BMC Public Health. 2017;17:470. https://doi.org/10.1186/s12889-017-4398-1
29. Altaras R, Nuwa A, Agaba B, Streat E, Tibenderana JK, Strachan CE. Why do health workers give anti-malarials to patients with negative rapid test results? A qualitative study at rural health facilities in western Uganda. Malar J. 2016;15:23. https://doi.org/10.1186/s12936-015-1020-9
30. Baker J, McCarthy J, Gatton M, Kyle DE, Belizario V, Luchavez J, et al. Genetic diversity of *Plasmodium falciparum* histidine-rich protein 2 (PfHRP2) and its effect on the performance of PfHRP2-based rapid diagnostic tests. J Infect Dis. 2005;192:870–7. https://doi.org/10.1086/432010
31. Gatton ML, Dunn J, Chaudhry A, Ciketic S, Cunningham J, Cheng Q. Implications of parasites lacking *Plasmodium falciparum* histidine-rich protein 2 on malaria morbidity and control when rapid diagnostic tests are used for diagnosis. J Infect Dis. 2017;215:1156–66. https://doi.org/10.1093/infdis/jix094
32. Crawley H. Migration: refugee economics. Nature. 2017; 544:26–7. https://doi.org/10.1038/544026a
33. Neumann K, Hermans F. What drives human migration in Sahelian countries? A meta-analysis. Popul Space Place. 2017;23:e1962. https://doi.org/10.1002/psp.1962
34. Quakyi IA, Adjei GO, Sullivan DJ, Jr., Laar A, Stephens JK, Owusu R, et al. Diagnostic capacity, and predictive values of rapid diagnostic tests for accurate diagnosis of *Plasmodium falciparum* in febrile children in Asante-Akim, Ghana. Malar J. 2018;17:468. https://doi.org/10.1186/s12936-018-2613-x https://doi.org/10.1186/s12936-018-2613-x
35. Hagen RM, Hinz R, Tannich E, Frickmann H. Comparison of two real-time PCR assays for the detection of malaria parasites from hemolytic blood samples—short communication. Eur J Microbiol Immunol (Bp). 2015;5:159–63. https://doi.org/10.1556/1886.2015.00006
36. Abakar MF, Schelling E, Béchir M, Ngandolo BN, Pfister K, Alfaroukh IO, et al. Trends in health surveillance and joint service delivery for pastoralists in West and Central Africa. Rev Sci Tech. 2016;35:683–91. https://doi.org/10.20506/rst.35.2.2549
37. World Health Organization. Evidence review group on border malaria: meeting report. World Health Organization, 2018 Malaria Policy Advisory Committee Meeting, October 17–19, 2018. Report no. WHO/CDS/GMP/MPAC/2018.13. Geneva: The Organization; 2018.
38. Watson OJ, Verity R, Ghani AC, Garske T, Cunningham J, Tshefu A, et al. Impact of seasonal variations in *Plasmodium falciparum* malaria transmission on the surveillance of *pfhrp2* gene deletions. eLife. 2019;8:e40339. https://doi.org/10.7554/eLife.40339

Address for correspondence: Christiane Prosser, Centre for Infectious Diseases and Microbiology, Westmead Institute for Medical Research, 176 Hawkesbury Rd, Westmead, Sydney, NSW 2145, Australia; email: christiane.prosser@sydney.edu.au

# Hepatitis C Virus Transmission Clusters in Public Health and Correctional Settings, Wisconsin, USA, 2016–2017[1]

Karli R. Hochstatter,[2] Damien C. Tully,[2] Karen A. Power, Ruth Koepke, Wajiha Z. Akhtar, Audrey F. Prieve, Thomas Whyte, David J. Bean, David W. Seal, Todd M. Allen,[3] Ryan P. Westergaard[3]

Ending the hepatitis C virus (HCV) epidemic requires stopping transmission among networks of persons who inject drugs. Identifying transmission networks by using genomic epidemiology may inform community responses that can quickly interrupt transmission. We retrospectively identified HCV RNA–positive specimens corresponding to 459 persons in settings that use the state laboratory, including correctional facilities and syringe services programs, in Wisconsin, USA, during 2016–2017. We conducted next-generation sequencing of HCV and analyzed it for phylogenetic linkage by using the Centers for Disease Control and Prevention Global Hepatitis Outbreak Surveillance Technology platform. Analysis showed that 126 persons were linked across 42 clusters. Phylogenetic clustering was higher in rural communities and associated with female sex and younger age among rural residents. These data highlight that HCV transmission could be reduced by expanding molecular-based surveillance strategies to rural communities affected by the opioid crisis.

Hepatitis C virus (HCV) infections have sharply increased in the United States, where an estimated 2.4 million persons are living with chronic infection (*1*). In 2013, ≈19,368 persons died of HCV-related complications, exceeding the number of deaths from all other nationally notifiable infectious diseases combined (*2*). During 2004–2014, prevalence of HCV increased by 2-fold, a direct result of the opioid epidemic and associated increases in the sharing of contaminated injection drug use equipment (*3*). Because the intersecting epidemics of opioid injection and infectious diseases are complex and dynamic, implementing community-specific comprehensive prevention services remains challenging.

Public health experts are increasingly using molecular-based surveillance techniques to identify and control emerging outbreaks (*4*–*7*). For example, the Centers for Disease Control and Prevention (CDC) has scaled up use of molecular HIV surveillance (*8*); however, the application of such programs for HCV surveillance has lagged. For molecular HCV surveillance and outbreak investigation, CDC developed a public health tool, Global Hepatitis Outbreak and Surveillance Technology (GHOST), which uses next-generation sequencing methods (*9*). GHOST integrates a suite of computational tools to accurately detect possible HCV transmission clusters from next-generation sequencing data in a simple fashion, regardless of the user's level of expertise.

During 2016–2017, the rate of opioid overdose in Wisconsin increased by 109%, the steepest increase observed in any US state and nearly 3 times the average national increase over that period (*10*). This sharp increase in opioid use was accompanied by substantial increases in HCV incidence. During

Author affiliations: Columbia University, New York, New York, USA (K.R. Hochstatter); University of Wisconsin School of Medicine and Public Health, Madison, Wisconsin, USA (K.R. Hochstatter, R. Koepke, W.Z. Akhtar, R.P. Westergaard); London School of Hygiene and Tropical Medicine, London, UK (D.C. Tully); Ragon Institute of MGH, MIT and Harvard, Cambridge, Massachusetts, USA (D.C. Tully, K.A. Power, D.J. Bean, T.M. Allen); Wisconsin Department of Health Services, Madison (R. Koepke, R.P. Westergaard); Wisconsin State Laboratory of Hygiene, Madison (A.F. Prieve, T. Whyte); Tulane University School of Public Health and Tropical Medicine, New Orleans, Louisiana, USA (D.W. Seal)

DOI: https://doi.org/10.3201/eid2702.202957

[1]The methods described in this article, along with preliminary results from the first 231 specimens analyzed, were presented in poster format at the 8th International Conference on Hepatitis Care in Substance Users; 2019 Sep 11–13; Montreal, Quebec, Canada.

[2]These first authors contributed equally to this article.

[3]These senior authors contributed equally to this article.

2011–2015, an average of 2,955 new HCV diagnoses were reported annually; during the previous 5-year period, the average was 2,396. As a result of recent injection drug use, the rate of new PCR-confirmed HCV diagnoses among persons 15–29 years of age more than doubled during that period, from 40 to 87 cases/100,000 population (*11*).

In this study, we integrated public heath surveillance and molecular analyses with GHOST to identify putative HCV transmission clusters among persons most likely infected through injection drug use during a period of expanded HCV transmission (*12*). We also investigated the network characteristics among members of this high-risk group.

## Materials and Methods

### Study Setting and Population

All HCV-positive test results in Wisconsin are routinely reported to the Wisconsin Electronic Disease Surveillance System (WEDSS), a secure, Internet-based health information system used for the reporting, investigation, and surveillance of communicable diseases in Wisconsin. Blood samples collected for HCV RNA confirmatory testing at sites supported by the Wisconsin Division of Public Health (e.g., syringe services programs [SSPs], correctional facilities, local health departments, community-based organizations, and public health clinics) are processed at the Wisconsin State Laboratory of Hygiene and stored for 5 years. Approximately 15% of all HCV cases reported to WEDSS represent persons who underwent fee-exempt HCV RNA confirmatory testing through the state laboratory. The cohort of persons tested comprised primarily younger persons with a history of injection drug use, resulting from the types of organizations that submit test results to the state laboratory.

We identified persons confirmed to have an HCV RNA–positive sample analyzed at the state laboratory and reported to WEDSS for the first time during 2016–2017 by 2 methods. First, we identified 241 persons residing in rural catchment areas. Of the 72 counties in Wisconsin, 51 were included in the rural catchment area and selected on the basis of participation in an ongoing federally funded research program. These counties were classified as rural because they were served by 1 of the 6 rural offices of the statewide SSP. Second, to improve network completeness and compare the extent of clustering between rural and nonrural populations, we identified 2 additional cohorts: 54 persons residing in nonrural catchment areas and 164 residing in correctional facilities. Because resource limitations prevented data collection from all HCV-infected persons in nonrural catchment areas and correctional facilities, we included those who were considered likely to represent recent or acute infections because they either had acute HCV when reported to WEDSS or were 15–39 years of age at diagnosis with an HCV viral load >1,000,000 IU/L. The nonrural catchment area included the other 21 Wisconsin counties served by 1 of the 4 SSP urban offices, and the correctional cohort included those incarcerated in a state correctional setting (i.e., state prison) at the time of testing.

### Specimen Processing

Per standard protocol, the state laboratory stores serum remaining after completion of HCV antibody and RNA PCR testing at -80°C. Specimens corresponding to the HCV RNA–positive persons identified in WEDSS were retrieved and shipped to the Ragon Institute of MGH, MIT and Harvard (Cambridge, MA, USA) for virus sequencing.

### Nucleic Acid Extraction and PCR Amplification

RNA was isolated from 140 µL of plasma by using a QIAamp Viral RNA Mini Kit (QIAGEN, https://www.qiagen.com). A 1-step reverse transcription PCR (RT-PCR) was performed to amplify a 305-bp segment at the E1/E2 junction of the HCV genome (H77 positions 1301–1606), which contains the hypervariable region (HVR) 1 (*13*). This region was chosen for its high variability and its ability to reliably detect transmission events in outbreak settings (*14*). The first round of RT-PCR consisted of an Illumina adaptor-specific portion, a sample-specific barcode segment, and an HCV HVR–specific primer segment F1-GTGACTGGAGTTCAGACGTGTGCTCTTCC-GATCT-NNNNNNNNNN-GGA-TAT-GAT-GAT-GAA-CTG-GT and R1-ACA-CTC-TTT-CCC-TAC-ACG-ACG-CTC-TTC-CGA-TCT-NNNNNNNNNN-ATG-TGC-CAG-CTG-CCG-TTG-GTG-T at a final concentration of 4 pM. Amplification conditions (SuperScript III One-Step RT-PCR System with Platinum Taq High Fidelity [ThermoFisher, https://www.thermofisher.com]) were cDNA synthesis for 30 min at 55°C followed by heat denaturation at 95°C for 2 min. PCR amplification conditions were 40 cycles of denaturation (94°C for 10 s), annealing (55°C for 10 s), and extension (68°C for 10 s) with a final extension at 68°C for 5 min. Amplified products were run on 1% agarose gel and either PCR purified with a QIAquick PCR Purification Kit (QIAGEN) or gel extracted and purified by using a PureLink Quick Gel Extraction Kit (Invitrogen, https://www.thermofisher.com). A second round of limited cycle PCR (94°C for 2 min, [94°C for 15 s; 55°C for 30 s; 68°C for 30 s] × 8 cycles, 68°C for 5 min) was performed to add barcode-specific indexes and sequencing-specific adapters and primers to each sample to allow for multiplexing as well as internal controls for cross-contamination. Negative controls were introduced at each stage, and all PCR procedures were performed under PCR clean room conditions by using established protocols. Indexed samples were purified by solid phase reversible immobilization (SPRI) 2 times at a bead-to-DNA ratio of 0.7× to remove excess primer dimer and short fragments that can interfere with the sequencing process.

### Deep Sequencing and Analysis

Resulting PCR amplicons were quantified by using a PicoGreen kit (Invitrogen) on a QuantiFluor ST fluorometer (Promega, https://www.promega.com), and the integrity of the fragment was evaluated by using a 2100 Bioanalyzer (Agilent, https://www.agilent.com). Samples were pooled and sequenced on an Illumina MiSeq platform (https://www.illumina.com) by using a 2 × 250–bp v2 Nano reagent kit. A sequence library consisted of 8–16 specimens, including 1 negative control for every 7 serum specimens. Paired-end reads were subject to stringent cleaning and quality control criteria as outlined previously (*15*–*17*). Duplicate reads were removed by using default settings with FastUniq version 1.1 (*18*) and quality trimmed by using Trimmomatic version 0.36 (*19*). Viral contigs were generated by using default settings with Vicuna version 1.1 (*20*), and a de novo consensus assembly was generated by using Viral Finishing and Annotation Toolkit (V-FAT) version 1.1 (https://www.broadinstitute.org/viral-genomics/v-fat). Read data are available from the National Center for Biotechnology Information Read Archive (https://www.ncbi.nlm.nih.gov) under BioProject accession no. PRJNA661611.

### Phylogenetic Reconstruction

We aligned the consensus sequences by using MEGA version 6.0 (*21*) and IQ-TREE version 1.6 (*22*). We then constructed a maximum-likelihood phylogenetic tree with 1,000 ultrafast bootstrap replicates (*23*).

### HCV Transmission Network Analyses

We uploaded Illumina paired-end reads to GHOST and subjected them to automatic quality control criteria. In brief, read pairs were filtered out if a read had >3 Ns (N indicates that software was not able to make a basecall for this base) or a length <185 bp. Each identifier on forward and reverse reads was examined, and the pair was discarded if either identifier was not an exact match to a given list of valid identifiers. We discarded pairs containing valid identifiers if they were not a constituent of the majority identifier tuple. If ≥11% of the read pairs contained valid identifiers that were not the majority tuple, we discarded the entire sample without further processing. Random subsampling of 5,000–20,000 read pairs was undertaken, and primer sequences were located in each read, allowing for a combined error total of ≤3. Read pairs were discarded when the primer could not be found. Remaining read pairs were then unified in a single error-corrected sequence, and only those sequences with a nonsense-free reading frame were collapsed into unique occurences with associated frequencies. Further methodologic details on quality filtering can be found elsewhere (*9*,*24*). We examined transmission links that represent the genetic similarity among virus populations from infected persons. For each case, we compared the intrahost populations between infected persons and calculated the genetic distance (defined as the Hamming distance) between their closest haplotypes. If the genetic distance is smaller than an empirically defined threshold of 3.77%, then samples are considered to be genetically related and indicate a transmission cluster (*14*). To further analyze each cluster's genetic relationship, we built k-step networks of intrahost HCV HVR1 variants, as previously described (*9*).

### Data Collection

Variables routinely reported to WEDSS for HCV-positive persons include age, sex, race/ethnicity, HCV-positive antibody and RNA test date(s), testing site(s), and residential address. In addition, persons tested by the multisite SSP provide risk information per standard HCV testing procedures. Reporting of risk information is voluntary. When possible, local health department staff members gather risk information from the healthcare provider or directly from patients and enter it into WEDSS. Persons with HCV originally reported from state correctional facilities are not interviewed by local public health officials, and risk information for them is typically not available. When risk information was missing from WEDSS, we were unable to determine whether a patient answered "no" to a risk behavior or whether the data were missing. For persons who reported risk behaviors, we assessed whether they ever engaged in injection drug use, shared injection equipment, were men who have sex with men (MSM), or were ever incarcerated. Persons were considered ever incarcerated if any result for an HCV test conducted at a state correctional facility was reported to WEDSS or if the person reported (on risk information forms) having ever been incarcerated. Because availability of risk information depends on the type of facility where the person was tested, we present demographic characteristics and risk behaviors by type of testing facility: SSP, correctional facility, local health department, or other public venue. Other venues include a limited number of community health centers, public health clinics, community-based organizations, and safety net hospitals. Local jails also were considered other venues because only 2 persons were tested in jails and local jails are more representative of where the person resides, whereas persons may be placed in other facilities anywhere across the state regardless of their county of residence.

This study was approved by the University of Wisconsin Health Sciences Institutional Review Board, which granted a waiver of informed consent, and the Massachusetts General Hospital Institutional Review Board. Data Use Agreements and a Materials Transfer Agreement were established between the University of Wisconsin, Wisconsin Division of Public Health, the state laboratory, and the Ragon Institute of MGH, MIT and Harvard.

### Statistical Analyses

To compare clustering by demographics and risk behaviors, we conducted $\chi^2$, Fisher exact, Student *t*, and analysis of variance tests by using Stata SE 16 (StataCorp, https://www.stata.com). Because sampling techniques differed in rural and nonrural catchment areas and the characteristics assessed were strongly determined by which catchment area persons were in, and because persons tested in correctional facilities could come from either rural or nonrural areas of the state, we compared persons who clustered with those who did not cluster, stratified by 3 groups based on testing location: the rural catchment area, the nonrural catchment area, and correctional facilities. We also compared characteristics between rural catchment area–only clusters, nonrural catchment area–only clusters, corrections-only clusters, and clusters that contained persons from >1 group. Statistical significance was determined by using $\alpha<0.05$.

## Results

### Study Sample

During 2016–2017, a total of 459 persons tested by the Wisconsin State Laboratory of Hygiene were HCV RNA positive for the first time. For those 459 persons, sufficient ($\geq$200 μL) residual serum was stored to enable virus sequencing for 424 (92.4%). Of these, virus was successfully amplified, sequenced, and passed GHOST quality control metrics for 379 (89.4%) samples. Among the samples that failed, 23 (5.4%) failed PCR and 22 (5.2%) failed GHOST quality control metrics. After quality control, the median number of error-corrected reads/person was 16,740 (interquartile range 13,302–18,262) and the median number of haplotypes was 3,322 (interquartile range 2,479–4,345).

### Patient Demographic Characteristics and Risk Behaviors

Among the 379 persons whose specimens were successfully analyzed by GHOST, positive HCV results were first obtained at an SSP for 119 (31.4%), a correctional facility for 154 (40.6%), a local health department for 38 (10.0%), and other settings for 68 (17.9%) (Table 1). The study population was primarily non-Hispanic white (83.9%), 18–39 years of age (90.8%), and male (75.5%). Self-reported injection drug use was documented for 177 (46.7%) persons. Of these, 145 (81.9%) self-reported having ever shared injection equipment. MSM status was reported by 8 (2.1%) persons. Most of the study population (335 [88.4%]) had been incarcerated; 154 received their first HCV-positive test result while at a correctional facility, and 180 reported a history of incarceration.

Among the 379 persons, 171 (45.1%) resided in the rural catchment area, of which 67 (39.2%) clustered; 54 (14.3%) resided in the nonrural catchment area, of which 14 (25.9%) clustered; and 154 (40.6%) resided in correctional facilities, of which 45 (29.2%) clustered. Among the 171 persons in the rural catchment area, women were significantly more likely to cluster (49%) than men (33%) ($p = 0.04$), and persons who clustered were significantly younger (mean age 28.7 years) than persons who did not cluster (mean age 34.1 years) ($p = 0.0001$). For in the nonrural catchment area or corrections groups, we found no statistically significant differences between those who clustered and those who did not cluster.

### Phylogenetic Analysis

We genetically characterized HCV strains by using HVR1 consensus sequences derived from isolates from all 379 persons. Phylogenetic analysis demonstrated a predominance of genotypes 1a (n = 255, 67.3%) and 3a (n = 88, 23.2%), followed by 2b (n = 22, 5.8%), 1b (n = 9, 2.4%), 2a (n = 4, 1.1%), and 4a (n = 1, 0.3%) (Figure 1).

### HCV Transmission Linkages

GHOST detected 42 clusters comprising 126 persons for an overall clustering rate of 33% (Figure 2). Cluster sizes ranged from 2 to 11 persons. Transmission net-

**Table 1.** Demographics and risk factor information, by type of testing facility, for all 379 persons tested for HCV while in public health or correctional settings, Wisconsin, USA, 2016–2017*

| | | Setting of first HCV-positive test result, no. (%) | | | |
|---|---|---|---|---|---|
| Variable | Overall no. (%) | Syringe services program | Corrections setting | Local health department | Other |
| Total | 379 (100) | 119 (31.4) | 154(40. 6) | 38 (10.0) | 68 (17.9) |
| Year first reported to WEDSS | | | | | |
| 2016 | 222 (58.6) | 68 (57.1) | 87 (56.5) | 22 (57.9) | 45 (66.2) |
| 2017 | 157 (41.4) | 51 (42.9) | 67 (43.5) | 16 (42.1) | 23 (33.8) |
| Age, y | | | | | |
| 18–29 | 190 (50.1) | 57 (47.9) | 77 (50.0) | 19 (50.0) | 37 (54.4) |
| 30–39 | 154 (40.6) | 39 (32.8) | 75 (48.7) | 16 (42.1) | 24 (35.3) |
| ≥40 | 35 (9.2) | 23 (19.3) | 2 (1.3) | 3 (7.9) | 7 (10.3) |
| Race/ethnicity | | | | | |
| Non-Hispanic white | 318 (83.9) | 103 (86.6) | 127 (82.5) | 34 (89.5) | 54 (79.4) |
| Hispanic or Latino | 18 (4.8) | 4 (3.4) | 7 (4.6) | 2 (5.3) | 5 (7.4) |
| American Indian or Alaska Native | 21 (5.5) | 7 (5.9) | 9 (5.8) | 1 (2.6) | 4 (5.9) |
| Asian | 2 (0.5) | 0 | 1 (0.7) | 0 | 1 (1.5) |
| Non-Hispanic black or African American | 12 (3.2) | 4 (3.4) | 5 (3.3) | 1 (2.6) | 2 (2.9) |
| Other/unknown | 8 (2.1) | 1 (0.8) | 5 (3.3) | 0 | 2 (2.9) |
| Sex | | | | | |
| F | 93 (24.5) | 44 (36.9) | 14 (9.1) | 13 (34.2) | 22 (32.3) |
| M | 286 (75.5) | 75 (63.0) | 14 (90.9) | 25 (65.8) | 46 (67.7) |
| Ever injected drugs | | | | | |
| Yes | 177 (46.7) | 98 (82.4) | 16 (10.4) | 32 (84.2) | 31 (45.6) |
| No or unknown | 202 (53.3) | 21 (17.7) | 138 (89.6) | 6 (15.8) | 37 (54.4) |
| Ever shared works | | | | | |
| Yes | 145 (38.3) | 88 (74.0) | 10 (6.5) | 29 (76.3) | 18 (26.5) |
| No, unknown, or NA | 234 (61.7) | 31 (26.1) | 144 (93.5) | 9 (23.7) | 50 (73.5) |
| MSM | | | | | |
| Yes | 8 (2.1) | 4 (3.4) | 0 | 2 (5.3) | 2 (2.9) |
| No or unknown | 371 (97.9) | 115 (96.6) | 154 (100) | 36 (94.7) | 66 (97.1) |
| Ever incarcerated | | | | | |
| Yes | 335 (88.4) | 92 (77.3) | 154 (100) | 34 (89.5) | 54 (79.7) |
| No or unknown | 44 (11.6) | 27 (22.7) | 0 | 4 (10.5) | 14 (20.6) |

*HCV, hepatitis C virus; MSM, men who have sex with men; NA, not applicable; WEDSS, Wisconsin Electronic Disease Surveillance System.

works were composed of mostly dyads (n = 23, 54.8%), followed by groups of 3 (n = 9, 21.4%), 4 (n = 3, 7.1%), and 5 (n = 6, 14.3%). The largest cluster involved 11 persons, all infected with genotype 3a. Among those 11 persons, 5 received their first HCV-positive test result from the same local health department and 3 from the same SSP. Also among those 11 persons, evidence of past injection drug use was available for 7 persons, 8 were male, and all 11 were non-Hispanic white with a history of incarceration.

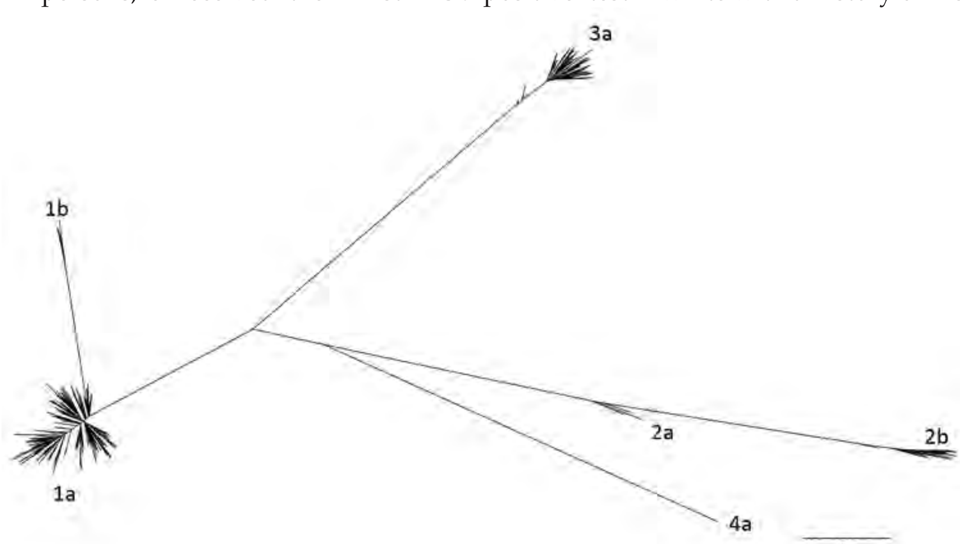


**Figure 1.** Maximum-likelihood phylogenetic tree of hepatitis C virus hypervariable region 1 consensus sequences from samples from 379 persons in public health and corrections settings, Wisconsin, USA, 2016–2017. The breadth of genetic diversity is shown, and genotypes are labeled. Scale bar indicates nucleotide subsitutions per site.

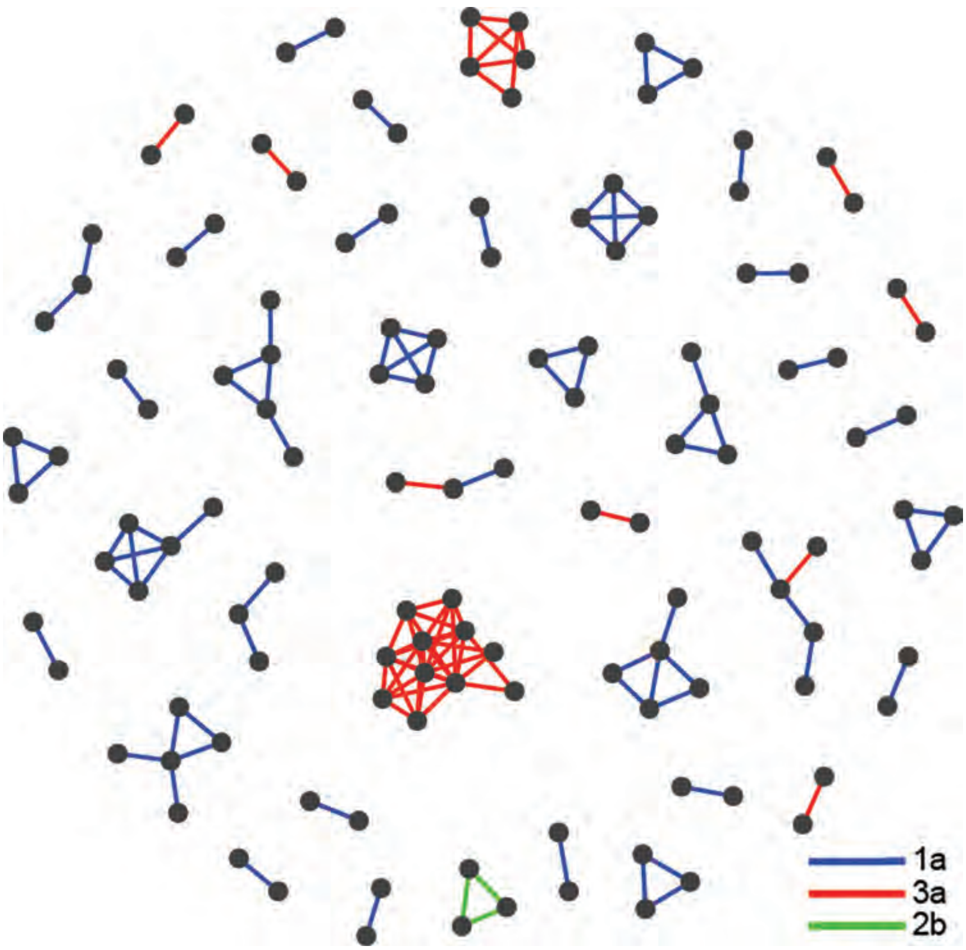


**Figure 2.** Hepatitis C virus (HCV) transmission network among persons in public health and corrections settings, Wisconsin, USA, 2016–2017, showing 42 clusters identified by Global Hepatitis Outbreak and Surveillance Technology (GHOST). Each node represents an HCV-infected person for whom HCV sequence data were generated. A transmission link is denoted as a line connecting persons where the minimal Hamming distance between sequences is smaller than the previously validated genetic threshold of 3.77%. Lines connecting clusters are colored according to genotype.

Among the 42 clusters identified, none comprised only persons residing in the nonrural catchment area, 12 comprised only persons residing in the rural catchment area (n = 34), 7 comprised only persons from corrections settings (n = 15), and 23 comprised persons from >1 group (n = 77). Rural catchment area–only clusters were more likely to comprise a higher percentage of women (47.1%) compared with 6.7% of corrections-only clusters and 27.3% of mixed clusters; this finding probably results from the higher incarceration rate among men. We found no other significant differences in demographics between rural-only, corrections-only, and mixed clusters. We were unable to compare risk behaviors between these cluster types because limited risk behavior data were available for corrections settings–only clusters, there were no urban-only clusters, and mixed clusters comprised many persons from corrections settings.

### Intrahost Genetic Variation within Transmission Clusters

GHOST analysis of the intrahost HVR1 variants revealed that 5 (1.3%) of the 379 persons were infected with multiple strains of HCV (Table 2). To further describe the nature of HCV transmission across clusters, we examined the population structure of HVR1 variants to address whether the same virus variant was shared among HCV-infected

**Table 2.** Characteristics of samples with mixed hepatitis C virus genotypes, collected from persons in public health or correctional settings, Wisconsin, USA, 2016–2017

| Sample/person no. | Major genotype (%) | Minor genotype (%) | Risk factor* |
|---|---|---|---|
| 116 | 1a (96.75) | 2a (3.25) | Unknown |
| 63 | 1a (99.38) | 3a (0.62) | Ever injected drugs, ever shared works |
| 318 | 1a (96.18) | 3a (3.82) | Unknown |
| 338 | 1a (99.72) | 6f (0.28) | Ever injected drugs |
| 306 | 1a (98.57) | 2b (0.59) | Ever injected drugs, ever shared works |

*When this evidence is available, the person can be classified as man who has sex with men, ever injected drugs, or ever shared works.

persons as previously described (*14*). Although it is not possible to illustrate the k-step networks for each sample, we highlight representative examples of clusters. One cluster comprised 3 persons (nos. 372, 338, and 362), and persons 338 and 362 harbored little viral intrahost genetic variation and shared 19 viral variants (modified Hamming distance = 0) (Figure 3, panel A). The third person, no. 372, was infected with many virus variants with a single subpopulation that is genetically similar to variants found in persons 338 (Figure 3, panel B) and 362 (Figure 3, panel C). Another representative cluster comprised a simple dyad of persons (nos. 84 and 86) who shared a virus variant (modified Hamming distance = 0.37) with only a minor difference between each (Figure 4, panel A). In contrast, the cluster of persons 281 and 367 shared a more distantly related variant (modified Hamming distance = 3.18) (Figure 4, panel B).

## Discussion

This study demonstrates the ability to link statewide public health surveillance to HCV transmission clusters identified by GHOST. The 33% rate of clustering that we found among key affected populations in Wisconsin is comparable to that found in Vancouver, British Columbia, Canada (where 31% of persons who inject drugs [PWIDs] cluster), and Baltimore, Maryland, USA (where 46% of PWIDs cluster) (*25*,*26*). However, those prior studies included only PWIDs from their respective metropolitan areas. Our study included both urban and rural populations. We found a higher rate of clustering in the rural catchment area, and rural persons who clustered were younger, a finding that aligns with the literature describing the particular burden of HCV on young persons in rural communities (*27*,*28*). Moreover, these data highlight that the increasing rurality of opioid injection and HCV transmission among young PWIDs could be better supported by the expansion of molecular-based surveillance strategies to reduce transmission. The availability of transmission networks would enable targeting of the underlying contact network structure such that persons who are highly central within a network contribute much more to infection than those on the periphery. This type of network-based disruption strategy has been shown to reduce incidence more than randomly targeted prevention strategies (*29*).

Use of molecular epidemiologic methods to investigate transmission of infectious diseases addresses many limitations of traditional contact tracing, for which data collection is often time-intensive and results may be subject to recall and social desirability biases. Contact tracing among persons who engage in illegal activity is especially challenging because these persons are often reluctant to disclose injecting behaviors or name injecting partners because of stigma or fear of criminal repercussions (*30*). Therefore, identifying transmission linkages with GHOST can support more targeted contact tracing strategies.

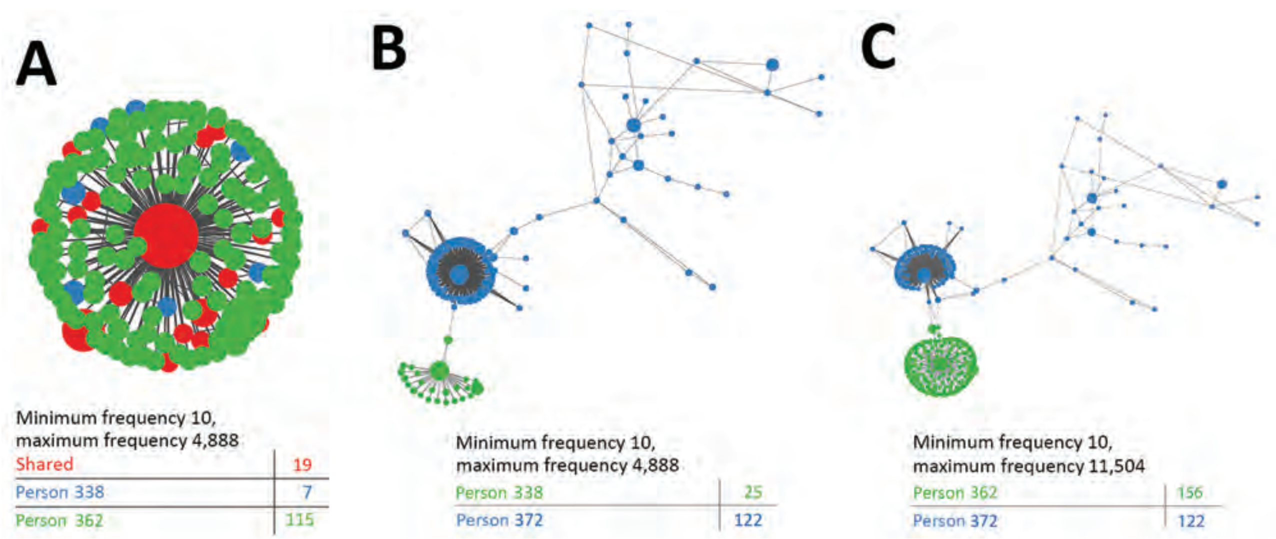


**Figure 3.** Hepatitis C virus (HCV) transmission network among persons in public health and corrections settings, Wisconsin, USA, 2016–2017, showing intrahost genetic heterogeneity within 1 representative transmission cluster. K-step network contains all possible minimum spanning trees and enables efficient visualization of genetic relatedness among all intrahost hypervariable region 1 (HVR1) variants for persons 338 and 362 (A), persons 338 and 372 (B), and persons 362 and 372 (B). Each node represents an HCV sequence, and the color of the node corresponds to the sample of origin: red, variant found in both samples; green, variant found only in the first sample; blue, variant found only in the second sample. Node size is based on frequency of the HVR1 variant, and edge length is proportional to the modified Hamming distance (does not count positions with insertions or deletions as differences).

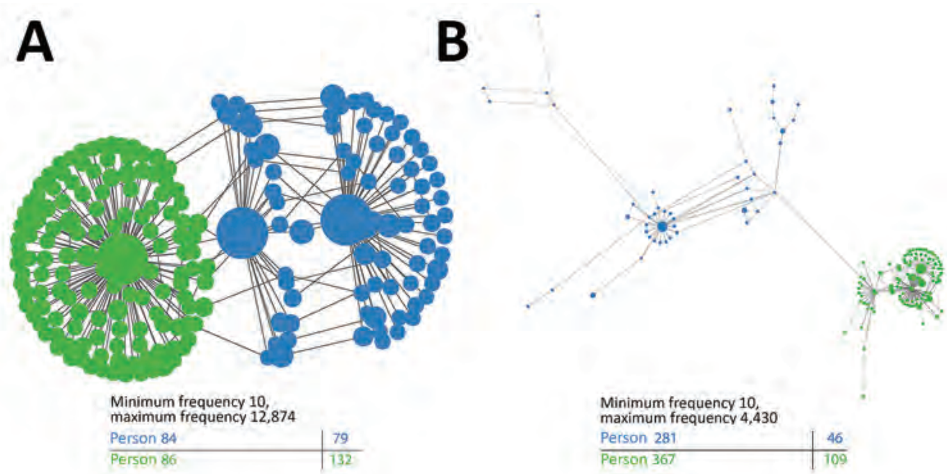


**Figure 4.** Intrahost genetic variation of representative transmission clusters of hepatitis C virus (HCV) among persons in public health and corrections settings, Wisconsin, USA, 2016–2017, highlighting the genetic relatedness of distinct variants. K-step network contains all possible minimum spanning trees and enables efficient visualization of genetic relatedness among all intrahost hypervariable region 1 (HVR1) variants for persons 84 and 86 (A) and persons 281 and 367 (B). Each node represents an HCV sequence. Color of the node corresponds to the sample of origin: green, found only in the first sample; blue, found only in the second sample. The node size is based on frequency of the HVR1 variant, and edge length is proportional to the modified Hamming distance (does not count positions with insertions or deletions as differences).

Unfortunately, contact tracing was not performed among our study population, precluding further analyses. Because modeling studies have demonstrated that HCV can be eliminated through scaling up and targeting treatment (*31,32*), a concept known as treatment as prevention, often used in HIV research (*33,34*), conducting routine molecular surveillance may also advance HCV prevention efforts by facilitating efficient allocation of limited resources to target and treat members in clusters.

The first limitation of our study is that HCV testing and surveillance challenges make identifying a complete cohort of HCV-infected PWIDs difficult. CDC estimates that approximately half of all HCV-infected persons are unaware of their infection status (*35*). Persons not included in our analysis include those who were never tested, were tested outside of Wisconsin, or were tested in other settings (e.g., primary care) that use commercial or hospital-based laboratories for HCV testing. Accordingly, the population studied is not fully representative of the Wisconsin general population. However, our results do provide a credible picture of the HCV epidemic across public health and correctional settings throughout rural and urban Wisconsin. Second, the association we found between clustering and younger age among rural residents could result from having sampled a larger number of younger persons. Third, risk-behavior data are missing for a large proportion of the sample because few agencies routinely collect and report these data. Data may also be missing because persons may choose to not disclose potentially stigmatizing drug use and sexual behaviors, particularly in settings such as correctional facilities ,where persons may fear further punishment. Fourth, we were unable to determine from which catchment area persons in corrections facilities orginated. Last, phylogenetic clustering alone cannot directly assert whether transmission has occurred between persons (*36*).

In conclusion, our findings provide a snapshot of the HCV epidemic throughout Wisconsin during 2016–2017. They illustrate the need to especially direct resources to rural communities affected by the opioid crisis.


### Acknowledgments

We thank Atkinson Longmire and Yury Khudyakov for specific discussions and the entire CDC GHOST team for their support and assistance.

This work was supported by grants from the National Institute on Drug Abuse at the National Institutes of Health: UG3 DA044826 to R.P.W. and D.W.S, U24 DA044801 to T.M.A, and R25 DA037190 to K.R.H. K.R.H. is also funded by National Institute on Drug Abuse: grant T32 DA037801.


## About the Author

Dr. Hochstatter is a postdoctoral research fellow at the Columbia University School of Social Work in New York, NY, USA, and an honorary fellow at the University of Wisconsin School of Medicine and Public Health in Madison. Her research focuses on preventing HIV and HCV transmission and improving screening and treatment uptake among populations disproportionately burdened by substance use disorders, especially PWIDs and adults involved in the criminal justice system.

## References


1. Hofmeister MG, Rosenthal EM, Barker LK, Rosenberg ES, Barranco MA, Hall EW, et al. Estimating prevalence of hepatitis C virus infection in the United States, 2013–2016. Hepatology. 2019;69:1020–31. https://doi.org/10.1002/hep.30297
2. Ly KN, Hughes EM, Jiles RB, Holmberg SD. Rising mortality associated with hepatitis C virus in the United States, 2003–2013. Clin Infect Dis. 2016;62:1287–8. https://doi.org/10.1093/cid/ciw111
3. Zibbell JE, Asher AK, Patel RC, Kupronis B, Iqbal K, Ward JW, et al. Increases in acute hepatitis C virus infection related to a growing opioid epidemic and associated injection drug use, United States, 2004 to 2014. Am J Public Health. 2018;108:175–81. https://doi.org/10.2105/AJPH.2017.304132
4. Gardy JL, Johnston JC, Sui SJH, Cook VJ, Shah L, Brodkin E, et al. Whole-genome sequencing and social-network analysis of a tuberculosis outbreak. N Engl J Med. 2011;364:730–9. https://doi.org/10.1056/NEJMoa1003176
5. Little SJ, Kosakovsky Pond SL, Anderson CM, Young JA, Wertheim JO, Mehta SR, et al. Using HIV networks to inform real time prevention interventions. PLoS ONE. 2014;9:e98443.
6. Poon AFY, Gustafson R, Daly P, Zerr L, Demlow SE, Wong J, et al. Near real-time monitoring of HIV transmission hotspots from routine HIV genotyping: an implementation case study. Lancet HIV. 2016;3:e231–8. https://doi.org/10.1016/S2352-3018(16)00046-1
7. Gardy JL, Loman NJ. Towards a genomics-informed, real-time, global pathogen surveillance system. Nat Rev Genet. 2018;19:9–20. https://doi.org/10.1038/nrg.2017.88
8. Fauci AS, Redfield RR, Sigounas G, Weahkee MD, Giroir BP. Ending the HIV epidemic: a plan for the United States. JAMA. 2019;321:844–5. https://doi.org/10.1001/jama.2019.1343
9. Longmire AG, Sims S, Rytsareva I, Campo DS, Skums P, Dimitrova Z, et al. GHOST: Global Hepatitis Outbreak and Surveillance Technology. BMC Genomics. 2017;18(Suppl 10):916. https://doi.org/10.1186/s12864-017-4268-3
10. Vivolo-Kantor AM, Seth P, Gladden RM, Mattson CL, Baldwin GT, Kite-Powell A, et al. Vital signs: trends in emergency department visits for suspected opioid overdoses—United States, July 2016–September 2017. MMWR Morb Mortal Wkly Rep. 2018;67:279–85. https://doi.org/10.15585/mmwr.mm6709e1
11. Wisconsin Department of Health Service, Wisconsin epidemiological profile on alcohol and other drugs [cited 2020 Dec 6]. https://www.dhs.wisconsin.gov/publications/p4/p45718-16.pdf
12. Centers for Disease Control and Prevention. Surveillance for viral hepatitis—United States, 2016 [cited 2020 Dec 6]. https://www.cdc.gov/hepatitis/statistics/2016surveillance/index.htm
13. Tully DC, Hjerrild S, Leutscher PD, Renvillard SG, Ogilvie CB, Bean DJ, et al. Deep sequencing of hepatitis C virus reveals genetic compartmentalization in cerebrospinal fluid from cognitively impaired patients. Liver Int. 2016;36:1418–24. https://doi.org/10.1111/liv.13134
14. Campo DS, Xia G-L, Dimitrova Z, Lin Y, Forbi JC, Ganova-Raeva L, et al. Accurate genetic detection of hepatitis C virus transmissions in outbreak settings. J Infect Dis. 2016;213:957–65. https://doi.org/10.1093/infdis/jiv542
15. Tully DC, Ogilvie CB, Batorsky RE, Bean DJ, Power KA, Ghebremichael M, et al. Differences in the selection bottleneck between modes of sexual transmission influence the genetic composition of the HIV-1 founder virus. PLoS Pathog. 2016;12:e1005619. https://doi.org/10.1371/journal.ppat.1005619
16. Henn MR, Boutwell CL, Charlebois P, Lennon NJ, Power KA, Macalalad AR, et al. Whole genome deep sequencing of HIV-1 reveals the impact of early minor variants upon immune recognition during acute infection. PLoS Pathog. 2012;8:e1002529. https://doi.org/10.1371/journal.ppat.1002529
17. Hedegaard DL, Tully DC, Rowe IA, Reynolds GM, Bean DJ, Hu K, et al. High resolution sequencing of hepatitis C virus reveals limited intra-hepatic compartmentalization in end-stage liver disease. J Hepatol. 2017;66:28–38. https://doi.org/10.1016/j.jhep.2016.07.048
18. Xu H, Luo X, Qian J, Pang X, Song J, Qian G, et al. FastUniq: a fast de novo duplicates removal tool for paired short reads. PloS One. 2012;7:e52249.
19. Bolger AM, Lohse M, Usadel B. Trimmomatic: a flexible trimmer for Illumina sequence data. Bioinformatics. 2014;30:2114–20. https://doi.org/10.1093/bioinformatics/btu170
20. Yang X, Charlebois P, Gnerre S, Coole MG, Lennon NJ, Levin JZ, et al. De novo assembly of highly diverse viral populations. BMC Genomics. 2012;13:475. https://doi.org/10.1186/1471-2164-13-475
21. Tamura K, Stecher G, Peterson D, Filipski A, Kumar S. MEGA6: Molecular Evolutionary Genetics Analysis version 6.0. Mol Biol Evol. 2013;30:2725–9. https://doi.org/10.1093/molbev/mst197
22. Nguyen L-T, Schmidt HA, von Haeseler A, Minh BQ. IQ-TREE: a fast and effective stochastic algorithm for estimating maximum-likelihood phylogenies. Mol Biol Evol. 2015;32:268–74. https://doi.org/10.1093/molbev/msu300
23. Hoang DT, Chernomor O, von Haeseler A, Minh BQ, Vinh LS. UFBoot2: improving the ultrafast bootstrap approximation. Mol Biol Evol. 2018;35:518–22. https://doi.org/10.1093/molbev/msx281
24. Sims S, Longmire AG, Campo DS, Ramachandran S, Medrzycki M, Ganova-Raeva L, et al. Automated quality control for a molecular surveillance system. BMC Bioinformatics. 2018;19(Suppl 11):358. https://doi.org/10.1186/s12859-018-2329-5
25. Jacka B, Applegate T, Krajden M, Olmstead A, Harrigan PR, Marshall B, et al. Phylogenetic clustering of hepatitis C virus among people who inject drugs in Vancouver, Canada. Hepatology. 2014;60:1571–80. https://doi.org/10.1002/hep.27310
26. Hackman J, Falade-Nwulia O, Patel EU, Mehta SH, Kirk GD, Astemborski J, et al. Correlates of hepatitis C viral clustering among people who inject drugs in Baltimore. Infect Genet Evol. 2020;77:104078. https://doi.org/10.1016/j.meegid.2019.104078
27. Suryaprasad AG, White JZ, Xu F, Eichler B-A, Hamilton J, Patel A, et al. Emerging epidemic of hepatitis C virus infections among young nonurban persons who inject drugs in the United States, 2006–2012. Clin Infect Dis. 2014;59:1411–9. https://doi.org/10.1093/cid/ciu643
28. Van Handel MM, Rose CE, Hallisey EJ, Kolling JL, Zibbell JE, Lewis B, et al. County-level vulnerability assessment for rapid dissemination of HIV or HCV infections among persons who inject drugs, United States. J Acquir Immune Defic Syndr. 2016;73:323–31.
29. Campo DS, Khudyakov Y. Intelligent Network DisRuption Analysis (INDRA): a targeted strategy for efficient interruption of hepatitis C transmissions. Infect Genet Evol. 2018;63:204–15. https://doi.org/10.1016/j.meegid.2018.05.028
30. Katzman C, Mateu-Gelabert P, Kapadia SN, Eckhardt BJ. Contact tracing for hepatitis C: the case for novel screening

strategies as we strive for viral elimination. Int J Drug Policy. 2019;72:33–9. https://doi.org/10.1016/j.drugpo.2019.04.003

31. Pitcher AB, Borquez A, Skaathun B, Martin NK. Mathematical modeling of hepatitis C virus (HCV) prevention among people who inject drugs: a review of the literature and insights for elimination strategies [cited 2020 Jun 13]. https://europepmc.org/article/pmc/pmc6522340
32. Heffernan A, Cooke GS, Nayagam S, Thursz M, Hallett TB. Scaling up prevention and treatment towards the elimination of hepatitis C: a global mathematical model. Lancet. 2019; 393:1319–29. https://doi.org/10.1016/S0140-6736(18)32277-3
33. Cohen MS, McCauley M, Gamble TR. HIV treatment as prevention and HPTN 052. Curr Opin HIV AIDS. 2012;7:99–105. https://doi.org/10.1097/COH.0b013e32834f5cf2
34. Cohen J. Breakthrough of the year. HIV treatment as prevention. Science. 2011;334:1628. https://doi.org/10.1126/science.334.6063.1628
35. Centers for Disease Control and Prevention. Hepatitis C kills more Americans than any other infectious disease [cited 2019 Sep 24]. https://www.cdc.gov/media/releases/2016/p0504-hepc-mortality.html
36. Villabona-Arenas CJ, Hanage WP, Tully DC. Phylogenetic interpretation during outbreaks requires caution. Nat Microbiol. 2020;5:876–7. https://doi.org/10.1038/s41564-020-0738-5

Address for correspondence: Karli Hochstatter, University of Wisconsin School of Medicine and Public Health, 1685 Highland Ave, Madison, WI 53705, USA; email: khochsta@medicine.wisc.edu

RESEARCH

# Prolonged Maternal Zika Viremia as a Marker of Adverse Perinatal Outcomes

Léo Pomar, Véronique Lambert, Séverine Matheus, Céline Pomar, Najeh Hcini, Gabriel Carles, Dominique Rousset, Manon Vouga, Alice Panchaud,[1] David Baud[1]

Whether prolonged maternal viremia after Zika virus infection represents a risk factor for maternal–fetal transmission and subsequent adverse outcomes remains unclear. In this prospective cohort study in French Guiana, we enrolled Zika virus–infected pregnant women with a positive PCR result at inclusion and noninfected pregnant women; both groups underwent serologic testing in each trimester and at delivery during January–July 2016. Prolonged viremia was defined as ongoing virus detection ≥30 days postinfection. Adverse outcomes (fetal loss or neurologic anomalies) were more common in fetuses and neonates from mothers with prolonged viremia (40.0%) compared with those from infected mothers without prolonged viremia (5.3%, adjusted relative risk [aRR] 7.2 [95% CI 0.9–57.6]) or those from noninfected mothers (6.6%, aRR 6.7 [95% CI 3.0–15.1]). Congenital infections were confirmed more often in fetuses and neonates from mothers with prolonged viremia compared with the other 2 groups (60.0% vs. 26.3% vs. 0.0%, aRR 2.3 [95% CI 0.9–5.5]).

The recent worldwide epidemic confirmed maternal–fetal transmission of Zika virus (ZIKV) and its association with adverse perinatal outcomes, particularly severe central nervous system lesions and fetal losses (*1*–*3*). Whether prolonged viremia after ZIKV infection in pregnant women represents a risk factor for maternal–fetal transmission, congenital Zika syndrome (CZS), or other adverse outcomes is on ongoing controversy (*4*).

Author affiliations: Lausanne University Hospital, Lausanne, Switzerland (L. Pomar, C. Pomar, M. Vouga, A. Panchaud, D. Baud); Centre Hospitalier de l'Ouest Guyanais Franck Joly, Saint-Laurent-du-Maroni, French Guiana (V. Lambert, C. Pomar, N. Hcini, G. Carles); Institut Pasteur, Paris, France (S. Matheus); Institut Pasteur of French Guiana, Cayenne, French Guiana (S. Matheus, D. Rousset); University of Bern, Bern, Switzerland (A. Panchaud)

DOI: https://doi.org/10.3201/eid2702.200684

ZIKV is detectable in maternal blood by reverse transcription PCR (RT-PCR) during the acute phase of infection. ZIKV viremia usually lasts from 2 days before to 16 days after symptom onset; median time of ZIKV RNA clearance is 5 days (*5*). Driggers et al. (*6*) detected ZIKV RNA in maternal serum samples 8 weeks after onset of clinical symptoms; they suggested that prolonged viremia might occur as a consequence of viral replication in the fetus or placenta and might be correlated with CZS. In other reports, however, prolonged maternal viremia has been described in pregnant women with both normal and adverse fetal outcomes (*6*–*10*).

In a cohort of pregnant women exposed to ZIKV in French Guiana, we investigated the impact of prolonged viremia on fetal and neonatal adverse outcomes (fetal loss or neurologic anomalies) compared with infected pregnant women without prolonged viremia and noninfected pregnant women. We also compared the rates of congenital infections between these groups.

## Methods

### Study Population, Recruitment, and Follow-up

The study was conducted at the Centre Hospitalier de l'Ouest Guyanais (CHOG; Saint-Laurent-du-Maroni, in French Guiana) during January 1–July 15, 2016, at the beginning of the ZIKV epidemic. Persons for inclusion were initially identified either through routine serologic testing of all pregnant women admitted to the prenatal diagnosis unit of CHOG (performed in each trimester of pregnancy and at birth), or through serologic and molecular testing in cases of maternal symptoms, acute exposure in the previous 2 weeks (patients who arrived in French Guiana from a nonendemic country or patients who arrived from an

[1]These senior authors contributed equally to this article.

endemic country [e.g., Brazil in January 2016] before the epidemic began in French Guiana), fetal or neonatal central nervous system anomalies, or in cases of amniocentesis performed for suspected CZS or other indications (i.e., aneuploidy diagnosis). All pregnant women with ZIKV testing available with ongoing follow-up at CHOG were invited to participate in the study. Written consent was obtained from all participants. The study received ethics approval from the CHOG institutional review board (*11*). Data regarding demographic, medical, and obstetrical characteristics and possible risk factors for congenital diseases were collected prospectively at inclusion.

Patients were monitored in accordance with the clinical standard of care in France, with the exception that prenatal ultrasound was performed monthly for patients who tested positive for ZIKV. Two supplementary ultrasounds were provided to patients who tested negative for ZIKV (at 26–28 and 36–38 weeks' gestation), as recommended by health authorities in France and other organizations (*12*–*15*). In cases of fetal loss (>14 weeks' gestation) or termination of pregnancy, a postmortem examination was offered, including macroscopic imaging and anatomic–pathologic examination.

In cases of live birth, a clinical examination (with particular attention to neurologic and systemic symptoms such as hypertonia, swallowing disorders, hypotonia, hepatomegaly, and jaundice) and testing for congenital ZIKV infection were performed for all neonates. Biologic, ophthalmologic, and imaging follow-up was offered for neonates from ZIKV-infected pregnant women (*16*).

Pregnant women not followed at the CHOG prenatal diagnosis unit after ZIKV testing, as well as patients who only delivered at CHOG without appropriate prenatal follow-up, were excluded from this study. Fetuses or neonates who did not undergo testing for ZIKV at birth or an appropriate postnatal or postmortem examination also were excluded.

#### Definition of Maternal ZIKV Infection

Molecular and serologic testing was performed at the French Guiana National Reference Center for arboviruses (Institut Pasteur of French Guiana, Cayenne, French Guiana) using the Realstar Zika Kit (Altona Diagnostics GmbH, https://altona-diagnostics.com) for RT-PCR, in-house IgM and IgG antibody-capture ELISA, and microneutralization assays for serologic testing. The limit of detection for serum samples tested using the Realstar Zika Kit was 0.61 (95% CI 0.39–1.27) copies/μL (*17*). A cycle threshold ($C_t$) value ≤37 was considered positive.

When ZIKV RNA was initially detected, molecular diagnosis was performed monthly and at delivery on maternal serum samples. Prolonged viremia was defined as ongoing viral detection ≥30 days after symptom onset or after initial detection of viremia in asymptomatic patients. Absence of prolonged viremia in infected patients was defined as a subsequent negative molecular test ≤30 days after symptom onset or after initial detection of viremia in asymptomatic patients.

In all cases, ZIKV serologic tests were performed in each trimester of pregnancy and at delivery. Patients with only positive IgM without RT-PCR testing or with a negative RT-PCR result were excluded from the analysis.

Maternal symptoms potentially related to ZIKV were recorded at each prenatal visit and at birth. These symptoms included rash, fever, asthenia, pruritus, arthralgia, retro-orbital headache, myalgia, conjunctival hyperemia, edema of the extremities, and neurologic complications (*18*). Asymptomatic pregnant women who remained ZIKV-negative on serologic tests during their pregnancy and at delivery were considered noninfected.

#### Definition of Fetal and Neonatal Adverse Outcomes and Congenital Infection

Fetal and neonatal outcomes were reviewed by 3 independent reviewers, including 2 maternal–fetal medicine specialists who had not been in contact with these patients previously. Cerebral anomalies were defined as ≥1 major cerebral sign, based on an extended definition of CZS (*14*,*19*,*20*) (Appendix 1 Table 1, https://wwwnc.cdc.gov/EID/article/27/2/20-0684-App1.pdf). Fetal loss was defined as a spontaneous fetal demise at >14 weeks' gestation, including late miscarriages (14–24 weeks' gestation) and stillbirths (fetal demise >24 weeks' gestation up to intrapartum); intrapartum and early postpartum deaths were excluded. For the analysis, fetuses and neonates who had major cerebral anomalies, fetal losses, or both were categorized as having adverse outcomes. Termination of pregnancy for reasons other than major cerebral abnormalities were not considered as adverse outcomes in this analysis.

All fetuses and neonates underwent ZIKV testing at birth or after fetal loss. Prenatal testing by amniocentesis was offered in those with fetal anomalies, if an amniocentesis was indicated for other indications (i.e., aneuploidy diagnosis), or both. A confirmed congenital ZIKV infection was defined either by ZIKV RNA amplification by RT-PCR from ≥1 fetal or neonatal sample (e.g., placenta, amniotic fluid, cerebrospinal fluid, urine, or blood) or identification of ZIKV-specific

IgM in the umbilical cord or neonatal blood or in cerebrospinal fluid. Details of congenital ZIKV testing are discussed elsewhere (*19*).

### Statistical Analyses

Standardized differences were calculated to compare baseline characteristics of patients with prolonged viremia to those of the reference groups (i.e., pregnant women with positive RT-PCR results without prolonged viremia and noninfected pregnant women). These characteristics were considered unbalanced when the standardized difference was >0.15.

Relative risks (RRs) and 95% CIs were calculated for fetal and neonatal adverse outcomes by using generalized linear regression. Adjusted RRs (aRRs) were calculated for variables reflecting unbalanced baseline characteristics that could represent confounding factors (maternal age and maternal underlying conditions). When fetuses from mothers with prolonged viremia were compared with those from infected mothers without prolonged viremia, RRs were also adjusted for the trimester of maternal infection diagnosis. A robust SE option was used for twins in order to not affect the variance in considering twins as separate cases.

We conducted a sensitivity analysis to test the robustness of our findings, using different criteria for the diagnosis of maternal prolonged viremia. We compared fetuses and neonates from patients with stable or increasing quantitative PCR (qPCR) values between the inclusion and the first follow-up with those from mothers with decreasing qPCR values.

The missing data were considered to be random, and thus we performed a complete case analysis. All statistical analyses were conducted by using Stata 15 (StataCorp, https://www.stata.com).

## Results

### Recruitment and Maternal ZIKV Diagnosis

During January 1–July 15, 2016, a total of 1,690 pregnant women were admitted to CHOG and tested for ZIKV infection (Figure 1). Among 498 women with a positive test, 198 were not prospectively followed in the CHOG prenatal diagnosis unit (including 20 patients with early miscarriages, 70 who were followed elsewhere after initial diagnosis of ZIKV infection, and 108 with a diagnosis at delivery without appropriate prenatal follow-up). A total of 300 pregnant women (including 5 with dichorionic twin pregnancies) with a positive ZIKV test were monitored in the unit. Full fetal and neonatal testing and follow-up was available for 287 of them (including 4 with twin pregnancies). Among these 287 ZIKV-positive patients, 254 (including 3 with twin pregnancies) had ZIKV infection diagnosed only by positive IgM, without molecular testing or with negative molecular testing, preventing calculation of the start of viremia. These patients were excluded from the analysis. Positive molecular testing was found in 33 patients (including 1 with a twin pregnancy); 30 were positive by RT-PCR in maternal blood, 9 were positive by RT-PCR in urine samples. Among these ZIKV RNA–positive pregnant women, 14 (including 1 with a twin pregnancy) exhibited a prolonged viremia, whereas the other 19 became subsequently negative within 30 days. Details of positive molecular testing are presented in Appendix 1 Table 2 and the evolution of qPCR values for each positive patient in Appendix 2 Figure (https://wwwnc.cdc.gov/EID/article/27/2/20-0684-App2.xlsx).

During the same period, 399 pregnant women (including 6 with dichorionic twin pregnancies) with negative serologic test results for ZIKV were followed for routine scans at CHOG. Full maternal, placental, and neonatal testing was available for 326 of them (including 6 with twin pregnancies). These patients remained negative for ZIKV during the entire pregnancy and at delivery, and constituted the noninfected group. The recruitment process is summarized in Figure 1.

### Baseline Characteristics of Participants

As shown in Appendix 1 Table 3, baseline characteristics were similar between pregnant women with prolonged viremia and the reference groups, except for a history of congenital abnormalities or intrauterine fetal demise, maternal underlying conditions, rate of dichorionic twins, and high risk for fetal aneuploidy (>1/250), for which standardized differences >0.15 were observed. Maternal ZIKV infections were diagnosed earlier in pregnancies with prolonged viremia than in those without prolonged viremia.

### Fetal and Neonatal Adverse Outcomes and Congenital Infections

ZIKV testing and outcomes were available for 15 fetuses from 14 infected pregnant women with prolonged viremia (including 1 with a dichorionic twin pregnancy) (Appendix 1 Tables 4, 5). Two pregnancies (2/15 [13.3%]) were terminated for severe neurologic anomalies, and 2 fetal losses (2/15 [13.3%]) were recorded. Among fetuses with imaging studies and examinations available, 4 (4/14 [28.6%]) exhibited neurologic anomalies and 4 (4/11 [36.4%]) ocular anomalies (Appendix 1 Table 4). Congenital ZIKV infections were confirmed in 9 (9/15 [60.0%]) of these fetuses or newborns, of which 6 (6/9 [66.7%]) cases resulted in adverse outcomes (4 suspected CZS and 2

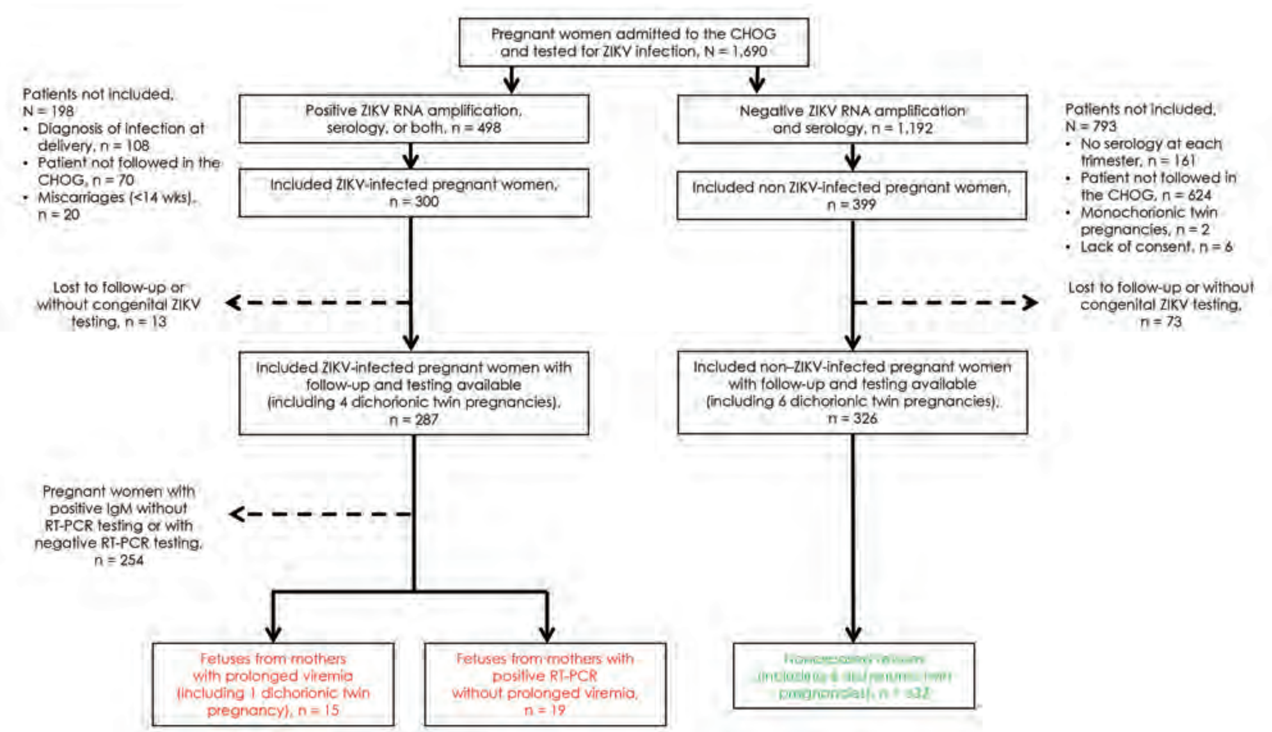


**Figure 1.** Flowchart of pregnant women admitted to CHOG, French Guiana, January 1–July 15, 2016. All women were routinely tested for ZIKV-specific IgM and IgG in each trimester of pregnancy and at delivery. In cases of maternal symptoms, acute exposure in the previous 2 weeks, fetal anomalies, or if an amniocentesis was indicated, pregnant women were also tested for ZIKV RNA by RT-PCR in blood and urine. Patients with a positive RT-PCR result were offered to participate in the study and underwent monthly RT-PCR testing up to clearance or delivery. Prolonged viremia was defined as ongoing viral detection $\geq$30 days after symptom onset or after initial detection of viremia. Asymptomatic patients who remained negative for ZIKV IgM during the whole pregnancy were recruited and considered as non–ZIKV-infected. Patients with only positive IgM without or with a negative RT-PCR test result were excluded of this analysis because of the inability to accurately date the onset and clearance of viremia. Patients without appropriate monthly follow-up were also excluded from this study (e.g., those who had early miscarriages, late diagnosis of infection at delivery, or were not followed in our center after the diagnosis). After expulsion, fetal losses were tested by RT-PCR (as well as by IgM, if available). Fetuses with anomalies were tested by RT-PCR on amniotic fluid. Neonates were tested for ZIKV at birth (RT-PCR on placenta, urine, blood and IgM on blood [as well as on cerebrospinal fluid, if symptomatic]). Fetuses and neonates without appropriate testing and examination after fetal loss or birth were excluded from this analysis. Overall, 15 fetuses from 14 infected pregnant women with prolonged viremia (including 1 with a twin pregnancy), 19 fetuses from 19 infected pregnant women without prolonged viremia, and 332 fetuses from 326 noninfected pregnant women (including 6 with twin pregnancies) were included. CHOG, Centre Hospitalier de l'Ouest Guyanais (Saint-Laurent-du-Maroni, French Guiana); RT-PCR, reverse transcription PCR; ZIKV, Zika virus.

fetal losses). All pregnancy outcomes for women with prolonged viremia are detailed in Figure 2. Figure 3 presents an example of CZS related to maternal prolonged viremia.

Among 19 fetuses from mothers with an initially positive RT-PCR result without prolonged viremia, no fetal loss or termination of pregnancy was recorded. Neurologic anomalies were found in 1 (1/19 [5.3%]) of these fetuses, who also had ocular anomalies (confirmed at birth). Congenital ZIKV infections were confirmed in 5 (5/19 [26.3%]) of these newborns, of which 1 (1/5 [20%]) resulted in adverse outcomes (suspected CZS).

ZIKV testing and outcomes were available for 332 fetuses or newborns from noninfected pregnant women (including 6 with dichorionic twin pregnancies). Four pregnancies (4/332 [1.2%]) resulted in termination of pregnancy (1 for severe neurologic anomalies and 3 for extraneurologic anomalies [congenital heart disease, skeletal dysplasia, and Down syndrome]). Four (4/332 [1.2%]) fetal losses were recorded. Among the fetuses with imaging studies and examination available, 17 (17/331 [5.1%]) had neurologic anomalies. None of these fetuses or neonates were found to be ZIKV-positive at birth.

### Associations between Prolonged Viremia, Fetal and Neonatal Adverse Outcomes, and Congenital Infections

Overall, fetuses or neonates from mothers with a prolonged viremia during pregnancy exhibited a higher risk for adverse outcomes (6/15 [40%] with fetal loss, neurologic anomalies, or both) compared with those from infected mothers without prolonged viremia (1/19 [5.3%], RR 7.6 [95% CI 1.0–56.5]) and noninfected mothers (20/332 [6.0%], RR 6.6 [95% CI 3.1–14.1]). Similar results were observed for fetal losses and neurologic anomalies when analyzed independently (Appendix 1 Table 4). After adjustment for maternal underlying conditions and considering the twin pregnancies in the variance, these associations and trends persisted (aRR 7.2 [95% CI 0.9–57.6] when compared with fetuses from infected mothers without prolonged viremia and aRR 6.7 [95% CI 3.0–15.1] when compared with fetuses from noninfected mothers). In the comparison with fetuses from infected mothers without prolonged viremia, the analysis was also adjusted for the trimester of maternal infection diagnosis (Appendix 1 Tables 4, 6).

Congenital infections were confirmed more frequently in fetuses from mothers with prolonged viremia (9/15 [60.0%]) when compared with those from infected mothers without prolonged viremia (5/19 [26.3%], RR 2.3 [95% CI 1.0–5.4]) and noninfected mothers (0/332 [0.0%]). After adjustment for the trimester of maternal infection diagnosis and consideration of twin pregnancies in the variance, this trend persists (aRR 2.3 [95% CI 0.9–5.5]) (Appendix 1 Tables 4, 6).

Our sensitivity analysis found similar results when considering the evolution of qPCR values between the inclusion and the first follow-up instead of prolonged viremia as a binary variable (Appendix 1 Table 7). Neurologic or systemic symptoms at birth were also more frequent in newborns from mothers with prolonged viremia compared with those from infected mothers without prolonged viremia or noninfected mothers (Appendix 1 Table 5).

## Discussion

The main findings of this cohort study are 2-fold. First, maternal ZIKV infection with prolonged viremia is associated with a 7-fold increased risk for fetal or neonatal adverse outcomes compared with pregnancies without prolonged viremia. Second, maternal prolonged

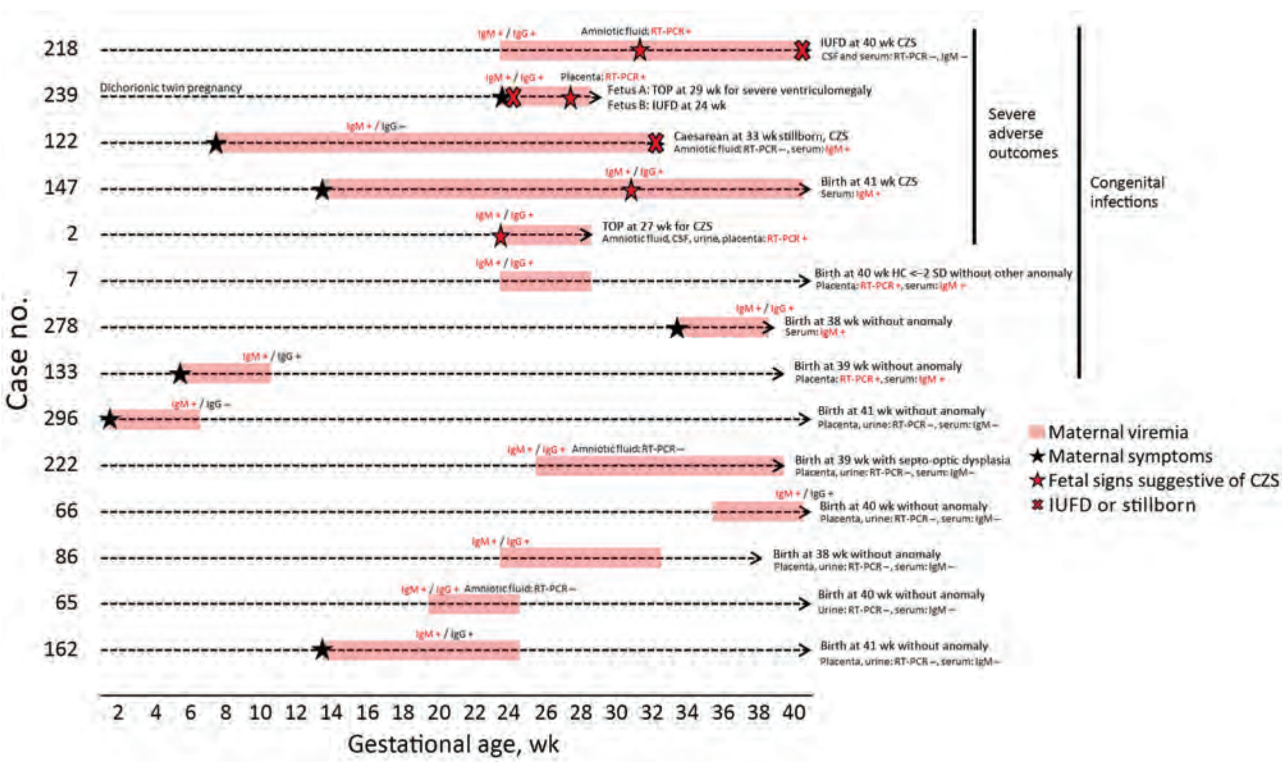


**Figure 2.** Pregnancy outcomes of patients with prolonged viremia in a cohort study of pregnant women admitted to Centre Hospitalier de l'Ouest Guyanais, French Guiana, January 1–July 15, 2016. Description and outcomes of 14 pregnancies with prolonged maternal ZIKV viremia (including 1 with dichorionic twin pregnancy). Congenital ZIKV infection was confirmed in 9/15 (60%) fetuses, and 6/15 (40%) fetuses had adverse outcomes. Four of them had multiple abnormalities consistent with CZS (1 live birth, 1 TOP, 1 IUFD, and 1 stillbirth). The 2 fetuses from the dichorionic twin pregnancy also had adverse outcomes, with an IUFD at 24 wk and a TOP for severe ventriculomegaly in the other fetus at 29 wk. CSF, cerebrospinal fluid; CZS, congenital Zika syndrome; HC, head circumference; IUFD, intrauterine fetal demise; RT-PCR, reverse transcription PCR; TOP, termination of pregnancy; ZIKV, Zika virus.

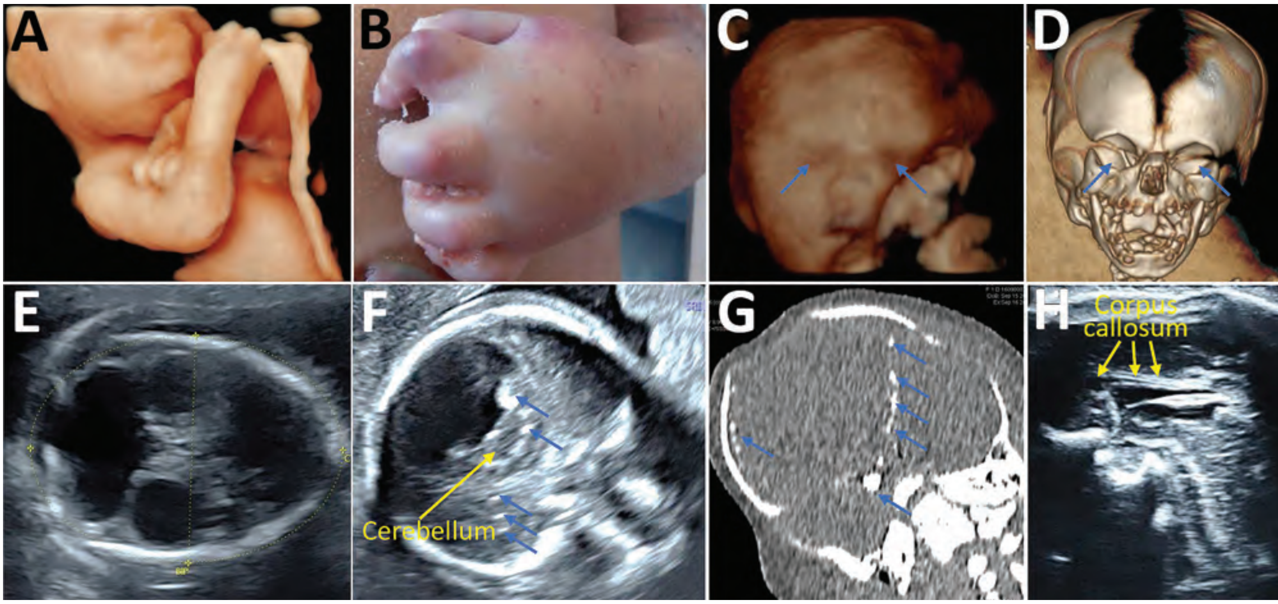


**Figure 3.** Prenatal ultrasound, computed tomography, and postmortem aspect of a fetus with congenital Zika syndrome related to maternal prolonged viremia in patient (case no. 122) in a cohort study of pregnant women admitted to Centre Hospitalier de l'Ouest Guyanais, French Guiana, January 1–July 15, 2016. The mother had symptomatic acute Zika virus infection at 8 weeks' gestation (and had ongoing viremia until birth of her stillborn child with signs of congenital Zika syndrome. Severe microcephaly, ventriculomegaly, and calcifications were detected by ultrasound at 13 weeks' gestation. Overall, this fetus had arthrogryposis detected on 3-D ultrasound (A) and postmortem (B); severe bilateral microphthalmia (blue arrows) detected on 3-D ultrasound (C) and fetal computed tomography (D); microcephaly with atrophic cortex detected on ultrasound (E) showing a head circumference of 160 mm at 25 weeks' gestation (−5 SDs); ventriculomegaly detected on ultrasound (E); brain calcifications (blue arrows) detected on ultrasound (F) and computed tomography (G); pontocerebellar hypoplasia (yellow arrows) detected on ultrasound (F); and corpus callosum dysgenesis (yellow arrows) detected on ultrasound (H).

viremia is associated with a 2-fold increased risk for confirmed congenital infection compared with infected mothers without prolonged viremia.

Our study was limited by the sample size of the infected group because only patients with a positive ZIKV RT-PCR result at enrollment were included in the analysis and followed up with monthly RT-PCR testing until clearance or delivery. Because the measured effect size was high, the sample size was sufficient to identify an association. The limited number of cases with prolonged viremia, however, forced us to group all adverse outcomes together to conduct an analysis with sufficient power and prevented the evaluation of its association with individual signs or symptoms or new characteristics (*21*,*22*).

Although ZIKV testing was based on the previous guidelines relevant during the 2015–2016 epidemic with adaptation to local capacities, testing does not follow the more recent CDC guidelines (*23*) (i.e., patients considered as noninfected underwent serologic testing in each trimester rather than nucleic acid testing, as is currently recommended). Patients included as noninfected, however, remained negative for IgM and IgG in each trimester and at delivery, limiting the risk for exposure misclassification. Similarly, women with only positive IgM testing were excluded from the study because some of them might have had undetected prolonged viremia, which would have led to an exposure misclassification and an underestimation of the consequences of prolonged viremia.

Information about the sensitivity and specificity of neonatal testing remains limited, and several studies have shown the progressive disappearance of ZIKV RNA in the maternal–fetal compartments (*24*). Although the identification of IgM in fetal or neonatal blood was used to avoid congenital ZIKV false negatives, we cannot exclude an outcome misclassification because some neonates with negative results could have been infected by ZIKV without viremia and immunity against ZIKV detectable at birth. This risk is likely low given that >80% of fetuses or neonates from infected pregnant women underwent testing in ≥3 different samples (including blood, urine, placenta, cerebrospinal, and amniotic fluid) (*19*), and all neonates from noninfected pregnant women underwent serologic testing at birth. Undetected congenital infections in the 2 reference groups might result in overestimation of the effect of prolonged viremia overall.

Neonates from noninfected mothers underwent postnatal transfontanellar ultrasound (as well as by computed tomography and magnetic resonance imaging, if available) only in the case of an abnormal prenatal ultrasound or symptoms at birth, in contrast to those from infected mothers who underwent routine postnatal imaging. However, when they are asymptomatic, some neonates from noninfected mothers might have undetected cerebral anomalies at birth, resulting in an overestimation of the consequences of prolonged Zika viremia. We cannot totally exclude this bias; however, all neonates from noninfected mothers underwent multiple prenatal ultrasound assessments (enhanced by 2 supplementary examinations with neurosonograms during the epidemic), reducing the risk for undetected cerebral anomalies.

Molecular testing has been proposed for use at different stages of pregnancy depending on the presence of maternal symptoms. Thus, symptomatic patients might have had ZIKV infection diagnosed earlier than asymptomatic patients for whom a molecular diagnosis was proposed in cases of fetal anomalies, amniocentesis (for fetal signs or other indications [i.e., aneuploidy diagnosis]), or both, occurring later in pregnancy. Among infected pregnant women without prolonged viremia, 7 were asymptomatic with a continuous exposure and did not have molecular testing before amniocentesis, preventing accurate identification of the time of infection during pregnancy. Thus, we cannot exclude that some of these patients were in fact infected earlier in pregnancy and had an undetected prolonged viremia resulting in an exposure misclassification. This bias would result in an underestimation of the consequences of prolonged viremia because a case that included neurologic anomalies (CZS) in the reference group from infected mothers without prolonged viremia could in fact be related to prolonged viremia. Similarly, we cannot exclude a potential selection bias given that some patients were tested by RT-PCR because their fetus had anomalies at inclusion. Because this proportion did not differ between the groups (3/14 vs. 4/19), even if we consider only anomalies suggestive of fetal infection at inclusion (2/14 vs. 2/19), we would not expect relative risks to be significantly affected. However, this potential selection bias could overestimate absolute frequencies of fetal anomalies in RT-PCR–positive patients, and this bias seems to be inherent in contemporary cohorts because inclusion after the observation of fetal anomalies potentially related to Zika were common.

Driggers et al. (*6*) were the first to highlight a possible association between prolonged maternal viremia and congenital infection with CZS. In their cohort study, Rodo et al. (*25*) described 9 cases of prolonged maternal viremia, among which 2 resulted in congenital ZIKV infection, with 1 of those 2 infections resulting in severe neurologic anomalies. The rates of congenital infection and fetal or neonatal adverse outcomes in women with prolonged viremia seem to be higher in our study (9/15 for congenital infections and 4/15 for CZS). This difference might be explained by the exclusive use of amniocentesis for diagnosis in the Rodo et al. cohort, whereas multiple fetal or neonatal samples were tested in our study (>80% of the fetuses or newborns had ≥3 different samples tested). Our results are congruent with Meaney et al. (*10*), who identified prolonged ZIKV RNA detection in 4 symptomatic pregnant women in the US Zika Pregnancy Registry, of which 1 pregnancy (25%) resulted in congenital Zika syndrome. Suy et al. (*8*) described a case of CZS with prolonged maternal viremia where the viral load in the maternal serum sample remained stable for 14 weeks and then became negative, instead of decreasing progressively, as would be expected. Suy et al. suggested that the prolonged viremia that was detected in the mother could be the result of viral replication in the fetus or placenta, which thus might act as a reservoir. However, their study still lacks a consensual threshold to define prolonged viremia. In our study, we defined prolonged viremia as ongoing viral detection ≥30 days after symptom onset or after initial detection of viremia for a question of feasibility. Indeed, many of our patients were living around the Maroni River, in isolated areas, and came monthly to CHOG for their clinical follow-up. In light of this geographic distance, we decided that monthly RT-PCR testing in case of initial detection of viremia was the most appropriate. In the context of a smaller area with local facilities, testing patients every 2 weeks to fulfill the threshold used in other studies might have been useful (*10*,*25*).

Negative and positive predictive values of prolonged maternal viremia for congenital infections and adverse outcomes related to ZIKV seem to be moderate because fetal and neonatal adverse outcomes and congenital infections also occur in pregnant women without identified prolonged viremia. One explanation could be that prolonged viremia might reflect viral replication in the placenta without further involvement for the fetus (*27*). In addition, some of our cases with prolonged maternal viremia (6/15) did not exhibit congenital infections, suggesting that prolonged maternal viremia might also reflect persistent viral replication in other reservoirs than the fetus or the placenta. The study of Rodo et al. (*10*) and the CDC report (*25*) also described fetuses without congenital infection or adverse outcomes from mothers with prolonged viremia (*10*,*25*).

Our results also indicate that noninfected women exhibited a 5.1% risk for fetal neurologic anomalies and 1.2% risk for fetal losses (higher than the estimation of 3% risk for neurologic anomalies and 0.5%–1.0% risk for fetal losses in developed countries), reflecting that other etiologies for adverse perinatal outcomes remain present even in the context of a ZIKV epidemic (*28*), particularly in French Guiana, where pregnant women are exposed to lead poisoning, poverty, and higher risk for underlying conditions (*29*). To reduce the impact of these cofounding factors on our assessment of adverse neonatal outcomes related to prolonged ZIKV viremia, we chose to adjust the RR estimates for unbalanced maternal underlying conditions that might have an effect on the exposure and on adverse perinatal outcomes.

In conclusion, prolonged maternal ZIKV viremia could be a marker for an increased risk for maternal–fetal transmission and subsequent adverse perinatal outcomes. Even if prolonged maternal viremia is not consistently present in cases of congenital infection, it might reflect active viral replication in the fetal–placental compartment and should lead to an enhanced prenatal and neonatal follow-up.


### Acknowledgments

We thank all involved personnel at Centre Hospitalier de l'Ouest Guyanais and Institut Pasteur of French Guiana.

L.P., V.L., A.P., and D.B. conceived and designed the study. L.P., V.L., C.P., G.C., and N.H. provided care to mothers and prospectively collected the clinical data and samples. D.R. and S.M. did all the viral investigations. L.P., A.P., M.V., and D.B. interpreted the results, did the literature review, and provided critical inputs to the paper. L.P., A.P., and D.B. wrote the first version of the report, and all authors critically reviewed and approved the final version. The corresponding author attests that all listed authors meet authorship criteria, that no others meeting the criteria have been omitted, that this manuscript is an honest, accurate, and transparent account of the study being reported, and that no important aspects of the study have been omitted.

Individual participant deidentified data that underlie the results will be shared with researchers who provide a methodologically sound proposal for multicentric study, particularly individual participant data metaanalysis. Proposals should be directed to L.P. (leo.pomar@chuv.ch).



### About the Author

Dr. Pomar was a midwife with a master's degree in ultrasound and fetal medicine and a specialization in fetal brain imaging when he enrolled and followed these patients. This research and other work led to his PhD degree at Lausanne University Hospital, Lausanne, Switzerland.


### References


1. Baud D, Gubler DJ, Schaub B, Lanteri MC, Musso D. An update on Zika virus infection. Lancet. 2017;390:2099–109. https://doi.org/10.1016/S0140-6736(17)31450-2
2. Rasmussen SA, Jamieson DJ, Honein MA, Petersen LR. Zika virus and birth defects—reviewing the evidence for causality. N Engl J Med. 2016;374:1981–7. https://doi.org/10.1056/NEJMsr1604338
3. Musso D, Bossin H, Mallet HP, Besnard M, Broult J, Baudouin L, et al. Zika virus in French Polynesia 2013–14: anatomy of a completed outbreak. Lancet Infect Dis. 2018;18:e172–82. https://doi.org/10.1016/S1473-3099(17)30446-2
4. Musso D, Ko AI, Baud D. Zika virus infection—after the pandemic. N Engl J Med. 2019;381:1444–57. https://doi.org/10.1056/NEJMra1808246
5. Fontaine A, de Laval F, Belleoud D, Briolant S, Matheus S. Duration of Zika viremia in serum. Clin Infect Dis. 2018;67:1143–4. https://doi.org/10.1093/cid/ciy261
6. Driggers RW, Ho CY, Korhonen EM, Kuivanen S, Jääskeläinen AJ, Smura T, et al. Zika virus infection with prolonged maternal viremia and fetal brain abnormalities. N Engl J Med. 2016;374:2142–51. https://doi.org/10.1056/NEJMoa1601824
7. Goncé A, Martínez MJ, Marbán-Castro E, Saco A, Soler A, Alvarez-Mora MI, et al. Spontaneous abortion associated with Zika virus infection and persistent viremia. Emerg Infect Dis. 2018;24:933–5. https://doi.org/10.3201/eid2405.171479
8. Suy A, Sulleiro E, Rodó C, Vázquez É, Bocanegra C, Molina I, et al. Prolonged Zika virus viremia during pregnancy. N Engl J Med. 2016;375:2611–3. https://doi.org/10.1056/NEJMc1607580
9. Schwartz KL, Chan T, Rai N, Murphy KE, Whittle W, Drebot MA, et al. Zika virus infection in a pregnant Canadian traveler with congenital fetal malformations noted by ultrasonography at 14-weeks gestation. Trop Dis Travel Med Vaccines. 2018;4:2. https://doi.org/10.1186/s40794-018-0062-8
10. Meaney-Delman D, Hills SL, Williams C, Galang RR, Iyengar P, Hennenfent AK, et al. Zika virus infection among U.S. pregnant travelers—August 2015–February 2016. MMWR Morb Mortal Wkly Rep. 2016;65:211–4. https://doi.org/10.15585/mmwr.mm6508e1
11. Pomar L, Malinger G, Benoist G, Carles G, Ville Y, Rousset D, et al. Association between Zika virus and fetopathy: a prospective cohort study in French Guiana. Ultrasound Obstet Gynecol. 2017;49:729–36. https://doi.org/10.1002/uog.17404
12. Picone O, Vauloup-Fellous C, D'Ortenzio E, Huissoud C, Carles G, Benachi A, et al. Zika virus infection during pregnancy [in French]. J Gynecol Obstet Biol Reprod (Paris). 2016;45:415–23. https://doi.org/10.1016/j.jgyn.2016.03.005
13. Vouga M, Musso D, Panchaud A, Baud D. Clinical management of pregnant women exposed to Zika virus.

Lancet Infect Dis. 2016;16:773. https://doi.org/10.1016/S1473-3099(16)30083-4
14. Pomar L, Musso D, Malinger G, Vouga M, Panchaud A, Baud D. Zika virus during pregnancy: from maternal exposure to congenital Zika virus syndrome. Prenat Diagn. 2019;39:420–30. https://doi.org/10.1002/pd.5446
15. Papageorghiou AT, Thilaganathan B, Bilardo CM, Ngu A, Malinger G, Herrera M, et al. ISUOG interim guidance on ultrasound for Zika virus infection in pregnancy: information for healthcare professionals. Ultrasound Obstet Gynecol. 2016;47:530–2. https://doi.org/10.1002/uog.15896
16. Adebanjo T, Godfred-Cato S, Viens L, Fischer M, Staples JE, Kuhnert-Tallman W, et al. Update: interim guidance for the diagnosis, evaluation, and management of infants with possible congenital zika virus infection—United States, October 2017. MMWR Morb Mortal Wkly Rep. 2017;66:1089–99. https://doi.org/10.15585/mmwr.mm6641a1
17. Ölschläger S, Enfissi A, Zaruba M, Kazanji M, Rousset D. Diagnostic validation of the RealStar Zika virus reverse transcription polymerase chain reaction kit for detection of Zika virus RNA in urine and serum specimens. Am J Trop Med Hyg. 2017;97:1070–1. https://doi.org/10.4269/ajtmh.17-0268
18. Flamand C, Fritzell C, Matheus S, Dueymes M, Carles G, Favre A, et al. The proportion of asymptomatic infections and spectrum of disease among pregnant women infected by Zika virus: systematic monitoring in French Guiana, 2016. Euro Surveill. 2017;22:17-00102. https://doi.org/10.2807/1560-7917.ES.2017.22.44.17-00102
19. Pomar L, Vouga M, Lambert V, Pomar C, Hcini N, Jolivet A, et al. Maternal-fetal transmission and adverse perinatal outcomes in pregnant women infected with Zika virus: prospective cohort study in French Guiana. BMJ. 2018;363:k4431. https://doi.org/10.1136/bmj.k4431
20. Kilby MD, Johnson A, Oepkes D, editors. Fetal therapy: scientific basis and critical appraisal of clinical benefits. Cambridge: Cambridge University Press; 2019 [cited 2020 Oct 17]. https://b-ok.org/book/5303728/45aadb
21. Wilder-Smith A, Wei Y, Araújo TVB, VanKerkhove M, Turchi Martelli CM, Turchi MD, et al.; Zika Virus Individual Participant Data Consortium. Understanding the relation between Zika virus infection during pregnancy and adverse fetal, infant and child outcomes: a protocol for a systematic review and individual participant data meta-analysis of longitudinal studies of pregnant women and their infants and children. BMJ Open. 2019;9:e026092. https://doi.org/10.1136/bmjopen-2018-026092
22. Panchaud A, Vouga M, Musso D, Baud D. An international registry for women exposed to Zika virus during pregnancy: time for answers. Lancet Infect Dis. 2016;16:995–6. https://doi.org/10.1016/S1473-3099(16)30255-9
23. Oduyebo T, Polen KD, Walke HT, Reagan-Steiner S, Lathrop E, Rabe IB, et al. Update: interim guidance for health care providers caring for pregnant women with possible Zika virus exposure–United States (including U.S. territories), July 2017. MMWR Morb Mortal Wkly Rep. 2017;66:781–93. https://doi.org/10.15585/mmwr.mm6629e1
24. Schaub B, Vouga M, Najioullah F, Gueneret M, Monthieux A, Harte C, et al. Analysis of blood from Zika virus–infected fetuses: a prospective case series. Lancet Infect Dis. 2017;17:520–7. https://doi.org/10.1016/S1473-3099(17)30102-0
25. Rodo C, Suy A, Sulleiro E, Soriano-Arandes A, Maiz N, Garcia-Ruiz I, et al. Pregnancy outcomes after maternal Zika virus infection in a non-endemic region: prospective cohort study. Clin Microbiol Infect. 2019;25:633.e5–9.
26. Meaney-Delman D, Oduyebo T, Polen KND, White JL, Bingham AM, Slavinski SA, et al.; U.S. Zika Pregnancy Registry Prolonged Viremia Working Group. Prolonged detection of Zika virus RNA in pregnant women. Obstet Gynecol. 2016;128:724–30. https://doi.org/10.1097/AOG.0000000000001625
27. Pomar L, Lambert V, Madec Y, Vouga M, Pomar C, Matheus S, et al. Placental infection by Zika virus in French Guiana. Ultrasound Obstet Gynecol. 2019. https://doi.org/10.1002/uog.21936
28. Vouga M, Baud D, Jolivet E, Najioullah F, Monthieux A, Schaub B. Congenital Zika virus syndrome…what else? Two case reports of severe combined fetal pathologies. BMC Pregnancy Childbirth. 2018;18:356. https://doi.org/10.1186/s12884-018-1998-4
29. Rimbaud D, Restrepo M, Louison A, Boukhari R, Ardillon V, Carles G, et al. Blood lead levels and risk factors for lead exposure among pregnant women in western French Guiana: the role of manioc consumption. J Toxicol Environ Health A. 2017;80:382–93. https://doi.org/10.1080/15287394.2017.1331490

Address for correspondence: Prof. David Baud, Materno-Fetal and Obstetrics Research Unit, Department "Woman–Mother–Child", Centre Hospitalier Universitaire Vaudois (CHUV), Avenue Pierre Decker 2, 1011 Lausanne, Switzerland; email: david.baud@chuv.ch

# Use of Commercial Claims Data for Evaluating Trends in Lyme Disease Diagnoses, United States, 2010–2018

Amy M. Schwartz, Kiersten J. Kugeler, Christina A. Nelson, Grace E. Marx, Alison F. Hinckley

We evaluated MarketScan, a large commercial insurance claims database, for its potential use as a stable and consistent source of information on Lyme disease diagnoses in the United States. The age, sex, and geographic composition of the enrolled population during 2010–2018 remained proportionally stable, despite fluctuations in the number of enrollees. Annual incidence of Lyme disease diagnoses per 100,000 enrollees ranged from 49 to 88, ≈6–8 times higher than that observed for cases reported through notifiable disease surveillance. Age and sex distributions among Lyme disease diagnoses in MarketScan were similar to those of cases reported through surveillance, but proportionally more diagnoses occurred outside of peak summer months, among female enrollees, and outside high-incidence states. Misdiagnoses, particularly in low-incidence states, may account for some of the observed epidemiologic differences. Commercial claims provide a stable data source to monitor trends in Lyme disease diagnoses, but certain important characteristics warrant further investigation.

Lyme disease is caused by infection with certain *Borrelia* spirochetes and transmitted to humans by *Ixodes* ticks (*1*). It is the most commonly reported vectorborne disease in the United States, despite a highly focal geographic distribution (*1*,*2*). Most reported cases of Lyme disease occur in 14 states in the Northeast, mid-Atlantic, and upper Midwest, although the geographic area with elevated disease risk is expanding (*2*,*3*). Lyme disease affects persons of all ages, but incidence peaks in children and older adults, presumably due to behaviors that put persons of these age groups in more frequent contact with infected ticks (*2*).

Lyme disease has been a nationally notifiable condition in the United States since 1991. Healthcare providers report cases to state or local health authorities, who evaluate the information and transmit it to the Centers for Disease Control and Prevention (CDC) through the National Notifiable Diseases Surveillance System (NNDSS) (*4*). Lyme disease surveillance was designed to provide public health officials with data to monitor trends and inform decision making. However, as the frequency and geographic distribution of Lyme disease cases have grown, so too has the burden of conducting surveillance. Several high-incidence jurisdictions are pursuing alternative ways to reduce the associated human resource and fiscal burden of conducting Lyme disease surveillance (*5*–*7*). As more jurisdictions adopt alternative sampling, estimation, or triage methods, the comparability of information gained from notifiable disease surveillance decreases (*5*,*7*).

Alternative data sources are increasingly more accessible and could supplement our understanding of the epidemiology of Lyme disease (*6*). Although intended for billing purposes, insurance claims data have been used to describe the epidemiology of many types of conditions (*8*–*10*), including the frequency and characteristics of clinician-diagnosed Lyme disease, its geographic distribution, and risk factors for disseminated illness (*11*,*12*). We expand on prior work by Nelson et al. (*11*) to examine the reliability of commercial claims data as an annual source of data on Lyme disease diagnoses. Specifically, we evaluated the stability and representativeness of a single commercial claims database during 2010–2018, variability in characteristics of identified Lyme disease diagnoses, and comparability to data obtained through routine passive surveillance.

## Methods

### Data Sources

IBM Watson Health MarketScan Commercial Claims and Encounters (CCAE) databases contain deidentified health encounter information on >25 million US

Author affiliation: Centers for Disease Control and Prevention, Fort Collins, Colorado, USA

DOI: https://doi.org/10.3201/eid2702.202728

residents <65 years of age who receive employer-sponsored health insurance, including early retirees and Consolidated Omnibus Budget Reconciliation Act (COBRA) continuees, and their dependents. Consistent with the methods described in Nelson et al., we restricted the MarketScan population to persons who had insurance coverage for an entire calendar year and who had the potential for associated pharmaceutical claims data to more accurately convey annual rates of coded Lyme disease diagnoses (*11*). State of primary beneficiary residence was used as a proxy for patient residence.

### Evaluation of the Stability and Representativeness of MarketScan

We evaluated characteristics of the insured population included in the MarketScan CCAE databases each year during 2010–2018 to define overall and annual population volume, composition, and representativeness with respect to sex, age, and geographic distribution. To evaluate the representativeness of the MarketScan population as compared with the US population <65 years of age, we used annual data from the US Census Bureau Vintage 2018 population estimates (*13*). To assess geographic representation given the focal nature of Lyme disease, we grouped states in geographic categories of Lyme disease endemicity in accordance with a recent Lyme disease surveillance summary (*2*). Connecticut, Delaware, Maine, Maryland, Massachusetts, Minnesota, New Hampshire, New Jersey, New York, Pennsylvania, Rhode Island, Wisconsin, Vermont, and Virginia were classified as high-incidence states. Illinois, Indiana, Iowa, Kentucky, Michigan, North Carolina, North Dakota, Ohio, South Dakota, Tennessee, West Virginia, and the District of Columbia all shared ≥1 border with a high-incidence state or were located between areas of high-incidence and thus were classified as neighboring states. All other states were classified as low-incidence for the purpose of this analysis.

### Identification of Lyme Disease Diagnoses in MarketScan

International Classification of Diseases (ICD) diagnosis codes are included in inpatient and outpatient healthcare encounter records in MarketScan; ≤15 diagnosis codes are included in each inpatient record and ≤4 diagnosis codes are included in each outpatient record. ICD-9-CM codes from the ICD, 9th Revision, Clinical Modification (ICD-9-CM), were used before October 2015; after this date, coding specialists were required to use codes from the ICD, 10th Revision, Clinical Modification (ICD-10-CM), in the United States (*14*).

For this analysis, we defined an outpatient Lyme disease diagnosis as the first outpatient healthcare encounter record per calendar year with a diagnosis code for Lyme disease (ICD-9-CM code 088.81 or ICD-10-CM code A69.2x) and a prescription for ≥7 days of treatment with an antimicrobial drug appropriate for Lyme disease and filled within ±30 days of the encounter date. This approach was highly similar to the previous effort by Nelson et al. but with the necessary addition of ICD-10-CM codes (*11*) (Appendix, https://wwwnc.cdc.gov/EID/article/27/2/20-2728-App1.pdf). We defined an inpatient Lyme disease diagnosis as a hospitalization record that contained a principal diagnosis code for Lyme disease, or a principal diagnosis code of a documented objective clinical manifestation of Lyme disease or a tickborne disease transmitted by the same vector (e.g., babesiosis) and a secondary diagnosis code for Lyme disease in the same record (Appendix). We included 1 Lyme disease diagnosis per person per calendar year; we used the earliest date of service on which all criteria were met as proxy for illness onset date for analysis of seasonality.

### Comparison of Lyme Disease Diagnoses in MarketScan with Cases Reported through Public Health Surveillance

Lyme disease cases are classified and reported by states according to the Council of State and Territorial Epidemiologists surveillance case definition in effect during the year of report (*4*). For our analysis, we used confirmed and probable cases among those <65 years of age reported to CDC during 2010–2018. We compared Lyme disease diagnoses as identified in MarketScan to those of cases reported through national public health surveillance with respect to incidence, seasonality, sex, age, and geographic distributions.

### Statistical Comparisons

To compare sex, age, and geographic distributions between the MarketScan population and the US population (2014 estimates) and compare distributions of select characteristics of Lyme disease diagnoses versus cases identified through public health surveillance, we used both $\chi^2$ tests and Cramer's V values, an approach similar to that used by Nelson et al. (*11*). Whereas $\chi^2$ tests are influenced by large cell sizes, Cramer's V is not and provides more insight into the magnitude of similarity between the 2 populations (*11*). We considered Cramer's V values <0.1 to indicate minimal to no difference between distributions because low values of Cramer's V suggest a high goodness-of-fit. We used SAS software version 9.4

(SAS Institute, https://www.sas.com) for data management and analysis.

## Results

Health insurance claims from a mean of 39,004,340 enrollees were captured in the MarketScan database annually from 2010–2018; the lowest annual total was 26,146,275 persons in 2017 and the highest 53,131,420 in 2012. When restricting this population to persons enrolled for an entire calendar year and with available prescription data, a mean of 22,869,944 persons met these criteria annually, with the lowest total of 18,166,082 persons in 2017 and the highest 28,747,962 in 2012 (Figure 1). Demographic characteristics of the restricted and unrestricted MarketScan populations did not notably differ (data not shown), although the number of persons in the restricted population was more stable over time (Figure 1). Henceforth, the MarketScan population figures we cite here reflect the restricted population.

### Stability and Representativeness of MarketScan as an Annual Data Source

Age, sex, and geographic distributions of the MarketScan population were qualitatively stable during the study period, showing <8% proportional variation among years. The annual median age in MarketScan was 35−36 years; median age of the US population <65 years was lower, 32 years. Overall, MarketScan contained a smaller proportion of children 0–9 years of age and adults 25–29 years of age and a larger proportion of adults 40–59 years of age compared with the US population ($p<0.0001$ by $\chi^2$ test; Cramer's V = 0.042); however, the low Cramer's V value suggests comparability in the age distributions (Figure 2). Female enrollees were slightly overrepresented in the MarketScan population during the study period (median 51.7% female, annual range 51.3%–51.9% female) compared with the US population <65 years of age (49.8%–49.9% female) ($p<0.0001$ by $\chi^2$ test; Cramer's V = 0.009); however, the very low Cramer's V value suggests this difference is unlikely to be meaningful.

Overall, the regional representation in the MarketScan population based upon geographic categories of Lyme disease endemicity differed slightly from that of the US population ($p<0.0001$ by $\chi^2$ test; Cramer's V = 0.026); however, the Cramer's V value suggests lack of a substantial difference between these geographic distributions. An average of 25.6% of the US population resided in high-incidence states for Lyme disease, and 23.7% of the MarketScan population (range 20.1%–28.1%) resided in high-incidence states. Whereas an average of 52.8% of the US population resided in low-incidence states during the study period, 51.0% (range 47.1%–54.0%) of the MarketScan population resided in low-incidence states.

### Characteristics of Lyme Disease Diagnoses in MarketScan vs. Cases Reported through Surveillance

We identified 140,281 MarketScan enrollees with Lyme disease diagnoses during 2010–2018, of whom 1.2% were hospitalized. The minimum in a year was 12,256 enrollees in 2010; the maximum, 19,880 in 2014. Median incidence of Lyme disease diagnoses during 2010–2018 was 73.3/100,000 enrollees; annual incidence ranged from a low of 49.1/100,000 enrollees in 2010 to a high of 87.9/100,000 enrollees in 2017 (Table 1). By comparison, median annual incidence of Lyme disease (among those <65 years of age) according to surveillance was 9.3 cases/100,000 population; incidence ranged from 7.9/100,000 population in 2012 to 11.8/100,000 population in 2017 (Table 1). Annual variability in incidence of Lyme disease diagnoses in MarketScan tracked with a similar trajectory to the annual variability in surveillance data (Figure 3).

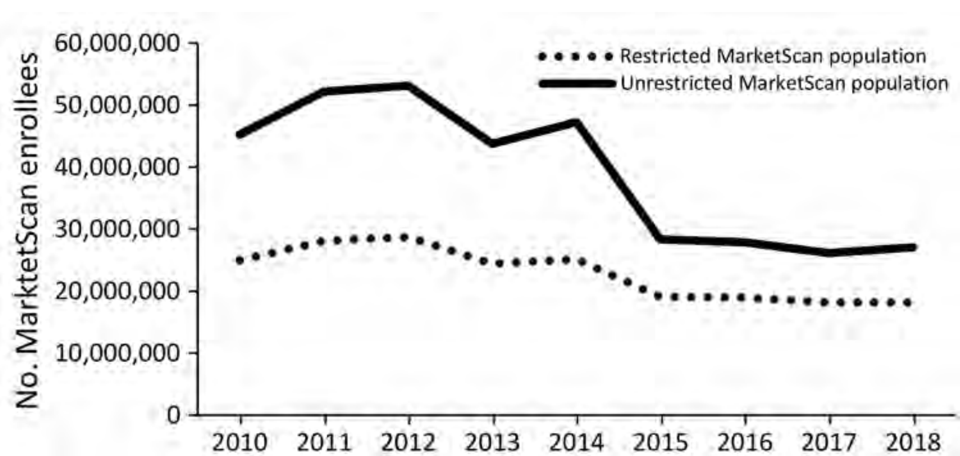


**Figure 1.** Annual restricted and unrestricted MarketScan database enrollment population by year, United States, 2010–2018. The restricted MarketScan population was limited to enrollees with insurance coverage for an entire calendar year, with the potential for pharmaceutical claims data, and a primary beneficiary residing in the United States (excluding territories when possible).

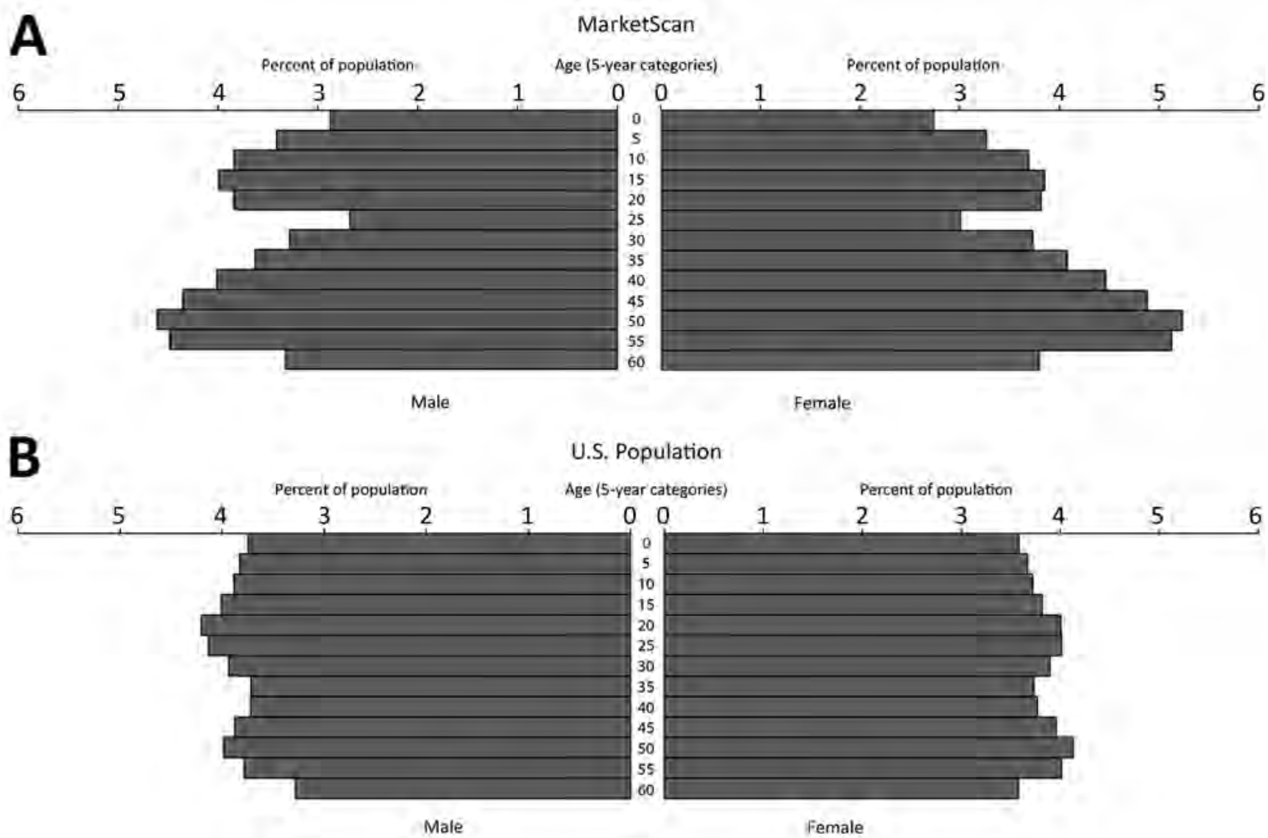


**Figure 2.** Population composition comparison of MarketScan enrollees (A) and US population (B) by age group and sex, United States, 2010–2018.

### Seasonality

The seasonal distribution of Lyme disease diagnoses peaked in the summer months, as it does for cases reported through surveillance (Table 1). Nevertheless, proportionally fewer coded diagnoses occurred during the historically higher incidence season for Lyme disease of May–August (57%) than among cases reported through surveillance (70%) ($p<0.0001$ by $\chi^2$ test; Cramer's V = 0.142) (Table 1).

### Sex and Age Distributions

Median annual incidence of Lyme disease diagnoses among male enrollees was 74.0 (range 46.8–88.9) diagnoses/100,000 enrollees; median annual incidence among female enrollees was similar at 72.0 (range 51.2–86.9) diagnoses/100,000 enrollees. In comparison, median incidence of cases among the male population according to surveillance was 10.6 (range 8.5–13.7) cases/100,000 population; median incidence among the

**Table 1.** Characteristics of Lyme disease diagnoses in MarketScan database versus national surveillance, United States, 2010–2018*

| Category | 2010 | 2011 | 2012 | 2013 | 2014 | 2015 | 2016 | 2017 | 2018 |
|---|---|---|---|---|---|---|---|---|---|
| Overall incidence | | | | | | | | | |
| MarketScan | 49.1 | 58.2 | 56.2 | 73.0 | 79.0 | 74.7 | 75.2 | 87.9 | 73.3 |
| Surveillance | 8.4 | 9.3 | 7.9 | 9.2 | 9.7 | 10.9 | 10.4 | 11.8 | 9.2 |
| Incidence among male enrollees | | | | | | | | | |
| MarketScan | 46.8 | 58.2 | 54.1 | 74.0 | 81.0 | 77.9 | 74.8 | 88.9 | 73.9 |
| Surveillance | 9.2 | 10.4 | 8.5 | 10.6 | 11.3 | 12.8 | 11.9 | 13.7 | 10.6 |
| Incidence among female enrollees | | | | | | | | | |
| MarketScan | 51.2 | 58.1 | 58.1 | 72.0 | 77.2 | 71.7 | 75.6 | 86.9 | 72.7 |
| Surveillance | 7.2 | 7.7 | 6.8 | 7.5 | 7.8 | 8.7 | 8.5 | 9.6 | 7.5 |
| Seasonality, peak month (% of total occurring during May−August) | | | | | | | | | |
| MarketScan | June (53.0) | June (55.2) | June (52.0) | July (59.4) | July (60.1) | July (60.5) | June (53.6) | July (57.9) | June (56.9) |
| Surveillance | June (68.8) | June (71.4) | June (64.6) | July (73.7) | July (72.8) | July (74.0) | June (69.2) | July (71.0) | June (66.0) |

*Incidence calculated as diagnoses/100,000 enrollees in MarketScan or cases/100,000 population among each subcategory.

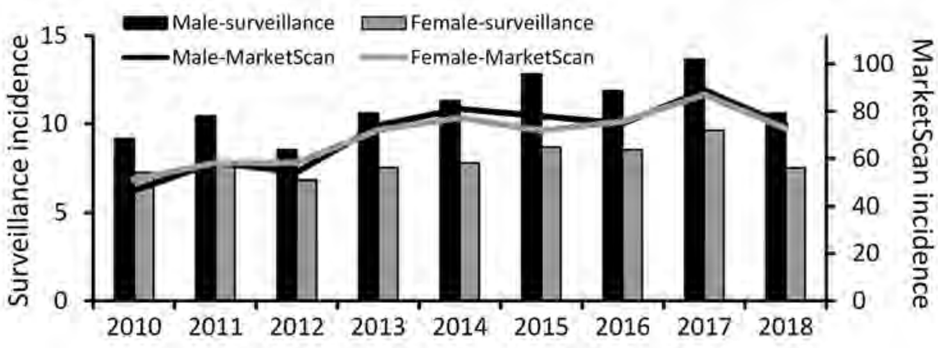


**Figure 3.** Incidence of patients with Lyme disease diagnoses in MarketScan database versus cases found by surveillance, by sex, United States, 2010–2018. Incidence was calculated as diagnoses/100,000 enrollees in MarketScan or cases/100,000 population among each subcategory. Scales for the primary and secondary y axes differ substantially to underscore sex-related incidence patterns but do not permit direct comparison of the magnitude of Lyme disease incidence between systems.

female population was generally lower at 7.7 (range 6.8–9.6) cases/100,000 population (Table 1; Figure 3). Proportionally more diagnoses in MarketScan were among female patients compared with cases identified through surveillance ($p<0.0001$ by $\chi^2$ test; Cramer's V= 0.095).

The sex and age distributions of Lyme disease diagnoses showed similar patterns across the years under study (Appendix Figure). Although both MarketScan and surveillance data display a bimodal age distribution with incidence peaks among children 5–9 years of age and adults >50 years of age, the peak among adults was more pronounced for diagnoses in MarketScan ($p<0.0001$ by $\chi^2$ test; Cramer's V = 0.126) (Appendix Figure).

#### Geographic Distribution

State of residence was available for 94.9% of Lyme disease diagnoses captured in MarketScan during 2010–2018. Of these, ≈80.5% (range 76.6%–83.6%) were from high-incidence states. Although that figure represents most diagnoses, it was smaller than the 93.2% of cases reported from high-incidence states through surveillance ($p<0.0001$ by $\chi^2$ test; Cramer's V = 0.216). Median annual incidence of Lyme disease diagnoses per 100,000 enrollees in MarketScan in high-incidence states was 242.8 (range 190.8–264.3); in neighboring states, 21.5 (range 14.8–32.0); and in low-incidence states, 15.0 (range 11.7–19.9). Median annual incidence per 100,000 population of Lyme disease according to surveillance in high-incidence states was 34.3 (range 28.7–43.0); in neighboring states, 2.1 (range 1.2–3.4); and in low-incidence states, 0.3 (range 0.3–0.5).

A smaller proportion of coded diagnoses identified in MarketScan occurred during the peak months of May–August compared with cases reported from surveillance across each geographic region ($p<0.0001$ by $\chi^2$ test and Cramer's V = 0.1–0.2 for all 3 regional comparisons). Among diagnoses identified in MarketScan, a higher proportion from high-incidence states (59%) occurred during the summer compared with diagnoses from neighboring (53%) and low-incidence states (42%) ($p<0.0001$ by $\chi^2$ test; Cramer's V = 0.113) (Table 2).

In both MarketScan and surveillance data, patient age distributions by sex differed across high-incidence, neighboring, and low-incidence states (Figure 4). Male patients accounted for a greater proportion of diagnoses in high-incidence states (50.8%) than in neighboring (41.9%) and low-incidence (36.6%) states

**Table 2.** Characteristics of Lyme disease diagnoses in MarketScan and reported cases in national surveillance by geographic category of Lyme disease endemicity, United States, 2010–2018*

| | Geographic category of Lyme disease endemicity | | | | | |
|---|---|---|---|---|---|---|
| | High-incidence states | | Neighboring states | | Low-incidence states | |
| Characteristic | MarketScan | Surveillance | MarketScan | Surveillance | MarketScan | Surveillance |
| No. cases | 107,125 | 220,320 | 10,891 | 11,435 | 15,117 | 4,627 |
| % M | 50.8 | 58.5 | 41.9 | 57.1 | 36.6 | 46.6 |
| % F | 49.2 | 41.5 | 58.1 | 42.9 | 63.4 | 53.4 |
| Incidence among male enrollees/population | 237.9 | 40.4 | 18.5 | 2.5 | 11.3 | 0.3 |
| Incidence among female enrollees/population | 220.5 | 28.5 | 24.1 | 1.9 | 18.2 | 0.4 |
| No. (%) occurring during May−August | 63,251 (59) | 112,660 (70) | 5,792 (53) | 6,631 (73) | 6,291 (42) | 2,172 (62) |
| % Change in incidence rate, 2010–2018 | 19.5 | 7.4 | 88.9 | 177.0 | 48.0 | 14.7 |

*Incidence calculated as diagnoses/100,000 enrollees in MarketScan or cases/100,000 population among each subcategory.

(Table 2). Among high-incidence states, the peak incidence of diagnoses was among children 5–9 years and adults >50 years of age, and incidence was elevated among male enrollees across all ages, similar to trends seen in surveillance (Figure 4). In the neighboring states, a peak in incidence among male children was apparent in both MarketScan and surveillance data; however, disproportionately more diagnoses were among female enrollees >15 years of age. In low-incidence states, we observed no obvious trend by age and sex, and overall, the rate of diagnoses among female enrollees was higher than for male enrollees across most age groups (Figure 4).

During 2010–2018, the overall rate of coded Lyme disease diagnoses as identified in MarketScan increased 20% in high-incidence states and 48% in low-incidence states and nearly doubled (89%) in neighboring states (Table 2). Lyme disease incidence according to surveillance during this period increased 7% in high-incidence states and 15% in low-incidence states and more than doubled (177%) in neighboring states.

## Discussion

MarketScan, containing data on >25 million persons annually, is one of the largest sources of health insurance claims data currently available for US residents. We evaluated this database for its potential to serve as a stable source of data on Lyme disease diagnoses. Despite annual fluctuations in the size of the covered population and its restriction to commercially insured persons <65 years of age, the MarketScan population was demographically similar to the US population. Temporal trends observed in MarketScan data were similar to those observed in surveillance data, although the relative rate of diagnoses was substantially higher than that of reported cases. The median

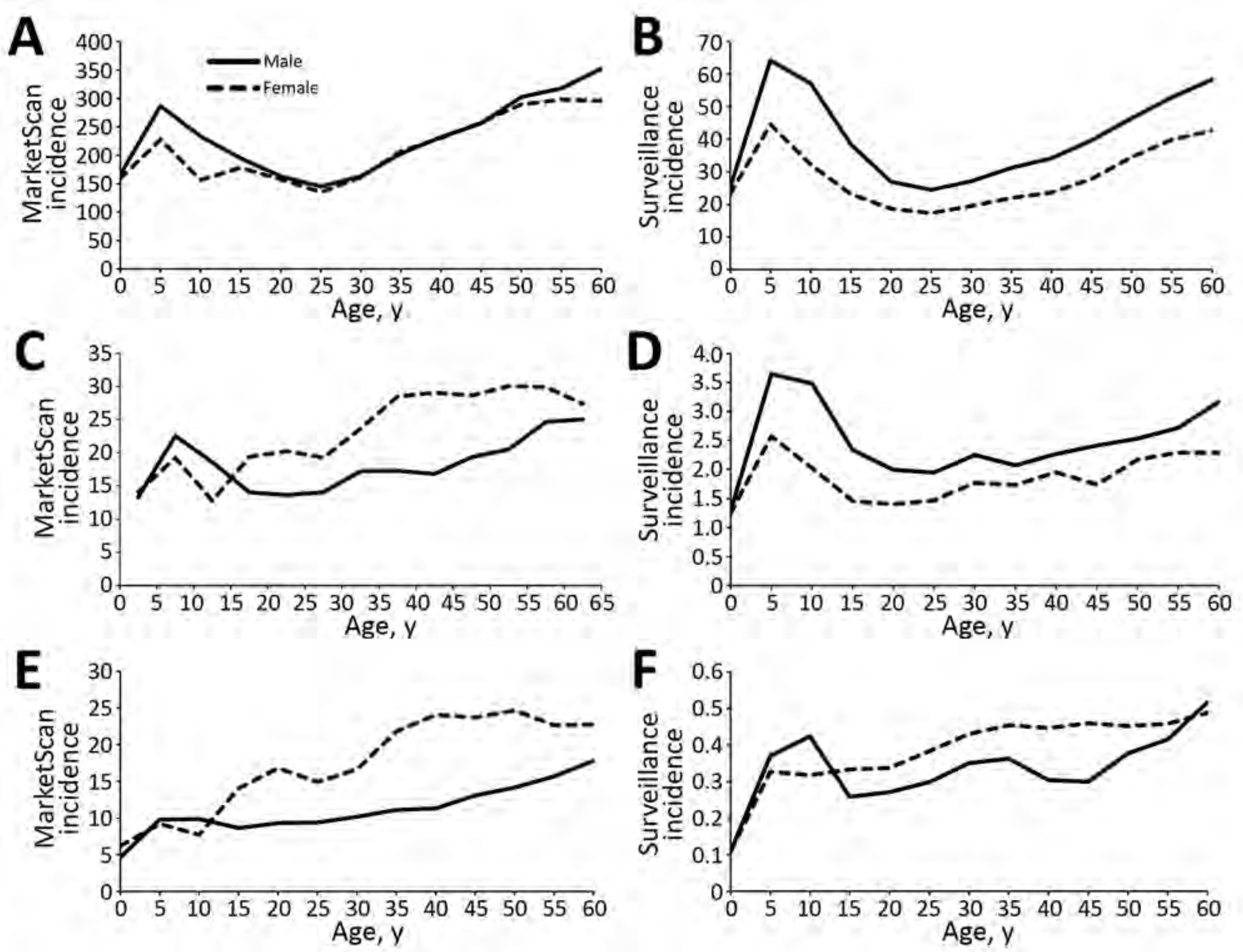


**Figure 4.** Lyme disease incidence by age group and sex in MarketScan enrollees (A, C, E) and from surveillance (B, D, F) by geographic category of Lyme disease endemicity (A– B, high-incidence states; C–D, neighboring states; E–F, low-incidence states), United States, 2010–2018. Incidence was calculated as diagnoses/100,000 enrollees in MarketScan or cases/100,000 population among each subcategory. Scales for each y-axis differ substantially to underscore overall age-related incidence patterns but do not permit direct comparison of the magnitude of Lyme disease between systems or geographic categories.

incidence of coded Lyme disease diagnoses in MarketScan was 73/100,000 enrollees during 2010–2018, ≈62% higher than the 45/100,000 enrollees observed in MarketScan during 2005–2010 (*11*), a temporal increase in Lyme diagnoses comparable to that reported in another insurance claims–based analysis (*15*). In addition, both the rate of Lyme disease diagnoses based on insurance claims and disease incidence as reported through surveillance increased substantially in states neighboring traditionally high-incidence states, a pattern consistent with ongoing geographic expansion of Lyme disease. Lyme disease diagnoses increased at a slower pace in traditionally high-incidence areas, a possible indication that disease risk is becoming more stable in these states. From this analysis, we conclude that MarketScan can serve as a stable source of data for annual evaluation of epidemiologic trends among Lyme disease diagnoses.

The higher incidence observed for Lyme disease diagnoses in MarketScan compared with cases identified through public health surveillance can be explained in large part by underreporting (*16*,*17*). However, variability in seasonal, demographic, and geographic distributions between data from these 2 systems suggest that some proportion of Lyme disease diagnoses captured through MarketScan are the result of misdiagnosis or miscoding. A larger proportion of Lyme disease diagnoses in MarketScan occurred outside of peak summer months, in female enrollees, and outside high-incidence states, compared with cases reported through surveillance. These characteristics may reflect the inclusion of other medical conditions for which Lyme disease may be considered in a differential diagnosis (*18*–*21*). In addition, given our objective of evaluating MarketScan for use on an annual, routine basis, our analysis treats each year independently. Individual patients could meet our designated criteria in multiple years, and consequently, a portion of identified diagnoses may actually reflect retreatment for a nonincident condition. Nevertheless, 91% of persons were diagnosed only once during the 9-year time frame.

In a recent evaluation of >1,200 persons referred for tertiary evaluation for Lyme disease in a high-incidence area, nearly three quarters lacked clinical or laboratory evidence of *Borrelia burgdorferi* infection; the majority of these persons referred with a diagnosis of Lyme disease were female and experiencing a long duration of constitutional symptoms (*18*). Given the relative scarcity of infected host-seeking ticks in low-incidence areas, the potential for locally acquired Lyme disease is often very low (*22*,*23*). Moreover, this low likelihood of Lyme disease translates to an increased probability of false-positive test results and, in turn, misdiagnoses for both humans and animals (*24*–*27*). In both MarketScan and surveillance data, the epidemiologic characteristics of Lyme disease differ between low- and high-incidence regions, consistent with proportionally more misdiagnoses in low-incidence states (*2*,*25*,*28*,*29*). Similarly, in a previous evaluation of Lyme disease cases reported through surveillance from low-incidence states (*25*), epidemiologic characteristics of cases with recent travel to high-incidence areas differed from those cases lacking reported travel. Further study would be helpful to understand which conditions, signs, or symptoms may be commonly mistaken for Lyme disease in these areas.

We used a Lyme disease−specific ICD code combined with appropriate antimicrobial treatment as a proxy measure for clinical diagnosis, a measure that is subject to limitations. Comprehensive laboratory data were not available for the majority of MarketScan enrollees and were not used to identify or rule out Lyme disease diagnoses. ICD codes are primarily used by medical institutions for billing, not for health studies, and practices are known to vary by coder and facility (*30*). We attempted to minimize use of rule-out codes by marrying temporally relevant treatment information, but some persons counted as Lyme disease diagnoses may not have received treatment for presumptive Lyme disease, but for another condition for which a similar antimicrobial therapy may be appropriate. Conversely, prior research suggests that Lyme disease−specific ICD codes are often omitted from medical records of patients with Lyme disease (*16*,*31*,*32*). Thus, the diagnoses summarized here using disease-specific codes likely reflect a fraction of all Lyme disease diagnoses and are therefore not comprehensive, even within the MarketScan database (*32*). Additional efforts analyzing coding patterns can be employed to create generalizable estimates regarding the incidence of clinician-diagnosed Lyme disease, which cannot be construed from these data alone (*11*,*33*). Despite statistical tests that indicated significant differences in the distributions of sex, age, and geographic representation between the MarketScan population and the US population, very low Cramer's V values together suggest minimal differences in these distributions. However, the MarketScan CCAE databases do not contain information on uninsured persons, adults ≥65 years of age, or members of the military; consequently, these data are not entirely representative of the US population. Exploration of Medicare and Medicaid data may provide more insight into patterns of Lyme disease in populations not reflected in this analysis.

As access to electronic data sources for health-related information increases, more diverse data can be queried to more comprehensively inform the epidemiology of Lyme disease. However, when using novel data sources, the volume, stability, and representativeness must be considered before drawing inference. We evaluated the potential for 1 commercial health insurance claims database, MarketScan, to provide reliable information on an annual basis about the epidemiology of Lyme disease diagnoses. Despite limitations in generalizability of the data source and incompleteness of use of Lyme disease–specific codes, MarketScan provided a stable source of data for Lyme disease diagnoses that is comparable across years and could serve as a resource-efficient adjunct to surveillance. Although Lyme disease diagnoses identified from claims data are not supported by the robust evidence of infection required for surveillance reporting, they are a consistent indicator of trends in the healthcare system. In addition, the sheer volume of data available through MarketScan provides potential for new insights into the epidemiology of Lyme disease diagnoses in the United States.

### Acknowledgments

We thank Paul Mead and William Mac Kenzie for providing valuable insight and Mark Delorey for providing statistical advice. We thank the public health personnel from state and local health departments for their contributions to the Lyme disease surveillance data used in this analysis.

## About the Author

Ms. Schwartz is an epidemiologist in the Bacterial Diseases Branch, Division of Vector-Borne Diseases, National Center for Emerging and Zoonotic Infectious Diseases, Centers for Disease Control and Prevention, Fort Collins, Colorado. Her primary research interests are the epidemiology and prevention of bacterial vectorborne infections.

### References

1. Steere AC. Lyme disease (Lyme borreliosis) due to *Borrelia burgdorferi*. In: Bennett JE, Dolin R, Blaser MJ, editors. Mandell, Douglas, and Bennett's principles and practice of infectious diseases. 8th ed. Philadelphia: Elsevier/Saunders; 2015. p. 2725–35.
2. Schwartz A, Hinckley A, Mead P, Hook S, Kugeler K. Surveillance for Lyme disease—United States, 2008–2015. MMWR Surveill Summ. 2017;66:1–12. https://doi.org/10.15585/mmwr.ss6622a1
3. Kugeler K, Farley G, Forrester J, Mead P. Geographic distribution and expansion of human Lyme disease, United States. Emerg Infect Dis. 2015;21:1455–7. https://doi.org/10.3201/eid2108.141878
4. Centers for Disease Control and Prevention. National Notifiable Diseases Surveillance System (NNDSS). 2019 [cited 2020 Feb 6]. https://wwwn.cdc.gov/nndss
5. Lukacik G, White J, Noonan-Toly C, Didonato C, Backenson PB. Lyme disease surveillance using sampling estimation: evaluation of an alternative methodology in New York State. Zoonoses Public Health. 2018;65:260–5. https://doi.org/10.1111/zph.12261
6. Cartter ML, Lynfield R, Feldman KA, Hook SA, Hinckley AF. Lyme disease surveillance in the United States: looking for ways to cut the Gordian knot. Zoonoses Public Health. 2018;65:227–9. https://doi.org/10.1111/zph.12448
7. Bjork J, Brown C, Friedlander H, Schiffman E, Neitzel D. Validation of random sampling as an estimation procedure for Lyme disease surveillance in Massachusetts and Minnesota. Zoonoses Public Health. 2018;65:266–74. https://doi.org/10.1111/zph.12297
8. Wallin TM, Culpepper JW, Campbell DJ, Nelson ML, Langer-Gould AA, Marrie RR, et al. The prevalence of MS in the United States. Neurology. 2019;92:e1029–40. https://doi.org/10.1212/WNL.0000000000007035
9. Li S, Peng Y, Weinhandl ED, Blaes AH, Cetin K, Chia VM, et al. Estimated number of prevalent cases of metastatic bone disease in the US adult population. Clin Epidemiol. 2012;4:87–93. https://doi.org/10.2147/CLEP.S28339
10. Broder M, Cai B, Chang E, Neary M. Epidemiology of gastrointestinal neuroendocrine tumors in a U.S. commercially insured population. Endocr Pract. 2017;23:1210–6. https://doi.org/10.4158/EP171879.OR
11. Nelson CA, Saha S, Kugeler KJ, Delorey MJ, Shankar MB, Hinckley AF, et al. Incidence of clinician-diagnosed Lyme disease, United States, 2005–2010. Emerg Infect Dis. 2015;21:1625–31. https://doi.org/10.3201/eid2109.150417
12. Kwit NA, Nelson CA, Max R, Mead PS. Risk factors for clinician-diagnosed Lyme arthritis, facial palsy, carditis, and meningitis in patients from high-incidence states. Open Forum Infect Dis. 2017;5. https://doi.org/10.1093/ofid/ofx254
13. US Census Bureau. Annual state resident population estimates for 6 race groups (5 race alone groups and two or more races) by age, sex, and Hispanic origin: April 1, 2010 to July 1, 2018. 2019 [cited 2020 Dec 9]. https://www2.census.gov/programs-surveys/popest/tables/2010-2018/state/asrh/sc-est2018-alldata6.csv
14. Centers for Medicare and Medicaid Services. ICD-10. 2020 [cited 2020 Mar 3]. https://www.cms.gov/Medicare/Coding/ICD10/index
15. Tseng Y-J, Cami A, Goldmann DA, DeMaria A Jr, Mandl KD. Using nation-wide health insurance claims data to augment Lyme disease surveillance. Vector Borne Zoonotic Dis. 2015;15:591–6. https://doi.org/10.1089/vbz.2015.1790
16. White J, Noonan-Toly C, Lukacik G, Thomas N, Hinckley A, Hook S, et al. Lyme disease surveillance in New York State: an assessment of case underreporting. Zoonoses Public Health. 2018;65:238–46. https://doi.org/10.1111/zph.12307
17. Schiffman EK, McLaughlin C, Ray JAE, Kemperman MM, Hinckley AF, Friedlander HG, et al. Underreporting of Lyme and other tick-borne diseases in residents of a high-incidence county, Minnesota, 2009. Zoonoses Public Health. 2018;65:230–7. https://doi.org/10.1111/zph.12291
18. Kobayashi T, Higgins Y, Samuels R, Moaven A, Sanyal A, Yenokyan G, et al. Misdiagnosis of Lyme disease with unnecessary antimicrobial treatment characterizes patients referred to an academic infectious diseases clinic. Open Forum Infect Dis. 2019;6:ofz299. https://doi.org/10.1093/ofid/ofz299

19. Rose CD, Fawcett PT, Gibney KM, Doughty RA. The overdiagnosis of Lyme disease in children residing in an endemic area. Clin Pediatr.(Phila) 1994;33:663–8. https://doi.org/10.1177/000992289403301105
20. Sigal LH. Summary of the first 100 patients seen at a Lyme disease referral center. Am J Med. 1990;88:577–81. https://doi.org/10.1016/0002-9343(90)90520-N
21. Steere AC, Taylor E, McHugh GL, Logigian EL. The overdiagnosis of Lyme disease. JAMA. 1993;269:1812–6. https://doi.org/10.1001/jama.1993.03500140064037
22. Maggi RG, Reichelt S, Toliver M, Engber B. *Borrelia* species in *Ixodes affinis* and *Ixodes scapularis* ticks collected from the coastal plain of North Carolina. Ticks Tick Borne Dis. 2010;1:168–71. https://doi.org/10.1016/j.ttbdis.2010.08.003
23. Oliver JH Jr, Lin T, Gao L, Clark KL, Banks CW, Durden LA, et al. An enzootic transmission cycle of Lyme borreliosis spirochetes in the southeastern United States. Proc Natl Acad Sci U S A. 2003;100:11642–5. https://doi.org/10.1073/pnas.1434553100
24. Tugwell P, Dennis DT, Weinstein A, Wells G, Nichol G, Shea B, et al. Laboratory evaluation in the diagnosis of Lyme disease. Ann Intern Med. 1997;127:1109–23. https://doi.org/10.7326/0003-4819-127-12-199712150-00011
25. Forrester JD, Brett M, Matthias J, Stanek D, Springs CB, Marsden-Haug N, et al. Epidemiology of Lyme disease in low-incidence states. Ticks Tick Borne Dis. 2015;6:721–3. https://doi.org/10.1016/j.ttbdis.2015.06.005
26. Mead P, Goel R, Kugeler K. Canine serology as adjunct to human Lyme disease surveillance. Emerg Infect Dis. 2011;17:1710–2. https://doi.org/10.3201/1709.110210
27. Millen K, Kugeler KJ, Hinckley AF, Lawaczeck EW, Mead PS. Elevated Lyme disease seroprevalence among dogs in a nonendemic county: harbinger or artifact? Vector Borne Zoonotic Dis. 2013;13:340–1. https://doi.org/10.1089/vbz.2012.1025
28. Bacon RM, Kugeler KJ, Mead PS. Surveillance for Lyme disease–United States, 1992–2006. MMWR Surveill Summ. 2008;57:1. https://www.cdc.gov/mmwr/pdf/ss/ss5710.pdf
29. Kwit NA, Dietrich EA, Nelson C, Taffner R, Petersen J, Schriefer M, et al. High volume of Lyme disease laboratory reporting in a low-incidence state—Arkansas, 2015–2016. MMWR Morb Mortal Wkly Rep. 2017;66:1156–7. https://doi.org/10.15585/mmwr.mm6642a8
30. Thomas N, Rutz HJ, Hook SA, Hinckley AF, Lukacik G, Backenson BP, et al. Assessing diagnostic coding practices among a sample of healthcare facilities in Lyme disease–endemic areas: Maryland and New York—a brief report. Zoonoses Public Health. 2018;65:275–8. https://doi.org/10.1111/zph.12414
31. Rutz H, Hogan B, Hook S, Hinckley A, Feldman K. Exploring an alternative approach to Lyme disease surveillance in Maryland. Zoonoses Public Health. 2018;65:254–9. https://doi.org/10.1111/zph.12446
32. Naleway AL, Belongia EA, Kazmierczak JJ, Greenlee RT, Davis JP. Lyme disease incidence in Wisconsin: a comparison of state-reported rates and rates from a population-based cohort. Am J Epidemiol. 2002;155:1120–7. https://doi.org/10.1093/aje/155.12.1120
33. Kugeler KJ, Schwartz AS, Delorey M, Mead P, Hinckley AF. Estimating the frequency of Lyme disease diagnoses, United States, 2010–2018. Emerg Infect Dis. 2020;27:616–9.


Address for correspondence: Alison Hinckley, Centers for Disease Control and Prevention, 3156 Rampart Rd, Fort Collins, CO 80521, USA; email: ahinckley@cdc.gov

# Highly Pathogenic Avian Influenza A(H5N8) Virus Spread by Short- and Long-Range Transmission, France, 2016–17

François-Xavier Briand, Eric Niqueux, Audrey Schmitz, Claire Martenot, Martine Cherbonnel, Pascale Massin, Florian Kerbrat, Marina Chatel, Carole Guillemoto, Cecile Guillou-Cloarec, Katell Ogor, Aurélie Le Prioux, Chantal Allée, Véronique Beven, Edouard Hirchaud, Yannick Blanchard, Axelle Scoizec, Sophie Le Bouquin, Nicolas Eterradossi, Béatrice Grasland

We detected 3 genotypes of highly pathogenic avian influenza A(H5N8) virus in France during winter 2016–17. Genotype A viruses caused dramatic economic losses in the domestic duck farm industry in southwestern France. Our phylogenetic analysis suggests that genotype A viruses formed 5 distinct geographic clusters in southwestern France. In some clusters, local secondary transmission might have been started by a single introduction. The intensity of the viral spread seems to correspond to the density of duck holdings in each production area. To avoid the introduction of disease into an unaffected area, it is crucial that authorities limit the movements of potentially infected birds.

Influenza A viruses are enveloped viruses of the *Alphainfluenzavirus* genus in the *Orthomyxoviridae* family. Their negative-stranded RNA genome consists of 8 segments encoding a total of 10–14 proteins. Avian influenza viruses (AIVs) are classified on the basis of antigenic differences in their surface glycoproteins, hemagglutinin (H1–H16) and neuraminidase (N1–N9) (*1*). H5 and H7 subtypes can become highly pathogenic avian influenza (HPAI) viruses after the evolution of multiple basic amino acids in the cleavage site of hemagglutinin protein (*2*,*3*). This mutation enables the virus to replicate efficiently in all organs, causing a severe and often fatal systemic disease. In contrast, the cleavage site of hemagglutinin in low pathogenicity AIVs lacks these multiple amino acids, restricting viral replication to the respiratory and digestive tracts. Low pathogenicity AIVs cause subclinical or mild disease that can be aggravated by secondary infections (*4*,*5*). Because H5 and H7 AIVs can evolve to be highly pathogenic, the diseases caused by these subtypes are notifiable to national and international bodies (*6*).

Since 1996, highly pathogenic H5 viruses of the A/goose/Guangdong/1/96 (Gs/GD/96) lineage have caused recurrent outbreaks with high death rates in birds. These HPAIs are categorized into 10 distinct clades (0–9) on the basis of hemagglutinin sequences (*7*). These clades are found in Asia; a few have spread to Africa, Europe, and North America (*8*–*10*). Europe experienced major introductions of H5N1 of clade 2.2 during 2005–2007 and H5N8 of clade 2.3.4.4 during 2014–2020 (*11*–*14*). Many reassortments were observed on Gs/Gd/1/96–like viruses, especially within clade 2.3.4.4. The reassortments generated several subtypes including H5N1, H5N2, H5N5, H5N6, and H5N8 (*11*,*15*–*17*). During winter 2016–17, twenty-nine countries in Europe reported 1,576 cases of Gs/Gd/1/96–like H5N8 infections in wild birds and 1,134 in poultry, especially domestic ducks (*18*).

During this outbreak, researchers identified 6 HPAI A(H5N8) genotypes in Europe; 2 of these genotypes were identified using 6 sequences from infected birds in France (*19*). France had 539 cases of HPAI A(H5N8) infections, 51 in wild birds and 488 in poultry flocks, most of which occurred at duck farms producing foie gras (*18*). A previous study used spatiotemporal analysis of clinical cases comprising 2 distinct epizootic periods in southwestern France (*20*). The first period spanned November 28, 2016–February 2, 2017 and comprised 4 spatiotemporal clusters (*20*). The second period spanned February 3–March 23, 2017 and comprised a single spatiotemporal cluster (*20*).

Author affiliation: Agence Nationale de Sécurité Sanitaire de l’Alimentation, de l’Environnement et du Travail, Ploufragan, France

DOI: https://doi.org/10.3201/eid2702.202920

During the first period, the disease spread mainly among local farms; during the second period, after local farm-to-farm spread, the average distance between affected farms increased (*20*). To limit viral spread among poultry farms, the French Ministry of Agriculture and Food established protection zones (3 km radius) and surveillance zones (1 km radius) around outbreak sites according to European Union regulations (*21*). Additional control measures included preventive culling of poultry inside surveillance zones and of outdoor palmipeds inside protection zones (*21*).

We sequenced 212 whole genomes of HPAI A(H5N8) viruses infecting wild and domestic birds during the outbreak in France. We used these molecular data to identify the geographic distribution and track the spread of H5N8 genotypes.

## Material and Methods

### Sampling

We collected oropharyngeal and cloacal swab samples from wild birds that had died of suspected H5N8 infection and from domestic or captive birds that had clinical signs of avian influenza. Official veterinarians from the Ministry of Agriculture and Food collected samples from poultry in surveillance zones before they were transferred or culled (*21*). Staff at district laboratories approved by the Ministry of Agriculture and Food suspended the swab samples in 2 mL of phosphate-buffered saline (PBS) and separated samples from domestic poultry into 5 pools.

### Detection and Characterization of HPAI A(H5N8) Genomes

Staff at the district laboratories extracted viral RNA from each pool using the RNeasy Mini Kit (QIAGEN, https://www.qiagen.com) according to the manufacturer's instructions. They tested RNA samples by real-time reverse transcription PCR selective for the matrix gene and H5 gene; pathotype was determined as described (*22*) at the French National Reference Laboratory for Avian Influenza (Ploufragan, France). Samples from domestic poultry that had a cycle threshold ($C_t$) value <30 underwent whole-genome sequencing at the Agence Nationale de Sécurité Sanitaire de l'Alimentation, de l'Environnement et du Travail (Ploufragan). All AIV-positive samples from wild birds, regardless of $C_t$ value, also underwent whole-genome sequencing at the Agence Nationale de Sécurité Sanitaire de l'Alimentation, de l'Environnement et du Travail. We amplified viral genomes with real-time reverse transcription PCR using specific primers at the 5′ and 3′ conserved ends of all 8 AIV genome segments (*23*). We sequenced amplicons with Ion Torrent technology (ThermoFisher Scientific, https://www.thermofisher.com). Libraries were prepared by using the Ion Xpress Plus Fragment Library Kit (ThermoFisher Scientific), selected by size, and cleaned by using the Agencourt AMPure XP (Beckman Coulter Life Sciences, https://www.beckman.com). We conducted emulsion PCR on the Ion OneTouch 2 system and subsequent enrichment of template particles on the Ion OneTouch ES system using the Ion PI template OT2 200 Kit version 3 (ThermoFisher Scientific). We loaded the samples onto a PI chip and sequenced them on an Ion Torrent Proton (ThermoFisher Scientific). We obtained the consensus sequence by comparing the de novo analysis with reference sequences from the Influenza Research Database (https://www.fludb.org) (*24*). We downsampled the reads to fit a coverage of 80× and submitted them to the SPAdes version 3.1.1 de novo assembler (http://cab.spbu.ru/software/spades). We submitted the de novo contigs to BLAST (https://blast.ncbi.nlm.nih.gov/Blast.cgi) on a local nucleotide database. For each segment, we selected the best matches for Bowtie 2 alignment (*25*). Finally, we compared de novo assemblies and alignment on the references and assessed their strict identities. We retained only the sequences with a coverage of ≥30× for all segments for further analysis. For the following analyses we considered only sequences from nucleotide positions 20–2248 for polymerase basic (PB) 2 protein, 4–2259 for PB 1 protein, 41–2151 for polymerase acidic (PA) protein, 49–1704 for hemagglutinin, 14–1458 for nucleoprotein (NP), 50–1385 for neuraminidase, 38–936 for matrix protein, and 28–815 for nonstructural protein, according to the first ATG. We submitted sequences to GenBank (Appendix Table 1, https://wwwnc.cdc.gov/EID/article/27/2/20-2920-App1.pdf).

### Phylogenetic Analysis

For the phylogenetic analysis, we used only samples with complete sequences for each segment. We aligned the sequences with ClustalW (http://www.clustal.org). We used MEGA version 7.0 software (*26*) to construct maximum-likelihood phylogenetic trees with 500 bootstrap replicates using the Tamura 3-parameter model. Then, we compared each segment that was representative of a phylogenetic group (i.e., closed sequences with >98% nucleotide identity) to sequences available in the GISAID database (https://www.gisaid.org).

For each sequence, we concatenated 8 AIV gene segments and tested them for reassortment using the RDP4 software (*27*) with the SIScan, Bootscan, RDP, MaxChi, and GENECOV methods. We estimated the time to most recent common ancestor (tMRCA) of the viral sequences by performing Bayesian coalescent phylogenetic analyses in BEAST version 1.7 (*28*). The models considered constant size, exponential growth, expansion growth, and Bayesian Skygrid for coalescent model in combination with a strict or uncorrelated lognormal clock model. We chose the best model on the basis of Akaike's Information Criterion value (*29*). We applied the uncorrelated lognormal molecular clock with the SDR06 model of nucleotide substitution and Bayesian Skygrid coalescent model (*30*) as in previous studies (*8*,*19*). We ran the model for 40 million generations with sampling evolutionary parameters every 4,000 generations. We visualized the trace files with Tracer 1.6 (http://beast.community/tracer) to check that the effective sample size values were >200, which corresponded to an acceptable number of independent samples (*31*). After removing a 10% burn-in with TreeAnnotator version 1.7.5 (https://beast.community/treeannotator), we generated maximum clade credibility trees. We annotated the trees with Figtree version 1.4 (http://tree.bio.ed.ac.uk/software/figtree). We visualized the evolution of the effective population size of A(H5N8) viruses in southwestern France using Icytree (*32*).

### Potential Transmission Networks

We reconstructed the potential transmission networks using a minimum spanning tree from PopART version 1.7 (*33*) corresponding to a parsimony method to reconstruct the relationships among highly similar genomes. We analyzed 197 genomes of H5N8 viruses from southwestern France and determined the number of local geographic clusters by testing the model using 2–8 clusters; 5 geographic clusters produced the most consistent relationship between geographic clustering and genome similarity.

## Results

### Epizootic Case Situation

During winter 2016–17, France declared 539 cases of HPAI H5 infection, the second-highest number of cases in Europe. In total, 488 cases were in domestic or captive birds, primarily ducks, and 51 cases were in wild birds (Figure 1). The 488 domestic cases were

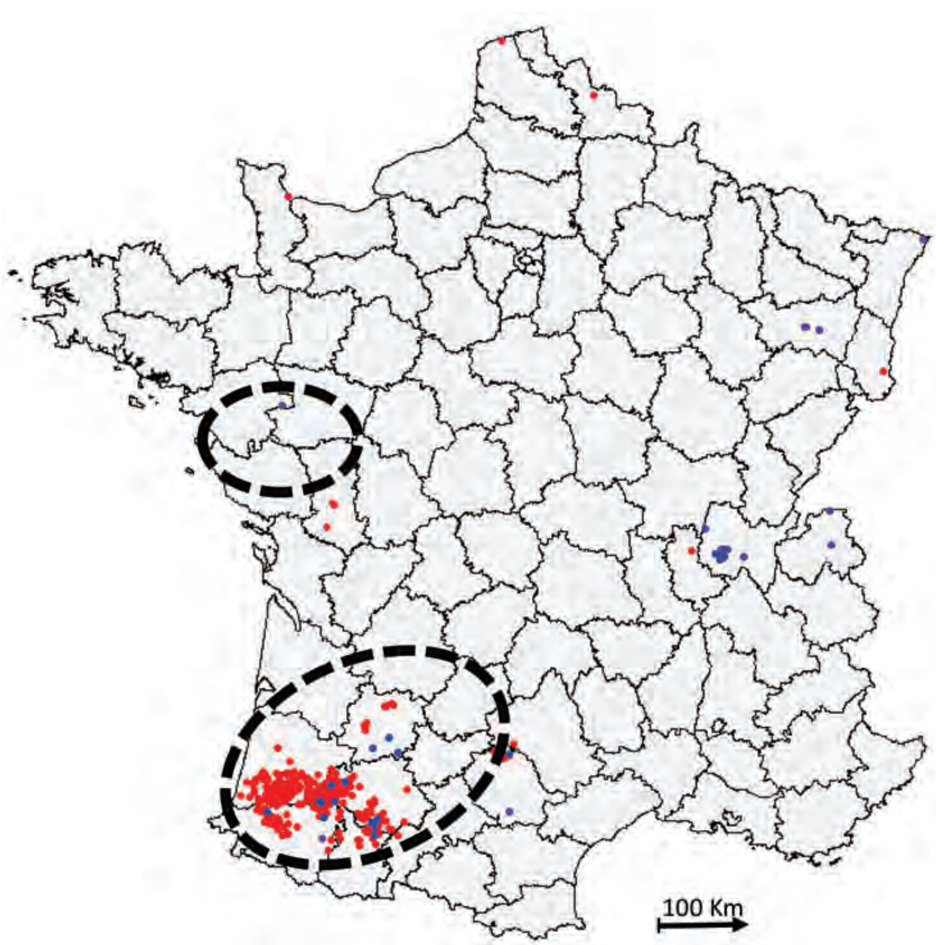


**Figure 1.** Distribution of highly pathogenic avian influenza H5N8 cases, France, 2016–17 (database of the French National Reference Laboratory for Avian Influenza). Blue indicates cases in wild birds; red indicates cases in domestic or captive birds. Dashed circles indicate zones of high duck farm density (*34*).

mainly in southwestern France, whereas H5N8 infection was more common in wild birds in other areas of France (Appendix Table 1). Seventeen cases were detected in wild birds, mostly common buzzards, in southwestern France, whereas cases in wild birds from other areas were in waterfowl (mostly swans). During this period in southwestern France, other AIVs were also identified, indicating viral cocirculation within poultry farms (data not shown).

### H5N8 Genotypes

Of the 539 detected HPAI H5 viruses, we characterized 212 viral genomes: 15 from wild birds (Appendix Table 2) and 197 from domestic or captive birds. Phylogenetic analyses of 8 genes indicated that the H5N8 viruses from France formed a monophyletic cluster for only the hemagglutinin, neuraminidase, matrix, and nonstructural genes (a monophyletic cluster has >98% similarity and a bootstrap value of ≥75), whereas the PB2, PB1, PA, and NP sequences formed 2 different phylogenetic clusters. We identified 3 genotypes (A–C) in France on the basis of all segment sequences. Genotype A differed from genotype B in segments PB2, PA, and NP and differed from genotype C in only segment PB1. Genotype A comprised 197 viruses and was a H5N8-A/mute_swan/Croatia/70/2016–like virus (*35*). Although genotype A was the most common genotype in our study, we found it only in southwestern France (Figure 2). We detected 192 genotype A viruses in poultry but only 5 in wild birds. Genotype B was a A/wild_duck/Poland/82A/2016–like virus (*35*,*36*). We found genotype B viruses in northern, western, and eastern France and detected 3 viruses in captive/domestic birds and 5 in wild birds. Genotype C was a A/domestic_goose/Poland/33/2016–like virus (*37*). We detected 7 genotype C viruses: 2 in captive/domestic birds in southwestern France and 5 in wild birds in eastern France.

### Geographic Clustering of Genotype A Viruses

On November 28, 2016, we detected genotype A virus in domestic breeding ducks in southwestern France. In total, we found 496 cases of HPAI

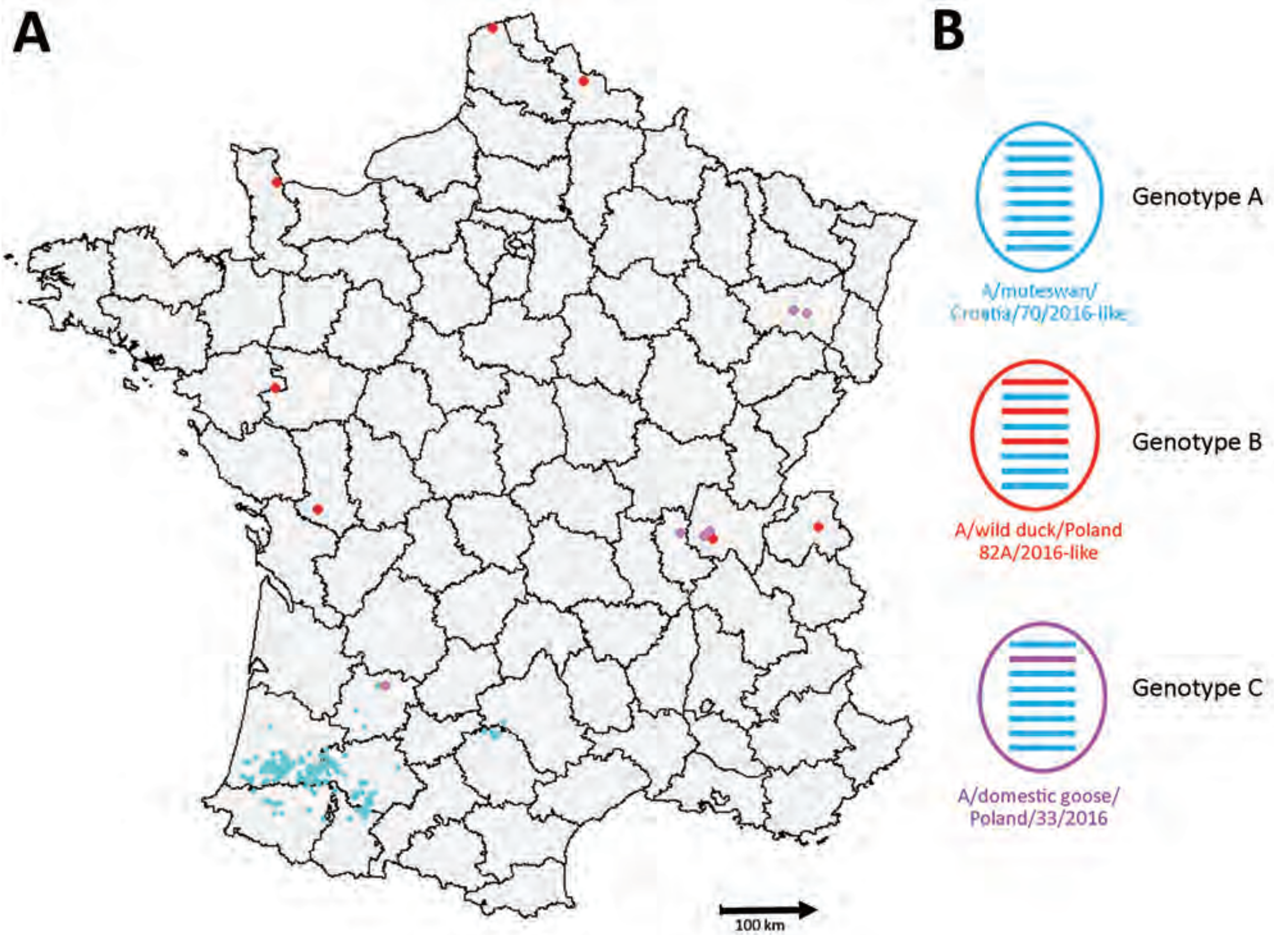


**Figure 2.** Distribution of the 3 detected genotypes of highly pathogenic avian influenza H5N8 viruses, France, 2016–17. A) Geographic distribution of genotypes. B) Representation of viral genome. Horizontal bars correspond to the 8 gene segments of each characterized genotype. Segments colored according to phylogenetic cluster.

A(H5N8) infection in southwestern France. Of the 496 cases, we determined full genome sequences for 197 (41.25%) viruses, all of which were genotype A. The 197 genomes comprised 5 geographic clusters: geocluster 1 contained 10 viruses in France departments nos. 12 and 81; geocluster 2 contained 5 viruses in department no. 47; geocluster 3 contained 41 viruses mostly in departments nos. 32 and 65; geocluster 4 contained 74 viruses in the east of the department no. 40 and a few viruses in departments nos. 32 and 64; geocluster 5 contained 67 sequences in departments nos. 40 and 64 (Figure 3).

The viruses in geocluster 1 were closely related (Figure 3); the tMRCA was November 16, 2016 (highest posterior density [HPD] 95% CI November 9–23) (Appendix Table 3). The viruses in geocluster 5 had a common ancestor that emerged on January 15, 2017 (HPD 95% CI January 7–23) from geocluster 3 (Appendix Table 4). This date probably corresponds with introduction of HPAI A(H5N8) into geocluster 5; the first case in geocluster 5 was documented in domestic ducks on January 30, 2017 (Figure 4). The first sequences to emerge in geoclusters 2, 3, and 4 were similar; afterwards, the sequences diverged into each geocluster. We did not calculate the viral transmission dates for geoclusters 2, 3, and 4 because these phylogenetic groups were not monophyletic and did not have posterior probabilities >0.8 for their ancestral nodes.

We constructed a phylogenetic tree of the 197 analyzed genomes (Figure 3). The tree had several principle nodes composed of identical sequences; many leaves were linked, indicating the evolution of numerous sequences from the principal nodes. The mean nucleotide difference between 2 related sequences belonging to distinct nodes was ≈3.1 mutations (range 1–11 mutations). The mean mutation rate of the complete genome was $6.68 \times 10^{-3}$ (HPD 95% CI $5.96–7.43 \times 10^{-3}$) substitutions/site/year.

### Dynamic Evolution of Genotype A

We used a Bayesian Skygrid plot to analyze the population growth of H5N8 viruses in southwestern France (Figure 5). The overall population increased during November 2016–January 2017, which corresponds to the period in which moderate viral spread occurred in geoclusters 1 and 2 and more pronounced spread occurred in geoclusters 3 and 4. After this time, we noted an overall population decrease corresponding with the last cases reported in geoclusters 3 and 4. The population dramatically increased during February 2017, when cases began in geocluster 5. The HPAI A(H5N8) population size declined in March 2017.

## Discussion

The 2016–17 HPAI A(H5N8) outbreak in Europe affected 1,576 wild birds and 1,134 domestic birds (*18*).

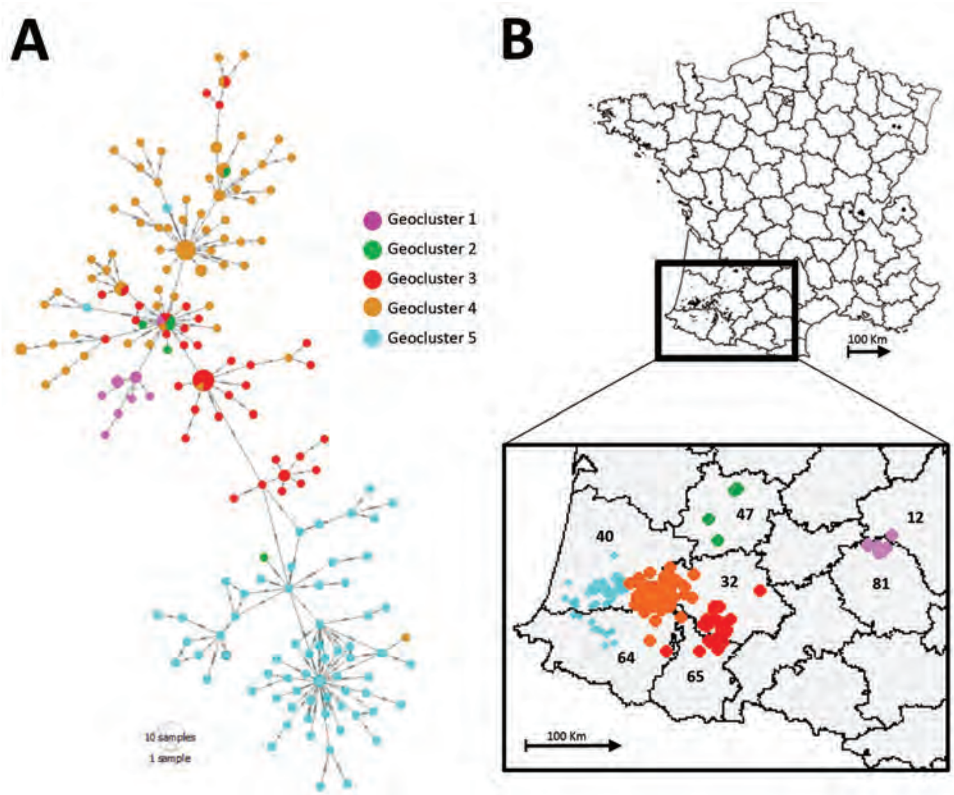


**Figure 3.** Minimum spanning tree and map of clusters of highly pathogenic avian influenza H5N8 genotype A viruses, France, 2016–17. A) Geographic clusters. Number of dashes indicates the number of observed mutations between 2 nodes. Circle size corresponds to the number of identical sequences. B) Geographic repartition of genotype in southwestern France. Inset shows identification numbers of affected departments: 12, Aveyron; 31, Haute-Garonne; 32, Gers; 47, Lot et Garonne; 40, Landes; 64, Pyrénées-Atlantiques; 65, Hautes-Pyrénées. Trees created using PopART (*32*).

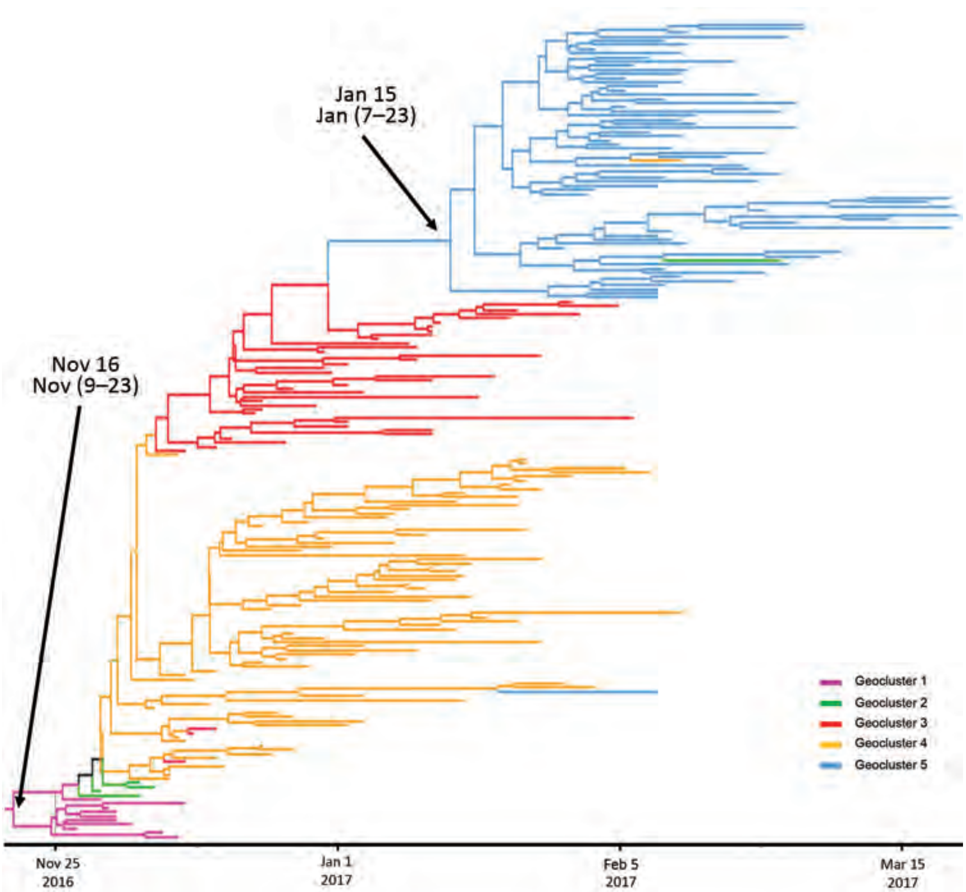


**Figure 4.** Maximum credibility tree of the 8 concatenated gene segments in highly pathogenic avian influenza H5N8 genotype A viruses, France, 2016–17. Tree generated using SDR06 model according to Bayesian method (*38*). Branch and leaf color indicates geoclusters. The estimated dates of common ancestors and their 95% CIs are indicated for geocluster 1 and geocluster 5.

In France, we identified 3 genotypes that had previously been described elsewhere in Europe (*19*,*35*–*7*), indicating that H5N8 was introduced into France $\geq$3 times during November 2016–April 2017. We found sporadic cases of genotypes B and C, mostly in wild birds. We found 197 viruses of genotype A, almost all of which were in domestic ducks in southwestern France. Only 2 viruses of genotype A were in backyard poultry, an observation that corresponds to the findings of Souvestre et al. (*39*), which showed the minor role of backyards in the H5N8 transmission dynamic. Of the 6 genotypes characterized during this outbreak in Europe, 3 genotypes resemble the sequences now described in France (i.e., genotype A corresponds with reassortants 6-like, B with reassortants 3-like, and C with reassortants 7-like) (*19*).

Similar sequences to genotype A viruses were identified in Croatia, Italy, Belgium, Poland, and the Czech Republic; they also were found in domestic ducks in Hungary (*19*). France and Hungary are the main producers of foie gras in Europe. Areas with high duck farm density (*34*) had an increased number of H5N8 cases in domestic birds during this outbreak (*18*,*19*). The H5N8 sequences found in Hungary are closely related to the genotype A viruses described in this study, an observation that might indicate an epidemiologic link between these 2 regions. Alternatively, the viral similarity could have been caused by the common use of mule ducks for foie gras, which might be more susceptible to genotype A than other H5N8 viruses.

All genotype A viruses found in France were closely related and formed a monophyletic cluster, strongly suggesting that this genotype was introduced only once into southwestern France. Genotype A viruses might have spread among domestic duck farms in a multistep process. First, genotype A viruses were introduced into southwestern France, where they spread and formed geocluster 1. According the tMRCA values, this introduction probably occurred around November 16, 2016. Second, the apparent transfer of infected ducks enabled H5N8 to spread to other areas of southwest France, prompting the formation of geoclusters 2, 3, and 4 (*40*). Third, the virus spread among farms in newly affected areas, possibly through airborne transmission or movements of animals, materials, or personnel among farms, as suggested by Andronico et al. (*41*). Fourth, the virus

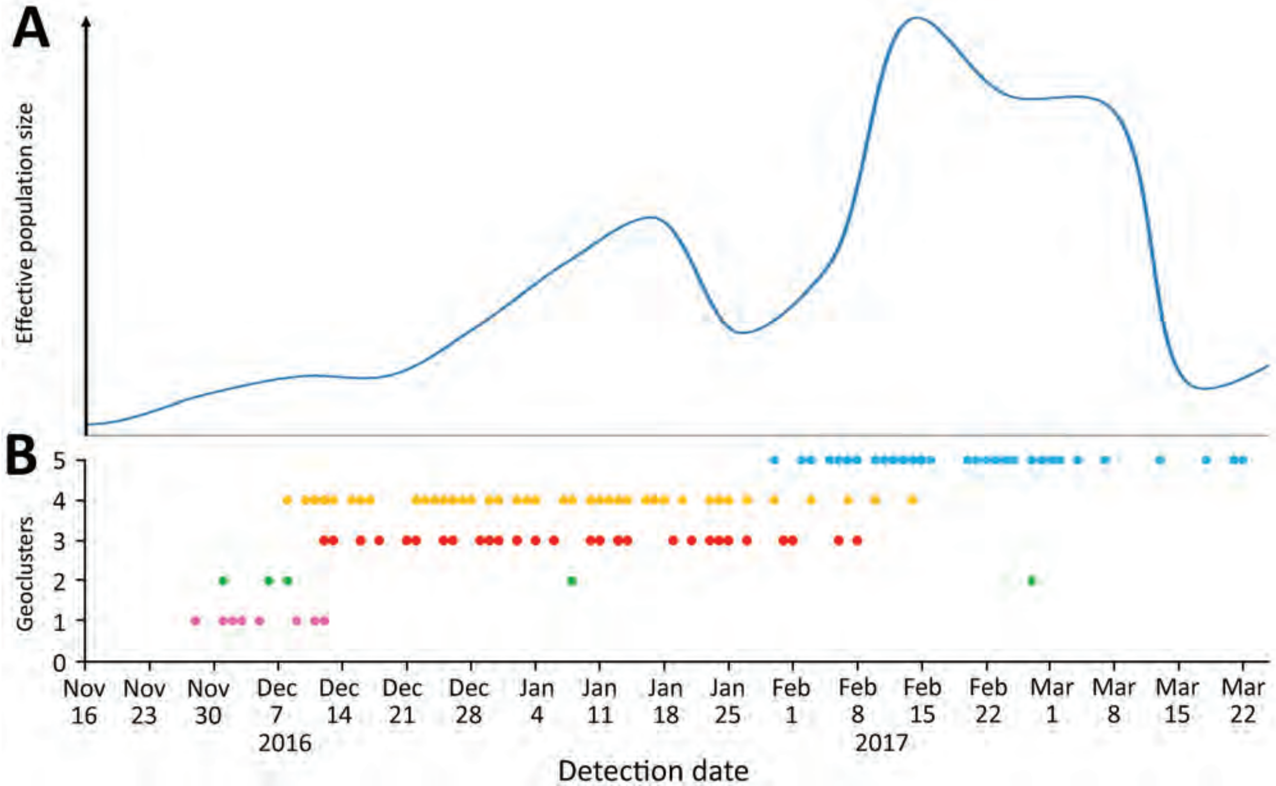


**Figure 5.** Evolution of highly pathogenic avian influenza H5N8 genotype A viruses, France, 2016–17. A) Bayesian Skygrid plot of viral population size over time. B) Timeline of cases of H5N8 genotype A. Pink indicates geocluster 1; green indicates geocluster 2; red indicates geocluster 3; orange indicates geocluster 4; blue indicates geocluster 5.

entered the geographic area corresponding to geocluster 5. This geocluster included viral genome sequences closely related to those of geocluster 3. This finding was unexpected because the geographic area of geocluster 5 is closer to that of geocluster 4 than geocluster 3. The low variability among geocluster 5 sequences suggests that the virus was introduced through a single viral transmission. We estimated that this event occurred around January 15, 2017, approximately 2 weeks before we first sequenced virus in this geocluster (i.e., January 30, 2017). This delay suggests that we might not have sampled all cases. In addition, the precision of our model could have been increased by using path and stepping-stone sampling methods. The single introduction seems to have been the origin of all subsequent infections in this area. This long-range viral transmission could have occurred through animal transport or the movement of wild birds. Once this new area was infected, the virus spread among nearby farms, resulting in the formation of geocluster 5.

Our results correspond with the estimation of the effective population size of the HPAI A(H5N8) viruses in southwestern France. The first increase of the viral population coincided with the emergence of geoclusters 3 and 4. The subsequent population decrease might reflect governmental actions to control viral dissemination, such as the preventive culling of poultry and ducks in farms with confirmed infection. In addition, the 5 geoclusters identified in this study correspond with the geoclusters characterized by Guinat et al. (*20*) on the basis of the dates and locations of clinical reports. According to Guinat et al., the depopulation of poultry farms and restrictions on movement of animals, materials, or personnel among farms could have substantially reduced viral spread within each geocluster. The second increase in the viral population coincided with the introduction of H5N8 into a new area (i.e., that of geocluster 5) with a high density of poultry farms (*41*). These results highlight the importance of controlling poultry movements to prevent viral spread, especially because these movements were identified as a risk factor for transmission in southwest France during this outbreak (*42*). Our data suggest that viral spread was directly related to the density of duck holdings. For example, the virus was effectively restrained in geoclusters 1 and 2, which corresponded to areas of low duck-holding density. The other 3 geoclusters had a higher density of duck farms, facilitating the local (inside the same geocluster) and long distance (between geoclusters) spreads of the virus. These results should be further combined with the epidemiologic data and Bayesian discrete trait phylogeography analysis to identify transmission factors.

In conclusion, during winter 2016–17, Europe faced a large outbreak of HPAI A(H5N8). Three viral genotypes were detected in France, but only genotype A caused dramatic economic losses. In southwestern France, a major producer of foie gras, genotype A viruses were detected in 5 separate geographic clusters. Our data show that local dissemination and long-distance transmission contributed to the severity of the outbreak, especially in areas of high duck-holding density. This study highlights the importance of limiting introduction of infected birds into a disease-free area. Implementing control measures for infected flocks is crucial to avoiding the spread of AIVs.

#### Acknowledgments

We thank the veterinarians, farmers, and Office National de la Chasse de la et de la Faune Sauvage staff involved for the collection of field samples. We are also grateful to the screening laboratories for the initial screening samples and to the local Directions Départementales de la Protection des Populations and central Direction Générale de l'Alimentation official veterinary services for the outbreak management.

This study was supported by Fonds de la Recherche pour l'Influenza Aviaire 2019 from the French Ministry of Agriculture.

### About the Author

Mr. Briand is a scientist at the French Reference Laboratory for Avian Influenza and Newcastle Disease. His research interests include phylogeny, virology, and molecular epidemiology, especially for avian influenza virus and Newcastle disease virus.

#### References

1. Olsen B, Munster VJ, Wallensten A, Waldenström J, Osterhaus AD, Fouchier RA. Global patterns of influenza A virus in wild birds. Science. 2006;312:384–8. https://doi.org/10.1126/science.1122438
2. Nao N, Yamagishi J, Miyamoto H, Igarashi M, Manzoor R, Ohnuma A, et al. Genetic predisposition to acquire a polybasic cleavage site for highly pathogenic avian influenza virus hemagglutinin. MBio. 2017;8:e02298–16. https://doi.org/10.1128/mBio.02298-16
3. OFFLU. Influenza A cleavage sites. 2020 Jul 8 [cited 2020 Nov 30]. http://www.offlu.net/fileadmin/home/en/resource-centre/pdf/Influenza_A_Cleavage_Sites.pdf
4. Pantin-Jackwood MJ, Swayne DE. Pathogenesis and pathobiology of avian influenza virus infection in birds. Rev Sci Tech. 2009;28:113–36. https://doi.org/10.20506/rst.28.1.1869
5. Lee DH, Criado MF, Swayne DE. Pathobiological origins and evolutionary history of highly pathogenic avian influenza viruses. Cold Spring Harb Perspect Med. 2020 Jan 21 [Epub ahead of print]. https://doi.org/10.1101/cshperspect.a038679
6. European Commission. Council directive 2005/94/EC on community measures for the control of avian influenza and repealing directive 92/40/EEC. 2019 Jan 1 [cited 2020 Nov 30]. https://eur-lex.europa.eu/legal-content/EN/TXT/?uri=celex%3A32005L0094
7. World Health Organization/World Organisation for Animal Health/Food and Agriculture Organization H5N1 Evolution Working Group. Toward a unified nomenclature system for highly pathogenic avian influenza virus (H5N1). Emerg Infect Dis. 2008;14:e1. https://doi.org/10.3201/eid1407.071681
8. Fusaro A, Zecchin B, Vrancken B, Abolnik C, Ademun R, Alassane A, et al. Disentangling the role of Africa in the global spread of H5 highly pathogenic avian influenza. Nat Commun. 2019;10:5310. https://doi.org/10.1038/s41467-019-13287-y
9. Saito T, Tanikawa T, Uchida Y, Takemae N, Kanehira K, Tsunekuni R. Intracontinental and intercontinental dissemination of Asian H5 highly pathogenic avian influenza virus (clade 2.3.4.4) in the winter of 2014–2015. Rev Med Virol. 2015;25:388–405. https://doi.org/10.1002/rmv.1857
10. Lee DH, Torchetti MK, Winker K, Ip HS, Song CS, Swayne DE. Intercontinental spread of Asian-origin H5N8 to North America through Beringia by migratory birds. J Virol. 2015;89:6521–4. https://doi.org/10.1128/JVI.00728-15
11. Lee DH, Bertran K, Kwon JH, Swayne DE. Evolution, global spread, and pathogenicity of highly pathogenic avian influenza H5Nx clade 2.3.4.4. J Vet Sci. 2017;18:269–80. https://doi.org/10.4142/jvs.2017.18.S1.269
12. Cattoli G, Fusaro A, Monne I, Capua I. H5N1 virus evolution in Europe—an updated overview. Viruses. 2009;1:1351–63. https://doi.org/10.3390/v1031351
13. Global Consortium for H5N8 and Related Influenza Viruses. Role for migratory wild birds in the global spread of avian influenza H5N8. Science. 2016;354:213–7. https://doi.org/10.1126/science.aaf8852
14. King J, Schulze C, Engelhardt A, Hlinak A, Lennermann SL, Rigbers K, et al. Novel HPAIV H5N8 reassortant (clade 2.3.4.4b) detected in Germany. Viruses. 2020;12:281. https://doi.org/10.3390/v12030281
15. Hill NJ, Hussein IT, Davis KR, Ma EJ, Spivey TJ, Ramey AM, et al. Reassortment of influenza A viruses in wild birds in Alaska before H5 clade 2.3.4.4 outbreaks. Emerg Infect Dis. 2017;23:654–7. https://doi.org/10.3201/eid2304.161668
16. Antigua KJC, Choi WS, Baek YH, Song MS. The emergence and decennary distribution of clade 2.3.4.4 HPAI H5Nx. Microorganisms. 2019;7:156. https://doi.org/10.3390/microorganisms7060156
17. Pohlmann A, Starick E, Grund C, Höper D, Strebelow G, Globig A, et al. Swarm incursions of reassortants of highly pathogenic avian influenza virus strains H5N8 and H5N5, clade 2.3.4.4b, Germany, winter 2016/17. Sci Rep. 2018;8:15. https://doi.org/10.1038/s41598-017-16936-8
18. Brown I, Kuiken T, Mulatti P, Smietanka K, Staubach C, Stroud D, et al.; European Food Safety Authority; European Centre for Disease Prevention and Control; European Union Reference Laboratory for Avian influenza.

Avian influenza overview September–November 2017. EFSA J. 2017;15:e05141.
19. Lycett SJ, Pohlmann A, Staubach C, Caliendo V, Woolhouse M, Beer M, et al. Global Consortium for H5N8 and Related Influenza Viruses. Genesis and spread of multiple reassortants during the 2016/2017 H5 avian influenza epidemic in Eurasia. Proc Natl Acad Sci U S A. 2020; 117:20814–25. https://doi.org/10.1073/pnas.2001813117
20. Guinat C, Nicolas G, Vergne T, Bronner A, Durand B, Courcoul A, et al. Spatio-temporal patterns of highly pathogenic avian influenza virus subtype H5N8 spread, France, 2016 to 2017. Euro Surveill. 2018;23. https://doi.org/10.2807/1560-7917.ES.2018.23.26.1700791
21. Bronner A, Niqueux E, Schmitz A, Le Bouquin S, Huneau-Salaûn A, Guinat C, et al. Description of the highly pathogenic avian influenza episode in France in 2016–2017 [in French]. Bulletin épidémiologique, santé animale et alimentation. 2017;79:13–7.
22. Slomka MJ, Coward VJ, Banks J, Löndt BZ, Brown IH, Voermans J, et al. Identification of sensitive and specific avian influenza polymerase chain reaction methods through blind ring trials organized in the European Union. Avian Dis. 2007;51:227–34. https://doi.org/10.1637/7674-063006R1.1
23. Zhou B, Donnelly ME, Scholes DT, St George K, Hatta M, Kawaoka Y, et al. Single-reaction genomic amplification accelerates sequencing and vaccine production for classical and swine origin human influenza A viruses. J Virol. 2009;83:10309–13. https://doi.org/10.1128/JVI.01109-09
24. Briand FX, Schmitz A, Ogor K, Le Prioux A, Guillou-Cloarec C, Guillemoto C, et al. Emerging highly pathogenic H5 avian influenza viruses in France during winter 2015/16: phylogenetic analyses and markers for zoonotic potential. Euro Surveill. 2017;22:30473. https://doi.org/10.2807/1560-7917.ES.2017.22.9.30473
25. Langmead B, Salzberg SL. Fast gapped-read alignment with Bowtie 2. Nat Methods. 2012;9:357–9. https://doi.org/10.1038/nmeth.1923
26. Kumar S, Stecher G, Tamura K. MEGA7: Molecular Evolutionary Genetics Analysis version 7.0 for bigger datasets. Mol Biol Evol. 2016;33:1870–4. https://doi.org/10.1093/molbev/msw054
27. Martin DP, Murrell B, Golden M, Khoosal A, Muhire B. RDP4: detection and analysis of recombination patterns in virus genomes. Virus Evol. 2015;1:vev003. https://doi.org/10.1093/ve/vev003
28. Drummond AJ, Suchard MA, Xie D, Rambaut A. Bayesian phylogenetics with BEAUti and the BEAST 1.7. Mol Biol Evol. 2012;29:1969–73. https://doi.org/10.1093/molbev/mss075
29. Baele G, Lemey P, Bedford T, Rambaut A, Suchard MA, Alekseyenko AV. Improving the accuracy of demographic and molecular clock model comparison while accommodating phylogenetic uncertainty. Mol Biol Evol. 2012;29:2157–67. https://doi.org/10.1093/molbev/mss084
30. Hill V, Baele G. Bayesian estimation of past population dynamics in BEAST 1.10 using the Skygrid coalescent model. Mol Biol Evol. 2019;36:msz172. https://doi.org/10.1093/molbev/msz172
31. Lanfear R, Hua X, Warren DL. Estimating the effective sample size of tree topologies from Bayesian phylogenetic analyses. Genome Biol Evol. 2016;8:2319–32. https://doi.org/10.1093/gbe/evw171
32. Vaughan TG. IcyTree: rapid browser-based visualization for phylogenetic trees and networks. Bioinformatics. 2017;33:2392–4. https://doi.org/10.1093/bioinformatics/btx155
33. Leigh J, Bryant D. POPART: full-feature software for haplotype network construction. Methods Ecol Evol. 2015;6:1110–6. https://doi.org/10.1111/2041-210X.12410
34. Agence nationale de sécurité sanitaire de l'alimentation, de l'environnement et du travail. Assessing avian influenza risk levels and their evolution [in French]. 2017 [cited 2017 Nov 07]. https://www.anses.fr/fr/system/files/SABA2017SA0203-partie2.pdf
35. Fusaro A, Monne I, Mulatti P, Zecchin B, Bonfanti L, Ormelli S, et al. Genetic diversity of highly pathogenic avian influenza A(H5N8/H5N5) viruses in Italy, 2016–17. Emerg Infect Dis. 2017;23:1543–7. https://doi.org/10.3201/eid2309.170539
36. Świętoń E, Śmietanka K. Phylogenetic and molecular analysis of highly pathogenic avian influenza H5N8 and H5N5 viruses detected in Poland in 2016–2017. Transbound Emerg Dis. 2018;65:1664–70. https://doi.org/10.1111/tbed.12924
37. Savić V. Novel reassortant clade 2.3.4.4 avian influenza A(H5N5) virus in wild birds and poultry, Croatia, 2016–2017. Vet Arh. 2017;87:377–96. https://doi.org/10.24099/vet.arhiv.170509
38. Shapiro B, Rambaut A, Drummond AJ. Choosing appropriate substitution models for the phylogenetic analysis of protein-coding sequences. Mol Biol Evol. 2006;23:7–9. https://doi.org/10.1093/molbev/msj021
39. Souvestre M, Guinat C, Niqueux E, Robertet L, Croville G, Paul M, et al. Role of backyard flocks in transmission dynamics of highly pathogenic avian influenza A(H5N8) clade 2.3.4.4, France, 2016–2017. Emerg Infect Dis. 2019;25:551–4. https://doi.org/10.3201/eid2503.181040
40. Moisson M, Hamon M, Malhere C, Donguy M, Niqueux E, Scoizec A, et al. The situation of HP H5N8 avian influenza in France as of 05/12/2016. 2016 [cited 2016 Dec 06]. https://www.plateforme-esa.fr/article/situation-de-l-influenza-aviaire-hp-h5n8-en-france-au-05122016
41. Andronico A, Courcoul A, Bronner A, Scoizec A, Lebouquin-Leneveu S, Guinat C, et al. Highly pathogenic avian influenza H5N8 in south-west France 2016–2017: a modeling study of control strategies. Epidemics. 2019; 28:100340. https://doi.org/10.1016/j.epidem.2019.03.006
42. Guinat C, Artois J, Bronner A, Guérin JL, Gilbert M, Paul MC. Duck production systems and highly pathogenic avian influenza H5N8 in France, 2016–2017. Sci Rep. 2019;9:6177. https://doi.org/10.1038/s41598-019-42607-x

Address for correspondence: François-Xavier Briand, Anses, Ploufragan-Plouzané-Niort Laboratory, Avian and Rabbit Virology Immunology and Parasitology Unit, National Reference Laboratory for Avian Influenza, BP53, 22440 Ploufragan, France; email: francois-xavier.briand@anses.fr

# Outbreak of Severe Vomiting in Dogs Associated with a Canine Enteric Coronavirus, United Kingdom

Alan D. Radford, David A. Singleton, Chris Jewell, Charlotte Appleton, Barry Rowlingson, Alison C. Hale, Carmen Tamayo Cuartero, Richard Newton, Fernando Sánchez-Vizcaíno, Danielle Greenberg, Beth Brant, Eleanor G. Bentley, James P. Stewart, Shirley Smith, Sam Haldenby, P.-J. M. Noble, Gina L. Pinchbeck

The lack of population health surveillance for companion animal populations leaves them vulnerable to the effects of novel diseases without means of early detection. We present evidence on the effectiveness of a system that enabled early detection and rapid response to a canine gastroenteritis outbreak in the United Kingdom. In January 2020, prolific vomiting among dogs was sporadically reported in the United Kingdom. Electronic health records from a nationwide sentinel network of veterinary practices confirmed a significant increase in dogs with signs of gastroenteric disease. Male dogs and dogs living with other vomiting dogs were more likely to be affected. Diet and vaccination status were not associated with the disease; however, a canine enteric coronavirus was significantly associated with illness. The system we describe potentially fills a gap in surveillance in neglected populations and could provide a blueprint for other countries.

Population health data is lacking for companion animals such as dogs, cats, and rabbits, leaving a surveillance gap for endemic diseases and delayed detection of incursions of disease, such as equine influenza virus (H3N8) (*1*), avian influenza (H3N2) (*2*,*3*), and parvoviruses (*3*). In the absence of legislated programs of population surveillance, several attempts have been made to fill this gap using secondary data, particularly from pet insurance providers (*4*). More recently, researchers have exploited the rapid digitization of electronic health records (EHRs) for passive surveillance. Data can be collected at great scale and analyzed in near–real time. EHR data are now routinely used in human heath efforts (*5*–*8*), in which their timeliness, simplicity, and breadth of coverage complements surveillance based on diagnostic data (*9*,*10*). Such approaches are beginning to find healthcare value in veterinary species, especially among companion animals (*4*,*11*–*13*), a high proportion of which visit veterinarians (*14*).

In January 2020, one of the authors of this article (D.G.), a primary care veterinarian in northwest England, contacted the other authors about seeing an unusually high number of cases (≈40) of severe vomiting in dogs; responses to a social media post suggested other veterinarians might have been experiencing similar events. Vomiting is a common complaint among dogs whose owners seek treatment for them (*15*,*16*). However, documented outbreaks are rare because established vaccines are available for most common known pathogens (*17*). In the absence of robust populationwide data, such sporadic reports frequently do not raise awareness of outbreaks.

For the response we describe, we obtained data from syndromic surveillance and text mining of EHRs collected from sentinel veterinary practices and diagnostic laboratories, which we then linked with data from field epidemiology and enhanced genomic testing. In 8 weeks, using this approach, we described the temporal and spatial epidemiology, identified a possible causative agent, and provided targeted advice to control the outbreak. Ethics approval was given by Liverpool University Research Ethics Committees (Liverpool, UK; VREC922/RETH000964).

Author affiliations: Institute of Infection, Veterinary and Ecological Sciences, University of Liverpool Leahurst Campus, Neston, UK (A.D. Radford, D.A. Singleton, B. Brant, E.G. Bentley, J.P. Stewart, S. Smith, P.-J.M. Noble, G.L. Pinchbeck);Lancaster University Centre for Health Informatics, Lancaster, UK (C. Jewell, C. Appleton, B. Rowlingson, A.C. Hale); University of Bristol, UK (C.T. Cuartero, F. Sánchez-Vizcaíno); Animal Health Trust, Lanwades Park, Kentford, UK (R. Newton); The Liverpool Vets, Liverpool, UK (D. Greenberg); Centre for Genomic Research, University of Liverpool, Liverpool (S. Haldenby)

DOI: https://doi.org/10.3201/eid2702.202452

## Methods

### Data Sources

#### Veterinary Practices

During March 17, 2014–February 29, 2020, we collected data from 7,094,397 consultation records (4,685,732 from dogs and 1,846,493 from cats) from EHRs from the Small Animal Veterinary Surveillance Network (SAVSNET), a volunteer network of 301 veterinary practices (663 sites) in the United Kingdom, recruited based on convenience (*11*). In brief, EHRs included data collected during individual consultations on species, breed, sex, neuter status, age, owners' postcodes, and vaccination status. Each EHR is also compulsorily annotated by the veterinary clinician with a main presenting complaint (MPC) at time of visit, using a questionnaire window embedded in the practice management system. Options for reasons for visit included gastroenteric, respiratory, pruritus, tumor, kidney disease, other unwell, post-op check, vaccination, or other healthy.

Given that severe vomiting was a key outbreak feature, we undertook 2 complementary analyses. First, we used regular expressions to identify clinical narratives describing frequent vomiting, but excluded common false positive search results (Appendix Table 1, https://wwwnc.cdc.gov/EID/article/27/2/20-2452-App1.pdf). Second, we used data on prescriptions to describe the frequency of all veterinary-authorized products containing the antiemetic maropitant (*18*). We calculated trend lines using Bayesian binomial generalized linear modeling trained on weekly prevalence during 2014–2019 (*19*), which allowed us to identify extreme (>99% credible interval [CrI]) or moderate (>95% CrI) observations.

#### Laboratories

SAVSNET also collects EHRs from participating diagnostic laboratories on samples submitted from more than half of UK veterinary practices. Canine diagnostic test results from January 2017 through February 2020 were queried from 6 laboratories for 6 gastroenteric pathogens. Test numbers, percentage of positive results, and associated 95% CIs were summarized (Table 1). The number of sites was surmised from the submitting practices' postcodes.

#### Questionnaires

Online questionnaires to enable case reporting were made available to both veterinarians and owners beginning January 29, 2020. The required case definition of ≥5 vomiting episodes in a 12-hour period was based on clinical observations of early cases. Veterinarians were also asked to complete control questionnaires. Initially, we requested only controls matched to veterinary practices contributing case data; however, to increase recruitment, a nonmatched control questionnaire open to any veterinarian was deployed on February 5. The questionnaires (Appendix) requested a range of information including owner postcode, animal signalment, vaccination status, clinical signs, treatment and diagnostic testing, animal contacts, diet, and recovery status.

We performed all statistical analyses using R version 3.6.1 (https://cran.r-project.org). Case details were described for both veterinarian- and owner-reported data. We calculated proportions and 95% CIs for categorical variables and median and range for continuous variables. We constructed univariable and multivariable mixed-effects logistic regression models using data submitted by veterinarians using R package lme4. Explanatory variables from univariable logistic regression were considered in

**Table 1.** Results of laboratory diagnostic tests for pathogens associated with gastroenteric disease in dogs for samples collected during January 2017–February 2020, United Kingdom*

| Pathogen | Method | No. tests | No. laboratories† | Unique sites‡ | % Positive (95% CI) | Peak month, % positive (95% CI) |
|---|---|---|---|---|---|---|
| CeCoV | PCR | 5,167 | 4 | 839 | 20.69 (19.58–21.79) | 2020 Feb, 34.8 (27.81–41.85) |
| Canineparvovirus | PCR | 5,499 | 6 | 965 | 6.62 (5.96–7.28) | 2017 Nov, 13.28 (7.38–19.18) |
| Giardia | PCR | 5,636 | 6 | 894 | 23.78 (22.66–24.89) | 2018 Jan, 33.96 (26.58–41.35) |
| *Salmonella* spp. | Culture | 114,722 | 6 | 2,951 | 0.87 (0.81–0.92) | 2018 Nov, 1.28 (0.87–1.70) |
| *Campylobacter* spp. | Selective culture | 111,983 | 6 | 2,947 | 16.10 (15.88–16.31) | 2017 Dec, 23.02 (21.44–24.60) |
| *Clostridium perfringens* | Enterotoxin PCR | 5,138 | 3 | 2,947 | 16.10 (15.88–16.31) | 2017 Dec, 23.02 (21.44–24.60) |

*CeCoV, canine enteric coronavirus.
†Number of diagnostic laboratories contributing test results.
‡Number of unique veterinary practices sites submitting samples to the laboratories.

multivariable models for likelihood ratios of p≤0.20, which underwent manual stepwise backward elimination to reduce Akaike's and Bayesian information criteria. Practice was included as a random effect. We assessed confounding by the effect on model fit with sequential removal of variables and assessed 2-way interaction terms for improved model fit. We defined final statistical significance as p <0.05.

### Spatiotemporal Analysis of Cases

We obtained records of consults weekly during November 4, 2019–March 21, 2020; cases were geolocated by pet owners' postcodes. We considered records of gastroenteric MPC as a binary outcome (i.e., 1 for gastroenteric consult, 0 for nongastroenteric consult). We used a logistic geostatistical model to investigate spatial clustering of cases for each week. We defined a spatial hotspot as a location having 95% posterior probability of prevalence exceeding the national mean prevalence over any 1-week period. With no discernible epidemic wave apparent over successive weeks, we aggregated weekly measures across the study period to show the number of weeks each location was a hotspot (Appendix).

### Sample Collection, PCR, and Phylogenetic Analyses

Veterinarians submitting questionnaires were also asked to submit samples for microbiological testing including mouth swabs, fecal samples, and for gastrointestinal cases, vomit. In brief, we extracted nucleic acids using a QIAGEN QIAamp viral RNA kit (https://www.qiagen.com), reverse transcribed samples using ThermoFisher Superscript III (https://www.thermofisher.com), and tested for canine enteric coronavirus (CeCoV) by M-gene PCR (*20*). To expedite results and reduce contamination risks, the PCR was run as a single-stage PCR rather than as the published nested reaction. We purified positive samples using QIAquick (QIAGEN) and sequenced them bidirectionally (Sanger sequencing; Source Biosciences, https://www.sourcebioscience.com) to produce consensus sequences (ChromasPro 2.1.8, http://technelysium.com.au).

To rapidly explore the potential involvement of other viruses, we extracted nucleic acid from 19 random cases and 5 controls for deep sequencing. RNA was amplified by sequence-independent, single-primer-amplification (*21*), multiplexed libraries were prepared using 30 ng of cDNA with an Oxford Nanopore SQK-LSK109 ligation sequencing kit (Oxford Nanopore, https://nanoporetech.com) and sequenced using an Oxford Nanopore MinION Mk1B device for 48 hours. To perform real-time fast basecalling, we used the Oxford Nanopore MinKNOW Guppy toolkit and FASTQ files uploaded to an Oxford Nanopore EPI2ME data analysis platform for identification.

For deeper sequencing coverage, we also processed 10 samples (6 CeCoV-positive cases, 3 negative cases, 1 control) for Illumina sequencing at the University of Liverpool Centre for Genomic Research (https://www.liverpool.ac.uk/genomic-research). We treated nucleic acids with RNase and prepared fragment libraries using a NEBNext Ultra II kit (https://www.neb.com) before performing paired-end, 2 × 150–bp sequencing on an Illumina HiSeq 4000 system (https://www.illumina.com). Adaptor sequences were trimmed using cutadapt (https://cutadapt.readthedocs.io) and sickle (https://github.com), with a minimum quality score of 20. Reads >19 bp matching the dog genome (CanFam3.1, http://genome.ucsc.edu) using Bowtie2 sequence alignment tool (http://bowtie-bio.sourceforge.net) were removed. Remaining reads were assembled using the SPAdes toolkit (https://github.com) and contigs >700 nt blasted against the NCBI RefSeq nonredundant proteins database (https://www.ncbi.nlm.nih.gov/refseq). Sequences matching CeCoV were aligned using the ClustalW multiple sequence alignment program (https://www.genome.jp) and phylogenies reconstructed using bootstrap analyses and neighbor-joining in MEGA6 software (https://www.megasoftware.net). Each sequence was assigned a local laboratory number based on the order in which the sequences were analyzed.

## Results

### Syndromic Surveillance

On the basis of MPCs identified in the EHRs, we found a specific and significant increase in the number of dogs recorded as exhibiting gastroenteric signs; the final 10 weeks, during December 2019–March 2020, were outside the 99% CrI (extreme outliers; Figure 1, panel A). A similar trend was observed in maropitant therapy for dogs (Figure 1, panel B). Both measures, peaked in the week ending February 2, 2020, at approximately double the preceding baseline. We observed no similar trends for respiratory disease in dogs, for gastroenteric MPCs, for maropitant treatment in cats (Figure 1, panels C–E), or for antibiotic use in dogs (data not shown), together suggesting the signal was specific to canine gastroenteric disease, a finding supported by similar increases in the regular expression identifying vomiting dogs (Figure 1, panel F).

Spatiotemporal mapping of weekly cases of gastroenteric MPC showed prevalence was spatially clustered (Figure 2). In particular, locations in northwest and southwest England and in Edinburgh, Scotland, had strong evidence of many weeks of prevalence higher than the national mean.

### Diagnostic Tests

The patterns of test results for different PCR tests, generally carried out concurrently, were broadly similar (Figure 3, panels A–C). The same was true for results based on cultured samples (Figure 3, panels D, E). Of particular interest, CeCoV showed strong seasonality, positive tests peaking during the winter months (Figure 3, panel A). However, similar peaks seen in previous years suggested the observed peak in February 2020 could not itself explain this outbreak.

### Questionnaire

By March 1, 2020, a total of 1,258 case questionnaires had been received. After excluding 59 questionnaires missing key data, we used data from 165 veterinary-reported cases, 1,034 owner-reported cases (Table 2), and 60 veterinary-reported controls (Appendix Table 2) for analyses.

Most cases were from households in England (Table 2). Median case age at examination was 4.0 years (range 0.3–15.0 years) based on veterinary reports and 4.8 years (range 0.2–15.5 years) based on owner reports. Most animals had been vaccinated against core pathogens (*17*) and leptospirosis within the preceding 3 years and dewormed within the previous 3 months. A range of breeds (data not presented) were observed, broadly corresponding to previous studies (*6*). Most cases were fed dog food, but

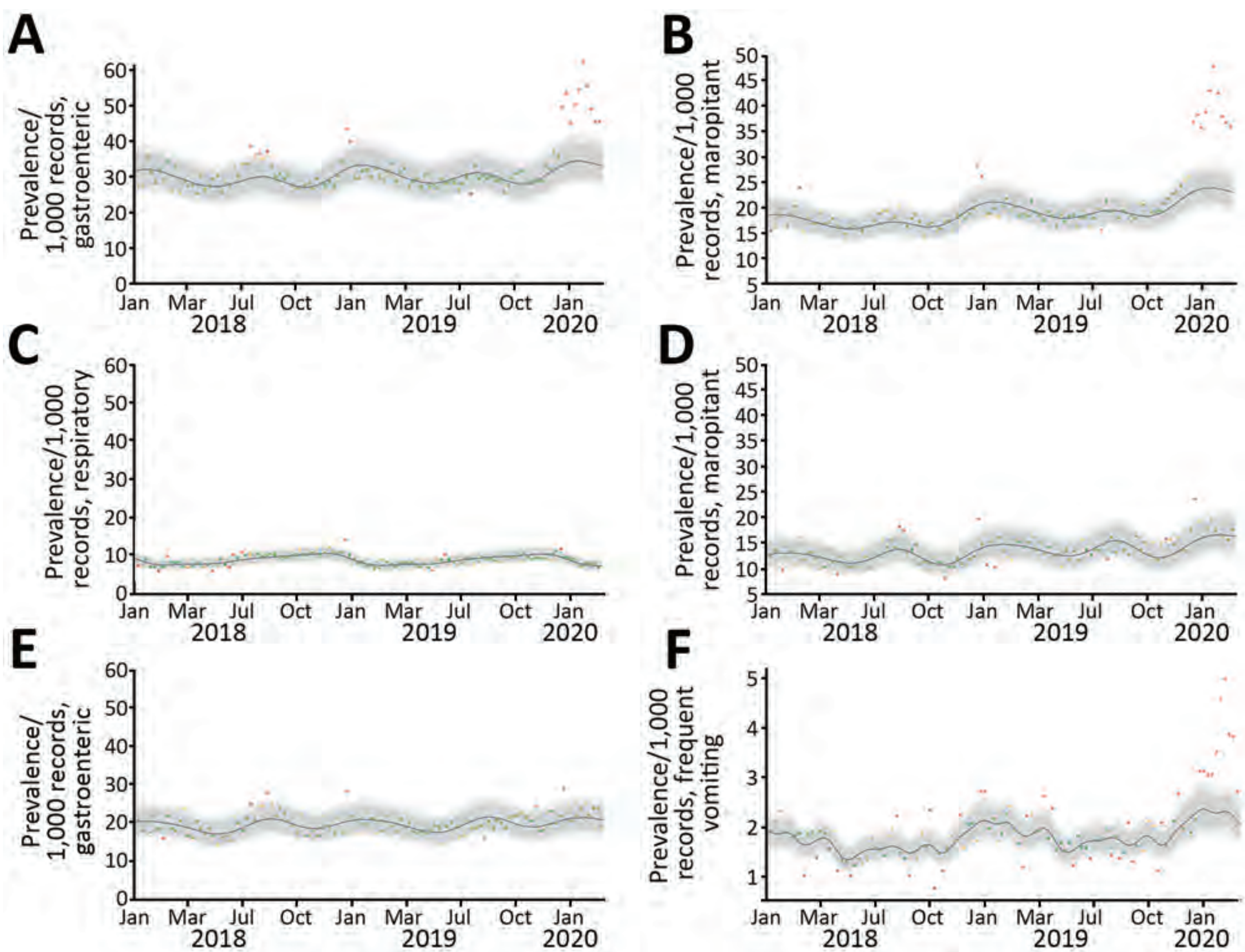


**Figure 1.** Observed prevalence of main presenting complaint (MPC) and maropitant use in cats and dogs, per 1,000 consultations, in investigation of dogs with vomiting, United Kingdom, January 2017–February 2020. A) Canine records labeled as gastroenteric MPC; B) canine records in which maropitant was prescribed; C) canine records labeled as respiratory MPC; D) feline records in which maropitant was prescribed; E) feline records labeled as gastroenteric MPC; and F) frequent vomiting in dogs based on regular expression searches of the clinical narratives. Red points represent the extreme outliers (outside the 99% credible interval [CrI]), orange points the moderate outliers (outside the 95% CrI, but within the 99% CrI), and green points the average trend (within the 95% CrI).

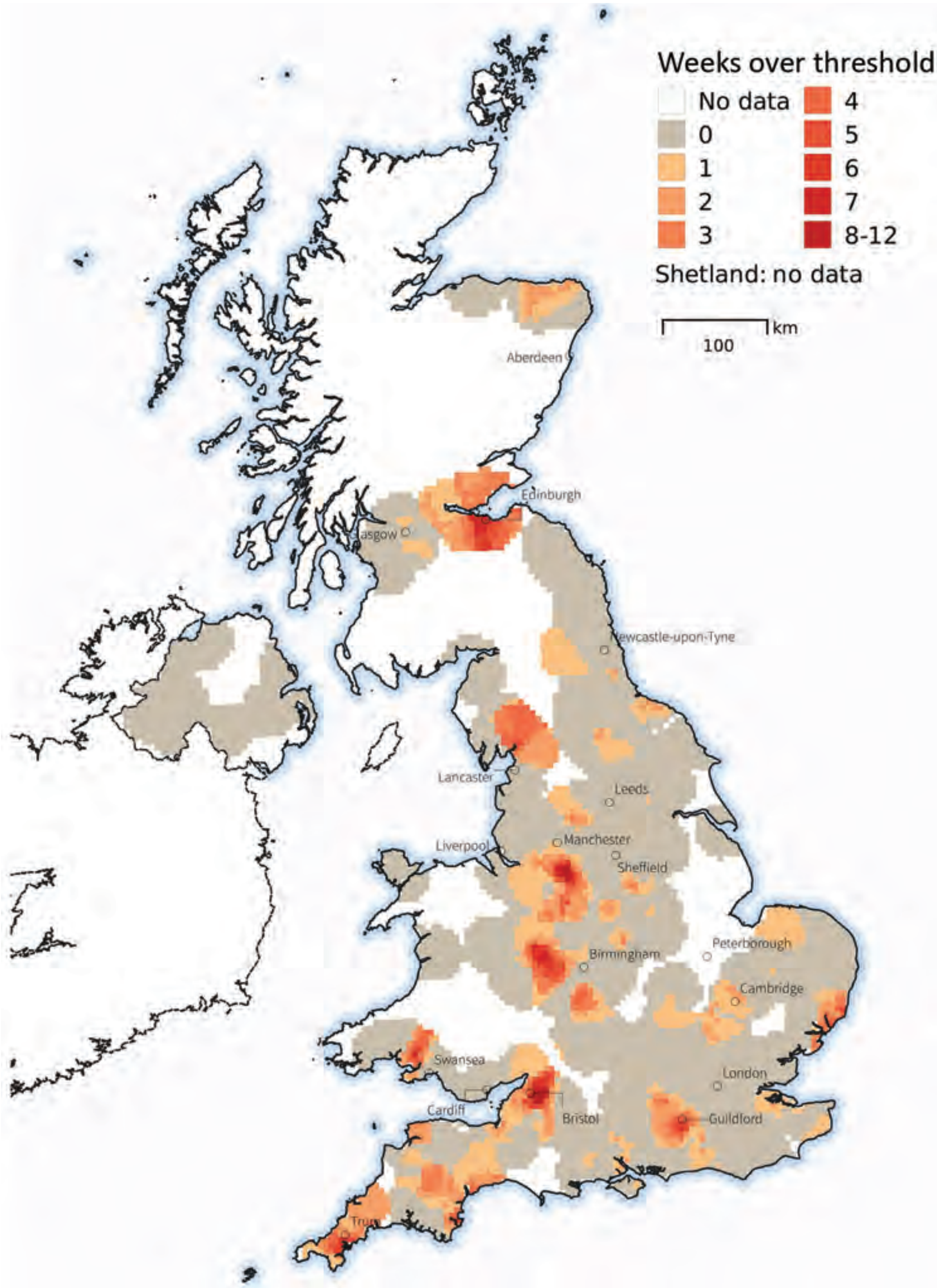


**Figure 2.** Rates of gastroenteric veterinary consults for dogs during November 4, 2019–March 21, 2020, in investigation of dogs with vomiting, United Kingdom. Consults were geolocated to owners' postcodes, with gastroenteric main presenting complaint as a binary outcome (1 for gastroenteric consult, 0 for a nongastroenteric consult). Colored areas represent the number of weeks a given location had a 95% posterior probability of prevalence exceeding the national mean prevalence in any week. The geostatistical modeling approach used is further detailed in the Appendix (https://wwwnc.cdc.gov/EID/article/27/2/20-2452-App1.pdf).

≈20%–37% of dogs scavenged food when walked. Of those from multidog households, just over half reported the presence of another dog recently vomiting within the same household. Around 30% of dogs had recently traveled, most commonly visiting a daycare facility.

Date of onset of clinical signs ranged from November 16, 2019, through February 28, 2020, for veterinary-reported cases, and September 4, 2019, through March 1, 2020, for owner-reported cases. Most cases involved inappetence (75.6%–86.1%) and vomiting without blood (88.7%–91.5%) (Table 3). Approximately half of cases reported diarrhea, most without blood. Diagnostic testing was performed in 32.1% of veterinary-reported cases, most (78.9%) using hematology or biochemistry assays, or both.

Dogs in >90% of veterinary-reported cases were treated, compared with in 61.7% of owner-reported cases. In both, antiemetics were most often prescribed: in 89.1% (CrI 84.3%–93.9%) of veterinary-reported cases and in 48.1% (CrI 45.0%–51.1%) of owner-reported cases. The most common recovery time was

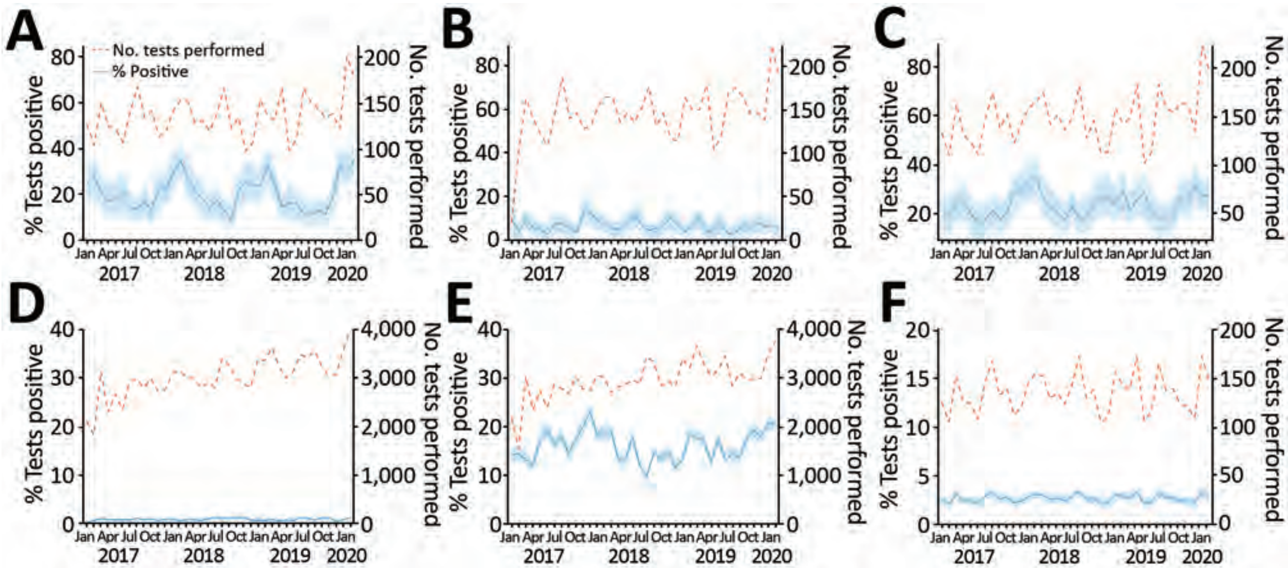


**Figure 3.** Diagnostic test findings during January 2017–February 2020 in investigation of dogs with vomiting, United Kingdom. A) Canine enteric coronavirus PCR; B) canine parvovirus PCR; C) *Giardia* PCR; D) *Salmonella* spp. selective culture; E) *Campylobacter* spp. selective culture; F) *Clostridium perfringens* enterotoxin PCR results. Blue shading represents 95% CI.

3–7 days; the dogs died in 0.6% of veterinary-reported and 1.0% of owner-reported cases.

Descriptive data about the control population, submitted by veterinarians, and univariable findings from analyses of the veterinary case controls are presented in Appendix Tables 2 and 3; multivariable findings are shown in Table 4. Both neutered and nonneutered male dogs were at significantly increased odds of contracting the illness, compared with neutered females, as were dogs living in the same household as another dog that had also been vomiting compared to those in households where other dogs were healthy. However, dogs living in a single-dog household were at increased odds of contracting the illness compared with dogs living in the same household as another dog that had not recently vomited. Dogs that had been in recent contact with another animal species (including humans) that had recently vomited were at reduced odds of vomiting, compared with those who had not. Other potential causes considered early in the outbreak, including foodborne etiologies, vaccine preventable diseases, or the possibility of interspecies transmission, were not significantly associated (Appendix Table 3).

### Sampling and Molecular Testing

During January 30–March 12, 2020, we collected a total of 95 samples from 71 animals (50 cases, 21 controls): 22 from feces, 60 from oral swabs, and 13 from vomit. Dogs with prolific vomiting were significantly more likely to test positive for CeCoV in $\geq$1 sample (17/50, 34%) compared with controls (0/21) ($p = 0.002$ by Fisher exact test). Positive test results were most likely in samples from feces (10/16 [62.5%] cases, 0/6 controls; $p = 0.01$) and vomit (6/13 [46%] cases, 0 controls). Samples from oral swabs were least likely to test positive (7/43 [16%] cases, 0/17 controls; $p = 0.17$). Of 17 CeCoV-positive cases, 12 met the case definition, 2 did not (<5 episodes of vomiting in 12 hours), and 3 lacked questionnaire data.

We gathered useable M-gene sequences from 21 samples (16 dogs). When we sequenced 2 samples from the same animal, the sequences were identical and subsequently represented only once in analyses (Figure 4). All sequences clustered with previously reported type II CeCoVs (22) in 1 of 3 lineages. Sequences from 14 of 16 dogs were identical, suggesting a single outbreak strain geographically distributed across England. Sequences from dogs 15 and 16 were phylogenetically distinct.

Results of MinION sequencing rapidly confirmed an alphacoronavirus as the predominant virus (24,190 out of 33,826,933 reads) and failed to identify any other prevalent candidates (next highest, betabaculovirus: 4,541 reads). Although bacterial reads were present in high numbers, none showed consistently high results across most samples.

Complete CeCoV genomes were assembled from 6 PCR-positive cases by Illumina sequencing. We identified no coronavirus sequences in 3 cases and 1 control that tested negative for CeCoV by PCR. The only other mammalian virus sequence detected matched a canine rotavirus (1 case, 1 control; data not presented). Consistent with M-gene sequencing, 5 of the CeCoV genomes clustered together (>99% similarity), distinct from the genome from dog 15 (Figure 4). The outbreak strain was most similar to a virus from Taiwan isolated in 2008 from a young dog with diarrhea (94.5% similarity; L. Chueh, pers. comm. [email] Apr. 27, 2020) and did not show any obvious sequence differences to published strains that might explain the unusual pattern of disease observed in the outbreak. Based on spike gene analyses, the outbreak strain clustered with IIb, having a TGEV-like N-terminal spike domain (*23*). Sequences were submitted to GenBank (accession nos. MT877072, MT906864, and MT906865).

## Discussion

Using EHRs annotated with syndromic information by veterinarians, we rapidly identified an outbreak of canine gastroenteric disease that had started in November 2019. This finding was corroborated by parallel increases in relevant prescriptions and records

**Table 2.** Veterinary- and owner-reported case questionnaire responses pertaining to signalment, health history, contacts, and feeding habits among dogs with vomiting, United Kingdom, January 2017–February 2020*

| | Veterinarian-reported cases, n = 165 | | Owner-reported cases, n = 1,034 | |
|---|---|---|---|---|
| Question | % Responses (95% CI) | No. unknown | % Responses (95% CI) | No. unknown |
| Veterinary practice location | | | | |
| England | 80.6 (74.6–86.7) | NA | 89.8 (87.9–91.6) | NA |
| Wales | 12.1 (7.1–17.1) | NA | 4.5 (3.2–5.7) | NA |
| Scotland | 4.9 (1.6–8.1) | NA | 4.5 (3.2–5.7) | NA |
| North Ireland | 1.2 (0.0–2.9) | NA | 1.1 (0.4–1.7) | NA |
| Republic of Ireland | 1.2 (0.0–2.9) | NA | 0.1 (0.0–0.3) | NA |
| Isle of Man | 0 | NA | 0.2 (0.0–0.5) | NA |
| Sex | | | | |
| F | 42.4 (34.9-50.0) | NA | 43.7 (40.7-46.7) | NA |
| M | 57.6 (50.0–65.1) | NA | 56.3 (53.3–59.3) | NA |
| Neutered‡ | 69.1 (62.0–76.2) | NA | 70.1 (67.3–72.9) | NA |
| Intact‡ | 30.9 (23.8-37.9) | NA | 29.9 (27.1-32.7) | NA |
| Vaccinated within past 3 y† | 94.6 (91.1–98.0) | NA | 88.4 (86.5–90.4 | 13 |
| Distemper | 92.7 (88.8–96.7) | NA | 49.7 (46.7–52.8) | NA |
| Infectious hepatitis | 92.1 (88.0–96.2) | NA | 40.4 (37.4–43.4) | NA |
| Parvo | 92.1 (88.0–96.2) | NA | 55.4 (52.4–58.5) | NA |
| Parainfluenza | 53.9 (46.3–61.6) | NA | 37.4 (34.5–40.4) | NA |
| Leptospirosis | 92.7 (88.8–96.7) | NA | 49.2 (46.2–52.3) | NA |
| Kennel cough | 46.7 (39.0–54.3) | NA | 40.4 (37.4–43.4) | NA |
| Rabies | 2.4 (0.1–4.8) | NA | 1.3 (0.6–1.9) | NA |
| Herpes | 0.6 (0.0–1.8) | NA | NA | NA |
| Dewormed within past 3 mo | 86.2 (80.5–92.0) | 27 | 69.8 (67.0–72.7) | 50 |
| Lives in multidog household | 34.6 (27.3–41.8) | NA | 47.4 (44.3–50.4) | NA |
| ≥1 dogs in household vomited | 54.4 (41.3–67.4) | NA | 55.9 (51.5–60.3) | NA |
| Regular contact with other species† | 54.9 (46.1–63.8) | 43 | 44.1 (41.1–47.1) | NA |
| Cats | 64.2 (52.6–75.8) | NA | 62.3 (57.8–66.7) | NA |
| Horses | 20.9 (11.1–30.7) | NA | 28.3 (24.2–32.4) | NA |
| Cattle or sheep or both | 25.4 (14.9–35.9) | NA | 22.2 (18.3–26.0) | NA |
| Pigs | 3.0 (0.0–7.1) | NA | 1.5 (0.4–2.7) | NA |
| Poultry | 13.4 (5.2–21.7) | NA | 14.0 (10.8–17.2) | NA |
| Rabbits | 7.5 (1.1–13.8) | NA | 5.7 (3.6–7.8) | NA |
| Other species | 11.9 (4.1–19.8) | NA | 20.6 (16.9–24.3) | NA |
| Contact with other vomiting species | 13.5 (7.1–19.9) | 54 | 17.4 (14.6–20.2) | 320 |
| Recent travel history† | 31.4 (23.0–39.8) | 47 | 26.7 (24.0–29.4) | NA |
| Boarding kennel | 8.1 (0.0–17.0) | NA | 9.1 (5.7–12.5) | NA |
| Group training/behavior classes | 24.3 (10.3–38.3) | NA | 35.5 (29.9–41.2) | NA |
| Doggie day care facility | 48.7 (32.3–65.0) | NA | 39.5 (33.7–45.3) | NA |
| Overseas | 2.7 (0.0–8.0) | NA | 0.7 (0.0–1.7) | NA |
| Rescue kennel | 0.0 (0.0–0.0) | NA | 0.4 (0.0–1.1) | NA |
| Other | 18.9 (6.1–31.7) | NA | 20.3 (15.5–25.0) | NA |
| Provided known food type† | 95.2 (91.9–98.4) | 8 | 100.0 (100.0–100.0) | NA |
| Proprietary dog food | 95.5 (92.3–98.8) | NA | 85.9 (83.8–88.0) | NA |
| Home-cooked diet | 6.4 (2.5–10.2) | NA | 10.4 (8.6–12.3) | NA |
| Raw meat | 5.1 (1.6–8.6) | NA | 15.9 (13.6–18.1) | NA |
| Table scraps | 14.7 (9.1–20.2) | NA | 16.1 (13.8–18.3) | NA |
| Scavenged food | 36.6 (28.7–44.4) | 20 | 19.9 (17.4–22.4) | 24 |

*NA, not available.
‡Includes both female and male animals.
†Multiple responses for the same dog are possible.

**Table 3.** Veterinarian reported and owner-reported case questionnaire responses pertaining to clinical signs, diagnostic and management strategies, and case recovery likelihood and time among dogs with vomiting, United Kingdom, January 2017–February 2020*

| | Veterinarian-reported cases, n = 165 | | Owner-reported cases, n = 1,034 | |
|---|---|---|---|---|
| Question | % Responses (95% CI) | No. unknown | % Responses (95% CI) | No. unknown |
| Clinical signs | | | | |
| Vomiting without blood | 91.5 (87.3–95.8) | NA | 88.7 (86.8–90.6) | NA |
| Vomiting with blood | 8.5 (4.2–12.8) | NA | 11.3 (9.4–13.3) | NA |
| Diarrhea without blood | 37.0 (29.6–44.4) | NA | 46.2 (43.2–49.3) | NA |
| Diarrhea with blood | 10.9 (6.1–15.7) | NA | 12.3 (10.3–14.3) | NA |
| Melaena | 1.8 (0.0–3.9) | NA | NA | NA |
| Pyrexia | 12.7 (7.6–17.8) | NA | 15.4 (13.2–17.6) | NA |
| Inappetence | 86.1 (80.8–91.4) | NA | 75.6 (73.0–78.3) | NA |
| Weight loss | 18.2 (12.3–24.1) | NA | 34.9 (32.0–37.8) | NA |
| Lethargy | 9.1 (4.7–13.5) | NA | 6.3 (4.8–7.8) | NA |
| Diagnostic testing performed | 32.1 (25.0–39.3) | NA | 18.3 (15.9–20.7) | NA |
| Treatment provided to dog | 92.1 (88.0–96.2) | NA | 61.7 (58.7–64.7 | 13 |
| Recovery status known | 88.5 (83.6–93.4) | 19 | 98.4 (97.6–99.1) | 17 |
| Recovery <24 h | 5.5 (2.0–8.9) | NA | 2.9 (1.8–3.9) | NA |
| Recovery in 24–48 h | 17.6 (11.8–23.4) | NA | 21.1 (18.6–23.7) | NA |
| Recovery in 3–7 d | 30.9 (23.8–38.0) | NA | 36.2 (33.2–39.1) | NA |
| Recovery in 7–14 d | 2.4 (0.1–4.8) | NA | 5.9 (4.5–7.4) | NA |
| Recovery in over 14 d | 2.4 (0.1–4.8) | NA | 2.1 (1.2–2.9) | NA |
| Dog currently vomiting | 7.9 (3.8–12.0) | NA | 9.4 (7.6–11.2) | NA |
| Dog not vomiting but still unwell | 21.2 (15.0–27.5) | NA | 21.4 (18.9–24.0) | NA |
| Dog died | 0.6 (0.0–1.8) | NA | 1.0 (0.4–1.6) | NA |

*NA, not available.

of frequent vomiting. Those data were augmented by data from responses to a questionnaire, diagnostic laboratories, and enhanced microbiological analyses. This system enabled us to determine case definitions and outcomes and to identify risk factors as well as a potential viral cause, within a 3-month period; findings were rapidly disseminated to veterinarians (*24*,*25*) and owners. This combined approach represents an efficient system that can fill a previously neglected national population health surveillance need for companion animals.

The first indication of an outbreak came from time-series analyses of syndromic data. Such syndromic surveillance is increasingly being used to monitor the impact of national events like natural disasters and bioterrorism on human population health, as well as changes in gastroenteric and influenza-like illness (*6*–*9*). Such data can be simple to collect, provide real-time wide geographic coverage, and be flexibly applied to different conditions (*10*,*11*). Although in some cases these data can identify outbreaks earlier than more active surveillance, their predictive value can sometimes be low, particularly where there is a low signal to noise complaint ratio. In our case, the outbreak was large compared with background levels, associated with near doubling of the gastroenteric syndrome, and had many weeks in which the syndrome statistically exceeded the baseline.

The richness of data within EHRs enabled us to validate this outbreak using numbers of antiemetic prescriptions and text mining. Prescription data have been used to understand, for example, human health inequalities (*26*), and the use of critical antimicrobials in both humans (*27*) and animals (*28*,*29*). We used

**Table 4.** Mixed effects multivariable logistic regression model investigating odds of being a veterinarian-reported prolific vomiting case among 165 cases and 60 controls in investigation of dogs with vomiting, United Kingdom, January 2017–February 2020*

| Variable | β | SE | OR (95% CI) | p value† |
|---|---|---|---|---|
| Intercept | –0.36 | 0.42 | NA | NA |
| F, neutered | NA | NA | Referent | NA |
| F, intact | 0.77 | 0.55 | 2.15 (0.74–6.26) | 0.16 |
| M, neutered | 0.81 | 0.40 | 2.25 (1.03–4.91) | 0.04 |
| M, intact | 1.34 | 0.59 | 3.82 (1.20–12.15) | 0.02 |
| Multidog household, no other dogs vomiting in the same household | NA | NA | Referent | NA |
| Multidog household, other dogs vomiting in the same household | 1.15 | 0.53 | 3.16 (1.11–8.97) | 0.03 |
| Single-dog household | 1.17 | 0.40 | 3.23 (1.47–7.11) | <0.01 |
| No contact with other species vomiting | NA | NA | Referent | NA |
| Confirmed contact with other species vomiting | –1.23 | 0.48 | 0.29 (0.12–0.74) | 0.01 |
| Unknown contact with vomiting other species | 0.63 | 0.42 | 1.88 (0.83–4.26) | 0.13 |

*β, β-value (coefficient).
†p value <0.05 indicates significant findings.

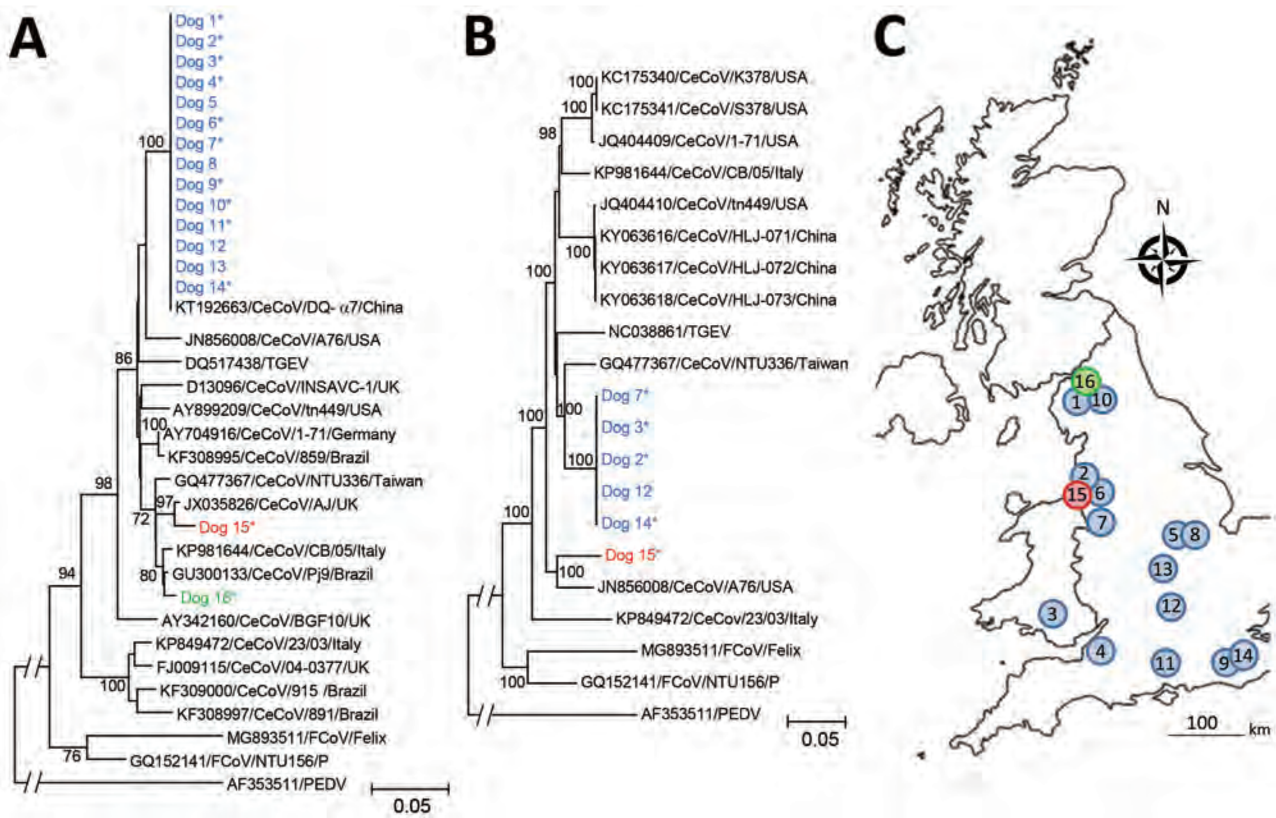


**Figure 4.** Phylogenetic analysis of canine enteric coronavirus strains, including locations were sequences were obtained, in investigation of dogs with vomiting, United Kingdom. Trees are based on nucleotide sequences for M-gene (final alignment 299 positions) (A) and whole genome (final alignment 26,564 positions) (B). Evolutionary analysis was performed using the neighbor-joining method. Bootstrap testing using 1,000 replicates was applied; only values >70 are indicated. Sequences identified in this study are indicated in blue (strain 1), red (strain 2), and green (strain 3). Asterisks (*) indicate samples from animals meeting the case definition. Each phylogeny included closest matches in GenBank, as well as representative published canine coronavirus, feline coronavirus, and transmissible gastroenteritis virus isolates. Scale bars indicate substitutions per site. C) Approximate geographic location of sequences obtained in this study, number- and color-matched to sequences shown in panels A and B.

these data to identify and track an outbreak, benefitting from a clear link between the syndrome (vomiting) and its therapy (antiemetic). It will be useful to identify other disease-therapy associations that could be used for similar surveillance.

We used text mining to identify records of frequent vomiting in clinical narratives. Such approaches can circumvent the need for practitioner-derived annotation and be flexibly and rapidly adapted to emerging syndromes as soon as case-definitions are determined. Similar approaches have been described in human health for conditions such as fever (*30*–*32*) but can suffer low sensitivity (*31*). Indeed, the outbreak peak based on text mining was ≈20% of that based on MPC analysis. However, it is also likely the outbreak as defined by the MPC included a considerable number of animals with milder signs that would not be detected by data mining using the regular expression developed here. Although data from text mining are unlikely to give an accurate estimate of the true prevalence of a given condition, they can still be used to track outbreaks.

To compliment syndromic surveillance, we implemented a rapid case-control study, collecting >1,200 responses from veterinarians and owners in 4.5 weeks. There was no evidence for similar disease in people or other species. The timing of the outbreak as shown by case data was in broad agreement with our syndromic surveillance. Questionnaires from owners and veterinarians were in broad agreement on date of onset, geographic density, clinical signs, and recovery. These data informed targeted health messages posted online and on social media on February 28, 2020, 4 weeks after we first became aware of the outbreak.

Clearly, evidence of transmission driving the outbreak was vital to providing disease control advice. Dogs in multidog households were more likely to vomit if other dogs in the household were also affected, suggesting either transmission between dogs or a common environmental source; these observations informed advice to the public around isolating affected dogs. Of note, dogs in single-dog households were also at increased odds of being affected compared to multidog households where only a single dog was vomiting. Some authors have shown that dogs from single-dog households are walked more and therefore could be at greater risk for infection (*33*). Factors affecting dog walking are clearly likely to be important for control of infectious disease transmission and should be explored further.

In addition to collecting epidemiologic data, we collected microbiological samples from cases and controls. Based on its known (*34*) and observed seasonality (Figure 3, panel A), we tested all samples for CeCoV. Cases were significantly more likely to show positive results both when all samples (oral swabs, feces and vomit) were considered or when just fecal samples were considered, suggesting a possible role for CeCoV in the outbreak. However, many case samples tested negative: 33 of 50 overall, 6 of 16 dogs for which feces samples were submitted, and 7 of 13 dogs for which vomit samples were submitted. There are several potential reasons for these negative findings, including the sensitivity of the PCR, the high numbers of oral swabs (although simpler to collect, oral swabs were more likely to test negative), the timing of samples in relation to viral shedding, and the storage and transport of samples. In addition, it is important to note that our case definition, based as it was on a syndrome and lacking more specific confirmatory testing, is likely to include some animals that were not part of the outbreak. Indeed, at its peak, the outbreak only doubled the background level of gastroenteric disease seen at other times of the year; therefore, we might expect only half of our cases to be truly associated with the outbreak.

Sequencing results identified a predominant CeCoV strain in outbreak cases across the United Kingdom, in contrast with earlier studies showing that CeCoV strains tend to cluster in households, veterinary practices, or local areas (*35*). This finding lends further support to the role of this strain in the observed outbreak. In Sweden, a single strain was also implicated in several small wintertime canine vomiting outbreaks (*36*); genetically, however, the virus strain we identified was distinct from the strain from Sweden (data not shown). Ultimately, it will be necessary to perform a challenge study to confirm or refute the role of this CeCoV strain as the cause of this outbreak, as well as to explore the range of clinical signs associated with infection.

If this strain is proven to be the cause of the outbreak, several features mark the observed pattern of disease as unusual, including the outbreak scale, its geographic distribution, the severity of signs in some animals, a lack of notable viral co-infections, and the involvement of adult dogs. CeCoV is generally associated with mild gastroenteritis (*37*). Although sporadic outbreaks of more severe hemorrhagic diseases with high mortality (*38*–*40*), as well as systemic diseases (*41*,*42*), have been reported, these typically affect individual households, and are often associated with mixed infections (*43*). Such observations suggest that the genetic variability of CeCoVs may affect virulence and are supported by experimental infections recreating more severe disease (*38*). The genetic mechanism underlying such shifts in virulence in CeCoV have not been defined. However, mutations impacting virulence are described in closely related alphacoronaviruses (*44*–*47*).

In conclusion, this multidisciplinary approach enabled a rapid response to a newly described outbreak of canine gastroenteritis and identified a CeCoV as a potential cause. Previous CeCoV seasonality suggests further outbreaks may occur. Having such an efficient surveillance system provides the ideal platform to inform and target population health messaging. Several challenges remain for addressing the lack of national population health structures for companion animals: to systematically capture discussions of disease in social and mainstream media; to sustainably fund these activities, which currently are largely resourced by research grants; to understand and broaden the representativeness of such sentinel networks; and to link surveillance information with agencies empowered to act (*12*).

**Acknowledgments**

We thank data providers both in veterinary practice (VetSolutions, Teleos, CVS Group, and independent practitioners) and participating veterinary diagnostic laboratories (Axiom Veterinary Laboratories, Batt Laboratories, BioBest, Idexx, NationWide Laboratories Microbiology Diagnostics Laboratory at the University of Liverpool, the Department of Pathology and Infectious Diseases at the University of Surrey, and the Veterinary Pathology Group), without whose support and participation this research would not have been possible. We are especially grateful for the help and support provided by SAVSNET team members Susan Bolan and Steven Smyth.

This work was funded in part by the Dogs Trust as part of SAVSNET-Agile, and by the Biotechnology and Biological Sciences Research Council, and previously by the British Small Animal Veterinary Association.

## About the Author

Dr. Radford is a professor of veterinary health informatics at the University of Liverpool. His primary research interests are the molecular epidemiology of viral pathogens, particularly those of veterinary importance, and combining this subject with electronic health data to study animal diseases at a population level and their impact on people.

## References


1. Crawford PC, Dubovi EJ, Castleman WL, Stephenson I, Gibbs EP, Chen L, et al. Transmission of equine influenza virus to dogs. Science. 2005;310:482–5. https://doi.org/10.1126/science.1117950
2. Li G, Wang R, Zhang C, Wang S, He W, Zhang J, et al. Genetic and evolutionary analysis of emerging H3N2 canine influenza virus. Emerg Microbes Infect. 2018;7:1–15. https://doi.org/10.1038/s41426-018-0079-0
3. Allison AB, Kohler DJ, Fox KA, Brown JD, Gerhold RW, Shearn-Bochsler VI, et al. Frequent cross-species transmission of parvoviruses among diverse carnivore hosts. J Virol. 2013;87:2342–7. https://doi.org/10.1128/JVI.02428-12
4. O'Neill DG, Church DB, McGreevy PD, Thomson PC, Brodbelt DC. Approaches to canine health surveillance. Canine Genet Epidemiol. 2014;1:2. https://doi.org/10.1186/2052-6687-1-2
5. Smith S, Elliot AJ, Mallaghan C, Modha D, Hippisley-Cox J, Large S, et al. Value of syndromic surveillance in monitoring a focal waterborne outbreak due to an unusual *Cryptosporidium* genotype in Northamptonshire, United Kingdom, June–July 2008. Euro Surveill. 2010;15:19643. https://doi.org/10.2807/ese.15.33.19643-en
6. Fleming DM, Elliot AJ. Lessons from 40 years' surveillance of influenza in England and Wales. Epidemiol Infect. 2008; 136:866–75. https://doi.org/10.1017/S0950268807009910
7. Hiller KM, Stoneking L, Min A, Rhodes SM. Syndromic surveillance for influenza in the emergency department—a systematic review. PLoS One. 2013;8:e73832. https://doi.org/10.1371/journal.pone.0073832
8. Elliot AJ, Singh N, Loveridge P, Harcourt S, Smith S, Pnaiser R, et al. Syndromic surveillance to assess the potential public health impact of the Icelandic volcanic ash plume across the United Kingdom, April 2010. Euro Surveill. 2010;15:19583.
9. Thomas MJ, Yoon PW, Collins JM, Davidson AJ, Mac Kenzie WR. Evaluation of syndromic surveillance systems in 6 US state and local health departments. J Public Health Manag Pract. 2018;24:235–40. https://doi.org/10.1097/PHH.0000000000000679
10. Smith GE, Elliot AJ, Lake I, Edeghere O, Morbey R, Catchpole M, et al.; Public Health England Real-time Syndromic Surveillance Team. Syndromic surveillance: two decades experience of sustainable systems—its people not just data! Epidemiol Infect. 2019;147:e101. https://doi.org/10.1017/S0950268819000074
11. Sánchez-Vizcaíno F, Noble PM, Jones PH, Menacere T, Buchan I, Reynolds S, et al. Demographics of dogs, cats, and rabbits attending veterinary practices in Great Britain as recorded in their electronic health records. BMC Vet Res. 2017;13:218. https://doi.org/10.1186/s12917-017-1138-9
12. McGreevy P, Thomson P, Dhand NK, Raubenheimer D, Masters S, Mansfield CS, et al. VetCompass Australia: a national big data collection system for veterinary science. Animals (Basel). 2017;7:74. https://doi.org/10.3390/ani7100074
13. O'Neill DG, Church DB, McGreevy PD, Thomson PC, Brodbelt DC. Prevalence of disorders recorded in cats attending primary-care veterinary practices in England. Vet J. 2014;202:286–91. https://doi.org/10.1016/j.tvjl.2014.08.004
14. Asher L, Buckland EL, Phylactopoulos CI, Whiting MC, Abeyesinghe SM, Wathes CM. Estimation of the number and demographics of companion dogs in the UK. BMC Vet Res. 2011;7:74. https://doi.org/10.1186/1746-6148-7-74
15. Elwood C, Devauchelle P, Elliott J, Freiche V, German AJ, Gualtieri M, et al. Emesis in dogs: a review. J Small Anim Pract. 2010;51:4–22. https://doi.org/10.1111/j.1748-5827.2009.00820.x
16. O Neill DG, Church DB, McGreevy PD, Thomson PC, Brodbelt DC. Prevalence of disorders recorded in dogs attending primary-care veterinary practices in England. PLoS One. 2014;9:e90501. https://doi.org/10.1371/journal.pone.0090501
17. Day MJ, Horzinek MC, Schultz RD, Squires RA; Vaccination Guidelines Group (VGG) of the World Small Animal Veterinary Association (WSAVA). WSAVA guidelines for the vaccination of dogs and cats. J Small Anim Pract. 2016; 57:E1–45. https://doi.org/10.1111/jsap.2_12431
18. Singleton DA, Sánchez-Vizcaíno F, Arsevska E, Dawson S, Jones PH, Noble PJM, et al. New approaches to pharmacosurveillance for monitoring prescription frequency, diversity, and co-prescription in a large sentinel network of companion animal veterinary practices in the United Kingdom, 2014–2016. Prev Vet Med. 2018;159:153–61. https://doi.org/10.1016/j.prevetmed.2018.09.004
19. Arsevska E, Singleton DA, Jewell C, Paterson S, Jones PH, Smyth S, et al. Small animal disease surveillance: pruritus and *Pseudomonas* skin infections. Vet Rec. 2018;183:182–7. https://doi.org/10.1136/vr.k3462
20. Pratelli A, Tempesta M, Greco G, Martella V, Buonavoglia C. Development of a nested PCR assay for the detection of canine coronavirus. J Virol Methods. 1999;80:11–5. https://doi.org/10.1016/S0166-0934(99)00017-8
21. Chrzastek K, Lee DH, Smith D, Sharma P, Suarez DL, Pantin-Jackwood M, et al. Use of sequence-independent, single-primer-amplification (SISPA) for rapid detection, identification, and characterization of avian RNA viruses. Virology. 2017;509:159–66. https://doi.org/10.1016/j.virol.2017.06.019
22. Pratelli A, Martella V, Decaro N, Tinelli A, Camero M, Cirone F, et al. Genetic diversity of a canine coronavirus detected in pups with diarrhoea in Italy. J Virol Methods. 2003;110:9–17. https://doi.org/10.1016/S0166-0934(03)00081-8
23. Decaro N, Mari V, Elia G, Addie DD, Camero M, Lucente MS, et al. Recombinant canine coronaviruses in dogs, Europe. Emerg Infect Dis. 2010;16:41–7. https://doi.org/10.3201/eid1601.090726
24. Smith SL, Singleton DA, Noble PJ, Radford AD, Brant B, Pinchbeck GL, et al. Possible cause of outbreak of prolific vomiting in dogs. Vet Rec. 2020;186:324. https://doi.org/10.1136/vr.m972
25. Singleton DA, Noble PJ, Radford AD, Brant B, Pinchbeck GL, Greenberg D, et al. Prolific vomiting in dogs. Vet Rec. 2020;186:191. https://doi.org/10.1136/vr.m553
26. Rowlingson B, Lawson E, Taylor B, Diggle PJ. Mapping English GP prescribing data: a tool for monitoring health-service inequalities. BMJ Open. 2013;3:e001363. https://doi.org/10.1136/bmjopen-2012-001363
27. Zanichelli V, Monnier AA, Gyssens IC, Adriaenssens N, Versporten A, Pulcini C, et al. Variation in antibiotic use among

and within different settings: a systematic review. J Antimicrob Chemother. 2018;73(suppl_6):vi17–29. https://doi.org/10.1093/jac/dky115
28. Singleton DA, Sánchez-Vizcaíno F, Dawson S, Jones PH, Noble PJM, Pinchbeck GL, et al. Patterns of antimicrobial agent prescription in a sentinel population of canine and feline veterinary practices in the United Kingdom. Vet J. 2017;224:18–24. https://doi.org/10.1016/j.tvjl.2017.03.010
29. Hur BA, Hardefeldt LY, Verspoor KM, Baldwin T, Gilkerson JR. Describing the antimicrobial usage patterns of companion animal veterinary practices; free text analysis of more than 4.4 million consultation records. PLoS One. 2020;15:e0230049. https://doi.org/10.1371/journal.pone.0230049
30. South BR, Chapman WW, Delisle S, Shen S, Kalp E, Perl T, et al. Optimizing a syndromic surveillance text classifier for influenza-like illness: does document source matter? AMIA Annu Symp Proc. 2008;2008:692–6.
31. Haas SW, Travers D, Waller A, Mahalingam D, Crouch J, Schwartz TA, et al. Emergency Medical Text Classifier: new system improves processing and classification of triage notes. Online J Public Health Inform. 2014;6:e178. https://doi.org/10.5210/ojphi.v6i2.5469
32. Chapman WW, Dowling JN, Wagner MM. Classification of emergency department chief complaints into 7 syndromes: a retrospective analysis of 527,228 patients. Ann Emerg Med. 2005;46:445–55. https://doi.org/10.1016/j.annemergmed.2005.04.012
33. Westgarth C, Christian HE, Christley RM. Factors associated with daily walking of dogs. BMC Vet Res. 2015;11:116. https://doi.org/10.1186/s12917-015-0434-5
34. Duijvestijn M, Mughini-Gras L, Schuurman N, Schijf W, Wagenaar JA, Egberink H. Enteropathogen infections in canine puppies: (co-)occurrence, clinical relevance and risk factors. Vet Microbiol. 2016;195:115–22. https://doi.org/10.1016/j.vetmic.2016.09.006
35. Stavisky J, Pinchbeck GL, German AJ, Dawson S, Gaskell RM, Ryvar R, et al. Prevalence of canine enteric coronavirus in a cross-sectional survey of dogs presenting at veterinary practices. Vet Microbiol. 2010;140:18–24. https://doi.org/10.1016/j.vetmic.2009.07.012
36. Escutenaire S, Isaksson M, Renström LH, Klingeborn B, Buonavoglia C, Berg M, et al. Characterization of divergent and atypical canine coronaviruses from Sweden. Arch Virol. 2007;152:1507–14. https://doi.org/10.1007/s00705-007-0986-1
37. Decaro N, Buonavoglia C. An update on canine coronaviruses: viral evolution and pathobiology. Vet Microbiol. 2008;132:221–34. https://doi.org/10.1016/j.vetmic.2008.06.007
38. Buonavoglia C, Decaro N, Martella V, Elia G, Campolo M, Desario C, et al. Canine coronavirus highly pathogenic for dogs. Emerg Infect Dis. 2006;12:492–4. https://doi.org/10.3201/eid1203.050839
39. Tennant BJ, Gaskell RM, Jones RC, Gaskell CJ. Studies on the epizootiology of canine coronavirus. Vet Rec. 1993;132:7–11. https://doi.org/10.1136/vr.132.1.7
40. Evermann JF, Abbott JR, Han S. Canine coronavirus-associated puppy mortality without evidence of concurrent canine parvovirus infection. J Vet Diagn Invest. 2005;17:610–4. https://doi.org/10.1177/104063870501700618
41. Decaro N, Campolo M, Lorusso A, Desario C, Mari V, Colaianni ML, et al. Experimental infection of dogs with a novel strain of canine coronavirus causing systemic disease and lymphopenia. Vet Microbiol. 2008;128:253–60. https://doi.org/10.1016/j.vetmic.2007.10.008
42. Zicola A, Jolly S, Mathijs E, Ziant D, Decaro N, Mari V, et al. Fatal outbreaks in dogs associated with pantropic canine coronavirus in France and Belgium. J Small Anim Pract. 2012;53:297–300. https://doi.org/10.1111/j.1748-5827.2011.01178.x
43. Dowgier G, Lorusso E, Decaro N, Desario C, Mari V, Lucente MS, et al. A molecular survey for selected viral enteropathogens revealed a limited role of canine circovirus in the development of canine acute gastroenteritis. Vet Microbiol. 2017;204:54–8. https://doi.org/10.1016/j.vetmic.2017.04.007
44. Porter E, Tasker S, Day MJ, Harley R, Kipar A, Siddell SG, et al. Amino acid changes in the spike protein of feline coronavirus correlate with systemic spread of virus from the intestine and not with feline infectious peritonitis. Vet Res. 2014;45:49. https://doi.org/10.1186/1297-9716-45-49
45. Chang HW, Egberink HF, Halpin R, Spiro DJ, Rottier PJ. Spike protein fusion peptide and feline coronavirus virulence. Emerg Infect Dis. 2012;18:1089–95. https://doi.org/10.3201/eid1807.120143
46. Licitra BN, Millet JK, Regan AD, Hamilton BS, Rinaldi VD, Duhamel GE, et al. Mutation in spike protein cleavage site and pathogenesis of feline coronavirus. Emerg Infect Dis. 2013;19:1066–73. https://doi.org/10.3201/eid1907.121094
47. Zhang X, Hasoksuz M, Spiro D, Halpin R, Wang S, Stollar S, et al. Complete genomic sequences, a key residue in the spike protein and deletions in nonstructural protein 3b of US strains of the virulent and attenuated coronaviruses, transmissible gastroenteritis virus and porcine respiratory coronavirus. Virology. 2007;358:424–35. https://doi.org/10.1016/j.virol.2006.08.051

Address for correspondence: Alan Radford, University of Liverpool, Leahurst Campus, Chester High Road, Neston, S. Wirral, CH64 7TE, UK; email; alanrad@liverpool.ac.uk

# Spread of Multidrug-Resistant *Rhodococcus equi*, United States

Sonsiray Álvarez-Narváez, Steeve Giguère,[1] Noah Cohen, Nathan Slovis, José A. Vázquez-Boland

Multidrug resistance has been detected in the animal and zoonotic human pathogen *Rhodococcus equi* after mass macrolide/rifampin antibioprophylaxis in endemically affected equine farms in the United States. Multidrug-resistant (MDR) *R. equi* emerged upon acquisition of pRErm46, a conjugative plasmid conferring resistance to macrolides, lincosamides, streptogramins, and, as we describe, tetracycline. Phylogenomic analyses indicate that the increasing prevalence of MDR *R. equi* since it was first documented in 2002 is caused by a clone, *R. equi* 2287, attributable to coselection of pRErm46 with a chromosomal *rpoB*$^{S531F}$ mutation driven by macrolide/rifampin therapy. pRErm46 spillover to other *R. equi* genotypes has given rise to a novel MDR clone, G2016, associated with a distinct *rpoB*$^{S531Y}$ mutation. Our findings illustrate that overuse of antimicrobial prophylaxis in animals can generate MDR pathogens with zoonotic potential. MDR *R. equi* and pRErm46-mediated resistance are currently disseminating in the United States and are likely to spread internationally through horse movements.

*Rhodococcus equi* is a soilborne facultative intracellular actinobacterium that causes pyogranulomatous infections in multiple animal species, including humans. Rhodococcal infection is particularly severe in young foals and immunocompromised persons, in whom it typically manifests as a life-threatening purulent bronchopneumonic disease (*1*–*3*). *R. equi* is able to colonize equids, pigs, and ruminants through 3 different host-specific virulence plasmid types (designated pVAPA, pVAPB, and pVAPN) (*4*). Analysis of the virulence plasmids carried by the isolates and comparison of genomic profiles indicate that human *R. equi* infections originate from animals (*4*–*6*).

Author affiliations: University of Georgia, Athens, Georgia, USA (S. Álvarez-Narváez, S. Giguère); Texas A&M University, College Station, Texas, USA (N. Cohen); Hagyard Equine Medical Institute, Lexington, Kentucky, USA (N. Slovis); University of Edinburgh, Edinburgh, Scotland, UK (J.A. Vázquez-Boland)

DOI: https://doi.org/10.3201/eid2702.203030

*R. equi* is highly prevalent in horse-breeding farms worldwide (*7*). For decades, the standard treatment for *R. equi* pneumonia in foals has been a combination macrolide/rifampin therapy (*8*). In the absence of effective preventive methods, many horse-breeding farms rely on early ultrasonographic detection of infected foals and initiation of macrolide/rifampin prophylaxis before clinical manifestation of the disease (*9*). In the United States, where foal rhodococcosis is often endemic, implementation of this practice has been linked to the emergence of dual macrolide/rifampin–resistant (MR$^R$) *R. equi* (*10*–*12*). First detected in the late 1990s, *R. equi* MR$^R$ isolates are increasingly prevalent (*11*–*14*), posing a substantial problem because no clinically proven therapeutic alternative is currently available for the treatment of affected foals (*8*). The MR$^R$ isolates also represent a potential hazard to human health because of the risk for zoonotic transmission.

We recently determined that the emerging MR$^R$ phenotype among *R. equi* equine isolates was linked to a novel methyltransferase gene, *erm*(46), which confers cross-resistance to macrolides, lincosamides, and streptogramins (MLS$^R$ phenotype) (*13*). *erm*(46) is part of a 6.9-kb transposable element, Tn*RErm46*, which is carried by the conjugative resistance plasmid pRErm46 (*15*). Upon pRErm46 acquisition, Tn*RErm46* stabilizes itself in *R. equi* by transposing to the host genome, including the conjugative virulence plasmid pVAPA. Despite its high potential for horizontal spread, we found that pRErm46/Tn*RErm46* was restricted to a specific *R. equi* clone, designated 2287, likely because of co-selection with a chromosomal rifampin-resistance *rpoB*$^{S531F}$ mutation in response to macrolide/rifampin therapy (*15*).

We identified the multidrug-resistant (MDR) *R. equi* 2287 clone by analyzing isolates collected during 2002–2011 (*15*). Here, we investigate the spread of the *erm*(46) determinant in a contemporary sample

[1]Deceased.

of macrolide-resistant isolates and horizontal spread of pRErm46/Tn*RErm46*, leading to emergence of a further MDR *R. equi* clone associated with a novel *rpoB*$^{S531Y}$ mutation.

## Materials and Methods

### Bacteria

We sequenced the genomes of a random selection of 30 macrolide-resistant and 18 macrolide-susceptible *R. equi* equine clinical strains recovered from pneumonic foals in 5 US states (Florida, Kentucky, Louisiana, New York, and Texas) during 2012–2017 (Appendix Table 1, https://wwwnc.cdc.gov/EID/article/27/2/20-3030-App1.pdf). Whenever possible, at least 1 strain from each category was chosen for each year and US state. The strains from Louisiana were a random collection of 10 convenience-sampled isolates from a single farm. All strains were routinely grown in brain-heart infusion medium (BD, https://www.bd.com) for 48 h at 37°C. Detection of the *erm*(46) gene by PCR was performed as previously described (*13*,*15*).

### Antimicrobial Susceptibility Testing

Susceptibility tests were performed at the Hagyard Equine Medical Institute diagnostic laboratory (Lexington, Kentucky, USA), Texas A&M Veterinary Medical Diagnostic Laboratory (College Station, Texas, USA), and University of Georgia Veterinary Diagnostic Laboratory (Athens, Georgia, USA) according to Clinical and Laboratory Standards Institute (CLSI) guidelines (https://clsi.org). In the absence of specific disk susceptibility interpretive criteria for *R. equi*, CLSI guidelines for *Staphylococcus aureus* were used in accordance with routine practices in veterinary diagnostic laboratories (*11*,*16*). MICs were determined in tryptone soy agar medium by using Etest strips (bioMérieux, https://www.biomerieux.com) according to the manufacturer's recommendations (*16*). *Staphylococcus aureus* ATCC 29213 was used as a control in all susceptibility tests.

### Genome Sequencing and Phylogenetic Analysis

We extracted bacterial genomic DNA by using DNeasy UltraClean Microbial Kit (QIAGEN, https://www.qiagen.com) following the manufacturer's instructions. DNA quality (optical density 260/280, ratio 1.8:2) and concentration (>1 µg) of each gDNA sample were verified by using a NanoDrop apparatus (Thermo Fisher Scientific, https://www.thermofisher.com). Single-molecule real-time long-read DNA sequencing was performed at Duke Center for Genomic and Computational Biology (Duke University, Durham, North Carolina, USA). SMRTbell Template Prep Kit 2.0 was used for library preparation of 4–6-kb insert for 8 multiplexed bacterial samples. Samples were run on a PacBio Sequel II system (Pacific Bioscience, https://www.pacb.com). Genomes were assembled de novo by using Canu version 1.9 (*17*). Whole-genome phylogenetic analysis was performed with ParSNP in the Harvest suite, designed for single-nucleotide polymorphism analysis between closely related species or strains ($\geq$97% average nucleotide identity) (*18*). The program uses FastTree 2 (*19*) to build approximately maximum-likelihood trees from core-genome single-nucleotide polymorphisms. Trees were visualized in FigTree 1.4.4 (http://tree.bio.ed.ac.uk/software/figtree). Principal component analysis was performed by feeding VCF files extracted from ParSNP alignments to ggfortify package in R software version 3.6.1 (https://cran.r-project.org/web/packages/ ggfortify/index.html).

### Statistical Analysis

Statistical significance of tetracycline susceptibility data was determined by $\chi^2$ test and Student t-test. All tests were conducted using Prism software version 8 (https://www.graphpad.com).

## Results

The 30 macrolide-resistant *R. equi* genome sequences determined in this study were subjected to phylogenetic analysis alongside a sample of 18 susceptible isolates from the same period and geographic origins to examine their relationships. The macrolide-resistant isolates had previously tested positive to *erm*(46) by PCR and most (n = 22, 73%) were also resistant to rifampin (MR$^R$ phenotype). Of note, 8 of the 2012–2017 *R. equi* isolates examined here were macrolide-only–resistant (Appendix Table 1); to date, dual MR$^R$ resistance had been invariably observed (*10*,*11*,*13*,*15*). We also included in our analysis Illumina whole-genome assemblies from 22 equine isolates characterized in our earlier study (n = 16 belonging to the 2287 clone, n = 6 control susceptible isolates) and 23 macrolide-susceptible strains representative of the global genomic diversity of *R. equi* (*20*). Figure 1 shows the core-genome phylogeny of the 93 *R. equi* strains.

### Clonal Spread of MDR *R. equi* 2287

Of 22 in total, 20 (91%) of the new MR$^R$ isolates clustered together at short genetic distances with the previously characterized MDR 2287 isolates, indicating

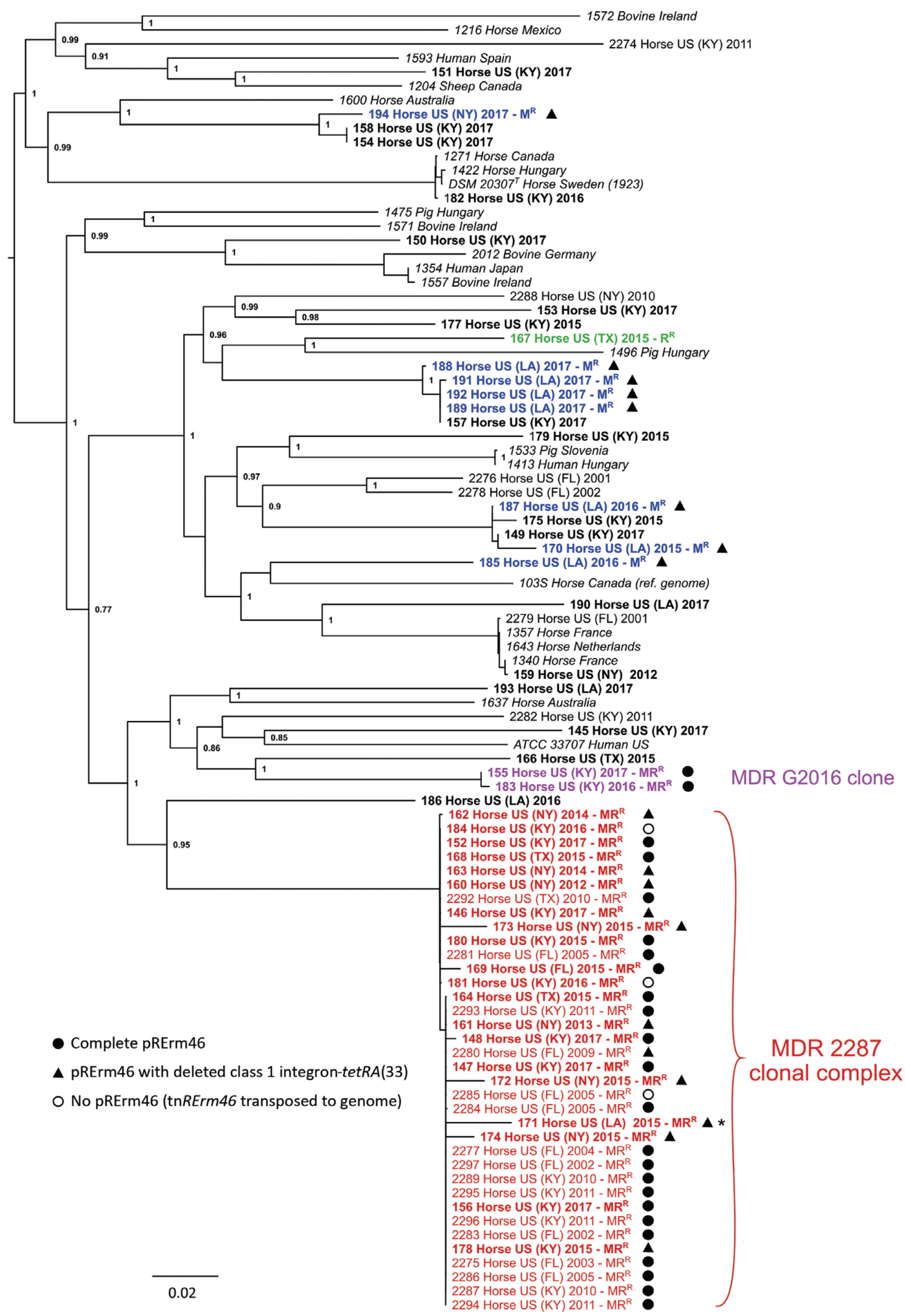


**Figure 1.** Spread and phylogenetic relationships of MDR *Rhodococcus equi*, United States. Phylogenetic tree of 93 *R. equi* isolates based on core-genome single-nucleotide polymorphism analysis by using ParSNP (*18*). The genomes analyzed are from 58 *erm*(46)-positive $M^R$ isolates, 24 control-susceptible isolates from same period and geographic origins, and 23 isolates representative of the genomic diversity of *R. equi*, including the reference genome 103S (*33*) and the type strain DSM 20307$^T$ (Appendix Table 1, https://wwwnc.cdc.gov/EID/article/27/2/20-3030-App1.pdf). Tip labels show year of collection and resistance phenotype for the 2001–2017 equine clinical isolates analyzed (the 50 genomes determined in this study are shown in bold, and other genomes are from previous study [*15*]). Red indicates MDR 2287 clonal complex, violet indicates novel MDR G2016 clone, blue indicates genetically diverse $M^R$ isolates recovered from a farm in Louisiana during 2015–2017 (MDR 2287 isolate from which they likely acquired the pRErm46 plasmid is indicated by an asterisk), and green indicates an $R^R$ isolate (*rpoB* S531K mutation). pRErm46 carriage status is indicated by symbols. Tree graph constructed with FigTree (http://tree.bio.ed.ac.uk/software/figtree). MDR, multidrug-resistant; $M^R$, macrolide-resistant; $MR^R$, dual macrolide/rifampin resistant; $R^R$, rifampin-resistant.

they correspond to the same clonal population (Figure 1). Accordingly, all of the newly sequenced $MR^R$ strains possessed the *rpoB*$^{S531F}$ mutation unique to the 2287 clone. Of those, 2 had lost the pRErm46 plasmid and only carried the Tn*RErm46* transposon (Figure 1), as previously observed in 1 of the 18 isolates from the 2002–2011 series (*15*). Collection times and locations encompassed the entire 2012–2017 period and the 5 US states for the MDR 2287 clonal population. The lack of spatial-temporal circumscription of MDR 2287 in the analyzed sample is illustrated by a principal components analysis in which the only grouping factor for the 93 *R. equi* isolates included in this study is the genetic background of the 2287 clone (Figure 2).

We repeated the phylogenomic analysis with the 36 *R. equi* 2287 sequences from 2002–2017 to assess the microevolution of the clone. This analysis

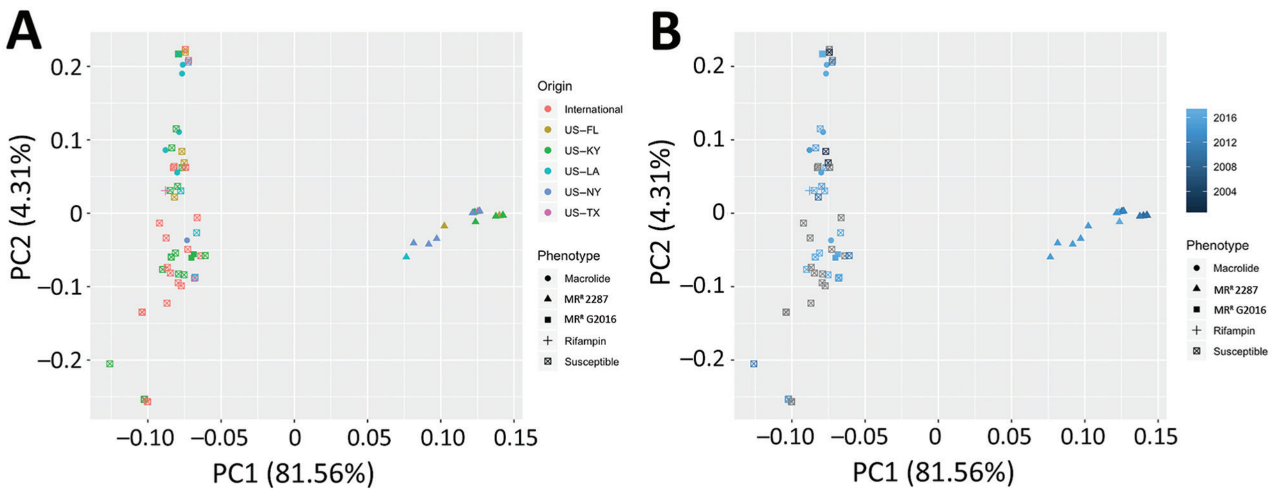


**Figure 2.** Lack of spatial-temporal circumscription of multidrug-resistant *Rhodococcus equi* clone 2287, United States. Principal component analysis plot was constructed on the basis of the single-nucleotide polymorphism variant calls obtained in the phylogenetic analysis. Isolates are identified by resistance group and color-coded by geographic origin (A) or year of isolation (B). $MR^R$, dual macrolide/rifampin resistant; PC1, principal component 1; PC2, principal component 2.

revealed that MDR 2287 had diversified into 3 major radiations (Figure 3), consistent with the clonal structure of *R. equi* evolution (*20*). Of note, 1 of these subclades gathered 11 of the 16 older isolates from 2002–2011, all originating from Florida or Kentucky. The remaining 5 older isolates were distributed in the 2 other subclades in which strains were grouped independently of year of collection or geographic origin. This distribution suggests a pattern of spread defined by the diversification of MDR 2287 into subclonal lineages and increasing exchange between horse farms of a progressively diverse clonal population.

### Dissemination of pERm46 and Emergence of Novel MDR *R. equi* Clone

Ten macrolide-resistant isolates also carried pERm46 but did not belong to the MDR 2287 clone and were genetically diverse. Most appeared as singletons interspersed among the different lines of descent in the *R. equi* tree (Figure 1). In this group, 8 strains corresponded to the previously mentioned macrolide-only–resistant isolates (i.e., rifampin susceptible, no *rpoB* mutation; MIC <0.125–1.25 µg/mL). All but 1 of these isolates originated from the same farm in Louisiana in which an MDR 2287 isolate (no. 171) was recovered during the same period. This circumstance suggests a scenario in which the entry of MDR 2287 into this farm resulted in the conjugal spread of pERm46 to different members of the heterogeneous *R. equi* populations that are typically found colonizing horse-breeding environments, or even individual animals within the same farm (*21*,*22*).

Of interest, 2 of the non-2287 macrolide-resistant isolates, numbers 155 (recovered in Kentucky in 2017) and 183 (recovered in Kentucky in 2016), were also resistant to rifampin (MIC>32 µg/mL) (Figure 1). These 2 nearly genomically identical $MR^R$ strains carried the pERm46 plasmid and a chromosomal *rpoB* mutation, Ser531Tyr (*Escherichia coli* numbering), distinct from that in MDR 2287 and novel in *R. equi*. Both $MR^R$ isolates constitute a new emerging MDR *R. equi* clone, first detected in 2016, which we designated G2016.

Collectively, these data indicate that the pERm46 macrolide-resistance plasmid, until now unique to the 2287 clone, has recently undergone horizontal transfer events to multiple *R. equi* genotypes. These transfers gave rise to novel MDR clones when associated with an *rpoB* mutation.

### pERm46 Variability and Tetracycline Resistance

pERm46 also harbors a class 1 integron (C1I) with a *tetR-tetA* cassette encoding a putative tetracycline efflux pump homologous to TetA(33) from the corynebacterial plasmid pTET3 (*15*,*23*). TetA efflux pumps are often carried by transposons and are one of the most prevalent tetracycline-resistance mechanisms (*24*). Both the C1I and *tetRA* determinant from pERm46 are virtually identical to those from pTET3, including flanking IS*6100* insertion sequences (*15*). Blast alignments revealed that the C1I-*tetRA*(33) region was deleted in 17 of the 43 (40%) pERm46 plasmids (Figures 1, 3), presumably because of recombination between the duplicated IS*6100*s (Figure 4). Similar rearrangements have been reported in other integrons carrying directly repeated IS*6100* copies (*25*,*26*). Confirming the predicted functionality of pRErm46's *tetRA*(33) determinant, pRErm46-positive isolates were resistant to tetracycline, in contrast to those carrying the ΔC1I-*tetRA*(33) form of the resistance plasmid (Table). However, all *R. equi* isolates were susceptible to the semisynthetic tetracycline derivative doxycycline, regardless of pRErm46 plasmid carriage (Table). This finding is consistent with previous data on *Corynebacterium glutamicum* showing that TetA(33) does not confer substantial cross-resistance to doxycycline (*23*).

Whereas a ΔC1I-*tetRA*(33) plasmid deletion was detected in only 1 of the older (2002–2011) MDR 2287 isolates, the deletion was found in 10 of the 18 pRErm46-positive clonal isolates recovered during 2012–2017 (Figure 1). Deleted pRErm46s are observed in each of the clonal radiations of the MDR 2287 population and coexist with complete plasmids in more basal branches (Figure 3), indicating increasing occurrence because of repeated independent deletion events. The deletion was detected in all of the genetically heterogeneous macrolide-only–resistant *R. equi* isolates and the MDR 2287 (isolate no. 171) recovered from the Louisiana farm during the same period. This finding supports the notion that the latter was the source from which pRErm46 had spread to other locally prevalent *R. equi* genotypes in that particular farm.

## Discussion

This study demonstrates that the increasing prevalence of MR[R] *R. equi* since its emergence in the late 1990s–early 2000s in equine farms in the United States (*11*–*14*) is primarily caused by the spread of the recently identified MDR 2287 clone (*15*). The oldest characterized MDR 2287 isolate dates from 2002 and was recovered in Kentucky (*15*) (Figure 1), where the clone likely emerged after the implementation of mass macrolide/rifampin antibiotic prophylaxis in foals (*10*). Since then, *R. equi* MDR 2287 has been frequently transferred between geographically distant farms, presumably through carrier horses. Active exchange of *R. equi* populations, previously noted in our earlier study (*20*), is evident in the United States

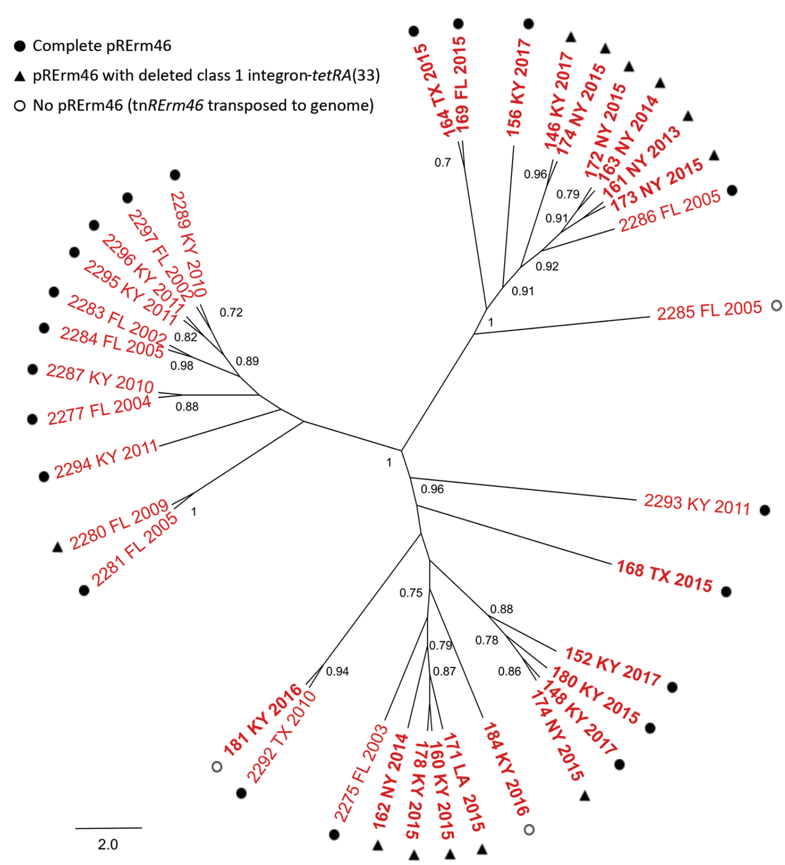


**Figure 3.** Phylogenetic population structure of multidrug-resistant *Rhodococcus equi* clonal complex 2287, United States. ParSNP core-genome tree of multidrug-resistant 2287 isolates shown in Figure 1. Nodes indicate bootstrap support for 1,000 replicates (values >0.7 shown). Tip labels indicate strain name, source (US state), and year of isolation.

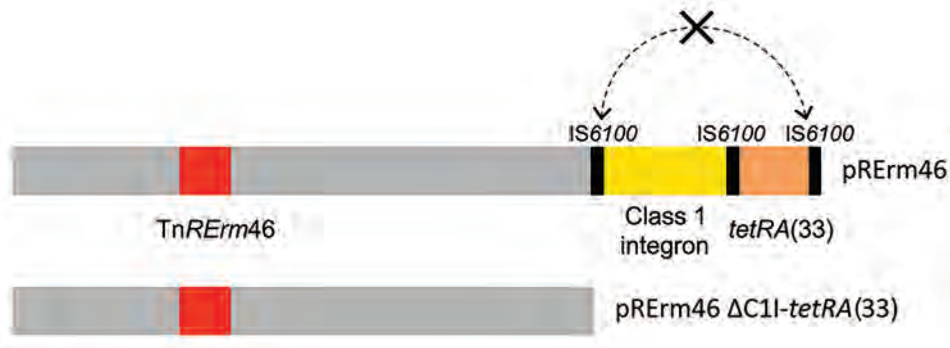


**Figure 4.** Schematic of ΔC1I-*tetRA*(33) deletion in *Rhodococcus equi* pRErm46 macrolide resistance plasmid. Top bar shows full-size plasmid with the Tn*RErm46* transposon carrying the macrolide-resistance *erm*(46) gene (in red, represented at nt position 32,567 [pRErm46 (PAM 2287) coordinates] common to all pRErm46 plasmids; additional Tn*RErm46* copies generated by transposition from original insertion may be present) and class 1 integron (C1I, in yellow) with associated *tetRA*(33) tetracycline-resistance cassette (peach). Bottom bar shows pRErm46 plasmid with the ΔC1I-*tetRA*(33) deletion. The deletion likely occurs through double crossover between the directly repeated flanking IS6100 sequences (dotted double arrow). Álvarez-Narváez et al. (*15*) includes detailed descriptions of pRErm46 plasmid and Tn*RErm46* transposon.

and internationally when considering the phylogenetic tree in Figure 1. For example, the strains recovered from the Louisiana farm in this study are essentially identical to others found elsewhere in the United States. Also, terminal branches of the *R. equi* tree contain nearly identical equine isolates from different countries (e.g., the United States, France, and the Netherlands, or, in another case, Canada, Hungary, Sweden, and the United States) (Figure 1).

Despite the diversity of *R. equi* genotypes that typically circulate in farms (*21*,*22*), the highly horizontally transferable *erm*(46) (Tn*RErm46*) determinant remains largely confined to MDR 2287. This paradoxical clonal restriction is the probable consequence of the simultaneous requirement for *erm*(46) and the *rpoB* mutation under dual macrolide/rifampin pressure. More specifically, the clonal restriction is likely determined by the low odds of pRErm46/Tn*RErm46* and a high-resistance *rpoB* mutation (such as Ser531Phe in MDR 2287 or Ser531Tyr in MDR G2016) being acquired concurrently, and the latter effectively linking the mobile *erm*(46) determinant to a specific chromosomal background (*15*).

This interpretation implies several predictions. First, under dual macrolide/rifampin pressure, spread of an existing $MR^R$ strain through horse movements is more likely to contribute to the bulk of resistance than the generation of new $MR^R$ strains (*15*). Second, continued macrolide/rifampin therapy might eventually lead to the emergence of new $MR^R$ clones, such as G2016 identified in this study, detected in 2016 in Kentucky and characterized by a novel *rpoB*$^{S531Y}$ mutation. Third, and importantly, if dual macrolide/rifampin selection ceases, unrestricted pRErm46/Tn*RErm46* horizontal transfer to other *R. equi* strains might occur. Our data appear to support these 3 possibilities.

The first and second scenarios are expected in horse-breeding areas such as Kentucky, Texas, or Florida, where *R. equi* is endemic and macrolide/rifampin antibiotic prophylaxis has been commonly practiced (*10*,*27*,*28*). Less intensive and more targeted antibiotic therapy is more likely in areas with smaller horse populations such as Louisiana (*29*), where pRErm46 spillover outside the MDR 2287 clone was detected (the third scenario). We hypothesize that a less intensive antibiotic

**Table.** Effect of absence of *tetRA*(33) determinant from pRErm46 plasmid on *R. equi* susceptibility to tetracycline and doxycycline, determined on macrolide-resistant isolates collected during 2012–2017*

| | pRErm46 | | pRErm46 ΔC1I-*tetRA*(33) | |
|---|---|---|---|---|
| Antibiotic | Phenotype† | MIC, µg/mL‡ | Phenotype | MIC, µg/mL |
| Tetracycline | Resistant (100)§ | 21.33 (8–48)¶ | Susceptible (100)§ | 1.97 (0.38–3)¶ |
| Doxycycline | Susceptible (100) | 3.35 (0.75–6)** | Susceptible (100) | 1.06 (0.25–3)** |

*Susceptibility data to other relevant antimicrobials are shown in Appendix Table 2 (https://wwwnc.cdc.gov/EID/article/27/2/20-3030-App1.pdf).
†Determined by disk diffusion technique. Isolate percentage shown in parenthesis. Zone diameter susceptibility breakpoints based on Clinical and Laboratory Standards Institute interpretive criteria for *Staphylococcus aureus*, routinely used for *R. equi* susceptibility testing in the absence of specific approved criteria for this species (*11*,*16*).
‡Minimal inhibitory concentration determined using Etest strips. Mean value (range in parenthesis).
§p<0.001 by $\chi^2$ test.
¶p<0.001 by t-test.
**p<0.001 by t-test. Presence of TetRA(33) appears to induce a small, statistically significant MIC increase, but MIC remains below the Clinical and Laboratory Standards Institute susceptibility breakpoint for doxycycline (susceptible ≤4 µg/mL, intermediate 8 µg/mL, resistant ≥16 µg/mL).

pressure, perhaps involving macrolide monotherapy or a macrolide in combination with non-rifampin antibiotic drugs, disrupted the linkage between *erm*(46) and *rpoB*$^{S531F}$ in the MDR 2287 strain found in the Louisiana farm, enabling the transfer of the plasmid to other locally prevalent *R. equi* strains (Figure 1).

Our analyses show that MDR 2287 has diversified since its first documented isolation into a clonal complex with several radiations (Figure 3). We also detected signs of microevolution in pRErm46, with a substantial rate of deletion of the C1I-*tetRA*(33) region in the 2012–2017 macrolide-resistant *R. equi* cohort, resulting in loss of tetracycline resistance. The clinical significance of this finding is unclear because tetracyclines are not used to treat *R. equi* infections in foals. An exception is doxycycline, which, because of its higher oral bioavailability in foals, greater tissue penetration, and better activity against gram-positive bacteria, might be used in cases of macrolide intolerance (or resistance) (*2*,*8*,*30*). However, our data indicate that the pRErm46-encoded TetA33 does not confer clinically relevant cross-resistance to this semisynthetic tetracycline derivative. Genetic dispensability due to lack of antibiotic selection or fitness advantage might therefore be the likely reason for the increasing occurrence of ΔC1I-*tetRA*(33) pRErm46 plasmids in the macrolide-resistant *R. equi* population.

MDR *R. equi* shows resistance to several clinically relevant antibiotic drugs, including macrolides, lincosamides; streptogramins, and, in a substantial proportion, also tetracycline, all conferred by the pRErm46 conjugative plasmid; and rifampin conferred by a chromosomal *rpoB*$^{S531F/Y}$ mutation. MDR *R. equi* also demonstrates intrinsic resistance to chloramphenicol (Appendix Table 2), which is often observed in *R. equi*. All of these antibiotic drugs are listed as critically or highly important for human medicine by the World Health Organization (*31*). Around 9% of human *R. equi* infections are caused by equine-derived (pVAPA-positive) strains, and about half of human cases are caused by porcine-derived (pVAPB-positive) isolates (*5*), which recent in vitro data demonstrate can also acquire pRErm46 (*32*). Therefore, in addition to compromising the therapeutic management of equine *R. equi* infection, these isolates represent a potential hazard to human health because of the risk of zoonotic transmission (or horizontal spread of the pRErm46 resistance plasmid to other pathogens, either directly or through environmental microbiota [*32*]).

Although our study is not systematic and therefore probably underestimates the extent of MDR *R. equi* spread, our results provide valuable insight into the determinants underlying its emergence and dissemination. The data suggest a pattern of MDR *R. equi* spread and evolution directly determined by antibiotic pressure in equine farms. The stable therapeutic regimen applied over years for *R. equi* facilitates a unique understanding of the factors affecting the generation and evolution of MDR clones, and specifically how combination therapy might help in limiting the horizontal transfer of resistance. Although MDR *R. equi* is, to our knowledge, still limited to the equine population in the United States, our data predict a scenario of international spread through horse movements, indicating the need for interventions to control its dissemination and potential zoonotic transmission.

### Acknowledgments

We thank L. Berghaus and A. Hanafi for technical support, L. Huber for help with the R commands, and G. Okem for preliminary experiments as part of a summer project.

This work was supported by grants from the Morris Animal Foundation (project no. D18EQ-401), the Hodgson Chair of Equine Research endowment of University of Georgia, the Link Equine Research Endowment at Texas A&M University, and Horserace Betting Levy Board, UK (project no. prj796 to JV-B).

S.A.-N., S.G., N.C. and J.V.-B. designed the study. S.A.-N. performed the research. N.S. and N.C. collected isolates and susceptibility data. S.A.-N. and J.V.-B. analyzed and interpreted the data. J.V.-B. conceptualized the findings. S.A.-N. and J.V-.B. wrote the article.

New *R. equi* genome assemblies were deposited in GenBank under the accession numbers indicated in Appendix Table 1.

## About the Author

Dr. Álvarez-Narváez is a clinical assistant professor at the University of Georgia. Her primary research interests include antimicrobial resistance mechanisms and host-pathogen interactions at the molecular level.

### References

1. Prescott JF. *Rhodococcus equi*: an animal and human pathogen. Clin Microbiol Rev. 1991;4:20–34. https://doi.org/10.1128/CMR.4.1.20
2. Vázquez-Boland JA, Giguère S, Hapeshi A, MacArthur I, Anastasi E, Valero-Rello A. *Rhodococcus equi*: the many facets of a pathogenic actinomycete. Vet Microbiol. 2013;167:9–33. https://doi.org/10.1016/j.vetmic.2013.06.016

3. Yamshchikov AV, Schuetz A, Lyon GM. *Rhodococcus equi* infection. Lancet Infect Dis. 2010;10:350–9. https://doi.org/10.1016/S1473-3099(10)70068-2
4. MacArthur I, Anastasi E, Alvarez S, Scortti M, Vázquez-Boland JA. Comparative genomics of *Rhodococcus equi* virulence plasmids indicates host-driven evolution of the *vap* pathogenicity island. Genome Biol Evol. 2017;9:1241–7. https://doi.org/10.1093/gbe/evx057
5. Ocampo-Sosa AA, Lewis DA, Navas J, Quigley F, Callejo R, Scortti M, et al. Molecular epidemiology of *Rhodococcus equi* based on *traA, vapA*, and *vapB* virulence plasmid markers. J Infect Dis. 2007;196:763–9. https://doi.org/10.1086/519688
6. Vázquez-Boland JA, Meijer WG. The pathogenic actinobacterium *Rhodococcus equi*: what's in a name? Mol Microbiol. 2019;112:1–15. https://doi.org/10.1111/mmi.14267
7. Muscatello G, Leadon DP, Klayt M, Ocampo-Sosa A, Lewis DA, Fogarty U, et al. *Rhodococcus equi* infection in foals: the science of 'rattles'. Equine Vet J. 2007;39:470–8. https://doi.org/10.2746/042516407X209217
8. Giguère S. Treatment of infections caused by *Rhodococcus equi*. Vet Clin North Am Equine Pract. 2017;33:67–85. https://doi.org/10.1016/j.cveq.2016.11.002
9. Giguère S, Cohen ND, Chaffin MK, Slovis NM, Hondalus MK, Hines SA, et al. Diagnosis, treatment, control, and prevention of infections caused by *Rhodococcus equi* in foals. J Vet Intern Med. 2011;25:1209–20. https://doi.org/10.1111/j.1939-1676.2011.00835.x
10. Burton AJ, Giguère S, Sturgill TL, Berghaus LJ, Slovis NM, Whitman JL, et al. Macrolide- and rifampin-resistant *Rhodococcus equi* on a horse breeding farm, Kentucky, USA. Emerg Infect Dis. 2013;19:282–5. https://doi.org/10.3201/eid1902.121210
11. Giguère S, Lee E, Williams E, Cohen ND, Chaffin MK, Halbert N, et al. Determination of the prevalence of antimicrobial resistance to macrolide antimicrobials or rifampin in *Rhodococcus equi* isolates and treatment outcome in foals infected with antimicrobial-resistant isolates of *R equi*. J Am Vet Med Assoc. 2010;237:74–81. https://doi.org/10.2460/javma.237.1.74
12. Huber L, Giguère S, Slovis NM, Carter CN, Barr BS, Cohen ND, et al. Emergence of resistance to macrolides and rifampin in clinical isolates of *Rhodococcus equi* from foals in central Kentucky, 1995 to 2017. Antimicrob Agents Chemother. 2018;63:e01714-18. https://doi.org/10.1128/AAC.01714-18
13. Anastasi E, Giguère S, Berghaus LJ, Hondalus MK, Willingham-Lane JM, MacArthur I, et al. Novel transferable *erm*(46) determinant responsible for emerging macrolide resistance in *Rhodococcus equi*. J Antimicrob Chemother. 2015;70:3184–90.
14. Erol E, Locke S, Saied A, Cruz Penn MJ, Smith J, Fortner J, et al. Antimicrobial susceptibility patterns of *Rhodococcus equi* from necropsied foals with rhodococcosis. Vet Microbiol. 2020;242:108568. https://doi.org/10.1016/j.vetmic.2019.108568
15. Álvarez-Narváez S, Giguère S, Anastasi E, Hearn J, Scortti M, Vázquez-Boland JA. Clonal confinement of a highly mobile resistance element driven by combination therapy in *Rhodococcus equi*. MBio. 2019;10:e02260–19. https://doi.org/10.1128/mBio.02260-19
16. Berghaus LJ, Giguère S, Guldbech K, Warner E, Ugorji U, Berghaus RD. Comparison of Etest, disk diffusion, and broth macrodilution for in vitro susceptibility testing of *Rhodococcus equi*. J Clin Microbiol. 2015;53:314–8. https://doi.org/10.1128/JCM.02673-14
17. Koren S, Walenz BP, Berlin K, Miller JR, Bergman NH, Phillippy AM. Canu: scalable and accurate long-read assembly via adaptive *k*-mer weighting and repeat separation. Genome Res. 2017;27:722–36. https://doi.org/10.1101/gr.215087.116
18. Treangen TJ, Ondov BD, Koren S, Phillippy AM. The Harvest suite for rapid core-genome alignment and visualization of thousands of intraspecific microbial genomes. Genome Biol. 2014;15:524. https://doi.org/10.1186/s13059-014-0524-x
19. Price MN, Dehal PS, Arkin AP. FastTree 2—approximately maximum-likelihood trees for large alignments. PLoS One. 2010;5:e9490. https://doi.org/10.1371/journal.pone.0009490
20. Anastasi E, MacArthur I, Scortti M, Alvarez S, Giguère S, Vázquez-Boland JA. Pangenome and phylogenomic analysis of the pathogenic actinobacterium *Rhodococcus equi*. Genome Biol Evol. 2016;8:3140–8. https://doi.org/10.1093/gbe/evw222
21. Cohen ND, Smith KE, Ficht TA, Takai S, Libal MC, West BR, et al. Epidemiologic study of results of pulsed-field gel electrophoresis of isolates of *Rhodococcus equi* obtained from horses and horse farms. Am J Vet Res. 2003;64:153–61. https://doi.org/10.2460/ajvr.2003.64.153
22. Morton AC, Begg AP, Anderson GA, Takai S, Lämmler C, Browning GF. Epidemiology of *Rhodococcus equi* strains on Thoroughbred horse farms. Appl Environ Microbiol. 2001;67:2167–75. https://doi.org/10.1128/AEM.67.5.2167-2175.2001
23. Tauch A, Götker S, Pühler A, Kalinowski J, Thierbach G. The 27.8-kb R-plasmid pTET3 from *Corynebacterium glutamicum* encodes the aminoglycoside adenyltransferase gene cassette *aadA9* and the regulated tetracycline efflux system Tet 33 flanked by active copies of the widespread insertion sequence IS6100. Plasmid. 2002;48:117–29. https://doi.org/10.1016/S0147-619X(02)00120-8
24. Chopra I, Roberts M. Tetracycline antibiotics: mode of action, applications, molecular biology, and epidemiology of bacterial resistance. Microbiol Mol Biol Rev. 2001;65:232–60. https://doi.org/10.1128/MMBR.65.2.232-260.2001
25. Targant H, Doublet B, Aarestrup FM, Cloeckaert A, Madec JY. IS6100-mediated genetic rearrangement within the complex class 1 integron In104 of the *Salmonella* genomic island 1. J Antimicrob Chemother. 2010;65:1543–5. https://doi.org/10.1093/jac/dkq163
26. Partridge SR, Recchia GD, Stokes HW, Hall RM. Family of class 1 integrons related to In4 from Tn1696. Antimicrob Agents Chemother. 2001;45:3014–20. https://doi.org/10.1128/AAC.45.11.3014-3020.2001
27. Huber L, Giguère S, Cohen ND, Slovis NM, Hanafi A, Schuckert A, et al. Prevalence and risk factors associated with emergence of *Rhodococcus equi* resistance to macrolides and rifampicin in horse-breeding farms in Kentucky, USA. Vet Microbiol. 2019;235:243–7. https://doi.org/10.1016/j.vetmic.2019.07.010
28. Álvarez-Narváez S, Berghaus LJ, Morris ERA, Willingham-Lane JM, Slovis NM, Giguere S, et al. A common practice of widespread antimicrobial use in horse production promotes multi-drug resistance. Sci Rep. 2020;10:911. https://doi.org/10.1038/s41598-020-57479-9
29. Kilby ER. The demographics of the US equine population. In: Salem DJ, Rowan AN, editors. The state of the animals. Washington (DC): Human Society Press; 2007. p. 175–205.
30. Womble A, Giguère S, Lee EA. Pharmacokinetics of oral doxycycline and concentrations in body fluids and bronchoalveolar cells of foals. J Vet Pharmacol Ther. 2007;30:187–93. https://doi.org/10.1111/j.1365-2885.2007.00857.x

31. Collignon PJ, Conly JM, Andremont A, McEwen SA, Aidara-Kane A, Agerso Y, et al.; World Health Organization Advisory Group, Bogotá Meeting on Integrated Surveillance of Antimicrobial Resistance. World Health Organization ranking of antimicrobials according to their importance in human medicine: a critical step for developing risk management strategies to control antimicrobial resistance from food animal production. Clin Infect Dis. 2016;63:1087–93. https://doi.org/10.1093/cid/ciw475
32. Álvarez-Narváez S, Giguère S, Berghaus LJ, Dailey C, Vázquez-Boland JA. Horizontal spread of *Rhodococcus equi* macrolide resistance plasmid pRErm46 across environmental *Actinobacteria*. Appl Environ Microbiol. 2020;86:e00108–20. https://doi.org/10.1128/AEM.00108-20
33. Letek M, González P, Macarthur I, Rodríguez H, Freeman TC, Valero-Rello A, et al. The genome of a pathogenic *Rhodococcus*: cooptive virulence underpinned by key gene acquisitions. PLoS Genet. 2010;6:e1001145. https://doi.org/10.1371/journal.pgen.1001145


Address for correspondence: Sonsiray Álvarez-Narváez, College of Veterinary Medicine, Department of Large Animal Medicine, 2200 College Station Rd, Athens, GA 30602, USA; email: Sonsiray.Alvarez@uga.edu; or José A. Vázquez-Boland, Microbial Pathogenesis Laboratory, Edinburgh Medical School (Biomedical Sciences-Infection Medicine), Edinburgh BioQuater, Chancellor's Building, Edinburgh EH16 4SB, Scotland, UK; email: v.boland@ed.ac.uk

# Emergence of Lyme Disease on Treeless Islands, Scotland, United Kingdom

Caroline Millins, Walter Leo, Isabell MacInnes, Johanne Ferguson, Graham Charlesworth, Donald Nayar, Reece Davison, Jonathan Yardley, Elizabeth Kilbride, Selene Huntley, Lucy Gilbert, Mafalda Viana, Paul Johnson, Roman Biek

Lyme disease is usually associated with forested habitats but has recently emerged on treeless islands in the Western Isles of Scotland. The environmental and human components of Lyme disease risk in open habitats remain unknown. We quantified the environmental hazard and risk factors for human tick bite exposure among treeless islands with low and high Lyme disease incidence in the Western Isles. We found a higher prevalence of *Borrelia burgdorferi* sensu lato–infected ticks on high-incidence than on low-incidence islands (6.4% vs. 0.7%); we also found that residents of high-incidence islands reported increased tick bite exposure. Most tick bites (72.7%) occurred ≤1 km from the home, including many in home gardens. Residents of high Lyme disease incidence islands reported increasing problems with ticks; many suggested changing deer distribution as a potential driver. We highlight the benefits of an integrated approach in understanding the factors that contribute to Lyme disease emergence.

To optimize public health responses to vectorborne disease emergence, knowledge of the factors affecting the density of infected vectors in different habitats, human interactions with the environment that lead to vector exposure, and how these factors affect disease incidence are essential. Lyme disease, caused by infection with the bacterium *Borrelia burgdorferi*, is the most commonly reported vectorborne zoonotic disease in Europe and North America (*1*,*2*). Higher densities of infected tick vectors (i.e., environmental hazard) and Lyme disease incidence are associated with wooded habitats (*3*–*5*). However, the recent emergence of Lyme disease on treeless islands in Scotland (*6*), United Kingdom, has challenged the current understanding of the relationship between habitat and Lyme disease.

Author affiliations: University of Liverpool, Liverpool, UK (C. Millins); University of Glasgow, Glasgow, Scotland, UK (C. Millins, W. Leo, D. Nayar, R. Davison, J. Yardley, L. Gilbert, M. Viana, P. Johnson, E. Kilbride, R. Biek); National Health Service Western Isles, Benbecula, Scotland, UK (I. MacInnes); Scottish Natural Heritage, South Uist, Scotland, UK (J. Ferguson); Southern Isles Veterinary Practice, Benbecula (G. Charlesworth); Heb Insights, North Uist, Scotland, UK (S. Huntley)

DOI: https://doi.org/10.3201/eid2702.203862

Lyme disease is an emerging zoonosis in the United Kingdom; the highest incidence is in the Highland region of Scotland (*7*,*8*). In the United Kingdom, Lyme disease surveillance is based on laboratory confirmed cases, following the best practice guidelines for serologic diagnosis published by the National Institute for Health and Care Excellence (*9*–*11*). This surveillance shows that some islands in the Highland region that lack woodland coverage have a Lyme disease incidence ≈40 times the national average (119 vs. 3.2 cases/100,000 persons per year) (*6*). These islands have had a higher Lyme disease incidence since at least 2010; other nearby, ecologically similar islands have a much lower incidence of 8.3 cases/100,000 persons (*6*). These islands also have a higher incidence of Lyme disease diagnoses made on the basis of an erythema migrans rash (*6*,*11*). Knowledge of the factors affecting the density of infected ticks in the environment, how persons interact with the environment and are exposed to tick bites, and possible drivers of emergence is urgently needed to examine, predict, and mitigate Lyme disease emergence in treeless habitats.

Evidence suggests that Lyme disease hazard (measured as the density of infected ticks) is lower in treeless habitats than in wooded areas; however, much about this relationship remains unknown (*12*–*18*). Many experts consider woodlands to be the optimal habitat for the Ixodid tick vector because of the humid microclimate, which improves off-host tick survival and the density of potential hosts for blood meals (*12*,*13*). Some studies have found lower tick densities in grassland than in nearby woodland habitats, prompting researchers to theorize that grassland might act as a sink for tick populations (*14*–*16*). Furthermore, many studies have found the density of the *Ixodes ricinus* tick, the main vector of Lyme disease in Europe, to be much lower in treeless habitats than woodlands (*17*). For example, surveys of open habitats in northern Spain found no questing *I. ricinus* ticks (*18*). In the United Kingdom, most studies have found relatively low tick densities in meadows (*19*), open hillside (*20*,*21*), and heather moorland (*22*,*23*).

The environmental hazard is linked to Lyme disease incidence through human interactions with the environment and exposure to infected tick bites (*24*). For example, a person's activities, knowledge of and attitude toward tickborne disease, and preventative behaviors will affect that person's risk for tick bites (*24*,*25*). Analysis of where people are exposed to tick bites and risk factors for tick bite exposure can be used to guide preventive public health interventions (*26*).

In the absence of longitudinal environmental data in treeless areas, alternative approaches are needed to assess trends in tick population abundance and distribution. Tick populations in treeless habitats are affected by many of the same environmental drivers as those in forested areas, such as changes in climate, land management, and host density, especially deer populations (*27*–*30*). Surveys of local communities can provide information on whether the tick hazard is perceived to have changed over time. Responses might also suggest environmental factors associated with these changes (*31*).

To identify possible causes of Lyme disease emergence in treeless habitats, we assessed factors influencing tick density and prevalence of *B. burgdorferi*–infected ticks; geographic, demographic, and behavioral factors associated with human tick bite exposure; and community recollections of tick distribution and numbers over time. We used treeless islands with high and low Lyme disease incidence in the Western Isles in Scotland, United Kingdom, as our study system.

## Methods

### Study Location and Site Selection

We classified each island as having a low or high Lyme disease incidence based on Lyme disease surveillance data (*6*). We compared the environmental hazard between 26 sites on islands with high Lyme disease incidence (North Uist, South Uist, and Benbecula) and 16 sites on islands with low incidence (Harris and Barra). We selected sites belonging to 2 dominant habitat types: improved grassland (mesotrophic grasslands, often used for livestock grazing) and heather moorland (a mixture of wet heathland and western blanket bog) (*32*). We used a spatially stratified sampling design and the random selection tool in QGIS (QGIS Development Team, https://www.qgis.org) to select sites (Figure 1). The vertebrate community of the Western Isles includes large ungulates, such as wild red deer (*Cervus elaphus*), farmed sheep, and cattle, all of which can maintain *I. ricinus* tick populations. The islands also have several *B. burgdorferi* sensu lato transmission hosts, including brown rats (*Rattus norvegicus*), Eurasian pygmy shrews (*Sorex minutus*), wood mice (*Apodemus sylvaticus*), hedgehogs (*Erinaceus europaeus*), field voles (*Microtus agrestis*), and certain species of passerine birds (*33*).

On islands where Lyme disease incidence is high (high-incidence islands), we also selected sites belonging to 3 additional habitats. We chose 8 sites in machair and 13 sites in bog and peatland habitats using the same stratified sampling approach. Machair is a sandy grassland along ocean coastline often used for grazing or cultivation (*32*). We also chose 12 sites in gardens that were randomly selected within each sector (Appendix Figure 1, https://wwwnc.cdc.gov/EID/article/27/2/20-3862-App1.pdf). Sampling was carried out during the peak questing period for *I. ricinus* ticks. We conducted sampling during April 19–June 5, 2018. To strengthen the comparison of tick infection prevalence, we sampled additional sites in low Lyme disease incidence (low-incidence) areas during May 17–June 22, 2019.

### Tick Collection

To estimate the density of questing *I. ricinus* ticks, we sampled from 20 randomized 10 m transects at each site. Transects were 30–50 m apart, or 20–30 m apart in gardens. We measured vegetation height and density, temperature, and humidity at the starting point of each transect (*34*). We dragged a 1 $m^2$ white woolen blanket across the surface of the vegetation for 10 m. We collected questing nymphs on the blanket, counted them, and placed them in 100% ethanol. To increase the sample size, we carried out continuous blanket dragging for ≤2 person-hours at each site.

### Screening of *I. ricinus* Ticks for *B. burgdorferi* s.l. and Genospecies Identification

Our pilot study on South Uist in 2017 estimated that 6.6% of *I. ricinus* nymphs were infected with *B. burgdorferi*; we used this preliminary prevalence to estimate a target sample size of 50 nymphs/site (C. Millins, unpub. data). We used an ammonia hydroxide technique (*35*) to extract approximately 50 *I. ricinus* questing nymphs collected by blanket dragging

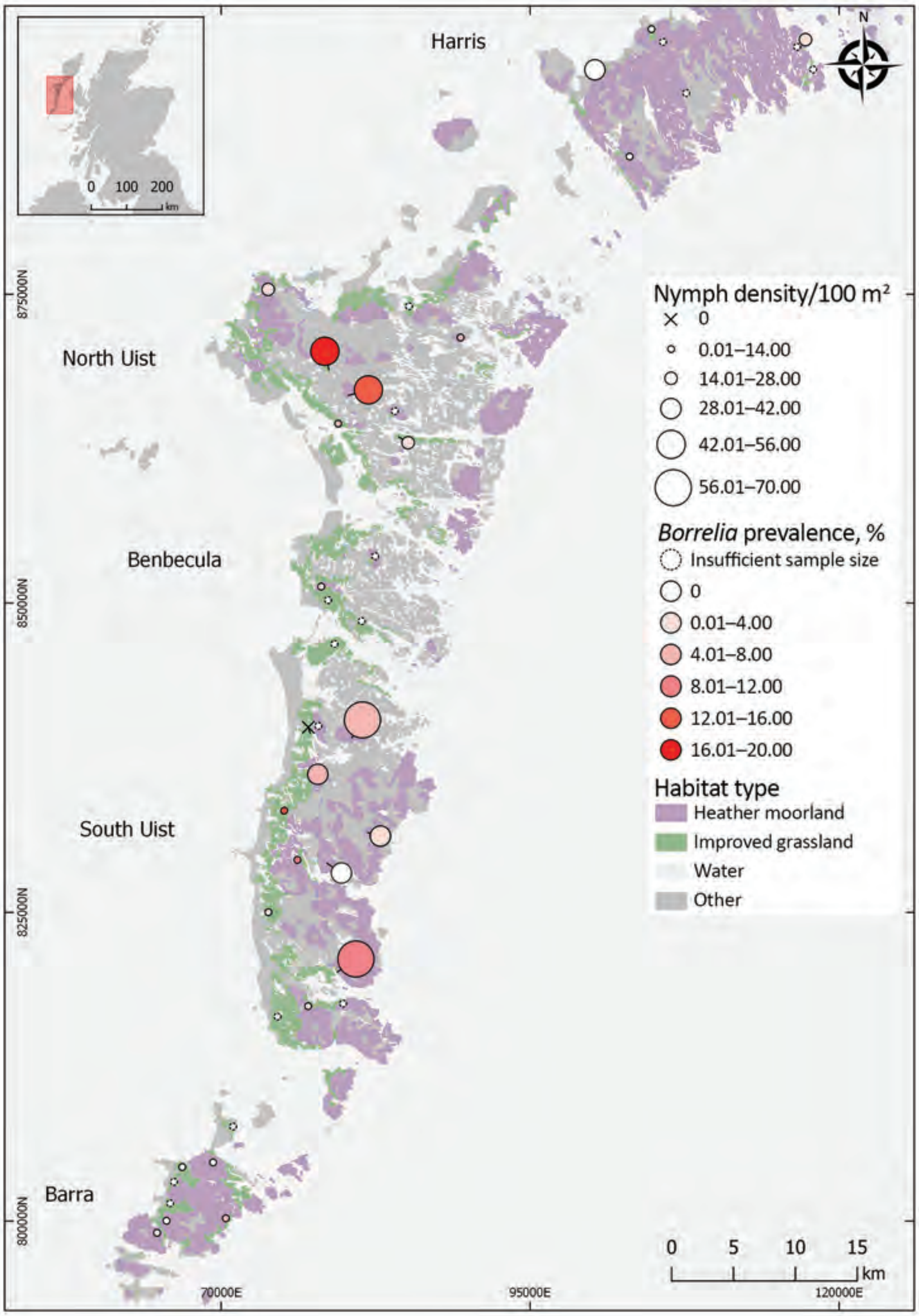


**Figure 1.** Tick collection sites for study on Lyme disease hazard, Western Isles, Scotland, UK, 2018–2019. Prevalence was not estimated at sites where <50 ticks were collected. Circle size indicates questing tick density. Circle color indicates *Borrelia burgdorferi* sensu lato prevalence. X indicates sites at which no ticks were detected.

at each site. We tested the ticks for *B. burgdorferi* s.l. infection using a nested PCR specific to the flagellin gene (*36*) with sequencing of the product to identify the genospecies.

### Geographic Locations of Human Tick Bite Exposure, Factors Associated with Tick Bite Risk, and Perceptions of Tick Problems Over Time

We invited residents to complete a questionnaire about tick bite exposure. We used the survey to collect data about differences in tick bite exposure between islands with high and low Lyme disease incidence, habitat types where tick bites occurred, the distance of tick bites from the home address, and social and behavioral factors associated with exposure to tick bites. Residents were asked if problems with ticks had changed over time. The survey was approved by the University of Glasgow College of Medical, Veterinary & Life Sciences Ethics Committee (reference no. 200170121). The survey was available online and in paper copy during April 18–October 31, 2018, and was publicized in local media and at community meetings.

### Statistical Analysis

We conducted statistical analyses and model selection in R version 4.0.0 (https://www.r-project.org) using the lme4 package for generalized linear mixed models (GLMMs) (*37*). We tested for correlations between explanatory variables using the variance inflation function in the car package (*38*). We tested each model for overdispersion. Starting from the maximum global model, we conducted stepwise model selection using likelihood-ratio tests (*39*).

Because Lyme disease incidence is reported at the island level (*6*), we assessed the relationship with the environmental hazard using a 2-step process. First, we investigated island as a predictor of nymph density, nymph infection prevalence, and the density of infected nymphs. Then, we made between-island comparisons from the best fit model using the Tukey test in the lsmeans package (*40*). We modeled nymph abundance (i.e., number of nymphs/10 m transect) from sites sampled in 2018 using a Poisson GLMM with a log link as a function of island, habitat type and wind (using the Beaufort wind force scale), vegetation density, temperature, and humidity with random effects of site and observation (*41*). We modeled the proportion of nymphs infected with *B. burgdorferi* s.l. from sites sampled in 2018 and 2019 using a binomial GLMM with a logit link as a function of island, habitat type, and mean nymph density with a random effect of site. We modeled the density of infected nymphs as the number of infected nymphs using a Poisson GLMM with a log link as a function of island and habitat, with an offset of the log estimated area to collect nymphs tested, using a random effect of site.

For high-incidence islands, where we had sampled additional habitat types, we used separate GLMM models to test for the effect of habitat and island on nymph density, nymph infection prevalence, and the density of infected nymphs. We did not include machair in the analyses because of the low number of nymphs detected.

We used survey responses to test for differences in human exposure to tick bites among islands with high and low Lyme disease incidence. We received 522 surveys from adult residents of the Western Isles, representing approximately 2% of the adult population. According to local census data, survey responses were broadly representative of island populations (Appendix). We modeled risk for tick bite exposure, classified as high ($\geq$5 tick bites/year) or low (<5 tick bites/year), using univariable analysis (Appendix Table 1) and then with a binomial GLM and a logit link as a function of island of residence, age, sex, frequency of outdoor activity, and pet ownership. Because awareness, attitudes and preventative behavior relating to tickborne disease could influence reported tick bite exposure, we tested for associations between risk for tick bite exposure and these explanatory variables in a separate model with an interaction of each variable with Lyme disease incidence.

Survey respondents commonly reported ticks in the home; we hypothesized that ticks could be transported indoors by clothing or pets and that this kind of exposure could vary among islands. To test this hypothesis, we used a binomial GLM and a logit link to model whether any tick (live and unfed, engorged, or dead) had ever been detected inside the home as a function of island, level of outdoor activity, and pet ownership.

We hypothesized that a higher proportion of respondents from high-incidence islands would report increasing tick numbers and associated problems than respondents from low Lyme disease incidence islands. We categorized free text responses as increased or not increased and used a binomial GLM with a logit link using Lyme disease incidence as an explanatory variable. We compared free text responses among residents of high- and low- incidence islands to assess factors associated with problems related to ticks. We used a corpus linguistic approach to extract common keywords and associated clusters of words for comparison (*42*; Appendix)

## Results

### Nymph Density

Nymph density did not vary significantly between islands with high and low Lyme disease incidence; island was not retained as an explanatory variable in the best fit model (Table 1; $\chi^2$ = 3.15; degree of freedom [df] = 4; p = 0.53) (Figure 2). In 2018, mean nymph density at improved grassland and heather moorland sites on low Lyme disease incidence islands was 1.36 nymphs/10 m$^2$ (SE = 0.28) compared to 1.60 nymphs/10 m$^2$ (SE = 0.25) on high-incidence islands (Figure 1; Appendix Table 2).

For sites sampled among different habitat types on high Lyme disease incidence islands (Appendix Figure 1), the best fit model to predict nymph density retained habitat type as a fixed effect ($\chi^2$ = 24.06; df = 4; p<0.01) (Figure 3; Appendix Table 3). We found significantly fewer nymphs in machair than in other

**Table 1.** Best-fit generalized linear mixed models of nymph density, *Borrelia burgdorferi* sensu lato prevalence, and density of infected nymphs among questing *Ixodes ricinus* ticks, Western Isles, Scotland, UK, 2018–2019

| Response variable | Explanatory variable | Estimate | SE | p value* |
|---|---|---|---|---|
| Nymph density | Intercept | –4.02 | 0.93 | |
| | Temperature, °C/10 | 2.11 | 0.64 | <0.01 |
| Nymph infection prevalence | Intercept | –2.94 | 0.30 | |
| | Island | | | <0.01 |
| | South Uist | Referent | | |
| | North Uist | 0.37 | 0.44 | |
| | Harris | –2.69 | 1.11 | |
| | Barra | –1.98 | 0.71 | |
| Density of infected nymphs | Intercept | –4.82 | 0.52 | |
| | Island | | | <0.01 |
| | South Uist | Referent | | |
| | North Uist | –0.07 | 0.79 | |
| | Harris | –2.96 | 1.45 | |
| | Barra | –4.07 | 1.15 | |

*p value determined from likelihood-ratio test of removing each variable from the best fit model.

habitat types (p<0.01 by Tukey post hoc analysis); we found no significant differences in nymph density between other habitat types.

### *B. burgdorferi* s.l. Nymph Infection Prevalence

We found that the prevalence of *B. burgdorferi* s.l. infection was significantly associated with island (Table 1; $\chi^2$ = 17.04; df = 3; p<0.01) (Figure 2). In total, 3 of 4 between-island comparisons showed that prevalence was significantly higher on high-incidence than on low-incidence islands. We found no significant differences in prevalence between islands with the same level of Lyme disease incidence (Appendix Table 4).

The mean infection prevalence on high-incidence islands (6.43%; 57/886; SE = 0.82) was higher than on low-incidence islands (0.66%; 4/609; SE = 0.33) (Appendix Table 2). Among sites on high-incidence islands, 98.25% (56/57) of infected nymphs carried *B. afzelii* and 1.75% (1/57) carried *B. garinii*. Among sites on low-incidence islands, 75% (3/4) of infected nymphs carried *B. garinii* and 25% (1/4) carried *B. valaisiana*. Among sites on high-incidence islands, prevalence did not differ by island or habitat type (Appendix Table 3).

### Density of Infected Nymphs

Variation in the density of infected nymphs was significantly associated with island (Table 1; $\chi^2$ = 16.98; df = 3; p<0.01) (Figure 2). In 2 of 4 between-island comparisons, the density of infected nymphs was significantly higher on high-incidence than on low-incidence islands. We found no significant differences between islands with the same level of Lyme disease incidence (Appendix Table 4).

The mean density of infected nymphs was 1.90 nymphs/100 m$^2$ (SE = 0.65) on high Lyme disease incidence islands, compared with 0.07 infected nymphs/100 m$^2$ (SE = 0.05) on low-incidence islands. Among sites on high-incidence islands, the density of infected nymphs did not differ by island or habitat type (Appendix Table 3).

### Geographic Locations of Tick Bite Risk

Most (64.4%; 333/517) participants provided information on their island of residence and the habitat where their most recent tick bite had occurred (Appendix). In addition, 51.7% (172/333) of these participants also provided the location of their most recent tick bite. Of these bites, 72.7% (125/172) occurred within 1 km of

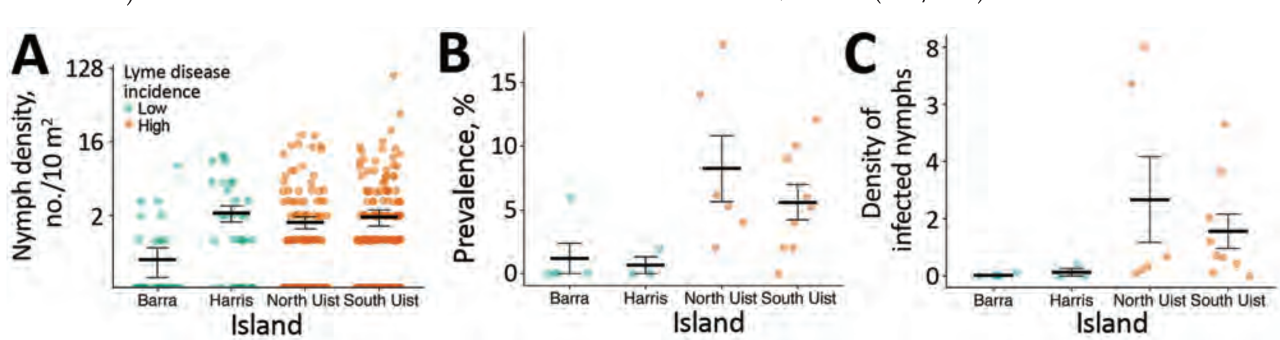


**Figure 2.** Comparison of nymph density, infection prevalence, and density of infected nymphs by island, Western Isles, Scotland, UK, 2018–2019. A) Nymph density shown by 10 m$^2$ blanket drag. B) Prevalence of *Borrelia burgdorferi* sensu lato shown by site. C) Density of infected nymphs per 100 m$^2$ shown by site. Green indicates islands with low incidence of Lyme disease; brown indicates islands with high incidence. Data shown from grassland and moorland sites shown in Figure 1. Horizontal bars indicate means and SEs.

**Table 2.** Best-fit general linear model of factors affecting risk for tick bite exposure in residents of the Western Isles, Scotland, UK, 2018–2019

| Variable | Estimate | SE | p value* | Odds ratio (95% CI) |
|---|---|---|---|---|
| Intercept | –1.99 | 0.54 | NA | NA |
| Island | | | <0.01 | |
| South Uist | Referent | | | |
| North Uist | 0.11 | 0.31 | | 1.12 (0.61–2.07) |
| Benbecula | –0.85 | 0.48 | | 0.43 (0.16–1.05) |
| Barra | 0.01 | 0.42 | | 1.01 (0.43–2.30) |
| Harris/Lewis | –1.14 | 0.33 | | 0.32 (0.16–0.61) |
| Age, y | | | 0.01 | |
| 18–30 | Referent | | | |
| 30–60 | 0.76 | 0.48 | | 2.14 (0.90–5.97) |
| >60 | 1.36 | 0.51 | | 3.88 (1.50–11.48) |
| Outdoor activity | | | 0.02 | |
| Less than most days | Referent | | | |
| Most days | 0.66 | 0.29 | | 1.94 (1.12–3.49) |

*p value determined from likelihood ratio tests of removing each variable from the best-fit model.

the participant's home address, including 81 (47.1%) at the home address (Appendix Figure 2).

### Factors Associated with Tick Bite Exposure Risk

In a multivariable model, the most significant explanatory variable for tick bite exposure risk was island of residence ($\chi^2 = 20.86$; df = 4; p<0.01) (Table 2). Persons >60 years of age had an increased risk for tick bite exposure (odds ratio [OR] 3.88, 95% CI 1.50–11.48). Persons who participated in outdoor activity most days also had an increased risk for tick bite exposure (OR 1.94, 95% CI 1.12–3.49). Residents of high Lyme disease incidence islands had significantly higher rates of tick bite exposure than those of low Lyme disease incidence islands (OR 2.41, 95% CI 1.55–3.82; Appendix Table 1). Awareness, attitudes, and preventative behaviors did not significantly differ between residents living on islands of high and low Lyme disease incidence.

### Factors Associated with Finding a Tick within the Home

The chances of finding a tick within the home increased with pet ownership (OR 4.07, 95% CI 2.61–6.41). Persons who participated in outdoor activity most days also had a slightly increased risk (OR 1.67, 1.05–2.64). The likelihood of finding a tick in the home did not vary among islands (Appendix Table 5).

### Changes in Tick Numbers and Problems Over Time

Approximately half (50.6%; 210/415) of respondents described an increase in tick-associated problems over time. Residents from high Lyme disease incidence islands were significantly more likely to report that tick numbers and associated problems had increased over time (OR 4.5, 95% CI 2.1–10.0) ($\chi^2 = 15.48$; df = 1; p<0.01) (Appendix Table 6). Linguistic analysis of free text comments revealed differences in themes between high and low Lyme disease incidence islands. Residents throughout the surveyed area reported an increased tick presence; residents of high Lyme disease incidence islands were more likely to describe the increase with words such as definitely or significantly than residents of low Lyme disease incidence islands. Residents of high Lyme disease incidence islands were also more likely to report deer near their homes (Appendix Table 7).

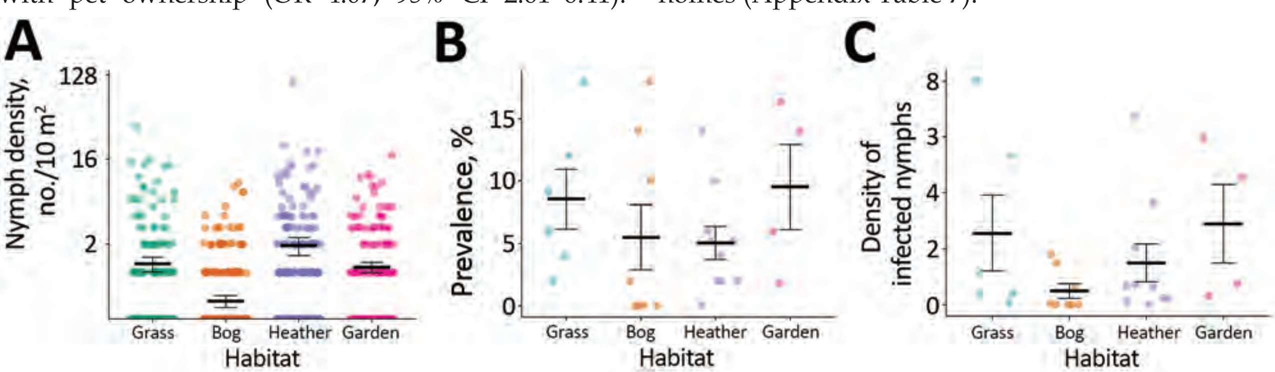


**Figure 3.** Comparison of nymph density, infection prevalence, and density of infected nymphs by habitat type in islands with high incidence of Lyme disease, Western Isles, Scotland, UK, 2018. A) Nymph density shown by 10 m$^2$ blanket drag. B) Prevalence of *Borrelia burgdorferi* sensu lato shown by site. C) Density of infected nymphs per 100 m$^2$ shown by site. Machair sites not shown because of low mean tick density (0.025 nymphs/10 m$^2$; SE = 0.015). Horizontal bars indicate means and SEs.

## Discussion

We investigated Lyme disease emergence in treeless habitats in Scotland. Our findings show that environmental hazard and human tick bite exposure risk contribute to higher Lyme disease incidence in these settings. In contrast to previous studies in Europe, we found that the density of infected nymphs in treeless habitats can be comparable to forested sites, which are traditionally associated with higher Lyme disease hazard (*34*,*43*).

We found a significantly higher prevalence of *B. burgdorferi* s.l. infected nymphs among high Lyme disease incidence islands, which contributed to a higher environmental hazard on these islands. Almost all infected ticks on these islands carried *B. afzelii,* a genospecies associated with mammalian transmission hosts (*44*). We did not detect *B. afzelii* infection in ticks collected from low Lyme disease incidence islands, where the prevalence of infection in ticks was extremely low (<1%). Because of the similarity in habitats and climate, we hypothesize that the presence or absence of this genospecies could be driven by differences in the host community. Alternatively, the introduction of *B. afzelii* from the mainland might have been limited to certain islands.

Within islands with a high incidence of Lyme disease, we found that improved grassland, heather moorland, bog and peatland, and domestic gardens had similar tick density and prevalence of *B. burgdorferi* s.l. infection among ticks as forested mainland sites in Scotland (*34*,*43*). Our results suggest that microclimatic conditions in these open habitats, possibly driven by the milder oceanic climate on the Western Isles, can be as conducive to tick survival as conditions in woodlands. Tick abundance was positively associated with vegetation density, which when combined with relatively high rainfall and humidity in this location, might contribute to a favorable microclimate and improved off-host tick survival. In contrast, we found significantly lower tick abundance within machair grassland, probably caused by a combination of short vegetation height, lack of a vegetation mat, and agricultural rotations and ploughing, which can reduce off-host tick survival (*45*,*46*). Tick abundance varied considerably within habitats (Appendix Table 2), a finding that warrants further investigation.

In addition to a higher environmental hazard on high Lyme disease incidence islands, residents of these islands reported more frequent exposures to tick bites. Tick bite exposure increased with the participant's age and amount of outdoor activity. Although outdoor activity and knowledge, attitudes, and prevention of tick bites did not contribute to differences in tick bite exposure between islands with high and low Lyme disease incidence, this finding might have been affected by the higher proportion of responses from older residents on high Lyme disease incidence islands. Although we found no significant differences in tick density between high- and low-incidence grassland and moorland sites, survey responses indicated that most tick bites occurred close to the home address, and frequently in gardens. On high Lyme disease incidence islands, we found a similar density of infected nymphs in gardens to surrounding habitats, indicating that spillover of infected ticks is common. Further research is required to test whether peridomestic tick exposure contributes to differences in tick bite exposure between islands. The findings that tick bites frequently occur within gardens and that residents might be exposed to ticks within their homes suggest that all members of a household could be at risk for tick bites. Our research suggests that environmental and educational public health interventions focused around residences could reduce tick bite exposure and potentially cases of Lyme disease.

Similar to previous studies, we found that in the absence of longitudinal data on vector populations and linked ecologic drivers, community surveys can be valuable indicators of ecologic trends (*31*). Residents of high Lyme disease incidence islands were significantly more likely to report that ticks were an increasing problem. In addition, many of these participants suggested that increased deer populations and presence near homes might contribute to increased numbers of ticks. Because deer habitat use and movements are established drivers of tick populations and distribution (*27*,*47*,*48*) and are associated with Lyme disease emergence in other areas of Europe (*49*), this association should be investigated in future research.

In summary, we have shown that treeless habitats can support similar tick densities and infection risk as forested areas and can be associated with Lyme disease emergence in humans. Our results suggest the potential for Lyme disease to emerge in open habitats with a suitable microclimate for off-host tick survival and host availability for blood meals elsewhere in Europe. Integrating these results with data on human exposure to tick bites revealed that most tick bites occurred close to homes. Furthermore, we found that the spillover of ticks and tickborne pathogens into gardens and homes is an emerging problem that residents attribute to increased deer populations and their changing distribution. Further research to understand the effects of ecologic drivers of tick populations in these regions, together with information on human use of these environments, is necessary to achieve more accurate prediction of areas of risk and suggest ways to prevent and mitigate this risk.

## Acknowledgments

We thank 2 anonymous reviewers for their helpful comments on the manuscript.

M.V. was funded by the European Research Council under the European Union's Horizon 2020 Research and Innovation Programme (grant agreement no. 852957). J.Y. was supported by a Collaborative Awards in Science and Engineering studentship funded by the Natural Environment Research Council, Swindon, UK.


## About the Author

Dr. Millins is a research fellow at the University of Liverpool. Her primary research interests include One Health approaches to the study of zoonotic pathogens, vectorborne pathogen ecology, and wildlife health.

## References


1. Dennis D, Hayes E. Epidemiology of Lyme borreliosis. In: Gray J, Kahl O, Lane R, Stanek G, editors. Lyme borreliosis: biology, epidemiology and control. New York: CABI; 2002. p. 251–80.
2. Rizzoli A, Hauffe H, Carpi G, Vourc H G, Neteler M, Rosà R. Lyme borreliosis in Europe. Euro Surveill. 2011;16:19906.
3. James MC. The ecology, genetic diversity and epidemiology of Lyme borreliosis in Scotland [PhD thesis]. Aberdeen (UK): University of Aberdeen; 2010.
4. Eisen RJ, Lane RS, Fritz CL, Eisen L. Spatial patterns of Lyme disease risk in California based on disease incidence data and modeling of vector-tick exposure. Am J Trop Med Hyg. 2006;75:669–76. https://doi.org/10.4269/ajtmh.2006.75.669
5. Dister SW, Fish D, Bros SM, Frank DH, Wood BL. Landscape characterization of peridomestic risk for Lyme disease using satellite imagery. Am J Trop Med Hyg. 1997;57:687–92. https://doi.org/10.4269/ajtmh.1997.57.687
6. National Health Service—Western Isles. The 'tick'-ing time bomb: the incidence of Lyme disease in the Outer Hebrides (2010–2017). 2018 [cited 2020 Aug 13]. https://www.wihb.scot.nhs.uk/wp-content/uploads/2020/08/A0-Template-The-ticking-time-bomb.-Incidence-of-Lyme-disease-in-the-Western-Isles-2010-2017.pdf
7. Slack GS, Mavin S, Yirrell D, Ho-Yen DO. Is Tayside becoming a Scottish hotspot for Lyme borreliosis? J R Coll Physicians Edinb. 2011;41:5–8. https://doi.org/10.4997/JRCPE.2011.102
8. Tulloch JSP, Decraene V, Christley RM, Radford AD, Warner JC, Vivancos R. Characteristics and patient pathways of Lyme disease patients: a retrospective analysis of hospital episode data in England and Wales (1998–2015). BMC Public Health. 2019;19:931. https://doi.org/10.1186/s12889-019-7245-8
9. Mavin S, Watson EJ, Evans R. Distribution and presentation of Lyme borreliosis in Scotland— analysis of data from a national testing laboratory. J R Coll Physicians Edinb. 2015;45:196–200. https://doi.org/10.4997/JRCPE.2015.304
10. Tulloch JSP, Semper AE, Brooks TJG, Russell K, Halsby KD, Christley RM, et al. The demographics and geographic distribution of laboratory-confirmed Lyme disease cases in England and Wales (2013–2016): an ecological study. BMJ Open. 2019;9:e028064. https://doi.org/10.1136/bmjopen-2018-028064
11. National Institute for Health and Care Excellence. Lyme disease. 2018 [cited 2020 Oct 20]. https://www.nice.org.uk/guidance/ng95
12. Medlock JM, Shuttleworth H, Copley V, Hansford KM, Leach S. Woodland biodiversity management as a tool for reducing human exposure to *Ixodes ricinus* ticks: a preliminary study in an English woodland. J Vector Ecol. 2012;37:307–15. https://doi.org/10.1111/j.1948-7134.2012.00232.x
13. Randolph SE. Tick ecology: processes and patterns behind the epidemiological risk posed by Ixodid ticks as vectors. Parasitology. 2004;129:S37–65. https://doi.org/10.1017/S0031182004004925
14. Boyard C, Barnouin J, Gasqui P, Vourc'h G. Local environmental factors characterizing *Ixodes ricinus* nymph abundance in grazed permanent pastures for cattle. Parasitology. 2007;134:987–94. https://doi.org/10.1017/S0031182007002351
15. Hoch T, Monnet Y, Agoulon A. Influence of host migration between woodland and pasture on the population dynamics of the tick *Ixodes ricinus*: a modelling approach. Ecol Modell. 2010;221:1798–806. https://doi.org/10.1016/j.ecolmodel.2010.04.008
16. Gilbert L. How landscapes shape Lyme borreliosis risk. In: Braks M, van Wieren SE, Takken W, Sprong H, editors. Ecology and control of vector borne diseases. Vol 4. Wageningen, the Netherlands: Wageningen Academic Publishers; 2016. p. 161–71.
17. Gray JS, Kahl O, Robertson JN, Daniel M, Estrada-Peña A, Gettinby G, et al. Lyme borreliosis habitat assessment. Zentralbl Bakteriol. 1998;287:211–28. https://doi.org/10.1016/S0934-8840(98)80123-0
18. Estrada-Peña A. Distribution, abundance, and habitat preferences of *Ixodes ricinus* (Acari: Ixodidae) in northern Spain. J Med Entomol. 2001;38:361–70. https://doi.org/10.1603/0022-2585-38.3.361
19. Gray JS. The ecology of ticks transmitting Lyme borreliosis. Exp Appl Acarol. 1998;22:249–58. https://doi.org/10.1023/A:1006070416135
20. Ogden NH, Nuttall PA, Randolph SE. Natural Lyme disease cycles maintained via sheep by co-feeding ticks. Parasitology. 1997;115:591–9. https://doi.org/10.1017/S0031182097001868
21. Walker AR, Alberdi MP, Urquhart KA, Rose H. Risk factors in habitats of the tick *Ixodes ricinus* influencing human exposure to *Ehrlichia phagocytophila* bacteria. Med Vet Entomol. 2001;15:40–9. https://doi.org/10.1046/j.1365-2915.2001.00271.x
22. Ruiz-Fons F, Gilbert L. The role of deer as vehicles to move ticks, *Ixodes ricinus*, between contrasting habitats. Int J Parasitol. 2010;40:1013–20. https://doi.org/10.1016/j.ijpara.2010.02.006
23. Harrison A, Newey S, Gilbert L, Haydon DT, Thirgood S. Culling wildlife hosts to control disease: mountain hares, red grouse and louping ill virus. J Appl Ecol. 2010;47:926–30. https://doi.org/10.1111/j.1365-2664.2010.01834.x
24. Bouchard C, Aenishaenslin C, Rees EE, Koffi JK, Pelcat Y, Ripoche M, et al. Integrated social-behavioral and ecological risk maps to prioritize local public health responses to Lyme disease. Environ Health Perspect. 2018;126:047008. https://doi.org/10.1289/EHP1943
25. Fischhoff IR, Keesing F, Ostfeld RS. Risk factors for bites and diseases associated with black-legged ticks: a meta-analysis. Am J Epidemiol. 2019;188:1742–50. https://doi.org/10.1093/aje/kwz130
26. Finch C, Al-Damluji MS, Krause PJ, Niccolai L, Steeves T, O'Keefe CF, et al. Integrated assessment of behavioral

and environmental risk factors for Lyme disease infection on Block Island, Rhode Island. PLoS One. 2014;9:e84758. https://doi.org/10.1371/journal.pone.0084758
27. Medlock JM, Hansford KM, Bormane A, Derdakova M, Estrada-Peña A, George J-C, et al. Driving forces for changes in geographical distribution of *Ixodes ricinus* ticks in Europe. Parasit Vectors. 2013;6:1. https://doi.org/10.1186/1756-3305-6-1
28. Werden L, Barker IK, Bowman J, Gonzales EK, Leighton PA, Lindsay LR, et al. Geography, deer, and host biodiversity shape the pattern of Lyme disease emergence in the Thousand Islands Archipelago of Ontario, Canada. PLoS One. 2014;9:e85640. https://doi.org/10.1371/journal.pone.0085640
29. Ostfeld RS, Brunner JL. Climate change and Ixodes tick-borne diseases of humans. Philos Trans R Soc Lond B Biol Sci. 2015;370:20140051. https://doi.org/10.1098/rstb.2014.0051
30. Simon JA, Marrotte RR, Desrosiers N, Fiset J, Gaitan J, Gonzalez A, et al. Climate change and habitat fragmentation drive the occurrence of *Borrelia burgdorferi*, the agent of Lyme disease, at the northeastern limit of its distribution. Evol Appl. 2014;7:750–64. https://doi.org/10.1111/eva.12165
31. Kimaro EG, Toribio JLML, Mor SM. Climate change and cattle vector-borne diseases: use of participatory epidemiology to investigate experiences in pastoral communities in Northern Tanzania. Prev Vet Med. 2017;147:79–89. https://doi.org/10.1016/j.prevetmed.2017.08.010
32. Angus S. The Outer Hebrides: moor and machair. Winwick (UK): White Horse Press; 2001. p. 78–81, 200.
33. National Biodiversity Network Atlas Partnership. National biodiversity network atlas. 2017 [cited 2020 Jul 1]. https://records.nbnatlas.org
34. Millins C, Gilbert L, Johnson P, James M, Kilbride E, Birtles R, et al. Heterogeneity in the abundance and distribution of *Ixodes ricinus* and *Borrelia burgdorferi* (sensu lato) in Scotland: implications for risk prediction. Parasit Vectors. 2016;9:595. https://doi.org/10.1186/s13071-016-1875-9
35. Gern L, Douet V, López Z, Rais O, Cadenas FM. Diversity of *Borrelia* genospecies in *Ixodes ricinus* ticks in a Lyme borreliosis endemic area in Switzerland identified by using new probes for reverse line blotting. Ticks Tick Borne Dis. 2010;1:23–9. https://doi.org/10.1016/j.ttbdis.2009.11.001
36. Johnson BJB, Happ CM, Mayer LW, Piesman J. Detection of *Borrelia burgdorferi* in ticks by species-specific amplification of the flagellin gene. Am J Trop Med Hyg. 1992;47:730–41. https://doi.org/10.4269/ajtmh.1992.47.730
37. Bates D, Maechler M, Bolker B, Walker S. lme4: Linear mixed-effects, models using Eigen and S4. 2020 [cited 2020 Jun 13]. https://tinyurl.com/lme42020
38. Fox J, Weisberg S. An R companion to applied regression. 3rd ed. Thousand Oaks (CA): Sage Publications, Inc.; 2019.
39. Johnson JB, Omland KS. Model selection in ecology and evolution. Trends Ecol Evol. 2004;19:101–8. https://doi.org/10.1016/j.tree.2003.10.013
40. Lenth RV. Least-squares means: the R package lsmeans. J Stat Softw. 2016;69:1–33. https://doi.org/10.18637/jss.v069.i01
41. Elston DA, Moss R, Boulinier T, Arrowsmith C, Lambin X. Analysis of aggregation, a worked example: numbers of ticks on red grouse chicks. Parasitology. 2001;122:563–9. https://doi.org/10.1017/S0031182001007740
42. Huntley SJ, Mahlberg M, Wiegand V, van Gennip Y, Yang H, Dean RS, et al. Analysing the opinions of UK veterinarians on practice-based research using corpus linguistic and mathematical methods. Prev Vet Med. 2018;150:60–9. https://doi.org/10.1016/j.prevetmed.2017.11.020
43. James MC, Bowman AS, Forbes KJ, Lewis F, McLeod JE, Gilbert L. Environmental determinants of *Ixodes ricinus* ticks and the incidence of *Borrelia burgdorferi* sensu lato, the agent of Lyme borreliosis, in Scotland. Parasitology. 2013;140:237–46. https://doi.org/10.1017/S003118201200145X
44. Hanincová K, Schäfer SM, Etti S, Sewell HS, Taragelová V, Ziak D, et al. Association of *Borrelia afzelii* with rodents in Europe. Parasitology. 2003;126:11–20. https://doi.org/10.1017/S0031182002002548
45. Milne A. Pasture improvement and the control of sheep tick (*Ixodes ricinus* L.) Ann Appl Biol. 1948;35:369–78. https://doi.org/10.1111/j.1744-7348.1948.tb07381.x
46. Owen NW, Kent M, Dale P. Ecological effects of cultivation on the machair sand dune systems of the Outer Hebrides, Scotland. J Coast Conserv. 2000;6:155–70. https://doi.org/10.1007/BF02913812
47. Gilbert L, Maffey GL, Ramsay SL, Hester AJ. The effect of deer management on the abundance of *Ixodes ricinus* in Scotland. Ecol Appl. 2012;22:658–67. https://doi.org/10.1890/11-0458.1
48. Hofmeester TR, Sprong H, Jansen PA, Prins HHT, van Wieren SE. Deer presence rather than abundance determines the population density of the sheep tick, *Ixodes ricinus*, in Dutch forests. Parasit Vectors. 2017;10:433. https://doi.org/10.1186/s13071-017-2370-7
49. Mysterud A, Easterday WR, Stigum VM, Aas AB, Meisingset EL, Viljugrein H. Contrasting emergence of Lyme disease across ecosystems. Nat Commun. 2016;7:11882. https://doi.org/10.1038/ncomms11882

Address for correspondence: Caroline Millins, Department of Livestock and One Health, Institute of Infection, Veterinary and Ecological Sciences, Leahurst Campus, University of Liverpool, Neston, CH64 7TE, UK; email: Caroline.Millins@Liverpool.ac.uk

# SARS-CoV-2 Transmission between Mink (*Neovison vison*) and Humans, Denmark

Anne Sofie Hammer, Michelle Lauge Quaade, Thomas Bruun Rasmussen, Jannik Fonager, Morten Rasmussen, Karin Mundbjerg, Louise Lohse, Bertel Strandbygaard, Charlotte Sværke Jørgensen, Alonzo Alfaro-Núñez, Maiken Worsøe Rosenstierne, Anette Boklund, Tariq Halasa, Anders Fomsgaard, Graham J. Belsham, Anette Bøtner

Severe acute respiratory syndrome coronavirus 2 has caused a pandemic in humans. Farmed mink (*Neovison vison*) are also susceptible. In Denmark, this virus has spread rapidly among farmed mink, resulting in some respiratory disease. Full-length virus genome sequencing revealed novel virus variants in mink. These variants subsequently appeared within the local human community.

Severe acute respiratory syndrome coronavirus 2 (SARS-CoV-2) has caused the ongoing coronavirus disease (COVID-19) pandemic (*1*). Ferrets, cats, dogs, Syrian hamsters, and nonhuman primates can be infected with the virus and, in some cases, transmit it (*2*); however, other species, such as pigs and chickens, appear resistant (*3,4*). Thus, the virus has a restricted host range. Infection with SARS-CoV-2 has occurred in farmed mink in the Netherlands (*5*).

In Denmark, there are ≈1,200 mink farms (*6*). Because of contacts between persons with COVID-19 and mink farms, investigation of SARS-CoV-2 infection within mink in Denmark was undertaken. We documented 3 premises in the Northern Jutland region of Denmark with SARS-CoV-2–infected mink and analyzed virus transmission in mink and the local human community.

## The Study

We collected blood and throat, nasal, and fecal swab samples from mink adults and kits (Table 1); we also sampled feed and air. We assayed viral RNA by quantitative reverse transcription PCR (qRT-PCR) (*7*). We performed SARS-CoV-2 Ab ELISA (Beijing Wantai Biological Pharmacy Enterprise, http://www.ystwt.cn) as described (R. Lassaunière et al., unpub. data, https://doi.org/10.1101/2020.04.09.20056325). SARS-CoV-2–positive RNA samples were sequenced and sequences aligned using Mafft (https://mafft.cbrc.jp/alignment/server/index.html). Phylogenetic analysis was performed in MEGA 10.1.7 (*8*) using the maximum-likelihood general time reversible plus invariant sites plus gamma (2 categories) method (*9*).

We selected mink farms for investigation because of COVID-19 in persons linked to them. During initial visits, we sampled 30 apparently healthy adult mink; we tested adults and kits in follow-up visits. We analyzed serum samples for SARS-CoV-2 antibodies and assayed swab samples for SARS-CoV-2 RNA (Table 1; Appendix, https://wwwnc.cdc.gov/EID/article/27/2/20-3794-App1.pdf). At initial sampling, seroprevalence was high on farm 1 (>95%) and farm 3 (66%) but, in contrast, only 3% on farm 2. However, after the infection spread widely on farm 2, indicated by the increased prevalence of viral RNA (Table 1), a large increase in seroprevalence occurred, to >95%.

Air samples from farm 1 tested negative. However, on farms 2 and 3, multiple samples collected from exhaled air from mink or within 1 m of the cages scored positive, albeit with fairly high (>31) $C_t$ values. None of the air samples collected outside the houses were positive. Feed samples collected at each farm tested negative.

We also sequenced SARS-CoV-2 RNA from samples from each mink farm. The viruses found on farms 1–3 were very similar (Table 2). These sequences and those from humans (H1–H9) linked to

Author affiliations: University of Copenhagen, Copenhagen, Denmark (A.S. Hammer, M.L. Quaade, K. Mundbjerg, A. Boklund, T. Halasa, G.J. Belsham, A. Bøtner); Statens Serum Institut, Copenhagen (T.B. Rasmussen, J. Fonager, M. Rasmussen, L. Lohse, B. Strandbygaard, C.S. Jørgensen, A. Alfaro-Núñez, M.W. Rosenstierne, A. Fomsgaard, A. Bøtner)

DOI: https://doi.org/10.3201/eid2702.203794

**Table 1.** Summary of laboratory analyses of mink samples from 3 mink farms tested for severe acute respiratory syndrome coronavirus 2 in Denmark, June–July 2020*

| | Test and specimen type, no. positive/no. tested (%) | | | | | |
|---|---|---|---|---|---|---|
| | ELISA | qRT-PCR | | | Date of sample | |
| Sample origin | Serum | Throat swabs | Nasal swabs | Fecal swabs | collection | Location |
| Live adult mink | 29/30 (97) | NA | NA | 5/30 (17) | 2020 Jun 14 | Farm 1 |
| Dead adult mink | NA | NA | 4/4 (100) | 3/4 (75) | 2020 Jun 14 | Farm1 |
| Live mink kits | 30/30 (100) | 3/30 (10) | 3/30 (10) | 1/30 (3) | 2020 Jun 17 | Farm 1 |
| Live adult mink | 30/30 (100) | 3/23 (13) | NA | 0/23 (0) | 2020 Jun 17 | Farm 1 |
| Retested adult mink | 4/4 (100) | 2/4 (50) | 2/4 (50) | 1/4 (25) | 2020 Jun 17 | Farm 1 |
| Live adult mink | 1/30 (3) | NA | NA | 0/8 (0) | 2020 Jun 18 | Farm 2 |
| Dead adult mink | NA | 1/8 (13) | NA | NA | 2020 Jun 18 | Farm 2 |
| Live mink kits | 1/50 (2) | 40/50 (80) | 39/50 (78) | NA | 2020 Jun 22 | Farm 2 |
| Live adult mink | 3/50 (6) | 46/50 (92) | NA | NA | 2020 Jun 22 | Farm 2 |
| Dead adult mink | 1/3 (33) | 2/3 (66) | 2/3 (66) | NA | 2020 Jun 22 | Farm 2 |
| Dead adult mink | NA | 3/3 (100) | 3/3 (100) | NA | 2020 Jun 30 | Farm 2 |
| Live adult mink (retest) | 36/37 (97) | 35/37 (95) | 37/37(100) | NA | 2020 Jun 30 | Farm 2 |
| Live adult mink | 20/30 (67) | 6/6†(100) | NA | NA | 2020 Jun 30 | Farm 3 |
| Dead adult mink | NA | 5/5 (100) | NA | NA | 2020 Jun 30 | Farm 3 |
| Live mink kits | 24/30 (80) | 30/30 (100) | 27/30 (90) | NA | 2020 Jul 2 | Farm 3 |
| Live adult mink | 23/30 (77) | 30/30 (100) | 26/30 (87) | NA | 2020 Jul 2 | Farm 3 |

*NA, not applicable; qRT-PCR, quantitative reverse transcription PCR.
†Samples from 30 mink were assayed in 6 pools of 5 swabs each.

**Table 2.** Location of nt differences identified in genome sequences of selected severe acute respiratory syndrome coronavirus 2 samples from mink and humans in Denmark, June–July 2020, compared with Wuhan and clade 20B reference sequences*

| | Genomic location and nt position | | | | | | | | | | | |
|---|---|---|---|---|---|---|---|---|---|---|---|---|
| | 5′ UTR | ORF1a | | | ORF1b | | Spike | | ORF3a | Nucleoprotein | | |
| Virus sample | 241 | 3037 | 5421 | 9534 | 14408 | 15656 | 22920 | 23403 | 25936 | 28881 | 28882 | 28883 |
| NC045512 (Wuhan) | C | C | A | C | C | C | A | A | C | G | G | G |
| Humans in Jutland (to 2020 Jun 10)† | T | T | A | C | T | C | A | G | C | G | G | G |
| EPI_ISL_455326 20B | T | T | A | C | T | C | A | G | C | A | A | C |
| Index case | T | T | A | C | T | T | A | G | ND | A | A | C |
| Mink_AD4_ Farm1 | T | T | G | C | T | T | T | G | T | A | A | C |
| Mink_AL3_ Farm1 | T | T | A | C | T | T | A | G | T | A | A | C |
| Mink_KL14_ Farm1 | T | T | A | C | T | T | A | G | T | A | A | C |
| Mink_KL11_ Farm1 | T | T | A | C | T | T | A | G | T | A | A | C |
| Mink_AD3_ Farm1 | T | T | G | C | T | T | T | G | T | A | A | C |
| Mink_AD6_ Farm1 | T | T | A | C | T | T | T | G | T | A | A | C |
| Mink_AL64_ Farm1 | T | T | A | C | T | T | A | G | T | A | A | C |
| Mink_AL25_ Farm1 | T | T | A | C | T | T | T | G | T | A | A | C |
| Mink_AD38_ Farm2 | T | T | A | C | T | T | T | G | T | A | A | C |
| Mink_M1-M47_Farm2‡ | T | T | A | C | T | T | T | G | T | A | A | C |
| Mink_AD37_ Farm3 | T | T | A | C | T | T | T | G | T | A | A | C |
| Mink_AD40_ Farm3 | T | T | A | C | T | T | T | G | T | A | A | C |
| Mink_AL35_ Farm3 | T | T | A | C | T | T | T | G | T | A | A | C |
| H1–H7 + H9 | T | T | A | C | T | T | T | G | T | A | A | C |
| H8 | T | T | A | T | T | T | T | G | T | A | A | C |
| In NB01 (NL)§ | T | T | A | C | T | C | A | G | C | G | G | G |
| In NB02 (NL)§ | C | C | A | C | C | C | T>A# | A | C | G | G | G |
| In NB03 (NL)§ | T | T | A | C | T | C | A | G | T | G | G | G |
| In NB04 (NL)§ | T | T | A | C | T | C | A | G | C | G | G | G |
| Humans in Jutland (to 2020 Jul 1) † | T | T | A | C | T | C>T | A>T | G | C>T | G>A | G>A | G>C |
| Encoded amino acid change¶ | NA | NA | I1719 V | T3083 I | P314 L | T730 I | Y453 F | D614 G | H182 Y | R203 K | R203 K | G204 R |

*Red text indicates nt differences from the Wuhan reference strain; pink shading indicates nt changes detected in mink and in human contacts (H1–H9) that differ from the clade 20 B and index case; gray shading indicates a reference clade 20B sequence and the human index case sequence. NA, not applicable, as nt change in the noncoding region; ND, not determined; NL, the Netherlands; ORF, open reading frame.
† The proportions of each nt present at each of these positions in human sequences in Jutland are shown in Appendix Table 1 (https://wwwnc.cdc.gov/EID/article/27/2/20-3794-App1.pdf).
‡nts present in farm 2 sequences obtained from throat swab specimens on June 22, 2020 (derived from 20 adult mink and 27 kits).
§The mink sequences from the Netherlands also differ at other locations compared with the Wuhan sequence (*5*).
¶Encoded amino acid substitutions (with residue number in each protein) compared to Wuhan reference strain are indicated using the single letter code.
#T in 5 of 6 sequences from farm NB02 (*5*).

the infected farms grouped within the European 20B clade of the global SARS-CoV-2 tree (*10,11*) (Figure; Appendix Table 1). We deposited the SARS-CoV-2 genome sequences of virus from farm 1 (SARS-CoV-2/mink/DK/AD3_Farm1/2020) in GenBank (accession nos. MT919525–36). The sequences closely matched those of a human case, diagnosed in mid-May, with a direct epidemiologic link to farm 1. This index sequence (only 91% complete) matched the mink viruses at nt 15656 (rare globally) but had A at nt 22920 (Table 2). The nt 25936 in the index case could not be determined. The local phylogeny (Appendix Figure) showed that mink sequences from farm 1 fell into 3 subclusters (defined by the nucleotide changes at positions 5421 and 22920), but sequences from linked humans (H1–H9) and mink in farms 2 and 3 were within subcluster 2 (Appendix Figure).

We found 9 to 11 nt differences (mainly nonsynonymous) between the mink sequences in Denmark and the Wuhan-Hu-1 reference sequence (Table 2). One mutation at nt 23403 (resulting in substitution D614G in the spike protein) was present in all sequences from mink in Denmark and the Netherlands, except for NB02 from the Netherlands (Table 2) and was predominant in the human population in Jutland (Appendix Table 1) and globally (*12*). However, another mutation (nt C25936T [as cDNA] encoding H182 to Y within ORF3a) appeared in all mink sequences from Denmark (Table 2) and in human cases (H1–H9) linked to them. This change was not found in human SARS-CoV-2 sequences from Jutland before June 10, 2020 (Appendix Table 1), but reached ≈40% frequency during June 10–July 1, 2020 (Table 2; Appendix Table 2). This mutation has been found only rarely in other SARS-CoV-2 sequences (*11*) (Appendix Table 1) but was in mink farm NB03 from the Netherlands (SARS-CoV-2/mink/NED/NB03_index/2020; GenBank accession no. MT457400.1).

Another mutation in the spike gene (A22920T, encoding Y453 to F) was present in 4 of 8 sequences from farm 1, in all sequences from farms 2 and 3, and in 5 of 6 sequences from farm NB02 in the

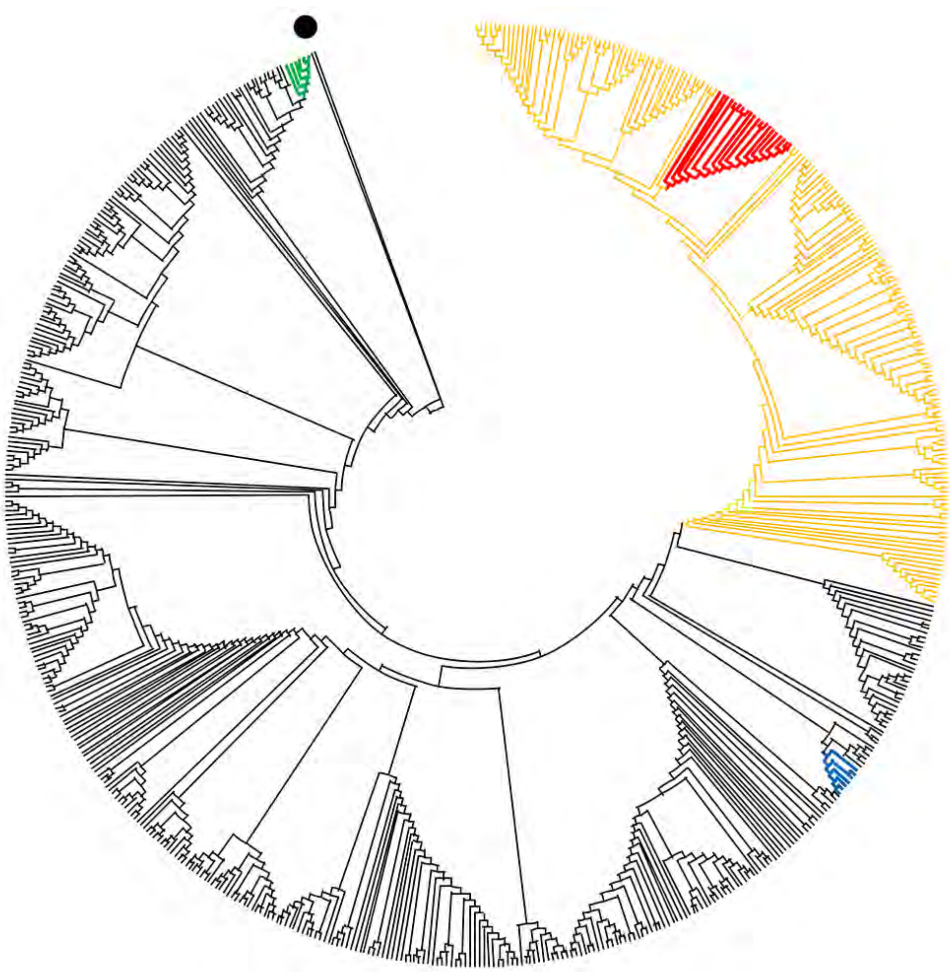

**Figure.** Phylogenetic tree showing relationships between genome sequences of severe acute respiratory syndrome coronavirus 2 from mink and humans at 3 mink farms in Denmark, June–July 2020 (red), and selected global full-length genome sequences. Black dot indicates Wuhan reference sequence NC_045512.2; green indicates mink farm NB02 in the Netherlands; blue indicates mink farms NB01, NB03, and NB04 in the Netherlands; orange indicates clade 20B.

Netherlands (*5*). This change was not in the index case or the human population anywhere before June 10 but was subsequently detected in farm-linked humans (H1–H9) and in Jutland (Table 2; Appendix Table 2). Finally, the mutation in the open reading frame 1b gene (C15656T, encoding T730 to I) was present only in mink/human sequences from Denmark (Table 2) and a sequence from New Zealand (Appendix Table 1).

## Conclusions

A high proportion of mink on farms can be infected with SARS-CoV-2 within a few days, which may provide major virus exposure to persons working with mink. The infections we describe here occurred with little clinical disease or increase in death (Appendix), making it difficult to detect the spread of infection; thus, mink farms could represent a serious, unrecognized animal reservoir for SARS-CoV-2. There is no evidence for spread of the virus outside of farm buildings, either in Denmark or in the Netherlands (*5*), except by infected persons. However, there appears to be some risk of virus transmission to persons working with infected mink as well as for their contacts and thus, indirectly, for the public.

On farm 1, the virus had probably been introduced some weeks before detection (Table 1). On farm 2, the low frequency (4%) of seropositivity and the high proportion of qRT-PCR positive animals at second sampling (Table 1) suggested that the virus had been recently introduced but was spreading. Indeed, a third sampling (8 days later) showed a much higher seroprevalence (>90%). Conceivably, the variant viruses that appeared in farm 1 and spread to farms 2 and 3 may be better adapted to mink and thus able to transmit rapidly. The infection at farm 3 was detected relatively late, with a high seroprevalence (66%) at first visit.

A likely scenario for the spread of infection in mink in Denmark is that the index human case-patient, who had nt T15656 introduced it into farm 1. Initially, we observed sequence heterogeneity at nt 22920 in mink on farm 1, but subsequently, we detected only the variant form (T22920) on farms 2 and 3 and in subsequent linked human cases (H1–H9) (Table 2). Remarkably, this heterogeneity also occurred on farm NB02 in the Netherlands. This change, possibly together with the mutation at nt 25936 (Table 2), may represent virus adaptation. It is not yet established whether these changes confer advantages in mink, but the variant viruses in farm 2 spread rapidly. It seems that the variant viruses on farm 1 spread to ≥1 human and were then transmitted, presumably by human–human contact, to other persons and to farms 2 and 3. The change at nt 22920 results in substitution Y453F in the S-protein (Table 2). This Y-residue, within the receptor-binding motif of the S-protein, is highly conserved among SARS-related coronaviruses and is close to residue L455 that is critical for interaction with the cellular ACE2 receptor (*13*).

### Acknowledgments

We thank Mads Albertsen for guidance with Nanopore sequencing and Henrik B. Krarup for providing human samples containing SARS-CoV-2. We gratefully acknowledge the provision of genetic sequence data shared via GISAID (https://www.gisaid.org; see Appendix Table 3, https://wwwnc.cdc.gov/EID/article/27/2/20-3794-App1.pdf). We also thank Amalie E. Bedsted and Thea Kristensen for careful reading of the manuscript.

### About the Author

Dr. Hammer, an associate professor at the University of Copenhagen, is a veterinary pathologist with special interest and expertise in pathological methods applied in diagnostics, research, and surveillance of diseases in fur animals and wildlife. Her research focus has been mainly on viral diseases of carnivorous species.

### References

1. Johns Hopkins University. Coronavirus resource center. 2020 [cited 2020 Nov 11]. https://coronavirus.jhu.edu
2. Cohen J. From mice to monkeys, animals studied for coronavirus answers. Science. 2020;368:221–2. https://doi.org/10.1126/science.368.6488.221
3. Schlottau K, Rissmann M, Graaf A, Schön J, Sehl J, Wylezich C, et al. SARS-CoV-2 in fruit bats, ferrets, pigs, and chickens: an experimental transmission study. Lancet Microbe. 2020;1:e218–25. https://doi.org/10.1016/S2666-5247(20)30089-6
4. Shi J, Wen Z, Zhong G, Yang H, Wang C, Huang B, et al. Susceptibility of ferrets, cats, dogs, and other domesticated animals to SARS–coronavirus 2. Science. 2020;368:1016–20. https://doi.org/10.1126/science.abb7015
5. Oreshkova N, Molenaar RJ, Vreman S, Harders F, Oude Munnink BB, Hakze-van der Honing RW, et al. SARS-CoV-2 infection in farmed minks, the Netherlands, April and May 2020. Euro Surveill. 2020;25:2001005. https://doi.org/10.2807/1560-7917.ES.2020.25.23.2001005
6. Miljø-og Fødevareministeriet, Fødevarestyrelsen [in Danish]. 2020 [cited 2020 Nov 11]. https://chr.fvst.dk/chri/faces/frontpage?_adf.ctrl-state=31prh7gzs_3
7. Corman VM, Landt O, Kaiser M, Molenkamp R, Meijer A, Chu DK, et al. Detection of 2019 novel coronavirus (2019-nCoV) by real-time RT-PCR. Euro Surveill. 2020;25:2000045. https://doi.org/10.2807/1560-7917.ES.2020.25.3.2000045
8. Kumar S, Stecher G, Li M, Knyaz C, Tamura K. MEGA X: Molecular Evolutionary Genetics Analysis across computing platforms. Mol Biol Evol. 2018;35:1547–9. https://doi.org/10.1093/molbev/msy096

9. Nei M, Kumar S. Molecular evolution and phylogenetics. Oxford (UK): Oxford University Press; 2000.
10. Alm E, Broberg EK, Connor T, Hodcroft EB, Komissarov AB, Maurer-Stroh S, et al. Geographical and temporal distribution of SARS-CoV-2 clades in the WHO European Region, January to June 2020. Euro Surveill. 2020;25: 2001410. https://doi.org/10.2807/1560-7917.ES.2020.25.32.2001410
11. Nextclade. 2020 [cited 2020 Nov 11]. https://clades.nextstrain.org
12. Korber B, Fischer WM, Gnanakaran S, Yoon H, Theiler J, Abfalterer W, et al. Tracking changes in SARS-CoV-2 spike: evidence that D614G increases infectivity of the COVID-19 virus. Cell. 2020;182:812–27.e19. https://doi.org/10.1016/j.cell.2020.06.043
13. Shang J, Ye G, Shi K, Wan Y, Luo C, Aihara H, et al. Structural basis of receptor recognition by SARS-CoV-2. Nature. 2020;581:221–4. https://doi.org/10.1038/s41586-020-2179-y


Address for correspondence: Anette Bøtner, Department of Veterinary and Animal Sciences, University of Copenhagen, Grønnegårdsvej 15, 1870 Frederiksberg C, Denmark; email: aneb@sund.ku.dk

# SARS-CoV-2 Infections among Recent Organ Recipients, March–May 2020, United States

Jefferson M. Jones, Ian Kracalik, Meenakshi M. Rana, Ann Nguyen, Brian C. Keller, Aaron Mishkin, Charles Hoopes, Thomas Kaleekal, Abhinav Humar, Juan Vilaro, Gene Im, Lou Smith, April Justice, Collette Leaumont, Stephen Lindstrom, Brett Whitaker, Ricardo M. La Hoz, Marian G. Michaels, David Klassen, Wendi Kuhnert, Sridhar V. Basavaraju

We conducted public health investigations of 8 organ transplant recipients who tested positive for severe acute respiratory syndrome coronavirus 2 infection. Findings suggest the most likely source of transmission was community or healthcare exposure, not the organ donor. Transplant centers should educate transplant candidates and recipients about infection prevention recommendations.

Although severe acute respiratory syndrome coronavirus 2 (SARS-CoV-2) infection has been reported in organ transplant recipients, it is unclear whether SARS-CoV-2 can be transmitted from organ donors to recipients (*1*) and if transplant recipients are at increased risk for severe illness from coronavirus disease (COVID-19) from SARS-CoV-2 infection compared with immunocompetent patients (*2*). In March 2020, organ procurement organizations (OPOs) and transplant centers in the United States began to report potential donor-derived SARS-CoV-2 transmission to the Organ Procurement and Transplantation Network (OPTN) for investigation by the Disease Transmission Advisory Committee (DTAC). These cases were referred to the Centers for Disease Control and Prevention (CDC), a member of DTAC, to determine if SARS-CoV-2 transmission from a donor had occurred and, if so, to identify the transmission source, and characterize clinical outcomes in the organ recipients.

Author affiliations: Centers for Disease Control and Prevention, Atlanta, Georgia, USA (J.M. Jones, I. Kracalik, C. Leaumont, S. Lindstrom, B. Whitaker, W. Kuhnert, S.V. Basavaraju); Icahn School of Medicine at Mount Sinai, New York, New York, USA (M.M. Rana, G. Im); University of Chicago, Chicago, Illinois, USA (A. Nguyen); The Ohio State University College of Medicine, Columbus, Ohio, USA (B.C. Keller); Temple University, Philadelphia, Pennsylvania, USA (A. Mishkin); University of Alabama at Birmingham School of Medicine, Birmingham, Alabama, USA (C. Hoopes); Robert Wood Johnson University, New Brunswick, New Jersey, USA (T. Kaleekal); University of Pittsburgh Medical Center, Pittsburgh, Pennsylvania (A. Humar, M.G. Michaels); University of Florida College of Medicine, Gainesville, Florida, USA (J. Vilaro); New York State Department of Health, Albany, New York, USA (L. Smith); Ohio Department of Health, Columbus (A. Justice); University of Texas Southwestern Medical Center, Dallas, Texas, USA (R.M. La Hoz); United Network of Organ Sharing, Richmond, Virginia, USA (D. Klassen)

DOI: https://doi.org/10.3201/eid2702.204046

## The Study

Current OPTN policy requires all US transplant centers and OPOs to report unanticipated potential donor-derived transmission events to the OPTN for investigation by DTAC. CDC coordinates investigations involving pathogens of special interest, including SARS-CoV-2 (Appendix, https://wwwnc.cdc.gov/EID/27/2/20-4046-App1.pdf).

For all reported potential donor-derived SARS-CoV-2 transmissions, CDC, OPO, or the transplant center staff reviewed medical records of organ donors and organ recipients. Recipients who initially tested positive for SARS-CoV-2 infection and triggered a notification to the OPTN of a potential donor-derived transmission were referred to as index recipients; recipients who shared a common donor with index recipients were referred to as co-recipients. CDC investigators asked OPO and index recipients' hospital staff about potential exposures to SARS-CoV-2. Transplant hospital providers monitored organ recipients for symptoms of COVID-19 for ≥14 days following the transplant. Recipients who developed symptoms and, depending on hospital capacity, some asymptomatic recipients were tested for SARS-CoV-2 infection by a nucleic acid test (NAT). All donor serum were tested for the presence of SARS-CoV-2 RNA. Donor respiratory specimens were tested if available.

During March–May 2020, a total of 8 potential donor-derived transmission events involving 8 deceased donors and 31 recipients were reported to OPTN. Each event was reported because an individual transplant recipient (the index recipient) tested positive for SARS-CoV-2 infection (Table 1; Appendix). For all donors included in this study, the cause of death was determined to be a noninfectious etiology. Donor next of kin reported that no donors had had symptoms of COVID-19 or contact with persons known to have COVID-19. One donor was screened for SARS-CoV-2 infection by the OPO using a NAT before organ procurement and tested negative.

Among the 8 index recipients, 4 received lung, 2 received liver, and 2 received heart transplants (Table 2, https://wwwnc.cdc.gov/EID/article/27/2/20-4046-T2.htm). The median age of index recipients was 65 years (range 37–75 years); the median duration from organ transplantation to symptom onset was 9 days (range 6–81 days). Seven (88%) index recipients experienced fever or lower respiratory tract symptoms. Seven index recipients required mechanical ventilation; 3 of them (2 liver recipients and 1 lung recipient) died. All index recipients had potential or confirmed community or healthcare exposure to persons infected with SARS-CoV-2.

Organs from the 8 deceased donors were transplanted into 31 recipients, including the 8 index recipients. Of the 23 co-recipients, 11 (48%) were tested for SARS-CoV-2 infection using a NAT; 1 tested positive 41 days after transplant. Twelve co-recipients were not tested because of absence of symptoms and need to conserve test supplies. Within 14 days after transplant, 3 co-recipients manifested symptoms related to COVID-19, but all tested negative.

## Conclusions

The 8 potential donor-derived SARS-CoV-2 transmissions reported to the OPTN during March–May 2020 were referred to CDC for public health investigation. Although the source of transmission was not definitively established, the available evidence did not suggest transmission occurred from donors.

**Table 1.** Epidemiologic and clinical characteristics of solid organ donors associated with potential SARS-CoV-2 transmission investigations, United States, March–May 2020*

| Donor | Cause of death | Organs procured from donor and transplanted into other recipients | Chest radiograph and chest CT findings | Donor lung disposition | Results of BAL PCR | Results of serum PCR | Results of nasopharyngeal PCR |
|---|---|---|---|---|---|---|---|
| A | Hemorrhagic stroke | Bilateral lungs, liver, left kidney | Bilateral lower lobe consolidations | Both lungs transplanted | Negative | Negative | NT |
| B | Ischemic stroke | Right lung, liver, left kidney | Bilateral lower lobe consolidations | Single lung not allocated in time | NT | Negative | NT |
| C | Opioid overdose | Bilateral lungs, liver, left kidney, right kidney, pancreas | Bilateral lower lobe consolidations | Both lungs transplanted | NT | Negative | NT |
| D | Head trauma | Liver, left kidney, right kidney, heart | Bilateral lower lobe consolidations | Lungs not transplanted because of traumatic damage | NT | Negative | NT |
| E | Hemorrhagic stroke | Bilateral lungs, right kidney, left kidney/split liver, split liver, heart | No focal infiltrates, small pneumomediastinum | Both lungs transplanted | NT | Negative | NT |
| F | Head trauma | Left lung, right lung, liver, and heart | Bilateral lower lobe consolidations | Both lungs transplanted | NT | Negative | NT |
| G | Head trauma | Heart/left kidney, liver, right kidney/pancreas | Bilateral lower lobe consolidations | Lungs not transplanted because of abnormal chest imaging | NT | Negative | NT |
| H | Opioid overdose | Heart, left kidney, right kidney, liver | Patchy ground glass in all lobes | Lungs not transplanted because of abnormal chest imaging | NT | Negative | Negative |

*In the 14 days before death, none of the donors had known contact with someone who had been sick with or received a diagnosis of coronavirus disease, had traveled, or had reported nosocomial transmission of SARS-CoV-2 in the donor hospital. None of the donors experienced symptoms consistent with COVID-19, including fever, cough, and shortness of breath. BAL, bronchoalveolar lavage; CT, computed tompgraphy; COVID-19: coronavirus disease; NT, not tested; SARS-CoV-2, severe acute respiratory syndrome coronavirus 2.

The risk for organ donor-derived SARS-CoV-2 transmission is unknown (*1*,*3*). Transmission of severe acute respiratory syndrome coronavirus, Middle East respiratory syndrome coronavirus, or SARS-CoV-2 from an organ or blood donor to a recipient has not been reported as of November 2020 (*1*). However, recent studies documented the presence of viral particles in organs of patients who had severe COVID-19 or died from COVID-19 (*4*–*6*). Infectious SARS-CoV-2 has been isolated from respiratory specimens, stool (*7*), and urine (*8*), suggesting transmissible virus might be present in extrapulmonary organs. Although these studies suggest that transplant transmission is plausible, the risk for SARS-CoV-2 transmission from extrapulmonary organs of asymptomatic infected deceased donors to organ recipients is unknown. Evidence suggests that the risk for viremia in persons with asymptomatic COVID-19 is low (*9*). However, OPOs should continue to evaluate donors for evidence of SARS-CoV-2 infection (*10*) because transmission of SARS-CoV-2 from organ donor to recipient might be possible and subsequent recipient infection might be severe; evaluating donors could also protect organ procurement and transplantation clinical teams. The American Society of Transplantation has recommended testing all donors by NAT since May 2020. No donors in this study had reported contact with persons with confirmed or suspected COVID-19.

COVID-19 has an estimated incubation period of 2–14 days (10), and all index recipients had confirmed or potential SARS-CoV-2 exposure during the 14 days before symptom onset or diagnosis. No co-recipients contracted COVID-19 within 14 days of transplant, providing further support that the donor was not the source of transmission. Transplant recipients and their healthcare providers should continue to take steps to reduce SARS-CoV-2 exposure.

Of the 8 index recipients in this study, 7 were intubated and 3 died. Seven of the index recipients received their COVID-19 diagnosis within 14 days of transplantation, which suggests that recipients of recent transplants may be at increased risk for severe disease compared with the general population (*11*) and possibly with organ recipients whose transplants were done months or years before SARS-CoV-2 infection (*12*). The advanced age of the index recipients in our study might have contributed to increased illness. Although some COVID-19 case series have suggested that organ transplant recipients are at higher risk for severe disease than the general population, others suggest that disease severity is similar (*2*,*11*). Data are sparse on the clinical severity of COVID-19 in recently transplanted organ recipients.

This study is subject to the following limitations. First, 7 of 8 donors were not tested for SARS-CoV-2 before transplant, and stored respiratory specimens were unavailable for retrospective testing. Although donor serum specimens were tested by NAT, limited performance and sensitivity data are available for this sample type using this test, and SARS-CoV-2 viremia is likely uncommon and intermittent (*1*). Second, donors and recipients might have had contact with unidentified persons with SARS-CoV-2 infection, including asymptomatic or presymptomatic persons (*13*). Asymptomatic SARS-CoV-2 infection might not have been detected in co-recipients given the low rate of testing (<50%). Finally, donor-derived SARS-CoV-2 transmission might not have been recognized by transplant clinicians and therefore not reported for investigation.

COVID-19 in the organ transplant recipients we report appears to have been community- or hospital-acquired. These findings suggest that organ transplant recipients, particularly in the immediate posttransplant period, might be at increased risk for severe COVID-19. Measures to limit household and healthcare-associated SARS-CoV-2 transmission to recipients should be implemented (*10*,*14*,*15*). All suspected donor-derived SARS-CoV-2 infections should be reported to the OPTN for further investigation.

**Acknowledgments**

We thank members of the Disease Transmission Advisory Committee and staff from the United Network of Organ Sharing staff, organ procurement organizations, and transplant centers for their assistance with the investigations.

## About the Author

Dr. Jones is a medical epidemiologist at the Office of Blood, Organ, and Other Tissue Safety, Division of Healthcare Quality Promotion, National Center for Emerging and Zoonotic Infectious Diseases, Centers for Disease Control and Prevention. Current research interests include infectious disease transmission through blood transfusion and organ transplantation and other medical product of human origin safety issues.

### References

1. Kates OS, Fisher CE, Rakita RM, Reyes JD, Limaye AP. Use of SARS-CoV-2-infected deceased organ donors: Should we always "just say no?". Am J Transplant. 2020;20:1787–94. https://doi.org/10.1111/ajt.16000
2. Molnar MZ, Bhalla A, Azhar A, Tsujita M, Talwar M, Balaraman V, et al.; STOP-COVID Investigators. Outcomes of

critically ill solid organ transplant patients with COVID-19 in the United States. Am J Transplant. 2020;20:3061–71. https://doi.org/10.1111/ajt.16280
3. Shah MB, Lynch RJ, El-Haddad H, Doby B, Brockmeier D, Goldberg DS. Utilization of deceased donors during a pandemic: argument against using SARS-CoV-2–positive donors. Am J Transplant. 2020;20:1795–9. https://doi.org/10.1111/ajt.15969
4. Puelles VG, Lütgehetmann M, Lindenmeyer MT, Sperhake JP, Wong MN, Allweiss L, et al. Multiorgan and renal tropism of SARS-CoV-2. N Engl J Med. 2020;383:590–2. https://doi.org/10.1056/NEJMc2011400
5. Wichmann D, Sperhake JP, Lütgehetmann M, Steurer S, Edler C, Heinemann A, et al. Autopsy findings and venous thromboembolism in patients with COVID-19. Ann Intern Med. 2020;173:268–77. https://doi.org/10.7326/M20-2003
6. Lindner D, Fitzek A, Bräuninger H, Aleshcheva G, Edler C, Meissner K, et al. Association of cardiac infection with SARS-CoV-2 in confirmed COVID-19 autopsy cases. JAMA Cardiol. 2020. https://doi.org/10.1001/jamacardio.2020.3551
7. Xiao F, Sun J, Xu Y, Li F, Huang X, Li H, et al. Infectious SARS-CoV-2 in feces of patient with severe COVID-19. Emerg Infect Dis. 2020;26:1920–2. https://doi.org/10.3201/eid2608.200681
8. Sun J, Zhu A, Li H, Zheng K, Zhuang Z, Chen Z, et al. Isolation of infectious SARS-CoV-2 from urine of a COVID-19 patient. Emerg Microbes Infect. 2020;9:991–3. https://doi.org/10.1080/22221751.2020.1760144
9. Chang L, Zhao L, Gong H, Wang L, Wang L. Severe acute respiratory syndrome coronavirus 2 RNA detected in blood donations. Emerg Infect Dis. 2020;26:1631–3. https://doi.org/10.3201/eid2607.200839
10. American Society of Transplantation. COVID-19 resources for transplant community. 2020 [cited 2020 June 24]. https://www.myast.org/covid-19-information
11. Kates OS, Haydel BM, Florman SS, Rana MM, Chaudhry ZS, Ramesh MS, et al.; UW COVID-19 SOT Study Team. COVID-19 in solid organ transplant: a multicenter cohort study. Clin Infect Dis. 2020;ciaa1097. https://doi.org/10.1093/cid/ciaa1097
12. Ravanan R, Callaghan CJ, Mumford L, Ushiro-Lumb I, Thorburn D, Casey J, et al. SARS-CoV-2 infection and early mortality of wait-listed and solid organ transplant recipients in England: a national cohort study. Am J Transplant. 2020;20:3008–18. https://doi.org/10.1111/ajt.16247
13. CDC COVID-19 Response Team. Characteristics of health care personnel with COVID-19—United States, February 12–April 9, 2020. MMWR Morb Mortal Wkly Rep. 2020;69:477–81.
14. Centers for Disease Control and Prevention. If you are immunocompromised, protect yourself from COVID-19. May 14, 2020 [cited 2020 June 24]. https://www.cdc.gov/coronavirus/2019-ncov/need-extra-precautions/immunocompromised.html
15. Centers for Disease Control and Prevention. Interim infection prevention and control recommendations for healthcare personnel during the coronavirus disease 2019 (COVID-19) pandemic. 2019 [cited 2020 June 24]. https://www.cdc.gov/coronavirus/2019-ncov/hcp/infection-control-recommendations.html.

Address for correspondence: Jefferson Jones, Centers for Disease Control and Prevention, 1600 Clifton Rd NE, Mailstop V18-4, Atlanta, GA 30329-4027, USA; email: ioe8@cdc.gov

# COVID-19 and Fatal Sepsis Caused by Hypervirulent *Klebsiella pneumoniae*, Japan, 2020

Tomohiro Hosoda, Sohei Harada, Koh Okamoto, Sumire Ishino, Makoto Kaneko, Masahiro Suzuki, Ryota Ito, Miyuki Mizoguchi

A patient in Japan with coronavirus disease and hypervirulent *Klebsiella pneumoniae* K2 sequence type 86 infection died of respiratory failure. Bacterial and fungal co-infections caused by region-endemic pathogens, including hypervirulent *K. pneumoniae* in eastern Asia, should be included in the differential diagnosis of coronavirus disease patients with acutely deteriorating condition.

For a minority of patients, bacterial and fungal co-infections can complicate the course of coronavirus disease (COVID-19) (*1*,*2*). Co-infection can contribute to the poor prognosis for patients with COVID-19, especially for high-risk populations such as elderly patients (*3*). Indeed, a large retrospective multicenter study reported that for half of the patients who died of COVID-19, secondary bacterial co-infection developed during hospitalization (*3*). In a retrospective study in China, the second most common respiratory pathogen detected from patients with COVID-19 was *Klebsiella pneumoniae*, following only *Streptococcus pneumoniae* (*4*).

Hypervirulent *K. pneumoniae* (hvKp) was originally recognized as a pathogen that causes severe community-acquired infections among relatively healthy persons. hvKp isolates carry virulence plasmids that harbor cardinal virulence genes, and with higher frequency than classical *K. pneumoniae* they cause disseminated infections involving liver, lungs, central nervous system, and eyes (*5*,*6*). Although hvKp infections have been reported mainly from hvKp-endemic areas such as eastern Asia, in recent years, sporadic cases have been increasingly reported worldwide (*7*). Furthermore, recent studies from hvKp-endemic areas demonstrated that hvKp is often associated with healthcare and hospitalization for elderly and debilitated populations (*8*,*9*). A multicenter study in Japan showed that more than half of bloodstream infections caused by hvKp occurred as healthcare-associated or hospital-acquired infections (*8*).

Therefore, hvKp infections may have the potential for seriously complicating the course of COVID-19, especially in hvKp-endemic areas. We describe a fatal case of superimposed hvKp infection in an elderly woman with COVID-19 in Japan.

## The Case

In August 2020, an 87-year-old woman sought care at an emergency department for a 4-day history of fever and dry cough. The day before, COVID-19 had been diagnosed for 2 family members living with her. The woman had hypertension, dyslipidemia, and dementia and had been receiving outpatient care at a nursing home 5 days a week. At admission, her vital signs were temperature 37.7°C, blood pressure 202/93 mm Hg, pulse rate 61 beats/min, respiratory rate 16 breaths/min, and oxygen saturation 95% while breathing ambient air. Physical examination findings were otherwise unremarkable. Laboratory studies revealed 2,660 leukocytes/µL, including 811 lymphocytes/µL; $13.8 \times 10^4$ platelets/µL; aspartic aminotransferase 36 U/L; alanine transaminase 22 U/L; creatinine 0.81 mg/dL; blood glucose 83 mg/dL; and ferritin 268.2 ng/mL. Coagulation studies showed elevated D-dimer of 0.8 µg/mL with prothrombin time or activated partial thromboplastin time within normal range. COVID-19 was diagnosed on the basis of a positive COVID-19 rapid antigen test result (ESPLINE SARS-CoV-2; Fujirebio Diagnostics,

Author affiliations: Kawasaki Municipal Hospital, Kanagawa, Japan (T. Hosoda, S. Ishino, M. Kaneko); The University of Tokyo Hospital, Tokyo, Japan (S. Harada, K. Okamoto, M. Mizoguchi); Fujita Health University School of Medicine, Aichi, Japan (M. Suzuki, R. Ito)

DOI: https://doi.org/10.3201/eid2702.204662

https://www.fujirebio.com). Shortly after admission, the patient became hypoxic (oxygen saturation 89% while breathing ambient air) and required supplemental oxygen delivered by nasal cannula at 2 L/min.

On hospitalization day 2, a chest radiograph showed no infiltrates (Figure 1, panel A); dexamethasone (6 mg/d) was initiated out of concern for hypoxia from COVID-19. Over the next 2 days, fever and dry cough subsided, and hypoxia gradually improved to an oxygen saturation of 96% while breathing ambient air. On hospitalization day 7, she experienced fever with productive cough and hypoxia (oxygen saturation of 90% while breathing supplemental oxygen at 6 L/min through a nonrebreathing oxygen mask). A chest radiograph revealed infiltrates in the left lung with pleural effusion (Figure 1, panel B). Ampicillin/sulbactam was started. On hospital day 8, her condition rapidly deteriorated; hypoxia and the lung infiltrates in the left lung worsened (Figure 1, panel C). The antimicrobial drug was switched to piperacillin/tazobactam. The patient and her family did not request escalation of her care to intensive care, which would have included mechanical ventilation; on hospitalization day 9, she died of respiratory failure.

Sputum and blood collected for culture on hospitalization day 7, along with sputum collected for culture on the day of admission, grew *K. pneumoniae*. All 3 isolates were positive by string test (showed viscous strings >5 mm when stretched with a standard inoculation rod) (Figure 2) and were susceptible to all antimicrobial drugs tested except ampicillin. We analyzed the virulence gene profiles of these isolates by using multiplex PCR as described previously (*10*), and we identified carriage of genes for capsular genotype K2, *iutA*, *rmpA*, *entB*, *mrkD*, and *ybtS*. Multilocus sequence typing with standardized protocol demonstrated that these isolates belonged to sequence type (ST) 86 (*11*). We further analyzed the isolate from blood (FUJ01174) with whole-genome sequencing by using Miseq (Illumina, https://www.illumina.com) as described previously (*8*), and we confirmed carriage of virulence genes *rmpA*, *rmpA2*, *iroBCDN*, *irp1*, *iucABCD*, *iutA*, *ybtARPQSTUX*, *kvgAS*, *fyuA*, and *mrkABDFHIJ* by using the *Klebsiella* locus/sequence definitions database (https://bigsdb.pasteur.fr/klebsiella). In addition, we identified *Peg-344* with a manual BLASTn (https://blast.ncbi.nlm.nih.gov) search (reference sequence, GenBank accession no. AP006726). Assembled contigs covered the nucleotide sequence of pLVPK (GenBank accession no. AY378100), a prototypical *K. pneumoniae* virulence plasmid, with 91.8% coverage and 99.9% identity (Appendix, https://wwwnc.cdc.gov/EID/article/27/2/20-4662-App1.pdf). We deposited genomic sequences of the FUJ01174 strain in the National Center for Biotechnology Information database under BioSample accession no. SAMN16787939.

## Conclusions

For this COVID-19 patient who died of superimposed *K. pneumoniae* infection, the causative strain recovered from blood and sputum belonged to K2-ST86, a prototypical hvKp, together with K1-ST23. Furthermore, the isolate carried the cardinal hvKp virulence genes *rmpA*, *rmpA2*, *iroBCDN*, *iucABCD*, and *peg-344*, which have been recognized as molecular markers for the identification of hvKp that carry high risk for disseminated and fatal infections (*6*,*8*).

This case highlights 2 implications for the management of COVID-19 patients. First, bacterial and fungal co-infection may occur relatively early in the

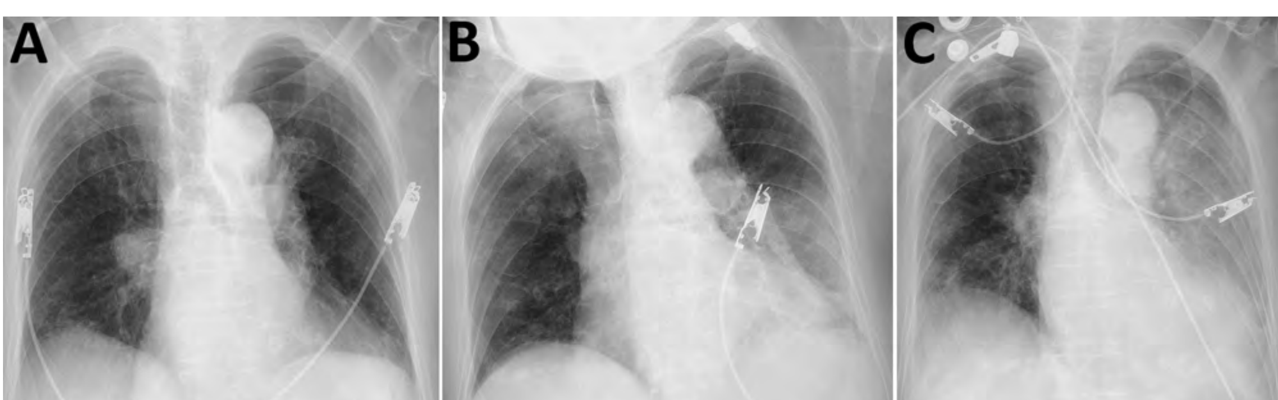


**Figure 1**. Chest radiographs (anteroposterior views) of hospitalized patient with coronavirus disease and fatal superimposed hypervirulent *Klebsiella pneumoniae* K2 sequence type 86 infection, Japan, 2020. A) Hospitalization day 1 (admission), showing no ground glass opacity and consolidation. B) Hospitalization day 7, showing asymmetric infiltrates with pleural effusion, mainly in left lung. C) Hospitalization day 8, showing infiltrate spread to right lower lung and worsened pleural effusion in left lung.

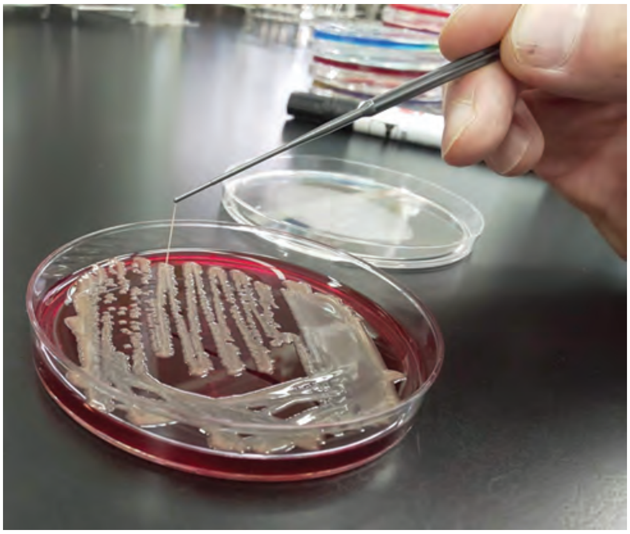

**Figure 2.** Positive string test result for *Klebsiella pneumoniae* isolate from blood of patient with coronavirus disease and fatal superimposed hypervirulent *Klebsiella pneumoniae* K2 sequence type 86 infection, Japan, 2020.

course of COVID-19. The condition of the patient reported here rapidly deteriorated 10 days after symptom onset; she had initially recovered after admission and treatment with dexamethasone. Although the timing (10 days after symptom onset) was typical for acute respiratory distress syndrome and acute cardiac injury resulting from COVID-19 itself (*12*), this patient instead experienced a fatal bacterial infection. Given the low prevalence of bacterial co-infections among COVID-19 patients, judicious use of antimicrobial drugs is recommended (*13*). However, this case emphasizes that timely antimicrobial treatment is crucial for patients with suspected or confirmed bacterial co-infection. Furthermore, corticosteroid treatment for COVID-19 may increase the risk for and severity of bacterial co-infection. Therefore, consideration for empiric antimicrobial therapy and thorough evaluation for bacterial co-infection should be considered for COVID-19 patients with acutely deteriorating condition. Second, local epidemiology should be considered when presuming a causative pathogen for patients with bacterial and fungal co-infections (*14*). Prevalence of hvKp infection in eastern Asia is exceptionally high (*8*). It is possible that a substantial number of superimposed hvKp infections complicating COVID-19 may have been unrecognized because the microbiological criteria for diagnosing hvKp widely used at microbiology laboratories in healthcare facilities (identifying carriage of genes for capsular genotype and string test) may not have been routinely available. For the case we report, respiratory colonization of hypermucoviscous *K. pneumoniae* was noted on culture at admission. Because colonization by hvKp is an established risk factor for subsequent hvKp invasive disease (*15*), additional caution is required for superimposed hvKp infections when caring for COVID-19 patients known to be colonized with hvKp.

In conclusion, we report a fatal case of hvKp infection superimposed on a patient with COVID-19. When the condition of COVID-19 patients worsens, bacterial and fungal infections, including region-endemic infections (hvKP in eastern Asia), should be included as a differential diagnosis and require appropriate evaluation and treatment in a timely fashion.

## About the Author

Dr. Hosoda is a clinician who specializes in infectious disease at the Kawasaki Municipal Hospital, Kawasaki, Japan. His research interests include hospitalization-associated disability resulting from COVID-19, especially for elderly patients.

## References

1. Rawson TM, Moore LSP, Zhu N, Ranganathan N, Skolimowska K, Gilchrist M, et al. Bacterial and fungal co-infection in individuals with coronavirus: a rapid review to support COVID-19 antimicrobial prescribing. Clin Infect Dis. 2020 May 2 [Epub ahead of print]. https://doi.org/10.1093/cid/ciaa530
2. Hughes S, Troise O, Donaldson H, Mughal N, Moore LSP. Bacterial and fungal coinfection among hospitalized patients with COVID-19: a retrospective cohort study in a UK secondary-care setting. Clin Microbiol Infect. 2020;26:1395–9. https://doi.org/10.1016/j.cmi.2020.06.025
3. Zhou F, Yu T, Du R, Fan G, Liu Y, Liu Z, et al. Clinical course and risk factors for mortality of adult inpatients with COVID-19 in Wuhan, China: a retrospective cohort study. Lancet. 2020;395:1054–62. https://doi.org/10.1016/S0140-6736(20)30566-3
4. Zhu X, Ge Y, Wu T, Zhao K, Chen Y, Wu B, et al. Co-infection with respiratory pathogens among COVID-2019 cases. Virus Res. 2020;285:198005. https://doi.org/10.1016/j.virusres.2020.198005
5. Siu LK, Yeh KM, Lin JC, Fung CP, Chang FY. *Klebsiella pneumoniae* liver abscess: a new invasive syndrome. Lancet Infect Dis. 2012;12:881–7. https://doi.org/10.1016/S1473-3099(12)70205-0
6. Russo TA, Marr CM. Hypervirulent *Klebsiella pneumoniae*. Clin Microbiol Rev. 2019;32:e00001–19. https://doi.org/10.1128/CMR.00001-19
7. Struve C, Roe CC, Stegger M, Stahlhut SG, Hansen DS, Engelthaler DM, et al. Mapping the evolution of hypervirulent *Klebsiella pneumoniae*. MBio. 2015;6:e00630. https://doi.org/10.1128/mBio.00630-15
8. Harada S, Aoki K, Yamamoto S, Ishii Y, Sekiya N, Kurai H, et al. Clinical and molecular characteristics of *Klebsiella pneumoniae* isolates causing bloodstream infections in Japan: occurrence of hypervirulent infections in

health care. J Clin Microbiol. 2019;57:e01206–19. https://doi.org/10.1128/JCM.01206-19

9. Liu C, Du P, Xiao N, Ji F, Russo TA, Guo J. Hypervirulent *Klebsiella pneumoniae* is emerging as an increasingly prevalent *K. pneumoniae* pathotype responsible for nosocomial and healthcare-associated infections in Beijing, China. Virulence. 2020;11:1215–24. https://doi.org/10.1080/21505594.2020.1809322
10. Compain F, Babosan A, Brisse S, Genel N, Audo J, Ailloud F, et al. Multiplex PCR for detection of seven virulence factors and K1/K2 capsular serotypes of *Klebsiella pneumoniae*. J Clin Microbiol. 2014;52:4377–80. https://doi.org/10.1128/JCM.02316-14
11. Diancourt L, Passet V, Verhoef J, Grimont PA, Brisse S. Multilocus sequence typing of *Klebsiella pneumoniae* nosocomial isolates. J Clin Microbiol. 2005;43:4178–82. https://doi.org/10.1128/JCM.43.8.4178-4182.2005
12. Sieswerda E, de Boer MGJ, Bonten MMJ, Boersma WG, Jonkers RE, Aleva RM, et al. Recommendations for antibacterial therapy in adults with COVID-19–an evidence based guideline. Clin Microbiol Infect. 2020 Oct 1 [Epub ahead of print].
13. Hu B, Guo H, Zhou P, Shi ZL. Characteristics of SARS-CoV-2 and COVID-19. Nat Rev Microbiol. 2020 Oct 6 [Epub ahead of print]. PubMed https://doi.org/10.1038/s41579-020-00459-7
14. Basso RP, Poester VR, Benelli JL, Stevens DA, Zogbi HE, Vasconcellos ICDS, et al. COVID-19-associated histoplasmosis in an AIDS patient. Mycopathologia. 2020 Nov 6 [Epub ahead of print]. PubMed
15. Gorrie CL, Mirceta M, Wick RR, Edwards DJ, Thomson NR, Strugnell RA, et al. Gastrointestinal carriage is a major reservoir of *Klebsiella pneumoniae* infection in intensive care patients. Clin Infect Dis. 2017;65:208–15. https://doi.org/10.1093/cid/cix270



Address for correspondence: Tomohiro Hosoda, Kawasaki Municipal Hospital, Infectious Diseases, 12-1 Shinkawadori Kawasaki-ku Kawasaki, Kanagawa 210-0013 Japan; email: ottotto723@gmail.com

# Non-Norovirus Viral Gastroenteritis Outbreaks Reported to the National Outbreak Reporting System, USA, 2009–2018

Claire P. Mattison, Molly Dunn, Mary E. Wikswo, Anita Kambhampati, Laura Calderwood, Neha Balachandran, Eleanor Burnett, Aron J. Hall

During 2009–2018, four adenovirus, 10 astrovirus, 123 rotavirus, and 107 sapovirus gastroenteritis outbreaks were reported to the US National Outbreak Reporting System (annual median 30 outbreaks). Most were attributable to person-to-person transmission in long-term care facilities, daycares, and schools. Investigations of norovirus-negative gastroenteritis outbreaks should include testing for these viruses.

In the United States, ≈179 million cases of acute gastroenteritis (AGE) occur annually (*1*). Norovirus is the leading cause of AGE in the United States; other viral causes include adenovirus (specifically group F or types 40 and 41), astrovirus, sapovirus, and rotavirus (*2*,*3*). These viruses are spread primarily through the fecal–oral route through person-to-person contact or through contaminated food, water, or fomites (*4*–*8*).

The epidemiology of outbreaks associated with sapovirus, another calicivirus, adenovirus types 40 and 41, and astrovirus is not well understood (*6*). In addition, our understanding of rotavirus is evolving in the postvaccine era. In 2009, the Centers for Disease Control and Prevention launched the National Outbreak Reporting System (NORS), which collects information from local, state, and territorial health departments on foodborne, waterborne, and enteric disease outbreaks (*9*). To inform prevention efforts, we describe AGE outbreaks caused by adenovirus, astrovirus, sapovirus, and rotavirus that were reported to NORS during 2009–2018.

Author affiliations: Centers for Disease Control and Prevention, Atlanta, GA, USA (C.P. Mattison, M. Dunn, M.E. Wikswo, A. Kambhampati, L. Calderwood, N. Balachandran, E. Burnett, A.J. Hall); Cherokee Nation Assurance, Arlington, Virginia, USA (C.P. Mattison, A. Kambhampati, N. Balachandran); Oak Ridge Institute for Science and Education, Oak Ridge, Tennessee, USA (L. Calderwood)

DOI: https://doi.org/10.3201/eid2702.203943

## The Study

NORS is a dynamic, voluntary outbreak reporting system. For each reported outbreak, health departments report the mode of transmission, number of confirmed and suspected cases, and aggregate epidemiologic and demographic information as available. NORS defines outbreaks as ≥2 cases of similar illness associated with a common exposure or epidemiologic link (*9*). Health departments determine reported outbreak etiologies on the basis of available laboratory, epidemiologic, and clinical data; specific laboratory testing protocols vary by health department. Outbreak etiologies are considered confirmed when ≥2 laboratory-confirmed cases are reported and considered suspected when <2 laboratory-confirmed cases are reported. Outbreaks are considered to have multiple etiologies when >1 etiology is confirmed or suspected.

Our analysis includes NORS data from outbreaks occurring during January 1, 2009–December 31, 2018 with adenovirus, astrovirus, rotavirus, or sapovirus as a confirmed or suspected etiology. NORS waterborne outbreak data were available through December 31, 2017. Data were extracted December 4, 2019.

Sex, age, symptom, and clinical outcomes percentages were calculated using the total number of cases for which information was available. Outbreak size and duration were compared by using the Kruskall–Wallis test. Analyses were performed by using SAS 9.4 (SAS Institute Inc., https://www.sas.com).

During 2009–2018, a total of 323 (1.2%) of 28,071 outbreaks reported to NORS had a reported etiology, including adenovirus, astrovirus, rotavirus, or sapovirus. A single etiology was reported in 244 (75.5%) outbreaks, of which 184 (57.0%) were confirmed (Table 1); of these 244 outbreaks, rotavirus accounted for 123 (50.4%), sapovirus for 107 (43.9%), astrovirus for 10 (4.1%), and adenovirus for 4 (1.6%). Multiple

**Table 1.** Summary of outbreak characteristics, by suspected or confirmed outbreak etiology, for outbreaks attributable to adenovirus, astrovirus, rotavirus, or sapovirus, National Outbreak Reporting System, USA, 2009–2018*

| | Etiology | | | | | |
|---|---|---|---|---|---|---|
| Characteristic | Adenovirus | Astrovirus | Rotavirus | Sapovirus | All single-etiology | Multiple etiologies† |
| No. outbreaks | | | | | | |
| Total | 4 | 10 | 123 | 107 | 244 | 79 |
| Annual median | 0 | 1 | 9 | 12 | 26 | 4 |
| States or territories | 3 | 6 | 28 | 22 | 32 | 22 |
| Confirmed or suspected | | | | | | |
| Confirmed | 3 (75) | 5 (50) | 70 (56.9) | 70 (65.4) | 148 (60.7) | 29 (36.7)‡ |
| Suspected, 1 positive | 1 (25) | 5 (50) | 30 (24.4) | 25 (23.4) | 61 (25.0) | 36 (45.6)‡ |
| Suspected, 0 positives | – | – | 23 (18.7) | 12 (11.2) | 35 (14.3) | 14 (17.7)‡ |
| Median duration, d (range) | 19 (6–39) | 11 (1–22) | 11 (1–39) | 9 (1–65) | 10 (1–65) | 18 (1–121) |
| Mode of transmission | | | | | | |
| Person-to-person | 3 (75) | 6 (60) | 104 (84.5) | 77 (72) | 190 (77.9) | 65 (82.3) |
| Foodborne | – | 1 (10) | 4 (3.3) | 15 (14) | 20 (8.2) | 4 (5.1) |
| Waterborne | 1 (25) | – | – | – | 1 (0.4) | – |
| Indeterminate or unknown | – | 3 (30) | 15 (12.2) | 15 (14) | 33 (13.5) | 10 (12.6) |
| Setting of exposure | | | | | | |
| Long-term care facility | – | 2 (20) | 80 (65.0) | 63 (58.9) | 145 (59.4) | 26 (32.9) |
| Child daycare | – | 2 (20) | 19 (15.4) | 6 (5.6) | 27 (11.1) | 28 (35.4) |
| School or university | 1 (25) | 3 (30) | 4 (3.3) | 12 (11.2) | 20 (8.2) | 10 (12.7) |
| Restaurant or catering | – | 1 (10) | 2 (1.6) | 13 (12.1) | 16 (6.6) | 2 (2.5) |
| Healthcare facility | 1 (25) | 1 (10) | 1 (0.8) | 1 (0.9) | 4 (1.6) | 3 (3.8) |
| Other, indeterminate, or missing | 2 (50) | 1 (10) | 17 (13.8) | 12 (11.2) | 32 (13.1) | 10 (12.7) |
| Year | | | | | | |
| 2009 | – | – | 8 (6.5) | 2 (1.9) | 10 (4.1) | 1 (1.3) |
| 2010 | – | – | 7 (5.7) | – | 7 (2.9) | 1 (1.3) |
| 2011 | – | 1 (10) | 6 (4.9) | 3 (2.8) | 10 (4.1) | 4 (5.1) |
| 2012 | 1 (25) | 1 (10) | 5 (4.1) | 10 (9.3) | 17 (7.0) | 3 (3.8) |
| 2013 | – | – | 10 (8.1) | 12 (11.2) | 22 (9.0) | 4 (5.1) |
| 2014 | – | – | 10 (8.1) | 21 (19.6) | 31 (12.7) | 3 (3.8) |
| 2015 | 1 (25) | 2 (20) | 37 (30.1) | 13 (12.1) | 53 (21.7) | 6 (7.6) |
| 2016 | – | 4 (40) | 8 (6.5) | 18 (16.8) | 30 (12.3) | 8 (10.1) |
| 2017 | 1 (25) | 1 (10) | 16 (13.0) | 16 (15.0) | 34 (13.9) | 25 (31.6) |
| 2018 | 1 (25) | 1 (10) | 16 (13.0) | 12 (11.2) | 30 (12.3) | 24 (30.4) |

*Values are no. (%) unless otherwise indicated. –, no outbreak reported.
†Outbreaks attributable to adenovirus (14), astrovirus (15), rotavirus (34), or sapovirus (33) along with ≥1 other etiology. The most common combinations reported were rotavirus and norovirus (19 outbreaks); sapovirus and norovirus (7 outbreaks); sapovirus, norovirus, and astrovirus (7 outbreaks); and adenovirus and norovirus (4 outbreaks).
‡Confirmed or suspected for ≥1 of the 4 viruses of interest. Suspected (1 positive) outbreaks include 7 outbreaks where 1 viral etiology of interest was confirmed and another viral etiology was suspected, with a single positive result.

etiologies were reported in 79 (24.5%) of the 323 outbreaks; 51 (64.5%) of the 79 also included norovirus as an etiology. The most common etiology combinations were rotavirus and norovirus (19 [24.1%]), sapovirus and norovirus (7 [8.9%]), and sapovirus, norovirus, and astrovirus (7 [8.9%]).

A median 30 outbreaks were reported per year (range 8–59 outbreaks). Reporting increased over time; most (62.0%) multiple-etiology outbreaks were reported during 2017–2018 (Table 1). Outbreaks were reported by 31 states and Puerto Rico; 5 states (Wisconsin [63 (19.5%)], Oregon [51 (15.8%)], Ohio [31 (9.6%)], Virginia [19 (5.9%)], and Illinois [19 (5.9%)]) accounted for >50% of reports. Subsequent results are presented for single-etiology outbreaks only.

Median outbreak size (17 cases [p = 0.62]) (Table 2) and outbreak duration (10 days [p = 0.30]) (Table 1) did not differ between etiologies. Most astrovirus (8 [80%]) and sapovirus (78 [72.9%]) outbreaks occurred during November–April. Most rotavirus outbreaks occurred during January–May (102 [82.9%]) (Figure 1).

The most common modes of transmission were person-to-person (190 [77.9%]), indeterminate or unknown (33 [13.5%]), and foodborne (20 [8.2%]) (Table 1). Most foodborne outbreaks were attributable to sapovirus (15 [75.0%]). Common outbreak settings included long-term care facilities (LTCFs) (145 [59.4%]), child daycares (27 [11.1%]), and schools (20 [8.2%]) (Table 1). Most rotavirus (80 [65.0%]) and sapovirus (63 [58.9%]) outbreaks occurred in LTCFs.

Among 3,688 cases for which data were available, 64.2% were in women and girls. Cases occurred among all age groups (Table 2). Compared with 20.4% of astrovirus outbreak cases, higher percentages (37.5%–42.0%) of adenovirus, rotavirus, and sapovirus outbreak cases were among persons >50 years old. Rotavirus outbreaks had the highest proportion of cases in children <1 year old (4.0%) and 1–4 years old (19.1%).

**Table 2.** Summary of outbreak case characteristics by suspected or confirmed outbreak etiology for outbreaks reporting adenovirus, astrovirus, rotavirus, or sapovirus — National Outbreak Reporting System, 2009–2018*

| | Etiology | | | | | |
|---|---|---|---|---|---|---|
| Characteristic | Adenovirus | Astrovirus | Rotavirus | Sapovirus | All single-etiology | Multiple etiologies† |
| No. outbreak cases | | | | | | |
| Total | 83 | 275 | 2,526 | 3,112 | 5,996 | 5,278 |
| Median | 19 | 20.5 | 16 | 17 | 17 | 18 |
| Range | 13–32 | 9–84 | 2–82 | 2–528 | 2–528 | 2–2,274 |
| Sex | | | | | | |
| No. cases with information | 82 | 162 | 1,750 | 1,694 | 3,688 | 4,070 |
| F | 36 (43.9) | 98 (60.5) | 1,171 (66.9) | 1,062 (62.7) | 2,367 (64.2) | 2,365 (58.1) |
| M | 46 (56.1) | 64 (39.5) | 579 (33.1) | 632 (37.3) | 1,321 (35.8) | 1,705 (41.9) |
| Age group, y | | | | | | |
| No. cases with information | 40 | 142 | 1,161 | 2,071 | 3,414 | 3,676 |
| <1 | 0 | 3 (2.1) | 47 (4.0) | 3 (0.1) | 53 (1.6) | 109 (3.0) |
| 1–4 | 1 (2.5) | 17 (12.0) | 222 (19.1) | 75 (3.6) | 314 (9.2) | 375 (10.2) |
| 5–9 | 7 (17.5) | 27 (19.0) | 185 (15.9) | 350 (16.9) | 569 (16.7) | 1,817 (49.4) |
| 10–49 | 17 (42.5) | 66 (46.5) | 221 (19) | 854 (41.2) | 1,158 (33.9) | 1,034 (28.1) |
| ≥50 | 15 (37.5) | 29 (20.4) | 487 (42.0) | 789 (38.1) | 1,320 (38.7) | 340 (9.3) |
| Clinical outcome‡ | | | | | | |
| Hospitalization | 21/71 (29.6) | 0/221 (0) | 87/2,030 (4.2) | 17/2,154 (0.8) | 125/4,476 (2.8) | 44/4,189 (1.1) |
| Death | 2/71 (2.8) | 0/275 (0) | 8/2,127 (0.4) | 2/2,283 (0.09) | 12/4,756 (0.25) | 5 /4,273 (0.1) |

*Values are no. (%) unless otherwise indicated.
†Outbreaks attributable to adenovirus (14), astrovirus (15), rotavirus (34), or sapovirus (33) along with ≥1 other etiology. The most common combinations reported were rotavirus and norovirus (19 outbreaks); sapovirus and norovirus (7 outbreaks); sapovirus, norovirus, and astrovirus (7 outbreaks); and adenovirus and norovirus (4 outbreaks).
‡No. cases/no. cases with data available (%).

Among adenovirus outbreaks, 58.8% of case-patients reported fever, 54.5% reported diarrhea, and 40.4% reported vomiting. Across the other 3 viral etiologies, diarrhea was the most reported symptom, followed by vomiting and fever (Figure 2). Bloody stools were reported for <2% of case-patients (data not shown). Adenovirus outbreaks were responsible for the highest proportions of hospitalized case-patients (21 [29.6%]) and deaths (2 [2.8%]) (Table 2).

## Conclusions

During 2009–2018, a total of 323 outbreaks caused by adenovirus, astrovirus, rotavirus, or sapovirus were reported to NORS. These 4 viral pathogens typically cause mild, self-limiting illness, as evidenced by the low reported hospitalization and case-fatality rates. In adenovirus outbreaks, >25% of case-patients were hospitalized and >50% reported fever, but because of the low number of outbreaks reported, these characteristics are likely not representative of all enteric adenovirus infections. Like norovirus outbreaks, astrovirus and sapovirus outbreaks often occurred in closed settings, were mostly transmitted through person-to-person contact or foodborne transmission, and had winter seasonality (*6*,*10*).

In the United States, rotavirus vaccination has substantially reduced incidence in younger, vaccinated populations and indirectly benefitted older, unvaccinated populations (*11*). Reported rotavirus outbreaks affected both young and older populations, and most occurred in LTCFs. Like other viral AGE etiologies, rotavirus is most often transmitted through person-to-person contact, spreads easily in closed settings, and most commonly causes diarrhea and vomiting. Sapovirus, astrovirus, and rotavirus should thus be considered in outbreaks initially suspected to be norovirus where case-patients have negative results.

All 4 viruses discussed in this report have low infectious doses, are shed asymptomatically and postsymptomatically, and can survive on surfaces, facilitating transmission in closed or semi-closed settings (*4*–*6*,*8*,*12*). Existing viral AGE outbreak prevention and control recommendations (i.e., handwashing, surface disinfection with appropriate products [e.g., bleach-based cleaners], exclusion of symptomatic persons from daycare, school, or work and food preparation for others until 48 hours after symptoms resolve [*13*]) are useful against viral AGE of all etiologies.

Many viral gastrointestinal outbreaks go unreported, and determination of outbreak etiology varies based on testing availability; adenovirus, astrovirus, and sapovirus testing only recently became widely available through multipathogen test panels (*14*). In 2012, the Centers for Disease Control and Prevention established the Unexplained Viral Diarrhea network in partnership with the California, Minnesota, and Oregon state public health laboratories to comprehensively test stool specimens from norovirus-negative outbreaks to better understand the burden of these viruses (*15*). This network partially explains the geographic heterogeneity of outbreak reports in NORS; as such, the observed geographic variability is most

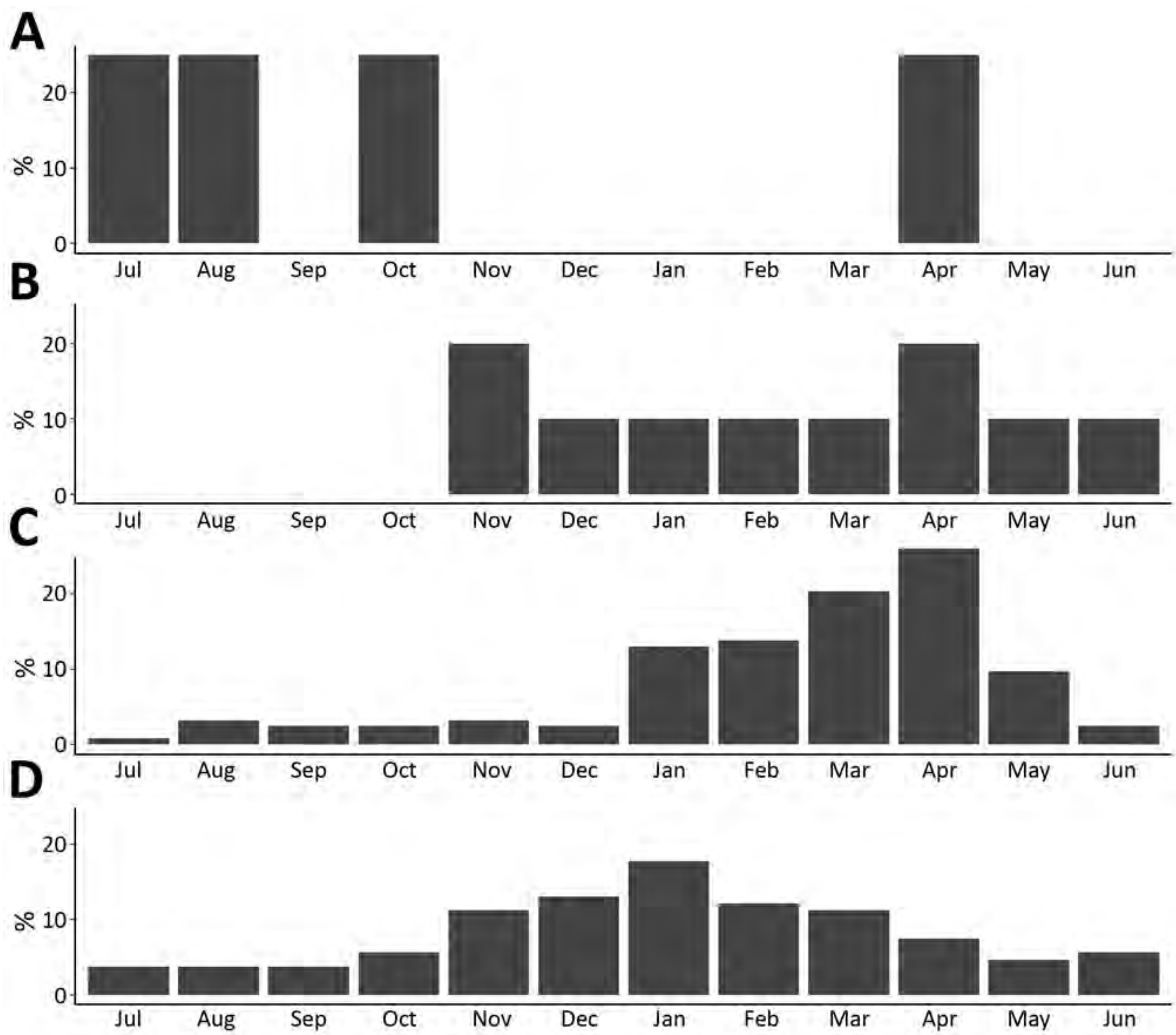


**Figure 1.** Percentage of outbreaks reported per month, by suspected or confirmed outbreak etiology, for single-etiology outbreaks attributable to adenovirus (A), astrovirus (B), rotavirus (C), or sapovirus (D), National Outbreak Reporting System, USA, 2009–2018.

likely attributable to differences in testing and reporting practices, not actual differences in incidence.

Multiple etiology outbreaks were reported more often in recent years, likely because of increased availability of multipathogen test panels. Multiple-etiology outbreaks involving adenovirus, astrovirus, rotavirus, or sapovirus were commonly found in combination with norovirus. Further study is needed to determine whether each of these detected pathogens contributed to outbreak illnesses or represent detection of asymptomatic shedding.

Adenovirus, astrovirus, rotavirus, and sapovirus remain important causes of AGE outbreaks in the United States and should be considered as potential etiologies, especially for norovirus-negative outbreaks. More widespread testing and reporting will help to advance understanding of the burden and epidemiology of these viruses.

### Acknowledgments

We thank Leslie Barclay and Mary Ann Kirkconnell Hall for their assistance on this manuscript.

### About the Author

Ms. Mattison is an epidemiologist in the Division of Viral Diseases, National Center for Immunization and Respiratory Diseases, Centers for Disease Control and Prevention. Her research interests include viral outbreak epidemiology and surveillance.

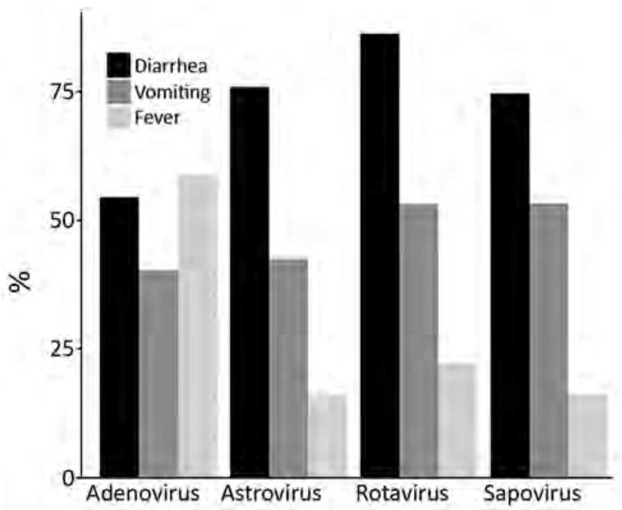


**Figure 2.** Percentage of cases with symptom information including diarrhea, vomiting, and fever, by suspected or confirmed outbreak etiology, for single-etiology outbreaks attributable to adenovirus, astrovirus, rotavirus, or sapovirus, National Outbreak Reporting System, USA, 2009–2018.

## References


1. Scallan E, Griffin PM, Angulo FJ, Tauxe RV, Hoekstra RM. Foodborne illness acquired in the United States—unspecified agents. Emerg Infect Dis. 2011;17:16–22. https://doi.org/10.3201/eid1701.P21101
2. Hall AJ, Wikswo ME, Manikonda K, Roberts VA, Yoder JS, Gould LH. Acute gastroenteritis surveillance through the National Outbreak Reporting System, United States. Emerg Infect Dis. 2013;19:1305–9. https://doi.org/10.3201/eid1908.130482
3. Chhabra P, Payne DC, Szilagyi PG, Edwards KM, Staat MA, Shirley SH, et al. Etiology of viral gastroenteritis in children <5 years of age in the United States, 2008–2009. J Infect Dis. 2013;208:790–800. https://doi.org/10.1093/infdis/jit254
4. Kurtz JB, Lee TW, Craig JW, Reed SE. Astrovirus infection in volunteers. J Med Virol. 1979;3:221–30. https://doi.org/10.1002/jmv.1890030308
5. Lynch JP III, Fishbein M, Echavarria M. Adenovirus. Semin Respir Crit Care Med. 2011;32:494–511. https://doi.org/10.1055/s-0031-1283287
6. Oka T, Wang Q, Katayama K, Saif LJ. Comprehensive review of human sapoviruses. Clin Microbiol Rev. 2015;28:32–53. https://doi.org/10.1128/CMR.00011-14
7. Steele JC Jr. Rotavirus. Clin Lab Med. 1999;19:691–703. https://doi.org/10.1016/S0272-2712(18)30111-2
8. Bosch A, Pintó RM, Guix S. Human astroviruses. Clin Microbiol Rev. 2014;27:1048–74. https://doi.org/10.1128/CMR.00013-14
9. Centers for Disease Control and Prevention. National Outbreak Reporting System (NORS): about NORS. 2018 [cited 2018 Aug 5]. http://www.cdc.gov/NORS/about.html
10. Wikswo ME, Kambhampati A, Shioda K, Walsh KA, Bowen A, Hall AJ; Centers for Disease Control and Prevention (CDC). Outbreaks of acute gastroenteritis transmitted by person-to-person contact, environmental contamination, and unknown modes of transmission—United States, 2009–2013. MMWR Surveill Summ. 2015;64:1–16. https://doi.org/10.15585/mmwr.ss6412a1
11. Pindyck T, Tate JE, Parashar UD. A decade of experience with rotavirus vaccination in the United States—vaccine uptake, effectiveness, and impact. Expert Rev Vaccines. 2018;17:593–606. https://doi.org/10.1080/14760584.2018.1489724
12. Pickering LK, Bartlett AV III, Reves RR, Morrow A. Asymptomatic excretion of rotavirus before and after rotavirus diarrhea in children in day care centers. J Pediatr. 1988;112:361–5. https://doi.org/10.1016/S0022-3476(88)80313-5
13. Centers for Disease Control and Prevention. Preventing norovirus infection. 2019 Nov 25 [cited 2020 Aug 24]. https://www.cdc.gov/norovirus/about/prevention.html
14. Bennett S, Gunson RN. The development of a multiplex real-time RT-PCR for the detection of adenovirus, astrovirus, rotavirus and sapovirus from stool samples. J Virol Methods. 2017;242:30–4. https://doi.org/10.1016/j.jviromet.2016.12.016
15. Centers for Disease Control and Prevention. Frequently asked questions and answers about CaliciNet. 2019 Feb 5 [cited 2019 Oct 30]. https://www.cdc.gov/norovirus/reporting/calicinet/faq.html#data-collection


Address for correspondence: Claire P. Mattison, Centers for Disease Control and Prevention, 1600 Clifton Rd NE, Atlanta, Georgia, 30329-4027, USA; email: cmattison@cdc.gov

# Shuni Virus in Cases of Neurologic Disease in Humans, South Africa

Thopisang P. Motlou, Marietjie Venter

We describe Shuni virus (SHUV) detection in human neurologic disease cases in South Africa. SHUV RNA was identified in 5% of cerebrospinal fluid specimens collected during the arbovirus season from public sector hospitals. This finding suggests that SHUV may be a previously unrecognized cause of human neurologic infections in Africa.

Arthropod-borne viruses (arboviruses) warrant attention in the global health landscape because of their potential to cause widespread epidemics worldwide (*1*). Epizootics in animals may signal an increase in virus activity and predict potential missed human outbreaks, as shown for West Nile virus neurologic infections in horses (*2–4*) and humans (*5*) and Rift Valley fever associated with abortion storms in livestock and cases of febrile and neurologic disease (*6*) and miscarriages in humans (*7,8*).

Arboviruses of African origin are largely responsible for the recent expansion in geographic range of emerging viruses worldwide. These viruses have been associated with human illness and death in new regions in recent years but remain underreported in Africa (*9*). Cases of neurologic arbovirus infections are thought to be underreported in humans in South Africa, with ≈3% of cerebrospinal fluid (CSF) samples of neurologic infections in humans testing positive for West Nile virus (*7*). This raised the question as to whether other neglected zoonotic arboviruses are circulating in Africa that may potentially cause future outbreaks in new regions (*10*).

Shuni virus (SHUV) has recently been described as a cause of neurologic infections in horses in South Africa (*11*) and emerged as a cause of neurologic infections and birth defects in livestock in Israel (*12*). Before this study, there had been only 1 confirmed human SHUV case since 1966 (*13*). We used real-time reverse transcription PCR (rRT-PCR) to investigate whether SHUV is associated with unsolved neurologic cases in humans in South Africa by screening archived CSF samples collected for viral diagnosis from hospitalized patients during the arbovirus season in January–May 2017.

Author affiliation: University of Pretoria, Pretoria, South Africa

DOI: https://doi.org/10.3201/eid2702.191551

## The Study

We obtained archived CSF specimens from public sector hospitals across Gauteng Province, South Africa, through the National Health Laboratory Service, Tshwane Academic division, from patients who had neurologic signs and symptoms during January–May 2017. We grouped the CSF specimens into 4 categories based on age: age group 1 was children (<1–12 years of age); age group 2, adolescents (13–18 years of age); age group 3, adults (19–59 years of age); and age group 4, senior adults (≥60 years of age). SHUV-positive cases were determined by an *Orthobunyavirus* genus-specific RT-PCR and confirmed using Sanger sequencing and phylogenetic analysis.

We extracted RNA from the CSF samples using the QIAamp Viral RNA Kit (QIAGEN, https://www.qiagen.com). We performed an *Orthobunyavirus* genus-specific RT-PCR using the Agpath-ID One Step RT-PCR (Thermo Fisher Scientific, https://www.thermofisher.com) with primers designed to amplify a 155-bp fragment of the nucleocapsid gene of the small (S) segment of orthobunyaviruses (*14*). We analyzed the sequences using the BioEdit DNA sequence alignment editor v7.0 5.3 software (*15*) and Blast search analysis (http://blast.ncbi.nlm.nih.gov/Blast.cgi). We performed phylogenetic analysis using maximum-likelihood analysis (MEGA X, http://www.megasoftware.net) as confirmation that the amplicons represent SHUV (Figure, panel A). A larger region of the S segment (≈460 bp) could be sequenced for only 1 of the positive samples (ZRUH131/17, GenBank accession no. MN937197) (Figure, panel B) because of low viral RNA concentration and sample volume in the other CSF samples.

A total of 7 of 130 (5.4%) CSF samples tested positive with an *Orthobunyavirus* rRT-PCR targeting the S segment and were confirmed by DNA sequencing to represent SHUV (Figure, panel A). A longer region was obtained for a CSF sample taken from a patient who was confirmed to have had neurologic diseases (meningitis, encephalitis, and seizures) with a clinical diagnosis of TB meningitis. Apart from neurological signs, additional clinical diagnoses in other patients included respiratory diseases (tuberculosis, upper respiratory tract infection, and pneumonia), gastrointestinal diseases, vomiting, and hydrops fetalis (Table 1). Only 3 patients' HIV status was recorded, of which 1 patient's mother was confirmed to be HIV positive and

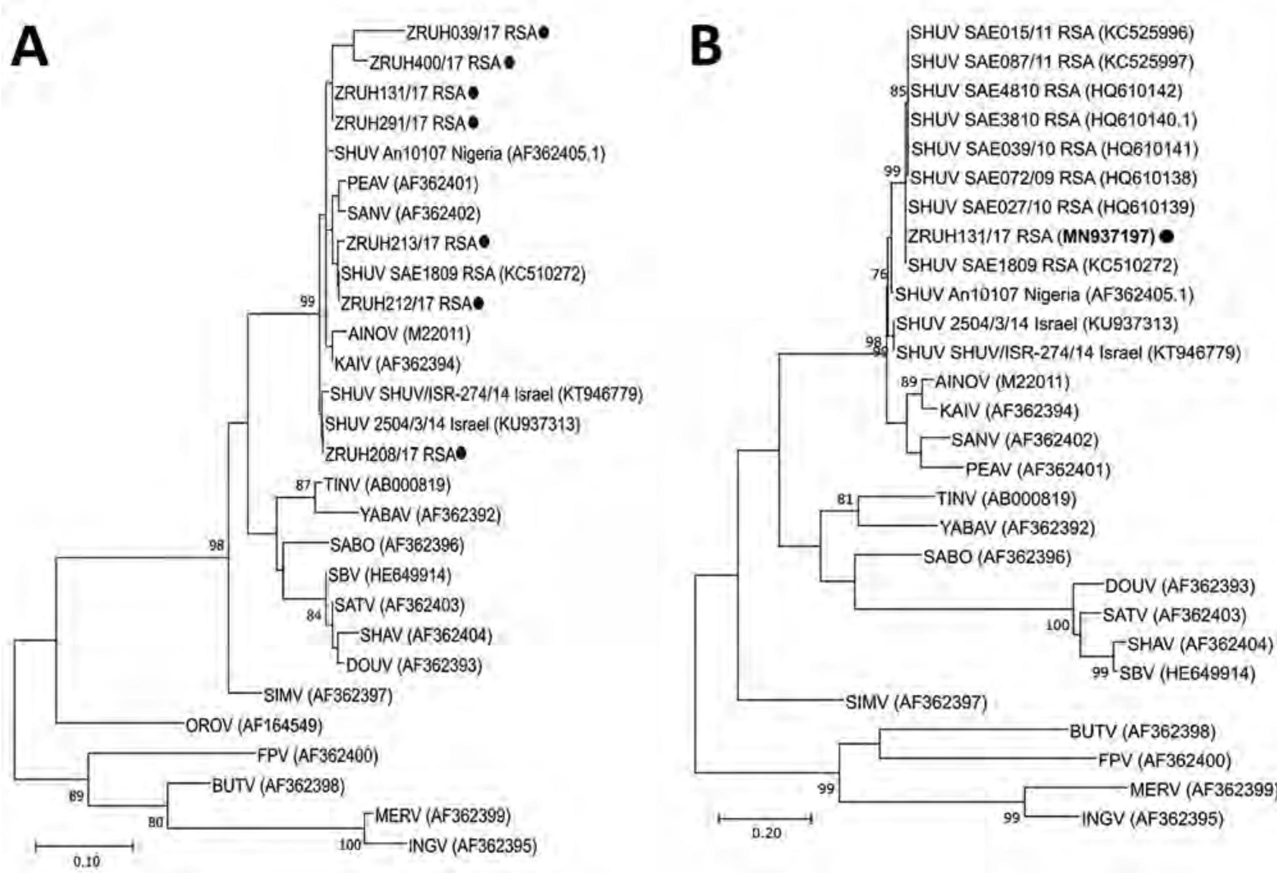


**Figure.** A) Phylogenetic confirmation that the orthobunyavirus small (S) segment specific reverse transcription PCR (14) positive products identified in this study clustered with SHUV strains. The 155-bp sequence of the nucleocapsid gene of the S segment of the human clinical isolates were aligned to SHUV strains previously identified in animals and other Orthobunyaviruses in the Simbu serogroup. The evolutionary history was inferred by using the maximum likelihood method and Kimura 2-parameter model. The tree with the highest log likelihood (–1043.27) is shown. The percentage of trees in which the associated taxa clustered together is shown next to the branches. Initial tree(s) for the heuristic search were obtained automatically by applying neighbor-joining and BioNJ algorithms to a matrix of pairwise distances estimated using the maximum composite likelihood (MCL) approach and then selecting the topology with superior log likelihood value. A discrete gamma distribution was used to model evolutionary rate differences among sites (5 categories [+G parameter = 0.6884]). This analysis involved 28 nt sequences. All positions containing gaps and missing data were eliminated (complete deletion option). There were a total of 151 positions in the final dataset. Evolutionary analyses were conducted in MEGA X (http://www.megasoftware.net). Black circles indicate the newly sequenced positive human samples (ZRUH208/17, ZRUH131/17, ZRUH219/17, ZRUH212/17, ZRUH213/17, ZRUH400/17, ZRUH039/17). B) Phylogenetic analysis of a human SHUV-positive case using a larger region of the S-segment amplified with SHUV-specific primers. The evolutionary history was inferred by using the maximum likelihood method and Tamura-Nei model. The tree with the highest log likelihood (–3135.73) is shown. The percentage of trees in which the associated taxa clustered together is shown next to the branches. Initial tree(s) for the heuristic search were obtained automatically by applying neighbor-joining and BioNJ algorithms to a matrix of pairwise distances estimated using the MCL approach and then selecting the topology with superior log likelihood value. A discrete gamma distribution was used to model evolutionary rate differences among sites (5 categories [+G, parameter = 0.3230]). This analysis involved 28 nt sequences. All positions containing gaps and missing data were eliminated (complete deletion option). There were a total of 324 positions in the final dataset. Evolutionary analyses were conducted in MEGA X. Black circle indicates the newly sequenced positive human strain (ZRUH131/17, GenBank accession no. MN937197). Sequence data are available upon request; numbers in parentheses for related strains indicate GenBank accession numbers. Scale bars indicate nucleotide substitutions per site. AINOV, Aino virus; AKAV, Akabane virus; BUTV, Buttonwillow virus; DOUV, Douglas virus; FPV, Faceys Paddock virus; INGV, Ingwavuma virus; KAIV, Kaikalur virus; KAIRV, Kairi virus; MERV, Mermet virus; OROV, Oropouche virus; PEAV, Peaton virus; SABOV, Sabo virus; SANV, Sango virus; SATV, Sathuperi virus; SBV, Schmallenburg virus; SHAV, Shamonda virus; SHUV, Shuni virus; SIMV, Simbu virus; TINV, Tinaroo virus; THIV, Thimiri virus; YABA, Yaba-7 virus.

**Table 1.** Demographic and clinical information of SHUV-positive CSF samples from 7 patients hospitalized with neurologic signs, Gauteng Province, South Africa, 2017*

| Sample ID | Patient age/sex | Other symptoms | Clinical diagnoses | HIV status | Other tests | Vaccination | Reason for discharge | Location |
|---|---|---|---|---|---|---|---|---|
| ZRUNH 039/17 | 29 y/F | Not stated | Meningitis | Unknown | Not stated | Unknown | Unknown | JHB |
| ZRUNH 131/17 | 1 y 9 mo/M | Not stated | TB, meningitis | Unknown | Not stated | Unknown | Unknown | JHB |
| ZRUNH 219/17 | 6 mo/F | Vomiting, diarrhea, fine maculopapular rash | Acute gastroenteritis and shock | Mother (positive), on HAART/ PMTCT, ART (FDC); baby received nevirapine | *H. influenzae* Ag (negative), *N. meningitidis* ACV W135 (negative), *E. coli* (negative), *S. pneumonia* (negative), GBS (negative), cryptococcal Ag (negative) | Mother did not have clinic card | Stable | Eastlynne, Pretoria |
| ZRUNH 212/17 | 2 y 8 mo/M | Coughing blood, otitis media, simple febrile seizures, fever (38°C), difficulty breathing, vomiting, diarrhea; had second episode of seizure | Upper respiratory tract infection/ hemoptysis/ febrile convulsions | Mother negative; baby received nevirapine | Not stated | Up to date: BGG, polio+DPT (3–18 mo), DT (5 y) not done | Stable | Pretoria |
| ZRUNH 208/17 | 4 y 11 mo/M | Seizures, ICU patient, decreased LOC, vomiting, seizures, fever, diarrhea | Encephalitis and aspiration pneumonia | Negative | Microbiology: negative for bacteria | Incomplete: no polio+DPT (4,5 mo) | Not stated | Eastlynne, Pretoria |
| ZRUNH 213/17 | 13 d/F | ICU patient, baby delivered normally, neonatal encephalopathy, second-degree congenital sepsis/TORCH, poor sucking, premature, low birthweight, nonimmune, subcutaneous edema, abdominal distension (HC, chest, AC), abdominal U/S (ascites, bilateral dense kidneys) | Nonimmune hydrops fetalis | Not stated | HSV (positive; patient tested negative following treatment), rubella PCR (IgG positive, IgM negative), CMV (IgG positive, IgM negative) | Up to date | Stable | Mamelodi East, Pretoria |
| ZRUNH 400/17 | 4 mo/M | Respiratory distress, vomiting bile | Viral pneumonia | Not stated | Not stated | Up to date | Not stated | Olieven-houtbosch, Pretoria |

*AC, abdominal circumference; Ag, antigen; BCG, bacille Calmette-Guérin; CMV, cytomegalovirus; DPT, diphtheria/pertussis/tetanus; *E. coli*, *Escherichia coli*; FDC, fixed-dose combination; GBS, group B *Streptococcus*; *H. influenzae*, *Haemophilus influenzae*; HAART, highly active antiretroviral therapy; HC, hepatitis C; HSV, herpes simplex virus; ICU, intensive care unit; ID, identification; JHB, Johannesburg; LOC, level of consciousness; *N. meningitis*, *Neisseria meningitidis*; PMTCT, prevention of mother-to-child transmission; SHUV, Shuni virus; TB, tuberculosis; TORCH, *Toxoplasma gondii*; U/S, ultrasound.

undergoing treatment. The baby of the positive mother subsequently received nevirapine. The other 2 patients were HIV negative; however, 1 of the children was given nevirapine for reasons not stated. No apparent travel history was recorded for any of these patients.

Most specimens screened were from children (63.1%). Groups with the lowest number of patients were adolescents (1.5%) and the elderly (4.6%) (Table 2). There was only a slight difference in the percentage of males and female patients tested (46.2% male and 51.7% female). A total of 6 (85.7%) of 7 positive cases were in children and 1 of 7 (14.3%) was in an adult. Three of the children with positive test results were <6 months of age. One of these positive children was a newborn admitted to the intensive care unit at 13 days of age who had not left the hospital since

**Table 2.** Demographics of the patient group screened for Shuni virus, Gauteng Province, South Africa, 2017

| Demographic | Total no. (%) | No. (%) positive | Odds ratio (95% CI) |
|---|---|---|---|
| Total | 130 | 7 (5.3) | |
| Age group, y* | | | |
| 1 | 82 (63.1) | 6 (4.9) | 0.05333 (0.01951–0.1458) |
| 2 | 2 (1.5) | 0 (0) | 0 |
| 3 | 40 (30.8) | 0 (0) | 0 |
| 4 | 6 (4.6) | 1 (16.7) | 0.2 (0.02337–1.71188) |
| Sex | | | |
| M | 60 (46.2) | 3 (42.9)† | |
| F | 67 (51.7) | 4 (57.1)† | |
| Not stated | 3 (2.3) | 0 | |

*The classification of the age groups is based on the neutral network using the FG-NET aging database and wavelets. Age group 1, children (<1–12 y); age group 2, adolescents (13–18 y); age group 3, adults (19–59 y); and age group 4, senior adults (≥60 y). p value = 0.6621.
†Percentages based on total no. positive cases.

birth. Aside from neurologic signs that were present in all patients, the most common recorded symptoms were vomiting, diarrhea, seizures, and fever.

SHUV was reported in horses with severe neurologic signs in South Africa during 2009–2012 (*11*), which prompted us to also investigate its occurrence in human cases. Screening of CSF specimens from hospitalized patients with neurologic signs around Gauteng Province in South Africa, where some of the equine cases were detected, suggests that up to 5.4% of unidentified neurologic human cases during the arbovirus season may be caused by SHUV. Six of the 7 patients who tested positive for SHUV were children <5 years of age, with 1 being a newborn 13 days of age; only 1 case was identified in a woman. Three of the 7 patients were discharged after being found to be stable; the outcomes of the other 4 are unknown.

These patients were also tested for other viral and bacterial infections, such as influenza, *Neisseria meningitidis*, pneumonia, herpes simplex virus (HSV), rubella, and cytomegalovirus (Table 1). All 7 patients showed negative results for all requested diagnostic assays except for the 13-day-old infant, who received a diagnosis of hydrops fetalis. He was IgG positive for rubella and cytomegalovirus but IgM negative for both, suggesting maternal antibody transmission. The patient was positive for HSV by PCR and was subsequently placed on treatment for 12 days postnatal until the HSV PCR yielded a negative result. Although the diagnosis of a HSV co-infection cannot rule out HSV as the cause of the hydrops fetalis, the fact that he had not left the hospital since birth suggests a likely vertical transmission of both HSV and SHUV. The patient was stable at discharge after 21 days; no death has been reported. None of the patients had any travel history, indicating that they may have been infected in or around their area of residence. Equine cases had previously been identified in these areas, suggesting possible similar vector exposure (*11*).

A limitation of this study was that all other potential causes of neurologic signs were not exhaustively investigated. Previous detection of SHUV in *Cullicoides* midges and *Culex theileri* mosquitoes (McIntosh BM, Epidemiology of arthropod-borne viruses in southern Africa. Unpublished thesis, University of Pretoria, 1980) suggests that SHUV has the potential to expand its geographic range and potentially emerge in new regions. The reservoir host for SHUV is not known but is thought to be ruminants and wildlife, from which transmission to humans would likely be accomplished through susceptible mosquitoes.

## Conclusions

Detection of SHUV RNA in the CSF is highly suggestive of SHUV contributing to neurologic signs and likely crossing of the blood–brain barrier. However, further investigations with larger cohorts are needed to determine the disease burden of SHUV in humans across all age groups. These investigations can also include determining the geographic range, clinical presentation, potential vectors, and reservoir hosts in Africa. Improved diagnoses that include IgM serology and early PCR detection of SHUV will aid in defining the true incidence and epidemiology of SHUV.

### Acknowledgments

We thank the National Health Laboratory Service of South Africa for contributing the CSF specimens and members of the Zoonotic, Arbo- and Respiratory Virus (ZARV) group at the Centre for Viral Zoonoses, Department of Medical Virology, University of Pretoria, for their assistance.

This study was funded in part through scholarships for T.P.M. by the National Research Foundation (nos. 107424 and 116385), Poliomyelitis Research Foundation (no. 17/37), and research funding from the German Federal Ministry of Education and Research (grant no.VN81204343) for the African Network for Improved Diagnostics, Epidemiology and Management of Common

Infectious Agents – ANDEMIA, Acute Febrile Disease of Unknown Origin Project (South Africa) and the G7 Global Health Fund Program (grant no. FKZ1368-1438TO08, Strengthening of the Expertise for the Investigation of Outbreaks of Haemorrhagic Fevers and Antibiotic-Resistant Germs [TP08], South Africa; collaboration project with Dr. F. Leendertz, Robert Koch Institute).

## About the Authors

Ms. Motlou is MSc graduate at the Centre for Viral Zoonoses at the University of Pretoria, South Africa. Her primary research focused on investigating SHUV as a cause of neurological disease in humans, horses, and mosquitoes.

Dr. Venter is a molecular virologist and head of the Respiratory and Emerging Neurological Virus Research Group at the Department of Medical Virology, University of Pretoria/National Health Laboratory Services in Pretoria. Her primary research interest is the pathogenicity and epidemiology of zoonotic arboviruses, as well as viral causes of pneumonia in southern Africa.

## References

1. Dash AP, Bhatia R, Sunyoto T, Mourya DT. Emerging and re-emerging arboviral diseases in Southeast Asia. J Vector Borne Dis. 2013;50:77–84.
2. Leblond A, Hendrikx P, Sabatier P. West Nile virus outbreak detection using syndromic monitoring in horses. Vector Borne Zoonotic Dis. 2007;7:403–10. https://doi.org/10.1089/vbz.2006.0593
3. Drummond R. Surveillance for West Nile virus in horses. Vet Rec. 2008;162:763. https://doi.org/10.1136/vr.162.23.763-a
4. Venter M, Pretorius M, Fuller JA, Botha E, Rakgotho M, Stivaktas V, et al. West Nile virus lineage 2 in horses and other animals with neurologic disease, South Africa, 2008–2015. Emerg Infect Dis. 2017;23:2060–4. https://doi.org/10.3201/eid2312.162078
5. Zaayman D, Venter M. West Nile virus neurologic disease in humans, South Africa, September 2008–May 2009. Emerg Infect Dis. 2012;18:2051–4. http://dx.doi.org/10.3201/eid1812.111208
6. Archer BN, Thomas J, Weyer J, Cengimbo A, Landoh DE, Jacobs C, et al. Epidemiologic investigations into outbreaks of Rift Valley fever in humans, South Africa, 2008–2011. Emerg Infect Dis. 2013;19:1918–25. https://dx.doi.org/10.3201/eid1912.121527
7. Budasha NH, Gonzalez J-P, Sebhatu TT, Arnold E. Rift Valley fever seroprevalence and abortion frequency among livestock of Kisoro district, South Western Uganda (2016): a prerequisite for zoonotic infection. BMC Vet Res. 2018;14:271. https://doi.org/10.1186/s12917-018-1596-8
8. Baudin M, Jumaa AM, Jomma HJE, Karsany MS, Bucht G, Näslund J, et al. Association of Rift Valley fever virus infection with miscarriage in Sudanese women: a cross-sectional study. Lancet Glob Health. 2016;4:e864–71. https://doi.org/10.1016/S2214-109X(16)30176-0
9. Reynolds ES, Hart CE, Hermance ME, Brining DL, Thangamani S. An overview of animal models for arthropod-borne viruses. Comp Med. 2017;67:232–41.
10. Venter M. The role of zoonotic vector borne viruses as neurological pathogens in horses in South Africa. Annual South African Equine Veterinary Association Congress; Limpopo, South Africa, February 13–17, 2011.
11. van Eeden C, Williams JH, Gerdes TG, van Wilpe E, Viljoen A, Swanepoel R, et al. Shuni virus as cause of neurologic disease in horses. Emerg Infect Dis. 2012;18:318–21. https://doi.org/10.3201/eid1802.111403
12. Golender N, Bumbarov V, Assis I, Beer M, Khinich Y, Koren O, et al. Shuni virus in Israel: neurological disease and fatalities in cattle. Transbound Emerg Dis. 2019;66:1126–31. https://doi.org/10.1111/tbed.13167
13. Causey OR, Kemp GE, Causey CE, Lee VH. Isolations of Simbu-group viruses in Ibadan, Nigeria 1964–69, including the new types Sango, Shamonda, Sabo and Shuni. Ann Trop Med Parasitol. 1972;66:357–62. http://dx.doi.org/10.1080/00034983.1972.11686835
14. Steyn J, Motlou P, van Eeden C, Pretorius M, Stivaktas VI, Williams J, et al. Shuni virus in wildlife and non-equine domestic animals, South Africa. Emerg Infect Dis. 2020;26:1521–5. https://doi.org/10.3201/eid2607.190770
15. Hall TA. BioEdit: a user-friendly biological sequence alignment editor and analysis program for Windows 95/98/NT. Nucleic acids symposium series. London: Information Retrieval Ltd., 1999. p. 95–8.

Address for correspondence: Marietjie Venter, University of Pretoria, Pretoria, South Africa; email: marietjie.venter@up.ac.za

# Murine Typhus in Canary Islands, Spain, 1999–2015

José María Robaina-Bordón, Cristina Carranza-Rodríguez, Michele Hernández-Cabrera, Margarita Bolaños-Rivero, Elena Pisos-Álamo, Nieves Jaén-Sánchez, Araceli Hernández-Betancor, Laura Suárez-Hormiga, José Luis Pérez-Arellano

To document the epidemiology, clinical features, and outcomes of murine typhus patients in the Canary Islands (Spain), we analyzed data that were retrospectively collected for 16 years for 221 patients. Murine typhus in the Canary Islands is characterized by a high rate of complications (31.6%), mainly liver, lung, kidney or central nervous system involvement.

Murine typhus is a febrile disease caused by *Rickettsia typhi* (*1*). Rickettsia are obligate, intracellular, gram-negative bacilli that are transmitted to mammals by various arthropod vectors, including ticks, lice, mites, and fleas (*2*). The classic *R. typhi* life cycle involves rats of the subgenus *Rattus* (such as *R. rattus* and *R. norvegicus*) and their fleas (especially *Xenopsylla cheopis*). Adaptation to new reservoirs (cats, dogs, opossums) and vectors, in particular *Ctenocephalides felis* (cat flea), has probably led to the reappearance of murine typhus in industrialized countries (*3*).

Murine typhus remains a neglected disease despite its worldwide distribution. It is one of the most frequent causes of fever of intermediate duration (FID), defined as fever of 7–28 days, and is not associated with localizing signs or diagnostic clues after a complete evaluation in southern Spain and the Canary Islands (*4*,*5*). Underdiagnosis represents a major health cost because unnecessary diagnostic tests might be performed and treatment might be inadequate (*6*). Although it is considered a mild disease, a large number of patients require hospital admission and show development of life-threatening complications (*7*). Our aim was to document the epidemiology, clinical features, and outcome of murine typhus in the Canary Islands (Spain).

Author affiliations: Universidad de Las Palmas de Gran Canaria, Las Palmas de Gran Canaria, Spain (J.M. Robaina-Bordón, C. Carranza-Rodríguez, M. Hernández-Cabrera, E. Pisos-Álamo, N. Jaén-Sánchez, L. Suárez-Hormiga, J.L. Pérez-Arellano); Hospital Universitario de Gran Canaria Doctor Negrín, Las Palmas de Gran Canaria (J.M. Robaina-Bordón); Complejo Hospitalario Universitario Insular-Materno Infantil de Gran Canaria, Las Palmas de Gran Canaria (C. Carranza-Rodríguez, M. Hernández-Cabrera, M. Bolaños-Rivero, E. Pisos-Álamo, N. Jaén-Sánchez, A. Hernández-Betancor, L. Suárez-Hormiga, J.L. Pérez-Arellano)

DOI: https://doi.org/10.3201/eid2702.191695

## The Study

The study included 221 adults >14 years of age who were inpatients and outpatients at the Hospital Universitario Insular of Las Palmas (Las Palmas de Gran Canaria, Spain), who received a diagnosis of murine typhus during June 1, 1999–December 31, 2015. Epidemiologic, clinical, and laboratory data were retrospectively collected from medical records. Diagnosis of murine typhus was based on detection of antibodies against *R. typhi* by using an indirect immunofluorescence test and 2 criteria. Criterion 1 was titer ≥1:1,280 for IgM in 1 sample, and criterion 2 was a 4-fold increase in IgG titers between 2 consecutive samples. A total of 72 (32.6%) patients were given a diagnosis according to criterion 1, and 149 (67.4%) patients were given a diagnosis according to criterion 2. Clinical and laboratory data for both groups were analyzed separately.

Murine typhus was more frequent during July–November (Figure 1). The mean ± SD number of cases diagnosed per year was 18 ± 5.33. We provide the annual distribution of cases (Figure 2). Most (91.4%, 202/221) case-patients lived in urban areas; 73.3% (162/221) were male; and the median age was 40 years (interquartile range 28.5–52.5 years). Most (88.7%, 188/212) reported close contact with animals, especially dogs (66%, 140/212) and cattle (42%, 89/212). Arthropod bites were reported by 34 (19.5%) of 174 case-patients.

We provide the main clinical features recorded (Table 1). A total of 180 (82.95%) of 217 patients had high fever (median temperature 39.8°C) of >1 week duration. Pharyngitis was more frequently observed

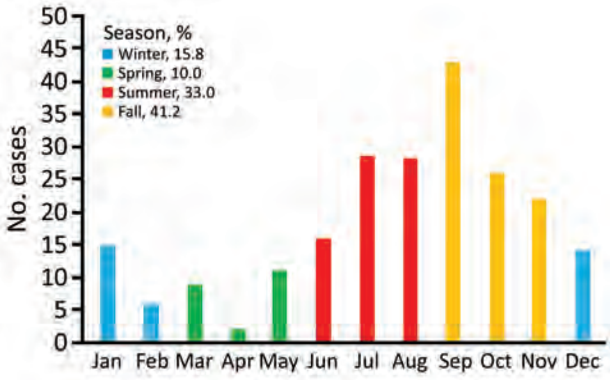


**Figure 1.** Monthly distribution of cases of endemic murine typhus, Canary Islands, Spain, 1999–2015.

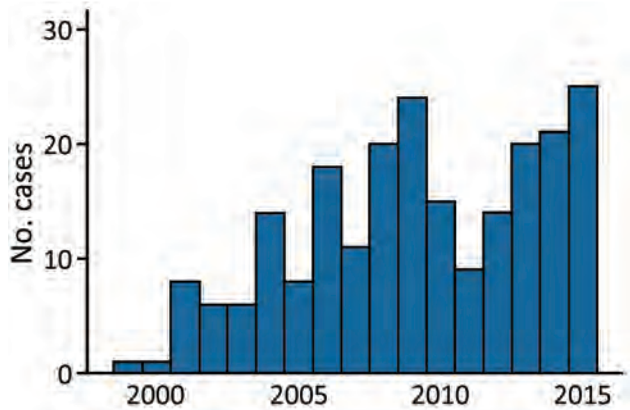


**Figure 2.** Annual distribution of cases of murine typhus, Canary Islands, Spain, 1999–2015.

for younger (<20 years of age) patients (7/20, 35%) than for older patients (12/169, 7.1%) ($p = 0.001$). Rash was present more often in younger patients (8/19, 42.1%) than in older patients (42/190, 22.1%) ($p = 0.05$). We also provide laboratory findings (Table 2). Most (184/195, 94.4%) had urinalysis alterations in the form of microhematuria, proteinuria, or leukocyturia.

Complications developed in 31.6% (68/215) of patients, especially hepatitis (22/221, 10.0%), acute renal failure (21/215, 9.8%), meningitis (12/215, 5.6%), and pneumonia (9/215, 4.2%). No differences were found between patients given a diagnosis by using criterion 1 or 2 (Appendix, https://wwwnc.cdc.gov/EID/article/27/2/19-1695-App1.pdf). Cerebrospinal fluid samples from patients who had meningitis were characterized by a clear appearance, moderate mononuclear pleocytosis (range 6–43 cells), mild proteinorachia, and standard glucose levels. Round pneumonia developed in 2 patients and retinitis in 1 patient.

A total of 51 (22.6%) of the 221 patients were hospitalized: 29 (56.9%) had complications, 12 (23.5%) experienced vomiting, and 10 (19.6%) needed a diagnostic workup. The average length of hospital stay was short (median 6 days; interquartile range 4–9 days). Seven patients did not receive treatment because of spontaneous recovery. The remaining patients received doxycycline. Two patients required admission

**Table 1.** Clinical findings for patients with cases of endemic murine typhus, Canary Islands, Spain, 1999–2015

| Finding | Total, no. (%) | IgM ≥1:1,280, no. (%)* | 4-fold IgG titer increase, no. (%)† | p-value |
|---|---|---|---|---|
| Symptom or sign | | | | |
| Headache, n = 206 | 181 (87.9) | 59 (88.1) | 122 (87.8) | 0.95 |
| Sweating, n = 175 | 129 (73.7) | 44 (74.6) | 85 (73.3) | 0.85 |
| Myalgias, n = 186 | 135 (72.6) | 39 (65) | 96 (76.2) | 0.11 |
| Nausea/vomiting, n = 206 | 103 (50) | 32 (47.8) | 71 (51.1) | 0.66 |
| Dry cough, n = 200 | 79 (39.5) | 23 (36.5) | 56 (40.9) | 0.56 |
| Rash, n = 211 | 56 (26.5) | 14 (21.2) | 36 (25.2) | 0.53 |
| Abdominal pain, n = 200 | 45 (22.5) | 15 (22.7) | 30 (22.4) | 0.96 |
| Classic triad, n = 201‡ | 46 (22.9) | 14 (21.5) | 32 (23.5) | 0.75 |
| Conjunctivitis, n = 201 | 41 (20.4) | 12 (18.8) | 29 (21.2) | 0.69 |
| Diarrhea, n = 221 | 41 (18.6) | 11 (15.3) | 30 (20.1) | 0.38 |
| Odynophagia, n = 182 | 24 (13.2) | 16 (13.1) | 8 (13.3) | 0.97 |
| Tachycardia, n = 164 | 75 (45.7) | 28 (54.9) | 47 (41.6) | 0.11 |
| Hepatomegaly, n = 209 | 37 (17.7) | 12 (17.9) | 25 (17.6) | 0.96 |
| Relative bradycardia, n = 162§ | 21 (13) | 3 (5.9) | 18 (16.2) | 0.07 |
| Pharyngitis, n = 189 | 19 (10.1) | 8 (12.7) | 11 (8.7) | 0.39 |
| Lymphadenopathy, n = 198 | 16 (8.1) | 10 (15.6) | 6 (4.5) | 0.01 |
| Splenomegaly, n = 209 | 17 (8.1) | 5 (7.5) | 12 (8.5) | 0.81 |
| Altered pulmonary auscultation, n = 210 | 17 (8.1) | 7 (10.3) | 10 (7) | 0.42 |
| Flea bite, n = 93 | 6 (6.5) | 0 (0) | 6 (9.4) | 0.17 |
| Costovertebral angle tenderness, n = 199 | 11 (5.5) | 6 (9.2) | 5 (3.7) | 0.18 |
| Jaundice, n = 210 | 11 (5.2) | 4 (5.9) | 7 (4.9) | 0.75 |

*Patients given a diagnosis by testing of 1 sample (criterion 1).
†Patients given a diagnosis by testing of 2 consecutive samples (criterion 2).
‡Fever, headache and rash.
§Temperature ≥38.9°C and heart rate ≤110 beats/min in the absence of treatment with β-blockers.

**Table 2.** Laboratory test results for patients with cases of endemic murine typhus, Canary Islands, Spain, 1999–2015*

| Finding | No. (%) | IgM ≥1:1,280, no. (%)† | 4-fold IgG titer increase, no. (%)‡ | p-value | Cutoff values |
|---|---|---|---|---|---|
| Anemia, n = 220 | 38 (17.3) | 16 (22.5) | 22 (14.8) | 0.15 | <12 g/dL Hb in women, <13 g/dL Hb in men |
| Leukopenia, n = 220 | 23 (10.5) | 7 (9.9) | 16 (10.7) | 0.26 | <4,000/μL |
| Leukocytosis, n = 220 | 42 (19.1) | 18 (25.4) | 24 (16.1) | 0.26 | >11,000/μL |
| Thrombocytopenia, n = 218 | 127 (58.3) | 28 (39.4) | 99 (67.3) | <0.01 | <150,000/μL |
| Increased ESR, n = 106 | 64 (60.4) | 27 (65.9) | 37 (56.9) | 0.42 | Upper limit of normality calculated according to age and sex |
| Prolonged PT, n = 197 | 82 (41.6) | 27 (42.9) | 55 (41) | 0.81 | <80% |
| Increased aPTTr, n = 188 | 6 (3.2) | 2 (3.4) | 4 (3.1) | 0.99 | >1.2 |
| Plasma Cr increase, n = 215 | 47 (21.9) | 16 (23.5) | 31 (21.1) | 0.72 | >1.2 mg/dL |
| Hyponatremia, n = 205 | 119 (58) | 30 (50) | 89 (61.4) | 0.13 | <135 mEq/L |
| Plasma CK increase, n = 97 | 20 (20.6) | 5 (13.5) | 15 (25) | 0.17 | >232 U/L |
| Plasma urea increase, n = 211 | 36 (17.1) | 12 (18.5) | 24 (16.4) | 0.72 | >40 mg/dL |
| Plasma LDH increase, n = 138 | 131 (94.9) | 40 (90.9) | 91 (96.8) | 0.21 | >190 U/L |
| Plasma ALT increase, n = 197 | 184 (93.4) | 59 (92.2) | 125 (94) | 0.76 | >35 U/L |
| Plasma AST increase, n = 196 | 182 (92.9) | 55 (88.7) | 127 (94.81) | 0.14 | >35 U/L |
| Plasma AP increase, n = 109 | 38 (34.9) | 10 (25.6) | 28 (40) | 0.15 | >136 U/L |
| Plasma GGT increase, n = 166 | 91 (54.8) | 29 (52.7) | 62 (55.9) | 0.74 | >85 U/L |
| Microhematuria, n = 195 | 146 (74.9) | 45 (72.6) | 101 (75.9) | 0.6 | >5 RBCs/mm$^3$ |
| Proteinuria, n = 195 | 169 (86.7) | 54 (87.1) | 115 (86.5) | 0.9 | Positive urine test strip |
| Leukocyturia, n = 194 | 123 (63.4) | 38 (62.3) | 85 (63.9) | 0.83 | >10 WBCs/mm$^3$ |

*ALT, alanine aminotransferase; AP, alkaline phosphatase; aPTTr, activated partial thromboplastin time ratio; AST, aspartate aminotransferase; Cr, creatinine; CK, creatine kinase; ESR, erythrocyte sedimentation rate; GGT, γ-glutamyl transpeptidase; Hb, hemoglobin; LDH, lactate dehydrogenase; PT, prothrombin Time; RBCs, red blood cells; WBCs, white blood cells.
†Patients given a diagnosis by testing of 1 sample (criterion 1).
‡Patients given a diagnosis by testing of 2 consecutive samples (criterion 2).

to the intensive care unit because of multiple organ failure, and no patients died. Low transient IgM titers and no IgG titers against other microorganisms were found in admission serum samples, especially against *Coxiella burnetii* (36/218, 16.5%) and Epstein-Barr virus (13/218, 6.0%).

## Conclusions

Murine typhus was diagnosed primarily in middle-age men and showed a similar male:female ratio as in other clinical series (*8*). The seasonal prevalence of murine typhus during late summer and fall has been described (*7*). This temporal pattern seems to be related to the increased propagation activity of the vector linked to higher temperatures. The number of annual cases is similar to that reported by others (*9–11*), and diagnoses increased over the study period. However, these data probably underestimate the incidence of murine typhus because of the absence of clinical hallmarks and the fact that this disease is self-limiting.

The clinical features of murine typhus observed in this study are consistent with those reported by Tsioutis et al. (*7*); high fever and intense headaches were the most common clinical features. Most of the patients fulfilled the criterion for FID. There were differences by age groups. The presence of a rash was rare among elderly patients, as reported (*12*,*13*). This finding makes the diagnostic utility of the classic triad of fever, headache, and rash somewhat debatable, especially for older patients. Furthermore, patients <20 years of age sometimes showed a clinical profile indistinguishable from that for infectious mononucleosis associated with pharyngitis, visceromegaly, lymphadenopathy, and atypical lymphocytosis.

The most common finding for blood counts was thrombocytopenia (127/218, 58.3%). A prolonged prothrombin time was common. No association was observed between a prolonged prothrombin time and complications, which is in contrast to the results of Chang et al. (*14*). Hypertransaminasemia was the most common serum alteration, which reached values typical for viral, toxic, or ischemic hepatitis in 10% of case-patients. However, clinical hepatitis, with the presence of hepatomegaly and increased levels of bilirubin, was much less frequent.

The higher incidence of renal damage for patients with murine typhus in the Canary Islands has been reported (*15*). This differential finding could be caused by specific strains of *R. typhi* that have a particular tropism, although there is no solid evidence to confirm this possibility.

Transient IgM titers against other microorganisms in admission serum samples are common. Obtaining 2 independent samples during an interval of 2 weeks is essential to avoid false-negative results or misdiagnoses.

A limitation of this study is its retrospective design, although based on an established protocol. Another limitation is the possibility of cross-reactivity; cross-reactivity is common in rickettsial diseases, and some cases diagnosed as murine typhus may have been caused by other rickettsial species. A third limitation is use of a single serum sample as a diagnostic criterion, which although used in most clinical case series is not rigorous, and previous exposure to pathogens as the cause of seroreactivity cannot be completely ruled out. However, the relatively high IgM cutoff point and the absence of relevant differences between patients given a diagnosis by using 1 sample and those with confirmed seroconversion support the data presented.

Murine typhus is a major cause of FID in the Canary Islands. Complications are frequent, especially in the elderly, usually with renal, hepatic, respiratory, or central nervous system involvement. These results should help raise awareness among physicians about the need to identify cases earlier, start treatment promptly, and thus improve clinical outcomes.

### Acknowledgment

We thank Janet Dawson for her help in revising the English version of the manuscript.

## About the Author

Dr. Robaina-Bordón is an internal medicine resident at the University Hospital of Gran Canaria Dr. Negrín, Las Palmas de Gran Canaria, Spain. His primary research interests are native and imported rickettsioses and fever of intermediate duration.

### References

1. Bolaños M, Angel-Moreno A, Pérez-Arellano JL. Murine typhus. A disease to think about here and now [in Spanish]. Med Clin (Barc). 2004;122:383–9.
2. Blanton LS. The rickettsioses, a practical update. Infect Dis Clin North Am. 2019;33:213–29. https://doi.org/10.1016/j.idc.2018.10.010
3. Gillespie JJ, Ammerman NC, Beier-Sexton M, Sobral BS, Azad AF. Louse- and flea-borne rickettsioses: biological and genomic analyses. Vet Res. 2009;40:12. https://doi.org/10.1051/vetres:2008050
4. Bernabeu-Wittel M, Pachón J, Alarcón A, López-Cortés LF, Viciana P, Jiménez-Mejías ME, et al. Murine typhus as a common cause of fever of intermediate duration: a 17-year study in the south of Spain. Arch Intern Med. 1999;159:872–6. https://doi.org/10.1001/archinte.159.8.872
5. Parra Ruiz J, Peña Monje A, Tomás Jiménez C, Parejo Sánchez MI, Vinuesa García D, Muñoz Medina L, et al. Clinical spectrum of fever of intermediate duration in the south of Spain. Eur J Clin Microbiol Infect Dis. 2008;27:993–5. https://doi.org/10.1007/s10096-008-0530-6
6. Vohra RF, Walker DH, Blanton LS. Analysis of health-care charges in murine typhus: need for improved clinical recognition and diagnostics for acute disease. Am J Trop Med Hyg. 2018;98:1594–8. https://doi.org/10.4269/ajtmh.17-0411
7. Tsioutis C, Zafeiri M, Avramopoulos A, Prousali E, Miligkos M, Karageorgos SA. Clinical and laboratory characteristics, epidemiology, and outcomes of murine typhus: a systematic review. Acta Trop. 2017;166:16–24. https://doi.org/10.1016/j.actatropica.2016.10.018
8. Miguélez M, Laynez P, Linares M, Hayek M, Abella L, Marañez I. Murine typhus in Tenerife. Clinicoepidemiological study and differential clinical features with Q fever [in Spanish]. Med Clin (Barc). 2003;121:613–5.
9. Psaroulaki A, Christou C, Chochlakis D, Tsiligianni I, Sandalakis V, Georgalis L, et al. Murine typhus in Cyprus: a 9-year survey. Trans R Soc Trop Med Hyg. 2012;106:489–95. https://doi.org/10.1016/j.trstmh.2012.02.010
10. Chaliotis G, Kritsotakis EI, Psaroulaki A, Tselentis Y, Gikas A. Murine typhus in central Greece: epidemiological, clinical, laboratory, and therapeutic-response features of 90 cases. Int J Infect Dis. 2012;16:e591–6. https://doi.org/10.1016/j.ijid.2012.03.010
11. Espinosa N, Cañas E, Bernabeu-Wittel M, Martín A, Viciana P, Pachón J. The changing etiology of fever of intermediate duration. Enferm Infecc Microbiol Clin. 2010;28:416–20. https://doi.org/10.1016/j.eimc.2009.07.014
12. Tsioutis C, Chaliotis G, Kokkini S, Doukakis S, Tselentis Y, Psaroulaki A, et al. Murine typhus in elderly patients: a prospective study of 49 patients. Scand J Infect Dis. 2014;46:779–82. https://doi.org/10.3109/00365548.2014.943283
13. Murray KO, Evert N, Mayes B, Fonken E, Erickson T, Garcia MN, et al. Typhus group rickettsiosis, Texas, USA, 2003–2013. Emerg Infect Dis. 2017;23:645–8. https://doi.org/10.3201/eid2304.160958
14. Chang K, Lee NY, Ko WC, Lin WR, Chen YH, Tsai JJ, et al. Characteristics of scrub typhus, murine typhus, and Q fever among elderly patients: prolonged prothrombin time as a predictor for severity. J Microbiol Immunol Infect. 2019;52:54–61. https://doi.org/10.1016/j.jmii.2016.08.023
15. Hernández Cabrera M, Angel-Moreno A, Santana E, Bolaños M, Francès A, Martín-Sánchez MS, et al. Murine typhus with renal involvement in Canary Islands, Spain. Emerg Infect Dis. 2004;10:740–3. https://doi.org/10.3201/eid1004.030532

Address for correspondence: José Luis Pérez-Arellano, Departamento de Ciencias Médicas y Quirúrgicas, Universidad de Las Palmas de Gran Canaria, 35080, Canary Islands, Spain; email: luis.perez@ulpgc.es

# Evidence of Zika Virus Infection in Pigs and Mosquitoes, Mexico

Daniel Nunez-Avellaneda, Rosa Carmina Cetina-Trejo, Emily Zamudio-Moreno, Carlos Baak-Baak, Nohemi Cigarroa-Toledo, Guadalupe Reyes-Solis, Antonio Ortega-Pacheco, Gerardo Suzán, Chandra Tandugu, Julián E. García-Rejón, Bradley J. Blitvich, Carlos Machain-Williams

Evidence suggests that pigs seroconvert after experimental exposure to Zika virus and are potential sentinels. We demonstrate that pigs are also susceptible to natural Zika virus infection, shown by the presence of antibodies in domestic pigs in Yucatan, Mexico. Zika virus RNA was detected in 5 species of mosquitoes collected inside pigpens.

Pigs are susceptible to experimental Zika virus infection (*1–4*), but evidence of natural infection is lacking. Microcephaly has occurred in fetal piglets after in utero inoculation, and neurologic disease has occurred in neonates after intracranial inoculation, suggesting that pigs are a suitable animal model for the study of Zika virus. Three-month-old pigs exposed to Zika virus through subcutaneous and intradermal injection produce antibodies but not viremias, indicating that pigs could be suitable sentinels. We performed a serologic investigation in the state of Yucatan, Mexico, to determine whether pigs are susceptible to natural Zika virus infection. Mosquitoes temporally and spatially associated with the pigs were tested for evidence of Zika virus infection to increase our understanding of the vector range of the virus.

## The Study

Pigs and mosquitoes were sampled at 4 sites. One site was a commercial farm in Xmatkuil, a suburb 16 km south of Merida, the largest city in Yucatan. The site contained a herd of Yucatan black hairless pigs and a commercial genetic line of breeding pigs. The other sites were Mayan villages to the east and southeast of Merida: Tzucacab (148 km southeast), Valladolid (159 km east), and Xkalakdzonot (155 km southeast). Each village maintained herds of Yucatan black hairless pigs as a food source for residents. We visited each site 1–3 times during 2018 and 2019, and no pigs were sampled more than once. An unusually high number of porcine fetal deaths occurred in Xmatkuil and Xkalakdzonot several weeks before our initial visits. The stillborn pigs displayed signs of mummification but no apparent neurologic malformations, according to their owners. During each visit, we searched human-made structures and vegetation for resting mosquitoes, which were collected by manual aspiration.

Serum samples were assayed by plaque-reduction neutralization test (PRNT) using dengue virus (DENV) serotype 1 (strain Hawaii), DENV serotype 2 (strain NGC), DENV serotype 3 (strain H-87), DENV serotype 4 (strain 241), Ilheus virus (original strain), St. Louis encephalitis virus (strain TBH-28), West Nile virus (strain NY99–35261–11), and Zika virus (strain PRVABC59). Serum specimens were initially screened at a dilution of 1:20 by using Zika virus. Positive samples were further diluted, then assayed using all 8 viruses. Titers were expressed as the reciprocal of serum dilutions yielding $\geq$90% reduction in the number of plaques ($PRNT_{90}$). For etiologic diagnosis, the $PRNT_{90}$ antibody titer to the respective virus was required to be $\geq$4-fold that of other flaviviruses tested.

Mosquitoes were transported alive to the arbovirus laboratory at the Universidad Autonoma de Yucatan and sorted into pools of $\leq$50 according to species, sex, date, study site, and location within the study site. Mosquitoes were transported in RNAlater (Sigma-Aldrich, https://www.sigmaaldrich.com) to Iowa State University, then homogenized by using mortars and pestles. Total RNA was extracted by using Trizol Reagent (ThermoFisher Scientific, https://www.thermofisher.com) and tested for Zika virus RNA by using reverse transcription PCR and Sanger sequencing using primers that amplify a 667-nt region of the envelope protein gene.

Author affiliations: Universidad Autonoma de Yucatan, Merida, Mexico (D. Nunez-Avellaneda, R. Carmina Cetina-Trejo, E. Zamudio-Moreno, C. Baak-Baak, N. Cigarroa-Toledo, G. Reyes-Solis, J.E. García-Rejón, C. Machain-Williams); Iowa State University, Ames, Iowa, USA (D. Nunez-Avellaneda, C. Tandugu, B.J. Blitvich); Universidad Autónoma de Yucatán, Xmatkuil, Mexico; (A. Ortega-Pacheco); Universidad Nacional Autónoma de México, Mexico City, Mexico (G. Suzán)

DOI: https://doi.org/10.3201/eid2702.201452

Serum specimens were collected from 297 pigs (20 from Tzucacab, 73 from Valladolid, 74 from Xkalakdzonot, and 130 from Xmatkuil). Thirty-eight (12.8%) pigs were positive for flavivirus-specific antibodies. Thirteen (4.8%) pigs were seropositive for Zika virus, 1 (0.3%) pig was seropositive for West Nile virus, and 24 (8.1%) pigs had antibodies to an undetermined flavivirus. Zika virus $PRNT_{90}$ titers ranged from 40 to 320 (Table 1). Eleven pigs seropositive for Zika virus were from Xmatkuil, and 1 each was from Tzucacab and Valladolid.

The entomologic investigation yielded 1,870 mosquitoes of 8 species that were sorted into 190 pools. Of these, 381 mosquitoes were collected inside pigpens, and >50% were engorged (Table 2). Mosquitoes were tested for Zika virus RNA by reverse transcription PCR, and resulting amplification products were analyzed by Sanger sequencing. Five pools, all of which contained ≥1 engorged mosquito, were positive for Zika virus sequence, and all consisted of mosquitoes collected inside pigpens in Xmatkuil (Genbank accession nos. MT309004–309008). One pool each of the following mosquito species tested positive: *Aedes aegypti, Ae. taeniorhynchus, Culex lactator, Cx. nigripalpus,* and *Cx. thriambus*. All sequences were identical and differed from the positive control, an isolate from the state of Chiapas, Mexico, in 2016 (Genbank accession no. KX446950.2) in 1 nucleotide position, a C→T substitution at genomic position 1893.

## Conclusions

We detected Zika virus RNA sequence in *Ae. aegypti, Ae. taeniorhynchus, Cx. lactator, Cx. nigripalpus,* and *Cx. thriambus* mosquitoes that were temporally and spatially associated with pigs seropositive for this virus. The role of *Culex* spp. mosquitoes in Zika virus transmission has been debated, but the consensus among the arbovirus community is that they are inefficient vectors (*5*,*6*). *Culex* spp. mosquitoes and Zika virus were first linked after experimental infection studies demonstrated that the *Cx. quinquefasciatus* mosquito is a competent vector of this virus (*7*). Many other studies have shown otherwise, including a study that demonstrated that *Cx. quinquefasciatus* mosquitoes in the state of Jalisco, Mexico, were refractory to Zika virus (*5*,*6*,*8*).

Vector competence experiments have also evaluated mosquitoes from ≥6 other *Culex* spp., although *Cx. lactator, Cx. nigripalpus,* and *Cx. thriambus* mosquitoes are not among them, and none were able to transmit Zika virus (*9*). We add to the small number of studies that have detected Zika virus nucleic acid in field-collected *Culex* spp. mosquitoes (*7*,*10*), but we did not isolate virus or provide evidence of a disseminated infection. We cannot dismiss the possibility that the Zika virus RNA–positive *Culex* spp. mosquitoes had recently fed upon a viremic host but virus replication had not occurred within the mosquito. Therefore, the link between *Culex* spp. mosquitoes and Zika virus remains tenuous. The *Ae. taeniorhynchus* mosquito is also considered an inefficient vector of Zika virus (*11*). In contrast, the *Ae. aegypti* mosquito is the principal urban vector of Zika virus in the Americas (*12*). *Ae. taeniorhynchus* and *Ae. aegypti* mosquitoes are not known to have a strong preference for porcine blood, although 2.4% of engorged *Ae. taeniorhynchus* mosquitoes in the Galapagos Islands had acquired blood from pigs, and the *Cx. nigripalpus* mosquito shifts seasonally to opportunistic feeding behavior (*13*,*14*). Porcine blood has occasionally been detected in *Ae. aegypti* mosquitoes (*15*,*16*).

**Table 1.** Plaque-reduction neutralization test data for pigs seropositive for Zika virus, Yucatan, Mexico, 2018–2019*

| Serum ID | Sample date† | Age category | Virus and $PRNT_{90}$ titer | | | | | | | |
|---|---|---|---|---|---|---|---|---|---|---|
| | | | DENV-1 | DENV-2 | DENV-3 | DENV-4 | ILHV | SLEV | WNV | Zika virus |
| XM-278-J‡ | 2018 Apr | J | – | 20 | – | – | – | – | – | 320 |
| XM-285-J | 2018 Apr | J | – | 40 | – | 20 | – | – | – | 160 |
| VA-265-A | 2018 Jun | A | – | – | – | – | – | – | – | 80 |
| XM-O2A-J | 2018 Jun | J | – | 20 | 20 | – | 40 | 20 | 40 | 160 |
| XM-177-J | 2018 Jun | J | – | – | – | – | – | – | – | 40 |
| XM-181-J | 2018 Jun | J | – | – | 20 | 20 | – | – | – | 80 |
| XM-183-S | 2018 Jun | S | – | – | – | – | – | – | – | 40 |
| XM-189-J | 2018 Jun | J | 80 | – | 20 | 20 | 40 | – | 40 | 320 |
| XM-199-J | 2018 Jun | J | – | – | – | – | – | – | – | 40 |
| XM-202-J | 2018 Jun | J | – | 20 | 20 | – | – | – | – | 80 |
| XM-212-J | 2018 Jun | J | – | – | – | – | – | – | – | 80 |
| XM-238-J | 2018 Jun | J | – | – | – | – | – | – | – | 40 |
| TZ-387-J | 2019 Jan | J | – | – | – | – | – | – | – | 80 |

*A, adult; DENV1, dengue virus type 1; DENV2, dengue virus type 2; DENV3, dengue virus type 3; DENV4, dengue virus type 4; ILHV, Ilheus virus; J, juvenile; $PRNT_{90}$, >90% reduction in the number of plaques on plaque-reduction neutralization test; S, suckling; SLEV, St. Louis encephalitis virus; WNV, West Nile virus; –, ≤20.
†Date (month/year) of serum collection.
‡Prefixes indicate pigs from these areas: TZ, Tzucacab; VA, Valladolid; XM, Xmatkuil.

**Table 2.** Summary of mosquitoes collected inside pigpens, Yucatan, Mexico, 2018–2019

| Study site | Mosquito species | No. collected | No. pools | No. pools positive for Zika virus RNA |
|---|---|---|---|---|
| Tzucacab | *Aedes aegypti* | 58 | 6 | 0 |
| | *Ae. taeniorhynchus* | 3 | 1 | 0 |
| | *Culex quinquefasciatus* | 63 | 7 | 0 |
| | *Cx. thriambus* | 1 | 1 | 0 |
| Valladolid | *Ae. aegypti* | 32 | 2 | 0 |
| | *Ae. cozumelensis* | 1 | 1 | 0 |
| | *Cx. quinquefasciatus* | 45 | 5 | 0 |
| Xkalakdzonot | *Ae. aegypti* | 46 | 5 | 0 |
| | *Ae. cozumelensis* | 2 | 1 | 0 |
| | *Anopheles albimanus* | 6 | 1 | 0 |
| | *Cx. lactator* | 1 | 1 | 0 |
| | *Cx. quinquefasciatus* | 60 | 6 | 0 |
| Xmatkuil | *Ae. aegypti* | 29 | 4 | 1 |
| | *Ae. taeniorhynchus* | 8 | 2 | 1 |
| | *Cx. lactator* | 1 | 1 | 1 |
| | *Culex nigripalpus* | 3 | 1 | 1 |
| | *Culex quinquefasciatus* | 21 | 2 | 0 |
| | *Culex thriambus* | 1 | 1 | 1 |

The mosquito infection rates in our study are high. All Zika virus RNA–positive mosquitoes and most seropositive pigs were sampled at the same site (Xmatkuil) on the same date (June 5, 2018). We speculate that these pigs were infected with Zika virus just before our visit and that some mosquitoes then bit them, without virus disseminating from the midguts of *Culex* spp. mosquitoes. Recent studies have demonstrated that pigs are susceptible to experimental Zika virus infection (*1*–*4*). We provide serologic evidence that pigs are also susceptible to natural Zika virus infection. A high number of stillbirths occurred at 2 study sites before sampling, but none displayed malformations typical of Zika virus infection.

We provide additional evidence that pigs produce neutralizing antibodies upon Zika virus exposure and are potential sentinels. This information will be useful for investigators and public and veterinary health personnel conducting surveillance in Zika virus–endemic areas where pigs are common and usually raised outdoors. One limitation of our study is that pig farmers were not tested for evidence of flavivirus infection. Future studies should investigate whether those persons are at increased risk for Zika disease.


## Acknowledgments

We thank the Institutional Animal Care and Use Committee at the Universidad Autonoma de Yucatan for reviewing and approving this study.

This study was supported by Consejo Nacional de Ciencia y Tecnologia de Mexico grant no. PDCPN 2014-247005 (Problemas Nacionales) and in part by intramural funding provided by Iowa State University.



## About the Author

Dr. Nunez-Avellaneda is a postdoctoral scientist in the College of Veterinary Medicine at Iowa State University. His research interests include studying the human and veterinary health impact and transmission dynamics of mosquito-transmitted viruses in Mexico.


## References


1. Wichgers Schreur PJ, van Keulen L, Anjema D, Kant J, Kortekaas J. Microencephaly in fetal piglets following in utero inoculation of Zika virus. Emerg Microbes Infect. 2018;7:42. https://doi.org/10.1038/s41426-018-0044-y
2. Darbellay J, Cox B, Lai K, Delgado-Ortega M, Wheler C, Wilson D, et al. Zika virus causes persistent infection in porcine conceptuses and may impair health in offspring. EBioMedicine. 2017;25:73–86. https://doi.org/10.1016/j.ebiom.2017.09.021
3. Darbellay J, Lai K, Babiuk S, Berhane Y, Ambagala A, Wheler C, et al. Neonatal pigs are susceptible to experimental Zika virus infection. Emerg Microbes Infect. 2017;6:e6. https://doi.org/10.1038/emi.2016.133
4. Ragan IK, Blizzard EL, Gordy P, Bowen RA. Investigating the potential role of North American animals as hosts for Zika virus. Vector Borne Zoonotic Dis. 2017;17:161–4. https://doi.org/10.1089/vbz.2016.2099
5. Roundy CM, Azar SR, Brault AC, Ebel GD, Failloux AB, Fernandez-Salas I, et al. Lack of evidence for Zika virus transmission by *Culex* mosquitoes. Emerg Microbes Infect. 2017;6:e90. https://doi.org/10.1038/emi.2017.85
6. van den Hurk AF, Hall-Mendelin S, Jansen CC, Higgs S. Zika virus and *Culex quinquefasciatus* mosquitoes: a tenuous link. Lancet Infect Dis. 2017;17:1014–6. https://doi.org/10.1016/S1473-3099(17)30518-2
7. Guedes DR, Paiva MH, Donato MM, Barbosa PP, Krokovsky L, Rocha SWDS, et al. Zika virus replication in the mosquito *Culex quinquefasciatus* in Brazil. Emerg Microbes Infect. 2017;6:e69. https://doi.org/10.1038/emi.2017.59
8. Elizondo-Quiroga D, Ramírez-Medina M, Gutiérrez-Ortega A, Elizondo-Quiroga A, Muñoz-Medina JE, Sánchez-Tejeda G, et al. Vector competence of *Aedes aegypti* and *Culex quinquefasciatus* from the metropolitan area of Guadalajara,

Jalisco, Mexico for Zika virus. Sci Rep. 2019;9:16955. https://doi.org/10.1038/s41598-019-53117-1
9. Epelboin Y, Talaga S, Epelboin L, Dusfour I. Zika virus: an updated review of competent or naturally infected mosquitoes. PLoS Negl Trop Dis. 2017;11:e0005933. https://doi.org/10.1371/journal.pntd.0005933
10. Elizondo-Quiroga D, Medina-Sánchez A, Sánchez-González JM, Eckert KA, Villalobos-Sánchez E, Navarro-Zúñiga AR, et al. Zika virus in salivary glands of five different species of wild-caught mosquitoes from Mexico. Sci Rep. 2018;8:809. https://doi.org/10.1038/s41598-017-18682-3
11. Hart CE, Roundy CM, Azar SR, Huang JH, Yun R, Reynolds E, et al. Zika virus vector competency of mosquitoes, Gulf Coast, United States. Emerg Infect Dis. 2017;23:559–60. https://doi.org/10.3201/eid2303.161636
12. Kauffman EB, Kramer LD. Zika Virus mosquito vectors: competence, biology, and vector control. J Infect Dis. 2017;216(suppl_10):S976–90. https://doi.org/10.1093/infdis/jix405
13. Edman JD, Taylor DJ. *Culex nigripalpus*: seasonal shift in the bird-mammal feeding ratio in a mosquito vector of human encephalitis. Science. 1968;161:67–8. https://doi.org/10.1126/science.161.3836.67
14. Bataille A, Fournié G, Cruz M, Cedeño V, Parker PG, Cunningham AA, et al. Host selection and parasite infection in *Aedes taeniorhynchus*, endemic disease vector in the Galápagos Islands. Infect Genet Evol. 2012;12:1831–41. https://doi.org/10.1016/j.meegid.2012.07.019
15. Olson MF, Ndeffo-Mbah ML, Juarez JG, Garcia-Luna S, Martin E, Borucki MK, et al. High rate of non-human feeding by *Aedes aegypti* reduces Zika virus transmission in south Texas. Viruses. 2020;12:E453. https://doi.org/10.3390/v12040453
16. Sivan A, Shriram AN, Sunish IP, Vidhya PT. Host-feeding pattern of *Aedes aegypti* and *Aedes albopictus* (Diptera: Culicidae) in heterogeneous landscapes of South Andaman, Andaman and Nicobar Islands, India. Parasitol Res. 2015;114:3539–46. https://doi.org/10.1007/s00436-015-4634-5


Address for correspondence: Carlos Machain-Williams, Laboratorio de Arbovirologia, Centro de Investigaciones Regionales Dr. Hideyo Noguchi, Edificio Inalámbrica, Calle 43 No. 613 x Calle 90, Colonia Inalámbrica, Universidad Autónoma de Yucatán, Mérida, Yucatán CP 97000, Mexico; email: carlos.machain@correo.uady.mx

# Novel Arterivirus Associated with Outbreak of Fatal Encephalitis in European Hedgehogs, England, 2019

Akbar Dastjerdi, Nadia Inglese, Tim Partridge, Siva Karuna, David J. Everest, Jean-Pierre Frossard, Mark P. Dagleish, Mark F. Stidworthy

In the fall of 2019, a fatal encephalitis outbreak led to the deaths of >200 European hedgehogs (*Erinaceus europaeus)* in England. We used next-generation sequencing to identify a novel arterivirus with a genome coding sequence of only 43% similarity to existing GenBank arterivirus sequences.

Arteriviruses are enveloped, spherical viruses with a positive-sense, single-stranded, linear RNA genome (*1*), and they are assigned to the order Nidovirales, family *Arteriviridae*. Arteriviruses infect equids, pigs, possums, nonhuman primates, and rodents. For example, equine arteritis virus causes mild-to-severe respiratory disease, typically in foals, or abortion in pregnant mares (*2*). In pigs, porcine reproductive and respiratory syndrome virus types 1 and 2 cause a similar clinical syndrome of reproductive failure and respiratory disease (*3*,*4*). Wobbly possum disease virus causes an often fatal neurologic syndrome in possums (*5*). Several other arteriviruses (Pebjah virus, simian hemorrhagic encephalitis virus, and simian hemorrhagic fever virus) cause highly lethal hemorrhagic fever in captive Asian macaques (*6*). Lactate dehydrogenase–elevating virus was discovered by Riley et al. during their work on plasma enzyme levels in tumor-bearing mice (*7*). Arteriviruses were detected in Chinese softshell turtles (*Pelodiscus sinensis*) that had hemorrhagic disease (*8*) and from healthy African giant shrews (*Crocidura olivieri*) by molecular assays (*9*). Arteriviruses are documented to be transmitted through respiratory, venereal, and transplacental routes (*10*,*11*); direct contact with infected possums has been the most efficient route of wobbly possum disease virus transmission.

Arteriviruses were recently classified into 6 subfamilies (*Crocarterivirinae*, *Equarterivirinae*, *Heroarterivirinae*, *Simarterivirinae*, *Variarterivirinae*, and *Zealarterivirinae*) and 12 genera (*12*). The arterivirus genome is composed of a single, 12–16 kb, polyadenylated, RNA strand that contains 2 major genomic regions. The 5′ region contains open reading frames (ORFs) 1a and 1b coding for the viral polymerase and other nonstructural proteins (*13*). The 3′ region encodes the structural components of the virions and contains $\geq$7 ORFs. These ORFs code for the envelope protein, glycoproteins (2b–5), membrane, and nucleocapsid proteins. The 2 regions also differ in their protein expression mechanisms (*1*).

We describe the disease history, histopathology, and the near complete genome sequence of a novel arterivirus, hedgehog arterivirus 1 (HhAV-1). This virus was detected in association with fatal encephalitis in European hedgehogs (*Erinaceus europaeus*) from England.

## The Study

An outbreak of neurologic disease began in October 2019 in wild hedgehogs admitted to the Vale Wildlife Hospital and Rehabilitation Centre (Tewkesbury, England) and lasted for 4 months. These hedgehogs were from within a 50-km radius of the hospital. Those initially admitted were housed in a room dedicated to sick and young animals, sharing airspace with birds, rabbits, and occasionally rodents. Those admitted later were housed separately with other

Author affiliations: Animal and Plant Health Agency–Weybridge, Addlestone, UK (A. Dastjerdi, N. Inglese, S. Karuna, D.J. Everest, J.P. Frossard); Vale Wildlife Hospital and Rehabilitation Centre, Tewkesbury, UK (T. Partridge); Moredun Research Institute, Penicuik, UK (M.P. Dagleish); International Zoo Veterinary Group, Keighley, UK (M.F. Stidworthy)

DOI: https://doi.org/10.3201/eid2702.201962

hedgehogs and occasionally with rabbits. Approximately 50% of hedgehogs admitted showed development of clinical signs, died, or were euthanized. Both juveniles and adults (≈15% of hedgehog admissions) were affected by this neurologic disease. In many instances, the animals became inappetent a few days after admission, although others took up to 6 weeks to become symptomatic.

Neurologic signs developed within 3 days of the onset of inappetence and included tremors, twitching, hyperaesthesia, ataxia/paresis, falling to 1 side, and paddling legs when laterally recumbent. Later signs included seizures, but most animals were euthanized before this stage. All described clinical signs developed after admission to the hospital; thus, all cases were considered nosocomial. Strict hygiene, biosecurity, and reduced juvenile admissions eventually resulted in the cessation of contagion. The outbreak resulted in >200 deaths.

The attending veterinarian at the wildlife hospital performed gross postmortem examinations of 3 newly dead hedgehogs. No major macroscopic lesions were identified. Histologic lesions in formalin-fixed brain were similar for all 3 hedgehogs (identification nos. 19-2271–3) examined by a specialist veterinary pathologist and consistent with a common etiology. Multiple coronal and longitudinal brain sections showed moderate-to-severe multifocal gliosis of highest severity in forebrain and hindbrain. Small numbers of neutrophils intermingled with microglia

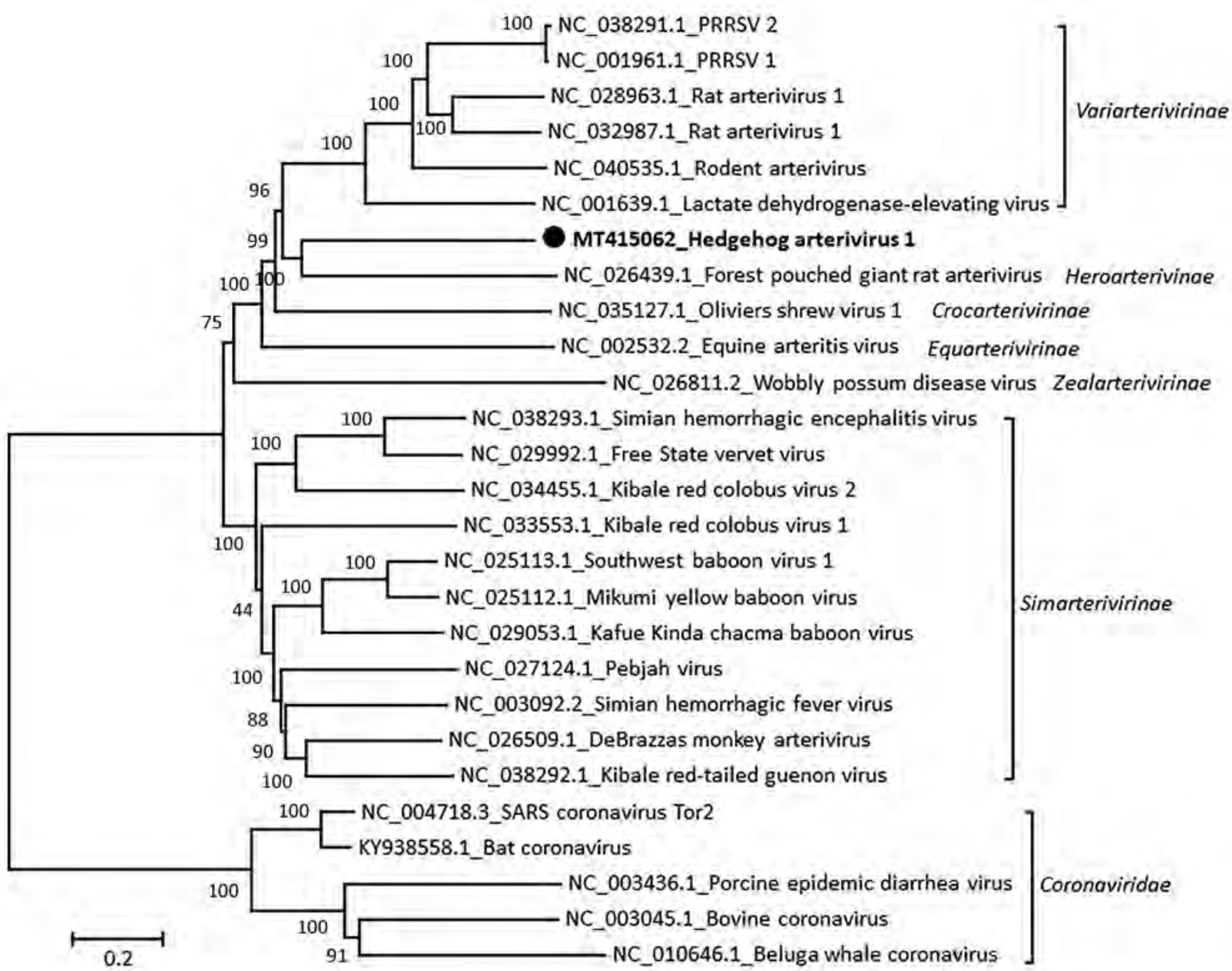


**Figure 1.** Phylogenetic analysis of the coding sequence of hedgehog arterivirus 1. The virus genome was aligned by using the MegAlign software of the DNASTAR Lasergene Core Suite (DNASTAR, Inc., https://www.dnastar.com), and phylogenetic analysis was performed by using MEGA 5.2 software (https://www.megasoftware.net). The rooted tree was constructed by using the neighbor-joining method and 1,000 bootstrap replications. Each virus on the tree is represented by its GenBank accession number and name. Designation of subfamilies was conducted as outlined in the International Committee on Taxonomy of Viruses 2018 release (https://talk.ictvonline.org/ictv-reports). Coronaviruses are included as an outgroup. Solid black circle and bold indicate strain detected in this study. Numbers along branches are bootstrap values. Scale bar indicates nucleotide substitutions per site.

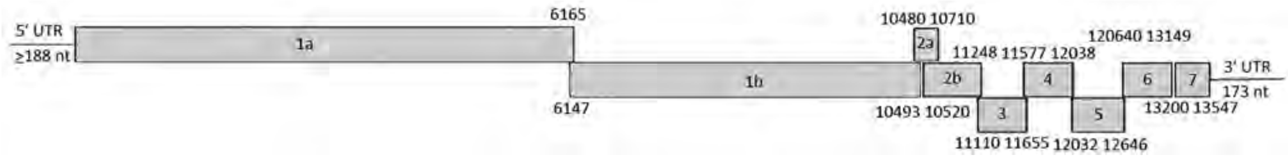


**Figure 2.** Genomic organization of hedgehog arterivirus-1. The genome arrangement resembles those of classical arteriviruses with open reading frames (ORFs) 1a/1b, 2a, 2b, 3, 4, 5, 6, and 7 that encode the polyproteins 1a/1ab, envelope protein, glycoproteins 2b–5, and membrane and nucleocapsid proteins, respectively. ORF1a and ORF1b are joined through a −1 ribosomal frameshift, encoding replicase precursor polyproteins pp1a/pp1ab. UTR, untranslated region.

in perivascular foci expanding into the surrounding parenchyma. Brainstem, cerebral cortex, hippocampus, and midbrain contained similar lesions. Minimal multifocal meningitis with mononuclear inflammatory cell cuffing (intermingled with small-to-moderate numbers of neutrophils) was also observed. Ventricles (particularly midbrain) had subependymal edema and were infiltrated by mixed mononuclear cells and fewer neutrophils. Reactive astrocytes with conspicuous nucleoli were present within areas of gliosis and inflammation. Neuronal necrosis was occasionally observed.

Epithelia in many proximal renal tubules had intracytoplasmic lipid vacuolation and occasional intracytoplasmic protein globules. Moderate numbers of glomerular capsules and distal tubules contained eosinophilic, proteinaceous fluid with infrequent interstitial and perivascular neutrophils. Splenic red pulp was packed with abundant extramedullary hematopoietic cells. Plentiful periarteriolar lymphoid populations frequently included central lymphocytes with pyknotic nuclei. Liver and heart were histologically unremarkable. No fungi, protozoa, or viral inclusion bodies were recognized. Clinical manifestations, histologic characteristics, and distribution of lesions were distinct from those of wobbly hedgehog syndrome (*14*).

We performed immunohistochemical analysis (*15*) of formalin-fixed brain tissue from the 3 hedgehogs for *Listeria* spp., louping-ill, and related flavivirus antigens. All results were negative.

Virologic investigation was conducted at the Animal and Plant Health Agency–Weybridge (Addlestone, UK). Freshly frozen brain tissues from 3 additional hedgehogs (identification nos. 3375, 4896, and 3777) initially were tested for herpesviruses and showed negative results. The 3 samples were then subjected to next-generation sequencing (NGS) by using an Illumina MiSeq (https://www.illumina.com). The HhAV-1 sequence was obtained by de novo assembly using the SeqMan NGen (DNASTAR, Inc., https://www.dnastar.com). No other microbial pathogen was detected.

The 3 identical HhAV-1 (UK 2019 strain) sequences had a genome coding sequence of ≥13,873 nt (GenBank accession no. MT415062). Genetic analysis of the sequence showed the highest similarity to arteriviruses detected in African giant-pouched rats (*Cricetomys gambianus)* (GenBank accession no. NC_026439) sampled in Guinea, but only 43% nt identity. Accordingly, the virus clustered phylogenetically with arterivirus in the African giant-pouched rat in the subfamily *Heroarterivirinae* (Figure 1). The virus genomic organization was determined to be typical of arteriviruses, in particular murine arteriviruses, and included ORF1a and 1b encoding replicase precursor polyproteins pp1a/pp1ab, followed by genes encoding envelope protein, the major structural glycoproteins (2b-5), matrix, and nucleocapsid proteins (Figure 2). At the amino acid level, the highest similarity was for the pp1b protein, where it showed a 50.6% similarity with the sequence from the African giant-pouched rat arterivirus.

To detect and quantify HhAV-1 load in samples from animals, we used reverse transcription quantitative PCR, primers forward 5′-CAG GAA CCC TCA CAG TAG-3′ and reverse 5′-TAA GAA GTT TGY GGC ATA G-3′, and probe (fluorescein) 5′-GGT TTC GTT CAA TGT TGA GGT-3′ (MGBEQ), which amplified a 100-nt segment of the ORF7 gene. Blood, brain, liver, lung, and spleen from these 3 animals were also positive for HhAV-1 in this PCR. The tissues tested had relatively high viral loads, and blood and brain had the highest load (measured by using the cycle threshold:β-actin ratio) but not much higher than those for other tissues.

## Conclusions

We detected a novel pathogenic arterivirus in the ever-expanding family *Arteriviridae*. Because no wild animals were identified as having neurologic signs, we infer that all cases were probably hospital acquired. Whether the virus was introduced to the hospital through an asymptomatic carrier hedgehog or other wildlife (e.g., birds, rabbits or rodents) that shared the same airspace in the hospital remains unknown. However, arteriviruses are known to cause persistent/

asymptomatic infections (e.g., equine arteritis virus, simian hemorrhagic fever virus, lactate dehydrogenase–elevating virus) and to be highly species specific (*10*,*13*). Therefore, the virus was most likely introduced by 1 or several asymptomatic hedgehogs.

This disease outbreak with neurologic signs highlights the requirement for strict biosecurity measures during rehabilitation involving intensive hospitalization of animals of this species, which are a frequent wildlife casualty submission in the United Kingdom. Hedgehogs are protected by the Biodiversity Action Plan in the United Kingdom.

#### Acknowledgments

We thank the Mammalian Virus Investigation Unit team at Animal and Plant Health Agency–Weybridge for helping to prepare samples for NGS, Clare Underwood for assistance with immunohistochemical analysis, Falko Steinbach for commenting on the manuscript, and Hannah Davies for helping with NGS data analysis.

This NGS portion of this study was supported by the British Hedgehog Preservation Society.

### About the Author

Dr. Dastjerdi is head of the Mammalian Virus Investigation Unit at the Animal and Plant Health Agency–Weybridge, Addlestone, UK. His primary research interests are detection and characterization of emerging viral pathogens.

#### References

1. Kuhn JH, Lauck M, Bailey AL, Shchetinin AM, Vishnevskaya TV, Bào Y, et al. Reorganization and expansion of the nidoviral family *Arteriviridae*. Arch Virol. 2016;161:755–68. https://doi.org/10.1007/s00705-015-2672-z
2. Bryans JT, Crowe ME, Doll ER, McCollum WH. Isolation of a filterable agent causing arteritis of horses and abortion by mares; its differentiation from the equine abortion (influenza) virus. Cornell Vet. 1957;47:3–41.
3. Wensvoort G, Terpstra C, Pol JM, ter Laak EA, Bloemraad M, de Kluyver EP, et al. Mystery swine disease in The Netherlands: the isolation of Lelystad virus. Vet Q. 1991; 13:121–30. https://doi.org/10.1080/01652176.1991.9694296
4. Collins JE, Benfield DA, Christianson WT, Harris L, Hennings JC, Shaw DP, et al. Isolation of swine infertility and respiratory syndrome virus (isolate ATCC VR-2332) in North America and experimental reproduction of the disease in gnotobiotic pigs. J Vet Diagn Invest. 1992;4:117–26. https://doi.org/10.1177/104063879200400201
5. Perrott MR, Meers J, Cooke MM, Wilks CR. A neurological syndrome in a free-living population of possums (*Trichosurus vulpecula*). N Z Vet J. 2000;48:9–15. https://doi.org/10.1080/00480169.2000.36150
6. Tauraso NM, Shelokov A, Palmer AE, Allen AM. Simian hemorrhagic fever. 3. Isolation and characterization of a viral agent. Am J Trop Med Hyg. 1968;17:422–31. https://doi.org/10.4269/ajtmh.1968.17.422
7. Riley V, Spackman DH, Santisteban GA, Dalldorf G, Hellstrom I, Hellstrom KE, et al. The LDH virus: an interfering biological contaminant. Science. 1978;200:124–6. https://doi.org/10.1126/science.263259
8. Liu L, Cao Z, Lin F, Ye XP, Xu Y. Partial sequence of a novel virus isolated from *Pelodiscus sinensis* hemorrhagic disease. Intervirology. 2015;58:197–204. https://doi.org/10.1159/000437354
9. Vanmechelen B, Vergote V, Laenen L, Koundouno FR, Bore JA, Wada J, et al. Expanding the arterivirus host spectrum: Olivier's shrew virus 1, a novel arterivirus discovered in African giant shrews. Sci Rep. 2018;8:11171. https://doi.org/10.1038/s41598-018-29560-x
10. Brinton MA. Arteriviruses (*Arteriviridae*). In: Granoff A, Webster R, editors. Encyclopedia of virology, 2nd ed. Amsterdam: Elsevier; 1999. p. 89–97.
11. London WT. Epizootiology, transmission and approach to prevention of fatal simian haemorrhagic fever in rhesus monkeys. Nature. 1977;268:344–5. https://doi.org/10.1038/268344a0
12. Siddell SG, Walker PJ, Lefkowitz EJ, Mushegian AR, Adams MJ, Dutilh BE, et al. Additional changes to taxonomy ratified in a special vote by the International Committee on Taxonomy of Viruses (October 2018). Arch Virol. 2019;164:943–6. https://doi.org/10.1007/s00705-018-04136-2
13. Snijder EJ, Kikkert M, Fang Y. Arterivirus molecular biology and pathogenesis. J Gen Virol. 2013;94:2141–63. https://doi.org/10.1099/vir.0.056341-0
14. Díaz-Delgado J, Whitley DB, Storts RW, Heatley JJ, Hoppes S, Porter BF. The pathology of wobbly hedgehog syndrome.Vet Pathol. 2018;55:711–8. https://doi.org/10.1177/ 0300985818768033
15. Dagleish MP, Benavides J, Chianini F. Immunohistochemical diagnosis of infectious diseases of sheep. Small Ruminant Research. 2010;92(1–3, Special Issue SI):19–35.

Address for correspondence: Akbar Dastjerdi, Animal and Plant Health Agency–Weybridge, Addlestone, Surrey KT15 3NB, UK; email: akbar.dastjerdi@apha.gov.uk

# Estimating Transmission Parameters for COVID-19 Clusters by Using Symptom Onset Data, Singapore, January–April 2020

Sheryl Hui-Xian Ng, Palvinder Kaur, Cécile Kremer, Woan Shin Tan, Aidan Lyanzhiang Tan, Niel Hens, Matthias Paul Toh, Kiok Liang Teow, Palvannan Kannapiran

We estimated the generation interval distribution for coronavirus disease on the basis of serial intervals of observed infector–infectee pairs from established clusters in Singapore. The short mean generation interval and consequent high prevalence of presymptomatic transmission requires public health control measures to be responsive to these characteristics of the epidemic.

A systematic review estimated that the basic reproduction number ($R_0$) for coronavirus disease (COVID-19) is 2–3 (*1*). However, alone is insufficient to characterize an epidemic. The distribution of the serial interval (i.e., the length of time between symptom onset of 2 cases) has been estimated for COVID-19; mean intervals range from 3.1 to 7.5 days (*2*,*3*). Estimation of the generation interval ($T_g$) (i.e., the length of time between the points of infection for 2 linked cases) is less common. Although studies have reported means of 3.3 and 5.0 days (*4*; Li et al., unpub. data, https://doi.org/10.1101/2020.02.26.20028431), Ganyani et al. (*5*) estimated the mean (± SD) of $T_g$ to be 3.9 (± 2.7) days on the basis of which they estimated that 66% (95% credible interval [CrI] 45%–84%) of transmission occurred before symptoms. Another study of 77 pairs estimated the same proportion to be 44% (95% CI 25%–69%) (*6*). Because conventional outbreak control measures are centered around isolation, contact tracing, and treatment of symptomatic case-patients, a high prevalence of presymptomatic transmission ($p$) would warrant shifting measures to address potential transmission among persons with no apparent symptoms (*7*). Hence, to inform control measures for the outbreak in Singapore, we generated estimates of $T_g$, $R_0$, and $p$ by using published symptom onset data for COVID-19 cases in Singapore.

Author affiliations: National Healthcare Group, Singapore (S.H.-X. Ng, P. Kaur, W.S. Tan, A.L. Tan, K.L. Teow, P. Kannapiran); Hasselt University, Hasselt, Belgium (C. Kremer, N. Hens); University of Antwerp, Antwerp, Belgium (N. Hens); National Centre for Infectious Diseases, Singapore (M.P. Toh); National University of Singapore, Singapore (M.P. Toh)

DOI: https://doi.org/10.3201/eid2702.203018

## The Study

We implemented a cross-sectional study design to estimate $T_g$, $R_0$, and $p$ for the COVID-19 outbreak in Singapore during January 23–April 6, 2020. Given that containment measures were initiated over the duration of the study, we considered $R_0$ *to* be the effective reproduction number of the outbreak. All confirmed COVID-19 cases classified by the Ministry of Health of Singapore (MOH) as linked to a local cluster were included in this analysis. Information on case number, cluster, patient age and sex, imported status, date of symptom onset (DOO), and known contacts who have also been confirmed as case-patients were extracted from daily press releases published by MOH. DOOs for cases that were not available from press releases were extracted from a similar anonymized dataset of COVID-19 admissions to the National Centre for Infectious Diseases, Singapore. Cases with DOOs not available from that dataset were subsequently excluded from analysis. Our study was approved by the ethics review board of National Healthcare Group, Singapore.

We identified index cases and potential infectors of each case-patient on the basis of available information of the case-patients' known contacts, published case links, and a heuristic to sensibly include potential infectors who could have transmitted the infection to the case-patients (Appendix, https://wwwnc.cdc.gov/EID/article/27/2/20-3018-App1.pdf). We subsequently used the infector–infectee pairs constructed to estimate the serial and generation interval distribution.

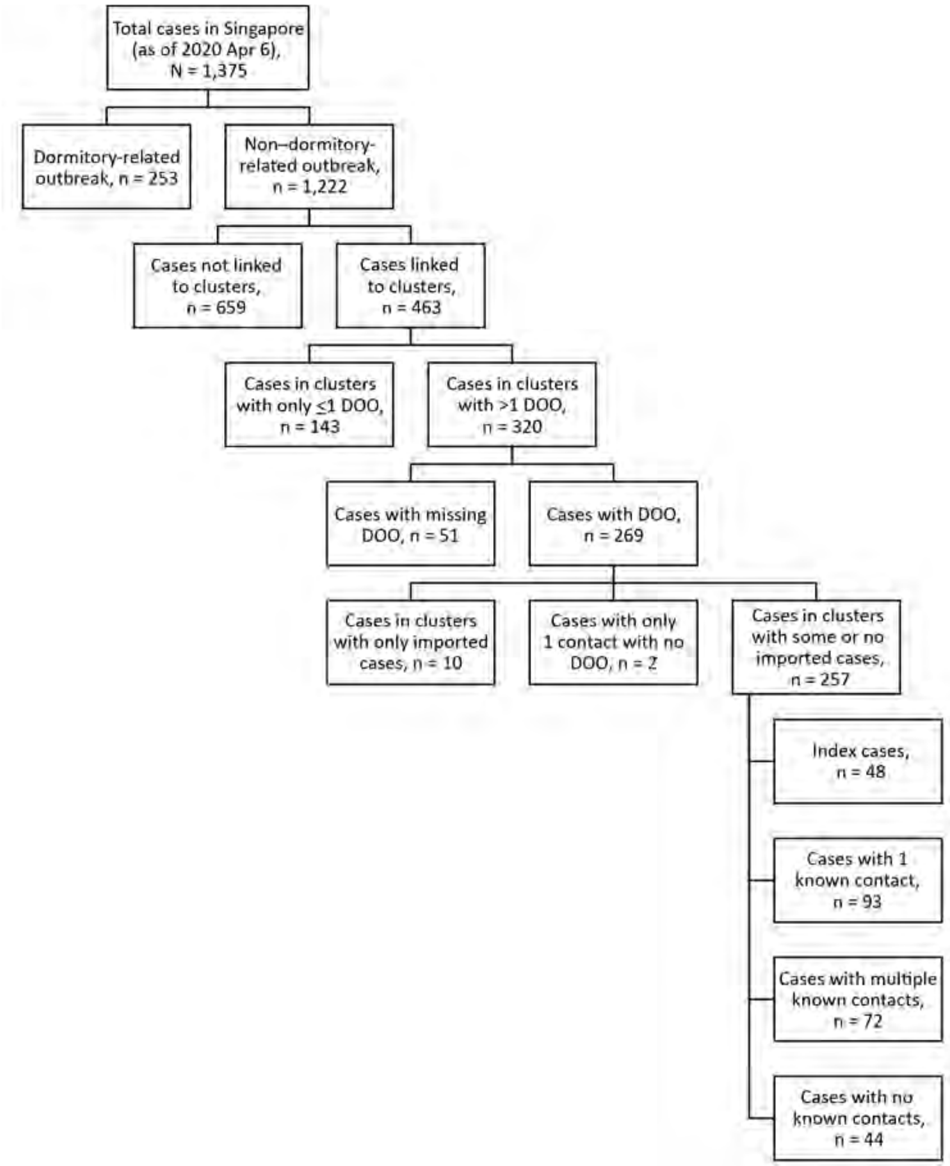


**Figure 1.** Inclusion and exclusion of coronavirus disease case-patients for analysis, Singapore, January–April 2020. DOO, date of symptom onset.

Assuming the same incubation period with mean (± SD) of 5.2 (± 2.8) days, we replicated the Bayesian Markov chain Monte Carlo procedure detailed in Ganyani et al. (*5*) to estimate the mean (SD) of the $T_g$ (Appendix). With the estimated parameters, we constructed the distribution of $R_0$ and subsequently $p$ by simulating infections and computing the proportion of presymptomatic transmissions. We conducted subgroup analyses for case-patients with multiple, family, or no contacts, and for clusters with no missing DOO. We conducted sensitivity analyses estimating the distribution of $R_0$ by using resampled values from a 95% CI of the epidemic growth rate and group-specific rates. For each distribution, we reported the median and 95% CrI. All analyses were conducted by using RStudio 1.2.5033 (https://rstudio.com).

A total of 1,375 confirmed cases had been reported as of April 6, 2020, and we applied our exclusion criteria to obtain a final sample size of 257 cases (Figure 1). We have summarized sample characteristics (Table 1) and the spread of cases over time (Figure 2). Because 48 index case-patients had no known infector, a maximum of 209 infector–infectee pairs were constructed for analysis.

Analyzing the 209 pairs, we estimated the mean $T_g$ to be 3.44 (95% CrI 2.79–4.11) days, with an SD of 2.39 (95% CrI 1.27–3.45) days (Table 2). This estimate corresponded to an $R_0$ of 1.09 (95% CrI 1.08–1.11) and $p$ of 0.72 (95% CrI 0.64–0.80). We estimated the serial interval distribution (Appendix Table 1) and convergence plots for all analyses (Appendix Figure 3).

**Table 1.** Characteristics of coronavirus disease case-patients in study estimating transmission parameters for coronavirus disease clusters by using symptom onset data, Singapore, January–April 2020

| Characteristic | No. (%)* |
|---|---|
| Age, y, median (25th–75th percentile) | 47 (30–59) |
| Sex | |
| M | 121 (47.1) |
| F | 136 (52.9) |
| Imported | 24 (9.3) |
| Cluster size, N = 51 | |
| 2 cases | 28 (54.9) |
| 3 cases | 12 (23.5) |
| ≥4 cases and above | 11 (21.6) |

*Values are no. (%) unless otherwise indicated.

Examining the 93 pairs with only 1 known contact, the estimates for mean $T_g$, SD $T_g$ and $R_0$ increased, whereas $p$ decreased (Table 2). The 116 pairs that required identification of potential infectors had a shorter mean $T_g$ and a higher $p$ in comparison (Table 2). Subgroup analyses are summarized in Appendix Table 2. However, the chains for pairs with family or no known contact exhibited poor convergence, and estimates were not reported. Sensitivity analyses using resampled growth rates and group-specific rates did not yield estimates differing from those of the main analyses (Appendix Table 3).

## Conclusions

The mean generation interval of the COVID-19 outbreak in Singapore was estimated at 3.44 days, suggesting that an infected person would be expected to pass on an infection to another person in 3 days, within the range of 3.3–5.0 days reported by other studies (*4,5*; Li et al., unpub. data). Pairs with only 1 known contact yielded a larger estimate of 3.93 days, whereas pairs for whom infectors were identified had a shorter mean generation interval of 3.03 days. These results suggest that we might best report the upper bound of estimates, accounting for the presence of unclear transmission links within the clusters.

The $R_0$ estimated was slightly >1, higher than other estimates reported as of March 31, 2020 (*8*). We observed a high $p$, potentially a result of prompt isolation of symptomatic case-patients (M. Casey et al., unpub. data, https://doi.org/10.1101/2020.05.08.20094870). This higher proportion might also be attributable to our allowance of infector DOOs to be up to 3 days after their infectees' DOOs, establishing the plausibility of presymptomatic transmission. We acknowledge that this cutoff would have an influence on our eventual estimates. Although negative serial intervals >3 days have occurred in other studies (*5*; Z. Du et al., unpub. data, https://doi.org/10.1101/2020.02.19.20025452), we chose a conservative cutoff of 3 days consistent with He et al. (*6*), where 9% of transmissions would occur before 3 days before DOO.

Nonetheless, the high prevalence of presymptomatic transmission in the community requires public health strategies to be responsive to this characteristic to remain effective. Universal wearing of masks in the community might reduce the likelihood of transmission through saliva and respiratory droplets (*9*). In place of testing when symptoms are observed,

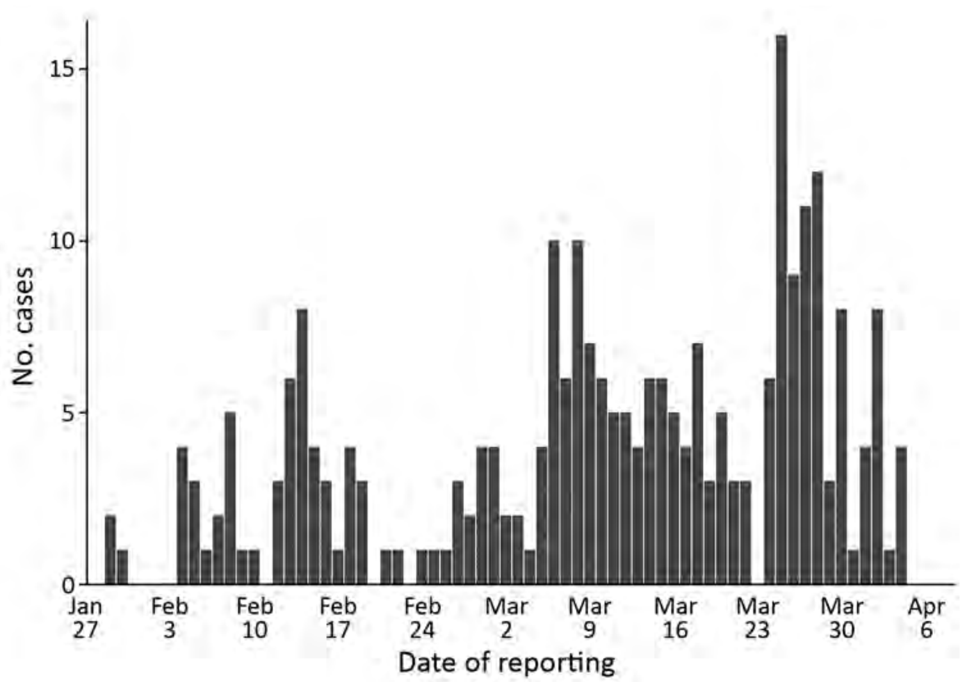


**Figure 2.** Epidemic curve of coronavirus disease clusters, Singapore, January–April 2020.

**Table 2.** Estimates of transmission parameters of coronavirus disease clusters, Singapore, January–April 2020 *

| Infectee type | Median (95% credible interval) | | | |
|---|---|---|---|---|
| | Mean $T_g$ | SD $T_g$ | $R_0$ | $p$ |
| All case-patients, N = 209 | 3.44 (2.79–4.11) | 2.39 (1.27–3.45) | 1.09 (1.08–1.11) | 0.72 (0.64–0.80) |
| Case-patients with only 1 known contact, n = 93 | 3.93 (3.00–4.93) | 2.63 (1.10–4.31) | 1.11 (1.08–1.14) | 0.65 (0.54–0.76) |
| Case-patients with only multiple or no known contacts, n = 116 | 3.03 (2.13–3.97) | 2.45 (0.86–4.21) | 1.08 (1.06–1.11) | 0.76 (0.65–0.86) |

*$p$, presymptomatic proportion; $R_0$, basic reproduction number; $T_g$, generation time.

universal testing of persons living in or working with confined populations should be prioritized to mitigate the risk for transmission of the infection into these populations (*10*). Contact tracing should be modified to include the period before symptom onset (*6,7*) and should adopt a digital approach to be more comprehensive and less labor intensive (*4*).

Our study generated estimates that accounted for the uncertainty arising from multiple potential infectors and a small sample size, which contributes to the scarce information about disease characteristics. Because we dropped cases without a reported DOO, and DOO data and contact information were self-reported, our estimates might be subject to selection, self-report, and recall biases. Our estimation approach assumed equal probability of infecting among potential infectors, although a higher likelihood of transmission among household contacts has been suggested (*11*). We also did not account for the potential formation of cyclical infector networks, although their effects on the estimates have been demonstrated to be limited (*12*). Nevertheless, our estimates contribute to knowledge about the transmission dynamics of COVID-19 and have implications for control measures.


### Acknowledgments

We thank the Singapore Ministry of Health for their tireless efforts in outbreak control and publication of the data for this manuscript.

N.H. acknowledges funding provided by the EpiPose project from the European Union's SC1-PHE-CORONAVIRUS-2020 programme (project no. 101003688) and by the European's Horizon 2020 research and innovation programme (grant agreement no. 682540–TransMID).


## About the Author

Ms. Ng is a research analyst with the National Healthcare Group in Singapore. Her research interests include the application of biostatistics in epidemiology and health services research.

### References


1. Park M, Cook AR, Lim JT, Sun Y, Dickens BL. A systematic review of COVID-19 epidemiology based on current evidence. J Clin Med. 2020;9:967. https://doi.org/10.3390/jcm9040967
2. Zhao S, Cao P, Chong MKC, Gao D, Lou Y, Ran J, et al. The time-varying serial interval of the coronavirus disease (COVID-19) and its gender-specific difference: a data-driven analysis using public surveillance data in Hong Kong and Shenzhen, China from January 10 to February 15, 2020. Infect Control Hosp Epidemiol. 2020;41:750–1.
3. Li Q, Guan X, Wu P, Wang X, Zhou L, Tong Y, et al. Early transmission dynamics in Wuhan, China, of novel coronavirus–infected pneumonia. N Engl J Med. 2020;382:1199–207. https://doi.org/10.1056/NEJMoa2001316
4. Ferretti L, Wymant C, Kendall M, Zhao L, Nurtay A, Abeler-Dörner L, et al. Quantifying SARS-CoV-2 transmission suggests epidemic control with digital contact tracing. Science. 2020 Mar 31 [Epub ahead of print]. https://doi.org/10.1126/science.abb6936
5. Ganyani T, Kremer C, Chen D, Torneri A, Faes C, Wallinga J, et al. Estimating the generation interval for coronavirus disease (COVID-19) based on symptom onset data, March 2020. Euro Surveill. 2020;25:2000257. https://doi.org/10.2807/1560-7917.ES.2020.25.17.2000257
6. He X, Lau EHY, Wu P, Deng X, Wang J, Hao X, et al. Author correction: temporal dynamics in viral shedding and transmissibility of COVID-19. Nat Med. 2020;26:1491–3. https://doi.org/10.1038/s41591-020-1016-z
7. Wei WE, Li Z, Chiew CJ, Yong SE, Toh MP, Lee VJ. Presymptomatic transmission of SARS-CoV-2—Singapore, January 23–March 16, 2020. MMWR Morb Mortal Wkly Rep. 2020;69:411–5. https://doi.org/10.15585/mmwr.mm6914e1
8. Tariq A, Lee Y, Roosa K, Blumberg S, Yan P, Ma S, et al. Real-time monitoring the transmission potential of COVID-19 in Singapore, March 2020. BMC Med. 2020;18:166. https://doi.org/10.1186/s12916-020-01615-9
9. Cheng VCC, Wong SC, Chuang VWM, So SYC, Chen JHK, Sridhar S, et al. The role of community-wide wearing of face mask for control of coronavirus disease 2019 (COVID-19) epidemic due to SARS-CoV-2. J Infect. 2020;81:107–14. https://doi.org/10.1016/j.jinf.2020.04.024
10. Gandhi M, Yokoe DS, Havlir DV. Asymptomatic transmission, the Achilles' Heel of current strategies to control Covid-19. N Engl J Med. 2020;382:2158–60. https://doi.org/10.1056/NEJMe2009758
11. Bi Q, Wu Y, Mei S, Ye C, Zou X, Zhang Z, et al. Epidemiology and transmission of COVID-19 in 391 cases and 1286 of their close contacts in Shenzhen, China: a retrospective cohort study. Lancet Infect Dis. 2020;20:911–9. https://doi.org/10.1016/S1473-3099(20)30287-5
12. Kremer C, Ganyani T, Chen D, Torneri A, Faes C, Wallinga J, et al. Authors' response: estimating the generation interval for COVID-19 based on symptom onset data. Euro Surveill. 2020;25: 2001269. https://doi.org/10.2807/1560-7917.ES.2020.25.29.2001269


Address for correspondence: Sheryl Hui-Xian Ng, National Healthcare Group, Health Services and Outcomes Research, 3 Fusionopolis Link, 03-08, Singapore 138543; email: sheryl_hx_ng@nhg.com.sg

# Population-Based Serosurvey for Severe Acute Respiratory Syndrome Coronavirus 2 Transmission, Chennai, India

Sriram Selvaraju, Muthusamy Santhosh Kumar, Jeromie Wesley Vivian Thangaraj, Tarun Bhatnagar, Velusamy Saravanakumar, Chethrapilly Purushothaman Girish Kumar, Krithikaa Sekar, Ezhilarasan Ilayaperumal, Ramasamy Sabarinathan, Murugesan Jagadeesan, Masanam Sriramulu Hemalatha, Manoj Vasant Murhekar, and the Chennai COVID Sero-Surveillance Team

We conducted a cross-sectional survey to estimate the seroprevalence of IgG against severe acute respiratory syndrome coronavirus 2 in Chennai, India. Among 12,405 serum samples tested, weighted seroprevalence was 18.4% (95% CI 14.8%–22.6%). These findings indicate most of the population of Chennai is still susceptible to this virus.

On August 15, 2020, India had the third highest number of coronavirus disease (COVID-19) cases globally (*1*). The Indian state of Tamil Nadu reported 332,105 cases and 5,641 deaths on August 15, and ≈35% cases were from the state capital, Chennai (*2*). Administratively, Greater Chennai Corporation (GCC) is divided into 15 zones that are further divided into 200 wards with populations ranging from 4,400–104,558 (*3*). The total population of GCC is 7.1 million and 31% of the population resides in slums.

As a part of nationwide containment strategy, Chennai was under lockdown beginning March 25, 2020; beginning May 4, the lockdown was relaxed in a phased manner. Wearing facemasks in public has been mandatory since April 13. However, the number of COVID-19 cases has been increasing in Chennai since May.

Serologic surveys can provide a comprehensive picture of community spread of severe acute respiratory syndrome coronavirus 2 (SARS-CoV-2), the causative agent of COVID-19 (*4*). During the first week of May, the unweighted seroprevalence in Chennai was 2% (*5*). We conducted a community-based serosurvey in July 2020, to estimate the seroprevalence of SARS-CoV-2 in GCC.

Author affiliations: Indian Council of Medical Research–National Institute for Research in Tuberculosis, Chennai, India (S. Selvaraju, K. Sekar, E. Ilayaperumal); ICMR–National Institute of Epidemiology, Chennai (M. Santhosh Kumar, J.W. Vivian Thangaraj, T. Bhatnagar, V. Saravanakumar, C.P. Girish Kumar, R. Sabarinathan, M.V. Murhekar); Greater Chennai Corporation, Chennai (M. Jagadeesan, M.S. Hemalatha)

DOI: https://doi.org/10.3201/eid2702.203938

## The Study

We conducted a household-based cross-sectional survey among usual residents ≥10 years of age in GCC. To estimate a seroprevalence of 2%, with 20% relative precision, design effect of 2.5, and 95% CI, we needed a sample size of 11,710 persons, which we rounded to 12,000. We used a multistage cluster sampling method to select the survey participants. In the first stage, we selected 51 wards by using probability proportion to population size method. In the second stage, we randomly selected 6 streets from each ward from which to recruit participants. The survey team selected a random starting point in each street and visited contiguous households to enroll ≥40 consenting persons ≥10 years of age. When no one was home or household members were unavailable, the team proceeded to the next house and completed the survey until ≥40 persons were enrolled from each street. We included all eligible persons in the household who consented.

After obtaining written consent from persons ≥18 years of age, and assent and parental or guardian approval from persons <18 years of age, we interviewed participants to collect information. We used the Open Data Kit application (https://opendatakit.org) to collect sociodemographic details, and information on exposure to laboratory-confirmed COVID-19 case, history of COVID-19 symptoms in the past 3 months, and COVID-19 testing status.

After the interview, we collected 3–5 mL of venous blood from each participant into BD Vacutainer Blood Collection Tubes (Becton Dickenson, https://www.bd.com). We later tested serum samples for IgG against SARS-CoV-2 by using SARS-CoV-2 IgG immunoassay (Abbott, https://www.corelaboratory.abbott) (Appendix, https://wwwnc.cdc.gov/EID/article/27/2/20-3938-App1.pdf) (*6*). The study protocol was approved by the Institutional Ethics Committee of ICMR-National Institute of Epidemiology.

We analyzed the data to estimate weighted seroprevalence of SARS-CoV-2 and 95% CI by using appropriate sampling weights. We further adjusted the seroprevalence for assay characteristics (*6*). We estimated the total number of SARS-CoV-2 infections among persons ≥10 years of age and infection-to-case ratio (ICR) (Appendix).

The survey teams visited 7,234 households from 321 streets across 15 zones. Of the 18,040 residents ≥10 years of age in the visited households, 14,839 (82.3%) were available at the time of survey, among whom 12,405 (83.6%) consented to participate (Appendix Table 1). The mean age of survey participants was 41.1 years (SD 17.3 years); 52.7% were female and 47.3% were male. Among 496 (4%) persons who reported prior reverse transcription-PCR (RT-PCR) testing for COVID-19, 119 (24%) reported testing positive (Table 1).

Among 12,405 serum samples tested, 2,673 were positive for IgG , a weighted prevalence of 18.7% (95% CI 15.1%–22.9%). After adjusting for the test sensitivity and specificity, seroprevalence was 18.4% (95% CI 14.8%–22.6%) (Table 2). The weighted seroprevalence was higher among female participants (20.6%, 95% CI 16.7%–25.3%) than male participants (16.6%, 95% CI 13.2%–20.6%) ($p<0.001$). Weighted seroprevalence was lowest among persons ≥60 years of age (13.4%, 95% CI 10.3%–17.4%) than younger persons ($p = 0.001$) (Table 2). We retested 100 seronegative and 40 seropositive samples and results were concordant.

From our data, we estimated a total of 1,509,701 (95% CI 1,212,711–1,856,190) SARS-CoV-2 infections in Chennai. ICR per laboratory-confirmed case was 21.4 (95% CI 17.2–26.3) until July 7 and 19.2 (95% CI 15.4–23.6) until July 14, 2020.

## Conclusions

Our community-based survey indicated that ≈1/5 persons in Chennai was exposed to SARS-CoV-2 by July 2020. We noted a wide variation in the extent of infection across wards and seroprevalence ranged from 2%–50% (Appendix Table 3).

Seroprevalence was higher in northern Chennai and adjoining wards of central Chennai than in

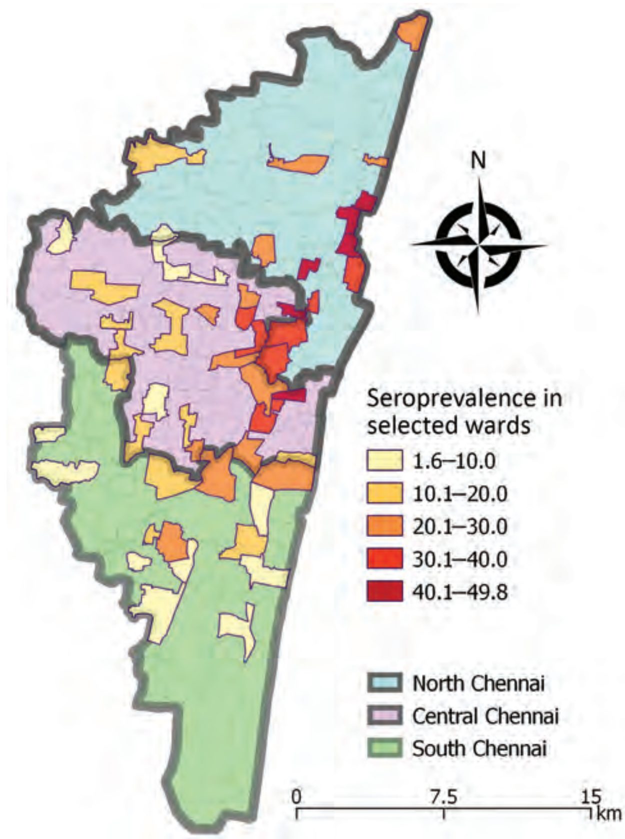


**Figure.** Seroprevalence of SARS-CoV-2 among residents of Chennai, India, July 2020. Values represent percent seroprevalence. SARS-CoV-2, severe acute respiratory syndrome coronavirus 2.

southern Chennai (Figure). Chennai witnessed a surge in COVID-19 cases in last week of April 2020 and >65% of cases were in northern Chennai (*7*). The number of cases showed a declining trend after the first week of July. Northern Chennai has a higher population density (55,000/km$^2$) than Chennai (27,000/km$^2$) and has several slum areas (*7*). High population density and persons living in close proximity might have contributed to the higher seroprevalence observed in northern Chennai.

Seroprevalence was lower among male participants. Laboratory surveillance data in India showed a higher proportion of laboratory-confirmed COVID-19 among male than female patients (*8*). Comparable seroprevalence between children and adults suggests exposure within and outside of the household settings. Lower prevalence among persons ≥60 years of age could be due to lower exposure to infected persons or stricter adherence to nonpharmaceutical interventions. Serosurveys conducted in Santa Clara County, California, USA reported lower seropositivity among persons ≥60 years of age (E. Bendavid,

**Table 1.** Characteristics of 12,405 participants in a SARS-CoV-2 serosurvey, Chennai, India, July 2020*

| Characteristics | No. (%) |
|---|---|
| Age, y, n = 12,319 | |
| 10–19 | 1,473 (12.0) |
| 20–29 | 2,105 (17.1) |
| 30–39 | 2,353 (19.1) |
| 40–49 | 2,353 (19.1) |
| 50–59 | 1,927 (15.6) |
| ≥60 | 2,108 (17.1) |
| Sex, n = 12,319 | |
| M | 5,785 (47.0) |
| F | 6,493 (52.7) |
| Transgender | 41 (0.3) |
| History of respiratory symptoms, n = 12,248 | 175 (1.4) |
| Symptomatic persons seeking medical care, n = 175 | 121 (69.1) |
| Hospitalization among persons seeking medical care, n = 121 | 71 (58.7) |
| Reported contact with COVID-19 case, n = 12,248 | 173 (1.4) |

*Among 12,405 persons enrolled in the survey, age and sex data were not available for 86 participants. COVID-19, coronavirus disease; SARS-CoV-2, severe acute respiratory syndrome coronavirus 2.

et al. unpub. data, https://doi.org/10.1101/2020.04.14.20062463); however, in Spain, seropositivity was similar across all age groups (*9*) and in Greece, seroprevalence was higher among persons ≥60 years of age (*10*).

Most seropositive participants in our survey did not report any symptoms nor had any known contact with COVID-19 patient. IgG developed among most (107/119; 90%) recovered COVID-19 patients in our survey. Among 105 participants for whom ≥15 days had passed between RT-PCR confirmation of COVID-19 and blood sample collection for our serosurvey, 99 (94.2%) had seroconverted. Even after accounting for a 2-week delay for development of antibodies (*11*), ≈6% of COVID-19 patients were seronegative. Discordance between RT-PCR test results and presence of IgG might be due to poor B cell response or antibodies waning over time (*12*).

The ICR ranged from 19–21 and was lower than the ICR of 82–130 reported during the nationwide seroprevalence survey in India conducted in May 2020 (*5*). Lower ICR reflects a high level of case detection, resulting from extensive COVID-19 testing in the city. By July 15, 2020, Chennai had conducted 14,270 tests/million population.

Our study had 2 limitations. First, ≈1/3 persons from the visited households did not participate in the survey. Among them, 17.7% were not available at the time of visit and 13.5% refused to participate. Due to time constraints, we did not revisit households where persons were not available. The proportion of female participants and children 10–19 years of age was higher among persons who did not participate in the survey (Appendix Table 2), which might have influenced the seroprevalence estimates in either direction. Second, we might have underestimated the seroprevalence because antibodies to

**Table 2.** Characteristics of persons with IgG against SARS-CoV-2, Chennai, India, July 2020*

| Characteristics | No. tested | No. positive | Unadjusted seroprevalence, % (95% CI) | Weighted seroprevalence, % (95% CI) | p value | Test performance-adjusted seroprevalence, % (95% CI) |
|---|---|---|---|---|---|---|
| Overall | 12,405 | 2,673 | 21.5 (20.8–22.3) | 18.7 (15.1–22.9) | NA | 18.4 (14.8–22.6) |
| Sex | | | | | | |
| M | 5,785 | 1,115 | 19.3 (18.3–20.3) | 16.6 (13.2–20.6) | <0.001 | 16.3 (12.9–20.3) |
| F | 6,493 | 1,538 | 23.7 (22.7–24.7) | 20.6 (16.7–25.3) | Referent | 20.3 (16.4–25.0) |
| Transgender | 41 | 5 | 12.2 (4.1–26.2) | 2.8 (0.2–27.6) | 0.093 | 2.4 (0.0–27.3) |
| Age, y | | | | | | |
| 10–19 | 1,473 | 351 | 23.8 (21.7–26.1) | 18.9 (14.7–24.0) | Referent | 18.6 (14.4–23.7) |
| 20–29 | 2,105 | 478 | 22.7 (20.9–24.6) | 21.1 (16.8–26.2) | 0.211 | 20.8 (16.5–25.9) |
| 30–39 | 2,353 | 535 | 22.7 (21.1–24.5) | 18.5 (14.6–23.1) | 0.802 | 18.2 (14.3–22.8) |
| 40–49 | 2,353 | 551 | 23.4 (21.7–25.2) | 19.6 (15.5–24.5) | 0.671 | 19.3 (15.2–24.2) |
| 50–59 | 1,927 | 408 | 21.2 (19.4–23.1) | 20.4 (16.1–25.5) | 0.419 | 20.1 (15.8–25.2) |
| ≥60 | 2,108 | 335 | 15.9 (14.4–17.5) | 13.4 (10.3–17.4) | 0.001 | 13.1 (9.9–17.1) |
| History of respiratory symptoms | | | | | | |
| Yes | 175 | 114 | 65.1 (57.6–72.7) | 59.8 (47.5–71.0) | <0.001 | 59.6 (47.3–70.9) |
| No | 12,073 | 2529 | 20.9 (20.2–21.7) | 18.3 (14.7–22.5) | Referent | 18.0 (14.4–22.2) |
| Contact with COVID-19 case | | | | | | |
| Yes | 173 | 94 | 54.3 (46.6–61.9) | 45.3 (34.6–56.6) | <0.001 | 45.1 (34.3–56.4) |
| No | 11,938 | 2,498 | 20.9 (20.2–21.7) | 18.3 (14.8–22.5) | Referent | 18.0 (14.5–22.2) |
| Don’t know | 137 | 51 | 37.2 (29.1–45.9) | 22.1 (14.0–33.1) | 0.363 | 21.8 (13.7–32.8) |
| Ever tested for COVID-19 | | | | | | |
| Yes | 496 | 198 | 39.9 (35.6–44.3) | 34.2 (26.9–42.5) | <0.001 | 33.9 (26.6–42.3) |
| No | 11,752 | 2,445 | 20.8 (20.0–21.6) | 18.0 (14.6–22.1) | Referent | 17.7 (14.3–21.8) |
| COVID- 19 test result, n = 496 | | | | | | |
| Positive | 119 | 107 | 89.9 (83.0–94.7) | NA | NA | NA |
| Negative | 342 | 83 | 24.3 (19.8–29.2) | NA | NA | NA |
| Don’t Know | 35 | 8 | 22.9 (10.4–40.1) | NA | NA | NA |

*COVID-19, coronavirus disease; NA, not applicable; SARS-CoV-2, severe acute respiratory syndrome coronavirus 2.

nucleocapsid protein have been shown to decline after infection (*13*).

In conclusion, ≈80% of the population in Chennai is still susceptible to SARS-CoV-2 infection. Transmission is expected to continue in wards with lower seroprevalence. Maintaining high testing rates and monitoring adherence to nonpharmacological interventions in GCC should be continued. In addition, periodic serosurveys would help monitor the trend of infection and assess the effects of varying containment measures in the city.

This study was funded by Greater Chennai Corporation public health department (PHDC no. 2797/20 dated July 9, 2020).

## Acknowledgments

We thank the Greater Chennai Corporation health officials for support in field operations. M.J. and M.S.H. are employees of Greater Chennai Corporation.

Chennai COVID Sero-surveillance team (in alphabetical order): Shravan Kumar Adavat, Akshitha, Vasudevan Arumugam, Ashwini, M. Balusamy, Chandrabalu, Sauvik Dasgupta, Tamil Mani Devi, Gomathi, R Gopinath, D. Gunasekaran, R. Harikrishnan, Satham Hussain, A. Jayakumar, Chitra Jayaprakash, Jayasree, Annamma Jose, I. Kalaimani, Kalayarasi, Anbarasan Kaliyappan, Bharath Kathavarayan, Krishna Yadav Kattagoni, T. Karunakaran, Maheshwari Krishnan, Ramesh Kumar Kumaraswamy, P. Ashok Kumar, K. Satish Kumar, Maheshkumar Madasamy, T. Magesh, Karthikesan Masilamani, A. Mohan, Rajesh Mondal, Murugesan, Nandhakumar, Kumaravel Padmanaban, R. Vijaya Prabha, C. Prabhakaran, Josephine Pradhan, E.B.Arun Prasath, G. Preethi, Michael Raj, Ranjithkumar, Rajmohan, K. Ramu, D. Sudha Rani, Catherine Rexy, N. Santhanakumar, S.Sarath Kumar, Anbalagan Selvaraj, Selvendiran, Sentrayan, Shalini, R. Sivakumar, Harshal Bhimrao Sonekar, A. Suresh, Suresh, Udhayakumar, V. Vettrichelvan, Hari Vignesh, and John Arokyadoss Yesuraj.

## About the Author

Dr. Selvaraju is a scientist at ICMR-National Institute for Research in Tuberculosis, Chennai, India. His research interests include estimation of burden of tuberculosis and building laboratory, surveillance, and workforce capacity to detect, respond and prevent drug resistant tuberculosis in India.

## References

1. World Health Organization. Coronavirus disease (COVID-19) situation report – 207 [cited 2020 Aug 15]. https://www.who.int/docs/default-source/coronaviruse/situation-reports/20200814-covid-19-sitrep-207.pdf
2. State Control Room, Directorate of Public Health and Preventive Medicine Health and Family Welfare Department, Government of Tamil Nadu. Media bulletin 15.18.2020: daily report on public health measures taken for COVID-19 [cited 2020 Aug 15]. https://stopcorona.tn.gov.in/wp-content/uploads/2020/03/Media-Bulletin-15-08-20-COVID-19-6-PM.pdf.
3. Greater Chennai Corporation. About Greater Chennai Corporation. [cited 2020 Sept 7]. https://www.chennaicorporation.gov.in/about-chennai-corporation/aboutCOC.htm
4. Koopmans M, Haagmans B. Assessing the extent of SARS-CoV-2 circulation through serological studies. Nat Med. 2020;26:1171–2. https://doi.org/10.1038/s41591-020-1018-x
5. Murhekar MV, Bhatnagar T, Selvaraju S, Rade K, Saravanakumar V, Vivian Thangaraj JW, et al. Prevalence of SARS-CoV-2 infection in India: findings from the national serosurvey, May–June 2020. Indian J Med Res. 2020;152:48–60. https://doi.org/10.4103/ijmr.IJMR_3290_20
6. SARS-CoV-2 IgG immunoassay. Instructions for use. Abbott. May 2020 [cited 2020 Sep 07]. https://www.corelaboratory.abbott/us/en/offerings/segments/infectious-disease/sars-cov-2
7. Special correspondent. Coronavirus: with over 65% of cases, all eyes on north Chennai. The Hindu. 2020 Apr 29 [citied 2020 Oct 26]. https://www.thehindu.com/news/cities/chennai/coronavirus-with-over-65-of-cases-all-eyes-on-north-chennai/article31467330.ece
8. ICMR COVID Study Group; In alphabetical order: Abraham P, Aggarwal N, Babu GR, Barani S, Bhargava B, et al. Laboratory surveillance for SARS-CoV-2 in India: performance of testing & descriptive epidemiology of detected COVID-19, January 22–April 30, 2020. Indian J Med Res. 2020;151:424–437. https://doi.org/10.4103/ijmr.IJMR_1896_20
9. Pollán M, Pérez-Gómez B, Pastor-Barriuso R, Oteo J, Hernán MA, Pérez-Olmeda M, et al. Prevalence of SARS-CoV-2 in Spain (ENE-COVID): a nationwide, population-based seroepidemiological study. Lancet. 2020396;535–44. https://doi.org/10.1016/S0140-6736(20)31483-5
10. Bogogiannidou Z, Vontas A, Dadouli K, Kyritsi MA, Soteriades S, Nikoulis DJ, et al. Repeated leftover serosurvey of SARS-CoV-2 IgG antibodies, Greece, March and April 2020. Euro Surveill. 2020;25:2001369. https://doi.org/10.2807/1560-7917.ES.2020.25.31.2001369
11. Long QX, Liu BZ, Deng HJ, Wu GC, Deng K, Chen YK, et al. Antibody responses to SARS-CoV-2 in patients with COVID-19. Nat Med. 2020;26:845–8. https://doi.org/10.1038/s41591-020-0897-1
12. Sekine T, Perez-Potti A, Rivera-Ballesteros O, Strålin K, Gorin JB, Olsson A, et al.; Karolinska COVID-19 Study Group. Robust T cell immunity in convalescent individuals with asymptomatic or mild COVID-19. Cell. 2020;183:158–168.e14. https://doi.org/10.1016/j.cell.2020.08.017
13. Ripperger TJ, Uhrlaub JL, Watanabe M, Wong R, Castaneda Y, Pizzato HA, et al. Orthogonal SARS-CoV-2 serological assays enable surveillance of low-prevalence communities and reveal durable humoral immunity. Immunity. 2020;53:925–933.e4. https://doi.org/10.1016/j.immuni.2020.10.004

Address for correspondence: Manoj V. Murhekar, ICMR – National Institute of Epidemiology, Second Main Road, Tamil Nadu Housing Board, Ayapakkam, Near Ambattur, Chennai 600077, Tamil Nadu, India; email: mmurhekar@nieicmr.org.in

# *Plasmodium cynomolgi* Co-infections among Symptomatic Malaria Patients, Thailand

Chaturong Putaporntip, Napaporn Kuamsab, Urassaya Pattanawong, Surasuk Yanmanee, Sunee Seethamchai, Somchai Jongwutiwes

Among 1,180 symptomatic malaria patients, 9 (0.76%) infected with *Plasmodium cynomolgi* were co-infected with *P. vivax* (n = 7), *P. falciparum* (n = 1), or *P. vivax* and *P. knowlesi* (n = 1). Patients were from Tak, Chanthaburi, Ubon Ratchathani, Yala, and Narathiwat Provinces, suggesting *P. cynomolgi* is widespread in this country.

*Plasmodium cynomolgi*, a simian malaria parasite, possesses biological and genetic characteristics akin to those of the most widespread human malaria parasite, *P. vivax*. Although *P. cynomolgi* circulates among monkey species such as long-tailed macaques (*Macaca fascicularis*) and pig-tailed macaques (*M. nemestrina*), experimental and accidental transmissions have been implicated in symptomatic infections in humans (*1*). Several mosquito vectors for human malaria can also transmit *P. cynomolgi*, posing the risk of cross-species transmission in areas where its natural hosts coexist with people (*1*,*2*). Among pig-tailed and long-tailed macaques living in various countries in Southeast Asia, including Thailand, *P. cynomolgi* infections are not uncommon (*3*,*4*). A case of naturally transmitted *P. cynomolgi* malaria in a human was reported from eastern Malaysia (*5*). Subsequent surveillance in western Cambodia and northern Sabah state in Malaysia revealed asymptomatic human infection, albeit at low prevalence (*6*,*7*). Symptomatic *P. cynomolgi* infection was diagnosed in a traveler returning to Denmark from Southeast Asia (*8*). During testing of symptomatic malaria patients in Thailand, we identified 9 co-infected with cryptic *P. cynomolgi* and other *Plasmodium* species.

## The Study

We examined 1,359 blood samples taken from febrile patients who sought treatment at malaria clinics or local hospitals in 5 Thailand provinces: Tak (n = 192, during 2007–2013), Ubon Ratchathani (n = 239, during 2014–2016), Chanthaburi (n = 144, during 2009), Yala (n = 592, during 2008–2018), and Narathiwat (n = 192, during 2008–2010). Using microscopy, we found 1,152 cases in which malaria was caused by *P. vivax* (869 patients, 75.43%), *P. falciparum* (272 patients, 23.61%), or co-infection with both species (11 patients, 0.96%). Using species-specific nested PCR, including for *P. cynomolgi* (Appendix, https://wwwnc.cdc.gov/EID/article/27/2/19-1660-App1.pdf), targeting the mitochondrial cytochrome *b* gene (*mtCytb*) of 5 human malaria species for molecular detection, as described elsewhere (*9*,*10*), we found malaria in 1,180 patients; *P. vivax* infections exceeded *P. falciparum* infections (Table 1). Submicroscopic parasitemia occurred in 28/1,180 (2.4%) patients: 19 infected with *P. vivax*, 7 with *P. falciparum*, 1 with *P. vivax* and *P. falciparum*, and 1 with *P. malariae*.

The mean age of all patients was 26.3 (range 7–85) years; 940/1,180 (79.7%) of patients were men. Febrile symptoms, lasting 1–7 days (mean 3.1, SD ±1.3 days) before blood sample collection, developed in all PCR-positive malaria patients. Monoinfection with *P. knowlesi* occurred in 4 patients, *P. malariae* in 3, and *P. ovale* in 1. We detected co-infections in 77 (0.93%) patients; of these co-infections, 55 were *P. falciparum* and *P. vivax*. In total (i.e., including both monoinfections and co-infections), *P. knowlesi* was detected in 18 patients, of which 10 cases were newly identified from Ubon Ratchathani Province, which borders Cambodia and Laos.

We detected *P. cynomolgi* in 9 patients, all of whom were co-infected with *P. vivax* (n = 7), *P. falciparum* (n = 1), or both *P. vivax* and *P. knowlesi* (n = 1). The overall prevalence of *P. cynomolgi* infections was 0.76%. Patients infected with *P. cynomolgi* were found in all provinces. Although 5 of these patients were from Yala Province, the proportion of *P. cynomolgi* infections among malaria cases in each malaria-endemic area (0.52%–0.87%) was comparable.

Author affiliations: Chulalongkorn University Faculty of Medicine, Bangkok, Thailand (C. Putaporntip, N. Kuamsab, U. Pattanawong, S. Yanmanee, S. Jongwutiwes); Naresuan University Faculty of Science, Pitsanulok, Thailand (S. Seethamchai)

DOI: https://doi.org/10.3201/eid2702.191660

**Table 1.** Distribution of *Plasmodium* infections diagnosed by PCR of blood samples taken from febrile patients who sought treatment at malaria clinics or local hospitals in 5 provinces, Thailand*

| Species | No. cases by province | | | | | Total no. cases | % Tota cases |
|---|---|---|---|---|---|---|---|
| | Tak | Ubon Ratchathani | Chanthaburi | Yala | Narathiwat | | |
| *P. vivax* | 98 | 57 | 141 | 467 | 59 | 822 | 69.66 |
| *P. falciparum* | 72 | 41 | 0 | 87 | 73 | 273 | 23.14 |
| *P. knowlesi* | 0 | 4 | 0 | 0 | 0 | 4 | 0.34 |
| *P. malariae* | 0 | 2 | 0 | 1 | 0 | 3 | 0.25 |
| *P. ovale* | 0 | 0 | 0 | 1 | 0 | 1 | 0.09 |
| *P. vivax* + *P. falciparum* | 21 | 8 | 0 | 11 | 15 | 55 | 4.66 |
| *P. vivax* + *P. knowlesi* | 0 | 3 | 2 | 0 | 4 | 9 | 0.76 |
| *P. vivax* + *P. cynomolgi* | 1 | 1 | 1 | 3 | 1 | 7 | 0.59 |
| *P. vivax* + *P. knowlesi* + *P. cynomolgi* | 0 | 0 | 0 | 1 | 0 | 1 | 0.09 |
| *P. falciparum* + *P. knowlesi* | 0 | 3 | 0 | 1 | 0 | 4 | 0.34 |
| *P. falciparum* + *P. cynomolgi* | 0 | 0 | 0 | 1 | 0 | 1 | 0.09 |
| PCR-positive | 192 | 119 | 144 | 573 | 152 | 1,180 | 100.00 |
| PCR-negative | 0 | 120 | 0 | 19 | 40 | 179 | NA |
| Total no. samples tested | 192 | 239 | 144 | 592 | 192 | 1,359 | NA |

*NA, not applicable.

DNA from 10 *P. knowlesi* isolates from Ubon Ratchathani Province and the 9 *P. cynomolgi* isolates were subject to nested PCR amplification spanning a 1,318-bp region of mitochondrially encoded cytochrome c oxidase I (*mtCOX1*). Direct sequencing of the purified PCR-amplified template was successfully performed from all 10 *P. knowlesi* and from 6 *P. cynomolgi* isolates. The remaining 3 *P. cynomolgi* isolates could not be further amplified due to inadequate DNA in the samples. All *mtCOX1* sequences of *P. knowlesi* from Ubon Ratchathani Province were different from one another and distinct from those from the previous case of natural human infection in Thailand (GenBank accession no. AY598141) (*11*). All 6 amplified *P. cynomolgi* isolates contained different sequences belonging to 2 clades. One was closely related to the Gombak strain (accession no. AB444129) and the remaining 5 isolates were clustered with the RO strain (accession no. AB444126) (Figure 1).

All but 1 *P. cynomolgi* infection occurred in male patients (age 15–53 years, median 32 years). Most *P. cynomolgi* malaria patients resided in areas where domesticated or wild macaques were living in proximity to humans. Infections with *P. cynomolgi* occurred in different annual periods; more cases were detected in rainy seasons than in dry seasons (Table 2). The parasite density of *P. cynomolgi* could not be determined from blood smears because of morphologic resemblance to *P. vivax*; an isolate co-infected with *P. falciparum* (YL3634) had very low parasitemia. Of 8 patients with *P. cynomolgi* co-infection, 6 had parasitemia <10,000 parasites/µL (<0.2% parasitemia). It remains unknown whether *P. cynomolgi* was co-responsible for symptomatic infections or merely coexisted asymptomatically with other human malaria parasites. However, self-reported defervescence among *P. cynomolgi*–co-infected patients occurred 1–3 days after antimalarial treatment with chloroquine plus primaquine after onsite microscopic diagnosis of *P. vivax* malaria or artesunate plus mefloquine for *P. falciparum* malaria. Unfortunately, data on long-term follow-up were not available.

## Conclusions

This report highlights the presence of *P. cynomolgi* in the human population of Thailand, where natural hosts, both pig-tailed and long-tailed macaques, are prevalent. All patients with *P. cynomolgi* infections harbored either *P. falciparum* or *P. vivax* in their blood, implying that this simian malaria species could share the same anopheline vectors or have different vectors with similar anthropophilic and zoophilic tendencies. The presence of *P. cynomolgi* in diverse malaria-endemic areas of Thailand suggests that cross-species transmission has occurred. Human infection with *P. cynomolgi* seems not to be newly emerging because it was detected among blood samples collected over a range of time periods since 2007. Undoubtedly, morphologic similarity between *P. cynomolgi* and *P. vivax* can hamper conventional microscopic diagnosis (*1*,*5*,*8*). Cryptic co-existence of simian and human malaria species could further preclude accurate molecular detection when inadequate diagnostic devices are used.

Previous surveys of *Plasmodium* infections in pig-tailed and long-tailed macaques have revealed the presence of *P. cynomolgi* and other simian malaria species in Thailand, mainly in the southern part of the country (*4*). Most patients infected with *P. cynomolgi* resided in areas where macaques were living in proximity to humans; therefore, the risk of acquiring malaria from this parasite could increase as people encroach into the habitats of infected macaques, as happened with malaria caused by *P. knowlesi*. Of note,

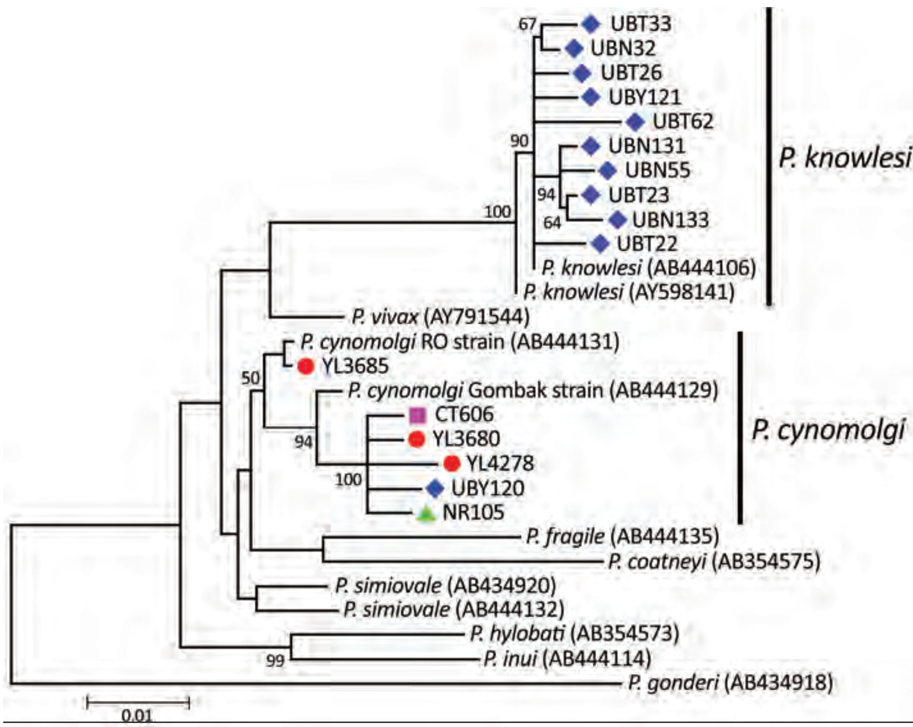


**Figure.** Maximum-likelihood phylogenetic tree inferred from mitochondrially encoded cytochrome *c* oxidase I of *Plasmodium cynomolgi* and *P. knowlesi* from Thailand compared with other closely related species. Tree spans 1,318-bp region. Colors indicate province where human isolates were found: red circles, Yala; green triangle, Narathiwat; purple square, Chanthaburi; and blue diamonds, Ubon Ratchathani. GenBank accession numbers of reference sequences are given in parentheses. Bootstrap values >50% based on 1,000 pseudoreplicates are shown on the branches. Scale bar indicates nucleotide substitution per site.

co-infection with *P. cynomolgi*, *P. knowlesi*, and *P. vivax* occurred in a patient in Yala Province whose housing area was surrounded by several domesticated pig-tailed and long-tailed macaques.

Analysis of the *mtCOX1* sequences of *P. cynomolgi* among 6 patients showed that all isolates possessed different genetic sequences, suggesting that several strains or clones of this simian parasite are capable of cross-transmission from macaques to humans. Meanwhile, *P. cynomolgi* seems to contain 2 divergent lineages (*12*), represented by RO and Gombak strains. The *mtCOX1* sequences of both *P. cynomolgi* lineages were found in human-derived isolates in this study, further supporting that diverse strains of this parasite can infect people. Likewise, sequence diversity in the *mtCOX1* of *P. knowlesi* from Ubon Ratchathani Province suggests that cross-transmission from macaques to humans may not be restricted to particular parasite strains.

**Table 2.** Demographic and parasitologic features of *Plasmodium cynomolgi*–co-infected patients among febrile patients who sought treatment at malaria clinics or local hospitals in 5 provinces, Thailand

| Patient* | Age, y/sex | Province | Month | Season | Monkey in proximity | Microscopy diagnosis | Parasites/µL‡ | PCR diagnosis |
|---|---|---|---|---|---|---|---|---|
| TSY1522 | 38/M | Tak | 2007 Nov | Dry | No | *P. vivax* | 12,160 | *P. vivax, P. cynomolgi* |
| CT606† | 30/M | Chanthaburi | 2009 Oct | Rainy | Yes | *P. vivax* | 86,535 | *P. vivax, P. cynomolgi* |
| UBY120 | 32/M | Ubon Ratchathani | 2015 Aug | Rainy | Yes | *P. vivax* | 570 | *P. vivax, P. cynomolgi* |
| NR105 | 53/M | Narathiwat | 2008 Jul | Rainy | Yes | *P. vivax* | 4,620 | *P. vivax, P. cynomolgi* |
| YL3179 | 15/M | Yala | 2016 Apr | Dry | Yes | *P. vivax* | 1,140 | *P. vivax, P. knowlesi P. cynomolgi* |
| YL3634 | 40/F | Yala | 2016 Dec | Rainy | Yes | *P. falciparum* | 60 | *P. falciparum, P. cynomolgi* |
| YL3680 | 49/M | Yala | 2016 Dec | Rainy | Yes | *P. vivax* | 3,720 | *P. vivax, P. cynomolgi* |
| YL3685 | 18/M | Yala | 2016 Dec | Rainy | Yes | *P. vivax* | 4,680 | *P. vivax, P. cynomolgi* |
| YL4278 | 21/M | Yala | 2017 Oct | Rainy | Yes | *P. vivax* | 7,440 | *P. vivax, P. cynomolgi* |

*Alphanumeric designations represent provinces and serial number of blood samples.
†Patient from Cambodia, but had lived in Thailand for 1 year just prior to illness, with no history of travel outside of the country.
‡All species of malaria parasites (all stages) were determined from ≥200 leukocytes on Giemsa-stained thick blood films.

Although human malaria from either parasite may be asymptomatic, infection with *P. knowlesi* can result in death, but patients infected with *P. cynomolgi* at worst had only benign symptoms (*5*–*8*). However, severe and complicated malaria has been observed in rhesus macaques experimentally infected with *P. cynomolgi* (*13*).

Whether severe cynomolgi malaria can occur in humans remains to be elucidated. However, if human infections with *P. cynomolgi* do become public health problems, diagnostic and control measures might be complicated by the morphological similarity between *P. vivax* and *P. cynomolgi*. This possibility makes further surveillance of this simian malaria in humans mandatory.

### Acknowledgments

We are grateful to all patients who provided blood samples and to staff at local malaria clinics and hospitals for assistance in field studies.

Funding for this study was provided to C.P. by the Thailand Research Fund (grant no. RSA5980054), to C.P. by the Asahi Glass Foundation (in fiscal year 2016), and to C.P. and S.J. by the Thai Government Research Budget for Chulalongkorn University (grant nos. GRB-APS-12593011 and GBA-600093004).

### About the Author

Dr. Putaporntip is a molecular parasitologist in the Molecular Biology of Malaria and Opportunistic Parasites Research Unit, Department of Parasitology, Faculty of Medicine, Chulalongkorn University, in Bangkok, Thailand. His work focuses on molecular diagnostics, population genetics, and the evolution of malarial parasites in human and nonhuman primates.

### References

1. Coatney GR, Collins WE, Warren M, Contacos PG. The primate malarias, version 1.0 [CD-ROM] [original book published 1971]. Atlanta: Centers for Disease Control and Prevention; 2003.
2. Klein TA, Harrison BA, Dixon SV, Burge JR. Comparative susceptibility of Southeast Asian *Anopheles* mosquitoes to the simian malaria parasite *Plasmodium cynomolgi*. J Am Mosq Control Assoc. 1991;7:481–7.
3. Fooden J. Malaria in macaques. Int J Primatol. 1994;15:573–96. https://doi.org/10.1007/BF02735972
4. Putaporntip C, Jongwutiwes S, Thongaree S, Seethamchai S, Grynberg P, Hughes AL. Ecology of malaria parasites infecting Southeast Asian macaques: evidence from cytochrome *b* sequences. Mol Ecol. 2010;19:3466–76. https://doi.org/10.1111/j.1365-294X.2010.04756.x
5. Ta TH, Hisam S, Lanza M, Jiram AI, Ismail N, Rubio JM. First case of a naturally acquired human infection with *Plasmodium cynomolgi*. Malar J. 2014;13:68. https://doi.org/10.1186/1475-2875-13-68
6. Imwong M, Madmanee W, Suwannasin K, Kunasol C, Peto TJ, Tripura R, et al. Asymptomatic natural human infections with the simian malaria parasites *Plasmodium cynomolgi* and *Plasmodium knowlesi*. J Infect Dis. 2019;219:695–702. https://doi.org/10.1093/infdis/jiy519
7. Grignard L, Shah S, Chua TH, William T, Drakeley CJ, Fornace KM. Natural human infections with *Plasmodium cynomolgi* and other malaria species in an elimination setting in Sabah, Malaysia. J Infect Dis. 2019;220:1946–9. https://doi.org/10.1093/infdis/jiz397
8. Hartmeyer GN, Stensvold CR, Fabricius T, Marmolin ES, Hoegh SV, Nielsen HV, et al. *Plasmodium cynomolgi* as cause of malaria in tourist to Southeast Asia, 2018. Emerg Infect Dis. 2019;25:1936–9. https://doi.org/10.3201/eid2510.190448
9. Putaporntip C, Buppan P, Jongwutiwes S. Improved performance with saliva and urine as alternative DNA sources for malaria diagnosis by mitochondrial DNA-based PCR assays. Clin Microbiol Infect. 2011;17:1484–91. https://doi.org/10.1111/j.1469-0691.2011.03507.x
10. Jongwutiwes S, Buppan P, Kosuvin R, Seethamchai S, Pattanawong U, Sirichaisinthop J, et al. *Plasmodium knowlesi* malaria in humans and macaques, Thailand. Emerg Infect Dis. 2011;17:1799–806. https://doi.org/10.3201/eid1710.110349
11. Jongwutiwes S, Putaporntip C, Iwasaki T, Sata T, Kanbara H. Naturally acquired *Plasmodium knowlesi* malaria in human, Thailand. Emerg Infect Dis. 2004;10:2211–3. https://doi.org/10.3201/eid1012.040293
12. Sutton PL, Luo Z, Divis PCS, Friedrich VK, Conway DJ, Singh B, et al. Characterizing the genetic diversity of the monkey malaria parasite *Plasmodium cynomolgi*. Infect Genet Evol. 2016;40:243–52. https://doi.org/10.1016/j.meegid.2016.03.009
13. Joyner CJ, The MaHPIC Consortium, Wood JS, Moreno A, Garcia A, Galinski MR. Case report: severe and complicated cynomolgi malaria in a rhesus macaque resulted in similar histopathological changes as those seen in human malaria. Am J Trop Med Hyg. 2017;97:548–55. https://doi.org/10.4269/ajtmh.16-0742

Address for correspondence: Chaturong Putaporntip, Molecular Biology of Malaria and Opportunistic Parasites Research Unit, Department of Parasitology, Faculty of Medicine, Chulalongkorn University, Bangkok 10330, Thailand; e-mail: p.chaturong@gmail.com

# Human Tacheng Tick Virus 2 Infection, China, 2019

Zhihui Dong,[1] Meihua Yang,[1] Zedong Wang,[1] Shuo Zhao, Songsong Xie, Yicheng Yang, Gang Liu, Shanshan Zhao, Jing Xie, Quan Liu, Yuanzhi Wang

We used metagenomic analysis to identify Tacheng tick virus 2 infection in a patient with a history of tick bite in northwestern China. We confirmed the virus with reverse transcription-PCR, virus isolation, and genomic analysis. We detected viral RNA in 9.6% of ticks collected from the same region.

Emerging pathogenic tickborne viruses have attracted much attention because of the increasing incidence of tickborne viral diseases and their effects on human health (*1*–*4*). In 2015, high-throughput sequencing of samples from ticks in China revealed several novel phleboviruses, including Tacheng tick virus 2 (TcTV-2), Changping tick virus 1, Bole tick virus 1 (BlTV-1), Lihan tick virus, Yongjia tick virus 1, and Dabieshan tick virus (*5*). However, the risk for human infection from these viruses is not yet known. We report on TcTV-2 infection in patient in China and describe methods for virus isolation and genomic analysis.

## The Study

The patient was a 38-year-old man who lived in northwestern China and had frequent contact with horses and sheep. On May 29, 2019, he noticed a tick embedded on his left upper arm and removed it himself. He noted a localized rash with slight pain and discomfort. On June 16, fever developed and soon after the patient had chills, severe fatigue, headache, anorexia, nausea, and vomiting. On June 20, he was admitted to the local hospital with a temperature of 37.9°C, which increased to 39.5°C the next day. The patient was initially given intravenous cefotaxime sodium and levofloxacin for 3 days for suspected tickborne bacterial disease, but these treatments did not alleviate his symptoms.

On June 24, the patient was admitted to the First Affiliated Hospital of Medical College of Shihezi University in Shihezi. Physical examination showed erythema at the bite site (Figure 1, panel A) and neck stiffness. Cerebrospinal fluid (CSF) analysis showed a total of $1.07 \times 10^8$ nucleated cells (92% hyaline leukocytes and 8% pleocaryocytes), an increased protein level (0.99 g/L), and decreased levels of CSF glucose (2.3 mmol/L) and chloridion (116.0 mmol/L). The patient was given intravenous ceftriaxone for 12 days, but still experienced headache, nausea, and vomiting, and his erythema was not decreasing.

Blood, throat swabs, urine, and CSF samples were obtained from the patient on days 9, 16, and 40 after illness onset. We tested the patient samples by PCR or reverse transcription-PCR (RT-PCR) for potential tickborne pathogens, including severe fever with thrombocytopenia syndrome virus, tickborne encephalitis virus, *Borrelia burgdorferi* sensu lato, *Anaplasma*, *Babesia*, *Rickettsia* spp., Tacheng tick virus 1, TcTV-2, Tacheng tick virus 5, BlTV-1, and Bole tick virus 4 (*2*). We detected TcTV-2 by metagenomic analysis on blood collected on day 9 and confirmed the virus by RT-PCR targeting the large (L) gene (Appendix Tables 1, 2, https://wwwnc.cdc.gov/EID/article/27/2/19-1486-App1.pdf). We detected TcTV-2 in blood, throat swabs, and urine samples from the patient. We ruled out bacterial infection in blood and CSF by using routine culture methods and 16S rRNA gene broad-range PCR, which confirmed that no bacterial infection occurred in this patient.

On July 18, the patient was admitted to the hospital again. He was given intravenous acyclovir for 12 days and his clinical symptoms and erythema vanished without any sequelae (Appendix Table 3).

Author affiliations: Shihezi University, Shihezi, China (Z. Dong, M. Yang, Shuo Zhao, Y. Yang, G. Liu, Shanshan Zhao, Y. Wang); Foshan University, Foshan, China (Z. Wang, Q. Liu); First Affiliated Hospital of Shihezi University, Shihezi (S. Xie, J. Xie); Shihezi People's Hospital, Shihezi (Y. Yang)

DOI: https://doi.org/10.3201/eid2702.191486

[1]These authors contributed equally to this article.

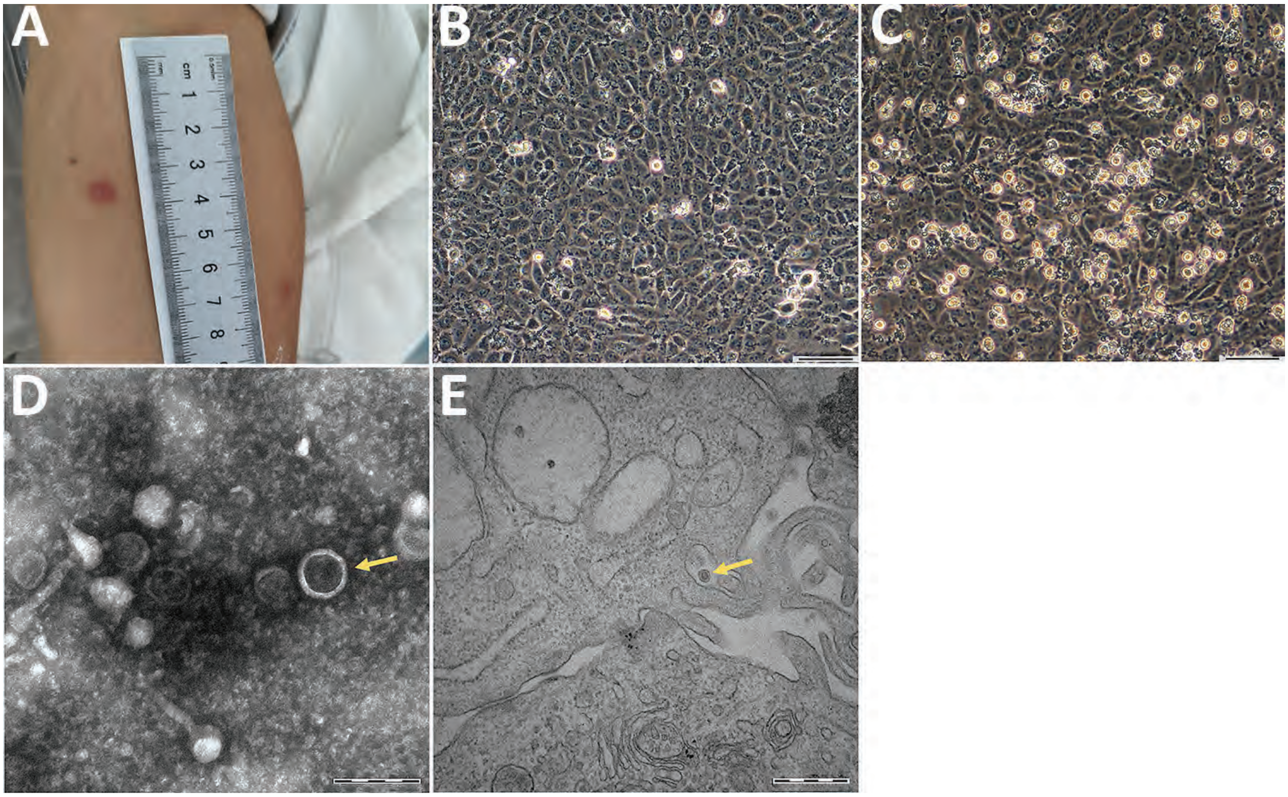


**Figure 1.** Clinical and morphological features of Tacheng tick virus 2 in a patient, China. A) Erythema at the site of tick bite on the anterior surface of the patient's left arm. B) Human hepatocellular carcinoma (SMMC-7721) cells without TcTV-2 infection; magnification × 100. Scale bar indicates 50 μm. C) TcTV-2–infected SMMC-7721 cells showing cytopathic effects visible by light microscopy; magnification × 100. Scale bar indicates 50 μm. D) Negatively stained virions purified from TcTV-2–infected SMMC-7721 cells (arrows); magnification × 25,000. Scale bar indicates 200 nm. E) Transmission electron microscopy image of TcTV-2–infected SMMC-7721 cells (arrows); magnification × 50,000. Scale bar indicates 500 nm. TcTV-2, Tacheng tick virus 2.

To isolate the virus, we inoculated human hepatocellular carcinoma (SMMC-7721) cells, African green monkey kidney (Vero) cells, baby hamster kidney cells, and human foreskin fibroblasts with the serum samples collected during early illness onset (Appendix Figure 2). We performed electron microscopy analysis on infected cells showing cytopathic effect, as described previously (*6*). After incubation, only the SMMC-7721 cells demonstrated cytopathic effect associated with TcTV-2 after several passages (Figure 1, panels B,C; Appendix Figure 3). The virions were spherical with a diameter of ≈90–100 nm (Figure 1, panel D). The virions could be seen in the cytoplasm of infected SMMC-7721 cells on transmission electron microscopy (Figure 1, panel E). We tested for TcTV-2–specific antibodies by using immunofluorescence assay. Serologic detection showed that TcTV-2 IgM titer in serum samples decreased from 1:40 on day 9 to 1:10 on day 40 after illness onset, and IgG titer increased from 1:10 on day 9 to 1:80 on day 40 (Table).

**Table.** Results of immunofluorescence assay in detection of Tacheng tick virus 2 infection in a human, China*

| | | IFA titer | |
|---|---|---|---|
| Days post illness onset | Sample type | IgM | IgG |
| Day 9 | Serum | 1:40 | <1:10 |
| | Urine | <1:10 | <1:10 |
| | CSF | <1:10 | <1:10 |
| Day 16 | Serum | 1:20 | 1:10 |
| | Urine | <1:10 | <1:10 |
| | CSF | <1:10 | <1:10 |
| Day 40 | Serum | <1:10 | 1:80 |
| | Urine | <1:10 | <1:10 |
| | CSF | <1:10 | <1:10 |

CSF, cerebrospinal fluid; IFA, immunofluorescence assay.

We isolated total RNA from infected cells and used the isolates to amplify the L and small (S) gene segment sequences by using primers based on our metagenomic analysis (Appendix Table 2, Table 4). The obtained L segment of TcTV-2 from the patient (GenBank accession no. MN567189) showed 98.8% (6,579/6,659) identity to the L segment of strain TC252 (GenBank accession no. KM817684) and the S segment from the isolate (GenBank accession no. MN567190) showed 99.2% (2,169/2,185) identity to the S of strain TC252 (GenBank accession no. KM817744).

Phylogenetic analysis suggested that TcTV-2, together with Phlebovirus sp. 20A L, Pacific coast tick phlebovirus, Changping tick virus 1, BlTV-1, Lihan tick virus, Yongjia tick virus 1, Dabieshan tick virus, American dog tick phlebovirus, *Rhipicephalus*-associated phlebovirus 1, Xinjiang tick phlebovirus, tick phlebovirus, and brown dog tick phlebovirus 2 formed a separate branch (Figure 2; Appendix Figure 1). An M segment has yet to be detected in any of these viruses (*5*,*7*–*12*).

To identify local natural virus hosts in the environment, 345 adult ticks were collected in the area where the patient lived, including 108 *Dermacentor marginatus*, 183 *D. nuttalli*, 12 *D. silvarum*, and 42 *Hyalomma asiaticum*. We extracted total RNA of each tick and detected TcTV-2 by using RT-PCR with TcTV-2–specific primers (Appendix Table 1). Among 345

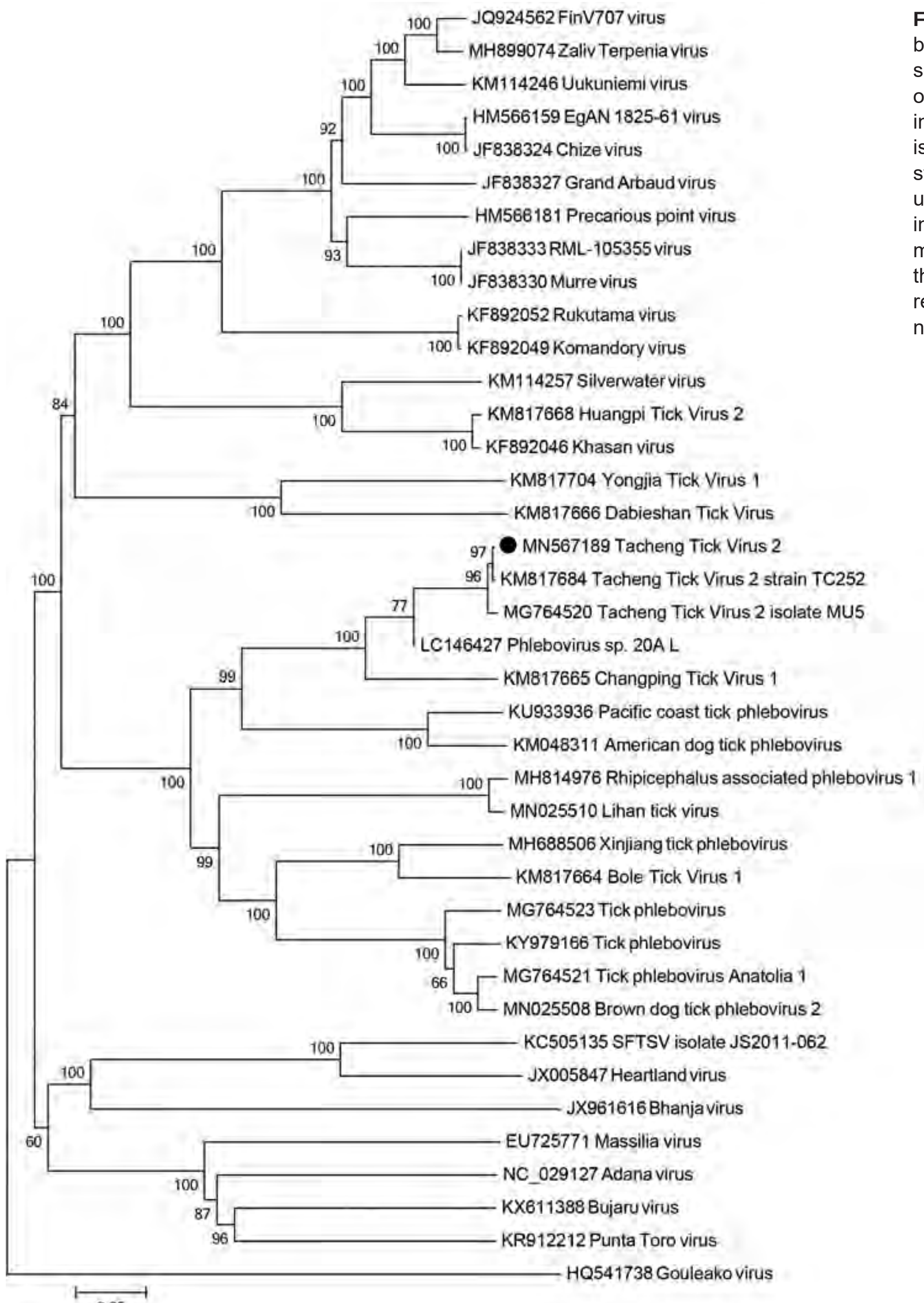


**Figure 2.** Phylogenetic analysis based on partial amino acid sequences of the L segment of tickborne viruses. Black dot indicates Tacheng tick virus 2 isolated from the patient in this study. The tree is constructed by using the neighbor-joining method in MEGA version 7.0 (https://www.megasoftware.net) and tested by the bootstrap method with 1,000 replications. Scale bar indicates nucleotide substitutions per site.

ticks, 33 (9.6%) carried TcTV-2. We noted high infection rates in *D. silvarum* (16.7%), *D. marginatus* (14.8%), *H. asiaticum* (11.9%), and *D. nuttalli* (5.5%). We obtained the partial fragments of the S segment of TcTV-2 in ticks and phylogenetic analyses showed that sequences from TcTv-2 in ticks were closely related to the isolate from the patient (Appendix Figure 1, Appendix Table 5).

We tried to obtain the medium (M) segment of TcTV-2 by designing a set of primers based on the conservative sequences of M segments from 15 typical phleboviruses (Appendix Table 6). We used these primers to amplify the M segment from both the patient and positive ticks detected by sequencing the L and S segments by using RT-PCR. We further analyzed the metagenomic sequences, but the results were negative.

## Conclusions

Among currently known emerging tickborne phleboviruses, severe fever with thrombocytopenia syndrome virus and Heartland virus have been reported to infect humans and cause multiple organ damage, including to the liver and kidneys (*1*,*13*). In this study, TcTV-2 did not show any growth in Vero, human foreskin fibroblasts, or baby hamster kidney 21 cells, but had low level replication and growth in SMMC-7721 cells, indicating that the virus is not well adapted to mammals and likely is more common in arthropods than in mammals.

Transmission electron microscopy showed that TcTV-2 might harbor glycoprotein encoded by the M gene segment. The lack of M sequence data on homology-based approaches could indicate that insufficient homology exists between these viruses to detect the M gene in this manner. Sequencing methods that obtain a greater depth of coverage might help obtain the missing M sequences. To increase the virus titer and the likelihood of obtaining the M sequence, we recommend performing deep sequencing on the isolated virus.

TcTV-2 previously was identified in *D. marginatus* ticks from China (*5*) and in *H. marginatum* ticks from Turkey (*12*). We detected TcTV-2 in *D. nuttalli*, *D. silvarum, H. asiaticum* ticks and in blood, urine, and throat swab samples from a patient with febrile illness. Our findings suggest that person-to-person transmission might be possible through direct contact with body fluids or by droplet transmission. In addition, we noted more tick species found in northwest China that could act as TcTV-2 vectors (*14*), but this finding should be verified in further studies. Nonetheless, our study demonstrates that TcTV-2 could be emerging and infecting humans. Clinicians should consider TcTV-2 infections in patients with febrile illness and recent history of tick bites.

This study was supported by the National Key Research and Development Program of China (approval no. 2018ZX10101002-002-007) and the National Natural Science Foundation of China (approval no. 81960379).

### About the Author

Dr. Dong is a scientist at the School of Medicine, Shihezi University, Shihezi, China. Her research interest is emerging tickborne diseases.

### References

1. Yu XJ, Liang MF, Zhang SY, Liu Y, Li JD, Sun YL, et al. Fever with thrombocytopenia associated with a novel bunyavirus in China. N Engl J Med. 2011;364:1523–32. https://doi.org/10.1056/NEJMoa1010095
2. Wang ZD, Wang B, Wei F, Han SZ, Zhang L, Yang ZT, et al. A new segmented virus associated with human febrile illness in China. N Engl J Med. 2019;380:2116–25. https://doi.org/10.1056/NEJMoa1805068
3. Jia N, Liu HB, Ni XB, Bell-Sakyi L, Zheng YC, Song JL, et al. Emergence of human infection with Jingmen tick virus in China: a retrospective study. EBioMedicine. 2019;43:317–24. https://doi.org/10.1016/j.ebiom.2019.04.004
4. Liu X, Zhang X, Wang Z, Dong Z, Xie S, Jiang M, et al. A tentative Tamdy Orthonairovirus related to febrile illness in northwestern China. Clin Infect Dis. 2020;70:2155–60. https://doi.org/10.1093/cid/ciz602
5. Li CX, Shi M, Tian JH, Lin XD, Kang YJ, Chen LJ, et al. Unprecedented genomic diversity of RNA viruses in arthropods reveals the ancestry of negative-sense RNA viruses. Elife. 2015;4:e05378. https://doi.org/10.7554/eLife.05378
6. Zhang L, Li S, Huang SJ, Wang ZD, Wei F, Feng XM, et al. Isolation and genomic characterization of lymphocytic choriomeningitis virus in ticks from northeastern China. Transbound Emerg Dis. 2018;65:1733–9. https://doi.org/10.1111/tbed.12946
7. Tokarz R, Williams SH, Sameroff S, Sanchez Leon M, Jain K,Lipkin WI. Virome analysis of *Amblyomma americanum, Dermacentor variabilis*, and *Ixodes scapularis* ticks reveals novel highly divergent vertebrate and invertebrate viruses. J Virol. 2014;88:11480–92. https://doi.org/10.1128/JVI.01858-14
8. Sameroff S, Tokarz R, Charles RA, Jain K, Oleynik A, Che X, et al. Viral diversity of tick species parasitizing cattle and dogs in Trinidad and Tobago. Sci Rep. 2019;9:10421. https://doi.org/10.1038/s41598-019-46914-1
9. Pereira A, Figueira L, Nunes M, Esteves A, Cotão AJ, Vieira ML, et al. Multiple Phlebovirus (Bunyaviridae) genetic groups detected in *Rhipicephalus, Hyalomma* and *Dermacentor* ticks from southern Portugal. Ticks Tick Borne Dis. 2017;8:45–52. https://doi.org/10.1016/j.ttbdis.2016.09.015
10. Dinçer E, Brinkmann A, Hekimoğlu O, Hacıoğlu S, Földes K, Karapınar Z, et al. Generic amplification and next generation sequencing reveal Crimean-Congo hemorrhagic fever virus AP92-like strain and distinct tick phleboviruses in Anatolia, Turkey. Parasit Vectors. 2017;10:335. https://doi.org/10.1186/s13071-017-2279-1

11. Souza WM, Fumagalli MJ, Torres Carrasco AO, Romeiro MF, Modha S, Seki MC, et al. Viral diversity of *Rhipicephalus microplus* parasitizing cattle in southern Brazil. Sci Rep. 2018;8:16315. https://doi.org/10.1038/s41598-018-34630-1
12. Brinkmann A, Dinçer E, Polat C, Hekimoğlu O, Hacıoğlu S, Földes K, et al. A metagenomic survey identifies Tamdy orthonairovirus as well as divergent phlebo-, rhabdo-, chu- and flavi-like viruses in Anatolia, Turkey. Ticks Tick Borne Dis. 2018;9:1173–83. https://doi.org/10.1016/j.ttbdis.2018.04.017
13. McMullan LK, Folk SM, Kelly AJ, MacNeil A, Goldsmith CS, Metcalfe MG, et al. A new phlebovirus associated with severe febrile illness in Missouri. N Engl J Med. 2012;367:834–41. https://doi.org/10.1056/NEJMoa1203378
14. Sheng J, Jiang M, Yang M, Bo X, Zhao S, Zhang Y, et al. Tick distribution in border regions of northwestern China. Ticks Tick Borne Dis. 2019;10:665–9. https://doi.org/10.1016/j.ttbdis.2019.02.011


Address for correspondence: Yuanzhi Wang or Quan Liu, Shihezi University, Shihezi, Xinjiang Uygur Autonomous Region 832002, China; email: wangyuanzhi621@126.com or liuquan1973@hotmail.com

# Combined Epidemiologic and Entomologic Survey to Detect Urban Malaria Transmission, Guinea, 2018

Dean Sayre, Alioune Camara, Yaya Barry, Touré Babacar Deen, Denka Camara, Mohamed Dioubaté, Ibrahima Camara, Kalil Keita, Nouman Diakité, Youssoufa Lo, Ibrahima Bah, Hadja Fanta Camara, Mohamed Saran Condé, Aissata Fofana, Abdoulaye Sarr, Eugène Lama, Seth Irish, Mateusz Plucinski

Malaria incidence is generally lower in cities than rural areas. However, reported urban malaria incidence may not accurately reflect the level of ongoing transmission, which has potentially large implications for prevention efforts. To guide mosquito net distribution, we assessed the extent of malaria transmission in Conakry, Guinea, in 2018. We found evidence of active malaria transmission.

Vector control strategies are an important tool for the reduction of malaria burden worldwide. However, these strategies, such as the distribution of mosquito nets (long-lasting insecticidal nets [LLINs]), are effective only in settings of ongoing malaria transmission. Malaria transmission is generally lower in urban areas compared with rural ones (*1*,*2*). Moreover, due to population mobility and increased urban access to medical services, malaria cases reported from cities may capture at least some infections acquired in the outlying rural areas, complicating use of incidence data to determine the need for LLINs in urban areas. To guide a recent LLIN distribution campaign, we rapidly assessed malaria transmission in Conakry, Guinea, using a combined epidemiologic and entomologic approach.

## The Study

During November 19–December 24, 2018, we conducted community and health facility cross-sectional surveys describing key malaria epidemiologic and entomologic indicators in 10 nonadjacent sites in Conakry, Guinea, by using the methods described by Camara et al. (*3*). In addition, a sample of outpatients seeking medical attention were tested for malaria at 25 health-care facilities across Conakry and asked about recent travel outside of the city (Appendix, https://wwwnc.cdc.gov/EID/article/27/2/19-1701-App1.pdf).

We conducted a community survey in 300 households throughout Conakry, yielding person-specific data from 2,164 persons and mosquito net access and use data for 1,016 unique sleeping spaces (Figure 1; Appendix Table 1). We performed rapid diagnostic tests (RDTs) to detect *Plasmodium falciparum*–specific antigens for 1,102 (50.9%) of these persons. Surveys conducted in 120 households in 4 villages within the neighboring rural district of Dubréka provided person-specific data for 919 participants and mosquito net access and use data for 486 unique sleeping spaces to serve as a control. We tested 451 (49.1%) control participants for malaria by RDT.

In Conakry, 43.3% of households surveyed claimed to own $\geq$1 mosquito net, compared with 89.2% ($p<0.001$) of households in Dubréka. Survey participants reported 18.8% (191/1,016) of documented sleeping spaces in Conakry had a mosquito net available at the time of the survey, compared with 63.8% (310/486, $p<0.001$) in Dubréka. Nets were hanging over 16.7% (170/1,016) of sleeping spaces in Conakry and 59.9% (291/486, $p<0.001$) of those in Dubréka. However, participant use of nets was similar; 89.0% (170/191) of the available nets in Conakry were in use at the time of the survey, compared with 93.8% (291/310, $p = 0.062$) in Dubréka (Table 1).

Mosquito net access and rates of use were found to be heterogeneous across Conakry. Availability of dedicated mosquito nets ranged from 11.6% (20/173) to 28.6% (63/220) of sleeping spaces when households were grouped by administrative sections (communes). Net use when available ranged from 65.0% (13/20) to 100% (26/26) by commune across Conakry (Table 1).

Author affiliations: Centers for Disease Control and Prevention, Atlanta, Georgia, USA (D. Sayre, A. Sarr, S. Irish, M. Plucinski); National Malaria Control Program, Conakry, Guinea (A. Camara, Y. Barry, T.B. Deen, D. Camara, M. Dioubaté, I. Camara, K. Keita, N. Diakité, Y. Lo, E. Lama); Catholic Relief Services, Conakry (I. Bah); Stop Palu+, Conakry (H.F. Camara, M.S. Condé, A. Fofana); Centers for Disease Control and Prevention, Conakry (A.Sarr)

DOI: https://doi.org/10.3201/eid2702.191701

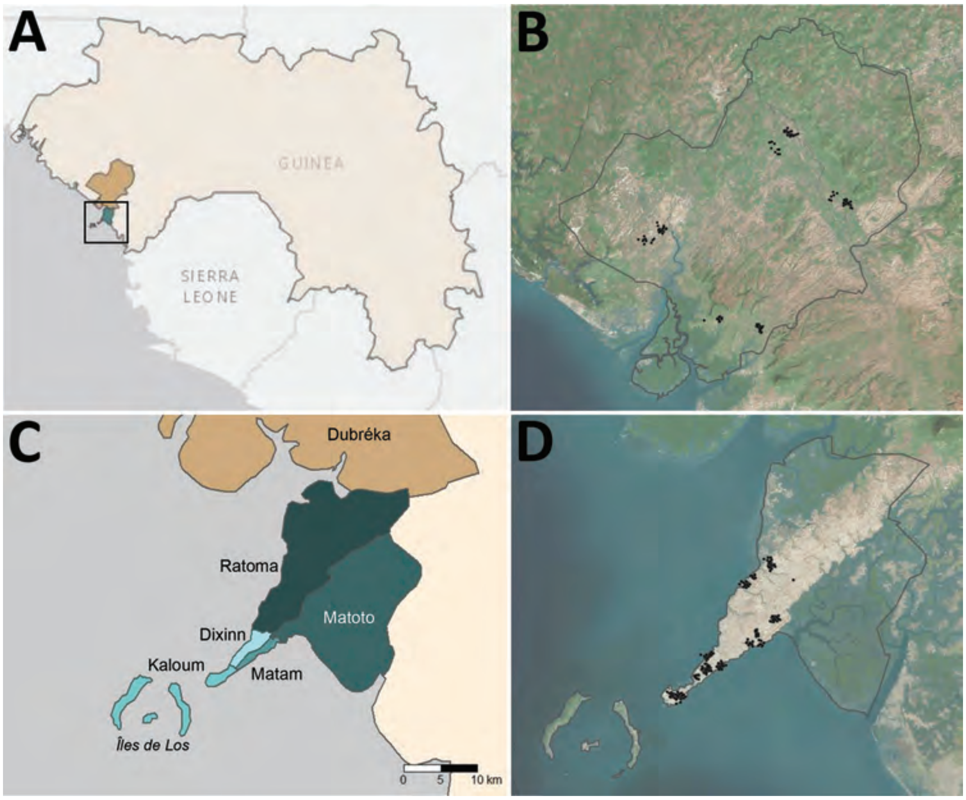


**Figure 1.** Administrative boundaries and location of communities visited as part of an epidemiologic–entomologic survey in Conakry and Dubréka, 2018. A) The positions of study sites are shown within the context of West Africa specifically Guinea. Turquoise area denotes Conakry and khaki Dubréka. Black square represents boundaries of the area depicted in panel B. B) Satellite imagery of Dubréka (outlined in black) and surrounding areas, with participating households shown as black points. C) Locations of 5 administrative communes within Conakry are shown in shades of turquoise; Dubréka is colored khaki. D) Satellite imagery of Conakry (outlined in black) and surrounding areas, with households participating in the survey shown as black points. Global positioning system coordinates of households were jittered for confidentiality before mapping in both (B) and (D).

**Table 1.** Coverage of malaria prevention interventions in and near Conakry, Guinea, 2018*

| | Conakry, no./total no. (%) | | | | | | | | |
|---|---|---|---|---|---|---|---|---|---|
| Characteristic | Kaloum | Dixinn | Matam | Matoto | Ratoma | Total | p value† | Dubréka | p value‡ |
| LLIN ownership | | | | | | | | | |
| Households receiving LLIN in last campaign | 50/60 (83.3) | 48/60 (80.0) | 54/60 (90.0) | 52/60 (86.7) | 52/60 (86.7) | 256/300 (85.3) | 0.61 | 102/120 (85.0) | 1 |
| Households with ≥1 LLIN at time of study | 14/60 (23.3) | 22/60 (36.7) | 38/60 (63.3) | 24/60 (40.0) | 32/60 (53.3) | 130/300 (43.3) | <0.001 | 107/120 (89.2) | <0.001 |
| LLIN access | | | | | | | | | |
| Sleeping spaces with LLIN available | 20/173 (11.6) | 28/169 (16.6) | 54/248 (21.8) | 26/206 (12.6) | 63/220 (28.6) | 191/1,016 (18.8) | <0.001 | 310/486 (63.8) | <0.001 |
| Population sleeping in space with LLIN available | 42/366 (11.5) | 66/383 (17.2) | 108/485 (22.3) | 63/445 (14.2) | 158/511 (30.9) | 437/2,190 (20.0) | <0.001 | 647/966 (67.0) | <0.001 |
| LLIN use | | | | | | | | | |
| Sleeping spaces with LLIN hanging | 13/173 (7.5) | 26/169 (15.4) | 45/248 (18.1) | 26/206 (12.6) | 60/220 (27.2) | 170/1,016 (16.7) | <0.001 | 291/486 (59.9) | <0.001 |
| Population sleeping in spaces with LLIN hanging | 27/366 (7.3) | 62/383 (16.2) | 89/485 (18.4) | 63/445 (14.2) | 146/511 (28.6) | 387/2,190 (17.3) | <0.001 | 617/966 (63.9) | <0.001 |
| Spaces with LLIN hanging among those where available | 13/20 (65.0) | 26/28 (92.9) | 45/54 (83.3) | 26/26 (100.0) | 60/63 (95.2) | 170/191 (89.0) | <0.001 | 291/310 (93.9) | 0.062 |
| Proportion sleeping under LLIN in population with access | 27/42 (64.3) | 62/66 (93.9) | 89/108 (82.4) | 63/63 (100.0) | 146/158 (92.4) | 387/437 (88.6) | <0.001 | 617/647 (95.4) | <0.001 |
| Used LLIN in previous night, <5 y | 5/52 (19.6) | 19/78 (24.4) | 21/99 (21.2) | 9/77 (11.7) | 24/86 (27.9) | 78/392 (19.9) | 0.021 | 137/204 (67.2) | <0.001 |
| Used LLIN in previous night, ≥5 y | 14/314 (4.5) | 44/298 (14.8) | 99/381 (26.0) | 40/371 (10.8) | 95/408 (23.3) | 292/1,772 (16.5) | <0.001 | 442/716 (61.7) | <0.001 |
| Indoor residual spraying | 4/60 (6.7) | 1/60 (1.7) | 0/60 (0.0) | 1/60 (1.7) | 0/60 (0.0) | 6/300 (2.0) | 0.11 | 1/120 (0.8) | 0.68 |
| Any insecticide use | 6/60 (10.0) | 9/60 (15.0) | 10/60 (16.7) | 16/60 (26.7) | 20/60 (33.3) | 61/300 (20.3) | 0.012 | 54/120 (45.0) | <0.001 |

*Populations determined by summing responses to number of persons sleeping in each space; total denominators do not necessarily match total number of persons reported as living in surveyed households. LLIN, long-lasting insecticidal nets.
†Comparison of results for communes within Conakry.
‡Comparison of results for Conakry and Dubréka.

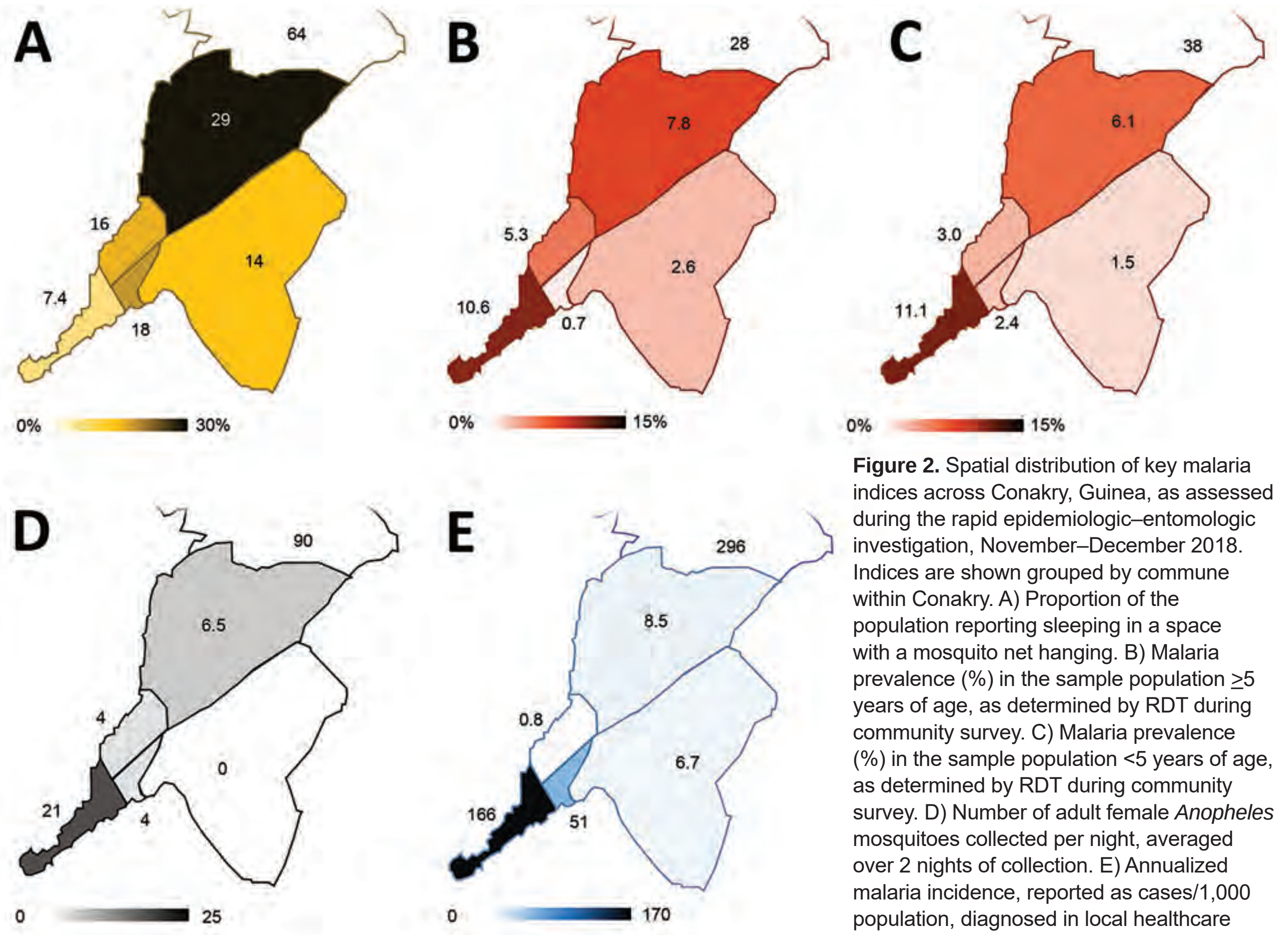


**Figure 2.** Spatial distribution of key malaria indices across Conakry, Guinea, as assessed during the rapid epidemiologic–entomologic investigation, November–December 2018. Indices are shown grouped by commune within Conakry. A) Proportion of the population reporting sleeping in a space with a mosquito net hanging. B) Malaria prevalence (%) in the sample population ≥5 years of age, as determined by RDT during community survey. C) Malaria prevalence (%) in the sample population <5 years of age, as determined by RDT during community survey. D) Number of adult female *Anopheles* mosquitoes collected per night, averaged over 2 nights of collection. E) Annualized malaria incidence, reported as cases/1,000 population, diagnosed in local healthcare facilities. RDT, rapid diagnostic test.

Malaria prevalence by RDT in both children <5 years and participants ≥5 years was lower in Conakry than in Dubréka (Appendix Table 2). RDT positivity among children <5 years was 4.3% (14/329) in Conakry and 38.0% (60/158) in Dubréka (p<0.001); in older participants positivity was 5.6% (43/773) in Conakry and 28.0% (82/293) in Dubréka (p<0.001). Within Conakry, the greatest malaria prevalence in both age groups collocated with the lowest rates of mosquito net use and access, although the differences observed between communes in the younger age group failed to reach statistical significance (p = 0.125 for age <5 years, p<0.001 for those ≥5 years) (Figure 2). Most participants tested in Conakry (717/1,102, 65.1%) denied having left the city within the last year. Considering only those reporting not having left the city in the past year, we found that 4.0% (29/717) were positive for *P. falciparum* antigen.

Of the 57 participants of all ages who were positive for malaria within Conakry, 75.4% (43/57) reported not leaving the city within the last 4 weeks (Table 2). Thirty-four of these participants (34/57, 59.6%) reported not having left Conakry within the 6 months before interview, and 50.9% (29/57) did not leave the city within the year before interview. Nearly one fifth of Conakry residents were positive for malaria reported never having left the city (17.5%, 10/57).

A random intercept, mixed effects regression model to identify risk factors for P. falciparum antigenemia demonstrated statistically significant associations with self-reported travel outside the city (p<0.23). Odds ratios were 2.2–7.3 and were higher for more recent travel (Appendix Table 3).

We collected recent travel history data from 4,678 persons seeking medical attention whose diagnostic workup included malaria testing by microscopy or RDT. Of these persons, 8.0% (376/4,678) reported travel outside Conakry within the 4 weeks before being tested. Malaria antigen was detected in 57.7% (217/376) of those reporting having left the city in the last 4 weeks, compared with 26.5% (1,139/4,302) of those who remained in Conakry in the same period (Appendix Table 4). The overall relative risk for malaria positivity associated with travel outside of Conakry within the last 4 weeks was 2.2 (95% CI 2.0–2.4). The corresponding population

**Table 2.** Characteristics of persons testing positive for malaria infection, Guinea, 2018*

| Characteristic, n/N (%) | Conakry: Kaloum | Dixinn | Matam | Matoto | Ratoma | Total | p value† | Dubréka | p value‡ |
|---|---|---|---|---|---|---|---|---|---|
| LLIN use previous night, <5 y | 0/5 (0.0) | 0/2 (0.0) | 0/2 (0.0) | 1/1 (100) | 0/4 (0.0) | 1/14 (7.1) | 0.07 | 41/60 (68.3) | <0.001 |
| LLIN use previous night, ≥5 y | 0/17 (0.0) | 0/8 (0.0) | 0/1 (0.0) | 1/4 (25.0) | 4/13 (30.8) | 5/43 (11.6) | 0.042 | 46/82 (56.1) | <0.001 |
| Fever ≤2 wk of RDT | 15/22 (68.2) | 3/10 (30.0) | 2/3 (66.7) | 5/5 (100) | 9/17 (52.9) | 34/57 (59.6) | 0.092 | 75/135 (55.6) | 0.64 |
| History of travel outside Conakry, ≤4 wks | 4/22 (18.2) | 5/10 (50.0) | 0/3 (0.0) | 1/5 (20.0) | 4/17 (23.5) | 14/57 (24.6) | 0.37 | NA | |
| History of travel outside Conakry, ≤6 mo | 5/22 (22.7) | 7/10 (70.0) | 0/3 (0.0) | 2/5 (40.0) | 9/17 (52.9) | 23/57 (40.4) | 0.04 | NA | |
| No travel outside Conakry within last year | 17/22 (77.3) | 2/10 (20.0) | 1/3 (33.3) | 2/5 (40.0) | 7/17 (41.2) | 29/57 (50.9) | 0.016 | NA | |

*In a joint epidemiologic–entomologic investigation of urban malaria transmission in Guinea, participants were tested by using rapid diagnostic test during community screening. LLIN, long-lasting insecticidal net; NA, not applicable; RDT, rapid diagnostic test.
†Comparison of results for communes within Conakry.
‡Comparison of results for Conakry and Dubréka.

attributable risk of travel outside the city was calculated as 8.7%. Although rates of malaria positivity and recent travel history both showed large variation, associated relative risks for individual communes were 1.56–3.57 and population-attributable fractions of risk were 4.6%–17.0% across different communes in Conakry.

Collection of adult mosquitoes as part of the study demonstrated the presence of female *Anopheles gambiae* sensu lato mosquitoes in 4/5 communes in Conakry. We captured an average of 21 adult female *A. gambiae* sl. mosquitoes nightly at the urban site yielding the greatest number of *Anopheles* mosquitoes in Conakry (Figure 2; Appendix Figure 1). In contrast, adult mosquito collection from 2 rural sites in Dubréka yielded an average of 90 female *Anopheles gambiae* sensu lato mosquitoes captured per night. However, the nightly yield was highly heterogeneous by site, with 1 of the 2 sites accounting for 99.4% (358/360) of the female *Anopheles* mosquitoes captured (Appendix Figure 2).

## Conclusions

We found multiple corroborating lines of evidence that strongly indicate malaria is actively transmitted in Conakry. The presence of *Anopheles* vectors, current or recent malaria infections in the absence of any plausible travel-related exposures, and the spatial distribution of infection mirroring that of risk factors for local acquisition of disease all suggest ongoing malaria transmission. Rural control sites had greater observed densities of competent vectors and higher prevalence of malaria. In addition, travel outside of the city was found to be a risk for malaria infection for persons living in Conakry. However, we found that the risk associated with travel was a minor contributor to the overall malaria burden in Conakry, indicating that residents appear to be at risk, albeit a decreased one, of acquiring malaria within the confines of the city.

Given the likely ongoing malaria transmission, coupled with the high rate of net use when available, LLIN distribution is a suitable malaria control strategy in Conakry. The observed heterogeneity of malaria transmission across the city raises the potential for more targeted distribution of prevention commodities. Additional studies are needed to confirm and further refine this finding.

This study was funded by the US President's Malaria Initiative.

## About the Author

Dr. Sayre is a physician trained in laboratory medicine in the Division of Parasitic Diseases and Malaria, Center for Global Health, Centers for Disease Control and Prevention, Atlanta, Georgia, USA. At the time of this work, he was an Epidemic Intelligence Service officer in the division. His research interests include the evaluation and optimization of programmatic interventions for malaria.

## References

1. De Silva PM, Marshall JM. Factors contributing to urban malaria transmission in sub-Saharan Africa: a systematic review. J Trop Med. 2012;2012:819563. https://doi.org/10.1155/2012/819563
2. Pond BS. Malaria indicator surveys demonstrate a markedly lower prevalence of malaria in large cities of sub-Saharan Africa. Malar J. 2013;12:313. https://doi.org/10.1186/1475-2875-12-313
3. Camara A, Guilavogui T, Keita K, Dioubaté M, Barry Y, Camara D, et al. Rapid epidemiological and entomological survey for validation of reported indicators and characterization of local malaria transmission in Guinea, 2017. Am J Trop Med Hyg. 2018;99:1134–44. https://doi.org/10.4269/ajtmh.18-0479

Address for correspondence: Dean Sayre, Centers for Disease Control and Prevention, 1600 Clifton Rd NE, Mailstop H24-3, Atlanta, GA 30333, USA; email: omp2@cdc.gov

# *Anopheles stephensi* Mosquitoes as Vectors of *Plasmodium vivax* and *P. falciparum*, Horn of Africa, 2019

Fitsum G. Tadesse,[1] Temesgen Ashine,[1] Hiwot Teka, Endashaw Esayas, Louisa A. Messenger, Wakweya Chali, Lisette Meerstein-Kessel, Thomas Walker, Sinknesh Wolde Behaksra, Kjerstin Lanke, Roel Heutink, Claire L. Jeffries, Daniel Abebe Mekonnen, Elifaged Hailemeskel, Surafel K. Tebeje, Temesgen Tafesse, Abrham Gashaw, Tizita Tsegaye, Tadele Emiru, Kigozi Simon, Eyuel Asemahegn Bogale, Gedeon Yohannes, Soriya Kedir, Girma Shumie, Senya Asfer Sabir, Peter Mumba, Dereje Dengela, Jan H. Kolaczinski, Anne Wilson, Thomas S. Churcher, Sheleme Chibsa, Matthew Murphy, Meshesha Balkew, Seth Irish, Chris Drakeley, Endalamaw Gadisa, Teun Bousema

*Anopheles stephensi* mosquitoes, efficient vectors in parts of Asia and Africa, were found in 75.3% of water sources surveyed and contributed to 80.9% of wild-caught *Anopheles* mosquitoes in Awash Sebat Kilo, Ethiopia. High susceptibility of these mosquitoes to *Plasmodium falciparum* and *vivax* infection presents a challenge for malaria control in the Horn of Africa.

Malaria control programs in Africa traditionally focus on rural settings, although transmission is also a health concern in some urban settings (*1*).

Author affiliations: Armauer Hansen Research Institute, Addis Ababa, Ethiopia (F.G. Tadesse, T. Ashine, H. Teka, E. Esayas, W. Chali, S.W. Behaksra, D.A. Mekonnen, E. Hailemeskel, S.K. Tebeje, T. Tafesse, A. Gashaw, T. Tsegaye, T. Emiru, E.A. Bogale, G. Shumie, S.A. Sabir, E. Gadisa); Radboud University Medical Center, Nijmegen, the Netherlands (F.G. Tadesse, L. Meerstein-Kessel, K. Lanke, R. Heutink, E. Hailemeskel, S.K. Tebeje, T. Bousema); Addis Ababa University, Addis Ababa (F.G. Tadesse, D.A. Mekonnen, E. Hailemeskel); United States Agency for International Development, Addis Ababa (H. Teka, S. Chibsa, M. Murphy); London School of Hygiene and Tropical Medicine, London, UK (L.A. Messenger, T. Walker, C.L. Jeffries, K. Simon, C. Drakeley, T. Bousema); President's Malaria Initiative VectorLink Ethiopia Project, Addis Ababa (G. Yohannes, P. Mumba, M. Balkew); Oromia Regional Health Bureau, Adama, Ethiopia (S. Kedir); President's Malaria Initiative VectorLink Project, Rockville, Maryland, USA (D. Dengela); World Health Organization, Geneva, Switzerland (J.H. Kolaczinski); Liverpool School of Tropical Medicine, Liverpool, UK; (A. Wilson); Imperial College London, London (T.S. Churcher); United States President's Malaria Initiative, Atlanta, Georgia, USA (S. Chibsa, M. Murphy, S. Irish); Centers for Disease Control and Prevention, Atlanta (S. Irish)

DOI: https://doi.org/10.3201/eid2702.200019

*Anopheles stephensi* mosquitoes breed predominantly in urban settings, prefer water storage containers (*2*), and are found throughout the Horn of Africa (*3*). To determine susceptibility of *An. stephensi* mosquito vectors to infection with local *Plasmodium* strains, we measured their abundance in an urban area of Ethiopia and characterized their aquatic habitats, biting and resting behavior, and competence to transmit local *P. vivax* and *P. falciparum*.

Study protocol was approved by the Institutional Ethical Review Board of the Aklilu Lemma Institute of Pathobiology of Addis Ababa University (ALIPB IRB/025/2011/2019), the Oromia Regional Health Bureau (BEFO/MBTFH/1331), and AHRI/ALERT Ethics Review Committee (AF-10-015.1, PO07/19). All participants or parents/legal guardians for participants <18 years of age provided written informed consent. Persons who volunteered for human landing collection also provided written informed consent, were monitored for 3 weeks after collections, and if symptomatic and positive received treatment for *Plasmodium* according to the treatment guidelines of the country.

## The Study

This study was conducted in Awash Sebat Kilo, Ethiopia, an area of perennial malaria transmission, during April–September 2019. We examined aquatic habitats for immature-stage *Anopheles* mosquitoes by standard dipping (10×/site) for 5 consecutive days (*4*). We assessed mosquito resting, feeding, and host-seeking behavior by 5 methods: CDC miniature light traps model 512 (John W. Hock Company,

[1]These authors contributed equally to this article.

https://www.johnwhock.com), human landing collection, pyrethrum spray sheet collection, aspiration from animal shelters, and cattle-baited traps (*5*). We identified adult mosquitoes by using standard keys and confirmed identification by targeted sequencing of nuclear internal transcribed spacer 2 (ITS2) and mitochondrial cytochrome oxidase subunit 1 gene (COI) (*6*). To generate clade topologies, we compared *An. stephensi* mosquito DNA sequences with those in publicly available libraries (*7*). We determined mosquito blood meal sources by using multiplex PCR targeting cytochrome b (*8*) and infection status by using 18S rRNA nested PCR (*9*).

Adult *An. stephensi* mosquitoes reared from immature mosquitoes from local water sources and a colony of *An. arabiensis* mosquitoes (≈120 each) were fed in the dark for 30 min on membrane feeders containing fresh blood from Adama malaria clinic patients with microscopy-confirmed mono- and mixed-species infections with *P. vivax* and *P. falciparum* (*10*). Unfed and partially fed mosquitoes were removed; fully engorged mosquitoes were maintained on sugar solution. At 7 or 12 days after feeding, mosquitoes were dissected, their midguts were examined for oocysts, and their salivary glands were examined for sporozoites. To compare infection status between *An. arabiensis* and *An. stephensi* mosquitoes, we performed logistic regression. We used individual mosquito data and a fixed effect for each patient to account for correlations between mosquito observations from the same donor. Bland-Altmann plots were generated for differences in infectivity between mosquito sources by using the Pitman test of difference in variance. For analyses, we used STATA version 13 (StataCorp., https://www.stata.com/company) and GraphPad Prism 5.3 (GraphPad Software Inc., https://www.graphpad.com). Raw data have been deposited in the DRYAD data depository (https://datadryad.org/stash/dataset/doi:10.5061/dryad.gf1vhhmnt).

*An. stephensi* larvae were detected in 75.3% (64/85) of the 85 artificial water sources surveyed (Table 1). A total of 49,393 immature *Anopheles* larvae and pupae were collected during 20 weekly collections in April–September 2019, of which 45,316 (91.7%) emerged as adult mosquitoes in the laboratory. Morphologic identification of adults confirmed that all were *An. stephensi*. During monthly rounds of entomologic surveillance in August and September (6 days each), we collected 89 adult female *Anopheles* mosquitoes (72 [80.9%] *An. stephensi*, 16 *An. gambiae*, and 1 *An. pharoensis*). We detected *P. vivax* in 2.8% (2/72) and *P. falciparum* in 1.4% (1/72) of wild-caught *An. stephensi* mosquitoes. Blood meal source was identified for 35.0% (28/80) blood-fed wild-caught *An. stephensi* mosquitoes; exclusive human blood meal was identified for 17.2% (5/29). The remainder fed (multiple blood meals) either on humans and animals (n = 9) or animals only (n = 14) such as goats (n = 21), cows (n = 4), and dogs (n = 5). Successful sequencing of ITS2 for 76 and COI for 45 *Anopheles* mosquitoes confirmed that all were *An. stephensi*. According to ITS2 sequences, *An. stephensi* mosquitoes from Ethiopia formed a well-supported monophyletic clade with isolates from the Arabian Peninsula and Southeast

**Table 1.** Characteristics of 85 aquatic habitats surveyed in study of *Anopheles stephensi* mosquitoes as vectors of *Plasmodium vivax* and f*alciparum*, Horn of Africa, 2019

| Characteristic | Habitats, no. | Mosquito larvae, no. larvae detected/no. habitats sampled (%) | Mosquito pupae, no. pupae detected/no. habitats sampled (%) |
|---|---|---|---|
| Localities (kebeles) within the town of Awash Sebat Kilo | | | |
| Sebat Kilo | 60 | 44/60 (73.3) | 19/44 (43.2) |
| Lemlefan | 17 | 12/17 (70.6) | 0/12 (0) |
| Alalamo | 8 | 8/8 (100.0) | 5/8 (62.5) |
| Artificial containers | | | |
| Permanent | 48 | 41/48 (85.4) | 17/41 (41.5) |
| Temporary | 37 | 23/37 (62.2) | 7/23 (30.4) |
| Shade status | | | |
| Fully | 22 | 14/22 (63.6) | 6/14 (42.9) |
| Partial | 24 | 22/24 (99.7) | 7/22 (31.8) |
| None | 39 | 28/39 (71.8) | 11/28 (39.3) |
| Use status | | | |
| In use | 71 | 54/71 (76.1) | 20/54 (37.0) |
| Not in use | 14 | 10/14 (71.4) | 4/10 (40.0) |
| Container material | | | |
| Fiber jar/tire | 23 | 10/23 (43.5) | 4/10 (40.0) |
| Metal/steel tanks/drum/barrel | 17 | 16/17 (94.1) | 5/16 (31.3) |
| Cement/ceramic | 45 | 38/4 (84.4) | 15/38 (39.5) |
| Water turbidity | | | |
| Clean | 56 | 45/56 (80.4) | 17/45 (37.8) |
| Turbid | 28 | 19/28 (67.9) | 7/19 (36.8) |

**Table 2.** Characteristics of blood meals and mosquito feeding outcomes in study of *Anopheles stephensi* mosquitoes as vectors of *Plasmodium vivax* and f*alciparum*, Horn of Africa, 2019*

| | *Plasmodium* species | | |
|---|---|---|---|
| Characteristic | *P. vivax*, n = 36 | *P. falciparum*, n = 7 | Mixed, n = 4 |
| Parasites/µL, median (IQR) | 7,783 (3,603–13,440) | 2,431 (867–8,756) | 4,516 (1,589–10,563) |
| Gametocyte positivity, no. positive/no. sampled (%) | 25/34 (73.5) | 1/7 (14.3) | 1/4 (25.0). |
| Infectious feeds, no. positive/no. sampled (%) | 26/36 (72.2) | 1/7 (14.3) | 2/4 (50.0) |
| Infected *An. stephensi* mosquitoes, no. positive/no. sampled (%) | 446/849 (52.5 | 2.2 | 36/104 (34.6) |
| Infected *An arabiensis* mosquitoes, no. positive/no. sampled (%) | 452/1,000 (45.2) | 18/200 (9.0) | 45/122 (36.9) |
| Oocysts in infected *An. arabiensis* mosquito midgut, mean (range) | 22.8 (1–115) | NA | 3.1 (1–22) |
| Oocysts in infected *An. stephensi* mosquito midgut, mean (range) | 24.1 (1–105) | NA | 2.8 (1–13) |

*Parasite and gametocyte densities were determined by microscopy; IQR, Interquartile range; NA, not available.

Asia (Appendix, https://wwwnc.cdc.gov/EID/article/27/2/20-0019-App1.pdf). The COI tree was more resolutive, suggesting that *An. stephensi* mosquitoes from Ethiopia were most closely related to mosquitoes from Djibouti (64%) and Pakistan (54%).

We conducted 47 paired-membrane feeding experiments by using blood from patients with microscopy-confirmed *P. vivax* or *P. falciparum* infection (Table 2). The proportion of blood-fed mosquitoes was generally higher for *An. arabiensis* (median 80.5%; interquartile range [IQR] 72.5–85.0) than *An. stephensi* mosquitoes (median 53.5%, IQR 44.0–68.0; p<0.001; Figure 1, panel A). The proportions of the 2 mosquito species infected with *P. vivax* were strongly associated (ρ = 0.82, p<0.001; Figure 1, panel B); a significantly higher proportion of *An. stephensi* (median 75.1%, IQR 60.0–85.9) than *An. arabiensis* mosquitoes were infected (median 58.4%, IQR 40.0–85.6; p<0.042). Allowing for the number of dissected mosquitoes for each set of paired feeding experiments, the odds of an individual mosquito becoming infected was higher for *An. stephensi* mosquitoes (odds ratio [OR] 1.99, 95% CI 1.52–2.59; p<0.001) (Figure 1, panel C). The number of oocysts per infected midgut was also higher for *An. stephensi* (median 17, IQR 6–33) than *An. arabiensis* mosquitoes (median 13, IQR 4–30); p<0.001 (Figure 2, panel A). The number of oocysts was positively associated with the proportion of infected mosquitoes for *An. stephensi* (ρ = 0.553, p<0.001) and *An. arabiensis* mosquitoes (ρ = 0.576, p<0.001; Figure 2, panel B). Among paired feedings, sporozoites were detected in 52.2% (47/90) *An. arabiensis* and 75.0% (84/112) *An. stephensi* mosquitoes. A much higher proportion of *An. stephensi* (51.8%, 58/112) than *An. arabiensis*

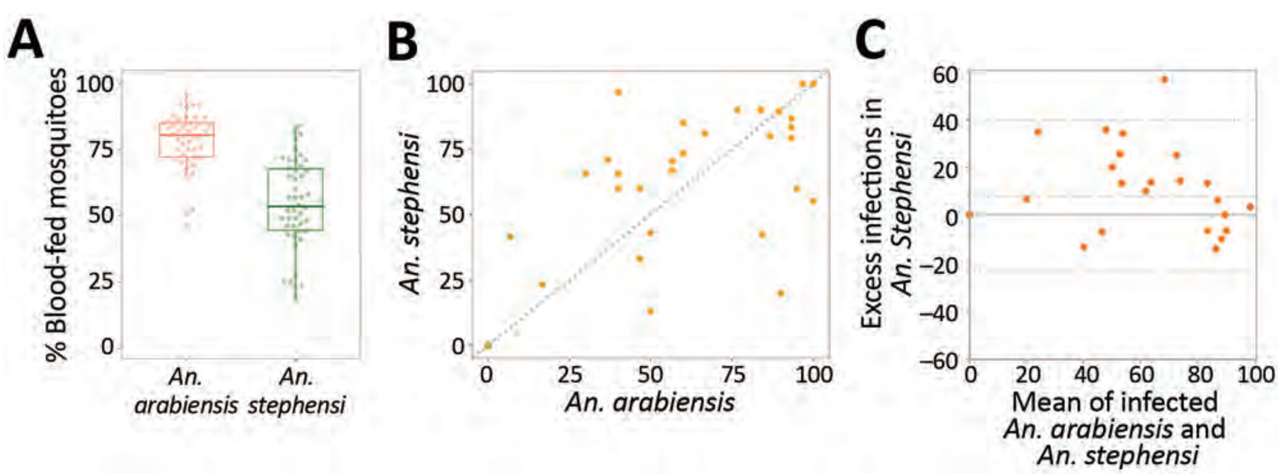


**Figure 1.** Comparison of feeding efficiency and infection rates for *Anopheles stephensi* and *An. arabiensis* mosquitoes in paired feeding experiments in study of *An. stephensi* mosquitoes as vectors of *Plasmodium vivax* and f*alciparum*, Horn of Africa, 2019. A) Percentage of fully fed *An. arabiensis* mosquitoes (red) and *An. stephensi* mosquitoes (green). Box plots indicate median (midline), 25th (lower line), and 75th (upper line) percentiles of proportion of blood-fed mosquitoes. Whiskers indicate lower and upper 25% scores. Vertical lines indicate minimum and maximum values. B) Percentage of infected mosquitoes. C) Bland-Altman plot (difference plots) for mosquito infection rates in different mosquito species. Symbols indicate differences in infection rates in *An. stephensi* versus *An. arabiensis* (y-axis) mosquitoes in relation to mean infection rates in these 2 species (x-axis). Positive values (57.1%; 16/28) indicate a higher infection rate in *An. stephensi* mosquitoes; dotted lines indicate the 95% limits of agreement. There was no evidence that the correlation coefficient between the paired differences and means differed significantly from 0 (Pitman test of difference in variance, r = 0.026, p = 0.864).

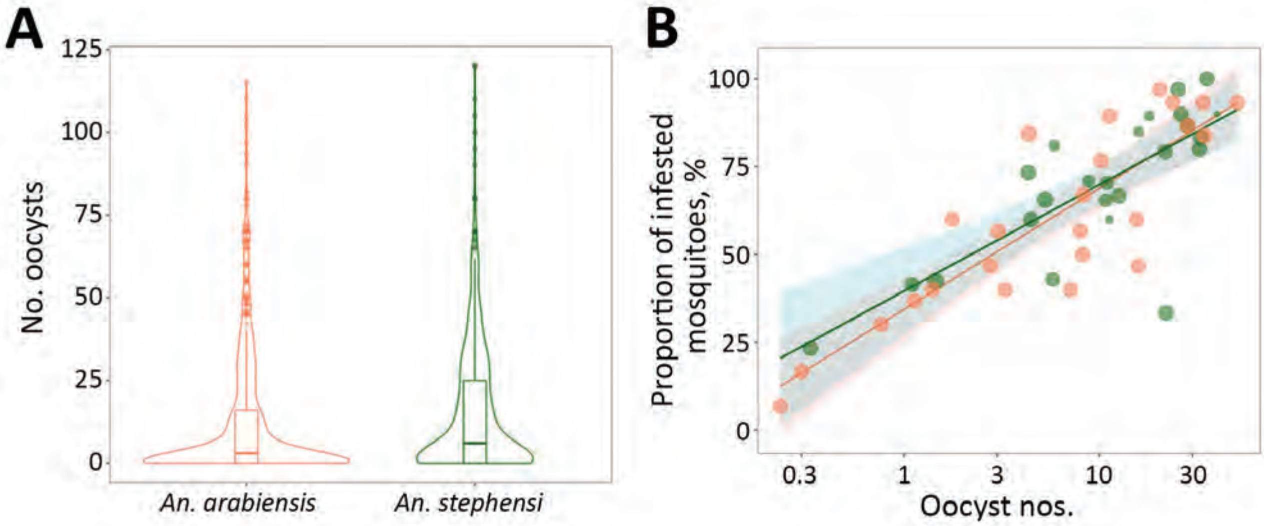


**Figure 2.** Comparison of relative oocyst numbers and infection rate for *Anopheles stephensi* and *An. arabiensis* mosquitoes in paired feeding experiments in study of *An. stephensi* mosquitoes as vectors of *Plasmodium vivax* and f*alciparum*, Horn of Africa, 2019. Number of oocysts per infected midgut for individual mosquitoes of each of the 2 species. A) Violin plot showing estimated kernel density. Horizontal lines indicate median; box indicates interquartile range; and spikes indicate upper and lower adjacent values. The proportion of midguts with detectable oocysts (y-axis) is indicated in association with $\log_{10}$ transformed oocyst numbers (x-axis) for *An. stephensi* (green dots) and *An. arabiensis* (orange dots) mosquitoes. B) Data for 24 feeding experiments in which 723 *An. arabiensis* and 643 *An. stephensi* mosquitoes were dissected. Shaded area indicates 95% CI around estimates for *An. stephensi* (green) and *An. arabiensis* (orange) mosquitoes.

mosquitoes (31.1%, 28/90) had high sporozoite load (+3 and +4); p = 0.011. After accounting for the number of examined salivary glands, the odds of detecting high sporozoite intensity were substantially higher for *An. stephensi* than *An. arabiensis* mosquitoes (OR 4.6, 95% CI 2.2–9.9; p<0.001).

## Conclusions

*An. stephensi* mosquitoes have spread from Asia throughout the Horn of Africa, detected in Djibouti in 2012 (*11*), Ethiopia in 2016 (*12*), and Sudan in 2019 (*3*). The widescale presence of *An. stephensi* mosquitoes in developmental stages in artificial water bodies demonstrates that these mosquitoes are firmly established in an urban setting in Ethiopia, located on the main transportation corridor from Djibouti to Addis Ababa. Detection of 4 haplotypes suggests independent arrival of different populations or heterogeneity arising after importation of the mosquito species. Our mosquito feeding experiments predominantly included highly infective patients with clinical *P. vivax* infection (*10*,*13*). Although feeding rates for the membrane-adapted colony of *An. arabiensis* mosquitoes were high, mosquito infection rates were significantly higher for *An. stephensi* mosquitoes. Our detection of salivary gland sporozoites establishes that sporogonic development of local *P. vivax* can be completed by *An. stephensi* mosquitoes. We recruited fewer patients with clinical *P. falciparum* infection, who were less likely than *P. vivax* patients to infect mosquitoes (*10*). Despite a modest number of observations, our findings demonstrate that local *P. falciparum* isolates are also capable of infecting *An. stephensi* mosquitoes and are further supported by detection of *P. falciparum*– and *P. vivax*–infected wild-caught adult mosquitoes.

Spread of *An. stephensi* mosquitoes poses risk for increased *P. falciparum* and *P. vivax* receptivity and local transmission in urban Africa. Given mosquito preference for human-made containers (*14*), our findings support integrated vector management recommended by the World Health Organization under the Global Vector Control Response (*15*). Management may include integrated surveillance and control of other vectors such as *Aedes aegypti* mosquitoes for larval source management.

### Acknowledgments

We acknowledge the study participants for their willingness to donate blood and allow assessment of mosquito exposure. We thank microscopists Tewabech Lema and Tsehay Orlando for their support. Appreciation also goes to the regional and district health officers for their collaboration and the PMI VectorLink Ethiopia Project for training the field team. Thanks also go to Gunawardena Dissanayake for insightful discussions. The drivers from Armauer Hansen Research Institute helped make the study successful.

The study was supported by the Bill and Melinda Gates Foundation grant (INDIE OPP1173572) to F.G.T., T.B., and C.D. The Armauer Hansen Research Institute supported W.C., T.A., E.H., and E.G. through its core funding from the Swedish International Development Cooperation Agency and the Norwegian Agency for Development Cooperation. The PMI VectorLink Ethiopia Project provided financial support for adult mosquito collection. C.L.J. and T.W. were supported by Wellcome Trust/Royal Society fellowships awarded to T.W. (101285/Z/13/Z).

H.T., P.M., S.C., M.M., M.B., S.I., C.D., E.G., T.B., and F.G.T. conceived the study; P.M., D.D., S.C., M.M., M.B., S.I., J.H.K., A.W., E.G., and F.G.T. participated in guiding the field activities; T.A. and E.E. collected mosquitoes in developmental stages; T.A., E.E., W.C., S.W.B., D.A.M., E.H., S.K.T., T.T., A.G., T.T., T.E., G.Y., S.K., G.S., and S.A.S. reared adult mosquitoes, collected blood samples, ran feeding experiments, and dissected mosquitoes; T.A., H.T., E.E., L.A.M., W.C., T.W., S.W.B., K.L., R.H., C.L.J., D.A.M., E.H., S.K.T., T.T., A.G., T.T., T.E., and F.G.T. conducted laboratory work; T.A., L.A.M., L.M.K., K.S., T.S.C., S.I., C.D., E.G., T.B., and F.G.T. analyzed data; T.A., H.T., E.E., L.A.M., T.W., C.L.J., C.D., E.G., T.B., and F.G.T. drafted the manuscript; and J.H.K., A.W., T.S.C., S.I., C.D., E.G., T.B., F.G.T. critically commented on the manuscript. All authors read and approved the final manuscript.

## About the Author

Dr. Tadesse is a molecular biologist leading the malaria research team of the Armauer Hansen Research Institute at the Federal Ministry of Health of Ethiopia and teaches at the Institute of Biotechnology at Addis Ababa University. His research interests include the biology and epidemiology of gametocytes of *P. vivax* and *P. falciparum*.

## References

1. Wilson ML, Krogstad DJ, Arinaitwe E, Arevalo-Herrera M, Chery L, Ferreira MU, et al. Urban malaria: understanding its epidemiology, ecology, and transmission across seven diverse ICEMR network sites. Am J Trop Med Hyg. 2015;93(Suppl):110–23. https://doi.org/10.4269/ajtmh.14-0834
2. Surendran SN, Sivabalakrishnan K, Sivasingham A, Jayadas TTP, Karvannan K, Santhirasegaram S, et al. Anthropogenic factors driving recent range expansion of the malaria vector *Anopheles stephensi*. Front Public Health. 2019;7:53. https://doi.org/10.3389/fpubh.2019.00053
3. World Health Organization. Vector alert: *Anopheles stephensi* invasion and spread [cited 2020 Sep 3]. https://www.who.int/publications/i/item/vector-alert-anopheles-stephensi-invasion-and-spread
4. World Health Organization. Larval source management: a supplementary measure for malaria vector control: an operational manual [cited 2020 Dec 21]. https://apps.who.int/iris/bitstream/handle/10665/85379/9789241505604_eng.pdf
5. St Laurent B, Oy K, Miller B, Gasteiger EB, Lee E, Sovannaroth S, et al. Cow-baited tents are highly effective in sampling diverse *Anopheles* malaria vectors in Cambodia. Malar J. 2016;15:440. https://doi.org/10.1186/s12936-016-1488-y
6. Folmer O, Black M, Hoeh W, Lutz R, Vrijenhoek R. DNA primers for amplification of mitochondrial cytochrome c oxidase subunit I from diverse metazoan invertebrates. Mol Mar Biol Biotechnol. 1994;3:294–9.
7. Kumar S, Stecher G, Li M, Knyaz C, Tamura K. MEGA X: Molecular Evolutionary Genetics Analysis across computing platforms. Mol Biol Evol. 2018;35:1547–9. https://doi.org/10.1093/molbev/msy096
8. Kent RJ, Norris DE. Identification of mammalian blood meals in mosquitoes by a multiplexed polymerase chain reaction targeting cytochrome B. Am J Trop Med Hyg. 2005;73:336–42. https://doi.org/10.4269/ajtmh.2005.73.336
9. Snounou G, Viriyakosol S, Zhu XP, Jarra W, Pinheiro L, do Rosario VE, et al. High sensitivity of detection of human malaria parasites by the use of nested polymerase chain reaction. Mol Biochem Parasitol. 1993;61:315–20. https://doi.org/10.1016/0166-6851(93)90077-B
10. Tadesse FG, Slater HC, Chali W, Teelen K, Lanke K, Belachew M, et al. The relative contribution of symptomatic and asymptomatic *Plasmodium vivax* and *Plasmodium falciparum* infections to the infectious reservoir in a low-endemic setting in Ethiopia. Clin Infect Dis. 2018;66:1883–91. https://doi.org/10.1093/cid/cix1123
11. Faulde MK, Rueda LM, Khaireh BA. First record of the Asian malaria vector *Anopheles stephensi* and its possible role in the resurgence of malaria in Djibouti, Horn of Africa. Acta Trop. 2014;139:39–43. https://doi.org/10.1016/j.actatropica.2014.06.016
12. Carter TE, Yared S, Gebresilassie A, Bonnell V, Damodaran L, Lopez K, et al. First detection of *Anopheles stephensi* Liston, 1901 (Diptera: culicidae) in Ethiopia using molecular and morphological approaches. Acta Trop. 2018;188:180–6. https://doi.org/10.1016/j.actatropica.2018.09.001
13. Kiattibutr K, Roobsoong W, Sriwichai P, Saeseu T, Rachaphaew N, Suansomjit C, et al. Infectivity of symptomatic and asymptomatic *Plasmodium vivax* infections to a Southeast Asian vector, *Anopheles dirus*. Int J Parasitol. 2017;47:163–70. https://doi.org/10.1016/j.ijpara.2016.10.006
14. Surendran SN, Sivabalakrishnan K, Gajapathy K, Arthiyan S, Jayadas TTP, Karvannan K, et al. Genotype and biotype of invasive *Anopheles stephensi* in Mannar Island of Sri Lanka. Parasit Vectors. 2018;11:3. https://doi.org/10.1186/s13071-017-2601-y
15. World Health Organization. Global vector control response 2017–2030 [cited 2020 Jun 7]. https://www.who.int/vector-control/publications/global-control-response/en/

Address for correspondence: Fitsum G. Tadesse, Malaria and NTD directorate, Armauer Hansen Research Institute, Federal Ministry of Health, PO Box 1005, Addis Ababa, Ethiopia; email: fitsum.tadesse@radboudumc.nl

# *Borrelia burgdorferi* Sensu Stricto DNA in Field-Collected *Haemaphysalis longicornis* Ticks, Pennsylvania, United States

Keith J. Price, Christine B. Graham, Bryn J. Witmier, Holly A. Chapman, Brooke L. Coder, Christian N. Boyer, Erik Foster, Sarah E. Maes, Ying Bai, Rebecca J. Eisen, and Andrew D. Kyle

We collected questing *Haemaphysalis longicornis* ticks from southeastern counties of Pennsylvania, USA. Of 263 ticks tested by PCR for pathogens, 1 adult female was positive for *Borrelia burgdorferi* sensu stricto, yielding a 0.4% infection rate. Continued monitoring of this invasive tick is essential to determine its public health role.

*Borrelia burgdorferi* sensu stricto is the causative agent of Lyme disease, the most commonly reported vectorborne disease in North America (*1*). In Pennsylvania, which is first in the United States in the number of reported Lyme disease cases, the spirochete has been identified in nearly 50% of adult *Ixodes scapularis* ticks, the primary vector (*2*). In 2018, Pennsylvania initiated a statewide active surveillance program to monitor tick distribution and density, by county, and tickborne pathogen prevalence. Although focused primarily on collecting and testing *Ixodes scapularis* ticks, initial surveillance efforts recovered, among other species, *Haemaphysalis longicornis* (Asian longhorned tick), an exotic species recently detected in North America (*3*), providing quantitative records of their presence in Pennsylvania public lands (*4*).

Since its US discovery in New Jersey during 2017, the number of states that have detected *H. longicornis* ticks has increased rapidly. In its native range, *H. longicornis* ticks have been found to carry a variety of pathogens endemic to Pennsylvania, including *B. burgdorferi* (*5*). However, because the ecologic characteristics and the pathogen diversity and prevalence of *H. longicornis* ticks in the United States are understudied, potential epidemiologic risks there remain unknown. We report surveillance program data on the presence of pathogen-infected *H. longicornis* in public areas in Pennsylvania.

Author affiliations: Pennsylvania Department of Environmental Protection, Harrisburg, Pennsylvania, USA (K.J. Price, B.J. Witmier, H.A. Chapman, B.L. Coder, C.N. Boyer, A.D. Kyle); Centers for Disease Control and Prevention, Fort Collins, Colorado, USA (C.B. Graham, E. Foster, S.E. Maes, Y. Bai, R.J. Eisen)

DOI: https://doi.org/10.3201/eid2702.201552

## The Study

We performed surveillance activities weekly in 38 Pennsylvania counties during May 1–September 6, 2019, capturing peak nymphal *I. scapularis* ticks, in addition to adult and nymphal *H. longicornis* tick densities (*6*). Sampling sites, primarily high-use public areas in deciduous forests, were selected for high risk of recreational and occupational tick encounters and suitable *I. scapularis* and reported *H. longicornis* tick habitat (*6*).

Collection processes were standardized to minimize spatial and temporal bias. We collected questing ticks by dragging a 1 $m^2$ white felt cloth over vegetation and leaf litter for 100–600 m. We examined cloths every 10 m and transferred recovered ticks into vials containing 80% ethanol, which we shipped to a central laboratory where they were stored at −80°C until being identified using morphological keys.

We tested the majority (84%) of collected *H. longicornis* nymphs and adults for pathogens, then retained the rest as voucher specimens. We prepared DNA extracts from individual *H. longicornis* tick homogenates on the KingFisher Flex Purification System with the MagMAX CORE Nucleic Acid Purification Kit (ThermoFisher Scientific, https://www.thermofisher.com). We tested each extract for *B. burgdorferi* sensu stricto, *B. mayonii*, *B. miyamotoi*, and *Babesia microti* using probe-based real-time PCR assays comprising multiple targets for each pathogen (Table). We amplified a segment of the *Borrelia* dipeptidyl aminopeptidase (PepX) gene using

**Table.** Pathogen targets included in real-time PCR testing of individual *Haemaphysalis longicornis* ticks, Pennsylvania, USA *†

| | Pathogen | | | | |
|---|---|---|---|---|---|
| PCR target | *Borrelia burgdorferi* sensu stricto | *B. mayonii* | *B. miyamotoi* | *Babesia microti* | Reference |
| *Borrelia* 16S rDNA | ‡ | ‡ | ‡ | NA | (*7*) |
| *B. burgdorferi* sensu lato *fliD* | ‡ | ‡ | NA | NA | (*8*) |
| *B. burgdorferi* sensu stricto *oppA2* | ‡ | NA | NA | NA | (*9*) |
| *B. mayonii oppA2* | NA | ‡ | NA | NA | (*9*) |
| *Borrelia miyamotoi purB* | NA | NA | ‡ | NA | (*9*) |
| *B. miyamotoi glpQ* | NA | NA | ‡ | NA | (*9*) |
| *B. microti sa1* | NA | NA | NA | ‡ | (*10*) |
| *B. microti* 18S rDNA | NA | NA | NA | ‡ | (*10*) |

**fliD*, flagellin gene; NA, not applicable; *oppA2*, oligopeptide permease periplasmic A2 gene; *purB*, adenylosuccinate lyase gene; *glpQ*, glycerophosphodiester phosphodiesterase gene; *sa1*, secreted antigen 1 gene.
†A sample was considered positive for a pathogen only if it was positive for all associated targets.
‡Targets associated with each pathogen.

seminested PCR and sequenced it to confirm *B. burgdorferi* sensu stricto–positive specimens. We followed real-time PCR and PepX amplification protocols published elsewhere (*9*). We amplified and sequenced a 667-nt fragment of the cytochrome oxidase subunit I (COI) gene using primers LCO1490 and HCO2198 (*11*) to confirm the tick species of positive specimens. The PCR mixture (25 μL) contained forward and reverse primers at a final concentration of 0.4 μmol and 5 μL of DNA template. Thermocycling conditions followed protocols published elsewhere (*11*). COI and PepX amplicons were sequenced as described elsewhere (*9*).

## Results

A total of 668 *H. longicornis* ticks (356 larvae, 166 nymphs, 146 adults) were collected from 4 counties in southeastern Pennsylvania (Figure). During the same period, 265 *I. scapularis* ticks (174 larvae, 78 nymphs, 13 adults) were collected from the same 4 counties. Of the subset of *H. longicornis* ticks tested by using real-time PCR (n = 263), 1 (0.4%) adult female collected from a county park in Bucks County on June 14, 2019 was positive for *B. burgdorferi* sensu stricto. A 570-nt segment of the PepX gene from this specimen was identical to *B. burgdorferi* sensu stricto reference sequences (GenBank accession nos. CP002312.1:657467–658036). The COI gene fragment from this tick showed 99.8% identity to an *H. longicornis* tick sequence in the GenBank database (accession no. JQ737090). No *H. longicornis* ticks were positive for *B. miyamotoi*, *B. mayonii*, or *B. microti*.

## Conclusions

We document detection of the Lyme disease spirochete, *B. burgdorferi* sensu stricto, in invasive *H. longicornis* ticks. The overall infection rate of 0.4% was low. In comparison, *B. burgdorferi* sensu lato infection rates in *I. scapularis* ticks collected during the same surveillance period and in the same counties ranged from 16.7% to 57.1% (K.P. Price et al., unpub. data). This finding is consistent with recent findings that *H. longicornis* ticks are relatively averse to feeding on white-footed mice (*Peromyscus leucopus*), the primary reservoir of *B. burgdorferi* sensu stricto (*12*). Our findings support laboratory studies demonstrating that *H. longicornis* ticks can acquire *B. burgdorferi* sensu stricto while feeding on experimentally infected mice; however, those studies suggested that *H. longicornis* ticks are unlikely to contribute to transmission of *B. burgdorferi* sensu stricto because infection is lost during molting (*13*). However, refeeding and transmission of Lyme spirochetes by partially-fed ixodid ticks has been documented (*14*).

On the basis of microscopy, we estimated that ≈10% of the host-seeking *H. longicornis* ticks that we recovered were partially fed, suggesting the possibility that transmission could occur before the ticks molt. Of note, however, although we detected *B. burgdorferi* sensu stricto DNA in the tick, we have no evidence to suggest the spirochetes were viable. Unique ecologic traits of *H. longicornis* ticks (e.g., cold hardiness, parthenogenetic reproduction, host generality), which may enable the species' rapid establishment and high density (*4*), could confound efforts to determine the extent to which the tick may be involved in maintenance of *B. burgdorferi* sensu stricto in nature.

Continued monitoring to identify infested areas is essential, especially in densely populated regions (e.g., southeastern Pennsylvania). Despite limited documentation of *H. longicornis* ticks biting humans in the United States (*15*), findings presented here support continued use of personal protective measures. *H. longicornis* ticks are a vector of human pathogens in its native range; further investigation is needed to determine its potential public health significance in the United States.

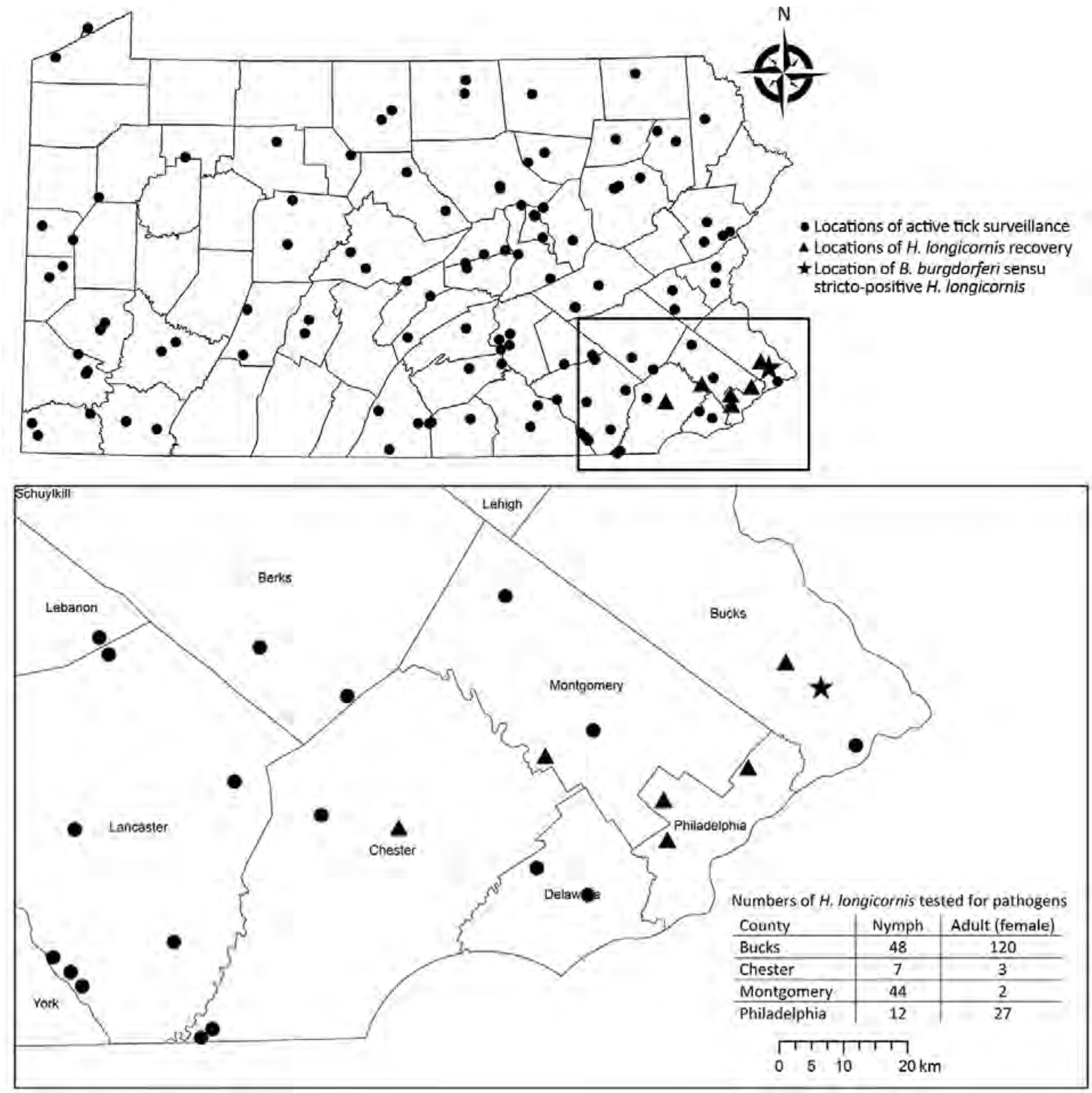


**Figure.** County map of Pennsylvania, USA, and the southeastern region (inset) showing locations of active tick surveillance, where *Haemaphysalis longicornis* ticks were recovered, and where *Borrelia burgdorferi* sensu stricto–positive *H. longicornis* ticks were found, May 1–September 6, 2019. Pennsylvania county map shows 38 counties sampled weekly and an additional 14 counties sampled opportunistically that yielded low tick recovery (*Ixodes scapularis* ticks only).


## Acknowledgments

We thank field personnel for collection efforts, Rebecca Eckert for helpful comments, and Pennsylvania Department of Health, especially Leah Lind, for cooperation and support.

Funding for this study was provided, in part, by an epidemiology subgrant (#4100082142) from the Pennsylvania Department of Health.


## About the Author

Dr. Price is a microbiologist at the Pennsylvania Department of Environmental Protection, Division of Vector Management, Harrisburg, PA. His research interests include vector ecology and vector-borne disease epidemiology.

## References

1. Mead PS. Epidemiology of Lyme disease. Infect Dis Clin North Am. 2015;29:187–210. https://doi.org/10.1016/j.idc.2015.02.010

2. Hutchinson ML, Strohecker MD, Simmons TW, Kyle AD, Helwig MW. Prevalence rates of *Borrelia burgdorferi* (Spirochaetales: Spirochaetaceae), *Anaplasma phagocytophilum* (Rickettsiales: Anaplasmataceae), and *Babesia microti* (Piroplasmida: Babesiidae) in host-seeking *Ixodes scapularis* (Acari: Ixodidae) from Pennsylvania. J Med Entomol. 2015;52:693–8. https://doi.org/10.1093/jme/tjv037
3. Rainey T, Occi JL, Robbins RG, Egizi A. Discovery of *Haemaphysalis longicornis* (Ixodida: Ixodidae) parasitizing a sheep in New Jersey, United States. J Med Entomol. 2018;55:757–9. https://doi.org/10.1093/jme/tjy006
4. Price KJ, Witmier BJ, Eckert RA, Boyer CN, Helwig MW, Kyle AD. Distribution and density of Haemaphysalis longicornis (Acari: Ixodidae) on public lands in Pennsylvania, United States. J Med Entomol. 2020 Dec 25 [Epub ahead of print]. https://doi.org/10.1093/jme/tjaa274
5. Zhao L, Li J, Cui X, Jia N, Wei J, Xia L, et al. Distribution of *Haemaphysalis longicornis* and associated pathogens: analysis of pooled data from a China field survey and global published data. Lancet Planet Health. 2020;4:e320–9. https://doi.org/10.1016/S2542-5196(20)30145-5
6. Tufts DM, VanAcker MC, Fernandez MP, DeNicola A, Egizi A, Diuk-Wasser MA. Distribution, host-seeking phenology, and host and habitat associations of *Haemaphysalis longicornis* ticks, Staten Island, New York, USA. Emerg Infect Dis. 2019;25:792–6. https://doi.org/10.3201/eid2504.181541
7. Kingry LC, Anacker M, Pritt B, Bjork J, Respicio-Kingry L, Liu G, et al. Surveillance for and discovery of *Borrelia* species in US patients suspected of tickborne illness. Clin Infect Dis. 2018;66:1864–71. https://doi.org/10.1093/cid/cix1107
8. Zeidner NS, Schneider BS, Dolan MC, Piesman J. An analysis of spirochete load, strain, and pathology in a model of tick-transmitted Lyme borreliosis. Vector Borne Zoonotic Dis. 2001;1:35–44. https://doi.org/10.1089/153036601750137642
9. Graham CB, Maes SE, Hojgaard A, Fleshman AC, Sheldon SW, Eisen RJ. A molecular algorithm to detect and differentiate human pathogens infecting *Ixodes scapularis* and *Ixodes pacificus* (Acari: Ixodidae). Ticks Tick Borne Dis. 2018;9:390–403. https://doi.org/10.1016/j.ttbdis.2017.12.005
10. Hojgaard A, Lukacik G, Piesman J. Detection of *Borrelia burgdorferi, Anaplasma phagocytophilum* and *Babesia microti*, with two different multiplex PCR assays. Ticks Tick Borne Dis. 2014;5:349–51. https://doi.org/10.1016/j.ttbdis.2013.12.001
11. Zhang R, Zhao A, Wang X, Zhang Z. Diversity of tick species on domestic animals in Shandong province, China, using DNA barcoding. Exp Appl Acarol. 2017;73:79–89. https://doi.org/10.1007/s10493-017-0161-7
12. Ronai I, Tufts DM, Diuk-Wasser MA. Aversion of the invasive Asian longhorned tick to the white-footed mouse, the dominant reservoir of tick-borne pathogens in the U.S.A. Med Vet Entomol. 2020;34:369–73. https://doi.org/10.1111/mve.12441
13. Breuner NE, Ford SL, Hojgaard A, Osikowicz LM, Parise CM, Rosales Rizzo MF, et al. Failure of the Asian longhorned tick, *Haemaphysalis longicornis*, to serve as an experimental vector of the Lyme disease spirochete, *Borrelia burgdorferi* sensu stricto. Ticks Tick Borne Dis. 2020;11:101311. https://doi.org/10.1016/j.ttbdis.2019.101311
14. Nakao M, Sato Y. Refeeding activity of immature ticks of *Ixodes persulcatus* and transmission of Lyme disease spirochete by partially fed larvae. J Parasitol. 1996;82:669–72. https://doi.org/10.2307/3283804
15. Wormser GP, McKenna D, Piedmonte N, Vinci V, Egizi AM, Backenson B, et al. First recognized human bite in the United States by the Asian longhorned tick, *Haemaphysalis longicornis*. Clin Infect Dis. 2020;70:314–6. https://doi.org/10.1093/cid/ciz449


Address for correspondence: Keith J. Price, Pennsylvania Department of Environmental Protection, 2575 Interstate Dr., Harrisburg, PA 17110, USA; email: keitprice@pa.gov

# Early Transmission Dynamics, Spread, and Genomic Characterization of SARS-CoV-2 in Panama

Danilo Franco,[1] Claudia Gonzalez,[1] Leyda E. Abrego,[1] Jean-Paul Carrera, Yamilka Diaz, Yaset Caicedo, Ambar Moreno, Oris Chavarria, Jessica Gondola, Marlene Castillo, Elimelec Valdespino, Melissa Gaitán, Jose Martínez-Mandiche, Lizbeth Hayer, Pablo Gonzalez, Carmen Lange, Yadira Molto, Dalis Mojica, Ruben Ramos, Maria Mastelari, Lizbeth Cerezo, Lourdes Moreno, Christl A. Donnelly, Juan Miguel Pascale, Nuno Rodrigues Faria, Sandra Lopez-Verges,[2] Alexander A. Martinez,[2] on behalf of Gorgas COVID19 team and Panama COVID19 Laboratory Network[3]

We report an epidemiologic analysis of 4,210 cases of infection with severe acute respiratory syndrome coronavirus 2 and genetic analysis of 313 new near-complete virus genomes in Panama during March 9–April 16, 2020. Although containment measures reduced $R_0$ and $R_t$, they did not interrupt virus spread in the country.

Coronavirus disease (COVID-19), caused by severe acute respiratory syndrome coronavirus 2 (SARS-CoV-2), was first reported in December 2019 in Wuhan, China (*1*,*2*). Of ≈23 million confirmed cases worldwide, as of October 20, 2020, a total of 28% (>6 million) had been reported in Latin America. SARS-CoV-2 was first reported in this region in São Paulo, Brazil, on February 25, 2020 (*3*).

In Panama, the first confirmed COVID-19 case was reported on March 9, 2020. Although Panama rapidly implemented disease control strategies, it is among the countries in Latin America with the highest cumulative rates of incidence and death (*4*). To elucidate the transmission and spread of SARS-CoV-2 in the region, we analyzed epidemiologic surveillance data and newly generated genetic data from Panama.

## The Study

To perform molecular detection of SARS-CoV-2, the Panama Ministry of Health implemented a surveillance program on January 20, 2020. The National Committee on Bioethics of Research of Panama approved protocol EC-CNBI-202–04–46.

We evaluated the early transmission dynamics of COVID-19 in Panama for the first 62 days of the epidemic (February 15–April 16, 2020) based on reported dates of symptom onset. We estimated the daily growth rate, doubling time, and basic ($R_0$) and time-varying ($R_t$) effective reproduction numbers. We performed genome amplification and sequencing according to ARTIC Network protocol (https://artic.network) for Illumina Sequencing (https://www.illumina.com) (*5*). Details of epidemic parameters, sequencing, and genome analysis are described in Appendix 2 (https://wwwnc.cdc.gov/EID/article/27/2/20-3767-App2.pdf).

A total of 18,559 suspected cases of COVID-19 had been investigated in Panama by April 16. Of these, 4,210 (22.7%) patients tested positive for SARS-CoV-2 infection by qualitative reverse transcription PCR. The first confirmed case, on March 9, corresponded to a patient who had arrived in Panama from Spain on March 8 and had exhibited symptoms beginning on March 6. The first case not related to travel was

Author affiliations: Gorgas Memorial Institute of Health Studies, Panama City, Panama (D. Franco, C. Gonzalez, L.E. Abrego, J.-P. Carrera, Y. Diaz, A. Moreno, O. Chavarria, J. Gondola, M. Castillo, E. Valdespino, M. Gaitán, J. Martínez-Mandiche, D. Mojica, R. Ramos, J.M. Pascale, S. Lopez-Verges, A.A. Martinez); Universidad de Panama, Panama City (D. Franco, C. Gonzalez, L.E. Abrego, J.M. Pascale, S. Lopez-Verges, A.A. Martinez); Ministry of Health of Panama, Panama City (L. Hayer, P. Gonzalez, C. Lange, Y. Molto, M. Mastelari, L. Cerezo, L. Moreno); University of Oxford, Oxford, UK (J.-P. Carrera, C.A. Donnelly, N.R. Faria); Fundación Valle del Lili, Cali, Colombia (Y. Caicedo); Imperial College, London, UK (C.A. Donnelly, N.R. Faria)

DOI: https://doi.org/10.3201/eid2702.203767

[1]These first authors contributed equally to this article.

[2]These senior authors contributed equally to this article.

[3]Members of the team are listed in Appendix 1 Table 1 (https://wwwnc.cdc.gov/EID/article/27/2/20-3767-App1.xlsx).

confirmed after the death on March 7 of a patient in whom symptoms first appeared on February 22. Epidemiologic investigation showed that the date of onset of symptoms for the earliest local case related to that fatal case dates back to February 15, 2020 (Figure 1). In most locally detected cases, patients had mild disease symptoms (Appendix 2 Figure 1, panel A).

By April 16, a total of 341 patients had been hospitalized (77 at time of diagnosis confirmation) and 116 had died (31 by time of diagnosis confirmation) (Appendix 2 Figure 1, panels B, C). The highest proportion of confirmed cases was observed in the 20–59 year age group (Appendix 2 Figure 2, panel A). A higher proportion (55.3%) of patients tested were female, but among those with positive results, 1.45 times more were male (Appendix 2 Figure 2, panel B). A rapid growth rate of 0.13 cases/day (Appendix 2 Figure 3, panel A) and a short doubling time were observed during the early stages of the epidemic; doubling time increased over the study period (Appendix 2 Figure 3, panel B). We estimated an $R_0$ for SARS-CoV-2 in Panama of 2.22 (95% CI 2.08–2.37).

Panama was the 11th country in Latin America to report SARS-CoV-2 and implemented epidemic control strategies rapidly compared with other countries in the region (Appendix 2 Figure 4). After the first confirmed case (March 9), school closures were implemented within 1 day, social distancing measures within 6 days, and 24-hour stay-at-home curfew within 14 days. Over the course of the next 17 days, $R_t$ dropped to 1.08 (95% Cl 1.00−1.17) (Appendix 2 Table 1, Figure 3, panel C). However, until April 16, Panama remained the country in Central America with the highest proportional number of cases and fatalities (Appendix 2 Figure 5).

To determine the diversity of SARS-CoV-2 in Panama and Latin America, we generated SARS-CoV-2 genomes from 313 patients, representing 7.4% of the total confirmed cases by April 16, 2020 (Appendix 2 Figure 6, panel A). We obtained complete genome coverage for samples using reverse transcription PCR cycle threshold values <25 (Appendix 2 Figure 6, panel B) and found circulation of ≥10 virus lineages (Figure 2, panel A; Appendix 2 Figure 7) (*6*). The most frequently identified was A.2 (71.2%), followed by B.1 (16.7%) and A.1 (3.5%), in contrast to other studies in Latin America, where B-like lineages largely predominate (*7*,*8*). Lineages A.3, B, and B.1.5 were identified in 79 cases detected early on in the epidemic, 11 (13.9%) of the cases imported (Figure 2, panel A; Appendix 2 Figure 7). Lineage A.2 was found in 51 patients; 4 (7.8%) belonged to a cluster (Appendix 2 Table 2) from a school outbreak associated with the first detected local case and 9 (17.6%) were police officers (Figure 2, panel C).

Phylogenetic analysis identified 3 main virus lineages (Figure 2). Lineage A.2.1/19B (n = 60; posterior support = 0.69; C12815T) comprised 54.3% of the sequenced cases in the study (Appendix 2 Figure 8, panel A); lineage B.1/20A (n = 15; posterior support = 0.97; G26143A) and lineage A.3/19B (n = 12; posterior support = 1.00; C3177T, T26729C) was third. Molecular clock estimates of the time to most recent common ancestor calculated from lineage A.2.1, made up just of cases with local transmission, placed the median time of mutation during February 19–March 9, 2020, just 2 weeks before the first COVID-19 case was confirmed, and in line with the time of onset of symptoms of the first case of local transmission (Figures 1, 2).

Central and western Panama had more diverse lineage distributions (Figure 2, panel B). Those regions encompass the capital and its surroundings, where more than 50% of the national population lives and the main international airport is located. Lineage A.2.1

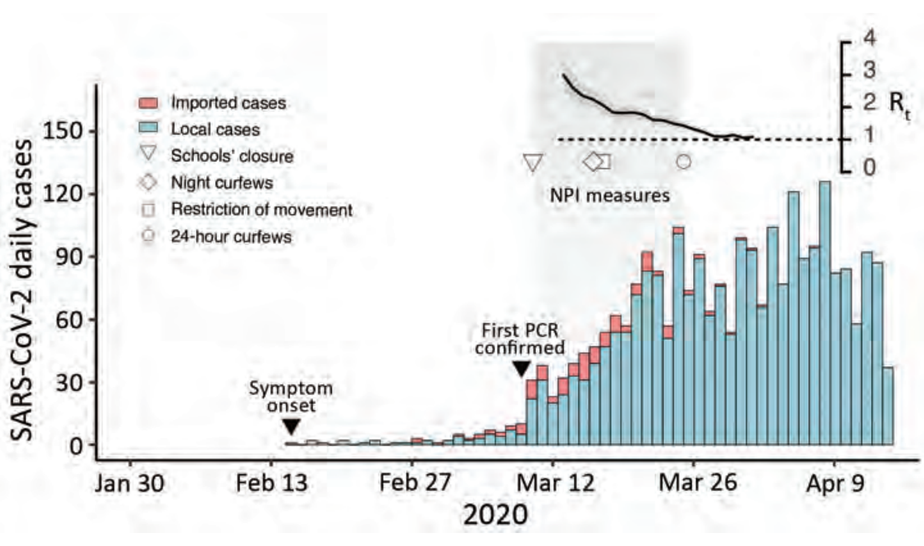


**Figure 1.** Epidemic curve of SARS-CoV-2 cases in Panama showing daily incidence of confirmed imported and local infections detected through April 16, 2020, with symptom onset during February 15–April 13, 2020. Gray shaded area indicates time period during which nonpharmaceutical interventions measures were initiated. Inset at top right shows the time-varying effective reproduction number ($R_t$) for a time frame of 45 days (x-axis); dark gray shading indicates 95% CI, and dashed line indicates threshold value $R_t$ = 1. SARS-CoV-2, severe acute respiratory syndrome coronavirus 2.

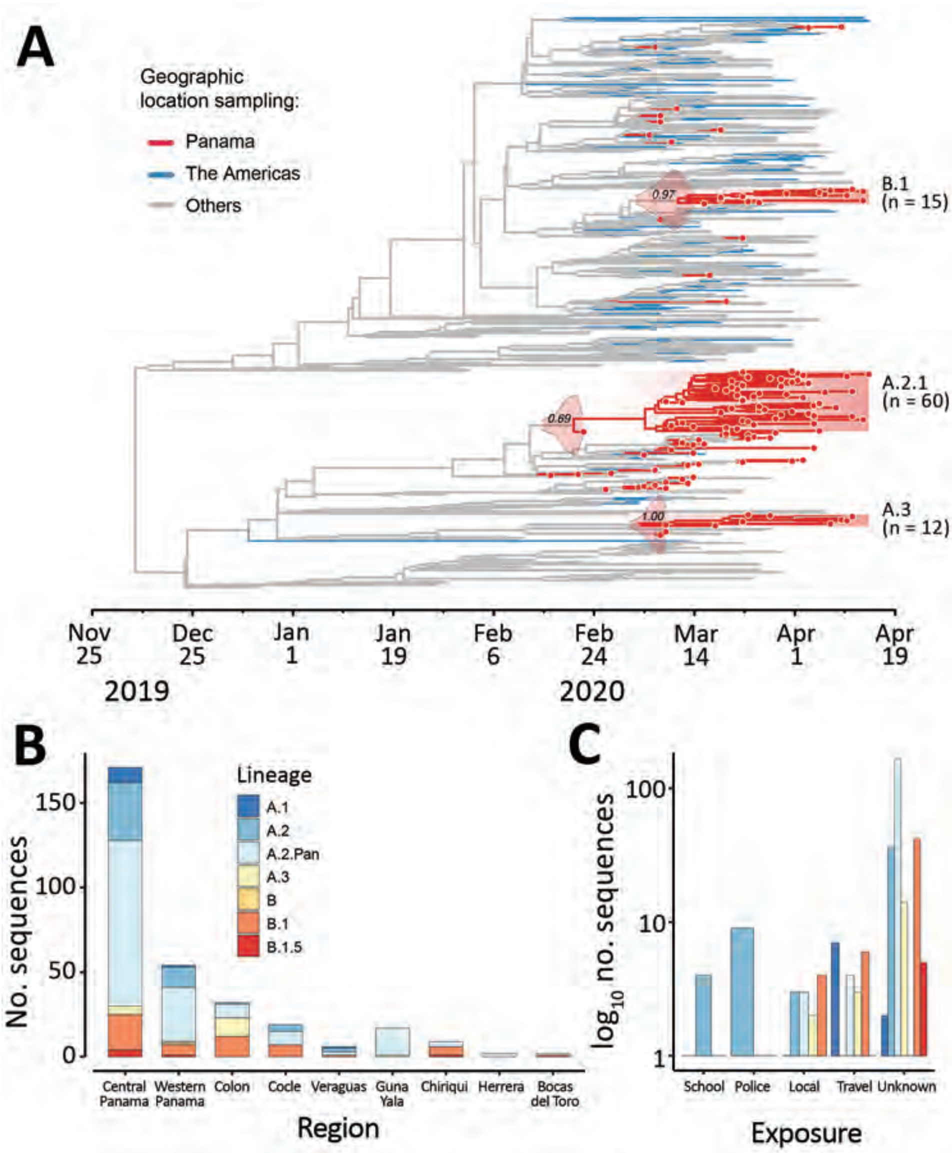


**Figure 2.** Genetic diversity of SARS-CoV-2 in Panama. A) Bayesian maximum clade credibility tree of 1,261 SARS-CoV-2 sequences: 133 from Panama; 492 from North or South America (443 genomes are from Brazil, 41 from the United States, 7 from Chile, 6 from Mexico, 3 from Argentina, 1 from Peru, and 1 from Canada); and 636 are from other locations. Posterior density estimates of time of the most recent common ancestor of each lineage with local transmission are shown in their branches. B) Distribution of lineages among regions in Panama. C) Distribution of lineages by channel of exposure detected by the surveillance system. SARS-CoV-2, severe acute respiratory syndrome coronavirus 2.

was found in all regions across the country with no obvious spatial pattern; according to a global analysis of SARS-CoV-2 lineages (https://cov-lineages.org), this lineage is composed of sequences predominantly from Panama. We also found that the spike glycoprotein variants D614 and G614 (*9*,*10*) were cocirculating early in the epidemic among all the regions analyzed and were comprised of multiple lineages (Appendix 2 Figure 8, panel B), but the G614 variant potentially associated with infectivity (*9*) was detected in only 18.8% of the sequenced cases (Appendix 2 Figure 8, panel C).

## Conclusions

Epidemiologic evidence suggested cryptic circulation of SARS-CoV-2 in Panama with a probable introduction during early February. A high median transmission potential of SARS-CoV-2 was estimated at $R_0$ = 2.22 (2.08–2.37), similar to estimates from China, Brazil, and Europe (*11*–*13*). $R_t$ rapidly dropped to 1.08 after implementation of control strategies.

Phylogenetic analysis detected circulation of ≥10 virus lineages, although the number of detected lineages could be underestimated because we did not sequence each positive case and there is a possibility of uncommon undetected lineages due to sample bias. Most of the lineages associated with imported cases (A.1, A.3, B, B.1, B.2.1) were detected and transmission controlled through active contact tracing. However, we detected early transmission of the lineage A.2.1/19B, which was introduced into the country ≥3 weeks before the first detected case. This lineage rapidly became widespread in Panama.

We conjecture that efforts to identify early suspected cases, which focused mainly in symptomatic travelers returning from China, precluded the opportunity to detect earlier cases imported from Europe and the United States, where the virus was already circulating at that time (*11*,*14*,*15*). Moreover, undetected early transmission occurring before control measures were implemented could help to explain the widespread distribution of SARS-CoV-2 across Panama.

Our findings on growth rates and $R_t$ show that mitigation measures undertaken shortly after the first reported case in March helped to reduce virus transmission. Measures such as active contact tracing and isolation, social distancing, and quarantine targeted to regions where active transmission clusters are found will help to effectively control the spread of SARS-CoV-2 in Panama.

### Acknowledgments

We thank the Gorgas administration and general services for their support and extra work during the COVID-19 response. We also thank all the health institutions from MINSA, CSS, and private hospitals. We gratefully acknowledge the authors, originating and submitting laboratories of the sequences from GISAID's EpiFlu Database on which this research is based (Appendix 1 Table 2).

A.A.M., J.M.P., S.L.V., and L.E.A. are members of the Sistema Nacional de Investigación from SENACYT, Panama. N.R.F. was supported by Wellcome Trust and Royal Society (204311/Z/16/Z) and by Medical Research Council-São Paulo Research Foundation's Center for Arbovirus Discovery, Diagnosis, Genomics and Epidemiology partnership award (MR/S0195/1 and FAPESP 18/14389-0).

## About the Author

Mr. Franco is responsible for respiratory virus surveillance and SARS-CoV-2 molecular diagnosis in the Department of Research in Virology and Biotechnology at the Gorgas Memorial Institute of Health Studies in Panama. His research is focused on epidemiological and genetic analysis of respiratory viruses circulating in Panama.

### References

1. Li Q, Guan X, Wu P, Wang X, Zhou L, Tong Y, et al. Early transmission dynamics in Wuhan, China, of novel coronavirus-infected pneumonia. N Engl J Med. 2020;382:1199–207. https://doi.org/10.1056/NEJMoa2001316
2. Zhu N, Zhang D, Wang W, Li X, Yang B, Song J, et al.; China Novel Coronavirus Investigating and Research Team. A novel coronavirus from patients with pneumonia in China, 2019. N Engl J Med. 2020;382:727–33. https://doi.org/10.1056/NEJMoa2001017
3. Jesus JG, Sacchi C, Candido DDS, Claro IM, Sales FCS, Manuli ER, et al. Importation and early local transmission of COVID-19 in Brazil, 2020. Rev Inst Med Trop São Paulo. 2020;62:e30. https://doi.org/10.1590/s1678-9946202062030
4. World Health Organization. Coronavirus disease (COVID-19) pandemic [cited 2020 August 26] https://www.who.int/emergencies/diseases/novel-coronavirus-2019
5. Quick J, Grubaugh ND, Pullan ST, Claro IM, Smith AD, Gangavarapu K, et al. Multiplex PCR method for MinION and Illumina sequencing of Zika and other virus genomes directly from clinical samples. Nat Protoc 2017;12;1261–76. https://doi.org/10.1101/098913
6. Rambaut A, Holmes EC, O'Toole Á, Hill V, McCrone JT, Ruis C, et al. A dynamic nomenclature proposal for SARS-CoV-2 lineages to assist genomic epidemiology. Nat Microbiol. 2020;5:1403–7. https://doi.org/10.1038/s41564-020-0770-5
7. Laiton-Donato K, Villabona-Arenas C, Usme-Ciro JA, Franco-Muñoz C, Álvarez-Díaz DA, Villabona-Arenas L, et al. Genomic epidemiology of severe acute respiratory syndrome coronavirus 2, Colombia. Emerg Infect Dis. 2020;26:2854–62. https://dx.doi.org/10.3201/eid2612.202969
8. Candido DS, Claro IM, de Jesus JG, Souza WM, Moreira FRR, Dellicour S, et al. Evolution and epidemic spread of SARS-CoV-2 in Brazil. Science. 2020;369:1255–60. https://doi.org/10.1126/science.abd2161
9. Korber B, Fischer WM, Gnanakaran S, Yoon H, Theiler J, Abfalterer W, et al.; Sheffield COVID-19 Genomics Group. Tracking changes in SARS-CoV-2 spike: evidence that D614G increases infectivity of the COVID-19 virus. Cell. 2020;182:812–827.e19. https://doi.org/10.1016/j.cell.2020.06.043
10. Ou X, Liu Y, Lei X, Li P, Mi D, Ren L, et al. Characterization of spike glycoprotein of SARS-CoV-2 on virus entry and its immune cross-reactivity with SARS-CoV. Nat Commun. 2020;11:1620. https://doi.org/10.1038/s41467-020-15562-9
11. Bartolini B, Rueca M, Gruber CEM, Messina F, Carletti F, Giombini E, et al. SARS-CoV-2 phylogenetic analysis, Lazio region, Italy, February–March 2020. Emerg Infect Dis J. 2020;26:1842–5. https://doi.org/10.3201/eid2608.201525
12. Lu J, du Plessis L, Liu Z, Hill V, Kang M, Lin H, et al. Genomic epidemiology of SARS-CoV-2 in Guangdong province, China. Cell. 2020;181:997–1003. https://doi.org/10.1016/j.cell.2020.04.023
13. de Souza WM, Buss LF, Candido DDS, Carrera J-P, Li S, Zarebski AE, et al. Epidemiological and clinical characteristics of the COVID-19 epidemic in Brazil. Nat Hum Behav. 2020;4:856–65. https://doi.org/10.1038/s41562-020-0928-4
14. Bedford T, Greninger AL, Roychoudhury P, Starita LM, Famulare M, Huang M-L, et al. Cryptic transmission of SARS-CoV-2 in Washington state. Science. 2020;370:571–5. https://doi.org/10.1126/science.abc0523
15. Deng X, Gu W, Federman S, du Plessis L, Pybus OG, Faria NR, et al. Genomic surveillance reveals multiple introductions of SARS-CoV-2 into northern California. Science. 2020;369:582–7. PubMed https://doi.org/10.1126/science.abb9263

Address for correspondence: Alexander Augusto Martinez Caballero or Sandra Lopez-Verges, Gorgas Memorial Institute of Health Studies, Justo Arosemena Avenue and Street 35th, Panama 0816-02593, Panama; email: almartinez@gorgas.gob.pa or slopez@gorgas.gob.pa

# Estimating the Frequency of Lyme Disease Diagnoses, United States, 2010–2018

Kiersten J. Kugeler, Amy M. Schwartz, Mark J. Delorey, Paul S. Mead, Alison F. Hinckley

By using commercial insurance claims data, we estimated that Lyme disease was diagnosed and treated in ≈476,000 patients in the United States annually during 2010–2018. Our results underscore the need for accurate diagnosis and improved prevention.

Lyme disease is caused by *Borrelia burgdorferi* spirochetes, which are transmitted to humans by certain *Ixodes* spp. ticks (*1*). The infection can involve multiple organ systems and is treatable with antimicrobial drugs; most persons recover fully, especially those who receive early and appropriate treatment (*1*). The geographic distribution of Lyme disease in the United States and the demographic characteristics of persons affected have been well documented through nearly 3 decades of public health surveillance (*2*).

However, the frequency of Lyme disease is less well understood. Although 30,000–40,000 cases are reported through surveillance each year, substantial underreporting occurs, as is typical for passively reported surveillance data (1). A previous analysis of insurance claims data for the years 2005–2010 estimated that Lyme disease was diagnosed in ≈329,000 persons annually in the United States (3). We use similar methods to develop an estimate for 2010–2018.

## The Study

The IBM Watson Health MarketScan Commercial Claims and Encounters Databases (https://www.ibm.com/products/marketscan-research-databases) are derived from insurance claims for inpatient, outpatient, and prescription services covering >25 million privately insured US residents <65 years of age. As detailed elsewhere, we identified Lyme disease diagnoses among the MarketScan population during 2010–2018 by linking specific billing codes for patient encounters with antimicrobial prescriptions (4). An outpatient Lyme disease diagnosis was identified by an International Classification of Diseases, 9th Revision, Clinical Modification (ICD-9-CM) or International Classification of Diseases, 10th Revision, Clinical Modification (ICD-10-CM) code for Lyme disease (ICD-9-CM: 088.81; ICD-10-CM: A69.2x) combined with an associated prescription of ≥7 days' duration for an appropriate antibiotic drug (3,4). Inpatient diagnoses were identified according to primary and secondary Lyme disease diagnosis codes (4). To minimize the influence of nonincident diagnoses, we excluded any events that occurred in the same person in subsequent years. Age, sex, geographic distribution, and seasonality of Lyme disease diagnoses in MarketScan during 2010–2018 are reported elsewhere (4).

To enable extrapolation of rates from the commercially insured population to the US population, we calculated directly standardized case counts according to 5-year age group and state using US Census Bureau 2015 population estimates. Because MarketScan does not include patients ≥65 years of age, we multiplied the sum of these counts by a factor derived from contemporaneous surveillance data (https://wwwn.cdc.gov/nndss) (Figure). Among confirmed and probable Lyme disease cases reported during 2010–2018, 80.3% were among persons <65 years of age. Thus, we multiplied the standardized case count by 1/0.803, or ≈1.25, to estimate the number of persons of all ages coded and treated for Lyme disease.

Previous research has demonstrated that medical records of patients with Lyme disease frequently lack the specific ICD-9 code for the condition (5,6). To adjust for this undercoding of medical records, we applied a correction factor by using data from 3 studies on the proportion of medical records that contain the ICD-9 code 088.81 and meet the confirmed, probable, and suspect Lyme disease surveillance case definitions (as a proxy for clinician diagnosis).

Author affiliation: Centers for Disease Control and Prevention, Fort Collins, Colorado, USA

DOI: https://doi.org/10.3201/eid2702.202731

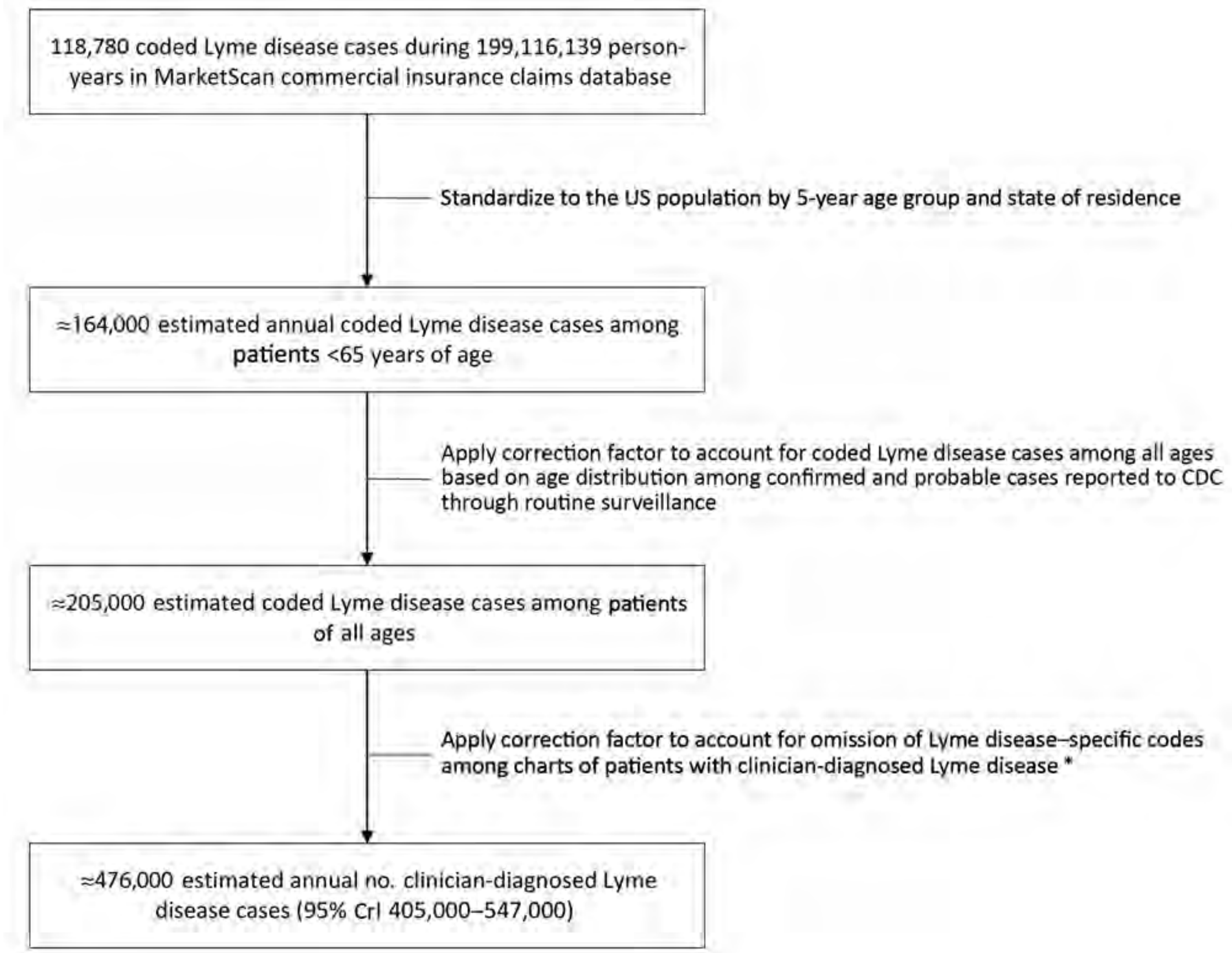


**Figure.** Estimated number of Lyme disease diagnoses annually, calculated by using commercial insurance claims data and 3 correction factors, United States, 2010–2018. Only those records that contained age and state information were included to enable calculation of standardized case counts for the US population. *Correction factor accounting for Lyme disease–specific codes is based on data from 3 studies that suggest only 43% of patients whose cases met the confirmed, probable, or suspect surveillance case definitions had the ICD-9-CM code for Lyme disease in their medical records (*5–7*; E. Schiffman, Minnesota Department of Health, pers. comm., 2020 Jan 17). CDC, Centers for Disease Control and Prevention; CrI, credible interval; ICD-9-CM, International Classification of Diseases, 9th Revision, Clinical Modification.

In New York, 114 (41.8%) of 273 records meeting these definitions contained 088.81 (*6*). In Maryland, 84 (35.6%) of 236 records contained 088.81 (*5*). Supplemental analysis of data from Minnesota captured as previously described (*7*) revealed that 91 (56%) of 163 charts contained 088.81 (E. Schiffman, Minnesota Department of Health, pers. comm., 2020 Jan 17). A total of 289 (43.0%) of 672 Lyme disease patients had 088.81 in their medical records. Thus, we multiplied the standardized and age-corrected number of cases by 1/0.430 or ≈2.33 to arrive at an estimate of the frequency of clinician-diagnosed Lyme disease (Figure). A 95% credible interval for this estimate was calculated as previously described (*3*).

A total of 118,780 persons with the requisite codes for Lyme disease were identified in MarketScan among 199,116,139 person-years of observation during 2010–2018. Overall, 81% of these diagnoses occurred among residents of 14 high-incidence states in the Northeast, mid-Atlantic, and upper Midwest; another 8% occurred among residents of adjoining states. After direct standardization and age correction, we found that an average of 205,000 patients were coded and treated for Lyme disease annually. Upon further correction for omission of Lyme disease–specific codes in patient records, we estimate an average of ≈476,000 patients received a diagnosis of Lyme disease each year (95% credible interval 405,000–547,000) during 2010–2018 (Figure).

## Conclusions

The public health burden of an infectious disease can be quantified in several ways: these include the number of illnesses meeting a specific definition that are reported to public health officials; the total number of actual infections resulting in illness in the community; or the number of patients in whom the presumed illness is diagnosed and treated, regardless of actual infection. Our estimate addresses the last of these; it reflects the overall societal and clinical burden of Lyme disease.

We estimate that ≈476,000 persons were diagnosed with Lyme disease annually during 2010–2018. This figure is greater than an estimate of ≈329,000 annual diagnoses for the period 2005–2010. Although both estimates were calculated by using similar methods, we implemented a slightly more restrictive approach that prohibited any patient with a diagnosis of Lyme disease from being counted more than once during the 9-year study period (3). The observed increase in Lyme disease diagnoses between these 2 periods parallels increases in cases reported through surveillance (1).

Our estimate is based on commercial insurance claims data that might not be representative of the US population with respect to disease risk and access to health care. In addition, the correction factor used to account for omission of Lyme disease–specific ICD-9-CM and ICD-10-CM codes in medical records is based on a review of codes in only 672 medical records, yet it more than doubles the estimated number of diagnoses. Without this correction factor, the observed rate of diagnoses in our study would be similar to the 76 diagnoses/100,000 persons per year reported by Tseng et al. (8) in a separate analysis of claims data. Further studies of coding patterns and improved access to and use of electronic health records could fill these data gaps, enabling more robust and precise estimates in the future (9).

The estimates we report are influenced by the uncertainties of clinical practice, in which patients are often treated presumptively, inevitably resulting in some degree of overdiagnosis and overtreatment (10). In contrast, cases reported through national Lyme disease surveillance meet a standardized case definition and are more likely to represent actual infections. However, routine surveillance is subject to substantial underreporting, previously estimated at between 3- and 12-fold for Lyme disease (1). The difference between our estimate and the ≈35,000 cases reported annually though surveillance is a result of the combined effects of underreporting of infections and overdiagnosis in clinical practice. Our analysis does not enable us to discern the relative contribution of each. Although we implemented restrictions to mitigate inclusion of retreatment for nonincident diagnoses, overdiagnosis could account for the proportionally higher number of diagnoses in residents of low-incidence states (19%) than what is typically seen in public health surveillance (≈5%).

Our findings underscore the large clinical burden associated with Lyme disease diagnoses in the United States. Evolving electronic medical and laboratory systems should help fill demonstrable data gaps and enable more robust and reliable monitoring of changes in the magnitude and spread of the disease. Effective interventions are needed, and improved awareness among clinicians and the public is paramount to foster early and accurate diagnosis and appropriate treatment.

### Acknowledgments

We thank Elizabeth Schiffman, Christina Nelson, and Sarah Hook for providing valuable data and insight.

This study was supported by the Centers for Disease Control and Prevention.

## About the Author

Dr. Kugeler is an epidemiologist in the Bacterial Diseases Branch, Division of Vector-Borne Diseases, National Center for Emerging and Zoonotic Infectious Diseases, Centers for Disease Control and Prevention, Atlanta, Georgia. Her professional interests lie in the surveillance and prevention of bacterial vector-borne infections.

### References

1. Mead PS. Epidemiology of Lyme disease. Infect Dis Clin North Am. 2015;29:187–210. https://doi.org/10.1016/j.idc.2015.02.010
2. Schwartz AM, Hinckley AF, Mead PS, Hook SA, Kugeler KJ. Surveillance for Lyme disease— United States, 2008–2015. MMWR Surveill Summ. 2017;66:1–12. https://doi.org/10.15585/mmwr.ss6622a1
3. Nelson CA, Saha S, Kugeler KJ, Delorey MJ, Shankar MB, Hinckley AF, et al. Incidence of clinician-diagnosed Lyme disease, United States, 2005-2010. Emerg Infect Dis. 2015;21:1625–31. https://doi.org/10.3201/eid2109.150417
4. Schwartz AM, Kugeler KJ, Nelson C, Marx GE, Hinckley AF. Use of commercial claims data for evaluating trends in Lyme disease diagnosis, United States. Emerg Infect Dis. 2021;27:. 499–507
5. Rutz H, Hogan B, Hook S, Hinckley A, Feldman K. Exploring an alternative approach to Lyme disease surveillance in Maryland. Zoonoses Public Health. 2018;65:254–9. https://doi.org/10.1111/zph.12446
6. White J, Noonan-Toly C, Lukacik G, Thomas N, Hinckley A, Hook S, et al. Lyme disease surveillance in New York state: an assessment of case underreporting. Zoonoses Public Health. 2016.

7. Schiffman EK, McLaughlin C, Ray JAE, Kemperman MM, Hinckley AF, Friedlander HG, et al. Underreporting of Lyme and other tick-borne diseases in residents of a high-incidence county, Minnesota, 2009. Zoonoses Public Health. 2018;65:230–7. https://doi.org/10.1111/zph.12291
8. Tseng YJ, Cami A, Goldmann DA, DeMaria A Jr, Mandl KD. Using nation-wide health insurance claims data to augment Lyme disease surveillance. Vector Borne Zoonotic Dis. 2015;15:591–6. https://doi.org/10.1089/vbz.2015.1790
9. Birkhead GS, Klompas M, Shah NR. Uses of electronic health records for public health surveillance to advance public health. Annu Rev Public Health. 2015;36:345–59. https://doi.org/10.1146/annurev-publhealth-031914-122747
10. Kobayashi T, Higgins Y, Samuels R, Moaven A, Sanyal A, Yenokyan G, et al. Misdiagnosis of Lyme disease with unnecessary antimicrobial treatment characterizes patients referred to an academic infectious diseases clinic. Open Forum Infect Dis. 2019;6:ofz299. https://doi.org/10.1093/ofid/ofz299

Address for correspondence: Kiersten Kugeler, Centers for Disease Control and Prevention, 3156 Rampart Rd, Fort Collins, CO, 80521, USA; email: kkugeler@cdc.gov

# Vaccine-Derived Polioviruses, Central African Republic, 2019

Marie-Line Joffret,[1] Joël Wilfried Doté,[1] Nicksy Gumede, Marco Vignuzzi, Maël Bessaud,[2] Ionela Gouandjika-Vasilache[2]

Since May 2019, the Central African Republic has experienced a poliomyelitis outbreak caused by type 2 vaccine-derived polioviruses (VDPV-2s). The outbreak affected Bangui, the capital city, and 10 districts across the country. The outbreak resulted from several independent emergence events of VDPV-2s featuring recombinant genomes with complex mosaic genomes. The low number of mutations (≤20) in the viral capsid protein 1–encoding region compared with the vaccine strain suggests that VDPV-2 had been circulating for a relatively short time (probably <3 years) before being isolated. Environmental surveillance, which relies on a limited number of sampling sites in the Central African Republic and does not cover the whole country, failed to detect the circulation of VDPV-2s before some had induced poliomyelitis in children.

Poliomyelitis results from infection of the central nervous system by poliovirus, a picornavirus of the species *Enterovirus C* (*1*). The Global Polio Eradication Initiative (https://polioeradication.org) managed to eradicate wild poliovirus of 2 of the 3 serotypes and to contain virus of the third serotype in Pakistan and Afghanistan. The Initiative relies on 2 pillars: surveillance of poliovirus circulation and vaccination. Contrary to the inactivated polio vaccine, the oral polio vaccine (OPV) induces strong intestinal immunity that blocks transmission of poliovirus in subsequent infections (*2*). Consequently, OPV is currently the only tool capable of stopping poliovirus transmission. However, because attenuated strains of OPV replicate in the gut and are excreted in feces, low vaccine coverage enables circulation of these strains and loss of their attenuated phenotype through genetic drift (*3*,*4*). Since May 2019, the Central African Republic (CAR) has experienced a poliomyelitis outbreak caused by serotype 2 vaccine-derived polioviruses (VDPV-2s). To ascertain the origin of these VDPV-2s, we determined and analyzed their full-length genomic sequences.

## The Study

During May–December 2019, using standardized procedures of the Global Polio Laboratory Network (https://polioeradication.org), we detected VDPV-2s in fecal samples of 19 children with acute flaccid paralysis (AFP). Positive samples came from 10 districts across the country, including Bangui, the capital city (Figure 1). In addition, we detected 49 VDPV-2s in fecal samples from healthy children living in the vicinity of the children with poliomyelitis; 17 were detected in environmental samples. In December 2017, routine environmental surveillance was implemented in CAR, restricted to 4 sampling sites in Bangui; 6 additional sites were gradually opened in 2019 (Figure 1). Compared with the vaccine Sabin-2 strain (reference strain), CAR VDPV-2s had 6–20 nt differences in the viral capsid protein 1 (VP1)–encoding region (903 nt), above the threshold used to discriminate VDPV-2s from Sabin-2 (≥6 mutations within the VP1-encoding sequence). Given the evolutionary rate of this genomic region (≈$10^{-2}$ nucleotide changes/site/year [*5*]), this range suggests that VDPVs had been circulating in CAR from a few months to a couple of years before detection.

Phylogenetic analysis based on VP1-encoding regions showed that the CAR VDPV-2s fell into different lineages (Figure 2, panel A; Appendix Figure https://wwwnc.cdc.gov/EID/article/27/2/20-3173-App1.pdf). Although the low number of nucleotide differences in young VDPVs makes precise marking of the boundaries of phylogenetic clusters challenging, we identified ≥12 main branches in this phylogram (Figure 2, panel A, branches A–L), indicating the concomitant emergence of multiple VDPV lineages. Branches A and J gathered sequences of VDPVs sampled from

Author affiliations: Institut Pasteur, Paris, France (M.-L. Joffret, M. Vignuzzi, M. Bessaud); Institut Pasteur, Bangui, Central African Republic (J.W. Doté, I. Gouandjika-Vasilache); World Health Organization African Region Office, Brazzaville, Congo (N. Gumede)

DOI: https://doi.org/10.3201/eid2702.203173

[1]These first authors contributed equally to this article.

[2]These senior authors contributed equally to this article.

districts located hundreds of kilometers apart (Figure 1), which suggests active circulation of these lineages in the country; by contrast, some lineages (F, I, K, L) were detected only 1 time. No isolates from patients with AFP were of lineages D, F, G, I, K, L; however, determining whether some AFP cases were missed or, alternately, whether surveillance managed to uncover VDPV lineages before they caused poliomyelitis, is not possible. Environmental surveillance is expected to detect poliovirus circulation before it causes the first poliomyelitis case, but the alert system is efficient only if the surveillance is dense enough to cover the entire country, a goal that is difficult to reach in CAR because of the political troubles.

Among the 70 CAR VDPV-2s for which genomes have been fully sequenced through gene walking and Sanger sequencing, only 4 (branches G and L, from healthy children) were free of recombination events and feature a global nucleotide divergence <1% compared with Sabin-2. The 66 other CAR VDPV-2 genomes comprised sequences derived from Sabin-2 and from other nonpolio enteroviruses in 12 recombinant patterns; polio/nonpolio breakpoints were within the 2A, 2B, 2C, 3A, 3C, and 3D-encoding regions (Figure 2, panel B; Appendix Figure). In the nonpolio region, the unique representative of recombinant pattern 5 (member of VP1 branch B) shared recent common ancestors through recombination with the genomes of patterns 3 and 6: it was closely related to genomes of pattern 6 from the 2A through the 3C genomic regions and to the genomes of pattern 3 downstream (Figure 2, panel C). Pattern 4 also shared a recent common ancestor with pattern 3, from which it diverged only near the 3′ extremity of the genome (Figure 2, panel B). Similarly, the genomes of patterns 7 and 8 were closely related from the 2B region through the middle of the 3C region and substantially diverged downstream. Genomic mosaicism is a common trait found in enterovirus ecosystems because of frequent recombination exchanges between cocirculating enteroviruses, including the poliovirus vaccine strains. Thus, VDPVs generally feature genomes resulting from multiple recombination events (*6*). Three VP1 branches (A, B, and D) contained various recombinant patterns (Figure 2, panel A); reciprocally, 2 recombinant patterns (3 and 11) were each found in several VP1 branches (Figure 2, panel B), thereby illustrating how recombination

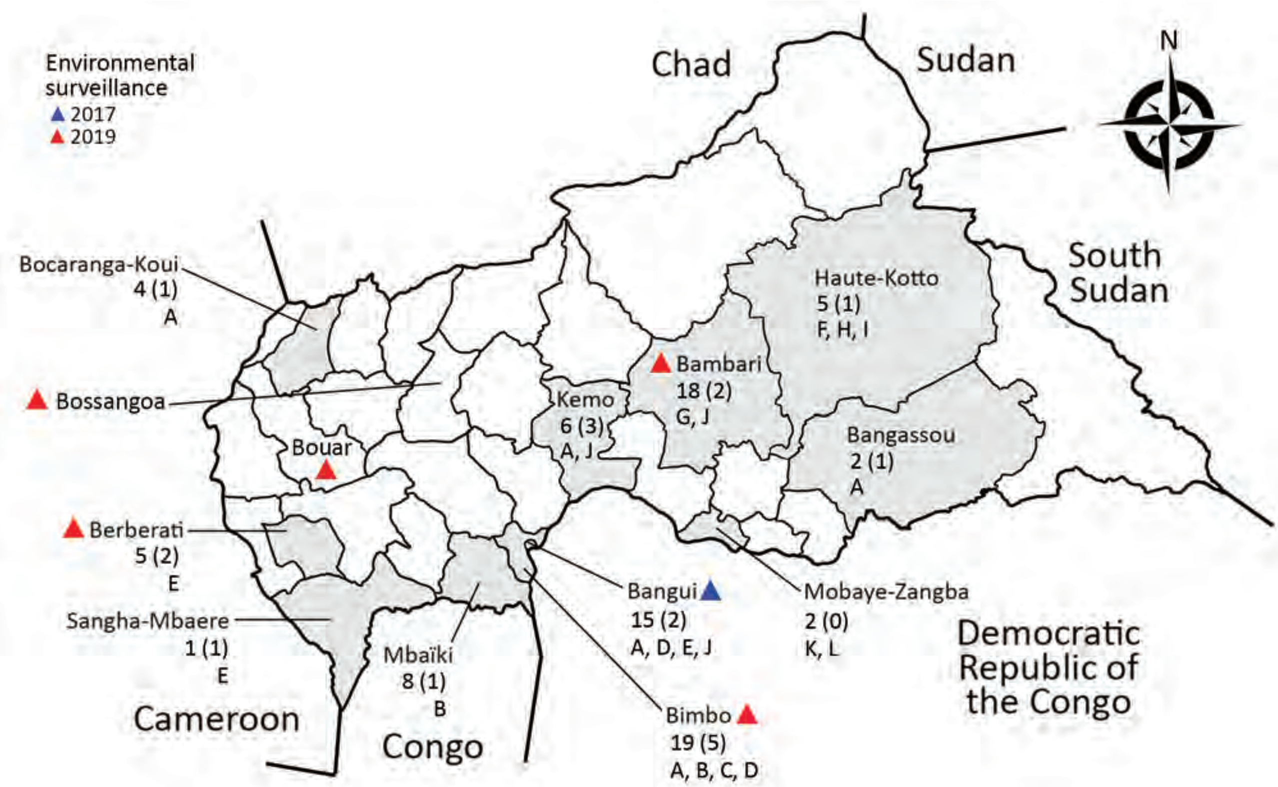


**Figure 1.** Central African Republic. Shading indicates districts where VDPV-2s were detected May–December 2019: triangles indicate districts where environmental surveillance has been implemented; numbers indicate total numbers of VDPVs; numbers in parentheses indicate number of confirmed poliomyelitis cases, letters A–L indicate VDPV lineages (based on the viral capsid protein 1–encoding region [Figure 2, panel A]). VDPV-2, type 2 vaccine-derived polioviruses.

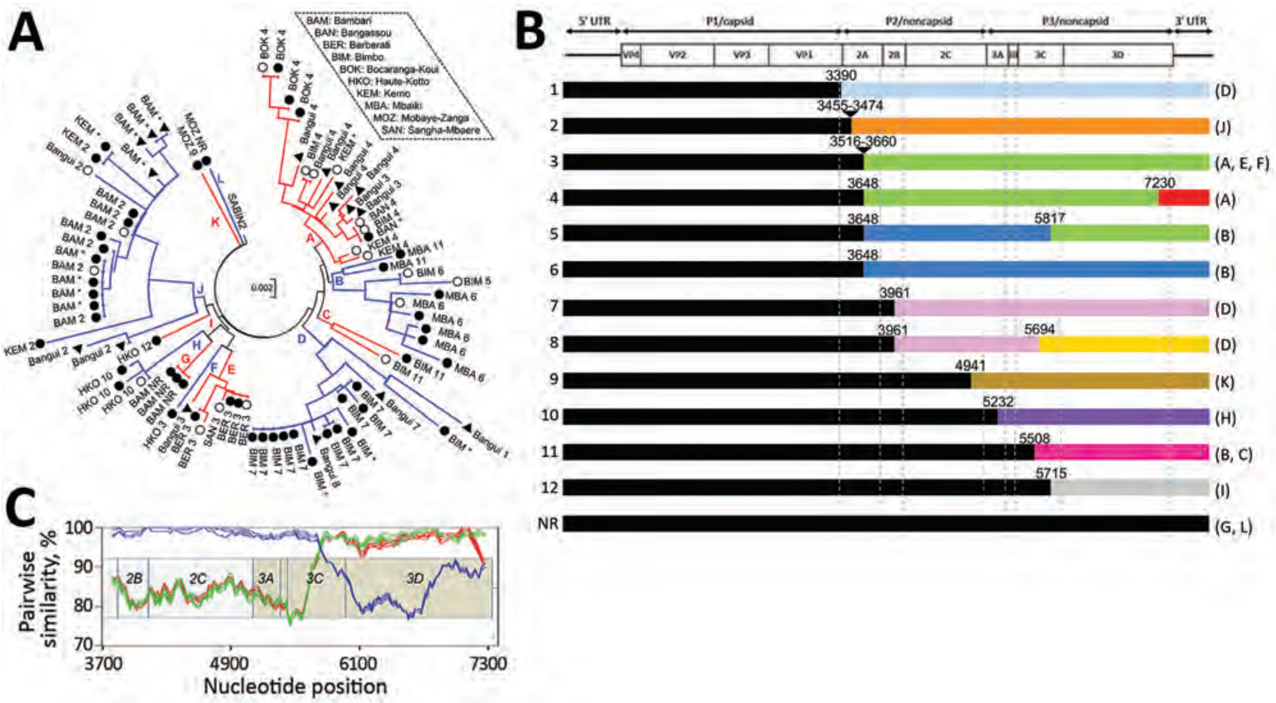


**Figure 2.** Molecular characterization of VDPV-2s isolated in the Central African Republic in 2019. A) Phylogram of the VP1-encoding sequence drawn by using the maximum-likelihood method based on the data-specific model. Alternating blue and red indicate evolutionary branches (A–L); open circles indicate sequences of VDPVs from patients with acute flaccid paralysis circles; closed circles indicate sequences of VDPVs from healthy children; black triangles indicate sequences of VDPVs from environmental samples. The district where the isolate was sampled and the recombinant pattern the isolate belongs to (patterns 1–12 or nonrecombinant [Figure 2, panel B]) are indicated; asterisks indicate isolates that have not been fully sequenced. Scale bar indicates nucleotide substitutions per site. B) Schematic representation of the genomic patterns of the VDPVs. Top row shows poliovirus genetic organization, with the main open reading frame flanked by the 5′ and 3′ untranslated regions (UTRs). Approximate locations of the recombination sites (1–12 on left) are shown. Sequences with different colors differ by <3%. Letters in parentheses on the right indicate the VP1 branches where each recombinant pattern can be found. NR, no recombination. C) Similarity plot drawn by comparing the sole genome of pattern 5 with genomes of patterns 3 (green), 4 (red), and 6 (blue) in the 3′ half of the genome. Sliding window width, 200 nt; step distance, 20 nt. VDPV-2s, type 2 vaccine-derived polioviruses; VP1, viral capsid protein 1.

can make different segments of the enterovirus genome evolve independently (*7*).

Although VDPV-2s commonly harbor a recombinant nonpolio 5′ untranslated region (UTR), all CAR VDPVs had a 5′ UTR from the vaccine Sabin-2 strain. Nonetheless, an A→G reversion was found in all genomes at nt position 481, which harbors one of the major determinants of attenuation of the Sabin-2 strain (*8*). A second major determinant of Sabin-2, located within the VP1-encoding region (nt position 2909), had also reverted (U→C, isoleucine-to-threonine) in all CAR VDPVs.

## Conclusions

The origin of the CAR VDPV-2s remains unknown. In April 2016, a switch from use of the trivalent OPV to the bivalent OPV, which contains the Sabin-1 and Sabin-3 attenuated strains (but not Sabin-2), was synchronized globally (*9*). The low nucleotide divergence observed within the VP1-encoding sequence between the CAR VDPV-2s and Sabin-2 makes the hypothesis of silent circulation of Sabin-2–derived strains originating from the trivalent OPV over $\geq$3 years unlikely. More likely, the CAR VDPV-2s may derive from the Sabin-2 strain contained in the monovalent OPV that was used to control a 2017–2018 VDPV-2 outbreak in the Democratic Republic of the Congo, which borders CAR (*10*). Population movements across the border between the 2 countries could have allowed introduction of Sabin-2–derived viruses into CAR, a country in which most children born after the global vaccine switch have no immunity against serotype 2. The silent circulation of these viruses for several months was probably rendered possible by the difficulties of implementing efficient surveillance in some regions of CAR because of the civil war that has been ongoing in the country since 2012.

We show that the CAR VDPV-2 outbreak resulted from several independent emergence events, involving recombinant genomes with no recombination in the 5′ UTR. Beyond the situation in CAR, 2019 was a dark year for the Global Polio Eradication Initiative; VDPV-2 outbreaks surged in many countries in Africa (*11*). OPV of serotype 2 remains the best tool to stop VDPV-2 outbreaks, but it also constitutes the seed for emergence of VDPVs. The pending release of a novel OPV that contains a genetically stabilized serotype 2 strain less prone to reversion is expected to put an end to this vicious cycle (*12*).

### Acknowledgments

We are indebted to Charlotte Balière and Aurelia Kwasiborski for Sanger sequencing.

### About the Author

Dr. Joffret is a scientist with the Institut Pasteur in Paris, France. Her main research interest is surveillance of poliovirus and other nonpolio enteroviruses in Africa.

### References

1. Zell R, Delwart E, Gorbalenya AE, Hovi T, King AMQ, Knowles NJ, et al.; Ictv Report Consortium. ICTV virus taxonomy profile: Picornaviridae. J Gen Virol. 2017;98:2421–2. https://doi.org/10.1099/jgv.0.000911
2. Bandyopadhyay AS, Garon J, Seib K, Orenstein WA. Polio vaccination: past, present and future. Future Microbiol. 2015;10:791–808. https://doi.org/10.2217/fmb.15.19
3. Combelas N, Holmblat B, Joffret ML, Colbère-Garapin F, Delpeyroux F. Recombination between poliovirus and coxsackie A viruses of species C: a model of viral genetic plasticity and emergence. Viruses. 2011;3:1460–84. https://doi.org/10.3390/v3081460
4. Burns CC, Diop OM, Sutter RW, Kew OM. Vaccine-derived polioviruses. J Infect Dis. 2014;210(Suppl 1):S283–93. https://doi.org/10.1093/infdis/jiu295
5. Jorba J, Campagnoli R, De L, Kew O. Calibration of multiple poliovirus molecular clocks covering an extended evolutionary range. J Virol. 2008;82:4429–40. https://doi.org/10.1128/JVI.02354-07
6. Bessaud M, Joffret ML, Blondel B, Delpeyroux F. Exchanges of genomic domains between poliovirus and other cocirculating species C enteroviruses reveal a high degree of plasticity. Sci Rep. 2016;6:38831. https://doi.org/10.1038/srep38831
7. Muslin C, Mac Kain A, Bessaud M, Blondel B, Delpeyroux F. Recombination in enteroviruses, a multi-step modular evolutionary process. Viruses. 2019;11:859. https://doi.org/10.3390/v11090859
8. Minor PD, Macadam AJ, Stone DM, Almond JW. Genetic basis of attenuation of the Sabin oral poliovirus vaccines. Biologicals. 1993;21:357–63. https://doi.org/10.1006/biol.1993.1096
9. Garon J, Seib K, Orenstein WA, Ramirez Gonzalez A, Chang Blanc D, Zaffran M, et al. Polio endgame: the global switch from tOPV to bOPV. Expert Rev Vaccines. 2016;15:693–708. https://doi.org/10.1586/14760584.2016.1140041
10. Mbaeyi C, Alleman MM, Ehrhardt D, Wiesen E, Burns CC, Liu H, et al. Update on vaccine-derived poliovirus outbreaks—Democratic Republic of the Congo and Horn of Africa, 2017–2018. MMWR Morb Mortal Wkly Rep. 2019;68:225–30. https://doi.org/10.15585/mmwr.mm6809a2
11. Jorba J, Diop OM, Iber J, Henderson E, Zhao K, Quddus A, et al. Update on vaccine-derived poliovirus outbreaks—worldwide, January 2018–June 2019. MMWR Morb Mortal Wkly Rep. 2019;68:1024–8. https://doi.org/10.15585/mmwr.mm6845a4
12. Van Damme P, De Coster I, Bandyopadhyay AS, Revets H, Withanage K, De Smedt P, et al. The safety and immunogenicity of two novel live attenuated monovalent (serotype 2) oral poliovirus vaccines in healthy adults: a double-blind, single-centre phase 1 study. Lancet. 2019;394:148–58. https://doi.org/10.1016/S0140-6736(19)31279-6

Address for correspondence Maël Bessaud, Institut Pasteur 25-28, rue du Dr Roux, 75 015 Paris, France; email: mael.bessaud@pasteur.fr

# Azithromycin-Resistant *Salmonella enterica* Serovar Typhi AcrB-R717Q/L, Singapore

Sophie Octavia, Ka Lip Chew, Raymond T. P. Lin, Jeanette W. P. Teo

Global travel has led to intermittent importation of multidrug-resistant *Salmonella enterica* serovar Typhi into industrialized countries. We detected azithromycin-resistant *Salmonella* Typhi in Singapore, of which 2 isolates were likely locally acquired. Ongoing vigilance and surveillance to minimize the public health risk for this serious pathogen is needed.

In Singapore, the incidence of typhoid fever is low (0.8–1.2 cases/100,000 population annually). Most cases are imported, particularly from the South Asia subcontinent (*1*). First-line treatments include ampicillin, trimethoprim/sulfamethoxazole, and chloramphenicol. With increasing multidrug-resistant and fluoroquinolone-resistant infections, ceftriaxone and azithromycin are the next treatment alternatives. However, resistance to ceftriaxone or azithromycin resistance has been reported (*2*).

Multidrug-resistant *Salmonella* Typhi isolates belong to haplotype H58 (genotype 4.3.1), which is predominant in Asia and Africa (*3*). Resistance in genotype 4.3.1 is characterized by nonsynonymous mutations in the quinolone resistance–determining-region (QRDR) of DNA gyrase genes *gyrA* and *gyrB*, DNA topoisomerase IV genes *parC* and *parE*, and acquisitions of IncHI1 plasmids (*3*,*4*). Azithromycin-resistant *Salmonella* Typhi is also seen in this genotype (*2*).

During September 2019–April 2020, increased MICs for azithromycin were detected for 3 *Salmonella* Typhi isolates identified at the National University Hospital, Singapore. To characterize the molecular mechanisms of azithromycin resistance and genetic lineage in these isolates, we performed whole-genome-sequencing.

Author affiliations: National Centre for Infectious Diseases, Singapore (S. Octavia, R.T. P. Lin); National University Hospital, Singapore (K.L. Chew, R.T. P. Lin, J.W.P. Teo)

DOI: https://doi.org/10.3201/eid2702.203874

## The Study

This study was approved by the National Healthcare Group Domain Specific Review Board (study no. 2020/01010). Apart from the 3 isolates tested for azithromycin resistance, an additional 21 *Salmonella* Typhi isolates (total 24 isolates) collected during 2016 and 2020 at the National University Hospital, a 1,200-bed tertiary hospital, were retrospectively investigated.

Genus was identified by using the Bruker MALDI Biotyper (Bruker Daltonics, https://www.bruker.com), and serotyping was performed by using slide agglutination and antiserum (Statens Serum Institute, Copenhagen, Denmark). After genus and serotype were confirmed, these isolates were submitted to the National Public Health Laboratory, Singapore, as part of the national surveillance program for *Salmonella* spp.

Drug susceptibility testing was routinely performed by using Vitek 2 (bioMérieux, https://www.biomerieux.com) and supplemented by using the Etest (bioMérieux) for ciprofloxacin and azithromycin. Azithromycin MICs were further confirmed by using broth microdilution. Quality control isolates used were *Escherichia coli* ATCC 25922, *Salmonella* Enteritidis ATCC 13076, *Salmonella* Typhimurium ATCC 14028, and *Staphylococcus aureus* ATCC 29213. EUCAST interpretative breakpoints were used, including for azithromycin resistance, which is based on the tentative epidemiologic cutoff value (https://eucast.org/fileadmin/src/media/PDFs/EUCAST_files/Breakpoint_tables/v_10.0_Breakpoint_Tables.pdf).

Whole-genome sequencing was performed by using MiSeq (Illumina, https://www.illumina.com) to generate 300-bp paired-end reads. Raw reads were assembled by using Shovill (https://github.com/tseemann/shovill). Isolates were genotyped by using the GenoTyphi tool (https://github.com/katholt/genotyphi), which separates *Salmonella* Typhi isolates into clades on the basis of the extended genotyping framework described by Wong et al. (*4*). SRST2 (*5*) was used to determine the presence of acquired antimicrobial drug resistance genes by using the ResFinder database (*6*). Chromosomal QRDR mutations in *gyrA*, *gyrB*, and *parC*, as well as the efflux pump AcrB (*acrB*-R717Q) mutations conferring resistance to azithromycin, were also investigated by using the GenoTyphi tool. PlasmidFinder (https://cge.cbs.dtu.dk/services/PlasmidFinder/) was used to detect replicons.

*Salmonella* Typhi CT18 (GenBank accession no. AL513382.1) was designated as the reference genome. We also downloaded all publicly available *Salmonella* Typhi genome sequences belonging to lineage 4.3.1 and its sublineages from the Pathogenwatch database (https://pathogen.watch) for comparison with our isolates belonging to lineage 4.3.1. Core-genome single-nucleotide polymorphisms were obtained by using snippy pipeline (https://github.com/tseemann/snippy) and then used to generate a phylogenetic tree by using FastTree (*7*). The resulting tree was visualized by using iTOL version 4 (*8*). Raw reads have been submitted to the Sequence Reads Archive under BioProject no. PRJNA660881.

Whole-genome sequencing results showed that 15 of the 24 *Salmonella* Typhi isolates belonged to subclade 4.3.1 (haplotype H58), which can be further differentiated into 4.3.1.1 (4/15), 4.3.1.2 (8/15), and 4.3.1.3 (3/15) (Table, https://wwwnc.cdc.gov/EID/article/27/2/20-3874-T1.htm). The 4.3.1 subclade is a dominant lineage disseminating from South Asia into East Africa (*3*). Signature mutations associated with this subclade are QRDR mutations at codon positions 83 and 87 in *gyrA* conferring fluoroquinolone resistance. The phylogenetic tree showed that these isolates did not form a unique group but were interspersed with isolates from countries in South Asia, particularly Bangladesh (Figure). The remaining 9/24 isolates belonged to subclades 0.0.2 (n = 1), 2.3.3 (n = 4), 3 (n = 2), 3.2.1 (n = 1), and 4.1 (n = 1).

The genomic antimicrobial drug–susceptibility profiles correlated with the phenotypic susceptibilities (Table). Six isolates harbored $bla_{\text{TEM-1}}$, but none had extended-spectrum-β-lactamases or carbapenemases. All isolates were resistant to ciprofloxacin and had QRDR mutations (Table). Four of 8 isolates belonged to subclade 4.3.1.2 and had the triple QRDR mutation combination. Only isolates with *dfrA7*, *sul1*, and *sul2* were phenotypically resistant to trimethoprim/sulfamethoxazole.

The 3 azithromycin-resistant isolates have not acquired macrolide-modifying enzymes, such as methylases [*erm(A)*, *erm(B)*, and *erm(C)*], esterases [*ere(A)* and *ere(B)*], or phosphotransferases [*mph(A)*, *mph(B)*, and *mph(D)*] observed in isolates belonging to the order Enterobacterales (*9*). There were no chromosomal alterations in the 50S ribosomal subunit proteins L4 (*rlpD*) and L22 (*rlpV*) (*11*). Instead, R717Q/L mutations in the efflux pump AcrB were detected. Increased MICs for azithromycin (R717Q: 32 mg/L, R717L: 16 mg/L) were observed for these isolates. Azithromycin MICs $\leq$4 mg/L were observed for all wild-type *acrB* isolates (Table). The AcrB-R717Q mutation was reported in azithromycin-resistant *Salmonella* Typhi 4.3.1.1 in Bangladesh (*2*) and subsequently in a Pakistan-specific 4.3.1.1 cluster (*10*). The mutation that emerged in Pakistan is believed to be a de novo spontaneous mutation, rather than spread of an azithromycin-resistant clone (*10*). AcrB-R717Q–associated azithromycin resistance has also been reported in India (*11*).

## Conclusions

The AcrB-R717L mutation (isolate SLT1105) is novel in *Salmonella* Typhi. This mutation was described in an azithromycin-resistant *Salmonella* Paratyphi A isolate in Bangladesh (*2*). Functional analysis of the R717L mutation conferred resistance to a sensitive *Salmonella* Paratyphi A strain resulted in a 4-fold increase in the MIC (7 mg/L vs. 28 mg/L; p = 0.0001) (*2*). In *Salmonella* Typhi, the mutation also appears to impart azithromycin resistance (Table).

These AcrB-R717Q/L mutations were in multidrug-resistant isolates. This finding is worrisome because of the unavailability of oral antimicrobial drug treatment options and increased relapses when treated with β-lactams without intracellular-acting antimicrobial drugs.

Most case-patients had relevant travel history within 2 months before onset of symptoms, including travel to India (n = 5), Bangladesh (n = 4), Pakistan (n = 1), Myanmar (n = 1), and the Philippines (n = 1). Three cases appeared to be local transmission, of which 2 had AcrB-R717Q/L mutations. The remaining case-patient, whose isolate had the AcrB-R717Q mutation, had traveled to Bangladesh and probably acquired the infection in this country (*2*).

Hooda et al. (*12*) analyzed 49,115 *Salmonella* genomes and found the AcrB-R717Q/L mutation in 16 *Salmonella* Typhi genomes (≈0.03%). Although this number was small, the rate of acquisition of such novel mechanisms might hasten, especially with increasing use of azithromycin, such as in mass drug administration with azithromycin as a key component for the control of neglected tropical diseases (*12*). The

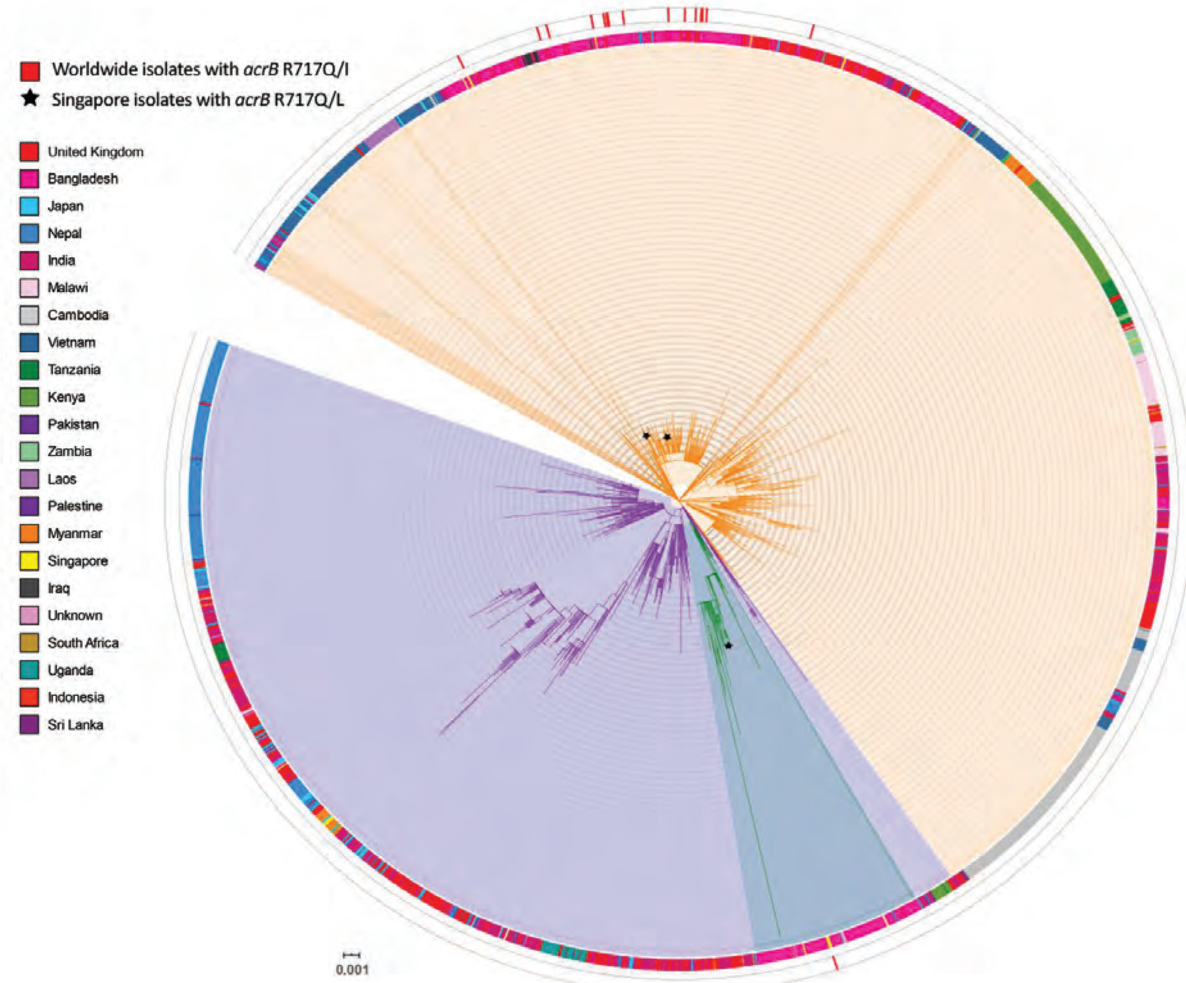


**Figure.** Core single-nucleotide polymorphism phylogenetic tree of 15 genotype 4.3.1 *Salmonella enterica* serovar Typhi isolates tested for azithromycin resistance, Singapore. Isolates sequenced in this study were compared with other publicly available *Salmonella* Typhi genomes, indicated by their corresponding GenBank accession number obtained from Pathogenwatch (https://pathogen.watch) on the basis of 3,104 core-genome single-nucleotide polymorphisms. Azithromycin-resistant isolates analyzed in this study are indicated by asterisks (*). *Salmonella* Typhi CT18 was designated as the reference genome (blue). Genotype information obtained from the GenoTyphi tool (*4*) was included for all genomes, and country of isolation was added when available. The tree was illustrated by using iTOL version (*8*). Scale bar indicates nucleotide substitutions per site.

proportion of isolates in our study with AcrB-717Q/L mutation (20%, 3/15) was unexpectedly higher than previously reported. The reasons for this finding are unclear. However, our study was a single-center study that had a limited number of cases.

Genotypic testing of the usual azithromycin resistance–associated genes in the order Enterobacterales cannot identify *acrB* mutations, and there are currently no formal breakpoints to guide phenotypic testing. An azithromycin MIC of 16 mg/L was observed for 1 isolate with the AcrB-R717L mutation. Although this azithromycin MIC was higher (≤8 mg/L) than that for isolates without the mutation, this isolate is still considered wild-type. Detection of increased MICs raises suspicion for resistance requiring further confirmation. Additional data are required to correlate resistance mutations, MICs, and treatment outcomes.

## About the Author

Dr. Octavia is a scientific officer at the National Public Health Laboratory, Singapore. Her primary research interest is laboratory surveillance of salmonellosis.

## References

1. Yew FS, Goh KT, Lim YS. Epidemiology of typhoid fever in Singapore. Epidemiol Infect. 1993;110:63–70. https://doi.org/10.1017/S0950268800050688

2. Hooda Y, Sajib MS, Rahman H, Luby SP, Bondy-Denomy J, Santosham M, et al. Molecular mechanism of azithromycin resistance among typhoidal *Salmonella* strains in Bangladesh identified through passive pediatric surveillance. PLoS Negl Trop Dis. 2019;13:e0007868–0007868. https://doi.org/10.1371/journal.pntd.0007868
3. Wong VK, Baker S, Pickard DJ, Parkhill J, Page AJ, Feasey NA, et al. Phylogeographical analysis of the dominant multidrug-resistant H58 clade of *Salmonella* Typhi identifies inter- and intracontinental transmission events. Nat Genet. 2015;47:632–9. https://doi.org/10.1038/ng.3281
4. Wong VK, Baker S, Connor TR, Pickard D, Page AJ, Dave J, et al.; International Typhoid Consortium. An extended genotyping framework for *Salmonella enterica* serovar Typhi, the cause of human typhoid. Nat Commun. 2016;7:12827. https://doi.org/10.1038/ncomms12827
5. Inouye M, Dashnow H, Raven L-A, Schultz MB, Pope BJ, Tomita T, et al. SRST2: rapid genomic surveillance for public health and hospital microbiology labs. Genome Med. 2014;6:90. https://doi.org/10.1186/s13073-014-0090-6
6. Bortolaia V, Kaas RS, Ruppe E, Roberts MC, Schwarz S, Cattoir V, et al. ResFinder 4.0 for predictions of phenotypes from genotypes. J Antimicrob Chemother. 2020;dkaa345. https://doi.org/10.1093/jac/dkaa345
7. Price MN, Dehal PS, Arkin AP. FastTree: computing large minimum evolution trees with profiles instead of a distance matrix. Mol Biol Evol. 2009;26:1641–50. https://doi.org/10.1093/molbev/msp077
8. Letunic I, Bork P. Interactive Tree Of Life (iTOL) v4: recent updates and new developments. Nucleic Acids Res. 2019;47:W256–9. https://doi.org/10.1093/nar/gkz239
9. Gomes C, Martínez-Puchol S, Palma N, Horna G, Ruiz-Roldán L, Pons MJ, et al. Macrolide resistance mechanisms in *Enterobacteriaceae*: focus on azithromycin. Crit Rev Microbiol. 2017;43:1–30. https://doi.org/10.3109/1040841X.2015.1136261
10. Iqbal J, Dehraj IF, Carey ME, Dyson ZA, Garrett D, Seidman JC, et al. A race against time: reduced azithromycin susceptibility in *Salmonella enterica* serovar Typhi in Pakistan. MSphere. 2020;5:e00215–20. https://doi.org/10.1128/mSphere.00215-20
11. Katiyar A, Sharma P, Dahiya S, Singh H, Kapil A, Kaur P. Genomic profiling of antimicrobial resistance genes in clinical isolates of *Salmonella* Typhi from patients infected with typhoid fever in India. Sci Rep. 2020;10:8299. https://doi.org/10.1038/s41598-020-64934-0
12. Hooda Y, Tanmoy AM, Sajib MS, Saha S. Mass azithromycin administration: considerations in an increasingly resistant world. BMJ Glob Health. 2020;5:e002446. https://doi.org/10.1136/bmjgh-2020-002446


Address for correspondence: Sophie Octavia, National Public Health Laboratory, National Centre for Infectious Diseases, 16 Jalan Tan Tock Seng, Singapore 308442; email: sophie.octavia@gmail.com or Ka Lip Chew, Department of Laboratory Medicine, National University Hospital, 5 Lower Kent Ridge Rd, Singapore 119074; email: ka_lip_chew@nuhs.edu.sg

# Prevalence of SARS-CoV-2–Specific Antibodies, Japan, June 2020

Takashi Yoshiyama, Yasuki Saito, Kunitsugu Masuda, Yoshiko Nakanishi, Yasutoshi Kido, Kazuhiro Uchimura, Satoshi Mitarai, Tadaki Suzuki, Yu Nakagama, Hiroshi Kubota, Maki Satomi, Sana Uchikoba, Makoto Ohnishi, Takaji Wakita, Seiya Kato, Katsunobu Kato

We used 2 commercially available antibody tests to estimate seroprevalence of severe acute respiratory syndrome coronavirus 2 infection in Japan during June 2020. Of 7,950 samples, 8 were positive by both assays. Using 2 reliable antibody tests in conjunction is an effective method for estimating seroprevalence in low prevalence settings.

During the first wave of the coronavirus disease (COVID-19) pandemic in Japan, a total of 16,884 persons tested positive for severe acute respiratory syndrome coronavirus 2 (SARS-CoV-2) by May 31, 2020, indicating a national cumulative incidence of 0.013% (*1*,*2*) (Appendix Figure, https://wwwnc.cdc.gov/EID/article/27/2/20-4088-App1.pdf). To establish a surveillance method in low prevalence settings, we assessed the seroprevalence of SARS-CoV-2 infection in Japan in early June 2020.

## The Study

By October 2020, no standard antibody test or standardized method for estimating the seroprevalence of SARS-CoV-2 infection had been established. We used 2 serologic tests, a neutralizing antibody assay, and participant questionnaires to estimate the seroprevalence of SARS-CoV-2 infection in Japan.

We conducted a seroprevalence survey of SARS-CoV-2 infection in 3 prefectures of Japan during June 1–7, 2020. We selected 2 prefectures with a relatively high cumulative incidence of confirmed COVID-19 cases as of May 31, 2020: Tokyo, with an incidence of 0.039% (5,408 cases/13.9 million population) and Osaka, with an incidence of 0.020% (1,785 cases/8.8 million population). To better estimate the range of seroprevalence of SARS-CoV-2 infection in Japan, we also chose a prefecture with a relatively low cumulative incidence, Miyagi, with an incidence of 0.004% (88 cases/2.3 million population).

Each prefecture was responsible for using its civil registration data to randomly select participants. The Tokyo metropolitan government used random sampling stratified by age and sex in 3 cities with a cumulative incidence resembling the average of the Tokyo metropolitan area. The Miyagi prefectural government used its residence registry to conduct random sampling with stratification for age, sex, and geographic region. The Osaka prefecture used age-adjusted random sampling to select resident users of an existing smartphone application on general health (Figure).

Eligible participants were persons ≥20 years of age living in Japan. The Tokyo and Miyagi prefectures excluded otherwise eligible participants with temperatures ≥37.5°C. All participants provided written informed consent. The study was approved by the internal review boards of the Research Institute of Tuberculosis (approval no. RIT/IRB 2020–04, 2020–05) and the National Institute of Infectious Diseases (approval no. 1140).

First, we asked participants to complete a questionnaire (Appendix Table 1). Trained healthcare workers collected blood samples from the participants. After centrifuging the samples, the workers collected serum and tested the samples with 2 commercially available antibody tests to detect the SARS-CoV-2 nucleocapsid antigen: a chemiluminescent microparticle immunoassay with published specificity results of 99.6%–99.9% at a cutoff index of 1.4 (SARS-CoV-2 IgG assay; Abbott, https://www.abbott.com) (*3*,*4*) and an electrochemiluminescence immunoassay for the

Author affiliations: Research Institute of Tuberculosis, Kiyose, Japan (T. Yoshiyama, K. Uchimura, S. Miatai, S. Kato); Fukujuji Kenshin Center of Miyagi Anti-Tuberculosis Association, Sendai, Japan (Y. Saito); Osaka Anti-Tuberculosis Association, Osaka, Japan (K. Masuda); Center for Comprehensive Health Check and Promotion of Japan Anti-Tuberculosis Association, Tokyo, Japan (Y. Nakanishi); Osaka City University, Osaka (Y. Kido, Y. Nakagama); National Institute of Infectious Diseases, Tokyo (T. Suzuki, M. Ohnishi, T. Wakita); Osaka City University Hospital, Osaka (H. Kubota); Ministry of Health, Labor and Welfare, Tokyo (M. Satomi, S. Uchikoba); Government of Japan, Tokyo (K. Kato)

DOI: https://doi.org/10.3201/eid2702.204088

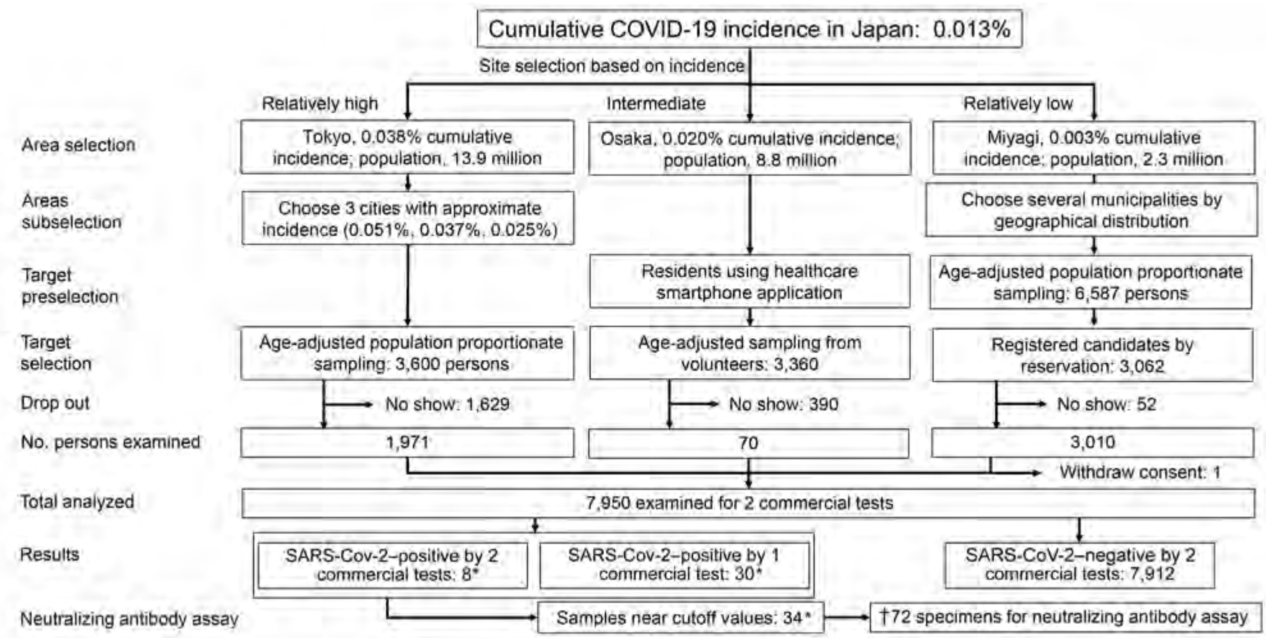


**Figure**. Flowchart of participants and results of SARS-CoV-2–specific antibody survey, Japan, 2020. Dagger (†) indicates sum of values marked with asterisks (*). SARS-CoV-2, severe acute respiratory syndrome coronavirus 2.

qualitative detection of antibodies with 99.8% specificity and 100% (manufacturer determined) sensitivity (Elecsys Anti-SARS-CoV-2 immunoassay; F. Hoffmann-La Roche Ltd, https://www.roche.com) (*5*). Samples that were positive or borderline negative by $\geq$1 assay (reference range 1.20–1.39 for the Abbott test and 0.70–0.99 titer for the Roche test) were sent to Japan's National Institute of Infectious Diseases (Tokyo) for a neutralizing antibody assay with VeroE6/TMPRSS2 cells (JCRB Cell Bank accession no. JCRB1819) (*6*). For the neutralizing antibody assay, we used an in vitro cytopathic effect assay, which is more accurate than serologic tests and therefore well-suited for confirmation of results; however, only a few laboratories in Japan have the resources to conduct the assay.

We compared the 2 groups using the $\chi^2$ test, considering values with $p<0.05$ to be significant. We compared ordinal scales by using the Mann-Whitney U test. We used Excel (Microsoft, https://www.microsoft.com) to conduct statistical analyses.

In total, 13,547 persons were invited to participate in the study; 7,950 (58.7%) accepted and gave informed consent. Of the participants, 3,660 (46.0%) were men and 4,290 (54.0%) were women. Persons 20–29 years of age (877 of 1,875 invitees) or 80–99 years of age (337 of 1,102 invitees) had the lowest response rate (Appendix Table 2). Participants from Osaka were more likely to have a history of fever within the past 4 months (2.7%) than participants from Tokyo (2.2%) and Miyagi (1.2%) (Appendix Table 1).

Of the 7,950 serum samples, 8 tested positive by both tests and 30 samples tested positive by only 1 test (15 by Abbott and 15 by Roche) (Table). All 8 specimens that were positive for both commercial tests also tested positive in the neutralizing antibody assay. No other specimens, including those that tested positive or borderline negative in 1 assay, tested positive by the neutralizing antibody assay.

The proportion of participants with 2 positive test results was significantly higher among those with fever (2.5%) than those without fever (0.05%; $p<0.001$). The proportion of participants with 1 positive test result was not significantly different among those with fever (1.2%) and those without fever (0.36%; $p = 0.25$) (Appendix Table 1). These findings, validated by the neutralizing antibody assay, indicated that 2 positive test results accurately identified seropositive participants. The proportion of participants that tested positive by both tests was 0.1% in Tokyo, 0.17% in Osaka, and 0.03% in Miyagi. The ratios of seroprevalence to cumulative incidence were 2.6 in Tokyo, 8.3 in Osaka, and 8.7 in Miyagi. Seropositivity rates were highest among participants 20–39 years of age.

## Conclusions

The US Centers for Disease Control and Prevention suggests using an orthogonal testing algorithm, which considers the results of 2 independent antibody tests, in settings with low SARS-CoV-2 prevalence (*7*). Some surveys in high SARS-CoV-2 prevalence areas such as

Spain (*8*), China (*9*), and Geneva, Switzerland (*10*) have not adopted this approach. We believe an orthogonal testing algorithm, such as the one used in this study, would be particularly valuable in our low prevalence setting. The 8 specimens that tested positive by both commercial antibody assays were confirmed to have neutralizing activity against SARS-CoV-2 with a neutralizing antibody assay. These results support our use of the neutralizing assay to confirm the validity of the commercial tests. Any 2 commercial tests with high sensitivity and specificity would be appropriate to use in this orthogonal testing strategy.

Our prefecture-level seroprevalence:cumulative case detection ratios (2.6–8.7) resemble those of the United States, which are ≈10 (*11*), and are lower than those of Switzerland (≈20–50) (*10*). These results indicate that Japan has monitored the pandemic as accurately as have other countries.

This study has several limitations. First, participant selection in Osaka was based on a volunteer population (i.e., users of a particular smartphone application) rather than the general community. In addition, the prefectures of Tokyo and Miyagi excluded otherwise eligible participants with temperatures ≥37.5°C. As a result, Osaka had the highest proportion of participants with fevers at the time of the survey and the highest seroprevalence. These factors might have introduced participation bias, skewing the results. Another limita-

**Table.** Patient characteristics and serologic results of 2 antibody tests for severe acute respiratory syndrome coronavirus 2, Japan, June 2020*

| Characteristic | Both + | Roche –, Abbott + | Roche +, Abbott – | Both – | Subtotal | % Patients positive by both tests (95% CI) |
|---|---|---|---|---|---|---|
| Total | 8 | 15 | 15 | 7,912 | 7,950 | 0.10 (0.04–0.20) |
| Area | | | | | | |
| Tokyo | 2 | 2 | 4 | 1,963 | 1,971 | 0.10 (0.01–0.37) |
| Osaka | 5 | 11 | 5 | 2,949 | 2,970 | 0.17 (0.05–0.39) |
| Miyagi | 1 | 2 | 6 | 3,000 | 3,009 | 0.03 (0.00–0.19) |
| Sex | | | | | | |
| M | 3 | 7 | 5 | 3,643 | 3,658 | 0.08 (0.02–0.24) |
| F | 5 | 8 | 10 | 4,269 | 4,292 | 0.12 (0.04–0.27) |
| Age, y | | | | | | |
| 20–29 | 3 | 0 | 0 | 875 | 878 | 0.34 (0.07–1.00) |
| 30–39 | 3 | 2 | 1 | 1,210 | 1,216 | 0.25 (0.05–0.72) |
| 40–49 | 0 | 3 | 7 | 1,589 | 1,599 | 0 (0.00–0.23) |
| 50–59 | 0 | 2 | 4 | 1,457 | 1,463 | 0 (0.00–0.25) |
| 60–69 | 1 | 4 | 0 | 1,315 | 1,320 | 0.08 (0.00–0.42) |
| 70–79 | 1 | 4 | 1 | 1,128 | 1,134 | 0.09 (0.00–0.49) |
| ≥80 | 0 | 0 | 2 | 338 | 340 | 0 (0.00–1.08) |
| Job setting | | | | | | |
| Working as before | 4 | 4 | 3 | 3,091 | 3,102 | 0.13 (0.04–0.33) |
| Working at home | 0 | 3 | 2 | 432 | 437 | 0 (0.00–0.84) |
| Working as before and at home | 1 | 1 | 5 | 1,974 | 1,981 | 0.05 (0.00–0.28) |
| Not working | 3 | 7 | 5 | 2,410 | 2,425 | 0.12 (0.03–0.36) |
| No information | 0 | 0 | 0 | 5 | 5 | 0 (0.00–52.20) |
| Time spent outside the home, h | | | | | | |
| 0 | 1 | 4 | 1 | 1,153 | 1,159 | 0.09 (0.00–0.48) |
| <2 | 1 | 5 | 6 | 2,871 | 2,883 | 0.03 (0.00–0.19) |
| 2–4 | 3 | 5 | 5 | 1,182 | 1,195 | 0.25 (0.05–0.73) |
| >4 | 3 | 1 | 3 | 2,704 | 2,711 | 0.11 (0.02–0.32) |
| No information | 0 | 0 | 0 | 2 | 2 | 0 (0.00–84.20) |
| Fever at time of study | | | | | | |
| Yes | 0 | 0 | 0 | 16 | 16 | 0 (0.00–20.60) |
| No | 8 | 15 | 15 | 7,886 | 7,924 | 0.10 (0.04–0.20) |
| No information | 0 | 0 | 0 | 10 | 10 | 0 (0.00–30.90) |
| History of fever lasting >4 days in past 4 months | | | | | | |
| Yes | 4 | 1 | 1 | 155 | 161 | 2.48 (0.68–6.24) |
| No | 4 | 14 | 14 | 7,756 | 7,788 | 0.05 (0.01–0.13) |
| No information | 0 | 0 | 0 | 1 | 1 | 0 (0.00–97.50) |
| Previous PCR result | | | | | | |
| Positive | 1 | 0 | 0 | 0 | 1 | 100.00 (2.50–100.00) |
| Negative | 0 | 0 | 0 | 33 | 33 | 0 (0.00–10.60) |
| Not applicable | 7 | 15 | 15 | 7,879 | 7,916 | 0.09 (0.04–0.18) |

*Roche, Elecsys Anti SARS-CoV-2 (F. Hoffmann-La Roche Ltd, https://www.roche.com); Abbott, ARCHITECT SARS-CoV-2 IgG assay (Abbott, https://www.abbott.com); +, positive; –, negative.

tion is that Tokyo had the lowest participation of participants 20–29 years of age. Because seroprevalences were higher in younger age groups, this sampling distribution might have reduced the seropositivity rate and prevalence:cumulative incidence ratio found in Tokyo. Furthermore, this study did not include participants <20 years of age. Although patients <20 years of age make up <10% of COVID-19 cases (*1*), excluding these patients might lead to an overestimation of SARS-CoV-2 infection prevalence. Finally, antibodies against SARS-CoV-2 might disappear after 60 days (*12*); however, the elapsed time might not affect levels of nucleocapsid protein antibody (*13*). Further studies on antibody levels after disease onset and recovery are essential for monitoring the course of infections.

We estimate that SARS-CoV-2 seroprevalence ranged from 0.03%–0.17% in Japan in early June 2020. Public health officials in low prevalence areas should consider using 2 antibody tests in conjunction for accurate surveillance.


### Acknowledgments

We thank the Tokyo, Osaka, and Miyagi prefecture governments, and Yukio Nakano and Shuji Ohgaki for conducting the survey. We also thank National Institute of Infectious Diseases' COVID-19 Antibody Testing Working Group (Akira Ainai, Hitomi Kinoshita, Kaori Sano, Kazu Okuma, Kiyoko Nojima, Ken Maeda, Naoko Iwata-Yoshikawa, Noriyo Nagata, Saya Moriyama, Shuetsu Fukushi, Souichi Yamada, Taishi Onodera, Takayuki Matsumura, Yoshimasa Takahashi, and Yu Adachi) for the laboratory examination. We are grateful to Kazuya Takemura, Hiroe Kawahara, Etsuko Takizawa, Yu Nagakura, Shinya Ueno, Yasuko Okui, Wataru Yamashita, Mika Nakamae, and Masayuki Hino for their support of the survey. We also thank Shutoku Matsuyama for providing samples of SARS-CoV-2 strain 2019-nCoVJPN/TY/WK-521/2020.

The survey was funded by the Ministry of Health, Labor and Welfare of Japan.


## About the Author

Dr. Yoshiyama is a senior researcher at the Research Institute of Tuberculosis, Kiyose, Japan. His primary interests are epidemiology and the clinical aspects of tuberculosis and other respiratory diseases, including COVID-19.

### References


1. Ohhamazaki T. Coronavirus COVID-19 Japan case by each prefecture. 2020 [cited 2020 Jun 5]. https://jagjapan.maps.arcgis.com/apps/opsdashboard/index.html#/641eba7fef234a47880e1e1dc4de85ce
2. Ministry of Internal Affairs and Communications. Population estimates. 2019 Oct 1 [cited 2020 Jun 5]. https://www.stat.go.jp/data/jinsui/2019np/index.html
3. Bryan A, Pepper G, Wener MH, Fink SL, Morishima C, Chaudhary A, et al. Performance characteristics of the Abbott Architect SARS-CoV-2 IgG assay and seroprevalence in Boise, Idaho. J Clin Microbiol. 2020;58:e00941–20. https://doi.org/10.1128/JCM.00941-20
4. Abbott Core Laboratory. SARS-CoV-2 immunoassays. 2020 [cited 2020 Jun 17]. https://www.corelaboratory.abbott/us/en/offerings/segments/infectious-disease/sars-cov-2
5. F. Hoffman–La Roche Ltd. Elecsys® Anti-SARS-CoV-2. 2020 [cited 2020 Aug 19]. https://diagnostics.roche.com/no/en/products/params/elecsys-anti-sars-cov-2.html
6. Matsuyama S, Nao N, Shirato K, Kawase M, Saito S, Takayama I, et al. Enhanced isolation of SARS-CoV-2 by TMPRSS2-expressing cells. Proc Natl Acad Sci U S A. 2020;117:7001–3. https://doi.org/10.1073/pnas.2002589117
7. US Centers for Disease Control and Prevention. Interim guidelines for COVID-19 antibody testing in clinical and public health settings. 2020 [cited 2020 Jul 20]. https://www.cdc.gov/coronavirus/2019-ncov/lab/resources/antibody-tests-guidelines.html
8. Pollán M, Pérez-Gómez B, Pastor-Barriuso R, Oteo J, Hernán MA, Pérez-Olmeda M, et al.; ENE-COVID Study Group. Prevalence of SARS-CoV-2 in Spain (ENE-COVID): a nationwide, population-based seroepidemiological study. Lancet. 2020;396:535–44. https://doi.org/10.1016/S0140-6736(20)31483-5
9. To KKW, Cheng VCC, Cai JP, Chan KH, Chen LL, Wong LH, et al. Seroprevalence of SARS-CoV-2 in Hong Kong and in residents evacuated from Hubei province, China: a multicohort study. Lancet Microbe. 2020;1:e111–8. https://doi.org/10.1016/S2666-5247(20)30053-7
10. Stringhini S, Wisniak A, Piumatti G, Azman AS, Lauer SA, Baysson H, et al. Seroprevalence of anti-SARS-CoV-2 IgG antibodies in Geneva, Switzerland (SEROCoV-POP): a population-based study. Lancet. 2020;396:313–9. https://doi.org/10.1016/S0140-6736(20)31304-0
11. Concepcion S. CDC: for every COVID-19 case reported 'there are actually 10' more. Talking Points Memo. 2020 Jun 25 [cited 2020 Jun 26]. https://talkingpointsmemo.com/news/cdc-covid-19-cases-10-times-higher-than-reported
12. Liu A, Wang W, Zhao X, Zhou X, Yang D, Lu M, et al. Disappearance of antibodies to SARS-CoV-2 in a -COVID-19 patient after recovery. Clin Microbiol Infect. 2020;26:1703–5; Epub ahead of print. https://doi.org/10.1016/j.cmi.2020.07.009
13. Bruni M, Cecatiello V, Diaz-Basabe A, Lattanzi G, Mileti E, Monzani S, et al. Persistence of anti-SARS-CoV-2 antibodies in non-hospitalized COVID-19 convalescent health care workers. J Clin Med. 2020;9:3188. https://doi.org/10.3390/jcm9103188


Address for correspondence: Takashi Yoshiyama, Research Institute of Tuberculosis, 3-1-24 Matsuyama Kiyose-shi, Tokyo 204-8533, Japan; email: Yoshiyama1962@yahoo.co.jp

# Strand-Specific Reverse Transcription PCR for Detection of Replicating SARS-CoV-2

Catherine A. Hogan, ChunHong Huang, Malaya K. Sahoo, Hannah Wang, Becky Jiang, Mamdouh Sibai, Marisa Holubar, Roshni Mathew, James Zehnder, Benjamin A. Pinsky

We developed an assay that detects minus-strand RNA as a surrogate for actively replicating severe acute respiratory syndrome coronavirus 2. We detected minus-strand RNA in 41 persons with coronavirus disease up to 30 days after symptom onset. This assay might inform clinical decision-making about patient infectiousness.

Real-time reverse transcription PCR (rRT-PCR) is the standard diagnostic method for coronavirus disease 2019, but it cannot differentiate between actively replicating and inactive virus. Active replication is a critical factor for infectiousness; however, its time course is difficult to estimate because of the typical 20–50 days before rRT-PCR negative conversion occurs (*1*,*2*). PCR cycle threshold ($C_t$) values might help physicians to determine a patient's infectiousness, but researchers have isolated replicating virus from patients with a wide range (28–33) of $C_t$ values (*3*–*7*). Given the stringent biosafety precautions needed for viral culturing of severe acute respiratory syndrome coronavirus 2 (SARS-CoV-2), physicians require additional diagnostic tools. Actively replicating virus produces minus-strand RNA intermediates that can be detected by PCR (*8*,*9*). We developed and validated a 2-step strand-specific rRT-PCR for the detection of actively replicating SARS-CoV-2 and assessed its clinical performance.

## The Study

We conducted standard nucleic acid and amplificaton testing at the Stanford Health Care Clinical Virology Laboratory (Stanford, CA, USA) using the Panther Fusion SARS-CoV-2 Assay (Hologic Inc., https://www.hologic.com), the Panther Aptima SARS-CoV-2 Assay (Hologic Inc.), or the in-house rRT-PCR specific to the SARS-CoV-2 envelope gene (permitted by Emergency Use Authorization) (*10*,*11*). We did not culture SARS-CoV-2 because we did not have access to a biosafety level 3 laboratory.

We developed a novel 2-step rRT-PCR specific to the minus strand of the envelope gene (Appendix, https://wwwnc.cdc.gov/EID/article/27/2/20-4168-App1.pdf). First, we used strand-specific primers to convert SARS-CoV-2 RNA to complementary DNA. Then, we amplified the complementary DNA by rRT-PCR in 3 separate positive, negative, and background (no primer) reactions using the Rotor-Gene Q instrument (QIAGEN, https://www.qiagen.com) (Appendix). We conducted the analytical validation during May–June 2020. We used in vitro transcribed minus- and plus-strand RNA to evaluate the linearity, precision, and lower limit of detection of the assay (Appendix).

We retrospectively collected a convenience set of upper respiratory specimens with a broad range of $C_t$ values. These samples had been collected and frozen from 93 inpatients and outpatients who were treated at Stanford Health Care and tested positive for SARS-CoV-2 during March 12–April 9, 2020. We also reviewed the electronic medical records of the participating patients. For the prospective phase of the study, we collected upper respiratory samples from 53 consecutive patients with confirmed SARS-CoV-2 infection by standard rRT-PCR during July 31–September 4, 2020 (Appendix). Treating physicians ordered strand-specific rRT-PCR on the basis of clinical need; we used samples from these patients in the prospective phase.

We conducted analytical validation (*12*) and statistical analysis using Stata version 15.1 (StataCorp LLC., https://www.stata.com) (Appendix). We considered a 2-tailed $p<0.05$ to be significant. This study was approved by the Stanford Institutional Review Board (protocol no. 48973).

In total, we analyzed specimens from 146 patients: 93 in the retrospective phase and 53 in the prospective

Author affiliations: Stanford University School of Medicine, Stanford, California, USA (C.A. Hogan, C. Huang, M.K. Sahoo, H. Wang, M. Holubar, R. Mathew, J. Zehnder, B.A. Pinsky); Stanford Health Care, Stanford (C.A. Hogan, B. Jiang, M. Sibai, B.A. Pinsky)

DOI: https://doi.org/10.3201/eid2702.204168

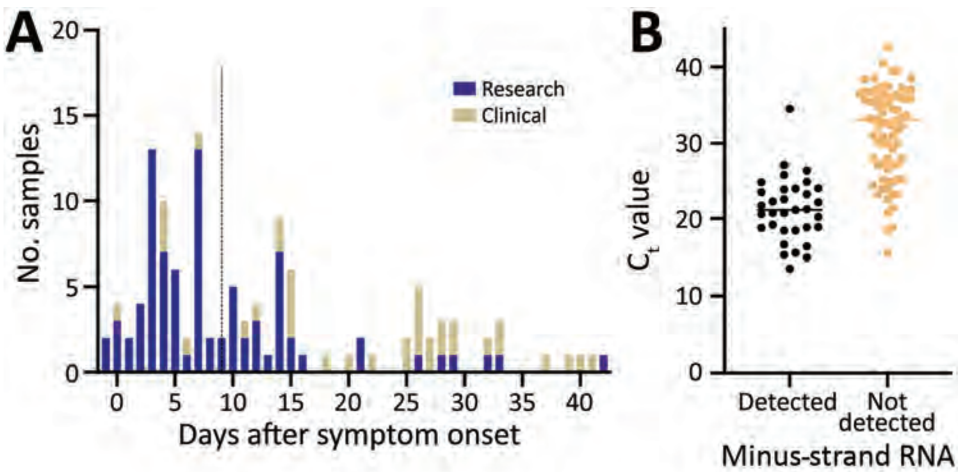


**Figure 1.** Frequency distribution of days between symptom onset and testing in study on strand-specific real-time reverse transcription PCR for detection of replicating severe acute respiratory syndrome coronavirus 2, California, USA, 2020. Dashed line indicates the median number of days since symptom onset. B) Distribution of standard real-time reverse transcription PCR cycle threshold values by results of strand-specific real-time reverse transcription PCR. Horizontal line indicates median.

phase (Appendix Tables 3, 4). The median age was 50 years (interquartile range 36–63 years); 73 (50.0%) were women, 26 (17.8%) were immunocompromised, and 30 (20.5%) were admitted to the intensive care unit for coronavirus disease during the course of the study (Table 1). Samples were collected a median of 9 days (interquartile range 4–18 days) after symptom onset (Figure 1, panel A). We detected minus-strand RNA in 41 (28.1%) patients. The median $C_t$ value of samples with detected minus-strand RNA (20.7) was significantly lower than those in which the minus strand was not detected (33.2; $p<0.01$) (Figure 1, panel B). The results of this strand-specific assay were closely correlated with the standard rRT-PCR results (Figure 2, panels A, B). The ratio of minus:plus strands varied by patient within 14 days after symptom onset (Appendix Figure 2).

We detected the minus strand in 7 patients in the prospective cohort (Table 1, https://wwwnc.cdc.gov/EID/article/27/2/20-4168-T1.htm). Two of these patients were nonimmunocompromised inpatients tested >10 days after symptom onset, including 1 who had been asymptomatic for >48 hours; the $C_t$ values for these samples were 39.0 and 38.6. We detected minus-strand SARS-CoV-2 RNA up to 30 days after symptom onset in an immunocompromised patient with persistent fever. For 2 patients in the prospective cohort, a negative result might have facilitated the approval of medical procedures despite prolonged positive results by standard rRT-PCR (Appendix).

## Conclusions

We described the performance of a 2-step strand-specific rRT-PCR for detection of SARS-CoV-2. The assay identified viral replication in patients with persistent positive results by standard rRT-PCR, possibly facilitating clinical decision-making.

Other assays that assess intermediates of viral replication, such as subgenomic RNA, have emerged in the literature (*5*,*13*). Perera et al. demonstrated high correlation between levels of presumptive SARS-CoV-2 active replication intermediates and standard rRT-PCR $C_t$ values (*13*). The standard SARS-CoV-2 rRT-PCR is appropriate for most routine clinical diagnostic applications. However, because this assay does not determine whether SARS-CoV-2 is actively replicating, it cannot infer infectiousness in samples with mid-level $C_t$ values (i.e., $C_t$ 25–35).

We detected minus-strand RNA up to 30 days after symptom onset, which is longer than the 14-day period previously reported for subgenomic RNA (*13*),

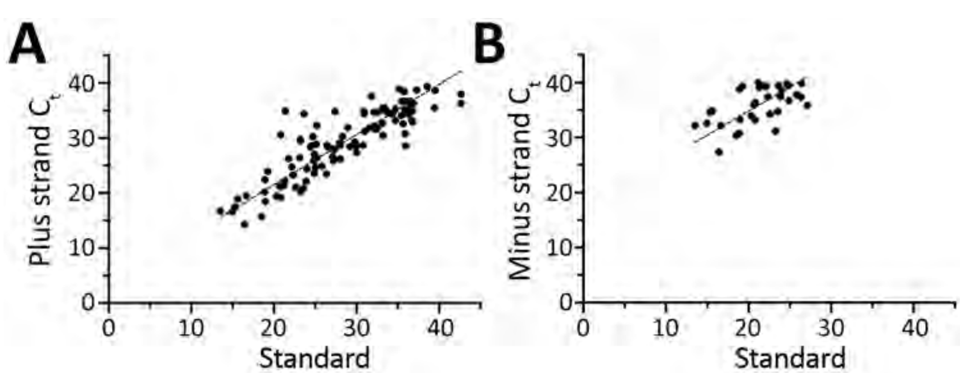


**Figure 2.** Deming regression analysis of $C_t$ values by strand-specific real-time reverse transcription PCR as a function of the $C_t$ values by standard real-time reverse transcription PCR for severe acute respiratory syndrome coronavirus 2. Results of PCR for plus strand (A; y = 0.91x + 3.26) and minus strand (B; y = 0.88x + 17.30). $C_t$, cycle threshold.

**Table 2.** Clinical characteristics of 7 patients with detected SARS-CoV-2 minus-strand RNA, California, USA, 2020*

| Patient ID | Age, y/sex | Immuno-compromised | Test order | Cycle threshold value for standard rRT-PCR specific to SARS-CoV-2 | Days after symptom onset | Symptomatic improvement at time of strand-specific testing† | Fever within 24 h of strand-specific testing | Minus strand detected beyond CDC isolation recommendations‡ |
|---|---|---|---|---|---|---|---|---|
| 102 | 75/M | No | 1 | 33.5 | Unclear | Unclear§ | No | Unclear |
| | | | 2 | 19.7 | Unclear | Unclear§ | No | Unclear |
| 111 | 58/M | Yes | 1 | NA¶ | 26 | No | Yes | No |
| 117 | 82/M | No | 1 | 18.5 | 12 | Unclear§ | No | Yes |
| 118 | 69/M | No | 1 | 20.8 | 4 | No | Yes | No |
| 127 | 61/M | No | 1 | 34.5 | 11 | Yes | No | Yes |
| 129 | 60/M | Yes | 1 | 22.6 | 18 | No | Yes | No |
| | | | 2 | 20.2 | 30 | No | Yes | No |
| 141 | 2/F | Yes | 1 | 18.1 | NA# | NA# | NA# | NA# |

*ID, identification; NA, not available; rRT-PCR, real-time reverse transcription PCR; SARS-CoV-2, severe acute respiratory syndrome coronavirus 2.
†From symptom onset to time of testing.
‡According to recommendations from the Centers for Disease Control and Prevention (*14*).
§Because of underlying condition.
¶Qualitative testing conducted at external reference laboratory.
#Data not available because patient was treated at external medical facility.

and 8–15 day period for viral culture (*3*–*6*,*13*). We detected minus-strand RNA in 2 patients beyond the typical period recommended for isolation. Isolation strategies on the basis of time and symptoms are simple to apply, reduce the number of tests that need to be conducted, thus saving resources, and are probably effective at a population level (*14*). However, it can be challenging to determine the infectiousness of patients in certain clinical contexts, such as immunocompromised hosts with persistent viral shedding, on the basis of time and symptoms alone. Tools such as strand-specific RNA testing might be helpful in determining the infectiousness of these patients. Strand-specific testing might also help avoid delays in required procedures or treatments such as chemotherapy, which might be postponed because of SARS-CoV-2–positive PCR results.

This study has several strengths, including a large patient cohort and analytical validation. This strand-specific assay is useful because it can be adapted for routine clinical laboratory testing, does not require emergency use authorization, and reports $C_t$ values and strand-specific RNA detection. The study was limited by its single-center design and combination of 2 patient cohorts chosen using different selection techniques. The assay lacks viral culture data and is hampered by longer turnaround time and complexity. In future studies, we will validate this assay against SARS-CoV-2 viral culture and within a household transmission study.

In summary, we described the test performance and clinical feasibility of a strand-specific rRT-PCR assay for SARS-CoV-2. Strand-specific rRT-PCR testing might be especially useful in patients with prolonged RNA shedding. It might also supplement existing strategies for estimating infectiousness on the basis of time and symptoms. Further work is required to correlate these findings with viral culture, compare different strand-specific RNA detection methods, and to assess clinical utility in large and longitudinal patient cohorts. These findings might improve understanding of the infectiousness of SARS-CoV-2, enabling optimization of infection control measures and resource use.


### Acknowledgments

We thank the staff from the Stanford Clinical Virology Laboratory for their testing of samples.


### About the Author

Dr. Hogan is a medical microbiologist in the Department of Pathology, Stanford University, Palo Alto, CA. Her research interests include novel and point-of-care diagnostics, clinical impact of diagnostic methods, and global health.

### References


1. Gombar S, Chang M, Hogan CA, Zehnder J, Boyd S, Pinsky BA, et al. Persistent detection of SARS-CoV-2 RNA in patients and healthcare workers with COVID-19. J Clin Virol. 2020;129:104477. https://doi.org/10.1016/j.jcv.2020.104477
2. Sun J, Xiao J, Sun R, Tang X, Liang C, Lin H, et al. Prolonged persistence of SARS-CoV-2 RNA in body fluids. Emerg Infect Dis. 2020;26:1834–8. https://doi.org/10.3201/eid2608.201097
3. Bullard J, Dust K, Funk D, Strong JE, Alexander D, Garnett L, et al. Predicting infectious severe acute respiratory syndrome coronavirus 2 from diagnostic samples. Clin Infect Dis. 2020;ciaa638. https://doi.org/10.1093/cid/ciaa638
4. La Scola B, Le Bideau M, Andreani J, Hoang VT, Grimaldier C, Colson P, et al. Viral RNA load as determined by cell culture as a management tool for discharge of SARS-CoV-2 patients from infectious disease wards. Eur J Clin Microbiol Infect Dis. 2020;39:1059–61. https://doi.org/10.1007/s10096-020-03913-9
5. Wölfel R, Corman VM, Guggemos W, Seilmaier M, Zange S, Müller MA, et al. Virological assessment of hospitalized patients with COVID-2019. Nature. 2020;581:465–9. https://doi.org/10.1038/s41586-020-2196-x

6. Jeong HW, Kim SM, Kim HS, Kim YI, Kim JH, Cho JY, et al. Viable SARS-CoV-2 in various specimens from COVID-19 patients. Clin Microbiol Infect. 2020;26:1520–4. https://doi.org/10.1016/j.cmi.2020.07.020
7. Tom MR, Mina MJ. To interpret the SARS-CoV-2 test, consider the cycle threshold value. Clin Infect Dis. 2020;71:2252–4. https://doi.org/10.1093/cid/ciaa619
8. Sztuba-Solińska J, Stollar V, Bujarski JJ. Subgenomic messenger RNAs: mastering regulation of (+)-strand RNA virus life cycle. Virology. 2011;412:245–55. https://doi.org/10.1016/j.virol.2011.02.007
9. Sawicki SG, Sawicki DL, Siddell SG. A contemporary view of coronavirus transcription. J Virol. 2007;81:20–9. https://doi.org/10.1128/JVI.01358-06
10. Hogan CA, Sahoo MK, Huang C, Garamani N, Stevens B, Zehnder J, et al. Comparison of the Panther Fusion and a laboratory-developed test targeting the envelope gene for detection of SARS-CoV-2. J Clin Virol. 2020;127:104383. https://doi.org/10.1016/j.jcv.2020.104383
11. U.S. Food and Drug Administration. Stanford Health Care Clinical Virology Laboratory SARS-CoV-2 test EUA Summary. 2020 Nov 24 [cited 2020 Dec 2]. https://www.fda.gov/media/136818/download
12. Chesher D. Evaluating assay precision. Clin Biochem Rev. 2008;29:S23–6.
13. Perera RAPM, Tso E, Tsang OTY, Tsang DNC, Fung K, Leung YWY, et al. SARS-CoV-2 virus culture and subgenomic RNA for respiratory specimens from patients with mild coronavirus disease. Emerg Infect Dis. 2020;26:2701–4. https://doi.org/10.3201/eid2611.203219
14. U.S. Centers for Disease Control and Prevention. Discontinuation of Transmission-Based Precautions and Disposition of Patients with COVID-19 in Healthcare Settings (Interim Guidance). 2020 [cited 2020 Sep 13]. https://www.cdc.gov/coronavirus/2019-ncov/hcp/disposition-hospitalized-patients.html


Address for correspondence: Benjamin A. Pinsky, Stanford University School of Medicine, 3375 Hillview Avenue, Room 2913, Palo Alto, CA 94304, USA; email: bpinsky@stanford.edu

# Seroprevalence of SARS-CoV-2 in Guilan Province, Iran, April 2020

Maryam Shakiba, Maryam Nazemipour, Arsalan Salari, Fardin Mehrabian, Seyed Saeed Hashemi Nazari, Seyed Mahmoud Rezvani, Zahra Ghasempour, Abtin Heidarzadeh, Mohammad Ali Mansournia

Author affiliations: Guilan University of Medical Sciences, Rasht, Iran (M. Shakiba, A. Salari, F. Mehrabian, S.M. Rezvani, Z. Ghasempour, A. Heidarzadeh); Iran University of Medical Sciences, Tehran, Iran (M. Nazemipour); Shahid Beheshti University of Medical Sciences, Tehran (S.S. Hashemi Nazari); Tehran University of Medical Sciences, Tehran (M.A. Mansournia)

DOI: https://doi.org/10.3201/eid2702.201960

We determined the seroprevalence of severe acute respiratory syndrome coronavirus 2 (SARS-CoV-2) in an affected area in northern Iran in April 2020. Antibodies to SARS-CoV-2 were detected in 528 persons by using rapid tests. Adjusted prevalence of SARS-CoV-2 seropositivity was 22.2% (95% CI 16.4%–28.5%).

Coronavirus disease (COVID-19) was first reported in China and has now spread throughout the world. Global estimates of disease spread are based on confirmed cases in symptomatic patients (*1*). However, these estimates do not accurately reflect actual infection rates in the community because they exclude persons with mild or no symptoms or for whom testing is unavailable. Knowledge about actual infection rates is vital for accurately estimating the case-fatality rate, a public health measure of COVID-19 (*2*), and for projecting the course of the pandemic and determining public policy guidelines (*3*).

Guilan Province was the second-largest province in Iran to have multiple confirmed cases of COVID-19 soon after the beginning of the pandemic. The epidemic curve has subsided in this province, making it an appropriate location to test for the presence of past infections through a seroprevalence survey. In this study, we provided a population-based seropositivity estimate of severe acute respiratory syndrome coronavirus 2 (SARS-CoV-2) infection based on World Health Organization protocol.

We conducted a cross-sectional population-based study among persons in Guilan Province during April 11–19, 2020. The study was approved by the Institutional Review Board of Guilan University of Medical Sciences (Rasht, Iran). All persons living in a household, regardless of age, were invited through multistage cluster random sampling. We selected clusters from the list of Comprehensive Healthcare Centers (CHCs) (the top units of the healthcare network in Iran) and used simple random sampling method to select households from those covered by CHCs. On the day participants arrived at the CHC, we took 10 µL capillary blood samples from each participant and collected information on demographics, disease history, COVID-19 symptoms in previous 3 months, and history of SARS-CoV-2 exposure. Samples were tested by using VivaDiag Rapid test kit (VivaChek, https://www.vivachek.com) for a SARS-CoV-2–specific serologic assay.

The design-adjusted prevalence of seropositivity was estimated by using inverse probability weighting with weights equal to the inverse of probability of selection for each participant (*4*). The prevalence estimates were then adjusted for test characteristics. We used a Monte Carlo bias analysis with 100,000 samples for sensitivity of 83.3% and specificity of 99% for IgM or IgG (*5*,*6*). The number of infections was calculated by multiplying infection prevalence by total population of Guilan Province. All analyses were performed in Stata version 14 (Stata, https://www.stata.com). Additional information about methods and results has been provided in the Appendix (https://wwwnc.cdc.gov/EID/article/27/2/20-1960-App1.pdf).

Of 632 households contacted, 196 households, consisting of a total of 551 persons, participated in this study. Eleven of those 551 participants refused blood sampling and could not be tested, and 12 had invalid test results. Of the remaining 528 participants, 117 were positive for either IgM or IgG (22.1% [95% CI 0.19%–0.26%]). Adjusted for design and test performance, prevalence was 22.2% (95% CI 16.4%–28.5%).

Seropositivity prevalence estimates varied most substantially according to age group, occupation, presence of COVID-19 symptoms in the previous 3 months, and county of residence (Table). Office workers had the highest prevalence of SARS-CoV-2 infection, followed by taxi drivers. Among counties, the highest prevalence of seropositivity was in Anzali, followed by Rasht.

In this study, the seroprevalence estimate of SARS-CoV-2 antibodies after adjusting for population and test characteristics was 22.2%. This result is much higher than those for previous seroprevalence estimates using an immunoassay test to detect antibodies in Spain (*7*); California, USA (*8*); and Geneva, Switzerland (*9*). Unlike Guilan Province, those places enacted severe lockdown policies to

**Table.** Severe acute respiratory syndrome coronavirus 2 seropositivity prevalence estimates according to study variables, Guilan Province, Iran, April 2020*

| Characteristic | Sample size (%), N = 528 | No. positive | Design-adjusted prevalence (95% CI) | Design- and test performance–adjusted prevalence (95% CI†) |
|---|---|---|---|---|
| Sex | | | | |
| M | 257 (48.7) | 55 | 16.8 (13.2–21.2) | 19.0 (12.7–25.4) |
| F | 271 (51.3) | 62 | 22.2 (14.7–32.1) | 25.6 (15.4–36.8) |
| Age group, y | | | | |
| <5 | 26 (4.9) | 4 | 8.7 (2.1–30.2) | 9.8 (0.9–22.6) |
| 5–17 | 101 (19.1) | 20 | 17.0 (11.6–24.2) | 19.1 (11.2–27.5) |
| 18–59 | 329 (62.3) | 74 | 21.0 (16.9–25.8) | 24.1 (17.5–31.6) |
| ≥60 | 72 (13.6) | 19 | 22.4 (15.7–31.0) | 25.7 (16.6–36.1) |
| Obesity, BMI >30 | | | | |
| No | 474 (89.8) | 107 | 19.8 (16.9–22.9) | 22.6 (16.8–29.0) |
| Yes | 54 (10.2) | 10 | 15.4 (7.8–28.2) | 17.3 (6.2–29.0) |
| SARS-CoV-2 exposure history | | | | |
| No | 452 (85.6) | 95 | 18.1 (12.7–25.1) | 20.4 (12.6–28.8) |
| Yes | 76 (14.4) | 22 | 26.9 (13.5–46.5) | 31.2 (13.4–50.8) |
| COVID-19 symptoms in previous 3 mo | | | | |
| No | 382 (69.3) | 65 | 15.3 (11.03–20.9) | 17.2 (10.3–24.1) |
| Yes | 169 (30.7) | 52 | 30.05 (25.3–36.4) | 35.5 (27.8–45.8) |
| Underlying condition | | | | |
| No | 420 (79.5) | 89 | 18.2(13.6–24.03) | 20.7 (13.5–28.3) |
| Yes | 108 (20.5) | 28 | 25.3 (18.3–33.9) | 29.2 (19.8–40.2) |
| Place of residence | | | | |
| Village | 162 (30.7) | 38 | 21.0 (16.0–27.1) | 24.0 (16.5–32.4) |
| Town | 366 (69.3) | 79 | 19.2 (16.0–23.0) | 21.9 (15.8–28.4) |
| Occupation‡ | | | | |
| Employee | 53 (10.04) | 19 | 46.0 (35.9–56.5) | 54.3 (41.8–71.1) |
| Housekeeper | 159 (30.1) | 39 | 21.8 (13.4–33.5) | 25.0 (13.6–37.5) |
| Student | 114 (21.6) | 22 | 15.6 (12.1–20.0) | 17.5 (11.3–23.7) |
| Unemployed | 67 (12.7) | 11 | 11.8 (7.6–18.0) | 12.9 (5.9–19.6) |
| Farmer | 16 (3.03) | 3 | 17.4 (9.9–28.8) | 19.7 (9.1–31.0) |
| Salesman | 46 (8.7) | 5 | 7.9 (2.0–26.7) | 8.7 (0.8–20.0) |
| Healthcare personnel | 43 (8.1) | 12 | 13.2 (6.5–24.9) | 14.5 (4.5–25.0) |
| Taxi driver | 13 (2.5) | 5 | 24.0 (7.1–56.7) | 28.0 (4.5–56.3) |
| Worker | 17 (3.2) | 1 | 2.5 (0.1–32.1) | 28.0 (4.5–56.3) |
| County | | | | |
| Rasht | 226 (42.8) | 56 | 20.8 (19.7–21.9) | 23.7 (18.6–29.6) |
| Anzali | 75 (14.2) | 23 | 30.0 (29.7–30.4) | 34.8 (29.7–43.2) |
| Astara | 78 (14.8) | 12 | 15.4 (14.3–16.6) | 17.4 (12.0–21.8) |
| Lahijan | 74 (14) | 12 | 15.0 (13.6–16.5) | 16.9 (11.5–21.4) |
| Rudbar | 75 (14.2) | 14 | 17.7 (15.5–20.2) | 20.1 (14.5–25.7) |

*BMI, body mass index; COVID-19, coronavirus disease 2019; SARS-CoV-2, severe acute respiratory syndrome coronavirus 2.
†Calculated using Monte Carlo simulation method.
‡Employee was defined as a government employee working in an office. Worker was defined as a person performing manual jobs in nongovernmental locations.

contain the pandemic, which might explain the higher prevalence of infection in our study.

Our study's limitations include possible selection bias if persons with previous COVID-19–like symptoms sought to participate in the study. However, in our study only 11 participants had a history of COVID-19 diagnosis. Otherwise, bias toward persons in good health who could participate in the study might result in an underestimation of actual prevalence. In addition, household sampling might result in an overestimation of prevalence compared with random sampling of persons because of clustering of infection in household contacts. We excluded persons in institutional residences (i.e., nursing homes, boarding schools, and prisons), for whom close contact with others might increase risk for infection, resulting in an underestimation of actual prevalence. Finally, our study used rapid test kits that have lower sensitivity than the ELISA test method, particularly for patients in the acute phase of infection. However, the study was designed to detect previous infection in healthy persons, in whom the test has better sensitivity.

In conclusion, our findings imply that ≈518,000 persons in Guilan Province may have been infected with SARS-COV-2 as of April 19, 2020, which is substantially higher than the 1,600 cumulative confirmed cases recorded. As of May 3, if we assume a 3-week lag from time of infection to death (*10*), 625 persons had died of confirmed COVID-19 in Guilan Province. This number would correspond to an infection-fatality rate of 0.12%.

## Acknowledgments

The authors are grateful to all healthcare centers' employees and personnel for cooperating and conducting the survey, as well as to all participants who took part in this research.

This research was supported by a grant from Iran's Ministry of Health and Deputy of Research at Guilan University of Medical Sciences.


## About the Author

Dr. Shakiba is an epidemiologist and faculty member at Guilan University of Medical Sciences. Her research interests include survey design and causal inference methodology.


## References

1. World Health Organization. Coronavirus disease (COVID-19) situation reports 2020 [cited 2020 Aug 10]. https://www.who.int/emergencies/diseases/novel-coronavirus-2019/situation-reports
2. Russell TW, Hellewell J, Jarvis CI, van Zandvoort K, Abbott S, Ratnayake R, et al.; Cmmid Covid-Working Group. Estimating the infection and case fatality ratio for coronavirus disease (COVID-19) using age-adjusted data from the outbreak on the Diamond Princess cruise ship, February 2020. Euro Surveill. 2020;25:2000256. https://doi.org/10.2807/1560-7917.ES.2020.25.12.2000256
3. Clapham H, Hay J, Routledge I, Takahashi S, Choisy M, Cummings D, et al. Seroepidemiologic study designs for determining SARS-COV-2 transmission and immunity. Emerg Infect Dis. 2020;26:1978–86. https://doi.org/10.3201/eid2609.201840
4. Mansournia MA, Altman DG. Inverse probability weighting. BMJ. 2016;352:i189. https://doi.org/10.1136/bmj.i189
5. Cassaniti I, Novazzi F, Giardina F, Salinaro F, Sachs M, Perlini S, et al.; Members of the San Matteo Pavia COVID-19 Task Force. Performance of VivaDiag COVID-19 IgM/IgG Rapid Test is inadequate for diagnosis of COVID-19 in acute patients referring to emergency room department. J Med Virol. 2020;92:1724–7. https://doi.org/10.1002/jmv.25800
6. Van Elslande J, Houben E, Depypere M, Brackenier A, Desmet S, André E, et al. Diagnostic performance of seven rapid IgG/IgM antibody tests and the Euroimmun IgA/IgG ELISA in COVID-19 patients. Clin Microbiol Infect. 2020;26:1082–7. https://doi.org/10.1016/j.cmi.2020.05.023
7. Pollán M, Pérez-Gómez B, Pastor-Barriuso R, Oteo J, Hernán MA, Pérez-Olmeda M, et al.; ENE-COVID Study Group. Prevalence of SARS-CoV-2 in Spain (ENE-COVID): a nationwide, population-based seroepidemiological study. Lancet. 2020;396:535–44. https://doi.org/10.1016/S0140-6736(20)31483-5
8. Sood N, Simon P, Ebner P, Eichner D, Reynolds J, Bendavid E, et al. Seroprevalence of SARS-CoV-2-specific antibodies among adults in Los Angeles County, California, on April 10–11, 2020. JAMA. 2020;323:2425–7. https://doi.org/10.1001/jama.2020.8279
9. Stringhini S, Wisniak A, Piumatti G, Azman AS, Lauer SA, Baysson H, et al. Seroprevalence of anti-SARS-CoV-2 IgG antibodies in Geneva, Switzerland (SEROCoV-POP): a population-based study. Lancet. 2020;396:313–9. https://doi.org/10.1016/S0140-6736(20)31304-0
10. Bhatraju PK, Ghassemieh BJ, Nichols M, Kim R, Jerome KR, Nalla AK, et al. Covid-19 in critically ill patients in the Seattle region—case series. N Engl J Med. 2020;382:2012–22. https://doi.org/10.1056/NEJMoa2004500



Address for correspondence: Mohammad Ali Mansournia, 5th Fl, Building of School of Public Health, Tehran University of Medical Sciences, Poursina St, 16 Azar St, Tehran 14155-6446, Iran; email: mansournia_ma@yahoo.com; Abtin Heidarzadeh, Pasdaran St, Deputy of Health, Guilan University of Medical Sciences, Rasht 41937-13111, Iran; email: heidarzadeh@gums.ac.ir


# Intrauterine Transmission of SARS-CoV-2


Emanuele Therezinha Schueda Stonoga,[1] Laura de Almeida Lanzoni,[1] Patricia Zadorosnei Rebutini,[1] André Luiz Permegiani de Oliveira, Jullie Anne Chiste, Cyllian Arias Fugaça, Daniele Margarita Marani Prá, Ana Paula Percicote, Andrea Rossoni, Meri Bordignon Nogueira, Lucia de Noronha, Sonia Mara Raboni

Author affiliations: Hospital de Clínicas da Universidade Federal do Paraná, Parana, Brazil (E.T.S. Stonoga, L.A. Lanzoni, J.A. Chiste, C.A. Fugaça, M.B. Nogueira); Pontifícia Universidade Católica do Paraná, Parana (P.Z. Rebutini, A.L.P. Oliveira, D.M. Marani Prá, L. de Noronha); Universidade Federal do Paraná, Parana (A.P. Percicote, A. Rossoni, S.M. Raboni)


DOI: https://doi.org/10.3201/eid2702.203824

We documented fetal death associated with intrauterine transmission of severe acute respiratory syndrome coronavirus 2. We found chronic histiocytic intervillositis, maternal and fetal vascular malperfusion, microglial hyperplasia, and lymphocytic infiltrate in muscle in the placenta and fetal tissue. Placenta and umbilical cord blood tested positive for the virus by PCR, confirming transplacental transmission.

[1]These first authors contributed equally to this article.

A woman 42 years of age at 27 weeks' gestation sought treatment at Hospital de Clínicas da Universidade Federal do Paraná, Parana, Brazil, for symptoms of coronavirus disease (COVID-19). Dyspnea, dry cough, high temperature (38.5°C), anosmia, nausea, vomiting, and diarrhea had developed 2 days before hospitalization. At admission, we collected a nasopharyngeal swab sample and tested it for severe acute respiratory syndrome coronavirus 2 (SARS-CoV-2) and rhinovirus by reverse transcription PCR (RT-PCR) (XGEN MASTER COVID-19 Kit; Mobius Life Science, Inc, https://mobiuslife.com.br) (Appendix Figure 1, https://wwwnc.cdc.gov/EID/article/27/2/20-3824-App1.pdf). The sample tested positive for both viruses. We prescribed azithromycin, oseltamivir, prophylactic enoxaparin, and corticosteroids for fetal lung maturation. A chest computed tomography scan revealed bilateral ground glass opacities and interlobular septal thickening. After 4 days, the patient needed ventilatory and hemodynamic support.

The patient's prenatal care had been uneventful. She had undergone routine tests and ultrasound scans; the most recent had been at 25 weeks' gestation. Her medical history included a previous pregnancy complicated by hypertension that resolved with delivery. The current pregnancy was her seventh; she previously had delivered 3 children and had 2 abortions and 1 ectopic pregnancy.

Six days after admission, obstetric ultrasound demonstrated a single intrauterine pregnancy. The fetus was in a transverse position with shoulder presentation; the ultrasound showed reduced amniotic fluid volume and absence of fetal movements and heart rate. Because misoprostol failed to induce labor, we conducted a cesarean delivery. The fetus was stillborn. Immediately after delivery, we used an aseptic technique to collect samples of amniotic fluid (before amniotic membranes ruptured), umbilical cord blood, placental membranes, and cotyledon fragments (Table).

We obtained informed written consent for fetal autopsy, placental grossing, and histologic examination. External examination showed a female concept with skin discoloration and moderate peeling; the fetus had gestational age of ≈28 weeks and weighed 1,020 g (50th percentile). Internal examination revealed red serous effusions in the chest and abdomen and petechial hemorrhage in the heart and lungs. We conducted evisceration using the Letulle method and separated the organs into functional groups. We noted hepatic discoloration and friability and lung and kidney hypoplasia (both <5th percentile). We did not identify other macroscopic abnormalities.

The placental disc was round, and had tan and glistening membranes peripherally attached. The umbilical cord had 3 vessels; it was 28 cm long, inserted eccentrically, and under coiled. The fetal surface was gray with normal chorionic plate vessels. The trimmed placental disc weighed 135 g and measured 12 × 12 cm (<3rd percentile) (Appendix Figure 2). We collected additional samples of fetal liver, spleen, lung, central nervous system tissue, ovary, and muscle for RT-PCR (Table). Tissue samples were fixed in 10% buffered formalin, routinely processed, stained in hematoxylin and eosin, and underwent immunohistochemical staining using CD68 antibodies (Figure; Appendix Figure 2).

Few reports have described the effects of SARS-CoV-2 infection in utero; because pathogen detection requires multiple samples, it has been difficult to characterize congenital infection (*1*,*2*). According to Shah et al. (*3*), congenital SARS-CoV-2 infection can be confirmed by PCR of placental tissue. We detected

**Table.** Results of PCR for severe acute respiratory syndrome coronavirus 2 in a pregnant woman and fetus, Brazil, 2020*

| | | Cycle threshold† | | |
|---|---|---|---|---|
| Sample | Day | ORF1ab | N | RNaseP‡ |
| Maternal nasopharyngeal swab sample | 0 | 21.0 | 24.0 | 23.0 |
| Maternal nasopharyngeal swab sample | 4 | 20.9 | 24.8 | 29.9 |
| Umbilical cord blood | 8 | 31.9 | 30.3 | 27.0 |
| Placenta§ | 8 | 24.5 | 25.5 | 25.6 |
| Fetal liver | 9 | Undetectable | Undetectable | 29.0 |
| Fetal spleen | 9 | Undetectable | Undetectable | 27.8 |
| Fetal lungs | 9 | Undetectable | Undetectable | 25.7 |
| Fetal central nervous system | 9 | Undetectable | Undetectable | 29.4 |
| Fetal skeletal muscle | 9 | Undetectable | Undetectable | 26.5 |
| Fetal heart | 9 | Undetectable | Undetectable | 26.5 |
| Fetal ovary | 9 | Undetectable | Undetectable | 25.4 |

*PCR conducted using XGEN MASTER COVID-19 Kit (Mobius Life Science, Inc, https://mobiuslife.com.br). N, nucleocapsid protein gene; ORF, open reading frame.
†Cycle threshold value is considered positive if both viral genes are <38.
‡PCR is selective for human RNaseP gene as a control for sample integrity.
§Insufficient sample.

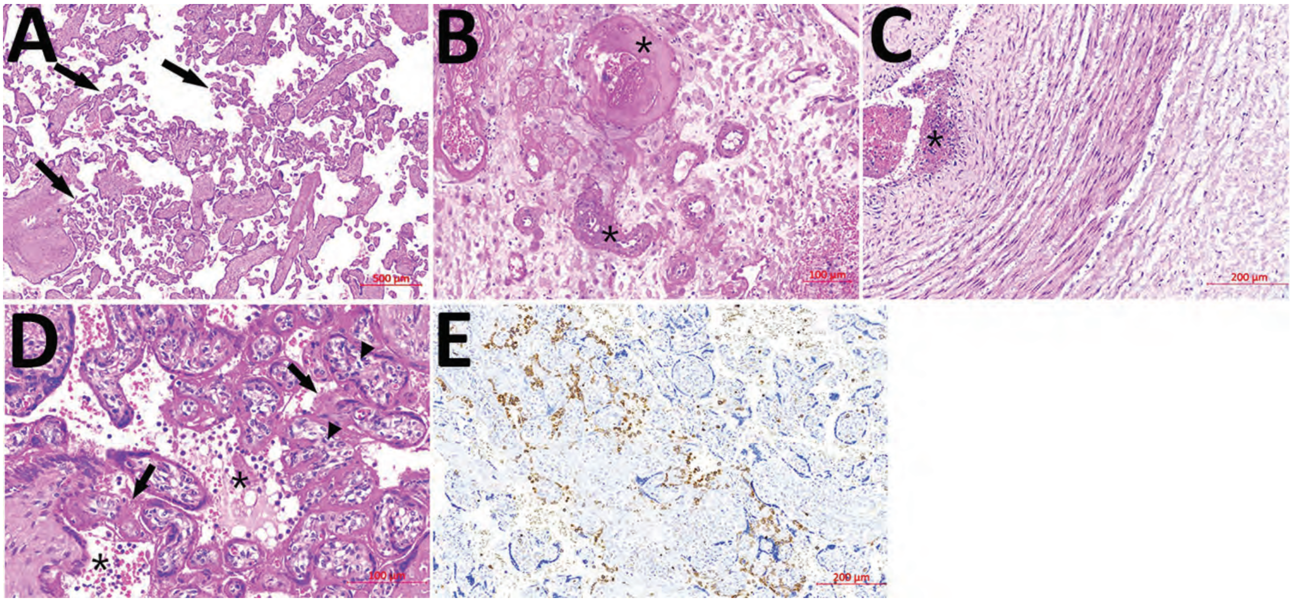


**Figure.** Histologic sections from the placenta of stillborn fetus of a woman with severe acute respiratory syndrome coronavirus 2 infection, Brazil, 2020. Tissue stained with hematoxylin and eosin. A) Placenta shows accelerated villous maturation with increase in syncytial knots. Black arrows indicate small or short hyper mature villi. B) Membranes and basal decidua show decidual arteriopathy, including fibrinoid necrosis with foam cells, mural hypertrophy, absence of spiral artery remodeling, and arterial thrombosis associated with decidual infarct. Asterisks (*) indicate fibrinoid necrosis. C) The umbilical cord shows subendothelial edema and nonocclusive arterial thrombosis, which was also focally observed in a chorionic plate and stem vessels. Asterisks (*) indicate arterial thrombosis. D–E) Photomicrographs show diffuse perivillous fibrin deposition associated with multifocal mononuclear inflammatory infiltrate in the intervillous space and occasional intervillous thrombi. Black arrows indicate fibrin deposition; asterisks (*) indicate mononuclear infiltrate; arrowheads indicate increase in number of Hofbauer cells. E) Immunohistochemical assay using CD68 antibodies highlights histiocyte infiltrate in paraffin-embedded samples (KP1 Clone; Biocare Medical LLC, https://biocare.net).

SARS-CoV-2 RNA in cotyledon samples, membranes, and umbilical cord blood aspirate, suggesting a breakdown of the placental barrier and fetal intrauterine viremia. We used immunohistochemical staining with CD68 antibodies to identify multifocal chronic histiocytic intervillositis in the placenta (Figure, panels D, E). This condition was also described in other pregnant women with COVID-19 (*4*,*5*). We also noted microglial hyperplasia, mild lymphocytic infiltrate, and edema in skeletal muscle (Appendix Figure 3). These findings might suggest infection. However, all fetal tissue samples tested negative for SARS-CoV-2 RNA (Table). Other findings might have been caused by intrauterine asphyxia (Appendix Figure 3).

COVID-19 is associated with cytokine storm, an exaggerated inflammatory response that is usually indicative of disease severity (*6*). Excessive inflammation could cause endothelial damage and disrupt the coagulation system; some evidence suggests that thrombotic and microvascular injury might affect manifestations of COVID-19 (*7*,*8*). We noted severe maternal vascular malperfusion injuries in the placenta, including substantial recent infarcts, decidual vasculopathy, accelerated villous maturation, and low placental weight. Similar findings are often observed in placentas from women with hypertensive disorders and have been associated with oligohydramnios, preterm birth, and stillbirth. Although the patient's blood pressure was within reference limits, her age and history of gestational hypertension are risk factors for such alterations and the probable cause of placental insufficiency and fetal demise (*9*,*10*). We also observed multifocal small intervillous thrombi and focal thrombosis of fetal placental vessels. Therefore, the extent and apparently rapid development of these findings suggests that infection contributed to vascular damage.

The effects of congenital transmission of SARS-CoV-2 remain largely unknown. This study highlights the need for placental and fetal gross and microscopic evaluation, which can help elucidate the pathophysiology of COVID-19.

## About the Author

Dr. Stonoga is a first-year pathology resident at Hospital de Clínicas da Universidade Federal do Paraná, Parana. Her research interests include perinatal pathology and infectious disease research.

## References


1. Alzamora MC, Paredes T, Caceres D, Webb CM, Valdez LM, La Rosa M. Severe COVID-19 during pregnancy and possible vertical transmission. Am J Perinatol. 2020;37:861–5. https://doi.org/10.1055/s-0040-1710050
2. Kirtsman M, Diambomba Y, Poutanen SM, Malinowski AK, Vlachodimitropoulou E, Parks WT, et al. Probable congenital SARS-CoV-2 infection in a neonate born to a woman with active SARS-CoV-2 infection. CMAJ. 2020;192:E647–50. https://doi.org/10.1503/cmaj.200821
3. Shah PS, Diambomba Y, Acharya G, Morris SK, Bitnun A. Classification system and case definition for SARS-CoV-2 infection in pregnant women, fetuses, and neonates. Acta Obstet Gynecol Scand. 2020;99:565–8. https://doi.org/10.1111/aogs.13870
4. Sisman J, Jaleel MA, Moreno W, Rajaram V, Collins RRJ, Savani RC, et al. Intrauterine transmission of SARS-COV-2 infection in a preterm infant. Pediatr Infect Dis J. 2020; 39:e265–7.
5. Vivanti AJ, Vauloup-Fellous C, Prevot S, Zupan V, Suffee C, Do Cao J, et al. Transplacental transmission of SARS-CoV-2 infection. Nat Commun. 2020;11:3572. https://doi.org/10.1038/s41467-020-17436-6
6. Huang C, Wang Y, Li X, Ren L, Zhao J, Hu Y, et al. Clinical features of patients infected with 2019 novel coronavirus in Wuhan, China. [Erratum in: Lancet. 2020;395:496]. Lancet. 2020;395:497–506. https://doi.org/10.1016/S0140-6736(20)30183-5
7. Nagashima S, Mendes MC, Camargo Martins AP, Borges NH, Godoy TM, Miggiolaro AFRDS, et al. Endothelial dysfunction and thrombosis in patients with COVID-19—brief report. Arterioscler Thromb Vasc Biol. 2020;40:2404–7. https://doi.org/10.1161/ATVBAHA.120.314860
8. Benhamou D, Keita H, Ducloy-Bouthors AS; CARO working group. Coagulation changes and thromboembolic risk in COVID-19 obstetric patients. Anaesth Crit Care Pain Med. 2020;39:351–3. https://doi.org/10.1016/j.accpm.2020.05.003
9. Shanes ED, Mithal LB, Otero S, Azad HA, Miller ES, Goldstein JA. Placental pathology in COVID-19. Am J Clin Pathol. 2020;154:23–32. https://doi.org/10.1093/ajcp/aqaa089
10. Baergen RN, Heller DS. Placental pathology in Covid-19 positive mothers: preliminary findings. Pediatr Dev Pathol. 2020;23:177–80. https://doi.org/10.1177/1093526620925569


Address for correspondence: Patricia Zadorosnei Rebutini, Postgraduate Program of Health Sciences, Pontifícia Universidade Católica do Paraná, Rua Imaculada Conceição, 1155, Prado Velho, Curitiba, Parana, Brazil; email: patricia.rebutini@hc.ufpr.br

# COVID-19 and Infant Hospitalizations for Seasonal Respiratory Virus Infections, New Zealand, 2020

Adrian Trenholme,[1] Rachel Webb,[1] Shirley Lawrence, Sharon Arrol, Susan Taylor, Shanthi Ameratunga, Catherine A. Byrnes

Author affiliations: Kidz First Children’s Hospital, Auckland, New Zealand (A. Trenholme, R. Webb, S. Lawrence); University of Auckland, Auckland (A. Trenholme, R. Webb, C.A. Byrnes); Department of Health Informatics, Auckland (R. Webb, S. Arrol); Middlemore Hospital, Auckland (S. Arrol, S. Taylor. S. Ameratunga); Population Health Directorate, Auckland (S. Ameratunga); Starship Children’s Health, Auckland (C.A. Byrnes)

DOI: https://doi.org/10.3201/eid2702.204041

In March 2020, a national elimination strategy for coronavirus disease was introduced in New Zealand. Since then, hospitalizations for lower respiratory tract infection among infants <2 years of age and cases of respiratory syncytial or influenza virus infection have dramatically decreased. These findings indicate additional benefits of coronavirus disease control strategies.

In New Zealand, the incidence of hospitalization of infants with lower respiratory tract infection (LRTI) is high. LRTIs disproportionately affect Māori and Pacific Islander children and are predominantly caused by respiratory syncytial virus (RSV) (*1*).

The first case of coronavirus disease (COVID-19) in New Zealand was identified on February 28, 2020. Subsequently, the government pursued an elimination strategy, commencing with a national lockdown on March 25, along with strict international border controls, mandatory 14-day isolation of all international arriving passengers, intensive community testing, school closures, and contact tracing. This strategy seems to have largely succeeded, although recent small clusters of cases in the Auckland region demonstrate continuing vulnerabilities (*2*).

Kidz First Children’s Hospital serves an urban population of ≈550,000 persons in South Auckland, where 50% of infants are of Māori or Pacific Islander ethnicity. Since 2007, clinicians have performed nasopharyngeal sampling for respiratory virus PCR

[1]These first authors contributed equally to this article.

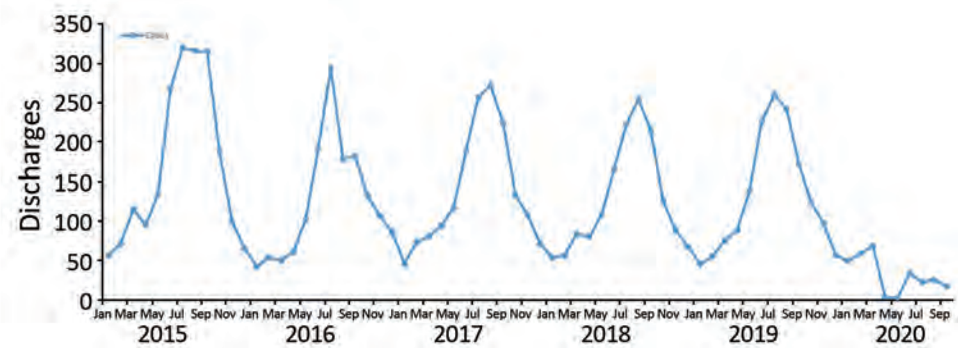


**Figure.** Hospital discharges among children <2 years of age with lower respiratory tract infection, South Auckland, New Zealand, 2015–2019.

when clinically indicated and have participated in the SHIVERS (Southern Hemisphere Influenza Vaccine Effectiveness Surveillance) program of multiplex PCR virus surveillance (*2*). Since March 2020, additional COVID-19 PCR testing has been routinely performed for hospitalized children with respiratory illness. Influenza vaccine, although recommended for pregnant women and high-risk infants and children, is not routinely administered. During winter–spring 2019, a large measles outbreak occurred in Auckland and hospitalizations increased. From 2016 through 2019, a randomized clinical trial of RSV vaccine for pregnant women was conducted with 152 South Auckland mother–infant pairs (*3*).

After COVID-19 lockdown measures were implemented, we observed a marked reduction in hospitalizations of infants for respiratory illness at Kidz First Hospital; the reduction was sustained after gradual easing of the national lockdown beginning on April 27, 2020. To confirm the decrease, we examined respiratory viral PCR test results and infant LRTI hospitalization data from January 1, 2015, through August 31, 2020. We reviewed clinical and laboratory records of infants <2 years of age hospitalized for >3 hours during that time for LRTI (codes J22, A37, J47, J10.0 J10.1 J11.1, J12–16, J20, J21, and J18 from the International Classification of Diseases, 10th Revision). All specimens submitted by a clinician for respiratory viral PCR testing were identified. Re-admissions and duplicate tests were not excluded from this dataset.

Annual numbers of hospitalizations for LRTI during 2015–2019 varied from 1,486 to 2,046. A characteristic winter peak in hospitalizations occurred during July and August; however, from January 1 through August 31, 2020, only 268 admissions were reported, with no winter peak observed (Figure). Numbers of clinician-directed PCR tests performed during March 1–August 31 during the 6-year study period are similar except for increased testing in 2019 during the major measles outbreak (Table). Since March 2020, the numbers of hospitalizations associated with a positive PCR result for RSV (n = 2) and influenza (n = 1) have plummeted; however, hospitalizations for adenovirus and rhinovirus/enterovirus (positive by PCR) have persisted at levels similar to previous years. No hospitalized children have received positive COVID-19 test results.

The New Zealand COVID-19 elimination strategy seems to have halted transmission of seasonal RSV and influenza virus to infants in South Auckland; similar findings have been reported for other populations around the world, focused mainly on influenza reductions (*4*–*8*). The most likely influence on the virtual absence of RSV and influenza disease affecting infants (during what would usually be the peak winter season in New Zealand) is international border controls, including mandatory 14-day isolation of arriving passengers, limiting seasonal virus ingress to the country, although physical distancing and hygiene measures undoubtedly play a part. This hypothesis is further supported by the persistence of rhinovirus/

**Table.** Data for children <2 years of age hospitalized for LRTI, South Auckland, New Zealand, March 1–August 31, 2015–2020*

| Variable | 2015 | 2016 | 2017 | 2018 | 2019 | 2020 |
|---|---|---|---|---|---|---|
| Total hospitalizations for LRTI | 1,249 | 881 | 1,012 | 916 | 1,031 | 159 |
| Total PCR tests for LRTI viruses | 7,259 | 6,642 | 8,876 | 7,676 | 14,881 | 6,735 |
| Positive PCR results | | | | | | |
| RSV | 214 | 224 | 317 | 204 | 388 | 2 |
| Influenza A | 28 | 16 | 56 | 53 | 85 | 1 |
| Influenza B | 11 | 6 | 11 | 1 | 97 | 0 |
| Rhinovirus/enterovirus | 285 | 274 | 378 | 283 | 495 | 252 |
| Adenovirus | 106 | 26 | 83 | 66 | 72 | 41 |

*LRTI, lower respiratory tract infection; RSV, respiratory syncytial virus.

enterovirus infections and lack of rebound of RSV and influenza infections when lockdown measures were gradually eased from late April on. The persistence of disease burdens from viruses that circulate all year suggests that although border controls have prevented entry of the seasonal viruses into the population, community preventive measures have had a more limited effect on the transmission of regional endemic viruses that cause infant hospitalizations.

Our findings are supported by the informative comparison of data across 6 years, during which time the clinician-directed investigation of infants with respiratory infections has remained consistent. Although these preliminary single-center findings need confirmation over a complete year and with national-level surveillance data, they closely align with emerging reports from Alaska, Australia, and Finland (*5*,*8*,*9*).

The current global situation emphasizes the need for ongoing comprehensive respiratory virus surveillance in vulnerable populations, as demonstrated by the unexpected benefit seen locally for Māori and Pacific Islander infants. As the Northern Hemisphere winter approaches, the population-level benefits of substantially reduced RSV and influenza burden may usefully inform policy makers about the merits of different COVID-19 control strategies (*10*).

## Acknowledgments

We acknowledge the Māori and Pacific Islander children of South Auckland and their families who bear an inequitable burden of childhood respiratory disease. We thank the SHIVERS team, particularly Sue Huang and Namrata Prasad, who have contributed to improved understanding of the local pediatric RSV disease burden. We thank colleagues Emma Best, Susan Morpeth, and Conroy Wong for their support. Drs. Wong and Prasad also provided helpful review of the manuscript.

A.T. and S.L. received funding from Novavax and Medimmune corporations during the conduct of the study. R.W. received grants from the Starship Foundation and University of Auckland. C.A.B. received grants from CureKids, the Health Research Council of New Zealand, Auckland Medical Research Foundation, and National Health and Medical and Health Research Council of Australia. S.A. received grants from the Health Research Council of New Zealand.

## About the Author

Dr. Trenholme is a pediatrician at Kidz First Hospital, South Auckland, and a clinician–researcher with a research interest in pediatric respiratory diseases, especially bronchiectasis, influenza, and RSV.

## References

1. Prasad N, Trenholme AA, Huang QS, Duque J, Grant CC, Newbern EC. Respiratory virus-related emergency department visits and hospitalizations among infants in New Zealand. Pediatr Infect Dis J. 2020;39:e176–82. https://doi.org/10.1097/INF.0000000000002681
2. Baker MG, Wilson N, Anglemyer A. Successful elimination of Covid-19 transmission in New Zealand. N Engl J Med. 2020;383:e56. https://doi.org/10.1056/NEJMc2025203
3. Madhi SA, Polack FP, Piedra PA, Munoz FM, Trenholme AA, Simões EAF, et al.; Prepare Study Group. Respiratory syncytial virus vaccination during pregnancy and effects in infants. N Engl J Med. 2020;383:426–39. https://doi.org/10.1056/NEJMoa1908380
4. Iacobucci G. Covid lockdown: England sees fewer cases of colds, flu, and bronchitis. BMJ. 2020;370:m3182. https://doi.org/10.1136/bmj.m3182
5. Kuitunen I, Artama M, Mäkelä L, Backman K, Heiskanen-Kosma T, Renko M. Effect of social distancing due to the COVID-19 pandemic on the incidence of viral respiratory tract infections in children in Finland during Early 2020. Pediatr Infect Dis J. 2020;39:e423–7.
6. Itaya T, Furuse Y, Jindai K. Does COVID-19 infection impact on the trend of seasonal influenza infection? 11 countries and regions, from 2014 to 2020. Int J Infect Dis. 2020;97:78–80. https://doi.org/10.1016/j.ijid.2020.05.088
7. Soo RJJ, Chiew CJ, Ma S, Pung R, Lee V. Decreased influenza incidence under COVID-19 control measures, Singapore. Emerg Infect Dis. 2020;26:1933–5. https://doi.org/10.3201/eid2608.201229
8. Nolen LD, Seeman S, Bruden D, Klejka J, Desnoyers C, Tiesinga J, et al. Impact of social distancing and travel restrictions on non-COVID-19 respiratory hospital admissions in young children in rural Alaska. Clin Infect Dis. 2020 Sept 5 [Epub ahead of print]. https://doi.org/10.1093/cid/ciaa1328
9. Britton PN, Hu N, Saravanos G, Shrapnel J, Davis J, Snelling T, et al. COVID-19 public health measures and respiratory syncytial virus. Lancet Child Adolesc Health. 2020;4:e42–3. https://doi.org/10.1016/S2352-4642(20)30307-2
10. Solomon DA, Sherman AC, Kanjilal S. Influenza in the COVID-19 Era. JAMA. 2020;324:1342–3. https://doi.org/10.1001/jama.2020.14661

Address for correspondence: Adrian Trenholme, Kidz First, Middlemore Hospital, Private Bag 93311, Auckland 1640, New Zealand; email: atrenholme@middlemore.co.nz

# COVID-19 Infection Control Measures in Long-Term Care Facility, Pennsylvania, USA

Scott T. Shimotsu, Ariel R.L. Johnson, Ethan M. Berke, Daniel O. Griffin

Residents of long-term care facilities are at risk for coronavirus disease. We report a surveillance exercise at such a facility in Pennsylvania, USA. After introduction of a testing strategy and other measures, this facility had a 17-fold lower coronavirus disease case rate than neighboring facilities.

Author affiliations: UnitedHealth Group, Minnetonka, Minnesota, USA (S.T. Shimotsu, A.R.L. Johnson, E.M. Berke, D.O. Griffin); Columbia University College of Physicians and Surgeons, New York, New York, USA (D.O. Griffin); ProHealth Care Optum, New York (D.O. Griffin)

DOI: 10.3201/2702.204265/ eid2702.204265

The coronavirus disease (COVID-19) pandemic created an urgency to accelerate data collection to better understand the outbreak in vulnerable populations and identify best strategies for containment (*1*). Data suggested that older adults living in long-term care facilities (LTCFs) were at high risk for infection (*2*,*3*). Guidance issued by the Centers for Disease Control and Prevention outlined the importance of restricting visitation, canceling group activities, and implementing symptom screening for residents and healthcare workers (HCWs). Mitigation was put in place to limit visitors to these facilities; however, residents rely on staff, who may be exposed to severe acute respiratory syndrome coronavirus 2 (SARS-CoV-2) outside the facility. As was seen in Seattle, Washington, USA, during early 2020 (*4*), once SARS-CoV-2 is introduced into a LTCF, infection and death can be common. We hypothesized that high-risk persons in group living situations would benefit from regular, proactive monitoring for COVID-19 to prevent infection and the high transmission rates that occur in LTCF (*5*).

In this surveillance exercise performed at Twin Pines, an LTCF in Chester County, Pennsylvania, USA, we selected participants based on their association with this LTCF through employment, frequent visits (e.g., deliveries, essential care), or residence. Although we were solely observing the impact of facility-wide quality improvement, we obtained approval from the UnitedHealth Group Research and Development Institutional Review Board (Minnetonka, Minnesota, USA) and proceeded with its oversight. All persons involved in daily activities of the LTCF, including residents, employees, and visitors, were asked to participate. They completed daily symptom surveys and provided samples by nasal swab. If a participant had trouble with the self-administered sampling, a healthcare provider assisted by overseeing or performing the process. Healthcare providers collected nasal swab tests from residents twice per week and staff daily for 10 weeks (June 23–October 1, 2020). All symptom surveys and tests were conducted at the LTCF.

In addition to all 92 of the staff (nurses, therapists, and other personnel), 9 frequent visitors completed a survey and test every time they entered the facility during the surveillance period. Delivery persons who did not enter the building were not required to participate. The use of personal protective equipment (PPE) was required for all staff and visitors; PPE consisted of masking at all times while in the facility and wearing N95 masks in isolation and quarantine areas. Strict hygiene practices for the staff and twice-daily cleaning were enforced. Only full-time staff worked during this period; no per-diem staff were engaged. New residents were admitted to the facility during the observation, but they were required to quarantine for 14 days or until they had 2 negative tests. Family visits and group activities were not allowed.

During this surveillance period, a total of 5,625 nasal swabs were evaluated. We processed swab test specimens by reverse transcription PCR using a SARS-CoV-2 nucleic acid amplification test platform (LabCorp, https://www.labcorp.com). Results were provided to participants; typical turnaround time was 3 days. Two of 111 residents who tested positive had confirmed positive SARS-CoV-2 tests (results available in 1 day for the first infected resident and 7 days for the second; the delay for the second patient resulted from increased testing and limited capacity). The 2 patients were isolated for 10 days, after which they were retested until they tested negative. Staff who tested positive waited 10 days from their initial positive test and were required to have 2 negative tests before returning to work. Frequent testing and symptom surveys enabled the detection of 1 infected staff member early enough to prevent spread within the facility. Based on data obtained September 28–October 9, 2020, this LTCF's case number was 17 times lower than that of neighboring facilities when adjusted for the facility census.

Although our findings were encouraging, several aspects of our study need confirmation in future studies. The introduction of testing, questionnaires, and infection control measures may not fully explain the low prevalence of SARS-CoV-2 infection. We do not have a clear explanation for how the 2 residents became infected after the introduction of these measures; we were unable to determine whether surveys were useful tools. It is possible that routine testing discouraged persons with symptoms from visiting. We observed a very low rate of positive tests in the LTCF staff; only 1 staff member tested positive. Potential explanations for this low rate could be that testing had an impact on behavior, symptom screening kept ill staff home, or the virus was less prevalent in the community surrounding the LTCF. Although symptom surveys were used and absentee rates were normal, staff did not report symptoms as a reason for missed work. Despite these limitations, this study suggests that a proper testing strategy coupled with other measures may result in protection of vulnerable populations.

## About the Author

Dr. Shimotsu is an epidemiologist at United Health Group. His research areas include clinical care model development, chronic disease treatment, and social determinants of chronic disease.

## References


1. Lai C-C, Wang J-H, Ko W-C, Yen M-Y, Lu M-C, Lee C-M, et al. COVID-19 in long-term care facilities: an upcoming threat that cannot be ignored. J Microbiol Immunol Infect. 2020;53:444–6. https://doi.org/10.1016/j.jmii.2020.04.008
2. Wortham JM, Lee JT, Althomsons S, Latash J, Davidson A, Guerra K, et al. Characteristics of persons who died with COVID-19–United States, February 12–May 18, 2020. MMWR Morb Mortal Wkly Rep. 2020;69:923–9. https://doi.org/10.15585/mmwr.mm6928el
3. Fisman DN, Bogoch I, Lapointe-Shaw L, McCready J, Tuite AR. Risk factors associated with mortality among residents with coronavirus disease 2019 (COVID-19) in long-term care facilities in Ontario, Canada. JAMA Netw Open. 2020;3:e2015957. https://doi.org/10.1001/jamanetworkopen.2020.15957
4. Rossen LM, Branum AM, Ahmad FB, Sutton P, Anderson RN. Excess deaths associated with COVID-19, by age and race and ethnicity—United States, January 26-October 3, 2020. MMWR Morb Mortal Wkly Rep. 2020;69:1522–7. https://doi.org/10.15585/mmwr.mm6942e2
5. McMichael TM, Clark S, Pogosjans S, Kay M, Lewis J, Baer A, et al.; Public Health – Seattle & King County, EvergreenHealth, and CDC COVID-19 Investigation Team. COVID-19 in a long-term care facility—King County, Washington, February 27–March 9, 2020. MMWR Morb Mortal Wkly Rep. 2020;69:339–42. https://doi.org/10.15585/mmwr.mm6912e1


Address for correspondence: Daniel Griffin, Columbia University Irving Medical Center—Medicine, 701 W 168th St, HHSC 1310, New York, NY 10032-3784, USA; email: DGriffin@ProHEALTHcare.com

# Severe Acute Respiratory Syndrome Coronavirus 2 Outbreak Related to a Nightclub, Germany, 2020

Nadine Muller,[1] Mareike Kunze,[1] Fabienne Steitz, Neil J. Saad, Barbara Mühlemann, Jörn I. Beheim-Schwarzbach, Julia Schneider, Christian Drosten, Lukas Murajda, Sandra Kochs, Claudia Ruscher, Jan Walter, Nadine Zeitlmann,[2] Victor M. Corman[2]

Author affiliations: European Centre for Disease Prevention and Control, Stockholm, Sweden (N. Muller, N.J. Saad); Robert Koch Institute, Berlin, Germany (N. Muller, N.J. Saad, J. Walter, N. Zeitlmann); Charité–Universitätsmedizin Berlin, Berlin (N. Muller, B. Mühlemann, J.I. Beheim-Schwarzbach, J. Schneider, C. Drosten, V.M. Corman); Local Health Authority Berlin-Mitte, Berlin (M. Kunze, F. Steitz, L. Murajda, S. Kochs); German Centre for Infection Research, Berlin (B. Mühlemann, C. Drosten, V.M. Corman); State Office for Health and Social Affairs, Berlin (C. Ruscher)

DOI: https://doi.org/10.3201/eid2702.204443

We report an outbreak of coronavirus disease with 74 cases related to a nightclub in Germany in March 2020. Staff members were particularly affected (attack rate 56%) and likely caused sustained viral transmission after an event at the club. This outbreak illustrates the potential for superspreader events and corroborates current club closures.

Severe acute respiratory syndrome coronavirus 2 (SARS-CoV-2) superspreading events are particularly linked to indoor settings, such as religious venues (*1*), restaurants (*2*), and bars or nightclubs (*3–6*). To provide further details on the extent and transmission dynamics in nightclubs, we describe a SARS-CoV-2 outbreak related to a Berlin, Germany, nightclub during the early phase of the coronavirus disease (COVID-19) pandemic, before infection prevention measures were applied.

On March 5, 2020, contact tracing activities in Berlin revealed several COVID-19 cases linked by visiting the same nightclub, club X, on February 29, 2020 (event 1). Estimates suggest ≈300 guests attended event 1. Club X then held other events: event 2 with ≈150 guests on March 2 and event 3 with ≈200 guests on March 5. On March 6, the local health

[1]These first authors contributed equally to this article.

[2]These senior authors contributed equally to this article.

authority of Mitte district, Berlin, published announcements in local newspapers and on social media to identify other attendees of the events. Everyone attending ≥1 event was categorized as a high-risk contact person and ordered to self-quarantine for 14 days. If symptoms occurred, laboratory testing was recommended. Mandatory case notification occurred from the laboratory to the local health authority based on Germany's Protection against Infection Act (*7*). Due to the increasing spread of COVID-19, on March 16, 2020, government authorities in Germany prohibited social gatherings, including events in nightclubs, until further notice.

Confirmed cases in the outbreak were defined as persons with laboratory-confirmed SARS-CoV-2 (Appendix, https://wwwnc.cdc.gov/EID/article/27/2/20-4443-App1.pdf). We retrieved dates of symptom onset and sociodemographic data of 64 outbreak cases from the national infectious diseases notification database. We considered staff and persons who attended any event at club X to have first-generation cases and their contacts to have second-generation cases.

We interviewed 44 persons with first-generation cases whose contact information was available and with all 16 club X staff members who worked any of the 3 events. For staff members who were not tested after the events or who tested negative despite reporting symptoms, we offered SARS-CoV-2 antibody testing 3 months after the outbreak to ascertain their infection status. We also mapped the space inside club X (Appendix Figure 1).

In total, 74 reported cases were linked to the outbreak. Median age was 30 (range 2–63) years; cases were equally distributed by sex, 37 female (50%) and 37 male (50%). Among 41 first-generation cases with known date of symptom onset and only 1 exposure, the median incubation period was 4 days (interquartile range 3–6 days). The calculated attack rates (ARs) show that guests attending event 1 were particularly affected. Staff pooled over all events had the highest risk for infection (AR 56%) (Table).

Among guests, 1 PCR-confirmed case had self-reported initial symptoms 1 day before attending event 1 and could be a potential source of the outbreak. The most probable source for continued viral transmission at event 3 was a PCR-confirmed case in a staff member working event 1 and event 3, with symptom onset 1 day before event 3. Overall, staff members reported symptom onset at a later stage of the outbreak than guests (Figure).

**Table.** Calculated attack rates for identified coronavirus disease outbreak cases among staff members and guests attending events in a nightclub, Berlin, Germany, March 2020*

| | | No. attending | | |
|---|---|---|---|---|
| Characteristics | Cases, no. (%) | Event 1 | Event 2 | Event 3 |
| Estimated guests† | – | 300 | 150 | 200 |
| Staff members, n = 16‡ | – | 11 | 6 | 11 |
| Total cases | 74 (100) | | | |
| Cases by generation§ | | | | |
| First-generation, n = 55 | 55 (74.3) | | | |
| Guests¶ | 46 (83.6) | 39 | 0 | 3 |
| Staff | 9 (16.4) | – | – | – |
| Second-generation, n = 10 | 10 (13.5) | – | – | – |
| Generation unknown, n = 9 | 9 (12.2) | – | – | – |
| Cases by case definition# | | | | |
| Confirmed cases, n = 72 | 72 (97.3) | – | – | – |
| PCR-confirmed | 70 (97.2) | – | – | – |
| Antibody testing-confirmed | 2 (2.8) | – | – | – |
| Probable cases | 2 (2.7) | – | – | – |
| Attack rate, %** | Pooled over all events | Event 1 | Event 2 | Event 3 |
| Guests | – | 13 | – | 2 |
| Staff | 56 | – | – | – |

*Event-related case numbers are shown only for first-generation guest cases as all of them confirmed to only have attended 1 of the 3 events. –, value not calculated.
†The exact number of guests attending the events is unknown. For event 1, an estimate of attending guests was based on the maximum capacity of the club; staff and contacted guests confirmed that the club was running at full capacity. For events 2 and 3, the club owner provided estimates listed here.
‡Most staff members attended ≥2 of the events.
§First-generation cases were defined as cases exposed during event 1, 2, or 3. Second-generation cases were defined as cases without exposure at club X but with exposure to first-generation cases. Cases of unknown generation were confirmed cases of the outbreak but without contact information to reveal whether they were first- or second-generation cases.
¶All guests contacted confirmed they attended only 1 of the 3 events. Information on the event of exposure was available for 42 first-generation cases among guests. No guest case reported visiting club X for event 2.
#The outbreak case definition is described in the Appendix (https://www.nc.cdc.gov/EID/article/27/2/20-4443-App1.pdf). All cases confirmed by antibody testing were otherwise probable cases.
**Calculation of primary attack rates for guests was based on approximations for the denominator, the number of guests attending. Because most staff members were exposed repeatedly while working at ≥1 event we separately calculated attack rates for staff pooled over all events.

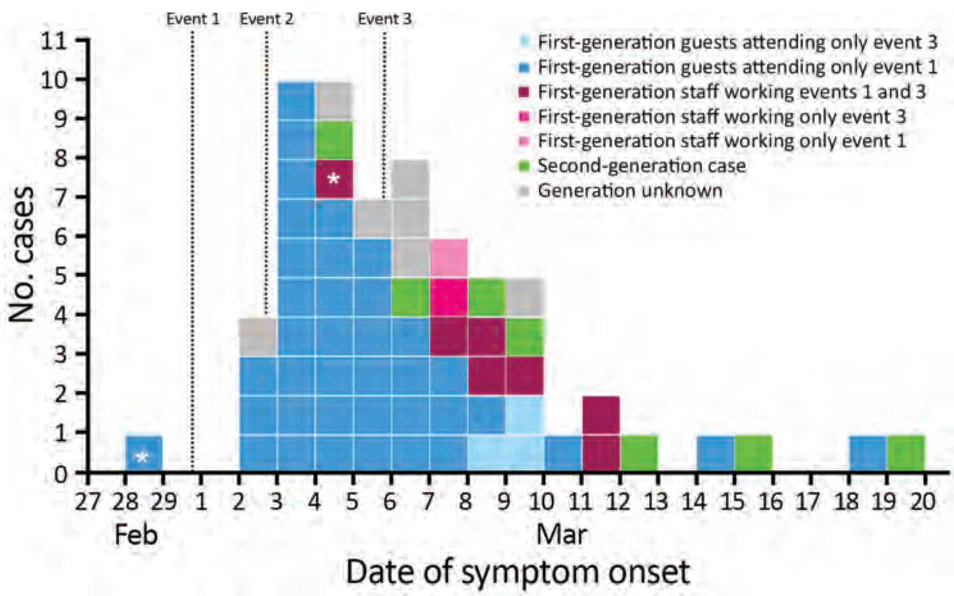


**Figure.** Date of symptom onset among 64 coronavirus disease cases linked to an outbreak in a nightclub, Berlin, Germany, March 2020. The asterisks indicate cases with symptom onset prior attending event 1 (symptom onset on February 28, 2020) and event 3 (symptom onset on March 4, 2020). No guests among cases reported attending event 2, but all attended either event 1 or event 3. No staff among cases attended only event 2; all attended event 1, event 3, or both events.

SARS-CoV-2 whole-genome sequencing was performed on 17 available patient samples to assess clustering of sequences. Sequencing revealed that 10 cases among event 1 guests, 2 second-generation cases, and 5 cases of unknown generation all grouped within clade G (GISAID, https://www.gisaid.org) and B.1 (Pangolin clade naming) (Appendix Figure 2). This clade also was observed in the SARS-CoV-2 outbreak in Italy and many later outbreaks in Europe (*8*). Sequences from 11 samples were identical. The other 6 samples were otherwise identical, but had slight differences; 1 sequence had 1 position with ambiguous nucleotides; 3 other sequences had 3 positions with ambiguous nucleotides; 1 sequence had a substitution in the 3′ untranslated region; and sequences from 2 cases, in a couple who attended event 1, had an identical substitution in the N gene (Appendix Table 1). This substitution could hint to a second independent transmission cluster comprising these 2 cases, but all observed sequence variants also can be explained by sporadic mutation events. Thus, the sequence data do not provide evidence against a single person as the outbreak source (Appendix Figure 2).

The large number of cases from event 1, the relatively low median incubation period (4 days) for first-generation cases, and the close genetic relatedness of the sequenced viruses corroborate the theory of transmission from a single person and the potential for superspreading in a nightclub when no social distancing measures are applied. This outbreak further illustrates the potential role of nightclub staff members in transmission. AR among staff was particularly high (56%), showing they had a particularly high risk for infection. Because 1 staff member appears to have been infected at event 1, then worked with symptoms at event 3, continued viral transmission could have been caused by staff. However, without sequencing data for all cases, staff contribution to viral transmission cannot be confirmed. Nonetheless, once ease of restrictions is considered, our study suggests that infection protection should be targeted particularly toward staff in nightclubs and bars.

#### Acknowledgments

We thank all our colleagues in the local health authority in Berlin and other federal states who actively collaborated in case finding activities, especially the team from the local health authority in the Berlin district Mitte for their unremitting commitment in managing cases and contact persons during the outbreak. We also thank the affected nightclub's owner and staff members for their trustful sharing of information. This study was only possible thanks to the collaboration of the affected individuals from the outbreak. We also gratefully acknowledge the authors, originating and submitting laboratories of the genetic sequence and metadata made available through GISAID on which the phylogenetic analysis presented in this paper is based.

N.M. is a fellow of Postgraduate Training for Applied Epidemiology, supported financially by the Robert Koch Institute. N.J.S. is a fellow of the European Centre for Disease Prevention and Control (ECDC) Fellowship Programme, supported financially by the ECDC. Contributions by V.M.C. and C.D. were funded by the German Ministry of Health (Konsiliarlabor für Coronaviren) and the German Center for Infection Research (DZIF).

## About the Author

Dr. Muller is a medical doctor working as a fellow of the Postgraduate Training for Applied Epidemiology at the Robert Koch Institute, Berlin, and has a research affiliation with the Department of Infectious Diseases and Respiratory Medicine, Charité University Medicine Berlin. Her main research interests include epidemiological investigations on respiratory diseases.

## References

1. Leclerc QJ, Fuller NM, Knight LE, CMMID COVID-19 Working Group, Funk S, Knight GM. What settings have been linked to SARS-CoV-2 transmission clusters? Wellcome Open Res. 2020;5:83. https://doi.org/10.12688/wellcomeopenres.15889.2
2. Lu J, Gu J, Li K, Xu C, Su W, Lai Z, et al. COVID-19 outbreak associated with air conditioning in restaurant, Guangzhou, China, 2020. Emerg Infect Dis. 2020;26:1628–31. https://doi.org/10.3201/eid2607.200764
3. Abbott S, Hellewell J, Thompson RN, Sherratt K, Gibbs HP, Bosse NI, et al. Estimating the time-varying reproduction number of SARS-CoV-2 using national and subnational case counts. Wellcome Open Res. 2020;5:112. https://doi.org/10.12688/wellcomeopenres.16006.1
4. Correa-Martínez CL, Kampmeier S, Kümpers P, Schwierzeck V, Hennies M, Hafezi W, et al. A pandemic in times of global tourism: superspreading and exportation of COVID-19 cases from a ski area in Austria. J Clin Microbiol. 2020;58:3. https://doi.org/10.1128/JCM.00588-20
5. Kang CR, Lee JY, Park Y, Huh IS, Ham HJ, Han JK, et al.; Seoul Metropolitan Government COVID-19 Rapid Response Team (SCoRR Team). Coronavirus disease exposure and spread from nightclubs, South Korea. Emerg Infect Dis. 2020;26:2499–501. https://doi.org/10.3201/eid2610.202573
6. Chau NVV, Hong NTT, Ngoc NM, Thanh TT, Khanh PNQ, Nguyet LA, et al. Superspreading event of SARS-CoV-2 infection at a bar, Ho Chi Minh City, Vietnam. Emerg Infect Dis. 2020 Oct 16 [Epub ahead of print]. https://doi.org/10.3201/eid2701.203480
7. Federal Ministry for Justice and Consumer Protection. Law on the Prevention and Control of Infectious Diseases in Humans [in German] [cited 2020 Nov 27]. https://www.gesetze-im-internet.de/ifsg/index.html
8. Rambaut A, Holmes EC, O'Toole Á, Hill V, McCrone JT, Ruis C, et al. A dynamic nomenclature proposal for SARS-CoV-2 lineages to assist genomic epidemiology. Nat Microbiol. 2020;5:1403–7. https://doi.org/10.1038/s41564-020-0770-5

Address for correspondence: Nadine Muller, Department of Infectious Disease Epidemiology, Robert Koch Institute, Seestrasse 10, Berlin 13353, Germany; email: mullern@rki.de

# Evidence of SARS-CoV-2 RNA in an Oropharyngeal Swab Specimen, Milan, Italy, Early December 2019

Antonella Amendola,[1] Silvia Bianchi,[1] Maria Gori, Daniela Colzani, Marta Canuti, Elisa Borghi, Mario C. Raviglione, Gian Vincenzo Zuccotti, Elisabetta Tanzi

Author affiliations: University of Milan, Milan, Italy (A. Amendola, S. Bianchi, M. Gori, D. Colzani, E. Borghi, M.C. Raviglione, G.V. Zuccotti, E. Tanzi); Memorial University of Newfoundland, St. John's, Newfoundland, Canada (M. Canuti)

DOI: https://doi.org/10.3201/eid2702.204632

We identified severe acute respiratory syndrome coronavirus 2 RNA in an oropharyngeal swab specimen collected from a child with suspected measles in early December 2019, ≈3 months before the first identified coronavirus disease case in Italy. This finding expands our knowledge on timing and mapping of novel coronavirus transmission pathways.

Coronavirus disease (COVID-19) symptoms can encompass a Kawasaki disease–like multisystem inflammatory syndrome and skin manifestations that accompany common viral infections such as chickenpox and measles (*1*,*2*). Some of the earliest reports of COVID-19 cutaneous manifestations came from dermatologists in Italy. In fact, Italy was the first Western country severely hit by the COVID-19 epidemic. The first known COVID-19 case in Italy was reported in the town of Codogno in the Lombardy region on February 21, 2020. However, some evidence suggests that severe acute respiratory syndrome coronavirus 2 (SARS-CoV-2) had been circulating unnoticed for several weeks in Lombardy before the first official detection (*3*). Phylogenetic studies highlighted an early circulation of SARS-CoV-2 in Italy and suggest multiple introductions of the virus from China and Germany, followed by an autochthonous transmission (*4*,*5*). Furthermore, environmental surveillance has unequivocally demonstrated the presence of the virus, at concentrations comparable to those obtained from samples collected at later stages of the pandemic, in the untreated wastewater of the Milan area as early as mid-December 2019 (*6*).

[1]These authors contributed equally to this article.

As participants in Italy's Measles and Rubella Network, a sensitive case-based surveillance system, we observed in Milan during late autumn 2019 cases of suspected measles in patients who eventually tested negative for measles. We therefore retrospectively explored a possible etiologic involvement of SARS-CoV-2 in these non–measles-linked rash cases.

We analyzed oropharyngeal swabs specimens collected during September 2019–February 2020 from 39 consenting patients (mean age 19.9 years [range 8 months–73 years]). All laboratory procedures were conducted in a university research laboratory, accredited according to World Health Organization standards, dedicated exclusively to the surveillance of measles and rubella, and therefore designated as free from SARS-CoV-2. RNA strands stored at −80°C were tested by an in-house heminested reverse transcription PCR assay for the amplification of a 470-bp fragment of the gene encoding the SARS-CoV-2 spike protein. Primers used during the first amplification step were Out_f 5′-AGGCTGCGTTATAGCTTGGA-3′ and MaSi_Ar 5′-ACACTGACACCACCAAAAGAAC-3′. Primers used for the second step were SiMa_Bf 5′-TCTTGATTCTAAGGTTGGTGGT-3′ and MaSi Ar 5′-ACACTGACACCACCAAAAGAAC-3′. Positive and negative controls also were included in each PCR test and performed as expected.

One oropharyngeal swab specimen tested positive. The amplicon was sequenced by using Sanger technology, resulting in a sequence of 409 bp. Sequence analysis performed by using BLAST (https://blast.ncbi.nlm.nih.gov/Blast.cgi) showed 100% identity to the reference sequence Wuhan-HU-1 (GenBank accession no. NC_045512.2) as well as to sequences of other SARS-CoV-2 strains circulating worldwide at a later stage; therefore, accurately determining the origin of the identified strain was not possible. The specimen was confirmed as positive by repeated amplification and sequencing, and all other specimens were repeatedly negative. The sequence (SARS-CoV-2_Milan_Dec2019 [GenBank accession no. MW303957]) was identified in a specimen collected from a 4-year-old boy who lived in the surrounding area of Milan and had no reported travel history. On November 21, the child had cough and rhinitis; about a week later (November 30), he was taken to the emergency department with respiratory symptoms and vomiting. On December 1, he had onset of a measles-like rash; on December 5 (14 days after symptom onset), the oropharyngeal swab specimen was obtained for diagnosis of suspected measles. This patient's clinical course, which included late skin manifestations, resembles what has been reported by other authors; maculopapular lesions have been among the most prevalent cutaneous manifestations observed during the COVID-19 pandemic, and several studies have noticed a later onset in younger patients (*7*).

We describe the earliest evidence of SARS-CoV-2 RNA in a patient in Italy, ≈3 months before Italy's first reported COVID-19 case. These findings, in agreement with other evidence of early SARS-CoV-2 spread in Europe, advance the beginning of the outbreak to late autumn 2019 (*6*,*8*–*10*). However, earlier strains also might have been occasionally imported to Italy and other countries in Europe during this period, manifesting with sporadic cases or small self-limiting clusters. These importations could have been different from the strain that became widespread in Italy during the first months of 2020. Unfortunately, the swab specimen, which was collected for measles diagnosis, was not optimal for SARS-CoV-2 detection because it was an oropharyngeal rather than a nasopharyngeal swab specimen and it was collected 14 days after the onset of symptoms, when viral shedding is reduced. In addition, thawing might have partially degraded the RNA, preventing the sequencing of longer genomic regions that could have been helpful in determining the origin of the strain.

This finding is of epidemiologic importance because it expands our knowledge on timing and mapping of the SARS-CoV-2 transmission pathways. Long-term, unrecognized spread of SARS-CoV-2 in northern Italy would help explain, at least in part, the devastating impact and rapid course of the first wave of COVID-19 in Lombardy. Full exploitation of existing virologic surveillance systems to promptly identify emerging pathogens is therefore a priority to more precisely clarify the course of outbreaks in a population. Further studies aimed at detecting SARS-CoV-2 RNA in archived samples suitable for whole-genome sequencing will be crucial at determining exactly the timeline of the COVID-19 epidemic in Italy and will be helpful for the preparedness against future epidemics.

**Acknowledgments**

The authors wish to thank Marino Faccini and the staff of local health authorities involved in outbreak investigation. They also wish to acknowledge Italy's Measles and Rubella Surveillance Network (MoRoNET), coordinated by the Infectious Diseases Epidemiology Unit of the National Health Institute (Istituto Superiore di Sanità [ISS]).

### About the Author

Prof. Amendola and Dr. Bianchi are researchers at the Department of Biomedical Sciences for Health, University of Milan, Italy. Their primary research interests include the epidemiology and prevention of viral infectious diseases. Prof. Amendola heads the subnational laboratory MoRoNET (Measles and Rubella Surveillance Network).

### References


1. Verdoni L, Mazza A, Gervasoni A, Martelli L, Ruggeri M, Ciuffreda M, et al. An outbreak of severe Kawasaki-like disease at the Italian epicentre of the SARS-CoV-2 epidemic: an observational cohort study. Lancet. 2020;395:1771–8. https://doi.org/10.1016/S0140-6736(20)31103-X
2. Recalcati S. Cutaneous manifestations in COVID-19: a first perspective. J Eur Acad Dermatol Venereol. 2020;34:e212–3. https://doi.org/10.1111/jdv.16387
3. Percivalle E, Cambiè G, Cassaniti I, Nepita EV, Maserati R, Ferrari A, et al. Prevalence of SARS-CoV-2 specific neutralising antibodies in blood donors from the Lodi Red Zone in Lombardy, Italy, as at 06 April 2020. Euro Surveill. 2020;25:2001031. https://doi.org/10.2807/1560-7917.ES.2020.25.24.2001031
4. Zehender G, Lai A, Bergna A, Meroni L, Riva A, Balotta C, et al. Genomic characterization and phylogenetic analysis of SARS-COV-2 in Italy. J Med Virol. 2020;92:1637–40. https://doi.org/10.1002/jmv.25794
5. Giovanetti M, Angeletti S, Benvenuto D, Ciccozzi M. A doubt of multiple introduction of SARS-CoV-2 in Italy: A preliminary overview. J Med Virol. 2020;92:1634–6. https://doi.org/10.1002/jmv.25773
6. La Rosa G, Mancini P, Bonanno Ferraro G, Veneri C, Iaconelli M, Bonadonna L, et al. SARS-CoV-2 has been circulating in northern Italy since December 2019: Evidence from environmental monitoring. Sci Total Environ. 2021;750:141711. https://doi.org/10.1016/j.scitotenv.2020.141711
7. Genovese G, Moltrasio C, Berti E, Marzano AV. Skin manifestations associated with COVID-19: current knowledge and future perspectives. Dermatology. 2020 Nov 24 [Epub ahead of print].
8. Deslandes A, Berti V, Tandjaoui-Lambotte Y, Alloui C, Carbonnelle E, Zahar JR, et al. SARS-CoV-2 was already spreading in France in late December 2019. Int J Antimicrob Agents. 2020;55:106006. https://doi.org/10.1016/j.ijantimicag.2020.106006
9. Olsen SJ, Chen MY, Liu YL, Witschi M, Ardoin A, Calba C, et al.; European COVID-19 Work Group. Early introduction of severe acute respiratory syndrome coronavirus 2 into Europe. Emerg Infect Dis. 2020;26:1567–70. https://doi.org/10.3201/eid2607.200359
10. Randazzo W, Truchado P, Cuevas-Ferrando E, Simón P, Allende A, Sánchez G. SARS-CoV-2 RNA in wastewater anticipated COVID-19 occurrence in a low prevalence area. Water Res. 2020;181:115942. https://doi.org/10.1016/j.watres.2020.115942


Address for correspondence: Elisabetta Tanzi, Coordinate Research Center "EpiSoMI," Department of Biomedical Sciences for Health, University of Milan, Via Pascal 36, 20133 Milan, Italy; email: elisabetta.tanzi@unimi.it

# COVID-19–Related Misinformation among Parents of Patients with Pediatric Cancer

Jeanine P.D. Guidry, Carrie A. Miller, Albert J. Ksinan, Jennifer M. Rohan, Marcia A. Winter, Kellie E. Carlyle, Bernard F. Fuemmeler

Author affiliation: Virginia Commonwealth University, Richmond, VA, USA

DOI: https://doi.org/10.3201/eid2702.203285

We conducted a survey among 735 parents to determine differences in endorsement of misinformation related to the coronavirus disease pandemic between parents of children in cancer treatment and those with children who had no cancer history. Parents of children with cancer were more likely to believe misinformation than parents of children without cancer.

Medical misinformation and unverifiable content about the coronavirus disease (COVID-19) pandemic have been propagated at an alarming rate, particularly on social media (*1*). Such misinformation may confer increased risk for nonadherence with COVID-19–related guidelines as well as ongoing medical regimens (*2*,*3*), which is particularly concerning for patients who are immunocompromised, such as children with cancer (*4*). The extent to which COVID-19 misinformation is believed by parents is not yet known, nor is it known whether parents of medically vulnerable children are more or less susceptible to misinformation than parents of children who are not medically vulnerable. Although parents of children with cancer may be more attentive to online medical information, rendering them more susceptible to misinformation, they may also be more discerning in what they endorse. We sought to determine whether parents of children with cancer are more or less vulnerable to COVID-19–related misinformation than their counterparts who have generally healthy children.

The panel survey firm Qualtrics (https://www.qualtrics.com) conducted a survey among 735 parents of children 2–17 years of age (n = 315 currently in cancer treatment, 38.7% female parent/caregiver; n = 420 without a cancer history, 67.1% female parent/caregiver) during May 1–31, 2020. Participants were asked to endorse a series of COVID-19–related misinformation statements taken from the World Health Organization's website, with the following scale: "Definitely untrue," "Likely untrue," "Not sure if untrue/true,"

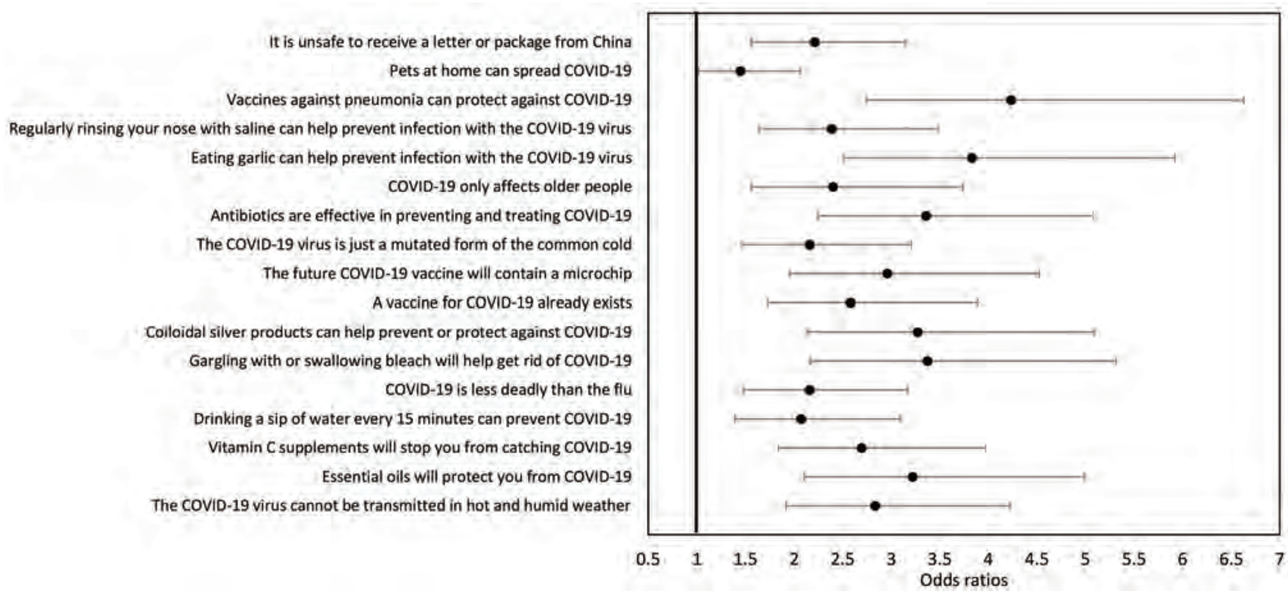


**Figure.** Forest plot of odds ratios for parents of children with cancer (as opposed to parents of children without cancer) predicting each dichotomized COVID-19 misinformation item ("definitely true" and "likely true" answers coded as 1, others as 0). Results are adjusted for sex, age, race, and education of parent as well as COVID-19–related stress. COVID-19, coronavirus disease.

"Likely true," and "Definitely true" (Figure) (*5*). Participants also answered questions about their highest attained education (dichotomized: college degree or less than college degree), sex, age, and race (dichotomized: white and nonwhite); an item also asked participants how much stress the COVID-19 pandemic has caused them, rated on a scale from 1 = "Not at all stressed" to 5 = "Extremely stressed."

First, we evaluated the fit of a single-factor confirmatory factor analysis model with misinformation items as indicators. The fit was adequate: $\chi^2$ (118) = 424.90, p<0.001, comparative fit index (CFI) = 0.94, root mean square error of approximation = 0.07. The reliability of the scale was α = 0.94. Next, we used the confirmatory factor analysis model as a dependent variable in a structural equation model, with parental age, sex, race, education, perceived stress from COVID-19, and parent group as predictors (Table). The fit was adequate: $\chi^2$ (198) = 608.60, p < 0.001, CFI = 0.93, root mean square error of approximation = 0.06. Parents of children with cancer were more likely to believe misinformation compared with parents of children without cancer. Believing misinformation was also more likely for fathers, younger parents, and parents with higher perceived stress from COVID-19. As a follow-up to this summative analysis, we evaluated each of the misconception items separately to determine the likelihood of endorsement of each item among parents of children with cancer compared with their counterparts using a logistic regression analysis (dichotomizing each item as definitely true and likely true = 1, others = 0) controlling for age, race, education, sex, and perceived stress (Figure).

This study's main finding was that parents of children with cancer were more likely to endorse misinformation about COVID-19, as well as more likely to believe myths associated with COVID-19 prevention as opposed to those related to COVID-19 susceptibility (Appendix, https://wwwnc.cdc.gov/EID/article/27/2/20-3285-App1.pdf). It is not completely clear why parents of children with cancer are more

**Table**. Results from structural model predicting belief in COVID-19 misinformation among parents of children with and without pediatric cancer*

| Characteristic | B | SE | p value | β |
|---|---|---|---|---|
| Male | 0.18 | 0.05 | <0.001 | 0.16 |
| Age | –0.01 | 0.01 | <0.001 | –0.16 |
| Nonwhite | –0.07 | 0.04 | 0.169 | –0.05 |
| College degree | –0.01 | 0.05 | 0.725 | –0.01 |
| COVID-19 stress | 0.06 | 0.02 | 0.001 | 0.12 |
| Parent of patient with pediatric cancer | 0.37 | 0.06 | <0.001 | 0.33 |

*B, unstandardized beta; COVID-19, coronavirus disease.

vulnerable to misinformation. Parents of children with cancer may be at greater risk of exposure to misinformation as a result of greater levels of COVID-19–related stress, resulting in more time spent looking for information online. Moreover, the increased stress levels reported by these parents could be affecting their information-processing abilities, making them more likely to use heuristics or cues rather than more critical, central processing routes of assessing information credibility (*6*).

From the perspective of health behavior theory, parents who feel high levels of fear should be most likely to seek out efficacious responses to ease their fears (*7*). This tendency could offer one explanation for why prevention-focused myths were more likely to be endorsed by parents of patients with pediatric cancer.

The mortality rate for pediatric cancer has increased during the COVID-19 pandemic as a result of delayed access to medical care; misinformation related to COVID-19 may also be a contributing factor (*8*). Although this study was focused on parents of children with cancer, it is possible that parents of children with other chronic diseases, as well as adult patients and caregivers, may experience similar patterns. Future studies should investigate the extent in which these findings hold in similar high-risk populations.

This study's results suggest that healthcare professionals working in pediatric oncology, in particular, should be aware of the potentially high endorsement of COVID-19 misinformation among parents of their patients across the illness trajectory, from new diagnosis to survivorship, and should proactively address this in routine visits as well as tailored written materials. The evolving nature of our understanding of COVID-19 necessitates coordinated and diligent efforts to reduce illness and death. Paramount among these efforts is the development of innovative preventive interventions to combat COVID-19–related misinformation.

This work was supported by the National Cancer Institute at the National Institutes of Health (grant nos. 2T32CA093423, P30 CA016059).

## About the Author

Dr. Guidry is an assistant professor at Virginia Commonwealth University's Richard T. Robertson School of Media and Culture, a member of the Institute for Women's Health (IWH) Sexual and Domestic Violence Research Development Group, and the director of the Media+Health Lab. Her research focuses on the use of visuals in infectious disease communication using digital media.

## References

1. Kouzy R, Abi Jaoude J, Kraitem A, El Alam MB, Karam B, Adib E, et al. Coronavirus goes viral: quantifying the COVID-19 misinformation epidemic on Twitter. Cureus. 2020;12:e7255. https://doi.org/10.7759/cureus.7255
2. Clarke S-A, Eiser C. Health behaviours in childhood cancer survivors: a systematic review. Eur J Cancer. 2007;43:1373–84. https://doi.org/10.1016/j.ejca.2007.03.002
3. Casanova M, Pagani Bagliacca E, Silva M, Patriarca C, Veneroni L, Clerici CA, et al. How young patients with cancer perceive the COVID-19 (coronavirus) epidemic in Milan, Italy: is there room for other fears? Pediatr Blood Cancer. 2020;67:e28318. https://doi.org/10.1002/pbc.28318
4. Balduzzi A, Brivio E, Rovelli A, Rizzari C, Gasperini S, Melzi ML, et al. Lessons after the early management of the COVID-19 outbreak in a pediatric transplant and hemato-oncology center embedded within a COVID-19 dedicated hospital in Lombardia, Italy. Estote parati. Bone Marrow Transplant. 2020;55:1900–5. https://doi.org/10.1038/s41409-020-0895-4>
5. World Health Organization. Coronavirus disease (COVID-19) advice for the public: myth busters. 2020 [cited 2020 Jun 22]. https://www.who.int/emergencies/diseases/novel-coronavirus-2019/advice-for-public/myth-busters
6. Cameron KA. A practitioner's guide to persuasion: an overview of 15 selected persuasion theories, models and frameworks. Patient Educ Couns. 2009;74:309–17. https://doi.org/10.1016/j.pec.2008.12.003
7. Witte K. Putting the fear back into fear appeals: The extended parallel process model. Commun Monogr. 1992;59:329–49. https://doi.org/10.1080/03637759209376276
8. Ding YY, Ramakrishna S, Long AH, Phillips CA, Montiel-Esparza R, Diorio CJ, et al. Delayed cancer diagnoses and high mortality in children during the COVID-19 pandemic. Pediatr Blood Cancer. 2020 Jun 26 [Epub ahead of print]. https:doi.org/10.1002/pbc.28427

Address for correspondence: Jeanine P.D. Guidry, Robertson School of Media and Culture, Virginia Commonwealth University, 901 W Broad St, Ste 2216, Richmond, VA 23284 USA; email: guidryjd@vcu.edu

# Rift Valley Fever and Crimean-Congo Hemorrhagic Fever Viruses in Ruminants, Jordan

Mohammad M. Obaidat, James C. Graziano, Maria Morales-Betoulle, Shelley M. Brown, Cheng-Feng Chiang, John D. Klena

Author affiliations: Jordan University of Science and Technology, Irbid, Jordan (M.M. Obaidat); Centers for Disease Control and Prevention, Atlanta, Georgia, USA (J.C. Graziano, M. Morales-Betoulle, S.M. Brown, C.-F. Chiang, J.D. Klena)

DOI: https://doi.org/10.3201/eid2702.203713

The epidemiology of Rift Valley fever virus (RVFV) and Crimean-Congo hemorrhagic fever virus (CCHFV) in Jordan is unknown. Our investigation showed 3% of 989 tested dairy cattle, sheep, and goats were RVFV seropositive and 14% were CCHFV seropositive. Ongoing surveillance is needed to assess risk to humans and protect public health.

Rift Valley fever (RVF) virus (RVFV) and Crimean-Congo hemorrhagic fever (CCHF) virus (CCHFV) are zoonotic arboviruses. RVFV has been causing sporadic outbreaks in East, West, and southern Africa; the Indian Ocean region; and the Arabian Peninsula (Saudi Arabia and Yemen) (*1*). Although Jordan is considered an at-risk country, the disease has not been reported in Jordan (*2*). Meanwhile, no seroprevalence studies for CCHFV in human or animals have been conducted in Jordan despite the endemicity of CCHF in neighboring countries (https://www.cdc.gov/vhf/crimean-congo/outbreaks/distribution-map.html), the presence of a necessary tick vector (*Hyalomma* sp.) (http://www.who.int/csr/disease/crimean_congoHF), and the classification of Jordan as an at-risk country (*3*). Accordingly, we aimed to determine whether livestock populations across Jordan have been exposed to CCHFV and RVFV (Appendix, https://wwwnc.cdc.gov/EID/article/27/2/20-3713-App1.pdf). Jordan University of Science and Technology Animal Care and Use Committee approved the study.

Using EpiTool (https://epitools.ausvet.com.au), we determined that a minimum of 665 samples were required based on an assumed prevalence of 0.5% and a 95% CI. We tested 989 serum samples from 109 farms (31 dairy cow farms, 44 sheep farms, and 20 goat farms, as well as 14 mixed sheep and goat farms) that were randomly selected from different regions of Jordan during 2015–2016. Serum samples were shipped to the US Centers for Disease Control and Prevention (Atlanta, Georgia USA) for laboratory testing by indirect ELISA (Appendix).

Overall seroprevalence was 14% for CCHFV and 3% for RVFV. The greatest differences in seroprevalence were among sheep, 16.7% (85/509) for CCHFV and 4.5% (23/509) for RVFV, followed by a similar difference for goats, 14.7% (48/327) for CCHFV and 0.6% (2/327) for RVFV (Table). CCHFV and RVFV seroprevalence did not differ in cows at ≈1% (4/152 for CCHF and 2/152 for RVF) (Table).

The provinces that had the highest respective seroprevalence for CCHFV or RVFV did not coincide (Figure). The highest CCHFV seroprevalence was found in the northwest and the highest RVFV seroprevalence in the provinces along the central western border area with Israel (Figure). In total, 29 farms had seropositivity for CCHFV: 19 sheep farms (10 in Irbid, 5 in Tafela, 2 in Jarash, 1 in Ma’an, and 1 in Mafraq), 5 mixed sheep and goat farms (1 in each of Irbid, Jarash, Ajloun,

**Table**. Seroprevalence of CCHFV and RVFV by location and animal species, Jordan, 2015–2016*

| | Seroprevalence, % | | | | | | | | | | | |
|---|---|---|---|---|---|---|---|---|---|---|---|---|
| | Sheep | | | Goat | | | Cow | | | All animals | | |
| Location | No. tested | CCHFV | RVFV | No. tested | CCHFV | RVFV | No. tested | CCHFV | RVFV | No. tested | CCHFV | RVFV |
| Ajloun | 36 | 80.5 | 5.6 | 42 | 85.7 | 0 | 0 | | | 78 | 83 | 2.6 |
| Zarqa (Al-Dulail area) | 0 | NA | NA | 0 | NA | 0 | 100 | 0 | 2 | 100 | 0 | 2 |
| Amman | 0 | | | 12 | 0 | 0 | 3 | 0 | 0 | 15 | 0 | 0 |
| Irbid and Northern Jordan Valley | 206 | 16.5 | 1.4 | 39 | 2.6 | 0 | 26 | 15.4 | 0 | 271 | 14.4 | 0.7 |
| Jarash | 78 | 8 | 0 | 127 | 4 | 0 | 10 | 0 | 0 | 215 | 5 | 0 |
| Karak | 8 | 0 | 0 | 24 | 0 | 4 | 1 | 0 | 0 | 33 | 0 | 3 |
| Ma’an | 12 | 8 | 0 | 13 | 0 | 0 | 0 | | | 25 | 5 | 0 |
| Mafraq | 94 | 5 | 13 | 42 | 5 | 0 | 8 | 0 | 0 | 144 | 5 | 8 |
| Balqa | 16 | 0 | 0 | 7 | 43 | 14 | 4 | 0 | 0 | 27 | 11 | 4 |
| Tafilah | 59 | 17 | 10 | 22 | 0 | 0 | 0 | | | 81 | 13 | 8 |
| Total | 509 | 16.7 | 4.5 | 328 | 14.7 | 0.6 | 152 | 2.6 | 1.3 | 989 | 14 | 3 |

*CCHFV, Crimean-Congo hemorrhagic fever virus; RVFV, Rift Valley fever virus.

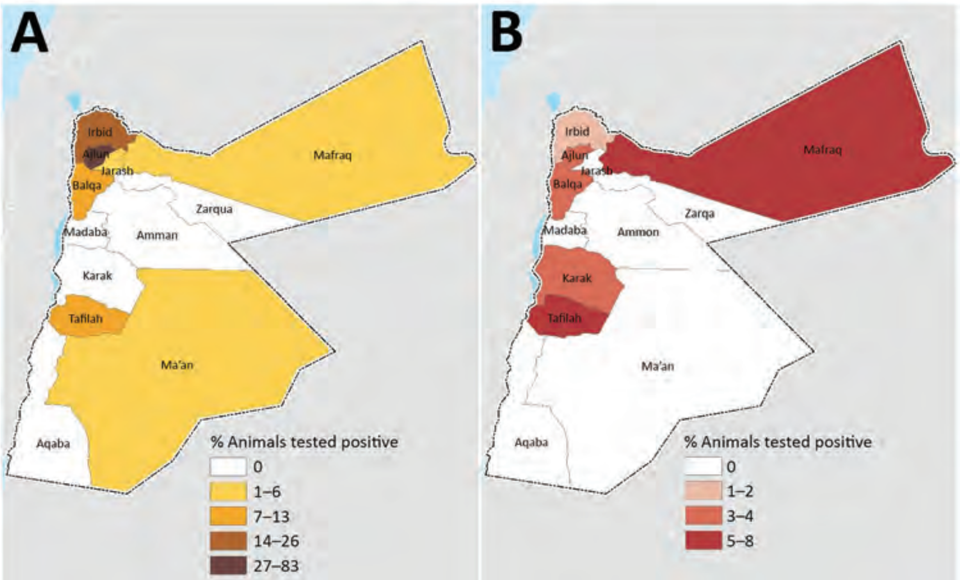


**Figure.** Seroprevalence of Crimean-Congo hemorrhagic fever (A) and Rift Valley fever (B) in ruminants, by province, Jordan, 2015–2016.

Mafraq, and Balqa), 3 goat farms (all in Jarash), and 2 dairy cow farms in Irbid. Ten farms had animals seropositive for RVFV: 5 sheep farms (2 in Tafelah, 2 in Irbid, and 1 in Mafraq), 3 mixed sheep and goat farms (1 in each of Ajloun, Mafraq, and Balqa), 1 goat farm in Karak, and 1 dairy-cow farm in Zarqa.

This study reports RVFV seropositivity in Jordan's ruminant population without any previously reported animal cases. Observing seropositive animals without disease, however, is not unique; 22% of the small ruminant population in Mayotte were seropositive (*4*) without any documented human or animal clinical cases. Similarly, South Africa reported high proportion of seropositive ruminants in the absence of a reported outbreak (*5*). In addition, IgG seroprevalence of 6.5% was detected in sheep and goats in southern Gabon without a reported outbreak (*6*).

In Jordan, small ruminants are short day breeders; June–September are breeding months. After a ≈5-month gestation period, lambing occurs during November–February, which places gestation and lambing periods during the rainy months in Jordan. The shift of RVF from enzootic to epizootic or epidemic cycle typically follows extended periods of heavy rainfall (*7*). Because rainy season and gestation periods overlap, RVFV spread poses a potential high risk for abortions and neonatal death in Jordan.

In light of the regional distribution and general expansion of RVFV and CCHFV into newly identified areas, it is not surprising that animals in Jordan tested seropositive to either virus. This finding is consistent with recent studies that reported other mosquitoborne viruses in Jordan, such as West Nile (*8*) and dengue viruses (*9*), and tickborne viruses such as *Coxiella burnetii* (*10*).

The findings of seropositive animals for CCHFV and RVFV in different regions of Jordan call for implementing an early warning contingency plan. Such a plan would include training field veterinary officers, developing strong epidemiologic capabilities, sustaining active disease surveillance, and enhancing laboratory diagnostic capabilities. On the basis of our identification of the subprovinces with the highest seroprevalence, small ruminant sentinel herds should be monitored for IgG and IgM to these viruses in conjunction with seasonal weather, particularly before and during the rainy months. Despite CCHF virulence in humans and the potential public health impact because of severe outbreaks, the virus is not pathogenic for the amplifying hosts (i.e., ruminants). Thus, farmers and veterinarians are at higher risk for infection compared with the general population. Future studies should be conducted to determine the prevalence and potential incident cases of CCHF and RVF in Jordan's human and animal populations. Ongoing surveillance will inform contemporaneous risk assessments and enable development of effective public health messaging for identified risk groups.


## Acknowledgments

We thank Alaa E. Bani Salman and Amany Rashaideh for their assistance. We thank the farmers and herdsmen for allowing the sampling of their herds and flocks.

Part of this study was supported by Deanship of Research at Jordan University of Science and Technology (grant no. 20160280).

## About the Author

Dr. Obaidat is associate professor at the faculty of veterinary medicine at Jordan University of Science and Technology. His research interest includes the epidemiology of zoonotic diseases in Jordan.

### References


1. Samy AM, Peterson AT, Hall M. Phylogeography of Rift Valley fever virus in Africa and the Arabian Peninsula. PLoS Negl Trop Dis. 2017;11:e0005226. https://doi.org/10.1371/journal.pntd.0005226
2. EFSA Panel on Animal Health and Welfare (AHAW). Scientific opinion on Rift Valley fever. EFSA J. 2013;11:3180. https://doi.org/10.2903/j.efsa.2013.3180
3. Spengler JR, Bente DA, Bray M, Burt F, Hewson R, Korukluoglu G, et al. Second international conference on Crimean-Congo hemorrhagic fever. Antiviral Res. 2018;150:137–47. https://doi.org/10.1016/j.antiviral.2017.11.019
4. Lernout T, Cardinale E, Jego M, Desprès P, Collet L, Zumbo B, et al. Rift Valley fever in humans and animals in Mayotte, an endemic situation? PLoS One. 2013;8:e74192. https://doi.org/10.1371/journal.pone.0074192
5. van den Bergh C, Venter EH, Swanepoel R, Thompson PN. High seroconversion rate to Rift Valley fever virus in cattle and goats in far northern KwaZulu-Natal, South Africa, in the absence of reported outbreaks. PLoS Negl Trop Dis. 2019;13:e0007296. https://doi.org/10.1371/journal.pntd.0007296
6. Maganga GD, Abessolo Ndong AL, Mikala Okouyi CS, Makiala Mandanda S, N'Dilimabaka N, Pinto A, et al. Serological evidence for the circulation of Rift Valley fever virus in domestic small ruminants in southern Gabon. Vector Borne Zoonotic Dis. 2017;17:443–6. https://doi.org/10.1089/vbz.2016.2065
7. Anyamba A, Linthicum KJ, Small J, Britch SC, Pak E, de La Rocque S, et al. Prediction, assessment of the Rift Valley fever activity in east and southern Africa 2006–2008 and possible vector control strategies. Am J Trop Med Hyg. 2010;83:Suppl 43–51. https://doi.org/10.4269/ajtmh.2010.09-0289
8. Obaidat MM, Stringer AP, Roess AA. Seroprevalence, risk factors and spatial distribution of West Nile virus in Jordan. Trans R Soc Trop Med Hyg. 2019;113:24–30. https://doi.org/10.1093/trstmh/try111
9. Obaidat MM, Roess AA. First report on seroprevalence and risk factors of dengue virus in Jordan. Trans R Soc Trop Med Hyg. 2018;112:279–84. https://doi.org/10.1093/trstmh/try055
10. Obaidat MM, Kersh GJ. Prevalence and risk factors of *Coxiella burnetii* antibodies in bulk milk from cattle, sheep, and goats in Jordan. J Food Prot. 2017;80:561–6. https://doi.org/10.4315/0362-028X.JFP-16-377


Address for correspondence: Mohammad M. Obaidat, Department of Veterinary Pathology and Public Health, Faculty of Veterinary Medicine, Jordan University of Science and Technology, Irbid, Jordan; email: mmobaidat@just.edu.jo; and John D. Klena, Centers for Disease Control and Prevention, 1600 Clifton Rd NE, Mailstop H18-SSB, Atlanta, GA 30329-4027, USA; email: irc4@cdc.gov

# Genomic Diversity of *Burkholderia pseudomallei* Isolates, Colombia

Carolina Duarte, Franco Montufar, Jaime Moreno, Dora Sánchez, Jose Yesid Rodríguez, Alfredo G. Torres, Soraya Morales, Adriana Bautista, Mónica G. Huertas, Julia N. Myers, Christopher A. Gulvik, Mindy G. Elrod, David D. Blaney, Jay E. Gee

Author affiliations: Instituto Nacional de Salud, Bogotá, Colombia (C. Duarte, J. Moreno, D. Sanchez, A. Bautista); Clínica León XIII Universidad de Antioquia, Medellín, Colombia (F. Montufar); Centro de Investigaciones Microbiológicas del Cesar, Valledupar, Colombia (J.Y. Rodriguez); University of Texas Medical Branch, Galveston, Texas, USA (A.G. Torres, J.N. Myers); Universidad de Santander, Valledupar, Colombia (S. Morales); Universidad El Bosque, Bogotá, Colombia (M.G. Huertas); Centers for Disease Control and Prevention, Atlanta, Georgia, USA (C.A. Gulvik, M.G. Elrod, D.D. Blaney, J.E. Gee)

DOI: https://doi.org/10.3201/eid2702.202824

We report an analysis of the genomic diversity of isolates of *Burkholderia pseudomallei*, the cause of melioidosis, recovered in Colombia from routine surveillance during 2016–2017. *B. pseudomallei* appears genetically diverse, suggesting it is well established and has spread across the region.

Melioidosis is caused by the environmental bacterium *Burkholderia pseudomallei*. Infections are acquired by direct contact with the pathogen, most commonly through traumatic inoculation with contaminated soil or water but also by ingestion or inhalation. Symptoms are nonspecific and can include pneumonia, skin lesions, abscess formation, and sepsis (*1*).

In Latin America, melioidosis is believed to be underdiagnosed because of the absence of reliable surveillance and the lack of available diagnostic tools and methods (*2*). Colombia has previously reported cases as sporadic, isolated events in a few geographic areas (*2*,*3*). The aim of this study was to genetically characterize isolates of *B. pseudomallei* recovered from clinical specimens in different departments of Colombia (*4*). (A department in Colombia is a geographic unit composed of municipalities led by a governor.) The goal was to better understand genetic relationships among the isolates from Colombia, as well as their relationships to isolates from other tropical and subtropical regions of the Americas. The study was internally reviewed at the US Centers for Disease

Control and Prevention (Atlanta, GA, USA) and determined not to involve human subject research.

Melioidosis is not an officially reportable disease in Colombia, but when cases are identified, department public health laboratories are required to send isolates of *B. pseudomallei* to the Instituto Nacional de Salud. During 2016–2017, a total of 11 isolates of *B. pseudomallei* were recovered from 10 melioidosis patients in the departments of Cesar (n = 4 isolates), Antioquia (n = 4), Casanare (n = 2), and Santander (n = 1) (Appendix, https://wwwnc.cdc.gov/EID/article/27/2/20-2824-App1.pdf). The most common risk factor was diabetes mellitus (n = 6); 4 of the patients died (Table). Cesar, Antioquia, Casanare, and Santander vary in population from a few hundred thousand to >6 million (*4*).

We performed whole-genome sequencing of the 11 isolates and deposited sequences at the National Center for Biotechnology Information under BioProject PRJNA638548. Sequences were used for multilocus sequence typing and single-nucleotide polymorphism (SNP) analysis (Appendix). The multilocus sequence types (ST) we observed were ones previously described, such as ST92, ST349, ST518, and ST1459. Two novel STs from this study were designated ST463 and ST1701. Previous entries in the PubMLST database (http://pubmlst.org) indicate that ST92 has been identified in cases associated with Puerto Rico and Brazil and in 1 person in Switzerland who had travelled to Martinique. ST349 was represented in 2 examples, one from Martinique and the other in a person from Spain who had travelled to West Africa; ST518 is represented in 4 examples. The first was in a person from Arizona, USA, in whom melioidosis developed after sustaining an injury while swimming in Costa Rica (*5*). In addition, ST518 was identified in *B. pseudomallei* isolates from 3 pet green iguanas, 2 of them in California, USA, and 1 in Belgium, all of which were presumably imported from Central or South America (*6*,*7*). ST1459 was noted in 1 isolate from Brazil.

SNP analysis determined from the whole genome sequences indicates that the Colombia isolates (N=11) are within the clade associated with Western Hemisphere *B. pseudomallei* based on a comparison with a panel of reference genomes (N=45) (Figure). Within this clade, a subgroup was resolved containing the Colombia genomes along with ones from Brazil and Guatemala. Also included is a genome from an isolate from a patient who had traveled to both Panama and Peru, as well as isolates from iguanas from California and Belgium, as noted, plus 1 from the Czech Republic that were presumably imported from Central or South America (Figure) (*6*–*8*).

The full panel (N = 56) was also used for quantifying SNP differences among the genomes. Patient isolates B107 and B108 had no SNPs between them, even though they were from different patients, suggesting a common source of infection or a clonal population of *B. pseudomallei* present in different sources. However, isolates B308 and B309 were from the same patient and had 1 SNP between them. The next closest relationship was for B199 (from Casanare), which diverged by 38 SNPs from B308 and by 39 SNPs from B309 (from Antioquia). The phylogenetic SNP tree indicates that isolates from Antioquia, Casanare, and Cesar for the most part do not uniformly group together by department. The largest divergence was seen between B109 and the genomes for B107 and B108, with >6,900 SNPs detected (all from Cesar). The amount of divergence plus the lack of grouping by department, even though we presume that patients' main exposures would have been within a given department, suggests *B. pseudomallei* is well established

**Table.** Epidemiologic and demographic characteristics of 10 melioidosis patients, Colombia

| Isolate | Sequence type | Department | Age, y/sex | Type of sample | Diagnosis | Medical history and risk factors | Outcome |
|---|---|---|---|---|---|---|---|
| B107 | 1459 | Cesar | 71/M | Blood | Sepsis | Arterial hypertension | Died |
| B108 | 1459 | Cesar | 54/M | Right leg injury | Soft tissue infection | Tibial fracture | Recovered |
| B109 | 349 | Cesar | 56/M | Urine | Urinary infection | Diabetes mellitus | Recovered |
| B197 | 1463 | Cesar | 51/F | Bronchoalveolar lavage | Pulmonary melioidosis | Diabetes mellitus, anemic syndrome | Recovered |
| B198 | 1701 | Casanare | 24/M | Blood | Pneumonia | None | Died |
| B199 | 518 | Casanare | 26/M | Blood | Unspecified sepsis | None | Died |
| B255 | 92 | Santander | 68/M | Blood | Sepsis | | Recovered |
| B308* | 518 | Antioquia | 64/M | Tracheal aspirate | Systemic inflammatory response syndrome | Diabetes mellitus | Died |
| B309* | | | | Blood | | | |
| B310 | 1740 | Antioquia | 81/F | Tracheal aspirate | Pneumonia | Kidney tumor (in studio), diabetes mellitus, arterial hypertension, hypothyroidism | Recovered |
| B411 | 1741 | Antioquia | 53/F | Blood | Sepsis | Diabetes mellitus | Recovered |

*Isolates from the same patient.

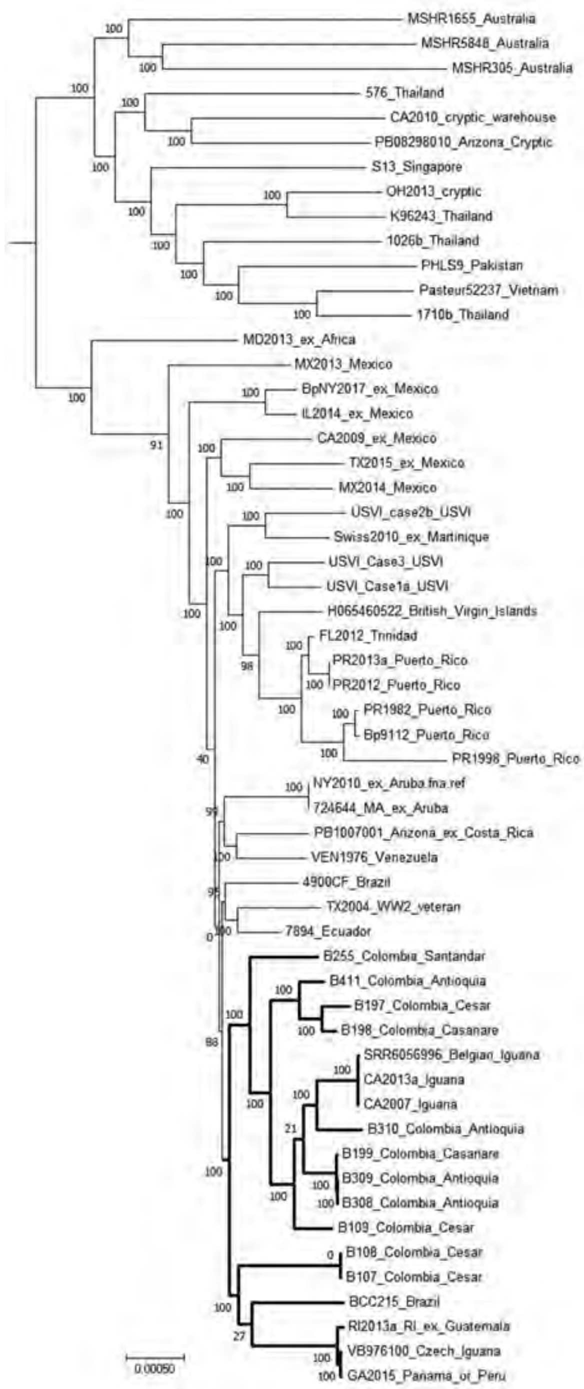


**Figure.** Dendrogram used for characterization of *Burkholderia pseudomallei* genomes from Colombia compared with reference genomes. Tree was generated in MEGA7 software (http://www.megasoftware.net) from results of maximum-parsimony phylogenetic analysis of core single-nucleotide polymorphisms conducted by using Parsnp, a component of the Harvest 1.3 software suite (https://github.com). Bold branches indicate the subclade containing the examples from Colombia along with reference genomes that group with them. Isolates from Colombia also include the department where they originated. Scale bar indicates number of substitutions per single nucleotide polymorphism.

in Colombia and has had time to diverge substantially since its introduction. In addition, the genomes from the 2 cases of melioidosis from pet iguanas from California and the 1 from Belgium cluster together with examples from Colombia, suggesting this region or a nearby region may have been the origin of the iguanas. Further studies, especially to recover and test environmental isolates, will improve our understanding of the population structure of *B. pseudomallei* in Colombia and improve the ability of public health stakeholders to respond to cases of melioidosis.


## Acknowledgments

We appreciate the Biotechnology Core Facility Branch, Division of Scientific Resources, National Center for Emerging and Zoonotic Infectious Diseases, Centers for Disease Control and Prevention, for performing Illumina MiSeq sequencing.

Our analysis made use of the *Burkholderia pseudomallei* MLST website (http://pubmlst.org/bpseudomallei) at the University of Oxford. The development of this site has been funded by the Wellcome Trust.


## About the Author

Ms. Duarte is the coordinator of the microbiology group (National Reference Library) at the Instituto Nacional de Salud in Colombia. Her primary research interest is laboratory surveillance of pathogens important for public health.

## References


1. Hoffmaster AR, AuCoin D, Baccam P, Baggett HC, Baird R, Bhengsri S, et al. Melioidosis diagnostic workshop, 2013. Emerg Infect Dis. 2015;21. https://doi.org/10.3201/eid2102.141045
2. Benoit TJ, Blaney DD, Doker TJ, Gee JE, Elrod MG, Rolim DB, et al. A review of melioidosis cases in the Americas. Am J Trop Med Hyg. 2015;93:1134–9. https://doi.org/10.4269/ajtmh.15-0405
3. Rodríguez JY, Morales-López SE, Rodríguez GJ, Álvarez-Moreno CA, Esquea K, Pinzon H, et al. Case series study of melioidosis, Colombia. Emerg Infect Dis. 2019;25:1534. https://doi.org/10.3201/eid2508.170786
4. DANE. Colombia. National and departmental estimates 1985–2005 and projections 2005–2020 disaggregated by sex, area and five-year age groups. [cited 2020 Dec 22] https://www.dane.gov.co/index.php/en/statistics-by-topic-1/population-and-demography/population-series-1985-2020
5. Gee JE, Gulvik CA, Elrod MG, Batra D, Rowe LA, Sheth M, et al. Phylogeography of *Burkholderia pseudomallei* Isolates, Western Hemisphere. Emerg Infect Dis. 2017;23:1133–8. https://doi.org/10.3201/eid2307.161978
6. Hellebuyck T, Wattiau P, Boyen F, Moeremans I, Roosens NH, Vanneste K, et al. Isolation of *Burkholderia pseudomallei* from a pet green iguana, Belgium. Emerg Infect Dis. 2018;24:2331–3. https://doi.org/10.3201/eid2412.171661

7. Zehnder AM, Hawkins MG, Koski MA, Lifland B, Byrne BA, Swanson AA, et al. *Burkholderia pseudomallei* isolates in 2 pet iguanas, California, USA. Emerg Infect Dis. 2014;20:304–6. https://doi.org/10.3201/eid2002.131314
8. Elschner MC, Hnizdo J, Stamm I, El-Adawy H, Mertens K, Melzer F. Isolation of the highly pathogenic and zoonotic agent *Burkholderia pseudomallei* from a pet green iguana in Prague, Czech Republic. BMC Vet Res. 2014;10:283. https://doi.org/10.1186/s12917-014-0283-7

Address for correspondence: Jay E. Gee, Centers for Disease Control and Prevention, 1600 Clifton Rd NE, Mailstop H17-2, Atlanta, GA 30329-4027, USA; email: xzg4@cdc.gov

# Puumala Virus Infection in Family, Switzerland

Pauline Vetter, Arnaud G. L'Huillier, Maria F. Montalbano, Fiona Pigny, Isabella Eckerle, Giulia Torriani, Sylvia Rothenberger, Florian Laubscher, Samuel Cordey, Laurent Kaiser, Manuel Schibler

Author affiliations: University of Geneva, Geneva, Switzerland (P. Vetter, A.G. L'Huillier, F. Pigny, G. Torriani, F. Laubscher, S. Cordey, L. Kaiser, M. Schibler); Geneva University Hospitals, Geneva (P. Vetter, M.F. Montalbano, F. Pigny, I. Eckerle, G. Torriani, F. Laubscher, S. Cordey, L. Kaiser, M. Schibler); Geneva Centre for Emerging Viral Diseases, Geneva (P. Vetter, I. Eckerle, G. Torriani, L. Kaiser); Spiez Laboratory, Spiez, Switzerland (S. Rothenberger); University of Lausanne, Lausanne, Switzerland (S. Rothenberger)

DOI: https://doi.org/10.3201/eid2702.203770

We report 3 cases of Puumala virus infection in a family in Switzerland in January 2019. Clinical manifestations of the infection ranged from mild influenza-like illness to fatal disease. This cluster illustrates the wide range of clinical manifestations of Old World hantavirus infections and the challenge of diagnosing travel-related hemorrhagic fevers.

Puumala orthohantavirus (PUUV), a species of the genus *Orthohantavirus* within the *Hantaviridae* family, is an enveloped single-strand negative-sense RNA virus (*1*). The case-fatality ratio of Old World hantaviruses ranges from 1%–10% for Dobrava-Belgrade and Hantaan orthohantaviruses to <1% for PUUV. Infection is transmitted by direct inhalation of virion-containing aerosols from rodent urine and feces. PUUV causes nephropathia epidemica, a limited form of hemorrhagic fever with renal syndrome (*1*). In Russia, 6,000–8,000 cases of hemorrhagic fever with renal syndrome are reported annually. Most cases occur in Western Russia and are caused by PUUV and Dobrava-Belgrade orthohantaviruses (*2*).

Asthenia, fever, chills, diffuse myalgia, and lumbar pain developed in a man 45 years of age 4 days after he returned to Switzerland from Samara, his hometown in central Russia (Appendix, https://wwwnc.cdc.gov/EID/article/27/2/20-3770-App1.pdf). Four days later, he sought treatment at the Geneva University Hospitals (Geneva, Switzerland) for septic shock with disseminated intravascular coagulation and kidney and liver failure. He had severe thrombocytopenia and elevated levels of C-reactive protein, procalcitonin, and leukocytes (Appendix Table 2). We transferred him to the intensive care unit for mechanical ventilation and hemodynamic support because of severe metabolic acidosis and confusion. We began treatment with broad-spectrum antimicrobial drugs, including doxycycline for possible leptospirosis. The day after admission, the patient tested positive for PUUV by real-time reverse transcription PCR (*3*) with a cycle threshold of 28. His serum sample tested positive for IgM and IgG against hantaviruses (Appendix Table 1). Shortly after his diagnosis, we administered 2 doses of 30 mg subcutaneous icatibant 6 hours apart. The patient died of multiple organ failure ≤60 hours after admission.

The next day, fever, lymphopenia, moderate thrombocytopenia, and hepatitis developed in the index patient's daughter, who was 12 years of age (Appendix). She was hospitalized and tested positive for PUUV by PCR with a cycle threshold of 26. We prescribed a 5-day course of oral ribavirin starting with an initial dose of 30 mg/kg followed by 15 mg/kg every 6 hours (*4*). The viral load in plasma rapidly decreased. We did not detect viral RNA in urine (Appendix Table 3). Interstitial nephropathy briefly developed and subsided; she was discharged without sequelae after 7 days.

The wife of the index patient had had influenza-like symptoms in Russia during the week before her husband's illness. Her serum sample tested positive for IgM and IgG against hantaviruses. We used a pseudovirus-based neutralization assay to confirm serologic results (Appendix Figure 1).

We sequenced the viral genome from blood samples taken from the father (GenBank accession no. MT822196) and the daughter (GenBank accession no. MT822195) using high-throughput sequencing (Appendix Figure 2). Both sequences showed a 100% s segment match and were related to PUUV sequences in GenBank from Samara (Figure), confirming that the patients were exposed there. Regular outbreaks occur in Samara (*5*), where annual rodent control measures were delayed in 2019. In Switzerland, local acquisition of PUUV is rare (*6*).

This familial cluster highlights the wide spectrum of clinical manifestations of PUUV, which can range from an influenza-like illness (mother) to the classical nephropathy (daughter) to a rapidly fatal hemorrhagic fever with shock and multiple organ failure (father). Such a large spectrum of disease might be caused by the viral inoculum or host factors. Uncontrolled immune response and subsequent cytokine storm have been identified as key factors in the development of critical disease (*7*). Smoking, enzymatic polymorphisms, and gene variants such as HLA-B8 DRB1*03:02 (*8*) might be risk factors for severe disease, whereas HLA-B57 might have a protective effect (*9*). High procalcitonin levels, severe thrombocytopenia, increased interleukin 6 levels, and leukocytosis are known markers for severe disease.

Although specific antimicrobial drugs have been tested against PUUV infections, treatment is limited to supportive care. A small trial in Russia showed no effect of ribavirin on PUUV viral load or risk for death (*10*). We decided to treat the daughter with ribavirin because of her early diagnosis and treatment, the potential genetic factors that might predispose her to severe disease, and the emotional context of her father's death. We treated the father with icatibant, a selective antagonist of the bradykinin type 2 receptor that reduces capillary leakage. This treatment has been used with apparent success in 2 patients with severe PUUV infection (Appendix).

PUUV usually causes limited renal disease but has a broad spectrum of clinical manifestations. Human hantavirus infections are rare in Switzerland and mostly acquired outside of the country. Physicians should consider viral hemorrhagic fevers when a patient has worsening influenza-like illness, thrombocytopenia, renal and hepatic impairment, and a plausible epidemiologic link to a region to which these viruses are endemic.

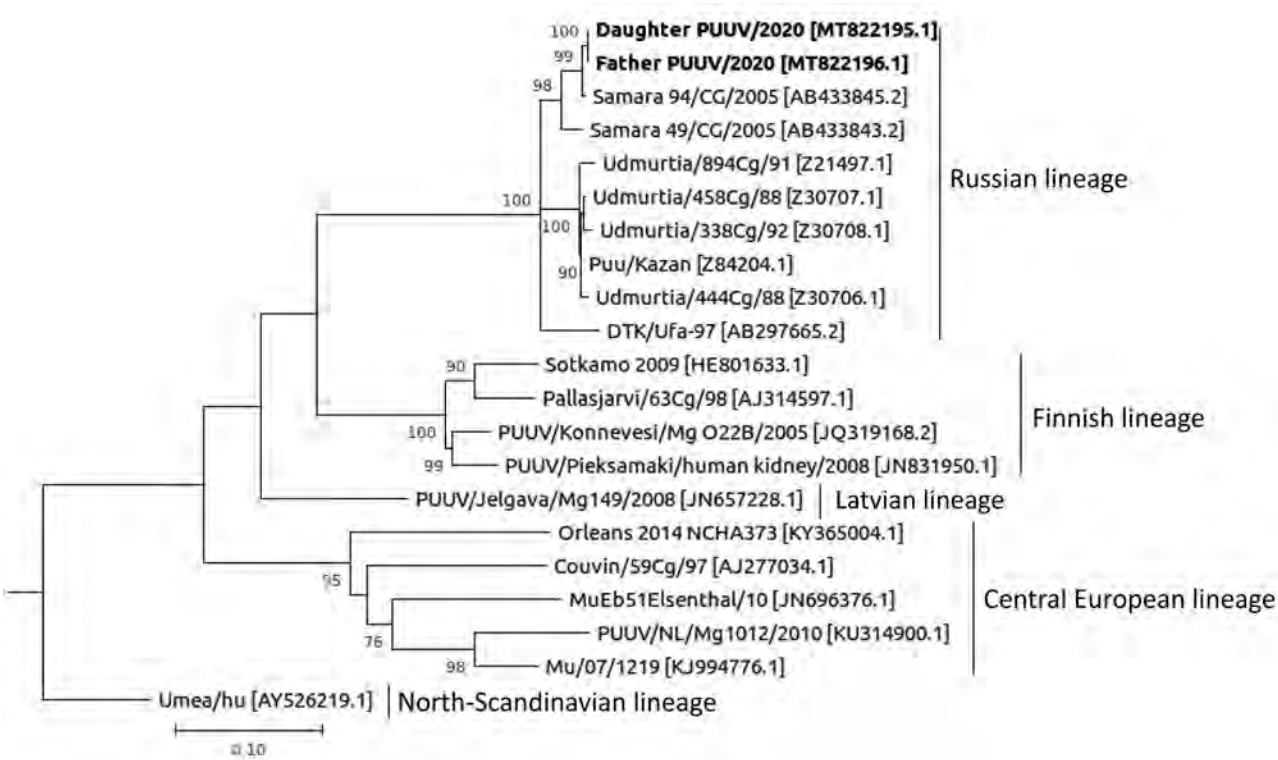


**Figure.** Phylogenetic tree of Puumala virus using S segment nucleotide sequences. Bold text indicates sequences isolated from family in Switzerland. GenBank accession numbers are provided in brackets. Lineages are indicated at right. Scale bar indicates number of substitutions per site.

## Acknowledgments

We thank Erik Boehm for editorial assistance. We thank Gert Zimmer for the donation of vesicular stomatitis virus recombinant, Jay W. Hooper from the United States Army Medical Research Institute of Infectious Diseases for the plasmid encoding Puumala glycoprotein, and Jennifer Mayor for the production of recombinant vesicular stomatitis virus with Puumala virus glycoprotein. We are deeply grateful to the family for their permission to publish this article.

This work was supported by the Geneva Center for Emerging Viral Diseases and Geneva University, Faculty of Medicine.

## About the Author

Dr. Vetter is an infectious diseases physician at Geneva University Hospitals and Geneva Centre for Emerging Viral Diseases, Geneva. Her research interests include emerging viral diseases.

## References

1. Manigold T, Vial P. Human hantavirus infections: epidemiology, clinical features, pathogenesis and immunology. Swiss Med Wkly. 2014;144:w13937. https://doi.org/10.4414/smw.2014.13937
2. Tkachenko EA, Ishmukhametov AA, Dzagurova TK, Bernshtein AD, Morozov VG, Siniugina AA, et al. Hemorrhagic fever with renal syndrome, Russia. Emerg Infect Dis. 2019;25:2325–8. https://doi.org/10.3201/eid2512.181649
3. Kramski M, Meisel H, Klempa B, Krüger DH, Pauli G, Nitsche A. Detection and typing of human pathogenic hantaviruses by real-time reverse transcription-PCR and pyrosequencing. Clin Chem. 2007;53:1899–905. https://doi.org/10.1373/clinchem.2007.093245
4. World Health Organization. Clinical management of patients with haemorragic fever. 2016 [cited 2020 Sep 30]. https://apps.who.int/iris/bitstream/handle/10665/205570/9789241549608_eng.pdf
5. Alexeyev OA, Suzdaltsev AA, Verkhovtsev VN, Efratova ES, Roschupkin VI. A major outbreak of hemorrhagic fever with renal syndrome in the Samara region, European Russia. Infection. 1998;26:322. https://doi.org/10.1007/BF02962264
6. Fontana-Binard L, Schultze D, Rojanavisut BS, Krüger DH, Dollenmaier G, Zanetti G, et al. First case of nephropathia epidemica acquired in Switzerland [in French]. Rev Med Suisse. 2008;4:1572–5.
7. Garanina E, Martynova E, Davidyuk Y, Kabwe E, Ivanov K, Titova A, et al. Cytokine storm combined with humoral immune response defect in fatal hemorrhagic fever with renal syndrome case, Tatarstan, Russia. Viruses. 2019;11:601. https://doi.org/10.3390/v11070601
8. Mäkelä S, Mustonen J, Ala-Houhala I, Hurme M, Partanen J, Vapalahti O, et al. Human leukocyte antigen-B8-DR3 is a more important risk factor for severe Puumala hantavirus infection than the tumor necrosis factor-alpha(-308) G/A polymorphism. J Infect Dis. 2002;186:843–6. https://doi.org/10.1086/342413
9. Mustonen J, Partanen J, Kanerva M, Pietilä K, Vapalahti O, Pasternack A, et al. Association of HLA B27 with benign clinical course of nephropathia epidemica caused by Puumala hantavirus. Scand J Immunol. 1998;47:277–9. https://doi.org/10.1046/j.1365-3083.1998.00302.x
10. Malinin OV, Platonov AE. Insufficient efficacy and safety of intravenous ribavirin in treatment of haemorrhagic fever with renal syndrome caused by Puumala virus. Infect Dis (Lond). 2017;49:514–20. https://doi.org/10.1080/23744235.2017.1293841

Address for correspondence: Pauline Vetter, Geneva Center for Emerging Viral Diseases, Geneva University Hospitals, 4, rue Gabrielle-Perret Gentil, 1205 Geneva, Switzerland; email: pauline.vetter@hcuge.ch; Manuel Schibler, Division of Infectious Diseases, Geneva University Hospitals, 4, rue Gabrielle Perret-Gentil, 1205 Geneva, Switzerland; email: manuel.schibler@hcuge.ch

# Protective Immunity and Persistent Lung Sequelae in Domestic Cats after SARS-CoV-2 Infection

Shiho Chiba, Peter J. Halfmann, Masato Hatta, Tadashi Maemura, Shufang Fan, Tammy Armbrust, Olivia M. Swartley, LaTasha K. Crawford, Yoshihiro Kawaoka

Author affiliations: University of Wisconsin–Madison School of Veterinary Medicine, Madison, Wisconsin, USA (S. Chiba, P.J. Halfmann, M. Hatta, T. Maemura, S. Fan, T. Armbrust, O.M. Swartley, L.K. Crawford, Y. Kawaoka,); University of Tokyo Institute of Medical Science, Tokyo, Japan (Y. Kawaoka)

DOI: https://doi.org/10.3201/eid2702.203884

Severe acute respiratory syndrome coronavirus 2 readily transmits between domestic cats. We found that domestic cats that recover from an initial infection might be protected from reinfection. However, we found long-term persistence of inflammation and other lung lesions after infection, despite a lack of clinical symptoms and limited viral replication in the lungs.

Previous studies have demonstrated the transmissibility of severe acute respiratory syndrome coronavirus-2 (SARS-CoV-2) by direct or indirect contact between domestic cats (*1*,*2*). Given the close relationship between cats and humans, further characterization of the biology of SARS-CoV-2 in cats is warranted.

We inoculated domestic cats with SARS-CoV-2, and on postinfection days 3, 6, and 10, sampled organs to titrate virus (Appendix Figure 1, https://wwwnc.cdc.gov/EID/article/27/2/20-3884-App1.pdf). In plaque-forming assays in VeroE6/TMPRSS2 cells, infectious viruses were detected in the nasal turbinates and trachea of all animals on day 3, and most on day 6, whereas virus detection in the lungs was limited on day 3 and absent on day 6 (Appendix Figure 2, panel A). These results suggest that the virus replicated efficiently in upper respiratory organs, which might contribute to its high transmissibility among cats. Infectious virus was cleared from the upper and lower respiratory organs by day 10 (Appendix Figure 2, panel A). No animal showed any signs of respiratory illness during the study (Appendix Figure 3). Infectious virus was not detected (detection limit 10 pfu/g of tissue) in other examined organs (e.g., brain, liver, spleen, kidney, small and large intestine, heart, and eyelids). Viral antigen was detected in nasal turbinates and trachea but was sparse within the lungs at day 3 (Appendix Figure 4).

We conducted histopathologic examination of the lungs, trachea, and nasal turbinates. Lymphocytic inflammation within the tracheal submucosa was present on days 3 to 10, whereas lymphocytic to mixed inflammation in the nasal cavity was more severe on days 3 and 6 but minimal on day 10. In lungs, moderate lesions persisted despite clearance of virus. On day 3, we observed mild bronchitis with lymphoid hyperplasia, moderate to severe histiocytic bronchiolitis with partial to complete occlusion of lumina, and moderate to severe thickening of alveolar septa (Appendix Figure 2, panel B; Appendix Figures 4, 5). Interstitial inflammatory infiltrate decreased significantly over time ($p = 0.0012$, $F = 34.70$, by 1-way analysis of variance) (Appendix Figure 2, panel C); however, by day 10, alveolar septa remained thickened (Appendix Figure 5). Bronchiolitis remained with partial occlusion of bronchioles, even in regions with minimal alveolar lesions (Appendix Figure 2, panel B).

Because SARS-CoV-2 did not cause acute lethal respiratory disease in the cats in our study, cats are a compelling animal model for studying the long-term effects of nonfatal infections. Cats were infected with SARS-CoV-2 and euthanized at postinfection day 28 (Appendix Figure 6, 7). Persistent lung lesions were observed 28 days after infection, including histiocytic bronchiolitis with luminal plugs and thickened alveolar septa, similar to lesions observed on day 10 but with more chronic features such as peribronchiolar fibrosis and vascular

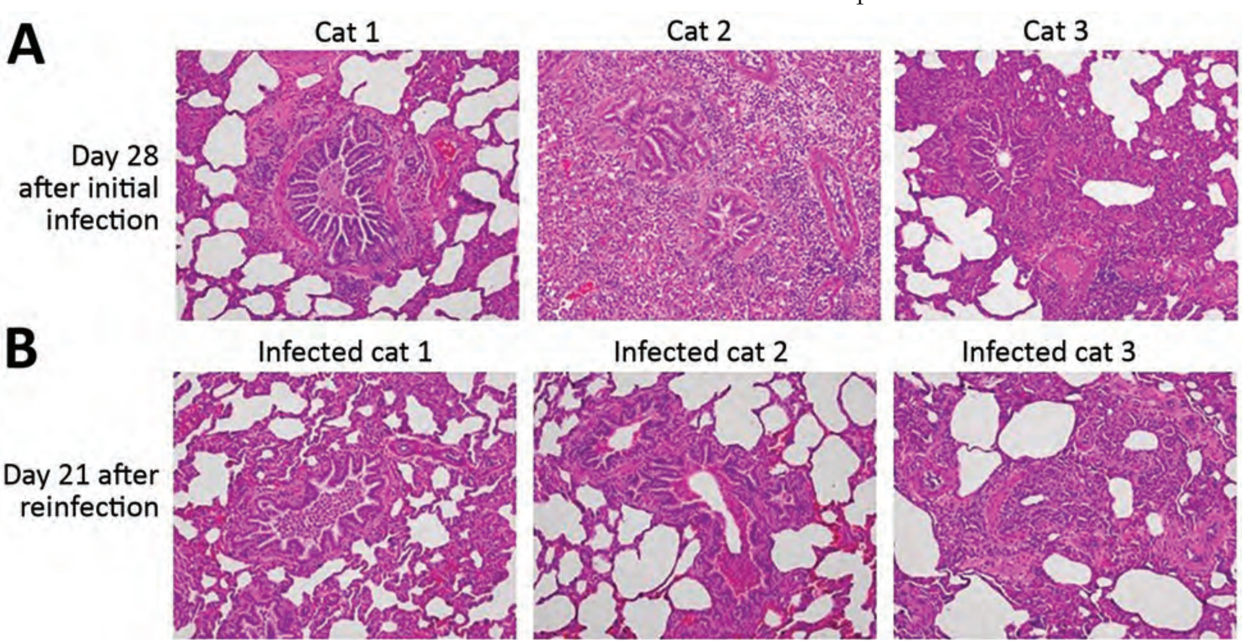


**Figure 1.** Comparison of histopathology between cats on day 28 after initial infection with severe acute respiratory syndrome coronavirus 2 and on day 21 after reinfection. Bronchioles and alveoli of cats (cats 1–3 in Appendix Figure 6; https://wwwnc.cdc.gov/EID/article/27/1/20-3884-App1.pdf) on day 28 after initial infection (A) and those of cats (infected cats 1–3 in Appendix Figure 6, upper half) on day 21 after reinfection (49 days after the initial infection) (B); original magnification 20 ×. Cats from both groups showed histiocytic bronchiolitis with occlusive plugs, peribronchiolar fibrosis, and thickening of alveolar septa. Mild acute hemorrhage was detected in affected and less affected regions of the lung on day 21 after reinfection, with a trend toward an increase compared with day 28 (severity score $1.8 \pm$ SEM 0.8 on day 21 vs. $0.3 \pm$ SEM 0.2 on day 28; $p = 0.187$ by unpaired *t*-test).

proliferation within the thickened interstitium. We observed a notable dearth of fibrosis within alveolar septa, in contrast to what has been reported for humans with severe acute respiratory syndrome or Middle East respiratory syndrome (*3*,*4*). One cat had severe pneumonia with fibrin in alveolar spaces and endothelialitis (Appendix Figure 8), similar to what has been reported in humans with fatal coronavirus disease (*5*), although this cat did not show any respiratory signs.

To determine whether previous infection provides protection from future potential infection by SARS-CoV-2, we performed a reinfection study with 2 groups of cats. We previously reported that SARS-CoV-2 was transmitted from cats inoculated with the virus to cohoused, naive cats (*1*). In the previous study, the 3 cats that had been inoculated with SARS-CoV-2, whose nasal swabs were virus-negative on day 6 or 7 after the initial infection (*1*), were reinoculated with the same virus 4 weeks after the initial infection (Figure 1; Figure 2, panel A). No infectious virus was detected in the nasal or rectal swabs after reinfection, suggesting that the animals were protected from reinfection. These cats were euthanized at 21 days after reinfection (49 days after the initial infection), and tissue was submitted for histopathologic examination. The reinfection group showed lesions that were comparable with lung lesions observed on day 28 but with less severe thickening of alveolar septa ($p = 0.041$, by unpaired *t*-test) (Figure 1; Figure 2 panel B). The 3 cats in the other group, which recovered from infection that was transmitted by contact with virus-inoculated cats, were reinfected with the virus at ≈4 weeks (29–32 days) after transmission. On day 3 after reinfection, organs were harvested; infectious virus was not detected (detection limit 10 pfu/g of tissue) in respiratory organs or other organs

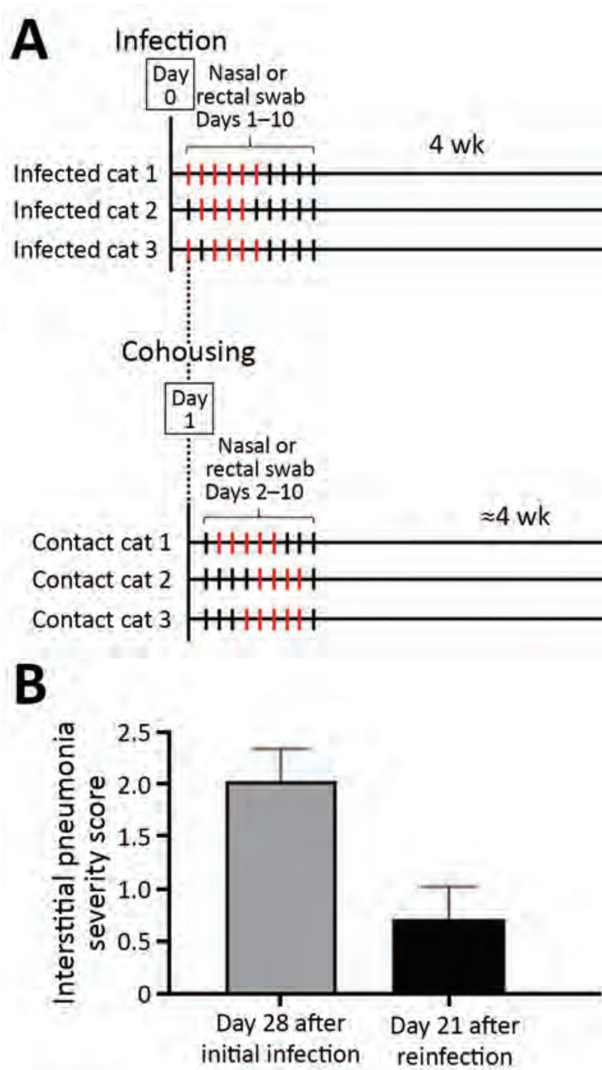


**Figure 2.** Timeline of severe acute respiratory syndrome coronavirus 2 infection and reinfection of cats and distribution of interstitial thickening. A) Timeline of infection and reinfection. As reported previously (*1*), a group of cats was inoculated with severe acute respiratory syndrome coronavirus 2 on day 0 (infected cats 1–3, upper half). A virus-naive cat was cohoused with each of the infected cats from day 1 (contact cats 1–3, lower half). The days on which infectious virus was detected in the nasal swabs are shown as red bars for each animal. In this study, we infected the cats with the same severe acute respiratory syndrome coronavirus 2 isolate at ≈4 weeks after initial infection or exposure to infected cats. After reinfection of the group shown in the upper half of the figure, no infectious virus was detected in the nasal swabs. The cats were confirmed to be seronegative before the initial infection or cohousing with infected cats, and seropositive before reinfection, on the basis of neutralization assay results. B) The distribution of interstitial thickening (interstitial pneumonia severity score) was decreased on day 21 after reinfection compared with day 28 ($p = 0.041$ by unpaired *t*-test).

analyzed (e.g., brain, liver, spleen, kidney, small and large intestine, heart, and eyelids). These results suggest that virus infection by natural transmission between cats, as well as by experimental inoculation, induces protective immunity against a second SARS-CoV-2 infection.

In conclusion, SARS-CoV-2 replicated effectively in the upper respiratory tract in cats, and infectious virus was cleared from the lungs within 6 days of infection; however, histopathologic examination demonstrated chronic lung sequelae in cats even a month after viral clearance. After initial infection with SARS-CoV-2, cats were protected from reinfection, with no virus replication in respiratory organs and no additional lung damage.

#### Acknowledgment

We thank Gillian McLellan for the cats used in this study and Sue Watson for scientific editing. We would also like to thank Angela Brice and Olga Gonzalez for sharing their expertise with our pathologists during consultation as well as Amanda Novak, Emily Tran, and Sara Stuedemann for their technical support.

This research was supported by the Center for Research on Influenza Pathogenesis, funded by the National Institutes of Allergy and Infectious Diseases, National Institutes of Health (grant no. HHSN272201400008C awarded to Y.K); the Research Program on Emerging and Re-emerging Infectious Disease from Japan Agency for Medical Research and Development (AMED) (grant no. JP19fk0108113 awarded to Y.K.); the Japan Initiative for Global Research Network on Infectious Diseases from AMED (grant no. JP19fm0108006 awarded to Y.K.); the Japan Program for Infectious Diseases Research and Infrastructure from AMED (grant no. JP20wm0125002 to Y.K.); and a University of Wisconsin K12 Career Development Award from the National Institute of Diabetes and Digestive and Kidney Diseases (grant no. K12DK100022 awarded to L.K.C.).

### About the Author

Dr. Chiba is a molecular virologist at the Influenza Research Institute at the University of Wisconsin–Madison, with a background in innate immunity studies and structural biology. Her primary research interests include mechanisms of virus infection, virus antigenicity, and host immune responses.

#### References

1. Halfmann PJ, Hatta M, Chiba S, Maemura T, Fan S, Takeda M, et al. Transmission of SARS-CoV-2 in domestic cats. N Engl J Med. 2020;383:592–4. https://doi.org/10.1056/NEJMc2013400
2. Shi J, Wen Z, Zhong G, Yang H, Wang C, Huang B, et al. Susceptibility of ferrets, cats, dogs, and other domesticated animals to SARS-coronavirus 2. Science. 2020;368:1016–20. https://doi.org/10.1126/science.abb7015
3. Cheung OY, Chan JW, Ng CK, Koo CK. The spectrum of pathological changes in severe acute respiratory syndrome (SARS). Histopathology. 2004;45:119–24. https://doi.org/10.1111/j.1365-2559.2004.01926.x
4. Das KM, Lee EY, Singh R, Enani MA, Al Dossari K, Van Gorkom K, et al. Follow-up chest radiographic findings in patients with MERS-CoV after recovery. Indian J Radiol Imaging. 2017;27:342–9. https://doi.org/10.4103/ijri.IJRI_469_16
5. Ackermann M, Verleden SE, Kuehnel M, Haverich A, Welte T, Laenger F, et al. Pulmonary vascular endothelialitis, thrombosis, and angiogenesis in Covid-19. N Engl J Med. 2020;383:120–8. https://doi.org/10.1056/NEJMoa2015432

Address for correspondence: Yoshihiro Kawaoka, 575 Science Dr, Madison, Wisconsin 53711, USA; email: yoshihiro.kawaoka@wisc.edu; or LaTasha K. Crawford, 2015 Linden Dr, Madison, Wisconsin 53706, USA; email: lkcrawford@wisc.edu

# Long-Term Humoral Immune Response in Persons with Asymptomatic or Mild SARS-CoV-2 Infection, Vietnam

Huynh Kim Mai, Nguyen Bao Trieu, Trinh Hoang Long, Hoang Tien Thanh, Nguyen Dinh Luong, Le Xuan Huy, Lam Anh Nguyet, Dinh Nguyen Huy Man, Danielle E. Anderson, Tran Tan Thanh, Nguyen Van Vinh Chau, Guy Thwaites, Lin-Fa Wang, Le Van Tan, Do Thai Hung

Author affiliations: Pasteur Institute, Nha Trang City, Vietnam (H.K. Mai, N.B. Trieu, T.H. Long, H.T. Thanh, N.D. Luong, L.X. Huy, D.T. Hung); Oxford University Clinical Research Unit, Ho Chi Minh City, Vietnam (L.A. Nguyet, T.T. Thanh, G. Thwaites, L.V. Tan); Hospital for Tropical Diseases, Ho Chi Minh City (D.N.H. Man, N.V.V. Chau); Duke-NUS Medical School, Singapore (D.E. Anderson, L.-F. Wang); Centre for Tropical Medicine and Global Health, Nuffield Department of Medicine, University of Oxford, Oxford, UK (G. Thwaites); SingHealth Duke-NUS Global Health Institute, Singapore (L.-F. Wang)

DOI: https://doi.org/10.3201/eid2702.204226

Antibody response against nucleocapsid and spike proteins of SARS-CoV-2 in 11 persons with mild or asymptomatic infection rapidly increased after infection. At weeks 18–30 after diagnosis, all remained seropositive but spike protein–targeting antibody titers declined. These data may be useful for vaccine development.

Severe acute respiratory syndrome coronavirus 2 (SARS-CoV-2) is the causative agent of the coronavirus disease (COVID-19) pandemic (*1*). Effective vaccines are vital for mitigating the impact of the pandemic. As such, synthesizing a long-term humoral immune response to SARS-CoV-2 remains essential to developing and implementing a SARS-CoV-2 vaccine. We report a longitudinal study of 11 persons with SARS-CoV-2 infection in Vietnam, in which we monitored antibody responses for up to 30 weeks after infection.

We included patients with a confirmed SARS-CoV-2 infection admitted to a COVID-19 treatment center in central Vietnam during January–March 2020. To enable long-term follow-up, we excluded all short-term visitors. We collected information from each participant about clinical status, travel history, contacts with persons with confirmed cases, and personal demographics. For plasma collection, we applied a flexible sampling schedule encompassing 30 weeks after diagnosis, stratified by collection at 1, 2–3, 4–7, and ≥18 weeks after diagnosis.

We measured antibodies against 2 main immunogens of SARS-CoV-2, the nucleocapsid (N) and spike (S) proteins, by using 2 well-validated sensitive and specific serologic assays, Elecsys Anti–SARS-CoV-2 assay (Roche, https://diagnostics.roche.com) (*2*) and SARS-CoV-2 Surrogate Virus Neutralization Test (sVNT) (GenScript, https://www.genscript.com) (*3*). The former is an electrochemiluminescence immunoassay that uses recombinant N protein for qualitative detection of pan Ig, including IgG, against SARS-CoV-2. The latter is a surrogate assay for measuring receptor-binding domain–targeting neutralizing antibodies (RBD-targeting NAbs) (*3*,*4*), in principle a blocking ELISA that quantifies antibodies that block the receptor–RBD interaction (*3*). Our study forms part of the national COVID-19 response and was approved by the institutional review board of the Pasteur Institute in Nha Trang, Vietnam.

During the study period, there were a total of 23 patients with confirmed SARS-CoV-2 infection in central Vietnam. Ten were tourists and were thus excluded from the study. Of the remaining 13, a total of 11 consented to participate in this study. Among study participants, 6 were female and 5 were male; the age range was 12–64 years (Table). Seven experienced mildly symptomatic infection and did not require supplemental oxygen during hospitalization; 4 were asymptomatic. Before becoming ill, 3 had traveled to a SARS-CoV-2–endemic country, including patients 2 and 3, who had traveled to Malaysia and patient 4 had traveled to the United States. Patient 4 transmitted the virus to 6 of her contacts, including 4 family members and 2 employees. Of these, 2 transmitted the virus to another family member (Table; Appendix Figure, https://wwwnc.cdc.gov/EID/article/27/2/20-4226-App1.pdf).

**Table.** Demographics, travel history, contact history, clinical status, and outcome for participants in study of long-term humoral immune response in persons with asymptomatic or mild SARS-CoV-2 infection, Vietnam, 2020*

| Patient no.† | Age, y/sex | Province | Presumed exposure | Symptoms developed | Diagnosed | Presumed incubation period, d | Recent travel history | Contact with confirmed patient | Clinical status | Hospital stay, d |
|---|---|---|---|---|---|---|---|---|---|---|
| 1 | 25/F | Khanh Hoa | Jan 14 | Jan 18 | Jan 24 | 4 | None | 1 of first 2 cases in Vietnam | Sympt | 11 |
| 2 | 42/M | Ninh Thuan | Feb 27–Mar 4 | Mar 9 | Mar 16 | 5–14 | Malaysia | Unknown | Sympt | 16 |
| 3 | 36/M | Ninh Thuan | Feb 27–Mar 4 | Mar 13 | Mar 17 | 9–15 | Malaysia | Unknown | Sympt | 15 |
| 4 | 51/F | Binh Thuan | Feb 22–29 | Mar 5 | Mar 9 | 7–14 | USA | Unknown | Sympt | 25 |
| 5‡ | 51/M | Binh Thuan | Mar 2–9 | Mar 11 | Mar 11 | 2–9 | None | Husband of patient 4 | Sympt | 23 |
| 6‡ | 64/F | Binh Thuan | Mar 2–10 | Asympt | Mar 10 | 5–8 | None | Domestic worker of patient 4 | Asympt | 31 |
| 7‡ | 28/F | Binh Thuan | Mar 7 | Asympt | Mar 10 | 3 | None | Daughter-in-law of patient 4 | Asympt | 24 |
| 8‡ | 28/M | Binh Thuan | Mar 2–9 | Mar 11 | Mar 11 | 2–9 | None | Son of patient 4 | Sympt | 23 |
| 9‡ | 47/F | Binh Thuan | Mar 3–8 | Mar 11 | Mar 11 | 3–8 | None | Mother of patient 7 | Sympt | 23 |
| 10‡ | 37/F | Binh Thuan | Mar 3–8 | Asympt | Mar 10 | 2–7 | None | Staff of patient 4 | Asympt | 24 |
| 11‡ | 12/M | Binh Thuan | Mar 3–8 | Asympt | Mar 11 | 2–7 | None | Son of patient 10 | Asympt | 30 |

*All patients made a full recovery. No patients required oxygen. All patients were of Vietnamese nationality. First enrollment was on January 24, 2020, and last was on March 17, 2020. Last follow up was on August 13, 2020. Asympt, asymptomatic; sympt, symptomatic.
†Patient numbers match those in Figure 1.
‡Patients from a cluster involving 3 household transmission chains (Appendix Figure, https://wwwnc.cdc.gov/EID/article/27/2/20-4226-App1.pdf).

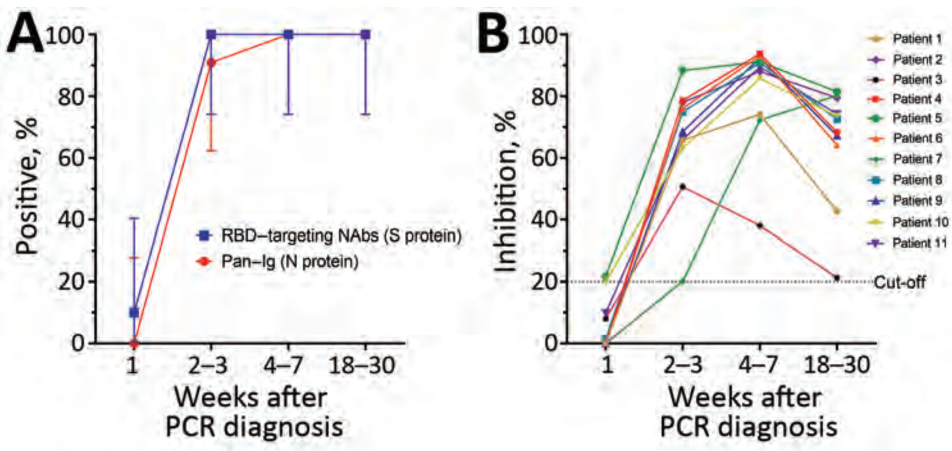


**Figure.** Antibody responses in 11 study participants, weeks 1–20 after PCR diagnosis of SARS-CoV-2 infection, Vietnam, 2020. A) Seroprevalence of SARS-CoV-2 among 11 COVID-19 patients. We followed testing protocols and the positive cutoff of 20% recommended in the Elecsys Anti–SARS-CoV-2 assay (Roche, https://diagnostics.roche.com) without any modification. Using these parameters, previous studies showed an excellent concordance between results from surrogate virus neutralization tests and conventional neutralizing antibody detection assays (*3*,*4*). Vertical bars denote 95% CIs. Graphs were created using GraphPad Prism version 8.0 (GraphPad software, https://www.graphpad.com). B) Kinetics of neutralizing antibodies measured by the surrogate neutralization assay (GenScript, https://www.genscript.com) with the 20% cutoff applied. We tested samples at 1:10 dilution as specified. Because of the limited availability of plasma samples, each sample was tested only once. RBD, receptor-binding domain; NAbs, neutralizing monoclonal antibodies; S, spike; N, nucleocapsid.

We collected 43 plasma samples from 11 participants within 4 time ranges after diagnosis: <1 week (n = 10), weeks 2–3 (n=11), weeks 4–7 (n=11), and weeks 18–30 (n = 11). During the first week after diagnosis, 1 patient (1/10, 10%) had detectable RBD-targeting NAbs, and none had antibodies against N protein. In subsequent weeks, all (100%) participants tested positive by surrogate virus neutralization. Antibodies against N protein were detected in 10/11 (91%) of the samples collected between the second and third weeks after diagnosis and 11/11 (100%) samples collected at subsequent time points (Figure, panel A).

Previous studies have demonstrated that the inhibition percentage measured by surrogate virus neutralization tests correlates well with neutralizing antibody titers measured by conventional virus neutralization assays or plaque-reduction neutralization tests (*3*,*4*). In our study, the inhibition percentage was below the assay cutoff in all but 1 plasma sample taken during the first week after diagnosis and then rapidly increased above the assay cutoff at subsequent time points. At weeks 18–30 after diagnosis, the inhibition percentage declined but remained detectable (Figure, panel B).

We demonstrate that antibodies against 2 main structural proteins (S and N) of SARS-CoV-2 in patients with asymptomatic or mild infections were almost undetectable within the first week after diagnosis. Antibodies rapidly increased in subsequent weeks and peaked around weeks 4–7 before declining during the later phase of infection, consistent with previously reported findings (*2*,*5*–*7*). However, few studies have reported the persistence of long-term humoral immune response to SARS-CoV-2 up to 18–30 weeks after diagnosis (*5*), especially among mildly symptomatic or asymptomatic infected patients.

The titers of RBD-targeting NAbs, which are well correlated with those of neutralizing antibodies, decayed by weeks 18–30 after infection, suggesting that humoral immunity to SARS-CoV-2 infection may not be long lasting. Because neutralizing antibodies are recognized as a surrogate for protection (*7*–*9*), follow-up studies beyond this period are needed to more conclusively determine the durability of these long-term responses and their correlation with protection.

Our collective findings offer insights into the long-term humoral immune response to SARS-CoV-2 infection. The data might have implications for COVID-19 vaccine development and implementation and other public health responses to the COVID-19 pandemic.


### Acknowledgments

We thank the patients for their participations in this study and the diagnostic team at the Hospital for Tropical Diseases, Le Nguyen Truc Nhu, Nguyen Thi Thu Hong for laboratory support.

This study was funded by the World Health Organization and the US Centers for Disease Control and Prevention through the Field Epidemiology of Training Programmes. L.V.T. and G.T. are supported by the Wellcome Trust of Great Britain (204904/Z/16/Z and 106680/B/14/Z, respectively). The serology work at Duke-NUS is supported by grants from the National Medical Research Council, Singapore (STPRG-FY19-001 and COVID19RF-003).

## About the Author

Ms. Mai is vice-head of the virology department of the Pasteur Institute in Nha Trang City, Vietnam. She has been part of a team responsible for COVID-19 diagnostics in an area of central Vietnam with a population of ≈25 million people.

## References


1. Zhu N, Zhang D, Wang W, Li X, Yang B, Song J, et al.; for the China Novel Coronavirus Investigating and Research Team. A novel coronavirus from patients with pneumonia in China, 2019. N Engl J Med. 2020;382:727–33. https://doi.org/10.1056/NEJMoa2001017
2. Chen SY, Lee YL, Lin YC, Lee NY, Liao CH, Hung YP, et al. Multicenter evaluation of two chemiluminescence and three lateral flow immunoassays for the diagnosis of COVID-19 and assessment of antibody dynamic responses to SARS-CoV-2 in Taiwan. Emerg Microbes Infect. 2020;9:2157–68. https://doi.org/10.1080/22221751.2020.1825016
3. Tan CW, Chia WN, Qin X, Liu P, Chen MI, Tiu C, et al. A SARS-CoV-2 surrogate virus neutralization test based on antibody-mediated blockage of ACE2-spike protein-protein interaction. Nat Biotechnol. 2020;38:1073–8. https://doi.org/10.1038/s41587-020-0631-z
4. Perera RAPM, Ko R, Tsang OTY, Hui DSC, Kwan MYM, Brackman CJ, et al. Evaluation of a SARS-CoV-2 surrogate virus neutralization test for detection of antibody in human, canine, cat and hamster sera. J Clin Microbiol. 2020;JCM.02504-20. https://doi.org/10.1128/JCM.02504-20
5. Gudbjartsson DF, Norddahl GL, Melsted P, Gunnarsdottir K, Holm H, Eythorsson E, et al. Humoral immune response to SARS-CoV-2 in Iceland. N Engl J Med. 2020;383:1724–34. https://doi.org/10.1056/NEJMoa2026116
6. Sun B, Feng Y, Mo X, Zheng P, Wang Q, Li P, et al. Kinetics of SARS-CoV-2 specific IgM and IgG responses in COVID-19 patients. Emerg Microbes Infect. 2020;9:940–8. https://doi.org/10.1080/22221751.2020.1762515
7. Folegatti PM, Ewer KJ, Aley PK, Angus B, Becker S, Belij-Rammerstorfer S, et al.; on behalf of the Oxford COVID Vaccine Trial Group. Safety and immunogenicity of the ChAdOx1 nCoV-19 vaccine against SARS-CoV-2: a preliminary report of a phase 1/2, single-blind, randomised controlled trial. Lancet. 2020;396:467–78. https://doi.org/10.1016/S0140-6736(20)31604-4
8. van Doremalen N, Lambe T, Spencer A, Belij-Rammerstorfer S, Purushotham JN, Port JR, et al. ChAdOx1 nCoV-19 vaccine prevents SARS-CoV-2 pneumonia in rhesus macaques. Nature. 2020;586:578–82. https://doi.org/10.1038/s41586-020-2608-y
9. Deng W, Bao L, Liu J, Xiao C, Liu J, Xue J, et al. Primary exposure to SARS-CoV-2 protects against reinfection in rhesus macaques. Science. 2020;369:818–23. https://doi.org/10.1126/science.abc5343


Address for correspondence: Huynh Kim Mai, 8-9-10 Tran Phu, Xuong Huan Ward, Nha Trang City, Khanh Hoa Province, Vietnam; email: mai064@yahoo.com and Le Van Tan, 764 Vo Van Kiet, District 5, Ho Chi Minh City, Vietnam; email: tanlv@oucru.org

# Prevalence and Time Trend of SARS-CoV-2 Infection in Puducherry, India, August–October 2020

Sitanshu Sekhar Kar, Sonali Sarkar, Sharan Murali, Rahul Dhodapkar, Noyal Mariya Joseph, Rakesh Aggarwal

Author affiliation: Jawaharlal Institute of Postgraduate Medical Education and Research, Puducherry, India

DOI: https://doi.org/10.3201/eid2702.204480

We conducted 3 population-based cross-sectional surveys, at 1-month intervals, to estimate the prevalence and time-trend of severe acute respiratory syndrome coronavirus 2 infection in Puducherry, India. Seropositivity rate increased from 4.9% to 34.5% over 2 months and was 20-fold higher than the number of diagnosed cases of infection.

The magnitude of the ongoing pandemic of coronavirus disease (COVID-19), caused by infection with severe acute respiratory syndrome coronavirus 2 (SARS-CoV-2), has not been fully assessed because most those infected have no or mild symptoms, and thus do not undergo viral nucleic acid or antigen testing (*1*–*3*). Determining the proportion of a population that has had infection at various time points is essential for understanding the dynamics of an epidemic in a particular area.

Puducherry district, population ≈1.25 million, is located in southern India. Its earliest recorded case of COVID-19 was in March 2020; it had 7 total cases by the end of May, 67 by end of June, and 663 by end of July 2020 (*4*). The district followed national COVID-19 management guidelines, including testing all symptomatic persons and their high-risk contacts.

We conducted 3 community-based serologic surveys for SARS-CoV-2 antibodies in Puducherry at 1-month intervals, i.e., during August 11–16, September 10–16, and October 12–16, 2020 (Figure). Each survey included 900 adults selected using a multistage sampling procedure. In the initial stages, we chose 30 clusters, including 21 of 90 urban wards and 9 of 62 villages, using a probability proportional to size with replacement method; this method replicated the urban-to-rural ratio (70:30) of the district's population. Thereafter, in each cluster, we chose 30 households by systematic random sampling; we collected blood from 1 adult (≥18 years of age) in each household using a modified Kish method (*5*,*6*). The data from these surveys represent the cumulative proportion of

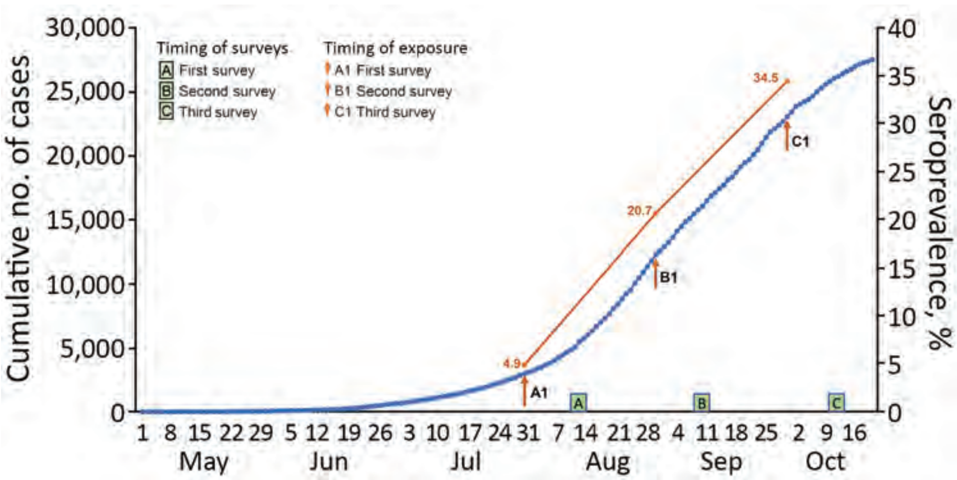


**Figure.** Prevalence of severe acute respiratory syndrome coronavirus 2 infection in 3 surveys in Puducherry district, India, 2020. Arrows indicate the timepoint 2 weeks before the midpoint of each of 3 surveillance periods.

population in Puducherry who had been infected with SARS-CoV-2 at ≈2 weeks before midpoint of each survey, i.e., at the end of July, August, and September 2020 (Figure). We obtained approval from Jawaharlal Institute's ethics committee and informed written consent from participants.

We tested all serum specimens using a commercial electrochemiluminescence-based microparticle immunoassay with 99.5% sensitivity and 99.8% specificity (Elecsys Anti-SARS-CoV-2; Roche, https://www.roche.com) (*7*) for qualitative detection of antibodies against recombinant nucleoprotein antigen of

**Table.** Seroprevalence of SARS-CoV-2 antibodies in 3 surveys in Puducherry, India, 2020*

| | August 11–16, n = 869 | | September 10–16, n = 898 | | October 12–16, n = 900 | |
|---|---|---|---|---|---|---|
| Variable | No, positive/ no. tested | % (95% CI) | No. positive/ no. tested | % (95% CI) | No. positive/ no. tested | % (95% CI) |
| Crude prevalence | 43/869 | 4.9 (3.5–6.4) | 186/898 | 20.7 (18.0–23.3) | 311/900 | 34.5 (31.5–37.7) |
| Age category, y | | | | | | |
| 18–29 | 8/170 | 4.7 (1.5–7.8) | 33/165 | 20.0 (13.9–26.1) | 58/180 | 32.2 (25.8–39.3) |
| 30–44 | 13/295 | 4.4 (2.1–6.7) | 58/277 | 20.9 (16.2–25.7) | 92/252 | 36.5 (30.8–42.6) |
| 45–59 | 13/242 | 5.4 (2.5–8.2) | 64/271 | 23.6 (18.5–28.7) | 101/259 | 39.0 (33.2–45.0) |
| ≥60 | 9/162 | 5.6 (2.0–9.1) | 31/185 | 16.7 (11.4–22.1) | 60/209 | 28.7 (23.0–35.1) |
| Sex | | | | | | |
| M | 16/439 | 3.6 (1.9–5.4) | 95/443 | 21.4 (17.6–25.2) | 126/406 | 31.0 (26.7–35.6) |
| F | 27/428 | 6.3 (4.0–8.6) | 91/455 | 20.0 (16.3–23.6) | 183/491 | 37.2 (33.1–41.6) |
| Residence setting† | | | | | | |
| Urban | 35/609 | 5.7 (3.9–7.5) | 130/629 | 20.7 (17.5–23.8) | 225/628 | 35.8 (32.1–39.7) |
| Rural | 8/260 | 3.1 (1.0–5.2) | 56/269 | 20.8 (16.0–25.7) | 86/272 | 31.6 (26.3–37.4) |
| Occupation‡ | | | | | | |
| Healthcare workers | 2/29 | 6.9 (1.0–22.8) | 4/32 | 12.5 (1.0–24.0) | 18/66 | 27.2 (18.0–39.0) |
| Other frontline workers | 0/22 | 0 | 8/23 | 34.8 (15.3–54.2) | 6/15 | 40.0 (19.0–64.2) |
| Others | 41/818 | 5.0 (3.5–6.5) | 174/843 | 20.6 (17.9–23.4) | 287/819 | 35.0 (31.8–38.3) |
| Other characteristics | | | | | | |
| COVID-19 | 4/34 | 11.8 (9.3–22.6) | 16/47 | 34.0 (20.5–47.6) | 82/184 | 44.5 (37.5–51.7) |
| COVID-19 diagnosis | 3/3 | 100 | 3/7 | 42.9 (6.1–79.5) | 25/29 | 86.2 (69.4–94.5) |
| COVID-19 symptoms in last 6 mo | 8/85 | 9.4 (3.2–15.6) | 10/44 | 22.7 (10.3–35.1) | 85/148 | 57.4 (49.3–65.1) |
| Cumulative case incidence (cumulative incidence ratio)§ | 2,987 (0.25%) | | 12,331 (1.03%) | | 23,080 (1.92%) | |
| Infection-to-case ratio¶ | 4.9%/0.25% = 19.6 | | 20.9%/1.03% = 20.0 | | 34.5%/1.92% = 18.0 | |
| Cumulative deaths | 43 | | 187 | | 441 | |
| Infection fatality ratio (cumulative deaths per 100,000 infected persons)# | 73.4 | | 75.8 | | 106.1 | |

*COVID-19, coronavirus disease; SARS-CoV-2, severe acute respiratory syndrome coronavirus 2.
†Definitions used by the Office of the Registrar General & Census Commissioner, Government of India.
‡Other frontline workers included police officers, teachers, revenue officers, persons involved in COVID-19 response.
§Calculated for data gathered until 2 weeks before the midpoint of the survey.
¶Infection-to-case ratio was calculated as crude seroprevalence / cumulative incidence ratio.
#Infection-fatality ratio was calculated as cumulative deaths/crude prevalence × estimated population of the district.

SARS-CoV-2, following manufacturer's instructions. Specimens with cutoff index ≥1.0 were considered seroreactive; cutoff index was the ratio of chemiluminescence signal of sample with that of the reference sample. For each timepoint, we calculated crude prevalence rate with 95% CI using a binomial model. In addition, we used the data on cumulative cases and deaths recorded until each timepoint (*4*) to calculate infection-to-case and infection-to-death ratios.

We visited 890 households and recruited 869 participants (response rate 97.8%) in August, 902 households from which we recruited 898 (99.8%) participants in September, and 900 households from which we recruited 900 (100%) participants in October. We tracked cumulative number of reported cases (cumulative incidence rates) of COVID-19 and deaths due to the disease in the district at each timepoint (Table) (*4*). In each survey, the median age was in the mid-40s with nearly equal numbers of men and women. Crude seroprevalence of SARS-CoV-2 antibodies increased from 4.9% (95% CI, 3.5%–6.4%) in August, to 20.7% (18.0%–23.3%) in September, to 34.5% (31.5%–37.7%) in October. These rates indicate that ≈16% of the district's population acquired SARS-CoV-2 infection during August and ≈14% during September 2020. These rates are much higher than those reported from other parts of the world (*8*), but are similar to a high seropositivity rate of 57% reported in slum areas of Mumbai (*9*).

The infection-to-case ratios were similar across the 3 surveys: 19.6 in August, 20.0 in September, and 18.0 in October. These results indicated that, despite implementing the strategies of testing all symptomatic persons and of aggressive contact tracing in the district, only a small proportion of SARS-CoV-2 infections had been diagnosed at each timepoint. This contrasts with the data from high-income countries (*10*) and could be related to the younger age distribution in the population of India, partial immunity due to other prior coronavirus or other infections, or both.

Strengths of our study include representativeness of the population by its random selection procedure and high participation rate; repeat testing in the same primary sampling units to reduce variability over time; and the use of an assay with high sensitivity and specificity. Limitations included the possibility that some persons did not show development of antibodies following infection, leading to a falsely low seroprevalence; possible loss of antibodies over time, leading to a falsely low rise of seroprevalence with time; and dependence of seroprevalence on the assay used.

Our data indicate a high rate of transmission of SARS-CoV-2 in Puducherry during August and September 2020, with some evidence of slowing over time. By the end of September, nearly one third of the population were infected with SARS-CoV-2, a much larger proportion than those diagnosed with COVID-19. These findings should help guide the response to COVID-19 in our district.

### Acknowledgments

We thank the members of our survey and laboratory teams, and the study participants for their help.

This project was funded by an intramural grant from the Jawaharlal Institute of Postgraduate Medical Education and Research, Puducherry, India.

## About the Author

Dr. Kar is an additional professor of preventive and social medicine at the Jawaharlal Institute of Postgraduate Medical Education and Research, Puducherry, India. His research interests include disease epidemiology.

### References

1. World Health Organization. Population-based age-stratified seroepidemiological investigation protocol for coronavirus 2019 (COVID-19) infection, 26 May 2020. 2020 [cited 2020 Aug 24]. https://apps.who.int/iris/handle/10665/332188
2. World Health Organization. Report of the WHO-China joint mission on coronavirus disease 2018 (COVID-19). 2020 [cited 2020 Aug 24]. https://www.who.int/docs/default-source/coronaviruse/who-china-joint-mission-on-covid-19-final-report.pdf
3. Varghese GM, John R, Manesh A, Karthik R, Abraham OC. Clinical management of COVID-19. Indian J Med Res. 2020;151:401–10. https://doi.org/10.4103/ijmr.IJMR_957_20
4. Health Department, Puducherry. COVID-19 Puducherry. 2020 [cited 2020 Oct 10]. https://covid19dashboard.py.gov.in
5. Lavrakas P. Kish selection method. In: Encyclopedia of survey research methods. 2020 Oct 30 [cited 2020 Nov 30]. https://methods.sagepub.com/reference/encyclopedia-of-survey-research-methods/n262.xml
6. Kumar MS, Bhatnagar T, Manickam P, Kumar VS, Rade K, Shah N, et al. National sero-surveillance to monitor the trend of SARS-CoV-2 infection transmission in India: protocol for community-based surveillance. Indian J Med Res. 2020;151:419–23. https://doi.org/10.4103/ijmr.IJMR_1818_20
7. Roche Diagnostics. Elecsys Anti-SARS-CoV-2. 2020 [cited 2020 Oct 10]. https://diagnostics.roche.com/global/en/products/params/elecsys-anti-sars-cov-2.html
8. Lai C–C, Wang J-H, Hsueh P-R. Population-based seroprevalence surveys of anti-SARS-CoV-2 antibody: an up-to-date review. Int J Infect Dis. 2020;101:314–322. https://doi.org/10.1016/j.ijid.2020.10.011
9. Tata Institute of Fundamental Research. Technical details: SARS-CoV2 serological survey in Mumbai by NITI-BMC-TIFR. 2020 [cited 2020 Nov 4]. https://www.tifr.res.in/TSN/article/Mumbai-Serosurvey%20Technical%20report-NITI.pdf

10. Stringhini S, Wisniak A, Piumatti G, Azman AS, Lauer SA, Baysson H, et al. Seroprevalence of anti-SARS-CoV-2 IgG antibodies in Geneva, Switzerland (SEROCoV-POP): a population-based study. Lancet. 2020;396:313–9. https://doi.org/10.1016/S0140-6736(20)31304-0

Address for correspondence: Sitanshu Sekhar Kar, Jawaharlal Institute of Postgraduate Medical Education—Preventive and Social Medicine, JIPMER Campus, Puducherry, Puducherry 605006 India; email: drsitanshukar@gmail.com

# SARS-CoV-2 Infection and Mitigation Efforts among Office Workers, Washington, DC, USA

Samira Sami, Nga Vuong, Halie Miller, Rachael Priestley, Matthew Payne, Garrett Licata-Portentoso, Jan Drobeniuc, Lyle R. Petersen

Author affiliations: Centers for Disease Control and Prevention, Atlanta, Georgia, USA (S. Sami, H. Miller, R. Priestley, J. Drobeniuc); Centers for Disease Control and Prevention, Fort Collins, Colorado, USA (N. Vuong, L.R. Petersen); Federal Emergency Management Agency, Washington, DC, USA (M. Payne, G. Licata-Portentoso)

DOI: https://doi.org/10.3201/eid2702.204529

Despite mitigation efforts, 2 coronavirus disease outbreaks were identified among office workers in Washington, DC. Moderate adherence to workplace mitigation efforts was reported in a serologic survey; activities outside of the workplace were associated with infection. Adherence to safety measures are critical for returning to work during the pandemic.

On March 19, 2020, the Federal Emergency Management Agency (FEMA) activated the National Response Coordination Center in Washington, DC, USA, in response to the coronavirus disease (COVID-19) pandemic. At that time, cases were rapidly increasing in Washington, DC; ≈200 cases had been reported since March 7. Although city officials ordered closure of nonessential businesses on March 24, FEMA remained open. To protect staff from severe acute respiratory syndrome coronavirus 2 (SARS-CoV-2) infection, all persons entering FEMA headquarters underwent symptom and temperature screening. On April 5, after a cluster of 6 epidemiologically linked cases was identified, additional mitigation efforts were implemented, including requiring face masks at all times, requiring that a distance of 6 feet be maintained between employees, and reducing occupancy in the open office space building from a daily average of 1,300 to 400 persons.

To examine workplace and community factors associated with infection, we conducted a serologic survey of SARS-CoV-2 antibodies among staff who worked on site after the mitigation efforts had been implemented. To assess the effect of mitigation efforts in the workplace, we examined occupational case surveillance data.

Staff who worked in the FEMA building during April 1–22 were identified by using turnstile records and were invited by email to participate in a survey. Persons who had had symptoms of COVID-19 within 2 weeks of the survey were ineligible to participate. During April 23–29, consenting participants completed a self-administered, online questionnaire assessing demographics and potential community and workplace exposure to SARS-CoV-2, and blood samples were collected.

Blood samples were tested for SARS-CoV-2 IgG by using ELISA targeting the SARS-CoV-2 receptor-binding domain protein (*1*). Indeterminate test results or incomplete questionnaires resulted in the exclusion of 10 participants. Characteristics of seropositive and seronegative groups were compared by using the Fisher exact test, and 2-sided p values $<0.05$ were considered statistically significant. Reports of confirmed COVID-19 cases among staff who worked at FEMA headquarters during March–October 2020 were obtained from occupational health records. This activity was reviewed by the Centers for Disease Control and Prevention and deemed public health surveillance.

Of the 466 survey participants, 15 (3.2%) tested positive for SARS-CoV-2 antibodies. Seroprevalence did not vary by sex or age (Table). Of those who tested positive, 11 (73%) reported never having been tested for SARS-CoV-2 by nasal or throat swab, and 8 (53%) reported no symptoms suggestive of SARS-CoV-2 infection since January 15, 2020 (*2*). On average, participants had spent 20.5 (± 12.0 SD) days in the FEMA building since March 2020. We found no significant difference in workplace

**Table.** Characteristics and workplace and community exposure for SARS-CoV-2 infection among workers in the FEMA headquarters, by serologic testing results, Washington, DC, USA, April 2020*

| Characteristic | SARS-CoV-2 result, no. (%) Positive (n = 15) | SARS-CoV-2 result, no. (%) Negative (n = 451) | p value† |
|---|---|---|---|
| Sex | | | |
| F | 4 (26.7) | 167 (37.0) | 0.588 |
| M | 11 (73.3) | 284 (63.0) | |
| Age group, y (n = 464) | | | |
| 18–34 | 5 (33.3) | 112 (24.9) | 0.503 |
| 35–49 | 3 (20.0) | 187 (41.5) | |
| 50–64 | 7 (46.7) | 139 (31.0) | |
| $\geq$65 | 0 (0.0) | 11 (2.4) | |
| Mitigation activities in the workplace | | | |
| Wear a face cover (most or all the time) | 9 (60.0) | 273 (60.5) | 0.298 |
| Maintain a distance $\geq$6 feet from others (most or all the time) | 12 (80.0) | 344 (76.3) | 1.000 |
| Wash your hands or use hand sanitizer ($\geq$5 times daily) | 13 (86.7) | 411 (91.1) | 0.147 |
| Exposure to someone who tested positive for SARS-CoV-2 in the FEMA building | | | |
| Any face-to-face contact | 2 (13.3) | 51 (11.4) | 0.224 |
| >10 min within 6 feet | 2 (13.3) | 46 (10.2) | 0.061 |
| Shared workspace | 2 (13.3) | 44 (9.8) | 0.062 |
| Shared breakroom | 1 (6.7) | 30 (6.7) | 0.286 |
| Within 6 feet while coughing or sneezing | 1 (6.7) | 10 (2.2) | 0.325 |
| Exposure to household member with confirmed COVID-19 | 2 (13.3) | 3 (0.7) | 0.001 |
| Community exposure during January 15–March 11 | | | |
| Traveled by bus, train, or subway | 8 (53.3) | 318 (70.5) | 0.161 |
| Traveled by taxi or rideshare | 9 (60.0) | 290 (64.3) | 0.787 |
| Attended social gatherings of >50 persons | 12 (80.0) | 254 (56.3) | 0.109 |
| Visited a healthcare facility | 8 (53.3) | 150 (33.3) | 0.162 |
| Community exposure during March 12 through date of blood draw | | | |
| Traveled by bus, train, or subway | 5 (33.3) | 204 (45.2) | 0.436 |
| Traveled by taxi or rideshare | 9 (60.0) | 147 (32.6) | 0.047 |
| Attended social gatherings of >50 persons | 2 (13.3) | 55 (12.2) | 0.704 |
| Visited a healthcare facility | 2 (13.3) | 64 (14.2) | 1.000 |

*COVID-19, coronavirus disease; FEMA, Federal Emergency Management Agency; SARS-CoV-2, severe acute respiratory syndrome coronavirus 2.
†Fisher exact test for categorical variables.

mitigation activities between seropositive and seronegative participants: 60.0% seropositive versus 60.5% seronegative participants used a face covering most of the time or always, 80.0% versus 76.3% maintained a distance of $\geq$6 feet from others most of the time or always, and 86.7% versus 91.1% washed their hands or used hand sanitizer $\geq$5 times per day. However, a higher, although not statistically significant, percentage of participants who shared a workspace were seropositive (13.3%) than seronegative (9.8%). The same was true for persons who spent >10 minutes $\leq$6 feet from someone who tested positive for SARS-CoV-2 in the FEMA building; 13.3% were seropositive and 10.2% were seronegative. A significantly higher percentage of seropositive participants lived with someone who had a confirmed positive test result for SARS-CoV-2 (13.3%) than those who were seronegative (0.7%). After the cancellation of nonessential gatherings on March 11, 60.0% of seropositive participants traveled by taxi or rideshare compared with 32.3% of seronegative participants who did not (p = 0.047).

By October 30, after mitigation efforts were implemented, 2 clusters of epidemiologically linked COVID-19 cases were identified: 4 cases among staff in cluster B and 5 cases in cluster D (Figure). We identified an additional 6 nonlinked cases among staff who worked in the FEMA building. Overall, 15 (71%) cases were linked to a cluster.

To our knowledge, evaluations of workplace SARS-CoV-2 mitigation strategies in office buildings have not been published. This study identified 2 factors outside of the workplace that are potentially associated with SARS-CoV-2 infection and transmission in the workplace (despite limited knowledge of whether infection occurred before or after potential exposure): residing with a household member with COVID-19 and using shared transportation. Although seroprevalence for SARS-CoV-2 antibodies was low among office workers, preventing workplace exposures to COVID-19 during March–April 2020 remained challenging. More than half of seropositive participants remained asymptomatic or were never tested for SARS-CoV-2, and 20%–40% of participants did not adhere to masking or physical distancing guidelines. This finding highlights the difficulties of adhering to mitigation efforts in the workplace and the importance of ensuring prevention efforts as persons return to work, such as engineering controls to reduce occupancy levels and modifying areas to

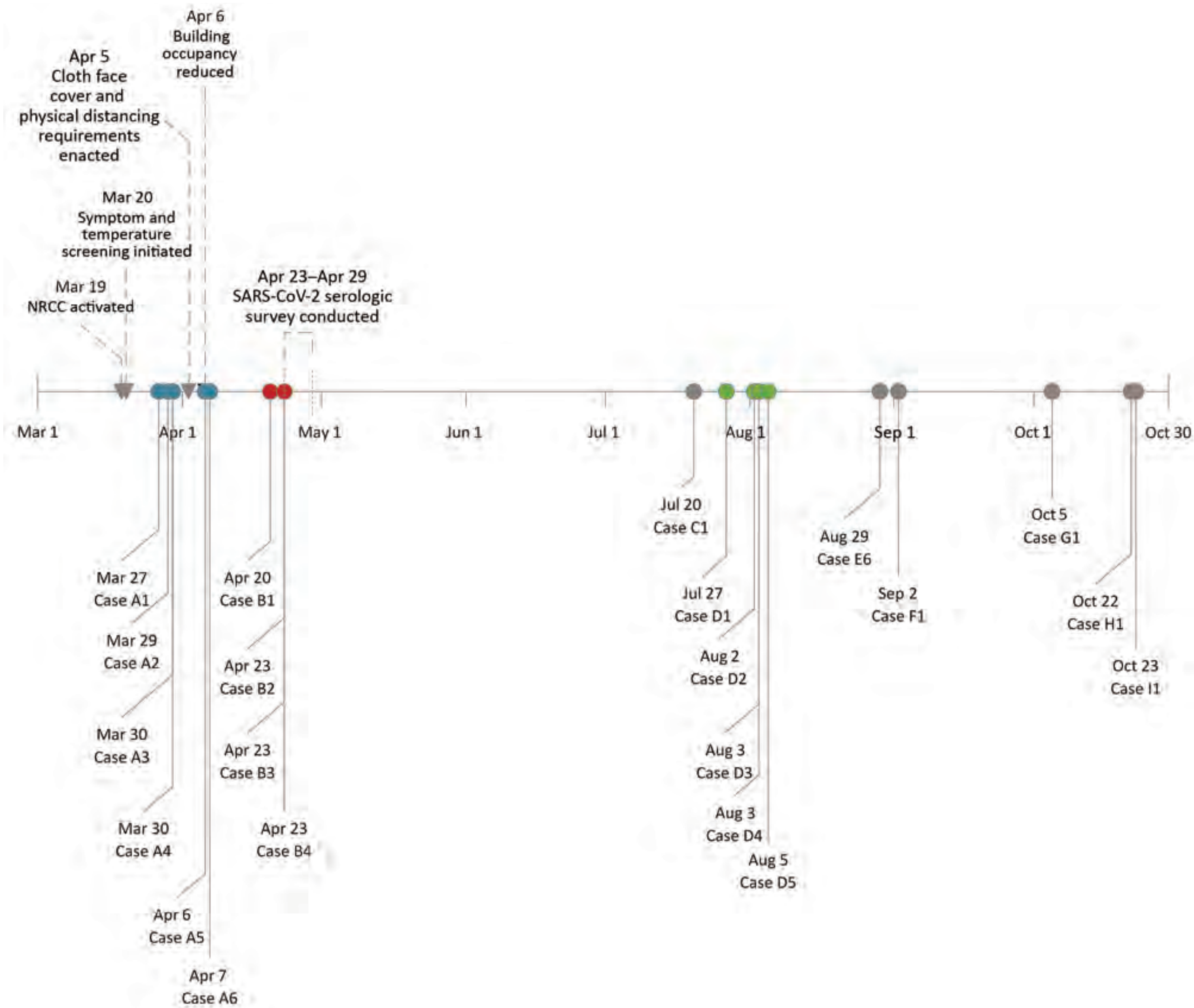


**Figure.** Coronavirus disease cases among workers in the Federal Emergency Management Agency, by case reporting date, and critical events, Washington, DC, USA, March–October 2020. Associated colors and A, B, and D indicate infection clusters. NRCC, National Response Coordination Center; SARS-CoV-2, severe acute respiratory syndrome coronavirus 2.

maintain a distance of 6 feet between employees (*3*). Despite hazard controls implemented in the workplace, activities outside of work and noncompliance with mitigation efforts probably contributed to cases and small clusters of COVID-19 among office workers. However, seroprevalence remained at the same level as the overall 3.2% seroprevalence estimate for Washington, DC residents (*4*).

**Acknowledgments**

We thank members of the Walter Reed National Military Medical Center for their assistance with specimen collection. We thank Anthony Macintyre and members of FEMA for their assistance with survey implementation. We also thank Emory University and the Centers for Disease Control and Prevention COVID-19 Lab Task Force for their assistance with specimen testing. Last, we are grateful to Concepcion Estivariz, Amanda Wilkinson, Susan Gerber, and Joe Bresee for input on the study protocol.

## About the Author

Dr. Sami is an epidemiologist in the Influenza Division, the National Center for Immunization and Respiratory Diseases, Centers for Disease Control and Prevention, Atlanta, Georgia, USA. She and her colleagues have undertaken this research while deployed in support of the federal coronavirus disease response.

References

1. US Food and Drug Administration. EUA authorized serology test performance. 2020 [cited 2020 Sep 26]. https://www.fda.gov/medical-devices/emergency-situations-medical-devices/eua-authorized-serology-test-performance
2. Centers for Disease Control and Prevention. Coronavirus disease 2019 (COVID-19): symptoms of coronavirus. 2020 May 13 [cited 2020 Sep 22]. https://www.cdc.gov/coronavirus/2019-ncov/symptoms-testing/symptoms.html
3. Centers for Disease Control and Prevention. Coronavirus disease 2019 (COVID-19): COVID-19 employer information for office buildings. 2020 Sep 11 [cited 2020 Sep 22]. https://www.cdc.gov/coronavirus/2019-ncov/community/office-buildings.html
4. Centers for Disease Control and Prevention. CDC COVID data tracker: commercial laboratory seroprevalence survey data. 2020 [cited 2020 Sep 5]. https://covid.cdc.gov/covid-data-tracker/#serology-surveillance

Address for correspondence: Samira Sami, Centers for Disease Control and Prevention, 1600 Clifton Rd NE, Atlanta, GA 30329, USA; email: ssami@cdc.gov

# Potential Association between Zika Infection and Microcephaly during 2007 Fever Outbreak, Gabon

Claudine A. Kombila Koumavor, Eric Elguero, Eric M. Leroy

Author affiliations: University of Health Sciences, Libreville, Gabon (C.A. Kombila Koumavor); Institute for Sustainable Development, IRD-CNRS-University of Montpellier Unit, Montpellier, France (E. Elguero, E. Leroy)

DOI: https://doi.org/10.3201/eid2702.202987

Although Zika virus (ZIKV) circulates in sub-Saharan Africa, no case of ZIKV-associated microcephaly has thus far been reported. Here, we report evidence of a possible association between a 2007 outbreak of febrile illness and an increase in microcephaly and possibly ZIKV infection in Gabon.

Since its 1947 discovery in Uganda, Zika virus (ZIKV) was restricted to sporadic human infections in Africa and Asia until 2007, when a large outbreak occurred in Micronesia, followed by another in French Polynesia 6 years later. This second outbreak spread to Brazil and throughout Central and South America, resulting in hundreds of thousands of cases (*1*). ZIKV infection leads to an asymptomatic or mildly symptomatic nonspecific disease in 80% of cases, but the outbreak in the Americas and French Polynesia coincided with a steep increase in the birth of babies with congenital microcephaly (*2*–*4*). However, no case of ZIKV-associated microcephaly has been recorded in sub-Saharan regions of Africa, where ZIKV also circulates.

During April–August 2007, Gabon's capital, Libreville, experienced simultaneous outbreaks of chikungunya and dengue (*5*). A retrospective study of 4,312 serum samples collected during this time found 5 ZIKV-positive cases (*6*). In addition, 2/137 (1.46%) pooled samples from *Aedes albopictus* mosquitoes tested positive for ZIKV, a proportion similar to that observed for dengue virus. Given that 80% of ZIKV infections are asymptomatic or subclinical, these findings suggest that an undetected ZIKV outbreak may have occurred in Gabon in 2007.

To determine if the incidence of microcephaly increased during this suspected ZIKV outbreak, we examined birth registers at the 2 main hospitals of Libreville: the Libreville Hospital Centre and the Regional Hospital of Melen in Estuaire Province. We recorded all births and cases of microcephaly occurring during January 2006–December 2008 (Figure). Most births in Libreville and its suburbs occur in these 2 hospitals; in addition, the hospitals receive newborns with malformations observed at birth who have been transferred from smaller healthcare facilities that lack neonatal departments. We collected most of the 4,312 samples from patients who visited these hospitals, so the 5 ZIKV case-patients likely lived in the 2 hospitals' coverage area.

In 2017, we searched birth registers for cases of microcephaly, identified when the head circumference was 2 SDs below the average, according to World Health Organization standards, depending on the age and sex of the neonate. For male-born infants, microcephaly corresponded to a cranial circumference of <31.9 cm, and for female-born infants, a cranial circumference of <31.5 cm, measured ≤48 hours after birth. We recorded only data from physical examination of newborns.

We collected details of 34,409 births and grouped them by 2-month periods from January–February 2006 through November–December 2008. Children were considered exposed if they were born during May 2007–June 2008 to mothers pregnant during April 2007–August 2007, as described elsewhere (*7*).

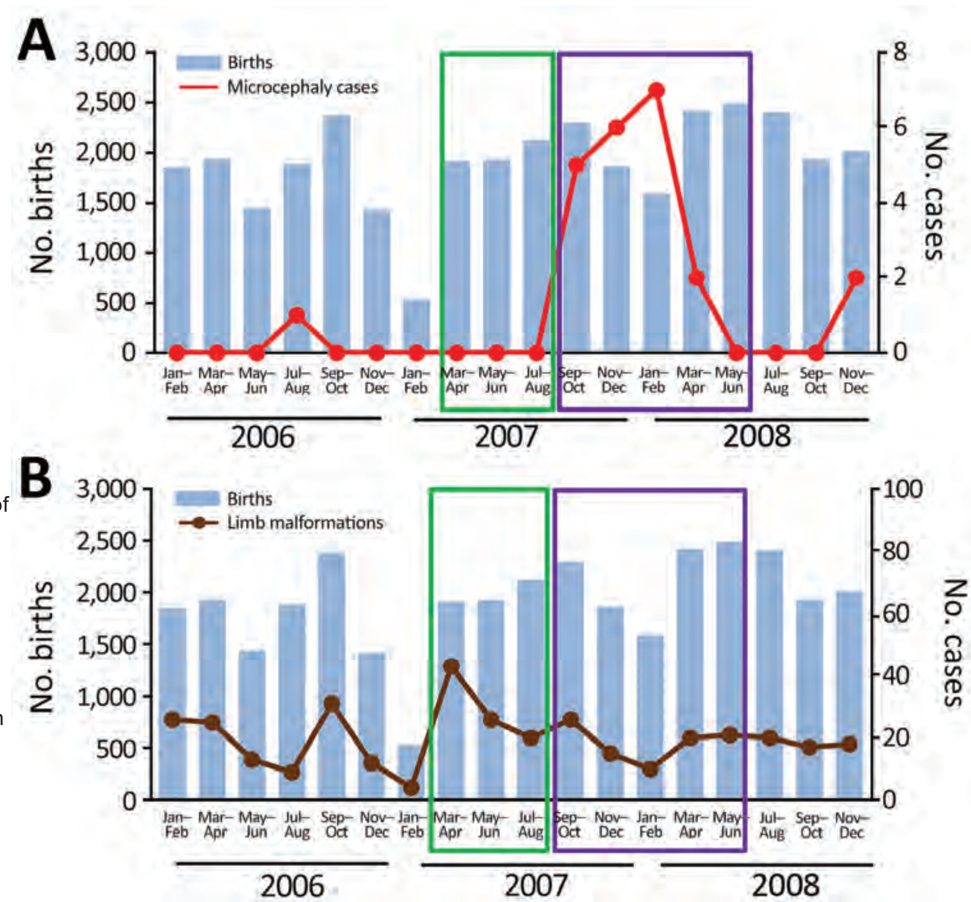


**Figure.** Cases of microcephaly (A) and limb malformations (B) in Libreville, Gabon, during January 2006–December 2008. Histograms correspond to the total number of births over the time of the study period. Scales for the y-axes differ to underscore patterns but do not permit direct comparisons. Green boxes encompass the time period when the febrile illness outbreak happened; purple boxes encompass the time period of births of infants whose mothers could have been exposed to Zika in their first trimester of pregnancy during the outbreak. Numbers of births were collected from birth registers by 2-month periods from January–February 2006 through November–December 2008. (Births are recorded in the registers in such a way that we were unable to obtain data for single months.) The duration of the febrile illness outbreak was estimated by the Health Ministry of Gabon during April 2007–August 2007, based on information communicated by hospitals. The febrile illness outbreak coincided with an increase in the number of patients seeking treatment for painful febrile illnesses at healthcare centers beginning in April 2007. The end of the outbreak in August 2017 coincided with the disappearance for ≥15 days of grouped clinical cases and with negative test results from samples.

We calculated statistical significance using the ratio of the odds of an infant with microcephaly being born within or outside of the exposure period. Only 1 case of microcephaly was recorded during January 2006–April 2007 (Figure, panel A), suggesting a baseline rate of ≈1 case/year.

Among 10,286 children born in the 14 months during May 2007–June 2008, a total of 20 microcephaly cases were recorded, compared with only 2 cases among 24,123 children born in the 20 months of the study period outside of the outbreak (OR 15.6, 95% CI 4.65–52.70; $p = 8.8 \times 10^{-6}$; Figure, panel A). In contrast, we found no increase in newborns with other types of malformation, such as limb malformations, during that period (Figure, panel B). Of note, 18 of the 20 outbreak-associated children with microcephaly were born during September 2007–February 2008, corresponding to mothers in the first trimester of pregnancy during the outbreak, when the risk of microcephaly in fetuses or neonates is highest. To eliminate potential artifacts in the data arising from unspecified environmental incidents, we used the same method of analysis to examine other congenital birth malformations such as facial, upper limb, and lower limb malformations. No significant associations were found.

Limitations of our study included that the tabulations (conducted in 2017) of ZIKV infections (from the 2007 disease outbreak) and microcephalic births were retrospective, meaning that no investigation of ZIKV infection was performed during the fever outbreak. Thus, there was no ZIKV diagnosis at the time of delivery for any of the mothers of infants born with microcephaly. Although fetal malformations are sometimes detected in obstetric ultrasounds, in Gabon they are usually discovered at birth. In addition, this study did not directly investigate the etiology of birth malformations for other possible explanations.

Despite these limitations, our findings support that the 2007 febrile illness outbreak in Libreville was associated with an increase in infants with microcephaly. Although microcephaly may be due to many other causes that were not investigated in our study, the detection of 5 ZIKV cases in samples collected during the febrile illness outbreak suggests a temporal association between ZIKV and microcephaly in this country. Given the risk of microcephaly in infants is ≈1% for mothers infected during the first trimester of pregnancy (*8*), the high number of microcephaly cases reported here indicates that ZIKV infections were likely prevalent during the outbreak. These observations highlight the need to provide specific priority care for pregnant women during future ZIKV outbreaks in Africa and to investigate possible ZIKV infections that have occurred in the past during the pregnancies of mothers of babies with microcephaly.

**Acknowledgments**

We thank Kurt McKean of Octopus Editing (https://octopusediting.com) for English-language editing of the manuscript.

## About the Author

Dr. Kombila Koumavor is a clinical infectious disease expert and a researcher in the Department of Virology and Bacteriology, University of Health Sciences, Libreville, Gabon. Her research interests include viral infectious diseases with an emphasis on arboviral, respiratory, and digestive infectious diseases in newborns and children.

### References

1. Baud D, Gubler DJ, Schaub B, Lanteri MC, Musso D. An update on Zika virus infection. Lancet. 2017;390:2099–109. PubMed https://doi.org/10.1016/S0140-6736(17)31450-2
2. de Araújo TVB, Rodrigues LC, de Alencar Ximenes RA, de Barros Miranda-Filho D, Montarroyos UR, de Melo APL, et al.; Investigators from the Microcephaly Epidemic Research Group; Brazilian Ministry of Health; Pan American Health Organization; Instituto de Medicina Integral Professor Fernando Figueira; State Health Department of Pernambuco. Association between Zika virus infection and microcephaly in Brazil, January to May, 2016: preliminary report of a case-control study. Lancet Infect Dis. 2016; 16:1356–63. https://doi.org/10.1016/S1473-3099(16)30318-8
3. Cauchemez S, Besnard M, Bompard P, Dub T, Guillemette-Artur P, Eyrolle-Guignot D, et al. Association between Zika virus and microcephaly in French Polynesia, 2013–15: a retrospective study. Lancet. 2016;387:2125–32. https://doi.org/10.1016/S0140-6736(16)00651-6
4. Moore CA, Staples JE, Dobyns WB, Pessoa A, Ventura CV, da Fonseca EB, et al. Characterizing the pattern of anomalies in congenital Zika syndrome for pediatric clinicians. JAMA Pediatr. 2017;171:288–95. https://doi.org/10.1001/jamapediatrics.2016.3982
5. Leroy EM, Nkoghe D, Ollomo B, Nze-Nkogue C, Becquart P, Grard G, et al. Concurrent chikungunya and dengue virus infections during simultaneous outbreaks, Gabon, 2007. Emerg Infect Dis. 2009;15:591–3. https://doi.org/10.3201/eid1504.080664
6. Grard G, Caron M, Mombo IM, Nkoghe D, Mboui Ondo S, Jiolle D, et al. Zika virus in Gabon (Central Africa)—2007: a new threat from *Aedes albopictus*? PLoS Negl Trop Dis. 2014;8:e2681. PubMed https://doi.org/10.1371/journal.pntd.0002681
7. Reefhuis J, Gilboa SM, Johansson MA, Valencia D, Simeone RM, Hills SL, et al. Projecting month of birth for at-risk infants after Zika virus disease outbreaks. Emerg Infect Dis. 2016;22:828–32. PubMed https://doi.org/10.3201/eid2205.160290
8. Saad-Roy CM, van den Driessche P, Ma J. Estimation of Zika virus prevalence by appearance of microcephaly. BMC Infect Dis. 2016;16:754. PubMed https://doi.org/10.1186/s12879-016-2076-z

Address for correspondence: Eric M. Leroy, unité MIVEGEC, Institut de Rechercher pour le Développement, Centre national pour la Rechercher scientifique, Université de Montpellier (UM), 911 avenue Agropolis, 34394, Montpellier, France; email: eric.leroy@ird.fr

# The Rules of Contagion: Why Things Spread—and Why They Stop

**Adam Kucharski; Basic Books, Hachette Book Group, New York, NY, USA, 2020; ISBN-13 (hardcover): 978-1541674318; ISBN-10: 1541674316; Pages: 341; Price: $30.00 (hardcover)**

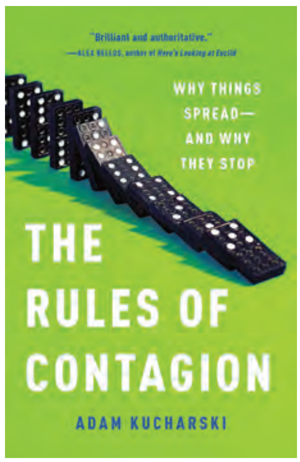


In 1902, Ronald Ross received the second Nobel Prize in Physiology or Medicine for discovering that mosquito bites transmit malaria. Determined to stop the spread of the disease, Ross developed mathematical models that demonstrated a key insight: mosquito control could effectively stop the spread of malaria without eliminating all mosquitos. This early insight showed the power of mechanistic models to inform efforts to slow the spread of infectious disease.

Over a century later, digital marketers repurposed epidemiologic models to tackle a new puzzle: spreading online content. They recognized that Instagram influencers have a lot in common with superspreaders of severe acute respiratory syndrome and that memes have $R_0$ values (mathematical terms that indicate how contagious an infectious disease is).

Although their goals were different, both the digital marketers and Ronald Ross turned to mathematical models to ask the same question: why do things spread, and why do they stop? This is the question that motivates Adam Kucharski's ambitious new book The Rules of Contagion. Kucharski, an associate professor at the London School of Hygiene and Tropical Medicine, has spent his career analyzing infectious disease outbreaks. In The Rules of Contagion, Kucharski zooms out to take a sweeping look at the science of how things, from viral infections to new ideas, spread.

Kucharski artfully interweaves the science of disease outbreaks with the spread of violent crime, financial bubbles, malware attacks, and folktales. Although this book covers a lot of ground, it is an incredibly fun ride. Kucharski shows how scientists and businessmen directly apply models of infectious disease dynamics to other contexts. For example, after the 2008 financial crisis, businesses on Wall Street recruited leading theoretical biologists to forecast financial contagion, such as the spread of an economic crisis from one country to another. However, social contagion fundamentally differs from infectious disease. For instance, influenza might be transmitted by a single exposure but the spread of new ideas might depend on cumulative exposure.

Against a backdrop of pandemic and political uncertainty, this book is a timely read. Models of disease outbreaks have never been more in the public eye. The science of contagion can help societies navigate not just disease, but also pressing political issues. For example, Kucharski makes a convincing case that violent crime behaves as a contagion; by viewing violence through this lens, public health experts have offered alternatives to traditional policing. Similarly, as misinformation spreads rampantly on social media during a US election year, understanding how ideas spread online has never been more crucial.

In one whirlwind of a book, The Rules of Contagion distills lessons learned from the Zika virus epidemic, the 2008 financial crisis, the ice bucket challenge, and more. Written in clear and accessible prose, this is a rewarding read for infectious disease professionals and members of the public alike. Whether you are looking to understand the coronavirus disease pandemic or promote your ideas to the public, Kucharski will convince you that understanding contagion is essential to understanding the modern world.

Valerie J. Morley

Author affiliation: The Pennsylvania State University, University Park, Pennsylvania, USA

DOI: https://doi.org/10.3201/eid2702.204255

Address for correspondence: Valerie J. Morley, Center for Infectious Disease Dynamics, W-235A Millennium Science Complex, The Pennsylvania State University, University Park, PA 16802, USA; email: vum84@psu.edu

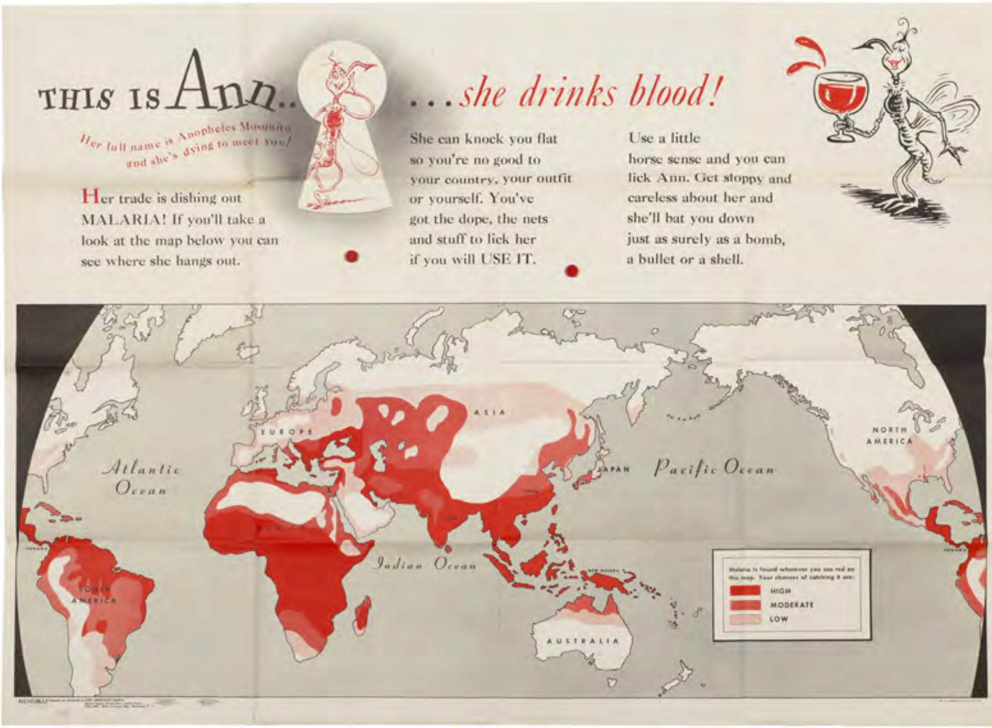


**Ted Geisel (aka Dr. Seuss) illustration; Munro Leaf, text; United States War Department Special Services Division and Government Printing Office. *This is Ann–: she drinks blood!* (1943).** Photomechanical print (poster): 35 inches x 47 inches/89 cm x 120 cm. National Library of Medicine, Bethesda, Maryland, USA. Public domain image.

# Public Health Posters Take Aim against Bloodthirsty Ann

Byron Breedlove

From June 1942 until September 1945, the United States Office of War used various media, including posters, as communication tools. Those posters—plastered in public areas, storefronts, factories, and military installations—employed motivation, guilt, and humor to boost morale and to encourage information security, buying war bonds, planting victory gardens, and, notably for military personnel deployed to tropical and subtropical areas during World War II, preventing malaria.

For military personnel deployed to tropical and subtropical areas during WWII, the number one health problem was malaria. Because of its lingering, debilitating, and recurring effects, this vector-borne infection hobbled the effectiveness of combat forces and support staff. Various official documents and publications issued by the Office of War and by the Office of Malaria Control in War Areas, a joint undertaking by the US Public Health Service and state health departments, detailed ways to reduce malaria infection, including using antimalarial drugs, insecticides, and bed nets. But the dense, bureaucratic language in such publications did not serve as a call to action. More accessible and persuasive messaging was needed to convince military personnel to protect their health for the good of the war effort.

Complicating matters, the traditional treatment for malaria, quinine, was in short supply. In 1942, Japan had seized control of the cinchona trees grown for quinine in the Dutch East Indies and other parts of Asia, and Germany had seized control of captured quinine reserves and manufacturing facilities in Amsterdam. The Allies turned to the synthetic drug quinacrine, known as Atabrine. Although effective, Atabrine had some disagreeable side effects: it often caused diarrhea, headaches, and nausea and had the unnerving, but temporary, tendency to turn skin bright yellow. Moreover, Japanese propaganda falsely proclaimed that using Atabrine could lead to infertility.

According to historical researcher Seth Paltzer, “It was clear to the Army that using antimalarials and

Author affiliation: Centers for Disease Control and Prevention, Atlanta, Georgia, USA

DOI: https://doi.org/10.3201/eid2702.AC2702

insecticides were key to the fight against disease but making sure troops at the front participated in these measures continued to be a problem. As a result, a third offensive front was opened against malaria, in the form of propaganda." Integral to that campaign were colorful, cartoonish posters for educating military personnel on malaria prevention.

Featured on this month's cover is a detail of an *Anopheles* mosquito from one such poster. At the top of the poster are the eye-catching words "This is Ann . . . and she drinks blood!" Drawings of Ann, whose full name is revealed to be "Anopheles Mosquito," appear twice, first glimpsed through a keyhole as a smiling red menace and then raising an oversized goblet brimming with blood (Figure).

The informal slang-based text calls attention to a world map showing where Ann "hangs out" and warns "She can knock you flat so you're no good to your country, your outfit or yourself. You've got the dope, the nets and stuff to lick her if you will USE IT." Bands of red indicate relative risks of contracting malaria in different locations when this poster was printed in late 1943. Among the highest risk locales are the South Pacific islands and southern Italy, where American forces were deployed.

Office of War Information posters and publications do not include credits. But the cartoonish images of Ann may look familiar. They are the handiwork of the young Army Captain Theodore Geisel, best known as Dr. Seuss, the pen name he used for writing and illustrating more than 60 children's books such as *Green Eggs and Ham* and *The Cat in the Hat*. Assigned to the Animation Department, First Motion Picture Unit, in Hollywood, California, USA, Geisel worked with a creative team of artists, cartoonists, writers, and filmmakers. Among them was Munro Leaf, another prolific author of childrens' books, including *The Story of Ferdinand*. Leaf drafted the text for this malaria poster and collaborated with Geisel on the related booklet *This Is Ann / She's Dying to Meet You*, featuring more of their text and illustrations.

Ginny A. Roth, Curator of Prints & Photographs, History of Medicine Division, National Library of Medicine, notes that Geisel and Leaf believed that the various military manuals and guides explaining how to prevent malaria were ". . . boring and concluded that soldiers were either not reading them or not making a connection between malaria and mosquitoes."

How much difference such posters made remains speculative, but the overall campaign yielded results. Paltzer writes, "Thanks to the educational efforts of the Army's propaganda, and the scientific and industrial base that supplied insecticides and antimalarials, the Army was able to significantly minimize the effects of malaria on the war effort, contributing in no small measure to final victory."

Effective September 15, 1945, an executive order by President Harry Truman shuttered the Office of War Information, which he had cited for its "outstanding contribution to victory." The war was over; however, the need to control malaria has persisted, although it has been largely controlled in many of the red-shaded areas on this WWII poster. Still the World Health Organization reports that in 2019, there were an estimated 229 million cases of malaria worldwide and an estimated 409,000 deaths, largely among children in the Africa region. Ann is still drinking blood and spreading malaria, especially in resource-limited tropical and subtropical areas.

### Bibliography


1. Beadle C, Hoffman SL. History of malaria in the United States Naval Forces at war: World War I through the Vietnam conflict. Clin Infect Dis. 1993;16:320–9. https://doi.org/10.1093/clind/16.2.320
2. Breedlove B, Arguin PM. Portrait of the coveted cinchona. Emerg Infect Dis. 2015;21:1280–1. https://doi.org/10.3201/eid2107.AC2107
3. Centers for Disease Control and Prevention. Malaria [cited 2021 Jan 2]. https://www.cdc.gov/parasites/malaria/index.html
4. Cornell University Library Digital Collections. This is Ann . . . She drinks blood [cited 2021 Dec 14]. https://digital.library.cornell.edu/catalog/ss:19343604
5. Malaria training manual and NAVMED. Prevention of malaria in military and naval forces in the South Pacific. Washington : U.S. G.P.O., 1944. U.S. National Library of Medicine Archive [cited 2021 Jan 14]. http://resource.nlm.nih.gov/101708640
6. Paltzer S. The other foe: the US Army's fight against malaria in the Pacific Theater, 1942–45 [cited 2020 Dec 17]. https://armyhistory.org/the-other-foe-the-u-s-armys-fight-against-malaria-in-the-pacific-theater-1942-45
7. Roth GA. Happy birthday, Dr. Seuss! [cited 2020 Dec 17]. https://circulatingnow.nlm.nih.gov/2019/03/04/happy-birthday-dr-seuss
8. Seuss D. Artist. United States. War Department Special Services Division, distributor. United States. Government Printing Office, printer. Army Orientation Course. This is Ann–: she drinks blood [cited 2020 Dec 14]. https://collections.nlm.nih.gov/catalog/nlm:nlmuid-101439358-img
9. United States. Office of Malaria Control in War Areas. Malaria control in war areas, 1943–44 [cited 2020 Dec 31]. https://stacks.cdc.gov/view/cdc/20727
10. World Health Organization. World Malaria Report 2020: 20 years of global progress and challenges. World malaria report 2020 (who.int) p. xv [cited 2021 Dec 31]. https://www.who.int/docs/default-source/malaria/world-malaria-reports/9789240015791-double-page-view.pdf?sfvrsn=2c24349d_5


Address for correspondence: Byron Breedlove, EID Journal, Centers for Disease Control and Prevention, 1600 Clifton Rd NE, Mailstop H16-2, Atlanta, GA 30329-4027, USA; email: wbb1@cdc.gov

# Earning CME Credit

To obtain credit, you should first read the journal article. After reading the article, you should be able to answer the following, related, multiple-choice questions. To complete the questions (with a minimum 75% passing score) and earn continuing medical education (CME) credit, please go to http://www.medscape.org/journal/eid. Credit cannot be obtained for tests completed on paper, although you may use the worksheet below to keep a record of your answers.

You must be a registered user on http://www.medscape.org. If you are not registered on http://www.medscape.org, please click on the "Register" link on the right hand side of the website.

Only one answer is correct for each question. Once you successfully answer all post-test questions, you will be able to view and/or print your certificate. For questions regarding this activity, contact the accredited provider, CME@medscape.net. For technical assistance, contact CME@medscape.net. American Medical Association's Physician's Recognition Award (AMA PRA) credits are accepted in the US as evidence of participation in CME activities. For further information on this award, please go to https://www.ama-assn.org. The AMA has determined that physicians not licensed in the US who participate in this CME activity are eligible for AMA PRA Category 1 Credits™. Through agreements that the AMA has made with agencies in some countries, AMA PRA credit may be acceptable as evidence of participation in CME activities. If you are not licensed in the US, please complete the questions online, print the AMA PRA CME credit certificate, and present it to your national medical association for review.

## Article Title

# Zika Virus–Associated Birth Defects, Costa Rica, 2016–2018

## CME Questions

**1. Your patient is a newborn infant born to a mother with confirmed Zika virus (ZIKV) infection. According to the descriptive analysis by Benavides-Lara and colleagues, which of the following statements about prevalence of Zika-related birth defects (ZBD) and microcephaly among live-born infants in Costa Rica, March 2016 to March 2018, is correct?**

A. Prevalence of ZBD was 5.3/100,000 births
B. Mortality within the first year of life among infants with ZBD was 6.6%
C. Provinces with the highest prevalence of ZBD were Limón and Puntarenas (58.8/100,000 and 37.1/100,000 live births, respectively)
D. Three-quarters of infants with confirmed or probable ZBD had microcephaly

**2. According to the descriptive analysis by Benavides-Lara and colleagues, which of the following statements about clinical and test findings of live-born infants with ZBD in Costa Rica, March 2016 to March 2018, is correct?**

A. 82% had brain anomalies; 95%, neurodevelopmental abnormalities; 41%, eye abnormalities; and 9% had hearing loss
B. Half of the evaluated cases had evidence of ≥1 brain defect on neuroimaging
C. Most cases were hypotonic
D. None of the cases had swallowing problems

**3. According to the descriptive analysis by Benavides-Lara and colleagues, which of the following statements about clinical and public health implications of ZBD among live-born infants in Costa Rica, March 2016 to March 2018, is correct?**

A. Timing of ZBD in Costa Rica relative to peak incidence of ZIKV infection in pregnant women differed substantially from that in Brazil, Colombia, and the United States
B. Enhancement of existing national birth defects surveillance identified affected babies and ensured referral of families to appropriate services
C. After ZIKV infection in a pregnant woman, microcephaly is the only congenital anomaly that should be monitored, and monitoring can stop at birth
D. Costa Rica's National Guidelines (CRNG) regarding surveillance of ZIKV disease in pregnant women contradict those of the Pan American Health Organization (PAHO)

# Earning CME Credit

To obtain credit, you should first read the journal article. After reading the article, you should be able to answer the following, related, multiple-choice questions. To complete the questions (with a minimum 75% passing score) and earn continuing medical education (CME) credit, please go to http://www.medscape.org/journal/eid. Credit cannot be obtained for tests completed on paper, although you may use the worksheet below to keep a record of your answers.

You must be a registered user on http://www.medscape.org. If you are not registered on http://www.medscape.org, please click on the "Register" link on the right hand side of the website.

Only one answer is correct for each question. Once you successfully answer all post-test questions, you will be able to view and/or print your certificate. For questions regarding this activity, contact the accredited provider, CME@medscape.net. For technical assistance, contact CME@medscape.net. American Medical Association's Physician's Recognition Award (AMA PRA) credits are accepted in the US as evidence of participation in CME activities. For further information on this award, please go to https://www.ama-assn.org. The AMA has determined that physicians not licensed in the US who participate in this CME activity are eligible for AMA PRA Category 1 Credits™. Through agreements that the AMA has made with agencies in some countries, AMA PRA credit may be acceptable as evidence of participation in CME activities. If you are not licensed in the US, please complete the questions online, print the AMA PRA CME credit certificate, and present it to your national medical association for review.

## Article Title

# *Plasmodium ovale wallikeri* and *P. ovale curtisi* Infections and Diagnostic Approaches to Imported Malaria, France, 2013–2018

## CME Questions

**1. You are advising an infectious disease practice regarding management of patients with *Plasmodium ovale* malaria. According to the retrospective multicenter analysis by Joste and colleagues, which of the following statements about epidemiologic and clinical characteristics of *P. ovale curtisi* (POC) and *P. ovale wallikeri* (POW) in infected patients treated in France from January 2013 to December 2018 is correct?**

A. Patients with POC vs POW infections had worse thrombocytopenia and shorter latency period
B. Patients with POC vs POW infections were significantly more likely to receive intensive care unit care
C. Among *P. ovale* cases, the proportion of POW infections increased from 44% to 59% between 2013 and 2018
D. Receipt of prophylactic treatment did not affect latency period

**2. According to the retrospective multicenter analysis by Joste and colleagues, which of the following statements about diagnostic test findings of POC- and POW- infected patients treated in France from January 2013 to December 2018 is correct?**

A. Rapid diagnostic tests (RDTs) detecting aldolase were more effective than those detecting *Plasmodium lactate* dehydrogenase (pLDH) (P < 0.001), with no difference in efficacy between POW and POC
B. Species identification for POW and POC were 97% accurate
C. Country of contamination was strongly associated with *P. ovale* tryptophan-rich antigen (potra) genotype
D. The potra gene was an excellent genetic marker of relapse

**3. According to the retrospective multicenter analysis by Joste and colleagues, which of the following statements about treatment and clinical implications of characteristics of POC- and POW-infected patients treated in France from January 2013 to December 2018 is correct?**

A. New recommendations from the French Infectious Diseases Society (SPILF) in 2017 led to marked increases in chloroquine treatment
B. POW- vs POC-infected patients were more frequently treated with artemisinin-based combination therapy (ACT) (29.2% vs 17.1%; P < 0.001)
C. ACT treatment was not associated with latency period
D. Currently, *P. ovale* relapses are diagnosed mainly by potra gene sequencing